frontiers | Research Topics

Molecular markers and targeted therapy for hepatobiliary tumors

Edited by
Yunfei Xu, Zongli Zhang, Hongda Liu and Xuesong Gu

Published in
Frontiers in Oncology

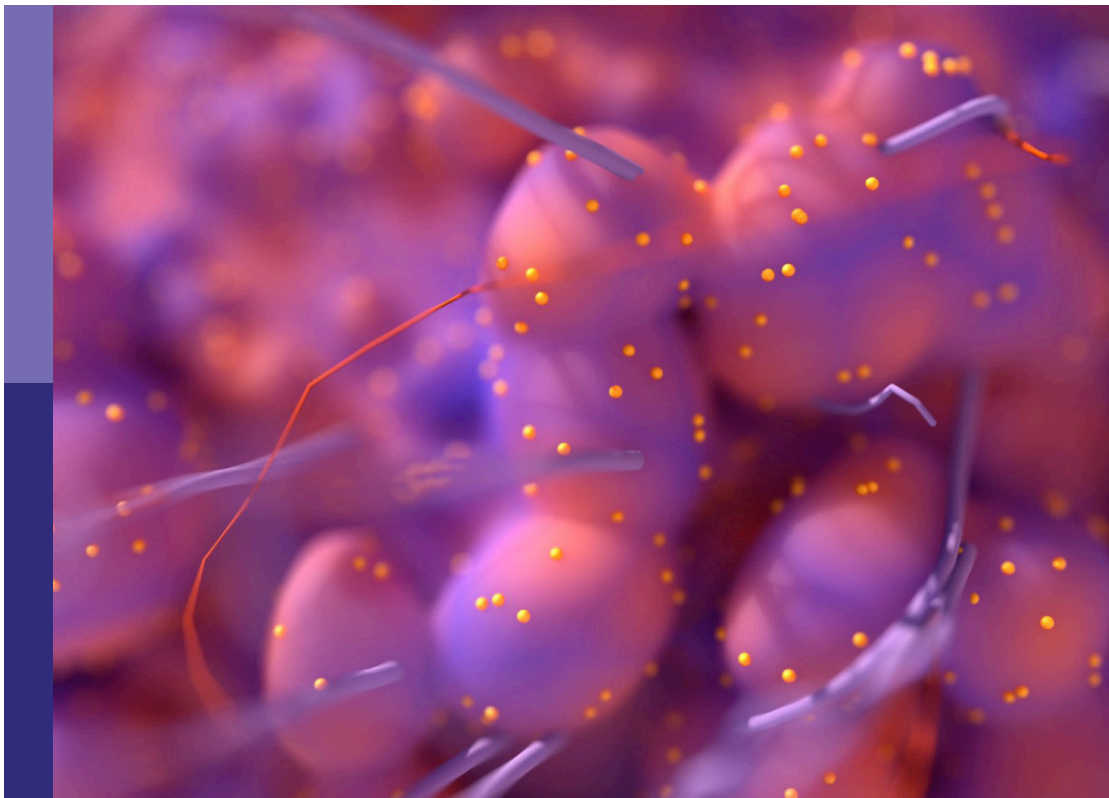

ISSN 1664-8714
ISBN 978-2-8325-4721-2
DOI 10.3389/978-2-8325-4721-2

About Frontiers

Frontiers is more than just an open access publisher of scholarly articles: it is a pioneering approach to the world of academia, radically improving the way scholarly research is managed. The grand vision of Frontiers is a world where all people have an equal opportunity to seek, share and generate knowledge. Frontiers provides immediate and permanent online open access to all its publications, but this alone is not enough to realize our grand goals.

Frontiers journal series

The Frontiers journal series is a multi-tier and interdisciplinary set of open-access, online journals, promising a paradigm shift from the current review, selection and dissemination processes in academic publishing. All Frontiers journals are driven by researchers for researchers; therefore, they constitute a service to the scholarly community. At the same time, the *Frontiers journal series* operates on a revolutionary invention, the tiered publishing system, initially addressing specific communities of scholars, and gradually climbing up to broader public understanding, thus serving the interests of the lay society, too.

Dedication to quality

Each Frontiers article is a landmark of the highest quality, thanks to genuinely collaborative interactions between authors and review editors, who include some of the world's best academicians. Research must be certified by peers before entering a stream of knowledge that may eventually reach the public - and shape society; therefore, Frontiers only applies the most rigorous and unbiased reviews. Frontiers revolutionizes research publishing by freely delivering the most outstanding research, evaluated with no bias from both the academic and social point of view. By applying the most advanced information technologies, Frontiers is catapulting scholarly publishing into a new generation.

What are Frontiers Research Topics?

Frontiers Research Topics are very popular trademarks of the *Frontiers journals series*: they are collections of at least ten articles, all centered on a particular subject. With their unique mix of varied contributions from Original Research to Review Articles, Frontiers Research Topics unify the most influential researchers, the latest key findings and historical advances in a hot research area.

Find out more on how to host your own Frontiers Research Topic or contribute to one as an author by contacting the Frontiers editorial office: frontiersin.org/about/contact

Molecular markers and targeted therapy for hepatobiliary tumors

This ebook is split into several files; this is part one of the ebook, please see the overview text of the Research Topic page to access the second part of the ebook.

Topic editors

Yunfei Xu — Shandong University, China

Zongli Zhang — Qilu Hospital of Shandong University, China

Hongda Liu — Nanjing Medical University, China

Xuesong Gu — Beth Israel Deaconess Medical Center, Harvard Medical School, United States

Citation

Xu, Y., Zhang, Z., Liu, H., Gu, X., eds. (2024). *Molecular markers and targeted therapy for hepatobiliary tumors*. Lausanne: Frontiers Media SA.

doi: 10.3389/978-2-8325-4721-2

Table of contents

frontiers in Oncology

SYSTEMATIC REVIEW
published: 28 June 2021
doi: 10.3389/fonc.2021.707742

Prognostic Value of Peripheral Whole Blood Cell Counts Derived Indexes in Gallbladder Carcinoma: A Systematic Review and Meta-Analysis

Bowen Xu[1†], Zhiqiang Chen[1†], Jing Zhang[2], Jianhua Chang[1], Wei Zhao[1], Zhaoru Dong[1], Xuting Zhi[1] and Tao Li[1,3*]*

[1] Department of Hepatobiliary Surgery, General Surgery, Qilu Hospital, Cheeloo College of Medicine, Shandong University, Jinan, China, [2] Department of Surgery, Yidu Central Hospital of Weifang City, Weifang, China, [3] Department of Hepatobiliary Surgery, The Second Hospital of Shandong University, Jinan, China

OPEN ACCESS

Edited by:
Xuesong Gu,
Beth Israel Deaconess Medical Center and Harvard Medical School, United States

Reviewed by:
Qi Pan,
Fudan University, China
Guoming Shi,
Fudan University, China
Liang Liu,
Fudan University, China

***Correspondence:**
Tao Li
litao7706@163.com
Zhiqiang Chen
chenzhq1982@hotmail.com

†These authors have contributed equally to this work and share first authorship

Specialty section:
This article was submitted to Cancer Molecular Targets and Therapeutics, a section of the journal Frontiers in Oncology

Received: *10 May 2021*
Accepted: *08 June 2021*
Published: *28 June 2021*

Citation:
Xu B, Chen Z, Zhang J, Chang J, Zhao W, Dong Z, Zhi X and Li T (2021) Prognostic Value of Peripheral Whole Blood Cell Counts Derived Indexes in Gallbladder Carcinoma: A Systematic Review and Meta-Analysis. Front. Oncol. 11:707742. doi: 10.3389/fonc.2021.707742

Background: Gallbladder carcinoma (GBC) is a rare gastrointestinal malignancy with poor prognosis. Adequate pre-treatment prediction of survival is essential for risk stratification and patient selection for aggressive surgery or adjuvant therapeutic strategy. Whole blood cell count (WBCC) derived indexes are broadly used as prognosticative biomarkers in various cancer types, but their utility in GBC needs to be validated.

Methods: An extensive literature review was conducted in line with PRISMA guideline until June 31 2020, to identify original studies concerning WBCC-derived indexes as prognostic indicators in GBC. All relative parameters were extracted and pooled for statistical analyses.

Results: Fourteen studies incorporating 2,324 patients were included with a high quality and low risk of biases. All 14 studies evaluated the prognostic value of NLR showing a significant correlation with OS in GBC patients (HR = 1.94, P <0.001). Elevated NLR was revealed to correlate with TNM stage (stages III and IV, OR = 4.65, P <0.001), tumor differentiation (OR = 2.37, P <0.042), CA 19-9 (SMD = 0.47, P = 0.01), but no significance was found with age, sex and CEA. Positive indicative value of MLR and PLR were also confirmed with a HR of 2.06 (P <0.001) and 1.34 (P <0.001), respectively.

Conclusion: The WBCC-derived indexes including NLR, MLR/LMR and PLR were validated to be useful prognostic parameters for predicting survival outcomes in GBC patients. These series of indexes, especially NLR, could improve risk stratification and facilitate better patient selection for surgical resection or aggressive chemotherapy in the decision making of GBC patients.

Keywords: gallbladder carcinoma (GBC), neutrophil-to-lymphocyte ratio (NLR), lymphocyte-to-monocyte ratio (LMR), platelet-to-lymphocyte ratio (PLR), prognosis

INTRODUCTION

Gallbladder carcinoma (GBC) is a relatively rare gastrointestinal malignancy with an estimated incidence rate about 1.0–3.0/100,000 in the United States and China (1, 2). It is unique in its characteristics that if diagnosed at an early stage (T1a and T1b, before invading beyond gallbladder mucosa), a nearly 100% 5-year survival could be achieved after surgery, but at its later stage (T2 especially T3 and T4, tumor penetrating beyond muscular layer), the long-term survival becomes dismal with only 25% of patients who could undergo potentially curative surgery and just 12–23% could survive for more than 5 years (3, 4). At present, no consensus has been achieved on the optimal treatment of GBC, and multidisciplinary therapy of surgery combined with adjuvant therapy may play a better role in prolonging the survival of patients with advanced GBC (3, 5).

Pathologic TNM staging from the American Joint Committee on Cancer (AJCC) is now the most widely adopted accurate and effective prognosis predicting system for various cancers including GBC (6). However, it could only be assessed after surgery which may account for only a minority of patients suffering GBC. Therefore, it is necessary to pursue preoperative biological markers that could predict survival outcomes of patients, aid in risk stratification and personalized decision making on whether patient could get potential benefits from more aggressive therapies (3).

There is growing evidence that systemic inflammation response (SIR) plays an important role in cancer development and progression, thus various SIR-related biomarkers have been developed and evaluated as prognostic indicators in different cancer types (7, 8). One series of SIR-related biomarkers is derived from peripheral whole blood cell counts (WBCC) which include neutrophil-to-lymphocyte ratio (NLR), lymphocyte-to-monocyte ratio (LMR) or monocyte-to-lymphocyte ratio (MLR), and platelet-to-lymphocyte ratio (PLR). These WBCC-derived indexes showed some great advantages over other pathology related markers, such as easy to perform, good replicability, low cost and preoperative application etc. (7, 8).

Despite the robust and growing data regarding the utility of these WBCC-derived indexes, findings are not uniform across all publications. Furthermore, previous studies mainly focused on colorectal, pancreatic, prostate, lung, esophageal-gastric and breast cancers (7), only few studies conducted investigations on GBC until recently (9–22). Based on the available data, we aimed to systematically review and rationalize the evidence for the prognostic value of these WBCC-derived indexes in predicting outcomes of GBC patients.

MATERIALS AND METHODS

This study was conducted in line with the PRISMA and AMSTAR guidelines that were well defined protocols for systemic reviews and meta-analysis (23, 24).

Inclusion and Exclusion Criteria

The inclusion criteria of studies in this meta-analysis were defined as: (i) randomized controlled trials (RCT), cohort studies or case control studies; (ii) patients diagnoses of GBC were confirmed by pathology; and (iii) any of the WBCC-derived markers (including NLR, PLR, MLR or LMR) were investigated objects of the studies, and clear cut-off values were given or could be extracted from the Kaplan–Meier curves. The exclusion criteria were: (i) basic researches or animal trials; (ii) abstracts, meta-analysis, case reports, letters, expert comments or reviews; (iii) hazard ratio (HR) investigating correlation between prognostic markers and overall survivals unavailable or cannot be extracted from the K–M curve; and (iv) patients suffered from other primary tumors or with severe infections.

Search Strategy

PubMed, Medline, Web of Science, Scopus, CNKI, and China Biology Medicine disc (CBMdisc) were searched by two independent researchers from inception to June 31 2020 without any other limits. The medical subject headings (MeSH) terms and free text terms were used to locate articles, combined with the Boolean operators to make an appropriate search strategy. The MeSH terms included "Gallbladder Neoplasms", "Lymphocytes", "Neutrophils", and the free text terms included "Neutrophil-lymphocyte (Ratio)", "Neutrophil (to) Lymphocyte (Ratio)".

Quality Assessment and Data Extraction

After eliminating duplicates, two researchers read titles and abstracts, then by reading full-texts to identify eligible literatures that met the inclusion and exclusion criteria for meta-analysis. The qualitative assessment of RCTs was based on Cochrane risk of bias tool. The Newcastle–Ottawa Scale (NOS) was used to assess risk of bias in non-RCTs. Two researchers used standardized Excel sheets to extract information from the final included studies, including basic information of the study (title, first author, year of publication, study types and number of patients), demographics (patient age and gender), oncology information (tumor types, predominant treatment arms, follow-up time, disease-free survival (DFS), overall survival (OS), hazard ratio (HR) and 95% confidence interval (95% CI), NLR, PLR, LMR and other tumor markers). In the absences of vital data from a study, the corresponding author of the study was inquired by email.

Statistical Analysis

In this meta-analysis, we mainly focused on the efficacy of NLR, MLR/LMR and PLR on predicting patient survival, and HR with 95% CI was employed to make analysis, as HR incorporates the impact of time-to-event outcomes and is more reliable to reflect survival status of patients over other statistical measures (25). Engauge Digitizer (version 10.8) and method described by Tierney et al. was used to calculate HR from available statistics and Kaplan–Meier curves if the included studies did not provide HR (26). The odds ratio (OR) was chosen to evaluate the association between NLR, MLR/LMR, PLR and clinical

features. The numerical data were expressed as means ± standard deviations (SD), and was calculated by using the method from Wan et al. and Luo et al., if the original studies only provided medians and interquartile ranges (27, 28). Heterogeneity between studies was evaluated by Chi-squared ($\chi 2$) Q test, and the extent of heterogeneity was quantified by I^2 index. The random-effects model was applied when the heterogeneity was low (I2 <50%), otherwise, the fixed effects model was adopted (I2 >50%). In addition, sensitivity and subgroup analyses were used to find the source of heterogeneity. The publication bias was assessed by Begg's funnel plot and Egger's test. All the statistical data were analyzed with STATA 12.0 (Version 12.0, Stata Corp LP, College Station, TX). A value of P <0.05 was considered statistically significant.

RESULTS

Search Results and Study Characteristics

The study selection was carried out in accordance with PRISMA flowchart (**Figure 1**). A total of 221 potentially relevant studies were identified from six databases by using the formulated search strategy. After removal of duplicates, we browsed the titles and abstracts of the remaining 134 studies, and 107 studies were excluded according to the inclusion and exclusion criteria. Then we assessed full-text review of the remaining 27 studies, another 13 studies were excluded and finally 14 retrospective cohort studies were included for meta-analysis (9–22). Basic characteristics of included studies were listed in **Table 1**. There were 2,324 patients in total from all studies with a mean NOS score of 7.6 ± 0.69, indicating a low risk of bias. NLR was evaluated by all the 14 studies enrolled, while MLR/LRM and PLR were investigated by only six and eight studies, respectively. Although we could calculate or directly withdraw HR data from all studies, it needs to be noted that different cut-off values were employed, as well as calculation methods for cut-off value among which ROC curve analysis was the mostly adopted by majority of authors.

Prognostic Value of NLR and Its Association With Clinical Features

NLR was evaluated in all 14 studies enrolled and HR data could be extracted directly from 14 studies and calculated from K–M curve from one study using the method as described above (26). The heterogeneity was not significant (P = 0.184, I^2 = 25%) among studies, so the fixed effect model was used for meta-analysis evaluating prognostic value between high NLR and low NLR groups. Compared with lower NRL group, higher pretreatment NLR was significantly correlated with shorter OS in GBC patients as shown in **Figure 2** with a HR value of 1.94 (95% CI=1.71–2.19, P <0.001).

As most included studies investigated the association between NLR and various clinical parameters including TNM stage, tumor differentiation, CA199 and CEA etc., we then summarized the

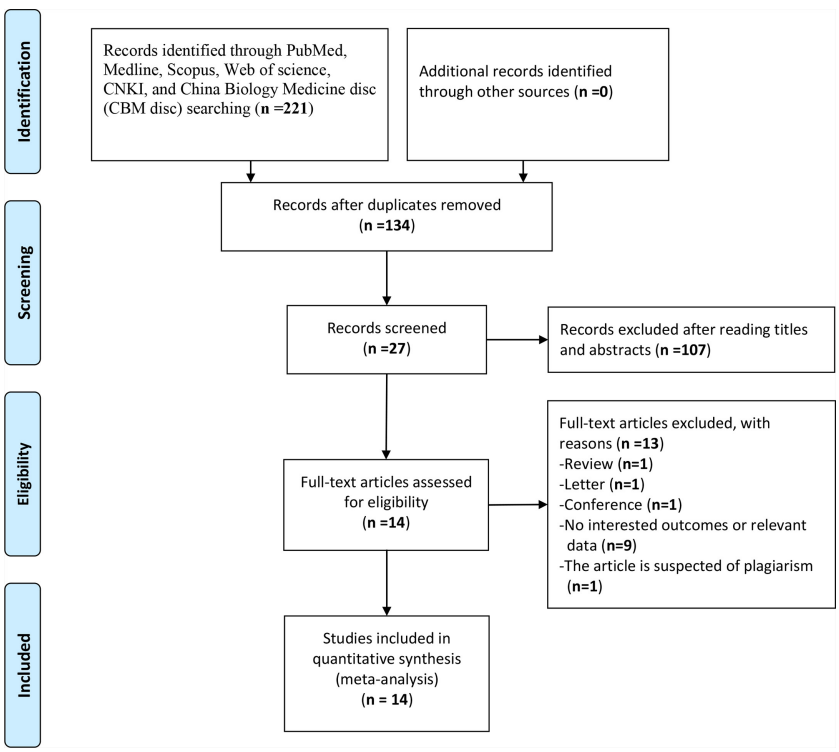

FIGURE 1 | Flow diagram following the PRISMA template of the search strategy for studies included in this meta-analysis.

TABLE 1 | Basic characteristics of included studies.

Study	Country	Patients (n)	Sex (M/F)	TNM stage (n)	cut-off value with HR (*P* value)			calculation method for cut-off value	NOS
					NLR	MLR/LMR	PLR		
Wu (9)	China	85	NR	I/II/III/IV (21/13/47/6)	2.3 1.77 (0.016)	NR	NR	median value of effect size	9
Gao (10)	China	90	47/43	I/II/III/IV (54/11/23/2)	5 3.09 (0.027)	NR	NR	refer to others	8
Zhang (11)	China	145	68/77	I/II/III/IV (7/12/75/51)	1.94 2.73 (0.001)	NR	113.3 1.74 (0.001)	ROC curve	8
Beal (12)	America	187	NR	NR	5 3.52 (0.02)	NR	NR	refer to others	8
Zhang (13)	China	316	215/101	I–II/III–IV (28/288)	2.61 1.65 (0.008)	NR	NR	ROC curve	8
Cui (14)	China	159	NR	I/II/III/IV (13/27/50/69)	4.39 1.57 (0.01)	0.30/NR 1.61 (0.006)	181 1.24 (0.23)	ROC curve	8
Tao (15)	China	84	28/56	III/IV (35/49)	3.2 2.348 (0.002)	0.25/NR 2.42 (0.001)	117.7 1.859 (0.024)	ROC curve	9
Du (16)	China	220	122/98	NR	5.1 1.38 (0.62)	NR/2.92 0.69 (0.03)	178 0.75 (0.44)	X-tile software	7
Choi (17)	South Korea	178	95/83	III/IV (39/139)	2 2.06 (0.001)	0.24/NR 2.53 (0.001)	108 1.69 (0.019)	refer to others	9
Deng (18)	China	169	55/114	I/II/III/IV (16/37/76/40)	2.61 3.30 (0.008)	NR/2.66 1.55 (0.027)	145.3 1.221 (0.376)	ROC curve	8
Liu (19)	China	90	NR	I–II/III–IV (20/70)	4.33 3.84 (0.01)	NR	NR	mean value of effect size	7
Navarro (20)	South Korea	197	83/114	II/III/IV (148/41/8)	2.4 1.80 (0.44)	NR/4 1.25 (0.739)	148 0.53 (0.432)	ROC curve	8
You (21)	South Korea	173	87/86	III/IV/IV (1/8/164)	3 1.65 (0.017)	NR	190 1.19 (0.405)	refer to others	8
Mady (22)	America	231	72/159	NR	5 1.70 (0.003)	NR	NR	refer to others	9

TNM, tumor/node/metastasis stages; HR, Hazard Ratio; NLR, neutrophil-to-lymphocyte ratio; MLR, monocyte-to-lymphocyte ratio; LMR, lymphocyte-to-monocyte ratio; PLR, platelet-to-lymphocyte ratio; NR, not reported; ROC, receiver operating characteristic; NOS, Newcastle–Ottawa Scale.

pooled OR of these parameters. As shown in **Table 2**, elevated NLR had significant correlation with TNM stage (stages III and IV, OR = 4.65, 95% CI = 1.96–11.03, P <0.001), tumor differentiation (OR = 2.73, 95% CI = 1.04–7.18, P <0.042), CA 19-9 (SMD = 0.47, 95% CI = 0.11–0.82, P = 0.01), but no significance was found with age, sex and CEA. Due to the significant heterogeneity between studies, random-effects models were used for analysis.

The Prognostic Value of MLR/LMR

Three studies incorporating 421patients reported the prognostic value of MLR in GBC patients (14–16). As shown in **Figure 3**, high MLR was significantly correlated with shorter OS in GBC patients compared to low MLR group, with a pooled HR of 2.06 (95% CI = 1.51–2.82, P <0.001). The heterogeneity was not significant (P = 0.193, I^2 = 39.2%) among studies, and the fixed effect model was used for meta-analysis. Another three studies enrolling 586 patients reported the relationship between LMR and OS in GBC patients (17, 18, 21). The primary results showed that there was no significant correlation between LMR and prognosis of GBC patients with a HR of 1.08 (95% CI = 0.58–2.07, P = 0.814, I^2 = 70%). Due to the high heterogeneity, we performed sensitivity analysis and revealed that the heterogeneity decreased significantly after excluding the study by Deng et al. (17), but the final result did not change either (HR = 0.73, 95% CI = 0.46–1.15, I^2 = 0%, P = 0.176). By re-reading the study by Deng et al., we found that they set the lower LMR group as experimental group instead of control group as the other two enrolled studies (18, 21). Therefore, we re-calculated the reciprocal of HR and 95% CI with a correction of pooled HR of 0.68 (95% CI = 0.51–0.91, I^2 = 0%, P = 0.011), showing significant correlation between low LMR and poor OS in GBC patients.

The Prognostic Value of PLR

Eight studies incorporating 1,325 patients investigated prognostic value of PLR in GBC patients (11, 14–18, 20, 21). No significant heterogeneity between groups was observed (I^2 = 33.4%, P = 0.162), and the pooled HR showed that low PLR group had significant better OS than high PLR group (**Figure 4**, HR = 1.34, 95% CI = 1.14–1.57, P <0.001).

Subgroup Analyses and Publication Bias

Our meta-analyses result above confirmed that NLR, LMR/MLR and PLR could be used as prognostic predictor of OS in GBC patients. Although there was no significant heterogeneity between groups, we still performed subgroup analysis in case of patient selection bias. Three stratification parameters were selected for subgroup analysis, that include cut-off value (≤3, 3–5 and ≥5), sample size (>100 and ≤100) and geographic area (Asian and America). Due to sample size and data availability, the subgroup analysis was only performed in NLR group, which confirmed a positive result as ungrouped analysis (**Figure 5**).

In the end, we run Begg's and Egger's test to examine the main effect indicators of this study. The results showed that there was no significant publication bias among included studies,

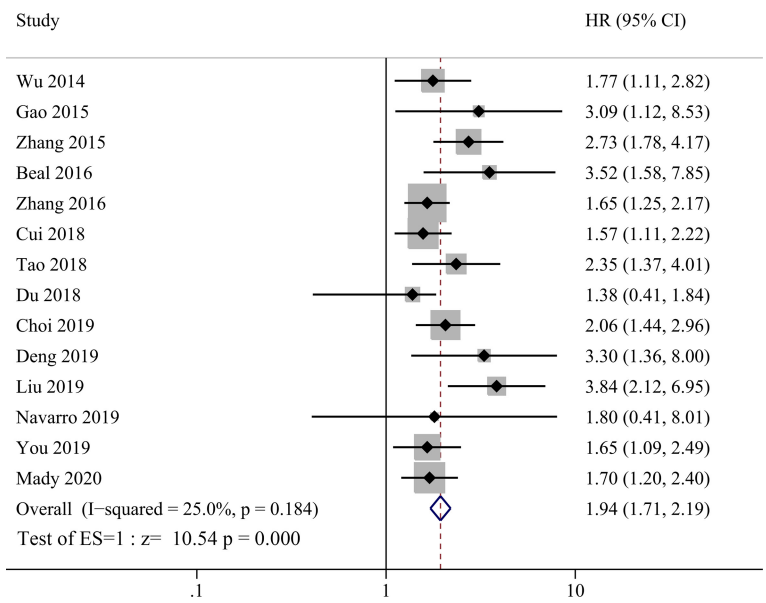

FIGURE 2 | Forest plot for the association between neutrophil-lymphocyte ratio (NLR) and overall survival of patients with Gallbladder carcinoma (GBC).

TABLE 2 | The association between elevated neutrophil-to-lymphocyte ratio (NLR) and clinical features.

Clinical parameter	Number of studies	Number of participants	Pooled results		*P* value
			Effect Size	95% CI	
Age (>60 years)	2	180	OR: 1.17	0.45–3.03	0.29
Age (>65years)	2	243	OR: 0.62	0.25–1.51	0.749
Gender (Male)	9	1,378	OR: 1.33	0.95–1.87	0.099
CEA (High)	3	320	SMD: 0.025	−0.198–0.249	0.826
CA-199 (High)	4	498	SMD: 0.47	0.11–0.82	0.01
TNM stage (III and IV)	7	969	OR: 4.65	1.96–11.03	<0.001
Tumor differentiation (Poor and undifferentiated)	5	726	OR: 2.73	1.04–7.18	0.042

OR, odds ratio; CI, confidence interval; CEA, carcinoembryonic antigen; CA-199, carbohydrate antigen 199; TNM, tumor/node/metastasis stage; SMD, Standard mean difference.

and the funnel plot was symmetrical (**Figure 6**, Begg's test P = 0.373, Egger's test P = 0.225).

DISCUSSION

GBC is rare and one of the most aggressive cancers with poor prognosis worldwide (29). Up to date, pathological TNM (pTNM) staging is still the gold standard risk stratification system and reversely correlated with survival of GBC patients, but with a limitation of being only assessable after surgery (6). Surgery still remains the only potentially curative therapy, but only a minority of patients has the chance of getting radical operation and adjuvant therapy still has its position in GBC treatment (3, 30). Thus, efficient pre-operative or pre-treatment parameters/indexes for prediction of prognosis should be pursued, as they may help identifying patients who might benefit from more aggressive adjuvant therapies (31, 32).

There are some kinds of predictive parameters/indexes advocated by different authors to be used for pre-treatment evaluation of survival in various cancer types (21, 33–39). These markers were derived mainly on the basis of three major groups of clinical parameters, specifically reflecting nutrition status (glucose, albumin and cholesterol), immune status (lymphocyte, monocyte), inflammation status (neutrophil, platelet and C-reactive protein) and their cross combinations. Examples may include GLR (glucose to lymphocyte ratio) (21), CONUT (controlling nutritional status score, calculated from albumin, lymphocyte and cholesterol) (34), PNI (prognostic nutritional index, calculated from albumin and lymphocyte) (35), GPS (Glasgow prognostic score, calculated from C-reactive protein and albumin) (38), SII (systemic immune-inflammation index, derived from platelet, neutrophil and lymphocyte) (39) and so on. Compared to pTNM or other pathology-based evaluators, these markers share similar advantages, such as easy to assess and replicable, low cost and

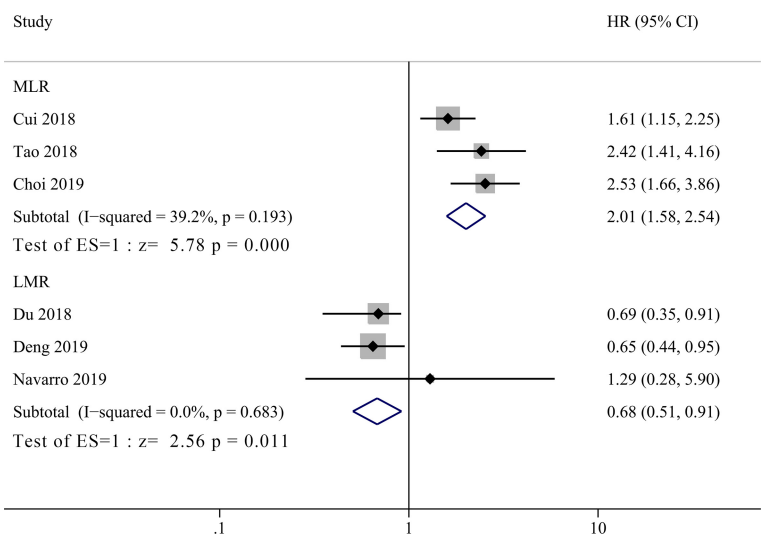

FIGURE 3 | Forest plot for the association between lymphocyte-to-monocyte ratio (LMR) or monocyte-to-lymphocyte ratio (MLR) and overall survival of patients with Gallbladder carcinoma (GBC).

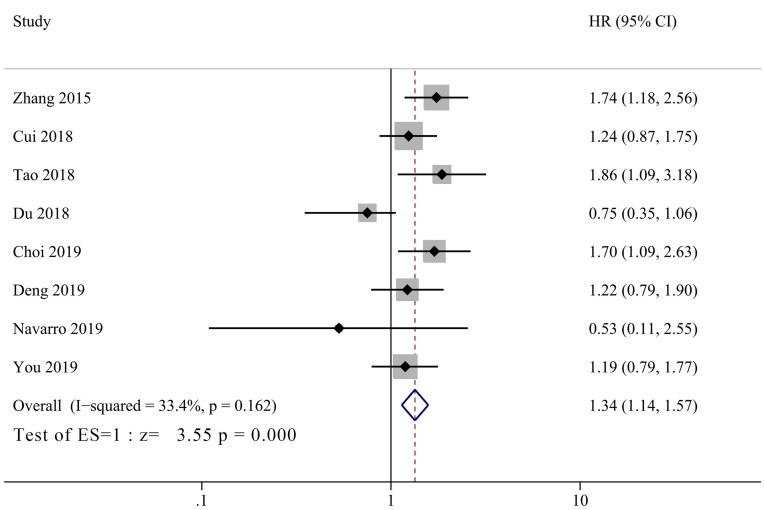

FIGURE 4 | Forest plot for the association between platelet-to-lymphocyte ratio (PLR) and overall survival of patients with Gallbladder carcinoma (GBC).

preoperative applicability etc. (7, 8). Although there were growing evidence of using these markers to predict survival in various cancers, no worldwide consensus has been achieved and concerns rise about the efficiency and accuracy of these makers, and thus their clinical utilities are still suspended and limited.

In the present review, we focused on the prognostic value of one series of the most easily accessible and investigated markers that is WBCC-derived indexes including NLR, LMR/MLR and PLR in GBC patients. Our meta-analysis showed that all these indexes could be used as prognostic factors for GBC patients, which was in compliance with results in other cancer types (31). And we also pooled available data together and revealed that elevated NLR was significantly correlated with TNM stage, tumor differentiation and CA19-9, which could explain in part the mechanisms of these indexes being used as prognostic markers for GBC patients.

Although WBCC-derived indexes are certified to be useful parameters for predicting prognosis in various cancer types, the underlying mechanisms largely remains to be elucidated. First of all, the theoretical foundation of their usage as prognostic biomarker lies in that different types of peripheral blood cells could be considered to reflect host immune and inflammation status, which play important role in systemic inflammatory response (SIR), carcinogenesis, tumor microenvironment

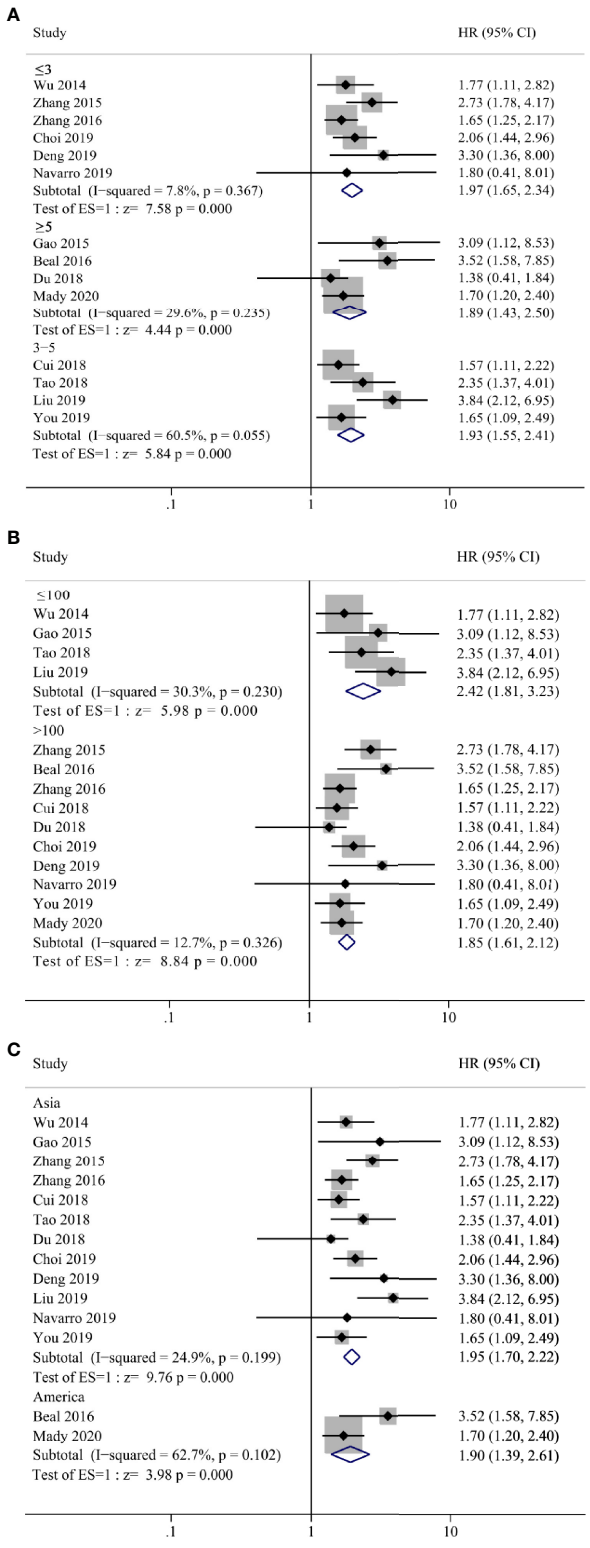

FIGURE 5 | Forest plot and subgroup analysis for **(A)** cut-off value, **(B)** sample size and **(C)** geographic area of the correlation between neutrophil–lymphocyte ratio (NLR) and overall survival of patients with Gallbladder carcinoma (GBC).

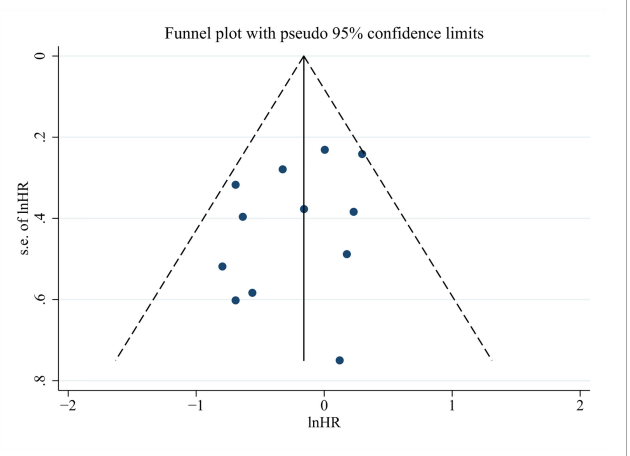

FIGURE 6 | Funnel plots for detecting publication bias of the association between neutrophil–lymphocyte ratio (NLR) and overall survival of Gallbladder carcinoma (GBC).

modulation and progression (40–42). Indeed, inflammatory microenvironment has been proposed as one hallmark of cancer (43), infiltrating immune and inflammatory cells are increasingly accepted to be generic constituents of tumors, and they exert conflicting ways for tumor development: tumor-antagonizing effect as for lymphocytes while tumor-promoting effect as for neutrophils and monocytes (37, 39). More specifically, infiltrating lymphocytes are major antitumor components that may induce cancer cell apoptosis *via* interaction of $CD4^+$ and $CD8^+$ T cells (44, 45). In contrast, low lymphocytes within or around tumor area may be responsible for an insufficient immune surveillance that leads to tumor progression and inferior survival of patient (44). On the other hand, neutrophils and monocytes play a tumor-promoting role in malignancies. In short, neutrophils, as another key component of SIR, are recruited to tumor area, produce various kinds of cytokines and chemokines that are implicated in promoting tumor progression *via* all kinds of pathophysiological process, such as matrix degradation, immunosuppression, angiogenesis etc. (43, 46, 47). Besides, peripheral monocytes are known for their association with the level of tumor-associated macrophages (TAMs) which could also produce cytokines and enzymes with protumoral functions, including tumor cell migration, invasion, metastasis as well as immunosuppression (48, 49). On the other hand, Deng and collogues revealed in their study that SIR biomarkers were significantly correlated with tumor differentiation, TNM stage or anemia, this could partially explain the positive correlation between SIR biomarkers and prognosis (17).

As we summarized above, most studies concluded with a favorable and positive results on prognosis predictive value of these WBCC-related biomarkers, but there are some limitations in these studies. Firstly, the cut-off value was discrepant through studies and different methods were employed to get it defined (**Table 1**). The receiver operating characteristic (ROC) curve

analysis was the mostly adopted method and the accuracy of it was determined by sample size and subjective populations (as parameters vary among different tumors, stage, treatment etc.) (50). So future large volume investigations among different populations should be considered to identify the optimal cut-off values for each index. Secondly, the WBCC parameters are continuous variables which may present quite different values, especially before and after treatment. For example, the neutrophils are more susceptible to antibiotics usage, and may differ greatly from before and after surgery. So dynamic observations at different time point or analysis on trend should be more significant and encouraged for future investigations. Thirdly and finally, it is impossible to have one index fit to all situations, and the prognostic value of each index varies between different tumors, and even between different stages and treatment strategies in same tumor. So, the accuracy and reliability of single index may be challenged and an optimized mathematical model should provide some benefits to solve this issue. For example, Deng and collogues proposed a predictive nomogram using all the significant independent predicators to predict the patient survival (17). Each variable could be assigned a weighted number of points in the model, and the sum of points for each patient could be used to predict prognosis.

There were some limitations in this meta-analysis. Firstly, all studies were retrospective with low quality of evidence, further high quality RCT studies should be designed for future investigations. Secondly, the cut-off value was different through studies. Although we performed sub-group analyses, a single defined cut-off value would provide better comparison between studies. Thirdly, although there was no significant heterogeneity among most included studies, the patient inclusion criteria varied through studies, such as operation method, tumor staging, chemotherapy strategy etc. Due to the limited sample size, subgroup analysis was not practicable. Finally, all the included 14 studies investigated NLR as prognosis marker for GBC, while only few studies investigated MLR, PLR, so the statistics for these latter meta-analyses are under-powered, and future studies on these markers should be expected and included for further meta-analysis.

In conclusion, our meta-analysis validated that WBCC-derived indexes including NLR, MLR/LMR and PLR could be used as prognostic parameters for predicting survival outcomes in GBC patients. These series of indexes, especially NLR, could improve risk stratification and facilitate better patient selection for surgical resection or aggressive chemotherapy in the management of GBC.

DATA AVAILABILITY STATEMENT

The original contributions presented in the study are included in the article/supplementary material. Further inquiries can be directed to the corresponding authors.

AUTHOR CONTRIBUTIONS

Study concepts: TL, ZC and BX. Study design: TL, ZC and BX. Data acquisition: BX, JC, ZC and WZ. Quality control of data and algorithms: BX, JC, ZD and XZ. Data analysis and interpretation: BX, ZC and JC. Statistical analysis: ZC, BX, JZ, JC and WZ. Manuscript preparation: BX, ZC, JZ and JC. Manuscript editing: ZC, BX and JZ. Manuscript review: TL, ZC and BX. All authors contributed to the article and approved the submitted version.

FUNDING

This study was supported by the Taishan Scholars Program for Young Experts of Shandong Province (tsqn20161064), the National Natural Science Foundation of China (81874178 & 82073200) for TL.

REFERENCES

1. Kakaei F, Beheshtirouy S, Nejatollahi SM, Zarrintan S, Mafi MR. Surgical Treatment of Gallbladder Carcinoma: A Critical Review. *Updates Surg* (2015) 67(4):339–51. doi: 10.1007/s13304-015-0328-x
2. WC L, Yun Z, S W, L J, WL F, XP G, et al. Analysis of the Incidence and Epidemic Trend of Gallbladder Cancer in China. *Chin J Digestive Surg* (2019) 18(2):186–9. doi: 10.3760/cma.j.issn.1673-9752.2019.02.015
3. Aloia TA, Jarufe N, Javle M, Maithel SK, Roa JC, Adsay V, et al. Gallbladder Cancer: Expert Consensus Statement. *HPB (Oxford)* (2015) 17(8):681–90. doi: 10.1111/hpb.12444
4. Jang JY, Heo JS, Han Y, Chang J, Kim JR, Kim H, et al. Impact of Type of Surgery on Survival Outcome in Patients With Early Gallbladder Cancer in the Era of Minimally Invasive Surgery: Oncologic Safety of Laparoscopic Surgery. *Med (Baltimore)* (2016) 95(22):e3675. doi: 10.1097/MD.0000000000003675
5. Hundal R, Shaffer EA. Gallbladder Cancer: Epidemiology and Outcome. *Clin Epidemiol* (2014) 6:99–109. doi: 10.2147/CLEP.S37357
6. Brierley J, Gospodarowicz MK, Wittekind C. *TNM Classification of Malignant Tumours. Eighth edition*. Chichester, West Sussex, UK; Hoboken, NJ: John Wiley & Sons, Inc (2017).
7. Dolan RD, Laird BJA, Horgan PG, McMillan DC. The Prognostic Value of the Systemic Inflammatory Response in Randomised Clinical Trials in Cancer: A Systematic Review. *Crit Rev Oncol Hematol* (2018) 132:130–7. doi: 10.1016/j.critrevonc.2018.09.016
8. Roxburgh CS, McMillan DC. Role of Systemic Inflammatory Response in Predicting Survival in Patients With Primary Operable Cancer. *Future Oncol* (2010) 6(1):149–63. doi: 10.2217/fon.09.136
9. Wu XS, Shi LB, Li ML, Ding Q, Weng H, Wu WG, et al. Evaluation of Two Inflammation-Based Prognostic Scores in Patients With Resectable Gallbladder Carcinoma. *Ann Surg Oncol* (2014) 21(2):449–57. doi: 10.1245/s10434-013-3292-z
10. Gao H, Zhang H, Xu X, Zou W, Lin K, Deng Y, et al. Neutrophil-Lymphocyte Ratio as a Prognostic Factor for Gallbladder Carcinoma After Radical Resection. *World Chin J Digestol* (2015) 23(35):5705. doi: 10.11569/wcjd.v23.i35.5705
11. Zhang Y, Jiang C, Li J, Sun J, Qu X. Prognostic Significance of Preoperative Neutrophil/Lymphocyte Ratio and Platelet/Lymphocyte Ratio in Patients With Gallbladder Carcinoma. *Clin Transl Oncol* (2015) 17(10):810–8. doi: 10.1007/s12094-015-1310-2
12. Beal EW, Wei L, Ethun CG, Black SM, Dillhoff M, Salem A, et al. Elevated NLR in Gallbladder Cancer and Cholangiocarcinoma - Making Bad Cancers Even Worse: Results From the US Extrahepatic Biliary Malignancy Consortium. *HPB (Oxford)* (2016) 18(11):950–7. doi: 10.1016/j.hpb.2016.08.006
13. Zhang L, Wang R, Chen W, Xu X, Dong S, Fan H, et al. Prognostic Significance of Neutrophil to Lymphocyte Ratio in Patients With Gallbladder Carcinoma. *HPB (Oxford)* (2016) 18(7):600–7. doi: 10.1016/j.hpb.2016.03.608

14. Cui X, Zhu S, Tao Z, Deng X, Wang Y, Gao Y, et al. Long-Term Outcomes and Prognostic Markers in Gallbladder Cancer. *Med (Baltimore)* (2018) 97(28): e11396. doi: 10.1097/MD.0000000000011396
15. Tao Z, Li SX, Cui X, Huang Y, Zhu S, Wang Y, et al. The Prognostic Value of Preoperative Inflammatory Indexes in Gallbladder Carcinoma With Hepatic Involvement. *Cancer Biomark* (2018) 22(3):551–7. doi: 10.3233/CBM-181230
16. Choi YH, Lee JW, Lee SH, Choi JH, Kang J, Lee BS, et al. A High Monocyte-to-Lymphocyte Ratio Predicts Poor Prognosis in Patients With Advanced Gallbladder Cancer Receiving Chemotherapy. *Cancer Epidemiol Biomarkers Prev* (2019) 28(6):1045–51. doi: 10.1158/1055-9965.EPI-18-1066
17. Deng Y, Zhang F, Yu X, Huo CL, Sun ZG, Wang S, et al. Prognostic Value of Preoperative Systemic Inflammatory Biomarkers In Patients With Gallbladder Cancer and The Establishment of A Nomogram. *Cancer Manag Res* (2019) 11:9025–35. doi: 10.2147/CMAR.S218119
18. Du JH, Lu J. Circulating CEA-dNLR Score Predicts Clinical Outcome of Metastatic Gallbladder Cancer Patient. *J Clin Lab Anal* (2019) 33(2):e22684. doi: 10.1002/jcla.22684
19. Liu F, Hu HJ, Ma WJ, Yang Q, Wang JK, Li FY, et al. Prognostic Significance of Neutrophil-Lymphocyte Ratio and Carbohydrate Antigen 19-9 in Patients With Gallbladder Carcinoma. *Med (Baltimore)* (2019) 98(8):e14550. doi: 10.1097/MD.0000000000014550
20. You MS, Ryu JK, Choi YH, Choi JH, Huh G, Paik WH, et al. Therapeutic Outcomes and Prognostic Factors in Unresectable Gallbladder Cancer Treated With Gemcitabine Plus Cisplatin. *BMC Cancer* (2019) 19(1):10. doi: 10.1186/s12885-018-5211-y
21. Navarro J, Kang I, Hwang HK, Yoon DS, Lee WJ, Kang CM. Glucose to Lymphocyte Ratio as a Prognostic Marker in Patients With Resected Pt2 Gallbladder Cancer. *J Surg Res* (2019) 240:17–29. doi: 10.1016/j.jss.2019.02.043
22. Mady M, Prasai K, Tella SH, Yadav S, Hallemeier CL, Rakshit S, et al. Neutrophil to Lymphocyte Ratio as a Prognostic Marker in Metastatic Gallbladder Cancer. *HPB* (2020) 22(10):1490–5. doi: 10.1016/j.hpb.2020.02.002
23. Shea BJ, Reeves BC, Wells G, Thuku M, Hamel C, Moran J, et al. AMSTAR 2: A Critical Appraisal Tool for Systematic Reviews That Include Randomised or non-Randomised Studies of Healthcare Interventions, or Both. *BMJ* (2017) 358:j4008. doi: 10.1136/bmj.j4008
24. Moher D, Liberati A, Tetzlaff J, Altman DG, Group P. Preferred Reporting Items for Systematic Reviews and Meta-Analyses: The PRISMA Statement. *BMJ* (2009) 339:b2535. doi: 10.1136/bmj.b2535
25. Michiels S, Piedbois P, Burdett S, Syz N, Stewart L, Pignon JP. Meta-Analysis When Only the Median Survival Times Are Known: A Comparison With Individual Patient Data Results. *Int J Technol Assess Health Care* (2005) 21 (1):119–25. doi: 10.1017/S0266462305050154
26. Jeng KS, Ohta I, Yang FS. Reappraisal of the Systematic Management of Complicated Hepatolithiasis With Bilateral Intrahepatic Biliary Strictures. *Arch Surg* (1996) 131(2):141–7. doi: 10.1001/archsurg.1996.01430140031008
27. Wan X, Wang W, Liu J, Tong T. Estimating the Sample Mean and Standard Deviation From the Sample Size, Median, Range and/or Interquartile Range. *BMC Med Res Methodol* (2014) 14:135. doi: 10.1186/1471-2288-14-135
28. Luo D, Wan X, Liu J, Tong T. Optimally Estimating the Sample Mean From the Sample Size, Median, Mid-Range, and/or Mid-Quartile Range. *Stat Methods Med Res* (2018) 27(6):1785–805. doi: 10.1177/0962280216669183
29. Bray F, Ferlay J, Soerjomataram I, Siegel RL, Torre LA, Jemal A. Global Cancer Statistics 2018: GLOBOCAN Estimates of Incidence and Mortality Worldwide for 36 Cancers in 185 Countries. *CA Cancer J Clin* (2018) 68(6):394–424. doi: 10.3322/caac.21492
30. Sharma A, Sharma KL, Gupta A, Yadav A, Kumar A. Gallbladder Cancer Epidemiology, Pathogenesis and Molecular Genetics: Recent Update. *World J Gastroenterol* (2017) 23(22):3978–98. doi: 10.3748/wjg.v23.i22.3978
31. Paramanathan A, Saxena A, Morris DL. A Systematic Review and Meta-Analysis on the Impact of Pre-Operative Neutrophil Lymphocyte Ratio on Long Term Outcomes After Curative Intent Resection of Solid Tumours. *Surg Oncol* (2014) 23(1):31–9. doi: 10.1016/j.suronc.2013.12.001
32. Chua W, Charles KA, Baracos VE, Clarke SJ. Neutrophil/Lymphocyte Ratio Predicts Chemotherapy Outcomes in Patients With Advanced Colorectal Cancer. *Br J Cancer* (2011) 104(8):1288–95. doi: 10.1038/bjc.2011.100
33. Shimose S, Kawaguchi T, Iwamoto H, Tanaka M, Miyazaki K, Ono M, et al. Controlling Nutritional Status (CONUT) Score Is Associated With Overall Survival in Patients With Unresectable Hepatocellular Carcinoma Treated With Lenvatinib: A Multicenter Cohort Study. *Nutrients* (2020) 12(4):1076. doi: 10.3390/nu12041076
34. Liang RF, Li JH, Li M, Yang Y, Liu YH. The Prognostic Role of Controlling Nutritional Status Scores in Patients With Solid Tumors. *Clin Chim Acta* (2017) 474:155–8. doi: 10.1016/j.cca.2017.09.021
35. Lee JY, Kim HI, Kim YN, Hong JH, Alshomimi S, An JY, et al. Clinical Significance of the Prognostic Nutritional Index for Predicting Short- and Long-Term Surgical Outcomes After Gastrectomy: A Retrospective Analysis of 7781 Gastric Cancer Patients. *Med (Baltimore)* (2016) 95(18):e3539. doi: 10.1097/MD.0000000000003539
36. Li SQ, Jiang YH, Lin J, Zhang J, Sun F, Gao QF, et al. Albumin-to-Fibrinogen Ratio as a Promising Biomarker to Predict Clinical Outcome of Non-Small Cell Lung Cancer Individuals. *Cancer Med* (2018) 7(4):1221–31. doi: 10.1002/cam4.1428
37. Saqib R, Pathak S, Smart N, Nunes Q, Rees J, Finch Jones M, et al. Prognostic Significance of Pre-Operative Inflammatory Markers in Resected Gallbladder Cancer: A Systematic Review. *ANZ J Surg* (2018) 88(6):554–9. doi: 10.1111/ans.14300
38. McMillan DC. The Systemic Inflammation-Based Glasgow Prognostic Score: A Decade of Experience in Patients With Cancer. *Cancer Treat Rev* (2013) 39 (5):534–40. doi: 10.1016/j.ctrv.2012.08.003
39. Yang R, Chang Q, Meng X, Gao N, Wang W. Prognostic Value of Systemic Immune-Inflammation Index in Cancer: A Meta-Analysis. *J Cancer* (2018) 9 (18):3295–302. doi: 10.7150/jca.25691
40. Grivennikov SI, Greten FR, Karin M. Immunity, Inflammation, and Cancer. *Cell* (2010) 140(6):883–99. doi: 10.1016/j.cell.2010.01.025
41. Coussens LM, Werb Z. Inflammation and Cancer. *Nature* (2002) 420 (6917):860–7. doi: 10.1038/nature01322
42. Diakos CI, Charles KA, McMillan DS, Clarke SJ. Cancer-Related Inflammation and Treatment Effectiveness. *Lancet Oncol* (2014) 15(11): e493–503. doi: 10.1016/S1470-2045(14)70263-3
43. Hanahan D, Weinberg RA. Hallmarks of Cancer: The Next Generation. *Cell* (2011) 144(5):646–74. doi: 10.1016/j.cell.2011.02.013
44. Pages F, Galon J, Dieu–Nosjean MC, Tartour E, Sautes–Fridman C, Fridman WH. Immune Infiltration in Human Tumors: A Prognostic Factor That Should Not be Ignored. *Oncogene* (2010) 29(8):1093–102. doi: 10.1038/onc.2009.416
45. Dunn GP, Old LJ, Schreiber RD. The Immunobiology of Cancer Immunosurveillance and Immunoediting. *Immunity* (2004) 21(2):137–48. doi: 10.1016/j.immuni.2004.07.017
46. Gregory AD, Houghton AM. Tumor-Associated Neutrophils: New Targets for Cancer Therapy. *Cancer Res* (2011) 71(7):2411–6. doi: 10.1158/0008-5472.CAN-10-2583
47. Imai Y, Kubota Y, Yamamoto S, Tsuji K, Shimatani M, Shibatani N, et al. Neutrophils Enhance Invasion Activity of Human Cholangiocellular Carcinoma and Hepatocellular Carcinoma Cells: An In Vitro Study. *J Gastroenterol Hepatol* (2005) 20(2):287–93. doi: 10.1111/j.1440-1746.2004.03575.x
48. Franklin RA, Liao W, Sarkar A, Kim MV, Bivona MR, Liu K, et al. The Cellular and Molecular Origin of Tumor-Associated Macrophages. *Science* (2014) 344(6186):921–5. doi: 10.1126/science.1252510
49. Condeelis J, Pollard JW. Macrophages: Obligate Partners for Tumor Cell Migration, Invasion, and Metastasis. *Cell* (2006) 124(2):263–6. doi: 10.1016/j.cell.2006.01.007
50. Walker SP. The ROC Curve Redefined - Optimizing Sensitivity (and Specificity) to the Lived Reality of Cancer. *N Engl J Med* (2019) 380(17):1594–5. doi: 10.1056/NEJMp1814951

Conflict of Interest: The authors declare that the research was conducted in the absence of any commercial or financial relationships that could be construed as a potential conflict of interest.

frontiers in Oncology

ORIGINAL RESEARCH
published: 09 August 2021
doi: 10.3389/fonc.2021.730615

Exosomal Cripto-1 Serves as a Potential Biomarker for Perihilar Cholangiocarcinoma

*Chunxiao Hu[1], Yanli Zhang[2], Mengjiao Zhang[3], Tingting Li[3], Xin Zheng[2], Qining Guo[3] and Xin Zhang[3]**

[1] Department of General Surgery, Qilu Hospital of Shandong University, Jinan, China, [2] Department of Clinical Laboratory, Shandong Provincial Third Hospital, Jinan, China, [3] Department of Clinical Laboratory, Qilu Hospital of Shandong University, Jinan, China

OPEN ACCESS

Edited by:
Xuesong Gu,
Beth Israel Deaconess Medical Center and Harvard Medical School, United States

Reviewed by:
Hua-Guo Xu,
Nanjing Medical University, China
Mingchen Zhu,
Nanjing Medical University, China
Laisheng Li,
The First Affiliated Hospital of Sun Yat-Sen University, China

***Correspondence:**
Xin Zhang
xinzhang@sdu.edu.cn

Specialty section:
This article was submitted to Cancer Molecular Targets and Therapeutics, a section of the journal Frontiers in Oncology

Received: 25 June 2021
Accepted: 26 July 2021
Published: 09 August 2021

Citation:
Hu C, Zhang Y, Zhang M, Li T, Zheng X, Guo Q and Zhang X (2021) Exosomal Cripto-1 Serves as a Potential Biomarker for Perihilar Cholangiocarcinoma. Front. Oncol. 11:730615. doi: 10.3389/fonc.2021.730615

Perihilar cholangiocarcinoma (PHCCA) has a poor prognosis, mainly due to diagnosis at an advanced stage. Cripto-1 functions as an oncogene and is highly expressed in several human cancers, however, its clinical application in PHCCA is poorly understood. Herein, we identified that Cripto-1 was released by PHCCA cells *via* exosomes *in vitro* and *in vivo*. Furthermore, an ELISA method was developed to detect exosomal Cripto-1 in the serum of 115 PHCCA patients, 47 cholangitis patients and 65 healthy controls, and it was found that exosomal Cripto-1 was increased in PHCCA patients and associated with metastasis. Compared with traditional serum tumor markers, CA19-9 and CEA, exosomal Cripto-1 demonstrated a larger area under ROC curve for PHCCA diagnosis. The cutoff value of exosomal Cripto-1 was 0.82, achieving a sensitivity of 79.1% and a specificity of 87.5%. As expected, exosomal Cripto-1 levels in immunohistochemically Cripto-1-high cases were significantly elevated compared to in Cripto-1-low cases. When measured 1-week postoperatively, Cripto-1 levels decreased on average from 1.25(0.96-3.26) to 0.85(0.62-1.82). Immunohistochemistry analysis showed Cripto-1 expression was negatively correlated with E-cadherin and was an independent prognostic biomarker for poor survival in PHCCA patients. In conclusion, exosomal Cripto-1 in sera can reflect its expression in the tissue of PHCAA patients and has the potential be a non-invasive biomarker for diagnosis and prognosis of PHCCA.

Keywords: exosomes, biomarker, diagnosis, prognosis, perihilar cholangiocarcinoma, Cripto-1

INTRODUCTION

Perihilar cholangiocarcinoma (PHCCA), also known as a Klatskin tumor, is a subtype of CCA, arising at or near the confluence of the right and left hepatic duct. It accounts for more than 50% of total CCA cases and is characterized by high surgical difficulty and poor prognosis (1–3). Even for those patients who undergo curative intent resection, the 5-year overall survival rate is only about 30% (4). Moreover, due to a lack of clear symptoms, most PHCCA patients are diagnosed at an advanced stage at which surgical treatment is not a viable option (5). If PHCCA could be diagnosed

before jaundice or intrahepatic biliary dilatation on imaging, patients might have better outcomes (6). However, until now there are no reliable biomarkers for early diagnosis of PHCCA.

Cripto-1, also known as teratocarcinoma-derived growth factor1 (TDGF-1), is a member of the epidermal growth factor/Cripto-1-FRL-1-Cryptic family (7). It is isolated and cloned from the human teratocarcinoma cDNA library of NTERA-2, and is indispensable for early embryonic development and maintenance of the pluripotency of embryonic stem cells (8). Recently, Cripto-1 has been reported to be an oncogene that plays an important role in the initiation and progression of several types of human cancers (9). Some studies have shown that Cripto-1 is involved in the epithelial-mesenchymal transition (EMT), whereby it enhances the invasion and metastasis of tumor cells (10, 11). Cripto-1 can also trigger mitogen activated protein kinase and Akt signaling pathways, to promote cell survival and migration *via* specific binding to Glypican-1 (12). In addition, overexpression of Cripto-1 enhances the proliferation of human endothelial cells. The subsequent increase in microvessel formation levels was detected by a directed angiogenesis assay *in vivo*, which confirmed the role of Cripto-1 in regulating tumor angiogenesis (13). Simultaneously, inhibition of Cripto-1 expression, by anti-Cripto-1 antibody (14) or microRNA-15b (15), exhibits a potential to suppress growth of cancer cells. Thus, Cripto-1 may represent a novel molecular target for diagnosis and prognosis of cancers.

Exosomes are cell-secreted bilayered membrane vesicles with a diameter of 30-120 nm (16). They originate from multivesicular bodies(MVB)/late endosomes inside the cell and are released into the external space upon fusion of MVBs with the cell membrane (17). Until now, it has been well-documented that almost all tumor cells secrete exosomes, and the presence of exosomes has been confirmed in a wide variety of body fluids, such as plasma/serum, urine, saliva, and bile (18). Moreover, it has been reported that cancer cell-secreted exosomes can be transferred to recipient cells and promote tumor progression by enhancing immunosuppression, angiogenesis and metastatic dissemination (19). More importantly, these extracellular vesicles contain specific components, such as lipids, proteins, and nucleic acids, mirroring their cellular origin (20). Thus, it is feasible that detection of enriched and specific molecules in cancer exosomes could serve as a liquid biopsy to aid in the diagnosis of malignancies. For instance, CKAP4 is detected in exosomes harvested from the serum of patients with pancreatic cancer and reflects its expression in tumor lesions, which may represent a biomarker for pancreatic cancer (21). However, whether Cripto-1 can be released from cancer cells, and its potential utility to act as a biomarker for detection of PHCCA, remain largely unclear.

In this study, exosomal Cripto-1 was quantitatively determined in a large number of patient serum samples by an exosome enzyme linked immunosorbent assay (exoELISA) method that was developed herein. The serum samples were collected from healthy control (HC) individuals, cholangitis patients and PHCCA patients. Furthermore, by analyzing a cohort of PHCAA patients with matched sera and tissues samples, we explored whether exosomal Cripto-1 in sera could be a surrogate of tissue biopsy. Finally, this study sought to assess the significance of Cripto-1 in prognosis in a retrospective cohort of PHCCA patients.

MATERIALS AND METHODS

Cell Culture

Human PHCAA cells, QBC-939 and FRH-0201 were purchased from the Cell Bank of the Chinese Academy of Sciences (Shanghai, China) and maintained in Dulbecco's Modified Eagle medium supplemented with 10% exosome-depleted fetal bovine serum in a humidified atmosphere containing 5% CO_2.

Tumor Xenograft Models

Four-week-old BALB/c nude mice were purchased from GemPharmatech (Nanjing, China). A total of 3×10^6 QBC939 cells transfected with an empty vector or the Cripto-1-OE vector, were subcutaneously injected into the flank of nude mice (24 mice for each group). Tumor diameters were measured every 2 days, and tumor volume was calculated as follows: volume= (length×width^2)/2. After 2, 4 and 6 weeks, the mice were sacrificed, and their blood and solid tumors were collected. All procedures were approved by the Animal Management Committee of Shandong University.

Patients and Samples

We obtained the approval of the local ethical committees, and all subjects gave written informed consent to participate. Three cohorts of subjects from Qilu Hospital of Shandong University and Shandong Provincial Third Hospital were enrolled in this study. In the first cohort, pre-operation serum samples were collected from a group of 217 cases with HC (n=65), cholangitis (n=47) and PHCCA (n=115). The PHCCA cases were newly diagnosed and previously untreated; their tumors were confirmed by postoperative histopathological analyses. In the second cohort, sera and matched tissue was collected from 34 PHCCA patients. Moreover, postoperative sera were collected from 15 of the PHCCA cases in the second cohort. The third cohort was comprised of 105 PHCCA patients with available formalin-fixed tumor tissues. These patients underwent radical resection and were followed up regularly. PHCCA was staged according to the 7th AJCC/UICC tumor-node-metastasis (TNM) classification system.

Serum was separated by 2-step centrifugation (1,600g for 10 minutes followed by 16,000g for 10 minutes as previously described (22). Tissues were embedded in paraffin and cut into 4μm sections. For tissue microarray (TMA) construction, core tissues of 1.5 mm in diameter from each tumor block, as confirmed by hematoxylin and eosin staining, were re-embedded into the recipient TMA block as we described previously (2).

Exosome Isolation and Identification

Exosomes were isolated from conditioned medium (CM) and serum using ultracentrifugation. CM was collected with

centrifugation of 800g for 10 min and 2,000g for 10 min. Next, the CM supernatant, or cell-free serum diluted with D-PBS, was filtered through a 0.22μm filter and then ultracentrifuged at 120,000g for 70 min at 4°C. The pellets were washed with D-PBS and purified by further ultracentrifugation at 120,000 g for 70 min at 4°C. Exosomal markers CD81, TSG101 and Calnexin were detected by western blotting assay.

Western Blotting

Cellular and exosomal lysates were prepared using RIPA buffer (Life Technologies) and quantified using a Pierce™ BCA Protein Assay Kit (Thermo Scientific). Proteins were separated by SDS-PAGE and transferred to PVDF membranes (Millipore). After blocking in 5% skimmed milk for 30 min, the membrane was incubated with primary antibodies overnight at 4°C. The following primary antibodies were used: CD81 (Abcam, ab79559, 1:1000 dilution), TSG101 (Abcam, ab83, 1:1000 dilution), Calnexin(Abcam,ab133615, 1:1000 dilution) and Cripto1 (Abcam, ab108391, 1:1000 dilution). Afterwards, an HRP-conjugated secondary antibody (Beyotime, Shanghai, China) was added at 1:5000 before incubation for 1h at room temperature. Chemiluminescence signal was detected using enhanced ECL Reagent (Vazyme, Nanjing, China) on the FluorChem E Chemiluminescent System (Cell Biosciences, Santa Clara, CA, USA).

ELISA Detection of Exosomal Cripto-1

The levels of exosomal Cripto-1 were detected using a Human Cripto-1 DuoSet ELISA kit (R&D) with some methodological alterations. In brief, 96 well-plates were coated with 100 μl of anti-CD81antibody (Abcam, ab79559, 1:250 dilution) per well, instead of the Capture Antibody in the kit, before incubation overnight at room temperature. After blocking plates with 300 μl/well Reagent Diluent for at least 1 h, 100 μl exosomes were added and incubated for 2 h at room temperature. Subsequently, we added 100 μl of the Detection Antibody before incubation for 2h, 100μl Streptavidin-HRP for 20 min, and then 100 μl Substrate Solution for 20 min. After blocking with 50 μl Stop Solution, the optical density (OD) of each well was determine immediately at 450 nm on an ELISA plate reader (Thermo Scientific, United States).

Carbohydrate Antigen 19-9 (CA19-9) and Carcinoembryonic Antigen (CEA) Assays

Serum CEA and CA19-9 levels were detected using an electrochemiluminescence method on the Cobas E601 Analyzer (Roche Diagnostics GmbH, Germany); the upper limits were defined as 5 ng/ml and 37 U/ml according to the manufacturer's directions.

Immunohistochemistry (IHC)

Slides were immersed in 3% hydrogen peroxide to inactivate endogenous peroxidase and incubated in EDTA buffer (pH = 9.0) for antigen retrieval. After blocking by 1% bovine serum albumin, sections were incubated with primary antibodies overnight at 4°C. Subsequently, the slides were incubated in secondary antibody prior to 3,3'-diaminobenzidine solution (Zsbio, Beijing, China), which enable visualization. The following primary antibodies were used: Cripto-1 Antibody (R&D, MAB2772, 1:100 dilution), Ki-67 (CST, #9027, 1:400 dilution), E-Cadherin (CST, #3195, 1:400 dilution). The IHC results were evaluated using the Quant Center software and calculated by a histochemistry score (H-score) system (23). The formula for the H-score was: H-score=(percentage of cells of weak intensity×1)+(percentage of cells of moderate intensity×2)+percentage of cells of strong intensity×3).

Statistical Analysis

A Kruskal-Wallis test was employed for global comparison of Cripto-1, CEA or CA19-9 level among multiple groups, and further *post hoc* multiple comparisons were examined using a Mann–Whitney U test. A chi-square test was used for comparison of categorical variables. Logistic regression modelling was performed to combine biomarkers and generated predicted probability value. The correlation between Cripto-1 and E-cadherin expression was assessed by spearman correlation analysis. Survival curves were generated using the Kaplan-Meier method, and compared by a log-rank test. A Cox regression model was applied for identifying the independent prognostic factors. All above statistical analyses were performed by SPSS software, 22.0 and figures were prepared using GraphPad Prism, 9.1. The area under the curve (AUC) was calculated on the receiver operating characteristic (ROC) curve and compared using MedCalc 9.3.9.0. The cutoff point was determined based on the Youden index (sensitivity+specificity-1). Statistical significance was defined as two-sided $P<0.05$.

RESULTS

Cripto-1 Is Secreted With Exosomes From PHCCA Cells

We isolated exosomes from the CM of two sets of PHCAA cells, QBC-939 and FRH-0201. Exosomes purified from PHCAA cells showed enrichment of exosomal markers, CD81 and TSG101, compared to total cell lysis, and had no Calnexin expression, an endoplasmic reticulum marker known to be absent in exosomes and present in cells lysis (**Figure 1A**). Western blotting analysis also showed Cripto-1 was expressed both in PHCAA cells and their exosomes (**Figure 1A**).

To observe whether Cripto-1 was released with exosomes *in vivo*, we subcutaneously injected QBC-939 cells into nude mice to establish a PHCCA mouse model. After 2 weeks, 4 weeks and 6 weeks post-injection the mice were bled, and tumors were harvested. As shown in **Figure 1B**, the concentration of serum exosomal Cripto-1 was gradually increased in mice xenografted QBC-939 cells (treated group), but not detected in normal mice (control group). Levels of exosomal Cripto-1 at 4 weeks and 6 weeks in the treated group were significantly higher than those in the control group and at 0 weeks in the treated group. IHC analysis showed the xenograft tumors had high Cripto-1 and ki-67 expression (**Figure 1C**), confirming exosomal Cripto-1 come from injected QBC-939 cells.

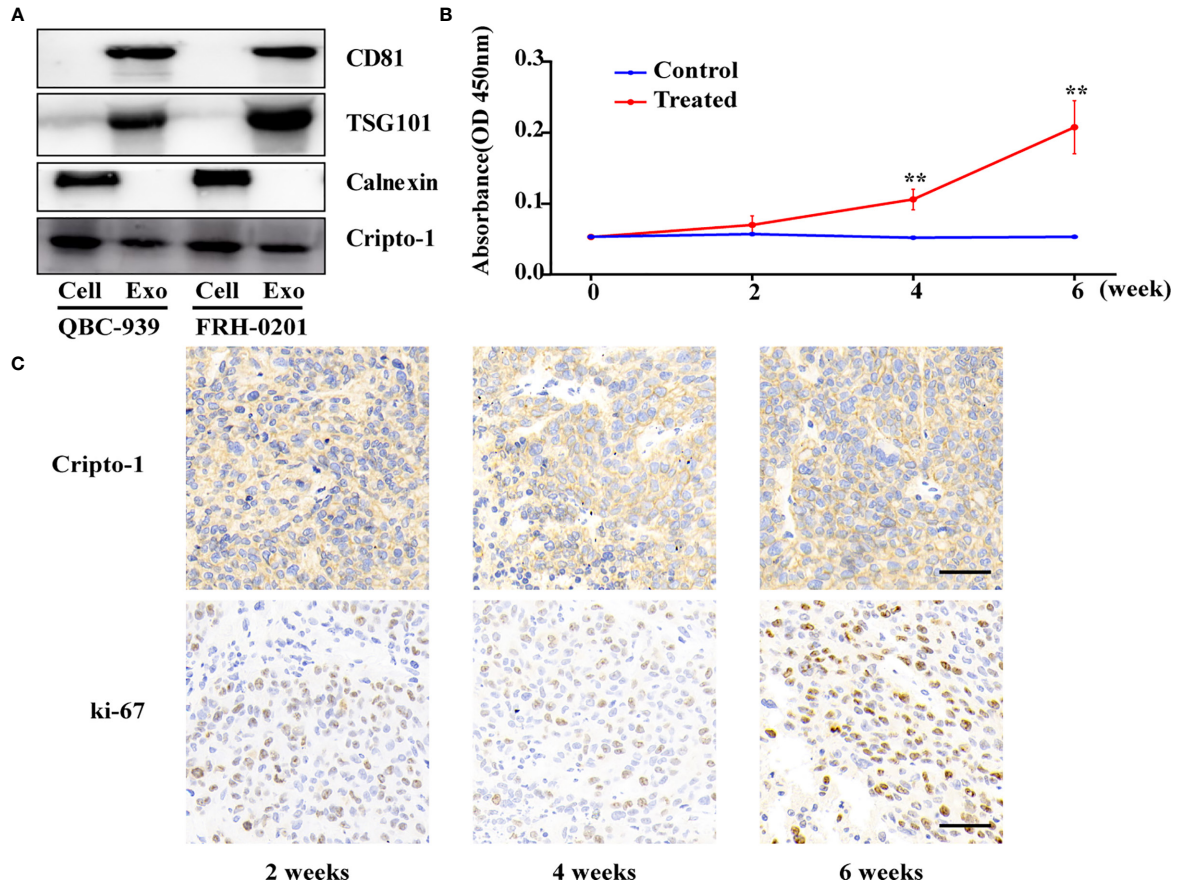

FIGURE 1 | Cripto-1 is secreted with exosomes from PHCCA cells. **(A)** Western blotting analysis of the exosomal markers (CD81, TSG101 and Calnexin) and Cripto-1 in PHCCA cells and exosomes isolated from CM of cells. **(B)** ELISA analysis of exosomal Cripto-1 purified from serum in BALB/c athymic nude mice (control) or mice subcutaneously injected with QBC-939 cells (treated). The levels of exosomal Cripto-1 at 4 week and 6 week in treated group were significantly higher than those in control group and at 0 week in treated group. $^{**}P < 0.01$(student's t-test). Data are presented as mean ± standard deviation. **(C)** Xenograft tumor and the corresponding immunohistochemistry of Cripto-1 and Ki-67 at 4 week and 6 week in treated group. Scale bars, 50μm.

Evaluation of exoELISA Method for Exosomal Cripto-1 Detection

An exoELISA method was developed for detection of exosomal Cripto-1 in serum as shown in **Figure 2A**. Repeat measurements of 3 serum samples, from the same batch or different batches, resulted in an average intra-assay coefficient of variation (CV) and inter-assay CV of 4.27% and 5.52% (**Figure 2B**). Then, the serum samples were evaluated following repeated freezing and thawing, with different lengths of room temperature incubation; the results of this experiment showed no significant changes to the levels of exosomal Cripto-1 (**Figures 2C, D**).

Levels of Exosomal Cripto-1 Were Increased in PHCCA Patients' Sera

By analyzing a large number of serum samples, measuring levels of exosomal Cripto-1 in serum showed a significant difference among HC, cholangitis and PHCCA groups (**Table 1**). Moreover, Cripto-1 levels were independent of age and sex (**Table 1**). Further pairwise comparison demonstrated exosomal Cripto-1 was significantly increased in the sera of the PHCCA group compared with the HC and cholangitis groups (both at $P<0.001$), whilst there was no significant difference between the HC and cholangitis groups (**Figure 3A**). In PHCCA patients, the levels of exosomal Cripto-1 increased as the TMN stage increased (**Figure 3B**). Further analysis showed exosomal Cripto-1 levels were significantly elevated in patients with lymph nodes metastasis (**Figure 3C**) or distant metastasis (**Figure 3D**), but not an advanced T stage (**Figure 3E**). Meanwhile, there were no significant differences observed when PHCCA cases were stratified by differentiation (**Figure 3F**), tumor size (**Figure 3G**) and neural invasion (**Figure 3H**). Cripto-1 showed no obvious association with age and sex (**Table S1**). Correlations between levels of exosomal Cripto-1 and clinicopathological characteristics are shown in **Table S1**.

Diagnosis Performance of Serum Exosomal Cripto-1 for PHCCA Patients

ROC curve analyses realized that exosomal Cripto-1 was robust in discerning PHCCA patients (n=115) from cholangitis (n=47)

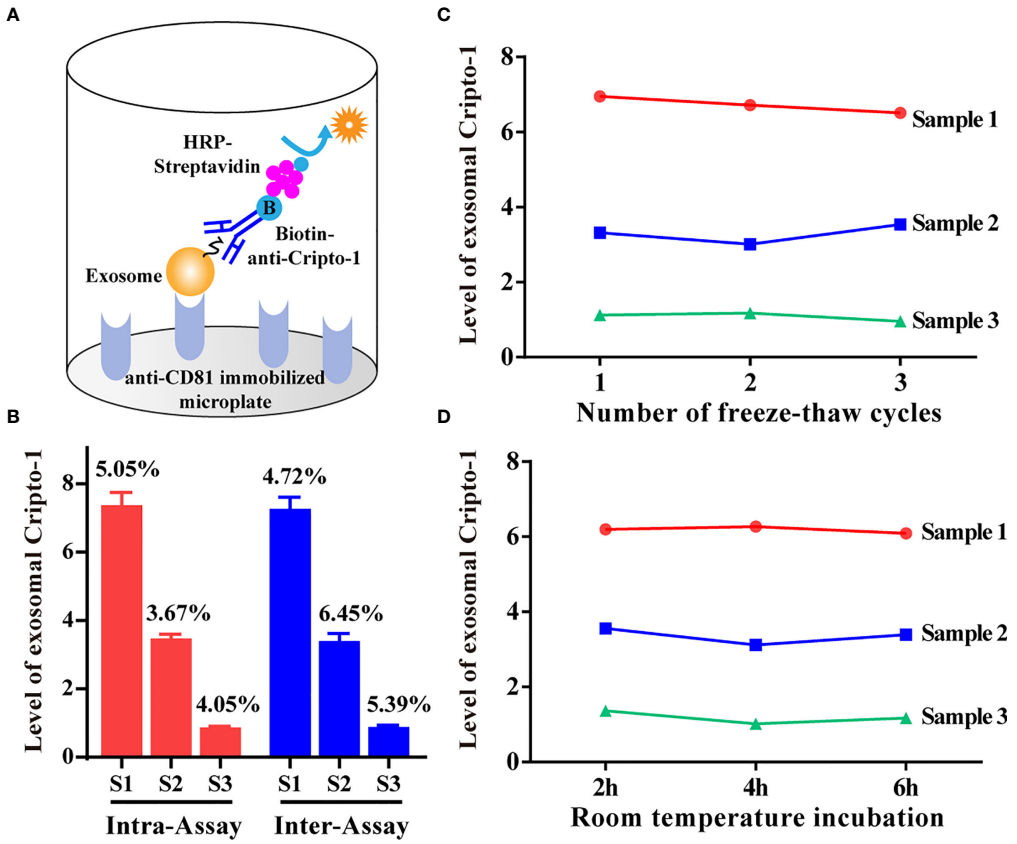

FIGURE 2 | Evaluation of exoELISA method for exosomal Cripto-1 detection. **(A)** Schematic representation of the established exoELISA set for exosomal Cripto-1 detection; **(B)** Coefficient of variation for the exoELISA; **(C)** Serum samples under re-peated freezing and thawing; **(D)** Serum samples incubating at room temperature for different time.

TABLE 1 | Characteristics and levels of biomarker of subjects.

	Healthy control	Cholangitis	PHCCA
Cases	65	47	115
Gender(Male/Female)	40/25	31/16	73/42
Age(y) [a]	59.4 ± 14.5	57.6 ± 14.9	61.3 ± 9.7
CEA (ng/ml) [bc]	2.78 (1.64-3.80)	2.63 (1.09-3.40)	3.12 (1.65-4.60)
CA19-9 (U/ml) [bc]	22.1 (13.3-31.0)	17.7 (7.98-23.3)	103 (22.1-441)
Cripto-1(pg/10mg) [bc]	0.44 (0.32-0.73)	0.34 (0.27-0.62)	1.03 (0.85-3.89)

[a]*Data are presented as mean ± standard deviation.*
[b]*Data are presented as median (interquartile range).*
[c]*Date are compared using Kruskal-Wallis test, P < 0.001.*

and HC subjects (n=65), with an AUC of 0.87 4 (**Figure 4A**). When the Youden index reached a maximum from the ROC curve, the corresponding cutoff value of exosomal Cripto-1 for diagnosing PHCCA was 0.82, achieving a sensitivity of 79.1% and a specificity of 87.5%. Moreover, it was highly capable in discerning different TNM stage of PHCCA patients from cholangitis and HC subjects (**Figure S1**). In contrast, exosomal Cripto-1 levels could not distinguish cholangitis cases from healthy controls (**Figure S2**). And, exosomal Cripto-1 had limited differential diagnosis value for PHCCA with or without lymph nodes metastasis (**Figure S3**).

To better understand the diagnostic performance of exosomal Cripto-1 for PHCCA, the levels of traditional serum tumor markers, CA19-9 and CEA, were assessed in all subjects. As shown in **Table 1**, there were significant differences between the HC, cholangitis and PHCCA groups. Further, CA19-9 in the PHCCA group was increased compared to the cholangitis and HC groups (both at $P< 0.001$), while CEA was only significantly higher than patients in the cholangitis group ($P< 0.01$) (**Figure S4**). The AUC values of CA19-9, CEA and the combined CA19-9 and CEA for PHCCA diagnosis were 0.773 (**Figure 4B**) and 0.596 (**Figure 4C**) and 0.773 (**Figure 4D**), much lower than that of

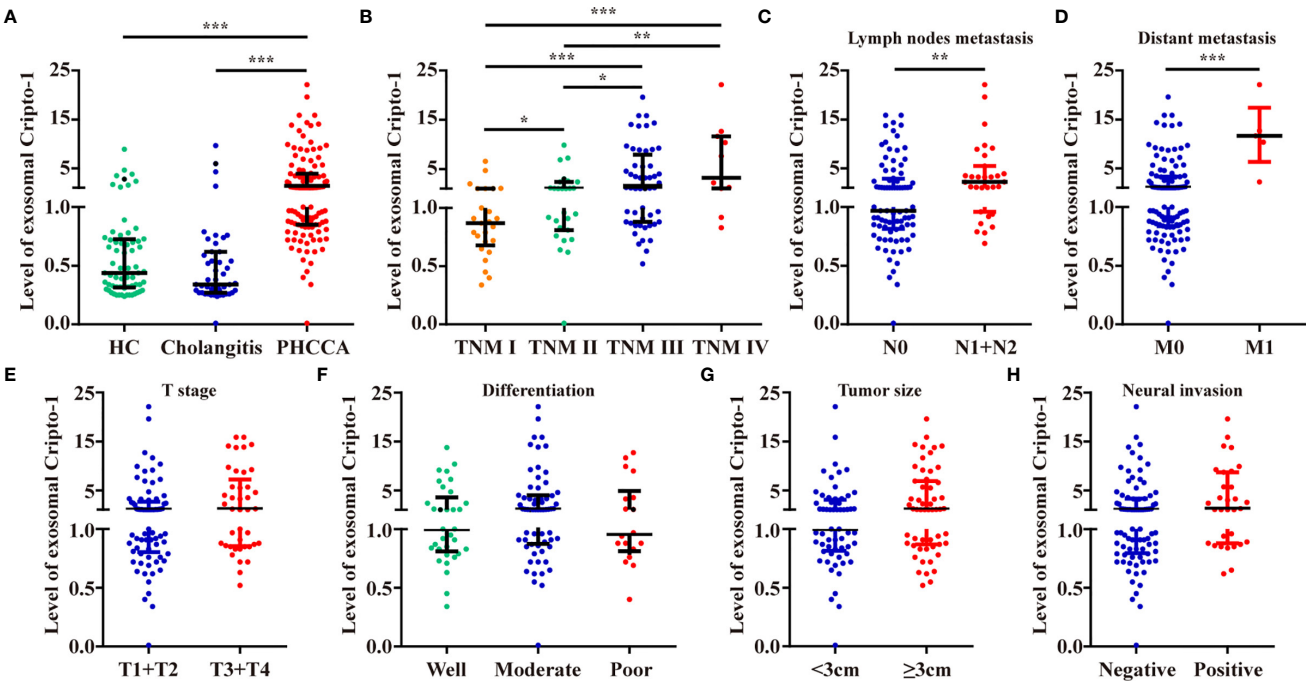

FIGURE 3 | Levels of exosomal Cripto-1 in PHCCA patient sera. **(A)** Levels of exosomal Cripto-1 were compared in sera among healthy control (HC) individuals, cholangitis patients and PHCCA patients. Comparison analysis of exosomal Cripto-1 between different TNM stage **(B)**, lymph nodes metastasis **(C)**, distant metastasis **(D)**, T stage **(E)**, differentiation **(F)**, tumor size **(G)**, neural invasion **(H)** in PHCCA patients. *$P < 0.05$, **$P < 0.01$, ***$P < 0.001$(Mann–Whitney U test). Data represents the median (interquartile range).

exosomal Cripto-1. When the combined exosomal Cripto-1, CA19-9 and CEA levels were used, the AUC was 0.888 (**Figure 4E**), not significantly enhanced compared to exosomal Cripto-1 alone. Since exosomal Cripto-1 had no significant association with CA19-9 and CEA, and no significant difference was observed between CA19-9 or CEA positive and negative groups (**Figure S5**), its diagnosis performance was assessed for CA19-9 or CEA negative individuals. As shown in **Figure 4F**, the exosomal Cripto-1 also had a high diagnostic capacity in subjects where diagnosis was missed in clinics. The diagnostic performance characteristics of exosomal Cripto-1, CA19-9 and CEA for PHCCA, such as sensitivity, specificity, positive likelihood ratio and negative likelihood ratio, are shown in **Table 2**.

Levels of Exosomal Cripto-1 in Sera of PHCAA Patients Reflects Their Expression in Tissues

To explore the relationship between Cripto-1 in the exosomes of sera and tissues, 34 pairs of tumor tissues and sera were collected from PHCCA patients who underwent radical resection. Western blot analysis showed Cripto-1 was increased in PHCCA tissues compared to the corresponding normal bile duct tissues (**Figure 5A**). Then, the expression of Cripto-1 in 34 PHCCA tissue samples was detected by immunohistochemical staining and classified into low and high Cripto-1 expression groups, according to median of H-score (**Figure 5B**). The corresponding sera detected by exoEILSA showed that exosomal Cripto-1 levels in immunohistochemically Cripto-1-high cases, were significantly higher than in Cripto-1-low cases (**Figure 5C**). Among the aforementioned cases, 15 further cases were detected 1-week post surgery. The quantitative assay showed that after surgery, the median levels of exosomal Cripto-1 decreased from 1.25 (0.96-3.26) to 0.85(0.62-1.82) (**Figure 5D**).

Expression and Prognostic Significance of Cripto-1 in PHCCA Tissues

Anti-Cripto-1 was used for immunohistochemical staining, in a retrospective cohort of 105 cases with PHCCA who had underwent radical resection. By evaluating the H-scores, the patients were divided into subgroups with low or high expression of Cripto-1 (**Figure 6A**). Data from **Table S2** showed Cripto-1 expression significantly associated with lymph nodes metastasis, whilst there was no relationship with other clinicopathological factors, such as gender, age, differentiation, tumor size, T stage and neural invasion. As patients with high exosomal Cripto-1 expression in tissues or serum tended to have metastasis and EMT was a critical event involved in tumor metastasis (10, 11), the expression of E-cadherin, a known EMT marker, was assessed (**Figure 6B**). As shown in **Figure 6C**, the Cripto-1 expression negatively correlated with E-cadherin expression and patients with high Cripto-1 expression lowly expressed E-cadherin.

To investigate the prognostic properties of PHCCA, univariate analysis was performed using a Kaplan–Meier survival curve. As shown in **Figure 6D**, patients with high Cripto-1 expression had

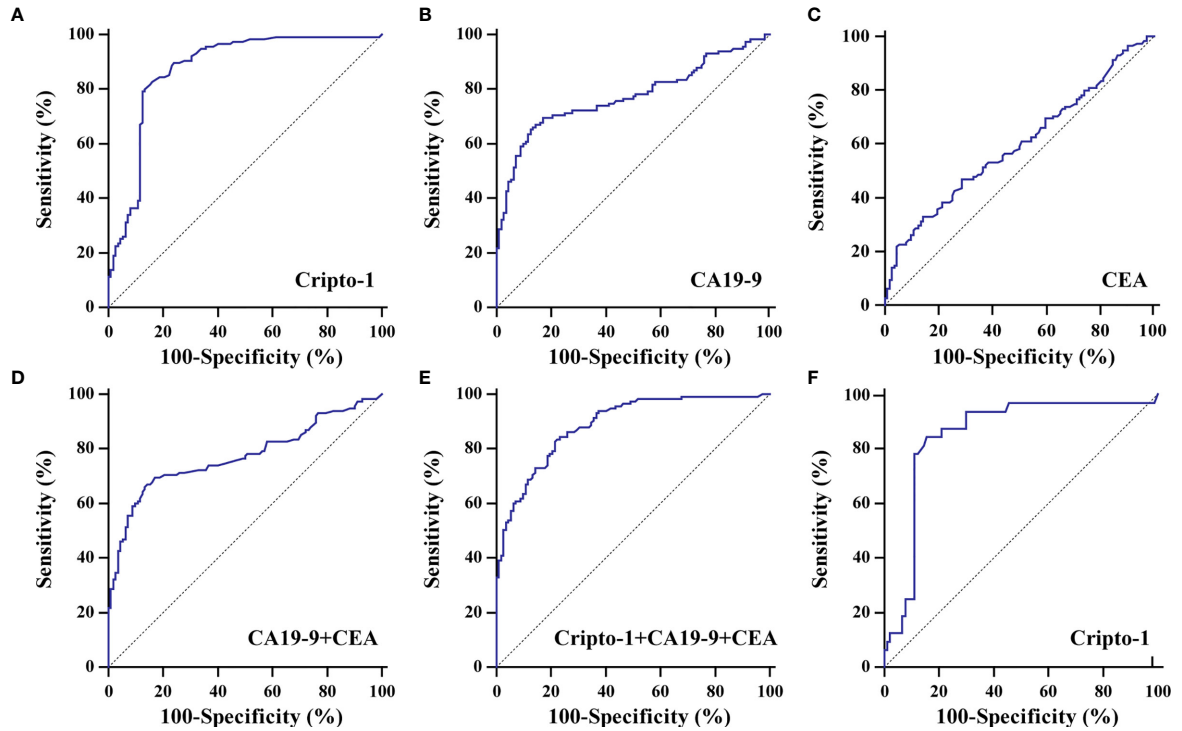

FIGURE 4 | Diagnostic significance analysis of exosomal Cripto-1 and traditional serum markers. ROC curves analysis for the detection of PHCCA using exosomal Cripto-1 **(A)**, CA19-9 **(B)**, CEA **(C)**, combined CA19-9 and CEA **(D)**, and combined exosomal Cripto-1, CA19-9 and CEA **(E)** in all subjects. **(F)** ROC curves analysis for the detection of PHCCA using exosomal Cripto-1 in both CA19-9 and CEA negative individuals.

TABLE 2 | The diagnosis performance of Cripto-1, CA19-9 and CEA for PHCCA.

Index	AUC	95% CI	Sensitivity	Specificity	+LR	-LR
Cripto-1	0.874	0.824-0.914	79.1	87.5	6.33	0.24
CA199	0.773	0.713-0.826	65.2	87.5	5.22	0.40
CEA	0.596	0.529-0.660	33.0	85.7	2.31	0.78
CA199+CEA	0.773	0.713-0.825	66.1	86.6	4.93	0.39
Cripto-1+CA199+CEA	0.888	0.840-0.926	82.6	78.6	3.86	0.22

AUC, Area under curve; CI, Confidence interval; +LR, Positive likelihood ratio; -LR, Negative likelihood ratio.

significantly lower survival rates than patients with low Cripto-1 expression. Moreover, patients with high Cripto-1 and low E-cadherin expression had the lowest probability of survival (**Figure 6E**). However, there were no significant survival differences between patients with low and high E-cadherin expression (**Figure S6**). In addition, patients with advanced T stage or positive lymph nodes metastasis had poor overall survival (**Figure S7**). Cripto-1 expression, along with the clinicopathological factors, was subjected to Cox model for multivariate analysis; except for T stage, Cripto-1 was identified as an independent prognostic biomarker (**Table 3**).

DISCUSSION

In the current study, it was first reported that Cripto-1 was released *via* exosomes by PHCCA cells. Next, an exoELISA method was developed and 3 cohorts were used to evaluate the clinical application value of Cripto-1. The study has achieved several new results. Firstly, exosomal Cripto-1 were increased in sera of PHCCA patients and associated with metastasis. Compared with traditional serum tumor markers, CA19-9 and CEA, exosomal Cripto-1 demonstrated as a more appropriate marker for PHCCA diagnosis. Secondly, it was found that exosomal Cripto-1 levels in sera reflect the expression in the tissues of PHCAA patients. Thirdly, it has been demonstrated in a prospective cohort analysis that Cripto-1 might be an independent factor for identifying poor prognosis in patients with PHCAA. Together, these findings verify that exosomal Cripto-1 is a potential biomarker for the diagnosis and prognosis of PHCCA.

In recent years, exosomes have emerged as an important liquid biopsy tool for a variety of malignant tumors (24). With the development of mass spectrometry and other detection

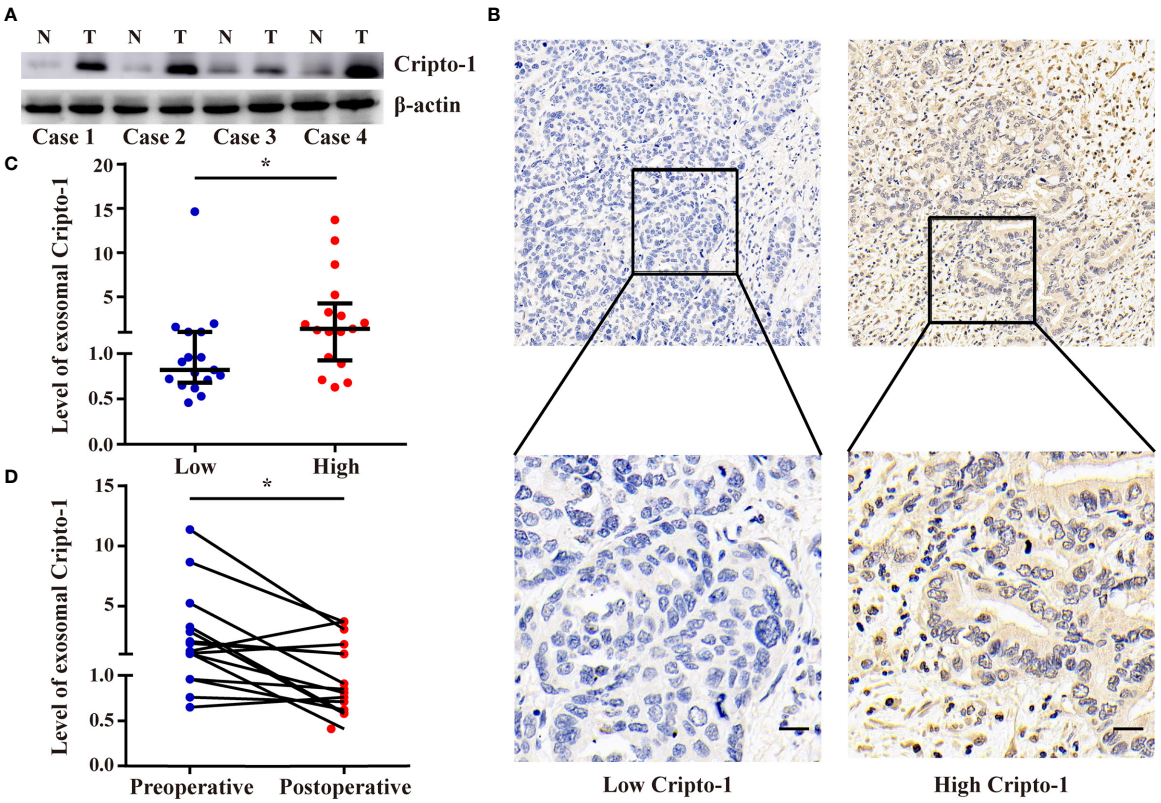

FIGURE 5 | Levels of exosomal Cripto-1 in sera of PHCAA patients reflects their expression in tissues. **(A)** Western blotting analysis of Cripto-1 expression in PHCCA tissues and adjacent normal tissues. **(B)** Immunohistochemistry analysis of Cripto-1 expression in PHCCA tissues. PHCCA patients were classified into low and high Cripto-1 expression groups according to median of histochemistry score (H-score). Scale bars, 50μm **(C)** exoELISA was performed to compare the levels of exosomal Cripto-1 in sera between PHCAA patients with low and high Cripto-1 expression in tissues. *$P < 0.05$ (Mann–Whitney U test). Data represents the median (interquartile range). **(D)** Preoperative and perioperative levels of exosomal Cripto-1 in sera were compared in PHCAA patients. *$P < 0.05$ (Wilcoxon matched-pairs signed rank test).

technologies, the protein composition of exosomes has been constantly identified; some of these are already used as tumor biomarkers due to their stability and specificity (20, 25). Amongst them, Glycosyl-Phosphatidyl-Inositol (GPI) anchored proteins (GPI-APs) are attractive as a source of exosomal candidates (26). This is because GPI-APs are preferentially embedded into lipid rafts through their GPI anchor and the lipid raft microdomains are believed to be involved in exosome biogenesis (27, 28). For example, Glypican-1 has been found in pancreatic carcinoma cell derived exosomes and can serve as a potential non-invasive diagnostic biomarker to facilitate the early detection of pancreatic cancer (29). CD24, located in lipid rafts through its GPI anchor, is demonstrated to be found in high levels in exosomes isolated from ovarian cancer cells, compared to other tumor biomarkers such as CA-125, EGFR and MUC18 (30). Since Cripto-1 has been reported as a cell surface GPI-linked glycoprotein (31), this study tested whether it can be found in exosomes. Cripto-1 was found in exosomes from the culture medium of PHCCA cell lines and the peripheral blood of mice implanted PHCCA cells. Thus, exosomal Cripto-1 might provide a noninvasive biomarker for the detection of PHCCA.

In previous studies, Cripto-1 has been detected at the mRNA or protein levels in tissues of several human solid cancers. Furthermore, Cripto-1 protein levels are also increased in serum/plasma obtained from patients with glioblastoma (32), renal cell carcinoma (33), colon cancer and breast cancer (34). In the present study, Cripto-1 levels were quantitatively determined in the exosomes of serum samples and showed increased levels in PHCCA patients compared to cholangitis patients and healthy controls. Moreover, the results are reliable, with batch differentiation, repeated freeze thawing and different lengths of incubation proving to have no significant effect on the result. To better assess the application of exosomal Cripto-1 as a potential diagnosis marker, the study compared its ability to detect PHCCA with current diagnostic tools CA19-9 and CEA, the traditional serum tumor markers routinely used in clinic. As shown in this data, exosomal Cripto-1 demonstrated improved sensitivity and specificity, associated with a markedly larger AUC, in distinguishing PHCCA from cholangitis patients and healthy controls. Furthermore, exosomal Cripto-1 also had a high diagnostic capacity in CA19-9 and CEA negative individuals. However, combined detection of Cripto-1, CA19-9

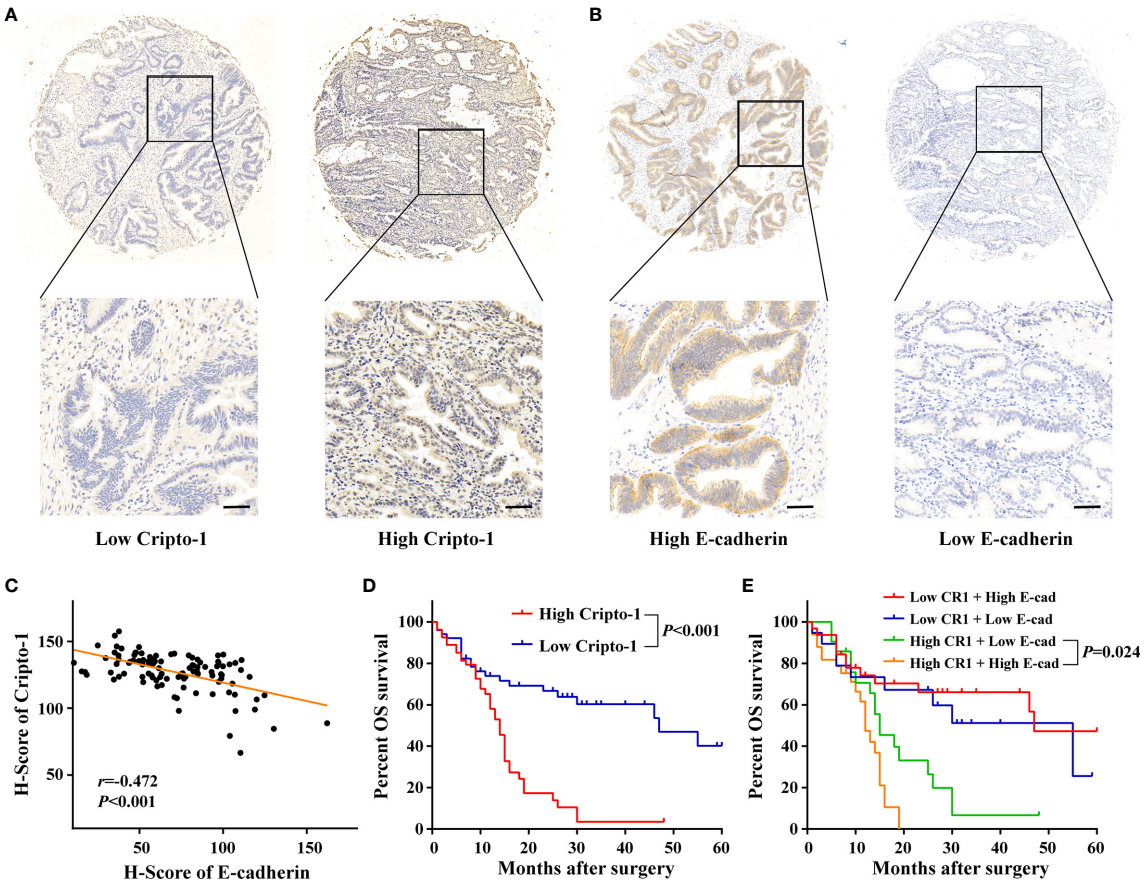

FIGURE 6 | Expression and prognostic significance of Cripto-1 in PHCCA tissues. **(A, B)** Immunohistochemistry analysis of Cripto-1 and E-cadherin expression in PHCCA tissues. PHCCA were classified into low and high Cripto-1/E-cadherin expression groups according to median of H-score. Scale bars, 50μm **(C)** Correlation analyses between Cripto-1 and E-cadherin expression in PHCCA tissues. **(D)** Kaplan–Meier curve for overall survival in PHCCA patients stratified according to Cripto-1 expression. **(E)** Kaplan–Meier curve for overall survival in PHCCA patients stratified according to Cripto-1 expression and E-cadherin expression.

and CEA did not enhance diagnostic performance compared to Cripto-1 alone. Another interesting finding of the current study is that exosomal Cripto-1 levels increased as the PHCCA TNM stage progressed. However, this phenomenon was not observed in CA19-9 or CEA. Thus, it can be concluded that exosomal Cripto-1 may detect PHCCA patients at an earlier stage.

Our previous study has reported that several long noncoding RNAs in exosomes of serum are associated their expression in tumor tissues (35). To better understand whether circulating exosomal Cripto-1 is represented in tissue biopsies, Cripto-1 expression was further examined in the tissues of PHCAA patients. Data from this study showed that Cripto-1 levels were increased in PHCCA tissues compared with the corresponding normal bile duct tissues. Exosomal Cripto-1 levels were especially elevated in immunohistochemically Cripto-1-high cases. These results infer that exosomal Cripto-1 levels in patient sera can reflect expression in tissues of PHCCA patients. Moreover, levels of exosomal Cripto-1 were decreased after surgery, which is conducive to monitoring disease status. Due to the limited follow-up time of collected serum, the prognostic value of Cripto-1 was analyzed using a previously established tissue microarray. It was found that patients with high expression of Cripto-1 had poor survival, which was an independent prognostic biomarker. This phenomenon is similar to some studies on other cancers, such as non-small cell lung cancer (36), hepatocellular carcinoma (37) and esophageal squamous cell carcinoma (38).

In the present study, it was demonstrated that Cripto-1 expression in both serum and tissues significantly associated with metastasis. Several studies have showed Cripto-1 plays an important role during developmental EMT. For example, the over-expression of Cripto-1 down-regulates E-cadherin whilst up regulating β-catenin in prostate cancer cells, thus inducing EMT through activation of the Wnt/β-catenin signaling pathway (39). In clear cell renal cell carcinoma, Cripto-1 promoted EMT properties, including the down-regulation of E-cadherin and the up-regulation of Vimentin, N-cadherin, ZEB-1, and Snail (33). EMT has been reported to increase the motility and invasiveness of cholangiocarcinoma cells (40–42). Functional loss of E-cadherin has been considered a hallmark of EMT (43) and this

TABLE 3 | Univariate and multivariate analysis of prognostic factors predicting overall survival in PHCAA patients.

Parameters	Univariate analysis		Multivariate analysis	
	5-year OS rate (%)	*P*-value[a]	HR(95%IC)	*P*-value[b]
Gender (Male *VS* Female)	0 *VS* 31.4	0.417	0.882 (0.491-1.582)	0.673
Age(<65y *VS* ≥65y)	29.1 *VS* 0	0.121	1.567 (0.877-2.800)	0.129
Differentiation(Well *VS* Moderate *VS* Poor)	36.7 *VS* 23.7 *VS* 14.1	0.056	1.373 (0.918-2.053)	0.123
Tumor size(<3cm *VS* ≥3cm)	30.7 *VS* 13.3	0.171	1.455 (0.862-2.455)	0.160
T stage (T1+T2 *VS* T3+T4)	32.1 *VS* 10.3	0.001	1.469 (1.115-1.936)	0.006
Lymph nodes metastasis(N0 *VS* N1+N2)	27.8 *VS* 7.3	0.008	1.396 (0.746-2.614)	0.297
Neural invasion(Negative *VS* Positive)	20.7 *VS* 34.7	0.930	1.341 (0.682-2.639)	0.395
Cripto-1 (Negative *VS* Positive)	40.2 *VS* 3.5	<0.001	2.460 (1.276-4.743)	0.007

OS, Overall survival; HR, Hazard ratio; CI, Confidence interval; [a]Calculated by log-rank test; [b]Calculated by Cox-regression Hazard model.

study showed that Cripto-1 expression negatively correlated with E-cadherin expression in PHCCA tissues; this suggests that Cripto-1 may also play a role as an EMT inducer to promote PHCCA cell migration and invasion. Additionally, it has also been shown that the combination of Cripto-1 and E-cadherin improved the power of the survival prediction.

Although the findings of this study are promising, some limitations need to be addressed. Firstly, it was found that there were increased exosomal Cripto-1 levels in some healthy individuals or cholangitis patients. The cause of this is not clear and whether these subjects develop tumors remains to be seen. Secondly, the prognostic value of exosomal Cripto-1 levels in the sera of PHCCA patients needs to be further studied, although it has been shown to correlate with tissue biopsies in this study. Thirdly, since currently there are not enough follow up serum samples for analysis, further ongoing perspective studies are necessary to address whether exosomal Cripto-1 can identify patients with reoccurring tumors. This is of particular importance for PHCCA patients because of the high recurrence rate (44).

In conclusion, this study developed a convenient and sensitive assay to detect exosomal Cripto-1 and for the first time demonstrated exosomal Cripto-1 as a potential noninvasive maker for PHCCA diagnosis and monitoring. Moreover, Cripto-1 shows promise as an independent predictor of poor prognosis for PHCCA patients. Since Cripto-1 has many advantages over conventional cancer markers, further multi-center prospective studies are needed to confirm whether exosomal Cripto-1 can be incorporated into routine clinical practice.

DATA AVAILABILITY STATEMENT

The raw data supporting the conclusions of this article will be made available by the authors, without undue reservation.

ETHICS STATEMENT

The studies involving human participants were reviewed and approved by Ethics Committee of Qilu Hospital of Shandong University. The patients/participants provided their written informed consent to participate in this study. The animal study was reviewed and approved by Medical Ethics Committee of Qilu Hospital of Shandong University.

AUTHOR CONTRIBUTIONS

CH, YZ, and XZhe performed all experiments. CH and MZ participated in data analysis and interpretation of results. CH, TL, and QG drafted the manuscript. XZha designed the study and revised the manuscript. All authors contributed to the article and approved the submitted version.

FUNDING

This work was supported by Shandong Province Natural Science Foundation (ZR2020MH238); Shandong Medical and Health Technology Development Project (2018WSB20002) and National Natural Science Foundation of China (No. 81900728).

SUPPLEMENTARY MATERIAL

The Supplementary Material for this article can be found online at: https://www.frontiersin.org/articles/10.3389/fonc.2021.730615/full#supplementary-material

REFERENCES

1. Siriwardena AK. Klatskin Tumor. *J Clin Oncol* (2017) 35(36):4091–2. doi: 10.1200/JCO.2017.75.1586
2. Liu Z, Sun R, Zhang X, Qiu B, Chen T, Li Z, et al. Transcription Factor 7 Promotes the Progression of Perihilar Cholangiocarcinoma by Inducing the Transcription of c-Myc and FOS-Like Antigen 1. *EBioMedicine* (2019) 45:181–91. doi: 10.1016/j.ebiom.2019.06.023
3. Xu YF, Liu ZL, Pan C, Yang XQ, Ning SL, Liu HD, et al. HMGB1 Correlates With Angiogenesis and Poor Prognosis of Perihilar Cholangiocarcinoma *via* Elevating VEGFR2 of Vessel Endothelium. *Oncogene* (2019) 38(6):868–80. doi: 10.1038/s41388-018-0485-8
4. Groot Koerkamp B, Wiggers JK, Gonen M, Doussot A, Allen PJ, Besselink MGH, et al. Survival After Resection of Perihilar Cholangiocarcinoma-Development and External Validation of a Prognostic Nomogram. *Ann Oncol* (2015) 26(9):1930–5. doi: 10.1093/annonc/mdv279

5. Nault JC, Villanueva A. Biomarkers for Hepatobiliary Cancers. *Hepatology* (2021) 73 Suppl 1:115–27. doi: 10.1002/hep.31175
6. Tsukahara T, Ebata T, Shimoyama Y, Yokoyama Y, Igami T, Sugawara G, et al. Residual Carcinoma *In Situ* at the Ductal Stump has a Negative Survival Effect: An Analysis of Early-Stage Cholangiocarcinomas. *Ann Surg* (2017) 266 (1):126–32. doi: 10.1097/SLA.0000000000001944
7. Watanabe K, Nagaoka T, Lee JM, Bianco C, Gonzales M, Castro NP, et al. Enhancement of Notch Receptor Maturation and Signaling Sensitivity by Cripto-1. *J Cell Biol* (2009) 187(3):343–53. doi: 10.1083/jcb.200905105
8. Park SW, Do HJ, Han MH, Choi W, Kim JH. The Expression of the Embryonic Gene Cripto-1 Is Regulated by OCT4 in Human Embryonal Carcinoma NCCIT Cells. *FEBS Lett* (2018) 592(1):24–35. doi: 10.1002/1873-3468.12935
9. Klauzinska M, Castro NP, Rangel MC, Spike BT, Gray PC, Bertolette D, et al. The Multifaceted Role of the Embryonic Gene Cripto-1 in Cancer, Stem Cells and Epithelial-Mesenchymal Transition. *Semin Cancer Biol* (2014) 29:51–8. doi: 10.1016/j.semcancer.2014.08.003
10. Rangel MC, Karasawa H, Castro NP, Nagaoka T, Salomon DS, Bianco C. Role of Cripto-1 During Epithelial-to-Mesenchymal Transition in Development and Cancer. *Am J Pathol* (2012) 180(6):2188–200. doi: 10.1016/j.ajpath.2012.02.031
11. Pilli VS, Gupta K, Kotha BP, Aradhyam GK. Snail-Mediated Cripto-1 Repression Regulates the Cell Cycle and Epithelial-Mesenchymal Transition-Related Gene Expression. *FEBS Lett* (2015) 589(11):1249–56. doi: 10.1016/j.febslet.2015.04.005
12. Bianco C, Strizzi L, Rehman A, Normanno N, Wechselberger C, Sun Y, et al. A Nodal- and ALK4-Independent Signaling Pathway Activated by Cripto-1 Through Glypican-1 and C-Src. *Cancer Res* (2003) 63(6):1192–7.
13. Bianco C, Strizzi L, Ebert A, Chang C, Rehman A, Normanno N, et al. Role of Human Cripto-1 in Tumor Angiogenesis. *J Natl Cancer Inst* (2005) 97 (2):132–41. doi: 10.1093/jnci/dji011
14. Ishii H, Zahra MH, Takayanagi A, Seno M. A Novel Artificially Humanized Anti-Cripto-1 Antibody Suppressing Cancer Cell Growth. *Int J Mol Sci* (2021) 22(4):1709. doi: 10.3390/ijms22041709
15. Sun G, Yan SS, Shi L, Wan ZQ, Jiang N, Fu LS, et al. MicroRNA-15b Suppresses the Growth and Invasion of Glioma Cells Through Targeted Inhibition of Cripto-1 Expression. *Mol Med Rep* (2016) 13(6):4897–903. doi: 10.3892/mmr.2016.5126
16. Soung YH, Ford S, Zhang V, Chung J. Exosomes in Cancer Diagnostics. *Cancers (Basel)* (2017) 9(1):94–100. doi: 10.3390/cancers9010008
17. Sung BH, von Lersner A, Guerrero J, Krystofiak ES, Inman D, Pelletier R, et al. A Live Cell Reporter of Exosome Secretion and Uptake Reveals Pathfinding Behavior of Migrating Cells. *Nat Commun* (2020) 11(1):2092. doi: 10.1038/s41467-020-15747-2
18. Li W, Li C, Zhou T, Liu X, Liu X, Li X, et al. Role of Exosomal Proteins in Cancer Diagnosis. *Mol Cancer* (2017) 16(1):145. doi: 10.1186/s12943-017-0706-8
19. Kalluri R. The Biology and Function of Exosomes in Cancer. *J Clin Invest* (2016) 126(4):1208–15. doi: 10.1172/JCI81135
20. Hoshino A, Kim HS, Bojmar L, Gyan KE, Cioffi M, Hernandez J, et al. Extracellular Vesicle and Particle Biomarkers Define Multiple Human Cancers. *Cell* (2020) 182(4):1044–61.e18. doi: 10.1016/j.cell.2020.07.009
21. Kimura H, Yamamoto H, Harada T, Fumoto K, Osugi Y, Sada R, et al. CKAP4, a DKK1 Receptor, Is a Biomarker in Exosomes Derived From Pancreatic Cancer and a Molecular Target for Therapy. *Clin Cancer Res* (2019) 25(6):1936–47. doi: 10.1158/1078-0432.CCR-18-2124
22. Zhang X, Yang X, Zhang Y, Liu X, Zheng G, Yang Y, et al. Direct Serum Assay for Cell-Free Bmi-1 mRNA and Its Potential Diagnostic and Prognostic Value for Colorectal Cancer. *Clin Cancer Res* (2015) 21(5):1225–33. doi: 10.1158/1078-0432.CCR-14-1761
23. Budwit-Novotny DA, McCarty KS, Cox EB, Soper JT, Mutch DG, Creasman WT, et al. Immunohistochemical Analyses of Estrogen Receptor in Endometrial Adenocarcinoma Using a Monoclonal Antibody. *Cancer Res* (1986) 46(10):5419–25.
24. Li S, Yi M, Dong B, Tan X, Luo S, Wu K. The Role of Exosomes in Liquid Biopsy for Cancer Diagnosis and Prognosis Prediction. *Int J Cancer* (2021) 148(11):2640–51. doi: 10.1002/ijc.33386
25. Pietrowska M, Zebrowska A, Gawin M, Marczak L, Sharma P, Mondal S, et al. Proteomic Profile of Melanoma Cell-Derived Small Extracellular Vesicles in Patients' Plasma: A Potential Correlate of Melanoma Progression. *J Extracell Vesicles* (2021) 10(4):e12063. doi: 10.1002/jev2.12063
26. Muller GA. The Release of Glycosylphosphatidylinositol-Anchored Proteins From the Cell Surface. *Arch Biochem Biophys* (2018) 656:1–18. doi: 10.1016/j.abb.2018.08.009
27. Vidal M. Exosomes and GPI-Anchored Proteins: Judicious Pairs for Investigating Biomarkers From Body Fluids. *Adv Drug Delivery Rev* (2020) 161-162:110–23. doi: 10.1016/j.addr.2020.08.006
28. Tan SS, Yin Y, Lee T, Lai RC, Yeo RW, Zhang B, et al. Therapeutic MSC Exosomes Are Derived From Lipid Raft Microdomains in the Plasma Membrane. *J Extracell Vesicles* (2013) 2:22614. doi: 10.3402/jev.v2i0.22614
29. Melo SA, Luecke LB, Kahlert C, Fernandez AF, Gammon ST, Kaye J, et al. Glypican-1 Identifies Cancer Exosomes and Detects Early Pancreatic Cancer. *Nature* (2015) 523(7559):177–82. doi: 10.1038/nature14581
30. Im H, Shao H, Park YI, Peterson VM, Castro CM, Weissleder R, et al. Label-Free Detection and Molecular Profiling of Exosomes With a Nano-Plasmonic Sensor. *Nat Biotechnol* (2014) 32(5):490–5. doi: 10.1038/nbt.2886
31. Alam MJ, Takahashi R, Afify SM, Oo AKK, Kumon K, Nawara HM, et al. Exogenous Cripto-1 Suppresses Self-Renewal of Cancer Stem Cell Model. *Int J Mol Sci* (2018) 19(11):3345. doi: 10.3390/ijms19113345
32. Pilgaard L, Mortensen JH, Henriksen M, Olesen P, Sorensen P, Laursen R, et al. Cripto-1 Expression in Glioblastoma Multiforme. *Brain Pathol* (2014) 24 (4):360–70. doi: 10.1111/bpa.12131
33. Xue YJ, Chen SN, Chen WG, Wu GQ, Liao YF, Xu JB, et al. Cripto-1 Expression in Patients With Clear Cell Renal Cell Carcinoma Is Associated With Poor Disease Outcome. *J Exp Clin Cancer Res* (2019) 38(1):378. doi: 10.1186/s13046-019-1386-6
34. Bianco C, Strizzi L, Mancino M, Rehman A, Hamada S, Watanabe K, et al. Identification of Cripto-1 as a Novel Serologic Marker for Breast and Colon Cancer. *Clin Cancer Res* (2006) 12(17):5158–64. doi: 10.1158/1078-0432.CCR-06-0274
35. Zhang Y, Liu H, Liu X, Guo Y, Wang Y, Dai Y, et al. Identification of an Exosomal Long Non-Coding RNAs Panel for Predicting Recurrence Risk in Patients With Colorectal Cancer. *Aging (Albany NY)* (2020) 12(7):6067–88. doi: 10.18632/aging.103006
36. Xu C, Yuan Q, Hu H, Wang W, Zhang Q, Li L, et al. Expression of Cripto-1 Predicts Poor Prognosis in Stage I Non-Small Cell Lung Cancer. *J Cell Mol Med* (2020) 24(17):9705–11. doi: 10.1111/jcmm.15518
37. Huang T, Guo YZ, Yue X, Zhang GP, Zhang Y, Kuang M, et al. Cripto-1 Promotes Tumor Invasion and Predicts Poor Outcomes in Hepatocellular Carcinoma. *Carcinogenesis* (2020) 41(5):571–81. doi: 10.1093/carcin/bgz133
38. Liu Q, Cui X, Yu X, Bian BS, Qian F, Hu XG, et al. Cripto-1 Acts as a Functional Marker of Cancer Stem-Like Cells and Predicts Prognosis of the Patients in Esophageal Squamous Cell Carcinoma. *Mol Cancer* (2017) 16 (1):81. doi: 10.1186/s12943-017-0650-7
39. Liu Y, Qin Z, Yang K, Liu R, Xu Y. Cripto-1 Promotes Epithelial-Mesenchymal Transition in Prostate Cancer *via* Wnt/Beta-Catenin Signaling. *Oncol Rep* (2017) 37(3):1521–8. doi: 10.3892/or.2017.5378
40. Chen T, Li K, Liu Z, Liu J, Wang Y, Sun R, et al. WDR5 Facilitates EMT and Metastasis of CCA by Increasing HIF-1alpha Accumulation in Myc-Dependent and Independent Pathways. *Mol Ther* (2021) 29(6):2134–50. doi: 10.1016/j.ymthe.2021.02.017
41. Li Z, Liu J, Chen T, Sun R, Liu Z, Qiu B, et al. HMGA1-TRIP13 Axis Promotes Stemness and Epithelial Mesenchymal Transition of Perihilar Cholangiocarcinoma in a Positive Feedback Loop Dependent on C-Myc. *J Exp Clin Cancer Res* (2021) 40(1):86. doi: 10.1186/s13046-021-01890-1
42. Sun R, Liu Z, Qiu B, Chen T, Li Z, Zhang X, et al. Annexin10 Promotes Extrahepatic Cholangiocarcinoma Metastasis by Facilitating EMT *via* PLA2G4A/PGE2/STAT3 Pathway. *EBioMedicine* (2019) 47:142–55. doi: 10.1016/j.ebiom.2019.08.062
43. Loh CY, Chai JY, Tang TF, Wong WF, Sethi G, Shanmugam MK, et al. The E-Cadherin and N-Cadherin Switch in Epithelial-to-Mesenchymal Transition: Signaling, Therapeutic Implications, and Challenges. *Cells* (2019) 8(10):1118. doi: 10.3390/cells8101118
44. Nakahashi K, Ebata T, Yokoyama Y, Igami T, Mizuno T, Yamaguchi J, et al. How Long Should Follow-Up be Continued After R0 Resection of Perihilar

Cholangiocarcinoma? *Surgery* (2020) 168(4):617–24. doi: 10.1016/j.surg.2020.04.068

Conflict of Interest: The authors declare that the research was conducted in the absence of any commercial or financial relationships that could be construed as a potential conflict of interest.

Publisher's Note: All claims expressed in this article are solely those of the authors and do not necessarily represent those of their affiliated organizations, or those of the publisher, the editors and the reviewers. Any product that may be evaluated in this article, or claim that may be made by its manufacturer, is not guaranteed or endorsed by the publisher.

frontiers in Oncology

REVIEW
published: 02 September 2021
doi: 10.3389/fonc.2021.714665

The Mechanism and Clinical Significance of Circular RNAs in Hepatocellular Carcinoma

Ziyue Huang[1†], Haoming Xia[1†], Shuqiang Liu[1], Xudong Zhao[1], Risheng He[1], Zhongrui Wang[1], Wenguang Shi[1], Wangming Chen[1], Pengcheng Kang[1], Zhilei Su[1], Yunfu Cui[1], Judy Wai Ping Yam[2*] and Yi Xu[1,2,3*]*

[1] Department of Hepatopancreatobiliary Surgery, Second Affiliated Hospital of Harbin Medical University, Harbin, China, [2] Department of Pathology, Li Ka Shing Faculty of Medicine, The University of Hong Kong, Hong Kong, Hong Kong, SAR China, [3] The Key Laboratory of Myocardial Ischemia, Harbin Medical University, Ministry of Education, Harbin, China

OPEN ACCESS

Edited by:
Zongli Zhang,
Qilu Hospital of Shandong University, China

Reviewed by:
Hanqing Liu,
Jiangsu University, China
Weijia Liao,
Affiliated Hospital of Guilin Medical University, China

***Correspondence:**
Yi Xu
xuyihmu@163.com
Judy Wai Ping Yam
judyyam@pathology.hku.hk
Yunfu Cui
yfcui777@hotmail.com

[†]These authors have contributed equally to this work and share first authorship

Specialty section:
This article was submitted to Cancer Molecular Targets and Therapeutics, a section of the journal Frontiers in Oncology

Received: 25 May 2021
Accepted: 09 August 2021
Published: 02 September 2021

Citation:
Huang Z, Xia H, Liu S, Zhao X, He R, Wang Z, Shi W, Chen W, Kang P, Su Z, Cui Y, Yam JWP and Xu Y (2021) The Mechanism and Clinical Significance of Circular RNAs in Hepatocellular Carcinoma. Front. Oncol. 11:714665. doi: 10.3389/fonc.2021.714665

Hepatocellular carcinoma (HCC) is one of the most prevalent malignant tumors worldwide. In view of the lack of early obvious clinical symptoms and related early diagnostic biomarkers with high specificity and sensitivity, most HCC patients are already at the advanced stages at the time of diagnosis, and most of them are accompanied by distant metastasis. Furthermore, the unsatisfactory effect of the follow-up palliative care contributes to the poor overall survival of HCC patients. Therefore, it is urgent to identify effective early diagnosis and prognostic biomarkers and to explore novel therapeutic approaches to improve the prognosis of HCC patients. Circular RNA (CircRNA), a class of plentiful, stable, and highly conserved ncRNA subgroup with the covalent closed loop, is dysregulated in HCC. Increasingly, emerging evidence have confirmed that dysregulated circRNAs can regulate gene expression at the transcriptional or post-transcriptional level, mediating various malignant biological behaviors of HCC cells, including proliferation, invasion, metastasis, immune escape, stemness, and drug resistance, etc.; meanwhile, they are regarded as potential biomarkers for early diagnosis and prognostic evaluation of HCC. This article reviews the research progress of circRNAs in HCC, expounding the potential molecular mechanisms of dysregulated circRNAs in the carcinogenesis and development of HCC, and discusses those application prospects in the diagnosis and prognosis of HCC.

Keywords: circular RNAs, hepatocellular carcinoma, sponge, biomarker, diagnosis, prognosis

INTRODUCTION

Hepatocellular carcinoma is the sixth most common hepatic malignancy and causes severe burden of mortality, making it rank as the third leading cause of cancer-associated deaths worldwide, with approximately 906,000 new cases and 830,000 deaths (1, 2). Epidemiological and experimental studies have demonstrated that the initiation and progression of HCC may be caused and promoted by hepatitis B virus (HBV) or hepatitis C virus (HCV), aflatoxin-contaminated foods, non-alcoholic fatty liver disease (NAFLD), excessive drinking, genetic factors, smoking, excess body weight, type 2 diabetes (3). At present, there are still many limitations to existing diagnostic methods for HCC.

On the one hand, the classical biomarkers for clinical diagnosis lead to some false-positive and false-negative results in HCC diagnosis, such as alpha-fetoprotein (AFP) was widely used in early detection of HCC, but it may also appear in varying degrees in liver diseases such as hepatitis and liver cirrhosis (LC); on the another hand, liver electronic computer tomography (CT) and magnetic resonance imaging (MRI) show unclear nodules <2 cm (4, 5). Currently, the main methods of treatment for HCC are liver resection, liver transplantation, percutaneous thermal ablation, radiotherapy, chemotherapy, and immunotherapy (6). Among them, surgical resection is the first-choice treatment for HCC. Because of the lack of effective biomarkers and insidious early clinical symptoms, most HCC patients are at the advanced stage when diagnosed, losing the opportunity of radical resection; furthermore, other palliative treatment options remain no satisfactory survival benefits, leading to the poor clinical prognosis of HCC patients. Therefore, it is extremely necessary to clarify the molecular mechanisms of the oncogenesis and development of HCC, find accurate and potent biomarkers for early diagnosis and prognostic prediction, and formulate effective HCC treatment strategies.

Approximately 93% of the DNA sequences of the eukaryotic organism genome can be transcribed into RNA, of which only 2% can be translated into protein, while 98% are non-coding RNAs (ncRNAs) with no protein coding capability or very low coding capability. The development of high-throughput RNA sequencing led to the discovery of a large number of ncRNAs. The number of identified ncRNA genes exceeds that of coding transcripts (7–10). According to the length of the transcript, ncRNAs can be divided into short ncRNAs (<200 nucleotides) and long non-coding RNAs (lncRNAs, >200 nucleotides) (11). Researches have shown that the dysregulated lncRNAs and short ncRNAs can play a vital role in regulating malignant tumor-related genes. For example, lncRNAs can interact with DNA, RNAs, or proteins, regulating gene expression at the transcription and post-transcriptional levels (12–14). MicroRNAs (MiRNAs) can specifically bind to target mRNAs, leading to mRNA degradation or inhibiting protein translation (15).

Over the past few years, circRNA, as a new type of ncRNA, has been widely concerned. Unlike traditional linear RNA, circRNA has a covalently closed, continuous loop structure without a 5' cap and a 3' tail, which makes it resistant to ribonuclease cleavage and expresses itself in a stable manner (16–19). Meanwhile, most circRNAs show high tissue specificity and developmental stage-related expression patterns, as well as a high conservation among species (20–22). Based on these characteristics, circRNAs also have great potential in disease diagnosis, progress monitoring, prognosis prediction, etc. CircRNAs are exon or intron sequences spliced in reverse from the precursor mRNA (pre-mRNA), which can be classified as exon circular RNAs (EcircRNAs), intron circular RNAs (ciRNAs), and exon-intron circular RNAs (EIciRNAs) (21). Among them, EcircRNAs account for the majority of circRNAs, which mainly exist in the cytoplasm, acting as miRNA sponge (23, 24), interacting with RNA binding protein (RBP) (25), or encode proteins (26); while ciRNAs and EIciRNAs are widely present in the nucleus, which can act as transcription/translation regulators (27) or affect the selective splicing of pre-mRNA (28) **(Figure 1)**.

Additionally, emerging evidence have indicated that circRNAs are involved in mediating the tumorigenesis and development of various tumors, exhibiting great potential as a molecular target of cancer therapy. For example, circSEPT9 regulated by E2F transcription factor 1 (E2F1) and eukaryotic translation initiation factor 4A3 (EIF4A3) pushes the cancerous derivation of triple-negative breast cancer through the circSEPT9/miR-637/Leukemia Inhibitory Factor (LIF) axis (29). CircNRIP1 acts as a microRNA-149-5p sponge to promote gastric cancer progression through the AKT1/mTOR pathway (30). CircMRPS35 can specifically bind to the forkhead box protein O1/3a (FOXO1/3a) promoter region to activate its transcription, subsequently triggering the expression of downstream target genes p21, p27, Twist1, and E-cadherin, thereby inhibiting the malignant biological behaviors of tumors (31). In this review, we summarized the functions and mechanisms of circRNAs in the oncogenesis and malignant progression of human HCC.

ROLE OF CircRNAs IN HCC

It is reported that circRNA, which is unregulated expressed in tumor tissues, plays a role in the promotion or suppression in the development of tumors. CircRNAs can participate in the mediation of tumorigenesis, cell proliferation and apoptosis, invasion and metastasis, cell cycle, epithelial-mesenchymal transition (EMT), immune escape, drug resistance, metabolic reprogramming, and other malignant biological behaviors in HCC patients, and can be used as HCC potential biomarkers for early diagnosis and clinical prognostic prediction **(Figure 2)**. In the following section, the role of circRNAs in the oncogenesis and development of HCC and the molecular mechanisms involved will be briefly described, and the application prospects of circRNAs in HCC diagnosis and prognostic evaluation will be described **(Table 1)**.

Regulation of Tumorigenesis

Tumorigenesis is a progressive process. Normal cells gradually transform into tumor cells, involving the accumulation of multiple cascades and genetic mutations, among which circRNAs play a crucial role.

E1A binding protein p300 (EP300) and WD repeat domain 5 (WDR5) are recruited to the circSOD2 promoter, stimulating the H3K27ac and H3K4me3-mediated modification to upregulate circSOD2, which further acts as a molecular sponge to inhibit the expression of miR-502-5p, in order to mediate the overexpression of its downstream target gene DNA methyltransferase 3 alpha (DNMT3a). Highly expressed DNMT3a reduces the expression of suppressor of cytokine signaling 3 (SOCS3) by promoting the over-methylation of CpG islands in the SOCS3 promoter, thereby activating the

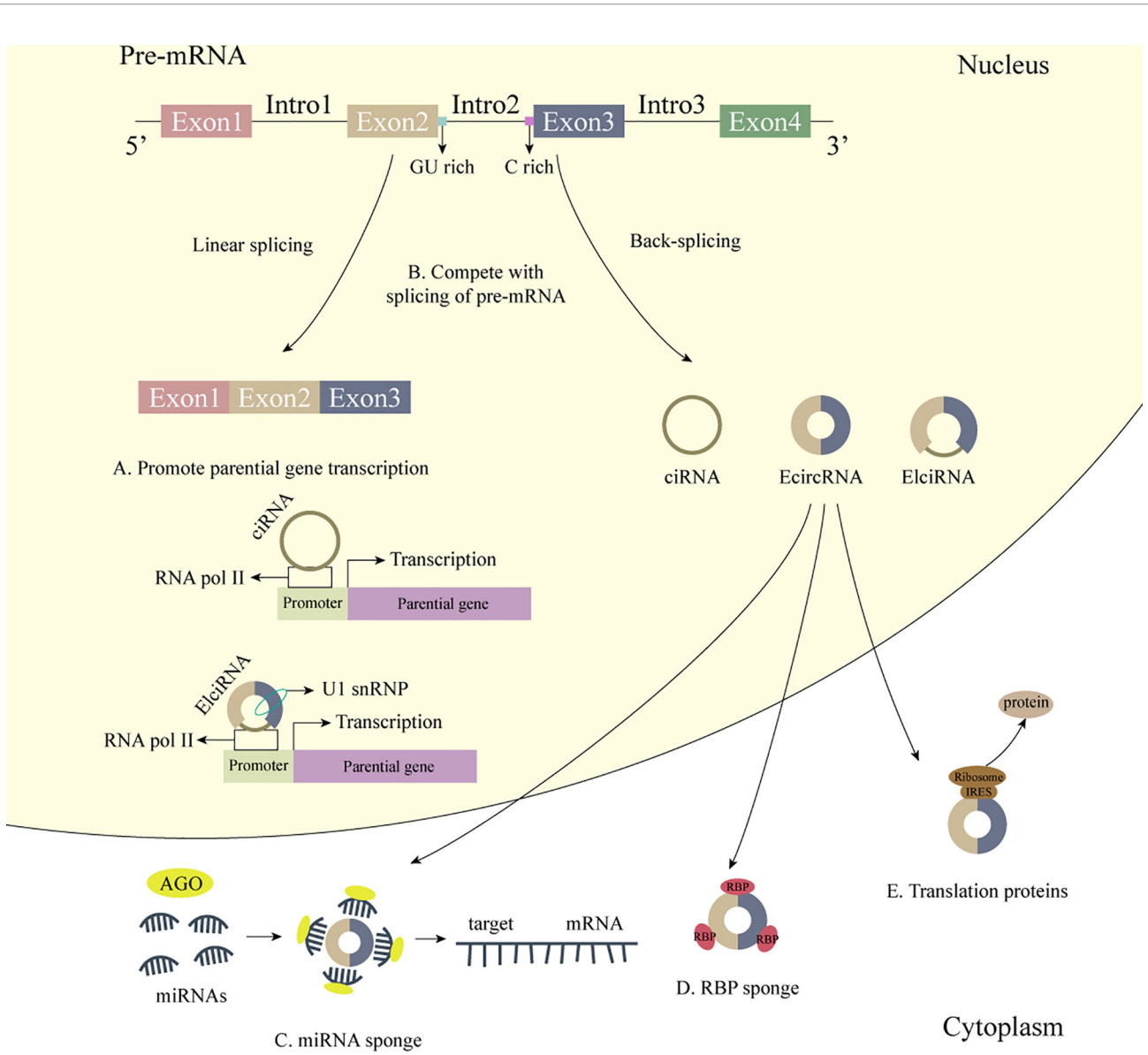

FIGURE 1 | The biogenesis and biological functions of circRNA. 1) The biogenesis of circRNA. CircRNAs are exon or intron sequences spliced in reverse from the pre-mRNA. 2) Some biological functions of circRNA. **(A)** CiRNAs interact with RNA Pol II, and ElciRNAs interact with RNA Pol II and U1 snRNP and further promote the transcription of their parental genes. **(B)** CircRNAs affect the selective splicing of pre-mRNA. **(C)** CircRNAs act as miRNA sponge. **(D)** CircRNAs act as RBP sponge. **(E)** CircRNAs bind to IRES to generate functional proteins.

Janus kinase 2/signal transducer and activator of transcription 3 (JAK2/STAT3) signaling pathway to drive the tumorigenesis of HCC. Meanwhile, STAT3 can combine with the circSOD2 promoter to form a positive feedback loop, persistently activating its transcription and maintaining a high-expression status (32). Hepatocyte nuclear factor 4 alpha (HNF4a) can bind to the circ_104075 promoter to activate its transcription, then upregulating YAP through sponge miR-582-3p to advance the process of HCC (33). circTMEM45A relieves the inhibition of insulin like growth factor 2 (IGF2) expression by interacting with miR-665 to promote HCC tumorigenesis (34). Knocking down circ_0001955 can significantly suppress the proliferation of HCC cells and subcutaneous xenografts growth *in vivo*, showing a smaller size and weight. Circ_0001955 can directly bind to miR-516a-5p as a competing endogenous RNA (ceRNA), which further mediates the upregulation of oncogenes TNF receptor associated factor 6 (TRAF6) and mitogen-activated protein kinase 11 (MAPK11) (35). Hsa_circ_0016788 also promotes the tumorigenesis of HCC through hsa_circ_0016788/miR-486/cyclin dependent kinase 4 (CDK4) axis (36). Functional assays revealed that overexpressed circSETD3 can restrain the proliferative capacity of HCC cells, as well as inducing G1/S phase arrest *in vitro*. Simultaneously, circSETD3 knockdown could effectively accelerate the growth rate of subcutaneous

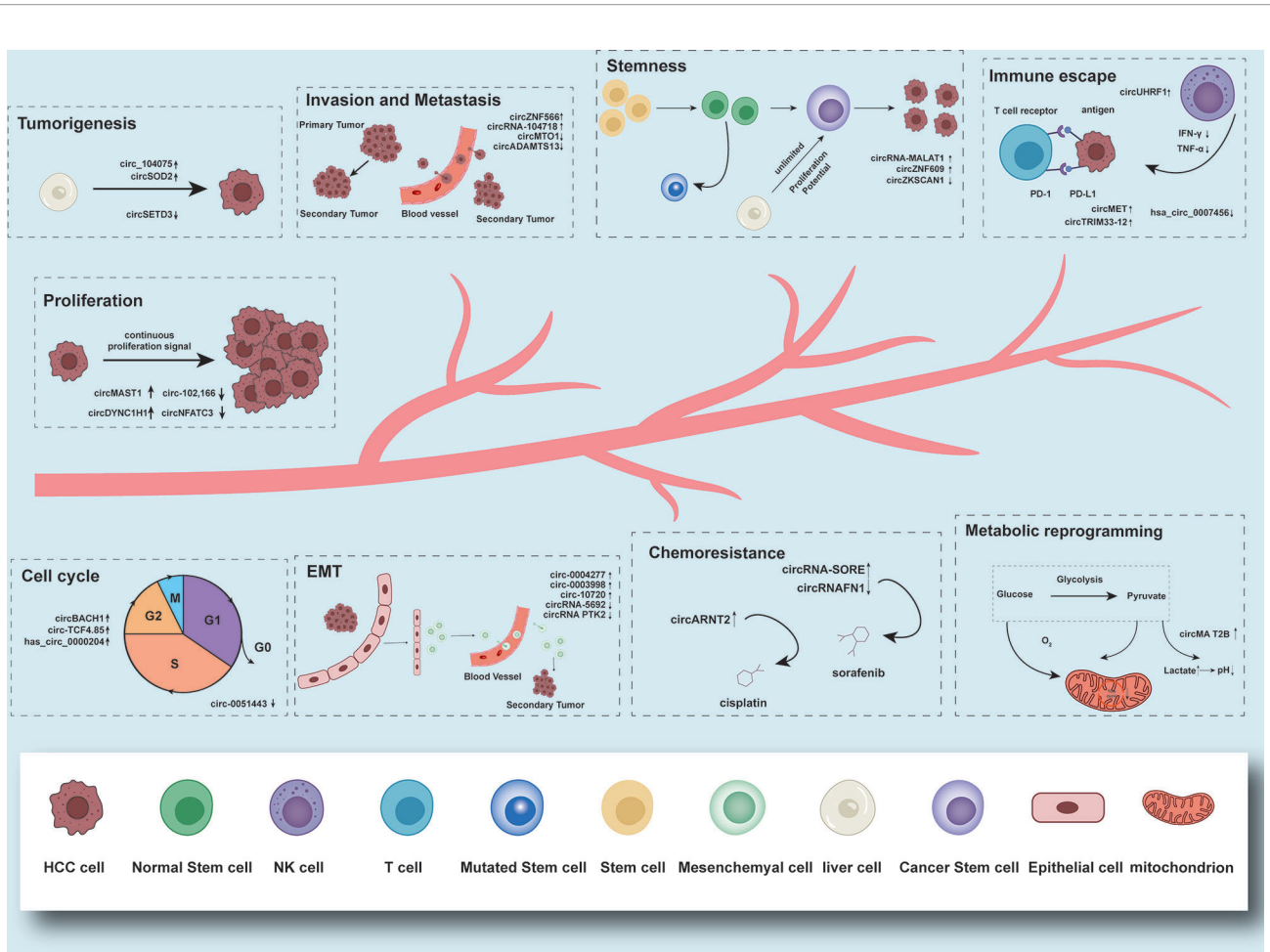

FIGURE 2 | Functions and brief mechanism of circRNAs in HCC tumorigenesis and progression. Aberrantly expressed circRNAs in HCC can participate in the mediation of tumorigenesis, cell proliferation and apoptosis, invasion and metastasis, cell cycle, EMT, immune escape, drug resistance, metabolic reprogramming, and stemness.

xenografts *in vivo*. CircSETD3 suppress the tumorigenesis of HCC through the circSETD3/miR-421/mitogen-activated protein kinase 14 (MAPK14) pathway (37).

Regulation of Malignant Biological Phenotypes

Affected by continuous proliferation signals, tumor cells with infinite growth potential can escape programmed cell apoptosis, accelerate the cell cycle process to achieve the long-term survival. Next, tumor cells originating from the primary tissues colonize other sites through body cavities, blood vessels, or lymphatic tracts, forming metastatic lesions. It is reported that circRNAs play an important regulatory role in the malignant biological behaviors of HCC cells.

Through binding to the 3'untranslated region (UTR) of stearoyl-CoA desaturase (SCD) mRNA, RNA binding motif protein 3 (RBM3) increases the production of SCD-circRNA 2, which enhances the phosphorylation of extracellular regulated protein kinase (ERK) and promotes the proliferation of HCC cells (38). Overexpressed circBACH1 activates the transport of human antigen R (HuR) from the nucleus to the cytoplasm, inhibiting p27 translation by abolishing the internal ribosome entry site (IRES) located at the 5'-UTR of p27, thereby promoting the proliferation of HCC cells and accelerating the cell cycle process (39). Has_circ_0000204 can sponge miR-191 to upregulate downstream target kruppel like factor 6 (KLF6), further promoting HCC cell proliferation and cell cycle transition (40). Exogenous knockdown of exosomal circRNA-100,338 can inhibit the invasive ability of HCC cells and the growth rate of xenografts, reducing the microvessel density in tumors and the number of lung metastatic nodules. Transported to human umbilical vein endothelial cells (HUVECs), exosomal circRNA-100,338 can stimulate the cell proliferation, and destroy the tight junctions between HUEVCs to affect their permeability. Meanwhile, the interaction with NOVA alternative splicing regulator 2 (NOVA2) induces angiogenesis and transfer ability of HCC cells (41). Enriched in HCC cell-derived exosomes characterized by high metastatic potential, circPTGR1 can upregulate MET proto-oncogene (MET) by competitively binding miR-449a, activating the metastatic activity of HCC

TABLE 1 | Representative circRNAs and related signaling pathways in HCC.

CircRNA	Current circBase ID	Genomic position	Spliced length (bp)	Expression	Biological functions	Regulatory axis	References
circSOD2	hsa_circ_0004662	chr6:160103505-160109274	462	up	promotes tumorigenesis	miR-502-5p/DNMT3a/JAK2/STAT3	(32)
circ_104075	hsa_circ_0075736	chr6:17669523-17669777	162	up	promotes tumorigenesis	miR-582-3p/YAP	(33)
circTMEM45A	hsa_circ_0066659	chr3:100274052-100296285	1254	up	promotes tumorigenesis	miR-665/IGF2	(34)
circ_0001955	hsa_circ_0001955	chr15:64495280-64508912	815	up	promotes tumorigenesis	miR-516a-5p/TRAF6/MAPK11	(35)
hsa_circ_0016788	hsa_circ_0016788	chr1:228581376-228594517	2691	up	promotes tumorigenesis	miR-486/CDK4	(36)
circSETD3	hsa_circ_0000567	chr14:99924615-99932150	683	down	inhibits tumorigenesis	miR-421/MAPK14	(37)
SCD-circRNA 2	/	/	/	up	enhances proliferation	SCD-circRNA 2/ERK	(37)
circBACH1	hsa_circ_0061395	chr21:30698379-30702014	1542	up	promotes proliferation, controls cell cycle	HuR/p27	(39)
hsa_circ_0000204	hsa_circ_0000204	chr10:1117078-1118233	1155	up	promotes proliferation, controls cell cycle	miR-191/KLF6	(40)
circRNA-100,338	/	/	/	up	promotes angiogenesis, migration	circRNA-100,338/NOVA2	(41)
circPTGR1 isoform	hsa_circ_0003731	chr9:114341075-114348445	442	up	promotes invasion, migration	miR-449a/MET	(42)
	hsa_circ_0008043	chr9:114332370-114348445	670				
	hsa_circ_0088030	chr9:114337013-114348445	551				
circASAP1	hsa_circ_0085616	chr8:131370262-131374017	229	up	promotes proliferation, invasion, migration, colony formation, TAM infiltration	miR-326/miR-532-5p/MAPK1/ERK1/2,miR-326/miR-532-5p/CSF-1	(43)
circMAST1	hsa_circ_0049613	chr19:12962747-12963209	303	up	promotes proliferation, invasion	miR-1299/CTNND1	(44)
circDYNC1H1	hsa_circ_0033351	chr14:102499401-102507010	1862	up	promotes proliferation, migration	miR-140-5p/SULT2B1	(45)
circSLC3A2	hsa_circ_0022587	chr11:62650379-62653080	669	up	promotes proliferation, invasion	miR-490-3p/PPM1F	(46)
circHIPK3	hsa_circ_0000284	chr11:33307958-33309057	1099	up	promotes proliferation, migration	miR-124/AQP3	(47)
hsa_circ_0001955	hsa_circ_0001955	chr15:64495280-64508912	815	up	promotes proliferation, invasion, migration	miR-145-5p/NRAS	(48)
circ-TCF4.85	/	/	/	up	promotes proliferation, invasion, migration, cell cycle, inhibits apoptosis	miR-486-5p/ABCF2	(49)
circZNF566	hsa_circ_0141434	chr19:36940300-36940903	603	up	promotes proliferation, invasion, migration	miR-4738-3p/TDO2	(50)
hsa_circRNA 103809	hsa_circ_0072088	chr5:32379220-32388780	693	up	promotes proliferation, migration, cell cycle	miR-377-3p/FGFR1	(51)
hsa_circ_104348	/	/	/	up	promotes proliferation, invasion, migration, inhibits apoptosis	miR-187-3p/RTKN2/Wnt/β-catenin	(52)
circRNA-104718	/	/	/	up	promotes growth, migration	miR-218-5p/TXNDC5	(53)
circFBLIM1	hsa_circ_0010090	chr1:16084668-16113084	3935	up	promotes growth, invasion, inhibits apoptosis	miR-346/FBLIM1	(54)
circ-DB	hsa_circ_0025129	chr12:6450941-6451283	342	up	promotes growth, invasion, modulates DNA damage	miR-34a/USP7/Cyclin2	(55)
circRASGRF2	hsa_circ_0073181	chr5:80338695-80409739	2182	up	promotes proliferation, invasion, migration, cell cycle, inhibits apoptosis	miR-1224/FAK	(56)
circ-LRIG3	hsa_circ_0027345	chr12:59277301-59308117	1080	up	promotes proliferation, invasion, migration, inhibits apoptosis	circ-LRIG3/EZH2/STAT3	(57)
circRHOT1	hsa_circ_0005397	chr17:30500849-30503232	233	up	promotes proliferation, invasion, migration, inhibits apoptosis	circRHOT1/NR2F6	(58)
circβ-catenin	hsa_circ-0004194	chr3:41265511-41268843	1129	up	promotes proliferation, invasion, migration, inhibits apoptosis	GSK3β/Wnt/β-catenin	(59)

(Continued)

TABLE 1 | Continued

CircRNA	Current circBase ID	Genomic position	Spliced length (bp)	Expression	Biological functions	Regulatory axis	References
circDLC1	hsa_circ_0135718	chr8:12945995-12948941	552	down	inhibits migration	KIAA1429/DHX9/HuR/MMP1	(60)
cSMARCA5	hsa_circ_0001445	chr4:144464661-144465125	269	down	inhibits proliferation, migration	miR-17-3p/miR-181b-5p/TIMP3	(61)
circARSP91	hsa_circ_0085154	chr8:101721360-101721451	91	down	inhibits colony formation and tumor growth	AR/ADAR1/circRNAARSP91	(62)
circ-ADD3	hsa_circ_0020007	chr10:111876016-111886261	1274	down	inhibits migration	CDK1/EZH2	(63)
circ-102,166	hsa_circ_0004913	chr17:62248459-62265775	495	down	inhibits proliferation, invasion	miR-182/miR-184/FOXO3a/MTSS1/SOX7	(64)
circMTO1	hsa_circ_0007874	chr6:74175931-74176329	318	down	inhibits proliferation, invasion, induces apoptosis	miR-9/p21	(65)
circNFATC3	hsa_circ_0000711	chr16:68155889-68160513	1298	down	inhibits proliferation, invasion, migration, induces apoptosis	miR-548l/JNK/c-jun/AKT/mTOR	(66)
hsa_circ_0091570	hsa_circ_0091570	chrX:131516205-131526362	711	down	inhibits proliferation, invasion, migration, induces apoptosis	miR-1307/ISM1	(67)
circ ADAMTS13	hsa_circ_0089372	chr9:136302868-136303486	270	down	inhibits proliferation, induces apoptosis	miR-484	(68)
circADAMTS14	hsa_circ_0018665	chr10:72468343-72496549	929	down	inhibits proliferation, invasion, migration, induces apoptosis	miR-572/RCAN1	(69)
circZKSCAN1	hsa_circ_0001727	chr7:99621041-99621930	668	down	inhibits proliferation, invasion, migration, stemness	FMRP/CCAR1/Wnt/β-catenin	(70, 71)
circ-0051443	hsa_circ_0051443	chr19:45667421-45668228	202	down	induces apoptosis, controls cell cycle	miR-331-3p/BAK1	(72)
circ-0004277	hsa_circ_0004277	chr10:1125950-1126416	161	up	induces EMT	HuR/ZO-1	(73)
circ-0003998	hsa_circ_0003998	chr20:47570092-47580435	304	up	induces EMT	miRNA-143-3p/FOSL2	(74)
circ10720	hsa_circ_0018189	chr10:35321362-35338693	747	up	promotes proliferation, invasion, migration, induces EMT	Twist1/circ10720/miRNA-490-5P/Vimentin	(75)
circRNA-5692	hsa_circ_0005692	chr16:4382215-4383520	411	down	inhibits EMT	miRNA-328-5p/DAB2IP	(76)
circPTK2	hsa_circ_0008305	chr8:141799572-141840625	584	down	inhibits EMT	miR-92a/E-cadherin	(77)
circUHRF1	hsa_circ_0048677	chr19:4941539-4945977	625	up	mediates immune escape	miR-449c-5p/TIM-3	(78)
circMET	hsa_circ_0082002	chr7:116339124-116340338	1214	up	induces EMT, participates in immune regulation	miR-30-5p/Snail/DPP4	(79)
circTRIM 33-12	/	/	/	down	inhibits proliferation, metastasis, mediates immune escape	miR-191/TET1	(80)
hsa_circ_0007456	hsa_circ_0007456	chr17:11984672-12016677	595	down	mediates immune escape	miR-6852-3p/ICAM-1	(81)
circARNT2	hsa_circ_0104670	chr15:80767350-80772264	4914	up	enhances drug resistance	miR-155-5p/PDK1	(82)
circRNA-SORE	hsa_circ_0087293	chr9:82267504-82268990	222	up	enhances drug resistance	YBX1/AKT/Raf1/ERK/c-Myc/TGF-β,miR-103a-2-5p/miR-660-3p/Wnt/β-catenin	(83, 84)
circFN1	hsa_circ_0058124	chr2:216270960-216274462	864	up	enhances drug resistance	miR-1205/E2F1	(85)
circ_0005075	hsa_circ_0005075	chr1:21377358-21415706	205	up	promotes proliferation, invasion, migration, inhibits apoptosis, induces drug resistance	miR-335/MAPK1	(86)
circMA T2B	hsa_circ_0074854	chr5:162940560-162944680	576	up	promotes metabolic reprogramming	miR-338-3p/PI3K/AKT/mTOR/PKM2	(87)
circ-MALAT1	hsa_circ_0002082	chr11:65271199-65272066	867	up	enhances stemness	miR-6887-3p/JAK2/STAT3/PAX5	(88)
circZNF609	hsa_circ_0000615	chr15:64791491-64792365	874	up	enhances proliferation, metastasis, stemness	miR-15a-5p/15b-5p/GLI2	(89)

cells with low or no metastatic potential, thereby destroying the tumor microenvironment homeostasis and promoting the invasion and metastasis of HCC cells (42). Silencing circASAP1 can restrain the proliferation, migration, and invasion of HCC cells, as well as impeding the growth and lung metastasis rate of xenografts. circASAP1 stimulates the expression of mitogen-activated protein kinase 1 (MAPK1) through sponging miR-326 and miR-532-5p, which further activates the ERK1/2 signaling pathway to promote the proliferation and invasion of HCC cells; additionally, MAPK1 de-inhibits colony stimulating factor 1 (CSF-1) and promotes the proliferation and chemotactic migration of tumor-associated macrophages (TAMs), mediating TAM infiltration into the tumor bed, which is benefit for the tumor metastasis (43). Through directly sponging miR-1299, circMAST1 rescues the expression suppression of catenin delta 1 (CTNND1), inducing the proliferation and invasion of HCC cells. Silencing circMAST1 reduces the growth rate of xenografts, while the expression levels of proliferating cell nuclear antigen (PCNA) protein and cell cycle-related proteins such as cyclin A, cyclin E, CDK1, and CDK2 are significantly decreased (44). CircDYNC1H1 negatively regulates the expression of miR-140-5p, relieving the expression inhibition of sulfotransferase family 2B member 1 (SULT2B1) mediated by miR-140-5p, further enhancing the proliferative and metastatic capacity of HCC cells (45). Highly expressed circSLC3A2 promotes the proliferation and invasion of HCC cells by circSLC3A2/miR-490-3p/protein phosphatase, Mg2+/Mn2+ dependent 1F (PPM1F) axis (36). CircHIPK3 acts as a miR-124 sponge to regulate its downstream target gene aquaporin 3 (AQP3), promoting the proliferation and metastasis of HCC cells, while silencing circHIPK3 inhibits the proliferation and migration of HCC cells *in vitro* and delaying the growth rate of subcutaneous xenografts *in vivo* (47). Hsa_circ_0001955 promotes the proliferation, invasion, and migration of HCC tumor cells through the miR-145-5p/NRAS pro-oncogene (NRAS) axis (48). Exogenous silencing circ-TCF4.85 can effectively inhibit the proliferation, invasion, and migration of HCC cells, as well as blocking the cell cycle process (49). Through competitively binding miR-4738-3p, circZNF566 blocks the direct interaction of miR-4738-3p and the 3'-UTR of tryptophan 2,3-dioxygenase (TDO2) mRNA, which further leads to the upregulation of TDO2, thereby promoting the proliferation, invasion, and metastasis of HCC cells, while cancer-promoting effect can be reversed by the knockdown of circZNF566 (50). Hsa_circRNA 103809 directly binds to miR-377-3p and negatively regulates its expression, releasing the inhibition of fibroblast growth factor receptor 1 (FGFR1), and then promotes the proliferation, metastasis, and cell cycle progression of HCC cells (51). Hsa_circ_104348 can act as a ceRNA of miR-187-3p, blocking its binding to the downstream target gene rhotekin 2 (RTKN2) to achieve the same trend expression of RTKN2 and hsa_circ_104348, and further activating the Wnt/β-catenin pathway, thereby affecting tumor cell proliferation, invasion, metastasis, and anti-apoptosis ability (52). Analogously, circRNA-104718 can also act as a ceRNA to directly bind to miR-218-5p, reducing the inhibition mediated by miR-218-5p upon its target gene thioredoxin domain containing 5 (TXNDC5), thereby promoting the growth and metastasis of HCC (53). CircFBLIM1 can acts as a miR-346 sponge through the ceRNA mechanism to regulate the expression of filamin binding LIM protein 1 (FBLIM1) and promote the progress of HCC (54). The expression of exosomal circ-DB is significantly upregulated in HCC patients with higher body fat ratio. The adipocyte-derived exosomes of HCC patients act as carriers of circ-DB, promoting the growth and reducing DNA damage *via* the suppression of miR-34a and the activation of deubiquitination-related ubiquitin specific peptidase (USP7) (55).

Overexpressed circRASGRF2 promotes the malignant biological behaviors of HCC through the circRASGRF2/miR-1224/focal adhesion kinase (FAK) signal axis. Moreover, knocking down circRASGRF2 can effectively suppress the proliferation, invasion, and migration of HCC tumor cells, and induce cell cycle arrest and apoptosis, as well as significantly slowing down the growth rate of xenografts in nude mice and inhibit the lung metastasis effect of tumors (56). Circ-LRIG3 can interact with enhancer of zeste homolog 2 (EZH2) and STAT3, acting as a scaffold to increase STAT3 methylation and subsequent phosphorylation induced by EZH2. Activated STAT3 can directly bind to the circ-LRIG3 promoter to enhance the transcriptional activity of circ-LRIG3, and then forms positive feedback loop to promote the progress of HCC (57). CircRHOT1 recruits Tat interactive protein 60 (Tip60) to the nuclear receptor subfamily 2 group F member 6 (NR2F6) promoter, subsequently recruiting NuA4 complex-related components to stimulate the expression of NR2F6. Meanwhile, the circRHOT1/Tip60/NR2F6 axis may partially activate the notch receptor 2 (NOTCH2) signaling pathway (58). β-catenin-370aa competitively interacts with glycogen synthase kinase 3β (GSK3β) and acts as a decoy, antagonizing GSK3β-induced β-catenin phosphorylation and degradation to stabilize full-length β-catenin, thereby activating the Wnt/β-catenin pathway to promote the malignant phenotypes of HCC (59). CircRNAs can also act as a tumor suppressor to inhibit the malignant biological behaviors of HCC. As a novel downstream effect target of m6A modification mediated by KIAA1429, the expression of circDLC1 in HCC can be inhibited by DExH-box helicase 9 (DHX9). Through interacting with HuR, circDLC1 reduces the stability of matrix metallopeptidase 1 (MMP1) mRNA and downregulates its expression to restrain HCC metastasis (60). DHX9 can also downregulate cSMARCA5, which promotes the expression of tissue inhibitor of metalloproteinase 3 (TIMP3) by sponging miR-17-3p (61). Androgen receptor (AR) suppresses the expression of circARSP91 by stimulating adenosine deaminase acting on RNA 1 (ADAR1) in combination with the ADAR1 promoter. CircARSP9 can act as a tumor suppressor in HCC to inhibit tumor growth (62). Circ-ADD3 can enhance the interaction between CDK1 and EZH2, mediating the increase of EZH2 ubiquitination, which mediates the degradation of EZH2. Reduced EZH2 significantly increases the expression of a series of antimetastatic genes, including circ-ADD3, by reducing the level of H3K27me3 in the promoter region

to form a regulatory circuit, thereby inhibiting the metastasis of HCC (63). By releasing the tumor-suppressor genes miR-182 and miR-184, circ-102 and circ-166 reduce the expression of downstream target genes FOXO3a, MTSS I-BAR domain containing 1 (MTSS1), and SRY-box transcription factor 7 (SOX7), as well as increasing the levels of c-myc protein and Rb phosphorylation, thereby inhibiting the proliferation and invasion of HCC cells (64). CircMTO1 promotes the expression of p21 by acting as a sponge for the oncogene miR-9 to inhibit the proliferation and invasion of HCC. Knocking down circMTO1 can effectively promote the proliferation and invasion of HCC cells and inhibit cell apoptosis. Meanwhile, the growth rate of xenografts in the knockdown group also significantly accelerates (65). CircNFATC3 acts as a ceRNA combined with miR-548 to protect the maternal gene nuclear factor of activated T cells 3 (NFATc3). NFATc3 and circNFATC3 can synergistically interfere with the phosphorylation of the c-Jun NK2-terminal kinase (JNK)/c-jun/serine/threonine kinase (AKT)/mechanistic target of rapamycin kinase (mTOR) cascade to inhibit the progression of HCC, while overexpressed circNFATC3 can inhibit the proliferation of HCC cells, inducing cell apoptosis and weakening the ability of invasion and migration; meanwhile, the size and weight of xenografts in the overexpression group were significantly reduced than those in the knockdown group, and the lung metastasis effect was inhibited (66). Hsa_circ_0091570 can also act as a ceRNA to bind miR-1307 and upregulate the expression of isthmin 1 (ISM1) to inhibit tumor progression (67). Circ ADAMTS13 can sponge miR-484 to inhibit the proliferation of HCC cells and induce apoptosis (68). CircADAMTS141 can competitively bind to miR-572 and inhibit its transcriptional activity, thereby promoting the expression of the downstream target gene regulator of calcineurin 1 (RCAN1) (69). Kyoto encyclopedia of genes and genomes (KEGG) enrichment analysis showed that after knocking down cirZKSCAN1, differentially expressed genes are more likely to be enriched in phosphatidylinositol 3-kinase (PI3K) pathway, migration pathway, actin cytoskeleton pathway, adhesion pathway, cytokine interaction pathway, and other tumor-related signal pathways. Zinc finger with KRAB and SCAN domains 1 (ZKSCAN1) mRNA regulates cell metabolism, suggesting that ZKSCAN1 mRNA and circZKSCAN1 may suppress HCC progression through interaction. The overexpression of cirZKSCAN1 can effectively inhibit cell proliferation, invasion, and migration. The xenografts in the knockdown group shows growth inhibitory effect (70). Exosomes transfer circ-0051443 from normal cells to HCC cells. Through competitive binding of miR-331-3p, circ-0051443 mediates the upregulation of downstream target gene BCL2 antagonist/killer 1 (BAK1), further promoting cell apoptosis, blocking cell cycle in G0/G1 phase, and inhibiting malignant biological behaviors of HCC cells (72).

Regulation of Epithelial-Mesenchymal Transition Process

EMT refers to the biological process in which differentiated epithelial cells transform into cells with a mesenchymal phenotype, which endows malignant tumor cells with abilities such as invasion and migration, stem cell characteristics, and immunosuppression.

Exogenous silencing circ-0004277 inhibits HCC cell proliferation and migration, mediating smaller volume and weight and lung metastasis inhibitory effect of xenografts. Studies have shown that circ-0004277 competitively binds to HuR, blocking its binding with zonula occludens-1 (ZO-1) mRNA, downregulating ZO-1, and stimulating the EMT process. Exosome circ-0004277 derived from HCC cells can mediate the communication between surrounding normal cells and HCC cells, stimulating the EMT process of surrounding normal cells, and promote the progress of HCC invading into surrounding normal tissues (73). Overexpressed circ-0003998 can promote the proliferation of HCC cells, significantly promoting the lung metastasis, while knockdown of circ-0003998 inhibits the opposite results. Circ-0003998 can act as a ceRNA of miRNA-143-3p to impair the expression inhibition of FOS-like antigen 2 (FOSL2) (EMT-related stimulator); meanwhile, circ-0003998 can also combine with poly(rC) binding protein 1 (PCBP1) to increase the expression of CD44v6 (EMT-related genes), then promote the EMT process of HCC (74). Twist1 directly binds to the cullin 2 (Cul2) promoter to activate its transcription and selectively promotes the expression of circ10720 in Cul2. Circ10720 induces EMT in HCC cells by sponging miRNA and upregulating the expression of the target gene Vimentin (75). The overexpression of circRNA-5692 significantly increased the expression of E-cadherin, while reducing the expression of Vimentin and Snail. CircRNA-5692 restrain the proliferative and invasive ability of tumor cells, as well as inducing apoptosis. Overexpressed circRNA-5692 can serve as ceRNA to spongy miRNA-328-5p, reducing its inhibitory effect on DAB2 interacting protein (DAB2IP) expression and promoting the demethylation of DAB2IP gene to weaken the EMT process (76). Similarly, circPTK2 can be used as ceRNA to absorb miR-92a, so as to upregulate E-cadherin and inhibit the EMT process of HCC (77).

Regulation of the Immune System

The immune escape of tumor cells is an important part of the progression of tumors. After cancer cells evade the body's immune surveillance and attack through various mechanisms, malignant biological behaviors such as proliferation, invasion, and metastasis are further enhanced, resulting in the loss control of tumor cell growth upon body's immune system.

CircUHRF1 was upregulated in HCC tissues and cancer cell–derived exosomes. Overexpressed plasma exosome circUHRF1 was associated with a decreased natural killer cell (NK) proportion and reduced NK cell tumor infiltration. HCC cell-derived exosomes can transfer circUHRF1 into peripheral NK cells and inhibit its activity by sponging miR-449c-5p to achieve the high expression of downstream target gene T-cell immunoglobulin mucin 3 (TIM-3), thereby inhibiting the secretion of interferon-γ (IFN-γ) and tumor necrosis factor-α (TNF-α) from NK cells, leading to impaired function and phenotypic exhaustion of NK cells to promote immune escape

of HCC cells (78). Highly expressed circMET can induce EMT or degrade C-X-C motif chemokine ligand 10 (CXCL10) *via* the circMET/miR-30-5p/Snail/dipeptidyl peptidase 4 (DPP4) axis to reduce CD8+ T lymphocyte transport, thereby enhancing the formation of the immunosuppressive tumor microenvironment to promote tumor progression (79). CircTRIM 33-12 acts as ceRNA and upregulates tet methylcytosine dioxygenase 1 (TET1) expression by competitively binding miR-191, promoting the expression of tumor-suppressor genes [WWC family member 3 (WWC3), tumor protein p53 nuclear protein 1 (TP53INP1), UL16 binding protein 1 (ULBP1), jumonji C domain containing hiatone demethylase 1 homolog D (JHDM1D)] in HCC cells, and reducing 5-hydroxy methylcytosine (5hmC) content, subsequently inhibiting the proliferation and metastasis of HCC cells and inducing immune evasion (80). The expression of hsa_circ_0007456 in HCC cell lines and clinicopathological tissues was significantly downregulated, which interferes with the sensitivity of HCC cells to NK cells by reducing the binding of NK cells and tumor cells. Hsa_circ_0007456 can also interact with miRNAs and endogenously adsorb miR-6852-3p, blocking its binding to the downstream target gene intercellular adhesion molecule 1 (ICAM-1) 3'-UTR, affecting the expression of ICAM-1 and promoting the immune escape of tumor cells (81).

Regulation of Drug Resistance

Chemotherapy is one of the main methods of tumor treatment, which can effectively reduce the recurrence and metastasis of tumors. While molecular targeting chemotherapy have recently experienced rapid progress, the existence of chemotherapy resistance still limits the advancement of long-term survival. Therefore, understanding the underlying molecular mechanism of HCC chemoresistance and developing mechanism-based therapies are urgently needed. CircRNA has been shown to be involved in the development of drug resistance.

CircARNT2 is upregulated in HCC tissues, cell lines, and cisplatin-resistant cells, and knocking down circARNT2 can significantly inhibit tumor cell proliferation and aggravate cisplatin-induced apoptosis. CircARNT2 can act as ceRNA to competitively bind miR-155-5p, regulating the autophagy induced by pyruvate dehydrogenase kinase 1 (PDK1) and then promoting the cisplatin resistance of HCC cells (82). circRNA-SORE is upregulated in sorafenib-resistant HCC cells. Knockdown of circRNA-SORE can significantly enhance the cytotoxicity of sorafenib, leading to cell morphology destruction and increased apoptosis. CircRNA-SORE binds to Y-box binding protein 1 (YBX1) in the cytoplasm to prevent it from translocating to the nucleus, thereby inhibiting PRP19-mediated ubiquitination and degradation of YBX1, affecting the expression of YBX1 downstream gene targets AKT, Raf1, ERK, c-Myc, and TGF-β1, thereby inducing the sorafenib resistance. CircRNA-SORE can also achieve the diffusion of sorafenib-resistant in HCC cells through the enrichment and transferation of HCC cell-derived exosomes (83). The increase in the expression level of m6A at the specific binding site of circRNA-SORE increases the stability of RNA, which in turn upregulates the expression level of circRNA-SORE in HCC sorafenib-resistant cells. The highly expressed circRNA-SORE acts as ceRNA to specifically sponge miR-103a-2-5p and miR-660-3p, activating Wnt/β-catenin pathway to induce sorafenib-resistant (84). Overexpression of circFN1 can positively regulate the expression of E2F transcription factor 1 (E2F1) by interacting with miR-1205 to achieve sorafenib-resistance in HCC cells, whereas silencing circFN1 can promote the expression of phosphatase and tensin homolog (PTEN) protein and inhibit the activation of AKT in HCC cells, enhancing sorafenib sensitivity in HCC cells (85). Circ_0005075 can bind to miR-335 and antagonize the inhibitory effect of miR-335 on the downstream target gene MAPK1, thereby enhancing the proliferation, migration, invasion, and anti-apoptotic abilities of HCC cells (86).

Regulation of Metabolic Reprogramming

Tumor cells adjust glucose metabolism from oxidative phosphorylation to glycolysis through metabolic reprogramming to adapt to hypoxic stress. Even in the case of sufficient oxygen supply, cancer cells still preferentially use glycolysis instead of the tricarboxylic acid cycle pathway of mitochondrial to decompose glucose, providing ATP and glycolysis intermediates for the metabolism and biosynthesis of cancer cells, as well as developing a tumor microenvironment suitable for cancer cells to survive, thus avoiding the immune and apoptotic procedures of the body, creating advantages for tumor cells to proliferate and metastasis (90).

In vivo and *in vitro* functional experiments have shown that siRNA-circMA T2B can inhibit the glycolysis capacity and rate of HCC cells, forming a low glucose uptake, low lactate production status, and reduced ATP levels of tumor cells. Meanwhile, it also activates mitochondrial oxidative phosphorylation, causing higher oxygen consumption of cells in the basal and maximum respiration state; under hypoxic stress, siRNA-circMA T2B can significantly suppress the proliferation, invasion, and migration of HCC cells and induce increased apoptosis. In the knockdown group, xenografts exhibit glycolysis, growth, and lung metastasis inhibitory effects, showing a lower level of glycolysis-related organic acids, a slower growth rate, and fewer lung metastasis nodules. Highly expressed circMA T2B acts as a sponge of miR-338-3p and inhibits its transcriptional activity, thereby increasing the expression of the target gene kinesin family member C1 (KIFC1), activating the PI3K/AKT/mTOR signaling pathway and upregulating the expression of pyruvate kinase M2 (PKM2), subsequently promoting glycolysis and malignant phenotypes of HCC cells under hypoxic conditions (87).

Regulation of Cellular Stemness

Cancer stem cells (CSCs) have the ability to self-renew and differentiate into different cell types. They can participate in the mediation of tumor initiation, metastasis, chemotherapy resistance, and recurrence, closely related to poor prognosis (91).

Under the mediation of AU-rich element RNA-binding factor 1 (AUF1), circ-MALAT1 was upregulated in HCC CSCs. Highly expressed circMALAT1 reduces the inhibitory effect of miR-6887-3p on JAK2 through molecular sponge action, thereby

upregulating the expression levels of JAK2 and enhancing its phosphorylation, then activating the JAK2/STAT3 signaling pathway to promote the self-renewal of HCC CSCs; meanwhile, circMALAT1 can also combine with ribosomal and paired box 5 (PAX5) mRNA coding sequences to form a specific ternary complex (ribosome-circRNA-mRNA) to exert mRNA braking. It directly hinders the translation of PAX5 mRNA and affects PAX5-related cell functions to promote the self-renewal of HCC CSCs (88). The expression of circZNF609 is higher in HCC tissues than in normal tissues. Knocking down circZNF609 represses the expression level of transfer-related proteins [matrix metalloproteinase (MMP2), (MMP7)], stemness-related transcription factors (OCT4 and Nanog), EMT-related proteins (N-cadherin, Twist), while the proliferation and spheroidizing ability of HCC cells are significantly inhibited. Further studies have shown that circZNF609 activates the Hedgehog pathway by inhibiting the expression of miR-15a-5p/15b-5p and upregulating the expression of GLI family zinc finger 2 (GLI2), a downstream target of miR-15a-5p/15b-5p, thereby enhancing proliferation, metastasis, and stemness of HCC cells (89). circZKSCAN1 is downregulated by Quaking (QKI) in HCC. CircZKSCAN1 blocks the binding of fragile X mental retardation protein (FMRP) to cell division cycle and apoptosis regulator 1 (CCAR1) mRNA by competitively binding to FMRP, and subsequently inhibits the transcriptional activity of the Wnt/β-catenin signaling pathway, thereby inhibiting the malignant biology behaviors of HCC cells by regulating the stemness of HCC cells (71).

CircRNAs as Indicators for Patient Outcomes

Dysregulated expression of circRNAs is closely related to the clinicopathological characteristics of HCC patients. Accurately predicting the clinical prognosis of HCC patients can help guide decision-making in HCC treatment, thereby effectively improving the survival benefits of patients. At the same time, due to the high abundance and high stability in HCC clinical samples, circRNA can be used as a potentially effective biomarker for the clinical prognosis of HCC patients.

Nine circRNAs, were greatly upregulated in HCC tissues, namely, circARNT2, circRASGRF2, circFN1, circRNA-104718, circSLC3A2, circ-10720, circSOD2, circ_0005075, and circRHOT1 (32, 46, 53, 56, 58, 75, 82, 85, 86). All these highly expressed circRNAs have been confirmed to be potential prognostic biomarkers for poor outcome in HCC by Kaplan-Meier (KM) analysis. Clinically, the expression of circARNT2 was closely related to tumor size, TNM stages, and distant metastasis (82), while the expression of circFN1 was correlated with HCC tumor size, TNM stages, and vascular infiltration (85). Higher expression of circRASGRF2 in HCC tissues indicates poor tumor differentiation, later tumor stages, larger tumor size (>5 cm), and the presence of microvascular infiltration (MVI) (56). circRNA-104718 expression was correlated with vascular infiltration (53); circ-10720 expression was related to serum AFP level and hepatitis B markers (75). Increased circSOD2 expression was associated with higher grade tumors (32). High expression of circRNAs not only in HCC tissues but also in HCC cell lines was also identified to be potential prognostic biomarkers for poor OS, circZNF566, has_circ_104348, circRNA_103809, and circBACH1, respectively (39, 50–52); simultaneously, highly expressed circZNF566 was negatively correlated with disease-free survival (DFS) (50). In terms of clinicopathological characteristics, upregulated circZNF566 was positively correlated with tumor size, tumor differentiation, and M stage (50). The expression of has_circ_104348 was further correlated with tumor size, lymph node invasion, and TNM stages (52), while circBACH1expression was associated with tumor size and histological differentiation (39). In other studies, higher expression of four circRNAs could predict poor prognosis of HCC patients by KM analysis, including circRNA-SORE, circMET, SCD-circRNA 2, circASAP1 (38, 43, 79, 84); in addition, HCC patients with high expression of circRNA-SORE have poor recurrence-free survival (RFS), so did SCD-circRNA 2. Moreover, patients in the high-expression group of circMET have higher cumulative recurrence rates (38, 79, 84). Clinically, circMET expression was closely correlated with MVI, multiple tumors, the presence or absence of tumor envelope, as well as advanced stages, while SCD-circRNA 2 expression was associated with serum AFP levels, alanine aminotransferase (ALT) and aspartate aminotransferase (AST) levels. Besides, circHIPK3 was reported to be upregulated in HCC tissues, and its expression was related to the degree of tumor differentiation, TNM stages, HBV-DNA replication, and the presence of LC (47). High circ0003998 expression has been observed in HCC tissues, which is also correlated with advanced TNM stages and high level of serum AFP (74). The expression of hsa_circ_0001955 in HCC tissues and cell lines was significantly elevated and positively correlated with larger tumor size and advanced TNM stages (48).

Except for HCC tissues and cell lines, several circRNAs upregulated in plasma, serum, and exosomes (serum-derived or cancer cell-derived) were identified as potent non-invasive prognostic biomarkers by KM analysis, such as circTMEM45A, circ-LRIG3, circUHRF1, circRNA-100,338, circPTGR1 (34, 41, 42, 57, 78). Among them, circTMEM45A expression was remarkably correlated with tumor size, TNM stages, vascular infiltration, and survival time of HCC patients (34). Patients in the high-expression group of circLRIG3 have larger tumor size, more vascular invasion, higher Edmondson's grade, TNM stages, and shorter OS and DFS. Multivariate analyses revealed that the expression of circLRIG3 may be used as an independent risk prognostic assessment factor (57). Higher expression of circUHRF1 was shown to be associated with larger tumor size, fewer NK cells in the blood, and more capillaries infiltration, and worse clinical prognosis. Moreover, circUHRF1 was confirmed to be an independent indicators of OS and postoperative recurrence in the disease by multivariable analyses (78). Interestingly, univariate and multivariate analyses demonstrated that the continuous high expression of circRNA-100,338 in the serum of HCC patients undergoing radical hepatectomy may serve as a risk factor of lung metastasis and

poor prognosis predictor (41). Similarly, circMA T2B was identified to be independent prognostic indicators for HCC patients by multivariable analyses. In addition, circMA T2B expression was related to tumor size, vascular infiltration, tumor multiplicity, tumor envelope, lymph node metastasis, as well as Edmonson stage (87).

Accumulating evidence has certificated that compared with these upregulated circRNAs, lower expression of other circRNAs could predict poor outcome of HCC patients. For instance, 12 circRNAs—namely, circDLC1, circ-102,166, circ-ADD3, circADAMTS13, circZKSCAN1, cSMARCA5, hsa_circ_0091570, circSETD3, circNFATC3, circTRIM33-12, hsa_circ_0007456, circMTO1—were significantly downregulated in HCC tissues and cell lines (37, 60, 61, 63–68, 70, 80, 81). Kaplan-Meier (KM) analysis demonstrated that lower expression of all these 12 circRNAs was associated with poor OS of HCC. Moreover, the first six lessened expression of circRNAs were correlated with shorter RFS of HCC patients as well. Of course, downregulated circRNAs were also associated with the clinicopathological characteristics of HCC patients. The low expression of circRNA-5692 was closely correlated with abnormally high levels of AFP, history of LC, larger tumor size, and distant metastasis (76). Other research shows that the expression of circ-102,166 significantly correlated with tumor size, TNM stages, Barcelona Clinic liver cancer (BCLC) stages, and vascular infiltration (64); lower expression of circ-ADD3 was correlated with vascular infiltration, intrahepatic metastasis, distant metastasis, and progression-free survival (PFS) (63). Lower expression of hsa_circ_0091570 was related to Edmondson Grade, portal vein tumor thrombus (67), while lower expression of circSETD3 was significantly associated with larger tumor size, poor tumor differentiation (37). Lower expression of circADAMTS13 was associated with the absence of LC, larger tumor size, and advanced BCLC stages (68). circZKSCAN1 was related with number of tumors, LC, tumor grade, and MVI (70, 71). Reduced expression of circTRIM33-12 was related to larger tumor size, multiple tumors, encapsulation invasion, and MVI, as well as elevated AFP levels (80), while decreased expression of cSMARCA5 is closely related to poor tumor differentiation, advanced tumor stage, larger tumor size, and MVI. Interestingly, multivariate analyses demonstrated that the expression of circTRIM33-12 and cSMARCA5 may serve as independent prognostic evaluation index for HCC patients (61). Similarly, multivariate analyses indicated that low circDLC1 and circNFATC3 expression in HCC tissues can be used as independent risk factors of poor prognosis for HCC patients (60, 66).

CircRNAs as Diagnostic Biomarkers for HCC

Insidious onset and lack of accurate and effective biomarkers for early diagnosis of HCC are the main reasons for low OS in HCC patients. Traditional diagnostic markers, such as AFP, AFP-L3, α-L-fucosidase (AFU), and protein induced by vitamin K absence or antagonist-II (PIVKA-II), have low sensitivity and specificity for the diagnosis of HCC. Studies have shown that lncRNAs and miRNAs have been reported as potential biomarkers for the diagnosis of HCC. Based on the high abundance of circRNA in HCC tissues, body fluids, and exosomes, the resistance to ribonuclease, and the highly conservative and specific expression of evolution, circRNA can be used as an ideal biomarker for the early diagnosis of HCC **(Table 2)**.

In HCC tissues, nine upregulated circRNAs, namely, circRASGRF2, circBACH1, circFN1, circ-LRIG3, circTCF4.85, hsa_circ_0016788, hsa_circ_0005075, hsa_circ_0128298, circ-CDYL (36, 39, 49, 56, 57, 85, 93–95), constitute potential diagnostic biomarkers in HCC. Among them, the first seven circRNAs reached higher area under the receiver operating characteristic curve (AUC) value of 0.882, 0.8506, 0.878, 0.8681, 0.891, 0.851, 0.94, respectively. At the same time, the sensitivity of circTCF4.85 to distinguish HCC patients from healthy controls was 86.8%, and the specificity was 87.0%, and the sensitivity and specificity of hsa_circ_0005075 were 83.3 and 90.0% (48, 93). In contrast, the upregulation of hsa_circ_0128298 (AUC value: 0.668, sensitivity: 0.674; specificity: 0.805) and circ-CDYL (AUC value: 0.64, sensitivity: 0.333; specificity: 0.928) demonstrated relatively poorer diagnostic value (94, 95). The downregulated expression of circRNAs in HCC tissues also has high diagnostic value. The AUC values of hsa_circ_0091570, circZKSCAN1, circADAMTS13, and hsa_circ_0004018 are 0.736, 0.834, 0.987, 0.848, respectively (50, 67, 68, 96). Among them, the sensitivity and the specificity of circZKSCAN1 as a diagnostic biomarker for HCC were 82.2 and 72.4%, as well as the sensitivity and the specificity of hsa_circ_0004018 were 71.6 and 81.5% (70, 96).

The expression of circRNAs was dysregulated not only in HCC tissues but also in serum, plasma, and exosomes, indicating that it may be used as a non-invasive circulating biomarker for HCC diagnosis. Study has shown that the expression levels of hsa_circ_000244 (AUC value: 0.974, sensitivity: 0.956; specificity: 0.927) and circ_104075 (AUC value: 0.973, sensitivity: 0.969; specificity: 0.983) in HCC tissues and serum were significantly higher than that of healthy individuals and showed a significant diagnostic value (33, 97). While four others circRNAs, namely, circ-0051443, circ-ADD3, cSMARCA5, hsa_circ_000520, and hsa_circ_001565, were reported to be downregulated in HCC tissues and serum/plasma of HCC patients and achieved diagnostic potential with AUC values of 0.8089, 0.8878, 0.938, 0.943, and 0.839, respectively (63, 72, 92, 97). Among them, the sensitivities of hsa_circ_000520 and hsa_circ_001565 as diagnostic biomarkers were 97.1 and 73.5%, the specificities were 89.6 and 82.3%, respectively. The sensitivity and specificity of cSMARCA5 were 86.7 and 89.3% (92, 97). In addition to the above circRNAs, dysregulated circRNAs in exosomes of HCC patients have potential diagnostic value as well. For example, upregulated exosomes circ-0004277 and exosomes circTMEM45A reached potent AUC values of 0.816, 0.818, respectively (34, 73). Moreover, the sensitivity and specificity of circ-0004277 used to distinguish HCC patients from healthy controls are 58.3 and 96.7%.

Combined detection can significantly improve the accuracy of HCC diagnosis. By a microarray screening and quantitative real-

TABLE 2 | CircRNAs as diagnostic biomarkers for HCC.

CircRNA	Expression	Samples	AUC	Sensitivity	Specificity	Youden index (YI)	Confidence interval (CI)	References
circRASGRF2	up	tissues	0.88	/	/	/	0.814–0.950	(56)
circBACH1	up	tissues	0.85	/	/	/	/	(39)
circFN1	up	tissues	0.88	/	/	/	0.794–0.963	(85)
circ-LRIG3	up	tissues	0.87	/	/	/	0.7843–0.9519	(57)
circTCF4.85	up	tissues	0.89	0.868	0.870	0.738	0.820–0.962	(49)
hsa_circ_0016788	up	tissues	0.85	/	/	/	/	(36)
hsa_circ_0091570	down	tissues	0.74	/	/	/	/	(67)
circZKSCAN1	down	tissues	0.83	0.822	0.724	0.546	/	(60)
circADAMTS13	down	tissues	0.99	/	/	/	/	(68)
circ_104075	up	tissues, serum	0.97	0.969	0.983	0.943	0.780–0.995	(33)
circ-0004277	up	serum exosomes	0.82	0.583	0.967	0.55	0.741–0.891	(73)
circTMEM45A	up	serum exosomes	0.89	/	/	/	0.823–0.954	(34)
circ-0051443	down	tissues, plasma	0.81	/	/	/	/	(72)
circ-ADD3	down	tissues, plasma	0.89	/	/	/	0.8094–0.9662	(63)
cSMARCA5	down	plasma	0.94	0.867	0.893	0.76	0.910–0.966	(92)
hsa_circ_0005075	up	tissues	0.94	0.833	0.9	0.733	/	(93)
hsa_circ_0128298	up	tissues	0.67	0.674	0.805	0.479	0.503–0.794	(94)
circ-CDYL	up	tissues	0.64	0.333	0.928	0.261	0.55–0.72	(95)
hsa_circ_0004018	down	tissues	0.85	0.716	0.815	0.531	0.803–0.894	(97)
hsa_circ_000244	up	tissues, serum	0.97	0.956	0.927	0.883	0.948–0999	(97)
hsa_circ_000520	down	tissues, serum	0.94	0.971	0.896	0.876	0.902–0.984	(97)
hsa_circ_001565	down	tissues, serum	0.84	0.735	0.823	0.555	0.771–0.907	(97)

time polymerase chain reaction (qRT-PCR) in a multicenter study, a circPanel containing three HBV-related HCC plasma upregulated expressions of circRNA (hsa_circ_0000976, hsa_circ_0007750, and hsa_circ_0139897) was identified. circPanel is superior to AFP in the diagnosis of HCC and small HCC. It can also effectively identify AFP-negative HCC and AFP-negative small HCC (AUC are greater than 0.80) (98). Studies have shown that the expression of circ_0009582, circ_0037120, and circ_0140117 in HBV-related HCC tissues is significantly higher than that in chronic hepatitis and healthy subjects. The combined detection of these three circRNA and alpha-fetoprotein has higher sensitivity and specificity (99).

CONCLUSION

HCC is one of the most malignant tumors, and the high mortality rate makes it urgent to develop effective tools for early diagnosis and clinical treatment. Emerging evidence reveals that the dysregulated circRNA expression in HCC clinical specimens was closely related to the clinicopathological characteristics of HCC patients and can act as a miRNA sponge, interact with RBP or a transcriptional regulator, and then participate in the regulation of the HCC cells tumorigenesis, proliferation and anti-apoptosis, invasion and metastasis, EMT, immune escape, drug resistance, metabolic reprogramming, and other biological processes. So, targeting of circRNA in HCC patients may reverse the progress of HCC, so as to develop new therapeutic strategies for HCC. For example, targeting of circRNA-SORE in sorafenib-treated HCC patients as a novel targeted therapy for advanced HCC, circRNA-SORE can sequester miR-103a-2-5p and miR-660-3p by acting as a miRNA sponge, thereby competitively activating the Wnt/β-catenin pathway and inducing sorafenib resistance (84). AR could suppress the formation of HCC vasculogenic mimicry (VM) by downregulating circRNA7/miRNA7-5p/VE-Cadherin/Notch4 signaling pathways in HCC, which will help in the design of novel therapies against HCC (100). In another study, under hypoxic conditions, AR can suppress HCC invasion/metastasis by targeting CIRC-LNPEP/miR-532e3p/RAB9A signal axis (101). Estrogen receptor α (ERα) can suppress HCC cell invasion *via* altering the ERα/circRNA-SMG1.72/miR-141-3p/GSN signaling, and targeting this newly identified signaling with small molecules may help in the development of novel therapies to better suppress the HCC progression (102). Except this, there are certain small molecular activators or inhibitors targeting the circRNAs signaling pathways in the treatment of HCC, including HNF4a, RBM3, KIAA1429, DHX9, Twist1, nudix hydrolase 21 (NUDT21), andQKI5 (33, 38, 60, 61, 71, 75, 103). However, the technique of specifically targeting a specified circRNA in HCC patients still needs further study, and development of novel targeted therapies remains the priority in hepatocellular carcinoma (HCC) treatments.

High stability and abundant circRNAs in tissues and various body fluids make it able to serve as biomarker for early diagnosis and prognosis prediction of HCC patients. At the same time, exosomes can carry circRNAs from tumor cells to recipient cells mediate cell–cell communication to regulate the behavior of recipient cells, suggesting that circRNAs can be used as non-invasive circulating biomarkers for cancer diagnosis. However, only a small number of functional circRNAs have been identified in HCC, and most of these studies have focused on miRNA sponge or ceRAN mechanism. Therefore, identifying functional circRNAs; clarifying their biogenesis, cell location, and function; further understanding the relationship between circRNA and the etiology, development, and molecular mechanism of HCC; screening target genes and corresponding signal pathways will help to improve HCC diagnosis and prognosis prediction and provide practical and reliable basis for clinical therapy.

AUTHOR CONTRIBUTIONS

HZY wrote the manuscript. XY and CYF revised and approved the manuscript. All authors contributed to the article and approved the submitted version.

FUNDING

This study was funded by Hong Kong Scholars Program (XJ2020012), National Natural Science Foundation of China (81902431), Excellent Youth Project of Natural Science Foundation of Heilongjiang (YQ2019H007), Special Project of China Postdoctoral Science Foundation (2019T120279), Special Project of Heilongjiang Postdoctoral Science Foundation (LBH-TZ1016), China Postdoctoral Science Foundation (2018M641849, 2018M640311), Heilongjiang Postdoctoral Science Foundation (LBH-Z18107 and LBH-Z18112), the Fundamental Research Funds for the Heilongjiang Provincial Universities (2018-KYYWF-0511, 2018-KYYWF-0498), Postgraduate Innovative Research Project of Harbin Medical University (YJSCX2016-21HYD), Foundation of Key Laboratory of Myocardial Ischemia, Ministry of Education (KF201810), and Chen Xiaoping Foundation for the Development of Science and Technology of Hubei Province (CXPJJH11800004-001, CXPJJH11800004-003).

REFERENCES

1. Sung H, Ferlay J, RL S, Laversanne M, Soerjomataram I, Jemal A, et al. Global Cancer Statistics 2020: GLOBOCAN Estimates of Incidence and Mortality Worldwide for 36 Cancers in 185 Countries. *CA Cancer J Clin* (2021) 71(3):209–49. doi: 10.3322/caac.21660
2. Siegel RL, Miller KD, Fuchs HE, Jemal A. Cancer Statistics, 2021. *CA Cancer J Clin* (2021) 71(1):7–33. doi: 10.3322/caac.21654
3. Tang A, Hallouch O, Chernyak V, Kamaya A, Sirlin CB. Epidemiology of Hepatocellular Carcinoma: Target Population for Surveillance and Diagnosis. *Abdom Radiol (NY)* (2018) 43(1):13–25. doi: 10.1007/s00261-017-1209-1
4. Huo TI, Hsu CY, Liu PH. Magic Mirror on the Wall: Which is the Best Biomarker for Hepatocellular Carcinoma? *Hepatology* (2018) 67(6):2482–3. doi: 10.1002/hep.29869
5. Hartke J, Johnson M, Ghabril M. The Diagnosis and Treatment of Hepatocellular Carcinoma. *Semin Diagn Pathol* (2017) 34(2):153–9. doi: 10.1053/j.semdp.2016.12.011
6. Sun JY, Yin T, Zhang XY, Lu XJ. Therapeutic Advances for Patients With Intermediate Hepatocellular Carcinoma. *J Cell Physiol* (2019) 234(8):12116–21. doi: 10.1002/jcp.28019
7. Cremer S, Michalik KM, Fischer A, Pfisterer L, Jaé N, Winter C, et al. Hematopoietic Deficiency of the Long Noncoding RNA MALAT1 Promotes Atherosclerosis and Plaque Inflammation. *Circulation* (2019) 139(10):1320–34. doi: 10.1161/CIRCULATIONAHA.117.029015
8. Ling H, Fabbri M, Calin GA. MicroRNAs and Other non-Coding RNAs as Targets for Anticancer Drug Development. *Nat Rev Drug Discov* (2013) 12 (11):847–65. doi: 10.1038/nrd4140
9. Fu XD. Non-Coding RNA: A New Frontier in Regulatory Biology. *Natl Sci Rev* (2014) 1(2):190–204. doi: 10.1093/nsr/nwu008
10. Iyer MK, Niknafs YS, Malik R, Singhal U, Sahu A, Hosono Y, et al. The Landscape of Long Noncoding RNAs in the Human Transcriptome. *Nat Genet* (2015) 47:199–208. doi: 10.1038/ng.3192
11. Peschansky VJ, Wahlestedt C. Non-Coding RNAs as Direct and Indirect Modulators of Epigenetic Regulation. *Epigenetics* (2014) 9(1):3–12. doi: 10.4161/epi.27473
12. Cho SW, Xu J, Sun R, Mumbach MR, Carter AC, Chen YG, et al. Promoter of lncRNA Gene PVT1 Is a Tumor-Suppressor DNA Boundary Element. *Cell* (2018) 173(6):1398–412.e22. doi: 10.1016/j.cell.2018.03.068
13. Dykes IM, Emanueli C. Transcriptional and Post-Transcriptional Gene Regulation by Long Non-Coding RNA. *Genomics Proteomics Bioinf* (2017) 15(3):177–86. doi: 10.1016/j.gpb.2016.12.005
14. Ferrè F, Colantoni A, Helmer-Citterich M. Revealing protein-lncRNA Interaction. *Brief Bioinform* (2016) 17(1):106–16. doi: 10.1093/bib/bbv031
15. Fabian MR, Sonenberg N, Filipowicz W. Regulation of mRNA Translation and Stability by microRNAs. *Annu Rev Biochem* (2010) 79:351–79. doi: 10.1146/annurev-biochem-060308-103103
16. Santer L, Bar C, Thum T. Circular RNAs: A Novel Class of Functional RNA Molecules With a Therapeutic Perspective. *Mol Ther* (2019) 27:1350–63. doi: 10.1016/j.ymthe.2019.07.001
17. Li Y, Ge YZ, Xu L, Jia R. Circular RNA ITCH: A Novel Tumor Suppressor in Multiple Cancers. *Life Sci* (2020) 254:117176. doi: 10.1016/j.lfs.2019.117176
18. Li D, Li Z, Yang Y, Zeng X, Li Y, Du X, et al. Circular RNAs as Biomarkers and Therapeutic Targets in Environmental Chemical Exposure-Related Diseases. *Environ Res* (2020) 180:108825. doi: 10.1016/j.envres.2019.108825
19. Suzuki H, Tsukahara T. A View of pre-mRNA Splicing From RNase R Resistant RNAs. *Int J Mol Sci* (2014) 15(6):9331–42. doi: 10.3390/ijms15069331
20. Kristensen LS, Andersen MS, Stagsted LVW, Ebbesen KK, Hansen TB, Kjems J. The Biogenesis, Biology and Characterization of Circular RNAs. *Nat Rev Genet* (2019) 20:675–91. doi: 10.1038/s41576-019-0158-7
21. Jeck WR, Sorrentino JA, Wang K, Slevin MK, Burd CE, Liu J, et al. Circular RNAs are Abundant, Conserved, and Associated With ALU Repeats. *RNA* (2013) 19(2):141–57. doi: 10.1261/rna.035667.112
22. Cui X, Wang J, Guo Z, Li M, Li M, Liu S, et al. Emerging Function and Potential Diagnostic Value of Circular RNAs in Cancer. *Mol Cancer* (2018) 17:123. doi: 10.1186/s12943-018-0877-y
23. Lu Q, Liu T, Feng H, Yang R, Zhao X, Chen W, et al. Circular RNA Circslc8a1 Acts as a Sponge of miR-130b/miR-494 in Suppressing Bladder Cancer Progression via Regulating PTEN. *Mol Cancer* (2019) 18(1):111. doi: 10.1186/s12943-019-1040-0
24. Xu SL, Deng YS, Liu J, Xu SY, Zhao FY, Wei L, et al. Regulation of Circular RNAs Act as ceRNA in a Hypoxic Pulmonary Hypertension Rat Model. *Genomics* (2021) 113(1 Pt 1):11–9. doi: 10.1016/j.ygeno.2020.11.021
25. Zang J, Lu D, Xu A. The Interaction of circRNAs and RNA Binding Proteins: An Important Part of circRNA Maintenance and Function. *J Neurosci Res* (2020) 98(1):87–97. doi: 10.1002/jnr.24356
26. Pamudurti NR, Bartok O, Jens M, Ashwal-Fluss R, Stottmeister C, Ruhe L, et al. Translation of CircRNAs. *Mol Cell* (2017) 66:9–21.e7. doi: 10.1016/j.molcel.2017.02.021
27. Li Z, Huang C, Bao C, Chen L, Lin M, Wang X, et al. Exon-Intron Circular RNAs Regulate Transcription in the Nucleus. *Nat Struct Mol Biol* (2015) 22:256–64. doi: 10.1038/nsmb.2959
28. Ashwal-Fluss R, Meyer M, Pamudurti NR, Ivanov A, Bartok O, Hanan M, et al. circRNA Biogenesis Competes With pre-mRNA Splicing. *Mol Cell* (2014) 56:55–66. doi: 10.1016/j.molcel.2014.08.019
29. Zhang X, Wang S, Wang H, Cao J, Huang X, Chen Z, et al. Circular RNA Circnrip1 Acts as a microRNA-149-5p Sponge to Promote Gastric Cancer Progression via the AKT1/mTOR Pathway. *Mol Cancer* (2019) 18(1):20. doi: 10.1186/s12943-018-0935-5
30. Jie M, Wu Y, Gao M, Li X, Liu C, Ouyang Q, et al. CircMRPS35 Suppresses Gastric Cancer Progression via Recruiting KAT7 to Govern Histone Modification. *Mol Cancer* (2020) 19(1):56. doi: 10.1186/s12943-020-01160-2
31. Zhao Z, Song J, Tang B, Fang S, Zhang D, Zheng L, et al. CircSOD2 Induced Epigenetic Alteration Drives Hepatocellular Carcinoma Progression Through Activating JAK2/STAT3 Signaling Pathway. *J Exp Clin Cancer Res* (2020) 39(1):259. doi: 10.1186/s13046-020-01769-7
32. Zhang X, Xu Y, Qian Z, Zheng W, Wu Q, Chen Y, et al. circRNA_104075 Stimulates YAP-Dependent Tumorigenesis Through the Regulation of

HNF4a and may Serve as a Diagnostic Marker in Hepatocellular Carcinoma. *Cell Death Dis* (2018) 9(11):1091. doi: 10.1038/s41419-018-1132-6
33. Zhang T, Jing B, Bai Y, Zhang Y, Yu H. Circular RNA Circtmem45a Acts as the Sponge of MicroRNA-665 to Promote Hepatocellular Carcinoma Progression. *Mol Ther Nucleic Acids* (2020) 22:285–97. doi: 10.1016/j.omtn.2020.08.011
34. Yao Z, Xu R, Yuan L, Xu M, Zhuang H, Li Y, et al. Circ_0001955 Facilitates Hepatocellular Carcinoma (HCC) Tumorigenesis by Sponging miR-516a-5p to Release TRAF6 and MAPK11. *Cell Death Dis* (2019) 10(12):945. doi: 10.1038/s41419-019-2176-y
35. Guan Z, Tan J, Gao W, Li X, Yang Y, Li X, et al. Circular RNA Hsa_Circ_0016788 Regulates Hepatocellular Carcinoma Tumorigenesis Through miR-486/CDK4 Pathway. *J Cell Physiol* (2018) 234(1):500–8. doi: 10.1002/jcp.26612
36. Xu L, Feng X, Hao X, Wang P, Zhang Y, Zheng X, et al. CircSETD3 (Hsa_circ_0000567) Acts as a Sponge for microRNA-421 Inhibiting Hepatocellular Carcinoma Growth. *J Exp Clin Cancer Res* (2019) 38(1):98. doi: 10.1186/s13046-019-1041-2
37. Dong W, Dai ZH, Liu FC, Guo XG, Ge CM, Ding J, et al. The RNA-Binding Protein RBM3 Promotes Cell Proliferation in Hepatocellular Carcinoma by Regulating Circular RNA SCD-circRNA 2 Production. *EBioMedicine* (2019) 45:155–67. doi: 10.1016/j.ebiom.2019.06.030
38. Liu B, Yang G, Wang X, Liu J, Lu Z, Wang Q, et al. CircBACH1 (Hsa_Circ_0061395) Promotes Hepatocellular Carcinoma Growth by Regulating P27 Repression via HuR. *J Cell Physiol* (2020) 235(10):6929–41. doi: 10.1002/jcp.29589
39. Tian F, Yu C, Wu M, Wu X, Wan L, Zhu X. MicroRNA-191 Promotes Hepatocellular Carcinoma Cell Proliferation by has_Circ_0000204/miR-191/KLF6 Axis. *Cell Prolif* (2019) 52(5):e12635. doi: 10.1111/cpr.12635
40. Huang XY, Huang ZL, Huang J, Xu B, Huang XY, Xu YH, et al. Exosomal circRNA-100338 Promotes Hepatocellular Carcinoma Metastasis via Enhancing Invasiveness and Angiogenesis. *J Exp Clin Cancer Res* (2020) 39(1):20. doi: 10.1186/s13046-020-1529-9
41. Wang G, Liu W, Zou Y, Wang G, Deng Y, Luo J, et al. Three Isoforms of Exosomal Circptgr1 Promote Hepatocellular Carcinoma Metastasis via the Mir449a-MET Pathway. *EBioMedicine* (2019) 40:432–45. doi: 10.1016/j.ebiom.2018.12.062
42. Hu ZQ, Zhou SL, Li J, Zhou ZJ, Wang PC, Xin HY, et al. Circular RNA Sequencing Identifies CircASAP1 as a Key Regulator in Hepatocellular Carcinoma Metastasis. *Hepatology* (2020) 72(3):906–22. doi: 10.1002/hep.31068
43. Yu X, Sheng P, Sun J, Zhao X, Zhang J, Li Y, et al. The Circular RNA Circmast1 Promotes Hepatocellular Carcinoma Cell Proliferation and Migration by Sponging miR-1299 and Regulating CTNND1 Expression. *Cell Death Dis* (2020) 11(5):340. doi: 10.1038/s41419-020-2532-y
44. Wang ZY, Zhu Z, Wang HF, Qin B, Liu J, Yao XH, et al. Downregulation of Circdync1h1 Exhibits Inhibitor Effect on Cell Proliferation and Migration in Hepatocellular Carcinoma Through miR-140-5p. *J Cell Physiol* (2019) 234(10):17775–85. doi: 10.1002/jcp.28403
45. Wang H, Chen W, Jin M, Hou L, Chen X, Zhang R, et al. CircSLC3A2 Functions as an Oncogenic Factor in Hepatocellular Carcinoma by Sponging miR-490-3p and Regulating PPM1F Expression. *Mol Cancer* (2018) 17(1):165. doi: 10.1186/s12943-018-0909-7
46. Chen G, Shi Y, Liu M, Sun J. Circhipk3 Regulates Cell Proliferation and Migration by Sponging miR-124 and Regulating AQP3 Expression in Hepatocellular Carcinoma. *Cell Death Dis* (2018) 9(2):175. doi: 10.1038/s41419-017-0204-3
47. Ding B, Fan W, Lou W. Hsa_Circ_0001955 Enhances *In Vitro* Proliferation, Migration, and Invasion of HCC Cells Through miR-145-5p/NRAS Axis. *Mol Ther Nucleic Acids* (2020) 22:445–55. doi: 10.1016/j.omtn.2020.09.007
48. Gao J, Dai C, Yu X, Yin XB, Zhou F. Circ-TCF4.85 Silencing Inhibits Cancer Progression Through microRNA-486-5p-Targeted Inhibition of ABCF2 in Hepatocellular Carcinoma. *Mol Oncol* (2020) 14(2):447–61. doi: 10.1002/1878-0261.12603
49. Li S, Weng J, Song F, Li L, Xiao C, Yang W, et al. Circular RNA Circznf566 Promotes Hepatocellular Carcinoma Progression by Sponging miR-4738-3p and Regulating TDO2 Expression. *Cell Death Dis* (2020) 11(6):452. doi: 10.1038/s41419-020-2616-8
50. Zhan W, Liao X, Chen Z, Li L, Tian T, Yu L, et al. Circular RNA Hsa_circRNA_103809 Promoted Hepatocellular Carcinoma Development by Regulating miR-377-3p/FGFR1/ERK Axis. *J Cell Physiol* (2020) 235(2):1733–45. doi: 10.1002/jcp.29092
51. Huang G, Liang M, Liu H, Huang J, Li P, Wang C, et al. CircRNA Hsa_circRNA_104348 Promotes Hepatocellular Carcinoma Progression Through Modulating miR-187-3p/RTKN2 Axis and Activating Wnt/β-Catenin Pathway. *Cell Death Dis* (2020) 11(12):1065. doi: 10.1038/s41419-020-03276-1
52. Yu J, Yang M, Zhou B, Luo J, Zhang Z, Zhang W, et al. CircRNA-104718 Acts as Competing Endogenous RNA and Promotes Hepatocellular Carcinoma Progression Through microRNA-218-5p/TXNDC5 Signaling Pathway. *Clin Sci (Lond)* (2019) 133(13):1487–503. doi: 10.1042/CS20190394
53. Bai N, Peng E, Qiu X, Lyu N, Zhang Z, Tao Y, et al. Circfblim1 Act as a ceRNA to Promote Hepatocellular Cancer Progression by Sponging miR-346. *J Exp Clin Cancer Res* (2018) 37(1):172. doi: 10.1186/s13046-018-0838-8
54. Zhang H, Deng T, Ge S, Liu Y, Bai M, Zhu K, et al. Exosome circRNA Secreted From Adipocytes Promotes the Growth of Hepatocellular Carcinoma by Targeting Deubiquitination-Related USP7. *Oncogene* (2019) 38(15):2844–59. doi: 10.1038/s41388-018-0619-z
55. Wu D, Xia A, Fan T, Li G. Circrasgrf2 Functions as an Oncogenic Gene in Hepatocellular Carcinoma by Acting as a miR-1224 Sponge. *Mol Ther Nucleic Acids* (2020) 23:13–26. doi: 10.1016/j.omtn.2020.10.035
56. Sun S, Gao J, Zhou S, Li Y, Wang Y, Jin L, et al. A Novel Circular RNA Circ-LRIG3 Facilitates the Malignant Progression of Hepatocellular Carcinoma by Modulating the EZH2/STAT3 Signaling. *J Exp Clin Cancer Res* (2020) 39(1):252. doi: 10.1186/s13046-020-01779-5
57. Wang L, Long H, Zheng Q, Bo X, Xiao X, Li B. Circular RNA Circrhot1 Promotes Hepatocellular Carcinoma Progression by Initiation of NR2F6 Expression. *Mol Cancer* (2019) 18(1):119. doi: 10.1186/s12943-019-1046-7
58. Liang WC, Wong CW, Liang PP, Shi M, Cao Y, Rao ST, et al. Translation of the Circular RNA Circβ-Catenin Promotes Liver Cancer Cell Growth Through Activation of the Wnt Pathway. *Genome Biol* (2019) 20(1):84. doi: 10.1186/s13059-019-1685-4
59. Liu H, Lan T, Li H, Xu L, Chen X, Liao H, et al. Circular RNA Circdlc1 Inhibits MMP1-Mediated Liver Cancer Progression via Interaction With HuR. *Theranostics* (2021) 11(3):1396–411. doi: 10.7150/thno.53227
60. Yu J, Xu QG, Wang ZG, Yang Y, Zhang L, Ma JZ, et al. Circular RNA Csmarca5 Inhibits Growth and Metastasis in Hepatocellular Carcinoma. *J Hepatol* (2018) 68(6):1214–27. doi: 10.1016/j.jhep.2018.01.012
61. Shi L, Yan P, Liang Y, Sun Y, Shen J, Zhou S, et al. Circular RNA Expression is Suppressed by Androgen Receptor (AR)-Regulated Adenosine Deaminase That Acts on RNA (ADAR1) in Human Hepatocellular Carcinoma. *Cell Death Dis* (2017) 8(11):e3171. doi: 10.1038/cddis.2017.556
62. Sun S, Wang W, Luo X, Li Y, Liu B, Li X, et al. Circular RNA Circ-ADD3 Inhibits Hepatocellular Carcinoma Metastasis Through Facilitating EZH2 Degradation via CDK1-Mediated Ubiquitination. *Am J Cancer Res* (2019) 9(8):1695–707.
63. Li R, Deng Y, Liang J, Hu Z, Li X, Liu H, et al. Circular RNA Circ-102,166 Acts as a Sponge of miR-182 and miR-184 to Suppress Hepatocellular Carcinoma Proliferation and Invasion. *Cell Oncol (Dordr)* (2021) 44(2):279–95. doi: 10.1007/s13402-020-00564-y
64. Han D, Li J, Wang H, Su X, Hou J, Gu Y, et al. Circular RNA Circmto1 Acts as the Sponge of microRNA-9 to Suppress Hepatocellular Carcinoma Progression. *Hepatology* (2017) 66(4):1151–64. doi: 10.1002/hep.29270
65. Jia C, Yao Z, Lin Z, Zhao L, Cai X, Chen S, et al. Circnfatc3 Sponges miR-548I Acts as a ceRNA to Protect NFATC3 Itself and Suppressed Hepatocellular Carcinoma Progression. *J Cell Physiol* (2021) 236(2):1252–69. doi: 10.1002/jcp.29931
66. Wang YG, Wang T, Ding M, Xiang SH, Shi M, Zhai B. Hsa_Circ_0091570 Acts as a ceRNA to Suppress Hepatocellular Cancer Progression by Sponging hsa-miR-1307. *Cancer Lett* (2019) 460:128–38. doi: 10.1016/j.canlet.2019.06.007
67. Qiu L, Huang Y, Li Z, Dong X, Chen G, Xu H, et al. Circular RNA Profiling Identifies Circadamts13 as a miR-484 Sponge Which Suppresses Cell

Proliferation in Hepatocellular Carcinoma. *Mol Oncol* (2019) 13(2):441–55. doi: 10.1002/1878-0261.12424
68. Song C, Li D, Liu H, Sun H, Liu Z, Zhang L, et al. The Competing Endogenous Circular RNA ADAMTS14 Suppressed Hepatocellular Carcinoma Progression Through Regulating microRNA-572/Regulator of Calcineurin 1. *J Cell Physiol* (2019) 234(3):2460–70. doi: 10.1002/jcp.26764
69. Yao Z, Luo J, Hu K, Lin J, Huang H, Wang Q, et al. ZKSCAN1 Gene and its Related Circular RNA (Circzkscan1) Both Inhibit Hepatocellular Carcinoma Cell Growth, Migration, and Invasion But Through Different Signaling Pathways. *Mol Oncol* (2017) 11(4):422–37. doi: 10.1002/1878-0261.12045
70. Zhu YJ, Zheng B, Luo GJ, Ma XK, Lu XY, Lin XM, et al. Circular RNAs Negatively Regulate Cancer Stem Cells by Physically Binding FMRP Against CCAR1 Complex in Hepatocellular Carcinoma. *Theranostics* (2019) 9 (12):3526–40. doi: 10.7150/thno.32796
71. Chen W, Quan Y, Fan S, Wang H, Liang J, Huang L, et al. Exosome-Transmitted Circular RNA Hsa_Circ_0051443 Suppresses Hepatocellular Carcinoma Progression. *Cancer Lett* (2020) 475:119–28. doi: 10.1016/j.canlet.2020.01.022
72. Zhu C, Su Y, Liu L, Wang S, Liu Y, Wu J. Circular RNA Hsa_Circ_0004277 Stimulates Malignant Phenotype of Hepatocellular Carcinoma and Epithelial-Mesenchymal Transition of Peripheral Cells. *Front Cell Dev Biol* (2021) 8:585565. doi: 10.3389/fcell.2020.585565
73. Song LN, Qiao GL, Yu J, Yang CM, Chen Y, Deng ZF, et al. Hsa_circ_0003998 Promotes Epithelial to Mesenchymal Transition of Hepatocellular Carcinoma by Sponging miR-143-3p and PCBP1. *J Exp Clin Cancer Res* (2020) 39(1):114. doi: 10.1186/s13046-020-01576-0
74. Meng J, Chen S, Han JX, Qian B, Wang XR, Zhong WL, et al. Twist1 Regulates Vimentin Through Cul2 Circular RNA to Promote EMT in Hepatocellular Carcinoma. *Cancer Res* (2018) 78(15):4150–62. doi: 10.1158/0008-5472.CAN-17-3009
75. Liu Z, Yu Y, Huang Z, Kong Y, Hu X, Xiao W, et al. CircRNA-5692 Inhibits the Progression of Hepatocellular Carcinoma by Sponging miR-328-5p to Enhance DAB2IP Expression. *Cell Death Dis* (2019) 10(12):900. doi: 10.1038/s41419-019-2089-9
76. Gong TT, Sun FZ-Y, Chen J, Liu JF, Yan Y, Li D, et al. The Circular RNA Circptk2 Inhibits EMT in Hepatocellular Carcinoma by Acting as a ceRNA and Sponging miR-92a to Upregulate E-Cadherin. *Eur Rev Med Pharmacol Sci* (2020) 24(18):9333–42. doi: 10.26355/eurrev_202009_23015
77. Zhang PF, Gao C, Huang XY, Lu JC, Guo XJ, Shi GM, et al. Cancer Cell-Derived Exosomal Circuhrf1 Induces Natural Killer Cell Exhaustion and may Cause Resistance to Anti-PD1 Therapy in Hepatocellular Carcinoma. *Mol Cancer* (2020) 19(1):110. doi: 10.1186/s12943-020-01222-5
78. Huang XY, Zhang PF, Wei CY, Peng R, Lu JC, Gao C, et al. Circular RNA circMET Drives Immunosuppression and Anti-PD1 Therapy Resistance in Hepatocellular Carcinoma via the miR-30-5p/Snail/DPP4 Axis. *Mol Cancer* (2020) 19(1):92. doi: 10.1186/s12943-020-01213-6
79. Zhang PF, Wei CY, Huang XY, Peng R, Yang X, Lu JC, et al. Circular RNA Circtrim33-12 Acts as the Sponge of MicroRNA-191 to Suppress Hepatocellular Carcinoma Progression. *Mol Cancer* (2019) 18(1):105. doi: 10.1186/s12943-019-1031-1
80. Shi M, Li ZY, Zhang LM, Wu XY, Xiang SH, Wang YG, et al. Hsa_circ_0007456 Regulates the Natural Killer Cell-Mediated Cytotoxicity Toward Hepatocellular Carcinoma via the miR-6852-3p/ICAM-1 Axis. *Cell Death Dis* (2021) 12(1):94. doi: 10.1038/s41419-020-03334-8
81. Li Y, Zhang Y, Zhang S, Huang D, Li B, Liang G, et al. circRNA Circarnt2 Suppressed the Sensitivity of Hepatocellular Carcinoma Cells to Cisplatin by Targeting the miR-155-5p/PDK1 Axis. *Mol Ther Nucleic Acids* (2020) 23:244–54. doi: 10.1016/j.omtn.2020.08.037
82. Xu J, Ji L, Liang Y, Wan Z, Zheng W, Song X, et al. CircRNA-SORE Mediates Sorafenib Resistance in Hepatocellular Carcinoma by Stabilizing YBX1. *Signal Transduct Target Ther* (2020) 5(1):298. doi: 10.1038/s41392-020-00375-5
83. Xu J, Wan Z, Tang M, Lin Z, Jiang S, Ji L, et al. N^6-Methyladenosine-Modified CircRNA-SORE Sustains Sorafenib Resistance in Hepatocellular Carcinoma by Regulating β-Catenin Signaling. *Mol Cancer* (2020) 19(1):163. doi: 10.1186/s12943-020-01281-8
84. Yang C, Dong Z, Hong H, Dai B, Song F, Geng L, et al. Circfn1 Mediates Sorafenib Resistance of Hepatocellular Carcinoma Cells by Sponging miR-1205 and Regulating E2F1 Expression. *Mol Ther Nucleic Acids* (2020) 22:421–33. doi: 10.1016/j.omtn.2020.08.039
85. Yang X, Song H, Zi Z, Kou J, Chen S, Dai Y, et al. Circ_0005075 Promotes Hepatocellular Carcinoma Progression by Suppression of microRNA-335. *J Cell Physiol* (2019) 234(12):21937–46. doi: 10.1002/jcp.28757
86. Li Q, Pan X, Zhu D, Deng Z, Jiang R, Wang X. Circular RNA MAT2B Promotes Glycolysis and Malignancy of Hepatocellular Carcinoma Through the miR-338-3p/PKM2 Axis Under Hypoxic Stress. *Hepatology* (2019) 70 (4):1298–316. doi: 10.1002/hep.30671
87. Chen L, Kong R, Wu C, Wang S, Liu Z, Liu S, et al. Circ-MALAT1 Functions as Both an mRNA Translation Brake and a microRNA Sponge to Promote Self-Renewal of Hepatocellular Cancer Stem Cells. *Adv Sci (Weinh)* (2019) 7 (4):1900949. doi: 10.1002/advs.201900949
88. He Y, Huang H, Jin L, Zhang F, Zeng M, Wei L, et al. CircZNF609 Enhances Hepatocellular Carcinoma Cell Proliferation, Metastasis, and Stemness by Activating the Hedgehog Pathway Through the Regulation of miR-15a-5p/15b-5p and GLI2 Expressions. *Cell Death Dis* (2020) 11(5):358. doi: 10.1038/s41419-020-2441-0
89. Lin YH, Wu MH, Huang YH, Yeh CT, Cheng ML, Chi HC, et al. Taurine Up-Regulated Gene 1 Functions as a Master Regulator to Coordinate Glycolysis and Metastasis in Hepatocellular Carcinoma. *Hepatology* (2018) 67(1):188–203. doi: 10.1002/hep.29462
90. Kreso A, Dick JE. Evolution of the Cancer Stem Cell Model. *Cell Stem Cell* (2014) 14(3):275–91. doi: 10.1016/j.stem.2014.02.006
91. Li Z, Zhou Y, Yang G, He S, Qiu X, Zhang L, et al. Using Circular RNA SMARCA5 as a Potential Novel Biomarker for Hepatocellular Carcinoma. *Clin Chim Acta* (2019) 492:37–44. doi: 10.1016/j.cca.2019.02.001
92. Shang X, Li G, Liu H, Li T, Liu J, Zhao Q, et al. Comprehensive Circular RNA Profiling Reveals That Hsa_Circ_0005075, a New Circular RNA Biomarker, Is Involved in Hepatocellular Crcinoma Development. *Med (Baltimore)* (2016) 95(22):e3811. doi: 10.1097/MD.0000000000003811
93. Chen D, Zhang C, Lin J, Song X, Wang H. Screening Differential Circular RNA Expression Profiles Reveal That Hsa_Circ_0128298 is a Biomarker in the Diagnosis and Prognosis of Hepatocellular Carcinoma. *Cancer Manag Res* (2018) 10:1275–83. doi: 10.2147/CMAR.S166740
94. Wei Y, Chen X, Liang C, Ling Y, Yang X, Ye X, et al. A Noncoding Regulatory RNAs Network Driven by Circ-CDYL Acts Specifically in the Early Stages Hepatocellular Carcinoma. *Hepatology* (2020) 71(1):130–47. doi: 10.1002/hep.30795
95. Fu L, Yao T, Chen Q, Mo X, Hu Y, Guo J. Screening Differential Circular RNA Expression Profiles Reveals Hsa_Circ_0004018 is Associated With Hepatocellular Carcinoma. *Oncotarget* (2017) 8(35):58405–16. doi: 10.18632/oncotarget.16881
96. Matboli M, Shafei AE, Ali MA, Ashry AM, Kamal KM, Agag MA, et al. circRNAs (Hsa_Circ_00156, Hsa_Circ _000224, and Hsa_Circ _000520) Are Novel Potential Biomarkers in Hepatocellular Carcinoma. *J Cell Biochem* (2018) 1–14. doi: 10.1002/jcb.28045
97. Yu J, Ding WB, Wang MC, Guo XG, Xu J, Xu QG, et al. Plasma Circular RNA Panel to Diagnose Hepatitis B Virus-Related Hepatocellular Carcinoma: A Large-Scale, Multicenter Study. *Int J Cancer* (2020) 146 (6):1754–63. doi: 10.1002/ijc.32647
98. Wu C, Deng L, Zhuo H, Chen X, Tan Z, Han S, et al. Circulating circRNA Predicting the Occurrence of Hepatocellular Carcinoma in Patients With HBV Infection. *J Cell Mol Med* (2020) 24(17):10216–22. doi: 10.1111/jcmm.15635
99. Bao S, Jin S, Wang C, Tu P, Hu K, Lu J. Androgen Receptor Suppresses Vasculogenic Mimicry in Hepatocellular Carcinoma *via* Circrna7/Mirna7-5p/VE-Cadherin/Notch4 Signalling. *J Cell Mol Med* (2020) 24(23):14110–20. doi: 10.1111/jcmm.16022
100. Ouyang X, Yao L, Liu G, Liu S, Gong L, Xiao Y. Loss of Androgen Receptor Promotes HCC Invasion and Metastasis via Activating Circ-LNPEP/miR-532-3p/RAB9A Signal Under Hypoxia. *Biochem Biophys Res Commun* (2021) 557:26–32. doi: 10.1016/j.bbrc.2021.02.120
101. Xiao Y, Liu G, Sun Y, Gao Y, Ouyang X, Chang C, et al. Targeting the Estrogen Receptor Alpha (Erα)-Mediated Circ-SMG1.72/miR-141-3p/

Gelsolin Signaling to Better Suppress the HCC Cell Invasion. *Oncogene* (2020) 39(12):2493–508. doi: 10.1038/s41388-019-1150-6
102. Li X, Ding J, Wang X, Cheng Z, Zhu Q. NUDT21 Regulates circRNA Cyclization and ceRNA Crosstalk in Hepatocellular Carcinoma. *Oncogene* (2020) 39(4):891–904. doi: 10.1038/s41388-019-1030-0
103. Zheng X, Huang M, Xing L, Yang R, Wang X, Jiang R, et al. The circRNA Circsept9 Mediated by E2F1 and EIF4A3 Facilitates the Carcinogenesis and Development of Triple-Negative Breast Cancer. *Mol Cancer* (2020) 19(1):73. doi: 10.1186/s12943-020-01183-9

Conflict of Interest: The authors declare that the research was conducted in the absence of any commercial or financial relationships that could be construed as a potential conflict of interest.

frontiers in Oncology

ORIGINAL RESEARCH
published: 09 September 2021
doi: 10.3389/fonc.2021.738477

Identification of a Ferroptosis-Related Signature Model Including mRNAs and lncRNAs for Predicting Prognosis and Immune Activity in Hepatocellular Carcinoma

Zi-An Chen, Hui Tian, Dong-Mei Yao, Yuan Zhang, Zhi-Jie Feng and Chuan-Jie Yang**

Department of Gastroenterology, The Second Hospital of Hebei Medical University, Shijiazhuang, China

OPEN ACCESS

Edited by:
Hongda Liu,
Nanjing Medical University, China

Reviewed by:
Tabish Hussain,
University of Texas MD Anderson Cancer Center, United States
Andrea Angeli,
University of Florence, Italy

***Correspondence:**
Chuan-Jie Yang
yangchuanjie2004@sina.com
Zhi-Jie Feng
zhijiefeng2005@163.com

Specialty section:
This article was submitted to Cancer Molecular Targets and Therapeutics, a section of the journal Frontiers in Oncology

Received: *08 July 2021*
Accepted: *17 August 2021*
Published: *09 September 2021*

Citation:
Chen Z-A, Tian H, Yao D-M, Zhang Y, Feng Z-J and Yang C-J (2021) Identification of a Ferroptosis-Related Signature Model Including mRNAs and lncRNAs for Predicting Prognosis and Immune Activity in Hepatocellular Carcinoma. Front. Oncol. 11:738477. doi: 10.3389/fonc.2021.738477

Background: Ferroptosis is a novel form of regulated cell death involved in tumor progression. The role of ferroptosis-related lncRNAs in hepatocellular carcinoma (HCC) remains unclear.

Methods: RNA-seq and clinical data for HCC patients were downloaded from The Cancer Genome Atlas (TCGA) Genomic Data Commons (GDC) portal. Bioinformatics methods, including weighted gene coexpression network analysis (WGCNA), Cox regression, and least absolute shrinkage and selection operator (LASSO) analysis, were used to identify signature markers for diagnosis/prognosis. The tumor microenvironment, immune infiltration and functional enrichment were compared between the low-risk and high-risk groups. Subsequently, small molecule drugs targeting ferroptosis-related signature components were predicted *via* the L1000FWD and PubChem databases.

Results: The prognostic model consisted of 2 ferroptosis-related mRNAs (SLC1A5 and SLC7A11) and 8 ferroptosis-related lncRNAs (AC245297.3, MYLK-AS1, NRAV, SREBF2-AS1, AL031985.3, ZFPM2-AS1, AC015908.3, MSC-AS1). The areas under the curves (AUCs) were 0.830 and 0.806 in the training and test groups, respectively. Decision curve analysis (DCA) revealed that the ferroptosis-related signature performed better than all pathological characteristics. Multivariate Cox regression analysis showed that the risk score was an independent prognostic factor. The survival probability of low- and high-risk patients could be clearly distinguished by the principal component analysis (PCA) plot. The risk score divided HCC patients into two distinct groups in terms of immune status, especially checkpoint gene expression, which was further supported by the Gene Ontology (GO) biological process, and Kyoto Encyclopedia of Genes and Genomes (KEGG) analysis. Finally, several small molecule drugs (SIB-1893, geldanamycin and PD-184352, etc) targeting ferroptosis-related signature components were identified for future reference.

Conclusion: We constructed a new ferroptosis-related mRNA/lncRNA signature for HCC patients. The model can be used for prognostic prediction and immune evaluation, providing a reference for immunotherapies and targeted therapies.

Keywords: hepatocellular carcinoma, LASSO regression analysis, ferroptosis-related mRNA and lncRNAs, tumor microenvironment, immune infiltration

INTRODUCTION

According to epidemiological studies, hepatocellular carcinoma (HCC) is considered the seventh most common malignancy and the second most common cause of cancer-related death (1). Many factors, including chronic infection with HBV/HCV, alcohol abuse, long-term obesity or exposure to aflatoxin, have been reported to be related to the progression of HCC (2). Considering that the early monitoring methods for HCC are still limited and that the tumor easily metastasizes and has a poor prognosis, it is necessary to develop new detection methods and identify new therapeutic targets for HCC.

Ferroptosis is a unique form of regulated cell death associated with iron metabolism, which is different from apoptosis, necrosis, and autophagy (3). Although the detailed mechanism underlying the role of ferroptosis in tumors is still unclear, several studies have reported that ferroptosis is involved in various cancers, including breast cancer (4–6), pancreatic cancer (7), ovarian cancer (8), and HCC (9–12). Compared to normal nontumor cells, cancer cells have a higher level of iron, which indicates the potential of ferroptosis inducers in new antitumor strategies (13, 14). For example, the triterpene saponin ardisiacrispin B and epunctanone exert cytotoxic effects on cancer cells with multiple drug resistance partly *via* ferroptosis (15, 16). In addition to ferroptosis-inducing agents, an increasing number of ferroptosis-related genes have been identified and found to be involved in the progression of cancers by serving as mediators of ferroptosis-related pathways. In HCC, CISD1 and a polymorphism of the TP53 gene (the S47 variant) are reported to negatively regulate ferroptosis, which proves that ferroptosis-related genes play a role in tumor progression (17, 18). In addition, several ferroptosis-related genes, including MI1G, NRF2, and Rb, were found to protect HCC cells from sorafenib-induced ferroptosis (19–21).

Based on the existing findings, we have noticed that ferroptosis plays a pivotal role in the progression of HCC; however, the specific function of ferroptosis-related long noncoding RNAs (lncRNAs) in HCC has not been fully elucidated. lncRNAs are a class of noncoding transcripts more than 200 nucleotides in length (22). It has been proved that lncRNAs serve as pivotal players in posttranscriptional regulatory mechanisms that target mRNA splicing, stability, or translation, the scope of which is still expanding (23). Dynamic alterations in the expression and mutation of lncRNAs are closely associated with tumorigenesis, tumor progression, metastasis, and cancer immunity indicating the emerging roles of lncRNAs as new biomarkers and therapeutic targets for cancer treatment strategies (24–26). Therefore, investigating lncRNAs related to ferroptosis and HCC is essential to our understanding of the mechanisms of tumor development. Recently, a model containing 3 ferroptosis-related lncRNAs was reported; however, it exhibited low predictive power for HCC with an area under the curve (AUC)=0.7 (27).

In this study, we constructed a new ferroptosis-related signature including mRNAs and lncRNAs by both weighted gene co-expression analysis (WGCNA) and least absolute shrinkage and selection operator (LASSO) regression analysis. We evaluated the predictive value of the ferroptosis-related signature and investigated the differential immune response in a variety of ways, including tumor microenvironment (TME) analysis and single-sample gene set enrichment analysis (ssGSEA). Furthermore, functional enrichment analysis was performed to clarify the biological functions of these differentially expressed genes (DEGs). Based on the DEG results, several small molecule drugs targeting ferroptosis-related signature components were identified *via* the L1000FWD database, and SIB-1893, geldanamycin and PD-184352 were visualized by PubChem.

MATERIAL AND METHODS

Data Collection and Preprocessing

The RNA sequencing (FPKM) and clinical data of HCC patients were downloaded from The Cancer Genome Atlas (TCGA) Genomic Data Commons (GDC) portal (https://portal.gdc.cancer.gov/repository). To reduce errors caused by confounding factors, we exclude samples with patient follow-up time < 30 d (n = 29) and without survival information (n = 1). Detailed information on the clinical data of the 377 samples is shown in **Table 1**. A list of 267 ferroptosis-related genes was compiled based on the FerrDb website (http://www.zhounan.org/ferrdb/) and previous literature (12, 13, 28–30) (**Supplementary Table 1**). The flowchart of this research is exhibited in **Figure 1**.

WGCNA

WGCNA was performed to identify coexpressed gene modules and investigate the relationships between gene networks and clinical traits. WGCNA was conducted with the "WGCNA" package. Pearson correlation tests were performed to construct a matrix to establish the module-trait relationships between ferroptosis-related genes and vital status according to the β value (soft-threshold value). The modules with a $p<0.05$ were

TABLE 1 | Clinical characteristics of patients in the TCGA LIHC cohort.

Characteristic		N = 348
Age	Median	61
	Range	16-90
	Male	238
Sex	Female	110
	G1	53
	G2	164
Grade	G3	113
	G4	13
	NA	5
	Stage I	165
	Stage II	78
Clinical stage	Stage III	81
	Stage IV	3
	NA	21
	T1	172
	T2	85
T stage	T3	75
	T4	13
	NA	3
	M0	250
M stage	MI	3
	NA	95
	NO	T6
N stage	N1	3
	NA	101
	Alive	223
Vital status	Dead	125

considered associated with vital status and were selected for further research.

Construction of the LASSO Cox Regression Model and Survival Analysis

Before establishing the model, the ferroptosis-related genes from WGCNA were tested by univariate Cox regression analysis (p <0.001). Furthermore, ferroptosis-related lncRNAs co-expressed with ferroptosis-related genes were screened by Pearson correlation test (correlation coefficient >0.4, and p <0.001). The lncRNAs were further screened by univariate Cox regression analysis (p <0.001). Then, the selected ferroptosis-related genes and lncRNAs were merged to establish the model. A network containing the ferroptosis-related mRNA-lncRNA network was constructed and visualized by Cytoscape (version 3.7.2)

HCC patients from the TCGA liver hepatocellular carcinoma (LIHC) cohort were randomly divided into a training group, and another 50% were set as the test group. The LASSO Cox regression algorithm was applied to select the ferroptosis-related signature. Finally, a formula for the risk score was established, and we calculated the risk score for each patient as follows:

$$\text{RiskScore} = \sum_{i=1}^{n} \text{Coef}_i \times X_i$$

Coefi indicates the correlation coefficient of each ferroptosis-related signature, and X indicates the level of gene expression. The median risk score in the training cohort was set as the cutoff value, and the training group and test group were divided into high-risk and low-risk groups according to the cutoff.

Determination of Immune Score, Stromal Score, and ESTIMATE Score

The Estimation of STromal and Immune cells in MAlignant Tumors using Expression data (ESTIMATE) algorithm was used to evaluate the ratio of the immune-stromal component in the TME by utilizing the "estimate" R package, which calculated three scores: the immune score (representing the level of immune cell infiltration), stromal score (representing the amount of stroma), and ESTIMATE score (representing the sum of both). A higher score indicated a larger ratio of the corresponding component in the TME.

Estimation of the Immune Cell Infiltration

To evaluate immune cell infiltration, ssGSEA was used to quantify the tumor-infiltrating immune cell subgroups and immune function between the two groups. The expression of potential immune checkpoint and m6A genes was also determined according to previous literature.

Functional and Pathway Enrichment Analysis

The DEGs between the low- and high-risk groups were then screened out by the "limma" package using the criteria false discovery rate (FDR) < 0.05 and |log2 fold change (FC)| ≥ 1. We then applied the "limma" and "clusterProfiler" packages to perform Gene Ontology (GO) analysis and Kyoto Encyclopedia of Genes and Genomes (KEGG) pathway enrichment analysis.

Identification of Potential Compounds

DEGs based on the ferroptosis-related signature were divided into up- and downregulated gene groups. The two groups of genes were then uploaded to the L1000FWD website (https://maayanlab.cloud/L1000FWD/), and then permuted results were obtained. The results were further visualized by the PubChem website (pubchem.ncbi.nlm.nih.gov).

Statistical Analysis

The data were analyzed with R software version 4.0.4. For comparisons, data conforming to normal and nonnormal distributions were assessed using the unpaired Student's t-test and the Wilcoxon test, respectively, and the statistical significance threshold was set at p <0.05. The survival of HCC patients based on the ferroptosis-related signature was assessed using Kaplan-Meier survival analysis. The receiver operating characteristic curve (ROC) and decision curve analysis (DCA) were performed with the timeROC and ggDCA packages, respectively.

RESULTS

Preprocessing of RNA Sequencing Data and Clinical Data

The RNA sequencing and clinical data of HCC patients were downloaded from the TCGA GDC portal on April 30, 2021

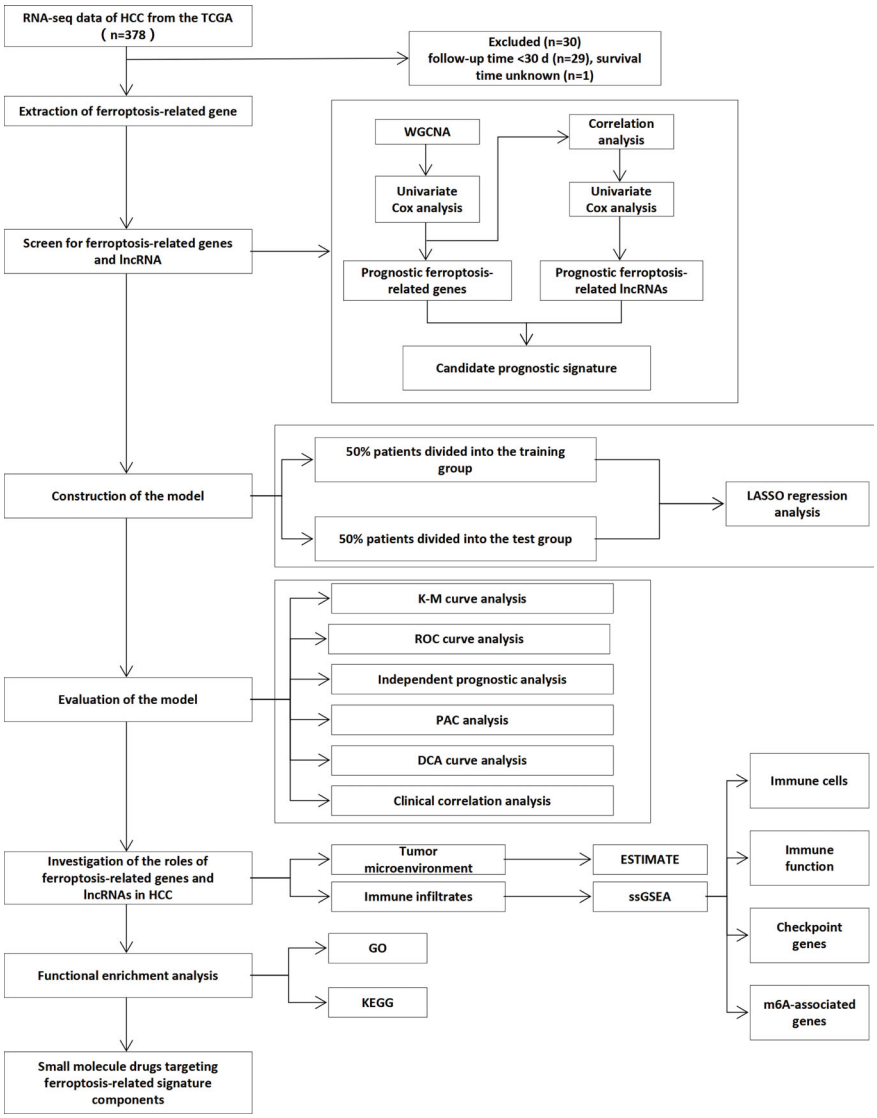

FIGURE 1 | Flowchart of overall study design.

(https://portal.gdc.cancer.gov/repository). After data curation, 30 cases were removed from the dataset (29 cases for survival time <30 d, 1 case for lack of survival information). The clinical data for 348 cases are listed in **Table 1**. A total of 267 ferroptosis-related genes were extracted from HCC patient datasets for further WGCNA.

Identification of Modules Associated With Survival Traits by WGCNA

The gene coexpression networks of the TCGA-LIHC dataset were established *via* the WGCNA package and are shown in **Figure 2**. To establish scale-free networks, the soft thresholding power was set to β=5 based on scale independence and mean connectivity (**Figures 2A, B**). The dynamic tree cut package was used to generate a gene cluster dendrogram containing 5 co-expression models (**Figure 2C**). The coexpression models are shown in blue, turquoise, brown, yellow and gray and contain 63, 110, 32, 28, and 15 genes, respectively (**Supplementary Table 2**). p <0.05 was considered to indicate a significant module-trait relationship between ferroptosis-related genes and vital status (**Figure 2D**). Based on these analyses, the blue, brown, yellow modules containing 123 genes were selected for further analysis.

Identification of Prognostic Ferroptosis-Related Genes and lncRNAs

According to the univariate Cox regression analysis, a total of 38 prognostic ferroptosis-related genes were screened. Then, by ferroptosis-related lncRNA co-expression analysis, we identified 526 ferroptosis-related lncRNAs (p <0.001, correlation coefficient >0.4). Univariate Cox regression analysis

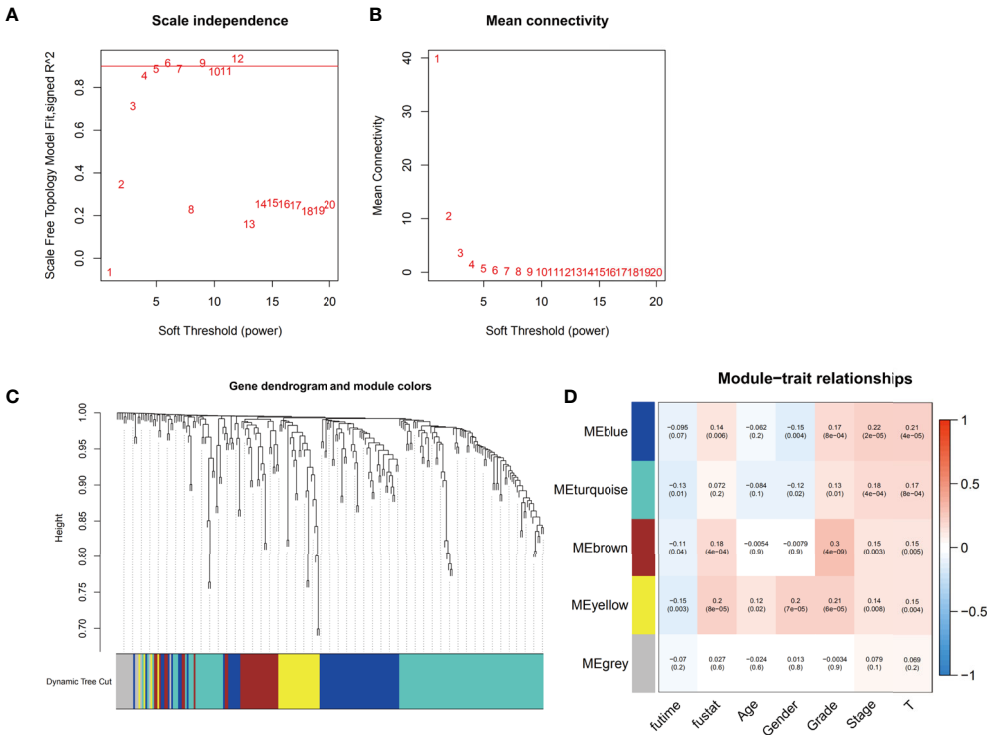

FIGURE 2 | Identification of the weighted gene coexpression network analysis (WGCNA) hub module and assessment of module-trait relationships. **(A, B)** Soft threshold selection to identify the WGCNA module. **(C)** The cluster dendrogram of 5 colored modules based on a dissimilarity measure (1-TOM) in HCC patients. **(D)** Correlation between the gene module and clinical traits, including survival time (futime), vital status (fustat), age, gender, grade, stage and T stage.

was further performed, and 70 prognostic ferroptosis-related lncRNAs were screened.

Construction and Validation of the LASSO-Cox Model

The prognostic ferroptosis-related genes and lncRNAs were merged and served as candidates for establishing the LASSO model (**Supplementary Table 3**). The HCC cohort was randomly divided into an equal training group and a test group. After the model reached the minimum lambda, a prognostic ferroptosis-related signature with 10 components was built (**Figures 3A, B**). In the training group, the median risk score classified patients into a high-risk group and a low-risk group and was calculated as follows: risk score = [expression level of AC245297.3×(0.003128)] + [expression level of MYLK-AS1×(0.086099)] + [expression level of NRAV×(0.061838)] + [expression level of SREBF2-AS1×(0.059227)] + [expression level of AL031985.3×(0.079650)]] + [expression level of ZFPM2-AS1×(0.028512)] + [expression level of AC015908.3×(-0.38804)] + [expression level of MSC-AS1×(0.161449)] + [expression level of SLC1A5×(0.023153)] + [expression level of SLC7A11×(0.090097)]. The correlations between ferroptosis-related genes and lncRNAs were used to construct a network, which was visualized in Cytoscape (**Figure 3C**). Among these, MSC-AS1, ZFPM2-AS1, NRAV and AL031985.3 have a co-expression relationship with more ferroptosis-related genes.

Prognostic Value of the Ferroptosis-Related Signature Model in the Training and Test Groups

Examination of the survival curves for the low-risk and high-risk patient groups was performed using the Kaplan-Meier method in both the training and test cohorts. The results from both cohorts showed that patients in the high-risk group had a statistically lower probability of survival ($p<0.001$ in both cohorts) (**Figures 4A, B**). The AUC for 1-year overall survival (OS) was 0.830 in the training cohort (**Figure 4C**) and 0.806 in the test cohort (**Figure 4D**).

The Ferroptosis-Related Signature is an Independent Prognostic Factor for HCC

Both univariate and multivariate analyses were performed to identify prognosis-related factors in the training group (**Figures 5A, B**). Stage, T stage and risk score were considered risk factors in the univariate analysis; however, only the risk score was an independent risk factor in the multivariate analysis. Therefore, the risk score calculated according to the 10-component ferroptosis-related signature was independently associated with the prognosis of patients (HR=3.038, 95% CI=2.023-4.563).

The distribution and status of OS were then analyzed by ranking the risk scores (**Figures 5C, D**). The results showed that patients with higher risk scores were more likely to be deceased.

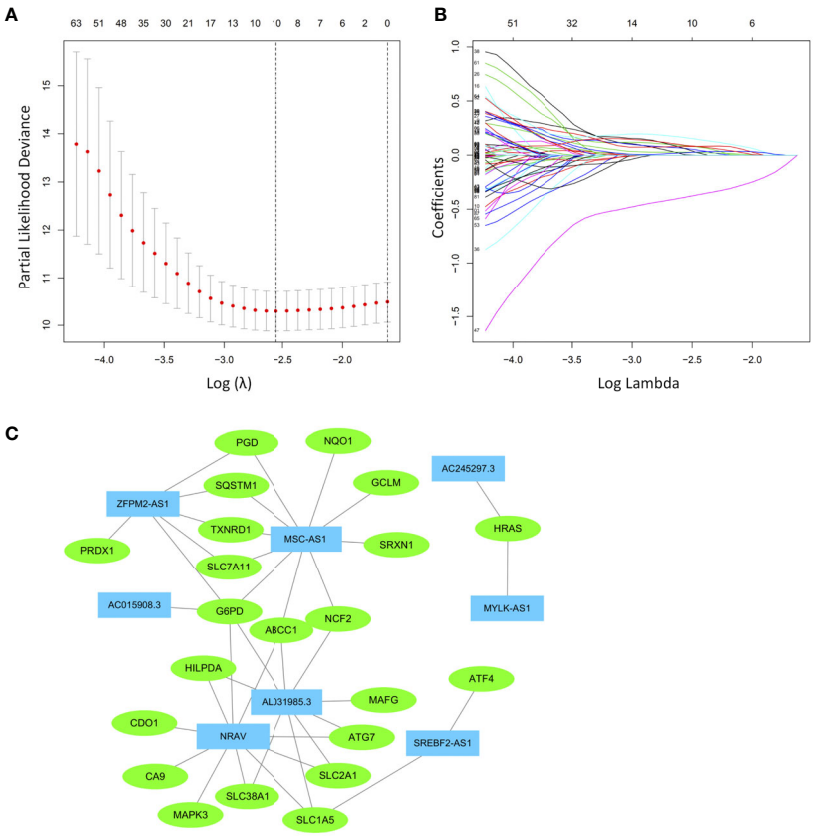

FIGURE 3 | Least absolute shrinkage and selection operator (LASSO) Cox regression analysis was conducted based on the ferroptosis-related signature. **(A)** LASSO coefficient profiles. **(B)** Candidate ferroptosis-related genes and lncRNAs from the univariate Cox regression analysis were filtered by the LASSO algorithm. **(C)** The network containing ferroptosis-related lncRNAs and mRNAs was visualized with Cytoscape. The green nodes indicate ferroptosis-related mRNAs, while the blue nodes indicate ferroptosis-related lncRNAs.

The differential expression profiles of the 10 ferroptosis-related signature are listed in the heatmap of **Figure 5E** between the low-risk group and the high-risk group. The principal component analysis (PCA) also proved that the ferroptosis-related signature prognostic model had the power to distinguish two separate subgroups of HCC patients (**Figure 5F**).

Verification of the Ferroptosis-Related Signature Model in the Testing Group

We next evaluated the prognostic efficiency of the ferroptosis-related signature by analyzing the data in the test cohort. Univariate and multivariate Cox regression analyses were performed to investigate the role of the ferroptosis-related signature in the prognosis of HCC patients (**Figures 6A, B**). Stage, T stage and risk score were risk factors in the univariate regression, and both T stage (HR=6.658, 95%CI=1.377-32.183) and risk score (HR=2.824, 95%CI=1.532-5.207) were further listed as risk factors in the multivariate regression. Similar to the results from the training group, the distribution and status of OS and the expression profiles of the risk-associated ferroptosis-related signature components were also analyzed by ranking the risk scores in the high-risk and low-risk HCC patient groups from the test cohort (**Figures 6C, D**). In addition, the expression trend of 10 ferroptosis-related signature components between the two groups was similar to that of the training group (**Figure 6E**). The PCA plot also showed that the HCC patients were divided into two subgroups by the ferroptosis-related signature model (**Figure 6F**). Overall, the accuracy of the ferroptosis-related signature model was confirmed in the independent validation liver cancer cohorts.

Evaluation of the Relationship Between Clinicopathological Characteristics and the Ferroptosis-Related Signature

To evaluate the differences between prediction methods, ROC curves were generated for the risk score and clinicopathological characteristics, as shown in **Figure 7A**. The AUC of the ferroptosis-related signature in HCC patients was higher than that of the clinical indexes (AUC=0.822, 1 year). DCA was performed and further showed that the risk score served as a better prognostic indicator than other variables in clinical decision-making (**Figure 7B**).

We next investigated the clinical and pathological features of the low-risk and high-risk groups. The heatmap in **Figure 7C**

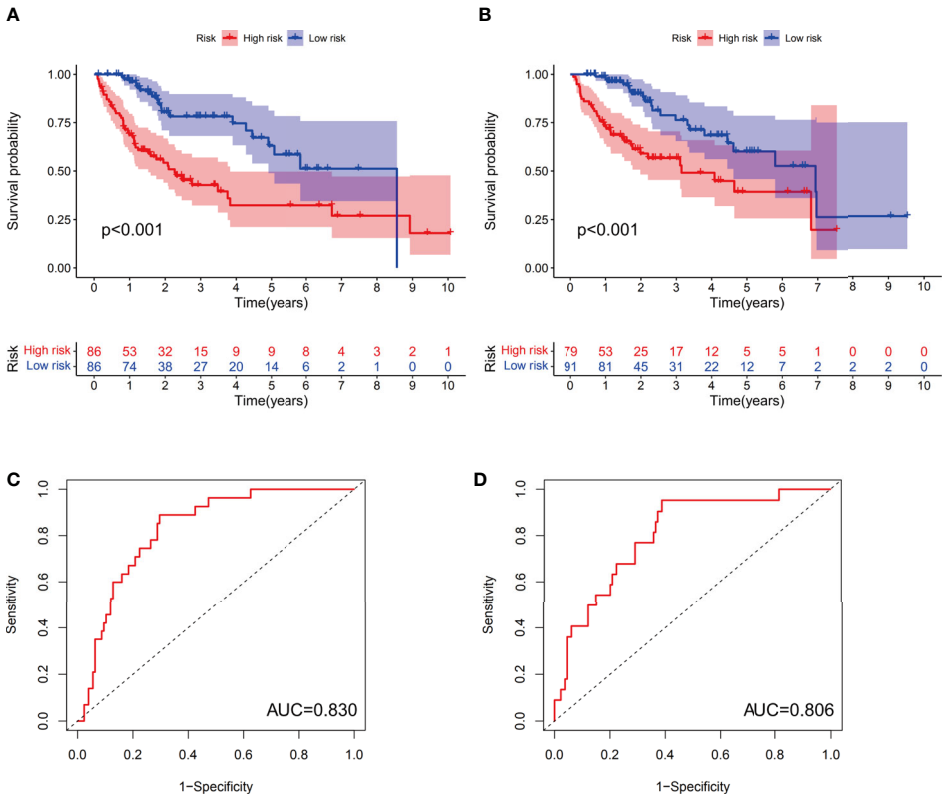

FIGURE 4 | The predictive value of the prognostic model in both the training and test groups. Kaplan-Meier curves were depicted based on the ferroptosis-related signature scores in the training group **(A)** and test group **(B)**. The receiver operating characteristic (ROC) curves of 1-year survival for HCC patients in the training group **(C)** and test group **(D)**.

shows the clinicopathological characteristics in both the high-risk and low-risk groups (grouped according to the ferroptosis-related signature score). The results showed a significant difference between the two groups with respect to HCC grade, stage, and T stage (all p<0.001).

Differential Immune Cell Infiltration and Function in the Low- and High-Risk Groups

Next, we investigated whether the expression of the ferroptosis-related signature components was associated with the TME. To determine the relationship between the proportion of immune and stromal components and the expression of ferroptosis-related signature components, the stromal score, immune score and ESTIMATE score were assessed in the low-risk and high-risk groups by using the ESTIMATE R package. The results showed no difference in stromal score (**Figure 8A**, p=0.23) but showed a significant difference in immune score (**Figure 8B**, p=0.0021) and ESTIMATE score (**Figure 8C**, p=0.01) between groups.

We next evaluated the relationship between immune infiltrates and the ferroptosis-related signature. The results showed activated dendritic cells (aDCs), immature dendritic cells (iDCs), macrophages, Th2 cells and Treg cells were distinct between high- and low-risk groups (all P <0.001). Besides, NK cells, plasmacytoid dendritic cells (pDCs) (both P <0.01), mast cells, T follicular helper (Tfh) cells, Th1 cells (all P <0.05) were also different in two groups (**Figure 9A**). Furtherly, almost all immune-related functions such as APC co-stimulation, APC co inhibition, CCR, and so on, were also different in the two groups (**Figure 9B**). In summary, the results from immune infiltration by ssGSEA showed that the immune status between low- and high-risk groups was totally different, which can be further elucidated to develop tumor immunotherapy in HCC.

Notably, the checkpoint pathway was significantly different between the low-risk and high-risk groups. Considering the clinical potential of checkpoint inhibition for immune therapy, we further explored the difference in the expression of immune checkpoints between the low- and high-risk groups. We observed a statistically significant difference between the two groups in terms of the expression of all checkpoint genes, most of which were more highly expressed in the high-risk group (**Figure 9C**). In addition, we investigated the expression of m6A-related genes between the low-risk group and the high-risk group, and the results showed that the expression of YTHDC1, FTO, YTHDF2, YTHDF1, WTAP, HNRNPC, METTL3, RBM15, and YTHDC2 in the high-risk group was obviously higher than that in the low-risk group (**Figure 9D**).

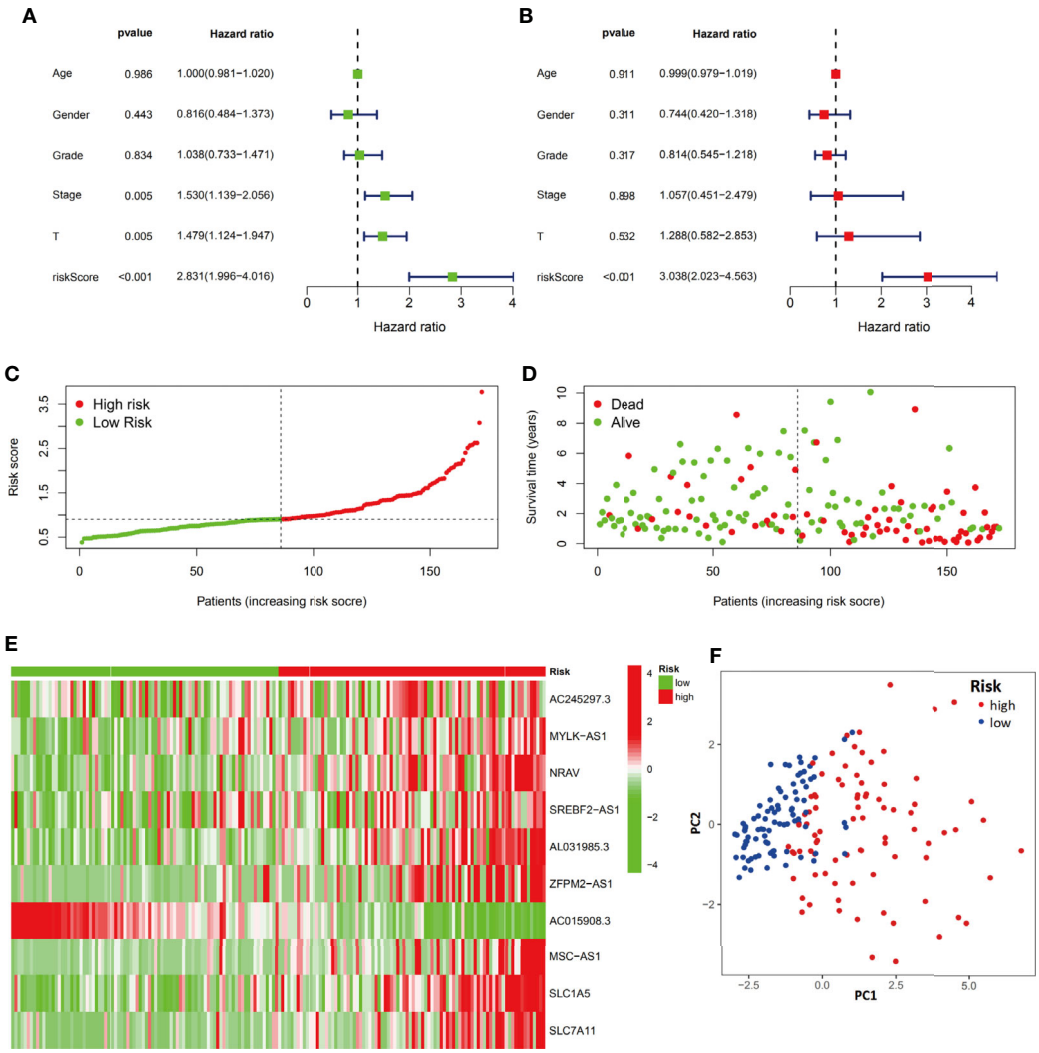

FIGURE 5 | Evaluation of the ferroptosis-related signature in the training group. Independent prognostic effects of the risk score model were assessed by univariate Cox regression analysis **(A)** and multivariate Cox regression analysis **(B)**. High- and low-risk group risk score rank **(C)**, survival status distribution **(D)**, expression of ferroptosis-related signature **(E)** and principal component analysis (PCA) plots **(F)**.

Functional Analysis

To investigate the biological functions and pathways associated with the risk score, the DEGs between the high-risk and low-risk groups were used to perform GO-BP enrichment and KEGG pathway analyses. Interestingly, the results showed that as many as 856 GO-BP terms and 63 KEGG pathways were identified between low- and high-risk groups (adj p<0.05, **Supplementary Table 4** and **Supplementary Table 5**), and the mainly enrichment results were listed in **Figure 10**. As expected, the DEGs were enriched in ferroptosis-associated pathways, such as the PI3K-Akt signaling pathway (31, 32), which is also one of the most frequently altered signaling pathways in human cancers (33–35). On the other hand, the DEGs were also obviously enriched in many immune-related biological processes, such as leukocyte migration, the humoral immune response and B cell-mediated immunity.

L1000FWD Analysis Identifies Candidate Compounds

To identify the potential drugs for HCC, we uploaded the upregulated and downregulated DEGs to the L1000FWD database. As a result, 10 significant candidate drugs were considered as potential drugs for HCC treatment. The mainly results were showed in **Table 2**. We can discover that these drugs were enriched in the glutamate receptor antagonist, HSP90 inhibitor, MEK inhibitor, c-Met inhibitor and so on. These mechanisms of action and potential small molecule drugs might provide reference for developing potential novel drugs targeting HCC. Among the highly correlated compounds, the structure of SIB-1893, geldanamycin, and PD-184352 were furtherly depicted in **Figure 11**. The 3D structure of geldanamycin isn't displayed since too many undefined stereocenters.

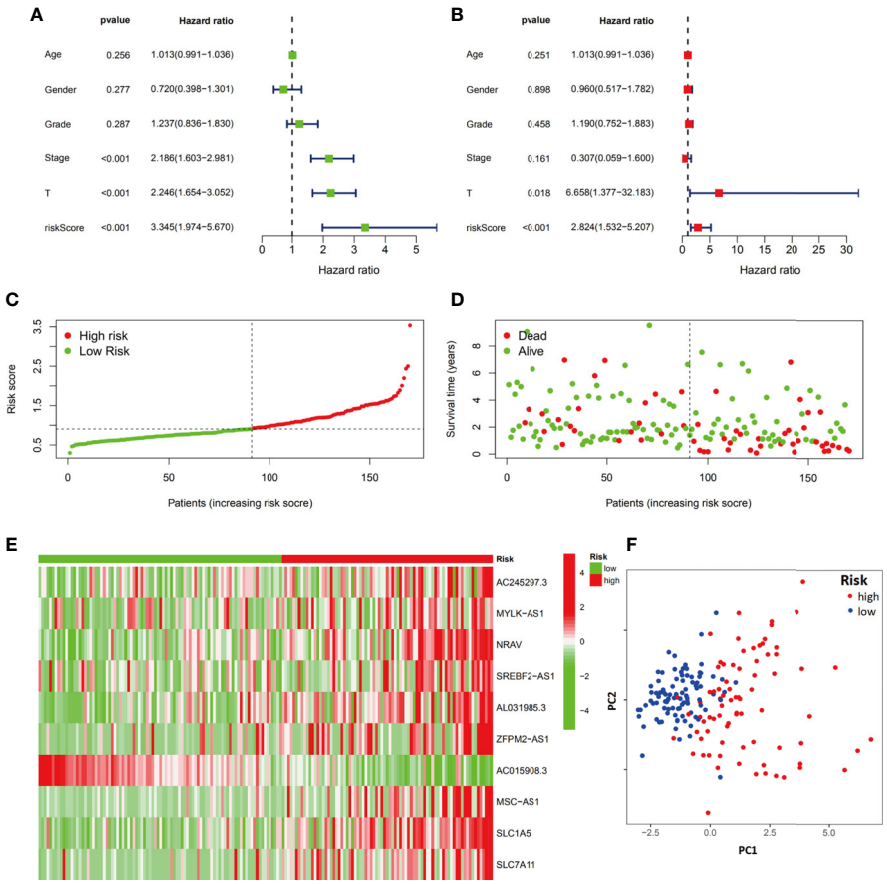

FIGURE 6 | Evaluation of the ferroptosis-related signature in the test group. The independent prognostic value of the risk score model was assessed by univariate Cox regression analysis **(A)** and multivariate Cox regression analysis **(B)**. Risk score rank **(C)**, survival status distribution **(D)**, ferroptosis-related signature component expression **(E)** and PCA plots **(F)** for the high- and low-risk groups.

DISCUSSION

In this study, we explored the role of the ferroptosis-related signature, which includes mRNAs and lncRNAs, in HCC. A prognostic model including 10 ferroptosis-related mRNAs/lncRNAs was first constructed and tested in the TCGA-LIHC dataset. Furthermore, immune analysis, including analysis with various bioinformatics tools, indicated obvious differences in the TME and immune cell infiltration between the low-risk and high-risk groups, especially in terms of checkpoint genes and m6A-associated genes. Functional analysis revealed that many tumor-related pathways were enriched. These findings strongly implied the great potential roles of ferroptosis in HCC.

The rapid progression of cancer is accompanied by the transformation and acceleration of a variety of metabolic pathways, which often means that a large number of metabolic byproducts, such as oxygen free radicals, accumulate in tumor cells to activate the oxidative stress pathway. Although tumor cells should have been vulnerable to ferroptosis, it has been found that cancer cells can acquire their resistance to ferroptosis through alteration of gene expression (36, 37). However, reactivation of the ferroptosis-related pathway in tumor cells may provide new therapeutic targets for tumor therapy. Although current therapeutic strategies, including surgical intervention, tumor-targeted drugs, immunotherapeutic agents or antiviral treatment, have improved OS in HCC patients in an inspiring way, their applications are still limited by tumor heterogeneity (38) and the development of drug resistance (39, 40).

The prognostic model in our study integrated 10 ferroptosis-related components, including 2 genes (SLC1A5 and SLC7A11) and 8 lncRNAs (AC245297.3, MYLK-AS1, NRAV, SREBF2-AS1, AL031985.3, ZFPM2-AS1, AC015908.3, MSC-AS1). Solute carrier family 1 member 5 (SLC1A5) is reported to be a driver gene of ferroptosis that mediates the uptake of glutamine, a conditionally essential amino acid in rapidly proliferating tumor cells (41, 42). In erastin- and RSL3-induced ferroptosis, glutamine importation and metabolism induce lipid ROS generation and promote cell death (43). Suppression of SLC1A5 by miR-137 or the small molecular inhibitor GPNA strongly inhibits glutaminolysis to cause ferroptotic cell death (44). As SLC1A5-mediated glutamine transport plays a key role in tumor cell metabolism, proliferation, and ferroptosis, blocking

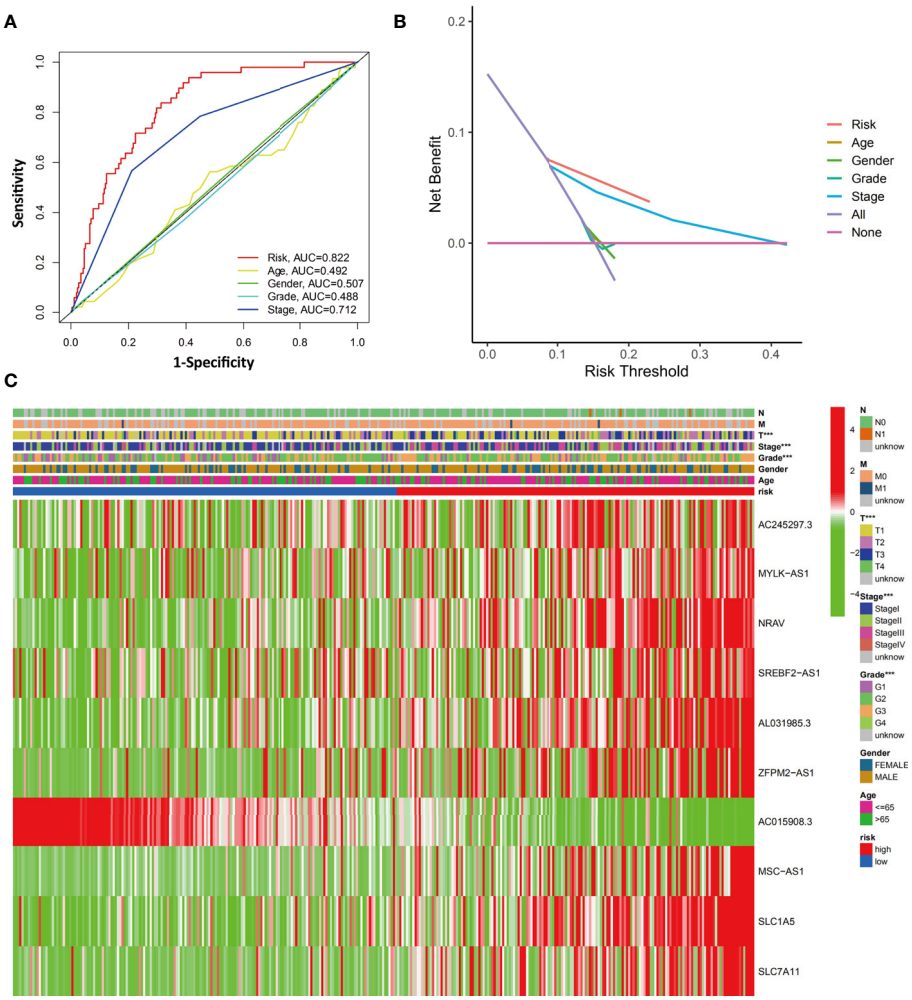

FIGURE 7 | Evaluation of the relationship between clinicopathological characteristics and the ferroptosis-related signature. **(A)** The AUC values of the risk factors and clinicopathological characteristics. **(B)** DCA of the risk factors and clinicopathological characteristics. **(C)** Heatmap of the ferroptosis-related lncRNA prognostic signature and clinicopathological features in HCC patients. ***p < 0.001.

SLC1A5 has been shown to successfully prevent tumor cell proliferation in melanoma (45), non-small-cell lung cancer (46, 47), prostate cancer (48) and acute myeloid leukemia (49). Solute carrier family 7 member 11 (SLC7A11) is a pivotal protein component of system Xc- that is responsible for maintaining redox homeostasis by importing cystine, where it is then reduced to cysteine and used to synthesize the major antioxidant GSH (50, 51). Numerous experiments have demonstrated its high expression in various cancers and multiple effects on cancer growth, invasion, metastasis and unfavorable prognosis (52–60). It has been demonstrated that SLC7A11 confers resistance to ferroptosis in cancer cells by importing cystine for the synthesis of GSH and indirectly relieving lipid ROS stress by activating the essential enzyme GPX4 to reduce lipid hydroperoxides (50, 61). Moreover, SLC7A11 has been demonstrated to be involved in the resistance to anticancer treatments, which was supported by experiments in which therapeutic resistance was reversed by directly targeting SLC7A11 (59, 60, 62–66). Therefore, targeting SLC7A11 exhibits good potential for the treatment of cancer, and several drugs targeting SLC7A11 are being prepared for clinical testing (54–58).

As the factor with the highest positive correlation coefficient in the prognostic model, lncRNA MSC-AS1 has been reported to be involved in HCC (67), lung adenocarcinoma (68), laryngeal cancer (69) and kidney renal clear cell carcinoma (70). It acts sponging miR-33b-5p to upregulate GPAM (68). Another study indicated that it activates the Wnt/β-catenin pathway to regulate tumor proliferation and migration *via* miR-3924/WNT5A (70). MYLK-AS1 was reported to be associated with tumor progression and angiogenesis in HCC. The mechanism involves targeting the miR-424-5p/E2F7 axis and activating the VEGFR-2 signaling pathway (71) or stimulating the EGFR/HER2-ERK1/2 signaling pathway (72). LncRNA NRAV has been reported to be involved in the antiviral immune response (73, 74). In addition, several independent bioinformatics analyses have demonstrated that it is a valuable clinical

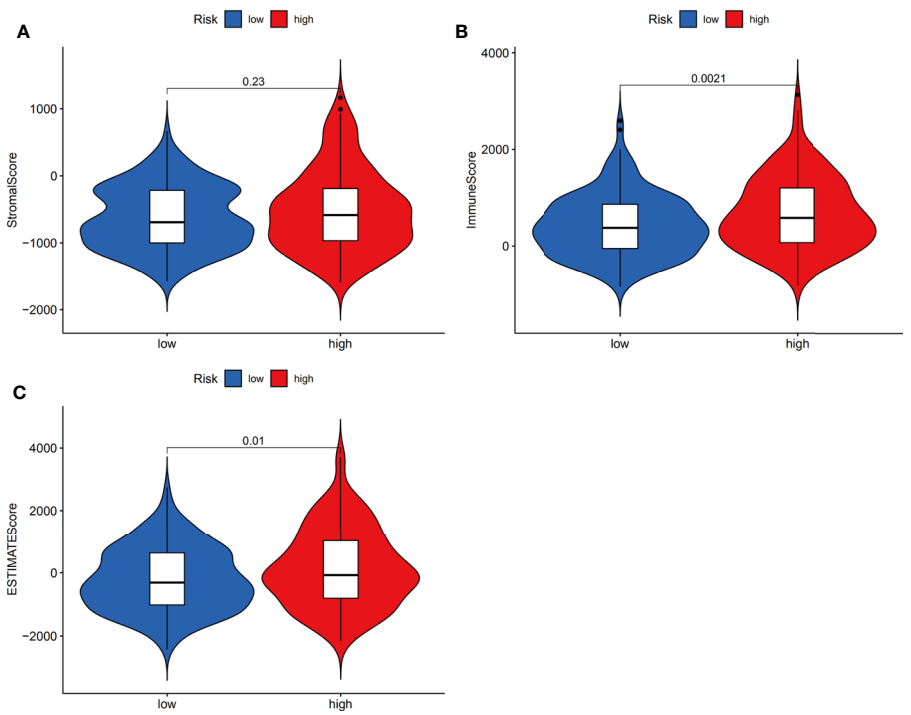

FIGURE 8 | Estimation of stromal and immune cells in malignant tumor tissues using expression data. Violin plots of tumor purity for the low- and high-risk groups according to the stromal score **(A)**, immune score **(B)** and ESTIMATE score **(C)**.

prognostic biomarker in HCC (75, 76) and lower-grade glioma (77). ZFPM2-AS1 is reported to be involved in numerous tumors, including lung adenocarcinoma (78), renal cell cancer (79), gastric carcinoma (80) and HCC (81). Mechanistically, it is reported to attenuate the p53 pathway by stabilizing MIF (80) or regulating miR-139/GDF10 (81).

Few studies have investigated lncRNA MSC-AS1, AL031985.3, and AC245297.3. However, they are indicated by different bioinformatics analyses to have prognostic value [MSC-AS1 (82, 83), AL031985.3 (84–86) in HCC, and AC245297.3 (87, 88) in breast cancer]. Therefore, these factors may be involved in multiple mechanisms in HCC and breast cancer, and their specific regulation mechanisms still further study. In particular, MSC-AS1 was the only protective lncRNA in the model and had a high correlation coefficient. There are no studies on lncRNA SREBF2-AS1 at present, so it needs further study. Notably, although several identified ferroptosis-related lncRNAs have not been well studied, in our study, the lncRNAs were closely co-expressed with many ferroptosis-related genes (**Figure 3C**).

The results from both immune infiltration analysis and enrichment analysis indicate that a higher level of APCs and humoral immunity including B cells and the complement system in the high-risk group. Besides, results from both difference in APC co-stimulation and co-inhibition appears contradictory in the immune microenvironment. However, we found the results are somewhat similar to the researches about ferroptosis-related signature in other cancers (6, 89–91). Though the mechanisms illustrating tumor susceptibility to ferroptosis have been an intense area of research in past decades, the complex relationship between tumor immunity and ferroptosis remains elusive. Tumor-infiltrating lymphocytic B cells (TIL-B) have been reported to be a main component of TILs in ovarian and breast cancers, which may be correlated with improved survival (92, 93). However, tumor development is enhanced when B cells are present have been reported in several mouse models (94, 95). For pancreatic carcinoma, several researches have demonstrated that TIL-Bs in supporting both early and more advanced stages of pancreatic tumorigenesis by multiple mechanisms, including suppression of other immune cells (e.g., CD8+ T cells and macrophages) in the tumor microenvironment and promoting pancreatic cancer cell proliferation (96).

Based on the DEGs between high- and low-risk groups, several small molecule drugs targeting ferroptosis-related signature components were identified *via* the L1000FWD database which was mainly enriched in the glutamate receptor antagonist, HSP90 inhibitor, MEK inhibitor and so on. As described above, glutamate metabolism was involved in the SLC1A5-induced ferroptosis, which may be inhibited by glutamate receptor antagonist, such as SIB-1893. HSP90-associated chaperone-mediated autophagy has been demonstrated to obviously promote ferroptosis (97, 98), which could be reduced by geldanamycin. The activation of the Raf-MEK-ERK pathway plays an important role in the proliferation, differentiation, invasion and metastasis of cancer cells (99). PD-184352 was the first MEK inhibitor to enter the clinical trial. It was terminated in phase II clinical trial because of its poor

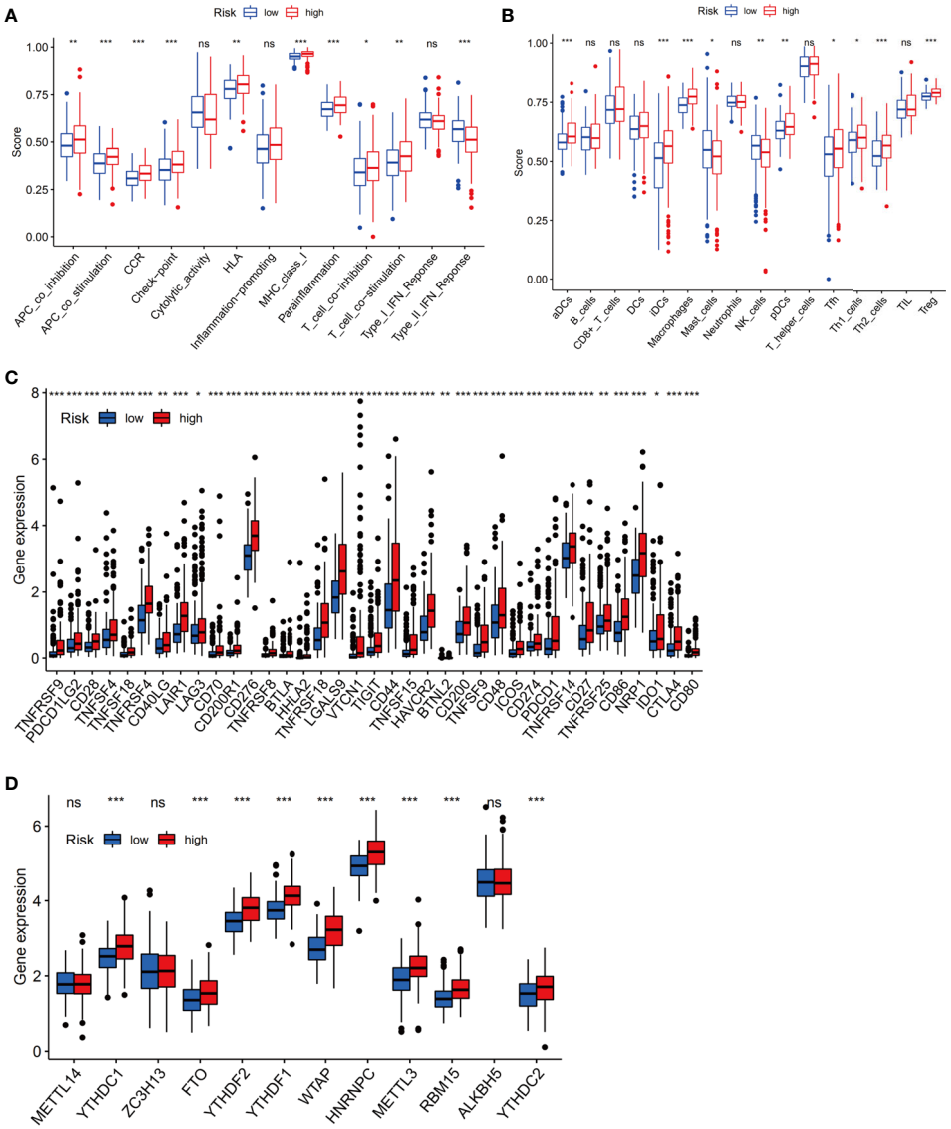

FIGURE 9 | The immune status difference between high-risk and low-risk HCC patients. **(A)** Comparison of immune cell abundance between the high-risk and low-risk groups of HCC patients. **(B)** Comparison of immune-related functions between the high-risk and low-risk groups of HCC patients. **(C)** Comparison of the expression of immune checkpoints between the high- and low-risk groups. **(D)** Comparison of the expression of m6A-associated genes between the high- and low-risk groups. *P < 0.05; **P < 0.01; ***P < 0.001. ns, no significance.

solubility, low oral bioavailability and large individual differences (100). Though the application of MEK inhibitor is limited by clinical efficacy and drug resistance, the development of novel MEK inhibitor is still one of the promising directions of anti-cancer treatment (101–103).

The model exhibited several advantages. 1) The prognostic model showed excellent performance in the ROC curve analysis, with AUCs as high as 0.830 and 0.806 in the training and test groups, respectively. As depicted in the DCA, the ferroptosis-related signature had better predictive value than all pathological characteristics. The risk score was identified as an independent risk factor, with HR=3.038 in the training group and 2.824 in the test group. Therefore, the model showed excellent clinical prognostic value. 2) According to the risk score from the model, the HCC patients were divided into two distinct groups. Analysis of the TME and immune infiltration showed that there were numerous variables with statistically significant differences between the two groups, especially the expression of checkpoint genes. These differences were consistent with the differences observed in the GO and KEGG analysis. Therefore, immunotherapies targeting the 10 components of the ferroptosis-related signature are promising methods for anti-tumor treatment. 3) Considering that there are frequent updates in the field of ferroptosis research, a large number of studies and ferroptosis-related databases were assessed (12, 13, 28–30). As many as 267 candidate ferroptosis-related genes were included in

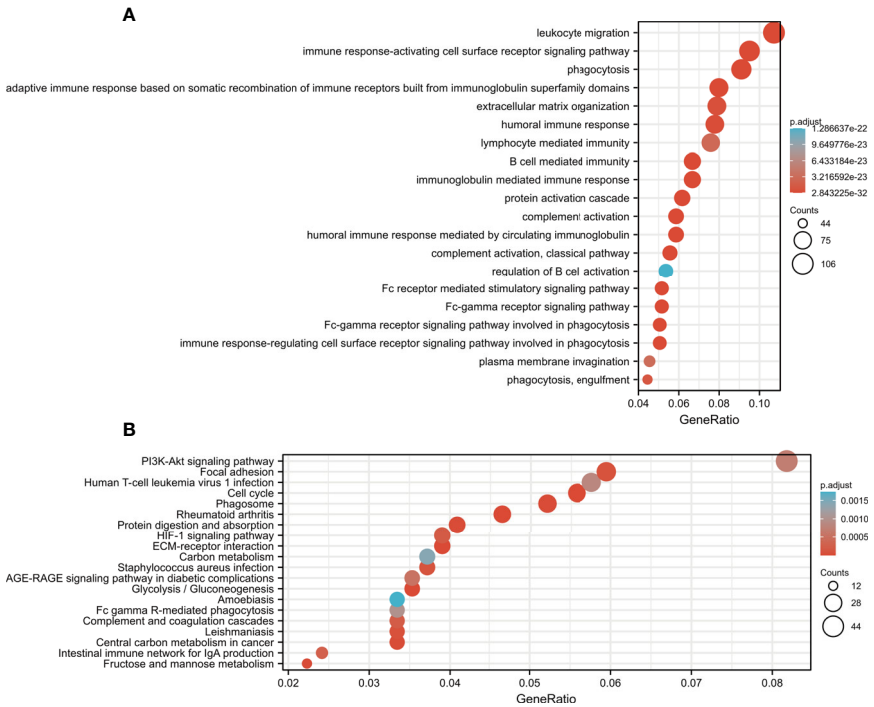

FIGURE 10 | Functional enrichment analysis of the ferroptosis-related signature. **(A)** GO-BP analysis. **(B)** KEGG analysis.

TABLE 2 | The mainly potential drugs identified by L1000FWD database.

Rank	Drug	Similarity Score	p-value	q-value	Z-score	Combined Score	MOA
1	SIB-1893	-0.0763	4.29E-20	2.59E-17	1.67	-32.29	glutamate receptor antagonist
2	geldanamycin	-0.0671	2.45E-16	7.08E-14	1.62	-25.31	HSP inhibitor
3	PD-184352	-0.0624	4.33E-15	9.56E-13	1.75	-25.2	MEK inhibitor
4	PF-04217903	-0.0509	3.27E-09	0.000000191	1.77	-15.06	c-Met inhibitor
5	PD-0325901	-0.0509	2.55E-09	0.000000154	1.68	-14.47	MEK inhibitor
6	FCCP	-0.0486	0.000000042	0.00000183	1.64	-12.06	Unknown
7	PD-198306	-0.0474	3.88E-08	0.00000171	1.68	-12.42	MAP kinase inhibitor, MEK inhibitor
8	BI-2536	-0.0474	0,000000161	0.00000612	1.74	-11.84	PLK inhibitor
9	PAROXETINE	-0.0462	0,000000554	0.0000179	1.63	-10.21	selective serotonin reuptake inhibitor (SSRI)
10	BRD-A66861218	-0.0462	0,000000199	0.00000733	1.76	-11.82	anti-inflammatory agent

the analysis. To our knowledge, this is the largest ferroptosis-related gene list used for bioinformatics analysis at present.

There are also some limitations to this study. Due to the limited knowledge of ferroptosis, most of the signature components in our research are involved not only in ferroptosis-related pathways but also in other pathways, such as immunity and autophagy. This may be more common for lncRNAs, which have nonspecific functions in biological processes. Therefore, it is difficult to evaluate the exact role of ferroptosis alone in HCC with our risk score. These results should be further validated in external HCC cohorts from multicenter research. In another attempt to investigate the role of ferroptosis-related in other cancers, we performed the survival analysis of SLC7A11, MSC-AS1 and MYLK-AS1 in gastrointestinal cancer including colon cancer, esophageal cancer, liver cancer, pancreatic cancer and stomach cancer (**Supplementary Figure**). Most of results showed that they are only play a specific role in liver cancer.

In conclusion, our research established a 10-component ferroptosis-related signature including mRNAs and lncRNAs for predicting the prognosis of HCC patients. The ferroptosis-related signature showed excellent performance in predicting clinical prognosis. The signature can be used to calculate the risk score, which accurately reflects the tumor environment and immune filtration of patients, thereby providing a reference for clinical treatment. Therefore, the ferroptosis-related signature is expected to be a new biomarker for both diagnosis and treatment decision making. Further investigation of the role and mechanism of the 10-component ferroptosis-related signature in the progression of HCC is still needed.

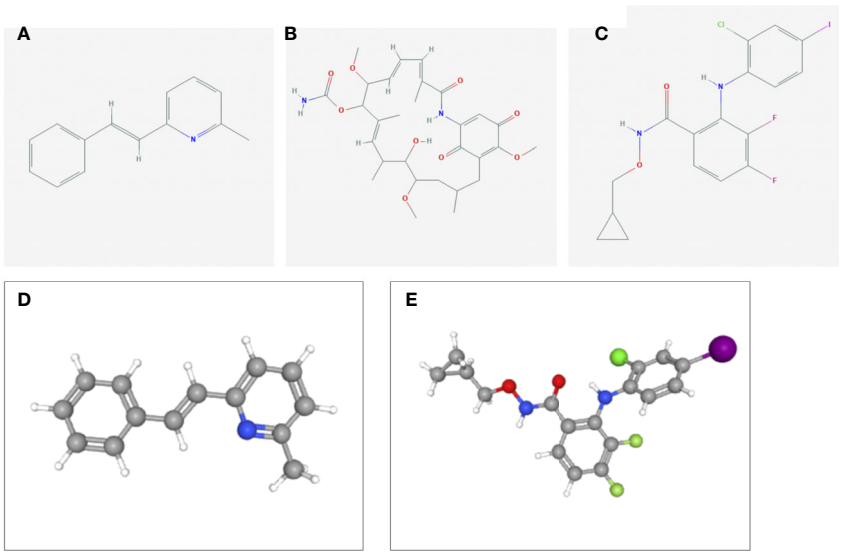

FIGURE 11 | The structure of screened small-molecule compounds. The DEGs were uploaded to L1000FWD website to screen the potential small molecule compounds. The top three compounds were visualized by Pubchem website. **(A)** The 2D structure of SIB-1893; **(B)** The 2D structure of geldanamycin; **(C)** The 2D structure of PD-184352; **(D)** The 3D structure of SIB-1893; **(E)** The 3D structure of PD-184352. The 3D structure of geldanamycin isn't displayed since too many undefined stereo centers.

DATA AVAILABILITY STATEMENT

The original contributions presented in the study are included in the article/**Supplementary Material**. Further inquiries can be directed to the corresponding authors.

AUTHOR CONTRIBUTIONS

Z-AC collected the papers and analyzed data, analyzed the conclusions, and drafted the manuscript. HT reviewed the data and conclusions. D-MY and YZ contributed to writing. C-JY and Z-JF presented the idea of this manuscript, supported the funding, analyzed the conclusions, drafted and revised the manuscript. All authors contributed to the article and approved the submitted version.

FUNDING

This study was funded by the Natural Science Foundation of Hebei Province (Grant No. H2020206337).

SUPPLEMENTARY MATERIAL

The Supplementary Material for this article can be found online at: https://www.frontiersin.org/articles/10.3389/fonc.2021.738477/full#supplementary-material

REFERENCES

1. Bray F, Ferlay J, Soerjomataram I, Siegel RL, Torre LA, Jemal A. Global Cancer Statistics 2018: GLOBOCAN Estimates of Incidence and Mortality Worldwide for 36 Cancers in 185 Countries. *CA Cancer J Clin* (2018) 68 (6):394–424. doi: 10.3322/caac.21492
2. Chimed T, Sandagdorj T, Znaor A, Laversanne M, Tseveen B, Genden P, et al. Cancer Incidence and Cancer Control in Mongolia: Results From the National Cancer Registry 2008-12. *Int J Cancer* (2017) 140(2):302–9. doi: 10.1002/ijc.30463
3. Dixon SJ, Lemberg KM, Lamprecht MR, Skouta R, Zaitsev EM, Gleason CE, et al. Ferroptosis: An Iron-Dependent Form of Nonapoptotic Cell Death. *Cell* (2012) 149(5):1060–72. doi: 10.1016/j.cell.2012.03.042
4. Kaplan GG, Ng SC. Understanding and Preventing the Global Increase of Inflammatory Bowel Disease. *Gastroenterology* (2017) 152(2):313–21.e2. doi: 10.1053/j.gastro.2016.10.020
5. Wang D, Wei G, Ma J, Cheng S, Jia L, Song X, et al. Identification of the Prognostic Value of Ferroptosis-Related Gene Signature in Breast Cancer Patients. *BMC Cancer* (2021) 21(1):645. doi: 10.1186/s12885-021-08341-2
6. Li H, Li L, Xue C, Huang R, Hu A, An X, et al. A Novel Ferroptosis-Related Gene Signature Predicts Overall Survival of Breast Cancer Patients. *Biol (Basel)* (2021) 10(2):151. doi: 10.3390/biology10020151
7. Tang R, Hua J, Xu J, Liang C, Meng Q, Liu J, et al. The Role of Ferroptosis Regulators in the Prognosis, Immune Activity and Gemcitabine Resistance of Pancreatic Cancer. *Ann Transl Med* (2020) 8(21):1347. doi: 10.21037/atm-20-2554a
8. Ye Y, Dai Q, Li S, He J, Qi H. A Novel Defined Risk Signature of the Ferroptosis-Related Genes for Predicting the Prognosis of Ovarian Cancer. *Front Mol Biosci* (2021) 8:645845. doi: 10.3389/fmolb.2021.645845
9. Deng T, Hu B, Jin C, Tong Y, Zhao J, Shi Z, et al. A Novel Ferroptosis Phenotype-Related Clinical-Molecular Prognostic Signature for

Hepatocellular Carcinoma. *J Cell Mol Med* (2021) 25(14):6618–33. doi: 10.1111/jcmm.16666
10. Shan Y, Yang G, Huang H, Zhou Y, Hu X, Lu Q, et al. Ubiquitin-Like Modifier Activating Enzyme 1 as a Novel Diagnostic and Prognostic Indicator That Correlates With Ferroptosis and the Malignant Phenotypes of Liver Cancer Cells. *Front Oncol* (2020) 10:592413. doi: 10.3389/fonc.2020.592413
11. Liu Y, Zhang X, Zhang J, Tan J, Li J, Song Z. Development and Validation of a Combined Ferroptosis and Immune Prognostic Classifier for Hepatocellular Carcinoma. *Front Cell Dev Biol* (2020) 8:596679. doi: 10.3389/fcell.2020.596679
12. Liang JY, Wang DS, Lin HC, Chen XX, Yang H, Zheng Y, et al. A Novel Ferroptosis-Related Gene Signature for Overall Survival Prediction in Patients With Hepatocellular Carcinoma. *Int J Biol Sci* (2020) 16 (13):2430–41. doi: 10.7150/ijbs.45050
13. Hassannia B, Vandenabeele P, Vanden Berghe T. Targeting Ferroptosis to Iron Out Cancer. *Cancer Cell* (2019) 35(6):830–49. doi: 10.1016/j.ccell.2019.04.002
14. Liang C, Zhang X, Yang M, Dong X. Recent Progress in Ferroptosis Inducers for Cancer Therapy. *Adv Mater* (2019) 31(51):e1904197. doi: 10.1002/adma.201904197
15. Mbaveng AT, Ndontsa BL, Kuete V, Nguekeu Y, Çelik İ, Mbouangouere R, et al. A Naturally Occuring Triterpene Saponin Ardisiacrispin B Displayed Cytotoxic Effects in Multi-Factorial Drug Resistant Cancer Cells *via* Ferroptotic and Apoptotic Cell Death. *Phytomedicine* (2018) 43:78–85. doi: 10.1016/j.phymed.2018.03.035
16. Mbaveng AT, Fotso GW, Ngnintedo D, Kuete V, Ngadjui BT, Keumedjio F, et al. Cytotoxicity of Epunctanone and Four Other Phytochemicals Isolated From the Medicinal Plants Garcinia Epunctata and Ptycholobium Contortum Towards Multi-Factorial Drug Resistant Cancer Cells. *Phytomedicine* (2018) 48:112–9. doi: 10.1016/j.phymed.2017.12.016
17. Yuan H, Li X, Zhang X, Kang R, Tang D. CISD1 Inhibits Ferroptosis by Protection Against Mitochondrial Lipid Peroxidation. *Biochem Biophys Res Commun* (2016) 478(2):838–44. doi: 10.1016/j.bbrc.2016.08.034
18. Jennis M, Kung CP, Basu S, Budina-Kolomets A, Leu JI, Khaku S, et al. An African-Specific Polymorphism in the TP53 Gene Impairs P53 Tumor Suppressor Function in a Mouse Model. *Genes Dev* (2016) 30(8):918–30. doi: 10.1101/gad.275891.115
19. Louandre C, Marcq I, Bouhlal H, Lachaier E, Godin C, Saidak Z, et al. The Retinoblastoma (Rb) Protein Regulates Ferroptosis Induced by Sorafenib in Human Hepatocellular Carcinoma Cells. *Cancer Lett* (2015) 356(2 Pt B):971–7. doi: 10.1016/j.canlet.2014.11.014
20. Sun X, Ou Z, Chen R, Niu X, Chen D, Kang R, et al. Activation of the P62-Keap1-NRF2 Pathway Protects Against Ferroptosis in Hepatocellular Carcinoma Cells. *Hepatology* (2016) 63(1):173–84. doi: 10.1002/hep.28251
21. Sun X, Niu X, Chen R, He W, Chen D, Kang R, et al. Metallothionein-1g Facilitates Sorafenib Resistance Through Inhibition of Ferroptosis. *Hepatology* (2016) 64(2):488–500. doi: 10.1002/hep.28574
22. Kung JT, Colognori D, Lee JT. Long Noncoding RNAs: Past, Present, and Future. *Genetics* (2013) 193(3):651–69. doi: 10.1534/genetics.112.146704
23. Yoon JH, Abdelmohsen K, Gorospe M. Posttranscriptional Gene Regulation by Long Noncoding RNA. *J Mol Biol* (2013) 425(19):3723–30. doi: 10.1016/j.jmb.2012.11.024
24. Bhan A, Soleimani M, Mandal SS. Long Noncoding RNA and Cancer: A New Paradigm. *Cancer Res* (2017) 77(15):3965–81. doi: 10.1158/0008-5472.CAN-16-2634
25. Huarte M. The Emerging Role of lncRNAs in Cancer. *Nat Med* (2015) 21 (11):1253–61. doi: 10.1038/nm.3981
26. Denaro N, Merlano MC, Lo Nigro C. Long Noncoding RNAs as Regulators of Cancer Immunity. *Mol Oncol* (2019) 13(1):61–73. doi: 10.1002/1878-0261.12413
27. Liang J, Zhi Y, Deng W, Zhou W, Li X, Cai Z, et al. Development and Validation of Ferroptosis-Related lncRNAs Signature for Hepatocellular Carcinoma. *PeerJ* (2021) 9:e11627. doi: 10.7717/peerj.11627
28. Stockwell BR, Friedmann Angeli JP, Bayir H, Bush AI, Conrad M, Dixon SJ, et al. Ferroptosis: A Regulated Cell Death Nexus Linking Metabolism, Redox Biology, and Disease. *Cell* (2017) 171(2):273–85. doi: 10.1016/j.cell.2017.09.021
29. Bersuker K, Hendricks JM, Li Z, Magtanong L, Ford B, Tang PH, et al. The CoQ Oxidoreductase FSP1 Acts Parallel to GPX4 to Inhibit Ferroptosis. *Nature* (2019) 575(7784):688–92. doi: 10.1038/s41586-019-1705-2
30. Doll S, Freitas FP, Shah R, Aldrovandi M, da Silva MC, Ingold I, et al. FSP1 Is a Glutathione-Independent Ferroptosis Suppressor. *Nature* (2019) 575 (7784):693–8. doi: 10.1038/s41586-019-1707-0
31. Liu L, Yang S, Wang H. α-Lipoic Acid Alleviates Ferroptosis in the MPP(+) -Induced PC12 Cells *via* Activating the PI3K/Akt/Nrf2 Pathway. *Cell Biol Int* (2021) 45(2):422–31. doi: 10.1002/cbin.11505
32. Yi J, Zhu J, Wu J, Thompson CB, Jiang X. Oncogenic Activation of PI3K-AKT-mTOR Signaling Suppresses Ferroptosis *via* SREBP-Mediated Lipogenesis. *Proc Natl Acad Sci USA* (2020) 117(49):31189–97. doi: 10.1073/pnas.2017152117
33. Fruman DA, Chiu H, Hopkins BD, Bagrodia S, Cantley LC, Abraham RT. The PI3K Pathway in Human Disease. *Cell* (2017) 170(4):605–35. doi: 10.1016/j.cell.2017.07.029
34. Saxton RA, Sabatini DM. mTOR Signaling in Growth, Metabolism, and Disease. *Cell* (2017) 168(6):960–76. doi: 10.1016/j.cell.2017.02.004
35. Zhang Y, Kwok-Shing Ng P, Kucherlapati M, Chen F, Liu Y, Tsang YH, et al. A Pan-Cancer Proteogenomic Atlas of PI3K/AKT/mTOR Pathway Alterations. *Cancer Cell* (2017) 31(6):820–32.e3. doi: 10.1016/j.ccell.2017.04.013
36. Friedmann Angeli JP, Krysko DV, Conrad M. Ferroptosis at the Crossroads of Cancer-Acquired Drug Resistance and Immune Evasion. *Nat Rev Cancer* (2019) 19(7):405–14. doi: 10.1038/s41568-019-0149-1
37. Mou Y, Wang J, Wu J, He D, Zhang C, Duan C, et al. Ferroptosis, a New Form of Cell Death: Opportunities and Challenges in Cancer. *J Hematol Oncol* (2019) 12(1):34. doi: 10.1186/s13045-019-0720-y
38. Gao Q, Wang XY, Zhou J, Fan J. Multiple Carcinogenesis Contributes to the Heterogeneity of HCC. *Nat Rev Gastroenterol Hepatol* (2015) 12(1):13. doi: 10.1038/nrgastro.2014.6-c1
39. Parikh ND, Singal AG, Hutton DW. Cost Effectiveness of Regorafenib as Second-Line Therapy for Patients With Advanced Hepatocellular Carcinoma. *Cancer* (2017) 123(19):3725–31. doi: 10.1002/cncr.30863
40. Nakagawa S, Wei L, Song WM, Higashi T, Ghoshal S, Kim RS, et al. Molecular Liver Cancer Prevention in Cirrhosis by Organ Transcriptome Analysis and Lysophosphatidic Acid Pathway Inhibition. *Cancer Cell* (2016) 30(6):879–90. doi: 10.1016/j.ccell.2016.11.004
41. Kanai Y, Clémençon B, Simonin A, Leuenberger M, Lochner M, Weisstanner M, et al. The SLC1 High-Affinity Glutamate and Neutral Amino Acid Transporter Family. *Mol Aspects Med* (2013) 34(2-3):108–20. doi: 10.1016/j.mam.2013.01.001
42. Cao JY, Dixon SJ. Mechanisms of Ferroptosis. *Cell Mol Life Sci* (2016) 73(11-12):2195–209. doi: 10.1007/s00018-016-2194-1
43. Gao M, Monian P, Quadri N, Ramasamy R, Jiang X. Glutaminolysis and Transferrin Regulate Ferroptosis. *Mol Cell* (2015) 59(2):298–308. doi: 10.1016/j.molcel.2015.06.011
44. Luo M, Wu L, Zhang K, Wang H, Zhang T, Gutierrez L, et al. miR-137 Regulates Ferroptosis by Targeting Glutamine Transporter SLC1A5 in Melanoma. *Cell Death Differ* (2018) 25(8):1457–72. doi: 10.1038/s41418-017-0053-8
45. Wang Q, Beaumont KA, Otte NJ, Font J, Bailey CG, van Geldermalsen M, et al. Targeting Glutamine Transport to Suppress Melanoma Cell Growth. *Int J Cancer* (2014) 135(5):1060–71. doi: 10.1002/ijc.28749
46. Hassanein M, Hoeksema MD, Shiota M, Qian J, Harris BK, Chen H, et al. SLC1A5 Mediates Glutamine Transport Required for Lung Cancer Cell Growth and Survival. *Clin Cancer Res* (2013) 19(3):560–70. doi: 10.1158/1078-0432.CCR-12-2334
47. Hassanein M, Qian J, Hoeksema MD, Wang J, Jacobovitz M, Ji X, et al. Targeting SLC1a5-Mediated Glutamine Dependence in Non-Small Cell Lung Cancer. *Int J Cancer* (2015) 137(7):1587–97. doi: 10.1002/ijc.29535
48. Wang Q, Hardie RA, Hoy AJ, van Geldermalsen M, Gao D, Fazli L, et al. Targeting ASCT2-Mediated Glutamine Uptake Blocks Prostate Cancer Growth and Tumour Development. *J Pathol* (2015) 236(3):278–89. doi: 10.1002/path.4518
49. Willems L, Jacque N, Jacquel A, Neveux N, Maciel TT, Lambert M, et al. Inhibiting Glutamine Uptake Represents an Attractive New Strategy for Treating Acute Myeloid Leukemia. *Blood* (2013) 122(20):3521–32. doi: 10.1182/blood-2013-03-493163

50. Lin W, Wang C, Liu G, Bi C, Wang X, Zhou Q, et al. SLC7A11/xCT in Cancer: Biological Functions and Therapeutic Implications. *Am J Cancer Res* (2020) 10(10):3106–26.
51. Shin CS, Mishra P, Watrous JD, Carelli V, D'Aurelio M, Jain M, et al. The Glutamate/Cystine xCT Antiporter Antagonizes Glutamine Metabolism and Reduces Nutrient Flexibility. *Nat Commun* (2017) 8:15074. doi: 10.1038/ncomms15074
52. Sugano K, Maeda K, Ohtani H, Nagahara H, Shibutani M, Hirakawa K. Expression of xCT as a Predictor of Disease Recurrence in Patients With Colorectal Cancer. *Anticancer Res* (2015) 35(2):677–82.
53. Zhang L, Huang Y, Ling J, Zhuo W, Yu Z, Luo Y, et al. Overexpression of SLC7A11: A Novel Oncogene and an Indicator of Unfavorable Prognosis for Liver Carcinoma. *Future Oncol* (2018) 14(10):927–36. doi: 10.2217/fon-2017-0540
54. Ye J, Jiang X, Dong Z, Hu S, Xiao M. Low-Concentration PTX And RSL3 Inhibits Tumor Cell Growth Synergistically By Inducing Ferroptosis In Mutant P53 Hypopharyngeal Squamous Carcinoma. *Cancer Manag Res* (2019) 11:9783–92. doi: 10.2147/CMAR.S217944
55. Hu K, Li K, Lv J, Feng J, Chen J, Wu H, et al. Suppression of the SLC7A11/glutathione Axis Causes Synthetic Lethality in KRAS-Mutant Lung Adenocarcinoma. *J Clin Invest* (2020) 130(4):1752–66. doi: 10.1172/JCI124049
56. Lachaier E, Louandre C, Godin C, Saidak Z, Baert M, Diouf M, et al. Sorafenib Induces Ferroptosis in Human Cancer Cell Lines Originating From Different Solid Tumors. *Anticancer Res* (2014) 34(11):6417–22.
57. Dolma S, Lessnick SL, Hahn WC, Stockwell BR. Identification of Genotype-Selective Antitumor Agents Using Synthetic Lethal Chemical Screening in Engineered Human Tumor Cells. *Cancer Cell* (2003) 3(3):285–96. doi: 10.1016/s1535-6108(03)00050-3
58. Ogihara K, Kikuchi E, Okazaki S, Hagiwara M, Takeda T, Matsumoto K, et al. Sulfasalazine Could Modulate the CD44v9-xCT System and Enhance Cisplatin-Induced Cytotoxic Effects in Metastatic Bladder Cancer. *Cancer Sci* (2019) 110(4):1431–41. doi: 10.1111/cas.13960
59. Lanzardo S, Conti L, Rooke R, Ruiu R, Accart N, Bolli E, et al. Immunotargeting of Antigen xCT Attenuates Stem-Like Cell Behavior and Metastatic Progression in Breast Cancer. *Cancer Res* (2016) 76(1):62–72. doi: 10.1158/0008-5472.CAN-15-1208
60. Roh JL, Kim EH, Jang HJ, Park JY, Shin D. Induction of Ferroptotic Cell Death for Overcoming Cisplatin Resistance of Head and Neck Cancer. *Cancer Lett* (2016) 381(1):96–103. doi: 10.1016/j.canlet.2016.07.035
61. Xie Y, Hou W, Song X, Yu Y, Huang J, Sun X, et al. Ferroptosis: Process and Function. *Cell Death Differ* (2016) 23(3):369–79. doi: 10.1038/cdd.2015.158
62. Wang L, Leite de Oliveira R, Huijberts S, Bosdriesz E, Pencheva N, Brunen D, et al. An Acquired Vulnerability of Drug-Resistant Melanoma With Therapeutic Potential. *Cell* (2018) 173(6):1413–25.e14. doi: 10.1016/j.cell.2018.04.012
63. Wada F, Koga H, Akiba J, Niizeki T, Iwamoto H, Ikezono Y, et al. High Expression of CD44v9 and xCT in Chemoresistant Hepatocellular Carcinoma: Potential Targets by Sulfasalazine. *Cancer Sci* (2018) 109(9):2801–10. doi: 10.1111/cas.13728
64. Horibe S, Kawauchi S, Tanahashi T, Sasaki N, Mizuno S, Rikitake Y. CD44v-Dependent Upregulation of xCT Is Involved in the Acquisition of Cisplatin-Resistance in Human Lung Cancer A549 Cells. *Biochem Biophys Res Commun* (2018) 507(1-4):426–32. doi: 10.1016/j.bbrc.2018.11.055
65. Drayton RM, Dudziec E, Peter S, Bertz S, Hartmann A, Bryant HE, et al. Reduced Expression of miRNA-27a Modulates Cisplatin Resistance in Bladder Cancer by Targeting the Cystine/Glutamate Exchanger Slc7a11. *Clin Cancer Res* (2014) 20(7):1990–2000. doi: 10.1158/1078-0432.CCR-13-2805
66. Miyoshi S, Tsugawa H, Matsuzaki J, Hirata K, Mori H, Saya H, et al. Inhibiting xCT Improves 5-Fluorouracil Resistance of Gastric Cancer Induced by CD44 Variant 9 Expression. *Anticancer Res* (2018) 38(11):6163–70. doi: 10.21873/anticanres.12969
67. Kou X, Zhu J, Xie X, Hao M, Zhao Y. Expression of lncRNA MSC-AS1 in Hepatocellular Carcinoma Cell Lines and Its Effect on Proliferation, Apoptosis, and Migration. *Turk J Gastroenterol* (2020) 31(12):860–7. doi: 10.5152/tjg.2020.19485
68. Li S, Yang S, Qiu C, Sun D. LncRNA MSC-AS1 Facilitates Lung Adenocarcinoma Through Sponging miR-33b-5p to Up-Regulate GPAM. *Biochem Cell Biol* (2021) 99(2):241–8. doi: 10.1139/bcb-2020-0239
69. Liu Y, Meng W, Cao H, Wang B. Identification of MSC-AS1, a Novel lncRNA for the Diagnosis of Laryngeal Cancer. *Eur Arch Otorhinolaryngol* (2021) 278(4):1107–18. doi: 10.1007/s00405-020-06427-4
70. Hu Z, Li L, Cheng P, Liu Q, Zheng X, Peng F, et al. lncRNA MSC-AS1 Activates Wnt/β-Catenin Signaling Pathway to Modulate Cell Proliferation and Migration in Kidney Renal Clear Cell Carcinoma *via* miR-3924/WNT5A. *J Cell Biochem* (2020) 121(10):4085–93. doi: 10.1002/jcb.29594
71. Teng F, Zhang JX, Chang QM, Wu XB, Tang WG, Wang JF, et al. LncRNA MYLK-AS1 Facilitates Tumor Progression and Angiogenesis by Targeting miR-424-5p/E2F7 Axis and Activating VEGFR-2 Signaling Pathway in Hepatocellular Carcinoma. *J Exp Clin Cancer Res* (2020) 39(1):235. doi: 10.1186/s13046-020-01739-z
72. Liu J, Zhao SY, Jiang Q, Qu Y, Huang X, Du J, et al. Long Noncoding RNA MYLK-AS1 Promotes Growth and Invasion of Hepatocellular Carcinoma Through the EGFR/HER2-ERK1/2 Signaling Pathway. *Int J Biol Sci* (2020) 16(11):1989–2000. doi: 10.7150/ijbs.43062
73. Ouyang J, Zhu X, Chen Y, Wei H, Chen Q, Chi X, et al. NRAV, a Long Noncoding RNA, Modulates Antiviral Responses Through Suppression of Interferon-Stimulated Gene Transcription. *Cell Host Microbe* (2014) 16(5):616–26. doi: 10.1016/j.chom.2014.10.001
74. Li J, Li M, Wang X, Sun M, Ma C, Liang W, et al. Long Noncoding RNA NRAV Promotes Respiratory Syncytial Virus Replication by Targeting the MicroRNA miR-509-3p/Rab5c Axis To Regulate Vesicle Transportation. *J Virol* (2020) 94(10). doi: 10.1128/JVI.00113-20
75. Xu Q, Wang Y, Huang W. Identification of Immune-Related lncRNA Signature for Predicting Immune Checkpoint Blockade and Prognosis in Hepatocellular Carcinoma. *Int Immunopharmacol* (2021) 92:107333. doi: 10.1016/j.intimp.2020.107333
76. Feng Y, Hu X, Ma K, Zhang B, Sun C. Genome-Wide Screening Identifies Prognostic Long Noncoding RNAs in Hepatocellular Carcinoma. *BioMed Res Int* (2021) 2021:6640652. doi: 10.1155/2021/6640652
77. Maimaiti A, Jiang L, Wang X, Shi X, Pei Y, Hao Y, et al. Identification and Validation of an Individualized Prognostic Signature of Lower-Grade Glioma Based on Nine Immune Related Long Non-Coding RNA. *Clin Neurol Neurosurg* (2021) 201:106464. doi: 10.1016/j.clineuro.2020.106464
78. Li J, Ge J, Yang Y, Liu B, Zheng M, Shi R. Long Noncoding RNA ZFPM2-AS1 Is Involved in Lung Adenocarcinoma *via* miR-511-3p/AFF4 Pathway. *J Cell Biochem* (2020) 121(3):2534–42. doi: 10.1002/jcb.29476
79. Liu JG, Wang HB, Wan G, Yang MZ, Jiang XJ, Yang JY. Long Noncoding RNA ZFPM2-AS1 Promotes the Tumorigenesis of Renal Cell Cancer *via* Targeting miR-137. *Eur Rev Med Pharmacol Sci* (2020) 24(18):9238. doi: 10.26355/eurrev_202009_22996
80. Kong F, Deng X, Kong X, Du Y, Li L, Zhu H, et al. ZFPM2-AS1, A Novel lncRNA, Attenuates the P53 Pathway and Promotes Gastric Carcinogenesis by Stabilizing MIF. *Oncogene* (2018) 37(45):5982–96. doi: 10.1038/s41388-018-0387-9
81. He H, Wang Y, Ye P, Yi D, Cheng Y, Tang H, et al. Long Noncoding RNA ZFPM2-AS1 Acts as a miRNA Sponge and Promotes Cell Invasion Through Regulation of miR-139/GDF10 in Hepatocellular Carcinoma. *J Exp Clin Cancer Res* (2020) 39(1):159. doi: 10.1186/s13046-020-01664-1
82. Zhang Q, Cheng M, Fan Z, Jin Q, Cao P, Zhou G. Identification of Cancer Cell Stemness-Associated Long Noncoding RNAs for Predicting Prognosis of Patients With Hepatocellular Carcinoma. *DNA Cell Biol* (2021) 40:1087–100. doi: 10.1089/dna.2021.0282
83. Zhao QJ, Zhang J, Xu L, Liu FF. Identification of a Five-Long Non-Coding RNA Signature to Improve the Prognosis Prediction for Patients With Hepatocellular Carcinoma. *World J Gastroenterol* (2018) 24(30):3426–39. doi: 10.3748/wjg.v24.i30.3426
84. Jia Y, Chen Y, Liu J. Prognosis-Predictive Signature and Nomogram Based on Autophagy-Related Long Non-Coding RNAs for Hepatocellular Carcinoma. *Front Genet* (2020) 11:608668. doi: 10.3389/fgene.2020.608668
85. Deng B, Yang M, Wang M, Liu Z. Development and Validation of 9-Long Non-Coding RNA Signature to Predicting Survival in Hepatocellular Carcinoma. *Med (Baltimore)* (2020) 99(21):e20422. doi: 10.1097/MD.0000000000020422

86. Kong W, Wang X, Zuo X, Mao Z, Cheng Y, Chen W. Development and Validation of an Immune-Related lncRNA Signature for Predicting the Prognosis of Hepatocellular Carcinoma. *Front Genet* (2020) 11:1037. doi: 10.3389/fgene.2020.01037
87. Li X, Jin F, Li Y. A Novel Autophagy-Related lncRNA Prognostic Risk Model for Breast Cancer. *J Cell Mol Med* (2021) 25(1):4–14. doi: 10.1111/jcmm.15980
88. Ma W, Zhao F, Yu X, Guan S, Suo H, Tao Z, et al. Immune-Related lncRNAs as Predictors of Survival in Breast Cancer: A Prognostic Signature. *J Transl Med* (2020) 18(1):442. doi: 10.1186/s12967-020-02522-6
89. Zhu G, Huang H, Xu S, Shi R, Gao Z, Lei X, et al. Prognostic Value of Ferroptosis-Related Genes in Patients With Lung Adenocarcinoma. *Thorac Cancer* (2021) 12(12):1890–9. doi: 10.1111/1759-7714.13998
90. Zhu L, Yang F, Wang L, Dong L, Huang Z, Wang G, et al. Identification the Ferroptosis-Related Gene Signature in Patients With Esophageal Adenocarcinoma. *Cancer Cell Int* (2021) 21(1):124. doi: 10.1186/s12935-021-01821-2
91. Liu J, Ma H, Meng L, Liu X, Lv Z, Zhang Y, et al. Construction and External Validation of a Ferroptosis-Related Gene Signature of Predictive Value for the Overall Survival in Bladder Cancer. *Front Mol Biosci* (2021) 8:675651. doi: 10.3389/fmolb.2021.675651
92. Nelson BH. CD20+ B Cells: The Other Tumor-Infiltrating Lymphocytes. *J Immunol* (2010) 185(9):4977–82. doi: 10.4049/jimmunol.1001323
93. Zhang Y, Morgan R, Podack ER, Rosenblatt J. B Cell Regulation of Anti-Tumor Immune Response. *Immunol Res* (2013) 57(1–3):115–24. doi: 10.1007/s12026-013-8472-1
94. Shalapour S, Font-Burgada J, Di Caro G, Zhong Z, Sanchez-Lopez E, Dhar D, et al. Immunosuppressive Plasma Cells Impede T-Cell-Dependent Immunogenic Chemotherapy. *Nature* (2015) 521(7550):94–8. doi: 10.1038/nature14395
95. Zhang Y, Gallastegui N, Rosenblatt JD. Regulatory B Cells in Anti-Tumor Immunity. *Int Immunol* (2015) 27(10):521–30. doi: 10.1093/intimm/dxv034
96. Roghanian A, Fraser C, Kleyman M, Chen J. B Cells Promote Pancreatic Tumorigenesis. *Cancer Discov* (2016) 6(3):230–2. doi: 10.1158/2159-8290.CD-16-0100
97. Chen C, Wang D, Yu Y, Zhao T, Min N, Wu Y, et al. Legumain Promotes Tubular Ferroptosis by Facilitating Chaperone-Mediated Autophagy of GPX4 in AKI. *Cell Death Dis* (2021) 12(1):65. doi: 10.1038/s41419-020-03362-4
98. Zhou B, Liu J, Kang R, Klionsky DJ, Kroemer G, Tang D. Ferroptosis Is a Type of Autophagy-Dependent Cell Death. *Semin Cancer Biol* (2020) 66:89–100. doi: 10.1016/j.semcancer.2019.03.002
99. Fernández-Medarde A, Santos E. Ras in Cancer and Developmental Diseases. *Genes Cancer* (2011) 2(3):344–58. doi: 10.1177/1947601911411084
100. Haura EB, Ricart AD, Larson TG, Stella PJ, Bazhenova L, Miller VA, et al. A Phase II Study of PD-0325901, An Oral MEK Inhibitor, in Previously Treated Patients With Advanced Non-Small Cell Lung Cancer. *Clin Cancer Res* (2010) 16(8):2450–7. doi: 10.1158/1078-0432.CCR-09-1920
101. Degirmenci U, Wang M, Hu J. Targeting Aberrant RAS/RAF/MEK/ERK Signaling for Cancer Therapy. *Cells* (2020) 9(1):198. doi: 10.3390/cells9010198
102. Kim C, Giaccone G. MEK Inhibitors Under Development for Treatment of Non-Small-Cell Lung Cancer. *Expert Opin Investig Drugs* (2018) 27(1):17–30. doi: 10.1080/13543784.2018.1415324
103. Subbiah V, Baik C, Kirkwood JM. Clinical Development of BRAF Plus MEK Inhibitor Combinations. *Trends Cancer* (2020) 6(9):797–810. doi: 10.1016/j.trecan.2020.05.009

Conflict of Interest: The authors declare that the research was conducted in the absence of any commercial or financial relationships that could be construed as a potential conflict of interest.

Publisher's Note: All claims expressed in this article are solely those of the authors and do not necessarily represent those of their affiliated organizations, or those of the publisher, the editors and the reviewers. Any product that may be evaluated in this article, or claim that may be made by its manufacturer, is not guaranteed or endorsed by the publisher.

frontiers in Oncology

ORIGINAL RESEARCH
published: 14 September 2021
doi: 10.3389/fonc.2021.724415

circRPS16 Promotes Proliferation and Invasion of Hepatocellular Carcinoma by Sponging miR-876-5p to Upregulate SPINK1

Shuwen Lin[1,2,3†], *Ye Lin*[2†], *Zhongshi Wu*[1,2], *Wuzheng Xia*[2], *Chenglong Miao*[4], *Tianyi Peng*[2], *Zhen Zhao*[2], *Chenggang Ji*[3], *Zhikang Mo*[3], *Xi Liu*[3] *and Zhixiang Jian*[1,2*]

[1] The Second School of Clinical Medicine, Southern Medical University, Guangzhou, China, [2] Department of General Surgery, Guangdong Provincial People's Hospital, Guangdong Academy of Medical Sciences, Guangzhou, China, [3] Department of General Surgery, Binhaiwan Central Hospital of Dongguan, (Also Called The Fifth People's Hospital of Dongguan), The Dongguan Affiliated Hospital of Medical College of Jinan University, Dongguan, China, [4] Department of General Surgery, Pizhou People's Hospital, Pizhou, China

OPEN ACCESS

Edited by:
Hongda Liu,
Nanjing Medical University, China

Reviewed by:
Dawei Zhang,
The Second Affiliated Hospital of Guangzhou Medical University, China
Zongpeng Li,
Linyi People's Hospital, China
Jiayun Pang,
Nanjing University, China

***Correspondence:**
Zhixiang Jian
jzx_118@163.com

[†]These authors have contributed equally to this work

Specialty section:
This article was submitted to Cancer Molecular Targets and Therapeutics, a section of the journal Frontiers in Oncology

Received: 13 June 2021
Accepted: 12 August 2021
Published: 14 September 2021

Citation:
Lin S, Lin Y, Wu Z, Xia W, Miao C, Peng T, Zhao Z, Ji C, Mo Z, Liu X and Jian Z (2021) circRPS16 Promotes Proliferation and Invasion of Hepatocellular Carcinoma by Sponging miR-876-5p to Upregulate SPINK1. Front. Oncol. 11:724415. doi: 10.3389/fonc.2021.724415

The roles of serine protease inhibitor Kazal type 1 (SPINK1) in multiple types of cancers have been significantly documented. However, its specific roles in hepatocellular carcinoma (HCC) remain to be investigated. This study found that SPINK1 is upregulated in HCC and its upregulation correlates with poor prognosis. Besides, functional assays revealed that SPINK1 promotes cell proliferation, cell cycle, and invasion *in vitro*. Through bioinformatics analysis, we speculate that circRPS16 regulates SPINK1 expression by sponging miR-876-5p. This was further verified by the dual-luciferase reporter and fluorescent *in situ* hybridization (FISH) assays. Subsequently, rescue assays verified that circRPS16 promotes cell proliferation, cell cycle, and invasion through miR-876-5p. Importantly, silencing circRPS16 inhibited tumor growth by downregulating SPINK1 expression *in vivo*. Collectively, our results confirm that SPINK1 is a downstream target of circRPS16. Besides, circRPS16 and SPINK1 are oncogenic factors in HCC progression; they provide novel diagnostic and therapeutic targets for HCC patients.

Keywords: hepatocellular carcinoma (HCC), circRPS16, miR-876-5p, SPINK1, proliferation, invasion, ceRNA

INTRODUCTION

Hepatocellular carcinoma (HCC) is the most prevalent primary liver cancer that has emerged as a critical global medical problem. Furthermore, HCC has ranked the fourth most common cause of cancer-related deaths and the sixth leading type of cancer in terms of incidence (1). Unlike that of the four major cancers, i.e., lung, breast, prostate, and colorectal cancers, whose mortality rates are reportedly declined, the death rate of HCC is still increasing worldwide (2).

Abbreviations: HCC, hepatocellular carcinoma; SPINK1, serine protease inhibitor Kazal type 1; FISH, fluorescent *in situ* hybridization; TATI, tumor-associated trypsin inhibitor; PSTI, pancreatic secretory trypsin inhibitor; GEO, Gene Expression Omnibus; ceRNA, competing endogenous RNAs; IHC, immunohistochemistry; ATCC, American Type Culture Collection; DMEM, Dulbecco's modified Eagle's medium; FBS, fetal bovine serum; qRT-PCR, quantitative reverse transcription PCR; CCK-8, Cell Counting Kit-8; PI, propidium iodide; NC, negative control; SD, standard deviation; TCGA, The Cancer Genome Atlas; AGO, Argonaute.

Circular RNAs (circRNAs) are a novel class of noncoding RNAs that exert critical regulatory roles in physiological and pathological processes. Unlike the linear RNAs, circRNAs are characterized by covalently closed-loop structures formed through a specific back-splicing mechanism of 5′ and 3′end (3). This specific structure enables circRNAs to tolerate RNase R digestion (4). Therefore, circRNAs have a longer half-life than linear RNA (5). Previous studies have reported abundant and conserved circRNAs across species showing tissue and development-stage-specific expression (6, 7). Based on the above characteristics, circRNAs may serve as potential diagnostic biomarkers and therapeutic molecules. Recent studies revealed the important roles of circRNAs in the progression of HCC. Nonetheless, its molecular mechanisms are not yet fully understood. Therefore, functional exploration of circRNAs may provide a novel diagnostic and therapeutic strategy for HCC.

Serine peptidase inhibitor, Kazal type1 (SPINK1) encodes a 79-amino acid peptide which is located at the chromosomal region 5q32 (8). It belongs to the family of protease inhibitors, also known as tumor-associated trypsin inhibitor (TATI) or pancreatic secretory trypsin inhibitor (PSTI) (9). SPINK1 was originally discovered in the urine of ovarian cancer patients (10). Subsequent studies indicate that SPINK1 has been detected in multiple types of cancers including bladder, renal, colorectal, prostate, and liver cancers (8, 11). For HCC, high SPINK1 expression acts as prognostic and diagnostic biomarkers that promote cell proliferation and metastasis (12, 13). This denotes the important roles of SPINK1 in HCC progression. Nonetheless, the regulatory mechanisms promoting the aberrant expression of SPINK1 remain to be investigated.

Herein, we found SPINK1 upregulation in HCC tissues and its high expression was closely associated with poor prognosis of HCC patients. Notably, functional assays revealed the oncogenic roles of SPINK1. Through bioinformatics analysis, we predicted that circRPS16 may regulate SPINK1 expression by sponging miR-876-5p; this was confirmed by mechanistic investigations and rescue assays. Additionally, *in vivo* assays demonstrated that circRPS16 knockdown inhibited tumor growth by inhibiting SPINK1 expression. In summary, our research provides potential diagnostic and therapeutic biomarkers for HCC patients.

MATERIALS AND METHODS

Bioinformatic Analysis

The microarray dataset (GSE14520) (14) analyzing gene expression patterns in tumor and paired nontumor tissue of HCC patients was downloaded from the Gene Expression Omnibus (GEO) database (https://www.ncbi.nlm.nih.gov/gds). The heatmap of the differentially expressed genes was performed using R studio. Kaplan-Meier Plotter (http://kmplot.com/analysis) was used to investigate the significance of SPINK1 expression and the survival of HCC patients (15). The miRWalk 2.0 (http://zmf.umm.uni-heidelberg.de) and starBase (http://starbase.sysu.edu.cn/) databases were used to predict the competing endogenous RNAs (ceRNA) networks (16). The immunohistochemistry (IHC) results of SPINK1 in normal and HCC tissues were obtained from the Human Protein Atlas (http://www.proteinatlas.org) (17).

Tissue Specimens and Cell Lines

A total of 25 paired HCC and adjacent noncancer tissues obtained from patients of the Guangdong Provincial People's Hospital, Guangdong Academy of Medical Sciences (Guangdong, China) were used to perform quantitative reverse transcription PCR (qRT-PCR) assays. All the specimens were confirmed through pathological examination. The patients signed the informed consent before surgery. This study was reviewed and approved by the Research Ethics Committee, Guangdong Provincial People's Hospital, Guangdong Academy of Medical Sciences. The specimens were preserved in liquid nitrogen after resection. Two HCC cell lines (Huh7 and HepG2) were procured from the American Type Culture Collection (ATCC). The cells were regularly cultured in Dulbecco's modified Eagle's medium (DMEM) with 10% fetal bovine serum (FBS) and 1% penicillin-streptomycin (Gibco Invitrogen, Grand Island, NY, USA) in a humidified 5% CO_2 atmosphere at 37°C.

RNA Extraction and qRT-PCR

Total RNA was extracted from HCC tissues using TRIzol reagent (Invitrogen, Camarillo, CA, USA) following the manufacturer's instruction; exactly 1 ml TRIzol was used per 30 mg of HCC tissue or 10^6 cells. After the concentration determination, the total RNA was stored at −80°C to prevent degradation. For qRT-PCR, PrimeScript RT reagent kit (Takara, Kusatsu, Japan) and an SYBR Premix Ex Taq II (Takara) were used for SPINK1 and circRPS16. β-Actin was used as an endogenous control. Meanwhile, Mir-X™ miRNA First-Strand Synthesis Kit (Takara) and SYBR® Premix Ex Taq™ II (Takara) were used for miR-876-5p, and RNU6-2 was used as an endogenous control. RiboBio (Guangzhou, China) synthesized the bulge-loop miRNA qRT-PCR primer sets specific for miR-876-5p. Sangon Biotech (Shanghai, China) synthesized the SPINK1 and circRPS16 primers. All the procedures were conducted according to the manufacturer's instructions. Primers for circRPS16: 5′ GCCCATCGTGACTCAAAACT 3′ (forward) and 5′ TTTTGGACTCGCAGCG AC 3′ (reverse). Primers for miR-876-5p included 5′ CGCGTGGATTTCTTT GTGAATCACCA-3′. Primers for SPINK1 included 5′ CCTGTCTGTGGGACTGA TGGAAATAC 3′ (forward) and 5′ TGAATGAGGATAGA AGTCTGGCGTTTC 3′ (reverse). Primers for RNU6-2: 5′ TGGCACCCAGCACAATGAA 3′ and 5′ CTAAGTCATAG TCCGCCTAGAAGCA 3′ (reverse). Primers for β-actin: 5′ CCTGGCACCCAGCACAAT 3′ (forward) and 5′ GGGCC GGACTCGTCATAC 3′ (reverse).

Transfection

Lentiviral-circRPS16-RNAi (Hanbio, Shanghai, China) was transfected to inhibit cicRNA RPS16 expression (10 μl, 1×10^8 TU/ml). circRPS16 siRNA (RiboBio, Guangzhou, China), (5 μl, 20 μM), circRPS16 overexpression plasmid (Hanbio, Shanghai,

China) (2 μg), miR-876-5p mimics (RiboBio, Guangzhou, China) (5 μl, 20 μM), miR-876-5p inhibitor (RiboBio, Guangzhou, China) (5 μl, 20 μM), SPINK1 siRNA (RiboBio, Guangzhou, China) (5 μl, 20 μM), and SPINK1 overexpression plasmid (Hanbio, Shanghai, China) were obtained for transient transfection. The Lipofectamine 3000 (Invitrogen, Camarillo, CA, USA) was used for transfection following the manufacturer's instructions. The siRNA sequences against SPINK1 included 5′ TGGCCCTGTTGAGTCTATCTGGTAA 3′ (sense), sequence 5′ TTACCAGATAGACTCAACAGG GCCA′ (antisense). Meanwhile, siRNA sequences against circRPS16 included 5′ TTCAAGAAATGTGGATGAG 3′ (sense), 5′ CTCATCCACATTTCTTG AA 3′ (antisense).

Protein Extraction and Western Blot

Protein lysates were extracted using RIPA (Beyotime Institute of Biotechnology, Shanghai, China) following the manufacturer's instructions. The concentrations of protein lysates were qualified by the BCA kit (Beyotime Institute of Biotechnology, Shanghai, China). Protein lysates were separated in 10% SDS-PAGE gel then transferred to polyvinylidene fluoride membranes (Millipore, Billerica, MA, USA). After incubation of primary and secondary antibodies, the belts were visualized under enhanced chemiluminescence reagents. The primary antibodies included anti-SPINK1 at dilution rate of 1:5,000 (Abcam, Shanghai, China), anti-β-actin at dilution rate of 1:5,000 (Proteintech, Wuhan, China), and secondary antibody at dilution rate of 1:2,000 (Proteintech, Wuhan, China).

CCK-8 Assay

Cell Counting Kit-8 (CCK-8) was purchased from Dojindo (Shanghai, China). Based on the manufacturer's instructions, 5,000 cells were seeded into 96-well plates, 4 h before detection, then 10 μl CCK-8 solution was added to each well. The OD values at 24, 48, 72, and 96 h were recorded for subsequent analyses.

EdU Assay

The EdU kit was purchased from Ribobio (Guangzhou, China), and the assay was conducted based on the manufacturer's instructions. In the present study, 10^5 cells were seeded into 96-well plates and incubated with EdU regents for 2 h. After fixation with 4% paraformaldehyde, the cells were incubated with Appllo® regents. The Hoechest® was then used for DNA dyeing. The pictures were collected with a fluorescence microscope.

Flow Cytometry

Flow cytometry was used to analyze the cell cycle. After transfection, HCC cells were fixed with 70% ethanol and stained with propidium iodide (PI) (Kaiji, Nanjing, China). Thereafter, the fixed cells were analyzed using a flow cytometer (Beckman FC500, Los Angeles, CA, USA).

Transwell Assay

The invasion assay was performed using Matrigel Invasion Chambers (8 μm) (MilliporeSigma, Burlington, MA, USA) following the manufacturer's instructions. Exactly 20,000 cells were seeded onto the upper chambers with serum-free DMEM; then DMEM with 10% FBS was added to the lower chambers. After 24 h incubation, cells on the upper surface of the insert chamber were eliminated. Cells migrating to the bottom of the insert membrane were fixed with 4% paraformaldehyde and stained with crystal violet.

Fluorescence *In Situ* Hybridization

Cell climbing was fixed in 4% paraformaldehyde. Then, proteinase K was used for digestion. After blocking with rabbit serum, hybridization in HCC cells were performed overnight using miR-876-5p, circRPS16 probes. Specimens were analyzed using positive fluorescence microscope. The miR-876-5p probe for fluorescent *in situ* hybridization (FISH) was 5′-TGGTGAT TCACAAAGAAATCCA-3′, whereas the circRPS16 probe for FISH was: 5′-AGCCTCATCCACATTTCTTGAAACTTTAA-3′.

Dual-Luciferase Reporter Assay

For the validation of circRPS16 and miR-876-5p combination, the wild and mutant types of the circRPS16 were directly synthesized into the psi-check2 vector. Then, 0.16 μg circRPS16 wild/mutant-type vector and 5 pmol miR-876-5p mimics/NC were cotransfected. For the validation of miR-876-5p and SPINK1 combination, the wild and mutant types of the 3′ UTR sequence of SPNK1 were directly synthesized into the psi-check2 vector. Subsequently, 0.16 μg plasmid comprising the wild/mutant types of SPINK1-3′UTR and 5 pmol miR-876-5p mimics/NC were cotransfected. After 48 h, firefly luciferase (internal reference) and Renilla luciferase activities were measured using the Promega Dual-Luciferase system.

Animal Experiment

Four-week female nude mice were obtained from the Peking University Animal Center (Beijing, China). After acclimatization for 1 week, 2×10^6 HepG2 cells transfected with either Lentiviral-circRPS16-RNAi or negative control (NC) were subcutaneously injected into the right back of each mouse. After four weeks, the mice were killed and tumor weights were measured then recorded in grams. The animal study was reviewed and approved by the Institutional Animal Care and Use Committee of the Guangdong Provincial People's Hospital, Guangdong Academy of Medical Sciences.

Immunohistochemistry

The tumor tissues were fixed by 4% paraformaldehyde. After paraffin embedding and pathological section, the slides were incubated with primary antibodies overnight at 4°C and then incubated with secondary antibodies at room temperature for 2 h. The expression was evaluated using a composite score obtained by multiplying the values of staining intensities (0, no staining; 1, weak staining; 2, moderate staining; 3, strong staining) and the percentage of positive cells (0, 0%; 1, <10%; 2, 10%–50%; 3, >50%). IHC kit was purchased from MXB® (Fuzhou, China), and the experiment was performed under the manufacturer's instructions.

Statistical Analysis

Statistical analysis was performed using GraphPad Prism 7 software. Quantitative data were presented as mean ± standard deviation (SD). The paired or unpaired *t*-test was used for quantitative data. Differences with *p*-values (*$p < 0.05$; **$p < 0.01$; ***$p < 0.001$) were considered statistically significant.

RESULTS

Upregulation of SPINK1 in HCC Is Associated With Poor Prognosis

Based on the GSE14520 dataset, we found that the SPINK1 mRNA levels were significantly upregulated in tumor samples (**Figure 1A**). The heatmap illustrated that SPINK1 was highly enriched in tumors (**Figure 1B**). Furthermore, qRT-PCR including 25 paired HCC and adjacent nontumor tissues confirmed that SPINK1 was upregulated in HCC tumors (**Figure 1C**). Analysis of The Cancer Genome Atlas (TCGA) using Kaplan-Meier plotter (18) revealed that high SPINK1 expression was closely related to low survival rate (**Figure 1D**). The IHC results from the Human Protein Atlas showed that SPINK1 protein was upregulated in HCC tissues and almost undetected in liver normal tissues (**Figure 1E**). Collectively, these findings suggest that SPINK1 is upregulated in HCC tissues and closely associated with the poor prognosis of HCC patients.

SPINK1 Exerts Oncogenic Roles of HCC *In Vitro*

Furthermore, the functions of SPINK1 were investigated *in vitro*. To downregulate or upregulate the SPINK1expression, siRNA or overexpressed plasmid vector and the corresponding NC were respectively transfected into HCC cell lines, HepG2 and Huh7. First, the transfection efficiency was examined through qRT-PCR. siRNA transfection downregulated SPINK1 expression, whereas overexpressed plasmid transfection upregulated it (**Figure 2A**). CCK-8 and EdU incorporation assays revealed that SPINK1 knockdown inhibited the cell proliferation and overexpression of SPINK1 promoted cell proliferation (**Figures 2B, C**). Furthermore, flow cytometry analysis showed that downregulation induced cell cycle arrest, while overexpression of SPINK1 accelerated the cell cycle (**Figure 2D**). Transwell assay was performed to find out whether SPINK1 regulates the invasion ability of HCC cells. Consequently, SPINK1 overexpression stimulated cell invasion, while its downregulation demonstrated the opposite effect (**Figure 2E**). Together, these results indicate that SPINK1 exerts important oncogenic roles in cell proliferation, cell cycle, and invasion of HCC cells *in vitro*.

circRPS16 Regulates SPINK1 *via* miR-876-5p

Reports indicate that circular RNAs act as sponges for miRNAs modulating the activity of miRNA on their target genes (19, 20). Unambiguously, circRNAs are considered a large class of posttranscriptional regulators (21). Therefore, we investigated whether SPINK1 is regulated by circular RNA. As a result, miR-876-5p was a potential miRNA regulating SPINK1, which was predicted by four databases including miRanda, Targetscan, starbase, and miRwalk (**Figure 3A**). Subsequently, the starBase database was used to investigate the potential upstream circRNAs of miR-876-5p. The results revealed that circRPS16 (circBase ID is hsa_circ_0050997) was the most potential one to bind miR-876-5p, which was supported by 32 Argonaute (AGO) CLIP seq experiments (**Figure 3B**) (22). The qRT-PCR results further demonstrated that circRPS16 is upregulated in HCC tissues (**Figure 3C**), nevertheless, miR-876-5p was downregulated in HCC tissues (**Figure 3D**). The FISH analysis confirmed that circRPS16 and miR-876-5p are colocalized in the cytoplasm of HCC cells (**Figure 3E**). Dual-luciferase system analysis was conducted for further validation. In contrast with the mutant type of circRPS16 plasmid, cotransfection of miR-876-5p mimics and wild type of circRPS16 plasmid significantly reduced the luciferase activity (**Figure 3F**). Moreover, unlike the transfection of plasmid containing mutant type of SPINK1 3′UTR, cotransfection of miR-876-5p mimics with wild-type plasmid decreased the luciferase activity (**Figure 3G**). Western blot assay was performed to find out whether circRPS16 regulates SPINK1 expression *via* miR-876-5p. As a result, transfection of miR-876-5p mimics downregulated SPINK1 expression, while miR-876-5p inhibitor upregulated SPINK1 expression. For the rescue assay, circRPS16 siRNA downregulated SPINK1 expression; this was restored by miR-876-5p inhibitor. Overexpressed circRPS16 vector upregulated SPINK1 expression, which was impaired by miR-876-5p mimics (**Figure 3H**).

In summary, the above findings prove that circRPS16 regulates SPINK1 expression *via* miR-876-5p.

miR-876-5p Regulates HCC Cell Proliferation, Cell Cycle, and Invasion

Considering that miR-876-5p directly targeted SPINK1 and was downregulated in HCC tissues, its functional roles were further explored. miR-876-5p mimics or inhibitor was transfected to ectopically upregulate or downregulate miR-876-5p expression, respectively. Meanwhile, the relevant NC were also transfected. CCK-8 and EdU assays identified that, unlike the NC group, miR-876-5p mimics inhibited HCC cell proliferation. In contrast, miR-876-5p inhibitor promoted HCC cell proliferation (**Figures 4A, B**). Additionally, flow cytometry analysis revealed that miR-876-5p mimics caused cell cycle arrest, while miR-876-5p inhibitor promoted cell cycle progression (**Figure 4C**). Transwell assays were further conducted to evaluate the effects of miR-876-5p on metastasis. In contrast with the NC group, miR-876-5p mimics inhibited the invasion capacity of HCC cells, whereas miR-876-5p inhibitor improved this capacity (**Figure 4D**). These results imply that miR-876-5p exerts inhibitory roles in HCC progression *in vitro*.

circRPS16 Regulates HCC Cell Proliferation, Cell Cycle, and Invasion by Sponging miR-876-5p

The independent roles of circRPS16 were confirmed through the transfection of circRPS16 siRNA. Then, to examine whether circRPS16 exerts regulatory roles by interacting with miR-876-5p,

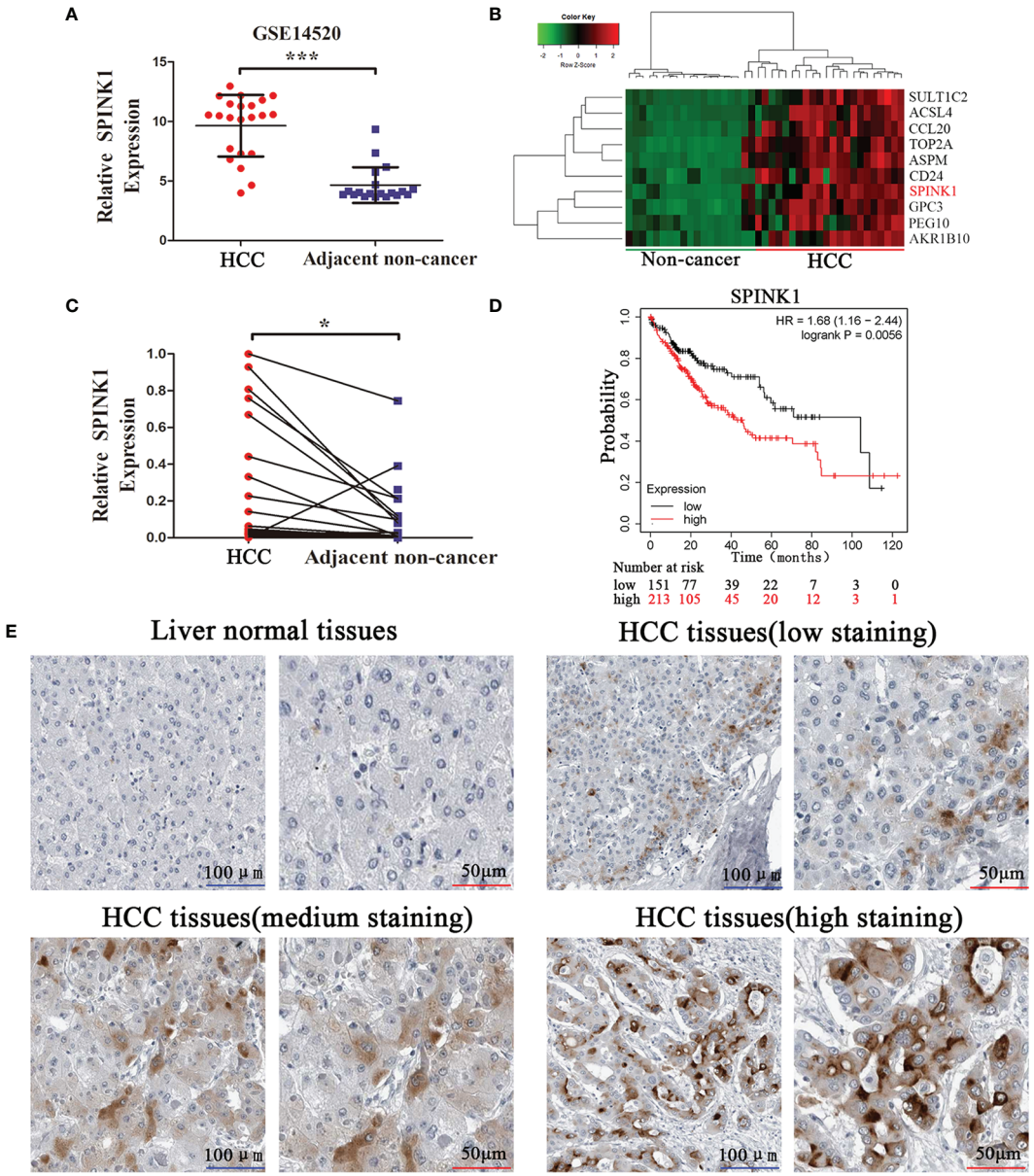

FIGURE 1 | SPINK1 is upregulated in HCC tissues, and high SPINK1 expression is associated with poor prognosis. **(A)** GEO dataset analysis (GSE14520) reveals that SPINK1 was upregulated in HCC tissues. Data are presented as mean ± SD; statistical significance was assessed by Student's t-test. ***$p < 0.001$. **(B)** The heatmap showed that SPINK1 was primarily clustered in HCC tissues. **(C)** The results of qRT-PCR reveal that SPINK1 was upregulated in HCC tissues. Data are presented as mean ± SD; statistical significance was assessed by paired *t*-test. *$p < 0.05$. **(D)** Kaplan-Meier analysis of overall survival from the TCGA dataset reveals that high SPINK1 expression was associated with poor prognosis; the log-rank test was used. $p = 0.0056$. **(E)** Immunochemistry (IHC) results from Human Protein Atlas reveal that SPINK1 was upregulated in HCC tissues.

rescue assays were performed through cotransfection of circRPS16 siRNA and miR-876-5p inhibitor. CCK-8 and EdU assays showed that knockdown of circRPS16 inhibited HCC cell proliferation (**Figures 5A, B**). Flow cytometry analyses demonstrated that circRPS16 siRNA caused cell cycle arrest, nonetheless (**Figure 5C**). Transwell assays identified that circRPS16 siRNA inhibited HCC cell invasion capacity (**Figure 5D**). Furthermore, rescue assays confirmed that reintroduction of miR-876-5p inhibitor rescued the inhibitory roles of circRPS16 siRNA on proliferation (**Figures 5A, B**), cell cycle (**Figure 5C**), and invasion (**Figure 5D**). These results indicate that circRPS16 regulates HCC cell proliferation, cell cycle, and invasion by sponging miR-876-5p.

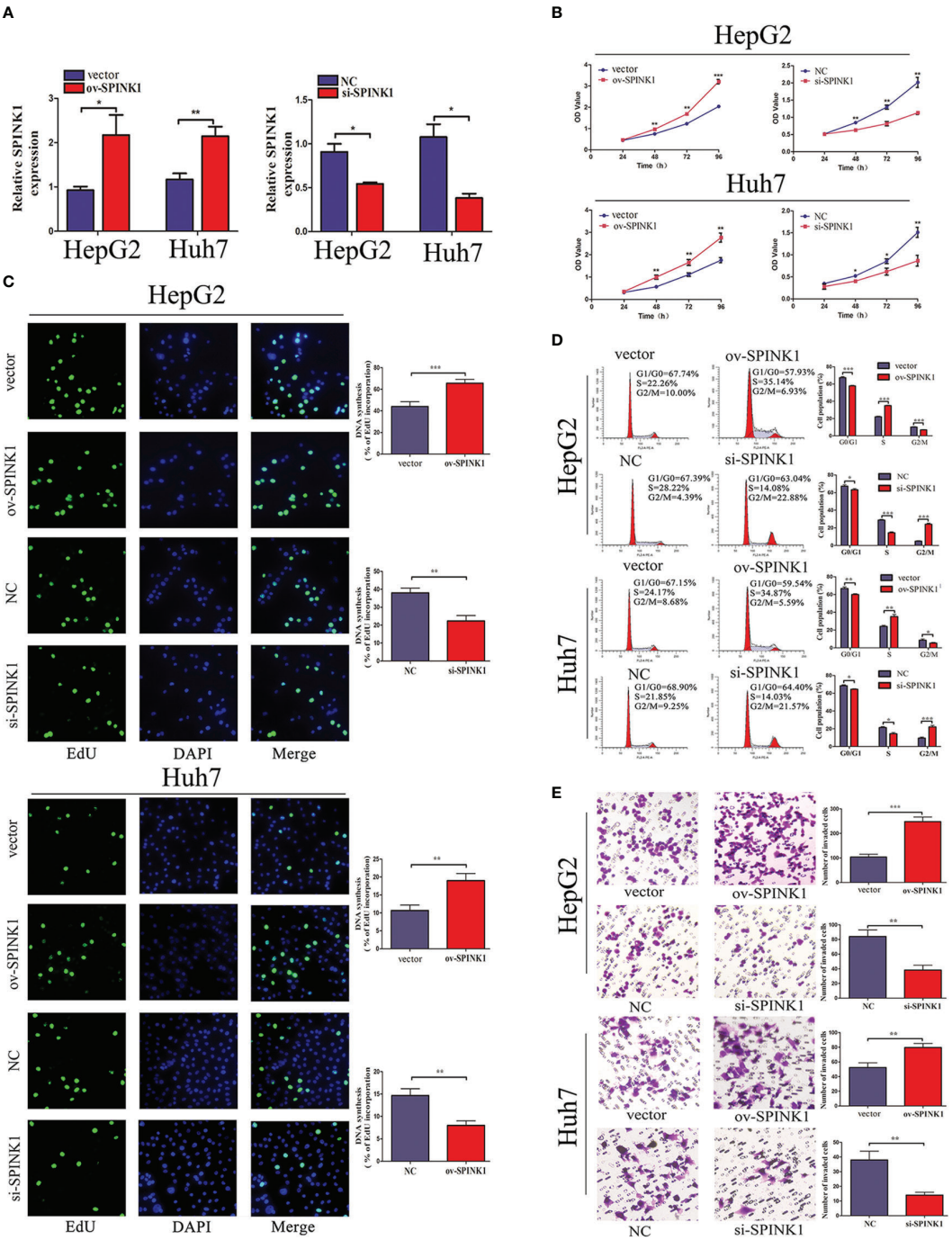

FIGURE 2 | SPINK1 regulates HCC cell proliferation, cell cycle, and invasion capacity. **(A)** The qRT-PCR results reveal the SPINK1 expression level after transfection of SPINK1 overexpression vector or siRNA. Independent experiments were repeated three times; data are presented as mean ± SD; statistical significance was assessed by paired *t*-test. $^{*}p < 0.05$, $^{**}p < 0.01$. **(B)** CCK-8 and **(C)** EdU assays reveal SPINK1 overexpression (ov) promotes and knockdown (si) inhibits the proliferation of HCC cells. Independent experiments were repeated three times; data are presented as mean ± SD; statistical significance was assessed by Student's *t*-test. $^{*}p < 0.05$, $^{**}p < 0.01$. **(D)** Flow cytometry shows SPINK1 overexpression accelerates cell cycle, while, SPINK1 knockdown induces cell cycle arrest. Independent experiments were repeated three times; data are presented as mean ± SD; statistical significance was assessed by Student's *t*-test. $^{*}p < 0.05$, $^{**}p < 0.01$, $^{***}p < 0.001$. **(E)** Transwell assays revealed SPINK1 overexpression promoted and its knockdown attenuated the invasion of HCC cells. Independent experiments were repeated three times; data are presented as mean ± SD; statistical significance was assessed by Student's *t*-test. $^{**}p < 0.01$, $^{***}p < 0.001$. ov, overexpressed plasmid vector; si, siRNA; NC, negative control.

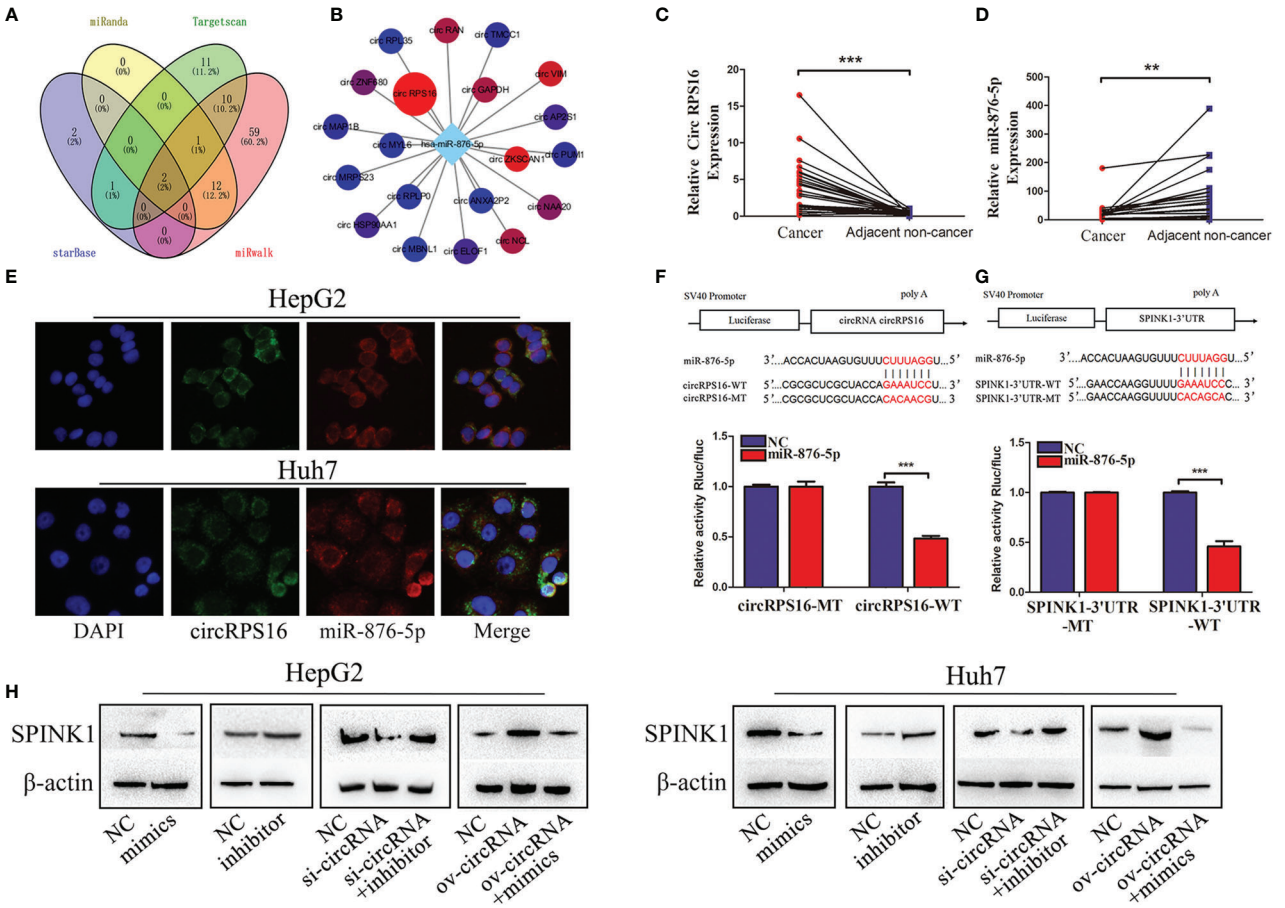

FIGURE 3 | circRPS16 regulates SPINK1 by sponging miR-876-5p. **(A)** The potential miRNA targeting SPINK1 were predicted by miRanda, Targetscan, starbase, and miRwalk database; the interaction is shown in the Venn diagram. **(B)** The potential circRNAs targeting miR-876-5p were predicted by starbase. **(C)** The circRPS16 and **(D)** miR-876-5p expression levels were qualified by qRT-PCR. Data are presented as mean ± SD; statistical significance was assessed by paired *t*-test. $^{**}p < 0.01$, $^{***}p < 0.001$. **(E)** The location of circRPS16 and miR-876-5p was determined by FISH. **(F)** Dual-luciferase reporter assays demonstrated that circRPS16 directly targets miR-876-5p and **(G)** miR-876-5p directly targets SPINK1. Independent experiments were repeated three times; data are presented as mean ± SD; statistical significance was assessed by Student's *t*-test. $^{***}p < 0.001$. **(H)** Western blot analysis shows that circRPS16 regulated SPINK1 expression *via* miR-876-5p. ov, overexpressed plasmid vector; si, siRNA; NC, negative control.

Knockdown of circRPS16 Inhibits Tumor Growth by Suppressing SPINK1 *In Vivo*

To detect the roles of circRPS16 on HCC growth *in vivo*, HepG2 cells with stable knockdown of circRPS16 and the NC cells were implanted into the nude mouse model. After 20 days, the xenograft mice were euthanized and tumor weight was recorded. The results revealed that tumors derived from circRPS16 knockdown cells have a lower weight than those from NC cells (**Figure 6A**). To further assess whether circRPS16 regulates SPINK1 expression *in vivo*, SPINK1 expression levels of the different group was detected through IHC assay. The results demonstrated that SPINK1 expression was significantly downregulated in the circRPS16 knockdown group (**Figure 6B**). As such, *in vivo* assay confirms that circRPS16 knockdown inhibits SPINK1 and tumor growth.

DISCUSSION

HCC is a major international health problem; while acknowledging significant progress in its prevention, detection, diagnosis, and treatment, its incidence and mortality rates are increasing (1). Notably, molecular alterations regulate the transition of dysplastic cells to full-blown hepatocellular carcinoma (23). Therefore, targeting the molecular targets implicated in its pathogenesis is a potential treatment approach (24). Studies indicate that SPINK1 regulates HCC progression. For instance, SPINK1 differentiates a well-differentiated HCC from a high-grade dysplastic nodule (12). Moreover, SPINK1 is significantly upregulated in HCC tissues compared with corresponding nonmalignant tissues (25, 26). It also causes the epithelial-mesenchymal transition (EMT) *via* MEK/ERK

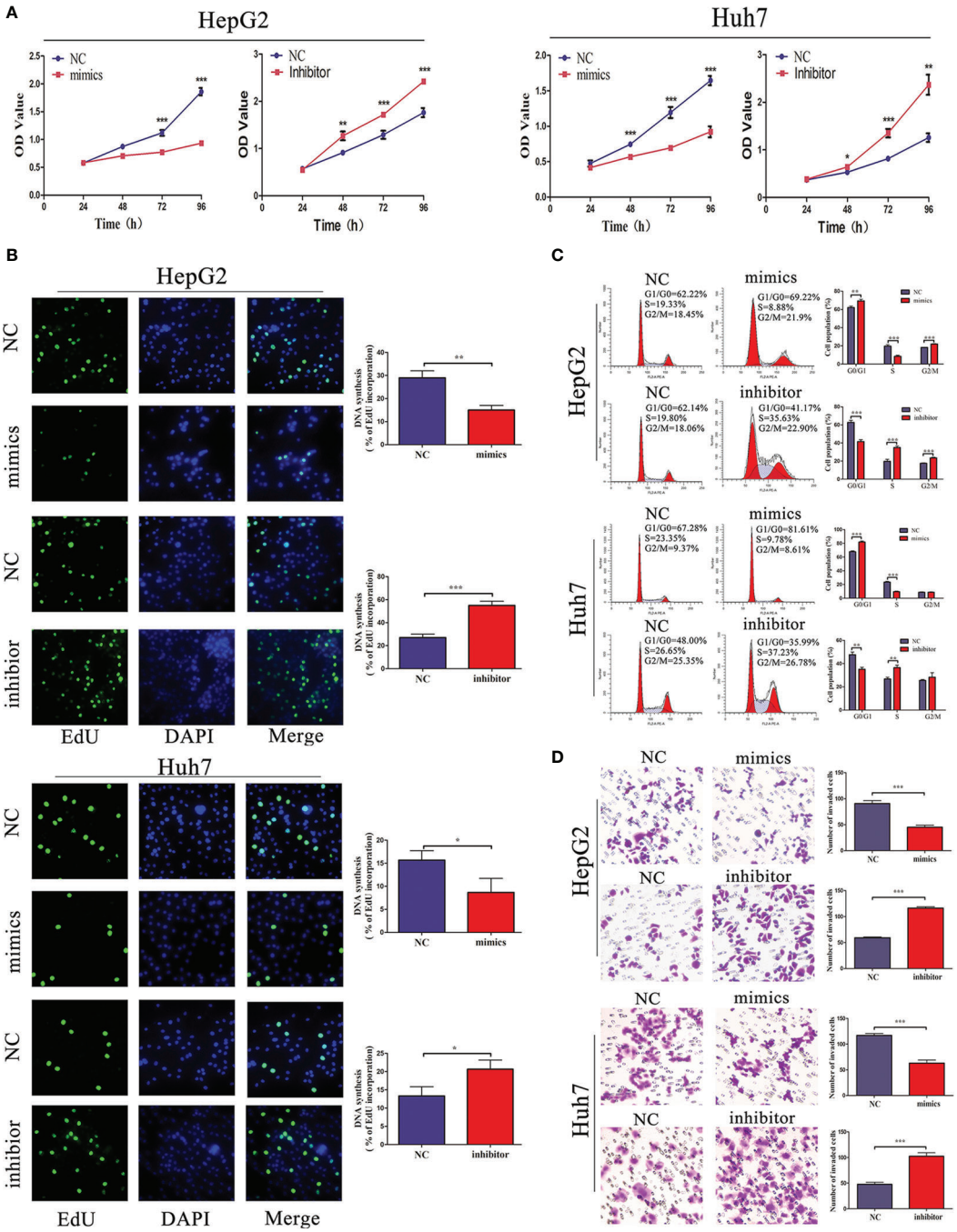

FIGURE 4 | miR-876-5p regulates HCC cell proliferation, cell cycle, and invasion capacity. **(A)** CCK-8 and **(B)** EdU assays reveal that miR-876-5p mimics inhibited and inhibitor promoted the proliferation of HCC cells. **(C)** Flow cytometry reveals that miR-876-5p mimics induced cell cycle arrest, while, miR-876-5p inhibitor accelerated cell cycle. **(D)** Transwell assays reveal miR-876-5p mimics attenuated, while, inhibitor promoted the invasion of HCC cells. All the above experiments were repeated three times independently; data are presented as mean ± SD; statistical significance was assessed by Student's *t*-test. $^{*}p < 0.05$, $^{**}p < 0.01$, $^{***}p < 0.001$.

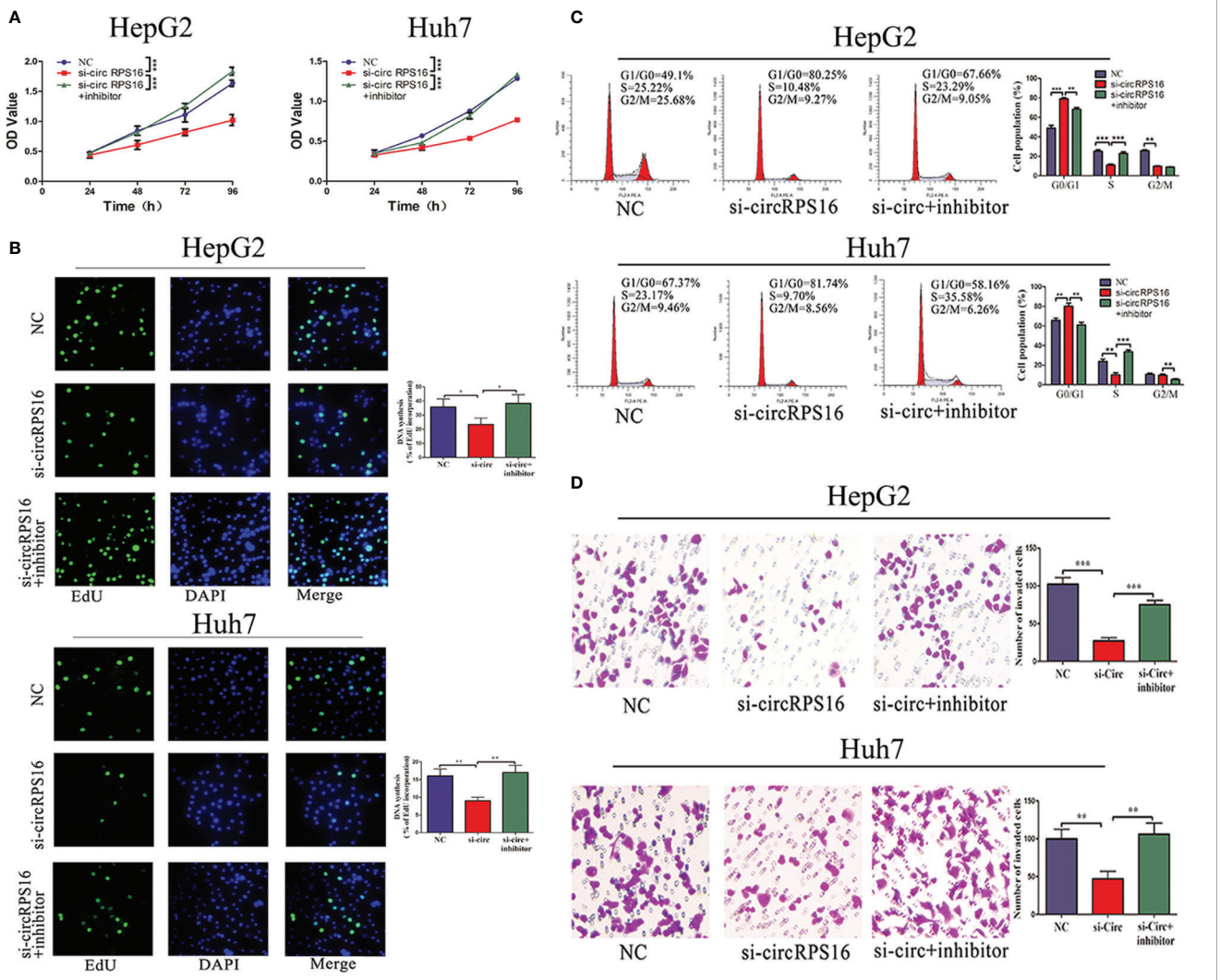

FIGURE 5 | circRPS16 regulates HCC cell proliferation, cell cycle, and invasion capacity *via* miR-876-5p. **(A)** CCK-8 and **(B)** EdU assays show that circRPS16 knockdown inhibited the proliferation of HCC cells and miR-876-5p inhibitor restored the proliferation of circRPS16 knockdown HCC cells. **(C)** Flow cytometry reveals that circRPS16 knockdown induced cell cycle arrest and miR-876-5p inhibitor accelerated cell cycle of circRPS16 knockdown HCC cells. **(D)** Transwell assays show that circRPS16 knockdown inhibited invasion capacity of HCC cells and miR-876-5p inhibitor restored invasion capacity of circRPS16 knockdown HCC cells. All the above experiments were repeated three times independently; data are presented as mean ± SD; statistical significance was assessed by Student's *t*-test. $^{*}p < 0.05$, $^{**}p < 0.01$, $^{***}p < 0.001$. NC, negative control; si, siRNA.

pathway (27) and acts as a downstream effector of the CDH17/β-catenin axis in HCC (28). By analyzing the GEO database, we found that SPINK1 was upregulated in the HCC tissues; this was further verified using qRT-PCR in 25 paired HCC tumors and adjacent nontumors. TCGA data showed that high SPINK1 expression is closely associated with poor prognosis. In addition, IHC results from the Human Protein Atlas revealed that SPINK1 was upregulated in HCC tissues. Functional assays confirmed that SPINK1 acts as an HCC oncogene. These results indicate the vital roles of SPINK1 in HCC progression and are urgently required to elucidate its upregulatory mechanism.

circRNA is a novel class of noncoding RNA with a covalent closed-loop structure through back splicing (29). This special structure offers circRNA distinct characteristics such as inhibiting digestion and cleavage of exonucleases and long half-life compared with linear RNAs (30). Previous studies have reported the vital roles of circRNA in tumorigenesis and tumor progression including HCC (31, 32). To a certain degree, the locations of circRNAs dictate their functions. Nuclear retained circRNAs are implicated in transcription regulation (33, 34). Additionally, the circular RNAs retained in the cytoplasm act as miRNA sponges then regulate the expression of the miRNA target genes (4, 35). Furthermore, circRNAs form specific circRNPs by interacting with different proteins and translate into protein and form pseudogenes (19). Through bioinformatic analysis, we hypothesized that circRPS16 acts as

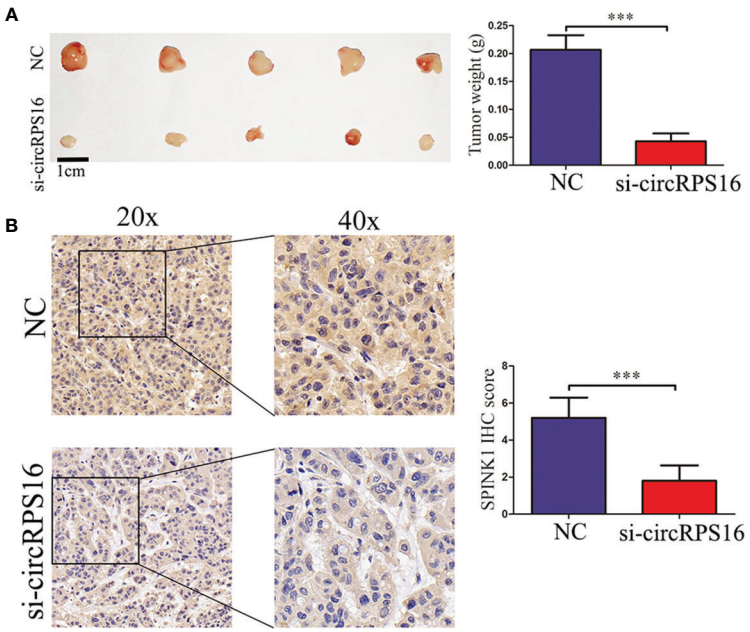

FIGURE 6 | circRPS16 knockdown inhibits tumor growth *in vivo*. **(A)** After four weeks, the implanted mice were killed and the tumor weights were recorded. Data are presented as mean ± SD; statistical significance was assessed by Student's *t*-test. ***$p < 0.001$. **(B)** The SPINK1 expression levels in each group were measured through IHC analysis. Data are presented as mean ± SD; statistical significance was assessed by Student's *t*-test. ***$p < 0.001$. NC, negative control; si, lentiviral-circRPS16-RNAi.

a miR-876-5p sponge to regulate the SPINK1 expression. Previous studies have investigated the regulating roles of miR-876-5p in prostate cancer, breast cancer, HCC, etc. (36, 37). In HCC, miR-876-5p acts as the targets of LncRNA PITPNA-AS1, long noncoding RNA SNHG14, and LINC-ROR and then regulates proliferation and sorafenib sensitivity of HCC (38–40). miR-876-5p also suppresses HCC progression by targeting DNMT3A and inhibits EMT and metastasis of HCC by targeting BCL6 corepressor like 1 (BCORL1) (36, 41). These findings strongly indicate the essential roles of miR-876-5p in HCC. In our study, qRT-PCR results confirmed that circRPS16 was significantly upregulated; this was inversely associated with miR-876-5p expression in HCC tissues. FISH assays revealed that circRPS16 and miR-876-5p were colocalized in the cytoplasm. Dual-luciferase reporter assays proved that miR-876-5p directly combined circRPS16 and SPINK1. Subsequently, Western blot analysis showed that circRPS16 regulated SPINK1 expression *via* miR-876-5p. Therefore, the mechanism assays demonstrated that circRPS16 acts as the sponge of miR-876-5p, then regulate the miR-876-5p target gene SPINK1. Furthermore, functional assays confirmed the oncogenic roles of circRPS16 and the tumor-suppressor roles of miR-876-5p. Rescue assays verified that circRPS16 regulated HCC cell proliferation, cell cycle, and invasion *via* miR-876-5p. Eventually, our results show that circRPS16 inhibits tumor growth *via* SPINK1 *in vivo*.

In conclusion, our findings suggest that SPINK1 is upregulated in HCC tissues and acts as an oncogene in HCC progression. Furthermore, SPINK1 is regulated by circRPS16 *via* sponging miR-876-5p. To our knowledge, this is the first study reporting the important roles of circRPS16/miR-876-5p/SPINK1 axis in HCC progression. circRPS16 and SPINK1 are the potential diagnostic biomarkers and therapeutic targets for HCC. Thus, our findings provide additional insights into the molecular and regulatory mechanisms in the progression of HCC.

DATA AVAILABILITY STATEMENT

The datasets presented in this study can be found in online repositories. The names of the repository/repositories and accession number(s) can be found in the article/supplementary material.

ETHICS STATEMENT

The studies involving human participants were reviewed and approved by the Research Ethics Committee, Guangdong Provincial People's Hospital, Guangdong Academy of Medical Sciences. The patients/participants provided their written informed consent to participate in this study. The animal study

was reviewed and approved by The Institutional Animal Care and Use Committee of the Guangdong Provincial People's Hospital, Guangdong Academy of Medical Sciences.

AUTHOR CONTRIBUTIONS

ZJ contributed to study design, technical support, and revision of the manuscript. SL and YL contributed to study design, experiment implementation, data acquisition, statistical analysis, and the first draft of the manuscript. ZW, WX, and TP collected the specimen and performed experiments. ZZ, ZM, and LM performed bioinformatics analysis and statistical analysis. CJ provided conceptual advice. All authors contributed to the article and approved the submitted version.

FUNDING

This work was supported by the Social Science and Technology Development Foundation of Dongguan (No. 202050715025194); National Natural Science Foundation of China (No. 81972792); National Science Foundation of Guangdong Province (No. 2020A1515010149).

REFERENCES

1. Villanueva A. Hepatocellular Carcinoma. *N Engl J Med* (2019) 380:1450–62. doi: 10.1056/NEJMra1713263
2. Yang JD, Hainaut P, Gores GJ, Amadou A, Plymoth A, Roberts LR. A Global View of Hepatocellular Carcinoma: Trends, Risk, Prevention and Management. *Nat Rev Gastroenterol Hepatol* (2019) 16:589–604. doi: 10.1038/s41575-019-0186-y
3. Chen LL, Yang L. Regulation of circRNA Biogenesis. *RNA Biol* (2015) 12:381–8. doi: 10.1080/15476286.2015.1020271
4. Jeck WR, Sorrentino JA, Wang K, Slevin MK, Burd CE, Liu J, et al. Circular RNAs Are Abundant, Conserved, and Associated With ALU Repeats. *RNA* (2013) 19:141–57. doi: 10.1261/rna.035667.112
5. Jeck WR, Sharpless NE. Detecting and Characterizing Circular RNAs. *Nat Biotechnol* (2014) 32:453–61. doi: 10.1038/nbt.2890
6. Salzman J, Chen RE, Olsen MN, Wang PL, Brown PO. Cell-Type Specific Features of Circular RNA Expression. *PloS Genet* (2013) 9:e1003777. doi: 10.1371/journal.pgen.1003777
7. Salzman J, Gawad C, Wang PL, Lacayo N, Brown PO. Circular RNAs Are the Predominant Transcript Isoform From Hundreds of Human Genes in Diverse Cell Types. *PloS One* (2012) 7:e30733. doi: 10.1371/journal.pone.0030733
8. Itkonen O, Stenman UH. TATI as a Biomarker. *Clin Chim Acta* (2014) 431:260–9. doi: 10.1016/j.cca.2014.02.014
9. Rasanen K, Itkonen O, Koistinen H, Stenman UH. Emerging Roles of SPINK1 in Cancer. *Clin Chem* (2016) 62:449–57. doi: 10.1373/clinchem.2015.241513
10. Huhtala ML, Pesonen K, Kalkkinen N, Stenman UH. Purification and Characterization of a Tumor-Associated Trypsin Inhibitor From the Urine of a Patient With Ovarian Cancer. *J Biol Chem* (1982) 257:13713–6. doi: 10.1016/S0021-9258(18)33505-1
11. Tiwari R, Manzar N, Bhatia V, Yadav A, Nengroo MA, Datta D, et al. Androgen Deprivation Upregulates SPINK1 Expression and Potentiates Cellular Plasticity in Prostate Cancer. *Nat Commun* (2020) 11:384. doi: 10.1038/s41467-019-14184-0
12. Holah NS, El-Azab DS, Aiad H, Sweed D. The Diagnostic Role of SPINK1 in Differentiating Hepatocellular Carcinoma From Nonmalignant Lesions. *Appl Immunohistochem Mol Morphol* (2017) 25:703–11. doi: 10.1097/PAI.0000000000000363
13. Huang K, Xie W, Wang S, Li Q, Wei X, Chen B, et al. High SPINK1 Expression Predicts Poor Prognosis and Promotes Cell Proliferation and Metastasis of Hepatocellular Carcinoma. *J Invest Surg* (2020) 34(9):1011–20. doi: 10.1080/08941939.2020.1728443
14. Roessler S, Jia HL, Budhu A, Forgues M, Ye QH, Lee JS, et al. A Unique Metastasis Gene Signature Enables Prediction of Tumor Relapse in Early-Stage Hepatocellular Carcinoma Patients. *Cancer Res* (2010) 70:10202–12. doi: 10.1158/0008-5472.CAN-10-2607
15. Gyorffy B, Lanczky A, Eklund AC, Denkert C, Budczies J, Li Q, et al. An Online Survival Analysis Tool to Rapidly Assess the Effect of 22,277 Genes on Breast Cancer Prognosis Using Microarray Data of 1,809 Patients. *Breast Cancer Res Treat* (2010) 123:725–31. doi: 10.1007/s10549-009-0674-9
16. Li JH, Liu S, Zhou H, Qu LH, Yang JH. Starbase V2.0: Decoding miRNA-ceRNA, miRNA-ncRNA and Protein-RNA Interaction Networks From Large-Scale CLIP-Seq Data. *Nucleic Acids Res* (2014) 42:D92–7. doi: 10.1093/nar/gkt1248
17. Uhlen M, Fagerberg L, Hallstrom BM, Lindskog C, Oksvold P, Mardinoglu A, et al. Proteomics. Tissue-Based Map of the Human Proteome. *Science* (2015) 347:1260419. doi: 10.1126/science.1260419
18. Gyorffy B, Lanczky A, Szallasi Z. Implementing an Online Tool for Genome-Wide Validation of Survival-Associated Biomarkers in Ovarian-Cancer Using Microarray Data From 1287 Patients. *Endocr Relat Cancer* (2012) 19:197–208. doi: 10.1530/ERC-11-0329
19. Li X, Yang L, Chen LL. The Biogenesis, Functions, and Challenges of Circular RNAs. *Mol Cell* (2018) 71:428–42. doi: 10.1016/j.molcel.2018.06.034
20. Salmena L, Poliseno L, Tay Y, Kats L, Pandolfi PP. A ceRNA Hypothesis: The Rosetta Stone of a Hidden RNA Language? *Cell* (2011) 146:353–8. doi: 10.1016/j.cell.2011.07.014
21. Memczak S, Jens M, Elefsinioti A, Torti F, Krueger J, Rybak A, et al. Circular RNAs Are a Large Class of Animal RNAs With Regulatory Potency. *Nature* (2013) 495:333–8. doi: 10.1038/nature11928
22. Xue Y, Ouyang K, Huang J, Zhou Y, Ouyang H, Li H, et al. Direct Conversion of Fibroblasts to Neurons by Reprogramming PTB-Regulated microRNA Circuits. *Cell* (2013) 152:82–96. doi: 10.1016/j.cell.2012.11.045
23. Torrecilla S, Sia D, Harrington AN, Zhang Z, Cabellos L, Cornella H, et al. Trunk Mutational Events Present Minimal Intra- and Inter-Tumoral Heterogeneity in Hepatocellular Carcinoma. *J Hepatol* (2017) 67:1222–31. doi: 10.1016/j.jhep.2017.08.013
24. Villani R, Vendemiale G, Serviddio G. Molecular Mechanisms Involved in HCC Recurrence After Direct-Acting Antiviral Therapy. *Int J Mol Sci* (2018) 20. doi: 10.3390/ijms20010049
25. Hass HG, Jobst J, Scheurlen M, Vogel U, Nehls O. Gene Expression Analysis for Evaluation of Potential Biomarkers in Hepatocellular Carcinoma. *Anticancer Res* (2015) 35:2021–8.
26. Xu W, Huang H, Yu L, Cao L. Meta-Analysis of Gene Expression Profiles Indicates Genes in Spliceosome Pathway Are Up-Regulated in Hepatocellular Carcinoma (HCC). *Med Oncol* (2015) 32:96. doi: 10.1007/s12032-014-0425-6
27. Ying HY, Gong CJ, Feng Y, Jing DD, Lu LG. Serine Protease Inhibitor Kazal Type 1 (SPINK1) Downregulates E-Cadherin and Induces EMT of Hepatoma Cells to Promote Hepatocellular Carcinoma Metastasis via The MEK/ERK Signaling Pathway. *J Dig Dis* (2017) 18:349–58. doi: 10.1111/1751-2980.12486
28. Shek FH, Luo R, Lam B, Sung WK, Lam TW, Luk JM, et al. Serine Peptidase Inhibitor Kazal Type 1 (SPINK1) as Novel Downstream Effector of the Cadherin-17/Beta-Catenin Axis in Hepatocellular Carcinoma. *Cell Oncol (Dordr)* (2017) 40:443–56. doi: 10.1007/s13402-017-0332-x
29. Ashwal-Fluss R, Meyer M, Pamudurti NR, Ivanov A, Bartok O, Hanan M, et al. circRNA Biogenesis Competes With pre-mRNA Splicing. *Mol Cell* (2014) 56:55–66. doi: 10.1016/j.molcel.2014.08.019
30. Harland R, Misher L. Stability of RNA in Developing Xenopus Embryos and Identification of a Destabilizing Sequence in TFIIIA Messenger RNA. *Development* (1988) 102:837–52. doi: 10.1242/dev.102.4.837
31. Lei M, Zheng G, Ning Q, Zheng J, Dong D. Translation and Functional Roles of Circular RNAs in Human Cancer. *Mol Cancer* (2020) 19:30. doi: 10.1186/s12943-020-1135-7

32. Beermann J, Piccoli M, Viereck J, Thum T. Non-Coding RNAs in Development and Disease: Background, Mechanisms, and Therapeutic Approaches. *Physiol Rev* (2016) 96:1297–325. doi: 10.1152/physrev.00041.2015
33. Li Z, Huang C, Bao C, Chen L, Lin M, Wang X, et al. Exon-Intron Circular RNAs Regulate Transcription in the Nucleus. *Nat Struct Mol Biol* (2015) 22:256–64. doi: 10.1038/nsmb.2959
34. Conn VM, Hugouvieux V, Nayak A, Conos SA, Capovilla G, Cildir G, et al. A circRNA From SEPALLATA3 Regulates Splicing of Its Cognate mRNA Through R-Loop Formation. *Nat Plants* (2017) 3:17053. doi: 10.1038/nplants.2017.53
35. Hansen TB, Jensen TI, Clausen BH, Bramsen JB, Finsen B, Damgaard CK, et al. Natural RNA Circles Function as Efficient microRNA Sponges. *Nature* (2013) 495:384–8. doi: 10.1038/nature11993
36. Wang Y, Xie Y, Li X, Lin J, Zhang S, Li Z, et al. MiR-876-5p Acts as an Inhibitor in Hepatocellular Carcinoma Progression by Targeting DNMT3A. *Pathol Res Pract* (2018) 214:1024–30. doi: 10.1016/j.prp.2018.04.012
37. Xu J, Zheng J, Wang J, Shao J. miR-876-5p Suppresses Breast Cancer Progression Through Targeting TFAP2A. *Exp Ther Med* (2019) 18:1458–64. doi: 10.3892/etm.2019.7689
38. Sun J, Zhang Y, Li B, Dong Y, Sun C, Zhang F, et al. PITPNA-AS1 Abrogates the Inhibition of miR-876-5p on WNT5A to Facilitate Hepatocellular Carcinoma Progression. *Cell Death Dis* (2019) 10:844. doi: 10.1038/s41419-019-2067-2
39. Liao Z, Zhang H, Su C, Liu F, Liu Y, Song J, et al. Long Noncoding RNA SNHG14 Promotes Hepatocellular Carcinoma Progression by Regulating miR-876-5p/SSR2 Axis. *J Exp Clin Cancer Res* (2021) 40:36. doi: 10.1186/s13046-021-01838-5
40. Zhi Y, Abudoureyimu M, Zhou H, Wang T, Feng B, Wang R, et al. FOXM1-Mediated LINC-ROR Regulates the Proliferation and Sensitivity to Sorafenib in Hepatocellular Carcinoma. *Mol Ther Nucleic Acids* (2019) 16:576–88. doi: 10.1016/j.omtn.2019.04.008
41. Xu Q, Zhu Q, Zhou Z, Wang Y, Liu X, Yin G, et al. MicroRNA-876-5p Inhibits Epithelial-Mesenchymal Transition and Metastasis of Hepatocellular Carcinoma by Targeting BCL6 Corepressor Like 1. *BioMed Pharmacother* (2018) 103:645–52. doi: 10.1016/j.biopha.2018.04.037

Conflict of Interest: The authors declare that the research was conducted in the absence of any commercial or financial relationships that could be construed as a potential conflict of interest.

Publisher's Note: All claims expressed in this article are solely those of the authors and do not necessarily represent those of their affiliated organizations, or those of the publisher, the editors and the reviewers. Any product that may be evaluated in this article, or claim that may be made by its manufacturer, is not guaranteed or endorsed by the publisher.

frontiers in Oncology

ORIGINAL RESEARCH
published: 29 September 2021
doi: 10.3389/fonc.2021.757498

Dual-Specificity Phosphatase 11 Is a Prognostic Biomarker of Intrahepatic Cholangiocarcinoma

Lin Xu[1†], Peng Wang[2†], Wei Zhang[2], Weiran Li[3], Tao Liu[3] and Xu Che[1,2]*

[1] Department of Hepatobiliary and Pancreatic Surgery, National Cancer Center/National Clinical Research Center for Cancer/Cancer Hospital & Shenzhen Hospital, Chinese Academy of Medical Sciences and Peking Union Medical College, Shenzhen, China, [2] Department of Pancreatic and Gastric Surgery, National Cancer Center/National Clinical Research Center for Cancer/Cancer Hospital, Chinese Academy of Medical Sciences and Peking Union Medical College, Beijing, China, [3] Department of Oncology Rehabilitation, Shenzhen Luohu People's Hospital, Shenzhen, China

Background: Cholangiocarcinoma (CCA), including intrahepatic (iCCA), perihilar (pCCA), and distal (dCCA) CCA, is a highly aggressive malignancy originating from bile duct. The prognosis of CCA is very poor, and the biomarker study is unsatisfactory compared with other common cancers.

Materials and methods: In our study, we investigated the expression of dual-specificity phosphatase 11(DUSP11) in eight pairs of iCCAs, pCCAs, and dCCAs, and their corresponding tumor-adjacent tissues, as well as their tumor-adjacent tissues with qPCR. Moreover, we investigated the expression of DUSP11 in 174 cases of CCAs with immunohistochemistry, including 74 iCCAs, 64 pCCAs, and 36 dCCAs. We classified these patients into subsets with low and high expressions of DUSP11, and evaluated the correlations between the DUSP11 subsets and clinicopathological factors. With univariate and multivariate analyses, we assessed the correlation between DUSP11 and the overall survival (OS) rates in these CCA patients.

Results: In all the CCA subtypes, DUSP11 was elevated in CCAs compared with their paired adjacent tissues. In iCCA, pCCA, and dCCA, the percentages of DUSP11 high expression were 44.59%, 53.85%, and 55.56%, respectively. In iCCA, high DUSP11 expression was significantly associated with an advanced T stage and a poor prognosis. However, the prognostic value of DUSP11 in pCCA and dCCA was not significant. To decrease the statistical error caused by the small sample size of the dCCA cohort, we merged pCCA and dCCA into extracellular CCA (eCCA). In the 101 cases of eCCA, DUSP11 expression was also not significantly associated with the prognosis.

Conclusions: DUSP11 expression was associated with tumor infiltration and the OS rate in iCCA, but not in pCCA and dCCA. DUSP11 was an independent biomarker of iCCA indicating a poor prognosis. Our results suggested that a high expression of DUSP11 was a post-operational risk factor, and detecting DUSP11 could guide the individual treatment for patients with CCA.

Keywords: DUSP11, prognosis, biomarker, intrahepatic cholangiocarcinoma, extrahepatic cholangiocarcinoma

OPEN ACCESS

Edited by:
Yunfei Xu,
Shandong University, China

Reviewed by:
Lanping Wang,
Shandong First Medical University, China
Xianqing Yang,
Shandong University, China

****Correspondence:***
Xu Che
chexu0192@163.com

[†]These authors have contributed equally to this work

Specialty section:
This article was submitted to Cancer Molecular Targets and Therapeutics, a section of the journal Frontiers in Oncology

Received: *12 August 2021*
Accepted: *31 August 2021*
Published: *29 September 2021*

Citation:
Xu L, Wang P, Zhang W, Li W, Liu T and Che X (2021) Dual-Specificity Phosphatase 11 Is a Prognostic Biomarker of Intrahepatic Cholangiocarcinoma. Front. Oncol. 11:757498. doi: 10.3389/fonc.2021.757498

INTRODUCTION

Cholangiocarcinoma (CCA) is a highly aggressive malignancy with extremely poor prognoses. Anatomically, CCA is further classified as three subtypes including intrahepatic (iCCA), perihilar (pCCA), and distal (dCCA) CCA based on their origin in the biliary tree (1). pCCA is the most prevalent type of CCA accounting for about 50%–60% of the total CCA cases, while dCCA and iCCA accounted for 20%–30% and 10%, respectively (2). The motility and morbidity of CCA are increasing rapidly in the recent decades, but the treatment options have few progresses (3). China has the highest incidence of CCA worldwide, and whether Chinese CCA patients have special molecular features is still unknown. In general, the rate of radical surgical resection of CCA is quite low, and the treatment options of unresectable or advanced-stage CCA are an urgent need. CCAs usually have poor responses to the classical adjuvant therapies such as chemotherapy or radiotherapy. Till 2020, there emerged the first FDA-approved target drug of CCA, pemigtinib, which was used for CCA with FGFR2 fusion or mutation (4). Overall, the 5-year overall survival rate (OS) of CCA is very unsatisfactory, remaining approximately 30% after radical resection (5). More biomarkers of CCA should be investigated because biomarker discovery is the initiation to find new drug targets and new treatment therapy.

Protein phosphorylation is a key post-translational modification mainly regulated by serine/threonine phosphatase and tyrosine phosphatase. Protein tyrosine phosphatase (PTP) family participates in numerous processes such as signal transduction and cell proliferation, *via* dephosphorylating the phosphor-tyrosine of substrates (6). In humans, PTPs consist of 107 members and are divided into four main subgroups, which are type-I cysteine-based PTP (including classical PTPs and dual-specific phosphatase), type-II cysteine-based PTP, type-III cysteine-based phosphatases, and aspartic acid-based PTPs (7). These PTPs have different tissue specificities, substrates, and functions. Genetic and epigenetic alterations in the PTP genes can result in aberrant tyrosine phosphorylation, and consequently lead to diverse effects including an uncontrollable cell proliferation and tumorigenesis (8, 9). Interestingly, both the tumor suppressing role and oncogenic functions of PTPs have been showed in cancer, and the putative oncogenic or tumor suppressive functions of PTP are considered to rely on the cellular context.

Dual-specificity phosphatases (DUSPs) have a dephosphorylating activity to both threonine/serine and tyrosine residues (10). There are 61 DUSPs out of the 107 PTP members, which have heterogeneous forms and functions, and are further classified based on the specific domains and sequence similarity. DUSP11, also known as PIR1 (phosphatase interacting with RNA and ribonucleoprotein 1), is a unique member of atypical DUSPs which could bind directly to RNA and possess RNA 5'-triphosphatase and diphosphatase activities (11, 12). DUSP11 converts the 5' triphosphate of microRNA precursors to a 5' monophosphate, and regulates cellular noncoding RNAs levels (12–14). In addition to a catalysis towards RNA, more evidence showed that DUSP11 could also dephosphorylate proteins. For example, DUSP11 could attenuate lipopolysaccharide-induced macrophage activation by targeting TGF-β-activated kinase 1 (15). DUSP11 was considered to participate in cancer progression by several previous studies (16, 17), but its functions and regulation mechanisms in cancer are still unclear to date. The tissue specificity and functions in tumor of DUSP11 have not been well studied.

In our study, we investigated the expression of DUSP11 in 174 cases of CCAs, including 74 iCCAs, 64 pCCAs, and 36 dCCAs. Moreover, we classified the patients into subsets with low and high expressions of DUSP11, and evaluated the clinicopathological factors in these subsets. With univariate and multivariate analyses, we assessed the correlation between DUSP11 and the OS rate in 74 iCCAs, 64 pCCAs, and 36 dCCAs.

MATERIALS AND METHODS

Patients and Ethics

A total of 258 patients were diagnosed with CCA in Chinese Academy of Medical Sciences and Peking Union Medical College and National Cancer Center Shenzhen Hospital from 2009 to 2016, which formed the primary cohort. A total of 174 cases of CCAs, including 74 iCCAs, 64 pCCAs, and 36 dCCAs, were selected from the primary cohort into the validation cohort, if they followed the criteria: (1) radical surgery with clear surgical margin was performed; (2) available formalin-fixed tumor tissues for IHC; (3) available follow-ups more than 3 months and complete medical records; and (4) no history of other malignancies. All samples were obtained with a prior consent from patients. The study was approved and supervised by the Ethics Committee of Chinese Academy of Medical Sciences and Peking Union Medical College and National Cancer Center Shenzhen Hospital.

Quantitative Real-Time PCR Analysis

A total of eight consecutive iCCAs, pCCAs, and dCCAs, and their corresponding tumor-adjacent tissues were collected for qPCR. Total mRNA was extracted from the frozen tissues using the TRIzol reagent (Thermo Fisher Scientific, Waltham, MA, USA), and then converted into cDNA using the ReverTra Ace qPCR RT kit (TOYOBO, Japan). Quantitative real-time PCR was performed using the SYBR Green Master (Roche, USA) and Light Cycler Roche 480 PCR instrument. The mRNA level was standardized with the $2^{-\Delta\Delta}$Ct method by normalization to GAPDH. The primer sequences were as follows:

DUSP11, forward:5'-GGCTGCCGAGTCTTTTCCT-3', Reverse5'-TTTCCACCTTTCGGGGATGTG-3'; GAPDH, forward:5'-GGAGCGAGATCCCTCCAAAAT-3', reverse: 5'-GGCTGTTGTCATACTTCTCATGG-3'.

Immunohistochemistry

Immunohistochemistry was performed with a streptavidin peroxidase complex method. Briefly, the paraffin-embedded

tissues were deparaffinized and rehydrated with xylene and graded alcohol. To inactivate the endogenous peroxidase, 3% hydrogen peroxide was used, and then, the slides were incubated in a citrate buffer (pH = 6.0) for the optimal antigen retrieval. The unspecific binding was blocked by incubation in 1% bovine serum albumin for 30 minutes. Primary antibody of DUSP11 (Santa Cruz Biotechnology, catalog: sc-393220) was used to incubate the tissues at 4°C overnight. Phosphate buffered saline was used to rinse the slides three times, and secondary antibodies labeled with streptavidin-biotin-peroxidase reagent were used to incubate the tissues for 1 hour. After that, slides were treated with the 3,3'-diaminobenzidine solution for 10 minutes for visualization. Slides were counterstained with hematoxylin and mounted at last.

Immunohistochemistry Results Evaluation

The IHC results were semi-quantified by two independent pathologists who were unaware of the clinical data. The final IHC scores was evaluated as the scores of the percentage of positive-stained cells multiplied by the scores of staining intensity. In brief, the scores of staining intensity were defined as: score 0 for negative staining, score 1 for weak staining, score 2 for moderate staining, and score 3 for strong staining. The scores for positive-stained cells were set as follows: score 1 for <25% of positive cells; score 2 for 25%–50% of positive cells; score 3 for 50%–75% of positive cells; and score 4 for 75%–100% of positive cells. The final IHC score ranged from from score 0 to 12, and was divided into subsets with different DUSP11 expression according to the cut-off, which was defined by the receiver operating characteristic (ROC) curve.

Statistical Analysis

SPSS 25.0 (IBM, Chicago, IL, USA) and GraphPad prism 5.0 software (California Resources Corporation, Los Angeles,CA, USA) were used for statistical analyses. The chi-square test was used to analyze the correlations between DUSP11 and the clinicopathological factors. The univariate analysis was analyzed with the log-rank test, and the survival curves were plotted with the Kaplan-Meier method. The Cox proportional hazards regression model was applied to identify the independent prognostic factors. P-values less than 0.05 in all experiments were considered statistically significant.

RESULTS

Expression of Dual-Specificity Phosphatase 11 in Cholangiocarcinoma Tissues and Tumor-Adjacent Tissues

The expression of DUSP11 was detected with qPCR in eight pairs of iCCAs, pCCAs, and dCCAs, as well as their corresponding tumor-adjacent tissues (**Figure 1A**). In these tissues, DUSP11 expressions in iCCAs, pCCAs, and dCCAs were substantially higher than those in their paired adjacent tissues. To better depict the expression of DUSP11 in CCA, the DUSP11 expression was investigated by IHC in 174 cases of CCAs, including 74 iCCAs, 64 pCCAs, and 36 dCCAs. In consistent with the DUSP11 function as a phosphatase toward phosho-RNA, the intracellular localization of DUSP11 was in the cell nucleus in CCA (**Figure 1B**). In iCCA, pCCA, and dCCA, the percentages of DUSP11 high expression were 44.59%, 53.85%, and 55.56%, respectively (**Table 1**). The basic information of CCA patients is shown in **Table 1**, including the sex, age, tumor size, differentiation, and T/N/M/TNM stage of the patients. The results of basic patients characters were consistent with previous studies (5, 18), supporting the validation of our cohort.

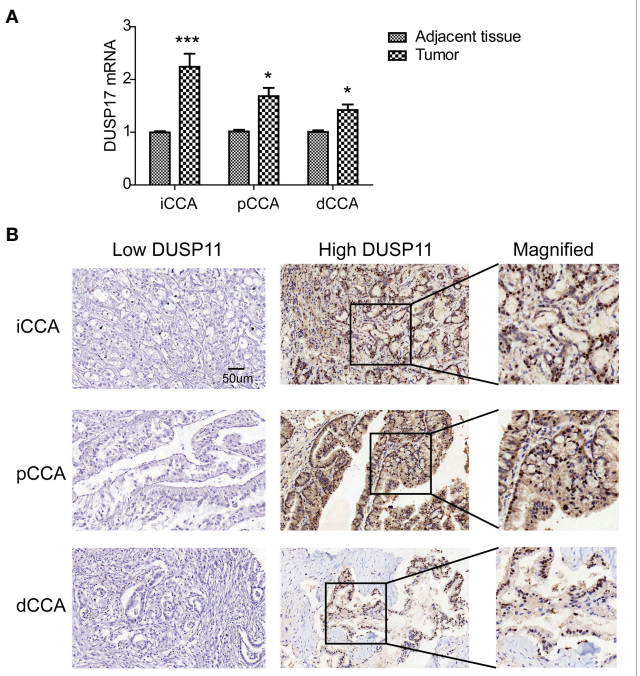

FIGURE 1 | Expression of DUSP11 in CCA tissues. **(A)** The expression of DUSP11 was detected with qPCR in eight pairs of iCCAs, pCCAs, and dCCAs, as well as their corresponding tumor-adjacent tissues. * represents $P < 0.05$ and *** represents $P < 0.0001$, calculated with paired t-test. **(B)** DUSP11 expression was investigated in 174 cases of CCAs, including 74 iCCAs, 64 pCCAs, and 36 dCCAs, by IHC. Representative images of low and high DUSP11 expressions were displayed.

Correlation Between Dual-Specificity Phosphatase 11 and Clinicopathological Factors

To screen the potential clinicopathological variables which may be associated with DUSP11 expression, we analyzed the correlation between the clinicopathological variables and DUSP11 with the chi-square test (**Table 2**). In iCCA, DUSP11 expression was significantly associated with the T stage. High expression of DUSP11 was positively correlated with an advanced T stage ($P = 0.008$), indicating that DUSP11 may be an attributor to iCCA infiltration. In pCCA and dCCA, no clinicopathological variables exhibited a significant correlation with DUSP11 expression.

TABLE 1 | Basic information of CCA patients.

Clinicopathologic parameters		iCCA		pCCA		dCCA	
		n	percentage	n	percentage	n	percentage
Age	<60	45	60.81%	40	61.54%	27	75.00%
(years)	≥60	29	39.19%	25	38.46%	9	25.00%
Sex	Male	37	50.00%	46	70.77%	21	58.33%
	Female	37	50.00%	19	29.23%	15	41.67%
Tumor size[#] (cm)	<3/5 cm	34	45.95%	37	56.92%	26	72.22%
	≥3/5 cm	40	54.05%	28	43.08%	10	27.78%
Differentiation	Well	17	22.97%	31	47.69%	17	47.22%
	Moderately	36	48.65%	25	38.46%	12	33.33%
	Poorly	21	28.38%	9	13.85%	7	19.44%
T stage	T1 + 2	52	70.27%	28	43.08%	16	44.44%
	T3 + 4	22	29.73%	37	56.92%	20	55.56%
N stage	N0	49	66.22%	52	80.00%	24	66.67%
	N1	25	33.78%	13	20.00%	12	33.33%
M stage	M0	70	94.59%	63	96.92%	36	100.00%
	M1	4	5.41%	2	3.08%	0	0.00%
TNM stage	I	27	36.49%	10	15.38%	13	36.11%
	II	8	10.81%	12	18.46%	22	61.11%
	III	15	20.27%	20	30.77%	1	2.78%
	IV	24	32.43%	23	35.38%	0	0.00%
DUSP11	Low	41	55.41%	30	46.15%	16	44.44%
	High	33	44.59%	35	53.85%	20	55.56%

[#]represents 5 cm for iCCA and 3 cm for pCCA/dCCA.

TABLE 2 | The correlations between clinicopathological factors and DUSP11.

Clinicopathologic parameters		iCCA			pCCA			dCCA		
		Low	High	P*	Low	High	P*	Low	High	P*
Age	<60	28	17	0.142	21	19	0.783	14	13	0.439
(years)	≥60	13	16		14	11		6	3	
Sex	Male	20	17	0.815	23	23	0.333	10	11	0.320
	Female	21	16		12	7		10	5	
Tumor size[#]	<3/5cm	22	12	0.138	19	18	0.643	14	12	0.739
(cm)	≥3/5cm	19	21		16	12		6	4	
Differentiation	Well	7	10	0.388	20	11	0.243[$]	10	7	0.753
	Moderately	22	14		11	14		7	5	
	Poorly	12	9		4	5		3	4	
T stage	T1+2	34	18	0.008	18	10	0.142	8	8	0.549
	T3+4	7	15		17	20		12	8	
N stage	N0	28	21	0.674	30	22	0.213	13	11	0.813
	N1	13	12		5	8		7	5	
M stage	M0	39	31	0.824[$]	34	29	0.933[$]	20	16	
	M1	2	2		1	1				
TNM stage	I	17	10	0.184	5	5	0.753	7	6	0.662
	II	6	2		8	4		12	10	
	III	5	10		11	9		1	0	
	IV	13	11		11	12				

**chi-square test, [#]represents 5 cm for iCCA and 3 cm for pCCA/dCCA, [$]represents Fisher test.*

Dual-Specificity Phosphatase 11 Was Correlated With Poor Prognosis in Intrahepatic Cholangiocarcinoma

We performed univariate analysis to evaluate the prognostic significance of DUSP11 and other clinicopathological factors in CCA. All clinicopathological factors and DUSP11 expression were enrolled into the univariate analysis. The Kaplan-Meier method was used to plot the OS curves, and the log-rank test was used to analyze the statistical difference between the subgroups (**Table 3**).

In iCCA, a high DUSP11 expression was significantly associated with a low OS rate (P = 0.002). The 5-year OS rates of patients with low and high DUSP11 were 52.6% and 9.4%, respectively (**Figure 2A**). However, the prognostic significance of DUSP11 in pCCA and dCCA was not remarkable (P = 0.354 and 0.459, respectively), though pCCA and dCCA patients with a high

TABLE 3 | The univariate analysis of DUSP11 and other clinicopathological factors.

Clinicopathologicparameters		iCCA		pCCA		dCCA	
		5-year OS	P*	5-year OS	P*	5-year OS	P*
Age	<60	36.1	0.435	40.6	0.142	43.8	0.600
(years)	≥60	28.3		36.4		54.7	
Sex	Male	31.5	0.288	37.8	0.789	37.8	0.789
	Female	35.3		35.1		35.1	
Tumor size#	<3/5 cm	44.7	0.007	41.9	0.329	41.9	0.389
(cm)	≥3/5 cm	22.8		41.1		32.9	
Differentiation	Well	35.6		49.0		64.3	
	Moderately	31.9	0.586	10.1	0	48.1	0.851
	Poorly	33.3		0		41.5	
T stage	T1 + 2	39.9	0.219	52.9	0.004	34.8	0.647
	T3 + 4	16.7		27.3		43.8	
N stage	N0	42.4	0.010	46.3	0.006	32.3	0.110
	N1	12.4		0		61.1	
M stage	M0	35.7	0.010	39.1	0.012		
	M1	0		0			
TNM stage	I	47.1		75.0		34.4	
	II	58.3	0.049	26.8	0.049	46.6	0.292
	III	22.5		30.8		0	
	IV	13.0		28			
DUSP11	Low	52.6	0.002	47.5	0.354	50.0	0.459
	High	9.4		25.2		45.9	

represents analysis with log-rank test; #represents 5 cm for iCCA and 3 cm for pCCA/dCCA.

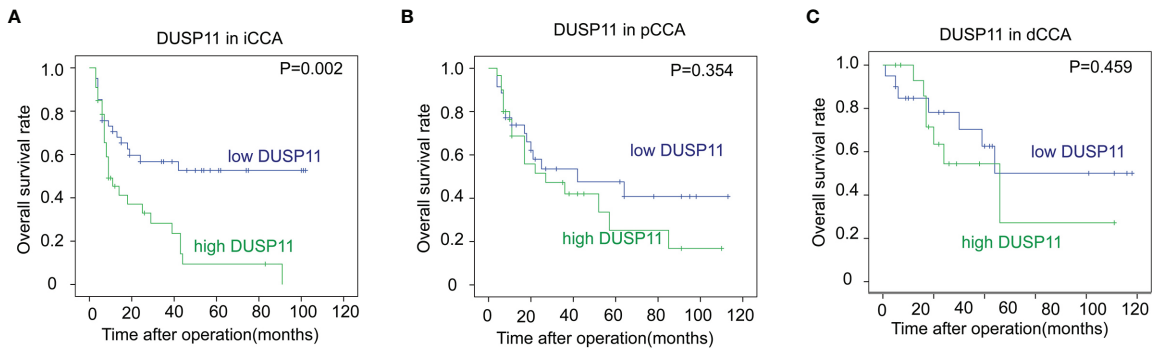

FIGURE 2 | The correlations between DUSP11 expression and the OS rates of CCA. **(A–C)** The survival curves of low and high expressions of DUSP11 in iCCA **(A)**, pCCA **(B)**, and dCCA **(C)** were plotted by the Kaplan-Meier method, and the statistical significance was analyzed with the log-rank test.

DUSP11 expression seemed to have poorer prognoses compared with those with a low DUSP11 expression (25.2% *vs.* 47.5% in pCCA, 45.9% *vs.* 50.0% in dCCA) (**Figures 2B, C**).

In iCCA, a large tumor size and advanced N stage and M stage, representing positive lymphatic invasion and distant metastasis, were also indicators of a poor prognosis (P = 0.007, 0.010 and 0.010 respectively) (**Figures 3A–C**). In addition, an advanced TNM stage was associated with the unfavorable outcome of iCCA as well (P = 0.049) (**Figure 3D**). In pCCA, poor differentiation was a notable indicator for a poor prognosis (P < 0.001) (**Figure 4A**). Moreover, advanced T stage, N stage, and M stage were also associated with a poor prognosis of pCCA (P = 0.004, 0.006, and 0.012, respectively) (**Figures 4B–D**). As expected, patients in an advanced TNM stage had a much poorer outcome than those in an early TNM stage (P = 0.049) (**Figure 4E**). In dCCA, no factors were defined to be associated with the OS time, which may be attributed to the small number of patients (n = 36).

Dual-Specificity Phosphatase 11 Was an Independent Prognostic Biomarker of Intrahepatic Cholangiocarcinoma

All the clinicopathological factors were enrolled into the Cox-regression hazard model for multivariate analysis (**Table 4**). In iCCA, DUSP11 was identified as an independent prognostic biomarker (P = 0.022, 95% confidence interval = 1.13–4.83). The hazard ratio (HR) of a high DUSP11 was 2.33, representing that patients with a high DUSP11 expression had a 2.33-fold time more than patients with a low DUSP11. However, the independent prognostic significance of

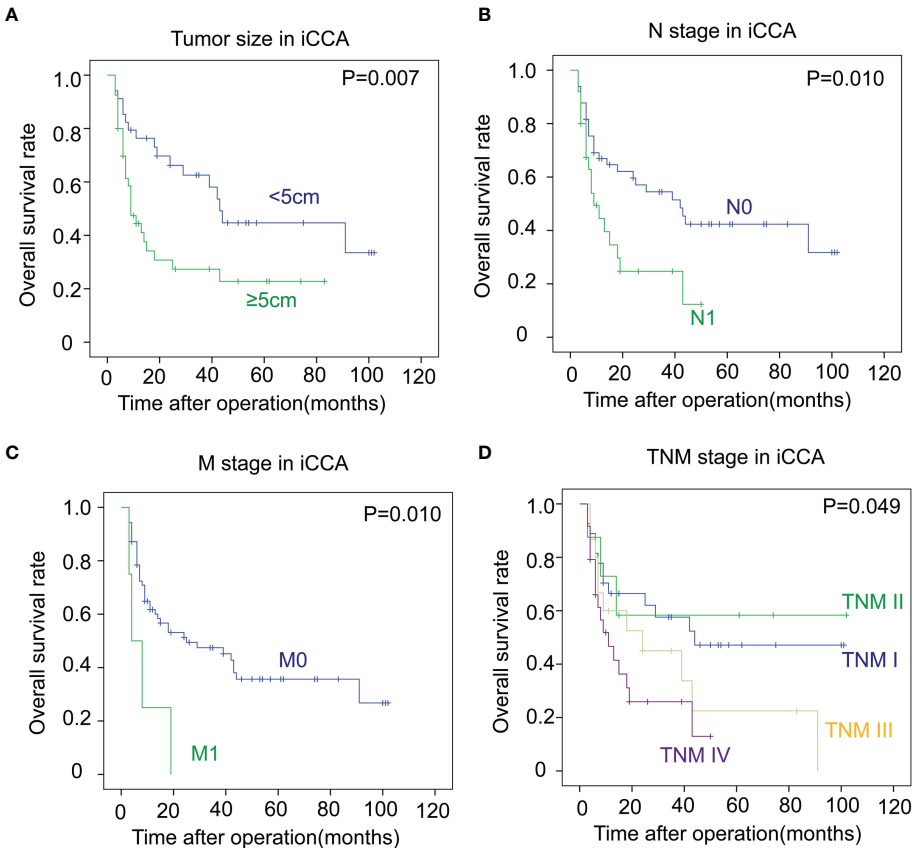

FIGURE 3 | The correlations between the clinicopathological factors and OS rates in iCCA. **(A–D)** In iCCA, the survival curves of tumor size **(A)**, N stage **(B)**, M stage **(C)**, and TNM stage **(D)** were plotted by the Kaplan-Meier method, and the statistical significance was analyzed with the log-rank test.

DUSP11 in pCCA and dCCA was not significant ($P = 0.993$ and 0.640, respectively).

Prognostic Significance of Dual-Specificity Phosphatase 11 in Extrahepatic Cholangiocarcinoma

To eliminate the effects of a small sample size towards the statistical significance, we merged pCCA and dCCA to extrahepatic CCA (eCCA), and performed the univariate analysis. In the 101 cases of eCCA, the prognostic significance of DUSP11 was still not remarkable ($P = 0.241$), but there existed a trend that a high DUSP11 expression seemed to correlate a low OS rate (**Table 5**). The 5-year OS rates of low and high DUSP11 were 48.7% and 26.0%, respectively (**Figure 5A**). Moreover, poor differentiation ($P = 0.016$), and advanced T stage ($P = 0.043$), M stage ($P = 0.003$), and TNM stage ($P = 0.012$) were all indicators for an unfavorable prognosis of eCCA (**Figures 5B–E**).

DISCUSSION

Compared with other common cancer types such as gastric cancer or lung cancer, CCA is characterized by its low rate of radical resection because of the specificity of the hepatic portal (19, 20). The low rate of radical surgery increases the difficulty of specimen obtainment and establishment of a large cohort (20, 21), which is the basement of biomarker identification and new drug target. However, more prognostic biomarkers of CCA are an urgent need to select the high-risk patients and help formulate the precise treatment. Our study collected a total of 174 cases of CCAs, which was a relatively large CCA cohort. We demonstrated for the first time that DUSP11 was an independent prognostic biomarker in CCA, suggesting that a high expression of DUSP11 was a post-operational risk and detecting DUSP11 could guide the individual treatment for patients with CCA.

In the seventh edition of AJCC/UICC in 2007, pCCA and dCCA were separated from eCCA and regarded as distinct subtypes (22). iCCA, pCCA, and dCCA have different morbidities, clinical characteristics, treatment strategies, and prognosis, but whether they have different biological features is still controversial (23). In some occasions, iCCA and eCCA have the same biomarkers such as EGFR and HER2 (24, 25), but several biomarkers exhibited a different prognostic significance in iCCA and eCCA (21, 26). In this study, we demonstrated that DUSP11 expression was correlated with a poor prognosis in iCCA but not eCCA. This result further supported that iCCA

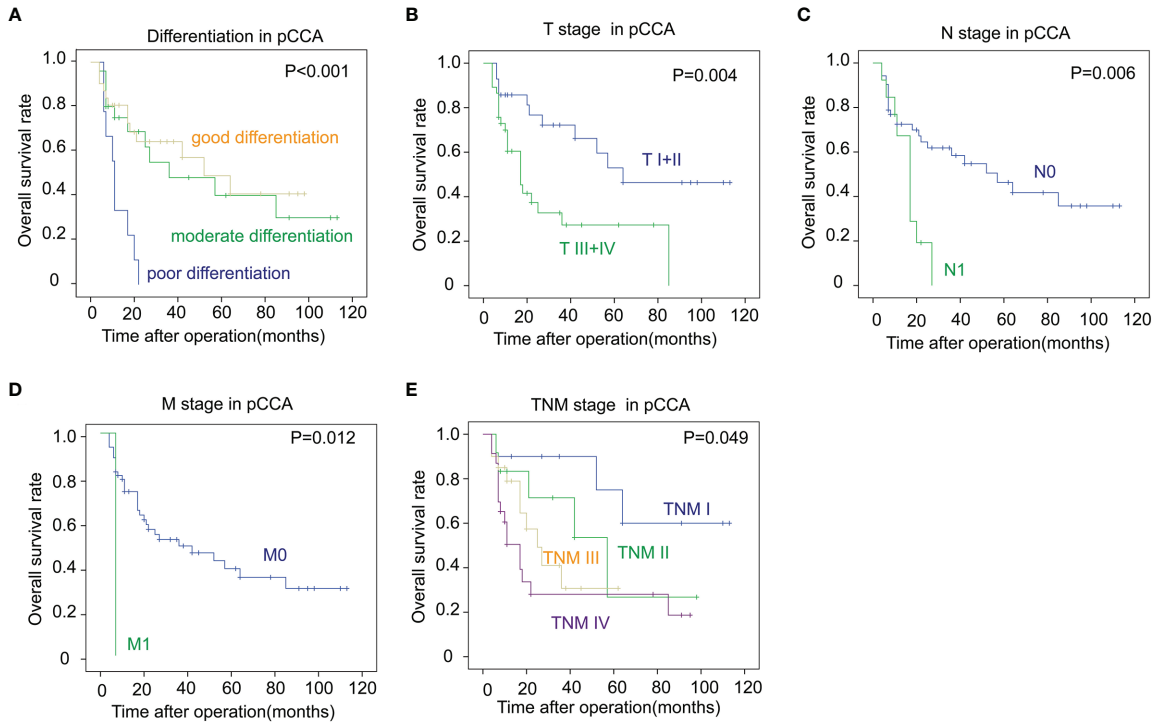

FIGURE 4 | The correlations between the clinicopathological factors and OS rates in pCCA. **(A–E)** Patients with pCCA were stratified according to the tumor differentiation **(A)**, T stage **(B)**, N stage **(C)**, M stage **(D)**, and TNM stage **(E)**, and the correlations between these factors and the OS rates were analyzed with the log-rank test.

TABLE 4 | Prognostic factors identified by multivariate analysis.

Clinicopathologic parameters		iCCA			pCCA			dCCA		
		HR	95%CI	P*	HR	95%CI	P*	HR	95%CI	P*
Age	<60	1			1			1		
(years)	≥60	1.34	0.69–2.57	0.387	1.98	0.82–4.75	0.129	0.83	0.17–3.93	0.810
Sex	Male	1			1			1		
	Female	0.84	0.45–1.62	0.575	0.85	0.36–1.99	0.702	0.59	0.17–2.10	0.415
Differentiation	Well	1			1			1		
	Moderately+Poorly	0.89	0.40–1.99	0.773	1.98	0.87–4.50	0.103	1.16	0.36–3.77	0.802
Size#	<3/5 cm	1			1			1		
	≥3/5 cm	1.76	0.89–3.48	0.107	1.29	0.60–2.74	0.516	0.49	0.09–2.55	0.397
T stage	T1 + T2	1			1			1		
	T3 + T4	0.83	0.40–1.71	0.604	2.15	0.99–4.71	0.057	1.60	0.45–5.72	0.467
N stage	N0	1			1			1		
	N1 + 2	1.66	0.81–3.40	0.167	2.67	1.14–6.23	0.023	0.37	0.06–2.12	0.262
M stage	M0	1			1					
	M1	2.63	0.78–8.78	0.117	5.44	1.02–28.96	0.047			
DUSP11	Low	1			1			1		
	High	2.33	1.13–4.83	0.022	1.01	0.47–2.13	0.993	1.31	0.42–4.17	0.643

Cox-regression model.
#*represents 5 cm for iCCA and 3 cm for pCCA/dCCA.*

and eCCA are two distinct cancer types, which have different biological factors and biomarkers.

In the era of high-throughput sequencing, numerous genetic alterations, such as the mutation, deletion, duplication, or translocation of PTP genes, are reported to be linked with diverse cancer phenotypes (27). The underlying mechanisms of the tumor suppressor or oncogenic role of PTPs in tumorigenesis or tumor progression are not fully understood. The loss or genetic alterations of several PTPs are shown to promote tumorigenesis, proliferation, and metastasis in *in vitro* and

TABLE 5 | The univariate analysis for eCCA.

Clinicopathologic parameters		eCCA	
		5-year OS	P*
Age (years)	<60	39.6	0.313
	≥60	39.6	
Sex	Male	38.1	0.372
	Female	39.0	
Tumor size[#] (cm)	<3 cm	39.5	0.886
	≥3 cm	40.4	
Differentiation	Well	45.7	
	Moderately	40.4	0.016
	Poorly	22.1	
T stage	T1 + 2	46.7	0.043
	T3 + 4	36.0	
N stage	N0	41.7	0.484
	N1	29.1	
M stage	M0	40	0.003
	M1	0	
TNM stage	I	51.9	
	II	37.3	0.012
	III	28.6	
	IV	28.0	
DUSP11	Low	48.7	0.241
	High	26.0	

*log-rank test.

[#]represents 5 cm for iCCA and 3 cm for pCCA/dCCA.

in vivo models, and these PTPs are generally considered to be tumor suppressors, including PTEN in prostate and breast cancer (28–30), SHP1 in leukemia and lymphomas (31, 32), PTPRF in colon, breast, and lung cancer (33, 34), and DUSP4 in breast, pancreas, and thyroid cancer (35–38). On the other hand, several tumor PTPs were identified as tumor suppressors because their genetic variations or loss facilitate tumorigenesis and tumor progression. For example, SHP2 was considered as an oncogene in breast cancer, leukemia, and gliomas (39–43), and PTP4A3 is an oncogene in breast, gastric, and colon cancer (44–46). The studies of DUSP11 in cancer are very few and the role of DUSP11 in tumor progression is nearly in vacancy. This is the first study reporting a definite role of DUSP11 as an oncogene because it is significantly associated with iCCA prognosis. Our results expand the understanding of the role of the DUSP family in cancer, and indicates DUSP11 as a potential drug target of CCA.

Although PTPs are attracting more and more attention as an onco-protein or a tumor suppressor, the improvement of PTP inhibitors as specific inhibitors or target drugs remains challenging. To obtain the specific small-molecule inhibitors are difficult because the catalytic domains of PTPs are very conserved. Till now, only a small proportion of PTPs have specific inhibitors, such as PTP1B, SHP2, and PTPN9 (47–50). However, the interacting proteins, substrates, and molecular

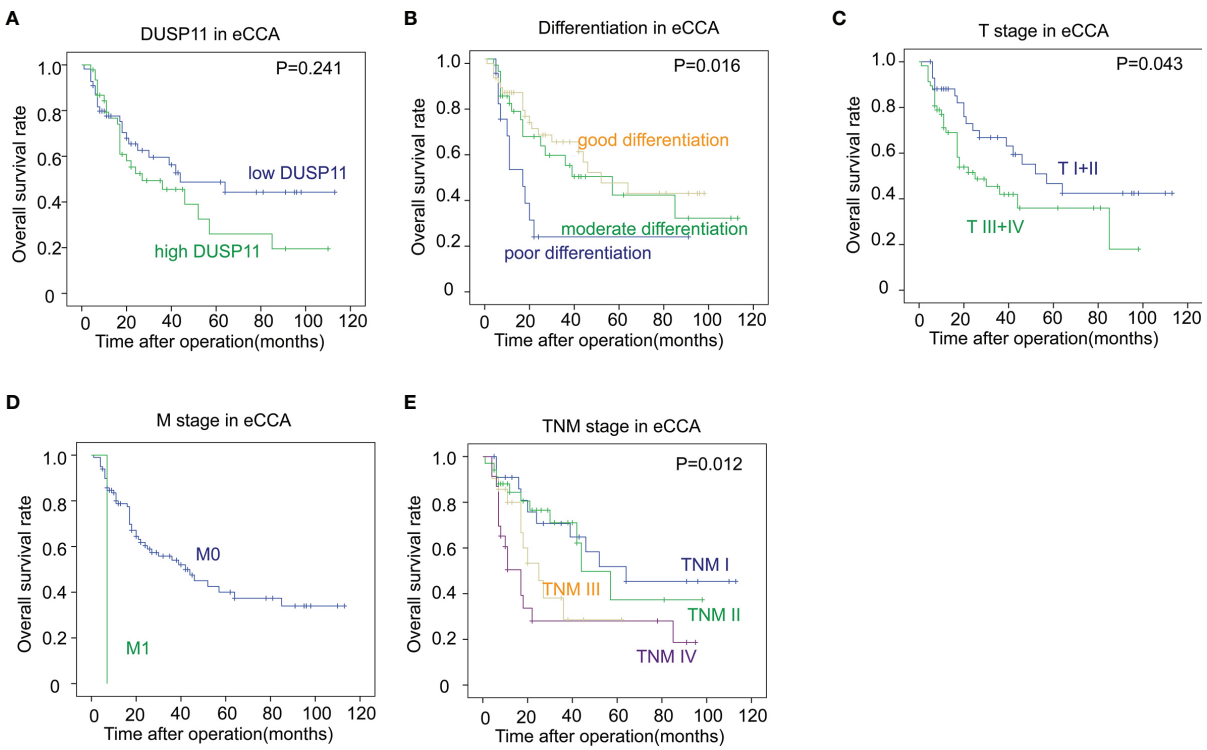

FIGURE 5 | The correlations between DUSP11, clinicopathological factors, and the OS rates in eCCA. **(A–E)** In the 101 cases of eCCA, the associations between the OS rate and DUSP11 expression **(A)** or clinicopathological factors including tumor differentiation **(B)**, T stage **(C)**, M stage **(D)**, and TNM stage **(E)** were analyzed with the log-rank test.

catalytic mechanism of DUSP11 are poorly understood, and there is still no available inhibitor of DUSP11. More studies on the expression profile of DUSP11 in cancer would help improve the therapeutic use of its potential inhibitor. We showed the clinical relevance of DUSP11 in CCA and suggested that the inhibitor towards DUSP11 may be a potential therapeutic strategy to CCA.

In conclusion, we, for the first time, investigated the expression of DUSP11 in 174 cases of CCAs, including 74 iCCAs, 64 pCCAs, and 36 dCCAs, and evaluated the clinical significance of DUSP11 by assessing DUSP11 correlation between the clinicopathological factors and prognosis. As a result, we demonstrated that DUSP11 expression was associated with tumor infiltration and the OS rate in iCCA, but not in pCCA or dCCA. DUSP11 was an independent biomarker of iCCA, indicating a poor prognosis. Our results suggested that a high expression of DUSP11 was a post-operational risk factor, and detecting DUSP11 could guide the individual treatment for patients with CCA.

DATA AVAILABILITY STATEMENT

The raw data supporting the conclusions of this article will be made available by the authors, without undue reservation.

ETHICS STATEMENT

The studies involving human participants were reviewed and approved by the Ethics Committee of Chinese Academy of Medical Sciences and Peking Union Medical College and National Cancer Center Shenzhen Hospital. The patients/participants provided their written informed consent to participate in this study.

AUTHOR CONTRIBUTIONS

Concept and design: XC. Administrative support: LX and PW. Specimen collection: XC, LX, PW, WZ, WL, and TL. Collection and assembly of data: XC, LX, PW, WZ, WL, and TL. Data analysis and interpretation: LX and PW. All authors contributed to the article and approved the submitted version.

FUNDING

The study is supported by Sanming Project of Medicine in Shenzhen (No. SZSM202011010) and Sanming Project of Medicine in Shenzhen (No. SZSM201911008).

REFERENCES

1. Rizvi S, Gores GJ. Emerging Molecular Therapeutic Targets for Cholangiocarcinoma. *J Hepatol* (2017) 67:632–44. doi: 10.1016/j.jhep.2017.03.026
2. Blechacz B. Cholangiocarcinoma: Current Knowledge and New Developments. *Gut liver* (2017) 11:13–26. doi: 10.5009/gnl15568
3. Sun R, Liu Z, Qiu B, Chen T, Li Z, Zhang X, et al. Annexin10 Promotes Extrahepatic Cholangiocarcinoma Metastasis by Facilitating EMT *via* PLA2G4A/PGE2/STAT3 Pathway. *EBioMedicine* (2019) 47:142–55. doi: 10.1016/j.ebiom.2019.08.062
4. Abou-Alfa GK, Sahai V, Hollebecque A, Vaccaro G, Melisi D, Al-Rajabi R, et al. Pemigatinib for Previously Treated, Locally Advanced or Metastatic Cholangiocarcinoma: A Multicentre, Open-Label, Phase 2 Study. *Lancet Oncol* (2020) 21:671–84. doi: 10.1016/S1470-2045(20)30109-1
5. Xu YF, Yang XQ, Lu XF, Guo S, Liu Y, Iqbal M, et al. Fibroblast Growth Factor Receptor 4 Promotes Progression and Correlates to Poor Prognosis in Cholangiocarcinoma. *Biochem Biophys Res Commun* (2014) 446:54–60. doi: 10.1016/j.bbrc.2014.02.050
6. Barr AJ, Ugochukwu E, Lee WH, King ON, Filippakopoulos P, Alfano I, et al. Large-Scale Structural Analysis of the Classical Human Protein Tyrosine Phosphatome. *Cell* (2009) 136:352–63. doi: 10.1016/j.cell.2008.11.038
7. Alonso A, Sasin J, Bottini N, Friedberg I, Osterman A, Godzik A, et al. Protein Tyrosine Phosphatases in the Human Genome. *Cell* (2004) 117:699–711. doi: 10.1016/j.cell.2004.05.018
8. Julien SG, Dube N, Hardy S, Tremblay ML. Inside the Human Cancer Tyrosine Phosphatome. *Nat Rev Cancer* (2011) 11:35–49. doi: 10.1038/nrc2980
9. Wang HM, Xu YF, Ning SL, Yang DX, Li Y, Du YJ, et al. The Catalytic Region and PEST Domain of PTPN18 Distinctly Regulate the HER2 Phosphorylation and Ubiquitination Barcodes. *Cell Res* (2014) 24:1067–90. doi: 10.1038/cr.2014.99
10. Patterson KI, Brummer T, O'Brien PM, Daly RJ. Dual-Specificity Phosphatases: Critical Regulators With Diverse Cellular Targets. *Biochem J* (2009) 418:475–89. doi: 10.1042/BJ20082234
11. Deshpande T, Takagi T, Hao L, Buratowski S, Charbonneau H. Human PIR1 of the Protein-Tyrosine Phosphatase Superfamily has RNA 5'-Triphosphatase and Diphosphatase Activities. *J Biol Chem* (1999) 274:16590–4. doi: 10.1074/jbc.274.23.16590
12. Yuan Y, Li DM, Sun H. PIR1, a Novel Phosphatase That Exhibits High Affinity to RNA . Ribonucleoprotein Complexes. *J Biol Chem* (1998) 273:20347–53. doi: 10.1074/jbc.273.32.20347
13. Burke JM, Kincaid RP, Nottingham RM, Lambowitz AM, Sullivan CS. DUSP11 Activity on Triphosphorylated Transcripts Promotes Argonaute Association With Noncanonical Viral microRNAs and Regulates Steady-State Levels of Cellular Noncoding RNAs. *Genes Dev* (2016) 30:2076–92. doi: 10.1101/gad.282616.116
14. Burke JM, Sullivan CS. DUSP11 - An RNA Phosphatase That Regulates Host and Viral Non-Coding RNAs in Mammalian Cells. *RNA Biol* (2017) 14:1457–65. doi: 10.1080/15476286.2017.1306169
15. Yang CY, Chuang HC, Tsai CY, Xiao YZ, Yang JY, Huang RH, et al. DUSP11 Attenuates Lipopolysaccharide-Induced Macrophage Activation by Targeting Tak1. *J Immunol* (2020) 205:1644–52. doi: 10.4049/jimmunol.2000334
16. Cai Y, Wu Q, Liu Y, Wang J. AZIN1-AS1, A Novel Oncogenic LncRNA, Promotes the Progression of Non-Small Cell Lung Cancer by Regulating MiR-513b-5p and DUSP11. *OncoTargets Ther* (2020) 13:9667–78. doi: 10.2147/OTT.S261497
17. Caprara G, Zamponi R, Melixetian M, Helin K. Isolation and Characterization of DUSP11, a Novel P53 Target Gene. *J Cell Mol Med* (2009) 13:2158–70. doi: 10.1111/j.1582-4934.2008.00616.x
18. Chen T, Li K, Liu Z, Liu J, Wang Y, Sun R, et al. WDR5 Facilitates EMT and Metastasis of CCA by Increasing HIF-1alpha Accumulation in Myc-Dependent and Independent Pathways. *Mol Ther J Am Soc Gene Ther* (2021) 29:2134–50. doi: 10.1016/j.ymthe.2021.02.017
19. DeOliveira ML, Cunningham SC, Cameron JL, Kamangar F, Winter JM, Lillemoe KD, et al. Cholangiocarcinoma: Thirty-One-Year Experience With 564 Patients at a Single Institution. *Ann Surg* (2007) 245:755–62. doi: 10.1097/01.sla.0000251366.62632.d3
20. Liu Z, Sun R, Zhang X, Qiu B, Chen T, Li Z, et al. Transcription Factor 7 Promotes the Progression of Perihilar Cholangiocarcinoma by Inducing the Transcription of C-Myc and FOS-Like Antigen 1. *EBioMedicine* (2019) 45:181–91. doi: 10.1016/j.ebiom.2019.06.023

21. Li Z, Liu J, Chen T, Sun R, Liu Z, Qiu B, et al. HMGA1-TRIP13 Axis Promotes Stemness and Epithelial Mesenchymal Transition of Perihilar Cholangiocarcinoma in a Positive Feedback Loop Dependent on C-Myc. *J Exp Clin Cancer Res CR* (2021) 40:86. doi: 10.1186/s13046-021-01890-1
22. Farges O, Fuks D, Le Treut YP, Azoulay D, Laurent A, Bachellier P, et al. AJCC 7th Edition of TNM Staging Accurately Discriminates Outcomes of Patients With Resectable Intrahepatic Cholangiocarcinoma: By the AFC-IHCC-2009 Study Group. *Cancer* (2011) 117:2170–7. doi: 10.1002/cncr.25712
23. Xu YF, Liu ZL, Pan C, Yang XQ, Ning SL, Liu HD, et al. HMGB1 Correlates With Angiogenesis and Poor Prognosis of Perihilar Cholangiocarcinoma *via* Elevating VEGFR2 of Vessel Endothelium. *Oncogene* (2019) 38:868–80. doi: 10.1038/s41388-018-0485-8
24. Claperon A, Mergey M, Nguyen Ho-Bouldoires TH, Vignjevic D, Wendum D, Chretien Y, et al. EGF/EGFR Axis Contributes to the Progression of Cholangiocarcinoma Through the Induction of an Epithelial-Mesenchymal Transition. *J Hepatol* (2014) 61:325–32. doi: 10.1016/j.jhep.2014.03.033
25. Pellat A, Vaquero J, Fouassier L. Role of ErbB/HER Family of Receptor Tyrosine Kinases in Cholangiocyte Biology. *Hepatology* (2018) 67:762–73. doi: 10.1002/hep.29350
26. Qiu B, Chen T, Sun R, Liu Z, Zhang X, Li Z, et al. Sprouty4 Correlates With Favorable Prognosis in Perihilar Cholangiocarcinoma by Blocking the FGFR-ERK Signaling Pathway and Arresting the Cell Cycle. *EBioMedicine* (2019) 50:166–77. doi: 10.1016/j.ebiom.2019.11.021
27. Andersen JN, Jansen PG, Echwald SM, Mortensen OH, Fukada T, Del Vecchio R, et al. A Genomic Perspective on Protein Tyrosine Phosphatases: Gene Structure, Pseudogenes, and Genetic Disease Linkage. *FASEB J Off Publ Fed Am Soc Exp Biol* (2004) 18:8–30. doi: 10.1096/fj.02-1212rev
28. Hollander MC, Blumenthal GM, Dennis PA. PTEN Loss in the Continuum of Common Cancers, Rare Syndromes and Mouse Models. *Nat Rev Cancer* (2011) 11:289–301. doi: 10.1038/nrc3037
29. Kinross KM, Montgomery KG, Kleinschmidt M, Waring P, Ivetac I, Tikoo A, et al. An Activating Pik3ca Mutation Coupled With Pten Loss Is Sufficient to Initiate Ovarian Tumorigenesis in Mice. *J Clin Invest* (2012) 122:553–7. doi: 10.1172/JCI59309
30. Petrocelli T, Slingerland JM. PTEN Deficiency: A Role in Mammary Carcinogenesis. *Breast Cancer Res BCR* (2001) 3:356–60. doi: 10.1186/bcr322
31. Cheng J, Zhang D, Zhou C, Marasco WA. Down-Regulation of SHP1 and Up-Regulation of Negative Regulators of JAK/STAT Signaling in HTLV-1 Transformed Cell Lines and Freshly Transformed Human Peripheral Blood CD4+ T-Cells. *Leukemia Res* (2004) 28:71–82. doi: 10.1016/S0145-2126(03)00158-9
32. Oka T, Ouchida M, Koyama M, Ogama Y, Takada S, Nakatani Y, et al. Gene Silencing of the Tyrosine Phosphatase SHP1 Gene by Aberrant Methylation in Leukemias/Lymphomas. *Cancer Res* (2002) 62:6390–4.
33. Shimozato O, Waraya M, Nakashima K, Souda H, Takiguchi N, Yamamoto H, et al. Receptor-Type Protein Tyrosine Phosphatase Kappa Directly Dephosphorylates CD133 and Regulates Downstream AKT Activation. *Oncogene* (2015) 34:1949–60. doi: 10.1038/onc.2014.141
34. Stevenson WS, Best OG, Przybylla A, Chen Q, Singh N, Koleth M, et al. DNA Methylation of Membrane-Bound Tyrosine Phosphatase Genes in Acute Lymphoblastic Leukaemia. *Leukemia* (2014) 28:787–93. doi: 10.1038/leu.2013.270
35. Balko JM, Cook RS, Vaught DB, Kuba MG, Miller TW, Bhola NE, et al. Profiling of Residual Breast Cancers After Neoadjuvant Chemotherapy Identifies DUSP4 Deficiency as a Mechanism of Drug Resistance. *Nat Med* (2012) 18:1052–9. doi: 10.1038/nm.2795
36. Balko JM, Schwarz LJ, Bhola NE, Kurupi R, Owens P, Miller TW, et al. Activation of MAPK Pathways Due to DUSP4 Loss Promotes Cancer Stem Cell-Like Phenotypes in Basal-Like Breast Cancer. *Cancer Res* (2013) 73:6346–58. doi: 10.1158/0008-5472.CAN-13-1385
37. Hijiya N, Tsukamoto Y, Nakada C, Tung Nguyen L, Kai T, Matsuura K, et al. Genomic Loss of DUSP4 Contributes to the Progression of Intraepithelial Neoplasm of Pancreas to Invasive Carcinoma. *Cancer Res* (2016) 76:2612–25. doi: 10.1158/0008-5472.CAN-15-1846
38. Mazumdar A, Poage GM, Shepherd J, Tsimelzon A, Hartman ZC, Den Hollander P, et al. Analysis of Phosphatases in ER-Negative Breast Cancers Identifies DUSP4 as a Critical Regulator of Growth and Invasion. *Breast Cancer Res Treat* (2016) 158:441–54. doi: 10.1007/s10549-016-3892-y
39. Bunda S, Burrell K, Heir P, Zeng L, Alamsahebpour A, Kano Y, et al. Inhibition of SHP2-Mediated Dephosphorylation of Ras Suppresses Oncogenesis. *Nat Commun* (2015) 6:8859. doi: 10.1038/ncomms9859
40. Dance M, Montagner A, Salles JP, Yart A, Raynal P. The Molecular Functions of Shp2 in the Ras/Mitogen-Activated Protein Kinase (ERK1/2) Pathway. *Cell Signalling* (2008) 20:453–9. doi: 10.1016/j.cellsig.2007.10.002
41. Xu R, Yu Y, Zheng S, Zhao X, Dong Q, He Z, et al. Overexpression of Shp2 Tyrosine Phosphatase Is Implicated in Leukemogenesis in Adult Human Leukemia. *Blood* (2005) 106:3142–9. doi: 10.1182/blood-2004-10-4057
42. Zhou X, Coad J, Ducatman B, Agazie YM. SHP2 Is Up-Regulated in Breast Cancer Cells and in Infiltrating Ductal Carcinoma of the Breast, Implying Its Involvement in Breast Oncogenesis. *Histopathology* (2008) 53:389–402. doi: 10.1111/j.1365-2559.2008.03103.x
43. Zhou XD, Agazie YM. Inhibition of SHP2 Leads to Mesenchymal to Epithelial Transition in Breast Cancer Cells. *Cell Death Differ* (2008) 15:988–96. doi: 10.1038/cdd.2008.54
44. Cramer JM, Zimmerman MW, Thompson T, Homanics GE, Lazo JS, Lagasse E. Deletion of Ptp4a3 Reduces Clonogenicity and Tumor-Initiation Ability of Colitis-Associated Cancer Cells in Mice. *Stem Cell Res* (2014) 13:164–71. doi: 10.1016/j.scr.2014.05.004
45. Fiordalisi JJ, Dewar BJ, Graves LM, Madigan JP, Cox AD. Src-Mediated Phosphorylation of the Tyrosine Phosphatase PRL-3 Is Required for PRL-3 Promotion of Rho Activation, Motility and Invasion. *PloS One* (2013) 8:e64309. doi: 10.1371/journal.pone.0064309
46. Walls CD, Iliuk A, Bai Y, Wang M, Tao WA, Zhang ZY. Phosphatase of Regenerating Liver 3 (PRL3) Provokes a Tyrosine Phosphoproteome to Drive Prometastatic Signal Transduction. *Mol Cell Proteomics MCP* (2013) 12:3759–77. doi: 10.1074/mcp.M113.028886
47. Erbe DV, Wang S, Zhang YL, Harding K, Kung L, Tam M, et al. Ertiprotafib Improves Glycemic Control and Lowers Lipids *via* Multiple Mechanisms. *Mol Pharmacol* (2005) 67:69–77. doi: 10.1124/mol.104.005553
48. Lantz KA, Hart SG, Planey SL, Roitman MF, Ruiz-White IA, Wolfe HR, et al. Inhibition of PTP1B by Trodusquemine (MSI-1436) Causes Fat-Specific Weight Loss in Diet-Induced Obese Mice. *Obes (Silver Spring)* (2010) 18:1516–23. doi: 10.1038/oby.2009.444
49. Xu YF, Chen X, Yang Z, Xiao P, Liu CH, Li KS, et al. PTP-MEG2 Regulates Quantal Size and Fusion Pore Opening Through Two Distinct Structural Bases and Substrates. *EMBO Rep* (2021) 22:e52141. doi: 10.15252/embr.202052141
50. Zhang X, He Y, Liu S, Yu Z, Jiang ZX, Yang Z, et al. Salicylic Acid Based Small Molecule Inhibitor for the Oncogenic Src Homology-2 Domain Containing Protein Tyrosine Phosphatase-2 (SHP2). *J Med Chem* (2010) 53:2482–93. doi: 10.1021/jm901645u

Conflict of Interest: The authors declare that the research was conducted in the absence of any commercial or financial relationships that could be construed as a potential conflict of interest.

Publisher's Note: All claims expressed in this article are solely those of the authors and do not necessarily represent those of their affiliated organizations, or those of the publisher, the editors and the reviewers. Any product that may be evaluated in this article, or claim that may be made by its manufacturer, is not guaranteed or endorsed by the publisher.

frontiers in Oncology

ORIGINAL RESEARCH
published: 05 October 2021
doi: 10.3389/fonc.2021.739660

Exploring the Expression and Prognostic Value of the TCP1 Ring Complex in Hepatocellular Carcinoma and Overexpressing Its Subunit 5 Promotes HCC Tumorigenesis

Jiahui Liu[1,2], Ling Huang[2], Yi Zhu[1,2], Yongyin He[1,2], Weiyun Zhang[2], Ting Lei[1,2], Junfeng Xuan[2], Bin Xiao[2,3], Linhai Li[2,3], Quan Zhou[2,4]* and Zhaohui Sun[1,2]**

[1] Graduate School, Guangzhou University of Chinese Medicine, Guangzhou, China, [2] Department of Laboratory Medicine, General Hospital of Southern Theater Command of People's Liberation Army (PLA), Guangzhou, China, [3] Qingyuan People's Hospital, The Sixth Affiliated Hospital of Guangzhou Medical University, Qingyuan, China, [4] Laboratory of Basic Medical Science, General Hospital of Southern Theater Command of PLA, Guangzhou, China

T-complex protein-1 ring complex (TRiC), also known as Chaperonin Containing T-complex protein-1 (CCT), is a multisubunit chaperonin required for the folding of nascent proteins. Mounting evidence suggests that TRiC also contributes to the development and progression of tumors, but there are limited studies on pathogenic functions in hepatocellular carcinoma (HCC). We comprehensively evaluated the expression pattern and biological functions of TRiC subunits using The Cancer Genome Atlas and The Human Protein Atlas. Expression levels of TRiC subunits TCP1, CCT2/3/4/5/6A/7/8 were significantly upregulated in HCC tissues at both transcript and protein levels, which predicted shorter overall survival (OS). Moreover, high mutation rates were found in several CCT subunits, and patients with altered CCT genes exhibited poorer clinical outcomes. Functional enrichment analysis showed that co-regulated genes were preferentially involved in 'protein folding' and 'microtubule-based process', while genes co-expressed with CCT subunits were primarily involved in 'ribosome' and 'spliceosome'. Knockout of CCT5 in a HCC cell line reduced while overexpression enhanced proliferation rate, cycle transition, migration, and invasion. In conclusion, these findings suggest that subunits of the TRiC may be potential biomarkers for the diagnosis of HCC and play an important role in the occurrence and development of HCC.

Keywords: TRiC complex, hepatocellular carcinoma, data mining, therapeutic target, prognosis

OPEN ACCESS

Edited by:
Zongli Zhang,
Qilu Hospital of Shandong University, China

Reviewed by:
Qianqian Song,
Wake Forest Baptist Medical Center, United States
Annette R. Khaled,
University of Central Florida, United States

***Correspondence:**
Zhaohui Sun
zhaohui3@126.com
Quan Zhou
springzhou@yeah.net
Linhai Li
mature303@126.com

Specialty section:
This article was submitted to Cancer Molecular Targets and Therapeutics, a section of the journal Frontiers in Oncology

Received: *11 July 2021*
Accepted: *08 September 2021*
Published: *05 October 2021*

Citation:
Liu J, Huang L, Zhu Y, He Y, Zhang W, Lei T, Xuan J, Xiao B, Li L, Zhou Q and Sun Z (2021) Exploring the Expression and Prognostic Value of the TCP1 Ring Complex in Hepatocellular Carcinoma and Overexpressing Its Subunit 5 Promotes HCC Tumorigenesis. Front. Oncol. 11:739660. doi: 10.3389/fonc.2021.739660

INTRODUCTION

Hepatocellular carcinoma (HCC) is one of the most frequent malignant tumors throughout the world. According to 2020 global cancer statistics, HCC mortality accounts for 8.3% of total cancer deaths, and there were an estimated 410,000 new HCC cases in China alone (1). Although HCC prognosis has improved greatly over the past 20 years, the five-year survival rate continues to be extremely low. Surgical resection and liver transplantation are the most effective therapeutic approaches for early-stage HCC, but most patients are diagnosed with intermediate- or advanced-stage disease. Several targeted drugs are now available that can prolong life, but again these have not markedly improved 5-year survival. The development of HCC is a complex process, and its occurrence, development, and metastasis are closely related to various gene mutations, the constantly activation of cell signal transduction pathways and abnormal neovascularization. A large number of studies have found the pathogenesis and therapeutic targets of HCC (2, 3), but there are currently no common therapeutic targets for broad-spectrum treatment. It may be possible to identify prognostic biomarkers and more efficacious treatment targets by screening tumor-related gene networks.

Molecular chaperonins aid in the proper folding of newly synthesized proteins. Group I chaperonins are found in bacterial cytosol and eukaryotic organelles, and include GroEL and the eukaryotic homology HSP60, while group II chaperonins are found in archaea and eukaryotic cytosol, and include the multisubunit T-complex protein-1 ring complex (TRiC), an ATP-dependent chaperone that may directly assist in the folding of about 10% of all cytosolic proteins (4). The TRiC is composed of eight paralogous subunits (TCP1, CCT2, CCT3, CCT4, CCT5, CCT6A, CCT6B, CCT7, CCT8) assembled into a double ring hexadecamer. Each subunit consists of three unique domains: an apical domain containing the substrate recognition site, an intermediate domain, and an equatorial domain containing the ATP-binding site. According to previous studies, the TRiC contributes to a variety of essential cellular functions and pathogenic processes such as tumorigenesis by stabilizing proteins involved in growth, proliferation, and apoptosis, including cyclin B and cyclin E (5–7). The TRiC also mediates the folding of cytoskeletal proteins such as actins and tubulins (8). Moreover, the TRiC contributes to carcinogenesis by directly regulating the folding and activity of oncogenic or tumor suppress proteins such as Von Hippel-Lindau (VHL), p53 and STAT3 (9–11).

Accumulating evidence also suggests that the expression levels of TRiC subunits are association with cancer development and progression. For instance, several studies have reported that elevated expression of subunit CCT3, a novel regulator of spindle integrity required for proper kinetochore–microtubule attachment during mitosis, is associated with poor HCC survival (12). Similarly, CCT8 overexpression has been linked to poor HCC prognosis (13) and glucose-regulated protein (GRP94)-mediated metastasis through CCT8 and JNK pathways (14). It was also found that CCT6A can accelerate the cell cycle G–S transition by upregulating cyclin D, thereby promoting HCC cell proliferation (15). Collectively, these findings suggest that TRiC subunits have potential utility as prognostic markers and treatment targets.

Therefore, we analyzed the expression levels and mutation rates of eight TRiC subunits in HCC by data mining. In the present study, the expression levels of TRiC subunits in HCC were significantly up-regulated compared to normal tissues except CCT6B. Moreover, high expression level of CCTs in HCC was associated with poor prognosis, also related to pathological grade and clinical stage. We also analyzed predicted functions and pathways of the mutations in CCTs and their frequently altered neighbor genes in HCC patients. Furthermore, significant correlations between expression levels of TRiC subunits in HCC were observed. Finally, gain/loss-of-function assays demonstrated that CCT5 plays an important role in proliferation, migration, invasion and cell cycle regulation of HCC cells. These findings may contribute to new targets and insights for diagnosis and treatment of HCC.

Abbreviations: TRiC/CCT, T-complex protein-1 ring complex; HCC, hepatocellular carcinoma; VHL, Von Hippel-Lindau; TCGA, The Cancer Genome Atlas; OS, overall survival; HR, hazard ratio (HR); DFS, disease-free survival; GO, gene ontology; KEGG, Kyoto encyclopedia of genes and genomes; BP, biological processes; CC, cellular components; MF, molecular function; PCNA, proliferating cell nuclear antigen; SCLC, small cell lung cancer; ESCC, esophageal squamous cell carcinoma; LNM, lymph node metastasis; PFDN, prefoldin; EMT, epithelial-mesenchymal transition; scaRNAs, small Cajal body RNAs; CNAS, copy number changes.

MATERIAL AND METHODS

ONCOMINE Analysis

The online cancer microarray database and data-mining platform ONCOMINE (www.oncomine.org), a compendium of dysregulated genes, pathways, and networks from 18,000 cancer gene expression profiles (16), was searched for genes differentially expressed between normal tissues and HCC tissues as evaluated by Student's t test. Datasets were extracted from TCGA pan cancer database using a cut-off p value of 0.01 and threshold fold-change of 2.

UALCAN Analysis

The online UALCAN database (http://ualcan.path.uab.edu) was used for analyzing and data mining based on The Cancer Genome Atlas (TCGA). UALCAN can be used to compare relative gene expression levels between normal and tumor samples, as well as between tumor subgroups stratified by pathological grade, clinical stage, age, sex, and other clinical features. We used the UALCAN to analyze the relationship between CCT subunit expression levels in the TCGA database and various clinicopathological features. Kaplan-Meier survival curves were also constructed to evaluate the associations of CCT subunit expression levels with clinical prognosis. Expression levels were compared by Student's t test, and $p < 0.05$ was considered statically significant. Kaplan-Meier curves were compared by log-rank test.

The Human Protein Atlas

The public Human Protein Atlas (https://www.proteinatlas.org) contains more than 10 million images of protein expression patterns at a single-cell level generated by immunocytochemistry and immunohistochemistry (17). It can be used to identify the protein expression profiles in normal and pathological human tissues, and to retrieve the related literature. In our study, the protein expression levels of TRiC subunits in normal human and HCC tissues were compared using immunohistochemical images and mass spectrometry-based quantitative proteomics analysis (18).

cBioPortal

The cBioPortal (www.cbioportal.org) is an online resource based on cancer genomics for exploring, visualizing, and analyzing multidimensional cancer genomics data. The types of genomic data integrated include somatic mutations, DNA copy number changes (CNAS), mRNA and miRNA expression, DNA methylation, and protein abundance. We used cBioPortal to analyze the genomic profiles and their correlations of TRiC subunits in the TCGA database. The search parameters included mutation, CNAS and mRNA expression z-Scores (RNASeq V2 RSEM), and somatic putative copy number alterations, which were generated from RNA-seq data by the GISTIC. Kaplan-Meier analysis was used to examine the associations of CCT mutation with overall survival (OS) and disease-free survival (DFS) in HCC, and $p<0.05$ by log-rank test was accepted as significant.

DAVID

The DAVID database (https://david.ncifcrf.gov/summary.jsp) provides information about systematic and comprehensive functional annotations for large-scale gene or protein lists. It is mainly used for function and pathway enrichment analysis of differentially expressed genes. In our study, GO and KEGG pathway enrichment were used to reveal the predominant functions and pathways of genes significantly associated with CCT mutations and co-expressed genes positively associated with CCT in the DAVID database. GO enrichment analysis included biological processes (BP), cellular components (CC), and molecular function (MF).

Cell Culture

The SK-HEP1 cell line was purchased from the Cell Bank of Shanghai Academy of Chinese Sciences and cultured in Dulbecco's Modified Eagle Medium (Gibco, USA) supplemented with 10% fetal bovine serum (Gibco, USA) at 37°C under a 5% CO_2 atmosphere.

Quantitative PCR

Total RNA was extracted using Trizol reagent (Invitrogen, Canada) and reverse transcribed using the Evo M-MLV RT Premix (Accurate Biology, China). Quantitative PCR was conducting using a CFX96 fluorescence quantitative PCR instrument and SYBR Green dye (Accurate Biology, China). Relative expression of CCT5 was calculated by $2^{-\Delta\Delta Ct}$ values. The primer sequences were as follows: 5'- AGTTAGCCAAGA GGCGGATAAG-3' (forward) and 5'-GACTTCGGTCATAG TCTGGATGG-3' (reverse) for CCT5, and 5'- GGTATGACAA CGAATTTGGC-3' (forward) and 5'- GAGCACAGGGTAC TTTATTG-3' (reverse) for GAPDH (the internal control).

Western Blotting

Total cellular proteins were extracted using RIPA lysis buffer, separated by 10% SDS-PAGE electrophoresis, and transferred to PVDF membranes. The membranes were incubated overnight at 4°C in blocking solution containing the following antibodies: CCT5 (Santa Cruz Biotechnology, USA, #SC374554), CDK2 (Cell Signaling Technology, USA, #2546), Cyclin D1 (Cell Signaling Technology, USA, #2978), CDK6 (Cell Signaling Technology, USA, #3136), Cyclin D3 (Cell Signaling Technology, USA, #2936), CDK4 (Cell Signaling Technology, USA, #12790), Cyclin A2 (Cell Signaling Technology, USA, #4656), Cyclin B1 (Cell Signaling Technology, USA, #12231), Cyclin E2 (Cell Signaling Technology, USA, #4132), Cyclin E1 (Cell Signaling Technology, USA, #4129), cdc2 (Cell Signaling Technology, USA, #9116), and GAPDH (Cell Signaling Technology, USA, #5174). After incubation with HRP-linked anti-rabbit/mouse IgG (Cell Signaling Technology, USA, #7074/ #7076) for 2 h, immunoreactive bands were visualized using ECL (Millipore, USA) and detected using the OI900 fully automatic chemiluminescence image analysis system. GAPDH was used as an internal reference.

Plasmid Construction, RNA Interference, and Transfection

The PCR products were resolved by 1% agarose gel electrophoresis and inserted into the pLVX-mCMV-ZsGreen-puro vector by NotI/EcoRI co-digestion and ligation using T4 DNA ligase to form overexpression plasmids. These plasmids were then electroporated into Escherichia coli DH5α competent cells and positive transformants selected on plates containing chloramphenicol. Correct insertion was confirmed by sequencing and comparison to the NCBI BLAST program.

Cultured SK-HEP1 cells were transfected with the indicated overexpression plasmid using Lipofectamine 3000 transfection reagent kit (Invitrogen, USA) strictly according to the manufacturer's instructions. After 48 h, cells were harvested for subsequent experiments. Other SK-HEP1 cell cultures were transfected with 50 nmol CCT5 siRNA (5'-CACCGACAG ATGGCTGAGA-3') (RiboBio, Guangzhou, China), and CCT5 gene silencing was confirmed by western blotting and PCR.

CCK8 Assay

After transfection for 48 h, SK-HEP1 cells were seeded onto 96-well plates at 5×10^3 cells/well in 100 µl DMEM with 10% FBS. The number of viable cells was estimated using a CCK-8 kit according to the manufacturer's instructions (Dojindo, Japan). At 1, 2, 3, and 4 days after seeding, 10 µl of CCK-8 solution was added to each well for 2 h at 37°C. The optical density of each well at 450 nm was determined using a microplate reader (Thermo Fisher Scientific, USA).

Colony Formation Assay

Cells were seeded in 6-well plates at a density of 1×10^3 and cultured at 37°C under 5% CO_2. After 10 days, colonies were washed twice with PBS, fixed with 4% paraformaldehyde for 60 min, and stained with 1% crystal violet (LEAGENE, China) for 30 min. Colonies were photographed and counted.

Wound Healing Assay

After transfection for 48 h, SK-HEP1 cells were seeded in 6-well plates at 8×10^4/well and cultured for 12 h. When cells reached 80%–90% confluence, a scratch was made through the center of each well using a 200-µl sterile pipette tip. The cells were then washed twice with PBS, incubated in serum-free DMEM, and photographed at 0 h and 24 h to assess cell migration into the bare region (wound healing). Images were analyzed by ImageJ software to calculate the % wound closure.

Transwell Assay

Cell migration was also evaluated by transwell migration assays (Corning, USA), and cell invasion was assessed using matrigel invasion chambers (Cat. Corning, USA). Briefly, the upper chambers were seeded with 8×10^4 cells in serum-free DMEM, and 800 µl DMEM containing 10% FBS was added to the lower chambers. After 24 h of culture at 37°C under 5% CO_2, cells on the reverse side of the insert (migrating/invading cells) were stained with 0.5% crystal violet and three fields were randomly selected and photographed at ×100 magnification.

Cell Cycle Assay

At 48 h after transfection, cells were collected and fixed overnight with 75% alcohol at −20°C. After washing with PBS, cells were incubated with propidium iodide (PI)/RNase A solution (Cat. #abs50005, Absin, China) for 20 min at 37°C. Samples were analyzed within 1 h of staining using a CytoFLEX flow cytometer (Beckman-Coulter, USA) and ModFit LT software.

Statistical Analysis

All statistical analyses were conducted using SPSS version 26 and GraphPad Prism 8. Data are presented as mean ± standard deviation (SD) of three independent experiments. Two group means were compared by Student's t test and more than two group means by one-way ANOVA. Overall and disease-free survival were compared by the Kaplan-Meier method and log-rank test. A P-value < 0.05 (two-tailed) was considered statistically significant for all tests.

Immunofluorescence Analysis

The cells were fixed in 4% paraformaldehyde for 10 min at −20°C and then permeabilized 10 min with 0.1% Triton X-100 at room temperature. Following blocking in 10% goat serum for 30 min at room temperature, cells were incubated with the primary antibodies anti−CCT5 (Santa Cruz Biotechnology, USA, #SC374554), and anti−β−tubulin (Sungene Biotech, China, #KM9003T) at 4°C overnight. After that, the cells were washed with TBST and incubated 1 h with 1µLAlexa Fluor®488 donkey anti-mouse lgG at room temperature (life technologies, USA, #A21202). After washing with TBST, nuclei were stained with DAPI (Solarbio, China) for 5 minutes. Images were acquired by confocal microscopy (Leica Microsystem SP8, Wetzlar, Germany). The fluorescence intensity was quantified using ImageJ software.

RESULTS

Differential Expression of TRiC Subunits in HCC

We first compared expression levels of TRiC subunits TCP1, CCT2/3/4/5/6A/6B/7/8 at both mRNA and protein levels between HCC patients and controls and among HCC subgroups using the ONCOMINE database, UALCAN database, and The Human Protein Atlas. We used the ONCOMINE database to compare the mRNA expression levels of the eight TRiC subunits in 20 different tumor types to corresponding normal tissues (**Figure 1A**) and found that all except CCT6B were significantly upregulated in multiple HCC datasets. For instance, in the Roessler Liver 2 dataset (**Supplementary Figure 1**), CCT2 was overexpressed by 2.084-fold in HCC tissues compared to adjacent non-tumor tissues (p=1.33E-53) (19). In the Wurmbach Liver dataset (20), CCT3 was also upregulated by 2.944-fold (p=4.60E-108). In the Roessler Liver dataset, CCT5 was overexpressed by 2.17-fold 3 (p=2.57E-72), while CCT6A was overexpressed by 2.897-fold in the Roessler dataset (p= 2.32E-85) and by 2.122-fold in the Wurmbach Liver dataset (p= 3.08E-5). Findings from the UALCAN database were generally consistent with those from ONCOMINE. As shown in **Figure 1B** and **Supplementary Figure 2**, the expression levels of TCP1, CCT/2/3/4/5/6A/7/8 were significantly upregulated, while CCT6B showed relatively stable low-level expression in HCC tissues (all p<0.01).

We then used The Human Protein Atlas to examine if these TRiC subunits were also differentially expressed in HCC tissues at the protein level. In accord with mRNA results, TCP1, CCT2/3/4/5/6A/7/8 (e.g., all except CCT6B) were highly expressed in HCC tissues but moderately expressed in normal liver tissues (**Figure 2A**). Since immunohistochemistry cannot accurately quantify protein abundance, we searched for additional mass spectrometry-based proteomics data (18) and obtained similar results (**Figure 2B**). Thus, most TRiC subunits appear overexpressed in HCC at both protein and mRNA levels, and thus could be prognostic predictors or even treatment targets.

The mRNA Expression of TRiC Subunits in HCC: Association With Clinical Pathological Parameters

The UALCAN database was used to further analyze the relationships between CCT expression and clinicopathological features. Overall, our results showed that the expression of CCT was significantly correlated with tumor grade and stage (both P<0.05) As shown in **Figure 3**, the mRNA expression level of CCT significantly increased with tumor grade except CCT6B. The mRNA expression levels of TCP1, CCT2/3/4/5/6A/7/8 in HCC patients were lower in grade 1/2 than grade 3/4, while CCT6B

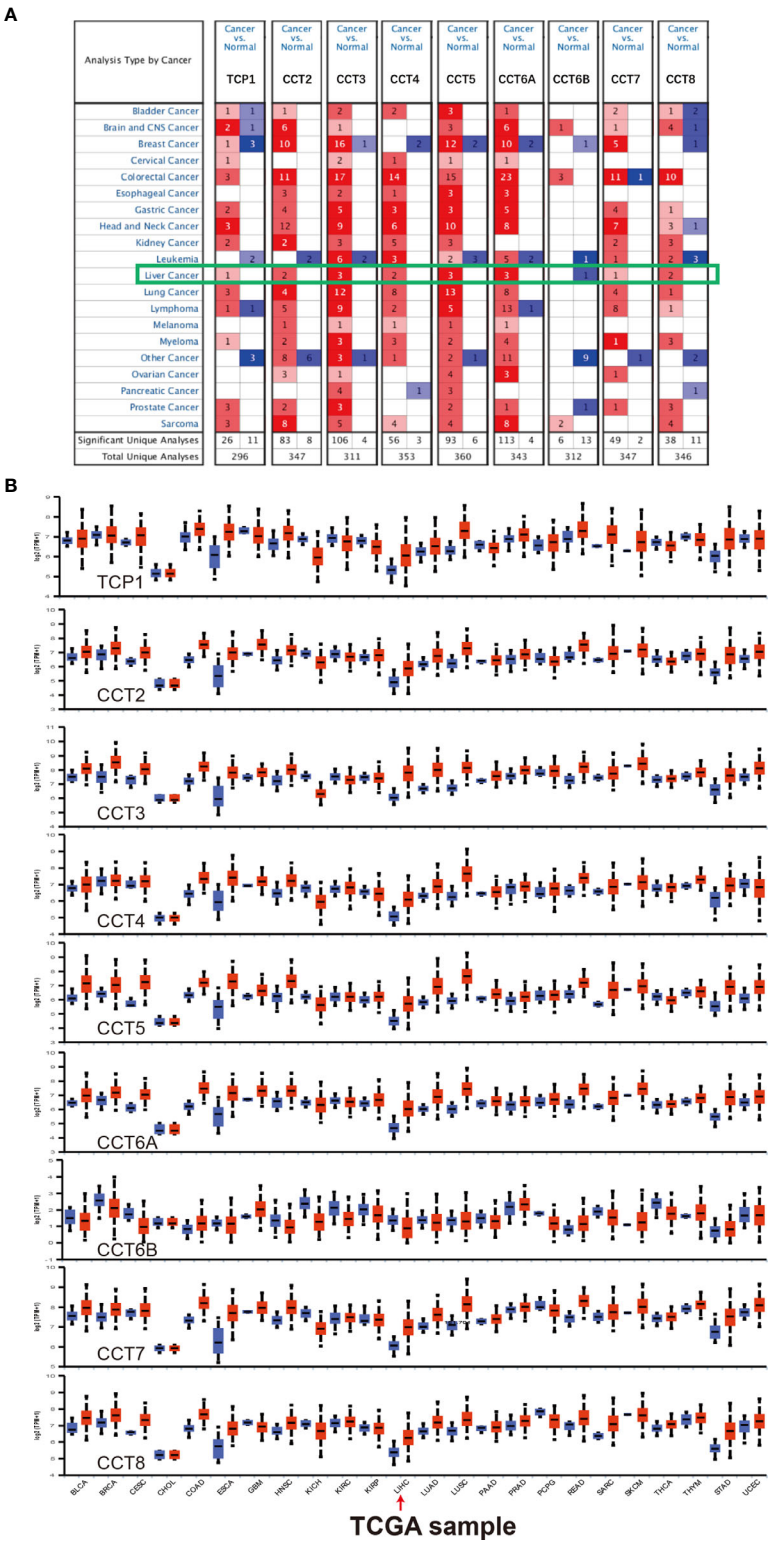

FIGURE 1 | Differential expression of TRiC subunits in 20 different cancer types (from ONCOMINE and UALCAN). **(A)** Differential expression of CCT mRNAs in various cancer types compared to corresponding normal tissues (from the ONCOMINE database). Red: overexpression; Blue: downregulated expression (threshold fold-change of 1.5, $p < 0.01$ for significance, gene rank: 10%, data type: mRNA). **(B)** Differential CCT mRNA expression levels in various cancer types compared to normal tissues (from the UALCAN database).

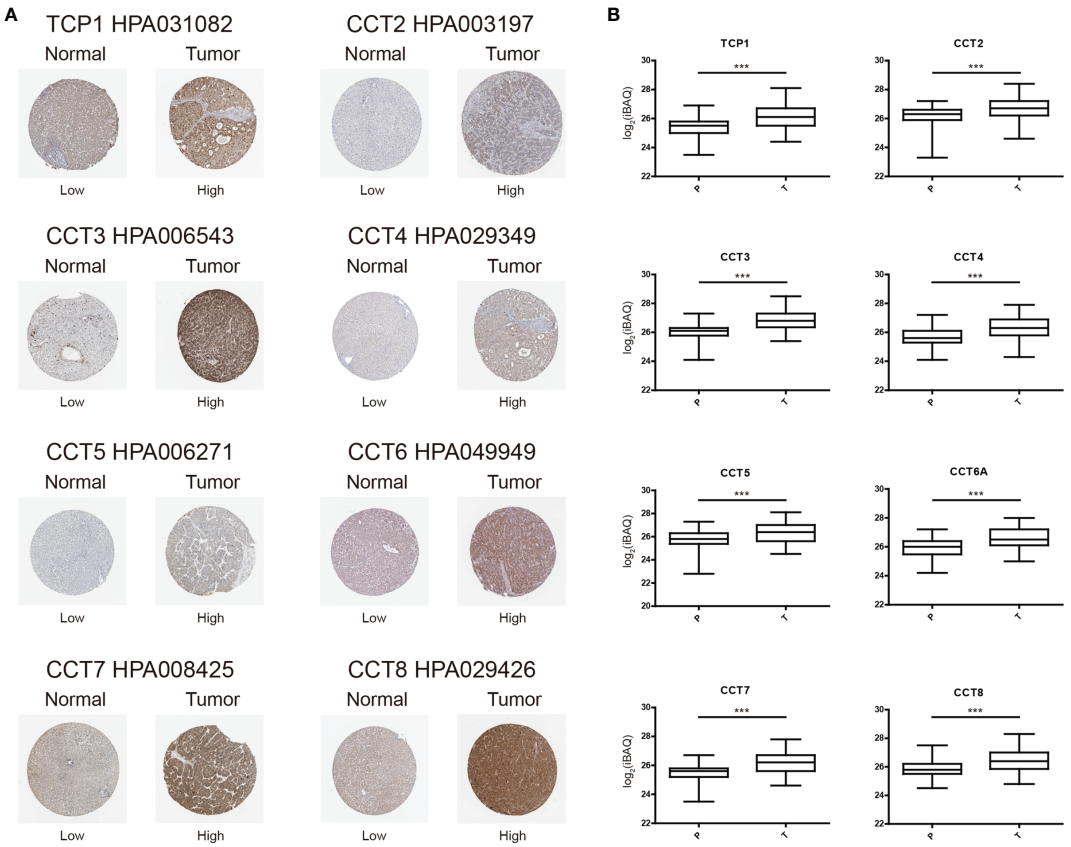

FIGURE 2 | Elevated expression levels of TRiC subunit proteins in HCC tissues *versus* normal tissues as evidenced by immunohistochemistry (from The Human Protein Atlas). **(A)** Representative images of tissues immunostained with the indicated HPA antibodies. **(B)** Mass spectrometry-based quantitative proteomics analysis. ***p < 0.001.

expression decreased as the tumor grade increased. Expression levels of CCT3 and CCT5 also differed significantly among grade 1, grade 2, and grade 3 by pair-wise comparisons (all P<0.05) and increased progressively with grade. However, expression in grade 4 did not differ significantly due to the low number of cases. Nonetheless, late-stage HCC patients tended to show higher TCP1, CCT2/3/4/5/6A/7/8 expression levels, while CCT6B expression was lower in the late stage (**Supplementary Figure 3**).

Elevated TRiC Subunit Expression Levels Were Associated Poorer HCC Prognosis

Consistent with the aforementioned associations between elevated TRiC subunit expression and higher HCC grade, Kaplan-Meier analysis revealed shorter OS among patients with higher TRiC complex expression (HR=2.53, 95% CI: 1.78–3.61, p<0.001) (**Figure 4**). Moreover, high expression of TCP1 (HR=1.51, 95%CI: 1.04–2.19, p=0.028), CCT2 (HR=2.31, 95%CI: 1.62–3.28, p<0.001), CCT3 (HR=2.01, 95%CI:1.42–2.48, p<0.001), CCT4 (HR=2.1, 95%CI: 1.48–2.97, p<0.001), CC5 (HR=2.35, 95%CI: 1.64–3.37, p<0.001), CCT6A (HR=2.42, 95% CI: 1.69–3.46, p<0.001), CCT7 (HR=1.86, 95%CI: 1.28–2.68, p<0.001), and CCT8 (HR=1.7, 95%CI: 1.21–2.57, p<0.001) predicted shorter OS, while overexpression of CCT6B (HR=0.57, 95%CI: 0.4–0.81, p<0.001) predicted longer survival. Collectively, these data suggest that transcriptional expression levels of TRiC subunits could be independent prognostic biomarkers for OS in HCC.

Genetic Mutations of TRiC Subunits in HCC

We then used cBioPortal to detect mutations and copy number alterations of TRiC subunits in HCC. Nearly half of the HCC patients in the database carried TRiC subunit gene alterations, with highest mutation rates in CCT3 (27%), CCT5 (18%), and TCP1 (12%) (**Figure 5**). The mRNA up-regulation and gene amplification were the most common CCT alterations in HCC patients. Moreover, we found significant correlations between subunit mRNA expression from TCGA and copy number alterations in HCC from cBioPortal for TCP1, CCT3, and CCT5, suggesting that alternations in CCT expression levels are caused by alternations at the genomic level. Furthermore, Kaplan-Meier survival analysis showed that patients with TRiC gene alterations demonstrated shorter OS (p<0.01) and DFS (p=0.018) than patients without these alterations.

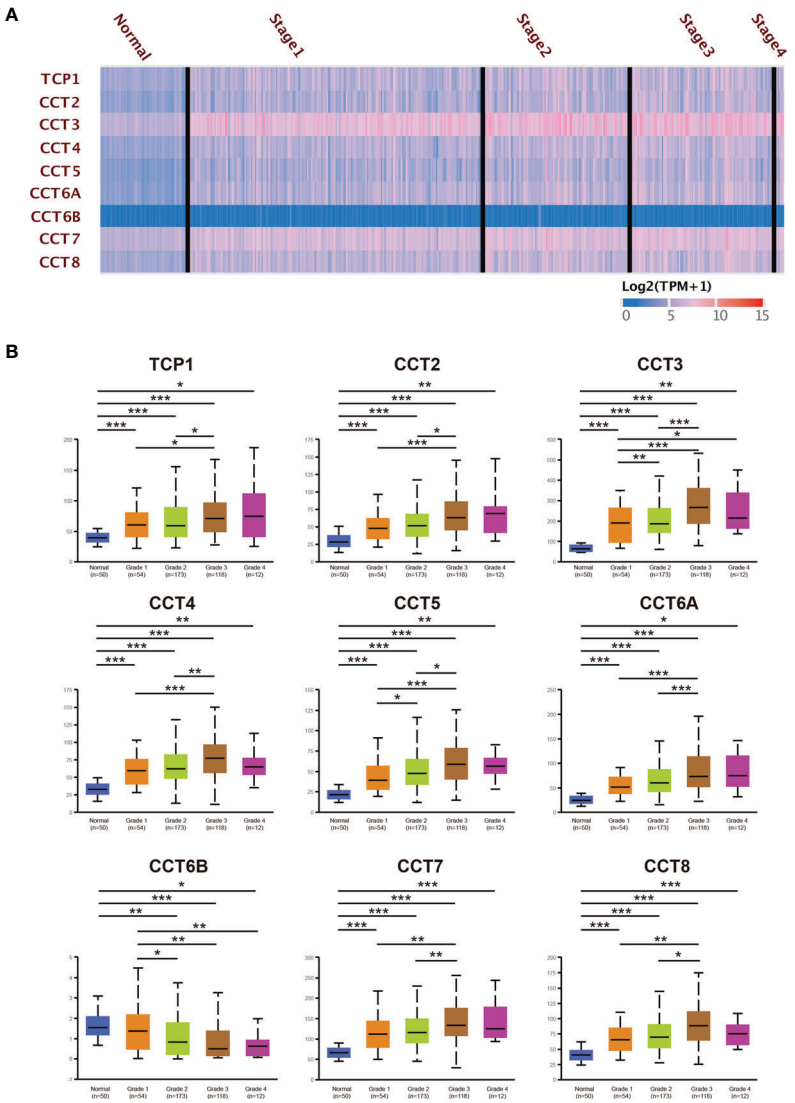

FIGURE 3 | Greater TRiC subunit mRNA expression levels are associated with higher HCC tumor grade (from UALCAN). **(A)** Heatmap shows the different expressed TRiC subunits in HCC patients with different grades. **(B)** The expression levels of TRiC subunits in HCC patients with different grades. *p < 0.05, **p < 0.01, ***p < 0.001.

Gene Network Construction and Functional Enrichment Analysis of CCT and Neighboring Genes in HCC

We also used cBioPortal to construct a biological interaction network of TRiC subunits with their associated altered neighbor genes. The results showed that, the neighbor genes of TRiC subunits with the most frequent alterations were TP53, PFDN2, GBA, and CCNE2 (**Figure 6A**). According to GO enrichment analysis (**Figure 6B**), CCT and their neighbor genes involved predominantly in 'protein folding', 'microtubule-based process', 'positive regulation of protein localization to Cajal body', 'cytoskeleton organization', and 'positive regulation of telomerase RNA localization to Cajal body'. The proteins encoded by these genes are mainly located in 'microtubule', 'chaperonin-containing T-complex', 'zona pellucida receptor complex', 'myelin sheath', and 'prefoldin complex', and enriched in the MF annotations 'structural constituent of cytoskeleton', 'GTPase activity' and 'unfolded protein binding'.

In addition to the CCT neighbor genes, we also investigated proteins with expression patterns similar to CCT subunits since such proteins may have similar functions. A total of 1,420 co-expressed proteins were identified with a threshold $r > 0.4$ and $P < 0.05$. According to the DAVID database, these proteins are involved mainly in 'rRNA processing', 'translational initiation', and 'translation', mainly located in 'nucleoplasm', 'ribosome', 'membrane', and 'intracellular ribonucleoprotein complex', and function in 'poly (A) RNA binding', 'structural constituent of ribosome', 'protein binding', and 'RNA binding' (**Figure 6C**).

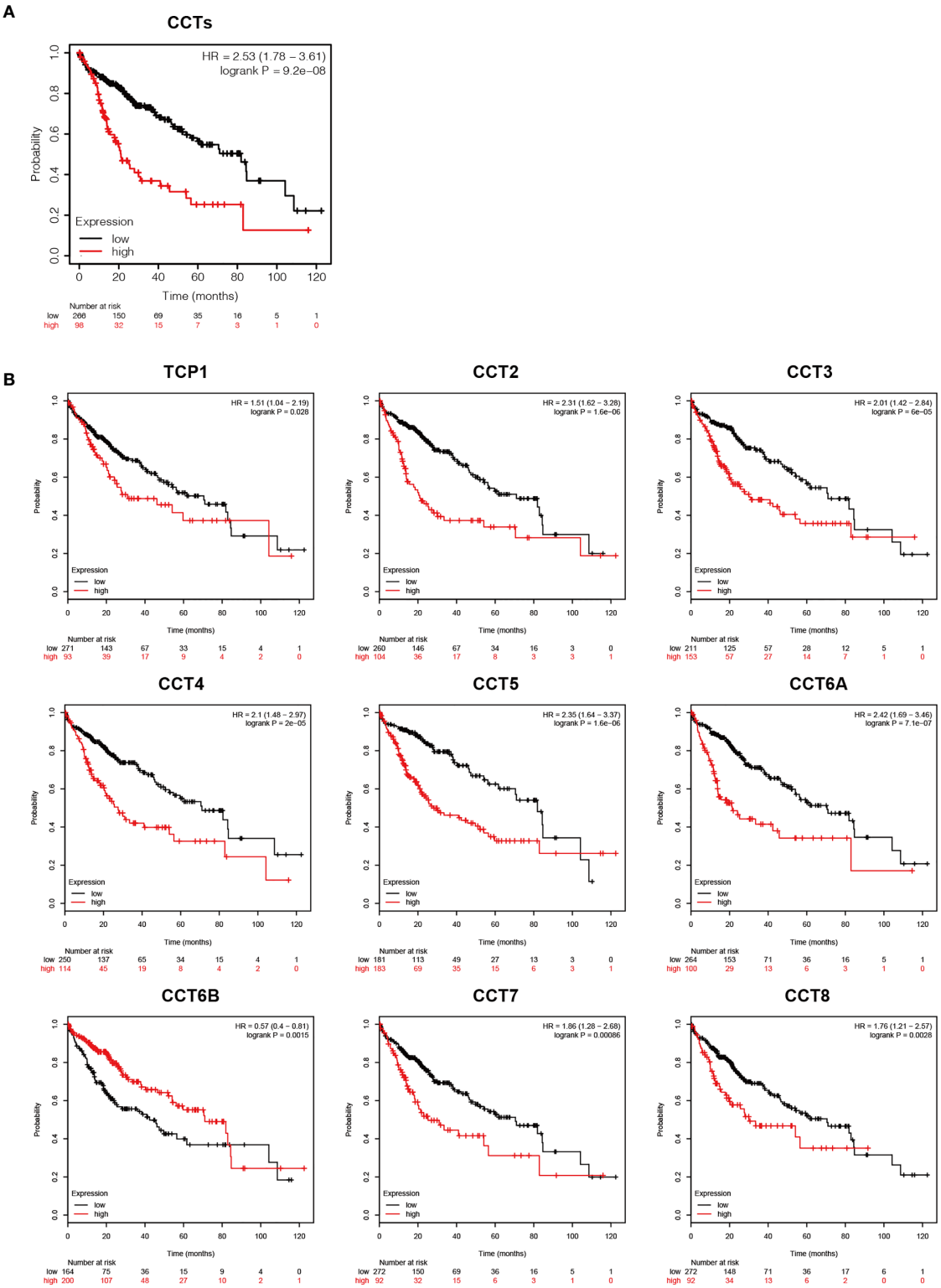

FIGURE 4 | Prognostic values of TRiC subunits for HCC (from UALCAN). **(A)** Survival analysis of the TRiC. **(B)** Survival analysis of individual TRiC subunits.

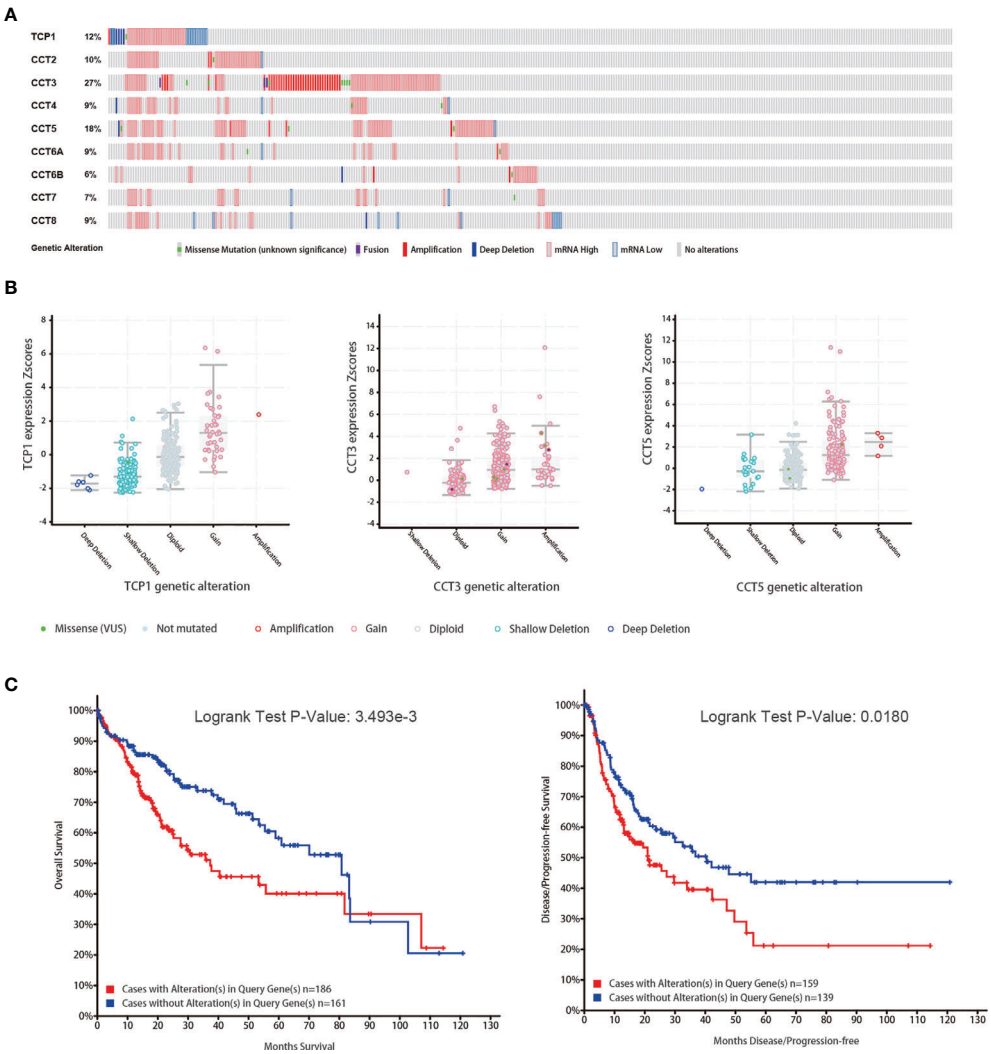

FIGURE 5 | TRiC gene mutations and altered mRNA copy numbers are association with overall survival (OS) and disease-free survival (DFS) (from cBioPortal). **(A)** Summary of CCT gene mutation rates. **(B)** CCT gene mutation types. **(C)** Associations of CCT mutations with OS and DFS.

According to KEGG enrichment analysis, these co-expressed proteins are involved in 'ribosome', 'spliceosome', 'RNA transport', 'cell cycle', 'pyrimidine metabolism', and 'proteasome'.

Significant Correlation Between Expression Levels of TRiC Subunits in HCC

After that, we explored the correlation between the eight subunits in the cBioportal database. It showed a positive correlation between TCP1, CCT2/3/4/5/6A/7/8 and a negative correlation between CCT6B and other eight subunits of TRiC (**Figure 7A**). We next investigated the impact of altered one single subunit expression on the expression of other subunits. Overexpression efficiency following CCT5 vector transfection and knockdown efficiency following siRNA transfection were first confirmed by WB and qPCR (**Figure 7B**). CCT5 overexpression significantly increased the expression levels of TCP1, CCT2/3/4/5/6A/7/8 while CCT6B decreased. Reverse validation experiment revealed that CCT5 knockdown reduced the expressions of TCP1, CCT2/3/4/5/6A/7/8 and elevated CCT6B instead (**Figure 7C**). The aberrant expression of a single TRiC subunit altered the expression level of other subunits which suggested the evident correlation between TRiC subunits.

CCT5 Overexpression Promoted Proliferation, Migration, Invasion, and G1–S Transition of HCC Cells

We then examined the specific cancer-related functions of the TRiC subunit CCT5 in the SK-HEP1 HCC cell line by targeted overexpression and knockdown. Knockdown of CCT5 significantly suppressed colony formation while CCT5

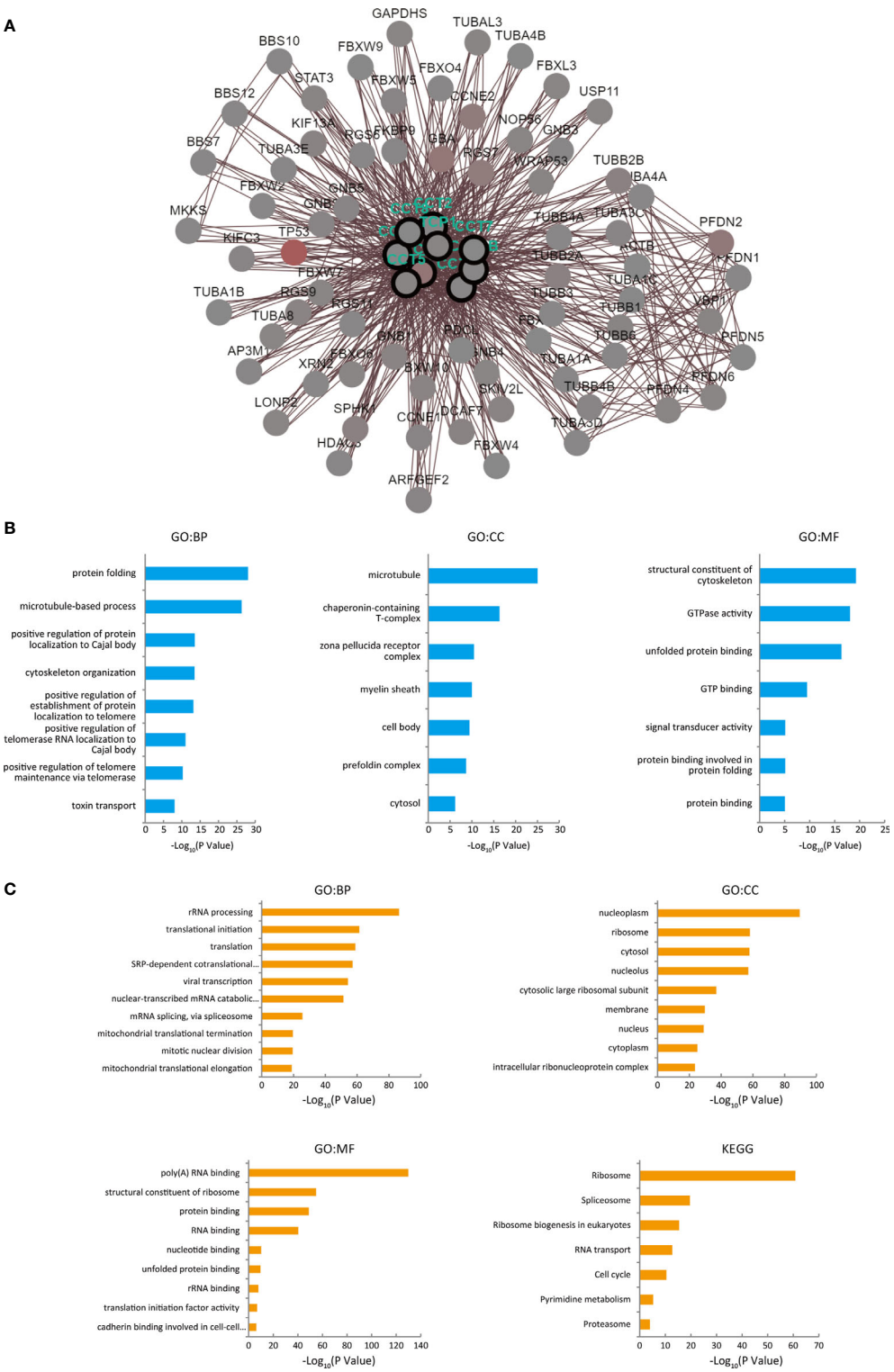

FIGURE 6 | Functional enrichment analyses of TRiC subunit genes, their neighbor genes and their co-expressed genes in HCC patients (from cBioPortal and DAVID). **(A)** Biological interaction network of CCT genes and their neighbor genes which were associated with CCT mutations. **(B)** GO enrichment analysis showing biological processes, cellular components, and molecular functions of CCT subunit and neighboring network genes. **(C)** GO functional annotation and KEGG pathway enrichment analysis of CCT subunit proteins and co-expressed genes were conducted proteins using DAVID.

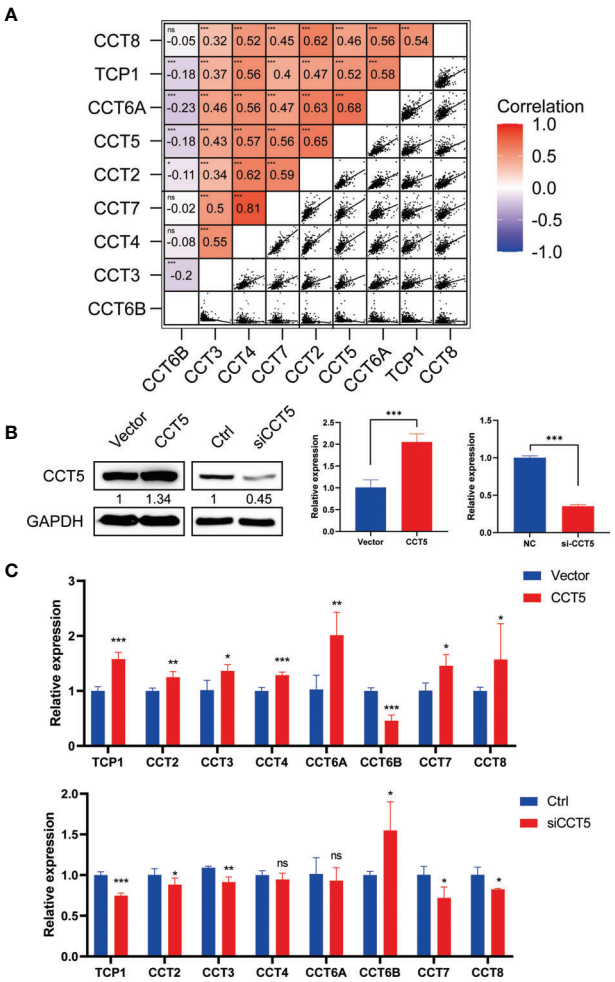

FIGURE 7 | Significant correlation between expression levels of TRiC subunits in HCC. **(A)** Pearson correlation analysis of the TRiC subunits in HCC (from cBioPortal). **(B)** Efficiencies of CCT overexpression and knockdown in SK-HEP1 cells following plasmid and siRNA transfection, respectively, as confirmed by western blotting (left) and qPCR (right). **(C)** CCT5 overexpression and knockdown-induced changes in the expression of other subunits were confirmed by qPCR. *p < 0.05, **p < 0.01, ***p < 0.001. ns, no significance.

overexpression significantly increased (**Figure 8A**). Consistent with CCK8 assay results, knockdown of CCT5 reduced viable HCC cell number after several days in culture while CCT5 overexpression significantly increased viable cell number as measured by CCK8 assay, suggesting that CCT5 acts to accelerate HCC cell proliferation (**Figure 8B**). Overexpression of CCT5 also promoted SK-HEP1 cell migration and invasion while CCT5 siRNA transfection repressed migration and invasion in transwell assays (**Figure 8C**). Similarly, overexpression promoted while knockdown suppressed cell migration in the wound healing assay (**Figure 8D**). Consistently, CCT5 could enhance the expression of Vimentin, Snail and Slug and downregulate the expression of E-cadherin, suggesting its roles in promoting epithelial-mesenchymal transition (EMT) of HCC cells (**Figure 8E**). These results demonstrate that CCT5 contributes to the migration and invasion ability of HCC cells.

Next, flow cytometry revealed that CCT5 knockdown reduced the proportion of cells in S phase compared to control cells and increased the proportion in G1 phase (**Figure 8F**). Furthermore, western blotting indicated that the expression levels of cell cycle regulators CDK2, 4, and 6 as well as CyclinA2, B1, D1, D3, and E2 were reduced by CCT5 knockdown compared to control cells (**Figure 8G**). Collectively, these results indicate that CCT5 is a positive regulator of cell cycle progression, while inhibiting CCT5 expression induces cell cycle arrest at the G1–S transition, thereby slowing proliferation rate. As a substrate for TRiC, tublin plays a major role in the mitotic process. We performed immunofluorescence experiments and found CCT5 co-localized with β-tublin (**Figure 8H**). The expression of β-tubulin was upregulated following CCT5 overexpression, while β-tubulin expression was suppressed through the knockdown of CCT5 (**Figure 8I**). It demonstrated that CCT5 aids in the proper folding of tublin in the cytoplasm, and full CCT activity is required for normal cell growth and division.

DISCUSSION

Most HCC patients are not diagnosed until intermediate or advanced stages of the disease, which may preclude transplantation and surgical resection as treatment options. Thus, biomarkers predictive of early-stage disease are urgently needed. Elevated serum alpha-fetoprotein (AFP) is the most widely used biomarker for HCC. However, not all tumors secrete AFP and AFP lacks adequate diagnostic sensitivity and specificity for HCC screening. Thus, its utility as a screening tool for HCC detection is not practical due to its poor performance (21). Further, many anticancer drugs show poor efficacy against HCC. For instance, median OS is only about one year for patients treated with the new first-line drug lenvatinib or the second-line drug regorafenib (3). Thus, novel drug targets as well as more sensitive and specific early biomarkers are required to prolong survival. The Cancer Genome Atlas is one of the largest publicly available cancer database of alterations in the oncogenic genome. Abundance of potential cancer biomarkers and cancer-associated gene in HCC have been discovered by using TCGA database and other public platforms (22, 23), however, the molecular mechanisms of HCC development are still incompletely understood. The ATP-dependent chaperone TRiC directly assists in the folding of up to 10% of all cytosolic proteins (4), and acts as an important regulator of cancer development by promoting the folding and activity of cancer-related proteins such as VHL, p53, and STAT3 (9–11). The clinical significance of TRiC subunit expression has been reported in a variety of cancers (24–27), but limited studies have been performed on HCC. To identify additional mechanisms underlying HCC regulation by CCTs, we conducted bioinformatics analysis of TCGA and other public

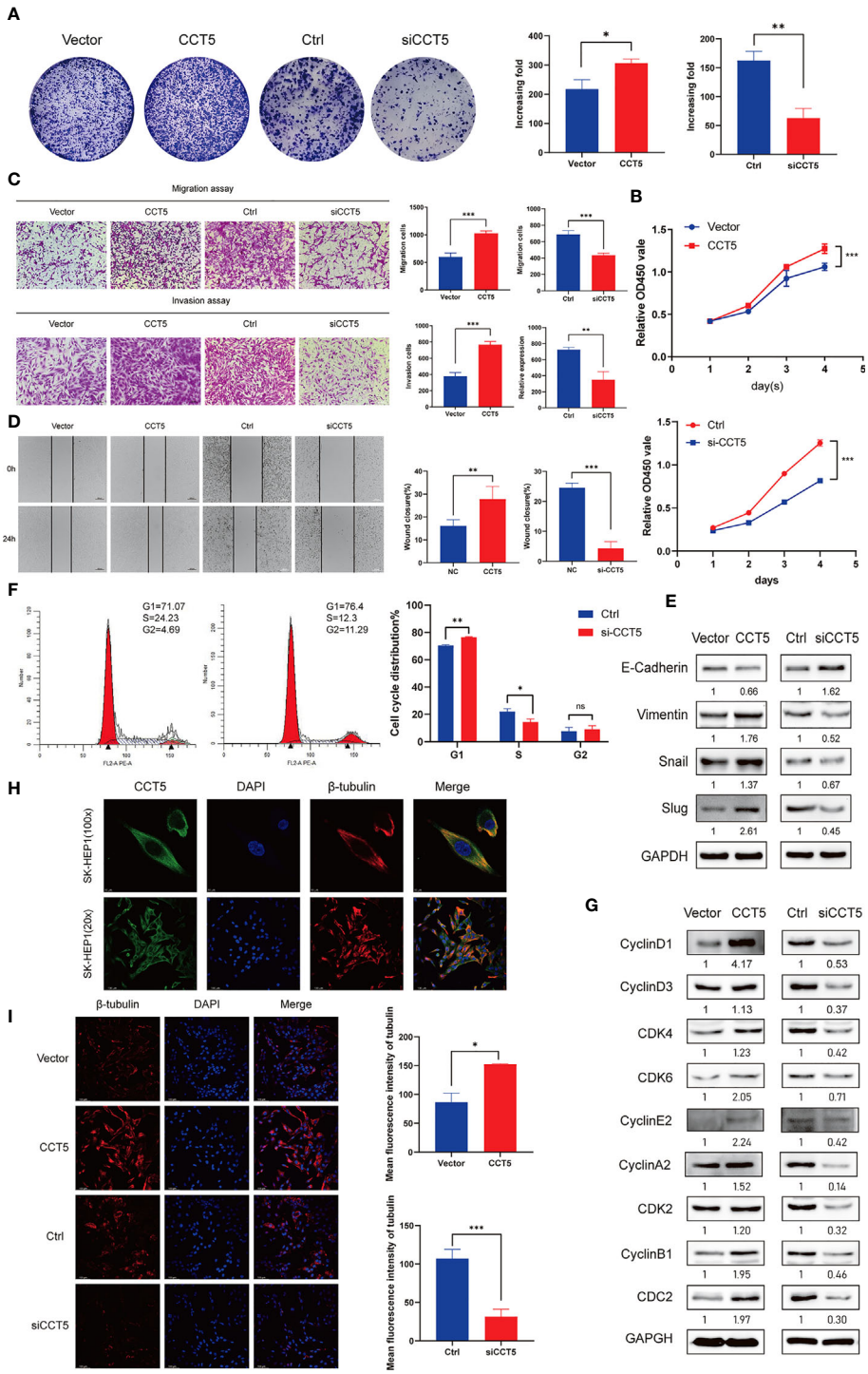

FIGURE 8 | Role of CCT5 in the proliferation, migration, invasion, and cell cycle regulation of HCC cells. **(A)** Colony formation assays showing the role of CCT5 on SK-HEP1 cell proliferation. **(B)** Cell viability of SK-HEP1cell line was determined by CCK-8 assays. **(C)** The effects of CCT5 on cell migration and invasion were determined by transwell assays in SK-HEP1 cell line. **(D)** The effects of CCT5 on cell migration were determined by wound healing assay in SK-HEP1 cell line. **(E)** The expression of EMT markers were examined by western blotting with CCT5 overexpression or downregulation. **(F)** The cell cycle distribution of SK-HEP1 cells were performed by flow cytometry analyses. **(G)** The relative expression levels of cyclin D1, cyclin D3, CKD4, CDK6, cyclin E2, cyclin A2, CDK2, cyclin B1, and CDC2 were examined by Western blotting in SK-HEP1 cells. **(H)** Fluorescence images show staining of CCT5 (green), DAPI (blue) and β-tubulin(red) in SK-HEP1 cells. Scale bar, 10 μm. **(I)** Representative images of β-tubulin(red) immunofluorescence staining in CCT5-overexpressing and CCT5-knockdown SK-HEP1 cells. Scale bar, 100 μm. Semi–quantitative analysis of β-tubulin fluorescence intensity using ImageJ software. *$p < 0.05$, **$p < 0.01$, ***$p < 0.001$. ns, no significance.

datasets. Our research revealed that the mRNA and protein expression levels of TCP1, CCT2/3/4/5/6A/7/8 were significantly upregulated in HCC tissues while CCT6B showed lower mRNA expression in HCC tissues compared to normal control liver tissue. However, CCT6B cannot be distinguished from CCT6A at the protein level due to a lack of specific antibodies, so the protein expression level of CCT6B in HCC is uncertain.

The mRNA expression levels of CCTs were also associated with clinicopathologic parameters, and higher expression levels of TCP1, CCT2/3/4/5/6A/7/8 predicted shorter OS, while overexpression of CCT6B predicted better prognosis. Mutations in TRiC subunit genes were found in nearly half of HCC patients, including CCT3 mutations in 27%, CCT5 mutations in 18%, and TCP1 mutations in 12%, and patients harboring such CCT gene mutations demonstrated poorer clinical outcome compared to patients without mutations. We analyzed functions and pathways of CCTs and their frequently altered neighbor genes in HCC patients and found that the neighbor genes of CCTs with the most frequent alterations were TP53, PFDN2, GBA, and CCNE2. In addition, the biological processes of co-altered genes were predominantly 'protein folding' and 'microtubule-based process', while functions were mainly related to the 'ribosome' and 'spliceosome'. Correlation analysis showed a positive correlation between TCP1, CCT2/3/4/5/6A/7/8 and a negative correlation between CCT6B and other eight subunits of TRiC. Finally, gain/loss-of-function assays demonstrated that CCT5 drives the proliferation, migration, invasion, and cell cycle progression of HCC cells. Thus, CCTs are potentially valuable biomarkers and therapeutic targets for HCC.

Significant upregulation of TCP1, CCT2/3/5/6A/8 levels have been found in a variety of cancers, with CCT3/6A/8 the best studied in HCC, while there are few studies on CCT4/5/7. Expression of TCP1 was upregulated in 93% of HCC patients and 76% of colon cancer patients, while CCT2 was overexpressed in 100% of HCC patients and 82% of colon cancer patients (24). Further, CCT2 expression level was strongly correlated with expression of proliferating cell nuclear antigen (PCNA), a biomarker of cellular proliferation (24). Similarly, CCT2 overexpression was found in small cell lung cancer (SCLC) and associated with poor prognosis (25). The mRNA and protein expression levels of CCT3 were upregulated in HCC tissues and strongly related to worse prognosis (12, 28, 29). In addition, the protein expression level of CCT3 was closely related to HCC tumor size, TNM stage, and Child-Pugh classification (30). Moreover, serum CCT3 protein demonstrated greater sensitivity than AFP as a diagnostic marker for HCC (28, 30). The prognostic values of other CCTs in HCC remain to be examined. Overexpression of CCT5 was found in breast cancer tissues with p53 mutations (26). Similar to CCT3, overexpression of CCT6A has been found in many malignancies, including liver cancers (15) as well as breast cancer (31) and lung cancer (32), and is associated with clinical prognosis and TNM stage. Recent studies have also found abnormal CCT8 expression associated with the occurrence and development of multiple cancers. In HCC patients, CCT8 expression was directly related to histologic grade and tumor size, and high expression was associated with poor clinical prognosis (13). Yang et al. also reported that CCT8 expression was higher in human esophageal squamous cell carcinoma (ESCC) patients with lymph node metastasis (LNM) than ESCC patients without LNM, and high CCT8 expression predicted shorter OS. Yi et al. found that CCT6B expression was significantly lower in active fibroblasts and that CCT6B overexpression significantly inhibited fibroblast function, suggesting that CCT6B upregulation can be used to inhibit cancer cell migration (33). Further, a CCT6B gene mutation that may lead to TRiC loss-of-function was found in Burkitt lymphoma, and it was suggested that CCT6B may be a potential tumor suppressor gene (34). In light of these results and the current findings, we suggest that TRiC subunits TCP1, CCT2/3/4/5/6A/7/8 may serve as HCC oncogenes while CCT6B may be a potential tumor suppressor gene. Further, all of these transcripts may serve as useful prognostic markers for HCC.

Previous studies have revealed that the complete TRiC is highly expressed in numerous malignant tumor types. In most cases, the TRiC exerts biological functions as a whole, so that overexpression or knockdown of any one of its subunits may alter function. Showalter and colleagues found that CCT2 overexpression enhanced the proliferation and invasion capacities of breast cancer cells (35). Mechanistically, Zhang et al. found that CCT3 was a novel regulator of spindle integrity and a requirement for proper kinetochore–microtubule attachment during mitosis. Further, CCT3 knockdown with a targeted siRNA induced cell apoptosis and suppressed cell proliferation by inducing mitotic arrest at prometaphase (12). Likewise, CCT3 depletion suppressed breast cancer cell proliferative and metastatic capacities, and ultimately induced apoptosis (36). Shi et al. also reported that CCT3 knockdown also significantly inhibited human papillary thyroid carcinoma cell proliferation and cell cycle progression and eventually induced cell apoptosis (27). Similarly, CCT5 siRNA knockdown increased docetaxel-induced apoptosis of MCF-7 breast cancer cells (26), suggesting that this knockdown strategy may potentiate the efficacy of anticancer drugs. Knockdown of CCT8 also markedly inhibited proliferation by arresting cells in G1-S phase (13). Knockdown of GRP94 depressed cell invasion and migration by inhibiting CCT8/c-Jun/EMT signaling (14). Silencing CCT8 also inhibited the proliferation and invasion capacities of glioma cells and dysregulated cytoskeletal dynamics (37). In addition, CCT8 has been shown to influence the migration and invasion of ESCC cells by regulating α-actin and β-tubulin (38). As shown in our **Figure 5**, there were few samples with high expression of all TRiC subunits in HCC. Therefore, the TRiC should be investigated as a whole since changes in the expression of a single subunit may alter multiple biological processes.

The Cancer Genome Atlas includes the results from a large number of gene level–mutation and gene level–copy number variation studies, so that we further investigated the alternation of CCT genes. Gene expression can be altered by mutations, copy number alterations (CNAs), and by epigenetic control

mechanisms. As shown in **Figure 5**, the highest mutation rate was found in CCT3 (27%), and mRNA upregulation and gene amplification were the most common CCT gene alterations in HCC patients. In addition, both CCT expression levels and HCC prognosis were affected by genetic alternation, and patients with gene amplifications showed the highest CCT expression levels. Altered CCT gene expression may in turn alter the expression levels of numerous downstream genes and signaling pathways. We also found that neighboring genes in the CCT network showed varying degrees of alteration, with TP53, CCNE2, PFDN2, TUBB2B, and TUBB2A showing particularly large changes in expression. TP53 is a classical tumor suppressor gene that can be classified as wild type or mutant type. TP53 mutation can induce the aberrant expression of many genes that lead to loss of tumor suppressor function (39). Correct folding of proteins is essential for the maintenance of normal cell functions, and the folding of wild-type p53 is thought to be promoted *via* interactions with CCTs. Cellular depletion of CCTs leads to accumulation of misfolded and unstable p53, resulting in enhanced motility and invasive capacity (10). In addition, CCT5 overexpression was found in breast cancer tissues with p53 mutations (26). Therefore, aberrant expression of CCT may modulate the expression of wild-type TP53, impacting tumorigenesis and cancer progression.

Cell cycle regulation is a complex biological process regulated by numerous cyclin proteins. The occurrence of cancer is strongly associated with abnormal cell cycle regulation. It was previously reported that aberrant CCT expression could lead to dysregulated cell cycle progression. Zeng et al. reported that CCT6A accelerated the G1–S transition and promoted HCC cell proliferation by maintaining cyclin D expression (15). In addition, there was a significant positive correlation between CCT6A and cyclin B2 or CCNA2 expression levels, implying an association between CCT6A expression and cell cycle progression (31). Overexpression of cyclin E may accelerate the G–S transition in hepatocytes and lead to the loss of p53 tumor-suppressor function, favoring hepatocarcinogenesis (40). However, TRiC is implicated in the proper folding and functional maturation of cyclin E (6). Therefore, TRiC may contribute to the initiation and progression of HCC by regulating cyclin E2 expression. The prefoldins (PFDNs) are important CCT-binding proteins that also bind to newly synthesized proteins and deliver them to the TRiC, thereby preventing misfolding (41). The PFDNs have been implicated in the EMT (42) and expression levels are correlated with cancer prognosis (43–45). In addition, the TRiC is required for proper folding of tubulin and actin. TUBB2A and TUBB2B are also critical TRiC substrates and were found to be associated with CCT mutations.

Assisting the folding of protein is the main biological function of TRiC complex and the primary substrates of the TRiC are tubulins and actins. The TRiC has also been found in association with a variety of proteins related to cell growth, proliferation, and apoptosis, such as cyclins B and E, in both normal cells and tumor cells. Our functional enrichment analysis on CCTs and co-altered genes revealed prominent functions in 'protein folding', 'microtubule-based process', and 'positive regulation of establishment of protein localization to telomere', consistent with the known physiological functions of CCT substrate proteins. Enhanced expression of CCTs and neighbor altered genes promotes proper protein folding, allowing more rapid proliferation and high metabolic activity. The synthesis of skeletal proteins such as tubulins requires high CCT gene expression as these are direct TRiC substrates. Telomeres are involved in DNA replication and play significant roles in cell mitosis. Telomerase is responsible for the extension of telomeres in cells, and enzyme activity is inhibited in most normal cells (post-mitotic cells) and reactivated in cancer cells, suggesting that telomerase activity may be involved in malignant transformation. The TRiC is required for folding of the telomerase cofactor TCAB1, which controls the transport of telomerase and small Cajal body RNAs (scaRNAs) (46). Therefore, the massive activation of telomerase in tumor cells requires TRiC and its co-altered genes. According to our functional enrichment analyses, CCTs and co-expressed genes are involved mainly in 'ribosome', 'spliceosome', and 'cell cycle'. Ribosomes are the specialized molecular machines mediating mRNA translation and synthesis of cellular proteins. Most CCT neighboring genes in the interaction network are involved in protein folding, while co-expressed genes are involved mainly in protein synthesis, so this network mediates the complete process from protein synthesis to folding and maturation. The division of tumor cells requires a large number of new proteins, including skeletal proteins such as tubulins, so TRiC, neighbor genes, and other co-expressed genes together promote the division and viability of tumor cells.

We believe that as a multisubunit complex, TRiC requires eight subunits to perform its molecular chaperone function. We found a positive correlation between TCP1, CCT2/3/4/5/6A/7/8 and a negative correlation between CCT6B and other eight subunits of TRiC. As expected, other subunit expressions were altered following CCT5 overexpression or knockdown. Thus, we hypothesize that TCP1, CCT2/3/4/5/6A/7/8 play a synergistic role in the regulation of HCC, while CCT6B has an antagonistic relationship with other subunits. However, it is not clear whether the alterations affect the development of HCC. We demonstrated that the aberrant expression of a single subunit (CCT5) affected the proliferation, migration, and invasion of HCC cells by gain/loss-of-function assay. Previous studies and the results of our GO enrichment analysis suggested that CCT subunits were closely related to cell cycle regulation, and we also confirmed it. There have been many studies on the CCT subunits for HCC but until now nothing was known about the role of CCT5 in HCC. Our results showed that CCT5 was significantly upregulated in HCC and it seemed to be a good indicator of prognosis in HCC. Although CCT5 has the highest ATP-binding affinity in the TCP1 ring complex (47), the exact molecular functions of CCT5 are still unclear. We found that CCT5 not only accelerated HCC cell proliferation and cell cycle progression, but also promoted metastasis and EMT progression. We suppose that CCT5 promotes the entire cell cycle and is mainly responsible for G1-S phase transition by

mediating the proper folding of cyclins and related cyclin-dependent kinases. TRiC function is related to the cell cycle. Tublin, which plays a major role in mitosis, is a known substrate of TRiC. We observed a co-localization of CCT5 and β-tubulin by immunofluorescence experiments, and β-tubulin expressions were altered following CCT5 overexpression or knockdown. This is probably because the reduction of TRiC activity decreases the rates of substrate processing by TRiC, causes a rapid degradation of misfolded tubulin due to insufficient TRiC levels and cell cycle arrest (48). We suppose that full CCTs activity is required for normal cell growth and division, which further explains why CCT5 promotes HCC proliferation. Therefore, CCT5 is required for proper mitotic progression, although further studies are needed to explore the underlying molecular mechanisms.

This study has several limitations. First, we did not verify the diagnostic and prognostic values of CCTs in HCC by sensitivity and specificity analyses. Further large-sample studies are needed to confirm our findings. Second, the pathogenic mechanism of CCTs in liver cancer were not investigated. Therefore, further studies should focus on CCTs such as CCT5 as potential targets for HCC therapy. Finally, although we utilized multiple datasets such as TCGA for analysis, all the data are from genomic and transcriptomic datasets sequencing. With the development of genomics, proteomics, single-cell sequencing cell sequencing and spatial transcriptomics have emerged, which have been conducted on a large scale, producing enormous amount of data and also obtaining breakthrough results (49, 50). We believe that applying bioinformatics methods and mining these data including data including the research of TCP complex will provide new perspectives on the pathogenesis of HCC in the future.

In conclusion, our study suggests that CCTs may be potential biomarkers for HCC diagnosis and prognosis as well as effect treatment targets due to critical functions in tumor cell transformation, proliferation, and metastasis.

CONCLUSIONS

In summary, we used several online bioinformatic platforms and web tools to analyze the expression, clinicopathological characteristics, prognosis, mutations, CNAs, correlated genes, and functions of the TCP1 ring complex in HCC. Expression levels of TRiC subunits were significantly upregulated in HCC compared to normal tissues except for subunit CCT6B. Gain/loss-of-function assays demonstrated that CCT5 can accelerate the proliferation, migration, and invasion of HCC cells. We speculate that the TCP1 ring complex plays an oncogenic role in HCC progression by facilitating the proper folding and function of cell cycle-related proteins. We are fully aware that the verification analysis using clinical specimens is necessary and further studies should be attached to the mechanism of TCP1 ring complex in HCC. Our results provide evidence that TRiC may be a novel therapeutic target and prognostic biomarker for HCC.

DATA AVAILABILITY STATEMENT

The original contributions presented in the study are included in the article/**Supplementary Material**. Further inquiries can be directed to the corresponding authors.

AUTHOR CONTRIBUTIONS

ZS and QZ designed the research. JL and QZ carried out the research. LH, YZ, YH, TL and JX analyzed the data. JL and QZ wrote the paper, QZ, LL, BX, and WZ assisted in manuscript revision. All authors contributed to the article and approved the submitted version.

FUNDING

This study was supported by the Science and Technology Program of Guangzhou, China (no. 202102021265), the National Natural Science Foundation of China (grant nos. 31901035), the Natural Science Foundation of Guangdong Province, China (no. 2020A1515010951), the Science and Technology Program of Guangzhou, China (no. 202002030078), and The Military Logistics Research Project (no. CLB19J033).

SUPPLEMENTARY MATERIAL

The Supplementary Material for this article can be found online at: https://www.frontiersin.org/articles/10.3389/fonc.2021.739660/full#supplementary-material

Supplementary Figure 1 | TRiC subunit mRNA expression levels in normal liver tissues and HCC tissues from the Roessler Liver 2 dataset.

Supplementary Figure 2 | Comparison of TRiC subunit mRNA expression levels between HCC and normal liver tissues (from UALCAN). **(A)** Heatmap shows the different expression levels of TRiC subunits between HCC and normal liver tissues **(B)** TRiC subunit expression in HCC tissues compared with normal liver tissues. **p<0.01, ***p<0.001.

Supplementary Figure 3 | Expression levels of TRiC subunit genes in HCC patients stratified by clinical stage (from UALCAN). The expression levels of TRiC subunits in HCC patients with different stages. *p<0.05, **p<0.01, ***p<0.001.

REFERENCES

1. Sung H, Ferlay J, Siegel RL, Laversanne M, Soerjomataram I, Jemal A, et al. Global Cancer Statistics 2020: GLOBOCAN Estimates of Incidence and Mortality Worldwide for 36 Cancers in 185 Countries. *CA* (2021) 71(3):1–14. doi: 10.3322/caac.21660
2. Zhang J, Gu C, Song Q, Zhu M, Xu Y, Xiao M, et al. Identifying Cancer-Associated Fibroblasts as Emerging Targets for Hepatocellular Carcinoma. *Cell Biosci* (2020) 10(1):127. doi: 10.1186/s13578-020-00488-y
3. Llovet JM, Montal R, Sia D, Finn RS. Molecular Therapies and Precision Medicine for Hepatocellular Carcinoma. *Nat Rev Clin Oncol* (2018) 15 (10):599–616. doi: 10.1038/s41571-018-0073-4

4. Yam AY, Xia Y, Lin HT, Burlingame A, Gerstein M, Frydman J. Defining the TRiC/CCT Interactome Links Chaperonin Function to Stabilization of Newly Made Proteins With Complex Topologies. *Nat Struct Mol Biol* (2008) 15 (12):1255–62. doi: 10.1038/nsmb.1515
5. Boudiaf-Benmammar C, Cresteil T, Melki R. The Cytosolic Chaperonin CCT/TRiC and Cancer Cell Proliferation. *PloS One* (2013) 8(4):e60895. doi: 10.1371/journal.pone.0060895
6. Won KA, Schumacher RJ, Farr GW, Horwich AL, Reed SI. Maturation of Human Cyclin E Requires the Function of Eukaryotic Chaperonin CCT. *Mol Cell Biol* (1998) 18(12):7584–9. doi: 10.1128/mcb.18.12.7584
7. Balchin D, Milicic G, Strauss M, Hayer-Hartl M, Hartl FU. Pathway of Actin Folding Directed by the Eukaryotic Chaperonin TRiC. *Cell* (2018) 174 (6):1507–21. doi: 10.1016/j.cell.2018.07.006
8. Sternlicht H, Farr GW, Sternlicht ML, Driscoll JK, Willison K, Yaffe MB. The T-Complex Polypeptide 1 Complex is a Chaperonin for Tubulin and Actin *In Vivo*. *Proc Natl Acad Sci USA* (1993) 90(20):9422–6. doi: 10.1073/pnas.90.20.9422
9. McClellan AJ, Scott MD, Frydman J. Folding and Quality Control of the VHL Tumor Suppressor Proceed Through Distinct Chaperone Pathways. *Cell* (2005) 121(5):739–48. doi: 10.1016/j.cell.2005.03.024
10. Trinidad AG, Muller PA, Cuellar J, Klejnot M, Nobis M, Valpuesta JM, et al. Interaction of P53 With the CCT Complex Promotes Protein Folding and Wild-Type P53 Activity. *Mol Cell* (2013) 50(6):805–17. doi: 10.1016/j.molcel.2013.05.002
11. Kasembeli M, Lau WC, Roh SH, Eckols TK, Frydman J, Chiu W, et al. Modulation of STAT3 Folding and Function by TRiC/CCT Chaperonin. *PloS Biol* (2014) 12(4):e1001844. doi: 10.1371/journal.pbio.1001844
12. Zhang Y, Wang Y, Wei Y, Wu J, Zhang P, Shen S, et al. Molecular Chaperone CCT3 Supports Proper Mitotic Progression and Cell Proliferation in Hepatocellular Carcinoma Cells. *Cancer Lett* (2016) 372(1):101–9. doi: 10.1016/j.canlet.2015.12.029
13. Huang X, Wang X, Cheng C, Cai J, He S, Wang H, et al. Chaperonin Containing TCP1, Subunit 8 (CCT8) Is Upregulated in Hepatocellular Carcinoma and Promotes HCC Proliferation. *Apmis* (2014) 122(11):1070–9. doi: 10.1111/apm.12258
14. Wei PL, Huang CY, Tai CJ, Batzorig U, Cheng WL, Hunag MT, et al. Glucose-Regulated Protein 94 Mediates Metastasis by CCT8 and the JNK Pathway in Hepatocellular Carcinoma. *Tumour Biol* (2016) 37(6):8219–27. doi: 10.1007/s13277-015-4669-3
15. Zeng G, Wang J, Huang Y, Lian Y, Chen D, Wei H, et al. Overexpressing CCT6A Contributes to Cancer Cell Growth by Affecting the G1-To-S Phase Transition and Predicts a Negative Prognosis in Hepatocellular Carcinoma. *Onco Targets Ther* (2019) 12:10427–39. doi: 10.2147/OTT.S229231
16. Rhodes DR, Kalyana-Sundaram S, Mahavisno V, Varambally R, Yu J, Briggs BB, et al. Oncomine 3.0: Genes, Pathways, and Networks in a Collection of 18,000 Cancer Gene Expression Profiles. *Neoplasia* (2007) 9(2):166–80. doi: 10.1593/neo.07112
17. Thul PJ, Lindskog C. The Human Protein Atlas: A Spatial Map of the Human Proteome. *Protein Sci* (2018) 27(1):233–44. doi: 10.1002/pro.3307
18. Jiang Y, Sun A, Zhao Y, Ying W, Sun H, Yang X, et al. Proteomics Identifies New Therapeutic Targets of Early-Stage Hepatocellular Carcinoma. *Nature* (2019) 567(7747):257–61. doi: 10.1038/s41586-019-0987-8
19. Roessler S, Jia HL, Budhu A, Forgues M, Ye QH, Lee JS, et al. A Unique Metastasis Gene Signature Enables Prediction of Tumor Relapse in Early-Stage Hepatocellular Carcinoma Patients. *Cancer Res* (2010) 70(24):10202–12. doi: 10.1158/0008-5472.CAN-10-2607
20. Wurmbach E, Chen Y, Khitrov G, Zhang W, Roayaie S, Schwartz M, et al. Genome-Wide Molecular Profiles of HCV-Induced Dysplasia and Hepatocellular Carcinoma. *Hepatology (Baltimore Md)* (2007) 45(4):938–47. doi: 10.1002/hep.21622
21. Attwa MH, El-Etreby SA. Guide for Diagnosis and Treatment of Hepatocellular Carcinoma. *World J Hepatol* (2015) 7(12):1632–51. doi: 10.4254/wjh.v7.i12.1632
22. Bian S, Ni W, Zhu M, Song Q, Zhang J, Ni R, et al. Identification and Validation of the N6-Methyladenosine RNA Methylation Regulator YTHDF1 as a Novel Prognostic Marker and Potential Target for Hepatocellular Carcinoma. *Front Mol Biosci* (2020) 7:604766. doi: 10.3389/fmolb.2020.604766
23. Zhu M, Wu M, Bian S, Song Q, Xiao M, Huang H, et al. DNA Primase Subunit 1 Deteriorated Progression of Hepatocellular Carcinoma by Activating AKT/mTOR Signaling and UBE2C-Mediated P53 Ubiquitination. *Cell Biosci* (2021) 11(1):42. doi: 10.1186/s13578-021-00555-y
24. Yokota S, Yamamoto Y, Shimizu K, Momoi H, Kamikawa T, Yamaoka Y, et al. Increased Expression of Cytosolic Chaperonin CCT in Human Hepatocellular and Colonic Carcinoma. *Cell Stress Chaperones* (2001) 6(4):345–50. doi: 10.1379/1466-1268(2001)006<0345:ieoccc>2.0.co;2
25. Carr AC, Khaled AS, Bassiouni R, Flores O, Nierenberg D, Bhatti H, et al. Targeting Chaperonin Containing TCP1 (CCT) as a Molecular Therapeutic for Small Cell Lung Cancer. *Oncotarget* (2017) 8(66):110273–88. doi: 10.18632/oncotarget.22681
26. Ooe A, Kato K, Noguchi S. Possible Involvement of CCT5, RGS3, and YKT6 Genes Up-Regulated in P53-Mutated Tumors in Resistance to Docetaxel in Human Breast Cancers. *Breast Cancer Res Treat* (2007) 101(3):305–15. doi: 10.1007/s10549-006-9293-x
27. Shi X, Cheng S, Wang W. Suppression of CCT3 Inhibits Malignant Proliferation of Human Papillary Thyroid Carcinoma Cell. *Oncol Lett* (2018) 15(6):9202–8. doi: 10.3892/ol.2018.8496
28. Liu Y, Zhang X, Lin J, Chen Y, Qiao Y, Guo S, et al. CCT3 Acts Upstream of YAP and TFCP2 as a Potential Target and Tumour Biomarker in Liver Cancer. *Cell Death Dis* (2019) 10(9):644. doi: 10.1038/s41419-019-1894-5
29. Hou J, Wu H, He R, Lin P, Dang Y, Chen G. Clinical and Prognostic Value of Chaperonin Containing T-Complex 1 Subunit 3 in Hepatocellular Carcinoma: A Study Based on Microarray and RNA-Sequencing With 4272 Cases. *Pathol Res Pract* (2019) 215(1):177–94. doi: 10.1016/j.prp.2018.11.006
30. Qian E, Han S, Ding S, Lv X. Expression and Diagnostic Value of CCT3 and IQGAP3 in Hepatocellular Carcinoma. *Cancer Cell Int* (2016) 16(1):55. doi: 10.1186/s12935-016-0332-3
31. Huang K, Zeng Y, Xie Y, Huang L, Wu Y. Bioinformatics Analysis of the Prognostic Value of CCT6A and Associated Signalling Pathways in Breast Cancer. *Mol Med Rep* (2019) 19(5):4344–52. doi: 10.3892/mmr.2019.10100
32. Zhang T, Shi W, Tian K, Kong Y. Chaperonin Containing T-Complex Polypeptide 1 Subunit 6A Correlates With Lymph Node Metastasis, Abnormal Carcinoembryonic Antigen and Poor Survival Profiles in Non-Small Cell Lung Carcinoma. *World J Surg Oncol* (2020) 18(1):156. doi: 10.1186/s12957-020-01911-x
33. Yi X, Wang Z, Ren J, Zhuang Z, Liu K, Wang K, et al. Overexpression of Chaperonin Containing T-Complex Polypeptide Subunit Zeta 2 (CCT6b) Suppresses the Functions of Active Fibroblasts in a Rat Model of Joint Contracture. *J Orthop Surg Res* (2019) 14(1):125. doi: 10.1186/s13018-019-1161-6
34. Love C, Sun Z, Jima D, Li G, Zhang J, Miles R, et al. The Genetic Landscape of Mutations in Burkitt Lymphoma. *Nat Genet* (2012) 44(12):1321–5. doi: 10.1038/ng.2468
35. Showalter AE, Martini AC, Nierenberg D, Hosang K, Fahmi NA, Gopalan P, et al. Investigating Chaperonin-Containing TCP-1 Subunit 2 as an Essential Component of the Chaperonin Complex for Tumorigenesis. *Sci Rep* (2020) 10 (1):798. doi: 10.1038/s41598-020-57602-w
36. Xu G, Bu S, Wang X, Zhang H, Ge H. Suppression of CCT3 Inhibits the Proliferation and Migration in Breast Cancer Cells. *Cancer Cell Int* (2020) 20 (1):1–12. doi: 10.1186/s12935-020-01314-8
37. Qiu X, He X, Huang Q, Liu X, Sun G, Guo J, et al. Overexpression of CCT8 and its Significance for Tumor Cell Proliferation, Migration and Invasion in Glioma. *Pathol Res Pract* (2015) 211(10):717–25. doi: 10.1016/j.prp.2015.04.012
38. Yang X, Ren H, Shao Y, Sun Y, Zhang L, Li H, et al. Chaperonin-containing T-complex Protein 1 Subunit 8 Promotes Cell Migration and Invasion in Human Esophageal Squamous Cell Carcinoma by Regulating α-actin and β-tubulin Expression. *Int J Oncol* (2018) 52(6):2021-30. doi: 10.3892/ijo.2018.4335
39. Viadiu H, Fronza G, Inga A. Structural Studies on Mechanisms to Activate Mutant P53. *Subcell Biochem* (2014) 85:119. doi: 10.1007/978-94-017-9211-0_7
40. Pok S, Wen V, Shackel N, Alsop A, Pyakurel P, Fahrer A, et al. Cyclin E Facilitates Dysplastic Hepatocytes to Bypass G1/S Checkpoint in Hepatocarcinogenesis. *J Gastroenterol Hepatol* (2013) 28(9):1545–54. doi: 10.1111/jgh.12216
41. Martin-Benito J, Gomez-Reino J, Stirling PC, Lundin VF, Gomez-Puertas P, Boskovic J, et al. Divergent Substrate-Binding Mechanisms Reveal an Evolutionary Specialization of Eukaryotic Prefoldin Compared to its Archaeal Counterpart. *Structure* (2007) 15(1):101–10. doi: 10.1016/j.str.2006.11.006

42. Zhou C, Guo Z, Xu L, Jiang H, Sun P, Zhu X, et al. PFND1 Predicts Poor Prognosis of Gastric Cancer and Promotes Cell Metastasis by Activating the Wnt/beta-Catenin Pathway. *Onco Targets Ther* (2020) 13:3177–86. doi: 10.2147/OTT.S236929
43. Penate X, Praena-Fernandez JM, Romero PP, Enguix-Riego M, Payan-Bravo L, Vieites B, et al. Overexpression of Canonical Prefoldin Associates With the Risk of Mortality and Metastasis in Non-Small Cell Lung Cancer. *Cancers (Basel)* (2020) 12(4):1052. doi: 10.3390/cancers12041052
44. Wang P, Zhao J, Yang X, Guan S, Feng H, Han D, et al. PFDN1, an Indicator for Colorectal Cancer Prognosis, Enhances Tumor Cell Proliferation and Motility Through Cytoskeletal Reorganization. *Med Oncol* (2015) 32(12):264. doi: 10.1007/s12032-015-0710-z
45. Yesseyeva G, Aikemu B, Hong H, Yu C, Dong F, Sun J, et al. Prefoldin Subunits (PFDN1-6) Serve as Poor Prognostic Markers in Gastric Cancer. *Biosci Rep* (2020) 40(2):BSR20192712. doi: 10.1042/BSR20192712
46. Freund A, Zhong FL, Venteicher AS, Meng Z, Veenstra TD, Frydman J, et al. Proteostatic Control of Telomerase Function Through TRiC-Mediated Folding of TCAB1. *Cell* (2014) 159(6):1389–403. doi: 10.1016/j.cell.2014.10.059
47. Reissmann S, Joachimiak LA, Chen B, Meyer AS, Nguyen A, Frydman J. A Gradient of ATP Affinities Generates an Asymmetric Power Stroke Driving the Chaperonin TRIC/CCT Folding Cycle. *Cell Rep* (2012) 2(4):866–77. doi: 10.1016/j.celrep.2012.08.036
48. Grantham J, Brackley KI, Willison KR. Substantial CCT Activity is Required for Cell Cycle Progression and Cytoskeletal Organization in Mammalian Cells. *Exp Cell Res* (2006) 312(12):2309–24. doi: 10.1016/j.yexcr.2006.03.028
49. Su J, Song Q, Qasem S, O Neill S, Lee J, Furdui CM, et al. Multi-Omics Analysis of Brain Metastasis Outcomes Following Craniotomy. *Front Oncol* (2021) 10:615472. doi: 10.3389/fonc.2020.615472
50. Song Q, Su J, Zhang W. scGCN Is a Graph Convolutional Networks Algorithm for Knowledge Transfer in Single Cell Omics. *Nat Commun* (2021) 12(1):3826. doi: 10.1038/s41467-021-24172-y

Conflict of Interest: The authors declare that the research was conducted in the absence of any commercial or financial relationships that could be construed as a potential conflict of interest.

Publisher's Note: All claims expressed in this article are solely those of the authors and do not necessarily represent those of their affiliated organizations, or those of the publisher, the editors and the reviewers. Any product that may be evaluated in this article, or claim that may be made by its manufacturer, is not guaranteed or endorsed by the publisher.

frontiers in Oncology

REVIEW
published: 11 October 2021
doi: 10.3389/fonc.2021.752725

Improving Outcomes of Tyrosine Kinase Inhibitors in Hepatocellular Carcinoma: New Data and Ongoing Trials

Lisha Mou[1,2†], Xiaohe Tian[2,3†], Bo Zhou[2,4†], Yongqiang Zhan[1], Jiao Chen[2], Ying Lu[2], Jing Deng[2], Ying Deng[2,5], Zijing Wu[1,2], Qi Li[6], Yi'an Song[6], Hongyuan Zhang[2,7], Jinjun Chen[1], Kuifeng Tian[1], Yong Ni[1*] and Zuhui Pu[6*]*

[1] Department of Hepatopancreatobiliary Surgery, Shenzhen Institute of Translational Medicine, The First Affiliated Hospital of Shenzhen University, Shenzhen Second People's Hospital, Shenzhen, China, [2] Shenzhen Xenotransplantation Medical Engineering Research and Development Center, Shenzhen Institute of Translational Medicine, The First Affiliated Hospital of Shenzhen University, Shenzhen Second People's Hospital, Shenzhen, China, [3] Rausser College of Natural Resources, University of California, Berkeley, Berkeley, CA, United States, [4] College of Engineering, Boston University, Boston, MA, United States, [5] Faculty of Science, University of Waterloo, Waterloo, ON, Canada, [6] Imaging Department, Shenzhen Institute of Translational Medicine, The First Affiliated Hospital of Shenzhen University, Shenzhen Second People's Hospital, Shenzhen, China, [7] The Faculty of Arts and Sciences, The University of British Columbia, Kelowna, BC, Canada

OPEN ACCESS

Edited by:
Yunfei Xu,
Shandong University, China

Reviewed by:
Luis E. Arias-Romero,
National Autonomous University of Mexico, Mexico
Ibrahim C. Haznedaroglu,
Hacettepe University Hospital, Turkey

***Correspondence:**
Lisha Mou
lishamou@gmail.com
Yong Ni
szniyong@sina.com
Zuhui Pu
pupeter190@163.com

†These authors have contributed equally to this work

Specialty section:
This article was submitted to Cancer Molecular Targets and Therapeutics, a section of the journal Frontiers in Oncology

Received: 03 August 2021
Accepted: 24 September 2021
Published: 11 October 2021

Citation:
Mou L, Tian X, Zhou B, Zhan Y, Chen J, Lu Y, Deng J, Deng Y, Wu Z, Li Q, Song Y, Zhang H, Chen J, Tian K, Ni Y and Pu Z (2021) Improving Outcomes of Tyrosine Kinase Inhibitors in Hepatocellular Carcinoma: New Data and Ongoing Trials. Front. Oncol. 11:752725. doi: 10.3389/fonc.2021.752725

Targeted therapies such as oral tyrosine kinase inhibitors (TKIs) are the main therapeutic strategy effective for advanced hepatocellular carcinoma (HCC). Currently six tyrosine kinase inhibitors for HCC therapy have been approved. The newly approved first-line drug donafenib represent the major milestones in HCC therapeutics in recent years. However, drug resistance in HCC remains challenging due to random mutations in target receptors as well as downstream pathways. TKIs-based combinatorial therapies with immune checkpoint inhibitors such as PD-1/PD-L1 antibodies afford a promising strategy to further clinical application. Recent developments of nanoparticle-based TKI delivery techniques improve drug absorption and bioavailability, enhance efficient targeting delivery, prolonged circulation time, and reduce harmful side effects on normal tissues, which may improve the therapeutic efficacy of the TKIs. In this review, we summarize the milestones and recent progress in clinical trials of TKIs for HCC therapy. We also provide an overview of the novel nanoparticle-based TKI delivery techniques that enable efficient therapy.

Keywords: sorafenib, lenvatinib, tyrosine kinase inhibitors, TKIs, hepatocellular carcinoma, HCC, targeted therapy

1 INTRODUCTION

According to GLOBOCAN 2020 statistics, estimated liver cancer summed up to 905,677 new cases and 830,180 deaths in 2020 worldwide (1). Hepatocellular carcinoma (HCC) is the most common type of primary liver cancer. It occurs in approximately 85% of cirrhosis cases (2). The first tyrosine kinase inhibitor (TKI) was approved early this century as a potential precision therapy for HCC. Its specificity to targets made it more efficient and safer compared to traditional chemotherapies due to

Abbreviations: TKI, tyrosine kinase inhibitor; HCC, hepatocellular carcinoma; OS, overall survival; ORR, overall response rate; PFS, progression-free survival; TACE, transcatheter arterial chemoembolization; RTK, receptor tyrosine kinase.

minimal impact on normal cells (3). Current systemic therapies for HCC are mainly based on TKIs, anti-angiogenesis drugs, and immunotherapy agents (**Figure 1**).

Since sorafenib was first approved for HCC and established its pioneer role in the field, a total of six TKIs have been approved for the treatments of HCC by regulatory authorities around the world. First-line drugs include sorafenib, lenvatinib, and the newly approved donafenib by Chinese National Medical Products Administration (NMPA). Second-line drugs are regorafenib, cabozantinib, and NMPA approved apatinib (**Table 1**) (4).

Other existing TKIs which were previously approved for the treatment of other cancer types are now under clinical trials for HCC, including sunitinib, erdafitinib, erlotinib, anlotinib, pazopanib an so on (**Table 2**). Most common targets of TKIs in HCC include vascular endothelial growth factor receptors (VEGFR), platelet-derived growth factors (PDGF), and tyrosine-protein kinases (5). Thus, TKIs would inhibit activation of corresponding signaling pathways through binding irreversibly or reversibly to various sites during the initial activation of receptor tyrosine kinases (RTKs) (6). This further prevents tumor growth and metastasis by preventing downstream signaling pathways from being activated (4, 7). TKIs which are discussed in the review are summarized in **Figure 2**.

2 DIFFERENT KIND OF TKIS FOR HCCS

2.1 VEGFR-TKIs

2.1.1 Sorafenib

Sorafenib was the first approved TKI for the treatment of advanced primary HCC by the FDA in 2007 (8). Sorafenib was first developed for the treatment of renal cell carcinoma and works through a dual mechanism, by targeting the serine/threonine kinase Raf or blocking autophosphorylation of multiple RTKs-VEGFR1, 2 and 3, PDGFR, c-Kit, and RET (9).

Sorafenib was termed the preferred first line therapy until recently replaced by the combination of atezolizumab and bevacizumab in 2021 according to the latest version of NCCN guidelines (10). In patients with unresectable hepatocellular carcinoma (HCC), the combination of atezolizumab and bevacizumab improved median progression-free survival (PFS)

Current Systemic Therapy for HCC

First-Line Systemic Therapy

Preferred Regimens	• Atezolizumab + bevacizumab (Child-Pugh Class A only)
Other Recommended	• Sorafenib (Child-Pugh Class A or B7) • Lenvatinib (Child-Pugh Class A only)
Useful in Certain Cases	• Nivolumab • FOLFOX

Subsequent-Line Systemic Therapy: Disease Progression

Options	• Regorafenib (Child-Pugh Class A only) • Cabozantinib (Child-Pugh Class A only) • Ramucirumab (AFP ≥400 ng/mL only) • Lenvatinib (Child-Pugh Class A only) • Sorafenib (Child-Pugh Class A or B7)
Other Recommended	• Nivolumab (Child-Pugh Class A or B) • Nivolumab + ipilimumab (Child-Pugh Class A only) • Pembrolizumab (Child-Pugh Class A only)

FIGURE 1 | Current systemic therapies for HCC.

TABLE 1 | Summary of approved TKIs.

No	Drug	Brand	Targets	Approved time/Organization
1	Sorafenib	Nexavar/Bayer	VEGFR1-3, TIE2, PDGFR, FGFR, BRAF, CRAF, KIT, FLT-3	2007/FDA
2	Regorafenib	Stivarga/Bayer	VEGFR1-3, TIE2, PDGFR, FGFR, BRAF, KIT, RET	2017/FDA
3	Lenvatinib	Lenvima/Eisai Inc	VEGFR1-3, PDGFR, FGFR1-4, RET, KIT	2018/FDA
4	Cabozantinib	Cometriq,Cabometyx/Exelixis Inc	VEGFR1-3, MET, ROS1, RET, AXL, NTRK, KIT	2019/FDA
5	Apatinib	Aitan/Jiangsu Hengrui	VEGFR2, KIT, RET, c-Src	2020/NMPA
6	Donafenib	Zepsun/Suzhou Zelgan	PDGFR, VEGFR, Raf	2021/NMPA

TABLE 2 | Representative clinical trials of tyrosine kinase inhibitors in hepatocellular carcinoma treatment.

Registered Trial Number	Duration (start-end)	Enrollment	Phase	Treatment	Targets	mPFS (months)	mOS (months)	ORR (%)	Adverse Events
NCT02645981 (ZGDH3)	2016.03 -2019.12	668	III	Donafenib *vs*. Sorafenib	VEGFR, PDGFR	3.7 *vs*. 3.6	12.1 *vs*. 10.3	4.6 *vs*. 2.7	hand-foot skin reaction, aspartate aminotransferase increased, blood bilirubin increased, platelet count decreased, and diarrhea
NCT01164202	2010.07 - 2017.07	78	II/III	Sunitinib + Doxorubincin-TACE	VEGFR, PDGFR, c-KIT, FLT3, RET	9.05	25	6	Hematologic toxicity, fatigue, transaminase elevation, hand-foot syndrome events
NCT03006926 (KEYNOTE 524)	2017.02 - 2019.10	104	Ib	Lenvatinib + Pembrolizumab	VEGFR, PDGFR	9.3	22	46	hypertension, diarrhea, fatigue, decreased appetite, hypothyroidism, hypertension, and Leukopenia/neutropenia
NCT03463876 (RESCUE)	2018.02 - 2020.02	190	II	Apatinib + Camrelizumab	VEGFR	5.7	N/A	34.3	hypertension, increased aspartate aminotransferase, proteinuria, hyperbilirubinemia, increased gammaglutamyltransferase, and neutropenia
ChiCTR-IPR-17012667	2018.01 - 2020.01	80	IV	Apatinib+TACE *vs* TACE	VEGFR	17.2 *vs* 12.5	N/A	55 *vs* 32.5 a	Fatigue, hand-foot syndrome, diarrhea, hypertension, proteinuria, oral ulcer
NCT04172571	2018.12 - 2020.06	30	Ib/II	Anlotinib + AK105	VEGFR, FGFR PDGFR, c-KiT, Ret	N/A	N/A	24	AST, increased ALT, asthenia, decreased platelet count, increased blood bilirubin, increased bilirubin conjugated, and rash
NCT02809534 (ALTER0802)	2016.09 - 2017.10	60	II	Anlotinib (with *vs*. without previous TKIs therapy)	VEGFR, FGFR PDGFR, c-KiT, Ret	80.8% *vs*. 72.5% b	20.1 *vs*. 7.9	N/A	hypertension, hypothyroidism, fatigue, hand-foot syndrome, elevated bilirubin, and diarrhea

a, ORR in three months; b,12-week mPFS rate; N/A, not available.

and overall survival (OS) (6.8 months *vs* 4.3 months) compared with sorafenib in the IMbrave150 trial (11).

Recently, studies on combination therapies based on sorafenib showed exciting results. The combination of sorafenib and transcatheter arterial chemoembolization (TACE) yielded an improved overall response rate (ORR) (55.9% *vs* 37.3%) and disease control rates (86.4% *vs* 67.8%) compared to TACE group (12). However, the sorafenib plus TACE therapy had increased AE. Besides, conflicting results were reported in other studies (ISRCTN93375053, NCT02425605) (13, 14). As a result, more studies are required to verify these findings.

2.1.2 Lenvatinib

Lenvatinib, which was approved by FDA in 2018, is another significant first-line TKI that differs from sorafenib in its mechanisms (15). It is developed by Eisai Inc and inhibits angiogenesis targeting a broad range of receptors, including VEGFR1-3 and PDGFRα, β (16). In addition, it inhibits tumor cell proliferation *via* inhibition of the proto-oncogenes KIT and RET (17). The alternative targets that differentiate lenvatinib from other HCC TKIs are the fibroblast growth factor receptors (FGFR) 1-4, which also contributes to angiogenesis in the progression of tumor growth and metastasis (18). Lenvatinib binds VEGFR2 at its ATP mimetic quinoline moiety to the ATP binding site and the neighboring region *via* a cyclopropane ring. In comparison to the other licensed VEGFR2 kinase inhibitors, these findings indicate that lenvatinib has a different binding mode of interaction (19).

Despite its role in first-line drugs for advanced HCC, lenvatinib is also considered a better alternative to TACE when treating patients in the BCLC intermediate stage with a high tumor burden. These patients were thought to be susceptible to decline in liver function and poor therapeutic response. A recent study compared the median PFS in TACE-refractory patients that were treated with lenvatinib (5.8 months), sorafenib (3.2 months), and TACE (2.4 months). This indicates treatment with lenvatinib in replacement of TACE has the potential to acquire good therapeutic responses while preserving normal liver function (20).

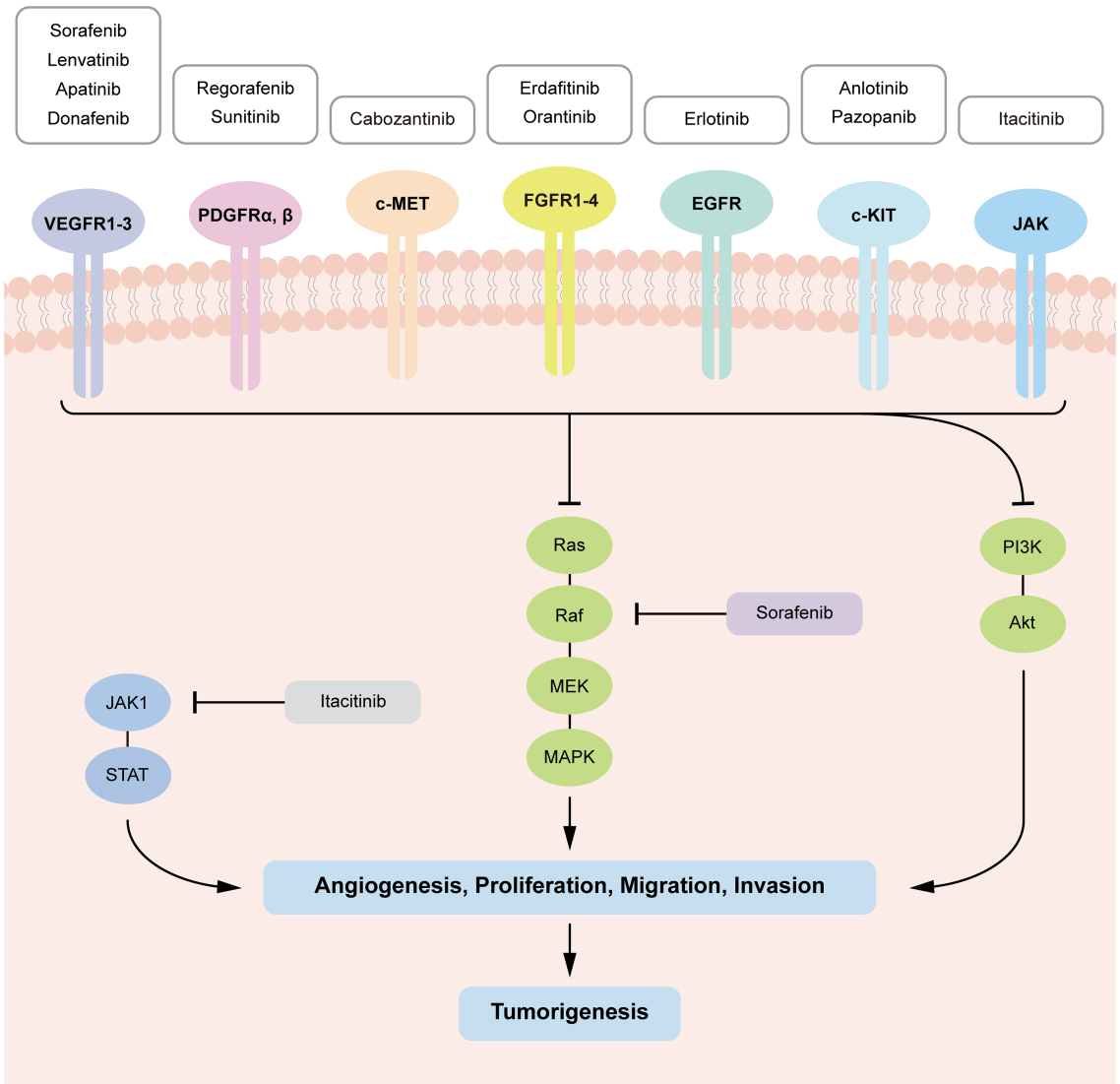

FIGURE 2 | Tyrosine kinase-mediated signaling pathways in HCC tumorigenesis and targets of the TKIs. TKIs bind with corresponding kinases from phosphorylating tyrosine residues in their substrates, which inhibit downstream signaling pathways (RAS–MAPK, PI3K–AKT and JAK–STAT) activation, preventing cell proliferation, migration, invasion, and angiogenesis in HCC.

In terms of combination therapies, lenvatinib plus pembrolizumab (an anti–PD-1 antibody) showed encouraging results with improved ORR and DCR for unresectable HCC (NCT03006926, **Table 2**) (21). The FDA granted lenvatinib plus pembrolizumab a breakthrough treatment designation for the first-line therapy of unresectable HCC which is not amenable to locoregional therapy. A phase III clinical trial of lenvatinib plus pembrolizumab as first-line therapy of unresectable HCC should further confirm the efficacy and safety (NCT03713593) (22). Besides, combination therapy of lenvatinib plus TACE also showed improved ORR (53.3% *vs* 23.3%) (23). The combination therapy of lenvatinib and microwave ablation indicated a better clinical effect with an OS of 14.89 ± 4.89 months and a PFS of 8.65 ± 2.68 months (24).

To conclude, the most prominent feature of lenvatinib would be its noninferiority compared to sorafenib as a first-line drug. The drug's different, as well as a wider range of targets compared to sorafenib would then mitigate the restrictions of using target therapy given tumor heterogeneity. On-going clinical trials of combination therapies in lenvatinib with antibodies also show better results than that of sorafenib.

2.1.3 Apatinib

Apatinib, or apatinib mesylate (YN968D1), is derived from Valantinib, with a predecessor YN968D11 (N- [4-(1-cyano-cyclopentyl) phenyl]-2-(4-pyridylmethyl) amino-3-pyridine carboxamide mesylate). By occupying the binding site of the VEGFR2, it selectively blocks VEGFR2, thus preventing new

blood vessel formation in tumor tissues. In October 2004, Chinese NMPA endorsed apatinib as the third-line treatment for advanced gastric cancer or adenocarcinoma of the gastroesophageal junction. Later in 2020, apatinib by Jiangsu Hengrui is approved for therapies of the second-line treatment in advanced HCC by Chinese NMPA. There exist some adverse events when taking apatinib, but the toxicity is still manageable (25). In terms of combinatorial therapies, the efficacy and safety of apatinib combined with camrelizumab or TACE application showed promising results with improved median PFS, short-term ORR and DCR (NCT03463876, ChiCTR-IPR-17012667, **Table 2**) (26). Therefore, the combination therapy of apatinib and TACE could be a potential treatment for future recurrent HCC patients.

2.1.4 Donafenib

Donafenib is formed by replacing the methyl group on a sorafenib molecule with a trideuteriomethyl group (**Figure 3**). By inhibiting phosphorylation of serine/threonine kinases (such as Raf kinase) and by blocking RTK signaling (such as VEGFR and PDGFR), donafenib shows similar antitumor activity as sorafenib for the advanced HCC patients (27). The donafenib group yielded an improved median OS (12.1 months *vs* 10.3 months, p=0.0363) compared to the sorafenib group (**Table 2**) (28). At the same time, the adverse effects of donafenib are fewer than sorafenib (28). According to the Guidelines of Chinese Society of Clinical Oncology (CSCO) on hepatocellular carcinoma that was published in July 2020, donafenib has been listed as a first-line treatment for advanced HCC (29). Donafenib is recommended by the first level specialists with 1A evidence by CSCO (29). On July 9th of 2021, according to Chinese NMPA, donafenib produced by Suzhou Zelgan was approved as a treatment for unresectable HCC patients without systemic therapy.

2.2 PDGFR-TKIs

PDGF family consists of PDGF-A to -D polypeptide homodimers and the PDGF-AB heterodimer. They bind to α- and β-tyrosine kinase receptors (PDGFRα and PDGFRβ, respectively) and activates downstream signaling pathways including MAPK, PI3K, phospholipase-γ (PLCγ) and reactive oxygen species (ROS)-dependent STAT3 signaling (30–32). Representative PDGFR-TKIs include regorafenib and sunitinib.

2.2.1 Regorafenib

Despite inhibiting VEGFR1-3, regorafenib inhibits angiogenic kinases PDGFRβ and FGFR1 and the mutant oncogenic kinases c-KIT, RET and B-RAF (33). It is more pharmacologically potent than sorafenib due to a broader spectrum of targets (34). Regorafenib was first approved for metastatic colorectal cancer by the FDA in 2012. In 2017, regorafenib was approved by the FDA as a second-line drug for treating HCC patients previously treated with sorafenib. Regorafenib blocks alpha-fetoprotein (AFP) secretion, further preventing cell migration and invasion in HCC cell lines at different drug doses. A high concentration of regorafenib impedes cell growth in both AFP-positive and AFP-negative HCC cell lines (35, 36). Adverse events of regorafenib are relatively serious yet manageable and clinically acceptable.

2.2.2 Sunitinib

Sunitinib (SU11248) is a low-molecular-weight multi-target TKI that inhibits PDGFRs, VEGFRs, c-KIT, fms-related tyrosine kinase 3 (FLT3), and RET. It was approved to treat imatinib-resistant gastrointestinal stromal tumor (GIST), renal carcinoma, and pancreatic neuroendocrine tumors (37). The most recent clinical trial on sunitinib consists of examining TACE plus sunitinib as first-line therapy in HCC (NCT01164202, **Table 2**) (38). The results showed possible use of TACE plus sunitinib as first-line treatment for patients with HCC who were not candidates for surgical resection.

2.2.3 c-MET TKIs

Hepatocyte growth factor (HGF) binds to c-Met for activation and deregulation, causing its dimerization and autophosphorylation, which further activates the mitogen-activated protein kinase (MAPK), phosphatidylinositol 3-

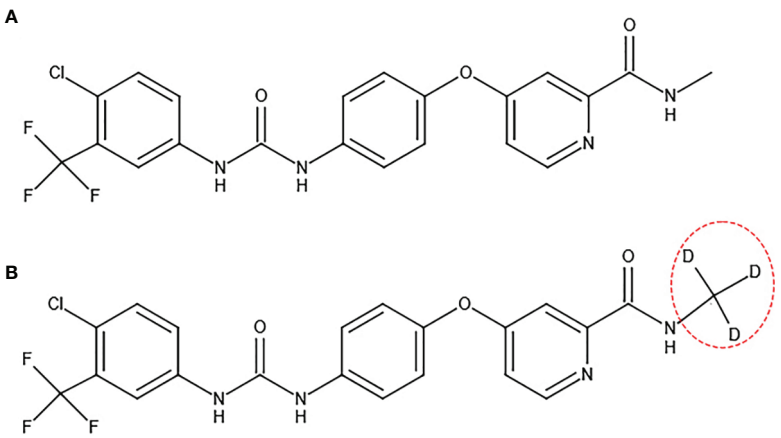

FIGURE 3 | Molecular structures of sorafenib **(A)** and donafenib **(B)**.

kinase (PI3K), v-src avian sarcoma viral oncogene homolog (Schmidt-Ruppin A-2), and signal transducer and activator of transcription (STAT) signaling pathways (39).

Met constitutive activation may be done either by creating HGF-Met autocrine loops, overexpression of Met, or having activating point mutations in the receptor coding sequence (40). An unusual multi-docking site for MET signals consists of two tyrosine that form a complex with MET when phosphorylated, whose cytoplasmic domain offers additional docking sites for PI3K and SHC. Cell proliferation and transformation are stimulated by increased SHC–GRB2–SOS–RAS pathway activation, whereas cell migration and survival is promoted by selective recruitment of PI3K (41). A representative c-MET-TKIs would be cabozantinib.

2.2.4 Cabozantinib

Cabozantinib, manufactured by Exelixis Inc, was approved by the FDA in 2019 as second-line therapy after treatment of sorafenib or lenvatinib. Cabozantinib is a more potent inhibitor of MET, AXL, RET, FLT3, and TIE-2 than regorafenib. Cabozantinib and regorafenib are structurally similar, yet impose different inhibitory effects on the kinase IC50 (42, 43). Clinical trials of cabozantinib showed promising results especially a recent phase I study (NCT03299946), which showed that cabozantinib plus nivolumab (an immune checkpoint inhibitor) could be an emerging option of neoadjuvant therapy for HCC as reported in 2021 the American Society of Clinical Oncology (ASCO) Symposium (44–46). This was the first clinical trial which investigated a TKI in combination with an immune checkpoint inhibitor in this setting. This pioneer study also provided the first prospective evidence of the above combinations aimed at downstaging HCC. However, this study only included a small patient size (n = 15). Larger sample clinical trials of neoadjuvant approaches are needed in order to confirm the findings in the future.

2.3 Other TKIs

The rest of TKIs for HCC targets FGFR (including erdafitinib and orantinib), EGFR (including erlotinib), c-Kit (including anlotinib and pazopanib), JAK (including itacitinib). Among these inhibitors, anlotinib (AL3818) is one of the promising drugs. In May 2018, anlotinib was first approved by Chinese NMPA as a third-line treatment for refractory advanced non-small-cell lung cancer (NSCLC). Then in June 2019, it was approved as a second-line treatment for advanced soft-tissue sarcoma (47). Hypertension, hand-foot skin reaction, fatigue, diarrhea, and anorexia are severe adverse events of anlotinib. In a phase II clinical trial testing the efficacy of anlotinib as first- or second-line treatment for advanced or metastatic HCC patients. Patients without or with prior TKI treatment were divided as cohort 1 or 2. The 12-week PFS rates for cohort 1 and 2 were 80.8% and 72.5%, and the median time to progression were 5.9 months and 4.6 months, respectively. In advanced HCC, anlotinib demonstrated potential effectiveness and safety as a first- or second-line therapy when used in conjunction with a continuous TKIs treatment approach (48). In the treatment for 13 advanced HCC patients with Anlotinib plus AK105, the ORR is 23.3%, and the DCR is 69.2%. At the same time, the adverse events did not exceed level three (49). Therefore, the effectiveness and safety of anlotinib in HCC make it a promising TKIs.

3 COMPARISON OF DIFFERENT TKIS

Because multiple signaling pathways are involved in tumorigenesis and tumor progression, all TKIs for HCC are multi-kinase inhibitors which are designed to target a wide range of targeted kinases. For first-line TKIs, sorafenib targets the serine/threonine kinase Raf or blocks autophosphorylation of multiple RTKs—VEGFR1, 2 and 3, PDGFR, c-Kit, and RET (9). This dual inhibition thus led to satisfactory efficacy with tolerable adverse events. In comparison, lenvatinib is the alternative choice for first-line treatment, but has a different mode of binding compared to sorafenib. When forming complexes with VEGFR2, sorafenib has slow binding kinetics, whereas lenvatinib exhibits a fast association rate constant. It also expresses prolonged residence time than expected due to its delayed dissociation rate constant. Thus, in terms of binding with VEGFR2, lenvatinib is more than 10 times as potent as sorafenib, which offsets sorafenib's dual inhibition, making lenvatinib confer noninferiority compared to sorafenib (19, 50).

For second-line TKIs, regorafenib, as the standard follow-up after sorafenib treatment, compensates for loss of efficacy by targeting a broader spectrum of targets compared to sorafenib. In addition to common targets such as VEGFR and PDGFR, regorafenib also targets angiogenic receptors TIE2, and oncogenic kinases BRAF V600E, RET, RAF-1, and KIT (34). Moreover, *in vitro* biochemical assays showed that regorafenib is a more potent inhibitor of VEGFR2,PDGFRβ, FGFR1 and c-Kit than sorafenib (43). When compared to regorafenib, cabozantinib offers an alternative choice as they are structurally similar but impose different inhibitory effects on the kinase IC50 (42). While data suggests cabozantinib is a more potent inhibitor of MET, AXL, RET, FLT3, and TIE-2 than regorafenib, it is also more toxic by inducing more frequent adverse events such as palmar-plantar erythrodysesthesia, diarrhea, and asthenia than regorafenib (45). In summary, patients with HCC had limited benefits with single TIK therapies and show better OS with combination therapies. The combination of cabozantinib plus nivolumab was the first step in this direction.

4 NANOTECHNOLOGY AS THE POTENTIAL DELIVERY SYSTEM

Emerging nanotechnology as the potential delivery system may improve the therapeutic efficacy of the TKIs, nanoparticle-based TKI delivery techniques are studied nowadays (51). Nanocarriers (NCs) are a form of drug delivery system that is often used to control the pharmacokinetic and pharmacodynamic features of medicines. Nanomaterials used as drug carriers have been shown to improve drug absorption and bioavailability, enhance efficient

targeting delivery, prolonged circulation time, and reduce harmful side effects on normal tissues due to their small particle size, large surface area, high surface reactivity and active sites, and desirable adsorption capacity (52).

Nanocarriers have been investigated for decades, and the most important carriers in drug delivery were polymeric, liposomal, nonorganic/metal, dendrimer, and micelle nanoparticles. There are multiple novel applications and researches on the delivery of TKIs through nanoparticles on some cancers recently, with most of them being liposomal, polymeric and polymeric micelle nano-carriers (**Figure 4**) (53).

Extracellular vesicles (EVs, 211.4 ± 3.83 nm) could be classified as a type of liposomal nanocarriers. In a research study, they were isolated from human primary adipose-derived stem cells. After incubation and sonication, TKI was loaded into EVs, which was further used to treat radioactive iodine-refractory thyroid cancer cells. The results showed a higher I125 uptake in the TKI treated EVs compared to a TKI-free treatment (54). In another research, polymeric nanoparticles were utilized. BSA-coated, dye-loaded nanoparticles were injected into prostate-specific PTEN/p53-deficient mice pretreated with cabozantinib. Their findings indicate that coating nanoparticles with BSA can improve cabozantinib-induced, neutrophil-mediated targeted intratumoral drug delivery while reducing off-target effects (55). The deliveries of apatinib and cediranib using polymeric nanoparticles were tested for osteosarcoma and glioblastoma, respectively. Both of the studies showed synergistic results compared to individual drugs (56, 57). Moreover, micelle nanoparticles were also studied in a study. A pH-sensitive ester link joins hyaluronic acid (HA) with dasatinib to create the HA-DAS polymer. Then, with rosiglitazone as the core and D-A-tocopheryl polydiethylene glycol isosuccinate (TPGS) and HA-DAS as carriers, a HA-DAS and TPGS mixed micelle system loaded with ROZ was created (THDR-NPs). The developed THDR-NPs showed better efficacy than the taking of free TKIs. In addition, the capacity of THDR-NPs to prevent tumor metastasis has been demonstrated (58). Another study using micelle nanoparticles to deliver anlotinib also showed a more effective uptake to the melanoma cells (59). Polymeric micelles were employed in other three studies relating liver fibrosis, glucose-avid pediatric sarcoma, and melanoma. Involved TKIs include nilotinib, dasatinib and sunitinib, and all of the treatments could enhance the clinical efficacy by utilizing nanoparticles relating to TKIs alone (60–62). Besides previously mentioned methods, electrospray technology was also applied to deliver nintedanib to treat idiopathic pulmonary fibrosis diseases. Higher bioavailability was demonstrated by using this technique (63). The newly developed techniques utilizing nanocarriers showed a higher bioavailability and reduction in the off-target tissues or organs. Noticeably, the bioavailability of nanocarrier involving erlotinib was almost 7 times greater than by orally taking (64).

In the presence of biological barriers *in vivo*, the physicochemical features of these nanocarriers modify their biological identity, which might drastically vary the therapeutic index of their payload and change the desired outcome. Furthermore, the challenges of producing effective medication nanocarriers have resulted in differing perspectives on their safety, permeability of biological barriers, and cellular absorption (65). During *in vivo* and *in vitro* cell exposure, nanoparticles can use a variety of distinct cellular entry pathways to penetrate the plasma membrane, either by endocytosis-based pathways or direct entry to the cells (66). Theoretically nanoparticles could be delivered to our body and focus on the desired target. However, there are only a few clinical studies going on for nanoparticle-based drugs, as the failure rate is high. For further stimulating cell-specific uptake and intracellular endosomal escape of therapeutic molecules, time- and space-controlled release techniques for TKIs delivery systems are necessary, and the responsive or "on-demand" release approach is vital for multidrug administration (51). Therefore, due to the limitations of current orally TKIs drugs, nanoparticle-based TKIs could be a potential way to deal with drug resistance and low bioavailability in future clinical trials, while it requires further investigations and more advanced techniques.

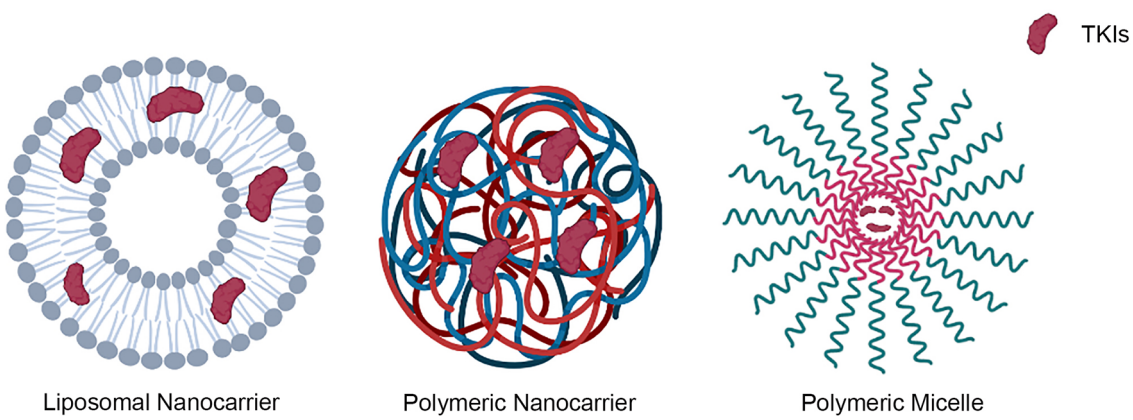

FIGURE 4 | Representative types of nanocarriers that were used in the delivery of TKIs, including liposomal, polymeric and polymeric micelle nano-carriers.

5 MOLECULAR CLASSIFICATIONS OF HCC

Molecular characterization of cancers has contributed to the improved patient outcomes. Recent advances of sequencing technologies have identified the molecular subtypes of HCC (67–74). The correlations between these molecular characterizations of HCC and outcome have been proposed. According to these previous studies, Rebouissou and Nault classified HCC into two major subtypes, "proliferation class" and "non-proliferation class". The proliferation class is related to HBV, including clinically aggressive tumors that are poorly differentiated. It is distinguished by an enrichment in TP53 inactivating mutations, amplification of FGF19 and CCND1, and frequent activation of pro-survival signaling pathways such as cell cycle, mTOR, RAS-MAPK, and MET. It could be then further divided into "Wnt-TGFβ subclass" and "progenitor subclass," involving Wnt and TGFβ pathways, and IGF1R and AKT pathways, respectively. Therefore, almost all tyrosine kinases inhibitors except Itacitinib would make contributions to the "proliferation class" of HCC. The non-proliferation class, on the other hand, relates to HCV or alcohol. These HCC cells are more differentiated and have hepatocyte-like characteristics. Non-proliferation class could be divided into "CTNB1 mutation" and "G4," involving Wnt/β-catenin pathway and IL6/JAK-STAT pathways, respectively (75). Itacitinib would affect this genre as it inhibits the JAK-STAT pathway.

6 BIOLOGICAL ALTERATIONS IN HCC GENESIS

Biological alterations in HCC genesis and the impact of TKIs on that pathobiological issues are important for the outcomes (76). Treatment of HCC by TKIs, however, still faces obstacles such as resistance by genetic mutation. For example, changes in the kinase gatekeeper residue may impede inhibitor binding by altering hydrophobic interactions, as suggested by the case of Thr 315 (coded by ACT) mutation in BCR-ABL kinase, which led to imatinib resistance (77). Moreover, overactivation of PI3K would prevent tumor cell from entering kinase-induced apoptosis, which was observed in sorafenib treatment (78). The amplification of the MET gene contributes to PI3K activation as well by driving ERBB3 (HER3)–dependent activation, which causes gefitinib and possible erlotinib resistance (79). Up-regulation of ATP-binding cassette (ABC) proteins can also lead to TKI resistance by exporting inhibitors (80). However, some TKIs such as sorafenib plays a dual role in multidrug resistance as it down-regulates ABCB1 and ABCC2 in HCC, hence opening new therapeutic options for TKI in the treatment of HCC (81). PHGDH was identified as an important driver gene for Sorafenib resistance in HCC by genome-wide CRISPR/Cas9 screening method (82). Although the molecular mechanisms of action of TKIs vary, previous progress have already identified attractive therapeutic approaches for TKI resistant HCC.

7 CONCLUSION

In the past 14 years, treatment of HCC by TKIs has evolved considerably. Although TKIs can delay HCC progression and prolong OS, they still have several challenges: (1) Drug resistance. Random mutations in target receptors lead to abnormal signaling. There are also problems for multi-targeted TKIs where off-target toxicity develops. Heterogeneity in tumor cells could also make TKI less effective due to its specificity of targets (83). The initial sensitivity of patients to TKIs are individually different, as a result, most patients who initially respond well to TKIs will eventually develop drug tolerance. Combination strategies of TKIs plus immune checkpoint inhibitors appearing as a promising strategy to circumvent resistance mechanisms that can be encountered with TKIs, aiming at a synergistic antitumor effect. For future studies, single cell RNA-sequencing could be applied for unraveling the tumor heterogeneity of HCC on a single cell level, further serving as a potential solution to decode the intricate mechanism behind the formation of drug resistance (84). (2) Side effects. Existing TKIs can cause serious side effects while treating HCC (e.g., Sorafenib treatment requires oral high-dose); (3) Low solubility. Only few of the substances could be utilized for targeting by orally taking for TKIs. Nanoparticle-based TKIs delivery techniques would be a promising field for research since they improve the therapeutic efficacy. All the efforts mentioned above will help to overcome TKI resistance and bring better therapy benefit for HCC patients in the future.

AUTHOR CONTRIBUTIONS

LM, XT, and BZ drafted the manuscript. YZ, JiaC, YL, YD, ZW, and QL collected data. YS, HZ, JinC, and KT proposed useful comments, suggestions, and revised the manuscript. JD proposed and drew the pictures in this manuscript. LM, YN, and ZP designed the structure and revised the manuscript. All authors contributed to the article and approved the submitted version.

FUNDING

This study was supported by Shenzhen Foundation of Science and Technology (grant number JCYJ20170817172116272), Sanming Project of Medicine in Shenzhen (SZSM201812079) and Shenzhen High-level Hospital Construction Fund (2019).

ACKNOWLEDGMENTS

We are grateful to Prof. Wenlong Huang (General Surgery, The First Affiliated Hospital of Shantou University Medical College) for valuable advice and discussions.

REFERENCES

1. Sung H, Ferlay J, Siegel RL, Laversanne M, Soerjomataram I, Jemal A, et al. Global Cancer Statistics 2020: GLOBOCAN Estimates of Incidence and Mortality Worldwide for 36 Cancers in 185 Countries. *CA Cancer J Clin* (2021) 71:201–49. doi: 10.3322/caac.21660
2. Asafo-Agyei KO, Samant H. Hepatocellular Carcinoma. In: *StatPearls*. Treasure Island (FL: StatPearls Publishing (2021). Available at: http://www.ncbi.nlm.nih.gov/books/NBK559177/ (Accessed March 12, 2021).
3. Forner A, Reig M, Bruix J. Hepatocellular Carcinoma. *Lancet* (2018) 391:1301–14. doi: 10.1016/S0140-6736(18)30010-2
4. Huang L, Jiang S, Shi Y. Tyrosine Kinase Inhibitors for Solid Tumors in the Past 20 Years (2001-2020). *J Hematol Oncol J Hematol Oncol* (2020) 13:143. doi: 10.1186/s13045-020-00977-0
5. Dimri M, Satyanarayana A. Molecular Signaling Pathways and Therapeutic Targets in Hepatocellular Carcinoma. *Cancers* (2020) 12:491. doi: 10.3390/cancers12020491
6. Thomson RJ, Moshirfar M, Ronquillo Y. Tyrosine Kinase Inhibitors. In: *StatPearls*. Treasure Island (FL: StatPearls Publishing (2021). Available at: http://www.ncbi.nlm.nih.gov/books/NBK563322/ (Accessed June 4, 2021).
7. Stacker SA, Achen MG. The VEGF Signaling Pathway in Cancer: The Road Ahead, Chin. *J Cancer* (2013) 32:297–302. doi: 10.5732/cjc.012.10319
8. Keating GM. Sorafenib: A Review in Hepatocellular Carcinoma. *Targeting Oncol* (2017) 12:243–53. doi: 10.1007/s11523-017-0484-7
9. Wilhelm S, Carter C, Lynch M, Lowinger T, Dumas J, Smith RA, et al. Discovery and Development of Sorafenib: A Multikinase Inhibitor for Treating Cancer. *Nat Rev Drug Discov* (2006) 5:835–44. doi: 10.1038/nrd2130
10. Benson A, D'Angelica MI, Abbott DE, Anaya DA, Anders R, Are C, et al. *National Comprehensive Cancer Network (NCCN) Clinical Practice Guidelines in Oncology. Hepatobiliary Cancers (Version1)* (2021). Available at: https://www.nccn.org/professionals/physician_gls/pdf/hepatobiliary.pdf.
11. Finn RS, Qin S, Ikeda M, Galle PR, Ducreux M, Kim T-Y, et al. Atezolizumab Plus Bevacizumab in Unresectable Hepatocellular Carcinoma. *N Engl J Med* (2020) 382:1894–905. doi: 10.1056/NEJMoa1915745
12. Liu Q, Dai Y. Sorafenib Combined With Transarterial Chemoembolization Prolongs Survival of Patients With Advanced Hepatocellular Carcinoma. *J BUON Off J Balk Union Oncol* (2020) 25:945–51.
13. Meyer T, Fox R, Ma YT, Ross PJ, James MW, Sturgess R, et al. Sorafenib in Combination With Transarterial Chemoembolisation in Patients With Unresectable Hepatocellular Carcinoma (TACE 2): A Randomised Placebo-Controlled, Double-Blind, Phase 3 Trial. *Lancet Gastroenterol Hepatol* (2017) 2:565–75. doi: 10.1016/S2468-1253(17)30156-5
14. Kim BK, Kim DY, Byun HK, Choi HJ, Beom S-H, Lee HW, et al. Efficacy and Safety of Liver-Directed Concurrent Chemoradiotherapy and Sequential Sorafenib for Advanced Hepatocellular Carcinoma: A Prospective Phase 2 Trial. *Int J Radiat Oncol* (2020) 107:106–15. doi: 10.1016/j.ijrobp.2020.01.027
15. Al-Salama ZT, Syed YY, Scott LJ. Lenvatinib: A Review in Hepatocellular Carcinoma. *Drugs* (2019) 79:665–74. doi: 10.1007/s40265-019-01116-x
16. Matsui J, Funahashi Y, Uenaka T, Watanabe T, Tsuruoka A, Asada M. Multi-Kinase Inhibitor E7080 Suppresses Lymph Node and Lung Metastases of Human Mammary Breast Tumor MDA-MB-231 *via* Inhibition of Vascular Endothelial Growth Factor-Receptor (VEGF-R) 2 and VEGF-R3 Kinase. *Clin Cancer Res* (2008) 14:5459–65. doi: 10.1158/1078-0432.CCR-07-5270
17. Tohyama O, Matsui J, Kodama K, Hata-Sugi N, Kimura T, Okamoto K, et al. Antitumor Activity of Lenvatinib (E7080): An Angiogenesis Inhibitor That Targets Multiple Receptor Tyrosine Kinases in Preclinical Human Thyroid Cancer Models. *J Thyroid Res* (2014) 2014:e638747. doi: 10.1155/2014/638747
18. Yamamoto Y, Matsui J, Matsushima T, Obaishi H, Miyazaki K, Nakamura K, et al. Lenvatinib, an Angiogenesis Inhibitor Targeting VEGFR/FGFR, Shows Broad Antitumor Activity in Human Tumor Xenograft Models Associated With Microvessel Density and Pericyte Coverage. *Vasc Cell* (2014) 6:18. doi: 10.1186/2045-824X-6-18
19. Okamoto K, Ikemori-Kawada M, Jestel A, von König K, Funahashi Y, Matsushima T, et al. Distinct Binding Mode of Multikinase Inhibitor Lenvatinib Revealed by Biochemical Characterization. *ACS Med Chem Lett* (2015) 6:89–94. doi: 10.1021/ml500394m
20. Hatanaka T, Naganuma A, Kakizaki S. Lenvatinib for Hepatocellular Carcinoma: A Literature Review, Pharm. *Basel Switz* (2021) 14:36. doi: 10.3390/ph14010036
21. Finn RS, Ikeda M, Zhu AX, Sung MW, Baron AD, Kudo M, et al. Phase Ib Study of Lenvatinib Plus Pembrolizumab in Patients With Unresectable Hepatocellular Carcinoma. *J Clin Oncol Off J Am Soc Clin Oncol* (2020) 38:2960–70. doi: 10.1200/JCO.20.00808
22. Finn RS, Ryoo B-Y, Merle P, Kudo M, Bouattour M, Lim H-Y, et al. Results of KEYNOTE-240: Phase 3 Study of Pembrolizumab (Pembro) *vs* Best Supportive Care (BSC) for Second Line Therapy in Advanced Hepatocellular Carcinoma (HCC). *J Clin Oncol* (2019) 37:4004–4. doi: 10.1200/JCO.2019.37.15_suppl.4004
23. Wang H. Analysis on the Clinical Effect and Safety of Lenvatinib Mesylate Combined With TACE in the Treatment of Patients With Metaphase and Advanced Primary Liver Cancer. *Med Innov China* (2020) 17:006–9. doi: 10.3969/j.issn.1674-4985.2020.31.002
24. Yue S. Clinical Effect of Microwave Ablation Combined With Lenvatinib in the Targeted Therapy of Advanced Liver Cancer and Its Influence on Prognosis. *Chin Foreign Med Res* (2020) 18:33–5. doi: 10.14033/j.cnki.cfmr.2020.28.013
25. Zhang X-H, Cao M-Q, Li X-X, Zhang T. Apatinib as an Alternative Therapy for Advanced Hepatocellular Carcinoma. *World J Hepatol* (2020) 12:766–74. doi: 10.4254/wjh.v12.i10.766
26. Gu H, Li J, You N, Wu K, Wang Z, Wang L, et al. Efficacy and Safety of Apatinib Combined With Transarterial Chemoembolization (TACE) in Treating Patients With Recurrent Hepatocellular Carcinoma. *Ann Transl Med* (2020) 8:1677. doi: 10.21037/atm-20-7244
27. Li X, Qiu M, Wang S, Zhu H, Feng B, Zheng L. A Phase I Dose-Escalation, Pharmacokinetics and Food-Effect Study of Oral Donafenib in Patients With Advanced Solid Tumours. *Cancer Chemother Pharmacol* (2020) 85:593–604. doi: 10.1007/s00280-020-04031-1
28. Qin S, Bi F, Cui C, Zhu B, Wu J, Xin X, et al. 982p Comparison of Donafenib and Sorafenib as Advanced Hepatocellular Carcinoma First-Line Treatments: Subgroup Analysis of an Open-Label, Randomized, Parallel-Controlled, Multicentre Phase II/III Trial. *Ann Oncol* (2020) 31:S688. doi: 10.1016/j.annonc.2020.08.1098
29. Qin S, Fan J, Shen F, Chen M, Luo R, Teng G, et al. *Guidelines of Chinese Society of Clinical Oncology in Hepatocellular Carcinoma* (2020). Available at: http://www.lcgdbzz.org/custom/news/id/10308.
30. Heldin C-H. Targeting the PDGF Signaling Pathway in Tumor Treatment. *Cell Commun Signal CCS* (2013) 11:97. doi: 10.1186/1478-811X-11-97
31. Blažević T, Schwaiberger AV, Schreiner CE, Schachner D, Schaible AM, Grojer CS, et al. 12/15-Lipoxygenase Contributes to Platelet-Derived Growth Factor-Induced Activation of Signal Transducer and Activator of Transcription 3. *J Biol Chem* (2013) 288:35592–603. doi: 10.1074/jbc.M113.489013
32. Papadopoulos N, Lennartsson J. The PDGF/PDGFR Pathway as a Drug Target. *Mol Aspects Med* (2018) 62:75–88. doi: 10.1016/j.mam.2017.11.007
33. Wilhelm SM, Dumas J, Adnane L, Lynch M, Carter CA, Schütz G, et al. Regorafenib (BAY 73-4506): A New Oral Multikinase Inhibitor of Angiogenic, Stromal and Oncogenic Receptor Tyrosine Kinases With Potent Preclinical Antitumor Activity. *Int J Cancer* (2011) 129:245–55. doi: 10.1002/ijc.25864
34. Rey J-B, Launay-Vacher V, Tournigand C. Regorafenib as a Single-Agent in the Treatment of Patients With Gastrointestinal Tumors: An Overview for Pharmacists. *Targeting Oncol* (2015) 10:199–213. doi: 10.1007/s11523-014-0333-x
35. Ettrich TJ, Seufferlein T. Regorafenib, Recent Results Cancer Res. Fortschritte Krebsforsch. Progres Dans Rech. *Sur Cancer* (2018) 211:45–56. doi: 10.1007/978-3-319-91442-8_3
36. Carr BI, Cavallini A, Lippolis C, D'Alessandro R, Messa C, Refolo MG, et al. Fluoro-Sorafenib (Regorafenib) Effects on Hepatoma Cells: Growth Inhibition, Quiescence, and Recovery. *J Cell Physiol* (2013) 228:292–7. doi: 10.1002/jcp.24148
37. Ferrari SM, Centanni M, Virili C, Miccoli M, Ferrari P, Ruffilli I, et al. Sunitinib in the Treatment of Thyroid Cancer. *Curr Med Chem* (2019) 26:963–72. doi: 10.2174/0929867324666171006165942
38. Turpin A, de Baere T, Heurgué A, Le Malicot K, Ollivier-Hourmand I, Lecomte T, et al. PRODIGE 16 Investigators Collaborators, Liver Transarterial

Chemoembolization and Sunitinib for Unresectable Hepatocellular Carcinoma: Results of the PRODIGE 16 Study. *Clin Res Hepatol Gastroenterol* (2021) 45:101464. doi: 10.1016/j.clinre.2020.05.012
39. Bouattour M, Raymond E, Qin S, Cheng A-L, Stammberger U, Locatelli G, et al. Recent Developments of C-Met as a Therapeutic Target in Hepatocellular Carcinoma. *Hepatol Baltim Md* (2018) 67:1132–49. doi: 10.1002/hep.29496
40. Gentile A, Trusolino L, Comoglio PM. The Met Tyrosine Kinase Receptor in Development and Cancer. *Cancer Metastasis Rev* (2008) 27:85–94. doi: 10.1007/s10555-007-9107-6
41. Trusolino L, Comoglio PM. Scatter-Factor and Semaphorin Receptors: Cell Signalling for Invasive Growth. *Nat Rev Cancer* (2002) 2:289–300. doi: 10.1038/nrc779
42. Lacy S, Hsu B, Miles D, Aftab D, Wang R, Nguyen L. Metabolism and Disposition of Cabozantinib in Healthy Male Volunteers and Pharmacologic Characterization of Its Major Metabolites. *Drug Metab Dispos Biol Fate Chem* (2015) 43:1190–207. doi: 10.1124/dmd.115.063610
43. Strumberg D, Schultheis B. Regorafenib for Cancer. *Expert Opin Investig Drugs* (2012) 21:879–89. doi: 10.1517/13543784.2012.684752
44. Kelley RK, Verslype C, Cohn AL, Yang T-S, Su W-C, Burris H, et al. Cabozantinib in Hepatocellular Carcinoma: Results of a Phase 2 Placebo-Controlled Randomized Discontinuation Study. *Ann Oncol Off J Eur Soc Med Oncol* (2017) 28:528–34. doi: 10.1093/annonc/mdw651
45. Kudo M. Cabozantinib as a Second-Line Agent in Advanced Hepatocellular Carcinoma. *Liver Cancer* (2018) 7:123–33. doi: 10.1159/000488542
46. Yarchoan M, Zhu Q, Durham JN, Gross N, Charmsaz S, Leatherman JM, et al. Feasibility and Efficacy of Neoadjuvant Cabozantinib and Nivolumab in Patients With Borderline Resectable or Locally Advanced Hepatocellular Carcinoma (HCC). *J Clin Oncol* (2021) 39:335–5. doi: 10.1200/JCO.2021.39.3_suppl.335
47. Gao Y, Liu P, Shi R. Anlotinib as a Molecular Targeted Therapy for Tumors. *Oncol Lett* (2020) 20:1001–14. doi: 10.3892/ol.2020.11685
48. Sun Y, Zhou A, Zhang W, Jiang Z, Chen B, Zhao J, et al. Anlotinib in the Treatment of Advanced Hepatocellular Carcinoma: An Open-Label Phase II Study (ALTER-0802 Study). *Hepatol Int* (2021) 15:621–9. doi: 10.1007/s12072-021-10171-0
49. Han C, Ye S, Hu C, Shen L, Qin Q, Bai Y, et al. Clinical Activity and Safety of Penpulimab (Anti-PD-1) With Anlotinib as First-Line Therapy for Unresectable Hepatocellular Carcinoma: An Open-Label, Multicenter, Phase Ib/II Trial (AK105-203). *Front Oncol* (2021) 11:684867. doi: 10.3389/fonc.2021.684867
50. Kudo M, Finn RS, Qin S, Han K-H, Ikeda K, Piscaglia F, et al. Lenvatinib *Versus* Sorafenib in First-Line Treatment of Patients With Unresectable Hepatocellular Carcinoma: A Randomised Phase 3 Non-Inferiority Trial. *Lancet* (2018) 391:1163–73. doi: 10.1016/S0140-6736(18)30207-1
51. Yin Y, Yuan X, Gao H, Yang Q. Nanoformulations of Small Molecule Protein Tyrosine Kinases Inhibitors Potentiate Targeted Cancer Therapy. *Int J Pharm* (2020) 573:118785. doi: 10.1016/j.ijpharm.2019.118785
52. Su C, Liu Y, Li R, Wu W, Fawcett JP, Gu J. Absorption, Distribution, Metabolism and Excretion of the Biomaterials Used in Nanocarrier Drug Delivery Systems. *Adv Drug Deliv Rev* (2019) 143:97–114. doi: 10.1016/j.addr.2019.06.008
53. Foroughi-Nia B, Barar J, Memar MY, Aghanejad A, Davaran S. Progresses in Polymeric Nanoparticles for Delivery of Tyrosine Kinase Inhibitors. *Life Sci* (2021) 278:119642. doi: 10.1016/j.lfs.2021.119642
54. Rajendran RL, Paudel S, Gangadaran P, Oh JM, Oh EJ, Hong CM, et al. Extracellular Vesicles Act as Nano-Transporters of Tyrosine Kinase Inhibitors to Revert Iodine Avidity in Thyroid Cancer. *Pharmaceutics* (2021) 13:248. doi: 10.3390/pharmaceutics13020248
55. Chaudagar KK, Landon-Brace N, Solanki A, Hieromnimon HM, Hegermiller E, Li W, et al. Cabozantinib Unlocks Efficient In Vivo Targeted Delivery of Neutrophil-Loaded Nanoparticles Into Murine Prostate Tumors. *Mol Cancer Ther* (2021) 20:438–49. doi: 10.1158/1535-7163.MCT-20-0167
56. Li X, Wang L, Wang L, Yu J, Lu G, Zhao W, et al. Overcoming Therapeutic Failure in Osteosarcoma *via* Apatinib-Encapsulated Hydrophobic Poly(Ester Amide) Nanoparticles. *Biomater Sci* (2020) 8:5888–99. doi: 10.1039/d0bm01296c
57. Kydd J, Jadia R, Rai P. Co-Administered Polymeric Nano-Antidotes for Improved Photo-Triggered Response in Glioblastoma. *Pharmaceutics* (2018) 10:E226. doi: 10.3390/pharmaceutics10040226
58. Wang H, Zhang Y, Zeng X, Pei W, Fan R, Wang Y, et al. A Combined Self-Assembled Drug Delivery for Effective Anti-Breast Cancer Therapy. *Int J Nanomed* (2021) 16:2373–88. doi: 10.2147/IJN.S299681
59. Zhang Y, Chen H, Feng N, Xin X, Xu Y, Huo P, et al. Construction and Antitumor Effects of Antitumor Micelles With Cyclic RGD-Modified Anlotinib, Nanomedicine Nanotechnol. *Biol Med* (2020) 28:102224. doi: 10.1016/j.nano.2020.102224
60. Fan Q-Q, Zhang C-L, Qiao J-B, Cui P-F, Xing L, Oh Y-K, et al. Extracellular Matrix-Penetrating Nanodrill Micelles for Liver Fibrosis Therapy. *Biomaterials* (2020) 230:119616. doi: 10.1016/j.biomaterials.2019.119616
61. Bukchin A, Pascual-Pasto G, Cuadrado-Vilanova M, Castillo-Ecija H, Monterrubio C, Olaciregui NG, et al. Glucosylated Nanomicelles Target Glucose-Avid Pediatric Patient-Derived Sarcomas. *J Control Release Off J Control Release Soc* (2018) 276:59–71. doi: 10.1016/j.jconrel.2018.02.034
62. Huo M, Zhao Y, Satterlee AB, Wang Y, Xu Y, Huang L. Tumor-Targeted Delivery of Sunitinib Base Enhances Vaccine Therapy for Advanced Melanoma by Remodeling the Tumor Microenvironment. *J Control Release Off J Control Release Soc* (2017) 245:81–94. doi: 10.1016/j.jconrel.2016.11.013
63. Liu H, Du K, Li D, Du Y, Xi J, Xu Y, et al. A High Bioavailability and Sustained-Release Nano-Delivery System for Nintedanib Based on Electrospray Technology. *Int J Nanomed* (2018) 13:8379–93. doi: 10.2147/IJN.S181002
64. Nottingham E, Sekar V, Mondal A, Safe S, Rishi AK, Singh M. The Role of Self-Nanoemulsifying Drug Delivery Systems of CDODA-Me in Sensitizing Erlotinib-Resistant Non-Small Cell Lung Cancer, J. *Pharm Sci* (2020) 109:1867–82. doi: 10.1016/j.xphs.2020.01.010
65. Zhao Z, Ukidve A, Krishnan V, Mitragotri S. Effect of Physicochemical and Surface Properties on *In Vivo* Fate of Drug Nanocarriers. *Adv Drug Deliv Rev* (2019) 143:3–21. doi: 10.1016/j.addr.2019.01.002
66. Donahue ND, Acar H, Wilhelm S. Concepts of Nanoparticle Cellular Uptake, Intracellular Trafficking, and Kinetics in Nanomedicine. *Adv Drug Deliv Rev* (2019) 143:68–96. doi: 10.1016/j.addr.2019.04.008
67. Boyault S, Rickman DS, Reyniès A, de, Balabaud C, Rebouissou S, Jeannot E, et al. Transcriptome Classification of HCC Is Related to Gene Alterations and to New Therapeutic Targets. *Hepatology* (2007) 45:42–52. doi: 10.1002/hep.21467
68. Chiang DY, Villanueva A, Hoshida Y, Peix J, Newell P, Minguez B, et al. Focal Gains of VEGFA and Molecular Classification of Hepatocellular Carcinoma. *Cancer Res* (2008) 68:6779–88. doi: 10.1158/0008-5472.CAN-08-0742
69. Hoshida Y, Nijman SMB, Kobayashi M, Chan JA, Brunet J-P, Chiang DY, et al. Integrative Transcriptome Analysis Reveals Common Molecular Subclasses of Human Hepatocellular Carcinoma. *Cancer Res* (2009) 69:7385–92. doi: 10.1158/0008-5472.CAN-09-1089
70. Lee J-S, Chu I-S, Heo J, Calvisi DF, Sun Z, Roskams T, et al. Classification and Prediction of Survival in Hepatocellular Carcinoma by Gene Expression Profiling. *Hepatology* (2004) 40:667–76. doi: 10.1002/hep.20375
71. Shimada S, Mogushi K, Akiyama Y, Furuyama T, Watanabe S, Ogura T, et al. Comprehensive Molecular and Immunological Characterization of Hepatocellular Carcinoma. *EBioMedicine* (2019) 40:457–70. doi: 10.1016/j.ebiom.2018.12.058
72. Wheeler DA, Roberts LR. Comprehensive and Integrative Genomic Characterization of Hepatocellular Carcinoma. *Cell* (2017) 169:1327–1341.e23. doi: 10.1016/j.cell.2017.05.046
73. Jiang Y, Sun A, Zhao Y, Ying W, Sun H, Yang X, et al. Chinese Human Proteome Project (CNHPP) Consortium. Proteomics Identifies New Therapeutic Targets of Early-Stage Hepatocellular Carcinoma. *Nature* (2019) 567:257–61. doi: 10.1038/s41586-019-0987-8
74. Gao Q, Zhu H, Dong L, Shi W, Chen R, Song Z, et al. Integrated Proteogenomic Characterization of HBV-Related Hepatocellular Carcinoma. *Cell* (2019) 179:561–77.e22. doi: 10.1016/j.cell.2019.08.052
75. Rebouissou S, Nault J-C. Advances in Molecular Classification and Precision Oncology in Hepatocellular Carcinoma. *J Hepatol* (2020) 72:215–29. doi: 10.1016/j.jhep.2019.08.017
76. Nenni M, Öncül S, Ercan >A, Çelebier M, Süslü* İ, Haznedaroğlu İC. Exposure of Hepatocellular Carcinoma Cells to Ankaferd Blood Stopper® Alters Cell Death Signaling Networks Confirmed by Oncoproteomic and Genomic Profiling Studies. *Curr Tradit Med* (2021) 7:246–58. doi: 10.2174/2215083806666200117093815

77. Xavier CPR, Lima CF, Preto A, Seruca R, Fernandes-Ferreira M, Pereira-Wilson C. Luteolin, Quercetin and Ursolic Acid Are Potent Inhibitors of Proliferation and Inducers of Apoptosis in Both KRAS and BRAF Mutated Human Colorectal Cancer Cells. *Cancer Lett* (2009) 281:162–70. doi: 10.1016/j.canlet.2009.02.041
78. Chen K-F, Tai W-T, Liu T-H, Huang H-P, Lin Y-C, Shiau C-W, et al. Sorafenib Overcomes TRAIL Resistance of Hepatocellular Carcinoma Cells Through the Inhibition of STAT3. *Clin Cancer Res Off J Am Assoc Cancer Res* (2010) 16:5189–99. doi: 10.1158/1078-0432.CCR-09-3389
79. Engelman JA, Zejnullahu K, Mitsudomi T, Song Y, Hyland C, Park JO, et al. MET Amplification Leads to Gefitinib Resistance in Lung Cancer by Activating ERBB3 Signaling. *Science* (2007) 316:1039–43. doi: 10.1126/science.1141478
80. Marin JJG, Monte MJ, Blazquez AG, Macias RIR, Serrano MA, Briz O. The Role of Reduced Intracellular Concentrations of Active Drugs in the Lack of Response to Anticancer Chemotherapy. *Acta Pharmacol Sin* (2014) 35:1–10. doi: 10.1038/aps.2013.131
81. Hoffmann K, Franz C, Xiao Z, Mohr E, Serba S, Büchler MW, et al. Sorafenib Modulates the Gene Expression of Multi-Drug Resistance Mediating ATP-Binding Cassette Proteins in Experimental Hepatocellular Carcinoma. *Anticancer Res* (2010) 30:4503–8.
82. Wei L, Lee D, Law CT, Zhang MS, Shen J, Chin DW, et al. Genome-Wide CRISPR/Cas9 Library Screening Identified PHGDH as a Critical Driver for Sorafenib Resistance in HCC. *Nat Commun* (2019) 10:4681. doi: 10.1038/s41467-019-12606-7
83. Cabral LKD, Tiribelli C, Sukowati CHC. Sorafenib Resistance in Hepatocellular Carcinoma: The Relevance of Genetic Heterogeneity. *Cancers* (2020) 12:1576. doi: 10.3390/cancers12061576
84. Dhanasekaran R. Deciphering Tumor Heterogeneity in Hepatocellular Carcinoma (HCC)-Multi-Omic and Singulomic Approaches, Semin. *Liver Dis* (2021) 41:9–18. doi: 10.1055/s-0040-1722261

Conflict of Interest: The authors declare that the research was conducted in the absence of any commercial or financial relationships that could be construed as a potential conflict of interest.

Publisher's Note: All claims expressed in this article are solely those of the authors and do not necessarily represent those of their affiliated organizations, or those of the publisher, the editors and the reviewers. Any product that may be evaluated in this article, or claim that may be made by its manufacturer, is not guaranteed or endorsed by the publisher.

frontiers in Oncology

ORIGINAL RESEARCH
published: 19 October 2021
doi: 10.3389/fonc.2021.747950

Surgery After Conversion Therapy With PD-1 Inhibitors Plus Tyrosine Kinase Inhibitors Are Effective and Safe for Advanced Hepatocellular Carcinoma: A Pilot Study of Ten Patients

Wenwen Zhang[1,2,3†], Bingyang Hu[1,2,3†], Jun Han[1,2,3†], Zhanbo Wang[4], Guangyu Ma[5], Huiyi Ye[6], Jing Yuan[4], Junning Cao[7], Ze Zhang[1,2,3,8], Jihang Shi[1,2,3,8], Mingyi Chen[1,2,3], Xun Wang[9], Yinzhe Xu[1,2,3], Yanshuang Cheng[1,2,3], Lantian Tian[10], Hongguang Wang[9] and Shichun Lu[1,2,3*]*

[1] Faculty of Hepato-Pancreato-Biliary Surgery, Chinese People's Liberation Army (PLA) General Hospital, Beijing, China, [2] Institute of Hepatobiliary Surgery of Chinese PLA, Beijing, China, [3] Key Laboratory of Digital Hepatobiliary Surgery, PLA, Beijing, China, [4] Department of Pathology, the First Medical Center of PLA General Hospital, Beijing, China, [5] Department of Nuclear Medicine, the First Medical Center of PLA General Hospital, Beijing, China, [6] Department of Radiology, the First Medical Center of PLA General Hospital, Beijing, China, [7] Organ Transplant Center, the Affiliated Hospital of Qingdao University, Qingdao, China, [8] Medical School of Chinese PLA, Beijing, China, [9] National Cancer Center/National Clinical Research Center for Cancer/Cancer Hospital, Chinese Academy of Medical Sciences and Peking Union Medical College, Beijing, China, [10] Department of Hepatopancreatobiliary Surgery, Affiliated Hospital of Qingdao University, Qingdao, China

Background and Aims: Immunotherapy with PD-1 inhibitors combined with tyrosine kinase inhibitors (TKIs) has been proven to be effective against advanced hepatocellular carcinoma (HCC). The aim of this study was to identify the feasibility and safety of subsequent salvage surgery after this combination therapy.

Methods and Patients: A retrospective analysis was performed on patients with primary HCC with major vascular invasion between 2018 and 2019. All cases were treated with a combination of a PD-1 inhibitor and TKI agents and subsequent surgery.

Results: A total of 10 HCC cases with major vascular invasion met the successful conversion criteria after the combination therapy, and eight patients underwent subsequent salvage surgery after both radiology and 3D quantitative oncological assessment. Partial response (PR) was recorded in 7 of 10 patients and complete response (CR) in 3 of 10 patients before salvage surgery. Salvage surgery included right hepatectomy, left hepatectomy, and anatomic segmental hepatectomy. The mean intraoperative blood loss was 1,650 ml (50–3,000 ml). No complications beyond Clavien–Dindo level III or postoperative mortality were observed. The viable tumor cell rate of the

OPEN ACCESS

Edited by:
Yunfei Xu,
Shandong University, China

Reviewed by:
Jinhong Chen,
Fudan University, China
Haitao Zhao,
Peking Union Medical College Hospital (CAMS), China

***Correspondence:**
Shichun Lu
lusc_301@163.com
Hongguang Wang
wanghongguang301@163.com

†These authors have contributed equally to this work

Specialty section:
This article was submitted to Cancer Molecular Targets and Therapeutics, a section of the journal Frontiers in Oncology

Received: *27 July 2021*
Accepted: *20 September 2021*
Published: *19 October 2021*

Citation:
Zhang W, Hu B, Han J, Wang Z, Ma G, Ye H, Yuan J, Cao J, Zhang Z, Shi J, Chen M, Wang X, Xu Y, Cheng Y, Tian L, Wang H and Lu S (2021) Surgery After Conversion Therapy With PD-1 Inhibitors Plus Tyrosine Kinase Inhibitors Are Effective and Safe for Advanced Hepatocellular Carcinoma: A Pilot Study of Ten Patients. Front. Oncol. 11:747950. doi: 10.3389/fonc.2021.747950

PR cases (modified response evaluation criteria in solid tumors, mRECIST) varied from 1.5% to 100%, and only one patient had pathology-proven pathological complete response (pCR). The postoperative median follow-up time was 19.7 months (9.1–24.9 months). The 12-month recurrence-free survival rate of all cases who underwent salvage surgery was 75%.

Conclusion: Salvage surgery was effective and safe after conversion therapy with PD-1 inhibitors plus TKIs and may increase the long-term oncological benefit for patients with unresectable HCC.

Keywords: hepatocellular carcinoma (HCC), conversion therapy, surgery, systematic treatment, PD-1 inhibitors, tyrosine kinase inhibitors (TKIs)

INTRODUCTION

Hepatocellular carcinoma (HCC) is a global public health challenge and socioeconomic burden, with nearly 906,000 new cases every year worldwide, including over 410,000 cases in China (1, 2). The overall 5-year survival rate was only 12.5% for the HCC population in China from 2003 to 2015 (3). Although surgical treatment is the most effective curative therapy for HCC in the early stages, with a 5-year survival rate exceeding 70%, no less than 44%–62.2% of all HCC patients were initially diagnosed with advanced HCC at Barcelona Clinic Liver Cancer (BCLC) classification stage C, most of which were accompanied by portal vein tumor thrombus (PVTT) (4–7). The majority of international guidelines recommend systemic treatment rather than curative radical surgery for these patients. However, the median overall survival (OS) values of the first- and the second-line targeted therapy were only 12 and 8 months, respectively (2, 8, 9).

In recent years, immune checkpoint inhibitors (ICIs) have achieved remarkable applications in cancer treatment. However, according to previous randomized clinical trials, ICI treatment alone did not show a significant survival benefit over targeted therapy with tyrosine kinase inhibitors (TKIs) for advanced HCC (10–12). Nevertheless, recent clinical studies have reported that combining PD-1/PD-L1 inhibitors and anti-angiogenesis targeted drugs achieved an objective response rate (ORR) of 33.2%–46.0% and a disease control rate (DCR) of 72.3%–88% for the treatment of unresectable HCC (13–15). The premium outcome of median OS was over 17 months, and 8.6%–11% of the included patients achieved complete response (CR) with good treatment safety.

On the other hand, a surprising discovery was that some of the cases with CR and partial response (PR) retrieved the opportunity for surgery. Moreover, ICIs enhanced the tumor-specific immunology, which can be maintained after subsequent surgery (16). This raised the possibility that combination therapy with PD-1 inhibitors plus TKIs can be utilized as a conversion therapy for advanced HCC. However, the effectiveness, safety, and long-term oncological benefit of salvage surgery need to be clarified. Furthermore, suitable indications and operative opportunities are also required for further investigation. As the initial exploration of a prospective clinical registration study (ChiCTR1900023914), in the past 2 years, we have initiated the clinical exploration of the PD-1 inhibitor in combination with TKIs as a conversion therapy for unresectable HCC with major vascular invasion. To date, 10 patients who underwent successful conversion therapy have been reported.

METHOD

Patients

A retrospective analysis was performed on patients with primary HCC at BCLC classification stage C without extrahepatic metastasis from August 2018 to December 2019. All of these cases were treated with a first- or a second-line combination of a PD-1 inhibitor and TKI agents (in the latter case, the first-line treatment did not include a systemic treatment regimen), and salvage surgery was performed after the combination therapy with sufficient evaluation and permission of patients. The study was censored on June 30, 2021.

All patients met the following criteria prior to enrollment in the combined drug therapy protocol: 1) confirmed histologically or in accordance with the clinical diagnosis criteria of the American Association for the Study of Liver Diseases (AASLD) as HCC; 2) Child–Pugh score <7; 3) BCLC stage C, without extrahepatic metastasis; 4) Eastern Cooperative Oncology Group (ECOG) performance status (PS) score ≤1; 5) expected survival time ≥12 weeks; 6) no esophageal or gastric varicose bleeding events caused by portal hypertension occurring in the proximate 6 months; and 7) no previous anti-PD-1, anti-PD-L1/L2 antibody, anti-CTLA4 antibody, or other immunotherapy or targeted therapy with TKI agents.

The treatment regimen was recorded. In this study, the majority of patients were treated with pemlizumab and lenvatinib combination regimens. Other PD-1 inhibitor options include sintilimab and toripalimab. Other molecularly targeted drugs include apatinib (**Table 1**).

Radiologic Assessment

Imaging examinations were performed before and after the combination treatment protocol. The imaging data, including enhanced magnetic resonance imaging (MRI), computed tomography (CT), and positron emission tomography computed

TABLE 1 | Clinical characteristics of patients.

	Patient/case no.									
	1	**2**	**3**	**4**	**5**	**6**	**7**	**8**	**9**	**10**
Age (years)	56	33	48	54	43	56	62	67	61	38
Sex	Female	Male	Male	Male	Male	Male	Male	Female	Male	Male
BMI (kg/m^2)	21.2	27.2	21.7	27.3	26.3	25.5	19.7	21.5	25.0	27.7
ECOG PS score	0	0	0	0	0	0	0	0	0	0
Child–Pugh grade	A	A	A	A	A	A	A	A	A	A
Cirrhosis/without cirrhosis	Cirrhosis	Cirrhosis	Cirrhosis	Cirrhosis	Cirrhosis	Cirrhosis	Cirrhosis	Cirrhosis	Cirrhosis	Cirrhosis
Largest tumor diameter (mm)	169.1	125.8	122.9	103.4	139.7	72.4	88.5	36.2	163.4	85.4
Tumor number	1	1	3	1	1	2	4	1	1	1
BCLC stage	C	C	C	C	C	C	C	C	C	C
Macrovascular invasion[a]	VP4	VP4	VP2/IVC	VP4	VP4	VP3	VP3	VP4	VP4	VP4/LHV
Etiology	HBV	HBV	HBV	HBV	HBV/NAFLD	HBV	HBV	HCV	HBV	HBV
Prior therapy	–	–	–	–	–	TACE	–	–	–	–
AFP (ng/ml)	1,552.3	1,534	6,951	14.6	>60500	10.8	846.4	3.4	>60500	216.7
Liver biopsy	–	HCC	–	–	–	HCC	HCC	HCC	HCC	HCC
PD-1 category	PEM	PEM	PEM	TRI	PEM	PEM	PEM	PEM	SIN	TRI
TKI category	LEN	LEN	LEN	APA	LEN	LEN	LEN	LEN	LEN	LEN
Treatment cycles[b]	10	4	6	6	4	6	6	5	5	6
mRECIST	PR	PR	PR	PR	PR	CR	PR	PR	CR	CR
RECIST 1.1	PR	PR	PR	PR	PR	PR	PR	SD	PR	PR

AFP, alpha fetoprotein; APA, apatinib; BCLC, Barcelona clinic liver cancer; BMI, body mass index; CR, complete response; ECOG PS, Eastern Cooperative Oncology Group performance status; HBV, hepatitis B virus; HCC, hepatocellular carcinoma; HCV, hepatitis C virus; IVC, inferior vena cava; LEN, lenvatinib; LHV, left hepatic vein; mRECIST, modified respond evaluation criteria solid tumors; NAFLD, non-alcoholic fatty liver disease; PEM, pembrolizumab; PR, partial response; RECIST 1.1, response evaluation criteria in solid tumors version 1.1; SIN, sintilimab; TACE, transcatheter arterial chemoembolization; TKI, tyrosine kinase inhibitor; TRI, toripalimab.

[a]*Macrovascular invasion was measured in the portal vein, inferior vena cava, and hepatic vein. Portal vein invasion grade was evaluated according to the Japanese VP classification.*

[b]*Treatment cycles were the period between the first treatment cycle of PD-1 inhibitor to the last cycle before the surgery or to the last evaluation.*

tomography (PET-CT), were evaluated by two independent physicians using the modified response evaluation criteria in solid tumors (mRECIST) and the response evaluation criteria in solid tumors, version 1.1 (RECIST 1.1) (17). The 3D assessment of quantitative oncology utilized the total tumor volume (TTV), portal vein tumor thrombus (PVTT) volume, and future liver remnant (FLR) volume before and after the combination treatment protocol, which were quantitatively analyzed using a 3D reconstruction software (IQQA-Liver; EDDA Technology, Princeton, NJ, USA). This software was used interactively based on original CT/MRI DICOM images. For comparison purposes, FLR was set in the software as the volume of the remaining liver after hemihepatectomy where the tumor was located.

Surgery Criteria

The criteria for successful conversion include the following: 1) Child–Pugh score <7; 2) ECOG PS score ≤1; 3) no extrahepatic lesion assessed by PET-CT (or pulmonary CT, bone scan, etc.); 4) intact vascular structure (such as the inflow and outflow) of the reserved liver: and 5) the expected ratios of FLR to standard liver volume (FLR/SLV) after resection of the tumor-bearing liver are ≥40% in compromised livers and 35% in normal livers.

All patients who met the criteria of successful conversion were informed of the benefits and risks of surgery. Patients who agreed to subsequent surgery signed written informed consent forms.

Clinicopathological Variables

Patient-related factors included age, sex, performance status, the etiology of liver disease, presence of cirrhosis, Child–Pugh grading, and alpha-fetoprotein (AFP) level. Tumor factors included tumor number, tumor size, macroscopic vascular invasion, and BCLC staging. Surgery-related factors included intraoperative blood loss, intraoperative blood transfusion, postoperative complications, fasting time, and abdominal drainage duration. Pathological specimens were analyzed according to the seven-point baseline sampling protocol as much as possible. Patients were followed up using the serum AFP level as well as the MRI or CT of the chest and abdomen once every 2 months for 6 months and then once every 3 months afterward.

RESULTS

In this study, 10 patients with HCC with major vascular invasion who were eligible for surgery after PD-1 inhibitor combined with TKI agents were examined between August 2018 and December 2019. Among these patients, eight underwent salvage surgery. Another two patients met the criteria of successful conversion, but refused surgical treatment and were willing to continue with the original treatment protocol.

Clinical Characteristics and Conversion Therapy

The pretreatment baseline level and treatment plan of the patients were recorded, as shown in **Table 1**. All patients had hepatitis-related cirrhosis [nine hepatitis B virus (HBV) and one hepatitis C virus (HCV)], and one had non-alcoholic fatty liver

disease (NAFLD). All cases were evaluated at a Child–Pugh grade A of liver function and an ECOG PS score of 0 before treatment. All the cases met the AASLD clinical diagnostic criteria for HCC, and six of them were pathologically proven to have HCC by biopsy. Seven of the patients had grade VP4 PVTT, two patients had grade VP3, and one patient had grade VP2 PVTT accompanied by inferior vena cava (IVC) invasion. One case also exhibited left hepatic vein invasion (18). Detailed demographic data are listed in **Table 1**.

Nine of the included patients were treated with four to six cycles of PD-1 inhibitor with TKI agents, and one patient received 10 cycles of the same treatment. All adverse events (AEs) associated with the combination therapy were evaluated and recorded in accordance with the National Cancer Institute (NCI) general term for adverse events (Common Terminology Criteria for Adverse Events, CTCAE) version 5.0. None of the patients presented with AEs or serious adverse events (SAEs) above CTCAE level 3.

Radiologic Assessment

At the first evaluation after the initiation of the combination therapy (after three cycles of immunotherapy), all patients had a significant reduction in tumor target lesion(s), accompanied by liquefactive necrosis or coagulative necrosis of the tumor(s). According to the mRECIST standard evaluation, PR was recorded in seven of 10 patients and in three patients with a complete response (CR) before salvage surgery (shown in **Table 1**). The complete necrosis rate of PVTT often precedes that of the primary tumor. In case no. 1, cavernous transformation of the portal vein (CTPV) and recanalization of the intrahepatic portal vein were observed in addition to dramatic enlargement of the remnant liver (shown in **Figure 1**).

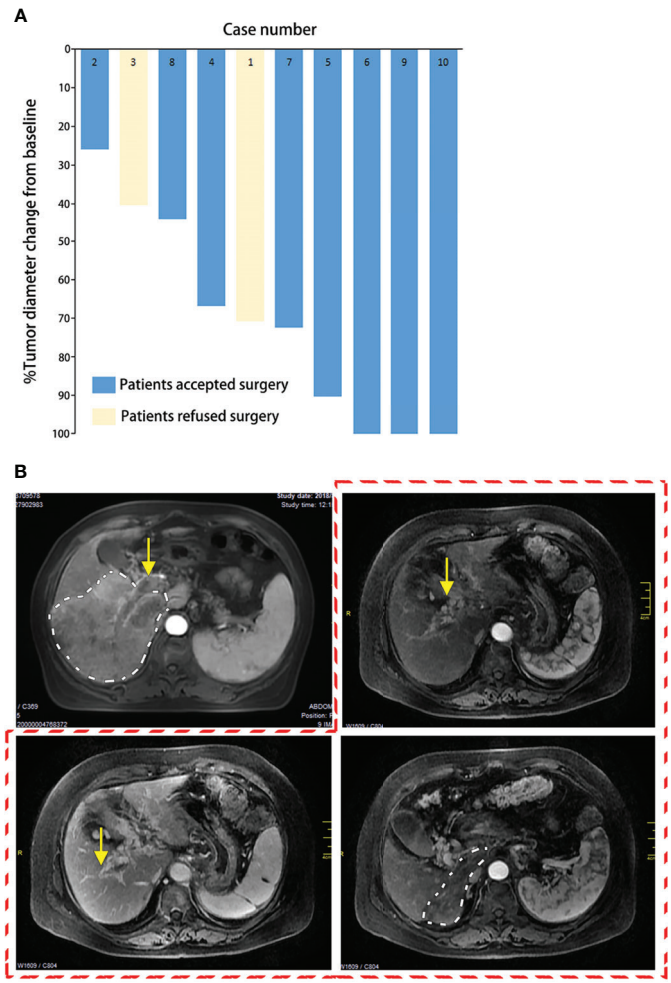

FIGURE 1 | Tumor shrinkage after the conversion therapy. **(A)** Waterfall plot of maximum tumor shrinkage based on the modified response evaluation criteria in solid tumors (mRECIST) per independent imaging review. **(B)** Radiologic change of case no. 1. Before treatment (*first image outside the red dotted line*): tumor located in the right liver (outlined in *white dotted line*) and portal vein tumor thrombus (PVTT) in the right portal vein (*yellow arrow*). After treatment (outlined in *red dotted line*): tumor shrinkage (outlined in *white dotted line*), future liver remnant (FLR) enlargement, cavernous transformation of portal vein, and recanalization of the intrahepatic portal vein (*yellow arrow*).

Three-dimensional reconstruction was utilized to quantitatively analyze the TTV, PVTT, and FLR before and after treatment. TTV decreased by an average of 357.29 and 4.15 ml/day, with a peak of 21.97 ml/day (accounting for 1.48%/day of the standard liver volume). The PVTT shrank by an average of 27.34 and 0.29 ml/day, with a peak of 56.27 ml/day. Radiologic features such as coagulative necrosis, poor blood supply, and size reduction can also be observed in PVTT after treatment. Although the tumor-free liver volume increased enormously, the FLR was not obviously elevated in the quantitative evaluation due to the software settings, as the volume of the remaining liver after hemihepatectomy where the tumor was located (shown in **Table 2** and **Figure 2**).

Perioperative Information

The preoperative surgical evaluation took place after informed consent was obtained at the time the patient met the criteria for successful conversion. All patients in this study were successfully converted to surgery candidates. Two patients decided to continue to rely on the combination therapy protocol and eight patients underwent salvage surgery in our center. Surgical options included right hepatectomy, left hepatectomy, and anatomic segmental hepatectomy, depending on the patient's tumor localization, degree of cirrhosis, and liver reserve. The perioperative information is listed in **Table 3**. **Figure 2** shows a typical case who had the combination therapy and underwent subsequent surgery (case no. 6).

In this case series, the interval between lenvatinib withdrawal and surgery was 3–7 days. The mean intraoperative blood loss was 1,650 ml (50–3000 ml). Endotracheal intubation was removed in all patients within 24 h. There was no postoperative mortality. There was no postoperative bleeding or bile leakage and no other postoperative complications beyond Clavien–Dindo level III (requiring surgery, endoscopy, or interventional intervention). The liver function indexes, such as transaminase and bilirubin, returned to normal within 7–10 days after surgery (within two times the upper limit of normal, ULN). All patients were discharged from the hospital within 10 days after surgery after successfully removing the abdominal drainage tube. Some of the patients suffered from postoperative elevated transaminase, hypoproteinemia, serosal effusion, and other manifestations of liver dysfunction, which could be significantly improved by conservative measures, such as both early enteral and parenteral nutrition.

Pathology and Postoperative Maintenance Treatment

Surgical specimens (such as tumor lesions and tumor thrombi) were analyzed by pathologists. Negative margins were achieved in all cases. The rate of residual viable tumor cells was reported in detail for every case. Residual viable tumor cells in the tumor thrombus were found in two of six cases with PVTT grade VP3/VP4. The rate of viable tumor cells of the PR cases (based on mRECIST) varied from 1.5% to 100%, as shown in **Table 3** and **Figure 3**. Only patient no. 10 had pathology-proven pathological complete response (pCR) among the three patients who achieved CR (using mRECIST), and sporadic viable tumor foci were found in specimens of the other two cases (see **Table 3** and **Figure 3**).

The combined therapy of an anti-PD-1 inhibitor and TKIs was continued for at least six cycles after surgery, except for the pCR case who was suggested a PD-1 inhibitor administration once every 3 weeks for at least six cycles. Every patient underwent reexamination 1–3 months after surgery.

Postoperative Follow-Up and Long-Term Survival

All the patients who underwent salvage surgery were well followed up, and the median follow-up time was 19.7 months (9.1–24.9 months). In all cases at the first visit. no tumor was found radiologically, and the AFP values were reduced to normal. But relapse occurred in case no. 2 (6.8 months after operation) and case no. 7 (3.8 months after operation), and the latter died of HCC 9.5 months postoperatively. Case no. 2 died of acute cholangitis and septic shock 14.4 months after surgery. Case no. 8 presented with advanced lung cancer (pathology-confirmed) and died 9.1 months postoperatively. The 12-month RFS rate of all cases who underwent salvage surgery was 75% (**Figure 4**).

TABLE 2 | Change in tumor characteristics before *vs*. after the combined therapy.

	Patient/case no.									
	1	**2**	**3**	**4**	**5**	**6**	**7**	**8**	**9**	**10**
ΔTTV (ml)	−739.7	−60.9	−433.9	−556.5	−1,054.5	−105.5	−170	−18.8	−1,072.7	−494.37
Time (days)	145	84	43	97	48	107	86	93	75	61
ΔTTV/day	−5.1	−0.73	−10.09	−5.74	−21.97	−0.99	−1.98	−0.2	−14.3	−8.1
ΔTTV/SLV*day	−0.48%	−0.06%	−0.77%	−0.43%	−1.48%	−0.07%	−0.17%	−0.02%	−1.21%	−0.58%
ΔFRLV (ml)	35.8	32.1	−2.1	−41.8	98.2	2.02	−70	−145	35.1	0
ΔFRLV/day	0.25	0.38	−0.05	−0.43	2.05	0.02	−0.81	−1.56	0.47	0
ΔFRLV/SLV*day	0.02%	0.03%	0.00%	−0.03%	0.14%	0.00%	−0.07%	−0.14%	0.04%	0.00%
ΔPVTTv (ml)	−30.07	−65.9	−6.9	−56.27	−9.35	–	–	−7.75	−44.89	−17.61
ΔPVTTv/day	−0.21	−0.78	−0.16	−0.58	−0.19	–	–	−0.08	−0.6	−0.29

Estimated standard liver volume (SLV) calculated using the Urata formula: SLV = 706.2 × BSA + 2.4. Body surface area (BSA) calculated using the DuBois formula: BSA (m^2) = BW (kg) 0.425 × BH (cm) 0.725 × 0.007184. Preoperative height (BH, measured to the nearest 1 cm), body weight (BW, measured to the nearest 1 kg).
FRLV, functional residue liver volume; PVTTv, portal vein tumor thrombus volume; SLV, standard liver volume; TTV, total tumor volume.

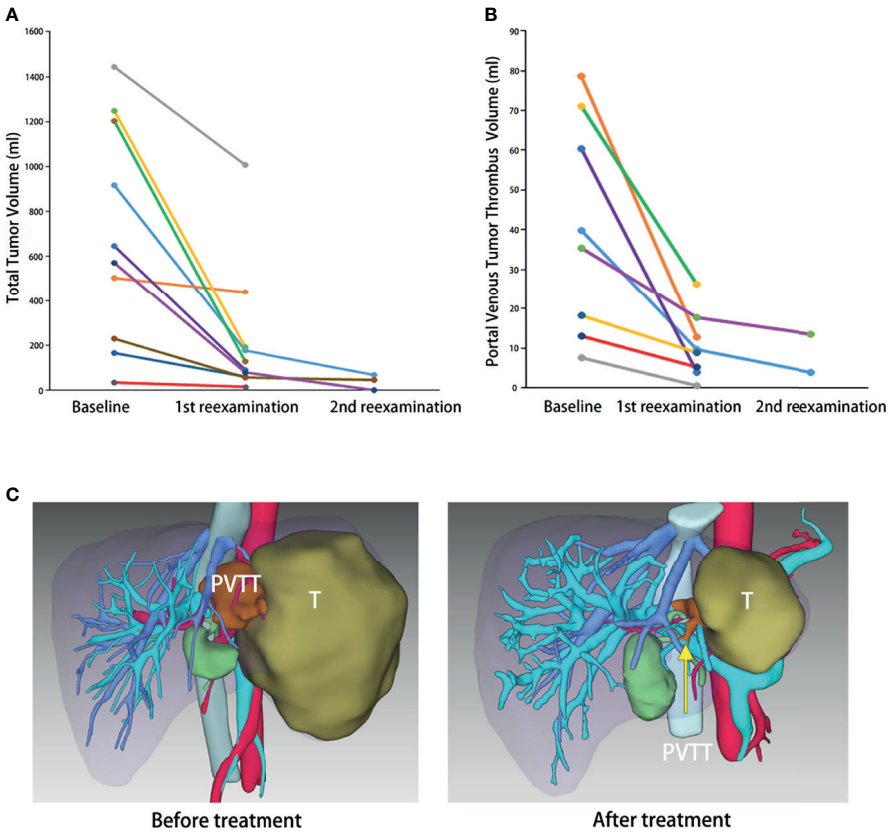

FIGURE 2 | The total tumor volume (TTV) and portal vein tumor thrombus volume (PVTTv) change demonstrated by 3D reconstruction. **(A)** Change in TTV over time by 3D reconstruction. **(B)** Change in PVTTv over time by 3D reconstruction. **(C)** Three-dimensional reconstruction of case no. 4 before and after the combination therapy. *T*, tumor. *Yellow arrow*: PVTT.

DISCUSSION

The Possibility of Immunotherapy Combined with Targeted Therapy as a Conversion Therapy

Based on the large population of advanced HCC in East Asia, some hepatobiliary institutions in Asia have performed surgical resection for a broader spectrum of advanced-stage HCC patients, but the long-term survival is still unsatisfactory (19, 20). We noted that both neoadjuvant therapy and conversion therapy have been successfully performed for colorectal cancer liver metastasis (CRLM) and locally advanced pancreatic cancer (21–25). Therefore, we initiated the conversion therapy scheme for unresectable HCC, stated above.

After the combination therapy of immunotherapy with TKI agents, the cases with objective response showed obvious tumor shrinkage with or without PVTT shrinkage and even FLR enlargement in reported clinical trials and case series in our center, which is noninvasive and safe with only a few AEs. When we evaluated the antitumor treatment, some of the patients had met the criteria to indicate surgery. Therefore, combination therapy may be promising as an effective and efficient conversion therapy protocol for advanced HCC, as shown in **Figure 5**.

Methods for Evaluating the Feasibility of Surgery

Both morphological and functional examinations need to be undertaken in order to estimate the therapeutic effect before salvage surgery. Both RECST1.1 and mRECIST were deemed feasible for the therapeutic evaluation of advanced HCC. The RECIST 1.1 criteria were intuitive and favorable for surgical decision-making, but only considered tumor shrinkage in a single diameter. mRECIST may be consistent with pathology and oncology better (17).

Our group introduced the method of quantitative oncology based on imaging (CT/MRI) in the evaluation process. The reductions in TTV and PVTT volume and the increase in FLR were evaluated and shown more individually and clearly. The integrity of the inflow and outflow of the reserved liver can be considered as an important criterion for successful conversion because PVTT necrosis also prevents intrahepatic metastasis through the portal vein. Combined with other liver reserve function tests, such as the indocyanine green (ICG) clearance

TABLE 3 | Operative and pathological information.

	Patient/case no.									
	1	**2**	**3**	**4**	**5**	**6**	**7**	**8**	**9**	**10**
Preoperative Child–Pugh grade	–	A	–	A	A	A	A	A	A	A
Preoperative ECOG PS score	–	0	–	0	0	0	0	0	0	0
Preoperative AFP (ng/ml)		1,673.5		1.7	323.1	5.1	2.5	2.2	2,198.3	127.6
Operation type	–	Right hepatectomy	–	Left hepatectomy	Right hepatectomy	Laparoscopic liver resection of S4, 5, 8	Liver resection of S5, 8	Right hepatectomy	Right hepatectomy	Left hepatectomy
Operation time	–	4 h, 25 min	–	4 h, 20 min	5 h, 50 min	4 h, 35 min	4 h, 23 min	3 h, 50 min	4 h, 20 min	5 h, 56 min
Blood loss (ml)	–	400	–	50	3,000	100	500	2,400	1,700	2,000
Blood transfusion	–	Autologous blood transfusion 2 U	–	–	RBC 2 U; plasma, 4.5 U	–	–	RBC, 2 U; plasma, 2.4 U	RBC, 4 U, plasma, 3.8 U	RBC, 4 U; plasma, 1.1 U
Mechanical ventilation time (days)	–	1	–	1	1	1	1	1	1	1
Abdominal drainage time (days)	–	6	–	5	9	5	8	8	7	7
Fasting time (days)	–	2	–	3	4	3	4	3	3	4
mRECIST before surgery	PR	PR	PR	PR	PR	CR	PR	PR	CR	CR
Viable tumor cell rate	–	90%	–	3%	1.5%	2.5%	<5% and 50% (for different lesions)	100%	15%	0% (pCR)

CR, complete response; mRECIST, modified respond evaluation criteria solid tumors; pCR, pathological complete response; PR, partial response; RBC, red blood cell.

test (26, 27), and general status assessment, such as the ECOG PS score, we could determine the feasibility and safety of large-volume hepatectomy after conversion therapy.

Timing of Surgery

How to determine the time of surgery is still under discussion: early operation may be risky and fail to take full advantage of the effects of the combination therapy, whereas secondary drug resistance and tumor progression may occur before late operation. It has been reported that most cases reach peak efficacy after three to six cycles of the treatment protocol (28, 29). As a result, we suggest that salvage surgeries can be performed after four to six cycles of combination therapy for PR or CR cases if the patient meets the surgery criteria listed in *Method*.

In the past, in the clinical practice of "neoadjuvant therapy" for CRLM, it was customary to perform surgery after the anti-angiogenic drugs were discontinued for a period of time to prevent intraoperative bleeding and poor healing (30, 31). In this case series, the interval between lenvatinib withdrawal and surgery was 3–7 days according to the half-life period data. There were no perioperative bleeding complications in all cases despite an increased number of transfusions. Poor wound healing and secondary suture were found in one case. However, this patient had significant hypoproteinemia secondary to decompensated liver function, which occurs frequently in cirrhotic subjects after surgery, and was considered the main reason for the poor wound healing.

Pathology: Accurate Response Evaluation and Predictor of Long-Term Survival?

In this case series, there seemed to be some discrepancy between the radiologic evaluation and pathology. We had three radiologic CR cases, but only one pCR, which was defined as: if no viable tumor cell found by pathology and patients with PR also had different percentages of viable tumor cells.

This could be attributed to an inadequate duration of the combined therapy, but further reflected the low response rate of the remaining tumors to therapy. There are two aspects that may result to this. Firstly, each HCC is composed of a unique combination of somatic alterations, including genetic, epigenetic, transcriptomic, and metabolic events, that form its unique molecular fingerprint, which is the underlying cause of the heterogeneity in HCC (32, 33). Moreover, tolerance to immunotherapy may be induced by T-cell exhaustion due to the absence of an effector T-cell response to neoantigens in some metastases, as a result of immunotherapy (21, 34). Regardless of the cause, inaccurate imaging assessment can lead to misjudgment of the next treatment choice. Therefore, we suggest surgery for all patients who meet the surgery criteria because: 1) pathology is the gold standard for response evaluation and 2) surgery is probably an effective measure to eliminate viable tumors caused by heterogeneity or secondary resistance to the combined therapy.

Furthermore, it seems that patients with a high viable tumor cell rate had worse prognosis, which means that pathology could be a predictor of long-term survival and offer information for the

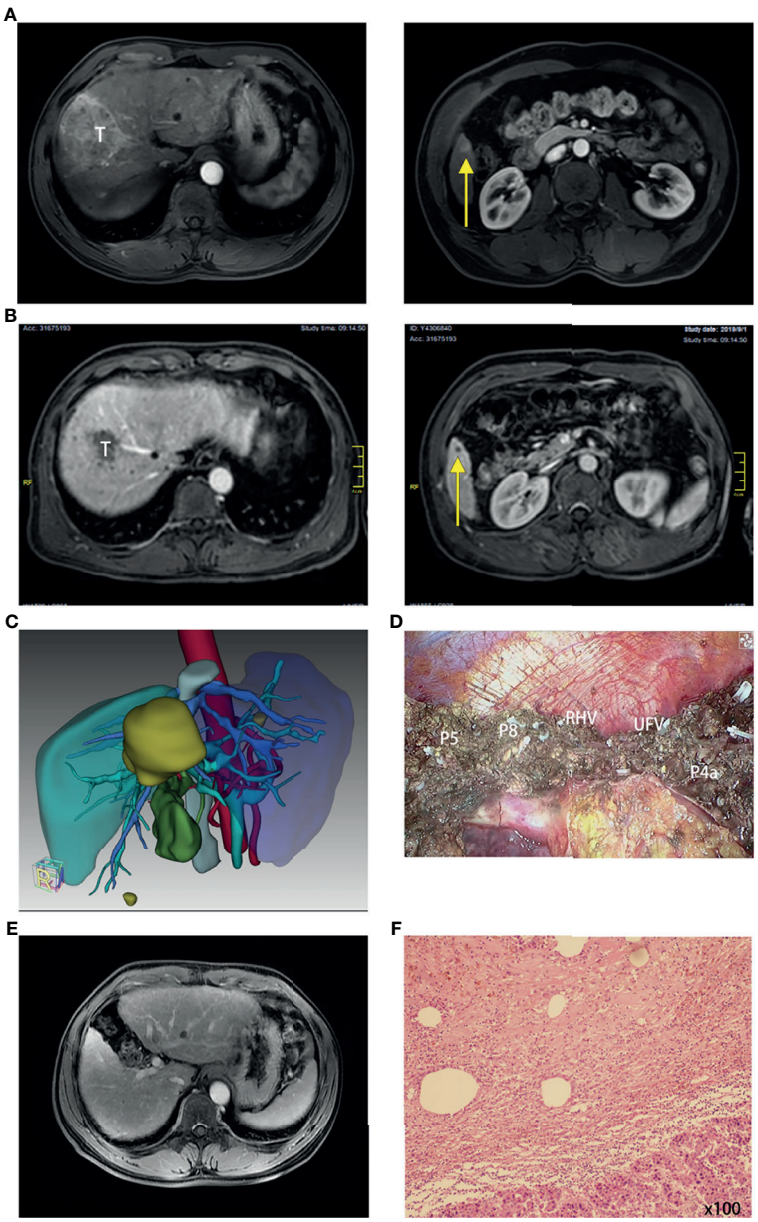

FIGURE 3 | A typical case had the combination therapy and underwent subsequent surgery (case no. 6). **(A)** Radiology of case no. 6 before treatment: *T* for tumor 1 and *yellow arrow* pointing tumor 2. **(B)** Radiology of case no. 6 after treatment: *T* for tumor 1 and *yellow arrow* pointing tumor 2. **(C)** Three-dimensional reconstruction and surgical plan of case no. 6 after the combination therapy. **(D)** Surgical photo of the margin (*P* for pedicle, *RHV* for right hepatic vein, and *UFV* for umbilical fissure vein). **(E)** Reexamination of the liver 6 months after the surgery: No tumor or relapse. **(F)** Pathology of tumor: moderately differentiated hepatocellular carcinoma (HCC) is focally distributed with extensive necrosis and several inflammatory cells (×100); viable tumor cell rate, 2.5%.

next step of treatment of patients. The small number of cases in this study was insufficient to draw conclusions with a higher level of evidence. Further prospective studies with a larger sample size are needed to confirm this.

Maintenance of Postoperative Antitumor Therapy

After a series of multidisciplinary treatment discussions focusing on the maintenance of postoperative antitumor therapy and sufficient informed consent, all patients continued using the PD-1 inhibitor for at least 6 months for the following reasons: as the body's antitumor immunity is activated, participants in antitumor immunity, such as $CD8^+$ T cells, tumor-associated macrophages (TAMs), and natural killer (NK) cells, exist not only in the tumor immune microenvironment but also in peripheral circulating blood. This is the intrinsic mechanism of the antitumor effect of immunotherapy. Among them, memory T-cell recruitment within the body plays a critical role in the

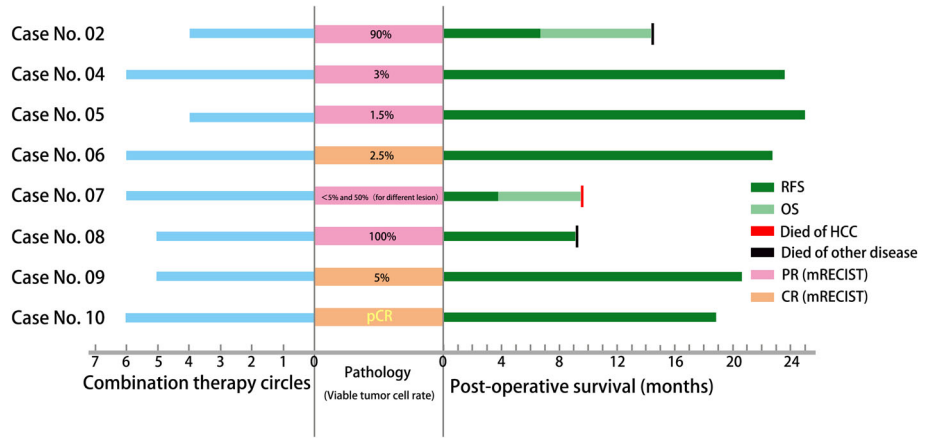

FIGURE 4 | General view of combination therapy, surgery, pathology, and post-surgery survival.

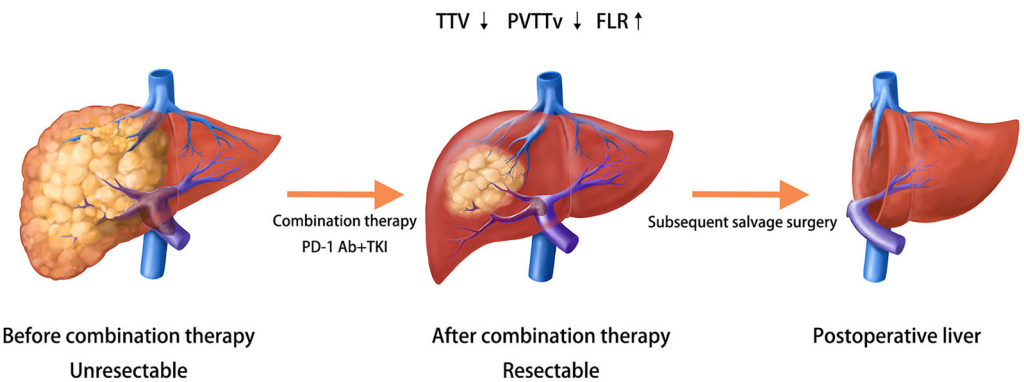

FIGURE 5 | Possibility of immunotherapy combined with targeted therapy as a conversion therapy.

long-term maintenance of the antitumor cytotoxic effects during postoperative immunological surveillance (35, 36). Therefore, continuous PD-1 inhibitor administration after surgery may elicit immunity against potential residual viable tumor cells, which was proven to be the origin of recurrence, as reported elsewhere in the literature (37). Patients for whom the pathology reported viable tumor cells should continue the lenvatinib therapy starting 1 month after surgery and last no less than 6 months.

CONCLUSION

The preliminary results of this case series suggest that immunotherapy based on PD-1 inhibitor combined with TKIs could be a reasonable and promising conversion therapy for advanced HCC with major vascular invasion. Salvage surgery was effective and safe after conversion therapy with PD-1 inhibitors plus TKIs for advanced HCC, and a combination therapy protocol including surgical treatment may increase the long-term oncological benefit.

However, this needs more prospective clinical trials in order to provide higher level evidence and discuss the preoperative radiologic assessment, pathology evaluation, and postoperative systematic treatment.

DATA AVAILABILITY STATEMENT

The original contributions presented in the study are included in the article/supplementary material. Further inquiries can be directed to the corresponding authors.

ETHICS STATEMENT

The studies involving human participants were reviewed and approved by the Medical Ethics Committee of PLA General

Hospital. The patients/participants provided written informed consent to participate in this study. Written informed consent was obtained from the individual(s) for the publication of any potentially identifiable images or data included in this article.

AUTHOR CONTRIBUTIONS

SL was responsible for concept and design. SL and HW provided administrative support. SL, BH, HW, WZ, and JH performed surgery. WZ, JH, JC, ZZ, JS, MC, XW, YC, YX, and LT collected and assembled the data. WZ, JH, BH, ZW, GM, HY, JY, and ZZ analyzed and interpreted the data. WZ, JH, and SL prepared the manuscript. SL, WZ, and JH critically revised the manuscript. All authors critically reviewed or revised the manuscript for intellectual content and approved the final version to be submitted.

FUNDING

This work was supported by the National Natural Science Foundation of China (no. 81670590) and the National Key Research and Development Program of China (2017YFA0103003).

REFERENCES

1. Bray F, Ferlay J, Soerjomataram I, Siegel RA, Torre LA, Jemal A. Global Cancer Statistics 2018: GLOBOCAN Estimates of Incidence and Mortality Worldwide for 36 Cancers in 185 Countries. *CA Cancer J Clin* (2018) 68 (6):394–424. doi: 10.3322/caac.21492
2. Wild CP, Weiderpass E, Stewart BW. *World Cancer Report: Cancer Research for Cancer Prevention*. Lyon, France: International Agency for Research on Cancer (2020). Available at: http://publications.iarc.fr/586. Licence: CC BY-NC-ND 3.0 IGO.
3. Chen WQ, Li H, Sun KX, Zheng RS, Zhang SW, Zeng HM, et al. Report of Cancer Incidence and Mortality in China, 2014. *Zhonghua Zhong Liu Za Zhi* (2018) 40(1):5–13. doi: 10.3760/cma.j.issn.0253-3766.2018.01.002
4. Marrero JA, Kulik LM, Sirlin CB, Zhu AX, Finn RS, Abecassis MM, et al. Diagnosis, Staging, and Management of Hepatocellular Carcinoma: 2018 Practice Guidance by the American Association for the Study of Liver Diseases. *Hepatology* (2018) 68(2):723–50. doi: 10.1002/hep.29913
5. Zhang ZM, Lai EC, Zhang C, Yu HW, Liu Z, Wan BJ, et al. The Strategies for Treating Primary Hepatocellular Carcinoma With Portal Vein Tumor Thrombus. *Int J Surg* (2015) 20:8–16. doi: 10.1016/j.ijsu.2015.05.009
6. Pons F, Varela M, Llovet JM. Staging Systems in Hepatocellular Carcinoma. *HPB (Oxford)* (2005) 7(1):35–41. doi: 10.1080/13651820410024058
7. Llovet JM, Brú C, Bruix J. Prognosis of Hepatocellular Carcinoma: The BCLC Staging Classification. *Semin Liver Dis* (1999) 19(3):329–38. doi: 10.1055/s-2007-1007122
8. European Association for the Study of the Liver. Electronic Address: easloffice@easloffice.eu, European Association for the Study of the Liver. EASL Clinical Practice Guidelines: Management of Hepatocellular Carcinoma. *J Hepatol* (2018) 69(1):182–236. doi: 10.1016/j.jhep.2018.03.019
9. Heimbach JK, Kulik LM, Finn RS, Sirlin CB, Abecassis MM, Roberts LR, et al. AASLD Guidelines for the Treatment of Hepatocellular Carcinoma. *Hepatology* (2018) 67(1):358–80. doi: 10.1002/hep.29086
10. Zhu AX, Finn RS, Edeline J, Cattan S, Ogasawara S, Palmer D, et al. Pembrolizumab in Patients With Advanced Hepatocellular Carcinoma Previously Treated With Sorafenib (KEYNOTE-224): A non-Randomised, Open-Label Phase 2 Trial. *Lancet Oncol* (2018) 19(7):940–52. doi: 10.1016/S1470-2045(18)30351-6
11. Kudo M. Targeted and Immune Therapies for Hepatocellular Carcinoma: Predictions for 2019 and Beyond. *World J Gastroenterol* (2019) 25(7):789–807. doi: 10.3748/wjg.v25.i7.789
12. Ikeda K, Kudo M, Kawazoe S, Osaki Y, Ikeda M, Okusaka T, et al. Phase 2 Study of Lenvatinib in Patients With Advanced Hepatocellular Carcinoma. *J Gastroenterol* (2017) 52(4):512–9. doi: 10.1007/s00535-016-1263-4
13. Finn RS, Ikeda M, Zhu AX, Sung MW, Baron AD, Kudo M, et al. Phase Ib Study of Lenvatinib Plus Pembrolizumab in Patients With Unresectable Hepatocellular Carcinoma. *J Clin Oncol* (2020) 38(26):2960–70. doi: 10.1200/JCO.20.00808
14. Finn RS, Qin S, Ikeda M, Galle PR, Ducreux M, Kim TY, et al. Atezolizumab Plus Bevacizumab in Unresectable Hepatocellular Carcinoma. *N Engl J Med* (2020) 382(20):1894–905. doi: 10.1056/NEJMoa1915745
15. Xu J, Shen J, Gu S, Zhang Y, Wu L, Wu J, et al. Camrelizumab in Combination With Apatinib in Patients With Advanced Hepatocellular Carcinoma (RESCUE): A Nonrandomized, Open-Label, Phase II Trial. *Clin Cancer Res* (2021) 27(4):1003–11. doi: 10.1158/1078-0432.CCR-20-2571
16. Blank CU, Rozeman EA, Fanchi LF, Sikorska K, van de Wiel B, Kvistborg P, et al. Neoadjuvant *Versus* Adjuvant Ipilimumab Plus Nivolumab in Macroscopic Stage III Melanoma. *Nat Med* (2018) 24(11):1655–61. doi: 10.1038/s41591-018-0198-0
17. Lencioni R, Llovet JM. Modified RECIST (mRECIST) Assessment for Hepatocellular Carcinoma. *Semin Liver Dis* (2010) 30(1):52–60. doi: 10.1055/s-0030-1247132
18. Chok KS, Cheung TT, Chan SC, Poon RT, Fan ST, Lo CM. Surgical Outcomes in Hepatocellular Carcinoma Patients With Portal Vein Tumor Thrombosis. *World J Surg* (2014) 38(2):490–6. doi: 10.1007/s00268-013-2290-4
19. Liu PH, Huo TI, Miksad RA. Hepatocellular Carcinoma With Portal Vein Tumor Involvement: Best Management Strategies. *Semin Liver Dis* (2018) 38 (3):242–51. doi: 10.1055/s-0038-1666805
20. Galle PR, Tovoli F, Foerster F, Wörns MA, Cucchetti A, Bolondi L. The Treatment of Intermediate Stage Tumours Beyond TACE: From Surgery to Systemic Therapy. *J Hepatol* (2017) 67(1):173–83. doi: 10.1016/j.jhep.2017.03.007
21. Liu J, O'Donnell JS, Yan J, Madore J, Allen S, Smyth MJ, et al. Timing of Neoadjuvant Immunotherapy in Relation to Surgery is Crucial for Outcome. *Oncoimmunology* (2019) 8(5):e1581530. doi: 10.1080/2162402X.2019.1581530
22. Wu Y, Liu F, Song W, Liang F, Wang L, Xu Y. Safety Evaluation of Simultaneous Resection of Colorectal Primary Tumor and Liver Metastasis After Neoadjuvant Therapy: A Propensity Score Matching Analysis. *Am J Surg* (2019) 218(5):894–8. doi: 10.1016/j.amjsurg.2018.09.019
23. Berardi G, De Man M, Laurent S, Smeets P, Tomassini F, Ariotti R. Radiologic and Pathologic Response to Neoadjuvant Chemotherapy Predicts Survival in Patients Undergoing the Liver-First Approach for Synchronous Colorectal Liver Metastases. *Eur J Surg Oncol* (2018) 44(7):1069–77. doi: 10.1016/j.ejso.2018.03.008
24. Miyasaka Y, Ohtsuka T, Kimura R, Matsuda R, Mori Y, Nakata K, et al. Neoadjuvant Chemotherapy With Gemcitabine Plus Nab-Paclitaxel for Borderline Resectable Pancreatic Cancer Potentially Improves Survival and Facilitates Surgery. *Ann Surg Oncol* (2019) 26(5):1528–34. doi: 10.1245/s10434-019-07309-8
25. Barnes CA, Chavez MI, Tsai S, Aldakkak M, George B, Ritch PS, et al. Survival of Patients With Borderline Resectable Pancreatic Cancer Who Received Neoadjuvant Therapy and Surgery. *Surgery* (2019) 166(3):277–85. doi: 10.1016/j.surg.2019.05.010
26. Møller S, la Cour Sibbesen E, Madsen JL, Bendtsen F. Indocyanine Green Retention Test in Cirrhosis and Portal Hypertension: Accuracy and Relation to Severity of Disease. *J Gastroenterol Hepatol* (2019) 34(6):1093–9. doi: 10.1111/jgh.14470
27. Shimizu S, Kamiike W, Hatanaka N, Yoshida Y, Tagawa K, Miyata M, et al. New Method for Measuring ICG Rmax With a Clearance Meter. *World J Surg* (1995) 19(1):113–8; discussion 118. doi: 10.1007/BF00316992
28. Ikeda M, Sung M, Kudo M, Kobayashi M, Baron A, Finn R, et al. A Phase 1b Trial of Lenvatinib (LEN) Plus Pembrolizumab (PEM) in Patients (Pts) With

Unresectable Hepatocellular Carcinoma (uHCC). *J Clin Oncol* (2018) 36:4076. doi: 10.1200/JCO.2018.36.15_suppl.4076
29. Llovet J, Finn RS, Ikeda M, Sung M, Baron AD, Kudo M, et al. A Phase 1b Trial of Lenvatinib Plus Pembrolizumab in Unresectable Hepatocellular Carcinoma: Updated Results. European Society for Medical Oncology (ESMO) Meeting (Barcelona, Spain). *Eur Soc Med Oncol (ESMO)* (2019). doi: 10.1093/annonc/mdz247.073
30. Kim JS, Cho SY, Min BS, Kim NK. Risk Factors for Anastomotic Leakage After Laparoscopic Intracorporeal Colorectal Anastomosis With a Double Stapling Technique. *J Am Coll Surg* (2009) 209(6):694–701. doi: 10.1016/j.jamcollsurg.2009.09.021
31. Kim CW, Baek SJ, Hur H, Min BS, Baik SH, Kim NK. Anastomotic Leakage After Low Anterior Resection for Rectal Cancer Is Different Between Minimally Invasive Surgery and Open Surgery. *Ann Surg* (2016) 263 (1):130–7. doi: 10.1097/SLA.0000000000001157
32. Marquardt JU, Andersen JB, Thorgeirsson SS. Functional and Genetic Deconstruction of the Cellular Origin in Liver Cancer. *Nat Rev Cancer* (2015) 15(11):653–67. doi: 10.1038/nrc4017
33. Schulze K, Nault JC, Villanueva A. Genetic Profiling of Hepatocellular Carcinoma Using Next-Generation Sequencing. *J Hepatol* (2016) 65 (5):1031–42. doi: 10.1016/j.jhep.2016.05.035
34. O'Donnell JS, Hoefsmit EP, Smyth MJ, Blank CU, Teng M. The Promise of Neoadjuvant Immunotherapy and Surgery for Cancer Treatment. *Clin Cancer Res* (2019) 25(19):5743–51. doi: 10.1158/1078-0432.CCR-18-2641
35. Fairfax BP, Taylor CA, Watson RA, Nassiri I, Danielli S, Fang H, et al. Peripheral CD8+ T Cell Characteristics Associated With Durable Responses to Immune Checkpoint Blockade in Patients With Metastatic Melanoma. *Nat Med* (2020) 26(2):193–9. doi: 10.1038/s41591-019-0734-6
36. Newton JM, Hanoteau A, Liu HC, Gaspero A, Parikh F, Gartrell-Corrado RD, et al. Immune Microenvironment Modulation Unmasks Therapeutic Benefit of Radiotherapy and Checkpoint Inhibition. *J Immunother Cancer* (2019) 7 (1):216. doi: 10.1186/s40425-019-0698-6
37. Sharma P, Allison JP. Immune Checkpoint Targeting in Cancer Therapy: Toward Combination Strategies With Curative Potential. *Cell* (2015) 161 (2):205–14. doi: 10.1016/j.cell.2015.03.030

Conflict of Interest: The authors declare that the research was conducted in the absence of any commercial or financial relationships that could be construed as a potential conflict of interest.

The reviewer HZ declared a shared affiliation with one of the authors HW to the handling editor at the time of the review.

Publisher's Note: All claims expressed in this article are solely those of the authors and do not necessarily represent those of their affiliated organizations, or those of the publisher, the editors and the reviewers. Any product that may be evaluated in this article, or claim that may be made by its manufacturer, is not guaranteed or endorsed by the publisher.

frontiers in Oncology

ORIGINAL RESEARCH
published: 02 November 2021
doi: 10.3389/fonc.2021.770997

Integrin-β6 Serves as a Potential Prognostic Serum Biomarker for Gastric Cancer

Zequn Li, Yuqi Sun, Jianfei Xu, Hao Yang, Xiaodong Liu, Yulong Tian, Shougen Cao and Yanbing Zhou**

Department of Gastrointestinal Surgery, The Affiliated Hospital of Qingdao University, Qingdao, China

Discovering novel biomarkers that easily accessed is a key step towards the personalized medicine approach for gastric cancer patients. Integrin-β6 (ITGB6) is a subtype of integrin that is exclusively expressed on the surface of epithelial cells and is up-regulated in various tumors. In the present study, a retrospective cohort with 135 gastric cancer patients and a prospective cohort with 34 gastric cancer patients were constructed, ITGB6 expression were detected in both the serum specimens and the tissue specimens. Detailed clinicopathological parameters as well as patients' survival were recorded. A nomogram including ITGB6 expression was also constructed and validated to predict the prognosis of gastric cancer patients. Results showed that serum ITGB6 expression was obviously increased and associated with tumor stage in gastric cancer patients, serum ITGB6 expression was relatively high in patients with liver metastasis. High ITGB6 expression indicated a poor prognosis, and nomogram including serum ITGB6 expression could predict the prognosis of gastric cancer patients effectively. Moreover, serum ITGB6 expression was associated with ITGB6 expression in tumor tissues. Furthermore, combined serum ITGB6 and CEA levels contributed to the risk stratification and prognostic prediction for gastric cancer patients. In addition, the serum expression of ITGB6 decreased significantly after radical surgery, and a new rise in serum ITGB6 expression indicated tumor recurrence or progression. The present study identified a novel serum biomarker for the risk stratification, prognostic prediction and surveillance of gastric cancer patients.

Keywords: ITGB6, gastric cancer, serum biomarker, risk stratification, prognosis, liver metastasis

OPEN ACCESS

Edited by:
Hongda Liu,
Nanjing Medical University, China

Reviewed by:
Yingfang Fan,
Zhujiang Hospital Southern Medical University, China
Zhixiong Li,
Teaching Hospital of Putian First Hospital of Fujian Medical University, China

****Correspondence:***
Yanbing Zhou
zhouyanbing999@aliyun.com
Shougen Cao
briancao@126.com

Specialty section:
This article was submitted to Cancer Molecular Targets and Therapeutics, a section of the journal Frontiers in Oncology

Received: *05 September 2021*
Accepted: *08 October 2021*
Published: *02 November 2021*

Citation:
Li Z, Sun Y, Xu J, Yang H, Liu X, Tian Y, Cao S and Zhou Y (2021) Integrin-β6 Serves as a Potential Prognostic Serum Biomarker for Gastric Cancer. Front. Oncol. 11:770997. doi: 10.3389/fonc.2021.770997

INTRODUCTION

Gastric cancer is the fifth most commonly diagnosed cancer and the third leading cause of cancer-related death worldwide (1, 2). Advanced gastric cancer accounts for the majority in China, and radical surgical resection remains to be the most effective treatment strategy (3). The prognosis of advanced gastric cancer has improved dramatically over the recent decades due to the implement of novel surgical techniques, progression of chemotherapeutics and targeted drugs (4–6). However, the survival for patients with local or distant metastasis remains poor (7). Discovering easily accessible biomarkers, such as serum biomarkers, is urgently needed for

optimizing patient care in patients with gastric cancer. At present, carcinoembryonic antigen (CEA) is one of the standard biomarkers for gastric cancer. However, it still exhibits low sensitivity and specificity (8).

Integrins are a family of heterodimeric cell membrane receptors that are expressed in most cells, where they mediate cell-cell and cell-extracellular matrix (ECM) interactions. Integrin β6 (ITGB6) was preliminarily identified in 1996 and it is exclusively expressed on epithelial cells during embryogenesis. ITGB6 expression also elevated during wound healing, fibrosis, and importantly, carcinogenesis (9, 10). As one of the key adhesion molecules on cell surface, ITGB6 was found to be involved in almost every step during tumor metastasis (11–14). Previous studies have demonstrated that ITGB6 was involved in the progression of gastric cancer. ITGB6 expression in gastric cancer tissues was closely associated with tumor stage, it also served as an independent prognostic indicator for the poor prognosis of gastric cancer. ITGB6 might be involved in the regulation of MMP expression, and contributed to tumor progression *via* ERK signaling (15–18). Nevertheless, the expression of serum ITGB6 in cancer is largely unknown so far.

Nomogram has been widely used in the prediction of cancer prognosis, which transforms traditional statistical predictive models into visualized probability estimates tailored to the needs of the individual patient. With continuous developments in molecular biology, applying biomarkers that reflect the malignant biological behaviors of tumors could potentially be a supplementary approach to the clinicopathological variables. Therefore, an effective and accurate model to predict the prognosis of gastric cancer is of vital importance for clinical-decision making.

The present study investigated whether serum ITGB6 level serves as a novel tumor biomarker for gastric cancer patients. Focusing on risk stratification, prognostic prediction and recurrence surveillance, we explored the clinical significance of serum ITGB6 levels for gastric cancer patients by both retrospective and prospective cohorts. This study provided a novel serum biomarker for gastric cancer patients, which might contribute to improving the prognosis and represent a key step forward towards the personalized medicine approach for advanced gastric cancer patients.

PATIENTS AND METHODS

Bioinformatics Analysis

The ITGB6 mRNA expression data and corresponding clinical information for gastric cancer patients were obtained from The Cancer Genome Atlas (TCGA; https://tcga-data.nci.nih.gov/tcga/). Meanwhile, the differential mRNA expression level of ITGB6 between a variety of cancer tissues and normal ones were obtained using the TIMER database (https://cistrome.shinyapps.io/timer/). Related gene expression analysis and disease-free survival (DFS) from TCGA and GTEx databases were performed using the GEPIA database (http://gepia.cancerpku.cn/) (19).

Retrospective Cohort

Between January 2017 and December 2017, we collected a total of 135 patients with gastric cancer that underwent surgical treatment at the Department of Gastrointestinal Surgery, the Affiliated Hospital of Qingdao University. The diagnosis was confirmed by routine pathological examination and inclusion criteria was as follows: (1) Serum samples with detailed clinicopathological data and medical records; (2) Postoperative survival time more than 1 month; (3) No history or signs of other malignancies. Follow-up data were recorded until June 2021, concerning survival time and progression of gastric cancer at the last visit. Tumor staging and histological classification were assessed according to the 8th edition of the American Joint Committee on Cancer (AJCC) classification. The expression levels of serum CEA were routinely detected for all the enrolled patients at least one time in the medical record. Follow-up was conducted every 3-6 months and serum tumor biomarkers including CEA were measured. Imaging examination, including computed tomography (CT), magnetic resonance imaging (MRI) or positron emission tomographic scanning (PET-CT) were also selectively conducted for the evaluation of metastasis or recurrence. This study was approved by the Ethics Committee of the Affiliated Hospital of Qingdao University, China. Written informed consent was obtained from all the subjects.

Prospective Cohort

A prospective study was carried out from Oct 2020 to Jun 2021, consisting of 34 patients with radical gastric cancer resection. Tumor tissues and corresponding adjacent normal tissues were obtained. None of the patients received chemotherapy or radiotherapy prior to surgery. Follow-up data was obtained until June 2021. Written informed consent was obtained from each patient, and this study was approved by the Ethics Committee of the Affiliated Hospital of Qingdao University, China. Registration of the prospective study was approved by the Chinese Clinical Trial Registry (ChiCTR1800018294).

Serum ITGB6 and CEA Detection

Serum ITGB6 levels were detected using human ITGB6 ELISA kit (SEC099Hu, USCN Life Science Inc., Wuhan; China) according to manufacturer's instructions. In brief, the tests were performed according to the instruction of the ELISA kit. Then added termination solution, incubated for 30 min in darkness (37 °C, 5% CO_2) and measured absorbance value at 450nm. Serum CEA levels were determined using radioimmunoassay kits manufactured by Abbott Laboratories (Chicago, IL, USA). The cut-off point for serum ITGB6 expression was defined 0.5ng/ml, which was verified by the X-tile program.

Nomogram Construction and Validation

Nomogram construction and validation were performed in accordance with the nomogram guidelines (20, 21). Univariate and multivariate Cox proportional hazard models were constructed to estimate the hazard ratios of prognostic factors

and to evaluate independent prognostic risk factors. A nomogram was constructed according to the independent prognostic factors of survival. Besides, the prognosis of nomograms was realized by using the RMS software package in R software version 3.1.3 (https://www.r-project.org/). To assess the model performance, the discrimination and calibration of the nomogram were performed (22). The discriminative power of the nomogram was computed by Harrell's concordance index (C-index) (23). The C-index ranges from 0.5-1.0, with 0.5 indicates the outcomes is no discrimination at all and 1.0 represents the perfect discrimination.

Immunohistochemistry (IHC)

IHC was performed using paraffin-embedded tissue sections (4 μm), and protocol was previously described (24, 25). Briefly, the sections were dewaxed and hydrated, followed by antigen retrieval (in 0.01 mol/L citrate buffer solution, pH 6.0, heated to boiling for 2-3 min). Endogenous peroxidase was blocked with 3% H_2O_2. The sections were blocked by goat serum for 15 min and then immunostained with mouse antibody against ITGB6 (dilution 1:500, Biogen Idec, USA) at 4°C overnight. Secondary staining was performed with HRP-conjugated antibody using a MaxVision Kit and a 3, 5-diaminobenzidine (DAB) peroxidase substrate kit (Maixin Co, Fuzhou, China). The sections were then counterstained with hematoxylin, and representative images were obtained under an Olympus inverted microscope.

Evaluation of Immunohistochemical Staining

Immunohistochemical staining was independently assessed by two experienced pathologists in a blinded manner. Staining was semi-quantitatively scored based on both the staining intensity (0, negative; 1, very weak; 2, weak; 3, moderate; 4, strong) and the percentage of positively stained cells (0, 0%; 1, 1%-25%; 2, 26%-50%; 3, 51%-75%; 4, 76%-100%). Both scores for each specimen were combined to obtain the final score of ITGB6 expression (ranging 0-8). The cut-off point for the sum of the scores was defined as follows, 0-5, low expression; 6-8, high expression, which was verified by the X-tile program.

Statistical Analysis

All the statistical analyses were performed by SPSS 22.0 software (SPSS, Chicago, IL, USA). The association between ITGB6 expression and clinicopathological parameters were assessed by chi-square test or Fisher's exact test. The receiver operating characteristic (ROC) curve analyses were conducted for the measurement of predictive accuracy index. The cumulative OS rates were calculated by Kaplan–Meier method, and the statistical differences between subgroups were calculated by log-rank test. Independent prognostic factors were identified by multivariate analysis with Cox-regression model. In cox regression analysis, cox model was built using forward stepwise method. P value < 0.05 was considered statistically significant.

RESULTS

Serum ITGB6 Was a Potential Biomarker for Gastric Cancer That Associated With Tumor Stage

To explore whether ITGB6 could be detected in the serum of gastric cancer patients, we investigated serum ITGB6 levels in a retrospective cohort containing 135 gastric cancer patients. The serum specimens of 32 healthy subjects that underwent physical health examination were used as control. Results showed that ITGB6 could be detected in the serum of gastric cancer patients, which ranged from 0-5.16ng/ml, and serum ITGB6 levels were significantly increased in gastric cancer patients (**Figure 1A**). Moreover, **Table 1** showed that increased ITGB6 serum levels were closely associated with the TNM stage of tumor size (P=0.001), T stage (P=0.050), N stage (P=0.001), TNM stage (P=0.007), neurovascular infiltration (P=0.008) and serum CEA levels (P<0.001). Importantly, ITGB6 levels gradually increased accompanied with advanced N stage and TNM stage (**Figures 1B–D**). Interestingly, serum ITGB6 expression was markedly increased in patients with liver metastasis (**Supplementary Figure 1**).

To confirm our conclusion, we further explored the clinical significance of serum ITGB6 expression in a prospective cohort that consisting 34 subjects. Serum ITGB6 expression was also elevated in gastric cancer patients compared with those healthy volunteers (**Figure 1E**), and elevated serum ITGB6 expression was also associated with lymph node metastasis in the prospective cohort (**Figure 1F**). These results confirmed our previous findings that serum ITGB6 possibly serve as a potential biomarker for gastric cancer.

High Serum ITGB6 Level Was Associated With Poor Survival of Gastric Cancer Patients

As our previous results demonstrated that serum ITGB6 expression was closely associated with tumor progression in gastric cancer. Then we explored the prognostic value of serum ITGB6 expression in overall survival (OS) of gastric cancer patients. In the retrospective cohort, we followed the enrolled subjects for 3-50 months after surgery with a median follow-up period of 42 moths, and the overall survival (OS) of the patients was 81.5%. Results showed that the OS of gastric cancer patients with high expression of ITGB6 was 66.7%, which was lower than those patients with low expression of ITGB6 (90.5%) (**Figure 2A**). Moreover, TNM stage (P=0.002), neurovascular infiltration (P=0.049) and serum CEA levels (P<0.001) were also correlated with the prognosis of patients (**Table 2**).

Moreover, multivariate analysis was conducted to evaluate the independent prognostic factors for this cohort. Results demonstrated that high expression of ITGB6 (P=0.011), TNM stage (P=0.029) and high CEA levels (P=0.002) were independent unfavorable prognostic factors (**Table 2**). Furthermore, to evaluate the predictive value of ITGB6 on the prognosis of gastric cancer patients, time-dependent ROC analysis was conducted and the AUC was 0.685 (95% CI:

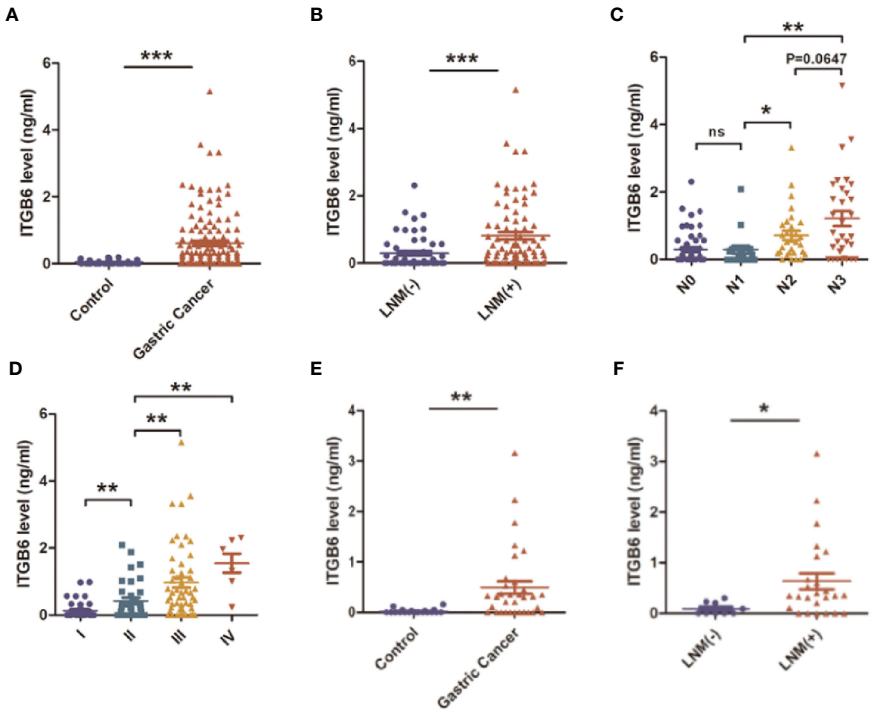

FIGURE 1 | The expression and clinical significance of serum ITGB6 in gastric cancer. **(A)** The expression of serum ITGB6 in gastric cancer patients and healthy controls from a retrospective cohort. **(B)** The serum ITGB6 levels in gastric cancer patients with or without lymph node metastasis. **(C)** The serum ITGB6 levels in gastric cancer patients with different N stage from the retrospective cohort. **(D)** The serum ITGB6 levels in gastric cancer patients with different pathological stage from the retrospective cohort. **(E)** The expression of serum ITGB6 in gastric cancer patients and healthy controls from the prospective cohort. **(F)** The serum ITGB6 levels in gastric cancer patients with or without lymph node metastasis from the prospective cohort. ns, not statistically different; **P*<0.05; ***P*<0.01; ****P*<0.001.

0.568-0.803, sensitivity: 69.1%, specificity: 68.0%) (**Figure 2B**). All these results verified that serum ITGB6 may serve as an unfavorable prognostic indicator for gastric cancer.

Serum ITGB6 Expression Was Associated With ITGB6 Expression in Tumor Tissues

Previous research demonstrated that elevated ITGB6 in gastric cancer tissues might serve as a potential biomarker for tumor progression and the prognosis of patients. By analyzing TCGA and GTEx public available database, we found that the mRNA expression level of ITGB6 in gastric cancer was significantly increased compared with that in normal tissues (**Supplementary Figure 2A**). Moreover, Kaplan-Meier analysis revealed that ITGB6 high-expressed patients had relatively less-optimistic prognostic outcome in terms of DFS (**Supplementary Figure 2B**).

To explore whether serum ITGB6 expression was associated with ITGB6 expression in tumor tissues, we detected the expression of ITGB6 in gastric cancer tissues using IHC. Consistent with previous findings, elevated ITGB6 protein expression was also shown in gastric cancer tissues compared with adjacent normal tissues (**Figures 3A, B**). Moreover, ITGB6 expression in tumor tissues was also associated with tumor N stage (**Figure 3C**). Furthermore, ITGB6 expression in tumor tissues was correlated with serum ITGB6 levels in advanced gastric cancer (**Figure 3D**). All these results indicated that ITGB6 was present in both serum and tumor tissue of gastric cancer patients, and serum ITGB6 may serve as a potential biomarker for advanced gastric cancer.

Construction and Validation of the Nomogram Based on Serum ITGB6 Level

To further assess how related clinicopathological parameters jointly impact on survival, the Cox regression model was used for univariate and multivariate survival analyses. Univariate analysis suggested that depth of invasion, TNM stage, neurovascular invasion, ITGB6 and CEA levels might be associated with the prognosis for gastric cancer patients (P<0.1). Subsequently, these variables were included in multivariate Cox proportional hazards analysis. Multivariate analysis confirmed that TNM stage, ITGB6 and CEA levels were independent prognostic factors for gastric cancer patients (**Table 2**).

According to the aforementioned results, the TNM stage, serum ITGB6 and CEA expression were included in the final model to develop the nomogram for predicting overall survival (**Figure 4**). C-index was used to appraise the discrimination. The accuracy of this prediction model was relatively high, with a C-index of 0.792 (95% CI: 0.721-0.863).

TABLE 1 | Correlation between serum ITGB6 expression and clinical characteristics of patients with gastric cancer.

Characteristic	Number	Serum ITGB6 expression		χ^2/t value	*P*-value
		Low (%)	High (%)		
Age (years)				0.263	0.608
≤60	70	45 (64.3)	25 (35.7)		
>60	65	39 (60.0)	26 (40.0)		
Gender				1.309	0.253
Male	104	62 (59.6)	42 (40.4)		
Female	31	22 (71.0)	9 (29.0)		
Tumor size				11.118	0.001*
<4	75	56 (74.7)	19 (25.3)		
≥4	60	28 (46.7)	32 (53.3)		
Tumor location				1.829	0.401
Cardia/Fundus	14	11 (78.6)	3 (21.34)		
Body	64	38 (59.4)	26 (40.6)		
Antrum/Pylorus	57	35 (61.4)	22 (38.6)		
Borrmann type				5.806	0.121
I	9	5 (55.6)	4 (44.4)		
II	86	48 (55.8)	38 (44.2)		
III	37	29 (78.4)	8 (21.6)		
IV	3	2 (66.7)	1 (33.3)		
T stage				7.827	0.050*
T1	28	22 (78.6)	6 (21.4)		
T2	27	19 (70.4)	8 (29.6)		
T3	59	34 (57.6)	25 (42.4)		
T4	21	9 (42.9)	12 (57.1)		
N stage				15.782	0.001*
N0	52	38 (73.1)	14 (26.9)		
N1	24	20 (83.3)	4 (16.7)		
N2	27	13 (48.1)	14 (51.9)		
N3	32	13 (40.6)	19 (59.4)		
AJCC pTNM stage[#]				7.202	0.007*
I-II	78	56 (71.8)	22 (28.3)		
III-IV	57	28 (49.1)	29 (50.9)		
Complications				1.058	0.304
Yes	17	13 (76.5)	4 (23.5)		
No	118	71 (60.2)	47 (39.8)		
Neurovascular infiltration				6.949	0.008*
Yes	90	49 (54.4)	41 (45.6)		
No	45	35 (77.8)	10 (22.2)		
CEA				16.683	<0.001*
Normal	85	64 (75.3)	21 (24.7)		
High	50	20 (40.0)	30 (60.0)		

[#]*The 8th AJCC classification criteria; *statistical difference.*

Combined Serum ITGB6 and CEA Levels Contributed to the Risk Stratification of Gastric Cancer

CEA is commonly used for the risk stratification and recurrence follow up nowadays. Here we compared serum ITGB6 levels with serum CEA levels using both the retrospective cohort and the prospective cohort. Kaplan-Meier analysis showed that the OS of the normal preoperative CEA group was 91.8%, whereas that of the elevated preoperative CEA group was 64.0% (**Figure 5A**). Then the ROC analysis was used to evaluate the predictive prognostic performance of CEA, which led to an AUC=0.715 (95% CI: 0.601-0.828, sensitivity: 70.9%, specificity: 72.0%) (**Figure 5B**).

To enhance the specificity of predict patient survival, we evaluated the clinical values of combined biomarkers of CEA and ITGB6. Patients were divided into two subgroups based on the expression of CEA and ITGB6: double negative or single positive (n=105, 77.78%) and double positive (n = 30, 22.22%). Patients with double positive had OS rate of 46.7% compared with 91.4% for patients with double negative or single positive (**Figure 5C**). Moreover, the AUC for the combined two biomarkers reached to 0.756 (95% CI, 0.638-0.875), with an estimated sensitivity and specificity of 64.0% and 87.3% (**Figure 5D**). All these results indicated that combined ITGB6 and CEA levels may improve the specificity of predicting clinical outcomes of gastric cancer patients.

Serum ITGB6 Served as a Potential Biomarker for Tumor Surveillance in Gastric Cancer Patients

To investigate whether serum ITGB6 could be used for tumor surveillance and monitoring of tumor recurrence during the follow-up of gastric cancer patients, we detected the expression of serum ITGB6 before and after surgery, and followed up the

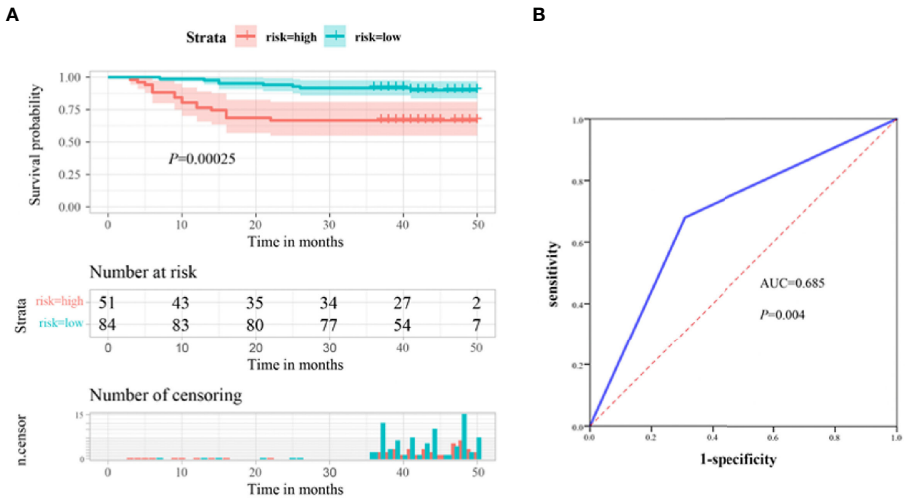

FIGURE 2 | Serum ITGB6 level may serve as an unfavorable prognostic indicator for gastric cancer patients. **(A)** Survival analysis according to serum ITGB6 expression in a total number of 135 gastric cancer patients from a retrospective cohort. **(B)** ROC analysis was constructed for the prediction of prognosis of gastric cancer patients using serum ITGB6 expression.

TABLE 2 | Univariate and multivariate Cox proportional hazard analyses of OS with gastric cancer patients.

	Univariate analysis		Multivariate analysis	
Variable	**HR (95%CI)**	***P*-value**	**HR (95%CI)**	***P*-value**
Sex (male *vs.* female)	0.423 (0.126-1.413)	0.162		
Age	1.171 (0.534-2.567)	0.694		
BMI	1.055 (0.954-1.168)	0.298		
Tumor size	1.007 (0.457-2.217)	0.987		
Tumor location		0.959		
Cardia/Fundus	Reference			
Body	0.851 (0.237-3.050)	0.804		
Antrum/Pylorus	0.936 (0.261-3.357)	0.920		
Borrmann type		0.415		
I	Reference			
II	0.605 (0.178-2.056)	0.421		
III	0.289 (0.065-1.293)	0.104		
IV	0.000 (0.000- ~)	0.981		
T stage		0.087		
T1	Reference			
T2	3.248 (0.338-31.225)	0.308		
T3	7.488 (0.984-56.966)	0.052		
T4	10.179 (1.252-82.779)	0.030*		
N stage		0.373		
N0	Reference			
N1	0.766 (0.203-2.889)	0.694		
N2	1.208 (0.395-3.691)	0.741		
N3	2.011 (0.775-5.217)	0.151		
AJCC pTNM stage	3.859 (1.611-9.248)	0.002*	2.599 (1.106-6.108)	0.029*
Complications	0.275 (0.037-2.030)	0.205		
Neurovascular infiltration	2.934 (1.007-8.552)	0.049*		
CEA	5.212 (2.174-12.494)	<0.001*	4.105 (1.692-9.961)	0.002*
ITGB6 expression	4.220 (1.820-9.789)	0.001*	3.138 (1.301-7.568)	0.011*

*HR, hazard ratio; CI, confidence interval; *statistical difference.*

patients for 6 months in the prospective cohort. Results showed that serum ITGB6 levels decreased dramatically after surgery for most of advanced gastric cancer patients (**Figures 6A, B**). Importantly, 7 patients presented recurrent disease during follow up. Among the patients with tumor recurrence, 4 of them had elevated serum ITGB6 levels, accompanied with increased tumor burden. One patient had sustained high serum ITGB6 level after surgery. In addition, serum ITGB6

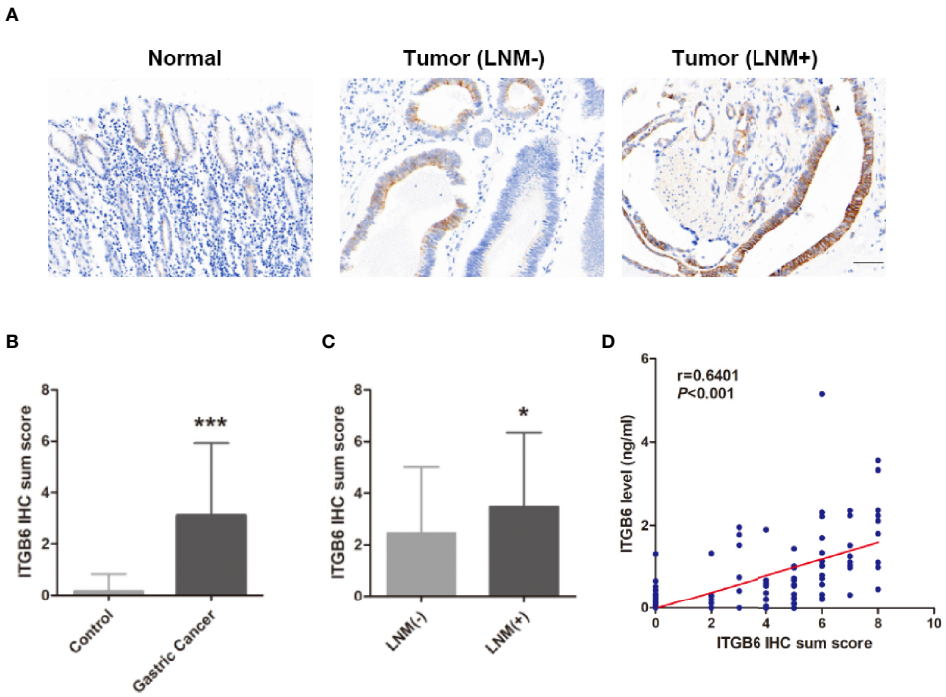

FIGURE 3 | Serum ITGB6 expression was associated with ITGB6 expression in tumor tissues. **(A)** Representative IHC staining of ITGB6 in adjacent normal tissue, gastric cancer tissues with or without lymph node metastasis. (200×, scale bar=50μM) **(B)** IHC sum scores were used to evaluate ITGB6 expression in gastric cancer tissues. **(C)** IHC sum scores were used to evaluate ITGB6 expression in gastric cancer tissues with or without lymph node metastasis. **(D)** Correlation between tissue ITGB6 expression and serum ITGB6 expression. *P<0.05; ***P<0.001.

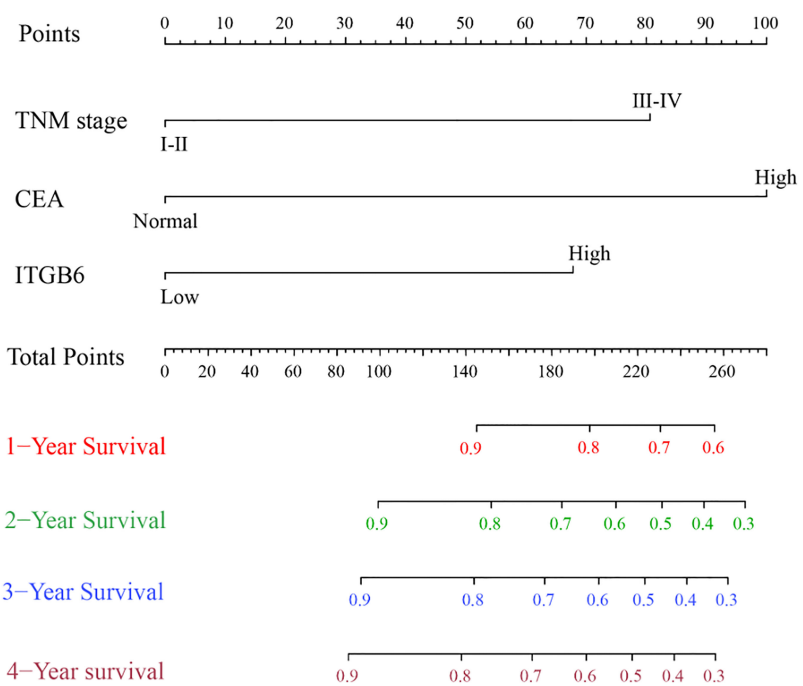

FIGURE 4 | Prognostic Nomogram of 1-year, 2-year, 3-year and 4-year overall survival of 135 gastric cancer patients.

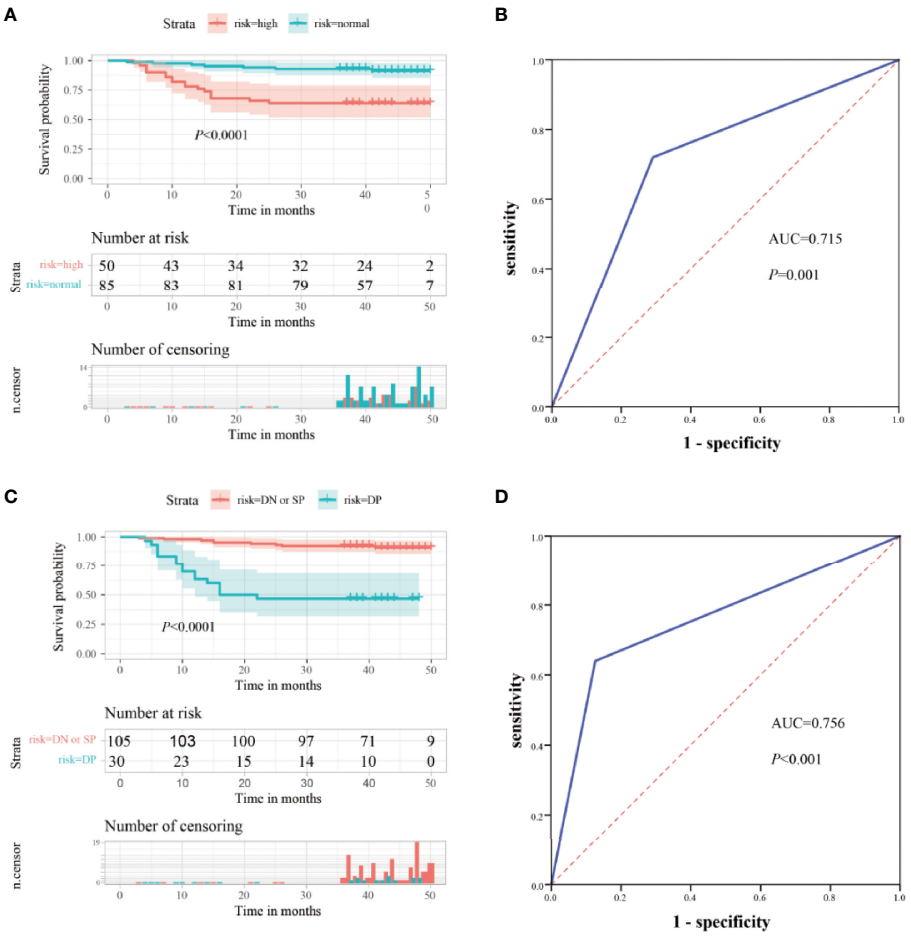

FIGURE 5 | Clinical significance of combined serum ITGB6 and CEA levels for gastric cancer patients. **(A)** Survival analysis according to serum CEA levels in a total number of 135 gastric cancer patients from a retrospective cohort. **(B)** ROC analysis was constructed for the prediction of prognosis of gastric cancer patients using serum CEA expression. **(C)** Survival analysis according to combined serum ITGB6 and CEA levels in gastric cancer patient from the retrospective cohort. **(D)** ROC analysis was constructed for the prediction of prognosis of gastric cancer patients using combined serum ITGB6 and CEA expression.

was not detected both before and after surgery for a patient, but there was a slight elevation in serum ITGB6 level during tumor recurrence (**Figure 6C**). These results indicated that serum ITGB6 may serve as a biomarker for tumor surveillance of gastric cancer patients, but a cohort with larger sample size is also warranted.

DISCUSSION

Discovering easily accessible tumor biomarkers is crucial for optimizing patient care in patients with gastric cancer (26). Here we identified serum ITGB6 level may serve as a novel tumor biomarker for gastric cancer. ITGB6 was identified as an epithelial-specific expressed subtype of integrin that induced during wound healing, inflammation and carcinogenesis (10, 27). As a member of cell surface adhesion molecules, ITGB6 was involved in the tumorigenesis and progression of several tumors. It has been demonstrated that ITGB6 participated in almost every step during tumor metastasis. The expression of ITGB6 in gastric cancer tissues was associated with matrix metalloproteinase 9 (MMP-9), and ITGB6 might participate in the invasiveness of gastric cancer as a downstream effector of vascular endothelial growth factor (VEGF), indicating that ITGB6 is a key molecule that involved in the invasiveness and metastatic potential of gastric cancer (14–17). Consistent with these findings, based on both retrospective and prospective cohorts, the present study found that high baseline serum ITGB6 levels were observed in patients with advanced gastric cancer, especially patients with lymph node metastasis or distant metastasis. Previous study also demonstrated that integrin αvβ6 may contribute to targeted liver metastasis of colorectal cancer *via* the SDF-1/CXCR4 axis (28), and we should notice the phenomenon that serum ITGB6 expression was markedly increased in patients with liver metastasis. Although the sample size was limited, further research focusing on the role

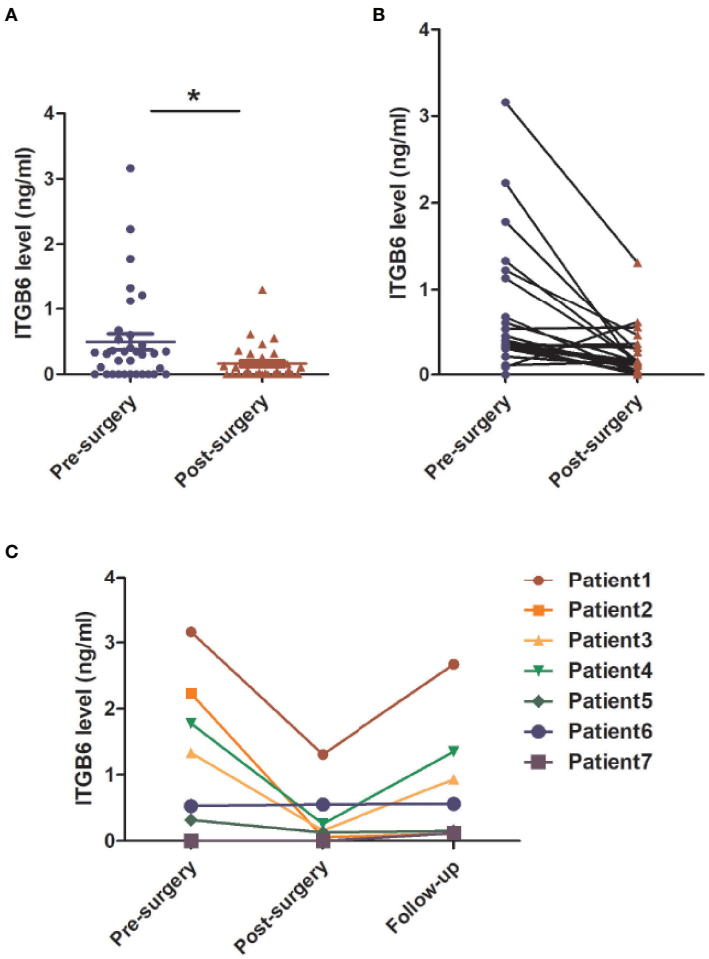

FIGURE 6 | The application of serum ITGB6 level for tumor surveillance in gastric cancer patients from a prospective cohort. **(A, B)** Changes of serum ITGB6 levels after radical gastrectomy for gastric cancer patients from a prospective cohort. **(C)** Trend line of serum ITGB6 levels from 7 patients with tumor recurrence during follow-up. *P<0.05.

of ITGB6 in liver metastasis of gastric cancer is warranted. The present study demonstrated that patients with a serum ITGB6 level >0.5ng/ml were highly suspected to have lymph node metastasis or distant metastasis, indicating that ITGB6 might serve as a potential marker for the risk stratification of gastric cancer patients.

ITGB6 was considered to be a prognostic indicator as its increased expression in tumor tissues was significantly associated with the prognosis of patients in various tumors (29–34). It has been demonstrated that positive ITGB6 expression in gastric cancer tissues was linked to significantly reduced survival times (15, 17). Importantly, our results showed that serum ITGB6 levels were closely associated with unfavorable prognosis of patients with gastric cancer. Based on the aforementioned findings, a nomogram for predicting the overall survival for gastric cancer patients based on ITGB6 expression was established, which showed a favorable predictive efficacy.

As one of the standard biomarker for gastric cancer, CEA is commonly used for the risk stratification and recurrence follow up nowadays (3, 35). The present study also showed that serum ITGB6 levels was associated with CEA expression for gastric cancer patients. Moreover, combined serum ITGB6 and CEA levels significantly improved the efficacy for the risk stratification of gastric cancer.

Importantly, the present study also constructed a prospective cohort for confirmation of the conclusion, as well as exploring the clinical significance of serum ITGB6 levels during follow-up. A dramatic decrease of serum ITGB6 expression showed after surgery for most of the enrolled subjects, indicating that serum ITGB6 levels may be associated with tumor burden for gastric cancer patients. Further results also preliminary confirmed that serum ITGB6 levels might serve as a potential biomarker for tumor surveillance and monitoring of tumor recurrence during follow up. Rebounded high serum ITGB6 expression may indicate tumor recurrence and a sustained high serum ITGB6 level might represent poor prognosis.

Most of previous research mainly focus on tissue-expressed ITGB6 and as far as we know, only one study detected serum

ITGB6 expression in patients with colorectal cancer, which revealed that serum ITGB6 may serve as a potential biomarker for diagnosis and surveillance of colorectal cancer (14, 36–38). For the first time, we demonstrated that serum ITGB6 level may serve as an effective biomarker for the risk stratification and prognostic prediction of gastric cancer patients. Interestingly, we should notice that serum ITGB6 expression was associated with ITGB6 expression in tumor tissues, and as an easily accessed specimen, serum is undoubtedly more convenient and more likely to be accepted during the perioperative period and follow-up visit, which represents a better applicative prospect. In order to evaluate the risk stratification and predict the prognosis of gastric cancer patients, we strongly recommend a routine serum ITGB6 level detection within the perioperative period and during follow-up.

A limitation of this study is the limited sample size for both the retrospective and the prospective cohort. And the follow-up results of the prospective cohort with larger size is also warranted. Moreover, as more and more gastric cancer patients receive chemotherapy before or after surgery nowadays, the effect of chemotherapy on both serum and tissue ITGB6 expression is also deserved further investigation. In addition, a multicenter prospective cohort study is also needed in the further research.

In conclusion, the present study identified a novel potential serum biomarker for the risk stratification, prognostic prediction and recurrence surveillance for gastric cancer, which deserves further validation and application. And such easily accessed biomarker might essentially contribute to an optimized patient care for patients with gastric cancer.

DATA AVAILABILITY STATEMENT

The raw data supporting the conclusions of this article will be made available by the authors, without undue reservation.

ETHICS STATEMENT

The studies involving human participants were reviewed and approved by the Ethics Committee of the Affiliated Hospital of Qingdao University. The patients/participants provided their written informed consent to participate in this study. Written informed consent was obtained from the individual(s) for the publication of any potentially identifiable images or data included in this article.

AUTHOR CONTRIBUTIONS

YZ, SC, and ZL designed the study. YS performed the experiments. JX and HY contributed to data analyses. XL and YT collected tissue specimens and clinical data. ZL and YS wrote the paper. YZ and SC revised the paper. All authors contributed to the article and approved the submitted version.

FUNDING

This work was supported by Shandong Provincial Natural Science Foundation, China (No. ZR2020QH225), Key Research Project of Shandong Province, China (2016GGB01022), Qingdao Minsheng Science and Technology Foundation, Shandong, China (No. 14-2-3-5-nsh) and Qingdao Science and Technology Plan Project (No. 13-1-4-220-jch).

SUPPLEMENTARY MATERIAL

The Supplementary Material for this article can be found online at: https://www.frontiersin.org/articles/10.3389/fonc.2021.770997/full#supplementary-material

REFERENCES

1. Siegel RL, Miller KD, Fuchs HE, Jemal A. Cancer Statistics, 2021. *CA: Cancer J Clin* (2021) 71(1):7–33. doi: 10.3322/caac.21654
2. Sung H, Ferlay J, Siegel RL, Laversanne M, Soerjomataram I, Jemal A, et al. Global Cancer Statistics 2020: GLOBOCAN Estimates of Incidence and Mortality Worldwide for 36 Cancers in 185 Countries. *CA: Cancer J Clin* (2021) 71(3):209–49. doi: 10.3322/caac.21660
3. Smyth EC, Nilsson M, Grabsch HI, van Grieken NC, Lordick F. Gastric Cancer. *Lancet* (2020) 396(10251):635–48. doi: 10.1016/S0140-6736(20)31288-5
4. Janjigian YY, Shitara K, Moehler M, Garrido M, Salman P, Shen L, et al. First-Line Nivolumab Plus Chemotherapy *Versus* Chemotherapy Alone for Advanced Gastric, Gastro-Oesophageal Junction, and Oesophageal Adenocarcinoma (CheckMate 649): A Randomised, Open-Label, Phase 3 Trial. *Lancet* (2021) 398(10294):27–40. doi: 10.1016/S0140-6736(21)00797-2
5. Yu J, Huang C, Sun Y, Su X, Cao H, Hu J, et al. Effect of Laparoscopic *vs* Open Distal Gastrectomy on 3-Year Disease-Free Survival in Patients With Locally Advanced Gastric Cancer: The CLASS-01 Randomized Clinical Trial. *JAMA* (2019) 321(20):1983–92. doi: 10.1001/jama.2019.5359
6. Zhang X, Liang H, Li Z, Xue Y, Wang Y, Zhou Z, et al. Perioperative or Postoperative Adjuvant Oxaliplatin With S-1 *Versus* Adjuvant Oxaliplatin With Capecitabine in Patients With Locally Advanced Gastric or Gastro-Oesophageal Junction Adenocarcinoma Undergoing D2 Gastrectomy (RESOLVE): An Open-Label, Superiority and Non-Inferiority, Phase 3 Randomised Controlled Trial. *Lancet Oncol* (2021) 22(8):1081–92. doi: 10.1016/S1470-2045(21)00297-7
7. Chen W, Zheng R, Baade PD, Zhang S, Zeng H, Bray F, et al. Cancer Statistics in China, 2015. *CA: Cancer J Clin* (2016) 66(2):115–32. doi: 10.3322/caac.21338
8. Duffy MJ, Lamerz R, Haglund C, Nicolini A, Kalousova M, Holubec L, et al. Tumor Markers in Colorectal Cancer, Gastric Cancer and Gastrointestinal Stromal Cancers: European Group on Tumor Markers 2014 Guidelines Update. *Int J Cancer* (2014) 134(11):2513–22. doi: 10.1002/ijc.28384
9. Dixit RB, Chen A, Chen J, Sheppard D. Identification of a Sequence Within the Integrin Beta6 Subunit Cytoplasmic Domain That Is Required to Support the Specific Effect of Alphavbeta6 on Proliferation in Three-Dimensional Culture. *J Biol Chem* (1996) 271(42):25976–80. doi: 10.1074/jbc.271.42.25976
10. Koivisto L, Bi J, Hakkinen L, Larjava H. Integrin Alphavbeta6: Structure, Function and Role in Health and Disease. *Int J Biochem Cell Biol* (2018) 99:186–96. doi: 10.1016/j.biocel.2018.04.013
11. Cantor DI, Cheruku HR, Nice EC, Baker MS. Integrin Alphavbeta6 Sets the Stage for Colorectal Cancer Metastasis. *Cancer metastasis Rev* (2015) 34(4):715–34. doi: 10.1007/s10555-015-9591-z
12. Hanahan D, Weinberg RA. Hallmarks of Cancer: The Next Generation. *Cell* (2011) 144(5):646–74. doi: 10.1016/j.cell.2011.02.013
13. Hanahan D, Weinberg RA. The Hallmarks of Cancer. *Cell* (2000) 100(1):57–70. doi: 10.1016/s0092-8674(00)81683-9

14. Niu J, Li Z. The Roles of Integrin Alphavbeta6 in Cancer. *Cancer Lett* (2017) 403:128–37. doi: 10.1016/j.canlet.2017.06.012
15. Zhang ZY, Xu KS, Wang JS, Yang GY, Wang W, Wang JY, et al. Integrin Alphanvbeta6 Acts as a Prognostic Indicator in Gastric Carcinoma. *Clin Oncol* (2008) 20(1):61–6. doi: 10.1016/j.clon.2007.09.008
16. Lian PL, Liu Z, Yang GY, Zhao R, Zhang ZY, Chen YG, et al. Integrin Alphavbeta6 and Matrix Metalloproteinase 9 Correlate With Survival in Gastric Cancer. *World J Gastroenterol* (2016) 22(14):3852–9. doi: 10.3748/wjg.v22.i14.3852
17. Zhuang Z, Zhou R, Xu X, Tian T, Liu Y, Liu Y, et al. Clinical Significance of Integrin Alphavbeta6 Expression Effects on Gastric Carcinoma Invasiveness and Progression *via* Cancer-Associated Fibroblasts. *Med Oncol* (2013) 30 (3):580. doi: 10.1007/s12032-013-0580-1
18. Zhao R, Liu XQ, Wu XP, Liu YF, Zhang ZY, Yang GY, et al. Vascular Endothelial Growth Factor (VEGF) Enhances Gastric Carcinoma Invasiveness *via* Integrin Alpha(V)Beta6. *Cancer Lett* (2010) 287(2):150–6. doi: 10.1016/j.canlet.2009.06.006
19. Tang Z, Li C, Kang B, Gao G, Li C, Zhang Z. GEPIA: A Web Server for Cancer and Normal Gene Expression Profiling and Interactive Analyses. *Nucleic Acids Res* (2017) 45(W1):W98–102. doi: 10.1093/nar/gkx247
20. Balachandran VP, Gonen M, Smith JJ, DeMatteo RP. Nomograms in Oncology: More Than Meets the Eye. *Lancet Oncol* (2015) 16(4):e173–80. doi: 10.1016/S1470-2045(14)71116-7
21. Iasonos A, Schrag D, Raj GV, Panageas KS. How to Build and Interpret a Nomogram for Cancer Prognosis. *J Clin Oncol* (2008) 26(8):1364–70. doi: 10.1200/JCO.2007.12.9791
22. Brentnall AR, Cuzick J. Use of the Concordance Index for Predictors of Censored Survival Data. *Stat Methods Med Res* (2018) 27(8):2359–73. doi: 10.1177/0962280216680245
23. Koziol JA, Jia Z. The Concordance Index C and the Mann-Whitney Parameter Pr(X>Y) With Randomly Censored Data. *Biometrical J Biometrische Z* (2009) 51(3):467–74. doi: 10.1002/bimj.200800228
24. Chen T, Liu H, Liu Z, Li K, Qin R, Wang Y, et al. FGF19 and FGFR4 Promotes the Progression of Gallbladder Carcinoma in an Autocrine Pathway Dependent on GPBAR1-cAMP-EGR1 Axis. *Oncogene* (2021) 40(30):4941–53. doi: 10.1038/s41388-021-01850-1
25. Liu H, Gong Z, Li K, Zhang Q, Xu Z, Xu Y. SRPK1/2 and PP1alpha Exert Opposite Functions by Modulating SRSF1-Guided MKNK2 Alternative Splicing in Colon Adenocarcinoma. *J Exp Clin Cancer Res CR* (2021) 40 (1):75. doi: 10.1186/s13046-021-01877-y
26. Joshi SS, Badgwell BD. Current Treatment and Recent Progress in Gastric Cancer. *CA: Cancer J Clin* (2021) 71(3):264–79. doi: 10.3322/caac.21657
27. Whilding LM, Vallath S, Maher J. The Integrin Alphavbeta6: A Novel Target for CAR T-Cell Immunotherapy? *Biochem Soc Trans* (2016) 44(2):349–55. doi: 10.1042/BST20150249
28. Wang B, Wang W, Niu W, Liu E, Liu X, Wang J, et al. SDF-1/CXCR4 Axis Promotes Directional Migration of Colorectal Cancer Cells Through Upregulation of Integrin Alphavbeta6. *Carcinogenesis* (2014) 35(2):282–91. doi: 10.1093/carcin/bgt331
29. Zheng X, Zhu Y, Wang X, Hou Y, Fang Y. Silencing of ITGB6 Inhibits the Progression of Cervical Carcinoma *via* Regulating JAK/STAT3 Signaling Pathway. *Ann Trans Med* (2021) 9(9):803. doi: 10.21037/atm-21-1669
30. Quigley NG, Czech N, Sendt W, Notni J. PET/CT Imaging of Pancreatic Carcinoma Targeting the "Cancer Integrin" Alphavbeta6. *Eur J Nucl Med Mol Imaging* (2021) 48(12):4107–8. doi: 10.1007/s00259-021-05443-8
31. Bagati A, Kumar S, Jiang P, Pyrdol J, Zou AE, Godicelj A, et al. Integrin Alphavbeta6-TGFbeta-SOX4 Pathway Drives Immune Evasion in Triple-Negative Breast Cancer. *Cancer Cell* (2021) 39(1):54–67.e9. doi: 10.1016/j.ccell.2020.12.001
32. Uusi-Kerttula H, Davies JA, Thompson JM, Wongthida P, Evgin L, Shim KG, et al. Ad5NULL-A20: A Tropism-Modified, Alphavbeta6 Integrin-Selective Oncolytic Adenovirus for Epithelial Ovarian Cancer Therapies. *Clin Cancer Res* (2018) 24(17):4215–24. doi: 10.1158/1078-0432.CCR-18-1089
33. Peng ZW, Ikenaga N, Liu SB, Sverdlov DY, Vaid KA, Dixit R, et al. Integrin Alphavbeta6 Critically Regulates Hepatic Progenitor Cell Function and Promotes Ductular Reaction, Fibrosis, and Tumorigenesis. *Hepatology* (2016) 63(1):217–32. doi: 10.1002/hep.28274
34. Li Z, Biswas S, Liang B, Zou X, Shan L, Li Y, et al. Integrin Beta6 Serves as an Immunohistochemical Marker for Lymph Node Metastasis and Promotes Cell Invasiveness in Cholangiocarcinoma. *Sci Rep* (2016) 6:30081. doi: 10.1038/srep30081
35. Montagnani F, Crivelli F, Aprile G, Vivaldi C, Pecora I, De Vivo R, et al. Long-Term Survival After Liver Metastasectomy in Gastric Cancer: Systematic Review and Meta-Analysis of Prognostic Factors. *Cancer Treat Rev* (2018) 69:11–20. doi: 10.1016/j.ctrv.2018.05.010
36. Bengs S, Becker E, Busenhart P, Spalinger MR, Raselli T, Kasper S, et al. Beta6 -Integrin Serves as a Novel Serum Tumor Marker for Colorectal Carcinoma. *Int J Cancer* (2019) 145(3):678–85. doi: 10.1002/ijc.32137
37. Feng X, Wang Y, Lu D, Xu X, Zhou X, Zhang H, et al. Clinical Translation of a (68)Ga-Labeled Integrin Alphavbeta6-Targeting Cyclic Radiotracer for PET Imaging of Pancreatic Cancer. *J Nucl Med* (2020) 61(10):1461–7. doi: 10.2967/jnumed.119.237347
38. Whilding LM, Halim L, Draper B, Parente-Pereira AC, Zabinski T, Davies DM, et al. CAR T-Cells Targeting the Integrin Alphavbeta6 and Co-Expressing the Chemokine Receptor CXCR2 Demonstrate Enhanced Homing and Efficacy Against Several Solid Malignancies. *Cancers* (2019) 11 (5):674. doi: 10.3390/cancers11050674

Conflict of Interest: The authors declare that the research was conducted in the absence of any commercial or financial relationships that could be construed as a potential conflict of interest.

frontiers in Oncology

ORIGINAL RESEARCH
published: 09 November 2021
doi: 10.3389/fonc.2021.762821

Identification and Validation of TYMS as a Potential Biomarker for Risk of Metastasis Development in Hepatocellular Carcinoma

Shuai Li[1], *Jingyuan Zhao*[2], *Linlin Lv*[1] *and Deshi Dong*[1]*

[1] Department of Pharmacy, The First Affiliated Hospital of Dalian Medical University, Dalian, China, [2] Regenerative Medicine Center, The First Affiliated Hospital of Dalian Medical University, Dalian, China

Metastasis is the major cause of hepatocellular carcinoma (HCC) mortality. Unfortunately, there are few reports on effective biomarkers for HCC metastasis. This study aimed to discover potential key genes of HCC, which could provide new insights for HCC metastasis. GEO (Gene Expression Omnibus) microarray and TCGA (The Cancer Genome Atlas) datasets were integrated to screen for candidate genes involved in HCC metastasis. Differentially expressed genes (DEGs) were screened, and then we performed enrichment analysis of Gene Ontology (GO), together with Kyoto Encyclopedia of Genes and Genomes (KEGG). A protein-protein interaction network was then built and analyzed utilizing STRING and Cytoscape, followed by the identification of 10 hub genes by cytoHubba. Four genes were associated with survival, their prognostic value was verified by prognostic signature analysis. Thymidylate synthase (TYMS) gene was identified as significant HCC metastasis-associated genes after mRNA expression validation and IHC analysis. TYMS silencing in HCC cells remarkedly inhibited growth and invasion. Finally, we found TYMS silencing dramatically decrease DNA synthesis and extracellular matrix (ECM) degradation, resulting in the inhibition of HCC metastasis, indicating TYMS had close associations with HCC development. These findings provided new insights into HCC metastasis and identified candidate gene prognosis signatures for HCC metastasis.

Keywords: hepatocellular carcinoma, metastasis, TYMS, prognostic biomarker, bioinformatics

OPEN ACCESS

Edited by:
Hongda Liu,
Nanjing Medical University, China

Reviewed by:
Wei Cao,
Shanghai Jiao Tong University, China
Limin Xia,
Huazhong University of Science and Technology, China

***Correspondence:**
Deshi Dong
dongdeshi@dmu.edu.cn

Specialty section:
This article was submitted to Cancer Molecular Targets and Therapeutics, a section of the journal Frontiers in Oncology

Received: *22 August 2021*
Accepted: *21 October 2021*
Published: *09 November 2021*

Citation:
Li S, Zhao J, Lv L and Dong D (2021) Identification and Validation of TYMS as a Potential Biomarker for Risk of Metastasis Development in Hepatocellular Carcinoma. Front. Oncol. 11:762821. doi: 10.3389/fonc.2021.762821

INTRODUCTION

Hepatocellular carcinoma (HCC) is the fourth most common cause of cancer-related deaths in the world (1). The 5-year overall survival remains relatively poor, because of the difficulty associated with the early diagnosis and metastasis (2). Metastasis is responsible for as much as 90% of most cancer-related deaths (3). The multistep process of invasion and metastasis has been schematized as a sequence of discrete steps, often termed the invasion-metastasis cascade (4). The acquisitions of extensive invasion potencies by cancer cells are key components in the metastatic cascade. To enter

the blood or lymphatic circulation, carcinoma cells must first degrade the ECM to break tissue barriers, which is considered a key step promoting tumor invasion and metastasis (5). Therefore, it is essential to elucidate the molecular mechanism of HCC metastasis and identify potential molecular biomarkers for prognosis prediction.

Along with the development of microarray and high-throughput sequencing technology, many tumor prognostic markers were reported by using GEO and TCGA. Databases based on the TCGA data set (GEPIA, cBioPortal, Human Protein Atlas, etc.) can analyze and confirm the expression of hub genes and the impact on survival. These identified genes are involved in the proliferation and metastasis of HCC, thereby affecting the survival and prognosis of HCC patients. The invasiveness and metastasis of HCC severely limit the improvement of the curative effect of HCC. Therefore, excavation of the genes involved in metastasis has been an important goal for the past several decades. Although many biomarkers for HCC have been identified, there are few reports on biomarkers for HCC metastasis. TYMS is an enzyme that catalyzes the conversion of dUMP to dTMP, and is the main intracellular target of the active 5-FU metabolite (6). There are many studies in the literature demonstrating prognostic and predictive values of TYMS presence in cancer (6–14), however, its role as a marker of HCC metastasis is not known.

In this study, the differential mRNA expression data of HCC from the TCGA and GEO databases were analyzed to identify key genes. The integrated bioinformatics analysis by investigating the functions and pathways of the gene was used to further investigated their potentiality of being biomarkers in HCC. Functional enrichment and protein interaction (PPI) analysis combined with survival analysis were used to further screen genes that are critical for HCC development. The prognostic value of the genes was evaluated using the ROC curve (Receiver Operating Characteristic Curve) and survival analysis. *In vitro* experiment was conducted to elaborate the potential roles of the biomarker in the proliferation and invasion of HCC cells.

MATERIALS AND METHODS

Data Collection and Data Preprocessing

The gene expression profiling datasets (GSE28248 and GSE27635) were obtained from the GEO database (https://www.ncbi.nlm.nih.gov/geo/). The dataset for GSE28248 includes intratumoral and peritumoral tissues of 20 paired HCC samples patients with lymph node-positive. GSE27635 incorporates 24 pairs of intratumoral and peritumoral tissue from HCC patients with bone metastases. TCGA HCC dataset, coupled with the clinical data, includes 50 normal and 369 tumor samples.

Screening of DEGs

To investigate DEGs among normal and tumor samples, the limma package in R was used with the cut-off criteria of |log 2-fold-change [FC]| > 1 and a corrected $p < 0.05$. The common DEGs in GSE28248 and TCGA were screened for subsequent analysis.

Gene Ontology and KEGG Pathway Analysis

Gene ontology (GO) term enrichment analysis and Kyoto Encyclopedia of Genes and Genomes (KEGG) pathway analysis were performed by using DAVID (https://david.ncifcrf.gov/). The KEGG pathway and GO enrichment analyses of upregulated and downregulated genes were based on the threshold of adjusted p-value < 0.05.

Protein-Protein Interaction (PPI) Network Construction and Hub Genes Identification

To evaluate the interrelationships behind the list of genes, we used the STRING database for analysis. The Cytoscape software for visualizing and analyzing molecular interaction networks, was used to build a PPI network. Hub genes were selected from genes intersection calculated by using the Cytoscape plugin cytoHubba.

Risk Stratification (RS) and ROC Curves

Multivariate Cox analysis was further used to determine whether the four prognostic genes were independent prognosis factors of the patient's OS (Overall survival). The risk score model was constructed based on a linear integration of the expression level multiplied regression model (β) using the following formula: Risk score= expRNA1×βRNA1 + expRNA2×βRNA2+… +expRNAn×βRNAn. The sensitivity and specificity of the risk model were calculated by the AUC (Area under the curve) of the ROC curve with the "survival ROC" R package.

Validation of the Key Genes Based on TCGA Data and HPA Database

Gene Expression Profiling Interactive Analysis (GEPIA: http://gepia.cancer-pku.cn/), a web-based tool to display the survival and expression patterns between tumor and normal groups was used to verify our results. Furthermore, the validation of the protein levels of the key genes was carried out using the Human Protein Atlas (HPA) database (https://www.proteinatlas.org/).

Validation of the TYMS in Clinical Tissue Samples

A total of 24 paired HCC patients specimens (tumor and adjacent nontumor tissues) were collected from the Biobank of the First Affiliated Hospital of Dalian Medical University (Liaoning, China). The samples were removed from hospitalized patients at the Department of Hepatobiliary Surgery, First Affiliated Hospital of Dalian Medical University (Liaoning, China) from 2018 to 2021. Samples used in this study were approved by the Committees for Ethical Review of Research

at the First Affiliated Hospital of Dalian Medical University. The TYMS gene mRNA expression between tumor and normal groups was assayed by real-time PCR.

Cell Culture and Cell Transfection

One immortalized normal liver cell line L02 and three human HCC cell line MHCC-97H, BEL-7402 and HuH-7 were obtained from the Chinese Type Culture Collection, Chinese Academy of Sciences. All cells were cultured in DMEM supplemented with 10% fetal bovine serum and kept in a humidified atmosphere of 5% CO_2 at 37∘C. In order to inhibit the expression of TYMS, we transfected two small interfering RNAs (siRNAs) targeting the TYMS coding sequence. The siRNAs were purchased from GenePharma (Shanghai, China) and sequences are as follows: 1. GGAGTTGACCAACTGCAAA 2. CAACCCTGACGACA GAAGA. The efficiency of infection was assayed by real-time PCR.

Quantitative Real-Time PCR

Total RNA was isolated using Trizol reagent (Thermo Fisher) and reverse-transcribed according to the manufacturer's instructions. The cDNA was subjected to quantitative Real-Time PCR using the SYBR Green PCR Master Mix (Thermo Fisher) and the assay was performed on a 7500 fast Real-Time PCR system (Applied Biosystems by Life Technologies). Relative expression levels were normalized to GAPDH. The $2^{-\Delta\Delta Ct}$ method was used to compare the fold differences in expression. Primer sequences were listed as follows: TYMS forward 5'- TGG GGCAGAATACAGAGATATGG-3' and reverse 5'- TGATGG TGTCAATCACTCTTTGC-3', GAPDH forward 5'- ACAACT TTGGTATCGTGGAAGG-3' and reverse 5'- GCCATCACGC CACAGTTTC-3'.

Western Blotting

The TYMS (#15047-1-AP) and GAPDH (#10494-1-AP) antibodies were purchased from Proteintech. Proteins were electrophoresed in SDS-PAGE gel and transferred onto PVDF membranes. The membranes were blocked with 5% skim milk in TBS/0.1% Tween 20 containing for 0.5 h and then incubated overnight with the primary antibodies at 4°C. The membrane was further incubated with HRP-conjugated secondary antibodies for 1 hours at room temperature. Protein bands were visualized with ECL substrates.

Cell Proliferation

Viable cells were measured using the Cell Counting Kit-8 (CCK-8) proliferation assay (APExBIO) according to the manufacturer's guidelines.

Colony Formation

For colony formation assay, 500 cells were plated in 6-well plates and culture for 14 days. Cells were stained with 0.1% crystal violet and the number of colonies was counted.

EdU (5-Ethynyl-2'-Deoxyuridine) Incorporation Assay

Cells were incubated with 10 μM EdU (APExBIO) for 2 h at 37°C. After incubation, the cells were washed with PBS and fixed with 4% paraformaldehyde (PFA) for 15 min and followed by incubation with 2.5% Triton X-100 for 10 min at room temperature. Cells were washed and a 100 μl Click-iT reaction cocktail was added to the sample incubated for 30 min at room temperature. 10 μg/ml hoechst33342 was added and incubated for 10 min at room temperature.

Wound Healing Assay

Cells were cultured in a 6-well plate until they reached 70–80% confluence. A scratch was made through the cell monolayer using a sterile pipette tip. The cells were allowed to migrate into the wound area for 48 h. The percent change in migration was determined by using ImageJ.

Transwell Invasion Assay

Cell invasion was performed using transwell chambers (8-μm pore size, Corning). For invasion assays, 1.0×10^5 cells were seeded into upper inserts with a Matrigel-coated membrane. The cells were allowed to migrate or invasion for 24 h. The cells remaining on the upper membrane were removed with cotton wool. The remaining cells were fixed, stained with crystal violet, and analyzed by inverted microscopy.

Matrix Degradation Assay

In brief, glass coverslips were coated with 0.2 mg/ml FITC-gelatin (Anaspec), cross-linked with 0.5% glutaraldehyde, and then treated with 5mg/ml sodium borohydride for 5 min. Cells were plated on FITC-gelatin for 8 h and fixed with 4% formaldehyde and analyzed for gelatin-degradation under a fluorescence microscope (Leica). Gelatin-degradation spots were quantified using ImageJ.

Statistical Analyses

Results are recorded as means ± standard error of the mean for at least three independent experiments, and analyzed by one-way ANOVA, two-tailed unpaired Student's t-test, or Mann-Whitney test. Statistical analyses were performed using the GraphPad Prism 6 software. Data were considered statistically significant as follows: $*P< 0.05$, $**P< 0.01$, and $***P< 0.001$.

RESULTS

Identification of DEGs and Functional Annotation

The gene expression profiling of GSE28248, which contained 20 pairs of HCC patients with bone metastases samples and normal samples, was analyzed with GEO2R. A total of 31DEGs were identified (23 upregulated and 8 downregulated genes were listed in **Supplementary Table 1**). The volcano plot of GSE28248 and TCGA DEGs is shown in **Figure 1A**. To confirm the reliability of

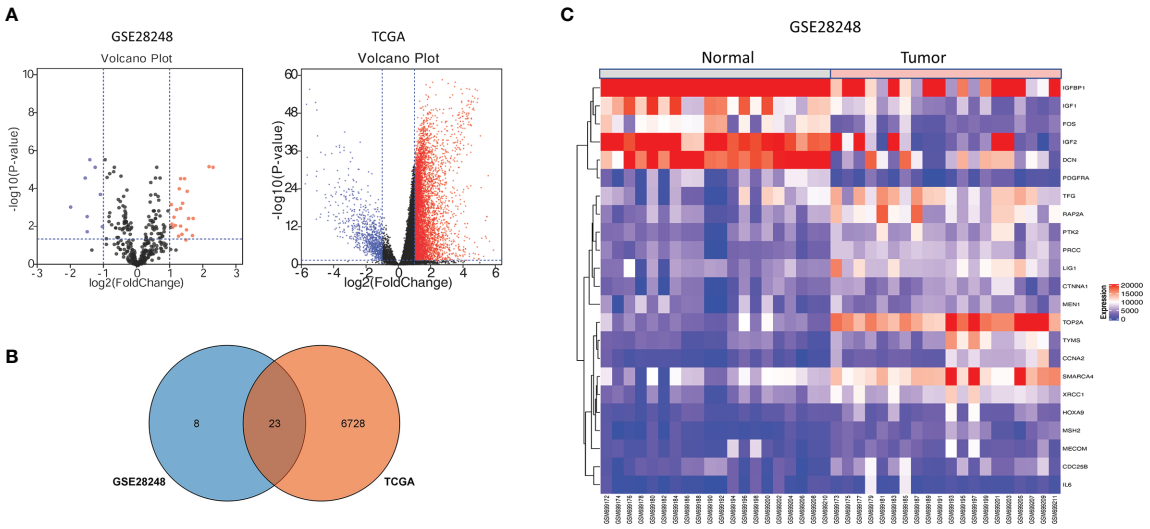

FIGURE 1 | DEGs identification from GEO and TCGA. **(A)** Volcano plot visualizing DEGs in GSE28248. **(B)** Overlapping DEGs between GEO and TCGA database. **(C)** The expression heatmap of the overlapping DEGs in GSE28248.

DEGs in HCC, we obtained overlapping DEGs (**Figure 1B**) of the two datasets including 16 upregulated and 7 downregulated genes. The heatmap of the top DEGs is shown in **Figure 1C**.

To further analyze the biological function of the DEGs, we processed GO function and KEGG pathway enrichment analysis with DAVID. With GO function analysis, we discovered that the DEGs are mostly enriched in the biological process of regulation of aging, regulation of phosphatidylinositol 3–kinase signaling (**Figure 2A**). As for molecular function, protein N–terminus binding and growth factor activity are contained in the top 10 enrichment classes (**Supplementary Figure 1A**). As we conducted the KEGG pathway analysis, we found that these DEGs are mainly enriched in the MAPK signaling pathway and PI3K–Akt signaling pathway (**Figure 2B**).

PPI Network Analysis and Screening for Hub Genes

STRING is an online tool for predicting protein-protein interactions (PPI) (15). After importing the overlapped DEGs into the online tool STRING, we obtained the PPI network of these genes (**Figure 3A**). Overlapped DEGs were imported into Cytoscape to screen the hub genes inside the network with Maximal Clique Centrality (MCC) algorithm. The MCC of each node was calculated by CytoHubba, a plugin in Cytoscape. In this study, the genes with the top 10 MCC values were considered as hub genes (**Figure 3B**).

Verification of the Prognostic Values of Hub Genes

We used GEPIA to evaluate the contribution of the 10 hub genes to clinical outcomes. The results demonstrated four genes CCNA2 (Cyclin-A2), MSH2 (MutS homolog 2), TOP2A (Topoisomerase 2-alpha) and TYMS were significantly positively correlated to patient outcomes, IGF2 was negatively correlated to patient outcomes (**Figure 3C**). The remaining hub gene survival analyses did not show statistical significance.

We calculated the risk score for each sample using the Sanger box website and used the cut-off values of the training set to classify the samples into high and low risk groups in TCGA HCC data. The distribution of risk score, survival status, and the expression of four genes for each patient were analyzed (**Figure 4A**). With the increase in riskscore, the expression levels of CCNA2, MSH2, TOP2A and TYMS showed an increasing trend. The AUC of the 1-, 3-, and 5-year ROC curve were 0.72, 0.65, and 0.62 (**Figure 4B**). Kaplan–Meier curve showed that the overall survival time of patients in the low-risk group was significantly longer than in the high-risk group (**Figure 4C**).

Validation of Genes Expressions

Validation of the expression of four prognosis-related genes with GEPIA, we detected the mRNA levels of four genes in TCGA database. CCNA2, MSH2, TOP2A and TYMS were found to be highly expressed in tumor tissues compared with normal tissues (**Figure 5A**). The significant correlation between four genes and the stage was also verified using the GEPIA (**Figure 5B**), they might be an oncogene for HCC that participates in tumorigenesis.

The protein expression of the genes was determined using immunohistochemistry (IHC) from the Human Protein Atlas database (HPA) to verify the transcriptome analysis results. The protein expression levels of TYMS showed upregulated (**Figure 5C**).

Validation in Clinical Tissue Samples

In order to validate the bioinformatics analysis results, 24 paired HCC tumor and peri-tumor samples were studied.

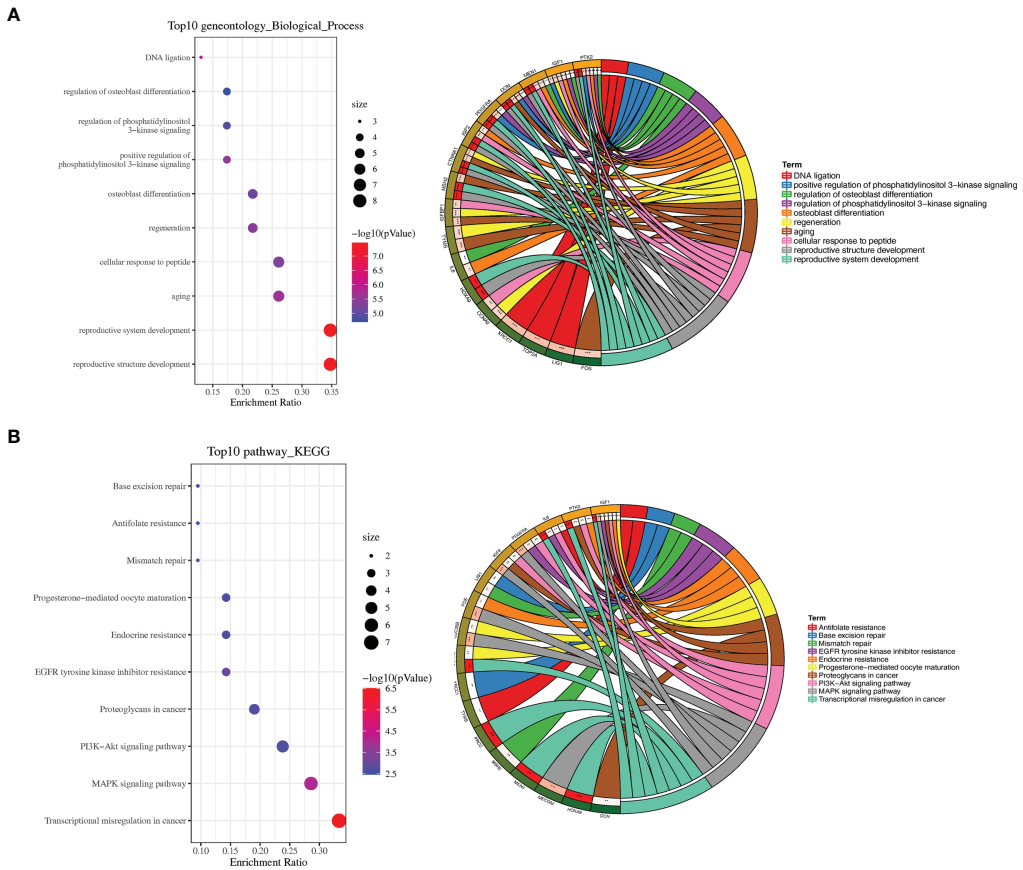

FIGURE 2 | GO and KEGG pathway enrichment analyses. **(A)** Bubble plot of biological processes enrichment analysis of DEGs and circle plot of biological processes enrichment analysis of DEGs. **(B)** Bubble plot of KEGG pathway enrichment analysis of DEGs and circle plot of KEGG pathway enrichment analysis of DEGs. *P < 0.05, **P < 0.01, and ***P < 0.001.

Comparing with peri-tumor controls, the expression of TYMS was significantly increased in HCC tissues (**Figure 6A**) which were consistent with the bioinformatics results obtained by the TCGA dataset. We studied the expression of TYMS in three HCC cell lines and one normal liver cell line (L02). Consistent with the results in cancer tissues, we observed that TYMS expression levels were higher in the liver cancer cell lines than in the normal liver cell line (**Figure 6A**).

TYMS Promotes HCC Cells Proliferation and Invasion

To analyze the impacts of TYMS on cancer cell proliferation and invasion. Two siRNA targeting TYMS were transfected into MHCC-97H and HuH-7. The silencing efficiency was verified by real-time PCR and western blot (**Figure 6B**). We performed a cell counting kit-8 assay to assess proliferation, the results showed that the downregulation of TYMS significantly decreased MHCC-97H and HuH-7 cells viability to a significant extent (**Figure 6C**). Colony formation assays found silencing of TYMS expression displayed significant differences in colony formation comparing with the control (**Figure 6D**), indicating that TYMS affects tumor growth.

To determine whether TYMS had a role in HCC cells invasion, we first investigated the effect of TYMS on migration. Wound healing assay was performed, the results suggested that TYMS promoted migration of MHCC-97H and HuH-7 cells (**Figure 6E**). Cells were subjected to chemotaxis invasion assays by seeding at equal numbers in a transwell invasion chamber with Matrigel. The invasion capabilities of MHCC-97H and HuH-7 cells were reduced by inhibition of TYMS expression compared with the control cells (**Figure 6F**). These findings suggest that TYMS promotes migration and invasion in HCC cells.

TYMS Promotes HCC Cells DNA Synthesis and Extracellular Matrix Degradation

EdU is a nucleoside analog of thymidine and is incorporated into DNA during active DNA synthesis (16). To further confirm the effect of TYMS on cell proliferation, we assessed DNA synthesis using an EdU incorporation assay.

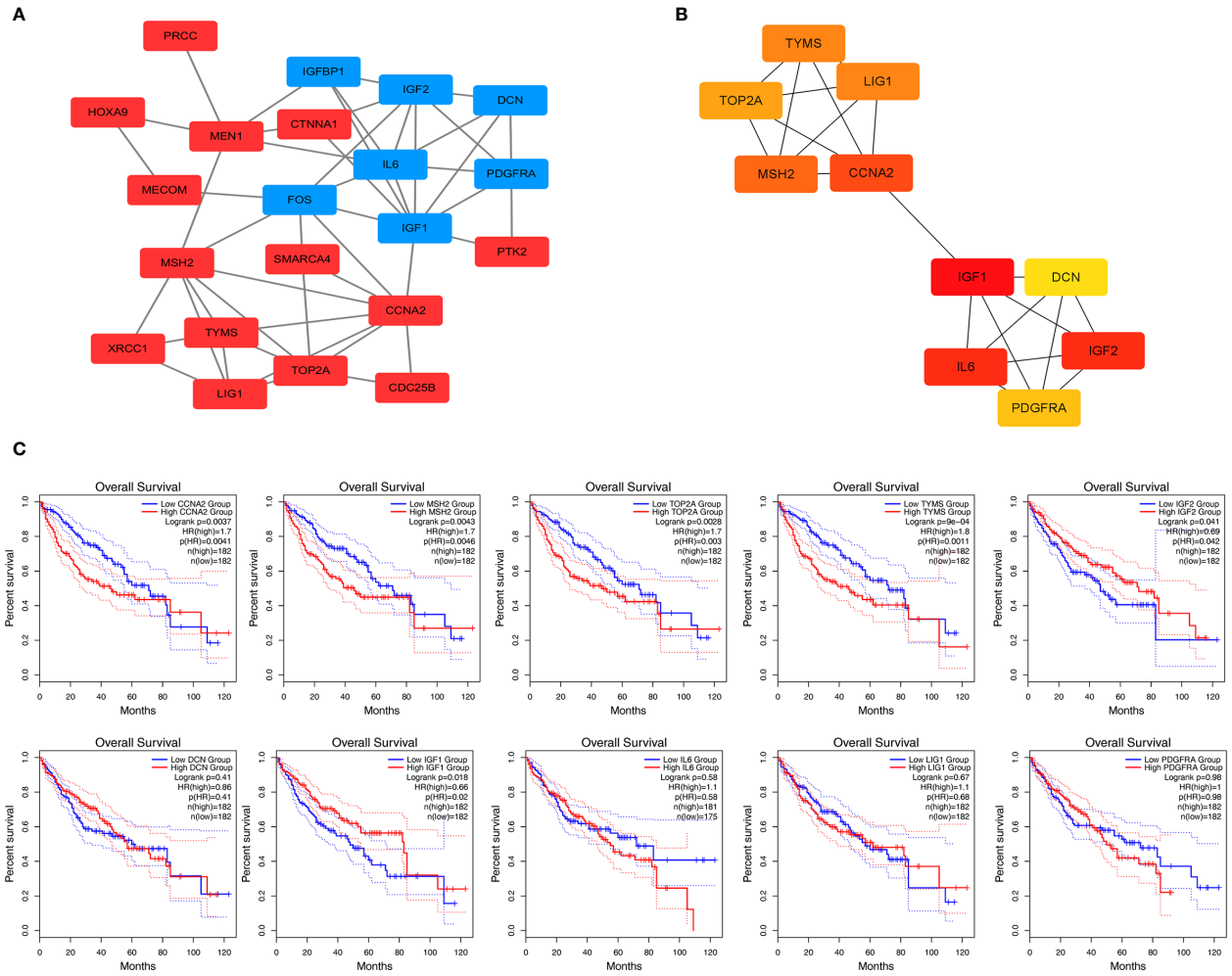

FIGURE 3 | Protein-protein interaction network and overall survival analysis of DEGs. **(A)** Based on the STRING online database, a PPI network was constructed containing 23 DEGs (upregulated DEGs labeled in red and downregulated DEGs labeled in blue). **(B)** Identification of hub genes MCC algorithm. **(C)** Survival analysis for TYMS in HCC from the GEPIA2 database.

The results showed that TYMS had an effect on the DNA synthesis of MHCC-97H and HuH-7 cells (**Figure 7A**). These results indicate that TYMS affects the proliferation of HCC cells.

Metastasis is a highly inefficient process, and certain steps of the invasion-metastasis cascade are extraordinarily inefficient (5). ECM degradation is an early and essential step in cancer metastasis, which is a key factor for determining patient survival in different types of solid tumors (3). To dissect the cellular functions of TYMS in promoting HCC cells invasion, we examined whether expression of TYMS was associated with ECM degradation. MHCC-97H and HuH-7 cells were plated on FITC–labeled gelatin matrix to assess their abilities to degrade the matrix. TYMS knockdown resulted in a potent reduction in matrix degradation in both cells (**Figure 7B**). These results indicate TYMS is necessary for extracellular matrix degradation in HCC cells.

DISCUSSION

In this study, the genes potentially affecting metastasis in HCC were identified based on two integrated GEO and TCGA HCC data sets. DEGs were screened out to investigate function and pathways enrichment. Enrichment analysis showed that the DEGs were significantly enriched in terms of MAPK signaling pathway and PI3K–Akt signaling pathway. The expressions of CCNA2, MSH2, TOP2A and TYMS mRNA were significantly upregulated in HCC. A combination of the identified genes was used as an indicator for risk stratification that helps to predict the prognosis of HCC. The overall survival rate indicated, HCC patients with high expression of CCNA2, MSH2, TOP2A and TYMS showed poor overall survival.

CCNA2 plays a critical role in the control of cell cycle transitions and has a potential role in tumorigenesis (17). CCNA2 belongs to the highly conserved cyclin family and is

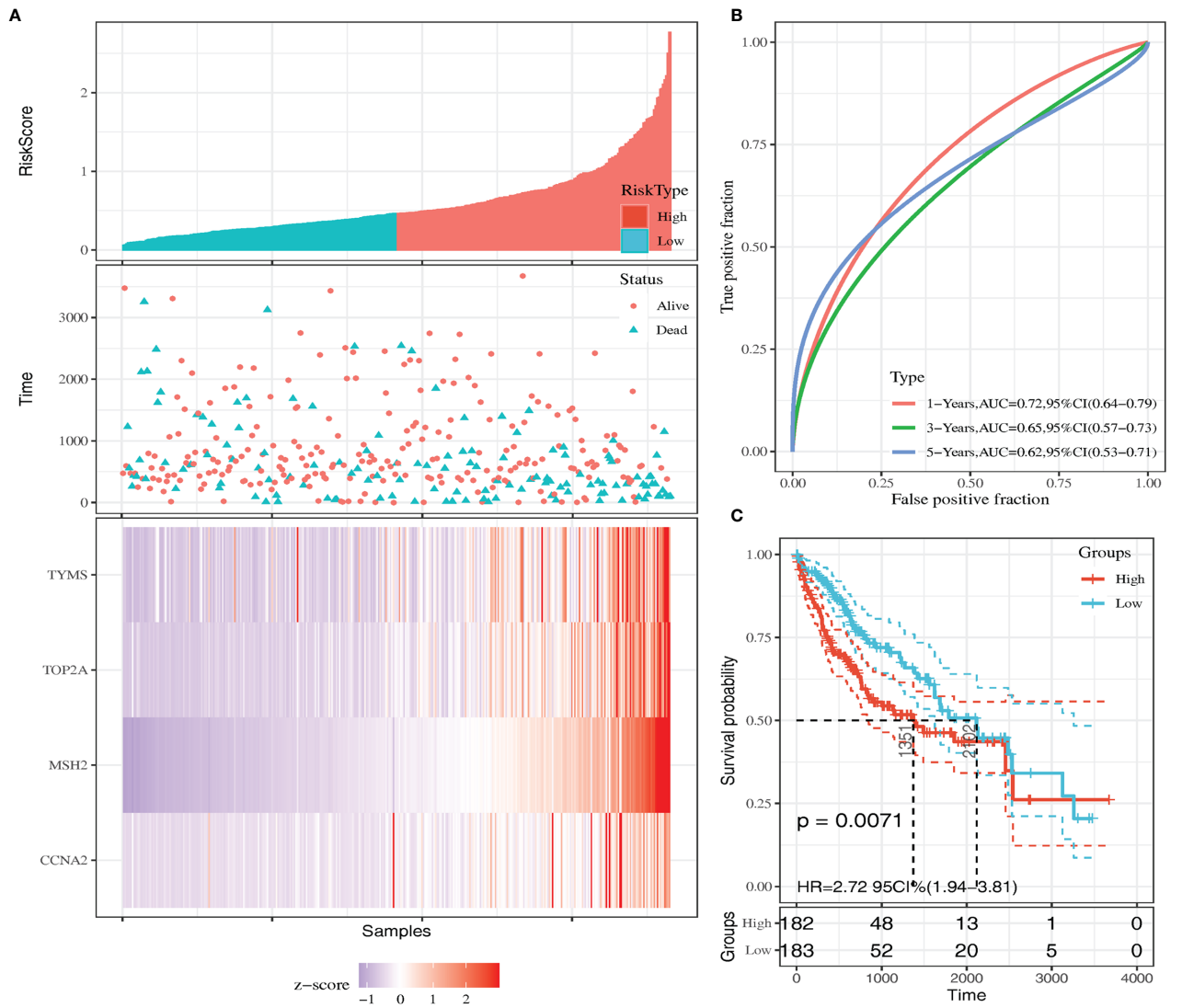

FIGURE 4 | Kaplan-Meier survival curve of overall survival between the high-risk group and low-risk group **(A)** Risk score, survival time, survival status, and expression of the four genes signature. **(B)** AUC for the four genes classification. **(C)** Kaplan-Meier survival curve of the four genes from the TCGA dataset.

expressed in almost all tissues in the human body (18). The MSH2 gene is responsible for recognizing nucleotide mismatches occurring during DNA replication (19), particularly in the case of microsatellite instability (20). TOP2A is a key enzyme in DNA replication and transcription (21). TOP2A expression is detected in various types of tumors (22), it is typically expressed at high levels in rapidly proliferating cells (23). TYMS is a highly conserved enzyme and essential for cell survival due to its important role in DNA biosynthesis (24–26). TYMS is also an mRNA-binding protein by binding mRNA to coordinately regulate the cellular gene expression (8). TYMS may regulate several key aspects of cell cycle control, including apoptosis and chemosensitivity (8). The high level of TYMS is conducive to the development of cancer, so it is considered to be an oncogene. TYMS is one of the most relevant targets for anti-tumor therapy, a lot of work has been done on TYMS as an anti-tumor target and drug resistance in the past (27–30). IHC staining obtained from the Human Protein Atlas database showed that the expression of TYMS was at high levels consistent with mRNA expression levels. The transcription is associated with promoter methylation (31), to discover the reason for the upregulation of the TYMS gene in HCC, TCGA database was used to analyze the expression of TYMS and its methylation status. We found that the methylation level of TYMS was negatively correlated with the transcription level (**Supplementary Figure 1B**), and its low methylation status in HCC may have contributed to the up-regulated expression. The gene expression profiling also proved that TYMS is up-regulated in metastatic tumor tissues from GSE27635 (**Supplementary Figure 1C**), which contained 24 pairs of intratumoral and peritumoral tissue from HCC

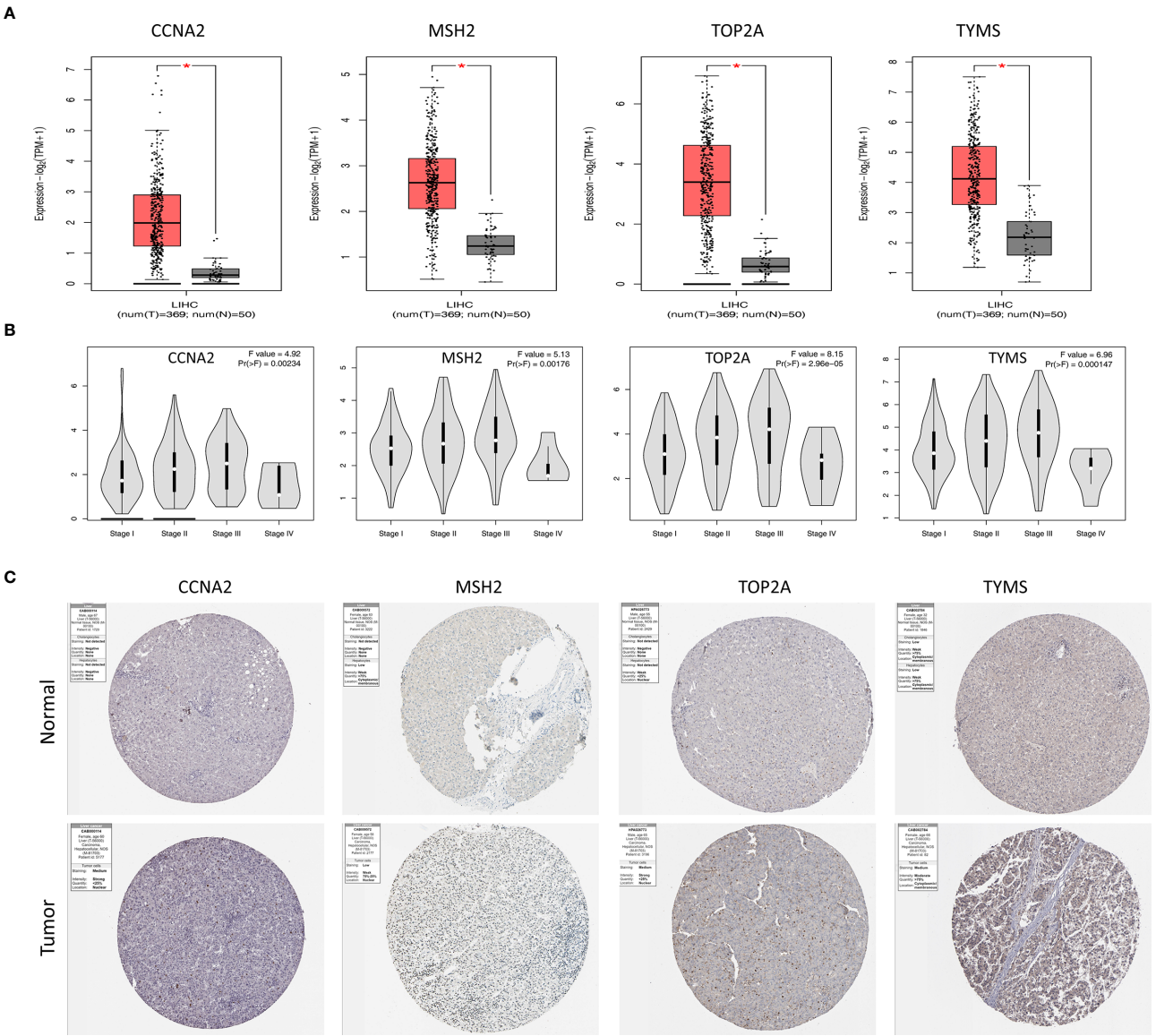

FIGURE 5 | Validation of genes expressions of four hub genes. **(A)** Box plots of CCNA2, MSH2, TOP2A and TYMS expression in TCGA tumor and normal tissues. **(B)** Correlations between differently expressed genes and the pathological TNM stage of HCC patients. **(C)** Representative immunohistochemistry staining of CCNA2, MSH2, TOP2A and TYMS in HCC tissue obtained from the Human Protein Atlas. *P < 0.05.

patients with bone metastases. Compare with microarrays, high-throughput sequencing offers higher accuracy and a larger dynamic range (32). Therefore, the TCGA HCC dataset using high-throughput sequencing technology has much more DEGs compare with GSE28248 and GSE27635 using microarrays. Therefore, the GSE28248 and GSE27635 used in the study may limit the discovery of more HCC metastasis biomarkers and also affect the further verification of biomarkers.

Although a large number of studies have focused on the association of TYMS with carcinogenesis, prognosis, chemotherapy reaction in colorectal cancer (13, 14), ovarian cancer (10), pancreatic cancer (11), cervical cancer (12), and breast cancer (9), few studies focused on the role of TYMS in metastatic HCC patients. More in-depth studies on molecular function and clinical relevance are needed to better understand the role of TYMS in promoting HCC progression and metastasis. Combined with bioinformatics and *vitro* experiments, we analyzed the gene changes and the role of TYMS in HCC. The downregulation of TYMS could reduce the proliferation and invasion of HCC cells. Colony formation assay indicated that the downregulation of TYMS could reduce the proliferation ability of HCC cells. It is possible that TYMS affects single cell proliferation ability. TYMS induces ECM degradation and invasion of HCC cells, which plays an active role in the

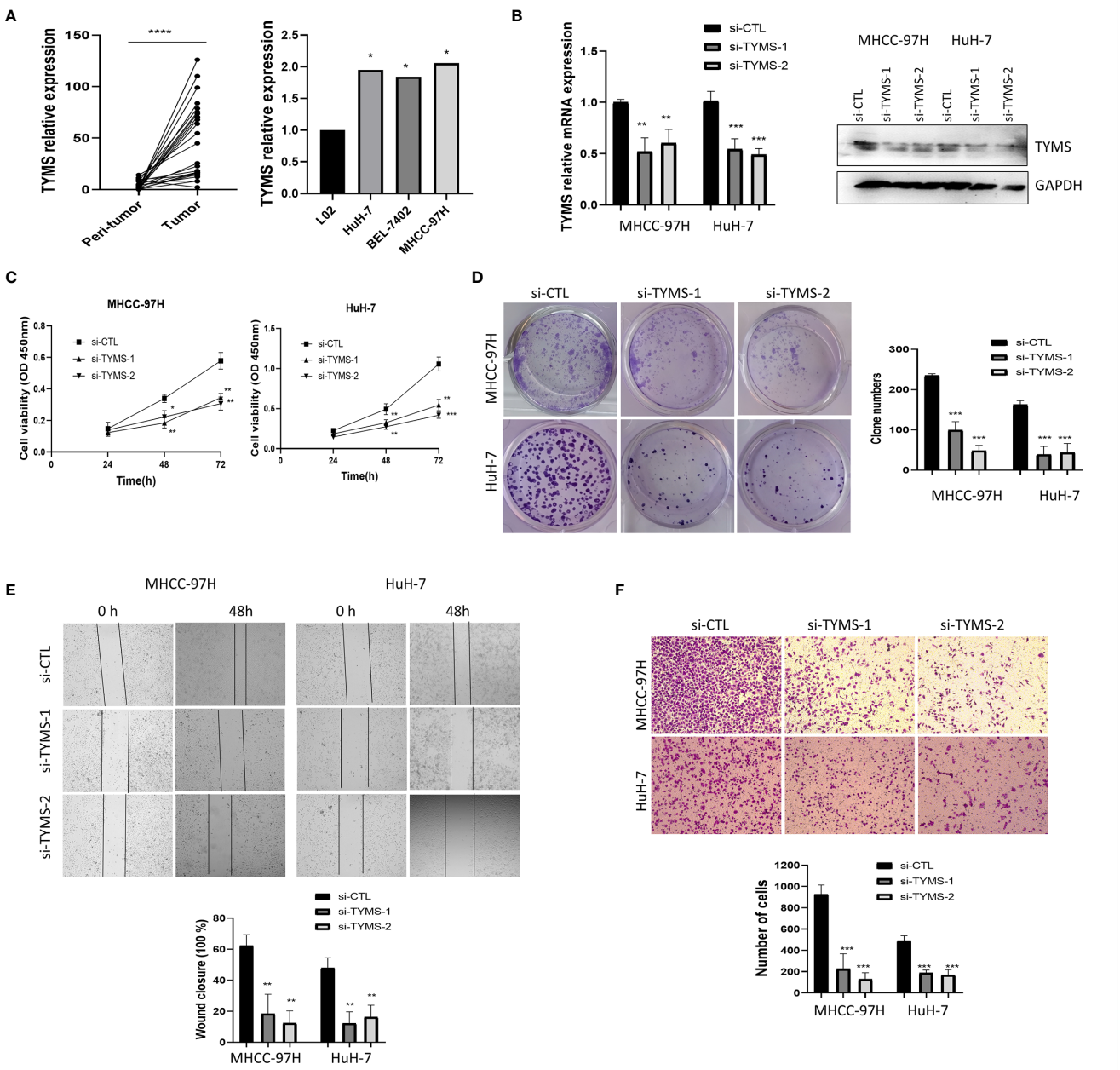

FIGURE 6 | TYMS affect cell growth and invasion in MHCC-97H and HuH-7 cells. **(A)** The mRNA expression of TYMS in 24 pairs of HCC tissues and HCC cell lines. **(B)** The expression of TYMS in MHCC-97H and HuH-7 cells. The expression of TYMS was detected by qPCR and western blot. The $2^{-\Delta\Delta Ct}$ method was used to quantify the mRNA fold changes, GAPDH was used as the internal control. **(C)** CCK8 assay was used to explore the effect of TYMS expression on cell viability. **(D)** Representative images and quantification of colony formation assay. The number of colonies with > 50 cells was scored after 14 days of incubation. **(E)** wound-healing analysis and **(F)** Transwell invasion assays represented the migration and invasion capacity of HCC cells. *P < 0.05, **P < 0.01, ***P < 0.001 and ****p < 0.0001.

metastatic progression of HCC. Results in the present work may reflect the role of TYMS in HCC metastasis and this raises the possibility to assess the clinical association of TYMS and metastasis of HCC. Detection of the TYMS expression in tumor cells is expected to make an early diagnosis of HCC metastasis. Our results provide new opportunities for the treatment of HCC metastasis targeting TYMS. In addition, in the follow-up work, a more detailed molecular mechanism analysis of TYMS is needed to clarify its role in promoting the metastasis of HCC.

As summarized in our work by bioinformatics analysis and *in vitro* experiment, we provided the evidence that TYMS is abnormally expressed in metastatic HCC, TYMS can be used as an indicator for risk stratification that helps to predict the prognosis of HCC. TYMS promotes cell DNA synthesis and ECM degradation, it has an impact on the proliferation and

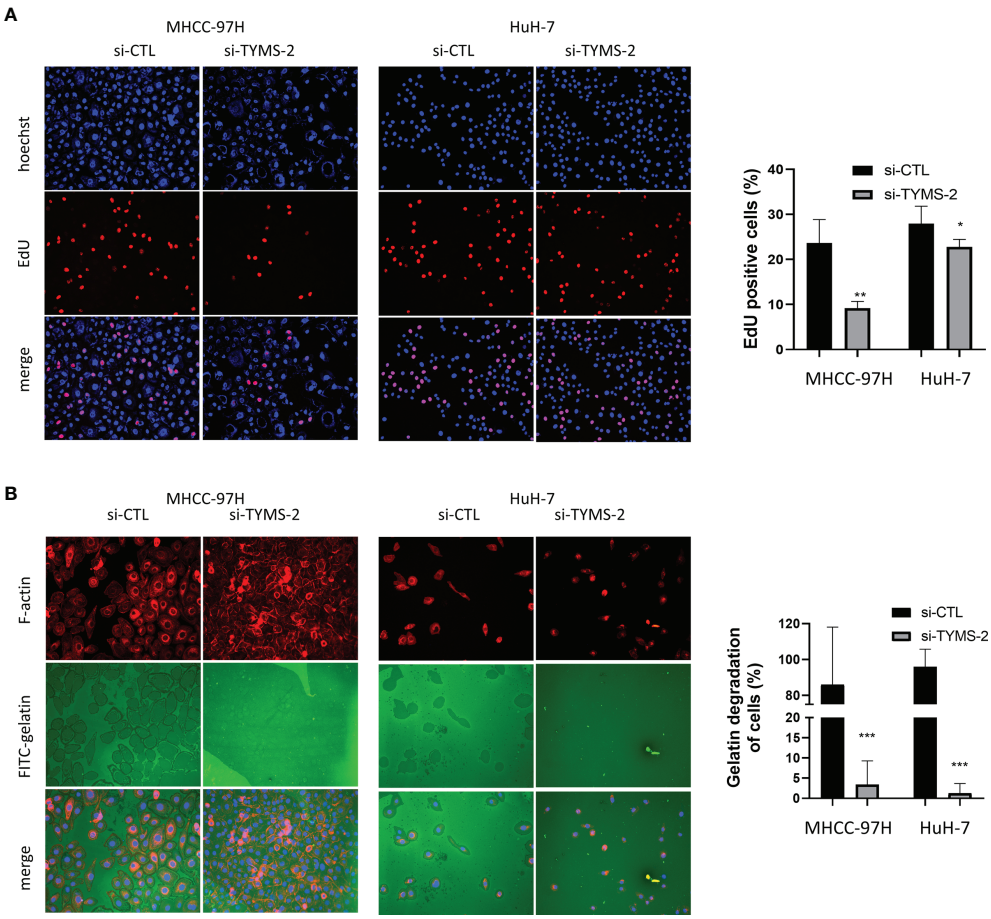

FIGURE 7 | TYMS plays a role in HCC cell's DNA synthesis and invasiveness. **(A)** The EdU incorporation analyses the effects of TYMS on cell proliferation. **(B)** TYMS is necessary for ECM degradation in MHCC-97H and HuH-7 cells. Cells were plated on coverslips coated with FITC- gelatin (green) for 8 h, F-actin was stained with phalloidin (red), and nuclei were stained with DAPI (blue). Gelatin degradation was shown as black areas. *P < 0.05, **P < 0.01, and ***P < 0.001.

invasion of HCC cells. As a prognostic biomarker, TYMS might provide essential information regarding personalized treatment decisions for individual patients and improve the therapeutic gain. It deserves more exploration and demonstration for its potentiality in diagnosis, prognosis, and therapeutic target.

DATA AVAILABILITY STATEMENT

The original contributions presented in the study are included in the article/**Supplementary Material**. Further inquiries can be directed to the corresponding author.

ETHICS STATEMENT

The studies involving human participants were reviewed and approved by Ethical Committee of First Affiliated Hospital of Dalian Medical University.

AUTHOR CONTRIBUTIONS

DD conceived and supervised the study. SL designed experiments. SL, JZ, and LL performed experiments. DD provided new tools and reagents. SL analyzed data. SL wrote the manuscript. DD made manuscript revisions. All authors contributed to the article and approved the submitted version.

FUNDING

This work is supported by a grant from the Natural Science Foundation of China (No. 62072070); Dalian Medical Science Research Project from the Dalian Municipal Health Commission (No. 2012006).

SUPPLEMENTARY MATERIAL

The Supplementary Material for this article can be found online at: https://www.frontiersin.org/articles/10.3389/fonc.2021.762821/full#supplementary-material

REFERENCES

1. Yang JD, Hainaut P, Gores GJ, Amadou A, Plymoth A, Roberts LR. A Global View of Hepatocellular Carcinoma: Trends, Risk, Prevention and Management. *Nat Rev Gastroenterol Hepatol* (2019) 16(10):589–604. doi: 10.1038/s41575-019-0186-y
2. El-Serag HB, Marrero JA, Rudolph L, Reddy KR. Diagnosis and Treatment of Hepatocellular Carcinoma. *Gastroenterology* (2008) 134(6):1752–63. doi: 10.1053/j.gastro.2008.02.090
3. Nguyen DX, Massague J. Genetic Determinants of Cancer Metastasis. *Nat Rev Genet* (2007) 8(5):341–52. doi: 10.1038/nrg2101
4. Fidler IJ. The Pathogenesis of Cancer Metastasis: The 'Seed and Soil' Hypothesis Revisited. *Nat Rev Cancer* (2003) 3(6):453–8. doi: 10.1038/nrc1098
5. Valastyan S, Weinberg RA. Tumor Metastasis: Molecular Insights and Evolving Paradigms. *Cell* (2011) 147(2):275–92. doi: 10.1016/j.cell.2011.09.024
6. Abdallah EA, Fanelli MF, Buim ME, Machado Netto MC, Gasparini Junior JL, Souza ESV, et al. Thymidylate Synthase Expression in Circulating Tumor Cells: A New Tool to Predict 5-Fluorouracil Resistance in Metastatic Colorectal Cancer Patients. *Int J Cancer* (2015) 137(6):1397–405. doi: 10.1002/ijc.29495
7. Amirfallah A, Kocal GC, Unal OU, Ellidokuz H, Oztop I, Basbinar Y. DPYD, TYMS and MTHFR Genes Polymorphism Frequencies in a Series of Turkish Colorectal Cancer Patients. *J Pers Med* (2018) 8(4):45. doi: 10.3390/jpm8040045
8. Liu J, Schmitz JC, Lin X, Tai N, Yan W, Farrell M, et al. Thymidylate Synthase as a Translational Regulator of Cellular Gene Expression. *Biochim Biophys Acta* (2002) 1587(2-3):174–82. doi: 10.1016/s0925-4439(02)00080-7
9. Wang J, Wang B, Bi J, Di J. The Association Between Two Polymorphisms in the TYMS Gene and Breast Cancer Risk: A Meta-Analysis. *Breast Cancer Res Treat* (2011) 128(1):203–9. doi: 10.1007/s10549-010-1314-0
10. Yang D, He Y, Wu B, Deng Y, Wang N, Li M, et al. Integrated Bioinformatics Analysis for the Screening of Hub Genes and Therapeutic Drugs in Ovarian Cancer. *J Ovarian Res* (2020) 13(1):10. doi: 10.1186/s13048-020-0613-2
11. Fu Z, Jiao Y, Li Y, Ji B, Jia B, Liu B. TYMS Presents a Novel Biomarker for Diagnosis and Prognosis in Patients With Pancreatic Cancer. *Med (Baltimore)* (2019) 98(51):e18487. doi: 10.1097/md.0000000000018487
12. Yang HJ, Xue JM, Li J, Wan LH, Zhu YX. Identification of Key Genes and Pathways of Diagnosis and Prognosis in Cervical Cancer by Bioinformatics Analysis. *Mol Genet Genomic Med* (2020) 8(6):e1200. doi: 10.1002/mgg3.1200
13. Jiang H, Li B, Wang F, Ma C, Hao T. Expression of ERCC1 and TYMS in Colorectal Cancer Patients and the Predictive Value of Chemotherapy Efficacy. *Oncol Lett* (2019) 18(2):1157–62. doi: 10.3892/ol.2019.10395
14. Ntavatzikos A, Spathis A, Patapis P, Machairas N, Peros G, Konstantoudakis S, et al. Integrating TYMS, KRAS and BRAF Testing in Patients With Metastatic Colorectal Cancer. *World J Of Gastroenterol* (2017) 23(32):5913–24. doi: 10.3748/wjg.v23.i32.5913
15. Szklarczyk D, Morris JH, Cook H, Kuhn M, Wyder S, Simonovic M, et al. The STRING Database in 2017: Quality-Controlled Protein-Protein Association Networks, Made Broadly Accessible. *Nucleic Acids Res* (2017) 45(D1):D362–d8. doi: 10.1093/nar/gkw937
16. Salic A, Mitchison TJ. A Chemical Method for Fast and Sensitive Detection of DNA Synthesis *In Vivo*. *Proc Natl Acad Sci USA* (2008) 105(7):2415–20. doi: 10.1073/pnas.0712168105
17. Arsic N, Bendris N, Peter M, Begon-Pescia C, Rebouissou C, Gadéa G, et al. A Novel Function for Cyclin A2: Control of Cell Invasion *via* RhoA Signaling. *J Cell Biol* (2012) 196(1):147–62. doi: 10.1083/jcb.201102085
18. Ko E, Kim Y, Cho EY, Han J, Shim YM, Park J, et al. Synergistic Effect of Bcl-2 and Cyclin A2 on Adverse Recurrence-Free Survival in Stage I Non-Small Cell Lung Cancer. *Ann Surg Oncol* (2013) 20(3):1005–12. doi: 10.1245/s10434-012-2727-2
19. Lo YL, Hsiao CF, Jou YS, Chang GC, Tsai YH, Su WC, et al. Polymorphisms of MLH1 and MSH2 Genes and the Risk of Lung Cancer Among Never Smokers. *Lung Cancer* (2011) 72(3):280–6. doi: 10.1016/j.lungcan.2010.10.009
20. Malik SS, Masood N, Asif M, Ahmed P, Shah ZU, Khan JS. Expressional Analysis of MLH1 and MSH2 in Breast Cancer. *Curr Probl Cancer* (2019) 43(2):97–105. doi: 10.1016/j.currproblcancer.2018.08.001
21. Tsavaris N, Lazaris A, Kosmas C, Gouveris P, Kavantzas N, Kopterides P, et al. Topoisomerase I and IIalpha Protein Expression in Primary Colorectal Cancer and Recurrences Following 5-Fluorouracil-Based Adjuvant Chemotherapy. *Cancer Chemother Pharmacol* (2009) 64(2):391–8. doi: 10.1007/s00280-008-0886-4
22. Liu T, Zhang H, Yi S, Gu L, Zhou M. Mutual Regulation of MDM4 and TOP2A in Cancer Cell Proliferation. *Mol Oncol* (2019) 13(5):1047–58. doi: 10.1002/1878-0261.12457
23. Woessner RD, Mattern MR, Mirabelli CK, Johnson RK, Drake FH. Proliferation- and Cell Cycle-Dependent Differences in Expression of the 170 Kilodalton and 180 Kilodalton Forms of Topoisomerase II in NIH-3T3 Cells. *Cell Growth Differ* (1991) 2(4):209–14.
24. Carreras CW, Santi DV. The Catalytic Mechanism and Structure of Thymidylate Synthase. *Annu Rev Biochem* (1995) 64:721–62. doi: 10.1146/annurev.bi.64.070195.003445
25. Garg D, Henrich S, Salo-Ahen OM, Myllykallio H, Costi MP, Wade RC. Novel Approaches for Targeting Thymidylate Synthase to Overcome the Resistance and Toxicity of Anticancer Drugs. *J Med Chem* (2010) 53(18):6539–49. doi: 10.1021/jm901869w
26. Ferrari S, Severi L, Pozzi C, Quotadamo A, Ponterini G, Losi L, et al. Human Thymidylate Synthase Inhibitors Halting Ovarian Cancer Growth. *Vitam Horm* (2018) 107:473–513. doi: 10.1016/bs.vh.2017.12.002
27. Rose MG, Farrell MP, Schmitz JC. Thymidylate Synthase: A Critical Target for Cancer Chemotherapy. *Clin Colorectal Cancer* (2002) 1(4):220–9. doi: 10.3816/CCC.2002.n.003
28. Gmeiner WH. Novel Chemical Strategies for Thymidylate Synthase Inhibition. *Curr Med Chem* (2005) 12(2):191–202. doi: 10.2174/0929867053363432
29. Danenberg PV. Pharmacogenomics of Thymidylate Synthase in Cancer Treatment. *Front Biosci* (2004) 9:2484–94. doi: 10.2741/1410
30. Rustum YM, Harstrick A, Cao S, Vanhoefer U, Yin MB, Wilke H, et al. Thymidylate Synthase Inhibitors in Cancer Therapy: Direct and Indirect Inhibitors. *J Clin Oncol* (1997) 15(1):389–400. doi: 10.1200/jco.1997.15.1.389
31. Cao W, Zhang ZY, Xu Q, Sun Q, Yan M, Zhang J, et al. Epigenetic Silencing of MAL, a Putative Tumor Suppressor Gene, can Contribute to Human Epithelium Cell Carcinoma. *Mol Cancer* (2010) 9:296. doi: 10.1186/1476-4598-9-296
32. Wang Z, Gerstein M, Snyder M. RNA-Seq: A Revolutionary Tool for Transcriptomics. *Nat Rev Genet* (2009) 10(1):57–63. doi: 10.1038/nrg2484

Conflict of Interest: The authors declare that the research was conducted in the absence of any commercial or financial relationships that could be construed as a potential conflict of interest.

frontiers in Oncology

ORIGINAL RESEARCH
published: 23 November 2021
doi: 10.3389/fonc.2021.711448

Norcholic Acid Promotes Tumor Progression and Immune Escape by Regulating Farnesoid X Receptor in Hepatocellular Carcinoma

Yihang Gong[1,2†], Kun Li[1,3†], Yunfei Qin[3†], Kaining Zeng[1], Jianrong Liu[1], Shaozhuo Huang[4], Yewu Chen[1,2], Haoyuan Yu[1,2], Wei Liu[1,2], Linsen Ye[1,2*] and Yang Yang[1*]*

[1] Department of Hepatic Surgery and Liver Transplantation Center, The Third Affiliated Hospital of Sun Yat-sen University, Guangzhou, China, [2] Guangdong Provincial Key Laboratory of Liver Disease Research, The Third Affiliated Hospital of Sun Yat-sen University, Guangzhou, China, [3] Department of Biotherapy Center, The Third Affiliated Hospital of Sun Yat-sen University, Guangzhou, China, [4] Department of General Surgery, The Third Affiliated Hospital, Sun Yat-sen University, Guangzhou, China

OPEN ACCESS

Edited by:
Zongli Zhang,
Qilu Hospital of Shandong University, China

Reviewed by:
Wendong Huang,
City of Hope, United States
Xufeng Tao,
Dalian University of Technology, China

***Correspondence:**
Yang Yang
yysysu@163.com
Linsen Ye
ye_linsen@163.com
Wei Liu
lwei6@mail.sysu.edu.cn

†These authors share first authorship

Specialty section:
This article was submitted to Cancer Molecular Targets and Therapeutics, a section of the journal Frontiers in Oncology

Received: *11 June 2021*
Accepted: *01 November 2021*
Published: *23 November 2021*

Citation:
Gong Y, Li K, Qin Y, Zeng K, Liu J, Huang S, Chen Y, Yu H, Liu W, Ye L and Yang Y (2021) Norcholic Acid Promotes Tumor Progression and Immune Escape by Regulating Farnesoid X Receptor in Hepatocellular Carcinoma. Front. Oncol. 11:711448. doi: 10.3389/fonc.2021.711448

Accumulating evidence shows a close association between various types of bile acids (BAs) and hepatocellular carcinoma (HCC), and they have been revealed to affect tumor immune response and progression mainly by regulating Farnesoid X receptor (FXR). Nevertheless, the roles of Norcholic acid(NorCA) in HCC progression remain unknown yet. In this study, herein we demonstrate that NorCA can promote HCC cell proliferation, migration and invasion through negatively regulating FXR. Additionally, NorCA can increase PD-L1 level on the surfaces of HCC cells and their exosomes, and NorCA-induced exosomes dramatically dampen the function of $CD4^+$T cells, thereby inducing an immunosuppressive microenvironment. Meanwhile, a negative correlation between PD-L1 and FXR expression in human HCC specimens was identified, and HCC patients with $FXR^{low}PD\text{-}L1^{high}$ expression exhibit a rather dismal survival outcome. Importantly, FXR agonist (GW4064) can synergize with anti-PD-1 antibody (Ab) to inhibit HCC growth in tumor-bearing models. Taken together, NorCA can promote HCC progression and immune invasion by inhibiting FXR signaling, implying a superiority of the combination of FXR agonist and anti-PD-1 Ab to the monotherapy of immune checkpoint inhibitor in combating HCC. However, more well-designed animal experiments and clinical trials are warranted to further confirm our findings in future due to the limitations in our study.

Keywords: hepatocellular carcinoma (HCC), bile acids, exosomes, immune microenvironment, Farnesoid X receptor

INTRODUCTION

Bile acids (BAs) are metabolites generated in the liver and synthesized from cholesterol *via* both the nonclassical and classical pathways, which are under the control of specific enzymes (1). The dysmetabolism of BAs can promote the development of HCC associated with obesity or fatty liver (2). In a mouse model of nonalcoholic steatohepatitis-associated HCC, the accumulation of

secondary BAs led to hepatocyte inflammation and contributed to carcinogenesis (3). When the BA pool was reduced by administering 2% cholestyramine in food, the sizes of malignant lesions were significantly decreased (4). The farnesoid X receptor (FXR) modulates BAs homeostasis *via* enterohepatic circulation (5). In the liver, FXR activates small heterodimer partner (SHP) expression, thereby suppressing the level of the cytochrome P450 A1 enzyme, which catalyzes the *de novo* synthesis of BAs from cholesterol (6). The FXR-KO model causes dysregulation of BAs metabolism and spontaneous hepatocarcinogenesis (7). Depletion of FXR is the causative factor for the induction of chronic inflammation, hepatocyte damage and the development of HCC (8, 9). Furthermore, FXR is considered to be a modulator of immune responses in a subset of immune disorders. Increased FXR modulates $CD8^+$ T cell metabolism (10) and downregulates the expression of inflammatory regulators (IFNγ, IL6, and IL1β) in a colitis mouse model (11).

Studies on BAs in HCC have focused on the direct effects of BAs on tumor cells, while the role of BAs in the cross talk between HCC and immune cells remains unclear. Recent studies have reported that Exos play pivotal roles in the cell-to-cell cross talk between HCC and immune cells (12). Exos are endosome-derived nanoscale (30–100 nm) lipid bilayer vesicles that contain several biological factors, including proteins, soluble substances, lipids, and miRNAs. They are transported to target cells to exert vital functions in intercellular cross talk. The characteristics and metabolism of immune cells can be modulated by tumor-derived Exos (13–17). Studies have shown that BAs regulate the immune microenvironment by stimulating the secretion of Exos from macrophages (18). In this study, we identified a new class of BAs and then tried to explore whether this BA class can affect the immune microenvironment of HCC by regulating Exos through FXR. Our study provides a new perspective for the protective effect of FXR in HCC patients. We recommend an FXR agonist combined with an anti-PD-1 antibody for immunotherapy of patients with advanced HCC.

MATERIALS AND METHODS

Patient Samples and Cell Lines

HCC and liver tissues were obtained from the Third Affiliated Hospital of Sun Yat-sen University. All patients had not received antitumor therapy before surgery. The contents of 31 BAs were determined by analyzing the peritumoral liver tissues and tumor samples of 6 patients with HCC who underwent radical resection from June to September in 2019. In our study, each pair of analyzed tumor tissue and peritumoral liver tissue are from the same patient. Samples for immunohistochemistry (IHC) were collected from patients who underwent surgical resection in the same hospital from July 2010 to November 2011. The written informed consent was obtained from each participant. This study was approved by the Ethics Review Board of the Third Affiliated Hospital, Sun Yat-sen University. Humanized Huh-7 and LM3 cells and murine Hepa1-6 cells were obtained from ATCC.

IHC Analysis

The tissues of HCC embedded in paraffin were cut into 4-μm thickness and IHC staining was performed as previously described (19). The following primary antibodies were used in follow-up experiments: SHP (sc-271511; Santa Cruz Biotechnology), FXR (ab129089; Abcam), and PD-L1 (13684S; CST). The staining results were independently analyzed by two pathologists who were blinded to the clinical outcomes. Because of their subcellular localization properties for normal functions, FXR and SHP in the nuclei and PD-L1 in the membranes of HCC cells were stained and scored for further analysis. The staining intensity of tumor cells was scored as 0 (negative), 1 (weak), 2 (moderate), 3 (high). The percentage of positive cells was categorized as follows: 0 (0%), 1 (1% to 25%), 2 (26% to 50%), 3 (51% to 75%), and 4 (76% to 100%). The total IHC staining score was obtained by multiplying the intensity score with the percentage score from 0 to 12. For FXR and SHP, staining scores 0–4 and 6–12 were considered as low and high expression, respectively. For PD-L1, staining scores 0–2 and 3–12 were defined as low and high expression, respectively (20).

BAs Analysis

Ultra-performance liquid chromatography/tandem mass spectrometry (UPLC-MS/MS) was applied to measure the levels of BAs, namely, GLCA, 3-DHCA, LCA, 7-ketoLCA, NorCA, 7-DHCA, LCA S, HCA, UDCA, DCA, TLCA, CDCA-3Gln, TDCA, GDCA, GLCA-S, bUDCA, GHDCA, GHCA, CA, TwMCA, CDCA, TaMCA, THDCA, TLCA-S, THCA, TUDCA, GUDCA, TCA, GCA, GCDCA, and TCDCA, in the tumor and peritumoral liver tissue.

Isolation of $CD4^+$ or $CD8^+$ T Cells and Flow Cytometry

Ficoll centrifugation (Axis-Shield) was used to isolate peripheral blood mononuclear from healthy donor blood samples. After 72 h of exposure to NorCA, LM3 cells or Exos were cocultured with $CD4^+$ and $CD8^+$ T cells that had been stimulated with anti-CD3/CD28 mAb beads. These results were analyzed by FlowJo 10.0 software. The fluorochrome-linked antibodies were applied as follow: anti-human Annexin V-FITC, PI-PE, CD4-APC-Cy7, CD8-FITC, PD-1-BV510, TIM3-PE, and CTLA4-PECY-Cy5.5 (eBioscience). Detailed staining protocols were followed previously described (21).

Bicinchoninic Acid Assay

Bicinchoninic Acid Assay was used to detect protein concentration. The diluted protein was performed by BCA kit (ThermoFisher). The absorbance was detected at a wavelength of 562 nm.

Quantitative Real-Time PCR (qRT-PCR)

Quantitative real-time PCR (qRT-PCR) was performed for mRNA detection using SYBR Green PCR Master Mix (Roche). The relative levels of mRNA were detected using the $2^{-\Delta\Delta Ct}$ method. Primer sequences are listed in **Supplementary Table 1**.

Migration and Invasion Assays

To detect the wound healing ability of Huh-7 and LM3 cells, using a 200 μL pipette tip to scratch a straight wound, then observed and measured immediately and 24 hours after scratching. A 24-well transwell chambers coated with Matrigel (Corning Costar, Cambridge, MA, USA) was used to check cell invasion. The chamber has two culture compartments (upper and lower) separated by a polycarbonate membrane (Corning costar) with a pore diameter of 8 microns. The bottom chamber was filled with 600μL complete medium. 5×10^4 per well cells were seeded in serum-free medium in the upper chamber. After culturing for 30 hours, cells that invaded to the bottom of the membrane were fixed with 4% paraformaldehyde and stained with 0.1% crystal violet, imaged, and counted under a microscope (Zeiss, Gottingen, Germany).

Cell Proliferation Assay

For Cell Counting Kit-8 (CCK-8) assay (Dojindo, Kumamoto, Japan), transfected cells were seeded into 96-well plates at 1000 cells/well, and then, 10 μL of CCK-8 solution was added to each well and incubated for 4 h at 37°C. The absorbance was detected at a wavelength of 450 nm. For 5-ethynyl-2′-deoxyuridine (EdU) assay, transfected cells were seeded in 48-well plates. Next, the cells were stained using the Cell-Light EdU *In Vitro* Kit (RIBOBIO). Nuclei were stained with DAPI before being observed with fluorescence microscopy (Solarbio).

Western Blot Analysis

Western blot analysis was employed as previously described (22). Anti-SHP (sc-271511; Santa Cruz Biotechnology), FXR (ab129089; Abcam), PD-L1 (13684S; CST), NSMase2 (ab68735; Abcam), RAB27A (ab55667; CST, USA), and β-Actin (ab8226; Abcam) were used according to concentration recommended by the manufacturers.

Exos Isolation From Cell Lines

Exos were isolated from HCC cells and collected as described previously (23).

Animal Studies

Male C57BL/6 and FXR-knockout mice aged 5 weeks were purchased from the Model Animal Research Center of Nanjing University (China) and Shanghai Nanfang Research Center for Model Organisms (China), respectively. All mice were raised under specific pathogen-free (SPF) conditions. Before orthotopic implantation operation, the mice were deprived of water for 4 hours and food for 8 hours. 10% chloral hydrate (0.07 mL/10 g) was injected intraperitoneally for anesthesia. The mouse was disinfected with iodophor and fixed in supine position, and then a 1 cm opening was cut out 0.5 cm below the xiphoid process. Cutting the skin, peritoneum and muscle layer in order. The right liver lobe was exposed by slowly pressing the ribs. Hepa1-6 cells (1×10^6 (50 μL)) were injected at an angle of 20° to the liver lobe. The injection extended for 1 cm and was performed slowly. After injection, the needle was pulled out and the hole was pressed for 1 minute until there was no active bleeding. Finally, the tissue was sealed layer by layer. After operation, water and food deprivation were performed for 4 hours. After 21 days, the liver tissues were harvested for detection. For the orthotopic implantation model, NorCA (5 mg/kg per mouse, Toronto Research Chemicals) and GW4064 (30 mg/kg per mouse, Sigma-Aldrich) were intraperitoneally injected. To generate subcutaneous xenograft tumors, Hepa1-6 cells (1×10^6) were suspended in 100 μL of phosphate-buffered saline and inoculated subcutaneously into the left flanks of mice. All mice were randomly divided into a control group and three treatment groups until the tumor volume reached 100 mm^3. IgG2a was given to the control group, and the treatment groups were given intraperitoneal injection of anti-mouse PD-1 *InVivo*MAb (200 μg per mouse, Bio X Cell) every 3 days or GW4064 every day. For the subcutaneous xenograft model, NorCA was intratumorally injected. The microcaliper was used to measure the volume of the tumors twice per week. Tumor volume = (length × $width^2$)/2. The animal research in this study were approved by the Institutional Animal Care and Use Committee of the Third Affiliated Hospital of Sun Yat-sen University (approval no 00256189).

Lentiviral Vectors and Cell Infection

For stable knockdown of SHP and overexpression FXR, Hepa1-6 cells were seeded in 6-well plates (2.5×10^5 cells) with antibiotic-free medium for 24 h. Then, they were infected with lentiviral hU6-SHP-ubiquitin-EGFP-IRES-puromycin and Ubi-FXR-CBh-gcGFP-IRES-puromycin or the corresponding control lentivirus (GeneChem Co., Ltd., Shanghai, China) at a multiplicity of infection (MOI) of 20 pfu/cell. The selection of stably transfected cells was performed 48 **h** later with 1 μg/mL puromycin (Sigma-Aldrich). The transfection efficiency of cherry fluorescent protein was observed by an inverted fluorescence microscope.

Statistical Analysis

SPSS 17.0 (SPSS, Inc., Chicago, IL, USA) and Prism 6.0 (GraphPad Software, La Jolla, CA, USA) were used to analyze the data. The quantitative data were expressed as the means ± SD. Mann–Whitney *U* test, Student's *t* test or Wilcoxon rank-sum test were used to compare two groups. $\chi 2$ test was used for correlation analysis. Kaplan-Meier survival analysis with log-rank test was performed to determine Overall survival (OS) and time-to-recurrence (TTR). The data were analyzed using two-sided test and *P* value of ≤ 0.05 was considered statistically significant in all analyses.

RESULTS

UPLC–MS/MS Metabolomic Analysis

UPLC–MS was used to measure the concentrations of the 31 BAs in the analysis. In the subsequent multidimensional data screening process, PLS-DA (**Figure 1A**) and OPLS-DA (**Figure 1B**) patterns

were used to show the aggregation trend of the tissue samples. The control group refers to 6 peritumoral liver tissues, and the model group refers to 6 tumor tissues paired with corresponding peritumoral tissues. The two groups showed obvious distinction, and these differences indicated that PLS-DA and OPLS-DA models were capable of distinguishing the tumor from the peritumoral liver tissue based on the BA levels. The permutation test was applied to estimate the effectiveness of the classification model. The intercept of Q2Y with a threshold less than zero indicates that this is a valid model (**Figure 1C**). The representative differential BAs were examined using the univariate statistical analysis Mann-Whitney U test (**Figure 1D**). The 31 differential BAs obtained by univariate statistical analysis are illustrated (**Figure 1E**). We found that NorCA was increased in peritumoral liver tissue compared to tumor tissue.

NorCA Promotes the Migration and Invasion of HCC Cells

Although different types of BAs may have opposite effects in tumorigenesis (24, 25), the effect of NorCA on tumors is still unknown. In order to explore the influence of NorCA on HCC, we used NorCA to stimulate LM3 and Huh-7 cells and detected the migration and invasion of cells. To exclude the activation of these proteins through apoptosis induced by NorCA, we used flow cytometry and CCK-8 assays to detect the apoptosis of HCC cells after NorCA exposure. The toxicity of 200 μM NorCA was negligible in Huh-7 and LM3 cells (**Supplementary Figures 1A, B**). Our results showed that coculture with NorCA resulted in enhanced the migration (3.5- and 2.5-fold) and invasion (2.3- and 1.9-fold) abilities of the LM3 (**Figures 2A, B**) and Huh-7 (**Figures 2C, D**) cells. Based on a mass spectrometry analysis of the properties of the 31 BAs, a Pearson's correlation analysis revealed that NorCA and GDCA were positively related (**Supplementary Figure 2**). The conjugated bile acid GDCA promoted the growth of tumors by downregulating the expression of FXR (26). Therefore, we hypothesized that NorCA can promote HCC migration and invasion by inhibiting FXR. GW4064 has been identified as an FXR agonist through experiments in which FXR was activated (27). As shown in **Figures 2A, B**, preincubation with while GW4064 efficiently prevented the HCC cells migration and invasion induced by NorCA. Meanwhile, in the cell proliferation assay, NorCA

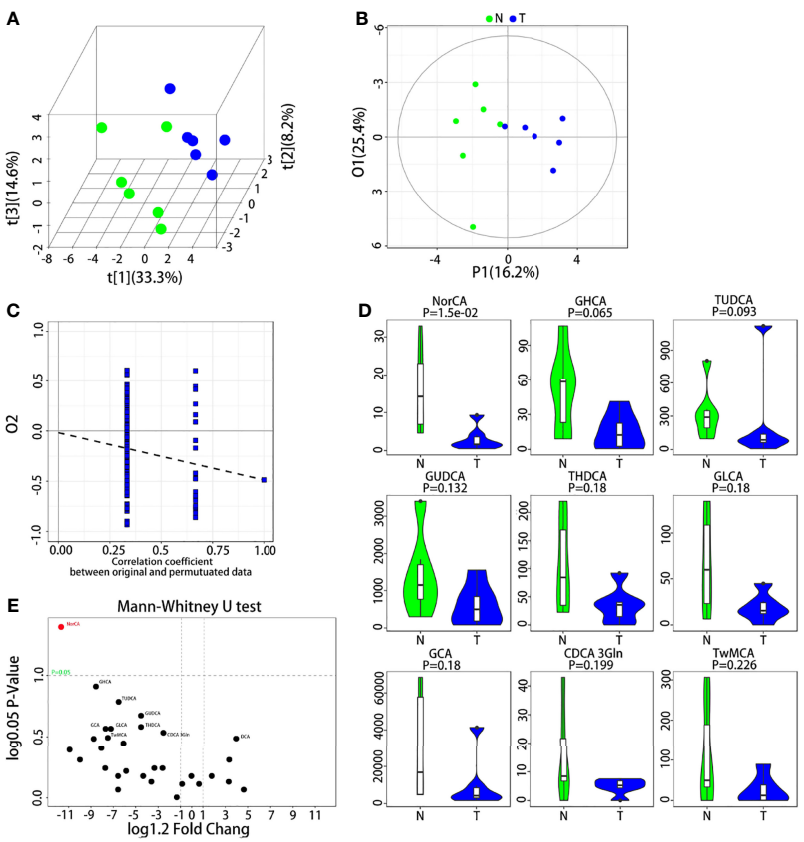

FIGURE 1 | UPLC-MS/MS analysis of BAs in the tumor and peritumoral liver tissue. **(A, B)** Quantitative data of the BAs in the tumor and peritumoral liver tissue were analyzed with a PLS-DA plot and OPLS-DA plot, respectively. **(C)** Permutation test was applied to estimate the effectiveness of the advanced model. **(D)** The differential BAs were examined by Mann-Whitney U test for univariate statistical analysis, and we used violin diagrams to display the top 9 representative BAs. **(E)** All BAs obtained through the univariate statistical analysis are shown.

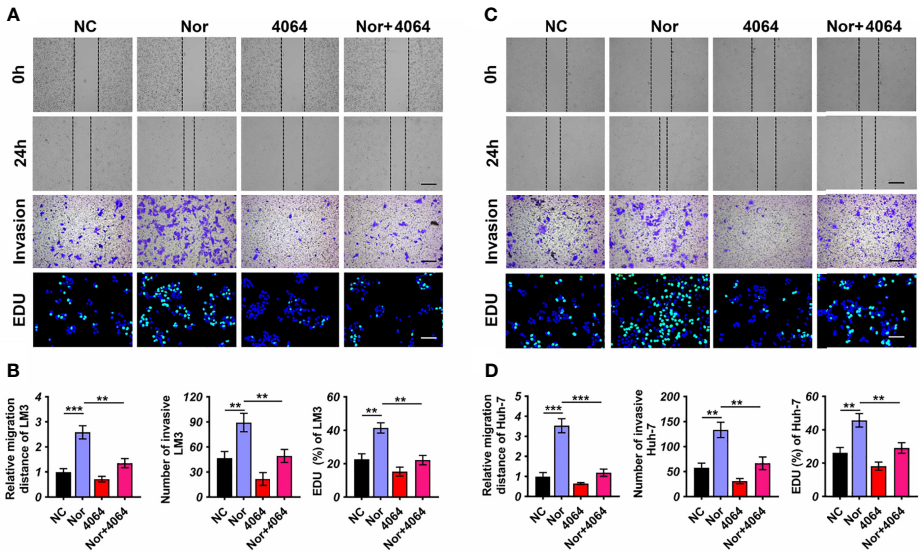

FIGURE 2 | NorCA enhances the ability of HCC cells to migrate and invade and promotes cell proliferation. **(A-D)** Data showed that after NorCA exposure, the migration and invasion abilities of Huh-7 cells and LM3 cells were enhanced, while the FXR agonist GW4064 restored these trends (scale bar, 100 μm). EdU assay showed the consistent results (scale bar, 100 μm). **p < 0.01, and ***p < 0.001, n = 3. Cells treated with BSA were used as a negative control.

markedly promoted the proliferation of Huh-7 and LM3 cells and GW4064 restored these phenomena (**Figures 2A–D**).

NorCA Upregulates PD-L1 Expression Through the FXR-SHP Axis

To further explore how NorCA exerts its protumorigenic effect through FXR, we first determined the effect of NorCA on mRNA levels on downstream targets of FXR, including SHP, BSEP, ABCB4, CYP3A4, FGF19, and OSTα1. Our results indicated that the mRNA level of SHP was significantly downregulated by NorCA (**Supplementary Figure 3**). FXR is a nuclear receptor that plays vital role in the tumorigenicity of the liver by regulating SHP (28), and SHP can regulate the level of PD-L1 in cancer cells (20, 29). Consistent with these studies, Western blot showed that the NorCA-induced upregulation of PD-L1 expression involves the FXR/SHP signaling pathway, and preincubation with GW4064 efficiently reversed the decreased level of FXR and SHP and downregulated the expression of PD-L1 in a dose-dependent manner. (**Figure 3A** and **Supplementary Figure 4**). To verify the safety of the drug, we intraperitoneally injected mice with NorCA and then assessed liver and kidney function, performed blood tests and weighed the mice. We found that the toxicity of NorCA to C57BL/6 mice was negligible (**Supplementary Figure 5** and **Supplementary Table 2**). Moreover, our results showed that NorCA promoted tumor growth compared with the control group, and GW4064 significantly reduced tumor sizes in the treatment groups (**Figure 3B**). Consistently, HE staining also supports this result (**Supplementary Figure 6**). We further examined the expression of FXR, SHP and PD-L1 in liver tissue. Consistently, PD-L1 protein was significantly increased while FXR and SHP proteins were downregulated in the liver tissue of the NorCA group. Moreover, GW4064 treatment reversed these trends (**Figure 3C** and **Supplementary Figure 7**). Next, stable FXR overexpression (OE-FXR) in Hepa1-6 cells was utilized to explore the role of FXR in hepatocarcinogenesis induced by NorCA. FXR overexpression was confirmed by Western blot in Hepa1-6 (**Supplementary Figure 8**). The results showed that compared with control group, OE-FXR mice exhibited significantly decreased tumor size under NorCA stimulation (**Figure 3D**). Furthermore, stable SHP silencing in murine cancer cells was verified (**Supplementary Figure 9**), and our data indicated that knocking down SHP expression obviously promoted the tumorigenicity of Hepa1-6 cells induced by NorCA in mice (**Figure 3E**). In summary, these data demonstrate that NorCA drives tumor growth and tumorigenicity *via* FXR-SHP-PD-L1 signaling.

NorCA Regulates Tumor-Derived Exos Through FXR to Affect the Immune Microenvironment

We further explored the impact of NorCA on the immune microenvironment. We characterized immune cell changes by flow cytometry using immune checkpoint-specific markers (PD-1, CTLA-4 and TIM3). However, we observed that the indicators of these immune checkpoints of $CD4^+$ T cells and $CD8^+$ T cells were not changed after coculture with LM3 cells induced by NorCA (**Figure 4A**). Moreover, we did not observe changes in these indicators when immune cells were cocultured in medium taken from cultures of LM3 cells induced by NorCA (**Figure 4A**).

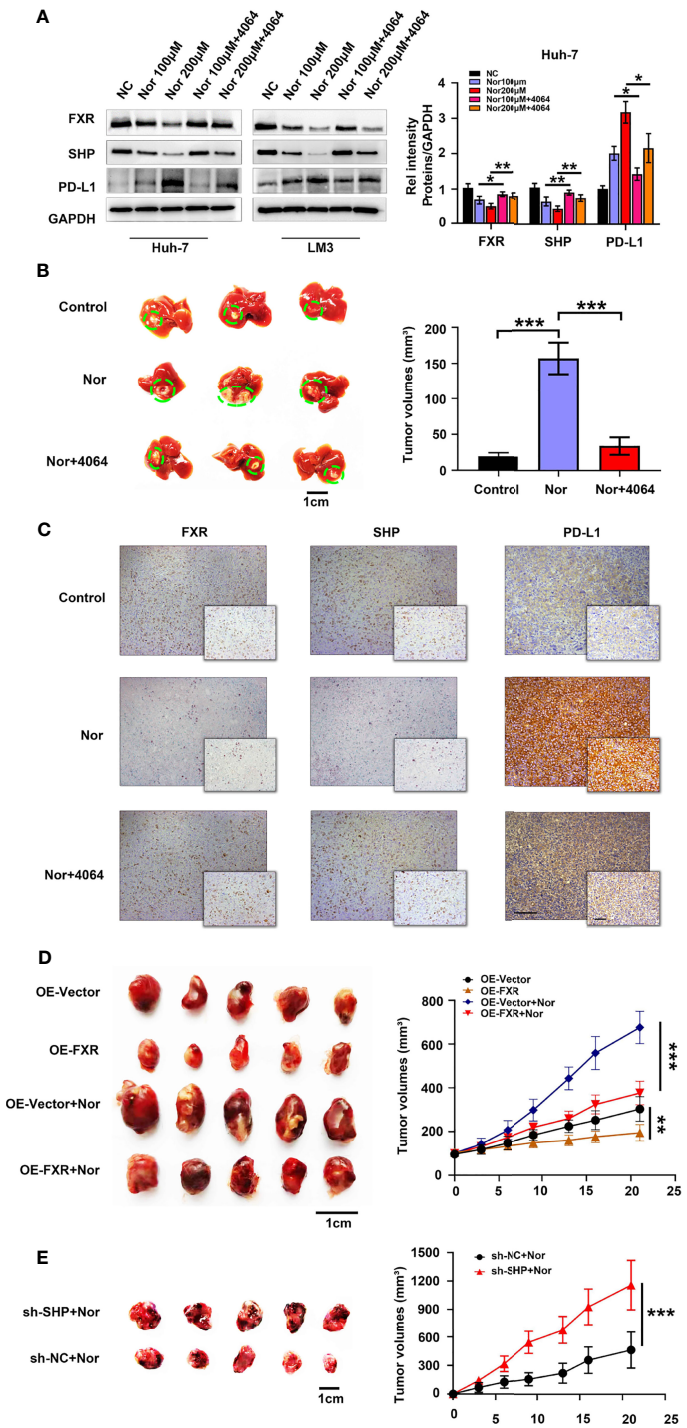

FIGURE 3 | NorCA contributes to tumor growth and tumorigenicity *via* FXR-SHP-PD-L1 signaling. **(A)** Left graph, the FXR, SHP, and PD-L1 levels in Huh-7 and LM3 cells were detected by western blot analysis. Right graph, gray value analysis of all proteins. **(B)** Left graph, schematic representation of the orthotopic implantation formed by Hep1-6 cells. Mice treated with PBS (n=5), NorCA alone (n=5) or NorCA plus GW4064 (n=5). Right graph, quantification of tumor volumes in different groups. **(C)** Typical pictures of FXR, SHP and PD-L1 staining in orthotopic implantation models (Large figure: 200× magnification, scale bar, 100 μm. Small figure: 400× magnification, scale bar, 100 μm). **(D)** Left image, comparing the tumor volume of OE-FXR mice (n=7) with the tumor volume of OE-Vector (n=7) mice with or without NorCA treatment. Right graph, quantification of the tumor volumes in different groups. **(E)** Left graph, Hep1-6 cells with or without SHP knocked down were subcutaneously injected into mice. Tumor volumes in the SHP-knockdown group (n=5) was obviously higher than that in the control group (n=5). Right graph, quantification of tumor volumes of different groups. *$p < 0.05$, **$p < 0.01$, and ***$p < 0.001$.

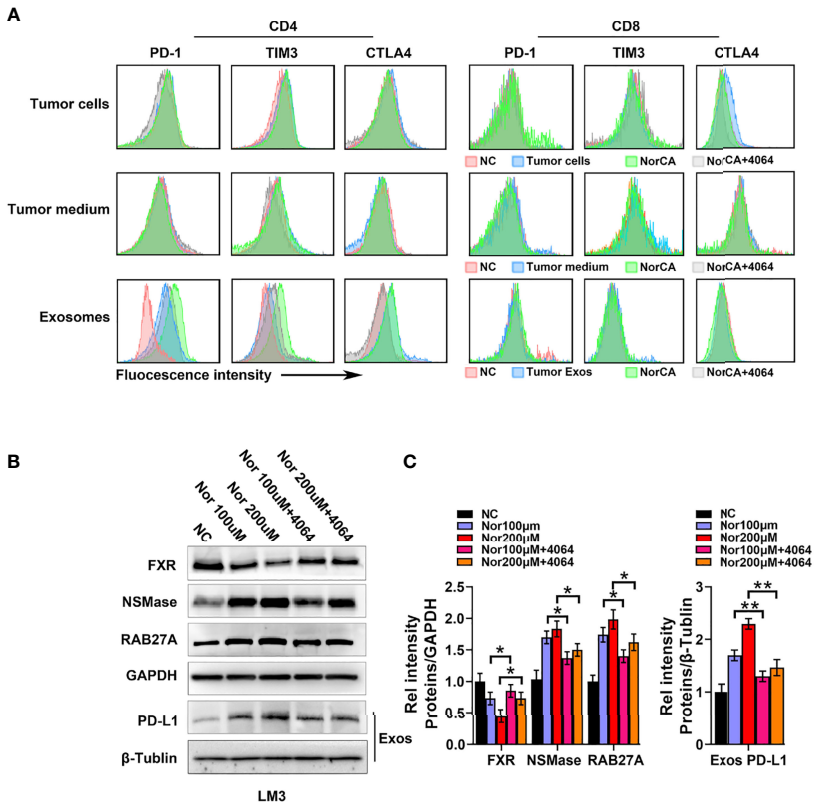

FIGURE 4 | NorCA mediates the immune microenvironment by promoting tumor-derived Exos secretion. **(A)** After cells were exposed to NorCA, flow cytometry was applied to analyze the change in immune checkpoint-specific markers (PD-1, CTLA-4, and TIM3) in $CD4^+$ T cells and $CD8^+$ T cells cocultured with tumor cells, medium from tumor cell or tumor-derived Exos. Tumor-derived Exos regulated $CD4^+$ T cells, as evidenced by the significantly higher expression of PD-1 and TIM3. **(B)** The FXR, NSMase, and RAB27A levels in tumor cells and PD-L1 levels in the tumor-derived Exos were detected using western blot analysis. **(C)** gray value analysis of all proteins. *$p < 0.05$ and **$p < 0.01$.

Deoxycholic acid can regulate macrophage-derived Exos to regulate the immune microenvironment (21). We hypothesized that NorCA-derived Exos (N-Exos) can play a role in modulating immune cells during tumor development. We found that N-Exos extracted from LM3 cells regulated $CD4^+$ T cell protein expression, as evidenced by significantly higher expression of PD-1 and TIM3 but did not affect the expression of CTLA-4. Furthermore, N-Exos treated with GW4064 reversed these trends. However, these phenomena were not observed in $CD8^+$ T cells (**Figure 4A**). To explore how NorCA affects tumor-derived Exos, we measured the protein expression of NSMase and RAB27A, which regulate the synthesis and secretion of Exos. Data showed that NorCA treatment increased the level of NSMase and RAB27A (**Figures 4B, C**). In addition, the total amount of exosomes in different treatment groups was detected by Bicinchoninic Acid Assay (BCA), the data was consistent with the previous results (**Supplementary Figure 10**). Furthermore, NorCA also upregulated PD-L1 expression on Exos secreted from HCC cells (**Figures 4B, C**). Moreover, GW4064 reversed the increased generation and secretion of Exos and the increased level of PD-L1. The results suggest that NorCA may create strong immunosuppressive microenvironment to promote the immune escape of HCC cells.

Upregulation of PD-L1 Level by FXR Is Used to Stratify HCC Patients

Taken together, these data showed that FXR can regulate PD-L1 through transrepression and SHP signaling in HCC cells. Considering this foundation, we first sought to explore the relationship between FXR and PD-L1 *in vivo*. A total of 156 HCC specimen cohorts were used to estimate PD-L1 and FXR expression by IHC staining. Interestingly, the intensity of the PD-L1 staining was distinctly higher in "FXR low" samples than in "FXR high" samples (**Figure 5A**). The spearman correlation analysis indicated a statistically significant negative correlation between PD-L1 and FXR in the HCC tissues (**Supplementary Figure 11**). We found that the proportion of $FXR^{low}PD\text{-}L1^{high}$ subgroup was 35% (55/156) in the HCC samples. OS is defined as the time from the end of the first operation to death (for any reason). TTR is defined as the time from the end of the first operation to the first recurrence. The OS and TTR for all 3 subgroups ($FXR^{low}PD\text{-}L1^{high}$, $FXR^{high}PD\text{-}L1^{low}$, and $FXR^{high}PD\text{-}L1^{high}$ and $FXR^{low}PD\text{-}L1^{low}$) are presented in **Figures 5B, C**. Here, we found that the $FXR^{low}PD\text{-}L1^{high}$ subgroup had a significantly shorter OS ($p<0.001$) and TTR ($p=0.001$) than the $FXR^{high}PD\text{-}L1^{low}$ HCC groups. In order to

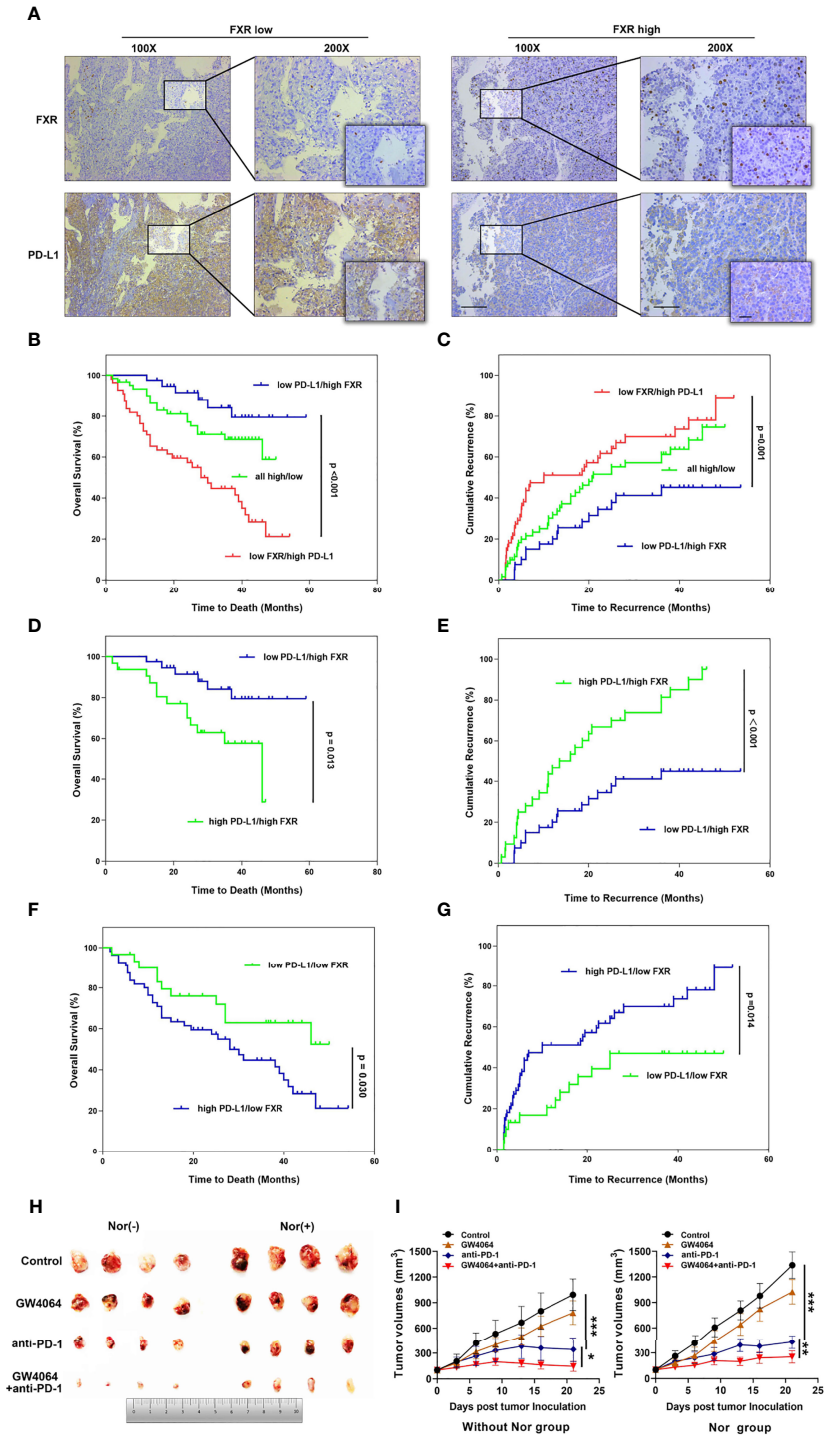

FIGURE 5 | The relevance of FXR to PD-L1 level in HCC samples and the FXR agonist exerting synergistic effects with anti-PD-1 Ab in the mouse model. **(A)** Immunohistochemical staining was performed with 156 HCC tissues. Representative images of $FXR^{low}PD\text{-}L1^{high}$ staining and $FXR^{high}PD\text{-}L1^{low}$ staining of serial sections of HCC tissues are displayed at 100× (left graph), 200× (right graph), 400× (right small graph) magnifications (scale bar, 100 μm). **(B, C)** The OS and TTR of postoperative HCC patients based on both FXR and PD-L1 expression. Patients with $FXR^{low}PD\text{-}L1^{high}$ displayed the shortest OS ($p<0.001$, log-rank test) and TTR ($p=0.001$, log-rank test). **(D–G)** The OS and TTR for 4 subgroups ($FXR^{high}PD\text{-}L1^{high}$ VS $FXR^{high}PD\text{-}L1^{low}$, and $FXR^{low}PD\text{-}L1^{high}$ and $FXR^{low}PD\text{-}L1^{low}$). **(H)** Mice were inoculated subcutaneously with 1×10^6 Hep1-6 cells and treated with anti-PD-1 Ab, IgG2a, GW4064 or anti-PD-1+GW4064 after the tumors reached 100 mm^3. **(I)** With (right graph) or without (left graph) NorCA exposure, the tumor growth in the single-agent therapy group (n = 5) was compared with the combination therapy group (n = 5). *$p < 0.05$, **$p < 0.01$, and ***$p < 0.001$.

further isolate the potential effect of the relationship between FXR and PD-L1, we next compare identical levels of FXR with different levels of PD-L1. The data showed that whether in the FXRhigh or FXRlow group, the PD-L1low subgroup showed better OS and TTR than the PD-L1high expression group (**Figures 5D–G**). These data indicated that PD-L1 is a prognostic factor independent of FXR.

FXR Agonist Combined With Anti-PD-1 Ab in the HCC Syngeneic Mouse Model

Because NorCA showed an immunomodulatory effect in $CD4^+$ T cells, we hypothesized that an FXR agonist in combination with an immune checkpoint inhibitor may have synergistic antitumor effect. Thus, we detected the antitumor therapeutic ability of GW4064 combined with anti-PD-1 Ab in the mouse model. In the group with or without NorCA, compared with the nontreatment group, GW4064 impeded tumor growth while the anti-PD-1 Ab significantly depressed tumor progress (**Figure 5H**). GW4064 combined with anti-PD-1 Ab treatment led to tumor regression and exhibited the most effective antitumor ability (**Figure 5I**). Thus, GW4064 combined with anti-PD-1 Ab treatment exhibited potent antitumor capacity because of the immune-activating efficacy of anti-PD-1 Ab.

DISCUSSION

Here, we identified a previously unrecognized subset of protumorigenic bile acid and employed various analytic strategies to assess the biological effects and mechanisms of this bile acid *in vivo* and *in vitro*. Our research illustrated that the FXR-SHP-PD-L1 axis may be a new way for NorCA to promote the tumorigenesis of HCC cells. Additionally, NorCA can increase the secretion of Exos from HCC cells, and N-Exos play roles in regulating $CD4^+$ cells during tumor progression. Specifically, compared with either therapy administered alone to the HCC tumor-bearing syngeneic model mice, a combination treatment consisting of FXR agonist plus an anti-PD-1 Ab obviously inhibited tumor development and showed potent antitumor ability.

Recently, BAs have been recognized as pivotal contributors to the etiopathogenesis of gastroenteric disorder and tumors. According to the report, BAs were enriched in cancer patients and were associated with poor prognosis (30). However, different BAs that exist in tumor microenvironments exhibit distinct efficiencies and functions (31, 32). Important secondary BAs, such as TCDCA, GCA, GCDCA, and GDCA, have all been revealed as etiologic agents in gastrointestinal tumors (33). Consistent with these studies, we illustrated that in the context of HCC, NorCA, a previously unrecognized BA subset, exhibited protumorigenic properties in the present study. FXR has been demonstrated to be a regulatory element of immune responses in different diseases in addition to its role in modulating BA metabolism (34, 35). However, the correlation between the immune microenvironment and FXR in HCC remains poorly understood. Here, we demonstrated that FXR decreases the level of PD-L1 in HCC cells under NorCA exposure. Exos have emerged as vital contributors in HCC etiopathogenesis, and the list of indicated tumor-derived Exos that regulate immunomodulatory effects is increasing (36, 37). However, few studies have focused on FXR and Exos, and the potential interaction between them remains largely unknown. Metastatic melanoma releases high levels of extracellular vesicles, mainly in the form of exosomes, carrying PD-L1 on its surface (38). Interestingly, our results indicated that FXR can impede the generation and secretion of tumor Exos, and an FXR agonist can inhibit the increased expression of PD-L1 on N-Exos while restoring the modulation of $CD4^+$ T cells by N-Exos. Therefore, we have identified a new function of FXR, which exerts pivotal effect in the immune microenvironment, not only by regulating the level of PD-L1 in HCC cells but also by affecting tumor-derived Exos to regulate $CD4^+$ T cell immune costimulatory targets.

Given that NorCA can exert an immunosuppressive effect by regulating PD-L1 through FXR in HCC cells, we further explored the relevance of FXR to PD-L1 *in vivo*. Moreover, a negative correlation between PD-L1 and FXR level was observed in 156 HCC patients. We identified the $FXR^{low}PD\text{-}L1^{high}$ and $FXR^{high}PD\text{-}L1^{low}$HCC subgroups. FXR clearly downregulated PD-L1 in HCC cells, and the $FXR^{high}PD\text{-}L1^{low}$ subgroup was associated with a better outcome for HCC patients. Our data indicate that this relevance may be due to the high expression of FXR in HCC cells, which inhibits PD-L1 level and thereby acting as a protective contributor against cancer progress. On the contrary, the $FXR^{low}PD\text{-}L1^{high}$ subgroup was correlated with a poor prognosis. In particular, immune checkpoint inhibitors represented by PD-L1/PD-1-blocking antibodies have obvious curative effect on the treatment of patients with advanced HCC (39). However, not all patients show a complete response or benefit from anti-PD-1/PD-L1 therapy. Because of the complexity of immunomodulatory mechanisms and the heterogeneity of tumors, combination therapy is a promising clinical treatment that can overcome the limitations of single-agent therapy (40). In agreement with this notion, our experiments indicated that combination treatment with an FXR agonist plus an anti-PD-1 Ab shows preferable antitumor ability in model mice.

There are several limitations in our study. First, evidence have demonstrated that other types of BAs can also increase or decrease FXR expression and participate in tumor progression (41). Therefore, we should have explored the effect of NorCA treatment on the concentrations and composition of other BAs, so as to determine whether NorCA regulates FXR signaling *via* multiple mechanisms. Second, we did not clarify whether OE-FXR or sh-SHP could affect the level of endogenous NorCA in tumor-bearing mouse models. If OE-FXR or sh-SHP really affected the endogenous NorCA level *in vivo*, the effect of NorCA treatment on tumor growth may be overestimated or underestimated. Last but not least, FXR has been uncovered to regulate the production of various inflammatory cytokines (42). Furthermore, a large number of studies have indicated that some cytokines play a critical role in tumor immune escape (43, 44). Hence, it would be very interesting to explore whether NorCA promotes tumor immune escape by inducing the secretion of specific inflammatory cytokines.

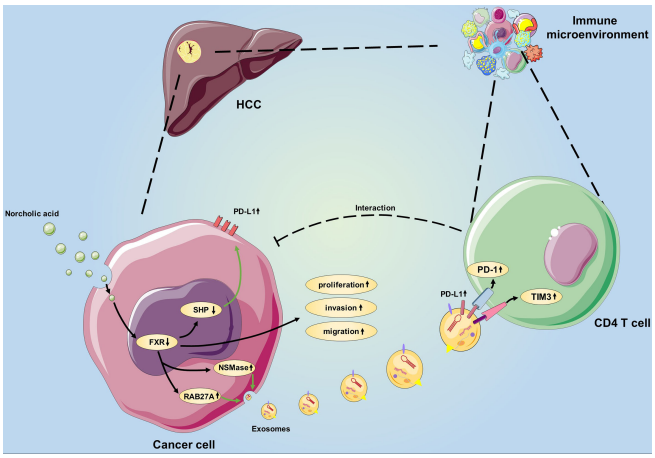

FIGURE 6 | Schematic showing the novel bile acid-mediated immune microenvironment in HCC progression. Considering our study results, we propose a model involving NorCA in HCC development. First, NorCA interacts with HCC cells to promote their ability to express PD-L1 through the FXR-SHP pathway. Second, NorCA enhances the synthesis and secretion of Exos from HCC cells by regulating NSMase and RAB27A. Third, N-Exos have the potential to create an immunosuppressive microenvironment by regulating the function of $CD4^+$ T cell, thus creates beneficial conditions for tumor development.

Herein, we for the first time demonstrate that NorCA can enhance HCC cell proliferation, migration and invasion by negatively regulating FXR. In addition, NorCA can increase PD-L1 levels on the surfaces of HCC cells and their exosomes, and NorCA-induced exosomes significantly impair the function of $CD4^+$ T cells. Furthermore, FXR agonist can synergize with anti-PD-1 Ab to inhibit HCC growth *in vivo*. Taken together, these results suggest that NorCA can facilitate HCC progression and tumor escape (**Figure 6**), and the combination of anti-PD-1 Ab and FXR agonist may be a promising strategy to combat HCC. However, more well-designed animal and clinical trials are warranted to further validate our findings in future due to the limitations in our study.

DATA AVAILABILITY STATEMENT

The original contributions presented in the study are included in the article/**Supplementary Material**. Further inquiries can be directed to the corresponding authors.

ETHICS STATEMENT

The studies involving human participants were reviewed and approved by the Institutional Animal Care and Use Committee of the Third Affiliated Hospital of Sun Yat-sen University. The patients/participants provided their written informed consent to participate in this study. The animal study was reviewed and approved by the Institutional Animal Care and Use Committee of the Third Affiliated Hospital of Sun Yat-sen University.

AUTHOR CONTRIBUTIONS

WL, LY, and YY was the principal investigator and designed the research. YG, KL, YQ, KZ, JL, and SH performed the experiments. YG, KL, YQ, YC, and HY analyzed the results and wrote the manuscript. All authors contributed to the article and approved the submitted version.

FUNDING

This work was supported by: National 13th Five-Year Science and Technology Plan Major Projects of China (2017ZX10203205); National Key R&D Plan (2017YFA0104304); National Natural Science Foundation of China (81770648, 81972286, 81970509); Guangdong Natural Science Foundation (2018A030313259, 2015A030312013); Science and Technology Program of Guangdong Province (2017B020209004, 20169013, 2020B1212060019); Science and Technology Program of Guangzhou city (201508020262); Guangdong Basic and Applied Basic Research Foundation (2019A1515110654); The Fundamental Research Funds for the Central Universities (20ykpy38); China Postdoctoral Science Foundation (2019TQ0369, 2020M672987).

SUPPLEMENTARY MATERIAL

The Supplementary Material for this article can be found online at: https://www.frontiersin.org/articles/10.3389/fonc.2021.711448/full#supplementary-material

REFERENCES

1. Chiang JYL, Ferrell JM. Bile Acids as Metabolic Regulators and Nutrient Sensors. *Annu Rev Nutr* (2019) 39:175–200. doi: 10.1146/annurev-nutr-082018-124344
2. Huang XF, Zhao WY, Huang WD. FXR and Liver Carcinogenesis. *Acta Pharmacol Sin* (2015) 36(1):37–43. doi: 10.1038/aps.2014.117
3. Manley S, Ding W. Role of Farnesoid X Receptor and Bile Acids in Alcoholic Liver Disease. *Acta Pharm Sin B* (2015) 5(2):158–67. doi: 10.1016/j.apsb.2014.12.011
4. Yang F, Huang X, Yi T, Yen Y, Moore DD, Huang W. Spontaneous Development of Liver Tumors in the Absence of the Bile Acid Receptor Farnesoid X Receptor. *Cancer Res* (2007) 67(3):863–7. doi: 10.1158/0008-5472.CAN-06-1078
5. Chávez-Talavera O, Tailleux A, Lefebvre P, Staels B. Bile Acid Control of Metabolism and Inflammation in Obesity, Type 2 Diabetes, Dyslipidemia, and Nonalcoholic Fatty Liver Disease. *Gastroenterology* (2017) 152(7):1679–94.e1673. doi: 10.1053/j.gastro.2017.01.055
6. Goodwin B, Jones SA, Price RR, Watson MA, McKee DD, Moore LB, et al. A Regulatory Cascade of the Nuclear Receptors FXR, SHP-1, and LRH-1 Represses Bile Acid Biosynthesis. *Mol Cell* (2000) 6(3):517–26. doi: 10.1016/S1097-2765(00)00051-4
7. Liu N, Meng Z, Lou G, Zhou W, Wang X, Zhang Y, et al. Hepatocarcinogenesis in FXR-/- Mice Mimics Human HCC Progression That Operates Through HNF1α Regulation of FXR Expression. *Mol Endocrinol* (2012) 26(5):775–85. doi: 10.1210/me.2011-1383
8. Iracheta-Vellve A, Calenda CD, Petrasek J, Ambade A, Kodys K, Adorini L, et al. FXR and TGR5 Agonists Ameliorate Liver Injury, Steatosis, and Inflammation After Binge or Prolonged Alcohol Feeding in Mice. *Hepatol Commun* (2018) 2(11):1379–91. doi: 10.1002/hep4.1256
9. Takahashi S, Tanaka N, Fukami T, Xie C, Yagai T, Kim D, et al. Role of Farnesoid X Receptor and Bile Acids in Hepatic Tumor Development. *Hepatol Commun* (2018) 2(12):1567–82. doi: 10.1002/hep4.1263
10. Campbell C, Marchildon F, Michaels AJ, Takemoto N, van der Veeken J, Schizas M, et al. FXR Mediates T Cell-Intrinsic Responses to Reduced Feeding During Infection. *Proc Natl Acad Sci U S A* (2020) 117(52):33446–54. doi: 10.1073/pnas.2020619117
11. Vavassori P, Mencarelli A, Renga B, Distrutti E, Fiorucci S. The Bile Acid Receptor FXR Is a Modulator of Intestinal Innate Immunity. *J Immunol (Baltimore Md 1950)* (2009) 183(10):6251–61. doi: 10.4049/jimmunol.0803978
12. Wu Q, Zhou L, Lv D, Zhu X, Tang H. Exosome-Mediated Communication in the Tumor Microenvironment Contributes to Hepatocellular Carcinoma Development and Progression. *J Hematol Oncol* (2019) 12(1):53. doi: 10.1186/s13045-019-0739-0
13. Kim JW, Wieckowski E, Taylor DD, Reichert TE, Watkins S, Whiteside TL. Fas Ligand-Positive Membranous Vesicles Isolated From Sera of Patients With Oral Cancer Induce Apoptosis of Activated T Lymphocytes. *Clin Cancer Res* (2005) 11(3):1010–20.
14. Taylor DD, Gercel-Taylor C. Exosomes/microvesicles: Mediators of Cancer-Associated Immunosuppressive Microenvironments. *Semin Immunopathol* (2011) 33(5):441–54. doi: 10.1007/s00281-010-0234-8
15. Kimura K, Hohjoh H, Fukuoka M, Sato W, Oki S, Tomi C, et al. Circulating Exosomes Suppress the Induction of Regulatory T Cells *via* Let-7i in Multiple Sclerosis. *Nat Commun* (2018) 9(1):17. doi: 10.1038/s41467-017-02406-2
16. Ludwig S, Floros T, Theodoraki MN, Hong CS, Jackson EK, Lang S, et al. Suppression of Lymphocyte Functions by Plasma Exosomes Correlates With Disease Activity in Patients With Head and Neck Cancer. *Clin Cancer Res* (2017) 23(16):4843–54. doi: 10.1158/1078-0432.CCR-16-2819
17. Gao L, Wang L, Dai T, Jin K, Zhang Z, Wang S, et al. Tumor-Derived Exosomes Antagonize Innate Antiviral Immunity. *Nat Immunol* (2018) 19(3):233–45. doi: 10.1038/s41590-017-0043-5
18. Xu X, Cheng J, Luo S, Huang D, Xu J, Qian Y, et al. Deoxycholic Acid-Stimulated Macrophage-Derived Exosomes Promote Intestinal Metaplasia and Suppress Proliferation in Human Gastric Epithelial Cells. *Eur J Pharmacol* (2020) 887:173566. doi: 10.1016/j.ejphar.2020.173566
19. Gong Y, Zou B, Peng S, Li P, Zhu G, Chen J, et al. Nuclear GAPDH Is Vital for Hypoxia-Induced Hepatic Stellate Cell Apoptosis and Is Indicative of Aggressive Hepatocellular Carcinoma Behavior. *Cancer Manage Res* (2019) 11:4947–56. doi: 10.2147/CMAR.S202268
20. You W, Li L, Sun D, Liu X, Xia Z, Xue S, et al. Farnesoid X Receptor Constructs an Immunosuppressive Microenvironment and Sensitizes FXR (high)PD-L1(low) NSCLC to Anti-PD-1 Immunotherapy. *Cancer Immunol Res* (2019) 7(6):990–1000. doi: 10.1158/2326-6066.CIR-17-0672
21. Deng Y, Cheng J, Fu B, Liu W, Chen G, Zhang Q, et al. Hepatic Carcinoma-Associated Fibroblasts Enhance Immune Suppression by Facilitating the Generation of Myeloid-Derived Suppressor Cells. *Oncogene* (2017) 36(8):1090–101. doi: 10.1038/onc.2016.273
22. Ding L, Gong Y, Yang Z, Zou B, Liu X, Zhang B, et al. Lactobacillus Rhamnosus GG Ameliorates Liver Injury and Hypoxic Hepatitis in Rat Model of CLP-Induced Sepsis. *Dig Dis Sci* (2019) 64(10):2867–77. doi: 10.1007/s10620-019-05628-0
23. Ye L, Zhang Q, Cheng Y, Chen X, Wang G, Shi M, et al. Tumor-Derived Exosomal HMGB1 Fosters Hepatocellular Carcinoma Immune Evasion by Promoting TIM-1(+) Regulatory B Cell Expansion. *J Immunother Cancer* (2018) 6(1):145. doi: 10.1186/s40425-018-0451-6
24. Dvorak K, Chavarria M, Payne CM, Ramsey L, Crowley-Weber C, Dvorakova B, et al. Activation of the Interleukin-6/STAT3 Antiapoptotic Pathway in Esophageal Cells by Bile Acids and Low Ph: Relevance to Barrett's Esophagus. *Clin Cancer Res* (2007) 13(18 Pt 1):5305–13. doi: 10.1158/1078-0432.CCR-07-0483
25. Tataranni T, Piccoli C. Dichloroacetate (DCA) and Cancer: An Overview Towards Clinical Applications. *Oxid Med Cell Longev* (2019) 2019:8201079. doi: 10.1155/2019/8201079
26. Dai J, Wang H, Shi Y, Dong Y, Zhang Y, Wang J. Impact of Bile Acids on the Growth of Human Cholangiocarcinoma *via* FXR. *J Hematol Oncol* (2011) 4:41. doi: 10.1186/1756-8722-4-41
27. Liu X, Guo GL, Kong B, Hilburn DB, Hubchak SC, Park S, et al. Farnesoid X Receptor Signaling Activates the Hepatic X-Box Binding Protein 1 Pathway *In Vitro* and in Mice. *Hepatology (Baltimore Md)* (2018) 68(1):304–16. doi: 10.1002/hep.29815
28. Wen LZ, Ding K, Wang ZR, Ding CH, Lei SJ, Liu JP, et al. SHP-1 Acts as a Tumor Suppressor in Hepatocarcinogenesis and HCC Progression. *Cancer Res* (2018) 78(16):4680–91. doi: 10.1158/0008-5472.CAN-17-3896
29. García-Rodríguez JL, Barbier-Torres L, Fernández-Álvarez S, Gutiérrez-de Juan V, Monte MJ, Halilbasic E, et al. SIRT1 Controls Liver Regeneration by Regulating Bile Acid Metabolism Through Farnesoid X Receptor and Mammalian Target of Rapamycin Signaling. *Hepatology (Baltimore Md)* (2014) 59(5):1972–83. doi: 10.1002/hep.26971
30. Huang H, Ren Z, Gao X, Hu X, Zhou Y, Jiang J, et al. Integrated Analysis of Microbiome and Host Transcriptome Reveals Correlations Between Gut Microbiota and Clinical Outcomes in HBV-Related Hepatocellular Carcinoma. *Genome Med* (2020) 12(1):102. doi: 10.1186/s13073-020-00796-5
31. Lin R, Zhan M, Yang L, Wang H, Shen H, Huang S, et al. Deoxycholic Acid Modulates the Progression of Gallbladder Cancer Through N(6)-Methyladenosine-Dependent microRNA Maturation. *Oncogene* (2020) 39(26):4983–5000. doi: 10.1038/s41388-020-1349-6
32. Soma T, Kaganoi J, Kawabe A, Kondo K, Tsunoda S, Imamura M, et al. Chenodeoxycholic Acid Stimulates the Progression of Human Esophageal Cancer Cells: A Possible Mechanism of Angiogenesis in Patients With Esophageal Cancer. *Int J Cancer* (2006) 119(4):771–82. doi: 10.1002/ijc.21917
33. Wehbe H, Henson R, Meng F, Mize-Berge J, Patel T. Interleukin-6 Contributes to Growth in Cholangiocarcinoma Cells by Aberrant Promoter Methylation and Gene Expression. *Cancer Res* (2006) 66(21):10517–24. doi: 10.1158/0008-5472.CAN-06-2130
34. Xu Z, Huang G, Gong W, Zhou P, Zhao Y, Zhang Y, et al. FXR Ligands Protect Against Hepatocellular Inflammation *via* SOCS3 Induction. *Cell Signal* (2012) 24(8):1658–64. doi: 10.1016/j.cellsig.2012.04.015
35. Meng Z, Wang X, Gan Y, Zhang Y, Zhou H, Ness CV, et al. Deletion of IFNγ Enhances Hepatocarcinogenesis in FXR Knockout Mice. *J Hepatol* (2012) 57(5):1004–12. doi: 10.1016/j.jhep.2012.06.016
36. Wang H, Lu Z, Zhao X. Tumorigenesis, Diagnosis, and Therapeutic Potential of Exosomes in Liver Cancer. *J Hematol Oncol* (2019) 12(1):133. doi: 10.1186/s13045-019-0806-6
37. Zhang L, Yu D. Exosomes in Cancer Development, Metastasis, and Immunity. *Biochim Biophys Acta Rev Cancer* (2019) 1871(2):455–68. doi: 10.1016/j.bbcan.2019.04.004

38. Chen G, Huang AC, Zhang W, Zhang G, Wu M, Xu W, et al. Exosomal PD-L1 Contributes to Immunosuppression and Is Associated With Anti-PD-1 Response. *Nature* (2018) 560(7718):382–6. doi: 10.1038/s41586-018-0392-8
39. El-Khoueiry AB, Sangro B, Yau T, Crocenzi TS, Kudo M, Hsu C, et al. Nivolumab in Patients With Advanced Hepatocellular Carcinoma (CheckMate 040): An Open-Label, Non-Comparative, Phase 1/2 Dose Escalation and Expansion Trial. *Lancet (London England)* (2017) 389 (10088):2492–502. doi: 10.1016/S0140-6736(17)31046-2
40. Wu X, Gu Z, Chen Y, Chen B, Chen W, Weng L, et al. Application of PD-1 Blockade in Cancer Immunotherapy. *Comput Struct Biotechnol J* (2019) 17:661–74. doi: 10.1016/j.csbj.2019.03.006
41. Dai J, Wang H, Dong Y, Zhang Y, Wang J. Bile Acids Affect the Growth of Human Cholangiocarcinoma *via* NF-kB Pathway. *Cancer Invest* (2013) 31 (2):111–20. doi: 10.3109/07357907.2012.762781
42. Anwer MS. Intracellular Signaling by Bile Acids. *J Biosci (Rajshari)* (2012) 20:1–23. doi: 10.3329/jbs.v20i0.17647
43. Jung IH, Choi JH, Chung YY, Lim GL, Park YN, Park SW. Predominant Activation of JAK/STAT3 Pathway by Interleukin-6 Is Implicated in Hepatocarcinogenesis. *Neoplasia* (2015) 17(7):586–97. doi: 10.1016/j.neo.2015.07.005
44. Nag S, Qin J, Srivenugopal KS, Wang M, Zhang R. The MDM2-P53 Pathway Revisited. *J BioMed Res* (2013) 27(4):254–71. doi: 10.7555/JBR.27.20130030

Conflict of Interest: The authors declare that the research was conducted in the absence of any commercial or financial relationships that could be construed as a potential conflict of interest.

Publisher's Note: All claims expressed in this article are solely those of the authors and do not necessarily represent those of their affiliated organizations, or those of the publisher, the editors and the reviewers. Any product that may be evaluated in this article, or claim that may be made by its manufacturer, is not guaranteed or endorsed by the publisher.

frontiers in Oncology

ORIGINAL RESEARCH
published: 30 November 2021
doi: 10.3389/fonc.2021.784067

Long Noncoding RNA *SNHG1* Regulates *LMNB2* Expression by Sponging *miR-326* and Promotes Cancer Growth in Hepatocellular Carcinoma

Wentao Mu[1,2], *Lingyu Guo*[3], *Yang Liu*[4], *Hui Yang*[5], *Shanglei Ning*[2*] and *Guoyue Lv*[1*]

[1] Department of Hepatobiliary and Pancreatic Surgery, The First Hospital of Jilin University, Changchun, China, [2] Department of Hepatobiliary Surgery, General Surgery, Qilu Hospital of Shandong University, Jinan, China, [3] Department of Urology, Second Affiliated Hospital of Xi'an Jiaotong University, Xi'an, China, [4] Department of Hepatobiliary Surgery, Taian City Central Hospital of Shandong Province, Tai'an, China, [5] Department of Colorectal and Anal Surgery, The First Affiliated Hospital of Shandong First Medical University, Jinan, China

OPEN ACCESS

Edited by:
Xuesong Gu,
Beth Israel Deaconess Medical Center and Harvard Medical School, United States

Reviewed by:
Chenyu Lin,
The Ohio State University, United States
Min Zhang,
Huazhong Agricultural University, China

***Correspondence:**
Shanglei Ning
shangleining@163.com
Guoyue Lv
lvgy@jlu.edu.cn

Specialty section:
This article was submitted to Cancer Molecular Targets and Therapeutics, a section of the journal Frontiers in Oncology

Received: 27 September 2021
Accepted: 09 November 2021
Published: 30 November 2021

Citation:
Mu W, Guo L, Liu Y, Yang H, Ning S and Lv G (2021) Long Noncoding RNA SNHG1 Regulates LMNB2 Expression by Sponging miR-326 and Promotes Cancer Growth in Hepatocellular Carcinoma. Front. Oncol. 11:784067. doi: 10.3389/fonc.2021.784067

Objective: The purpose of the study is to explore the potential competing endogenous RNA (ceRNA) network and investigate the molecular mechanism of long noncoding RNA (lncRNA) *small nucleolar RNA host gene 1* (*SNHG1*) in hepatocellular carcinoma (HCC) development.

Methods: By analyzing the data of HCC in The Cancer Genome Atlas (TCGA) database, we included differentially expressed lncRNA and microRNA (miRNA) profiles and constructed ceRNA networks related to the prognosis of HCC patients. qRT-PCR, Western blotting, 3-(4,5-Dimethylthiazol-2-yl)-2,5-diphenyltetrazolium bromide (MTT), transwell assay, and the nude mouse model were employed to test the effects of *SNHG1* and *LMNB2* on tumor proliferation and growth *in vitro* and *in vivo*.

Results: In the study, we identified 115 messenger RNAs (mRNAs), 12 lncRNAs, and 37 miRNAs by intersecting differentially expressed genes (DEGs) in TCGA and StarBase databases. Then, *SNHG1–miR-326–LMNB2* pathway came into notice after further survival analysis and hub gene screening. Our results showed that *SNHG1* expression was upregulated significantly in HCC tissues and cell lines. Downregulation of both *LMNB2*, the target of *miR-326* in HCC, and *SNHG1* inhibited tumor proliferation and growth *in vitro* and *in vivo*. Furthermore, *SNHG1* could regulate *LMNB2* expression through binding to *miR-326* in HCC cell lines.

Conclusion: *SNHG1* is a promising prognostic factor in HCC, and the *SNHG1–miR-326–LMNB2* axis may be a potential therapeutic target for HCC.

Keywords: hepatocellular carcinoma, *SNHG1*, *miR-326*, *LMNB2*, lncRNA, microRNA, bioinformatics

INTRODUCTION

Hepatocellular carcinoma (HCC) is the fourth most common cause of cancer-related death worldwide and the sixth leading cause of incident cancer cases (1, 2). The majority of HCC mainly occurs in patients with hepatitis B virus (HBV) infection, hepatitis C virus (HCV) infection, and alcohol abuse (3). Although the 5-year survival rate of early-stage HCC is about 60% these years, the prognosis of most patients with unresectable HCC is still very poor (4), despite recent advances in surgery and systematic therapy. Besides, HCC is a highly heterogeneous tumor that may be the main cause of treatment failure, so the biological diversity of HCC poses a considerable challenge for individualized therapy (5, 6). Therefore, it is urgent to explore the molecular mechanism of tumor progression and identify novel therapeutic targets for HCC.

Long noncoding RNAs (lncRNAs) are a set of RNA transcripts longer than 200 nucleotides that are not for translation but capable of regulating the expression of different genes (7). Emerging evidence has suggested that lncRNAs participate in tumor proliferation, invasion, apoptosis, and other biological processes (8–11). Generally, lncRNAs acted as a competing endogenous RNA (ceRNA) and bound with specific microRNA (miRNA), regulating the corresponding downstream messenger RNA (mRNA) translation (12–14). Although *SNHG1* has been reported to function as an oncogene through sponging *miR-195-5p* (15), *miR-377-3p* (16), and *miR-195* (17) in HCC, in the present study, we made use of The Cancer Genome Atlas (TCGA) database and identified a novel molecular mechanism of *SNHG1* in HCC growth.

Our data demonstrated the crucial roles of *SNHG1* in HCC proliferation and invasion *in vitro* and *in vivo*. Furthermore, we innovatively demonstrated that *SNHG1* promoted HCC growth through competitively binding to *microRNA-326* (*miR-326*) to regulate *LMNB2* expression, which provided a novel insight into the mechanism of HCC progression.

MATERIALS AND METHODS

Data Source

The published HCC cohort dataset, including gene expression profiles and relevant clinical information, can be downloaded from TCGA data portal (18). The clinical information of patients includes age, gender, preoperative diagnosis, Child–Pugh score of liver function, radical resection, postoperative pathological diagnosis, pathological grading and staging, survival time, last follow-up time, and so on. Only the survival time-related data in the complex clinical data are used, so only the data needed in the article are shown in (**Supplementary Tables 1** and **2**). Data acquisition and application were conducted in accordance with TCGA release guidelines and data access policy without additional approval from the local ethics committee.

Screening of Differentially Expressed mRNA, lncRNA, and miRNA

The limma package in R language (version 3.6.1) was subsequently used for the calculation of DEGs. Gene counts >0, the adjusted p value <0.05, and $|\log_2$ fold change$|>1$ were set as the cutoff criteria. Similarly, Differentially Expressed microRNAs (DEmiRs) were selected by the three cutoff values, Gene Counts >0, the adjusted p value <0.05, and $|\log_2$ fold change$|>1$. Heat maps and volcanic maps were drawn using R language. Then, the principal component analysis (PCA) figure about the samples was performed.

Function and Pathway Enrichment Analysis

In order to understand the biological functions of selected DEGs and DEmiRs, we performed the enrichment analysis of DEGs and DEmiRs in Gene Ontology (GO) terms and Kyoto Encyclopedia of Genes and Genomes (KEGG) Database Pathways. The clusterProfiler (version 3.12.0) (19) package in R language was used for revealing the roles of DEGs in biological process (BP), cellular component (CC), and molecular function (MF). The adjusted p value was less than 0.01 and considered statistically significant.

The ceRNA Network Construction

R language GDCRNATools package was used to search and match on StarBase database and find out the common miRNAs targeting mRNA and lncRNA (20, 21). The mRNA and lncRNA are negatively correlated with miRNA, but mRNA and lncRNA present a positive correlation. Hypergeometric distribution test was used to assess the importance between each pair of them. We used false discovery rate (FDR) to correct p values while FDR <0.05 is the cutoff value. Meanwhile, the regulation of similarity correlation with miRNAs (similarity of correlation between miRNA and lncRNA expression and correlation between miRNA and mRNA expression) is not equal to zero. All the competitive lncRNA and mRNA were mixed together after we identified them under the conditions above. Finally, ceRNA network diagram was established in the Cytoscape (3.7.2) for visualization.

Establishment of ceRNA Network Associated With Hepatocellular Carcinoma Patient Survival

In order to find out the survival-related lncRNA–miRNA–mRNA pathways, we conducted a single-factor survival analysis on each lncRNA, mRNA, and miRNA node in the ceRNA network. The node was marked in the ceRNA network diagram, and the survival-related ceRNA network was constructed through the survival-related node. Then, samples were divided into the high-expression group and the low-expression group according to the median expression of each gene. The Kaplan–Meier survival was used to evaluate the difference of overall survival (OS) time between the two groups. Finally the *SNHG1–miR-326–LMNB2* pathway was selected, and the effects of this pathway were experimentally verified in our study.

Cell Lines

The human hepatocellular cancer cell lines (Huh7 and PLC) were obtained from the Cell Bank of Chinese Academy of Sciences, Shanghai Branch. The Huh7 and PLC cells were

cultured in Dulbecco's modified Eagle's medium (DMEM) with 10% fetal bovine serum in 5% CO_2 and 90% humidity at 37°C.

Cell Transduction

The lentivirus vectors (sh-*SNHG1*, sh-*LMNB2*) and small interfering RNAs (siRNAs) against human *SNHG1* or *LMNB2* were synthesized by GenePharma Co. Ltd. The stable Huh7 cells with *SNHG1* and *LMNB2* knocked down were generated using lentiviral vectors. Infected cells were then treated with puromycin (2 μg/ml) for 2 days, and surviving cells were maintained in complete medium with puromycin (0.5 μg/ml). The siRNAs were transfected into hepatocellular cancer cells using Lipofectamine 2000 (Thermo Fisher Scientific, Inc.) according to their instructions. Besides, *miR-326* mimics, *miR-326* inhibitors, and negative controls were purchased from GenePharma Co. Ltd. When the cell confluence reached 50%, oligonucleotide transfection was performed using Lipofectamine 2000 according to the manufacturer's protocol.

Luciferase Reporter Assay

We constructed the wild-type plasmid *SNHG1*-WT and the mutant plasmid *SNHG1*-MUT. PLC and HuH7 cells that were seeded in 24-well plates were cotransfected with *miR-326* mimic or negative control and wild-type or mutant plasmids using Lipofectamine 2000. The luciferase intensity on the microplate was measured with the Dual-Luciferase Reporter Assay System (Promega Corp.), and Renilla luciferase activity was normalized to firefly luciferase activity.

Western Blotting

The total protein was extracted from the cells using radioimmunoprecipitation assay lysis buffer with protease inhibitors. Each lane is loaded with the same amount of total protein (20 μg), and the sample is separated by 10% sodium dodecyl sulfate polyacrylamide gel electropheresis (SDS PAGE) and then transferred to a polyvinylidene fluoride membrane (Roche Diagnostics). After blocking with 5% skim milk at room temperature for 1 h, primary antibody *LMNB2* (Abcam) or *glyceraldehyde 3-phosphate dehydrogenase* (*GAPDH*; Abcam) was used at 4°C overnight. Subsequently, the membranes were incubated with anti-rabbit (1:3,000, cat. no. 7074, Cell Signaling Technology, Inc.) horseradish peroxidase-conjugated secondary antibodies at 37°C for 1 h. Finally, ECL Western blot substrate (Promega corp.) and FluorChem E system (Protein Simple) were used to observe the immune response zone.

qPCR

According to the manufacturer's protocol, TRIzol reagent (Thermo Fisher Scientific, Inc.) was used to extract total RNA from cells and tissues. The RNA purity was evaluated based on the A260/280 ratio. RNA was reverse transcribed into cDNA using miRNA first-strand cDNA synthesis kit [Accurate Biotechnology (Hunan) Co., Ltd.]. SYBR Green Premix Pro Taq HS qPCR Kit II [Accurate Biotechnology (Hunan) Co., Ltd.] was used for qPCR to detect the relative expression of the target gene. Thermal cycling conditions are as follows: Initial denaturation at 95°C for 30 sec; 40 cycles of 5 sec at 95°C; 1 min at 60°C and 72°C for 15 sec; with a final extension cycle at 72°C for 5 min. Finally, it step in the dissociation stage. The relative levels were calculated using the $2^{-\Delta\Delta Cq}$ method. The endogenous control gene is GAPDH. The primer sequence is shown in **Table 1**.

Cell Migration and Invasion Assays

Cells (1×10^5) were seeded in the upper chamber of a Boyden chamber (8 μm aperture) in 200 μl of serum-free medium (Corning Corporation). The lower chamber was filled with 700 μl containing 10% fetal bovine serum (Gibco) as a chemical attractant. After 24 h of incubation at 37°C, cells remaining on the upper side of the membrane were removed with a cotton swab, and the cells that had migrated to the lower side of the membrane were fixed with 70% ethanol for 20 min and stained with 0.1% crystal violet for 20 min at room temperature. Then, the cells were counted with an optical microscope. The method of the invasion test is similar to cell migration assay except that the Boyden chamber is covered with a matrix before seeding the cells.

Wound Healing Test

The cells were seeded in six-well plates and cultured to 80% confluence before we scratched the cell layer with a 20-μl pipette tip. The cells were then incubated in fresh medium containing 10% fetal bovine serum for 48 h. Scratches were observed under a fluorescence microscope after 24 and 48 h.

In Vivo Assay

Female nude mice (aged 5–6 weeks, weight 18–22 g) were purchased from Hangzhou Ziyuan Biology and bred in a 12-h light/dark cycle and sterile conditions (temperature 26°C–28°C, humidity 40%–60%) with free access to water and food. We injected 3×10^6 cells into the fore limbs of nude mice to generate transplanted tumors and measure the tumor size with a caliper every 3 days. After 19 days, the mice were sacrificed, and tumor images were captured. Tumor volume was calculated with the formula: maximum diameter × (minimum diameter) 2 × 0.5.

Statistical Analysis

Statistical analysis was performed using SPSS 19.0 software (SPSS Inc., Chicago, IL, USA). The summary data are expressed as the mean ± standard error of the mean (SEM). We use the χ^2 test, Student's t-test, or one-way analysis of variance with the least significant difference correction to assess the differences between groups. Spearman rank correlation analysis was used to evaluate linear regression. p value less than 0.05 was considered to be statistically significant in all cases.

TABLE 1 | qPCR primers.

	Forward Primer	Reverse Primer
miR-326	CATCTGTCTGTTGGGCTGGA	AGGAAGGGCCCAGAGGCG
SNHG1	CTACTGACCTAGCTTGTTGCCA	GGCCCTGAATGAGCTACCTAC
U6	CTCGCTTCGGCAGCACA	AACGCTTCACGAATTTGCGT
GAPDH	GCACCGTCAAGGCTGAGAAC	TGGTGAAGACGCCAGTGGA
LMNB2	CTGGAGCTGGAGCAGACCTA	TCCCGAATGCGATCTTCAGC

Ethics Approval and Consent to Participate

The study protocol was approved by the research ethics committee of the Qilu Hospital of Shandong University.

RESULTS

Identification of Differentially Expressed Genes and Differentially Expressed microRNAs (DEmiR)

Firstly, 421 HCC patient samples with para-tumor tissue available from TCGA database were analyzed using R language tools. We used p value <0.05 and $|\log_2$ fold change$|$>1 as cutoffs to identify differential gene profiles. As a result, a total of 2,416 differentially expressed genes (DEGs), 2,181 differentially expressed mRNAs, and 148 differentially expressed lncRNAs were identified (**Figures 1A–C**). The green dots represent downregulated genes, and the red dots represent upregulated genes. Black dots represent genes without statistically significant change. The heatmap shows the DEGs between the primary tumor (red) and solid tissue normal (blue). Moreover, 131 differentially expressed miRNAs were screened using both R language and GDCRNATools (**Figures 1D–F**).

Gene Ontology Enrichment Analysis and Kyoto Encyclopedia of Genes and Genomes Enrichment Analysis

GO and KEGG enrichment analysis on these 2,416 DEGs was carried out to explore their functions (p value <0.01 was the cutoff value). The results showed that (**Figure 2A**) the differential genes mainly focus on the catabolic process of biological procedure extracellular matrix of cells and small molecular compounds bindings with the oxidative respiratory chains. Otherwise, KEGG enrichment analysis demonstrated that the differential genes concentrated upon the pathways participating in complement and coagulation cascades, cell cycle regulation, and cell metabolism (**Figure 2B**).

Construction of the ceRNA Network

Based on the 2,181 differentially expressed mRNAs and 148 differentially expressed lncRNAs mentioned above, we constructed the ceRNA network containing 115 mRNAs, 12 lncRNAs, and 37 miRNAs, in which 343 different lncRNA–miRNA–mRNA pathways were also described (**Figure 2C**). Then, we intersected the selected 37 miRNAs with DEmiRs obtained previously and only four differentially expressed miRNAs including *miR-326*, *miR-154-5p*, *miR-21-5p*, and *miR-93-5p* were found, which means that these four miRNA-associated lncRNA–miRNA–mRNA pathways may function in HCC development.

Survival Analysis of Candidate lncRNA–miRNA–mRNA Pathway in Hepatocellular Carcinoma Patients

In order to evaluate the prognostic significance of the obtained ceRNA network, we used univariate survival analysis, Cox regression, and Kaplan–Meier survival analysis and found that only *miR-326* was associated with HCC patient survival among the four potential miRNAs ($p < 0.01$) (**Figure 3C**). So, the lncRNA–miRNA–mRNA pathways that associated with *miR-326* were extracted from ceRNA as a whole (**Figure 2D**). And the heatmap of correlation matrix was drawn to visualize the gene expression correlation quantitatively (**Figure 2E**). We evaluated the prognostic significance of SNHG family members, such as *SNHG1 SNHG3*, *SNHG12*, and *SNHG20*; although the p value for *SNHG1* survival analysis is slightly greater than 0.05, the survival analysis p values for 25% and 75% of the quartile subgroups were both less than 0.05 (**Figures 3A, B**). Furthermore, previous studies have demonstrated that lncRNA *SNHG1* predicted a poor prognosis in HCC (16, 22), and the diagram showed that lncRNA *SNHG1* is a potential lncRNA in HCC progression. Although three candidate targets *ANKRD13B*, *LMNB2*, and *FANCE*, which were regulated by *miR-326*, were all associated with HCC patient survival (**Figure 3D**), only *LMNB2* has been investigated in a hepatocellular cancer study before (23). Previous studies showed that *ANKRD13B* and *FANCE* were associated with epidermal growth factor receptor (EGFR) activation (24) and Fanconi anemia (25, 26), respectively. Furthermore, correlation analysis indicated both lncRNA *SNHG1* and *LMNB2* were negatively correlated with *miR-326*, but *SNHG1* correlated with *LMNB2* positively in HCC (**Figures 4A–C**).

SNHG1 Promotes the Proliferation, Migration, and Invasion of Hepatocellular Cancer Cells

Firstly, *SNHG1* level were examined in five HCC cell lines. As shown in **Figure 5A**, Huh7 and PLC have a higher expression of *SNHG1*, so we chose the two cell lines for further research. Three independent siRNAs were designed to silence *SNHG1* expression. The results showed that *SNHG1* expression decreased significantly compared with control group (**Figure 5B**). MTT assay and colony formation demonstrated that *SNHG1* silencing inhibited cell proliferation significantly (**Figures 5C–F**). The transwell assay indicated that knockdown of *SNHG1* inhibited the migration and invasion of Huh7 and PLC cells (**Figures 5G, H**), and these results were confirmed in the wound healing experiment using both Huh7 and PLC cells (**Figure 5I**). The above results showed that *SNHG1* promoted the proliferation, migration, and invasion of hepatocellular cancer cells.

SNHG1 Knockdown Inhibits Tumor Growth *In Vivo*

To investigate the role of *SNHG1* in HCC growth *in vivo*, we cultured Huh7 cells stably expressing sh*SNHG1* using lentivirus (**Figure 6A**). As shown in **Figures 6B, C** (six mice per group), the knockdown of *SNHG1* inhibited tumor growth significantly compared with control group (**Figures 6A, B**). Furthermore, decreased tumor size and weight were observed after *SNHG1* was knocked down (**Figures 6D, E**). These results indicated that *SNHG1* knockdown could influence tumor growth significantly *in vivo*. The *miR-326* level of tumor increased markedly in the sh*SNHG1* group compared with control, whereas the expression of *LMNB2* decreased (**Figure 6F, G**).

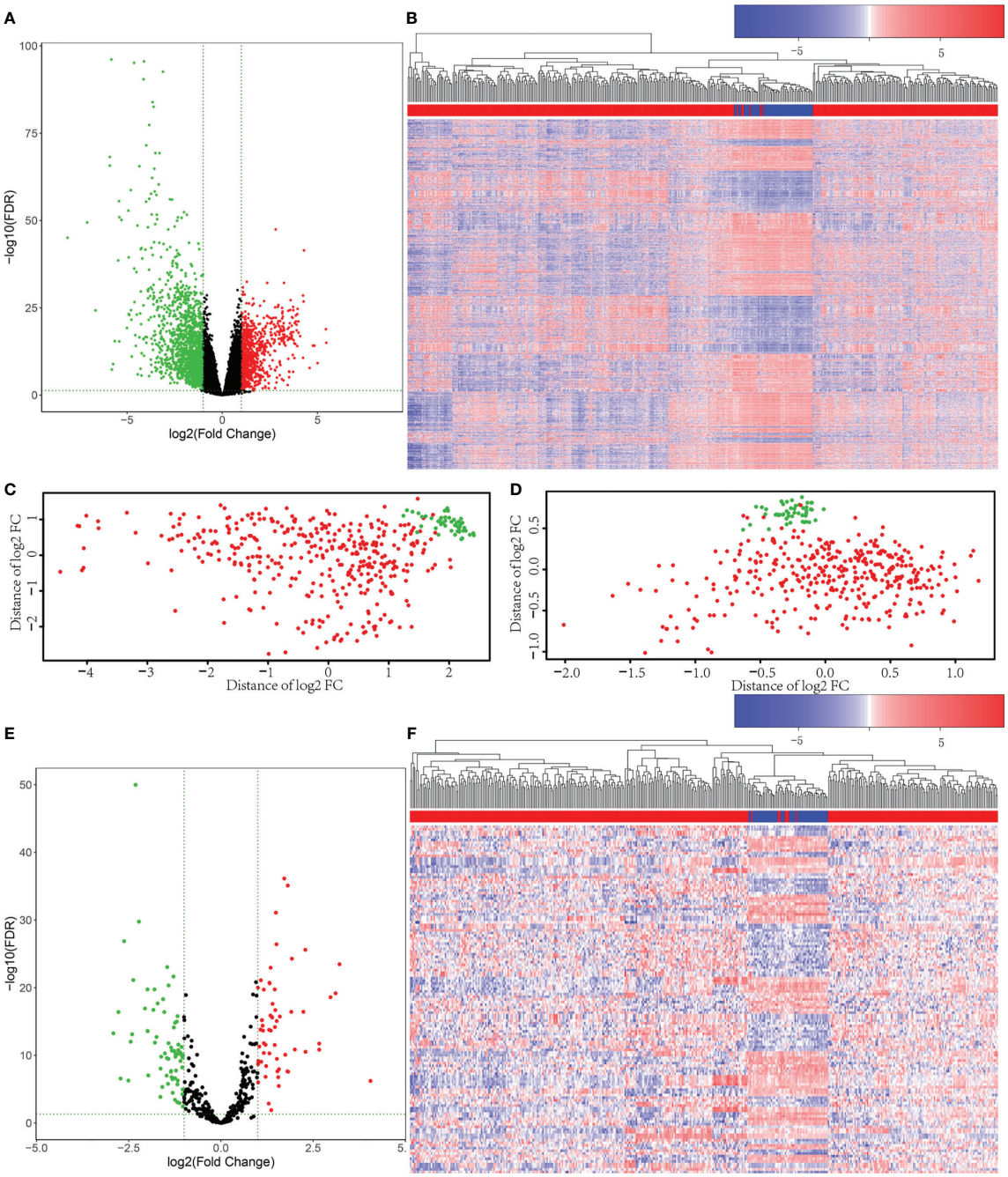

FIGURE 1 | Differentially expressed mRNAs and miRNAs were selected from The Cancer Genome Atlas (TCGA) database. **(A)** Volcano plots for 2,416 differentially expressed genes (DEGs). The green dots represent downregulated genes, and the red dots represent upregulated genes. Black dots represent genes without statistically significant change ($p < 0.05$ and |log2 fold change|>1). **(B)** Heatmap for DEGs in primary tumor (red) compared with solid tissue normal (blue). **(C)** The principal component analysis (PCA) figure of the samples based on the differentially expressed mRNAs. **(D)** The PCA figure of the samples based on the differentially expressed miRNAs. **(E)** Volcano plots for the 131 Differentially Expressed microRNAs (DEmiRs). The green dots represent downregulated miRNAs, and the red dots represent upregulated miRNAs. Black dots represent miRNAs without statistically significant change ($p < 0.05$ and |log2 fold change|>1). **(F)** Heatmap for DEmiRs in primary tumor (red) compared with solid tissue normal (blue).

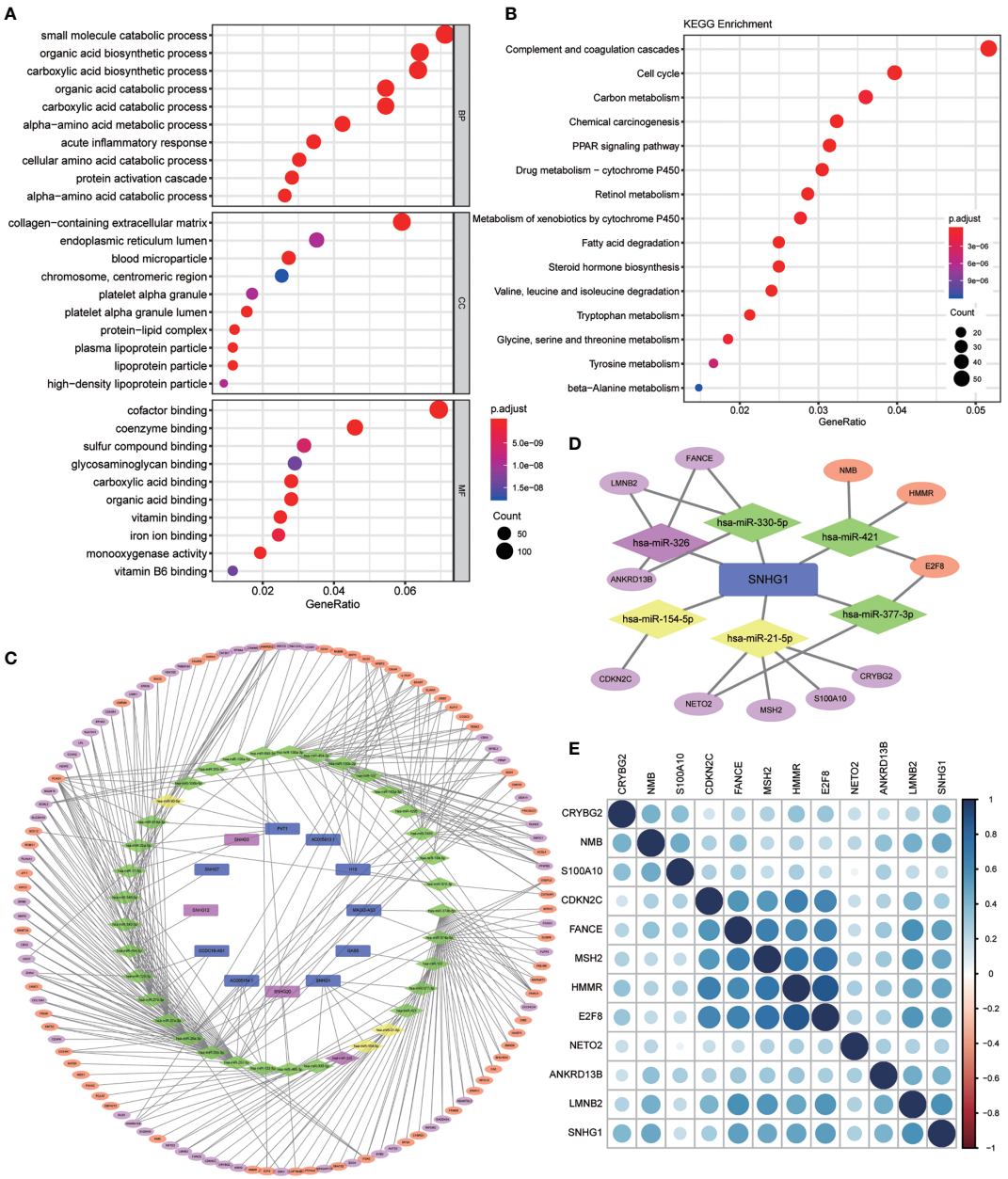

FIGURE 2 | Differential gene enrichment analysis and pathway construction. **(A)** Gene Ontology (GO) enrichment analysis of differentially expressed genes (BP, biological process; CC, cellular component; MF, molecular function) ($p < 0.01$). **(B)** Kyoto Encyclopedia of Genes and Genomes (KEGG) pathway analysis of differentially expressed genes ($p < 0.01$). **(C)** Competing endogenous RNA (ceRNA) network was established by Cytoscape for differentially expressed lncRNA–miRNA–mRNA. (All lncRNA nodes and mRNA nodes were differentially expressed; purple nodes were associated with survival. Yellow miRNA nodes were differentially expressed.). **(D)** A total of six miRNAs and 11 mRNAs were identified from the lncRNA *SNHG1*-related network. **(E)** Heatmap for correlation matrix to visualize the gene expression correlation quantitatively.

SNHG1 Regulates LMNB2 Expression in Hepatocellular Carcinoma *via* Sponging *miR-326* in Hepatocellular Carcinoma

In order to confirm the regulatory axis of *SNHG1–miR-326–LMNB2* in HCC mentioned above, we firstly perform the subcellular localization assay of *SNHG1*. Nucleocytoplasmic separation and RT-qPCR assay revealed that *SNHG1* was expressed in both nucleus and cytoplasm of HuH7 and PLC cells, whereas a larger proportion of *SNHG1* was located in the cytoplasm (**Figure 7A**). Many lncRNAs acted as ceRNAs through binding miRNAs (27). *SNHG1* has also been reported to be involved in tumor development including colorectal cancer and osteosarcoma

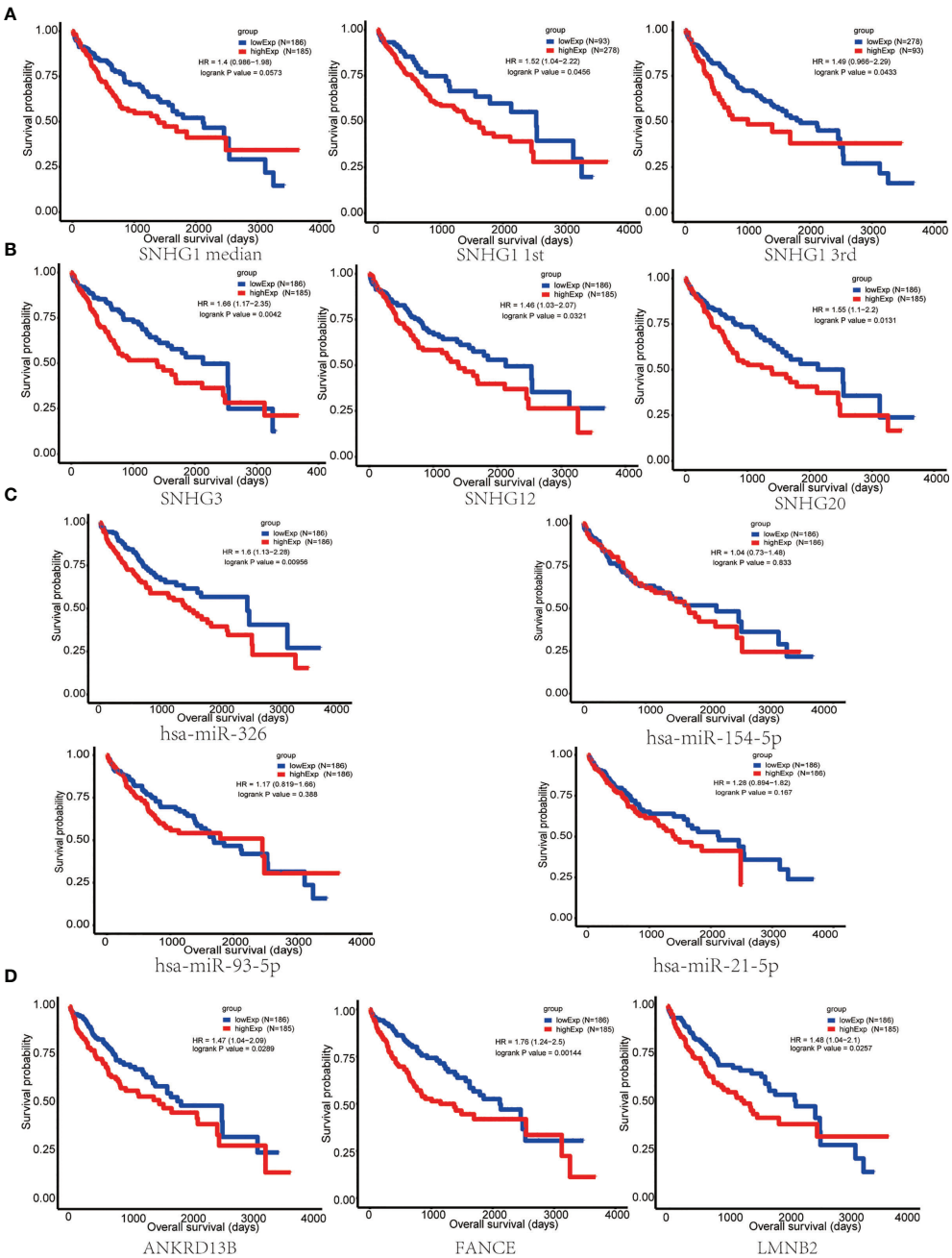

FIGURE 3 | Survival analysis of key nodes in hepatocellular carcinoma (HCC). **(A)** Kaplan–Meier curve of HCC patients with low or high *SNHG1* expression of the quartile subgroups. **(B)** *SNHG3*, *SNHG12*, and *SNHG20* were significantly associated with the overall survival in patients with HCC, as detected using the Kaplan–Meier curve. **(C)** Kaplan–Meier curve of HCC patients with low or high expression of *miR-326*, *miR-154-5p*, *miR-21-5p*, and *miR-93-5p*. **(D)** The Kaplan–Meier curve showed that *ANKRD13B*, *FANCE*, and *LMNB2* were significantly associated with the overall survival in patients with HCC.

(28–30). Therefore, we used dual-luciferase reporter assays to make sure whether *SNHG1* can directly interact with *miR-326* in Huh7 and PLC cells. The results showed that the *miR-326* mimics could reduce the luciferase activity in both Huh7 and PLC cells (**Figure 7B**). Meanwhile, wild-type and mutant *SNHG1* luciferase reporter vectors were constructed using binding sites predicted by StarBase (**Figure 7C**), and it was found that *miR-326* mimics reduced the luciferase activity significantly of wt-*SNHG1* but showed no effect on mut-*SNHG1*. Furthermore, addition of wt-*SNHG1* will attenuate the inhibition effect of *miR326* on the *LMNB2* expression level, while addition of mut-*SNHG1* will not (**Figure 7D**). Actually, *miR-326* level increased markedly after

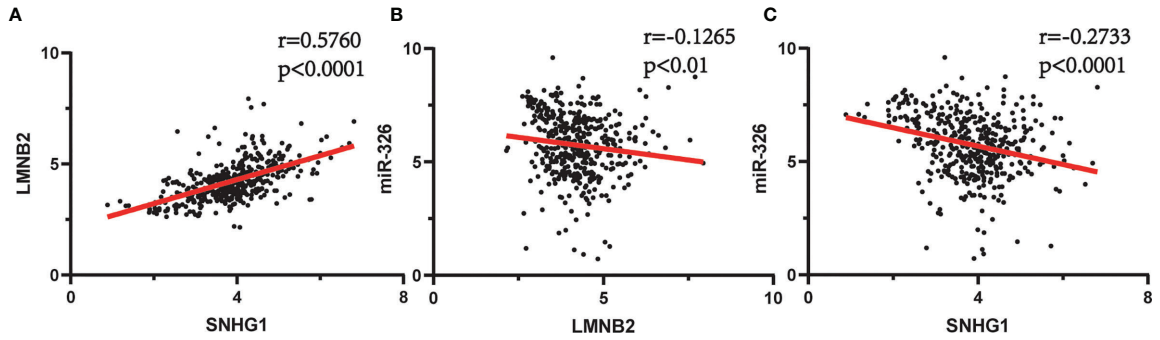

FIGURE 4 | Spearman's correlation analysis between *SNHG1*, *miR-326*, and *LMNB2* in hepatocellular carcinoma (HCC). **(A)** *SNHG1* is positively correlated with *LMNB2* (r = 0.5760, p < 0.0001). **(B)** *miR-326* is negatively correlated with *LMNB2* (r = 0.1256, p < 0.01). **(C)** *SNHG1* is negatively correlated with *miR-326* (r = 0.2733, p < 0.0001).

SNHG1 was knocked down in HuH7 and PLC cells (**Figure 7E**). These results were consistent with the correlation described in **Figure 4**. Additionally, *miR-326* mimics could inhibit cell proliferation significantly, while *miR-326* inhibitor could accelerate HuH7 cell proliferation (**Figure 7F**). Bioinformatics analysis has revealed that *LMNB2* is the potential target of *miR-326* in HCC. To test the effect of *miR-326* on *LMNB2* expression, as the results shown in **Figure 7G**, *LMNB2* level decreased markedly with *miR-326* mimic treatment in Huh7 cells compared with control, whereas the expression of *LMNB2* increased significantly with *miR-326* inhibitor treatment. In a word, *miR-326* could downregulate *LMNB2* expression in HCC. Moreover, *LMNB2* was observed to be upregulated in the HCC tissues with low expression of *miR-326* (**Figure 7H**). Furthermore, the *LMNB2* expression was also investigated after *SNHG1* silence in HCC cells (**Figure 7I**). Moreover, wild-type and mutant *LMNB2* luciferase reporter vectors were constructed using binding sites predicted by StarBase (**Figures 7J, K**), and it was found that *miR-326* mimics significantly reduced the luciferase activity of wt-*LMNB2* but showed no effect on mut-*LMNB2*. The data showed that *LMNB2* RNA expression was reduced significantly after *SNHG1* siRNA treatment. To sum up, *LMNB2* is the target of *miR-326* in HCC, and *SNHG1* regulates *LMNB2* expression *via* sponging *miR-326* in HCC.

LMNB2 Mediated the Positive Effects of *SNHG1* on Tumor Growth in Hepatocellular Carcinoma

In order to explore the biological effects of *LMNB2* in HCC, we also knocked down *LMNB2* expression using siRNAs or lentivirus-mediated shRNA. The results showed that *LMNB2* expression was reduced in HuH7 cells significantly from RNA to protein level (**Figures 8A, B**). It is worth noting that the proliferation ability of Huh7 cells decreased markedly with the silence of *LMNB2* expression (**Figure 8C**). Furthermore, we further studied the role of *LMNB2* on tumor growth *in vivo* (three mice per group). Twenty days after transfected HuH7 cells were injected into nude mice, the volume and weight of formed tumor were significantly smaller than those of control group (**Figures 8D, E**), also indicating that *LMNB2* knockdown could inhibit the growth of HCC cells *in vitro* and *in vivo*. Besides, *SNHG1* knockdown reduced *LMNB2* expression compared with control in Huh7 cells, but *SNHG1*-induced downregulation of *LMNB2* was reversed or enhanced by *miR-326* inhibitor or mimic treatment, respectively. The similar results were also confirmed by Western blotting assays (**Figures 8F, G**). In addition, MTT assay proved that *miR-326* inhibitor could rescue the role of *SNHG1* knockdown on HuH7 cell proliferation. (**Figure 8H**). These data demonstrated that the oncogenic *SNHG1* upregulated *LMNB2* expression and promoted tumor growth *via* suppressing *miR-326* level in HCC.

DISCUSSION

The present study was conducted to investigate potential lncRNA–miRNA–mRNA regulatory network based on TCGA database and elucidate the molecular signatures of HCC progression. Firstly, we screened 2,416 DEGs from RNA-seq of TCGA database through R language, including 148 lncRNAs and 2,181 mRNAs. After analyzing the miRNA data, a total of 131 differentially expressed miRNAs were screened. Then, GO enrichment analysis of DEGs indicated that differential genes are mainly concentrated in the small molecule catabolic process, collagen-containing extracellular matrix, and small molecular compounds bindings in the oxidative respiratory chain of molecular function. The results from KEGG enrichment analysis of DEGs showed that the enrichment of differential genes focused on the pathways associated with complement and coagulation cascades, cell cycle, and carbon metabolism. The GDCRNA Tools package was used to search and match in StarBase database the R language to figure out the miRNAs that linked lncRNAs with mRNAs described above. Finally, 164 related nodes and 343 correlations were found that contained 12 lncRNAs, 115 mRNAs, and 37 miRNAs. We utilized Cytoscape to visualize the relationships between them through the relational network. Then, we intersected the 37 miRNAs selected by DEGs with DEmiRs obtained previously; as a result, only four

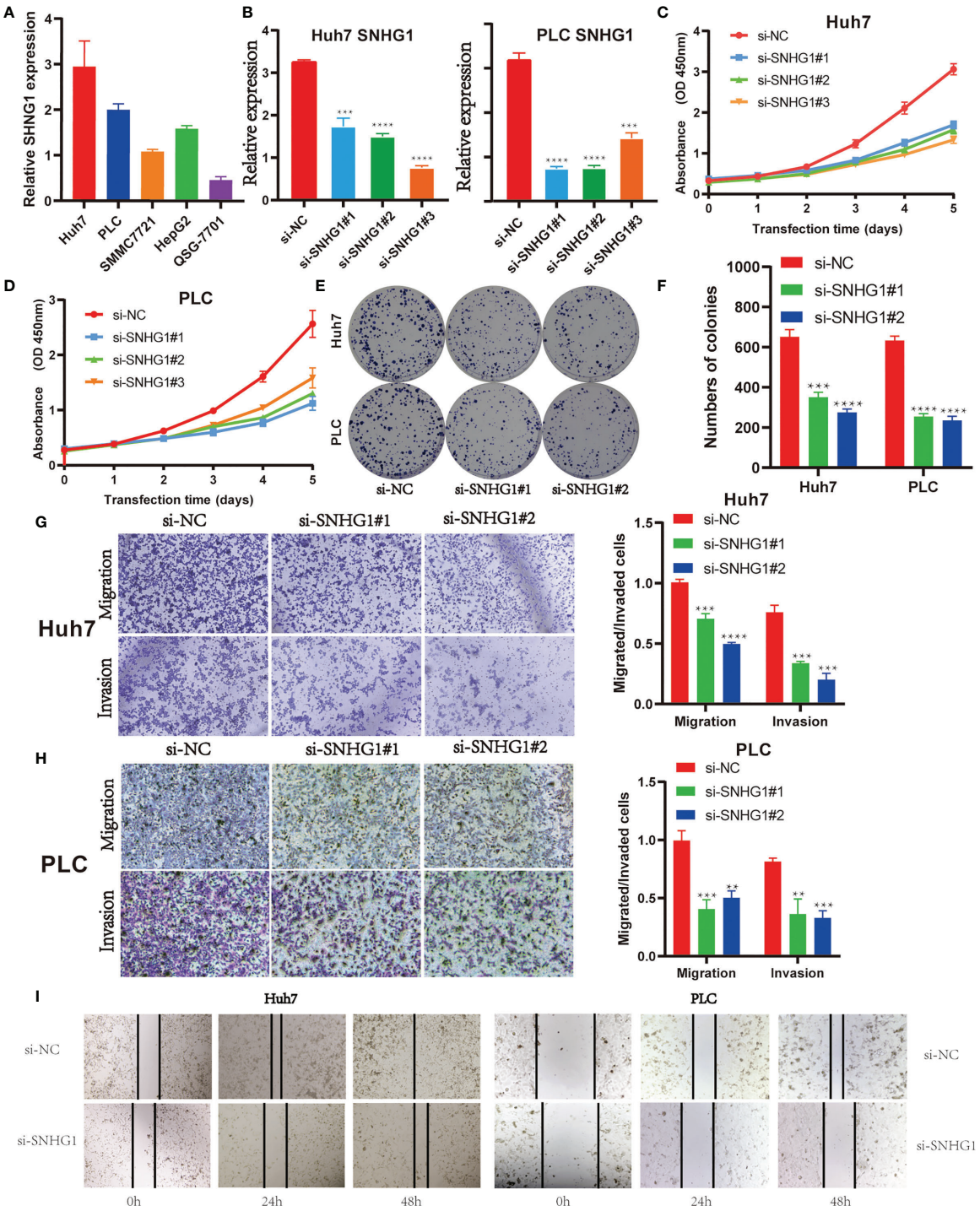

FIGURE 5 | *SNHG1* promotes proliferation, migration, and invasion of hepatocellular cancer cells. **(A)** Relative expression of *SNHG1* was detected in QSG-7701 and the other four hepatocellular carcinoma (HCC) cell lines by RT-qPCR. **(B)** Expression of *SNHG1* in Huh7 and PLC cells with *SNHG1* knockdown detected by RT-qPCR (***p < 0.001, ****p < 0.0001). **(C)** Optical density (OD) value of Huh7 cells with *SNHG1* knockdown and control cells in 3-(4,5-Dimethylthiazol-2-yl)-2,5-diphenyltetrazolium bromide (MTT) assay. **(D)** OD value of PLC cells with *SNHG1* knockdown and control cells in MTT assay. **(E)** Colonies of Huh7 and PLC cells with *SNHG1* knockdown and control cells in the colony formation assay. **(F)** The number of colonies was calculated 14 days after cell seeding (***p < 0.001, ****p < 0.0001). **(G)** Migratory and invasive potential of Huh7 cells with *SNHG1* knockdown and control cells (***p < 0.001, ****p < 0.0001). **(H)** Migratory and invasive potential of PLC cells with *SNHG1* knockdown and control cells (**p < 0.01, ***p < 0.001). **(I)** Wound healing assay was used to detect the migratory ability of Huh7 and PLC cells with *SNHG1* knockdown.

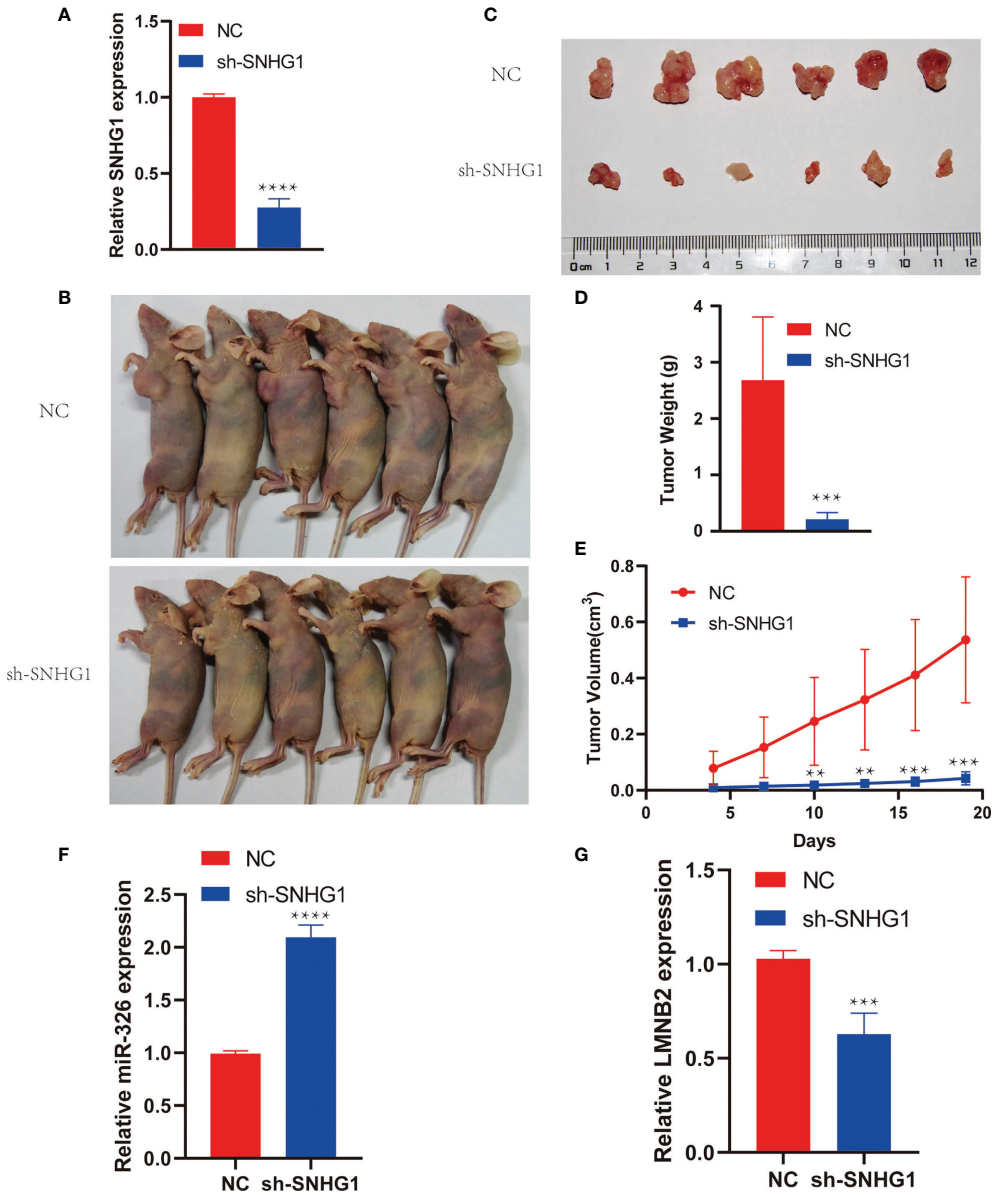

FIGURE 6 | *SNHG1* promotes hepatocellular carcinoma (HCC) tumor growth *in vivo*. **(A)** RNA levels of *SNHG1* in Huh7 cells with *SNHG1* knockdown detected by RT-qPCR (****p < 0.0001). **(B)** Representative images of mice bearing tumors from *SNHG1* knockdown group and control group. **(C)** Representative tumor images were shown. **(D, E)** Quantification of tumor weight and tumor volume of individual mice following the injection of HuH7 cells with *SNHG1* knockdown or control cells (**p < 0.01, ***p < 0.001). **(F, G)** Expression of *miR-326* and *LMNB2* in tumor of sh*SNHG1* group compared with control (***p < 0.001, ****p < 0.0001).

differentially expressed miRNAs were left including *miR-326*, *miR-154-5p*, *miR-21-5p*, and *miR-93-5p*. Univariate survival analysis showed that only *miR-326* was associated with OS among the four differentially expressed miRNAs. So the lncRNA–miRNA–mRNA axis that contained *miR-326* was extracted from the network, and we could see the direct relationship between *SNHG1* and *miR-326* in HCC; at the same time, *LMNB2*, *FANCE*, and *ANKRD13B*, three candidate targets, were involved in the diagram. In view of the reported role of *LMNB2* in HCC progression, recently, we selected *SNHG1–miR-326–LMNB2* axis as the hypothetic signaling involved in HCC development and progression (23).

Emerging evidence showed that lncRNAs acted as oncogenes or tumor suppressors in different types of cancer through regulating gene expression (31). Recently, many studies have unveiled the crucial role of *SNHG1* in various cancer tumorigeneses and progressions (28, 30, 32). In the present study, we found that *SNHG1* expression level was higher in HCC tissues and cancer cell lines and was a poor prognosis marker in HCC, which is consistent with previous reports (33–35). Furthermore, knockdown

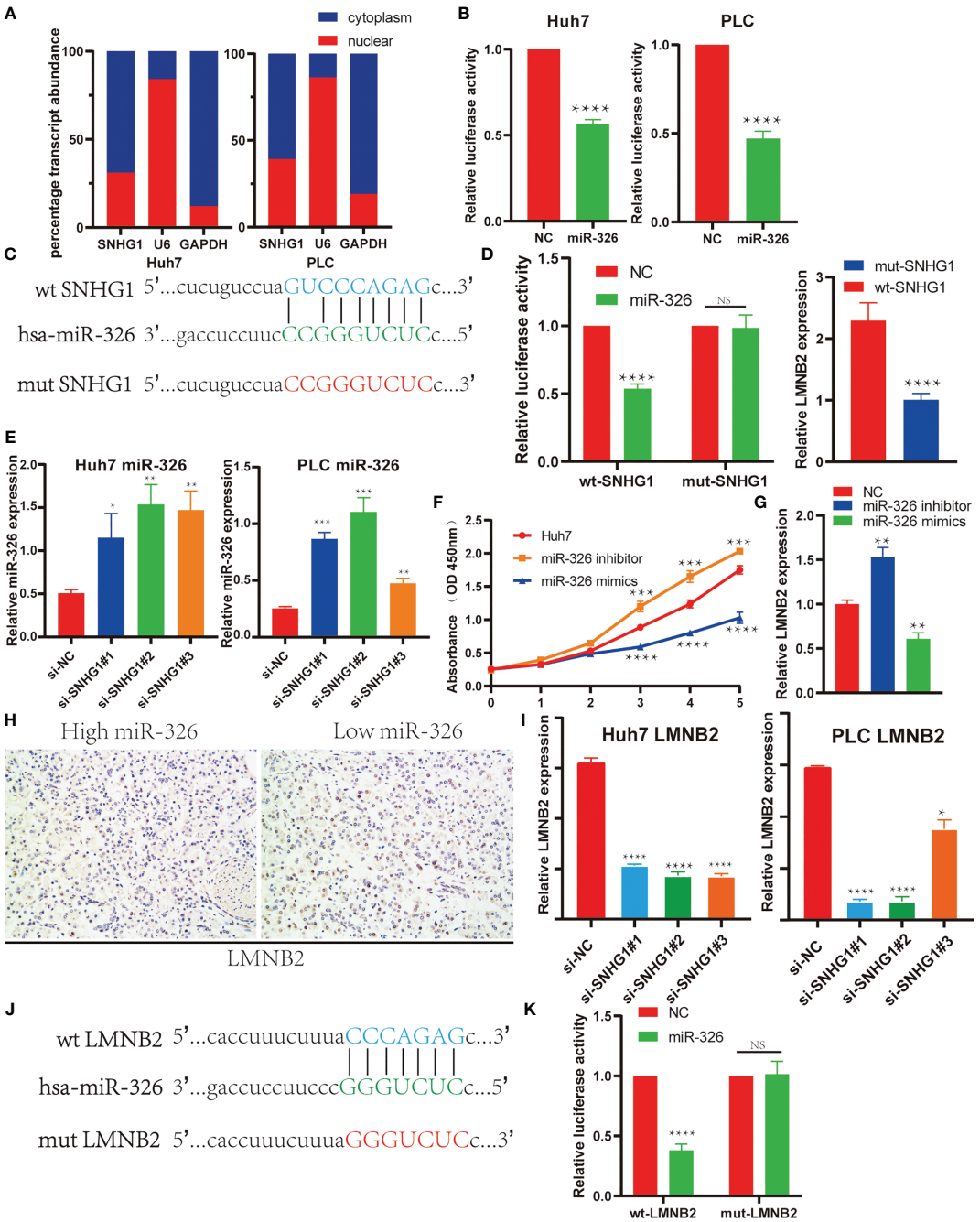

FIGURE 7 | *SNHG1* regulated *LMNB2* expression through sponging *miR-326* in hepatocellular carcinoma (HCC) cells. **(A)** Subcellular localization of *SNHG1* was detected by quantifying nuclear and cytoplasmic fractions. U6 and glyceraldehyde 3-phosphate dehydrogenase (GAPDH) were used as nuclear and cytosolic controls, respectively. **(B)** Dual-luciferase reporter assay showed that *miR-326* directly interacted with *SNHG1* in Huh7 and PLC cells (****p < 0.0001). **(C)** The potential binding site of *SNHG1* and *miR-326* predicted by StarBase. The sequence alignment of *miR-326* and the predicted binding region in *SNHG1* (green). Predicted *miR-326* binding sites (blue) in *SNHG1* and position of mutated nucleotides in *SNHG1* (red). **(D)** Dual-luciferase reporter assay was performed to detect the binding of *miR-326* with WT-*SNHG1* in Huh7 cells. Expression of *LMNB2* in Huh7 cells after addition of wt-*SNHG1* compared with mut-*SNHG1* (****p < 0.0001). **(E)** Expression of *miR-326* in Huh7 and PLC cells with *SNHG1* knockdown (*p < 0.05, **p < 0.01, ***p < 0.001). **(F)** OD value of Huh7 cells in the MTT assay demonstrated that *miR-326* mimics could inhibit cell proliferation significantly, while *miR-326* inhibitor could accelerate HuH7 cell proliferation (***p < 0.001, ****p < 0.0001). **(G)** Expression of *LMNB2* in Huh7 cells transfected with *miR-326* mimics and inhibitor was measured by qRT-PCR (**p < 0.01). **(H)** Representative immunohistochemistry (IHC) images of *LMNB2* are shown in hepatocellular carcinoma with different *miR-326* expression levels. **(I)** RNA levels of *LMNB2* in Huh7 and PLC cells with *SNHG1* knockdown detected by RT-qPCR (*p < 0.05, ****p < 0.0001). **(J)** The potential binding site of *LMNB2* and *miR-326* predicted by StarBase. The sequence alignment of *miR-326* and the predicted binding region in *LMNB2* (green). Predicted *miR-326* binding sites (blue) in *LMNB2* and position of mutated nucleotides in *SNHG1* (red). **(K)** Dual-luciferase reporter assay was performed to detect the binding of *miR-326* with wt-*LMNB2* in Huh7 cells (****p < 0.0001). NS, No Significant.

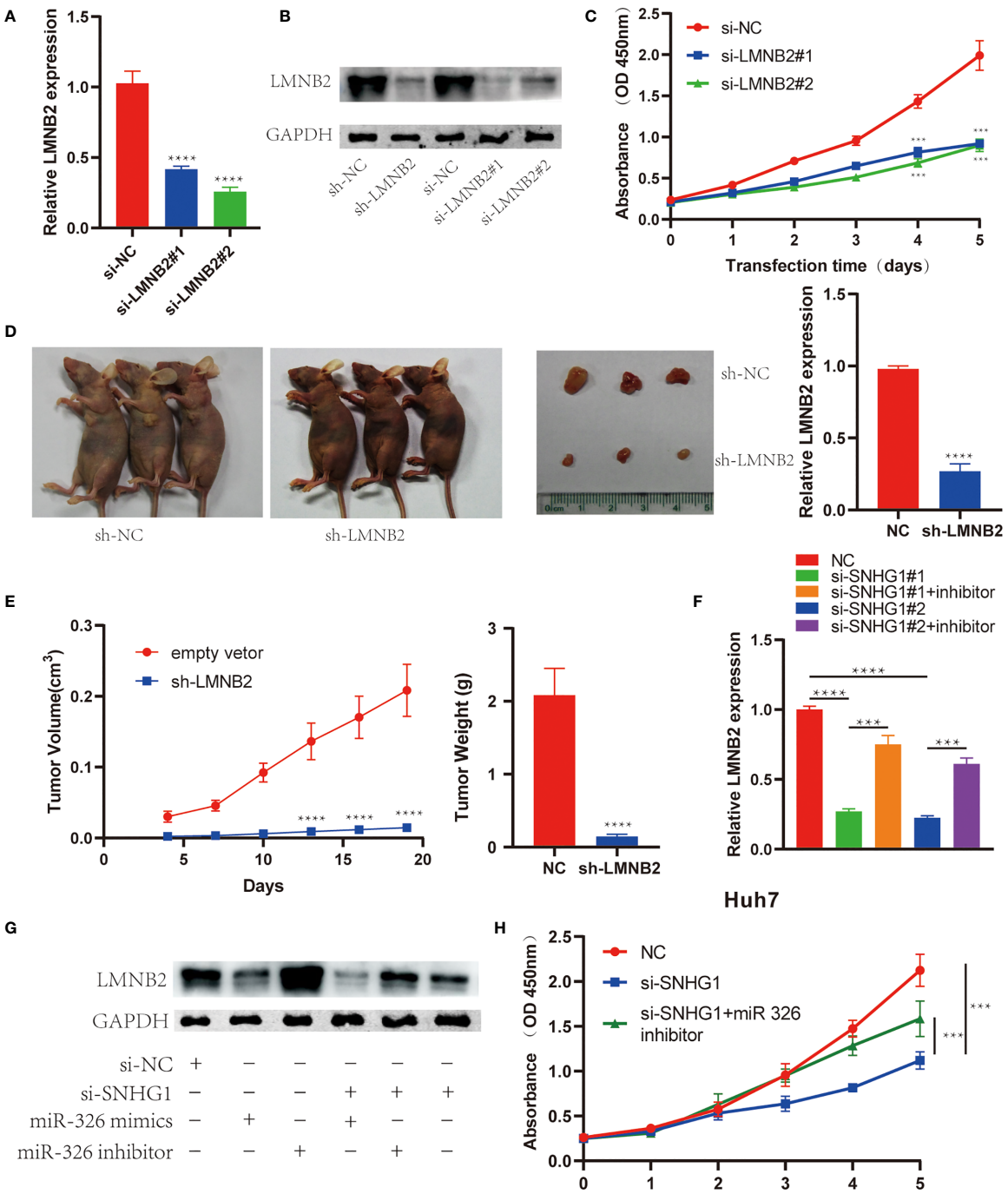

FIGURE 8 | *LMNB2* promotes hepatocellular carcinoma (HCC) growth and mediates the role of *SNHG1* in HCC. **(A)** *LMNB2* expression decreased significantly in Huh7 cells with *LMNB2* siRNA treatment (****p < 0.0001). **(B)** Western blotting was performed to detect the protein level of *LMNB2* in Huh7 cells. **(C)** OD value of Huh7 cells with *LMNB2* knockdown and control cells in the 3-(4,5-Dimethylthiazol-2-yl)-2,5-diphenyltetrazolium bromide (MTT) assay (***p < 0.0001). **(D, E)** Quantification of tumor volume and tumor weight of mice following the injection of HuH7 cells with *LMNB2* knockdown or control cells. Representative images of mice bearing tumors, and tumor images were shown (****p < 0.0001). **(F)** The qRT-PCR demonstrated that *miR-326* inhibitor rescued the decreased *LMNB2* expression caused by *SNHG1* knockdown (***p < 0.001, ****p < 0.0001). **(G)** Western blotting assay showed that *miR-326* regulated *LMNB2* expression, and *miR-326* inhibitor rescued *LMNB2* downregulation caused by *SNHG1* knockdown in Huh7 cells. **(H)** MTT assays demonstrated that *miR-326* inhibitor rescued tumor growth inhibition caused by *SNHG1* knockdown (***p < 0.0001).

of *SNHG1* expression could inhibit cell proliferation, migration, and invasion significantly, and the function of *SNHG1* was further confirmed in an *in vivo* xenograft model. However, the mechanism of *SNHG1* in HCC is still unclear. Zhang et al. (35) revealed that *SNHG1* promoted HCC proliferation and cell cycle progression through inhibiting *p53* and its target genes expression, and similar results were described in colorectal cancer (36). Recent further research found that binding to *DNMT1* mediated the role of *SNHG1*-induced *p53* inhibition in HCC (34). As we know, sponging miRNA is an important regulatory way of lncRNA functions. For example, *SNHG1* has been reported to regulate *PDCD4* expression by sponging *miR-195-5p* in HCC (15). Recent studies found that *SNHG1* promoted HCC progression *via* sponging *miR-377-3p* and *miR-195* (16, 17). Interestingly, our findings showed a new mechanism through which *SNHG1* promoted HCC growth by binding to *miR-326* directly. Our data indicated that *miR-326* level increased significantly after *SNHG1* knockdown and *SNHG1* level is correlated with *miR-326* expression negatively based on TCGA database. Consistent with our reports, *SNHG1* also accelerated tumorigenesis by sponging *miR-326* in osteosarcoma and promoted nucleus pulposus cell proliferation through regulating *miR-326* (30, 37).

Lamin B2 is a member of the lamin protein family known as the nuclear lamina, which included *lamin A*, *B1*, *B2*, *B3*, and *C* (38). It is reported to be involved in the formation of mitotic spindles (39). However, increasing evidence showed that *LMNB2* was associated with prostate and lung tumor progression and served as a prognostic marker (40–42). In our results, we also found that knockdown of *LMNB2* inhibited cell proliferation and growth *in vitro* and *in vivo*, consistent with the data in latest reports (23). miRNAs are small noncoding RNAs that regulate gene expression negatively by enhancing degradation of the target mRNA and inhibiting the following translation (43). Based on our data in bioinformatics analysis and cell experiments, we found that *miR-326* mimics could reduce *LMNB2* mRNA and protein expression compared with control in HCC cell lines, meaning we firstly identified *LMNB2* as the target of *miR-326* in HCC. To verify the hypothesis that *SNHG1* regulates *LMNB2* expression by sponging *miR-326* in HCC, we tested the effects of *miR-326* on *SNHG1*-induced *LMNB2* expression. The rescue experiments indicated that *miR-326* inhibitor reversed the *LMNB2* decrease induced by *SNHG1* knockdown, and correlation analysis also confirmed the *SNHG1–miR-326–LMNB2* axis in HCC. Although Zhang et al. (42) have demonstrated that *LMNB2* was responsible for the malignant phenotype of non-small cell lung carcinoma (NSCLC) through upregulating demethylation of *H3K9*, the mechanism of *SNHG1* in HCC progression still needs further investigation.

To sum up, we found that *SNHG1* acted as a ceRNA by sequestering miR-326 and regulating *LMNB2* expression in HCC. These findings contributed to a better understanding of the mechanisms underlying HCC progression. *SNHG1* may be a promising biomarker for predicting prognosis and a potential therapeutic target for HCC.

DATA AVAILABILITY STATEMENT

The datasets presented in this study can be found in online repositories. The names of the repository/repositories and accession number(s) can be found in the article/**Supplementary Material**.

ETHICS STATEMENT

The studies involving human participants were reviewed and approved by Qilu Hospital of Shandong University. The patients/participants provided their written informed consent to participate in this study. The animal study was reviewed and approved by Qilu Hospital of Shandong University.

AUTHOR CONTRIBUTIONS

WM, LG, and SN participated in the conceptual design of the study. WM participated in the operation of bioinformatics tools. WM, LG, and SN performed the experiments. SN and HY are responsible for fund acquisition. GL is responsible for resource acquisition. LG, YL, and GL participated in the data verification. WM and SN performed the data analysis and wrote the article. All authors have read and reviewed the article. All authors contributed to the article and approved the submitted version.

FUNDING

The present study was supported by the National Natural Science Foundation of China (grant nos. 31701013 and 81903044) and the Natural Science Foundation of Shandong Province (grant no. ZR2017BC032).

SUPPLEMENTARY MATERIAL

The Supplementary Material for this article can be found online at: https://www.frontiersin.org/articles/10.3389/fonc.2021.784067/full#supplementary-material

Supplementary Table 1 | Clinical data in TCGA LIHC mRNA data.

Supplementary Table 2 | Clinical data in TCGA LIHC miRNA data.

REFERENCES

1. Forner A, Reig M, Bruix J. Hepatocellular Carcinoma. *Lancet* (2018) 391:1301–14. doi: 10.1016/S0140-6736(18)30010-2
2. Villanueva A. Hepatocellular Carcinoma. *N Engl J Med* (2019) 380:1450–62. doi: 10.1056/NEJMra1713263
3. Marengo A, Rosso C, Bugianesi E. Liver Cancer: Connections With Obesity, Fatty Liver, and Cirrhosis. *Annu Rev Med* (2016) 67:103–17. doi: 10.1146/annurev-med-090514-013832
4. Yang JD, Hainaut P, Gores GJ, Amadou A, Plymoth A, Roberts LR. A Global View of Hepatocellular Carcinoma: Trends, Risk, Prevention and Management. *Nat Rev Gastroenterol Hepatol* (2019) 16:589–604. doi: 10.1038/s41575-019-0186-y

5. Lin DC, Mayakonda A, Dinh HQ, Huang P, Lin L, Liu X, et al. Genomic and Epigenomic Heterogeneity of Hepatocellular Carcinoma. *Cancer Res* (2017) 77:2255–65. doi: 10.1158/0008-5472.CAN-16-2822
6. Zheng H, Pomyen Y, Hernandez MO, Li C, Livak F, Tang W, et al. Single-Cell Analysis Reveals Cancer Stem Cell Heterogeneity in Hepatocellular Carcinoma. *Hepatology* (2018) 68:127–40. doi: 10.1002/hep.29778
7. Kopp F, Mendell JT. Functional Classification and Experimental Dissection of Long Noncoding RNAs. *Cell* (2018) 172:393–407. doi: 10.1016/j.cell.2018.01.011
8. Huarte M. The Emerging Role of Lncrnas in Cancer. *Nat Med* (2015) 21:1253–61. doi: 10.1038/nm.3981
9. Schmitt AM, Chang HY. Long Noncoding RNAs in Cancer Pathways. *Cancer Cell* (2016) 29:452–63. doi: 10.1016/j.ccell.2016.03.010
10. Wong CM, Tsang FH, Ng IO. Non-Coding RNAs in Hepatocellular Carcinoma: Molecular Functions and Pathological Implications. *Nat Rev Gastroenterol Hepatol* (2018) 15:137–51. doi: 10.1038/nrgastro.2017.169
11. Galamb O, Barták BK, Kalmár A, Nagy ZB, Szigeti KA, Tulassay Z, et al. Diagnostic and Prognostic Potential of Tissue and Circulating Long non-Coding RNAs in Colorectal Tumors. *World J Gastroenterol* (2019) 25:5026–48. doi: 10.3748/wjg.v25.i34.5026
12. Jiao M, Ning S, Chen J, Chen L, Jiao M, Cui Z, et al. Long non–Coding RNA ZEB1–AS1 Predicts a Poor Prognosis and Promotes Cancer Progression Through the MiR–200a/ZEB1 Signaling Pathway in Intrahepatic Cholangiocarcinoma. *Int J Oncol* (2020) 56:1455–67. doi: 10.3892/ijo.2020.5023
13. Thomson DW, Dinger ME. Endogenous MicroRNA Sponges: Evidence and Controversy. *Nat Rev Genet* (2016) 17:272–83. doi: 10.1038/nrg.2016.20
14. Wang JY, Yang Y, Ma Y, Wang F, Xue A, Zhu J, et al. Potential Regulatory Role of LncRNA-MiRNA-mRNA Axis in Osteosarcoma. *BioMed Pharmacother* (2020) 121:109627. doi: 10.1016/j.biopha.2019.109627
15. Huang D, Wei Y, Zhu J, Wang F. Long non-Coding RNA *SNHG1* Functions as a Competitive Endogenous RNA to Regulate *PDCD4* Expression by Sponging *MiR-195-5p* in Hepatocellular Carcinoma. *Gene* (2019) 714:143994. doi: 10.1016/j.gene.2019.143994
16. Qu A, Yang Q. LncRNA *SNHG1* Promotes Cell Progression and Metastasis *via* Sponging *MiR-377-3p* in Hepatocellular Carcinoma. *Neoplasma* (2020) 67:557–66. doi: 10.4149/neo_2020_190705N593
17. Zhang H, Zhou D, Ying M, Chen M, Chen P, Chen Z, et al. Expression of Long non-Coding RNA (LncRNA) Small Nucleolar RNA Host Gene 1 (*SNHG1*) Exacerbates Hepatocellular Carcinoma Through Suppressing MiR-195. *Med Sci Monit* (2016) 22:4820–9. doi: 10.12659/MSM.898574
18. Ding L, Bailey MH, Porta-Pardo E, Thorsson V, Colaprico A, Bertrand D, et al. Perspective on Oncogenic Processes at the End of the Beginning of Cancer Genomics. *Cell* (2018) 173:305–20.e10. doi: 10.1016/j.cell.2018.03.033
19. Yu G, Wang LG, Han Y, He QY. Clusterprofiler: An R Package for Comparing Biological Themes Among Gene Clusters. *Omics* (2012) 16:284–7. doi: 10.1089/omi.2011.0118
20. Li JH, Liu S, Zhou H, Qu LH, Yang JH. Starbase V2.0: Decoding Mirna-Cerna, Mirna-Ncrna and Protein-RNA Interaction Networks From Large-Scale CLIP-Seq Data. *Nucleic Acids Res* (2014) 42:D92–7. doi: 10.1093/nar/gkt1248
21. Li R, Qu H, Wang S, Wei J, Zhang L, Ma R, et al. Gdcrnatools: An R/Bioconductor Package for Integrative Analysis of Lncrna, Mirna and Mrna Data in GDC. *Bioinformatics* (2018) 34:2515–7. doi: 10.1093/bioinformatics/bty124
22. Zhang S, Song X. Long non-Coding RNA *SNHG1* Promotes Cell Proliferation and Invasion of Hepatocellular Carcinoma by Acting as a Molecular Sponge to Modulate MiR-195. *Arch Med Sci* (2020) 16:386–94. doi: 10.5114/aoms.2019.81311
23. Li XN, Yang H, Yang T. MiR-122 Inhibits Hepatocarcinoma Cell Progression by Targeting LMNB2. *Oncol Res* (2020) 28:41–9. doi: 10.3727/096504019X15615433287579
24. Mattioni A, Boldt K, Auciello G, Komada M, Rappoport JZ, Ueffing M, et al. Ring Finger Protein 11 Acts on Ligand-Activated EGFR *via* the Direct Interaction With the UIM Region of ANKRD13 Protein Family. *FEBS J* (2020) 287:3526–50. doi: 10.1111/febs.15226
25. Polito D, Cukras S, Wang X, Spence P, Moreau L, D'Andrea AD, et al. The Carboxyl Terminus of *FANCE* Recruits FANCD2 to the Fanconi Anemia (FA) E3 Ligase Complex to Promote the FA DNA Repair Pathway. *J Biol Chem* (2014) 289:7003–10. doi: 10.1074/jbc.M113.533976
26. Wang X, Kennedy RD, Ray K, Stuckert P, Ellenberger T, D'Andrea AD. Chk1-Mediated Phosphorylation of *FANCE* is Required for the Fanconi Anemia/BRCA Pathway. *Mol Cell Biol* (2007) 27:3098–108. doi: 10.1128/MCB.02357-06
27. Peng WX, Koirala P, Mo YY. Lncrna-Mediated Regulation of Cell Signaling in Cancer. *Oncogene* (2017) 36:5661–7. doi: 10.1038/onc.2017.184
28. Xu M, Chen X, Lin K, Zeng K, Liu X, Pan B, et al. The Long Noncoding RNA *SNHG1* Regulates Colorectal Cancer Cell Growth Through Interactions With EZH2 and MiR-154-5p. *Mol Cancer* (2018) 17:141. doi: 10.1186/s12943-018-0894-x
29. Zhang Y, Yu R, Li Q, Li Y, Xuan T, Cao S, et al. *SNHG1*/MiR-556-5p/TCF12 Feedback Loop Enhances the Tumorigenesis of Meningioma Through Wnt Signaling Pathway. *J Cell Biochem* (2020) 121:1880–9. doi: 10.1002/jcb.29423
30. Wang J, Cao L, Wu J, Wang Q. Long non-Coding RNA *SNHG1* Regulates NOB1 Expression by Sponging *MiR-326* and Promotes Tumorigenesis in Osteosarcoma. *Int J Oncol* (2018) 52:77–88. doi: 10.3892/ijo.2017.4187
31. Bhan A, Soleimani M, Mandal SS. Long Noncoding RNA and Cancer: A New Paradigm. *Cancer Res* (2017) 77:3965–81. doi: 10.1158/0008-5472.CAN-16-2634
32. Li X, Zheng H. LncRNA *SNHG1* Influences Cell Proliferation, Migration, Invasion, and Apoptosis of Non-Small Cell Lung Cancer Cells *via* the Mir-361-3p/FRAT1 Axis. *Thorac Cancer* (2020) 11:295–304. doi: 10.1111/1759-7714.13256
33. Li W, Dong X, He C, Tan G, Li Z, Zhai B, et al. LncRNA *SNHG1* Contributes to Sorafenib Resistance by Activating the Akt Pathway and is Positively Regulated by MiR-21 in Hepatocellular Carcinoma Cells. *J Exp Clin Cancer Res* (2019) 38:183. doi: 10.1186/s13046-019-1177-0
34. Li SJ, Wang L, Sun ZX, Sun SJ, Gao J, Ma RL. LncRNA *SNHG1* Promotes Liver Cancer Development Through Inhibiting *P53* Expression *via* Binding to DNMT1. *Eur Rev Med Pharmacol Sci* (2019) 23:2768–76. doi: 10.26355/eurrev_201904_17550
35. Zhang M, Wang W, Li T, Yu X, Zhu Y, Ding F, et al. Long Noncoding RNA *SNHG1* Predicts a Poor Prognosis and Promotes Hepatocellular Carcinoma Tumorigenesis. *BioMed Pharmacother* (2016) 80:73–9. doi: 10.1016/j.biopha.2016.02.036
36. Zhao Y, Qin ZS, Feng Y, Tang XJ, Zhang T, Yang L. Long non-Coding RNA (LncRNA) Small Nucleolar RNA Host Gene 1 (*SNHG1*) Promote Cell Proliferation in Colorectal Cancer by Affecting P53. *Eur Rev Med Pharmacol Sci* (2018) 22:976–84. doi: 10.26355/eurrev_201802_14379
37. Tan H, Zhao L, Song R, Liu Y, Wang L. The Long Noncoding RNA SNHG1 Promotes Nucleus Pulposus Cell Proliferation Through Regulating *MiR-326* and CCND1. *Am J Physiol Cell Physiol* (2018) 315:C21–c7. doi: 10.1152/ajpcell.00220.2017
38. Hale CM, Shrestha AL, Khatau SB, Stewart-Hutchinson PJ, Hernandez L, Stewart CL, et al. Dysfunctional Connections Between the Nucleus and the Actin and Microtubule Networks in Laminopathic Models. *Biophys J* (2008) 95:5462–75. doi: 10.1529/biophysj.108.139428
39. Zheng X, Kim Y, Zheng Y. Identification of Lamin B-Regulated Chromatin Regions Based on Chromatin Landscapes. *Mol Biol Cell* (2015) 26:2685–97. doi: 10.1091/mbc.E15-04-0210
40. Saarinen I, Mirtti T, Seikkula H, Boström PJ, Taimen P. Differential Predictive Roles of a- and B-Type Nuclear Lamins in Prostate Cancer Progression. *PloS One* (2015) 10:e0140671. doi: 10.1371/journal.pone.0140671
41. Ma Y, Fei L, Zhang M, Zhang W, Liu X, Wang C, et al. *Lamin B2* Binding to Minichromosome Maintenance Complex Component 7 Promotes non-Small Cell Lung Carcinogenesis. *Oncotarget* (2017) 8:104813–30. doi: 10.18632/oncotarget.20338
42. Zhang MY, Han YC, Han Q, Liang Y, Luo Y, Wei L, et al. *Lamin B2* Promotes the Malignant Phenotype of Non-Small Cell Lung Cancer Cells by Upregulating Dimethylation of Histone 3 Lysine 9. *Exp Cell Res* (2020) 393:112090. doi: 10.1016/j.yexcr.2020.112090
43. Rupaimoole R, Slack FJ. MicroRNA Therapeutics: Towards a New Era for the Management of Cancer and Other Diseases. *Nat Rev Drug Discov* (2017) 16:203–22. doi: 10.1038/nrd.2016.246

Conflict of Interest: The authors declare that the research was conducted in the absence of any commercial or financial relationships that could be construed as a potential conflict of interest.

this article, or claim that may be made by its manufacturer, is not guaranteed or endorsed by the publisher.

frontiers in Oncology

ORIGINAL RESEARCH
published: 02 December 2021
doi: 10.3389/fonc.2021.756419

Loss of FBP1 by aPKC-ι/Snail Pathway-Mediated Repression Promotes Invasion and Aerobic Glycolysis of Intrahepatic Cholangiocarcinoma

Meng Gao[1,2†], Chengjie Mei[1,2†], Yonghua Guo[1,2], Peng Xia[1,2], Hao Zhang[1,2], Yinyi Liu[1,2], Ye Yao[1,2], Xiang Jiang[1,2], Yufeng Yuan[1,2] and Yawei Qian[3*]*

[1] Department of Hepatobiliary and Pancreatic Surgery, Zhongnan Hospital of Wuhan University, Wuhan, China, [2] Clinical Medicine Research Center for Minimally Invasive Procedure of Hepatobiliary & Pancreatic Diseases of Hubei Province, Wuhan, China, [3] Department of General Surgery, The First Affiliated Hospital of Nanjing Medical University, Nanjing, China

OPEN ACCESS

Edited by:
Yunfei Xu,
Shandong University, China

Reviewed by:
Alessandro Rizzo,
Sant'Orsola-Malpighi Polyclinic, Italy
Kishor Pant,
University of Minnesota Twin Cities, United States

***Correspondence:**
Yawei Qian
ywess1990@163.com
Yufeng Yuan
yuanyf1971@whu.edu.cn

†These authors have contributed equally to this work and share first authorship

Specialty section:
This article was submitted to Cancer Molecular Targets and Therapeutics, a section of the journal Frontiers in Oncology

Received: 10 August 2021
Accepted: 15 November 2021
Published: 02 December 2021

Citation:
Gao M, Mei C, Guo Y, Xia P, Zhang H, Liu Y, Yao Y, Jiang X, Yuan Y and Qian Y (2021) Loss of FBP1 by aPKC-ι/Snail Pathway-Mediated Repression Promotes Invasion and Aerobic Glycolysis of Intrahepatic Cholangiocarcinoma. Front. Oncol. 11:756419. doi: 10.3389/fonc.2021.756419

Intrahepatic cholangiocarcinoma (ICC) is one of the most commonly diagnosed malignancies worldwide, and the second most common primary liver tumor. The lack of effective diagnostic and treatment methods results in poor patient prognosis and high mortality rate. Atypical protein kinase C-ι (aPKC-ι) is highly expressed in primary and metastatic ICC tissues, and regulates epithelial mesenchymal transition (EMT) through the aPKC-ι/P-Sp1/Snail signaling pathway. Recent studies have correlated aberrant glucose metabolism with EMT. Given the vital role of FBP1 in regulating glucose metabolism in cancer cells, we hypothesized that aPKC-ι downregulates FBP1 in ICC cells through the Snai1 pathway, and enhances glycolysis and metastasis. We confirmed the ability of aPKC-ι promotes glycolysis, invasion and metastasis of cancer cells, and further demonstrated that FBP1 inhibits the malignant properties of ICC cells by antagonizing aPKC-ι. Our findings provide novel insights into the molecular mechanisms of ICC progression and metastasis, as well as a theoretical basis for exploring new treatment strategies.

Keywords: aPKC-ι, intrahepatic cholangiocarcinoma, FBP1, Snai1, EMT, invasion, metastasis

INTRODUCTION

Intrahepatic cholangiocarcinoma (ICC) is a highly malignant tumor that originates from the epithelial cells of the intrahepatic secondary bile duct and its branches. It is the second most common primary liver tumor, and has poor prognosis (1) due to frequent metastasis and recalcitrance to radiotherapy and chemotherapy (2, 3). Although notable improvements have been made with different preclinical available cholangiocarcinoma models (4–6), such as the fibroblast growth factor receptor 2 inhibitor pemigatinib, the first approval of a molecularly targeted treatment in patients with advanced cholangiocarcinoma by US Food and Drug Administration, the prognosis of this disease remains unsatisfactory (7). Therefore, further studies on the molecular

mechanism of invasion and metastasis and exploring a novel and effective therapeutic target of ICC are urgently needed (8).

Atypical protein kinase C-ι (aPKC-ι) is a promising target for multiple tumor types, such as non-small cell lung cancer, pancreatic ductal adenocarcinoma and hepatocellular carcinoma (9–11). A recent study showed that targeted silencing of aPKC-ι reversed TGF-β-induced epithelial mesenchymal transition (EMT) of non-small cell lung cancer cells, implying that aPKC-ι may function to promote EMT (12). In addition, it is also involved in tumor cell transformation, adhesion, movement, invasion and metastasis (13).

Fructose-1,6-bisphosphatase (FBP1) is one of the rate-limiting enzymes of gluconeogenesis (14), and its epigenetic regulation is critical to the glucose metabolism in cancer cells (15, 16). Loss of FBP1 in basal-like breast cancer cells significantly increased glucose uptake, lactate secretion and glycolysis rate, which was conducive to EMT and the maintenance of the basal-like phenotype (17, 18). It is also reported that decreased FBP1 expression regulating by miR-18a-5p promotes liver cancer cells migration and invasion (19). Glucose metabolism is a determinant of cancer cell invasion and metastasis. Cancer cells preferentially use glycolysis to produce energy in the hypoxic tumor mass, a phenomenon known as the "Warburg effect" (20–23). Glucose uptake is significantly enhanced in the cancer cells during EMT, which coincides with increased glycolysis (24, 25) and lactate secretion that promote tumor invasion and distant metastasis (26, 27). It is also reported that the reprogramming of tumor cell metabolism is a macroscopic change, and the change of ICC from oxidative phosphorylation to glycolysis provides favorable conditions for the proliferation of tumor cells (5–7).

The Snail family of transcriptional repressors, including Snai1, Snai2 (Slug) and Snai3 (Smuc), have been implicated in EMT during embryonic development as well as carcinogenesis. Snai1-mediated inhibition of the tumor suppressor microRNA let-7 is associated with poor prognosis in several cancers (28). In our previous studies, we found that high levels aPKC-ι in ICC cells correlated to increased glycolysis and lactate production (29). Given that FBP1 deletion promotes tumorigenesis in some cancers (30), our aim of this study was to elucidate the mechanistic relationship between PKC-ι, FBP1 and Snai1 in the regulation of glycolysis and metastasis of ICC cells.

MATERIALS AND METHODS

Tissue Samples and Cell Culture

40 paired of ICC and para-cancerous tissue specimens were collected at the Zhongnan Hospital of Wuhan University (Hubei Province, China) after obtaining written consent from the patients. HCCC-9810 and RBE cell lines were obtained from the cell bank of the Chinese Academy of Sciences (Shanghai, China), and were cultured in RPMI-1640 medium supplemented with 10% fetal bovine serum (GIBCO, US) at 37°C under 5% CO_2. Cells in the logarithmic growth phase were selected for the experiments. The study was conducted according to the guidelines of the "Declaration of Helsinki" and approved by the Hospital Committee for the Protection of Human Subjects.

RNA Isolation and qRT-PCR

Total RNA was isolated form the cells and tissues using TRIzol reagent (Thermo Fisher Scientific, MA, USA) according to the manufacturer's instructions. A reverse transcription kit Vazyme, Hubei, China) was used to synthesize cDNA, and RT-PCR was performed using the SYBR Green PCR Kit (Vazyme, Hubei, China).

Histology and Immunohistochemistry (IHC)

The tumor tissue samples were fixed in 10% formalin, embedded in paraffin, and cut into 4μm-thick sections. After clearing with xylene and rehydrating with ethanol, the sections were incubated with 0.3% hydrogen peroxide to inactivate the endogenous peroxidases. The tissue sections were then incubated with the primary antibody, washed with PBS, and probed with the HRP-conjugated secondary antibody and streptavidin (Santa Cruz). Diaminobenzidine substrate was used for color development, followed by counterstaining with hematoxylin. The tissue microarray chips were probed with specific antibodies and digitally scanned.

Western Blotting

Western blotting was performed as previously described (31). The proteins extracted from the cells were quantified using the BCA protein assay method (Biyuntian, Wuhan, China), and equal amounts of protein per sample were separated *via* 6–15% SDS-PAGE and transferred to polyvinylidene fluoride membranes (Millipore, USA). After blocking with 5% skimmed milk, the membranes were incubated overnight with the primary antibodies at 4°C, washed thrice with TBST (10 minutes each), and probed with the secondary antibody at room temperature. The membranes were washed thrice with TBST and developed with ECL.

Glucose Uptake and Lactate Secretion Assay

The cells were seeded in a 6-well plate at the density of 5×10^5 cells per well, and cultured in the presence of EGF or 2-DG 48h. The glucose uptake was measured using a glucose uptake cell-based assay kit (Cayman Chemical) according to the manufacturer's instructions. The cells were analyzed by flow cytometry. The conditioned media were centrifuged at 13000 g for 10 minutes at 4°C, and the lactate concentration in the clarified supernatants was measured using the L-lactate detection kit (Eton Biosciences) according to the manufacturer's instructions. The absolute lactate level was calculated from the corresponding standard curve and normalized to the number of cells.

Seahorse XFp Metabolic Flux Analysis

The day before the experiment, ICC cells were planted on the Seahorse XF cell culture plate at 1×10^6 cells/well. Add the test solution prepared by Seahorse XF Base Medium to the plate, then use NaOH to adjust the pH to 7.4. 2 hours later, change the medium and place it in a carbon dioxide-free incubator for one hour. After adding mitochondrial inhibitors oligomycin, FCCP, and antimycin (AA) plus rotenone (AR), the baseline was

measured four times in sequence. Then use the XFp extracellular analyzer (Agilent Technologies, USA) to analyze the oxygen consumption rate (OCR). Similarly, after adding Gluoose, Oligomycin, 2-DG, we can calculate the extracellular acidification rate (ECAR).

Chromatin Immunoprecipitation (ChIP)

EZ ChIP™ Chromatin Immunoprecipitation Kit (Millipore, Billerica, MA) was used for ChIP assay. The treated cells were cross-linked in 1% formaldehyde at 37°C for 10 minutes, and sonicated to obtain chromatin fragments of 200-1000 bp. The lysates were incubated overnight with 3μg anti-Snai1 or anti-IgG antibody (Millipore) at 4°C, followed by magnetic beads for 2h. The protein/DNA complex was eluted and cross-linked, and the immunoprecipitated DNA was analyzed by qRT-PCR.

Dual Luciferase Assay

Cells were co-transfected with FBP1-3'UTR-WT or -MUT reporter plasmid and Renilla luciferase vector using Lipofectamine 3000 reagent (Invitrogen). Luciferase activity was measured 48h later using the dual luciferase reporter gene detection system (Promega), and the data was normalized to Renilla luciferase activity.

Establishment of Subcutaneous Tumor and Lung Metastasis Model

The animal experiments were approved by the Institutional Animal Ethics Committee of Wuhan University. 10 of four-week-old female BALB/c nude mice were injected subcutaneously with 1×10^6 HCCC-9810 cells to induce subcutaneous tumors. The mice were sacrificed 4 weeks later for further analysis. The lung metastasis model was established in four-week-old female BALB/c nude mice by intravenous injection of 3×10^6 HCCC-9810 cells (n=5 for each group), and the lungs were harvested 4 weeks later for IHC (32).

Statistical Analysis

All data are expressed as the mean ± SD of at least three independent experiments. Two groups were compared by Student's t test (SPSS statistical software package, version 12; SPSS Inc.). Overall survival rates were analyzed by the Kaplan-Meier method and Cox proportional hazards regression model. $P < 0.05$ was considered statistically significant.

RESULTS

FBP1 Expression Is Inversely Correlated With aPKC-ι in Intrahepatic Cholangiocarcinoma

Quantitative real-time PCR was employed to determine the expression levels of aPKC-ι and FBP1 in 40 paired ICC and adjacent nontumor tissues (**Figure 1A**). The results were confirmed by WB and IHC (**Figures 1C, D**). We found that aPKC-ι and FBP1 were both localized to the cytoplasm of cancer cells in IHC experiments. In addition, the expression level of aPKC-ι was significantly higher in tumor tissues compared to that in paired para-matched non-tumor specimens, while FBP1 expression was markedly lower. We next investigated whether the expression of aPKC-ι and FBP1 was associated with clinicopathological characteristics and prognosis. The clinical data of all ICC patients, including age, gender, tumor/non-tumor tissues, nodal invasion, tumor staging and tumor differentiation degree, are summarized in **Table 1**.

Overexpression of aPKC-ι was related to tumor–node–metastasis (TNM) stage III-IV ($\chi2 = 10.417$, P=0.004), and medium/poor differentiation ($\chi2 = 10.157$, P=0.005) in ICC patients. And, as expected, low expression of FBP1 was related to tumor–node–metastasis (TNM) stage III-IV ($\chi2 = 10.417$, P=0.004), and medium/poor differentiation ($\chi2 = 6.144$, P=0.034). We further investigated whether there was an correlation between aPKC-ι and FBP1 expression in ICC samples. As shown in **Figure 1B**, aPKC-ι level is significantly negatively associated with FBP1 (R=-0.605, $p<0.01$). Meanwhile, a Kaplan-Meier analysis indicated that patients with high expression of aPKC-ι displayed a shorter OS compared to those with low expression, while those with low FBP1 expression exhibited a shorter OS (**Figure 1E**). Multivariate Cox regression analyses also showed that aPKC-ι and FBP1 were independent prognostic factors for OS in ICC (**Table 2**). These above results suggested that aPKC-ι may interact with FBP1 and promote invasion and metastasis of ICC.

Silencing aPKC-ι Attenuates Aerobic Glycolysis and Retards EMT-Like Changes in ICC Cells

Previous studies reported that aPKC-ι may induce EMT-like changes and promote metastasis in cancer cells (33). In this study, we first established two stable human ICC cell lines, HCCC-9810 and RBE, with down-regulated aPKC-ι expression levels *in vitro* by transfection with human aPKC-ι siRNA (**Figure 2A**). Along with aPKC-ι down-regulation, the EMT-like protein expression profiles in both HCCC-9810 and RBE cell lines were reversed compared with negative controls (**Figure 2B**), including up-regulation of the epithelial markers E-cadherin and down-regulation of mesenchymal marker Vimentin. These indicated that aPKC-ι promoted early invasion and metastasis of ICC cells by accelerating EMT. Consistent with above findings, ICC cells with down-regulated aPKC-ι also reversed EMT-like cellular characteristics, including decreased cell proliferation, migration and invasion as compared to negative controls (**Figures 2C–E**). To further assess the effects of aPKC-ι in ICC, metabolism-related indices were determined by glucose uptake and lactate secretion assay. We found that knocking down aPKC-ι deceased the rate of glucose uptake and lactate production in the ICC cells (**Figures 2F, G**), which was according with its role in the aberrant glucose metabolism of cancer cells. Thus, we speculated that aPKC-ι promoted EMT and aerobic glycolysis of ICC cells, which could provide a competitive environment for ICC cells invasion and migration.

FBP1 Is Crucial for aPKC-ι Induced EMT-Like Changes and Glycolysis in Human ICC Cells

To investigate the causal relationship between aPKC-ι and FBP1, we first suppressed aPKC-ι expression in two ICC cell lines.

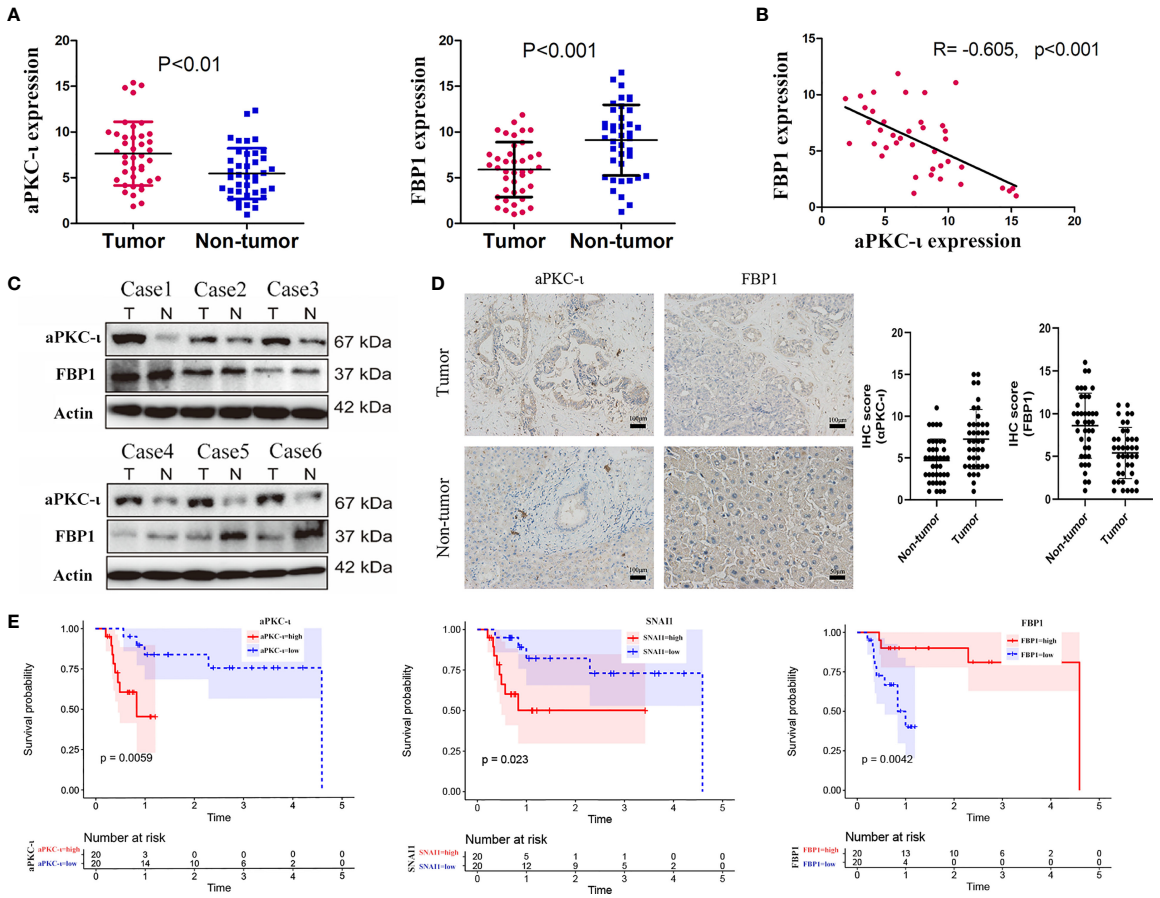

FIGURE 1 | FBP1 expression is inversely correlated with aPKC-ι in ICC. **(A)** mRNA expression levels of aPKC-ι and FBP1 in 40 paired ICC and adjacent nontumor tissues **(B)**. Pearson correlation analysis of aPKC-ι and FBP1 expression (R=-0.605,p<0.01). **(C)** Expression of aPKC-ι and FBP1 in 6 matched ICC samples. **(D)** IHC score and representative images showing *in situ* expression of aPKC-ι and FBP1 in ICC and normal bile duct tissues. **(E)** Overall survival rate in patient with aPKC-ι, FBP1 and SNAI1 expression.

FBP1 mRNA and protein levels were up-regulated in aPKC-ι-deficient HCCC-9810 and RBE cells (**Figures 2A, B**), which was suggestive of an inhibitory effect of aPKC-ι on FBP1 mRNA and protein. We further determined whether FBP1 was regulated by aPKC-ι. The mRNA and protein levels of FBP1 were down-regulated in aPKC-ι-overexpressing ICC cells by transfecting with aPKC-ι-cDNA (**Figures 3A, B**). Therefore, FBP1 expressions were markedly increased both in mRNA and protein levels by transfecting aPKC-ι-cDNA ICC cells with FBP1-cDNA, while aPKC-ι levels were no significant changes as compared with negative control.

Following the up-regulation of FBP1 expression in aPKC-ι-overexpressing ICC cells, EMT-like changes were almost reversed compared with negative control groups, including the expression levels of EMT markers (**Figure 3B**) and cell proliferation, invasion, and migration (**Figures 3C–E**). In addition, along with the up-regulation of FBP1 expression, FBP1-cDNA transfection significantly decreased the relative glucose uptake rate and lactate production (**Figures 3F, G**). Those suggested that FBP1 could reverse the aPKC-ι induced EMT-like changes and normalize glucose metabolism in ICC cells.

aPKC-ι and FBP1 Play the Roles of Accelerator and Speed Limiter in the Process of Glycolysis

Along with koncking down aPKC-i, four key glycolytic enzymes (HK2, ENO1, PKM, LDHA) were decreased at the protein level (**Figure 4A**), which additionally supported that aPKC-i could enhance the glycolysis level of ICC. The cellular oxygen consumption rate (OCR) and extracellular acidification rate (ECAR) were further measured in ICC cells (**Figure 4B**). According to ECAR and OCR curve chart (**Figures 4C, D**), the glycolysis level, glycolysis capacity and glycolysis capacity reserve were significantly increased in aPKC-i-overexpressing ICC cells compared to negative control, while OCR was decreased as compared with negative control. Following increased FBP1 expression in aPKC-i-overexpressing ICC cells, those glycolysis

TABLE 1 | Clinicopathological parameters of ICC patients.

Characteristics	Numberof case	aPKC-ι		P value	FBP1		P value
		Low	High		Low	High	
Age (years)				0.744			0.102
≤60	25	12	13		10	15	
>60	15	6	8		10	5	
Gender				0.507			0.185
Male	26	14	12		11	15	
Female	14	6	8		9	5	
Tumor/nontumor tissues				**0.025**			**<0.001**
Tumor	40	15	25		28	12	
Nontumor	40	25	15		12	28	
Nodal invasion				0.084			0.084
Yes	12	3	9		9	3	
No	28	17	11		11	17	
TNM staging				**0.004**			**0.004**
I-II	16	13	3		3	13	
III-IV	24	7	17		17	7	
Differentiation				**0.005**			**0.034**
Well	11	10	1		2	9	
Medium/poor	29	10	19		18	11	

The boldfaced part indicates a statistically significant value.

markers were markedly down-regulated, whereas the OCR was obviously up-regulated. The results reinforced that aPKC-i/FBP1 pathway palys a important role in glucose metabolism of ICC, which was consistent with our previous conclusions.

FBP1 Antagonizes aPKC-ι and Inhibits Tumor Growth and Metastasis *In Vivo*

To further evaluate the role of FBP1 in ICC, a xenograft tumor model and a pulmonary metastasis tumor model were established. We subcutaneously injected aPKC-ι-overexpressing HCCC-9810 cells transfected with FBP1-cDNA or vector into nude mice. The volumes of tumors from aPKC-ι-overexpressing cells transfected with FBP1-cDNA were dramatically smaller compared with negative control groups (**Figure 5A**). Furthermore, the *in situ* expression of FBP1 and E-cadherin detected by IHC were significantly higher in FBP1-cDNA treatment groups, while Vimentin expression was lower (**Figure 5B**). The *in situ* expression of HK2,ENO1,PKM,LDHA detected by IHC was higher in FBP1-cDNA treatment groups (**Figure 5C**). Moreover, fewer metastatic nodules were determined in the treatment groups than in the untreated groups, suggesting that FBP1 could significantly inhibit lung metastases of ICC cells induced by aPKC-ι (**Figure 5D**). In conclusion, the assay confirmed that FBP1 played an important role in aPKC-ι-mediated ICC progression and metastasis *in vivo*.

FBP1 Is a Direct Target of Snail in aPKC-ι Mediated EMT and "Warburg Effect"

To explore the underlying molecular mechanisms of decreased FBP1 by aPKC-ι, we first performed coimmunoprecipitation (CO-IP) experiments to assess whether aPKC-ι directly interacts with FBP1. Expression of aPKC-ι and FBP1 was not detected in the precipitated protein complex, suggesting that aPKC-ι indirectly regulated Snail through other ways. Snail, a very well-known transcription factor, was reported to be critical for epidermal growth factor–induced EMT of cancer cells (34). We noticed that nine consensus Snail-binding E-boxes domains (CAGGTG) were identified in the FBP1 promoter (17). Moreover, our previous studies had demonstrated that snail was also crucial for aPKC-ι-induced EMT-like changes in cholangiocarcinoma (29). Hence, we hypothesized that Snail may bind to the FBP1 promoter and is responsible for FBP1 repression in aPKC-ι-overexpressing ICC cells.

The expression of Snail was first examined by qRT-PCR in 40 pair-matched tumor specimens and non-tumor tissues. In agreement with existing results, higher Snail expression was in

TABLE 2 | Multivariate cox regression analyses.

Variable	*P*	HR	95% CI
aPKC-ι	0.00514	2.220e+01	[2.530355-194.7296]
FBP1	0.00192	6.626e-02	[0.011930-0.3680]
SNAI	0.00193	1.883e+01	[2.943553-120.4158]
SEX (Male *vs* Female)	0.21720	4.224e-01	[0.107480-1.6602]
AGE (<50 *vs* > = 50)	0.88377	1.187e+00	[0.118751-11.8722]
Differentiation degree (Low&Middle *vs* High)	0.01170	2.489e-02	[0.001409-0.4395]
Lymphatic metastasis	0.01610	5.681e+00	[1.380381-23.3765]

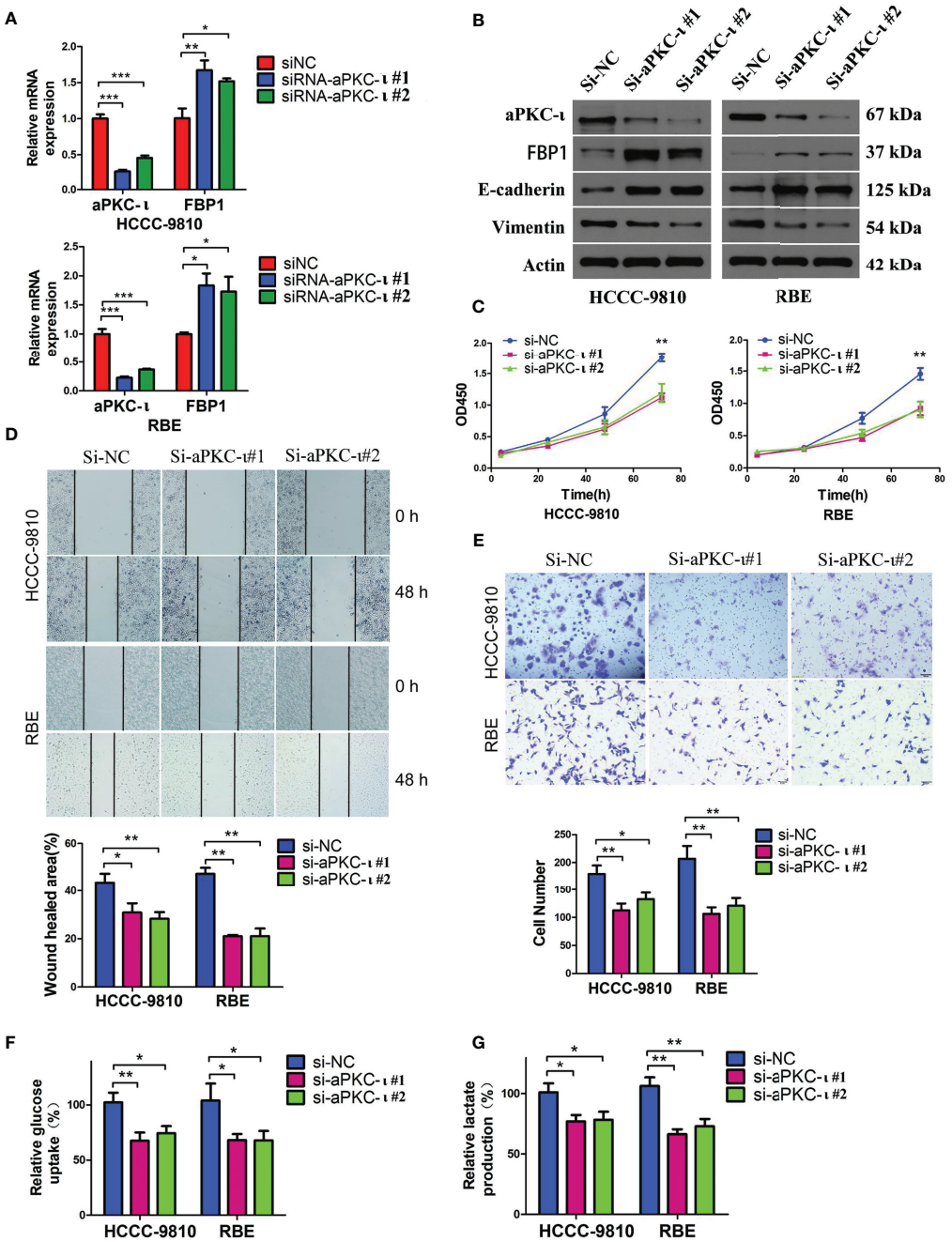

FIGURE 2 | Down-regulated aPKC-ι reversed EMT-like changes and metabolic advantages in cancer cells. **(A)** FBP1 mRNA level in aPKC-ι knockdown HCCC-9810 and RBE cell lines. **(B–E)** Expression levels of EMT-related proteins including the epithelial markers E-cadherin and mesenchymal marker Vimentin, viability, and *in vitro* migration and invasion of control and aPKC-ι knockdown ICC cells. **(F, G)** Glucose uptake rate and lactate production after knocking down aPKC-ι in HCCC-9810 and RBE cell lines. * means $P < 0.05$, ** means $P < 0.01$, *** means $P < 0.001$.

tumor samples (**Figure 6A**). Pearson correlation analysis showed a significant positive correlation between aPKC-ι and Snail expression (R=-0.643, p<0.001), whereas high Snail was related to low FBP1 (R=-0.484, p<0.01) (**Figure 6B**). In addition, ectopic expression of Snail in the HCCC-9810 and RBE cells markedly decreased FBP1 protein levels, suggesting that Snail is required for loss of FBP1 by aPKC-ι-mediated inhibition (**Figure 6E**).

To investigate whether Snail binds the promoter regions of FBP1, we constructed wild-type FBP1 (FBP1-WT) and mutant FBP1 (FBP1-MUT) eukaryotic expression vectors and generated

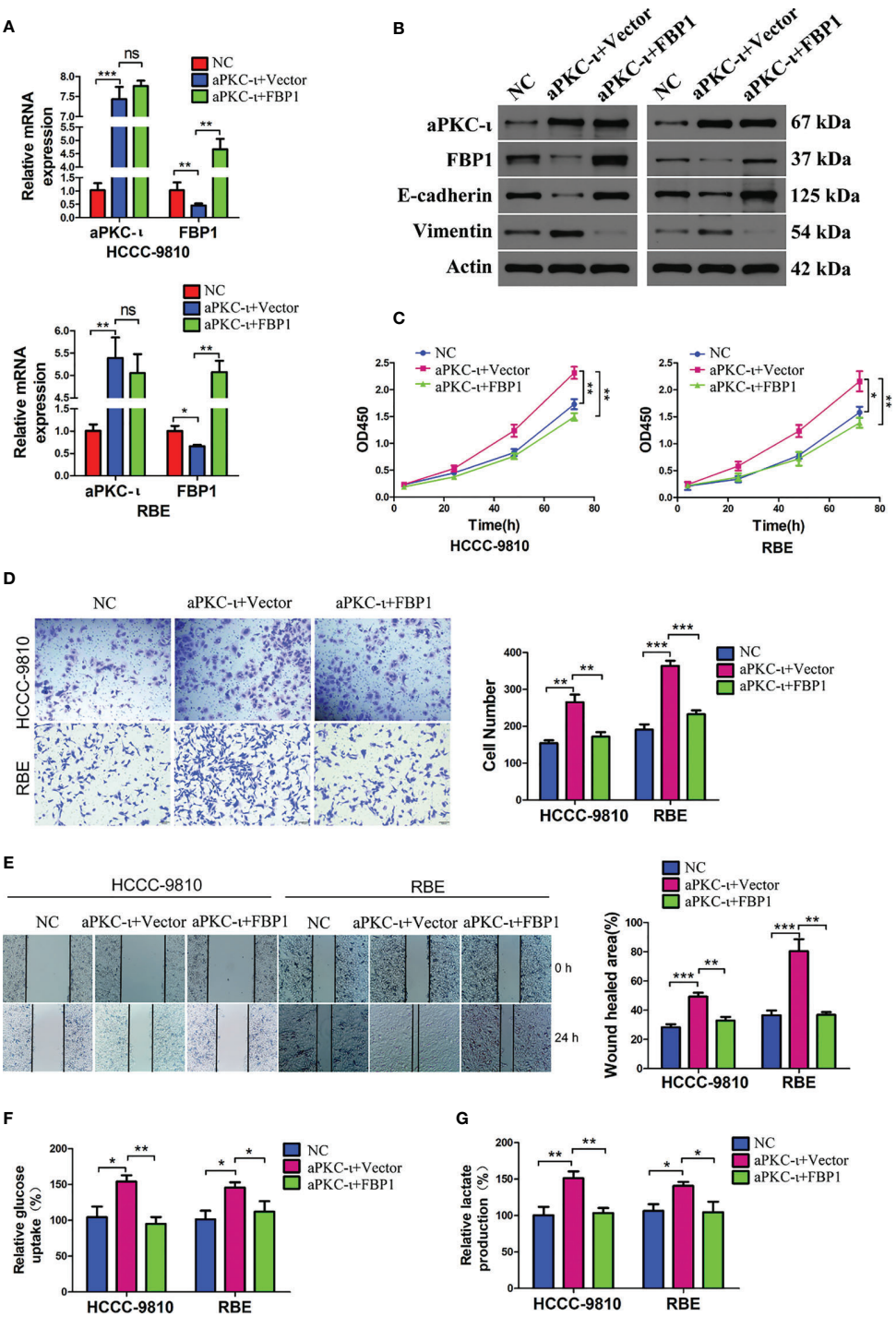

FIGURE 3 | FBP1 antagonizes aPKC-ι and inhibits tumor progression. **(A, B)** The mRNA and protein levels of FBP1 were down-regulated in aPKC-ι-overexpressing ICC cells by transfecting with aPKC-ι-cDNA. **(C–E)** EMT-like changes were reversed compared with negative control groups, including cell proliferation, invasion, and migration. **(F, G)** Glucose uptake rate and lactate production in aPKC-ι/aPKC-ι + FBP1 groups. * means $P < 0.05$, ** means $P < 0.01$, *** means $P < 0.001$. ns, no statistical difference.

ICC cells that stably expressed these two constructs. In dual luciferase assay, Snail significantly repressed the FBP1 promoter activity, indicated that Snail inhibited FBP1 transcription (**Figure 6C**). Therefore, chromatin immunoprecipitation (ChIP) was performed in the RBE cells by using three sets of FBP1 primers and confirmed a direct physical interaction between FBP1 promoter and Snail (**Figure 6D**). Taken together, these results implied that FBP1 is a direct target of Snail in ICC cells.

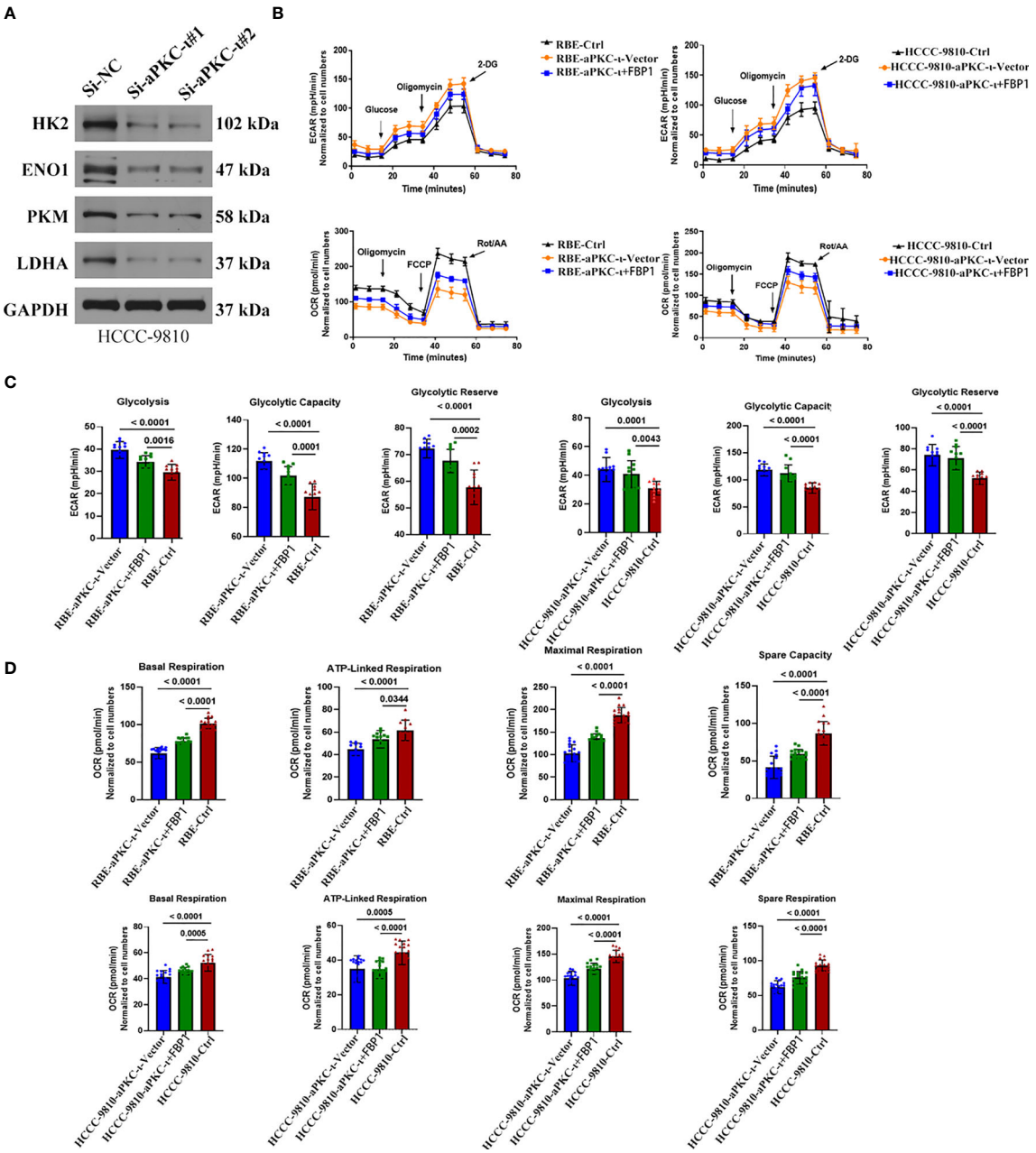

FIGURE 4 | aPKC-ι and FBP1 play the roles of accelerator and speed limiter in the process of glycolysis. **(A)** The protein levels of HK2,ENO1,PKM,LDHA were down-regulated in aPKC-ι knockdown ICC cells. **(B)** Oxygen consumption rate (OCR) and extracellular acidification rate (ECAR) of ICC cells which were transfected with aPKC-ι/aPKC-ι+FBP1 cDNA. **(C, D)** Glycolysis level, glycolysis capacity,glycolysis capacity,reserve basal respiration, ATP-linked respiration, maximum respiration, and spare respiration of ICC cells transfected with aPKC-ι/aPKC-ι+FBP1 cDNA.

DISCUSSION

As aPKC-ι, a polarization regulatory protein, regarded as human oncogene and potential therapeutic target in various epithelial cancers (35), we then found that aPKC-ι knockdown in ICC cells led to increase of E-cadherin, decreases of Vimentin expression and the abilities of migratory and invasive. These were in line with our previous studies indicating that aPKC-ι/Snail signaling pathway has a critical role in the regulation of EMT in cholangiocarcinoma *in vitro* and *in vivo* (29). The EMT constitutes a pivotal step in variety epithelial cancer cells invasion and metastasis, defined by loss of epithelial cell polarity and reorganization of the cytoskeleton (34). Therefore, a better understanding of EMT process regulating by aPKC-ι

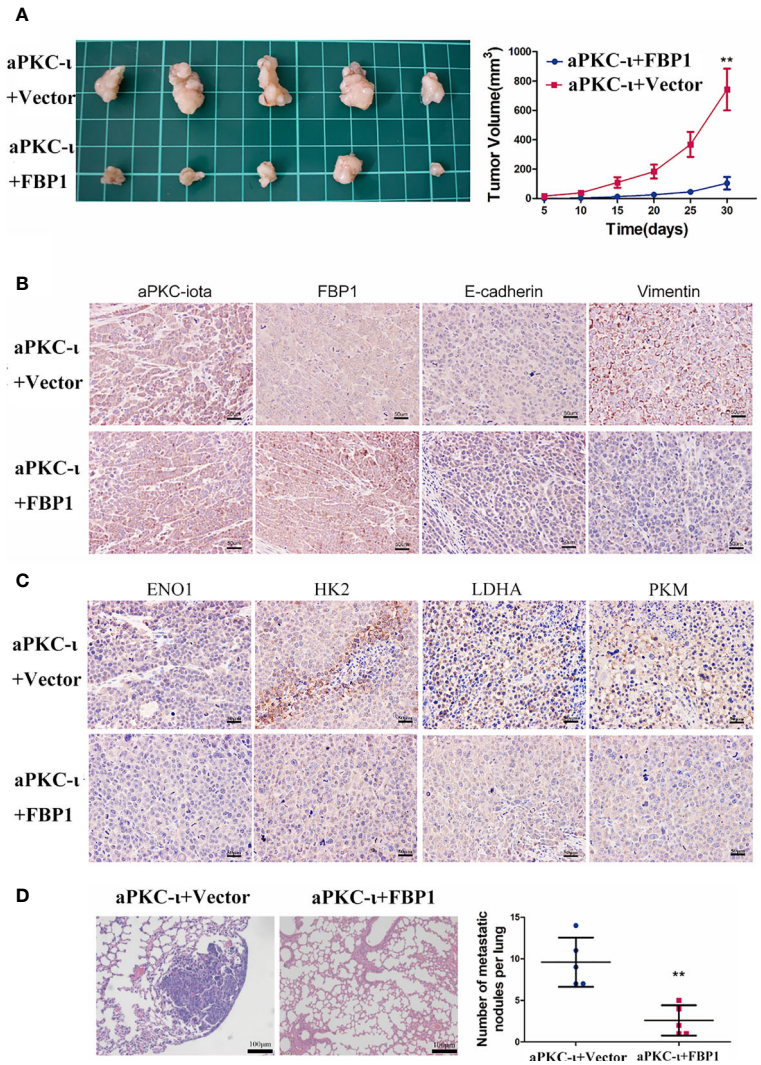

FIGURE 5 | FBP1 antagonizes aPKC-ι and inhibits tumor growth and metastasis *in vivo*. **(A)** Tumor volume changes in nude mice over a 30-day period after injection of HCCC-9810 cells transfected with aPKC-ι/aPKC-ι + FBP1. **(B)** *In situ* expression of aPKC-ι, FBP1, E-cadherin and vimentin in the tumor tissues of the indicated groups. **(C)** *In situ* expression of HK2,ENO1,PKM,LDHA in the tumor tissues of the indicated groups **(D)** Representative images of HE-stained lung metastatic nodules from the indicated groups. ** means $P < 0.01$.

may hold a great promise for the development of novel therapeutic approaches to eradicate ICC that are currently resistant to conventional therapies.

Despite a high genetic diversity, cancer cells still exhibit a common set of characteristics. Aberrant metabolic reprogramming constitutes one of its important features during the tumor progression, which could enhance glucose uptake and lactate production of cancer cells through aerobic glycolysis to meet the rapid energy requirements for catabolism and anabolism (36). Recent studies indicated that extracellular matrix (ECM) of cancer cells is remodeled by aerobic glycolysis, which could also increase the expression of EMT-inducing transcription factor and decrease the pH value of tumor microenvironment (37). It had shown that an increased glycolytic metabolism can facilitate cancer cells EMT and promote tumor progression. In our current study, the content of secreted lactate, the end product of glycolysis, were significantly increased in the ICC cells and correlated positively with aPKC-ι expression. These results first demonstrated that aPKC-ι could facilitate aerobic glycolysis and contributed to EMT process in ICC. However, the underlying mechanisms that aPKC-ι affect the biological behavior of ICC cells, are still unclear.

Intracellular glucose homeostasis is regulated by catabolic glycolysis, aerobic oxidation of sugars, and anabolic gluconeogenesis. Until now, metabolites that accumulated *via* aerobic glycolysis were considered as a building blocks or fuel source for cancer cells proliferation (38). Several studies reported that metabolic intermediates of gluconeogenesis regulate aerobic breakdown of glucose in cancer cells (22, 39, 40). FBP1 catalyzes

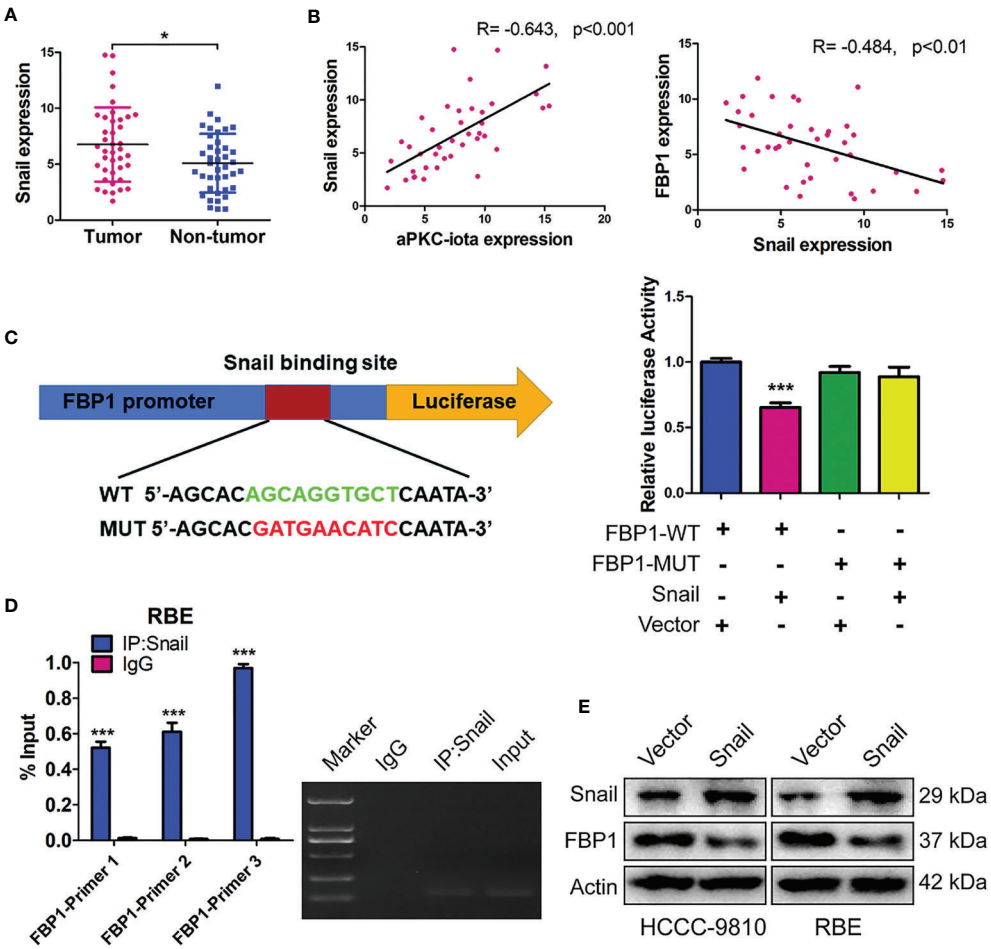

FIGURE 6 | FBP1 is a direct target of Snail in aPKC-ι mediated EMT and "Warburg effect". **(A)** Snai1 expression levels in 40 paired ICC and adjacent nontumor tissues. **(B)** Pearson correlation analysis showed a significant positive correlation between aPKC-ι and FBP1 expression (R=-0.643, p<0.001), whereas high Snail was related to low FBP1 (R=-0.484, p<0.01). **(C, D)** Snail significantly repressed the FBP1 promoter activity in dual luciferase assay and ChIP was performed in the RBE cells by using three sets of FBP1 primers and confirmed a direct physical interaction between FBP1 promoter and Snail. **(E)** Snai1 and FBP1 protein expression in HCCC-9810 and RBE cells transfected with Snai1.

the decomposition of fructose-1,6-bisphosphate into 6-phosphate fructose and inorganic phosphate, and its epigenetic regulation in cancer cells is an underlying factor of aberrant glucose metabolism (14). Interestingly, the loss of FBP1 was recently determined to be a critical oncogenic event in breast cancer and renal cell carcinoma progression (17). Consistent with previous findings, we found that FBP1 expression is negatively correlated with aPKC-ι and the malignant progression in ICC. Moreover, upregulating FBP1 expression in aPKC-ι-overexpressing ICC cells reversed EMT-like changes and aberrant metabolic reprogramming. These results further support the critical role of FBP1 for aPKC-ι induced EMT-like changes and glycolysis in ICC.

To elucidate the specific mechanism by which aPKC-ι regulates FBP1 in ICC, co-IP experiment was performed and showed that aPKC-ι indirectly regulated FBP1 through other molecules. Snail, a transcriptional repressor, could induce EMT, allowing cancer cells with invasive properties (41). It also could regulate many genes involved in glucose metabolism, such as glucose phosphate isomerase and aldolase, suggesting that Snail participates in complex metabolic reprogramming in cancer (42). Furthermore, some studies have confirmed that the Snail transcriptional factor Snai1 represses FBP1 to accelerate EMT of various tumor cells (43). Since we had previously observed that Snail is a major downstream target of aPKC-ι in triggering EMT (29), we hypothesized that aPKC-ι promotes EMT and provides metabolic advantages of ICC cells by repressing FBP1 *via* Snail. As expected, we identified that Snail inhibited the transcription of FBP1 by directly binding to its promoter by dual luciferase assay and ChIP experiment. In addition, the expression level of Snail correlated positively with that of aPKC-ι, whereas correlated negatively with FBP1.

Oxidative metabolism is impaired in cancer cells due to the increase in glycolysis and oxygen consumption. The Warburg effect,

wherein the tumor cells preferentially use glycolysis to produce energy under hypoxic conditions (44), protects the cells against metabolic stress, and promotes their invasion, migration and EMT (45). In the glycolytic pathway, lactate dehydrogenase A (LDHA) irreversibly catalyzes the conversion of pyruvate to lactate *via* the oxidative dehydrogenation of nicotinamide adenine dinucleotide (NADH) to NAD^+ (46). As an important carcinogen, lactate is closely related to tumor growth, immune escape, angiogenesis and EMT (47). Existed data had shown that LDHA is highly expressed in various cancers and its expression is positively associated with tumor progression (48). Based on our findings therefore, we speculated that aPKC-ι/Snail-mediated repression of FBP1 increases glycolysis and lactate production in the ICC cells, which in turn upregulates aPKC-ι to form a positive feedback loop, eventually enhancing EMT, invasion and migration. Further mechanism studies are needed to investigate.

In conclusion, we found that aPKC-ι, Snail and loss of FBP1 are significantly correlated with poor prognosis in ICC patients. FBP1 played a crucial role in aPKC-ι induced EMT and glycolysis in ICC cells. We illustrated aPKC-ι was confirmed to inhibit FBP1 expression by increasing Snail binding to the FBP1 promoter, which is conducive to EMT and metastasis. Our results strongly suggest that aPKC-ι induces EMT and promotes glycolysis in human ICC cells through an aPKC-ι/Snail/FBP1 pathway. It is known that cells always take the most economical way to carry out physiological activities, which is well verified in our study. The polarization regulatory protein, aPKC-ι, simultaneously regulated EMT and metabolic reprogramming *via* the same signal pathway, which eventually led to more effective metastasis of ICC cells. The above results provide a new perspective to illustrate the mechanism of tumor progression.

Our and recent observations implied that glucose metabolism is not simply a consequence but rather affects polarized states of cancer cells. Nevertheless, the specific interaction of enzymes associated with glucose metabolism regulating EMT-like characteristics is still unknown. One emerging idea on how changes in glucose metabolism induce EMT-like phenotype is that mitochondrial derived reactive oxygen species could serve as signaling molecules (49). It will be of interest how interaction between EMT process and glucose metabolism. Targeting this pathway may abolish cancer metastasis and metabolic advantages. This strategy will generate an entirely effective approach for treating ICC.

Radical surgical resection remains to be the only potential curative treatment option for ICC in the near future. Limitations of current clinical trials include small sample size, combined analysis of cholangiocarcinoma and gallbladder cancer, and lack of randomization (50). Precision medicine will be advocated to improve outcomes for patients with ICC, which is highly genetically heterogeneous tumor. More recently, a variety of genetic mutations implicated in causing ICC have been identified, and future studies will continue to focus on targeting genetic aberrations. In addition, the efficacy and safety of immunotherapies have also been widely reported in ICC. Although immunotherapy has been disappointing now, it could become an important part of the treatment landscape in the future. The road is rough, but the beauty lies ahead.

DATA AVAILABILITY STATEMENT

The original contributions presented in the study are included in the article/supplementary material. Further inquiries can be directed to the corresponding authors.

ETHICS STATEMENT

The studies involving human participants were reviewed and approved by the Committee for the Protection of Human Subjects, Zhongnan Hospital of Wuhan University. The patients/participants provided their written informed consent to participate in this study. The animal study was reviewed and approved by the Institutional Animal Ethics Committee of Wuhan University.

AUTHOR CONTRIBUTIONS

MG and CM designed the learning concept and design. MG drafted the manuscript. CM is in charge of statistics. XJ, PX, HZ, YL, YG, and YY made significant contributions to the research program. YQ and YFY reviewed and approved the final version of this article. All authors contributed to the article and approved the submitted version.

FUNDING

This work was supported by the National Science Fund for Young Scholars (No. 81802442) and Scientific Research Project of Hubei Province Health commission (WJ2017Z007).

REFERENCES

1. Razumilava N, Gores GJ. Cholangiocarcinoma. *Lancet (London England)* (2014) 383(9935):2168–79. doi: 10.1016/s0140-6736(13)61903-0
2. Zhang H, Yang T, Wu M, Shen F. Intrahepatic Cholangiocarcinoma: Epidemiology, Risk Factors, Diagnosis and Surgical Management. *Cancer Lett* (2016) 379(2):198–205. doi: 10.1016/j.canlet.2015.09.008
3. Gupta A, Dixon E. Epidemiology and Risk Factors: Intrahepatic Cholangiocarcinoma. *Hepatobiliary Surg Nutr* (2017) 6(2):101–4. doi: 10.21037/hbsn.2017.01.02
4. Rizzo A, Ricci AD, Brandi G. Pemigatinib: Hot Topics Behind the First Approval of a Targeted Therapy in Cholangiocarcinoma. *Cancer Treat Res Commun* (2021) 27:100337. doi: 10.1016/j.ctarc.2021.100337
5. Pant K, Richard S, Peixoto E, Gradilone SA. Role of Glucose Metabolism Reprogramming in the Pathogenesis of Cholangiocarcinoma. *Front Med* (2020) 7:113. doi: 10.3389/fmed.2020.00113
6. Fujiwara H, Tateishi K, Misumi K, Hayashi A, Igarashi K, Kato H, et al. Mutant IDH1 Confers Resistance to Energy Stress in Normal Biliary Cells Through PFKP-Induced Aerobic Glycolysis and AMPK Activation. *Sci Rep* (2019) 9(1):18859. doi: 10.1038/s41598-019-55211-w

7. Tang D, Xu L, Zhang M, Dorfman RG, Pan Y, Zhou Q, et al. Metformin Facilitates BG45–Induced Apoptosis *via* an Anti–Warburg Effect in Cholangiocarcinoma Cells. *Oncol Rep* (2018) 39(4):1957–65. doi: 10.3892/or.2018.6275
8. Florio AA, Ferlay J, Znaor A, Ruggieri D, Alvarez CS, Laversanne M, et al. Global Trends in Intrahepatic and Extrahepatic Cholangiocarcinoma Incidence From 1993 to 2012. *Cancer* (2020) 126(11):2666–78. doi: 10.1002/cncr.32803
9. Ma CQ, Yang Y, Wang JM, Du GS, Shen Q, Liu Y, et al. The Apkcι Blocking Agent ATM Negatively Regulates EMT and Invasion of Hepatocellular Carcinoma. *Cell Death Dis* (2014) 5(3):e1129. doi: 10.1038/cddis.2014.91
10. Justilien V, Fields AP. Ect2 Links the PKCiota-Par6alpha Complex to Rac1 Activation and Cellular Transformation. *Oncogene* (2009) 28(41):3597–607. doi: 10.1038/onc.2009.217
11. Garg R, Benedetti LG, Abera MB, Wang H, Abba M, Kazanietz MG. Protein Kinase C and Cancer: What We Know and What We do Not. *Oncogene* (2014) 33(45):5225–37. doi: 10.1038/onc.2013.524
12. Gunaratne A, Thai BL, Di Guglielmo GM. Atypical Protein Kinase C Phosphorylates Par6 and Facilitates Transforming Growth Factor β-Induced Epithelial-to-Mesenchymal Transition. *Mol Cell Biol* (2013) 33(5):874–86. doi: 10.1128/mcb.00837-12
13. Du GS, Qiu Y, Wang WS, Peng K, Zhang ZC, Li XS, et al. Knockdown on aPKC-ι Inhibits Epithelial-Mesenchymal Transition, Migration and Invasion of Colorectal Cancer Cells Through Rac1-JNK Pathway. *Exp Mol Pathol* (2019) 107:57–67. doi: 10.1016/j.yexmp.2018.11.007
14. Grasmann G, Smolle E, Olschewski H, Leithner K. Gluconeogenesis in Cancer Cells - Repurposing of a Starvation-Induced Metabolic Pathway? *Biochim Biophys Acta Rev Cancer* (2019) 1872(1):24–36. doi: 10.1016/j.bbcan.2019.05.006
15. Liu X, Wang X, Zhang J, Lam EK, Shin VY, Cheng AS, et al. Warburg Effect Revisited: An Epigenetic Link Between Glycolysis and Gastric Carcinogenesis. *Oncogene* (2010) 29(3):442–50. doi: 10.1038/onc.2009.332
16. Li B, Qiu B, Lee DS, Walton ZE, Ochocki JD, Mathew LK, et al. Fructose-1,6-Bisphosphatase Opposes Renal Carcinoma Progression. *Nature* (2014) 513(7517):251–5. doi: 10.1038/nature13557
17. Dong C, Yuan T, Wu Y, Wang Y, Fan TW, Miriyala S, et al. Loss of FBP1 by Snail-Mediated Repression Provides Metabolic Advantages in Basal-Like Breast Cancer. *Cancer Cell* (2013) 23(3):316–31. doi: 10.1016/j.ccr.2013.01.022
18. Cong J, Wang X, Zheng X, Wang D, Fu B, Sun R, et al. Dysfunction of Natural Killer Cells by FBP1-Induced Inhibition of Glycolysis During Lung Cancer Progression. *Cell Metab* (2018) 28(2):243–55.e5. doi: 10.1016/j.cmet.2018.06.021
19. Gao S, Zhu D, Zhu J, Shen L, Zhu M, Ren X. miR-18a-5p Targets FBP1 to Promote Proliferation, Migration, and Invasion of Liver Cancer Cells and Inhibit Cell Apoptosis. *Comput Math Methods Med* (2021) 2021:3334065. doi: 10.1155/2021/3334065
20. Hanahan D, Weinberg RA. Hallmarks of Cancer: The Next Generation. *Cell* (2011) 144(5):646–74. doi: 10.1016/j.cell.2011.02.013
21. Dang CV. Links Between Metabolism and Cancer. *Genes Dev* (2012) 26(9):877–90. doi: 10.1101/gad.189365.112
22. Vander Heiden MG, Cantley LC, Thompson CB. Understanding the Warburg Effect: The Metabolic Requirements of Cell Proliferation. *Science (New York NY)* (2009) 324(5930):1029–33. doi: 10.1126/science.1160809
23. Lu J, Tan M, Cai Q. The Warburg Effect in Tumor Progression: Mitochondrial Oxidative Metabolism as an Anti-Metastasis Mechanism. *Cancer Lett* (2015) 356(2 Pt A):156–64. doi: 10.1016/j.canlet.2014.04.001
24. Liu M, Quek LE, Sultani G, Turner N. Epithelial-Mesenchymal Transition Induction is Associated With Augmented Glucose Uptake and Lactate Production in Pancreatic Ductal Adenocarcinoma. *Cancer Metab* (2016) 4:19. doi: 10.1186/s40170-016-0160-x
25. Yu J, Li J, Chen Y, Cao W, Lu Y, Yang J, et al. Snail Enhances Glycolysis in the Epithelial-Mesenchymal Transition Process by Targeting FBP1 in Gastric Cancer. *Cell Physiol Biochem* (2017) 43(1):31–8. doi: 10.1159/000480314
26. Zhao J, Huang X, Xu Z, Dai J, He H, Zhu Y, et al. LDHA Promotes Tumor Metastasis by Facilitating Epithelial–Mesenchymal Transition in Renal Cell Carcinoma. *Mol Med Rep* (2017) 16(6):8335–44. doi: 10.3892/mmr.2017.7637
27. Hua Q, Mi B, Huang G. The Emerging Co-Regulatory Role of Long Noncoding RNAs in Epithelial-Mesenchymal Transition and the Warburg Effect in Aggressive Tumors. *Crit Rev Oncol Hematol* (2018) 126:112–20. doi: 10.1016/j.critrevonc.2018.03.028
28. Wang H, Chirshev E, Hojo N, Suzuki T, Bertucci A, Pierce M, et al. The Epithelial-Mesenchymal Transcription Factor SNAI1 Represses Transcription of the Tumor Suppressor miRNA Let-7 in Cancer. *Cancers* (2021) 13(6):1–18. doi: 10.3390/cancers13061469
29. Qian Y, Yao W, Yang T, Yang Y, Liu Y, Shen Q, et al. aPKC-ι/P-Sp1/Snail Signaling Induces Epithelial-Mesenchymal Transition and Immunosuppression in Cholangiocarcinoma. *Hepatology (Baltimore Md)* (2017) 66(4):1165–82. doi: 10.1002/hep.29296
30. Li F, Huangyang P, Burrows M, Guo K, Riscal R, Godfrey J, et al. FBP1 Loss Disrupts Liver Metabolism and Promotes Tumorigenesis Through a Hepatic Stellate Cell Senescence Secretome. *Nat Cell Biol* (2020) 22(6):728–39. doi: 10.1038/s41556-020-0511-2
31. Jiang X, Liu Y, Wang G, Yao Y, Mei C, Wu X, et al. Up-Regulation of CLIC1 Activates MYC Signaling and Forms a Positive Feedback Regulatory Loop With MYC in Hepatocellular Carcinoma. *Am J Cancer Res* (2020) 10(8):2355–70.
32. Massa A, Varamo C, Vita F, Tavolari S, Peraldo-Neia C, Brandi G, et al. Evolution of the Experimental Models of Cholangiocarcinoma. *Cancers* (2020) 12(8):1–31. doi: 10.3390/cancers12082308
33. Tian L, Deng Z, Xu L, Yang T, Yao W, Ji L, et al. Downregulation of ASPP2 Promotes Gallbladder Cancer Metastasis and Macrophage Recruitment *via* aPKC-ι/GLI1 Pathway. *Cell Death Dis* (2018) 9(11):1115. doi: 10.1038/s41419-018-1145-1
34. Goossens S, Vandamme N, Van Vlierberghe P, Berx G. EMT Transcription Factors in Cancer Development Re-Evaluated: Beyond EMT and MET. *Biochim Biophys Acta Rev Cancer* (2017) 1868(2):584–91. doi: 10.1016/j.bbcan.2017.06.006
35. Atwood SX, Li M, Lee A, Tang JY, Oro AE. GLI Activation by Atypical Protein Kinase C ι/λ Regulates the Growth of Basal Cell Carcinomas. *Nature* (2013) 494(7438):484–8. doi: 10.1038/nature11889
36. Ganapathy-Kanniappan S, Geschwind JF. Tumor Glycolysis as a Target for Cancer Therapy: Progress and Prospects. *Mol Cancer* (2013) 12:152. doi: 10.1186/1476-4598-12-152
37. Su Z, Yang Z, Xu Y, Chen Y, Yu Q. Apoptosis, Autophagy, Necroptosis, and Cancer Metastasis. *Mol Cancer* (2015) 14:48. doi: 10.1186/s12943-015-0321-5
38. Hirschhaeuser F, Sattler UG, Mueller-Klieser W. Lactate: A Metabolic Key Player in Cancer. *Cancer Res* (2011) 71(22):6921–5. doi: 10.1158/0008-5472.Can-11-1457
39. Lunt SY, Vander Heiden MG. Aerobic Glycolysis: Meeting the Metabolic Requirements of Cell Proliferation. *Annu Rev Cell Dev Biol* (2011) 27:441–64. doi: 10.1146/annurev-cellbio-092910-154237
40. Vaupel P, Multhoff G. Revisiting the Warburg Effect: Historical Dogma Versus Current Understanding. *J Physiol* (2021) 599(6):1745–57. doi: 10.1113/jp278810
41. Kim NH, Cha YH, Lee J, Lee SH, Yang JH, Yun JS, et al. Snail Reprograms Glucose Metabolism by Repressing Phosphofructokinase PFKP Allowing Cancer Cell Survival Under Metabolic Stress. *Nat Commun* (2017) 8:14374. doi: 10.1038/ncomms14374
42. Wang Y, Shi J, Chai K, Ying X, Zhou BP. The Role of Snail in EMT and Tumorigenesis. *Curr Cancer Drug Targets* (2013) 13(9):963–72. doi: 10.2174/15680096113136660102
43. Liu GM, Li Q, Zhang PF, Shen SL, Xie WX, Chen B, et al. Restoration of FBP1 Suppressed Snail-Induced Epithelial to Mesenchymal Transition in Hepatocellular Carcinoma. *Cell Death Dis* (2018) 9(11):1132. doi: 10.1038/s41419-018-1165-x
44. Liberti MV, Locasale JW. The Warburg Effect: How Does it Benefit Cancer Cells? *Trends Biochem Sci* (2016) 41(3):211–8. doi: 10.1016/j.tibs.2015.12.001
45. Upadhyay M, Samal J, Kandpal M, Singh OV, Vivekanandan P. The Warburg Effect: Insights From the Past Decade. *Pharmacol Ther* (2013) 137(3):318–30. doi: 10.1016/j.pharmthera.2012.11.003
46. Pathria G, Scott DA, Feng Y, Sang Lee J, Fujita Y, Zhang G, et al. Targeting the Warburg Effect *via* LDHA Inhibition Engages ATF4 Signaling for Cancer Cell Survival. *EMBO J* (2018) 37(20):1–17. doi: 10.15252/embj.201899735
47. Le A, Cooper CR, Gouw AM, Dinavahi R, Maitra A, Deck LM, et al. Inhibition of Lactate Dehydrogenase A Induces Oxidative Stress and Inhibits Tumor Progression. *Proc Natl Acad Sci U S A* (2010) 107(5):2037–42. doi: 10.1073/pnas.0914433107
48. Urbańska K, Orzechowski A. Unappreciated Role of LDHA and LDHB to Control Apoptosis and Autophagy in Tumor Cells. *Int J Mol Sci* (2019) 20(9):1–15. doi: 10.3390/ijms20092085

49. Laura AS, Navdeep SC. Physiological Roles of Mitochondrial Reactive Oxygen Species. *Mol Cell* (2012) 48(2):158–67. doi: 10.1016/j.molcel.2012.09.025
50. Boris B. Cholangiocarcinoma: Current Knowledge and New Developments. *Gut Liver* (2017) 11(1):12–26. doi: 10.5009/gnl15568

Conflict of Interest: The authors declare that the research was conducted in the absence of any commercial or financial relationships that could be construed as a potential conflict of interest.

Publisher's Note: All claims expressed in this article are solely those of the authors and do not necessarily represent those of their affiliated organizations, or those of the publisher, the editors and the reviewers. Any product that may be evaluated in this article, or claim that may be made by its manufacturer, is not guaranteed or endorsed by the publisher.

frontiers in Oncology

ORIGINAL RESEARCH
published: 17 December 2021
doi: 10.3389/fonc.2021.788635

A Retrospective Study of Lenvatinib Monotherapy or Combined With Programmed Cell Death Protein 1 Antibody in the Treatment of Patients With Hepatocellular Carcinoma or Intrahepatic Cholangiocarcinoma in China

Sihui Zhu[1,2], *Chenxi Liu*[1], *Yanbing Dong*[1], *Jie Shao*[1,2], *Baorui Liu*[1,2*] *and Jie Shen*[1,2*]

[1] *Comprehensive Cancer Centre of Drum Tower Hospital, Medical School of Nanjing University, Clinical Cancer Institute of Nanjing University, Nanjing, China,* [2] *Comprehensive Cancer Centre of Nanjing Drum Tower Hospital, Clinical College of Nanjing Medical University, Nanjing, China*

Lenvatinib has been ratified as a first-line medication for advanced liver tumors by the American Food and Drug Administration. To assess the effectiveness and security of Lenvatinib in the Chinese population in a real-world setting, we enrolled 48 patients with unresectable liver cancer, managed from December 2018 to March 2021. Among them, 9 and 39 (83.30% men) patients had intrahepatic cholangiocarcinoma (ICC) and hepatocellular carcinoma (HCC), respectively. Twenty-one (43.75%) patients had progressive disease after first-line treatment, and others (56.25%) had not receiving systemic treatment. Lenvatinib was administered alone or in combination with a programmed cell death protein 1 antibody (anti-PD-1). Treatment duration, median progression-free survival (mPFS), and median overall survival (mOS) were examined. The mOS and mPFS were 22.43 and 8.93 months, respectively. Of HCC patients treated with Lenvatinib only, the mOS and mPFS were 22.43 and 11.60 months, respectively. The corresponding values for HCC cases managed with anti-PD-1 combined with Lenvatinib were 21.77 and 7.10 months, respectively. ICC patients did not reach the mOS and their mPFS was 8.63 months. The present findings support the efficacy and security of Lenvatinib in the real-world therapy of Chinese patients with unresectable liver cancer.

Keywords: lenvatinib, hepatocellular carcinoma, intrahepatic cholangiocarcinoma, anti-PD-1, progression-free survival, overall survival

OPEN ACCESS

Edited by:
Hongda Liu,
Nanjing Medical University, China

Reviewed by:
Anna Crispo,
National Cancer Institute G. Pascale Foundation (IRCCS), Italy
Luca Rinaldi,
University of Campania Luigi Vanvitelli, Italy

***Correspondence:**
Jie Shen
shenjie2008nju@163.com
Baorui Liu
baoruiliu@nju.edu.cn

Specialty section:
This article was submitted to Cancer Molecular Targets and Therapeutics, a section of the journal Frontiers in Oncology

Received: *03 October 2021*
Accepted: *30 November 2021*
Published: *17 December 2021*

Citation:
Zhu S, Liu C, Dong Y, Shao J, Liu B and Shen J (2021) A Retrospective Study of Lenvatinib Monotherapy or Combined With Programmed Cell Death Protein 1 Antibody in the Treatment of Patients With Hepatocellular Carcinoma or Intrahepatic Cholangiocarcinoma in China. Front. Oncol. 11:788635. doi: 10.3389/fonc.2021.788635

INTRODUCTION

There were an estimated 905,700 new cases of liver cancer, and approximately 830,200 associated deaths in 2020 worldwide (1). Globally, liver cancer has being the second most common causation of cancer-related deaths (1).

Sorafenib, a multikinase inhibitor that targets raf, platelet-derived growth factor, vascular endothelial growth factor, and tyrosine kinases (2, 3) was made offical by the Food and Drug Administration in November 2007 for the treatment of advanced liver cancer and it remained the standard of care for over a decade, prolonging the median survival of patients in clinical trials (4). In August 2018, data from the Phase III REFLECT trial (NCT01761266) have enabled the same agency to approve another small-molecule tyrosine kinase inhibitor as first-line medication of advanced liver cancer, Lenvatinib, which inhibits the activity of the vascular endothelial growth factor receptor, platelet-derived growth factor receptor α, stem cell factor receptor, fibroblast growth factor receptor, and rearrangement during transfection (5, 6). However, the median survival time of patients receiving Lenvatinib monotherapy was 13.6 months in a clinical trial (7).

ICIs are monoclonal antibodies that can block the interaction between immune checkpoint proteins and their ligands, thereby enhancing the anti-tumor immune response by preventing T cell inactivation and restoring immune recognition and immune attack. At present, it mainly includes anti-PD-1, anti-PD-L1 and anti-CTLA-4 (8). Anti-PD-1 can bind to its ligands PD-L1 or PD-L2 which expressed in various tumors, including HCC (9). It was found that pembrolizumab treatment shown promising clinical effects in patients with advanced hepatocellular carcinoma after sorafenib treatment fails in KEYNOTE-224 clinical trial. The mPFS is 4.9 months and the median overall survival is 12.9 months in this trial (10). In 2017, the PD-1 inhibitor nivolumab received accelerated approval in the United States for the second-line treatment of patients with advanced HCC after sorafenib treatment (11).

Combination of immunotherapy strategies are being developed to enhance liver tumor response to immune checkpoint inhibitors (12). The combination of tyrosine kinase inhibitors or vascular endothelial growth factor inhibitors and immune checkpoint inhibitors may enhance dendritic cell and cytotoxic T lymphocyte activity and inhibit tumor-associated macrophage, regulatory T-cell, and myeloid-derived suppressor cell regulation of the immune microenvironment, thereby creating an inflammatory microenvironment associated with relatively effective and long-lasting responses to checkpoint inhibitors (13). In a phase Ib trial (KEYNOTE-524), the mPFS and mOS of HCC patients treated with Lenvatinib and anti-PD-1 were 8.6 and 22 months, respectively (14).

However, clinical trials may not fully reflect real-world treatment efficacy, while risk factors for liver cancer may differ among populations (15). In China, the dominating causation of HCC is chronic hepatitis B virus infection. While the major risk factor for HCC in developed countries is nonalcoholic fatty liver disease (16). Furthermore, clinical trials tend to exclude patients with clear invasion into the bile duct or main portal vein. Patients who had received systemic treatment such as chemotherapy or sorafenib tend to be also excluded (7). Therefore, this retrospective study comprised 48 patients with HCC or ICC treated with Lenvatinib alone or combined with anti-PD-1, aiming to appraise the efficacy and safety of these treatments in clinical practice in China.

MATERIALS AND METHODS

We included 56 cases with unresectable liver cancer treated with Lenvatinib from December 2018 to March 2021 at the Comprehensive Cancer Center of Drum Tower Hospital of Nanjing University. There were 48 patients analyzable and well-documented. A total of 21 HCC patients were managed with Lenvatinib only, while a total of 18 and 9 patients with HCC and ICC, respectively, were treated with combination therapy. The patients' average age was 59.7 years. Eight patients were female; 6 cases of them were HCC and other 2 cases were ICC. Twenty-one (43.75%) patients had progressive disease after receiving first-line treatment; meanwhile, 27 (56.25%) patients received no systemic treatment. According to the Child-Pugh score, 4 patients had grade B liver function, of which 3 were HCC; the remaining patients had grade A liver function. Forty patients had cirrhosis at baseline, including all ICC cases and 31 HCC cases. There were 4 ICC patients and 35 HCC patients had hepatitis B virus infection, respectively. Most patients had tumor node metastasis (TNM, American Joint Commission on Cancer 8th edition) stage IV; only 11 patients had stage III disease, and all of them were HCC cases. In addition, in HCC patients, 39 cases all presented with microvascular invasion; 33 cases had tumor invasion into the macroscopic portal vein or extrahepatic spread, or both; 12 cases had lung metastases. Only one HCC patient had no liver lesions. Six HCC patients were classified as Barcelona Clinic Liver Cancer stage B; the remaining patients were classified as stage C. The specific characteristics of HCC patients are presented in **Supplementary Table 1**.

Treatment Measures

A total of 21 patients with HCC were managed with Lenvatinib only (8 mg daily), as they were in good general condition. Twenty-seven patients received combined treatment, including 18 cases with HCC and other 9 cases with ICC (Lenvatinib plus anti-PD-1 treatment at a dose of 8 mg daily and 200 mg every 3 weeks, respectively). These patients tended to be in later stage of disease than their monotherapy counterparts, including larger tumor burden, more advanced disease stage, and pathology findings indicative of poorer prognosis.

Study Design

This retrospective cohort study was founded on medical records of patients with unresectable liver cancer, undergoing the treatment of interest. Disease progression and mortality were examined; the primary outcome was PFS, defined as the time from medication inaugural to tumor progression or death (clinical response was evaluated with the Response Evaluation Criteria in Solid Tumors). The minor endpoints involved OS,

defined as the time from medication inaugural to death, objective remission rate (ORR), and performance status scores. Safety assessment evaluation included vital signs, and blood and biochemical examination findings, among others. Adverse events were recorded based on the National Cancer Institute Common Terminology Criteria for Adverse Events.

Data Analysis

The Kaplan-Meier method was used to estimate time-to-event outcomes. All statistical analyses were performed by Graphpad 7.0. P-values of < 0.05 were considered statistically significant.

RESULTS

Twenty patients died at the termination of the follow-up duration. The overall mOS was 22.43 months (95% confidence interval (CI) was not reached, range: 4.20-28.30 months, **Figure 1**). The 6-month, 1-year, and 18-month OS rates were 95.74% (95% CI, 84.01-98.92), 73.08% (95% CI, 57.45-83.74), and 63.22% (95% CI, 46.99-75.70), respectively. The overall mPFS was 8.93 months. (95% CI, 6.76-11.10, range: 3.20-28.30 months, **Figure 1**). The mOS and mPFS of HCC patients treated with monotherapy were 22.43 months (95% CI was not reached, **Figure 2**) and 11.60 months (95% CI, 7.46-15.74, **Figure 2**), respectively. In the HCC combination treatment group, the corresponding were 21.77 months (95% CI, 3.68-39.86, **Figure 3**) and 7.10 months (95% CI, 2.8-11.4, **Figure 3**), respectively. However, patients with ICC in the combination treatment group did not reach mOS (**Figure 4**); meanwhile, the mPFS was 8.63 months (95% CI, 0-17.67, **Figure 4**).

Safety

Overall, Lenvatinib was well-tolerated (**Supplementary Table 2**). Twenty-one (43.8%) and 12 (25%) patients had elevated transaminase levels (grades 1-2 and 3-4, respectively). The administration of liver protection treatments returned transaminase levels to the normal range; other patients presented no abnormalities. Ten (20.8%) and 8 (16.7%) patients had bilirubin elevation of grades 1-2 and 3-4, respectively; 30 (62.5%) patients had decreased albumin levels of grades 1-2. Twenty-one (43.8%) and 6 (12.5%) patients had platelet decrease of grades 1-2 and 3-4, respectively. Nineteen (39.6%) and 3 (6.3%) patients had grades 1-2 and 3-4 of alkaline phosphatase increase, respectively. In addition, 16 (33.3%) patients developed rash grades 1-2; no other serious adverse

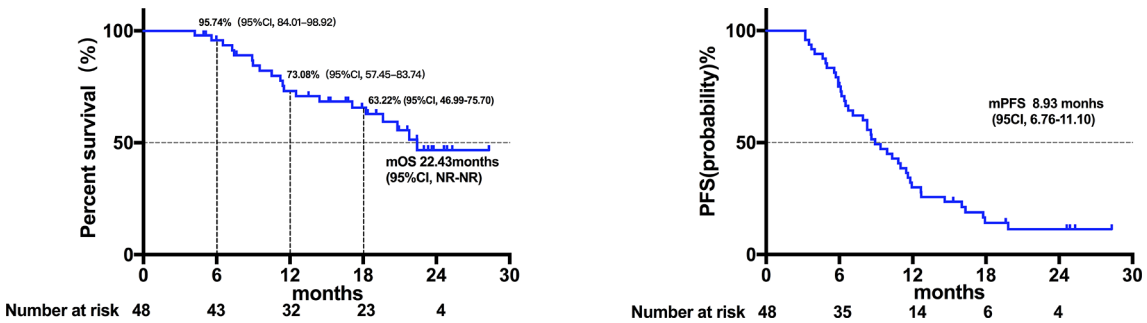

FIGURE 1 | Kaplan-Meier estimates of overall and progression-free survival in all patients. The mOS of all patients was 22.43 months (95% confidence interval was not reached; range: 4.20-28.30 months), and the mPFS of all patients was 8.93 months (95% CI, 6.76-11.10; range, 3.20-28.30 months).

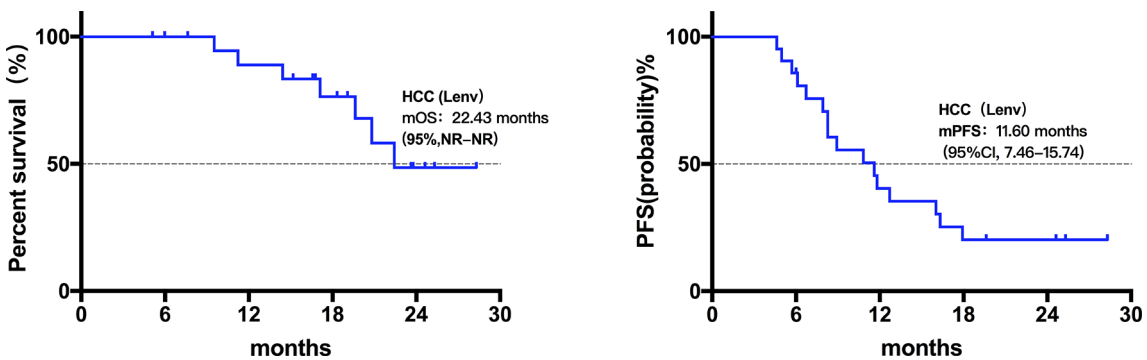

FIGURE 2 | Kaplan-Meier estimates of overall and progression-free survival in HCC patients treated with Lenvatinib monotherapy. The mOS of HCC patients treated with Lenvatinib only was 22.43 months (95% CI was not reached), the mPFS was 11.60 months (95% CI, 7.46-15.74).

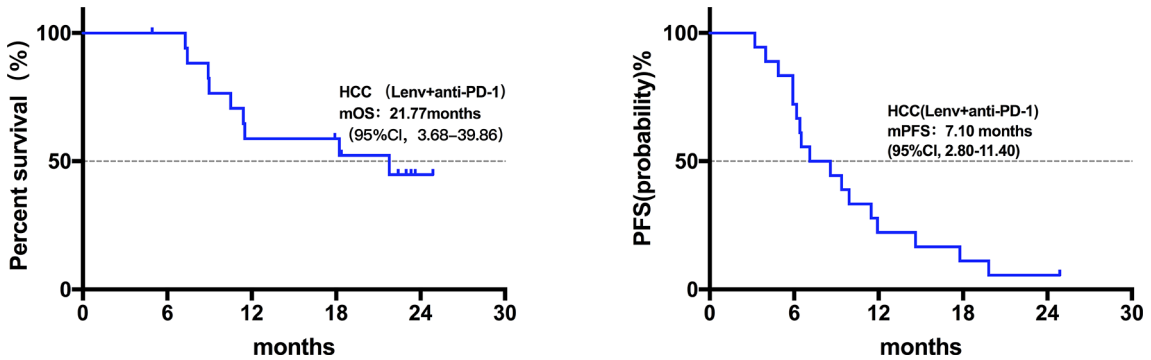

FIGURE 3 | Kaplan-Meier estimates of overall and progression-free survival in HCC patients treated with anti-PD-1 combine with Lenvatinib. The mOS of HCC patients treated with anti-PD-1 combined with Lenvatinib was 21.77 months (95% CI, 3.68-39.86), mPFS was 7.10 months (95% CI, 2.8-11.4).

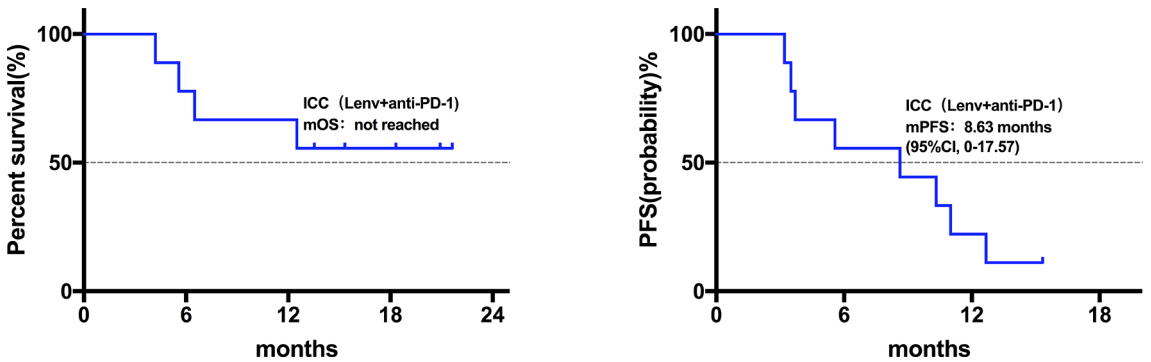

FIGURE 4 | Kaplan-Meier estimates of overall and progression-free survival in ICC patients treated with anti-PD-1 combine with Lenvatinib. The ICC patients did not reach mOS; mPFS was 8.63 months (95% CI, 0-17.67).

events were observed. At the end of the study, 13 (27.1%) and 29 (60.4%) patients had a performance status score of 1 and 2 points, respectively; the remaining patients had a score of 0 points.

Efficacy

One patient with HCC treated with combination therapy achieved complete response at the first review. Further, 14 patients achieved partial response (including two HCC patients treated with Lenvatinib monotherapy, and 4 and 8 ICC and HCC patients treated with combination therapy, respectively). In addition, 33 patients had stable disease (including 19 HCC patients treated with monotherapy, and 5 and 9 ICC and HCC patients, respectively, treated with combination therapy). Imaging studies revealed the overall ORR of 31.25%; the corresponding rate among the patients treated with monotherapy was 9.52%. The corresponding rates for ICC and HCC patients treated with combination therapy were 44.44% and 50.00%, respectively (**Figure 5**). The disease control rate in this study was 100%; there was no case of progressive disease at first review.

Impact of α-Fetoprotein (AFP) and Carbohydrate Antigen 19-9 (CA19-9) Levels on Liver Cancer Prognosis

Among 39 patients with HCC, 6 patients had negative baseline AFP data. We divided the remaining 33 patients into low (≤ 200 ng/mL) (n=18) and high (> 200 ng/mL) (n=15) AFP level groups. In the low AFP group, 3 and 15 patients had partial remission and stable disease, respectively; the corresponding counts for the high AFP group were 5 and 10 patients. There was no association between baseline AFP levels and treatment efficacy assessed with imaging. However, OS (**Figure 6**, P = 0.0108) and PFS (**Figure 6**, P = 0.0330) in the low AFP group were greater than those in the high AFP group. There was no association between baseline CA19-9 level of HCC patients and clinical efficacy or prognosis in the present study.

In addition, we found that in 9 ICC patients, the OS between patients with high CA-199 (>150 ng/mL) (n=4) and low CA-199 (≤150 ng/mL) (n=5) has no significant difference (**Figure 7**, P=0.1401). However, PFS was significantly different (**Figure 7**, P=0.0230).

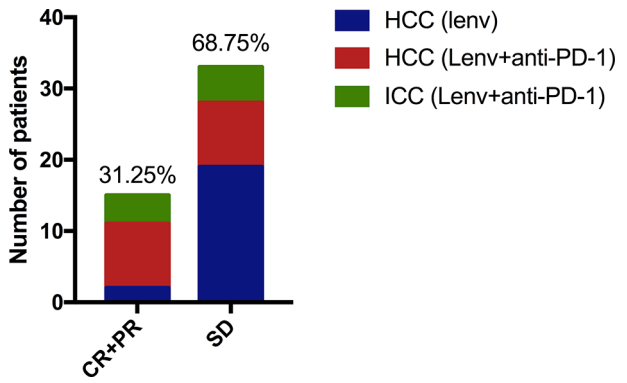

FIGURE 5 | One case of HCC treated with anti-PD-1 combined with Lenvatinib achieved complete remission, and 14 patients achieved partial remission (including two HCC patients treated with Lenvatinib monotherapy. Another 4 ICC cases and 8 HCC cases were treated with anti-PD-1 combined with Lenvatinib. Thirty-three patients had SD (19 cases of HCC were treat with monotherapy, 5 cases of ICC and 9 cases of HCC received combined treatment).

DISCUSSION

Lenvatinib was approved in 2018 as a first-line treatment for advanced HCC (6). This study used real-world data to assess the clinical efficacy of Lenvatinib used with or without anti-PD-1. The present ORR of patients with HCC conducted with Lenvatinib monotherapy was lower than that reported by the REFLECT trial; however, both mOS (22.43 vs. 13.6 months) and mPFS (11.60 vs. 7.3 months) in the present research were greater than those reported by the REFLECT trial (7). However, the present mOS of combined therapy were similar to those reported by the KEYNOTE-524 trial (14), which used Lenvatinib plus pembrolizumab (an anti-PD-1 antibody) in the treatment of unresectable liver cancer (21.77 vs. 22 months). The present ORR were comparable to those reported by the KEYNOTE-524 study (50.00% vs. 36%) (14). The mPFS (7.10 vs. 8.6 months) was slightly shorter than that previously reported, which may be attributed to the later disease condition of patients treated with combination therapy than that of those treated with monotherapy.

In the present study, nine patients with ICC did not reach mOS, and their mPFS was slightly greater than that previously reported by Zhao et al. (8.63 vs. 4.9 months); the present ORR was also higher than that previously reported by these authors (44.44% vs. 25%) (16). These findings suggest that PD-1 combined with Lenvatinib may benefit patients with ICC. However, the number of ICC patients included in this study was small and the follow-up time was short. In order to make our results more credible, we will enroll more patients for analysis and extend the follow-up time of patients.

The quality of life is becoming the focus of oncology research. The incidence of serious adverse events in clinical trials of sorafenib was 52% (4); the rates associated with Lenvatinib were comparable to those associated with sorafenib (7). In phase III clinical REFLECT trial, a 12-mg therapeutic dose was used for patients weighing >60 kg; in contrast, patients weighing ≤60 kg were given a dose of 8 mg (7). Reducing the dose may delay the onset of treatment-related adverse events; however, it may affect efficacy (13). In the present study, given disease stage, large tumor burden, and the overall poor liver function of the included patients, the dose of 8 mg was used. At the end of the follow-up period, patients with body weight of > 60 kg had slightly poorer mOS and mPFS than did those with body weight of ≤60 kg; however, this difference was not statistically significant. In the present study, the 8 mg dose did not affect treatment efficacy especially in the combined therapy group. However, further studies are required to validate the present findings and elucidate the relationship between drug dosage and treatment efficacy and safety.

HCC is a complex disease with multiple pathogenic mechanisms and associated with multiple risk factors; the use of a single

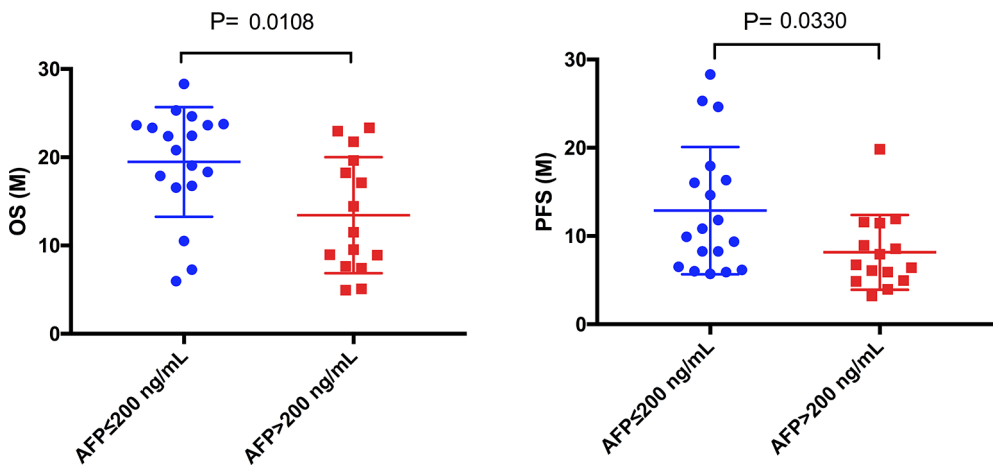

FIGURE 6 | Comparison of mOS and mPFS between the low AFP and high AFP groups in HCC patients. The mOS of the low AFP group was significantly longer than that of the high AFP group (19.48 months vs. 13.43 months, P = 0.0108), as was the mPFS (12.88 months vs. 8.16 months, P = 0.0330).

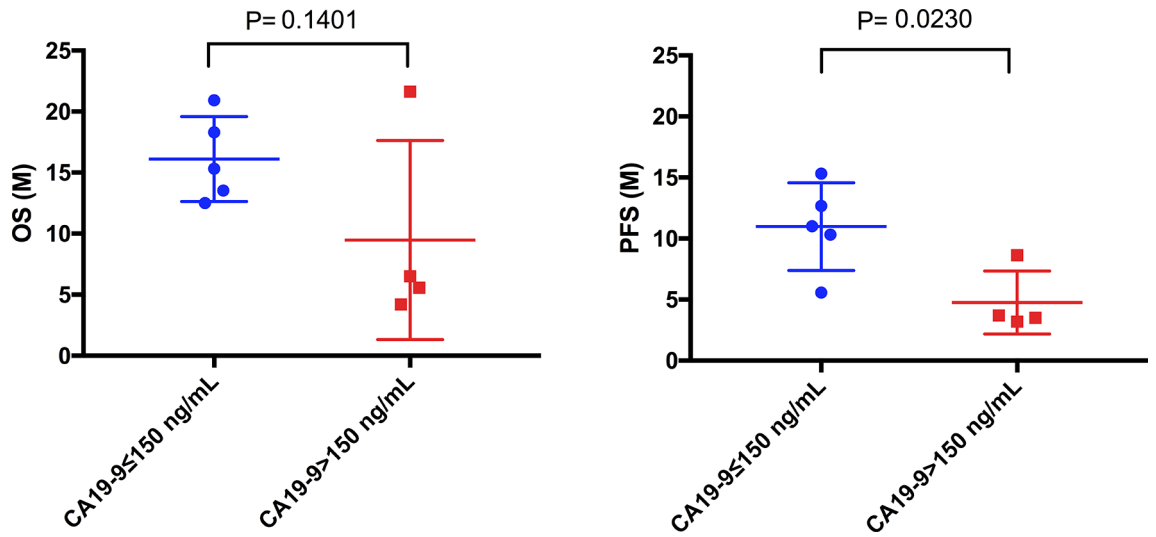

FIGURE 7 | Comparison of mOS and mPFS between the low CA19-9 and high CA19-9 groups in ICC patients. The mPFS of the low CA19-9 group was significantly longer than that of the high CA19-9 group (10.78 months vs. 4.76months, P = 0.0230), but there was no significant difference in mOS (16.12months vs. 9.48 months, P = 0.1401).

biomarker is insufficient for prognostication (17). AFP is the most widely used and recognized serum marker in this context. Zhang found that AFP- and ultrasound-based screening every 2 years may reduce HCC mortality by 37% (18). However, this approach remains controversial. In the present study, baseline AFP levels correlated with survival, including the mOS of HCC patients; this findings is consistent with that of the REFLECT trial. However, the associated mechanism remains unclear and further research is needed. In addition, CA19-9 is a biomarker for the diagnosis of cholangiocarcinoma (19, 20). We found that CA19-9 may have a certain relationship with the prognosis of ICC. However, due to the low incidence of cholangiocarcinoma, our center currently collects very little data, and we would expand the sample size to further support our conclusion.

At present, there are many clinical studies on lenvatinib and anti-PD-1 in the treatment of advanced liver cancer malignancies, such as NCT02579616 (21), NCT03006926 (14), NCT04044313 (22), NCT03895970 (16). There are also some retrospective analysis of the efficacy of lenvatinib in the real world (23–26). In our central study, based to the limited data available so far, it was found that Lenvatinib alone or in combination with anti-PD-1 could be an effective treatment for unresectable HCC and ICC. Moreover, baseline AFP and CA19-9 levels may contribute to predict the prognostication. However, the relationships among body weight and Lenvatinib dose and toxicity require further studies. Of course, in the future work, we will expand the sample size and extend the follow-up time to collect more data to make our conclusion more credible.

DATA AVAILABILITY STATEMENT

The raw data supporting the conclusions of this article will be made available by the authors, without undue reservation.

ETHICS STATEMENT

The studies involving human participants were reviewed and approved by Ethics committee of Comprehensive Cancer Center of Drum Tower Hospital of Nanjing University. The patients/participants provided their written informed consent to participate in this study.

AUTHOR CONTRIBUTIONS

SZ, JShe, and BL conceived and designed the experiments. SZ, CL, YD, JShe, and JSha performed the experiments and analyzed the samples. SZ, CL, YD, and JSha analyzed the data. SZ, JShe, and BL wrote the manuscript. All authors interpreted the data, critically revised the manuscript for important intellectual contents and approved the final version.

FUNDING

This study was supported by National Natural Science Foundation of China (No. 81902914); Jiangsu Provincial Medical Youth Talent (No. QNRC2016043); and the Key Medical Science and Technology Development Project of Nanjing (No. ZKX16032).

SUPPLEMENTARY MATERIAL

The Supplementary Material for this article can be found online at: https://www.frontiersin.org/articles/10.3389/fonc.2021.788635/full#supplementary-material

REFERENCES

1. Ferlay J, Colombet M, Soerjomataram I, Parkin DM, Piñeros M, Znaor A, et al. Cancer Statistics for the Year 2020: An Overview. *Int J Cancer* (2021). doi: 10.1002/ijc.33588
2. Wilhelm S, Carter C, Tang L, Wilkie D, McNabola N, Rong H, et al. BAY 43-9006 Exhibits Broad Spectrum Oral Antitumor Activity and Targets the RAF/MEK/ERK Pathway and Receptor Tyrosine Kinases Involved in Tumor Progression. And Angiogenesis. *Cancer Res* (2004) 64:7099–109. doi: 10.1158/0008-5472.CAN-04-1443
3. Chang Y, Adnane J, Trail P, Levy J, Henderson A, Xue D, et al. Sorafenib (BAY 43-9006) Inhibits Tumor Growth and Vascularization and Induces Tumor Apoptosis and Hypoxia in RCC Xenograft Models. *Cancer Chemother Pharmacol* (2007) 59:561–74. doi: 10.1007/s00280-006-0393-4
4. Llovet J, Ricci S, Mazzaferro V, Hilgard P, Gane E, Blanc J, et al. Sorafenib in Advanced Hepatocellular Carcinoma. *N Engl J Med* (2008) 359:378–90. doi: 10.1056/NEJMoa0708857
5. Yamamoto Y, Matsui J, Matsushima T, Obaishi H, Miyazaki K, Nakamura K, et al. Lenvatinib, an Angiogenesis Inhibitor Targeting VEGFR/FGFR, Shows Broad Antitumor Activity in Human Tumor Xenograft Models Associated With Microvessel Density and Pericyte Coverage. *Vasc Cell* (2014) 6:18. doi: 10.1186/2045-824X-6-18
6. Singal A, Nagar S, Hitchens A, Davis K, Iyer S. Real-World Effectiveness of Lenvatinib Monotherapy Among Patients With Unresectable Hepatocellular Carcinoma Patients in the USA. *Future Oncol* (2021) 21:2759–68. doi: 10.2217/fon-2021-0242
7. Kudo M, Finn R, Qin S, Han KH, Ikeda K, Piscaglia F, et al. Lenvatinib Versus Sorafenib in First-Line Treatment of Patients With Unresectable Hepatocellular Carcinoma: A Randomised Phase 3 non-Inferiority Trial. *Lancet* (2018) 391:1163–73. doi: 10.1016/S0140-6736(18)30207-1
8. Zongyi Y, Xiaowu L. Immunotherapy for Hepatocellular Carcinoma. *Cancer Lett* (2020) 470:8–17. doi: 10.1016/j.canlet.2019.12.002
9. Okazaki T, Honjo T. PD-1 and PD-1 Ligands: From Discovery to Clinical Application. *Int Immunol* (2007) 19:813–24. doi: 10.1093/intimm/dxm057
10. Zhu A, Finn R, Edeline J, Cattan S, Ogasawara S, Palmer D, et al. Pembrolizumab in Patients With Advanced Hepatocellular Carcinoma Previously Treated With Sorafenib (KEYNOTE-224): A non-Randomised, Open-Label Phase 2 Trial. *Lancet Oncol* (2018) 19:940–52. doi: 10.1016/s1470-2045(18)30351-6
11. Liu Z, Liu X, Liang J, Liu Y, Hou X, Zhang M, et al. Immunotherapy for Hepatocellular Carcinoma: Current Status and Future Prospects. *Front Immunol* (2021) 12:765101. doi: 10.3389/fimmu.2021.765101
12. Zappasodi R, Merghoub T, Wolchok J. Emerging Concepts for Immune Checkpoint Blockade-Based Combination Therapies. *Cancer Cell* (2018) 33:581–98. doi: 10.1016/j.ccell.2018.03.005
13. Llovet J, Kelley R, Villanueva A, Singal A, Pikarsky E, Roayaie S, et al. Hepatocellular Carcinoma. *Nat Rev Dis Primers* (2021) 7:6. doi: 10.1038/s41572-020-00240-3
14. Finn R, Ikeda M, Zhu A, Sung M, Baron A, Kudo M, et al. Phase Ib Study of Lenvatinib Plus Pembrolizumab in Patients With Unresectable Hepatocellular Carcinoma. *J Clin Oncol* (2020) 38:2960–70. doi: 10.1200/JCO.20.00808
15. Yang J, Hainaut P, Gores G, Amadou A, Plymoth A, Roberts L. A Global View of Hepatocellular Carcinoma: Trends, Risk, Prevention and Management. *Nat Rev Gastroenterol Hepatol* (2019) 16:589–604. doi: 10.1038/s41575-019-0186-y
16. Lin J, Yang X, Long J, Zhao S, Mao J, Wang D, et al. Pembrolizumab Combined With Lenvatinib as non-First-Line Therapy in Patients With Refractory Biliary Tract Carcinoma. *Hepatobiliary Surg Nutr* (2020) 9:414–24. doi: 10.21037/hbsn-20-338
17. Galle P, Foerster F, Kudo M, Chan SL, Llover JM, Qin S, et al. Biology and Significance of Alpha-Fetoprotein in Hepatocellular Carcinoma. *Liver Int* (2019) 39:2214–29. doi: 10.1111/liv.14223
18. Zhang BH, Yang BH, Tang ZY. Randomized Controlled Trial of Screening for Hepatocellular Carcinoma. *J Cancer Res Clin Oncol* (2004) 130:417–22. doi: 10.1007/s00432-004-0552-0
19. Levy C, Lymp J, Angulo P, Gores G, Larusso N, Lindor K. The Value of Serum CA 19-9 in Predicting Cholangiocarcinomas in Patients With Primary Sclerosing Cholangitis. *Dig Dis Sci* (2005) 50:1734–40. doi: 10.1007/s10620-005-2927-8
20. Charatcharoenwitthaya P, Enders F, Halling K, Lindor K. Utility of Serum Tumor Markers, Imaging, and Biliary Cytology for Detecting Cholangiocarcinoma in Primary Sclerosing Cholangitis. *Hepatology (Baltimore Md)* (2008) 48:1106–17. doi: 10.1002/hep.22441
21. Ueno M, Ikeda M, Sasaki T, Nagashima F, Mizuno N, Shimizu S, et al. Phase 2 Study of Lenvatinib Monotherapy as Second-Line Treatment in Unresectable Biliary Tract Cancer: Primary Analysis Results. *BMC Cancer* (2020) 20:1105. doi: 10.1186/s12885-020-07365-4
22. He M, Liang R, Zhao Y, Xu Y, Chen H, Zhou Y, et al. Versuslenvatinib, Toripalimab, Plus Hepatic Arterial Infusion Chemotherapy Lenvatinib Alone for Advanced Hepatocellular Carcinoma. *Ther Adv Med Oncol* (2021) 13:17588359211002720. doi: 10.1177/17588359211002720
23. Koroki K, Kanogawa N, Maruta S, Ogasawara S, Iino Y, Obu M, et al. Posttreatment After Lenvatinib in Patients With Advanced Hepatocellular Carcinoma. *Liver Cancer* (2021) 10:473–84. doi: 10.1159/000515552
24. Goh M, Oh J, Park Y, Kim J, Kang W, Sinn DH, et al. Efficacy and Safety of Lenvatinib Therapy for Unresectable Hepatocellular Carcinoma in a Real-World Practice in Korea. *Liver Cancer* (2021) 10:52–62. doi: 10.1159/000512239
25. Tsuchiya K, Kurosaki M, Sakamoto A, Marusawa H, Kojima Y, Hasebe C, et al. The Real-World Data in Japanese Patients With Unresectable Hepatocellular Carcinoma Treated With Lenvatinib From a Nationwide Multicenter Study. *Cancers* (2021) 13. doi: 10.3390/cancers13112608
26. Chen K, Wei W, Liu L, Deng Z, Li L, Liang X, et al. Lenvatinib With or Without Immune Checkpoint Inhibitors for Patients With Unresectable Hepatocellular Carcinoma in Real-World Clinical Practice. *Cancer Immunol Immunother* (2021). doi: 10.1007/s00262-021-03060-w

Conflict of Interest: The authors declare that the research was conducted in the absence of any commercial or financial relationships that could be construed as a potential conflict of interest.

The handling editor HL declared a shared parent affiliation with the authors at the time of the review.

frontiers in Oncology

REVIEW
published: 20 December 2021
doi: 10.3389/fonc.2021.756334

A New Antitumor Direction: Tumor-Specific Endothelial Cells

Jing Liang[1], *Shouqi Wang*[2], *Guowei Zhang*[2], *Baoyu He*[1], *Qingli Bie*[1,3*] *and Bin Zhang*[1,3*]

[1] Department of Laboratory Medicine, Affiliated Hospital of Jining Medical University, Jining Medical University, Jining, China, [2] Department of Gastrointestinal Surgery, Affiliated Hospital of Jining Medical University, Jining Medical University, Jining, China, [3] Institute of Forensic Medicine and Laboratory Medicine, Jining Medical University, Jining, China

Targeting tumor blood vessels is an important strategy for tumor therapies. At present, antiangiogenic drugs are known to have significant clinical effects, but severe drug resistance and side effects also occur. Therefore, new specific targets for tumor and new treatment methods must be developed. Tumor-specific endothelial cells (TECs) are the main targets of antiangiogenic therapy. This review summarizes the differences between TECs and normal endothelial cells, assesses the heterogeneity of TECs, compares tumorigenesis and development between TECs and normal endothelial cells, and explains the interaction between TECs and the tumor microenvironment. A full and in-depth understanding of TECs may provide new insights for specific antitumor angiogenesis therapies.

Keywords: tumor-specific endothelial cells, tumor heterogeneity, tumor angiogenesis, tumor microenvironment, antiangiogenic therapy

OPEN ACCESS

Edited by:
Hongda Liu,
Nanjing Medical University, China

Reviewed by:
Laura Gatti,
Fondazione IRCCS Istituto Neurologio Carlo Besta (IRCCS), Italy
Alessandro Fantin,
University of Milan, Italy
Simona D'Aguanno,
Istituti Fisioterapici Ospitalieri (IRCCS), Italy

***Correspondence:**
Bin Zhang
zhb861109@163.com
Qingli Bie
xiaobie890101@163.com

Specialty section:
This article was submitted to Cancer Molecular Targets and Therapeutics, a section of the journal Frontiers in Oncology

Received: *10 August 2021*
Accepted: *25 November 2021*
Published: *20 December 2021*

Citation:
Liang J, Wang S, Zhang G, He B, Bie Q and Zhang B (2021) A New Antitumor Direction: Tumor-Specific Endothelial Cells. Front. Oncol. 11:756334. doi: 10.3389/fonc.2021.756334

1 INTRODUCTION

Tumor angiogenesis refers to the formation of new blood vessels in tumors.Tumor blood vessels provide oxygen and nutrients for tumor growth, remove waste from tumor tissues, and provide pathways for tumor metastasis.If a solid tumor has insufficient amounts of blood vessels, then it can only grow to a critical size of 1–2 mm (or approximately 10^6 cells) (1). In recent years, many studies have identified significant differences in the structure and function between tumor vasculature and normal vasculature. Normal blood vessels have regular hierarchical structures that are responsible for blood flow throughout the body and maintain normal physiological activities, and these structures include arteries, veins and capillaries. Tumor blood vessels, however, are highly irregular in shape, and they are swollen and twisting and have many blind ends, which results in abnormal vascular function, including increased vascular permeability, leakage and bleeding, and blood flow disorder (2, 3).

The specificity of tumor-specific endothelial cells (TECs) is one of the main reasons for tumor vascular anomalies. Blood vessels are composed of ECs and pericytes, which are responsible for the contraction and relaxation of blood vessels. In normal blood vessels, ECs are mostly in a static state. In tumors, hypoxia and chronic growth factor stimulation may cause endothelial dysfunction (4). Increasing evidence has shown that these abnormalities can lead to the development of cancer. Initial hypotheses suggested that TECs were genetically stable normal somatic cells that were not prone to mutation and drug resistance and remained consistent in various tumors, which would allow multiple types of cancer to be treated by a single antiangiogenic drug (5). However, in recent

years, many researchers have found that TECs are not ordinary somatic cells but rather are heterogeneous in many aspects relative to normal endothelial cells (NECs), which contradicts previous assumptions (6, 7). Therefore, the study of TECs will provide targets or directions for tumor therapy. Because most current antiangiogenic drugs are nonspecific, they cause damage to NECs, thus leading to fatal side effects, such as intestinal perforation and bleeding in the later stages (8, 9).Therefore, exploring specific targets for TECs have potential for antitumor therapy.

The tumor microenvironment (TME) is essential for tumor progression, which accelerates metastasis and increases tumor malignancy. TME refers to the local environment for tumor survival. A large number of tumor cells infiltrate in TME, includes stromal cells, TECs and immune cells (10). TME provides an acidic and hypoxic environment containing a large number of cytokines (11). TME plays an important role in the process that TECs promote tumor progression and drug resistance (12). Among them, tumor-associated macrophages (TAMs) and tumor-associated fibroblasts (CAFs) have been found to promote the proliferation, migration and tube formation of HUVECs (13–15). And Myeloid-Derived Suppressor Cells (MDSCs) and extracellular matrix (ECM) alsoregulate the function of ECs (16, 17). Therefore, to study the interaction between TECs and TME is necessary to target for TECs therapy.

2 ANTITUMOR ANGIOGENESIS THERAPY

Fifty years ago, Judah Folkman first emphasized that angiogenesis was an important process for the growth and proliferation of solid tumors (18) and proposed that antiangiogenesis may be a potential method for treatment various cancers. In recent years, many factors and related receptors that promote angiogenesis have been confirmed, including vascular endothelial growth factor (VEGF) (19), platelet-derived growth factor (PDGF) (20, 21) and angiopoietin (Ang) (22), and antitumor angiogenesis drugs have been developed.

VEGF is considered a key factor in inducing tumor angiogenesis and is research hotspot as a key target for antitumor vascular therapy. VEGF activates MAPK, PI3K and other signals in ECs by binding to VEGF receptors (VEGFR1-3) to promote the formation of new blood vessels, increase vascular permeability, and regulate tumor angiogenesis (23–25). In recent decades, VEGF has been used as a therapeutic target to inhibit angiogenesis and promote the normalization of tumor blood vessels, and has achieved great success. Bevacizumab is the first approved antitumor angiogenesis therapy monoclonal antibody, and it can specifically bind to VEGF to inhibit tumor angiogenesis (26). But, the effect of bevacizumab treatment alone is limited. Minjian et al. observed that a significant upregulation of VEGF and downregulation of β-FGF and ANG1 in colon cancer-derived endothelial cells treated with bevacizumab alone, which might activate a potential self-regulating mechanism of angiogenic growth factors and also explained why current antiangiogenic therapy with bevacizumab alone has limited effects in prolonging the survival of colon cancer patients (27). Clinical studies have confirmed that a combination of bevacizumab and chemotherapy drugs can significantly prolong the survival period of tumor patients and achieve antitumor effects (28–30). Nadine et al. found that telomerase regulates VEGF expression and secretion through its catalytic subunit hTERT in gastrointestinal cancer cells, and VEGF inhibition with bevacizumab increased hTERT expression which further increased VEGFR1 and VEGFR2 expression. They suggested the combination of bevacizumab with telomerase inhibitors could improve tumor cell response to anti-VEGF treatment (31). The VEGF pathway coordinates with many other signaling pathways, such as Ang/Tie receptor and PDGF/PDGFR signaling targeted by specific inhibitors nesvacumab and olaratumab, participates in tumor angiogenesis. Tyrosine kinase inhibitors (TKIs) are small molecule drugs that can inhibit the kinase activity of different receptors and their downstream signal transduction. Several studies revealed sunitinib, a TKI, not only targets VEGFR (32) but also inhibits PDGFR (33) and FGFR (34).Sunitinib has been used to treat a variety of cancers. Similarly, studies have reported that sunitinib treatment alone can cause ECs senescence, loose ECs connections, and promote tumor cell migration through the endothelial barrier (35). Based on the above research reports, treatment with one antitumor angiogenesis drug alone have great limit effects on cancer therapy (**Figure 1**).

Previously, antiangiogenic drugs were thought to be less toxic than other cytotoxic drugs; however, they subsequently been found have serious side effects (hypertension (36), bleeding (37), gastrointestinal perforation (8), etc.), with vascular toxicity particularly prominent. Theseside effects are associated with the inhibitory role of most current antiangiogenic drugs on cell signaling pathways, such as VEGF/VGEFR, which has a negative impact on the survival of NECs (38).Antiangiogenic drugs and their side effects are shown in (**Table 1**) (39–49). An important goal of cancer treatment is to develop new and safer tumor-specific antiangiogenic drugs.

3 TUMOR-SPECIFIC ENDOTHELIAL CELLS

At present, tumor angiogenesis research and antiangiogenic drug development use cultured ECs, such as human umbilical vein ECs (HUVECs). A number of studies have clarified the molecular differences between TECs and NECs through global analysis and compare TECs with NECs to try to find specific molecules for TECs. For example, Alam et al. conducted a DNA chip analysis and found that suprabasin might be a new marker for TECs. Compared with NECs, suprabasin, the upstream factor of the AKT pathway, was highly expressed in TECs and positively correlated with the migration and tube formation ability of TECs (50). Microarray and immunohistochemical analyses revealed that biglycan was a specific marker and an autocrine angiogenic factor of TECs (51). Goveia et al. performed single-cell RNA (scRNA) sequencing on 56,771 ECs from human/mouse tumor in lungs and cultured human lung TECs, and detected 17 known and 16 previously unrecognized phenotypes. And found that collagen modification was a

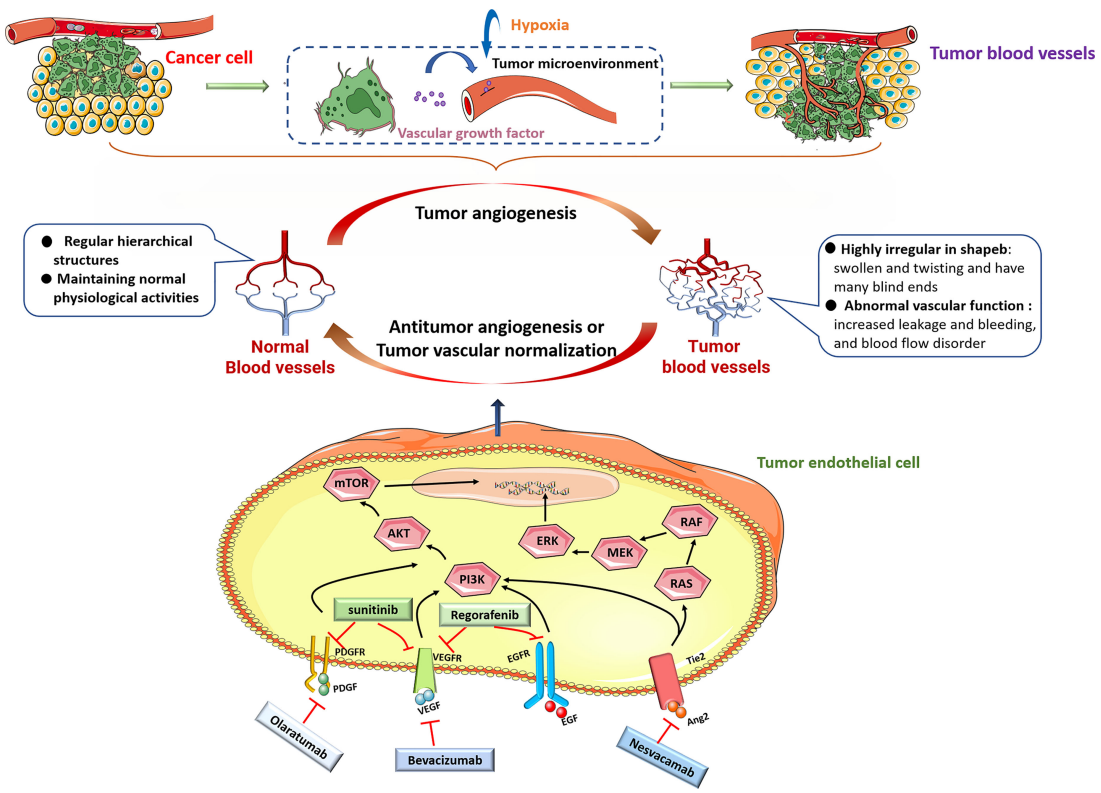

FIGURE 1 | Under pathological conditions including hypoxia, most tumor cells upregulate the expression of many angiogenic factors, including VEGF, PDGF, EGF and Ang, and secrete them into the tumor microenvironment. When these molecules bind to their cognate receptors, then stimulate downstream signaling, including PI3K/AKT and RAS/MEK/ERK signaling pathways to promote tumor growth and angiogenesis. Monoclonal antibodies beracizumab, olaratumab, nesvacamab and small molecule drugs sunitinib and regorafenib can block the interaction between pro-angiogenic factors and their receptors, and inhibit tumor angiogenesis.

candidate pathway for angiogenesis (52). Among the abovementioned studies, a few have focused on the function of TECs because human primary TECs culture have several limits, including small amounts from surgical specimens, difficult to separate, a short life span *in vitro*, easily lose their specificity and cannot be cultured in large quantities. In 2019, NakoMaishi and others established immortalized human TECs (h-imTECs) and their normal counterparts (h-imNECs) by transfecting with a lentivirus that produces simian virus 40 large T antigens and human telomerase reverse transcriptase to overcome replication barriers. These ECs exhibited an extended life span and retained their characteristic endothelial morphology, endothelial marker expression, and tube formation ability. Hence, these h-imTECs could be a valuable tool for drug screening to develop novel therapeutic agents specific to TECs or functional biological assays in tumor angiogenesis research (53).

3.1 Heterogeneity of Tumor-Specific Endothelial Cells

As a component of blood vessels, TECs are also different from NECs in many aspects (54). The whole tumor can be heterogeneous and biopsy may not be representative of the whole tumor. Angiogenesis contributes to the development of pathological conditions, such as tumor progression and metastasis, diabetic retinopathy, psoriasis, atherosclerosis, and rheumatoid arthritis (55).

As a component of blood vessels, TECs are also different from NECs in many aspects. Compared with most normal ECs, TECs have a higher proliferation rate and do not form a regular monolayer; the tumor vascular basement membrane is discontinuous or nonexistent, and the tumor endothelium is variably covered by pericytes with abnormal morphology (56, 57). Due to the phenotypic difference between tumor blood vessels and normal blood vessels, studies have concluded that may also exist genotype changes. Kyoko Hida found that the nucleus of TECs was larger than that of NECs and showed increased aneuploidy, abnormal centrosomes, and abnormalities, such as chromosome deletion, markers of unknown origin, and double microchromosomes (58). Chromosomal aberrations are also found in human renal carcinoma ECs and human B-cell lymphoma microvascular ECs (59, 60). These findings can be used as evidence of genetic instability of TECs. High-throughput expression profiles reveal changes in gene and protein expression profiles in the tumor endothelium. Li C et al. analyzed the expression differences between cervical cancer-derived ECs and NECs by scRNA-seq, and found several marker genes such as

TABLE 1 | Anti-angiogenic drugs.

Type	Drug	Target	Manufacturer	Approval	Indication	Side Effects
Monoclonal antibodies	Bevacizumab	VEGF	Genentech	2004	Colorectal cancer, Lung cancer, Cervical cancer, Glioblastoma, Ovarian cancer	Fatigue, pain, headache, abdominal pain, constipation, diarrhea, nausea, vomiting, anorexia, hemorrhage, dyspnea, Hypertension
	Cetuximab	EGFR	ImClone	2004	Colorectal cancer, Head and neck cancers	Fatigue, weakness, pain, headache, insomnia, weight loss, skin toxicities, GI toxicities, cough, dyspnea, fever, pharyngitis
	Panitumumab (Vectibix)	EGFR	Amgen	2005	Colorectal cancer	Fatigue, ocular toxicity, nausea, diarrhea, vomiting, skin toxicity, dyspnea reactions
	Ramucirumab	VEGFR2	Imclone	2014	Colorectal cancer, Lung cancer, Gastric cancer,	Hypertension, diarrhea
	Necitumumab	EGFR	Eli Lilly	2015	Lung cancer	Acne, diarrhea, vomiting, mouth sores, vision changes, tearing or itching, red and swollen nails, itching
	Olaratumab	PDGFR	Eli Lilly	2016	Sarcoma	Nausea, fatigue, musculoskeletal pain, mucositis, hair loss, vomiting, diarrhea, loss of appetite, abdominal pain, neuropathy, headache
Tyrosine kinase inhibitors	Imatinib	PDGFR, SCFR	Novartis Abl	2001	Chronic myelocytic leukemia, Gastrointestinal Stromal Tumors	Difficulty breathing, rapid heartbeat, insomnia, coughing up blood or pink mucus, chest pain, frequent urination, fever, jaundice, bloody stools, skin bruises, fatigue
	Gefitinib	EGFR	AstraZeneca	2003	Nonsmall-cell lung cancer	Diarrhea, rash, itching, dry skin, acne
	Nilotinib	PDGFR	Novartis Bcr-Abl	2004	Chronic myelocytic leukemia	Fatigue, diarrhea, anorexia, skin discoloration, rash, hand-foot syndrome, edema, muscle cramps, joint pain, headache, abdominal discomfort, anemia, cough and itching, heart failure, pancreatitis, kidney failure
	Sorafenib	VEGFR, PDGER	Bayer Raf	2005	Renal cell carcinoma	Diarrhea, fatigue, hair loss, constipation, skin rash, high blood pressure
	Sunitinib	PDGFR, VEGFR	Pfizer	2006	Renal cell carcinoma	Hand and foot skin reactions, rash, diarrhea, fatigue, increased blood pressure, mucositis, fever, yellow skin, edema
	Dasatinib	SRC, PDGFR	Bristol-Myers Squibb Bcr-Abl	2006	Chronic myelocytic leukemia	Diarrhea, headache, nausea, rash, dyspnea, bleeding, fatigue, musculoskeletal pain, infection, vomiting, cough, abdominal pain, fever
	Lapatinib	EGFR	GlaxoSmithKline	2007	Breast cancer	Nausea, diarrhea, stomatitis and indigestion, dry skin, rash, breathing difficulties and insomnia
	Pazopanib	VEGFR, PDGFR, FGFR	GlaxoSmithKline	2009	Renal cell carcinoma, soft tissue sarcoma, Nonsmall-cell lung cancer	Diarrhea, high blood pressure, hair color changes, nausea, anorexia, vomiting
	Crizotinib	ALK	Pfizer	2011	Nonsmall-cell lung cancer	Abnormal vision, nausea, diarrhea, vomiting, constipation, edema, fatigue
	Vandetanib	VEGFR, EGFR	AstraZeneca	2011	Thyroid cancer	Diarrhea, skin rash, acne, nausea, high blood pressure, headache, fatigue, loss of appetite, abdominal pain
	Axitinib	VEGFR	Pfizer	2012	Renal cell carcinoma	Diarrhea, high blood pressure, fatigue, loss of appetite, nausea, dysphonia, weight loss, vomiting, fatigue, constipation
	Afatinib	EGFR	Boehringer	2013	Nonsmall-cell lung cancer	Diarrhea, skin rash, stomatitis, paronychia, loss of appetite, nose bleeding, dry skin
	Erlotinib	EGFR	Roche	2013	Nonsmall-cell lung cancer	Skin rash, diarrhea, loss of appetite, fatigue, dyspnea, cough, nausea, infection, vomiting, stomatitis, itching, dry skin, conjunctivitis, keratoconjunctivitis, abdominal pain
	Ceritinib	ALK	Novartis	2014	Nonsmall-cell lung cancer	Diarrhea, nausea, vomiting, abdominal pain, fatigue, loss of appetite, constipation
	Osimertinib	EGFR	AstraZeneca	2015	Nonsmall-cell lung cancer	Skin rash, mouth ulcers, paronychia
	Regorafenib	VEGFR, EGFR	Bayer	2017	Colorectal cancer, Hepatocellular carcinoma, Gastrointestinal Stromal Tumors	Fatigue, loss of appetite, diarrhea, oral mucositis, weight loss, high blood pressure, dysphonia.
	Lorbrena	ALK	Pfizer	2018	Nonsmall-cell lung cancer	Edema, cognitive effects, dyspnea, fatigue, weight gain, joint pain, diarrhea
	Dacomitinib		Pfizer	2018		Diarrhea, skin rash, paronychia, stomatitis

(Continued)

TABLE 1 | Continued

Type	Drug	Target	Manufacturer	Approval	Indication	Side Effects
	Cabozantinib	EGFR/HER2/HER4 MET/VEGFR1/VEGFR2/VEGFR3/ROS1/RET/AXL/NTRK/KIT	Exelixis		Nonsmall-cell lung cancer Medullarythyroidcance (2012) Renal cell carcinoma (2016) Hepatocellular carcinoma (2018)	Diarrhea, stomatitis, weight loss, loss of appetite, nausea, fatigue, oral pain, changes in hair color, dysgeusia, high blood pressure, abdominal pain, constipation

TAGLN2, KLF5, STAT1 and STAT2 (7). ScRNA sequencing revealed that 2590 genes were differentially expressed between TECs isolated from human hepatocellular carcinoma and NECs isolated from normal liver tissues (61). Proteomics analysis identified 127 highly expressed proteins in ECs isolated from human renal cancer, colon cancer, and lung cancer compared with NECs, among which CD146, CD31, and VWF might be tumor endothelial cell markers (62). In addition to expressing common vascular endothelial markers,TECs also show upregulated expression of VEGFR-2, VEGFR-3, e-selectin, ICAM-1, CD44, integrin and MUC-18 (63) and the nontraditional angiogenic factors biglycan, lysyl oxidase and pentraxin 3, which together promote tumor angiogenesis (64). These data indicate that the huge differences between TECs and NECs can be exploited to specifically target TECs for tumor treatment.

In addition to differing from NECs, different TECs also show heterogeneity. TECs have long been regarded as normal somatic cells without tumor characteristics, such as susceptibility to mutation and drug resistance. However, in glioblastoma, some ECs were found to originate from the glioblastoma stem cell population (65). In lymphoma and neuroblastoma, ECs derived from tumor cells were also confirmed (60, 66). In recent years, bone marrow-derived endothelial progenitor cells have been found to be involved in the formation of tumor pathological blood vessels, although the mechanism of action is still unclear (67). These findings provide new targets and directions for antitumor therapies that specifically target TECs but also increase the difficulty of developing such therapies.

In addition to the different origins of TECs, TEC phenotypes are affected by TME. Comparing the TECs stimulated by two different metastatic tumor supernatants, found that the treatment of highly metastatic tumor conditioned medium increased the resistance of TECs to 5-fluorouracil (5-FU) (68). After coculture with lung cancer cells, human umbilical vein ECs showed enhanced cell motility and microvascular formation and a decrease in the percentage of apoptosis (69). Conditional culture can also cause epigenetic changes in gene expression in cultured ECs (70). This evidence reveals the influence of the tumor microenvironment on the characteristics of TECs and leads to heterogeneity among TECs. Therefore, studying the heterogeneity and diversity of TECs in the development of tumors will contribute to the development of antitumor angiogenesis drugs. Antitumor research about specifically targeting TECs has become a trend (**Figure 2**).

3.2 Function of Tumor-Specific Endothelial Cells in Cancer Progression

3.2.1 Tumorigenesis

The cellular origin of cancer and the nature of cells responsible for the maintenance and progression of tumors are still unsolved challenges for cancer therapy (71). Predictably, cancer originating from a single cell expands with the development of the cancer (72). Cancer stem cells (CSCs) have stem cell-like properties and can renew themselves. A number of studies have found that CSCs may cause cancer (73), thus leading to tumor recurrence (74). In melanoma,ECs can interact with CD133+ cancer stem cells to promote the occurrence and development of tumors (75). Targeting Cxcl12+ECs can inhibit the formation of the niche of gastric stem cells around blood vessels and inhibit the occurrence of diffuse gastric cancer (76). The specific regulatory mechanism of TECs on tumor stem cells is not very clear. *In vitro* experiments found that HUVECs co-cultured with human liver cancer cells (MHCC97H) enhanced the spheroidizing ability of MHCC97H cells and the expression of CD133 (77). Jia et al. found that TECs could release soluble factors through paracrine action and increasedthe CSCs ratio, clonal sphere formation, tumorigenicity and chemoresistance (78). These effects are caused by the activation of Notch signaling in TECs and changes in the CSCs phenotype (78, 79). Knocking out the specific Notch ligand Dll4 inECs inhibits Epithelial-Mesenchymal Transition(EMT) and results in a reduction in the number of CSCs and decreased tumor metastasis (80). The above evidence shows that TEC may regulate cancer stem cells through the Notch signaling pathway. In addition, studies have found that TECs may also regulate the phenotype and chemotherapy resistance of CSCs through the AKT, Src, and FAK signaling pathways (81, 82).

The transcriptional regulator YAP/TAZ has strong activity in malignant tumors and has been found to promote the occurrence of many tumors, including gastric cancer, colorectal cancer, liver cancer, and neuroblastoma. The YAP/TAZ signaling could influence the function of ECs to promote the tumor progression (83). Up-regulation of the tumor suppressor gene DLC1 in ECs activated YAP signal and ECs lost the contact inhibition function,which leaded to the occurrence and proliferation of angiosarcoma (84, 85). YAP also controls the activation of ECs and regulates tumorigenesis and angiogenesis (86). Thus, interference with the YAP/TAZ signaling pathway is expected to suppress tumorigenesis and tumor angiogenesis (**Figure 3**).

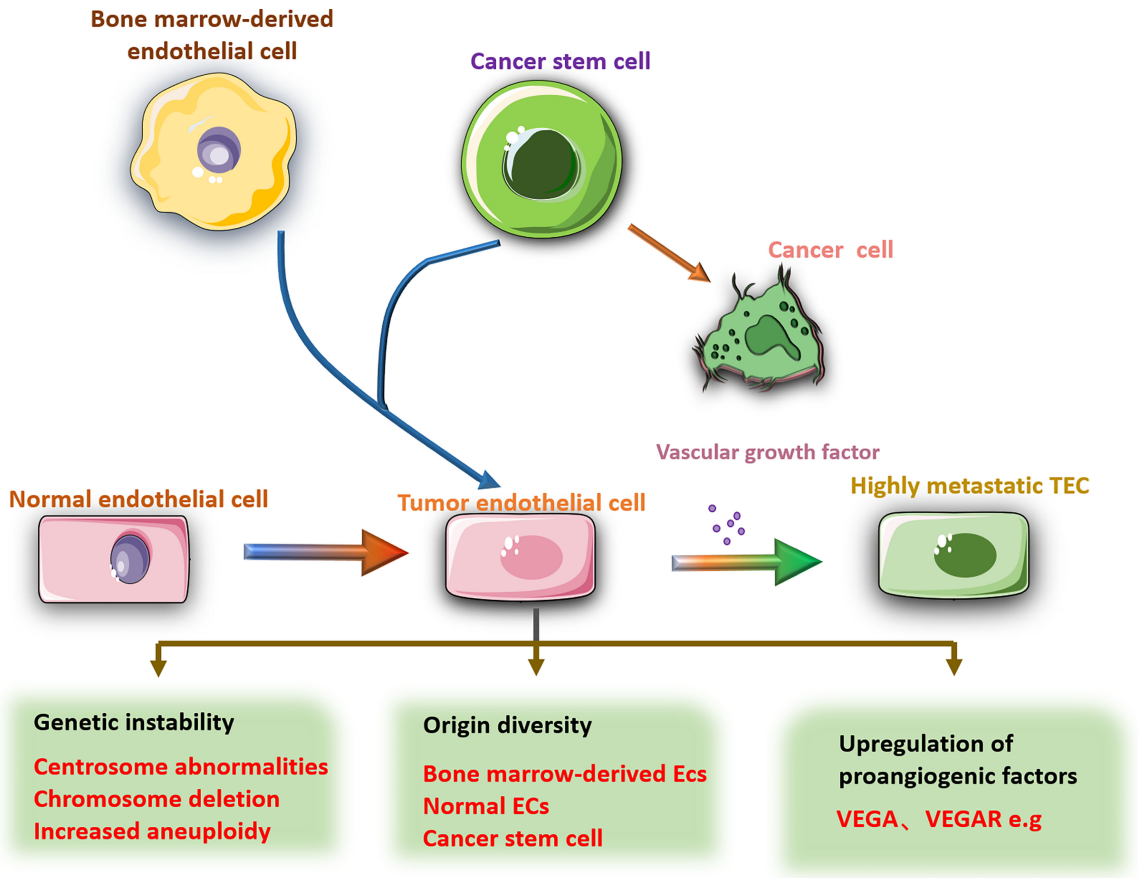

FIGURE 2 | There are obvious differences between TECs and NECs. Compared with NECs, TECs have larger nuclei, increased aneuploidy, abnormal centrosomes, and chromosomal deletions. The source of TECs is diverse, including NECs mutations, bone marrow-derived ECs, cancer stem cells and other cell transformations. The gene changes lead to high expression of pro-angiogenic factors in TECs, such as VEGF, VEGFR, etc., which promote tumor angiogenesis. In addition, the phenotype of TECs is also affected by the tumor microenvironment.

3.2.2 Tumor Transendothelial Migration

Metastasis is the main cause of cancer patient death, which has not yet been resolved by current tumor treatments. Tumor cell migration across the endothelium is an important step in the process of tumor invasion and metastasis. Tumor cells cross the basement membrane and enter peripheral blood circulation to reach distant organs, then adhere to vascular ECs through cell adhesion molecules, and migrate through vascular endodermis to colonize these organs. Endothelial-to-mesenchymal transition (EndoMT) is considered a necessary process for tumor migration across the endothelium. EndoMT is a complex cell differentiation process in which ECs break away from the cell population and migrate, which reduces the characteristics of ECs to varying degrees, and these cells then acquire mesenchymal characteristics. The main hallmark of EndoMT is that TGF-β inducesECs to transform into CAF-like cells, thus leading to the loss of endothelial adhesion molecules and endothelial cytoskeleton reorganization through the Rho and Rac-1 signaling pathway (87) (**Figure 4**). EndoMT helps to destroy the endothelial barrier, which leads to tumor extravasation and increase metastasis. Studies have confirmed that EndoMT increases the transendothelial migration of melanoma (88). Similarly, EndoMT, which is mediated by osteopontin (OPN) through the PI3K/Akt/TSC2 and mTORC1 signaling pathways, promotes the growth and metastasis of colorectal cancer (89). EndoMT caused by endoglin deficiency causeincreased liver and lung metastasis in pancreatic cancer model mice (90). Therefore, it is feasible to use EndoMT as a target to inhibit tumor metastasis. Moreover, some studies have pointed out that EndoMT may be the cause of drug resistance in antitumor therapy (91). Therefore, the role of EndoMT needs to be explored and fully understood.

Cell adhesion molecules are essential for tumor migration across the endothelium. Laferriere et al. found that E-selectin expressed by TECs ensured that colon cancer cells adhered to ECs and activated the SAPK2/P38 signaling pathway to promote tumor transendothelial migration (92). In addition, the activation of ERK by E-selectin regulates the opening of the endothelial space by initiating the activation of Src kinase activity and the dissociation of the VE-cadherin/β-catenin complex (93).

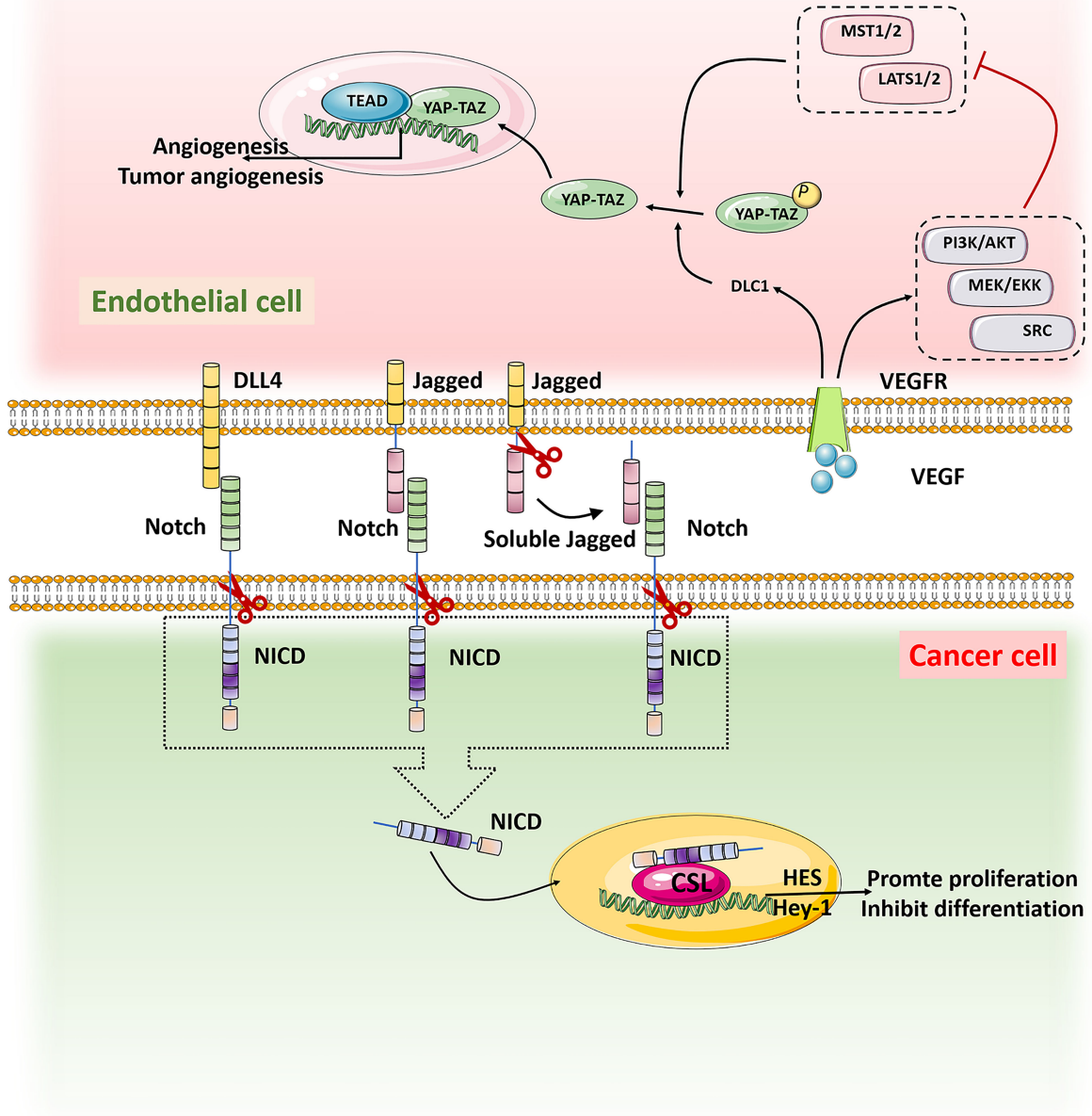

FIGURE 3 | When Notch on tumor cells binds to ligands DLL4 and Jagged on TECs, it is activated and cut by Y secretion to release the Notch intracellular domain NICD, which is translocated into the nucleus by activating transcriptional targets HES and Hey1 to inhibit differentiation and maintain stemness. VEGF in the tumor microenvironment binds to the receptor VEGFR on TECs, promoting the expression of tumor suppressor gene DLC1 and the activation of signaling pathways such as PI3K/AKT, MEK/EKK and SRC, thus inhibiting the activation of MST1/2-LATS1/2 kinase cassette. YAP/TAZ was dephosphorylated and translocated into the nucleus. In the nucleus, YAP/TAZ interacts with the transcription factor TEAD to promote tumor genesis and angiogenesis.

In melanoma, ICAM-1 expressed in TECs interacts with its receptor integrin LFA-1 to promote tumor cell migration across the endothelium *in vitro* (94). The VE-cadherin binding domain of fibrinogen induces the permeability of the endothelial barrier and enhances the transendothelial migration of malignant breast epithelial cells (95). Therefore, blocking the production of cell adhesion molecules or inhibiting their function has great potential to inhibit tumor metastasis.

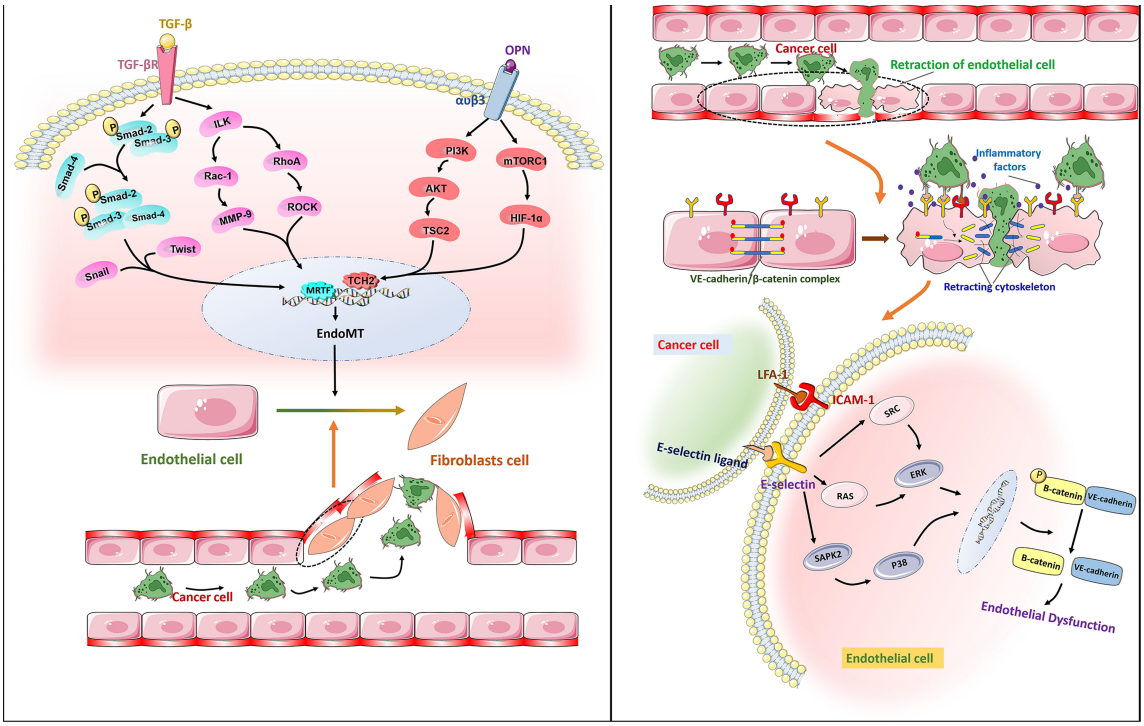

FIGURE 4 | Right: Free TGF-β binds to receptors on the surface of ECs membranes, phosphorylates Smad2 and Smad3, then binds to Smad4, enters the nucleus, and binds to Snail, Twist and other transcription factors to initiate EndoMT by promoting transcription of mesenchymal markers and reducing transcription of endothelial markers. It leads to endothelial dysfunction and promotes the transendothelial migration of cancer cells. Osteopontin (OPN) interacts with a variety of integrins. The combination of OPN and α V β3 activates PI3K/AKT and mTORC1 pathways and promotes the metastasis of cancer cells.Left: The adhesion molecule ICAM-1 binds to e-selectin through ligand receptor, which enables tumor cells to bind to endothelial cells. The dissociation of the VE-cadherin/β -catenin complex is associated with endothelial barrier dysfunction. E-selectin regulates the transendothelial migration of cancer cells by activating the ERK and P38 signaling pathways and mediating the dissociation of the VE-cadherin/β -catenin complex.

Studies have confirmed that anti-cell adhesion molecule antibodies can inhibit tumor growth and metastasis. For example, after treatment with an anti-L1CAM antibody, the cancer growth (up to 75%) of SKOV3ip ovarian cancer cells was significantly reduced (96). Unfortunately, such treatment cannot effectively eliminate highly malignant tumors. In view of this situation, additional in-depth research is required to find more effective treatment strategies that target cell adhesion molecules (**Figure 4**).

3.2.3 Tumor Resistance

Drug resistance is an obstacle that impairs the success of cancer therapies. In some cases, relapse occurs in initially responsive patients after repeated cycles of chemotherapy due to the acquisition of tumor resistance (97). In the early stage, TECs were considered to be homogenous, these genetic stable cell populations did not cause drug resistance. With the progression of tumor, as we previously mentioned, TECs occurred considerable heterogeneity and genetic instability which might lead to drug resistance (98). A number of experiments have proven that ECs show resistance to some drugs. For example, kidney cancer ECs are resistant to vincristine (63) while liver cancer ECs are resistant to adriamycin (99) and 5-fluorouracil (100). However, it is not clear whether this resistance is related to the genomic characteristics of TECs. The resistance of ECs to antiangiogenic treatment appears to be related to the increased expression of multidrug resistance proteins, such as P-glycoprotein (Pgp, ABCB1) and breast cancer resistance protein (BCRP,ABCG2), which serve as cellular efflux pumps (101, 102). In addition, Ca2+ transporters are also changed in stromal cancer cells, including ECs and endothelial colony forming cells (103). The remodeling of the endothelial Ca2+ toolkit may enhance the resistance of anticancer treatments by supporting tumor angiogenesis and reducing the sensitivity to proapoptotic stimuli (104). VEGF is an important target for antitumor angiogenesis. Studies have found that the failure of anti-VEGF drugs in anticancer treatment may be due to the recruitment of endothelial progenitor cells. VEGF inhibitors can induce the expression of placental growth factor, IL-6 and stem cell factors in nontumor tissues, and these cytokines can recruit bone marrow-derived ECs and myeloid progenitor cells to promote the formation of a premetastatic environment. Some of these recruited cells express VEGFR-1 and are resistant to VEGF inhibitors that target VEGFR-2 (105).

3.3 Interaction of Tumor-Specific Endothelial Cells and the Tumor Microenvironment

The interaction between a tumor and mesenchymal cells may be the reason for the abnormal structure of mesenchymal cells. The TME consists of stromal cells (including fibroblasts, macrophages, regulatory T cells, myeloid suppressor cells, ECs, pericytes and platelets) and extracellular matrix components (including inflammatory cytokines, chemokines and Matrix metalloproteinases), which enhance invasion and metastasis of cancer cells through mutual signal transduction. The TME induces gene expression in ECs to develop in a direction that is conducive to angiogenesis (**Figure 5**).

3.3.1 Tumor-Associated Macrophages

TAMs are the key cells that control tumor angiogenesis and the main source of angiogenic factors. TAMs can secrete angiogenesis factors, such as VEGF (106–108), basic fibroblast growth factor (Fgf2) (109), insulin-like growth factor-1 (Igf1) (110), chemokine ligand 2 (Ccl2) (111, 112) and placental growth factor (Pgf) (113)ect. These factors can stimulate ECs and promote proliferation rapidly of cells, which leads to tumor angiogenesis (14). Recent studies have found that TAMs highly express certain cytokines in gastric cancer, such as VEGF-A, VEGF-C, matrix metalloproteinase 1 (MMP-1) and amphiregulin (114), and induces capillary morphogenesis in human gastric cancer lymphatic ECs (115). Another study showed that CCL18 released

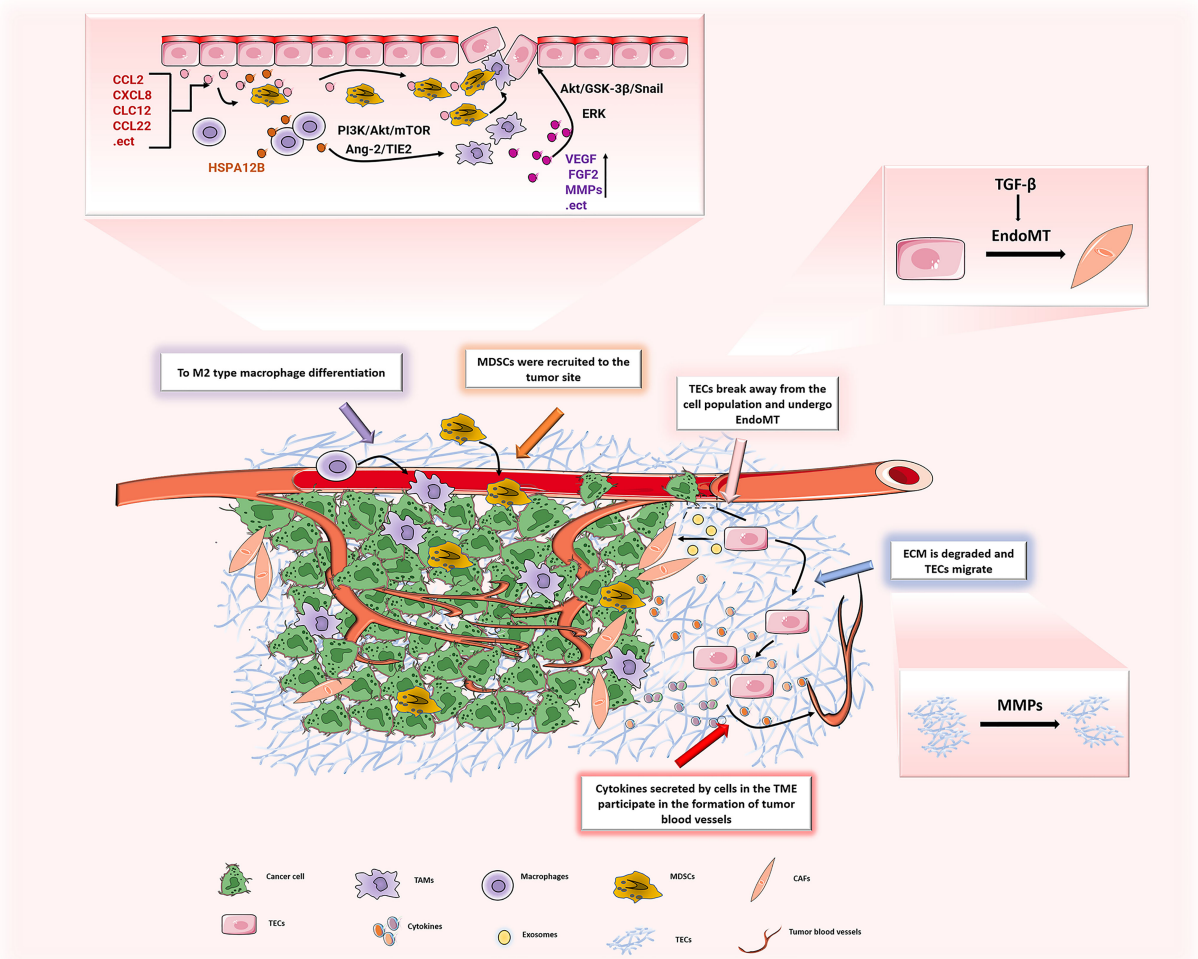

FIGURE 5 | In TME, the various components interact to promote the development of ECs in the direction of promoting angiogenesis. ECs can induce M2 polarization of macrophages through PI3K/Akt/mTOR, and may recruit TAMs to tumor sites through the Ang-2/TIE2 signaling pathway to promote tumor progression. TAMs secrete a large number of pro-angiogenic factors (VEGF, FGF2, MMPs, etc.) to promote the proliferation of ECs, leading to tumor angiogenesis. The chemokines (CCL2, CXCL8, etc.) secreted by ECs recruit MDSCs to the tumor and play a tumor-promoting effect. ECs generate CAFs through EndoMT, and the generated CAFs secrete pro-angiogenic factors to stimulate ECs and promote tumor angiogenesis. After ECM is degraded by MMPs, it increases the migration of ECs and promotes tumor angiogenesis.

by TAMs cooperated with VEGF to promote the migration of ECs, induce EndoMT, and activate ERK and Akt/GSK-3β/Snail signals in HUVECs, thereby promoting breast cancer angiogenesis (116). The latest breakthrough study found that an M1-like macrophage subtype might keep vascular cells quiescent, and at the same time, Matrix-remodeling macrophages might assist invasive cancer cells to co-opt vessels (117). Therefore, TAMs regulate the phenotype and function of ECs in the process of tumor angiogenesis and vascular remodeling. There is no doubt that TECs can also act on TAMs. First, TECs can recruit TAMs to tumor sites, which are mediated by several signaling pathways including the Ang-2/TIE2 signaling (118, 119). Second, changes in the permeability ofECs will also increase the infiltration of TAMs, thereby promoting the development of tumors (120). In addition, studies have found that ECs could selectively activate the differentiation of tumor-promoting M2 macrophages and promoted tumor angiogenesis (121). The latest research confirms that TECs may induce M2 polarization of macrophages by secreting HSPA12B to activate the PI3K/Akt/mTOR signal pathway (122). The above evidence shows that ECs play a key role in inducing the differentiation of macrophages and promoting further polarization to a pro-angiogenic phenotype. Therefore, studying the interaction between TECs and TAMs may provide a novel therapeutic approach on specifically targeting TECs.

3.3.2 Tumor-Associated Fibroblasts

In the TME, CAFs are a major matrix component that helps build the extracellular matrix and provides necessary growth factors for tumor cell growth and development. There are various sources of CAFs, such as activated tissue cells, transdifferentiated pericytes and adipocytes. However, CAFs can also be generated from transdifferentiated ECs through EndoMT (123). Studies have speculated that approximately 40% of CAFs are formed from ECs (124). As mentioned above, this process is mainly mediated by TGF-β. TGF-β secreted by tumor cells stimulates the phosphorylation of TGF-β receptors on the surface of ECs and activates Smad, which in turn activates the downstream signal transduction cascade, then leads to the occurrence of EndoMT and to generate CAFs (125, 126). A study found that exosomes secreted by tumors may also mediate the differentiation of ECs into CAFs and promote tumor invasion (123). Another study confirmed that melanoma-derived exosomes increased the number of CAFs differentiated from HUVECs by promoting EndoMT, which showed obvious morphological, molecular changes and motility (127). It is worth mentioning that the generated CAFs secrete a large number of cytokines, which can react with TECs and promote tumor angiogenesis. For example, CAFs release a large amount of angiogenic factors, such as VEGF-A (128) and FGF2 (129), in the TME to activate ECs and promote tumor angiogenesis. Interestingly, CAFs can also recruit endothelial progenitor cells by secreting CXCL12 to accelerate tumor growth and increase angiogenesis (130). In addition, early studies have found that platelet-derived growth factor C (PDGF-C) produced by CAFs can act on ECs and enhance the resistance to anti-angiogenesis and anti-VEGF treatments (131). Later studies showed that CAFs enhanced the motility and permeability of ECs by upregulating the LPP gene and promoted chemotherapy resistance in ovarian cancer (132). Overall, studies on the relationship between TECs and CAFs will provide a deeper understanding of tumor angiogenesis and chemotherapy drug resistance. Inhibiting the generation of CAFs or killing existing CAFs might represent effective therapeutic targets for antitumor angiogenesis.

3.3.3 Myeloid-Derived Suppressor Cells

MDSCs are immature myeloid cells that are normally produced and secreted by the bone marrow in the state of local inflammation. They have strong immunosuppressive activity, which can inhibit excessive inflammation and protect the host from autoimmune diseases (133). In the tumor state, MDSCs are abnormally produced and recruited to the TME to help establish an immunosuppressive TME and promote tumor angiogenesis and metastasis to support tumor progression. There are two main types of MDSCs, mononuclear MDSCs (M-MDSCs) and polymorphonuclear MDSCs (PMN-MDSCs) (134). In tumors, M-MDSC can quickly differentiate into TAMs (135, 136), and the relationship between TAMs and ECs and the promotion of tumors have been discussed above. However, evidence has shown that PMN-MDSCs are mainly recruited to tumor tissues by chemokines to play a pro-tumor effect. Sushil et al. found that CXCL2 and CCL22 promoted MDSC recruitment to primary tumors and metastatic sites in triple-negative breast cancer (137). However, inhibiting the expression of CXCL1 and CXCL2 reduces the recruitment of MDSCs in ovarian cancer (138). ECs are the main sources of chemokines. Studies have shown that in a variety of tumors, TECs can secrete a large number of chemokines, such as CCL2, CXCL8 and CXCL12 (139, 140). Chemokine receptors are distributed on the cell membrane of MDSCs, and chemokine recruit MDSCs to the tumor site by binding these chemokine receptors and promote tumor progression (141). After knocking down the chemokine receptor (CXCR2) in myeloid cells, the recruitment of MDSCs is reduced and vascular remodeling is inhibited (142). The above studies show that TECs play a key role in MDSCs recruitment and tumor progression. Similarly, MDSCs can also regulate TECs. A study found that MDSCs may interact with lysosomal acid lipase to cause dysfunction of ECs (16). Moreover, *in vitro* experiments have shown that the culture supernatant of PMN-MDSCs can significantly promote the tube formation of HUVECs (143). This finding indicates that PMN-MDSCs may secrete some pro-angiogenic factors. Later studies confirmed that MDSCs might promote endothelial cell angiogenesis through the production of VEGF-A, Ang2 and HIF-1α and unregulated angiogenesis by activating the STAT3 signaling pathway (144). In summary, TECs play key roles in the pro-tumor effect of MDSCs and exploring the mechanisms involved in MDSCs-induced tumor angiogenesis will provide new insights for anti-angiogenesis therapy.

3.3.4 Extracellular Matrix

Along with stromal cells, the extracellular matrix is another important part of the TME. The extracellular matrix (ECM) is a noncellular three-dimensional polymer network composed of

collagen, elastin, fibronectin, laminin and other proteins. It can regulate a variety of cellular functions and is essential for maintaining normal homeostasis. The production and maintenance of the ECM is an important aspect of endothelial cell function. The ECM provides mechanical support to ECs and mediates signaling (145) *via* secreted molecules (146) and mechanical strain (147)between cells. In the absence of angiogenesis stimulation, ECM helps ECs to maintain in a quiescent state. In the tumor growth stage, the ECM is degraded in the TME and the basement membrane is destroyed, which cause ECs migrate from existing blood vessels to newly formed blood vessels. In this progress, MMPs play a major role. MMPs are the main enzyme in degradatingextracellular matrix proteins, and can participate in the occurrence and development of tumors in different ways. On the one hand, MMPs can regulate the expression of VEGF to promote formation of neovascularization and increase blood vessel permeability (148). Moreover, MMPs can also degrade collagen to promote the migration of ECs, which adhere to the temporary ECM through specific integrins to form a tubular structure and obtain a continuous lumen (149). On the other hand, it can degrade a variety of extracellular matrix components to promote tumor progression. For example, MMP-2 promotes the transendothelial migration of breast cancer cells by degrading the laminin component of the ECM (150). MMP9 can bind to CD44 to degrade fibronectin, which leads to the active form of TGF-βreleasing (151), then TGF-β enhances the conversion of ECs to endothelial mesenchyme and increases the quantity of CAFs to promote tumor progression (152). In short, the ECM is the main regulator of angiogenesis and vascular stability. However, it is not a stable component and will undergo tremendous changes under a variety of pathological conditions including tumors. Therefore, promoting the normalization of ECM composition can be used as a new therapy for antitumor angiogenesis.

4 CONCLUSION

This review summarizes the tissue differences between tumor blood vessels and normal blood vessels. Tumor blood vessels are highly irregular in shape with increased vascular permeability and leakage, which contributes to the tumor metastasis. Contrary to previous ideas, recent studies suggest that TECs differ from NECs in many aspects. Different studies have revealed TECs originate from various cell types, for example bone marrow-derived endothelial progenitor cells and tumor cells. The development of TECs and angiogenesis are affected by the intricate TME including infiltrated various cells and inflammatory cytokines, growth factors and so on. All the above described factors can contribute to the different gene expression profile between TECs and NECs, which affects the formation and function of tumor blood vessels. Moreover, identification of relevant factors influencing the structural and functional differences between TECs and NECs are also imminent to provide clues for target therapies of angiogenesis. Taken together, this review summarizes the most recent research developments in the field of the molecular and cellular features of angiogenesis of cancer biology. Importantly, this review systematically introduces the current knowledge on TECs, and provides new insights into the potential of targeted therapies.

AUTHOR CONTRIBUTIONS

JL drafted the manuscript, SW and GZ drew the figures, BH contributed equally to plot the table, BZ and QB revised the review. All authors contributed to the article and approved the submitted version.

FUNDING

This study was supported by grants from the National Natural Science Foundation of China (No. 82173371, 81802446), project tsqn201909192 supported by Tai Shan Young Scholar Foundation of Shandong Province, project ZR2019BH050, ZR2020YQ59, ZR202103020202 supported by Shandong Provincial Natural Science Foundation; PhD Research Foundation of the Affiliated Hospital of Jining Medical University (No. 2018-BS-001, 2018-BS-013), project 202003031182, 202003031183 supported by the Project of Medicine Health and Technology Development Plan of Shandong Province, project CX2020081, CX2020042, CX2020035 supported by University Student Innovation Training Program of Jining Medical University, the Miaopu Research of the Affiliated Hospital of Jining Medical University (No. MP-ZD-2020-005).

ACKNOWLEDGMENTS

The work was supported by the Laboratory Medicine Department of the Affiliated Hospital of Jining Medical University,and I would like to show great gratitude to them all. In addition, we are very grateful to Dr. Huabao Xiong for editing the manuscript.

REFERENCES

1. Brown LF, Guidi AJ, Schnitt SJ, Van De Water L, Iruela-Arispe ML, Yeo TK, et al. Vascular Stroma Formation in Carcinoma *in Situ*, Invasive Carcinoma, and Metastatic Carcinoma of the Breast. *Clin Cancer Res* (1999) 5:1041–56.
2. Tilki D, Kilic N, Sevinc S, Zywietz F, Stief CG, Ergun S. Zone-Specific Remodeling of Tumor Blood Vessels Affects Tumor Growth. *Cancer* (2007) 110:2347–62. doi: 10.1002/cncr.23024
3. Viallard C, Audiger C, Popovic N, Akla N, Lanthier K, Legault-Navarrete I, et al. BMP9 Signaling Promotes the Normalization of Tumor Blood Vessels. *Oncogene* (2020) 39:2996–3014. doi: 10.1038/s41388-020-1200-0
4. Lin PP. Aneuploid Circulating Tumor-Derived Endothelial Cell (CTEC): A Novel Versatile Player in Tumor Neovascularization and Cancer Metastasis. *Cells* (2020) 9:1539. doi: 10.3390/cells9061539
5. Dhanabal M, Jeffers M, Larochelle WJ. Anti-Angiogenic Therapy as a Cancer Treatment Paradigm. *Curr Med Chem Anticancer Agents* (2005) 5:115–30. doi: 10.2174/1568011053174882

6. Nagl L, Horvath L, Pircher A, Wolf D. Tumor Endothelial Cells (Tecs) as Potential Immune Directors of the Tumor Microenvironment - New Findings and Future Perspectives. *Front Cell Dev Biol* (2020) 8:766. doi: 10.3389/fcell.2020.00766
7. Li C, Guo L, Li S, Hua K. Single-Cell Transcriptomics Reveals the Landscape of Intra-Tumoral Heterogeneity and Transcriptional Activities of Ecs in CC. *Mol Ther Nucleic Acids* (2021) 24:682–94. doi: 10.1016/j.omtn.2021.03.017
8. Pfisterer J, Shannon CM, Baumann K, Rau J, Harter P, Joly F, et al. Bevacizumab and Platinum-Based Combinations for Recurrent Ovarian Cancer: A Randomised, Open-Label, Phase 3 Trial. *Lancet Oncol* (2020) 21:699–709. doi: 10.1016/S1470-2045(20)30142-X
9. Zhao B, Zhao H, Zhao J. Risk of Fatal Adverse Events in Cancer Patients Treated With Sunitinib. *Crit Rev Oncol Hematol* (2019) 137:115–22. doi: 10.1016/j.critrevonc.2019.03.007
10. Ni Y, Zhou X, Yang J, Shi H, Li H, Zhao X, et al. the Role of Tumor-Stroma Interactions in Drug Resistance Within Tumor Microenvironment. *Front Cell Dev Biol* (2021) 9:637675. doi: 10.3389/fcell.2021.637675
11. Yamaguchi R, Perkins G. Animal Models for Studying Tumor Microenvironment (TME) and Resistance to Lymphocytic Infiltration. *Cancer Biol Ther* (2018) 19:745–54. doi: 10.1080/15384047.2018.1470722
12. Luis G, Godfroid A, Nishiumi S, Cimino J, Blacher S, Maquoi E, et al. Tumor Resistance to Ferroptosis Driven by Stearoyl-Coa Desaturase-1 (SCD1) in Cancer Cells and Fatty Acid Biding Protein-4 (FABP4) in Tumor Microenvironment Promote Tumor Recurrence. *Redox Biol* (2021) 43:102006. doi: 10.1016/j.redox.2021.102006
13. Sun M, Qiu S, Xiao Q, Wang T, Tian X, Chen C, et al. Synergistic Effects of Multiple Myeloma Cells and Tumor-Associated Macrophages on Vascular Endothelial *Cells in Vitro*. *Med Oncol* (2020) 37:99. doi: 10.1007/s12032-020-01426-1
14. Jetten N, Verbruggen S, Gijbels MJ, Post MJ, De Winther MP, Donners MM. Anti-Inflammatory M2, But Not Pro-Inflammatory M1 Macrophages Promote Angiogenesis *in Vivo*. *Angiogenesis* (2014) 17:109–18. doi: 10.1007/s10456-013-9381-6
15. Pausch TM, Aue E, Wirsik NM, Freire Valls A, Shen Y, Radhakrishnan P, et al. Metastasis-Associated Fibroblasts Promote Angiogenesis in Metastasized Pancreatic Cancer *via* the CXCL8 and the CCL2 Axes. *Sci Rep* (2020) 10:5420. doi: 10.1038/s41598-020-62416-x
16. Zhao T, Ding X, Du H, Yan C. Myeloid-Derived Suppressor Cells Are Involved in Lysosomal Acid Lipase Deficiency-Induced Endothelial Cell Dysfunctions. *J Immunol* (2014) 193:1942–53. doi: 10.4049/jimmunol.1301941
17. Bagulho A, Vilas-Boas F, Pena A, Peneda C, Santos FC, Jeronimo A, et al. the Extracellular Matrix Modulates H2O2 Degradation and Redox Signaling in Endothelial Cells. *Redox Biol* (2015) 6:454–60. doi: 10.1016/j.redox.2015.09.006
18. Folkman J. Tumor Angiogenesis: Therapeutic Implications. *N Engl J Med* (1971) 285:1182–6. doi: 10.1056/NEJM197111182852108
19. Zhu CC, Chen C, Xu ZQ, Zhao JK, Ou BC, Sun J, et al. CCR6 Promotes Tumor Angiogenesis *via* the AKT/NF-Kappab/VEGF Pathway in Colorectal Cancer. *Biochim Biophys Acta Mol Basis Dis* (2018) 1864:387–97. doi: 10.1016/j.bbadis.2017.10.033
20. Balamurugan K, Koehler L, Durig JN, Hempel U, Rademann J, Hintze V, et al. Structural Insights Into the Modulation of PDGF/PDGFR-Beta Complexation by Hyaluronan Derivatives. *Biol Chem* (2021) 402:1441–52. doi: 10.1515/hsz-2021-0173
21. Ma J, Tang W, Gu R, Hu F, Zhang L, Wu J, et al. SHP-2-Induced Activation of C-Myc is Involved in PDGF-B-Regulated Cell Proliferation and Angiogenesis in Rmecs. *Front Physiol* (2020) 11:555006. doi: 10.3389/fphys.2020.555006
22. Mueller T, Freystein J, Lucas H, Schmoll HJ. Efficacy of a Bispecific Antibody Co-Targeting VEGFA and Ang-2 in Combination With Chemotherapy in a Chemoresistant Colorectal Carcinoma Xenograft Model. *Molecules* (2019) 24:2865. doi: 10.3390/molecules24162865
23. Cheng W, Cheng Z, Weng L, Xing D, Zhang M. Asparagus Polysaccharide Inhibits the Hypoxia-Induced Migration, Invasion and Angiogenesis of Hepatocellular Carcinoma Cells Partly Through Regulating HIF1alpha/VEGF Expression *via* MAPK and PI3K Signaling Pathway. *J Cancer* (2021) 12:3920–9. doi: 10.7150/jca.51407
24. Wagner MJ, Lyons YA, Siedel JH, Dood R, Nagaraja AS, Haemmerle M, et al. Combined VEGFR and MAPK Pathway Inhibition in Angiosarcoma. *Sci Rep* (2021) 11:9362. doi: 10.1038/s41598-021-88703-9
25. Liao ZH, Zhu HQ, Chen YY, Chen RL, Fu LX, Li L, et al. the Epigallocatechin Gallate Derivative Y6 Inhibits Human Hepatocellular Carcinoma by Inhibiting Angiogenesis in MAPK/ERK1/2 and PI3K/AKT/HIF-1alpha/VEGF Dependent Pathways. *J Ethnopharmacol* (2020) 259:112852. doi: 10.1016/j.jep.2020.112852
26. Ferrara N, Hillan KJ, Gerber HP, Novotny W. Discovery and Development of Bevacizumab, an Anti-VEGF Antibody for Treating Cancer. *Nat Rev Drug Discov* (2004) 3:391–400. doi: 10.1038/nrd1381
27. Zhao M, Yu Z, Li Z, Tang J, Lai X, Liu L. Expression of Angiogenic Growth Factors VEGF, Bfgf and ANG1 in Colon Cancer After Bevacizumab Treatment in vitro: A Potential Self-Regulating Mechanism. *Oncol Rep* (2017) 37:601–7. doi: 10.3892/or.2016.5231
28. Bamias A, Gibbs E, Khoon Lee C, Davies L, Dimopoulos M, Zagouri F, et al. Bevacizumab With or After Chemotherapy for Platinum-Resistant Recurrent Ovarian Cancer: Exploratory Analyses of the AURELIA Trial. *Ann Oncol* (2017) 28:1842–8. doi: 10.1093/annonc/mdx228
29. Cheng Y, Wu G, Zhang S, Liu Y, Qu J, Qu X. Complete Pathologic Response of Multiple Liver Metastases and Clinical Complete Response of Rectal Cancer in a Patient With Ataxia-Telangiectasia Mutated Gene Mutations After XELOXIRI Plus Bevacizumab: A Case Report. *Onco Targets Ther* (2021) 14:4201–9. doi: 10.2147/OTT.S320477
30. Ilic I, Jankovic S, Ilic M. Bevacizumab Combined With Chemotherapy Improves Survival for Patients With Metastatic Colorectal Cancer: Evidence From Meta Analysis. *PloS One* (2016) 11:e0161912. doi: 10.1371/journal.pone.0161912
31. Mahfouz N, Tahtouh R, Alaaeddine N, El Hajj J, Sarkis R, Hachem R, et al. Gastrointestinal Cancer Cells Treatment With Bevacizumab Activates a VEGF Autoregulatory Mechanism Involving Telomerase Catalytic Subunit Htert *via* PI3K-AKT, HIF-1Alpha and VEGF Receptors. *PloS One* (2017) 12:e0179202. doi: 10.1371/journal.pone.0179202
32. Brossa A, Grange C, Mancuso L, Annaratone L, Satolli MA, Mazzone M, et al. Sunitinib But Not VEGF Blockade Inhibits Cancer Stem Cell Endothelial Differentiation. *Oncotarget* (2015) 6:11295–309. doi: 10.18632/oncotarget.3123
33. Alamon C, Davila B, Garcia MF, Sanchez C, Kovacs M, Trias E, et al. Sunitinib-Containing Carborane Pharmacophore With the Ability to Inhibit Tyrosine Kinases Receptors FLT3, KIT and PDGFR-Beta, Exhibits Powerful *In Vivo* Anti-Glioblastoma Activity. *Cancers (Basel)* (2020) 12:3423. doi: 10.3390/cancers12113423
34. Tran TA, Leong HS, Pavia-Jimenez A, Fedyshyn S, Yang J, Kucejova B, et al. Fibroblast Growth Factor Receptor-Dependent and -Independent Paracrine Signaling by Sunitinib-Resistant Renal Cell Carcinoma. *Mol Cell Biol* (2016) 36:1836–55. doi: 10.1128/MCB.00189-16
35. Wang D, Xiao F, Feng Z, Li M, Kong L, Huang L, et al. Sunitinib Facilitates Metastatic Breast Cancer Spreading by Inducing Endothelial Cell Senescence. *Breast Cancer Res* (2020) 22:103. doi: 10.1186/s13058-020-01346-y
36. Carvalho B, Lopes RG, Linhares P, Costa A, Caeiro C, Fernandes AC, et al. Hypertension and Proteinuria as Clinical Biomarkers of Response to Bevacizumab in Glioblastoma Patients. *J Neurooncol* (2020) 147:109–16. doi: 10.1007/s11060-020-03404-z
37. Lai XX, Xu RA, Yu-Ping L, Yang H. Risk of Adverse Events With Bevacizumab Addition to Therapy in Advanced non-Small-Cell Lung Cancer: A Meta-Analysis of Randomized Controlled Trials. *Onco Targets Ther* (2016) 9:2421–8. doi: 10.2147/OTT.S96156
38. Small HY, Montezano AC, Rios FJ, Savoia C, Touyz RM. Hypertension Due to Antiangiogenic Cancer Therapy With Vascular Endothelial Growth Factor Inhibitors: Understanding and Managing a New Syndrome. *Can J Cardiol* (2014) 30:534–43. doi: 10.1016/j.cjca.2014.02.011
39. Middleton G, Lapka DV. Bevacizumab (Avastin). *Clin J Oncol Nurs* (2004) 8:666–9. doi: 10.1188/04.CJON.663-669
40. Graham J, Muhsin M, Kirkpatrick P. Cetuximab. *Nat Rev Drug Discov* (2004) 3:549–50. doi: 10.1038/nrd1445
41. Tyagi P. Recent Results and Ongoing Trials With Panitumumab (ABX-EGF), a Fully Human Anti-Epidermal Growth Factor Receptor Antibody, in Metastatic Colorectal Cancer. *Clin Colorectal Cancer* (2005) 5:21–3. doi: 10.1016/s1533-0028(11)70161-x

42. Poole RM, Vaidya A. Ramucirumab: First Global Approval. *Drugs* (2014) 74:1047–58. doi: 10.1007/s40265-014-0244-2
43. Thatcher N, Hirsch FR, Luft AV, Szczesna A, Ciuleanu TE, Dediu M, et al. Necitumumab Plus Gemcitabine and Cisplatin Versus Gemcitabine and Cisplatin Alone as First-Line Therapy in Patients With Stage IV Squamous non-Small-Cell Lung Cancer (SQUIRE): An Open-Label, Randomised, Controlled Phase 3 Trial. *Lancet Oncol* (2015) 16:763–74. doi: 10.1016/S1470-2045(15)00021-2
44. Olaratumab Approved for Soft-Tissue Sarcoma. *Cancer Discov* (2016) 6:1297. doi: 10.1158/2159-8290.CD-NB2016-141
45. Hartmann JT, Haap M, Kopp HG, Lipp HP. Tyrosine Kinase Inhibitors - a Review on Pharmacology, Metabolism and Side Effects. *Curr Drug Metab* (2009) 10:470–81. doi: 10.2174/138920009788897975
46. Zhao Y, Bilal M, Raza A, Khan MI, Mehmood S, Hayat U, et al. Tyrosine Kinase Inhibitors and Their Unique Therapeutic Potentialities to Combat Cancer. *Int J Biol Macromol* (2021) 168:22–37. doi: 10.1016/j.ijbiomac.2020.12.009
47. Chaar M, Kamta J, Ait-Oudhia S. Mechanisms, Monitoring, and Management of Tyrosine Kinase Inhibitors-Associated Cardiovascular Toxicities. *Onco Targets Ther* (2018) 11:6227–37. doi: 10.2147/OTT.S170138
48. Lipsky A, Lamanna N. Managing Toxicities of Bruton Tyrosine Kinase Inhibitors. *Hematol Am Soc Hematol Educ Program* (2020) 2020:336–45. doi: 10.1182/hematology.2020000118
49. Jiao Q, Bi L, Ren Y, Song S, Wang Q, Wang YS. Advances in Studies of Tyrosine Kinase Inhibitors and Their Acquired Resistance. *Mol Cancer* (2018) 17:36. doi: 10.1186/s12943-018-0801-5
50. Alam MT, Nagao-Kitamoto H, Ohga N, Akiyama K, Maishi N, Kawamoto T, et al. Suprabasin as a Novel Tumor Endothelial Cell Marker. *Cancer Sci* (2014) 105:1533–40. doi: 10.1111/cas.12549
51. Yamamoto K, Ohga N, Hida Y, Maishi N, Kawamoto T, Kitayama K, et al. Biglycan is a Specific Marker and an Autocrine Angiogenic Factor of Tumour Endothelial Cells. *Br J Cancer* (2012) 106:1214–23. doi: 10.1038/bjc.2012.59
52. Rohlenova K, Goveia J, Garcia-Caballero M, Subramanian A, Kalucka J, Treps L, et al. Single-Cell RNA Sequencing Maps Endothelial Metabolic Plasticity in Pathological Angiogenesis. *Cell Metab* (2020) 31:862–877 e814. doi: 10.1016/j.cmet.2020.03.009
53. Maishi N, Kikuchi H, Sato M, Nagao-Kitamoto H, Annan DA, Baba S, et al. Development of Immortalized Human Tumor Endothelial Cells From Renal Cancer. *Int J Mol Sci* (2019) 20:4595. doi: 10.3390/ijms20184595
54. Hida K, Maishi N, Annan DA, Hida Y. Contribution of Tumor Endothelial Cells in Cancer Progression. *Int J Mol Sci* (2018) 19:1272. doi: 10.3390/ijms19051272
55. Eelen G, de Zeeuw P, Simons M, Carmeliet P. Endothelial Cell Metabolism in Normal and Diseased Vasculature. *Circ Res* (2015) 116:1231–44. doi: 10.1161/CIRCRESAHA.116.302855
56. Chen WZ, Jiang JX, Yu XY, Xia WJ, Yu PX, Wang K, et al. Endothelial Cells in Colorectal Cancer. *World J Gastrointest Oncol* (2019) 11:946–56. doi: 10.4251/wjgo.v11.i11.946
57. Morikawa S, Baluk P, Kaidoh T, Haskell A, Jain RK, McDonald DM. Abnormalities in Pericytes on Blood Vessels and Endothelial Sprouts in Tumors. *Am J Pathol* (2002) 160:985–1000. doi: 10.1016/S0002-9440(10)64920-6
58. Hida K, Hida Y, Amin DN, Flint AF, Panigrahy D, Morton CC, et al. Tumor-Associated Endothelial Cells With Cytogenetic Abnormalities. *Cancer Res* (2004) 64:8249–55. doi: 10.1158/0008-5472.CAN-04-1567
59. Akino T, Hida K, Hida Y, Tsuchiya K, Freedman D, Muraki C, et al. Cytogenetic Abnormalities of Tumor-Associated Endothelial Cells in Human Malignant Tumors. *Am J Pathol* (2009) 175:2657–67. doi: 10.2353/ajpath.2009.090202
60. Streubel B, Chott A, Huber D, Exner M, Jager U, Wagner O, et al. Lymphoma-Specific Genetic Aberrations in Microvascular Endothelial Cells in B-Cell Lymphomas. *N Engl J Med* (2004) 351:250–9. doi: 10.1056/NEJMoa033153
61. Chai ZT, Zhang XP, Ao JY, Zhu XD, Wu MC, Lau WY, et al. AXL Overexpression in Tumor-Derived Endothelial Cells Promotes Vessel Metastasis in Patients With Hepatocellular Carcinoma. *Front Oncol* (2021) 11:650963. doi: 10.3389/fonc.2021.650963
62. Mesri M, Birse C, Heidbrink J, McKinnon K, Brand E, Bermingham CL, et al. Identification and Characterization of Angiogenesis Targets Through Proteomic Profiling of Endothelial Cells in Human Cancer Tissues. *PloS One* (2013) 8:e78885. doi: 10.1371/journal.pone.0078885
63. Bussolati B, Deambrosis I, Russo S, Deregibus MC, Camussi G. Altered Angiogenesis and Survival in Human Tumor-Derived Endothelial Cells. *FASEB J* (2003) 17:1159–61. doi: 10.1096/fj.02-0557fje
64. Maishi N, Annan DA, Kikuchi H, Hida Y, Hida K. Tumor Endothelial Heterogeneity in Cancer Progression. *Cancers (Basel)* (2019) 11:1511. doi: 10.3390/cancers11101511
65. Ricci-Vitiani L, Pallini R, Biffoni M, Todaro M, Invernici G, Cenci T, et al. Tumour Vascularization *via* Endothelial Differentiation of Glioblastoma Stem-Like Cells. *Nature* (2010) 468:824–8. doi: 10.1038/nature09557
66. Pezzolo A, Parodi F, Corrias MV, Cinti R, Gambini C, Pistoia V. Tumor Origin of Endothelial Cells in Human Neuroblastoma. *J Clin Oncol* (2007) 25:376–83. doi: 10.1200/JCO.2006.09.0696
67. Marcola M, Rodrigues CE. Endothelial Progenitor Cells in Tumor Angiogenesis: Another Brick in the Wall. *Stem Cells Int* (2015) 2015:832649. doi: 10.1155/2015/832649
68. Torii C, Maishi N, Kawamoto T, Morimoto M, Akiyama K, Yoshioka Y, et al. Mirna-1246 in Extracellular Vesicles Secreted From Metastatic Tumor Induces Drug Resistance in Tumor Endothelial Cells. *Sci Rep* (2021) 11:13502. doi: 10.1038/s41598-021-92879-5
69. Cheng HW, Chen YF, Wong JM, Weng CW, Chen HY, Yu SL, et al. Cancer Cells Increase Endothelial Cell Tube Formation and Survival by Activating the PI3K/Akt Signalling Pathway. *J Exp Clin Cancer Res* (2017) 36:27. doi: 10.1186/s13046-017-0495-3
70. Ciesielski O, Biesiekierska M, Panthu B, Vialichka V, Pirola L, Balcerczyk A. The Epigenetic Profile of Tumor Endothelial Cells. Effects of Combined Therapy With Antiangiogenic and Epigenetic Drugs on Cancer Progression. *Int J Mol Sci* (2020) 21:2606. doi: 10.3390/ijms21072606
71. Brooks MD, Burness ML, Wicha MS. Therapeutic Implications of Cellular Heterogeneity and Plasticity in Breast Cancer. *Cell Stem Cell* (2015) 17:260–71. doi: 10.1016/j.stem.2015.08.014
72. Sotgia F, Fiorillo M, Lisanti MP. Hallmarks of the Cancer Cell of Origin: Comparisons With "Energetic" Cancer Stem Cells (E-Cscs). *Aging (Albany NY)* (2019) 11:1065–8. doi: 10.18632/aging.101822
73. Zhao H, Yan C, Hu Y, Mu L, Liu S, Huang K, et al. Differentiated Cancer Cell-Originated Lactate Promotes the Self-Renewal of Cancer Stem Cells in Patient-Derived Colorectal Cancer Organoids. *Cancer Lett* (2020) 493:236–44. doi: 10.1016/j.canlet.2020.08.044
74. O'Brien CA, Kreso A, Ryan P, Hermans KG, Gibson L, Wang Y, et al. ID1 and ID3 Regulate the Self-Renewal Capacity of Human Colon Cancer-Initiating Cells Through P21. *Cancer Cell* (2012) 21:777–92. doi: 10.1016/j.ccr.2012.04.036
75. Kumar D, Kumar S, Gorain M, Tomar D, Patil HS, Radharani NNV, et al. Notch1-MAPK Signaling Axis Regulates CD133(+) Cancer Stem Cell-Mediated Melanoma Growth and Angiogenesis. *J Invest Dermatol* (2016) 136:2462–74. doi: 10.1016/j.jid.2016.07.024
76. Hayakawa Y, Ariyama H, Stancikova J, Sakitani K, Asfaha S, Renz BW, et al. Mist1 Expressing Gastric Stem Cells Maintain the Normal and Neoplastic Gastric Epithelium and Are Supported by a Perivascular Stem Cell Niche. *Cancer Cell* (2015) 28:800–14. doi: 10.1016/j.ccell.2015.10.003
77. Feng C, Yang X, Sun J, Luo Q, Song G. [Effect of Conditioned Medium From Endothelial Cells on Cancer Stem Cell Phenotype of Hepatoma Cells]. *Sheng Wu Yi Xue Gong Cheng Xue Za Zhi* (2015) 32:1061–6.
78. Lu J, Ye X, Fan F, Xia L, Bhattacharya R, Bellister S, et al. Endothelial Cells Promote the Colorectal Cancer Stem Cell Phenotype Through a Soluble Form of Jagged-1. *Cancer Cell* (2013) 23:171–85. doi: 10.1016/j.ccr.2012.12.021
79. Wang Y, Wang Y, Chen H, Liang Q. Endothelial Cells Promote Formation of Medulloblastoma Stem-Like Cells *via* Notch Pathway Activation. *J Mol Neurosci* (2017) 63:152–8. doi: 10.1007/s12031-017-0965-2
80. Mendonca L, Trindade A, Carvalho C, Correia J, Badenes M, Gigante J, et al. Metastasis is Impaired by Endothelial-Specific Dll4 Loss-of-Function Through Inhibition of Epithelial-to-Mesenchymal Transition and Reduction of Cancer Stem Cells and Circulating Tumor Cells. *Clin Exp Metastasis* (2019) 36:365–80. doi: 10.1007/s10585-019-09973-2
81. Kong DH, Kim MR, Jang JH, Na HJ, Lee S. A Review of Anti-Angiogenic Targets for Monoclonal Antibody Cancer Therapy. *Int J Mol Sci* (2017) 18:1786. doi: 10.3390/ijms18081786

82. Sun L, Pan J, Yu L, Liu H, Shu X, Sun L, et al. Tumor Endothelial Cells Promote Metastasis and Cancer Stem Cell-Like Phenotype Through Elevated Epiregulin in Esophageal Cancer. *Am J Cancer Res* (2016) 6:2277–88.
83. Thomann S, Weiler SME, Marquard S, Rose F, Ball CR, Toth M, et al. YAP Orchestrates Heterotypic Endothelial Cell Communication *via* HGF/C-MET Signaling in Liver Tumorigenesis. *Cancer Res* (2020) 80:5502–14. doi: 10.1158/0008-5472.CAN-20-0242
84. Ritchey L, Ha T, Otsuka A, Kabashima K, Wang D, Wang Y, et al. DLC1 Deficiency and YAP Signaling Drive Endothelial Cell Contact Inhibition of Growth and Tumorigenesis. *Oncogene* (2019) 38:7046–59. doi: 10.1038/s41388-019-0944-x
85. Ye C, Hu Y, Wang J, Liu D, Du J. Mono (2-Ethylhexyl) Phthalate (MEHP) Triggers the Proliferation of Hemangioma-Derived Endothelial Cells *via* YAP Signals. *Chem Biol Interact* (2019) 311:108773. doi: 10.1016/j.cbi.2019.108773
86. Hooglugt A, van der Stoel MM, Boon RA, Huveneers S. Endothelial YAP/TAZ Signaling in Angiogenesis and Tumor Vasculature. *Front Oncol* (2020) 10:612802. doi: 10.3389/fonc.2020.612802
87. Ciszewski WM, Sobierajska K, Wawro ME, Klopocka W, Chefczynska N, Muzyczuk A, et al. the ILK-MMP9-MRTF Axis is Crucial for Endmt Differentiation of Endothelial Cells in a Tumor Microenvironment. *Biochim Biophys Acta Mol Cell Res* (2017) 1864:2283–96. doi: 10.1016/j.bbamcr.2017.09.004
88. Krizbai IA, Gasparics A, Nagyoszi P, Fazakas C, Molnar J, Wilhelm I, et al. Endothelial-Mesenchymal Transition of Brain Endothelial Cells: Possible Role During Metastatic Extravasation. *PloS One* (2015) 10:e0119655. doi: 10.1371/journal.pone.0119655
89. Fan CS, Chen WS, Chen LL, Chen CC, Hsu YT, Chua KV, et al. Osteopontin-Integrin Engagement Induces HIF-1alpha-TCF12-Mediated Endothelial-Mesenchymal Transition to Exacerbate Colorectal Cancer. *Oncotarget* (2018) 9:4998–5015. doi: 10.18632/oncotarget.23578
90. Anderberg C, Cunha SI, Zhai Z, Cortez E, Pardali E, Johnson JR, et al. Deficiency for Endoglin in Tumor Vasculature Weakens the Endothelial Barrier to Metastatic Dissemination. *J Exp Med* (2013) 210:563–79. doi: 10.1084/jem.20120662
91. Kim SH, Song Y, Seo HR. GSK-3beta Regulates the Endothelial-to-Mesenchymal Transition *via* Reciprocal Crosstalk Between NSCLC Cells and Huvecs in Multicellular Tumor Spheroid Models. *J Exp Clin Cancer Res* (2019) 38:46. doi: 10.1186/s13046-019-1050-1
92. Laferriere J, Houle F, Taher MM, Valerie K, Huot J. Transendothelial Migration of Colon Carcinoma Cells Requires Expression of E-Selectin by Endothelial Cells and Activation of Stress-Activated Protein Kinase-2 (SAPK2/P38) in the Tumor Cells. *J Biol Chem* (2001) 276:33762–72. doi: 10.1074/jbc.M008564200
93. Tremblay PL, Auger FA, Huot J. Regulation of Transendothelial Migration of Colon Cancer Cells by E-Selectin-Mediated Activation of P38 and ERK MAP Kinases. *Oncogene* (2006) 25:6563–73. doi: 10.1038/sj.onc.1209664
94. Ghislin S, Obino D, Middendorp S, Boggetto N, Alcaide-Loridan C, Deshayes F. LFA-1 and ICAM-1 Expression Induced During Melanoma-Endothelial Cell Co-Culture Favors the Transendothelial Migration of Melanoma Cell Lines In Vitro. *BMC Cancer* (2012) 12:455. doi: 10.1186/1471-2407-12-455
95. Sahni A, Arevalo MT, Sahni SK, Simpson-Haidaris PJ. the VE-Cadherin Binding Domain of Fibrinogen Induces Endothelial Barrier Permeability and Enhances Transendothelial Migration of Malignant Breast Epithelial Cells. *Int J Cancer* (2009) 125:577–84. doi: 10.1002/ijc.24340
96. Arlt MJ, Novak-Hofer I, Gast D, Gschwend V, Moldenhauer G, Grunberg J, et al. Efficient Inhibition of Intra-Peritoneal Tumor Growth and Dissemination of Human Ovarian Carcinoma Cells in Nude Mice by Anti-L1-Cell Adhesion Molecule Monoclonal Antibody Treatment. *Cancer Res* (2006) 66:936–43. doi: 10.1158/0008-5472.CAN-05-1818
97. Huang L, Perrault C, Coelho-Martins J, Hu C, Dulong C, Varna M, et al. Induction of Acquired Drug Resistance in Endothelial Cells and Its Involvement in Anticancer Therapy. *J Hematol Oncol* (2013) 6:49. doi: 10.1186/1756-8722-6-49
98. Yu Z, Mouillesseaux KP, Kushner EJ, Bautch VL. Tumor-Derived Factors and Reduced P53 Promote Endothelial Cell Centrosome Over-Duplication. *PloS One* (2016) 11:e0168334. doi: 10.1371/journal.pone.0168334
99. Xiong YQ, Sun HC, Zhang W, Zhu XD, Zhuang PY, Zhang JB, et al. Human Hepatocellular Carcinoma Tumor-Derived Endothelial Cells Manifest Increased Angiogenesis Capability and Drug Resistance Compared With Normal Endothelial Cells. *Clin Cancer Res* (2009) 15:4838–46. doi: 10.1158/1078-0432.CCR-08-2780
100. Ohga N, Ishikawa S, Maishi N, Akiyama K, Hida Y, Kawamoto T, et al. Heterogeneity of Tumor Endothelial Cells: Comparison Between Tumor Endothelial Cells Isolated From High- and Low-Metastatic Tumors. *Am J Pathol* (2012) 180:1294–307. doi: 10.1016/j.ajpath.2011.11.035
101. Huang L, Hu C, Di Benedetto M, Varin R, Liu J, Wang L, et al. Induction of Multiple Drug Resistance in HMEC-1 Endothelial Cells After Long-Term Exposure to Sunitinib. *Onco Targets Ther* (2014) 7:2249–55. doi: 10.2147/OTT.S67251
102. Akiyama K, Ohga N, Hida Y, Kawamoto T, Sadamoto Y, Ishikawa S, et al. Tumor Endothelial Cells Acquire Drug Resistance by MDR1 Up-Regulation *via* VEGF Signaling in Tumor Microenvironment. *Am J Pathol* (2012) 180:1283–93. doi: 10.1016/j.ajpath.2011.11.029
103. Nielsen N, Lindemann O, Schwab A. TRP Channels and STIM/ORAI Proteins: Sensors and Effectors of Cancer and Stroma Cell Migration. *Br J Pharmacol* (2014) 171:5524–40. doi: 10.1111/bph.12721
104. Moccia F. Endothelial Ca(2+) Signaling and the Resistance to Anticancer Treatments: Partners in Crime. *Int J Mol Sci* (2018) 19:217. doi: 10.3390/ijms19010217
105. Ebos JM, Lee CR, Christensen JG, Mutsaers AJ, Kerbel RS. Multiple Circulating Proangiogenic Factors Induced by Sunitinib Malate Are Tumor-Independent and Correlate With Antitumor Efficacy. *Proc Natl Acad Sci USA* (2007) 104:17069–74. doi: 10.1073/pnas.0708148104
106. Song Y, Tang C, Yin C. Combination Antitumor Immunotherapy With VEGF and PIGF SiRNA *via* Systemic Delivery of Multi-Functionalized Nanoparticles to Tumor-Associated Macrophages and Breast Cancer Cells. *Biomaterials* (2018) 185:117–32. doi: 10.1016/j.biomaterials.2018.09.017
107. Ohashi K, Wang Z, Yang YM, Billet S, Tu W, Pimienta M, et al. NOD-Like Receptor C4 Inflammasome Regulates the Growth of Colon Cancer Liver Metastasis in NAFLD. *Hepatology* (2019) 70:1582–99. doi: 10.1002/hep.30693
108. Wang D, Wang X, Si M, Yang J, Sun S, Wu H, et al. Exosome-Encapsulated Mirnas Contribute to CXCL12/CXCR4-Induced Liver Metastasis of Colorectal Cancer by Enhancing M2 Polarization of Macrophages. *Cancer Lett* (2020) 474:36–52. doi: 10.1016/j.canlet.2020.01.005
109. Huang JK, Ma L, Song WH, Lu BY, Huang YB, Dong HM, et al. Lncrna-MALAT1 Promotes Angiogenesis of Thyroid Cancer by Modulating Tumor-Associated Macrophage FGF2 Protein Secretion. *J Cell Biochem* (2017) 118:4821–30. doi: 10.1002/jcb.26153
110. Lv J, Liu C, Chen FK, Feng ZP, Jia L, Liu PJ, et al. M2like Tumourassociated Macrophagesecreted IGF Promotes Thyroid Cancer Stemness and Metastasis by Activating the PI3K/AKT/Mtor Pathway. *Mol Med Rep* (2021) 24:604. doi: 10.3892/mmr.2021.12249
111. Liu Q, Song J, Pan Y, Shi D, Yang C, Wang S, et al. Wnt5a/Camkii/ERK/CCL2 Axis is Required for Tumor-Associated Macrophages to Promote Colorectal Cancer Progression. *Int J Biol Sci* (2020) 16:1023–34. doi: 10.7150/ijbs.40535
112. Lee S, Lee E, Ko E, Ham M, Lee HM, Kim ES, et al. Tumor-Associated Macrophages Secrete CCL2 and Induce the Invasive Phenotype of Human Breast Epithelial Cells Through Upregulation of ERO1-Alpha and MMP-9. *Cancer Lett* (2018) 437:25–34. doi: 10.1016/j.canlet.2018.08.025
113. Rolny C, Mazzone M, Tugues S, Laoui D, Johansson I, Coulon C, et al. HRG Inhibits Tumor Growth and Metastasis by Inducing Macrophage Polarization and Vessel Normalization Through Downregulation of Plgf. *Cancer Cell* (2011) 19:31–44. doi: 10.1016/j.ccr.2010.11.009
114. Yamaguchi T, Fushida S, Yamamoto Y, Tsukada T, Kinoshita J, Oyama K, et al. Tumor-Associated Macrophages of the M2 Phenotype Contribute to Progression in Gastric Cancer With Peritoneal Dissemination. *Gastric Cancer* (2016) 19:1052–65. doi: 10.1007/s10120-015-0579-8
115. Tauchi Y, Tanaka H, Kumamoto K, Tokumoto M, Sakimura C, Sakurai K, et al. Tumor-Associated Macrophages Induce Capillary Morphogenesis of Lymphatic Endothelial Cells Derived From Human Gastric Cancer. *Cancer Sci* (2016) 107:1101–9. doi: 10.1111/cas.12977
116. Lin L, Chen YS, Yao YD, Chen JQ, Chen JN, Huang SY, et al. CCL18 From Tumor-Associated Macrophages Promotes Angiogenesis in Breast Cancer. *Oncotarget* (2015) 6:34758–73. doi: 10.18632/oncotarget.5325
117. Teuwen LA, De Rooij L, Cuypers A, Rohlenova K, Dumas SJ, Garcia-Caballero M, et al. Tumor Vessel Co-Option Probed by Single-Cell Analysis. *Cell Rep* (2021) 35:109253. doi: 10.1016/j.celrep.2021.109253

118. Mazzieri R, Pucci F, Moi D, Zonari E, Ranghetti A, Berti A, et al. Targeting the ANG2/TIE2 Axis Inhibits Tumor Growth and Metastasis by Impairing Angiogenesis and Disabling Rebounds of Proangiogenic Myeloid Cells. *Cancer Cell* (2011) 19:512–26. doi: 10.1016/j.ccr.2011.02.005
119. Kang JH, Woo JK, Jang YS, Oh SH. Radiation Potentiates Monocyte Infiltration Into Tumors by Ninjurin1 Expression in Endothelial Cells. *Cells* (2020) 9:1086. doi: 10.3390/cells9051086
120. Yin M, Zhou HJ, Zhang J, Lin C, Li H, Li X, et al. ASK1-Dependent Endothelial Cell Activation is Critical in Ovarian Cancer Growth and Metastasis. *JCI Insight* (2017) 2:e91828. doi: 10.1172/jci.insight.91828
121. He H, Xu J, Warren CM, Duan D, Li X, Wu L, et al. Endothelial Cells Provide an Instructive Niche for the Differentiation and Functional Polarization of M2-Like Macrophages. *Blood* (2012) 120:3152–62. doi: 10.1182/blood-2012-04-422758
122. Zhou J, Zhang A, Fan L. HSPA12B Secreted by Tumor-Associated Endothelial Cells Might Induce M2 Polarization of Macrophages *via* Activating PI3K/Akt/Mtor Signaling. *Onco Targets Ther* (2020) 13:9103–11. doi: 10.2147/OTT.S254985
123. Kim K, Sohn YJ, Lee R, Yoo HJ, Kang JY, Choi N, et al. Cancer-Associated Fibroblasts Differentiated by Exosomes Isolated From Cancer Cells Promote Cancer Cell Invasion. *Int J Mol Sci* (2020) 21:8153. doi: 10.3390/ijms21218153
124. Sobierajska K, Ciszewski WM, Sacewicz-Hofman I, Niewiarowska J. Endothelial Cells in the Tumor Microenvironment. *Adv Exp Med Biol* (2020) 1234:71–86. doi: 10.1007/978-3-030-37184-5_6
125. van Meeteren LA, ten Dijke P. Regulation of Endothelial Cell Plasticity by TGF-Beta. *Cell Tissue Res* (2012) 347:177–86. doi: 10.1007/s00441-011-1222-6
126. Sanchez-Duffhues G, Orlova V, Ten Dijke P. in Brief: Endothelial-to-Mesenchymal Transition. *J Pathol* (2016) 238:378–80. doi: 10.1002/path.4653
127. Yeon JH, Jeong HE, Seo H, Cho S, Kim K, Na D, et al. Cancer-Derived Exosomes Trigger Endothelial to Mesenchymal Transition Followed by the Induction of Cancer-Associated Fibroblasts. *Acta Biomater* (2018) 76:146–53. doi: 10.1016/j.actbio.2018.07.001
128. Fukumura D, Xavier R, Sugiura T, Chen Y, Park EC, Lu N, et al. Tumor Induction of VEGF Promoter Activity in Stromal Cells. *Cell* (1998) 94:715–25. doi: 10.1016/s0092-8674(00)81731-6
129. Pietras K, Pahler J, Bergers G, Hanahan D. Functions of Paracrine PDGF Signaling in the Proangiogenic Tumor Stroma Revealed by Pharmacological Targeting. *PloS Med* (2008) 5:e19. doi: 10.1371/journal.pmed.0050019
130. Orimo A, Gupta PB, Sgroi DC, Arenzana-Seisdedos F, Delaunay T, Naeem R, et al. Stromal Fibroblasts Present in Invasive Human Breast Carcinomas Promote Tumor Growth and Angiogenesis Through Elevated SDF-1/CXCL12 Secretion. *Cell* (2005) 121:335–48. doi: 10.1016/j.cell.2005.02.034
131. Crawford Y, Kasman I, Yu L, Zhong C, Wu X, Modrusan Z, et al. PDGF-C Mediates the Angiogenic and Tumorigenic Properties of Fibroblasts Associated With Tumors Refractory to Anti-VEGF Treatment. *Cancer Cell* (2009) 15:21–34. doi: 10.1016/j.ccr.2008.12.004
132. Leung CS, Yeung TL, Yip KP, Wong KK, Ho SY, Mangala LS, et al. Cancer-Associated Fibroblasts Regulate Endothelial Adhesion Protein LPP to Promote Ovarian Cancer Chemoresistance. *J Clin Invest* (2018) 128:589–606. doi: 10.1172/JCI95200
133. Khaled YS, Ammori BJ, Elkord E. Myeloid-Derived Suppressor Cells in Cancer: Recent Progress and Prospects. *Immunol Cell Biol* (2013) 91:493–502. doi: 10.1038/icb.2013.29
134. Zheng W, Zhu Y, Chen X, Zhao J. CD73 Expression in Myeloid-Derived Suppressor Cells is Correlated With Clinical Stages in Head and Neck Squamous Cell Carcinomas. *Ann Transl Med* (2021) 9:1148. doi: 10.21037/atm-21-2589
135. Kumar V, Cheng P, Condamine T, Mony S, Languino LR, McCaffrey JC, et al. CD45 Phosphatase Inhibits STAT3 Transcription Factor Activity in Myeloid Cells and Promotes Tumor-Associated Macrophage Differentiation. *Immunity* (2016) 44:303–15. doi: 10.1016/j.immuni.2016.01.014
136. Kumar V, Patel S, Tcyganov E, Gabrilovich DI. the Nature of Myeloid-Derived Suppressor Cells in the Tumor Microenvironment. *Trends Immunol* (2016) 37:208–20. doi: 10.1016/j.it.2016.01.004
137. Kumar S, Wilkes DW, Samuel N, Blanco MA, Nayak A, Alicea-Torres K, et al. Deltanp63-Driven Recruitment of Myeloid-Derived Suppressor Cells Promotes Metastasis in Triple-Negative Breast Cancer. *J Clin Invest* (2018) 128:5095–109. doi: 10.1172/JCI99673
138. Taki M, Abiko K, Baba T, Hamanishi J, Yamaguchi K, Murakami R, et al. Snail Promotes Ovarian Cancer Progression by Recruiting Myeloid-Derived Suppressor Cells *via* CXCR2 Ligand Upregulation. *Nat Commun* (2018) 9:1685. doi: 10.1038/s41467-018-03966-7
139. Pellegrino A, Ria R, Di Pietro G, Cirulli T, Surico G, Pennisi A, et al. Bone Marrow Endothelial Cells in Multiple Myeloma Secrete CXC-Chemokines That Mediate Interactions With Plasma Cells. *Br J Haematol* (2005) 129:248–56. doi: 10.1111/j.1365-2141.2005.05443.x
140. Salazar N, Zabel BA. Support of Tumor Endothelial Cells by Chemokine Receptors. *Front Immunol* (2019) 10:147. doi: 10.3389/fimmu.2019.00147
141. Li BH, Garstka MA, Li ZF. Chemokines and Their Receptors Promoting the Recruitment of Myeloid-Derived Suppressor Cells Into the Tumor. *Mol Immunol* (2020) 117:201–15. doi: 10.1016/j.molimm.2019.11.014
142. Oliveira AC, Fu C, Lu Y, Williams MA, Pi L, Brantly ML, et al. Chemokine Signaling Axis Between Endothelial and Myeloid Cells Regulates Development of Pulmonary Hypertension Associated With Pulmonary Fibrosis and Hypoxia. *Am J Physiol Lung Cell Mol Physiol* (2019) 317:L434–44. doi: 10.1152/ajplung.00156.2019
143. Yin J, Shen Y, Yu A, Liu C, Yao J, Gong W, et al. The Proangiogenic Role of Polymorphonuclear Myeloid-Derived Suppressor Cells in Mice Infected With Echinococcus Granulosus. *Biosci Trends* (2018) 12:338–41. doi: 10.5582/bst.2018.01105
144. Wang W, Zuo R, Long H, Wang Y, Zhang Y, Sun C, et al. Advances in the Masquelet Technique: Myeloid-Derived Suppressor Cells Promote Angiogenesis in PMMA-Induced Membranes. *Acta Biomater* (2020) 108:223–36. doi: 10.1016/j.actbio.2020.03.010
145. Sack KD, Teran M, Nugent MA. Extracellular Matrix Stiffness Controls VEGF Signaling and Processing in Endothelial Cells. *J Cell Physiol* (2016) 231:2026–39. doi: 10.1002/jcp.25312
146. Bao M, Chen Y, Liu JT, Bao H, Wang WB, Qi YX, et al. Extracellular Matrix Stiffness Controls VEGF165 Secretion and Neuroblastoma Angiogenesis *via* the YAP/RUNX2/SRSF1 Axis. *Angiogenesis* (2021). doi: 10.1007/s10456-021-09804-7
147. Davidson CD, Jayco DKP, Wang WY, Shikanov A, Baker BM. Fiber Crimp Confers Matrix Mechanical Nonlinearity, Regulates Endothelial Cell Mechanosensing, and Promotes Microvascular Network Formation. *J Biomech Eng* (2020) 142:111009. doi: 10.1115/1.4048191
148. Chetty C, Lakka SS, Bhoopathi P, Rao JS. MMP-2 Alters VEGF Expression *via* Alphavbeta3 Integrin-Mediated PI3K/AKT Signaling in A549 Lung Cancer Cells. *Int J Cancer* (2010) 127:1081–95. doi: 10.1002/ijc.25134
149. Bayless KJ, Salazar R, Davis GE. RGD-Dependent Vacuolation and Lumen Formation Observed During Endothelial Cell Morphogenesis in Three-Dimensional Fibrin Matrices Involves the Alpha(V)Beta(3) and Alpha(5)Beta(1) Integrins. *Am J Pathol* (2000) 156:1673–83. doi: 10.1016/s0002-9440(10)65038-9
150. Peyri N, Berard M, Fauvel-Lafeve F, Trochon V, Arbeille B, Lu H, et al. Breast Tumor Cells Transendothelial Migration Induces Endothelial Cell Anoikis Through Extracellular Matrix Degradation. *Anticancer Res* (2009) 29:2347–55.
151. Krzyzanowska-Golab D, Lemanska-Perek A, Katnik-Prastowska I. Fibronectin as an Active Component of the Extracellular Matrix. *Postepy Hig Med Dosw (Online)* (2007) 61:655–63.
152. Yoshimatsu Y, Wakabayashi I, Kimuro S, Takahashi N, Takahashi K, Kobayashi M, et al. TNF-Alpha Enhances TGF-Beta-Induced Endothelial-to-Mesenchymal Transition *via* TGF-Beta Signal Augmentation. *Cancer Sci* (2020) 111:2385–99. doi: 10.1111/cas.14455

Conflict of Interest: The authors declare that the research was conducted in the absence of any commercial or financial relationships that could be construed as a potential conflict of interest.

Publisher's Note: All claims expressed in this article are solely those of the authors and do not necessarily represent those of their affiliated organizations, or those of the publisher, the editors and the reviewers. Any product that may be evaluated in this article, or claim that may be made by its manufacturer, is not guaranteed or endorsed by the publisher.

frontiers in Oncology

REVIEW
published: 12 January 2022
doi: 10.3389/fonc.2021.763539

Anti-Hepatocellular Carcinoma Effect and Molecular Mechanism of the Estrogen Signaling Pathway

Yusheng Guo[1], Guohui Wu[1], Junrong Yi[1], Qin Yang[2], Wengong Jiang[2], Shaoqiang Lin[1], Xiaorong Yang[3], Xiangsheng Cai[4]* and Liufeng Mao[1]**

[1] Scientific Research Center, The First Affiliated Hospital of Guangdong Pharmaceutical University, Guangzhou, China, [2] Nephrology Department, The First Affiliated Hospital of Guangdong Pharmaceutical University, Guangzhou, China, [3] Clinical Laboratory, The First Affiliated Hospital of Guangdong Pharmaceutical University, Guangzhou, China, [4] Center for Medical Experiments, University of Chinese Academy of Science-Shenzhen Hospital, Shenzhen, China

OPEN ACCESS

Edited by:
Yunfei Xu,
Shandong University, China

Reviewed by:
Andrea Angeli,
University of Florence, Italy
Giuseppe Carruba,
ARNAS Ospedali Civico Di Cristina Benfratelli, Italy

***Correspondence:**
Liufeng Mao
mlf_9295@126.com
Xiangsheng Cai
xiangshengcai@yeah.net
Xiaorong Yang
122424818@qq.com

Specialty section:
This article was submitted to Cancer Molecular Targets and Therapeutics, a section of the journal Frontiers in Oncology

Received: *24 August 2021*
Accepted: *14 December 2021*
Published: *12 January 2022*

Citation:
Guo Y, Wu G, Yi J, Yang Q, Jiang W, Lin S, Yang X, Cai X and Mao L (2022) Anti-Hepatocellular Carcinoma Effect and Molecular Mechanism of the Estrogen Signaling Pathway. Front. Oncol. 11:763539. doi: 10.3389/fonc.2021.763539

There are significant gender differences in the incidence and mortality of hepatocellular carcinoma (HCC). Compared with men, the incidence and mortality of HCC in women are relatively low. The estrogen signaling pathway, composed of estrogen and estrogen receptors, has been postulated to have a protective effect on the occurrence and development of HCC. There have been multiple studies that have supported anti-HCC effects of the estrogen signaling pathways, including direct and indirect pathways such as genomic pathways, rapid transduction pathways, non-coding RNA, tumor microenvironment, estrogen metabolites, and inhibition of hepatitis infection and replication. Based on the evidence of an anti-HCC effect of the estrogen signaling pathway, a number of strategies have been investigated to determine the potential therapeutic effect. These have included estrogen replacement therapy, targeting the estrogen receptor, key molecules, inflammatory mediators, and regulatory pathways of the estrogen signaling pathway. In this review, we have systematically summarized the latest developments in the complex functions and molecular mechanisms of the estrogen signaling pathway in liver cancer. Furthermore, we have highlighted the potential targets of treatment strategies based on the estrogen signaling pathway in the treatment of liver cancer and the principal obstacles currently encountered for future investigation.

Keywords: hepatocellular carcinoma (HCC), estrogen signaling pathway, tumor therapy, molecular mechanism, estrogen receptor

1 INTRODUCTION

Hepatocellular carcinoma (HCC) is a highly lethal malignant tumor with a growing worldwide incidence that remains a leading cause of cancer-related death. Chronic infection with hepatitis B virus (HBV) and hepatitis C virus (HCV), and nonalcoholic fatty liver disease (NAFLD) are strongly linked to HCC. Traditional treatment methods for HCC offer limited cure options, including surgical resection, local ablative treatments, chemotherapy, targeted therapy and immunotherapy (1). Targeted therapy prevents the growth, progression and metastasis of cancer by interfering with specific molecules. The only systemic agent with proven clinical efficacy for patients with

unresectable HCC over the past decade is sorafenib. However, sorafenib has the detrimental characteristic of high-level drug-resistance development, and is therefore associated with poor patient tolerance (2). The estrogen signaling pathway is a signal transduction pathway composed of estrogen and its related receptors. It has multiple functions such as regulation of reproduction, growth and development, and immunity (3). Epidemiological studies have confirmed that females have a lower incidence and reduced mortality from HCC than males, which suggests that the estrogen signaling pathway may play a protective role in the pathogenesis of HCC (4).

The protective effect of the estrogen signaling pathway in the development of liver cancer has been studied and established in pre-clinical models including *in vitro* cellular experiments and animal studies. Regulatory actions of estrogen and the estrogen receptor can antagonize liver cancer through modulation of proliferation, cell cycle, apoptosis and invasive potential of liver cancer cells. In animal models of both castrated and uncastrated males, chemically induced liver cancer can be effectively inhibited with estrogen treatment (5). Our most recent study demonstrated that estrogen could regulate the ERα-36/AKT/Foxo3a signal axis to reduce the transcription of related oxidative stress scavenger enzymes and trigger oxidative stress, thereby inducing liver cancer cells to undergo apoptosis (6). This was the first report of the application of estrogen to HCC cells to induce oxidative stress, an important initial step to further clarify the anti-HCC effect and mechanism of the estrogen signaling pathway.

Dating back twenty years, based on the estrogen signaling pathway, estrogen antagonism was used in both prospective and retrospective studies for treatment of liver cancer, but the results were unsatisfactory (7–10). However, in recent years, estrogen replacement therapy has been applied to the treatment of liver cancer with good results from multiple retrospective studies. These data support an anti-HCC effect of estrogen replacement therapy (11, 12). These new treatment methods based on the estrogen signaling pathway represent a potentially valuable therapeutic strategy in the treatment of liver cancer. However, it is vital to elucidate the functions and regulatory mechanisms of the estrogen signaling pathway as they pertain to hepatocellular cancer.

This review is intended to describe the functions and pathways of the estrogen signaling pathway constituted by estrogen and estrogen receptors, as well as the complex functions and molecular mechanisms of the estrogen signaling pathway in the occurrence and development of liver cancer.

2 OVERVIEW OF THE ESTROGEN SIGNALING PATHWAY

Estrogens are important steroid hormones that are responsible for the control of functions of the female reproductive system, and the development of secondary sexual characteristics. They exert their actions by binding to the estrogen receptors (ERs), activating transcriptional processes and signaling events that control gene expression. In addition to regulation of reproductive physiology and function, they influence cell growth, proliferation, immune response and metabolism. The estrogen signaling pathway is mainly composed of estrogens, estrogen receptors, estrogen related receptor (ERR), and a series of target molecules regulated by them.

2.1 Estrogen

Estrogens include endogenous estrogens, phytoestrogens, xenoestrogens and selective estrogen receptor modulators (SERMs). Endogenous estrogens are the physiological estrogens that are naturally produced and metabolized in the human body, principally including estrone (E1), 17-β-estradiol (E2), estriol (E3), and estretrol (E4) (**Figure 1**); E2 is the main estrogen hormone in humans due to its predominance and physiological relevance during reproductive years (3).

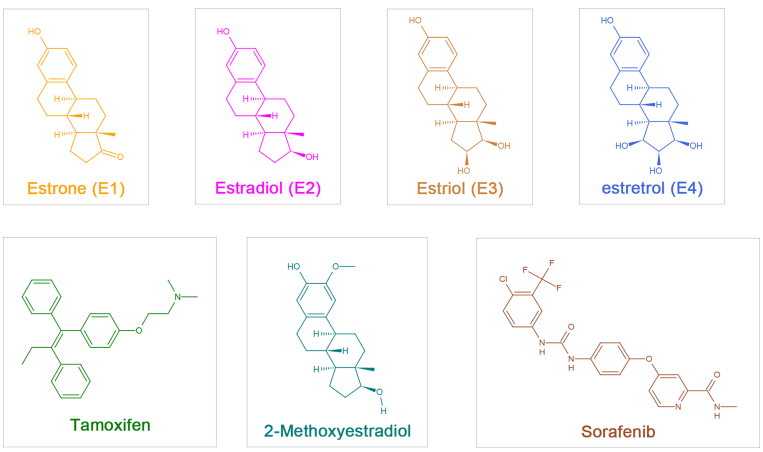

FIGURE 1 | The chemical structure of estrogen, estrogen metabolites and sorafenib. Estrogen:estrone (E1), 17-β-estradiol (Estradiol,E2), Estriol (E3), Estretrol (E4) and Tamoxifen; Estrogen metabolites: 2-Methoxyestradiol (2-ME); Sorafenib.

Selective estrogen receptor modulators (SERMs) are compounds that have tissue-specific activation or antagonism of estrogen receptors. SERMs were originally developed to be used in the treatment of estrogen-dependent tumors such as breast cancer. Among them, tamoxifen has been widely used in the treatment of breast cancer and has been highly successful in the adjuvant setting and in breast cancer prevention (13).

2.2 Biosynthesis, Secretion, and Metabolism of Estrogen

In premenopausal women, estrogen is mainly synthesized and secreted by the ovaries, and the granulosa cells in the ovaries synthesize estrogen from androgens. Additionally, there are other organs and tissues that can synthesize estrogen and use it in a paracrine or endocrine manner, such as liver, pancreas, adrenal glands, and adipose and breast tissues. Placental tissue also produces estrogen (E3) during pregnancy (14). In postmenopausal women, circulating estrogen is mainly synthesized and secreted by the adrenal gland and adipose tissue. Aromatase mediates the one-way reaction of the conversion of androgen into estrogen in local tissues, and it is the only enzyme responsible for local estrogen formation, which is essential for maintaining normal estrogen levels in premenopausal and postmenopausal women (15). Estrogen metabolism is principally carried out in liver tissues that highly express members of the cytochrome P450 enzyme superfamily (CYP1A1, CYP1B1, and CYP1A2) that catalyze estrogen hydroxylation. After a series of binding reactions, estrogen becomes water-soluble and is excreted through the urine, feces, and bile. Hydroxylation of estrogen produces catechol estrogens (2-hydroxyestrone, 4-hydroxyestrone, 2-hydroxyestradiol, 4-hydroxyestradiol, and 16α-hydroxyestrone), which have the pharmacological properties of catecholamines and estrogen (16–18).

CYP1B1, which is highly expressed in breast, uterus and ovarian tissues, specifically catalyzes the 4-hydroxylation of estradiol. Because the reduction-oxidation cycle of 4-hydroxyestradiol itself generates free radicals that cause cell damage, the local specific formation of 4-hydroxyestradiol carries great significance for cancerization of breast, uterine and ovarian tissues (17). Catechol-estrogen-3, 4-quinone, the oxidative product of 4-hydroxyestradiol, reacts with specific purine bases in DNA to form depurinating estrogen-DNA adducts. The resulting apurinic sites can lead to oncogenic mutations. Because of this unique carcinogenic reaction, catechol estrogen-3, 4-quinone plays a central role in breast cancer initiation (19).

In addition, catechol-O-methyltransferase can catalyze the conversion of catechol estrogens into methoxy estrogens, which have anti-proliferative properties and the ability to control estrogen synthesis (20). Estrogen metabolites may have either anti-tumor or tumor-promoting effects dependent on their different configurations. These in turn depend on the type of CYP isoforms expressed by target tissues and are tissue specific. Of note, CYP enzymes are regulated by the estrogen signaling pathway, which has physiological significance for maintaining homeostasis of estrogen in local organs (21).

2.3 Estrogen Receptor

There are two classical isoforms of estrogen receptor, ERα and ERβ, which are encoded by ESR1 and ESR2 genes, respectively. ERα and ERβ are expressed in a variety of tissues, such as uterus, ovary, breast, liver and brain. The specific isoform and expression level of the ER are the main factors that determine its tissue-specific estrogen responsiveness (22).

ERα includes ERα-66, ERα-46, ERα-36 and other isoforms. The classic isoform of ERα is 66KDa ERα-66, which can be divided into 6 different regions in structure (A-F) (**Figure 2**) (23).

ERα-46 is a truncated amino-terminal isoform that lacks the A/B region which encodes transcription activation domain (AF-1). High expression of ERα-46 found in breast cancer reduces the sensitivity of tamoxifen to breast cancer cells (24).

ERα-36 is a recently discovered ERα isoform. It lacks the AF-1 and AF-2 transcriptional activation function domains,

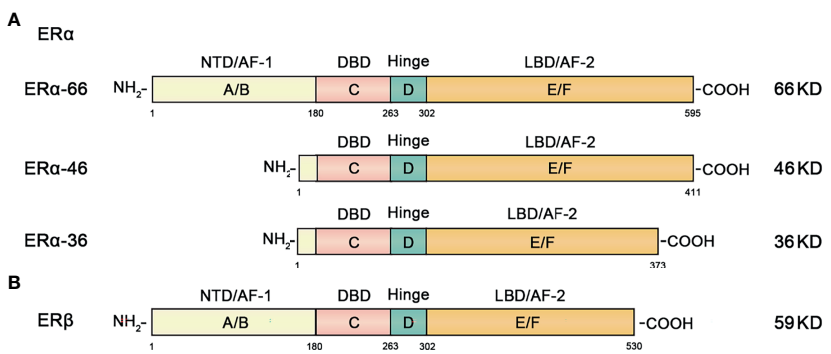

FIGURE 2 | Structural and functional domains of the major classical subtypes of estrogen receptors. **(A)** The three main isotypes of ERα include ERα-66, ERα-46 and ERα-36. The full-length form of ERα-66 has six different structural domains (functional domains): A/B domain (NTD, AF-1), DNA binding domain or C domain (DBD), D domain (hinge region), and ligand-containing binding domain or E/F domain (LBD, AF-2). **(B)** ERβ has 6 different domains (functional domains) similar to ERα.

retaining only the DNA binding domain (DBD), ligand binding domain (LBD) and hinge region. The overall characteristics of ERα-36 and ERα-46 are similar, but their ends contain a characteristic 27 amino acid domain that is different from the 138 amino acids encoded by ERα-66 and ERα-46 isoform genes (25, 26).

ERβ is an ER subunit that also consists of 6 regions and contains the A-F domain (**Figure 2**). The main difference from ERα is that the amino terminal domain of ERβ is relatively short.

In addition to the classic nuclear receptors ERα and ERβ, the membrane receptor G-Protein-Coupled Estrogen Receptor (GPER) isoform has recently been found on the cell membrane. This is a typical G protein-coupled receptor that acts as a molecular switch signal transducing molecule. Its structure consists of 7 transmembrane α-helix regions, 4 extracellular and 4 cytoplasmic segments. The characteristic structure of GPER allows it to respond quickly to estrogen stimulation (27).

2.4 Transduction Pathway of the Estrogen Signaling Pathway

Estrogen can enter the plasma membrane and interact with the intracellular ER, binding to DNA sequences; this is known as the genomic pathway (**Figure 3**). The main mediating genomic pathway is the classical estrogen nuclear receptors (nERs), including ERα-66, ERα-46, and Erβ (27). Estrogen can bind to nERs to form homodimers and/or heterodimers and translocate to the nucleus, bind DNA on estrogen response elements (EREs) and activate the expression of ERE-dependent genes (28). Under the mediation of stimulating protein (SP-1), the estrogen receptor complex can also interact with other transcription factors and response elements to regulate non-targeted transcriptome activities, and ultimately affect cell proliferation and apoptosis signals (29).

Estrogen can also interact with ERs that do not contain ERE-like sequences but rather activate the intracellular signal transduction cascade, which is called the non-genomic pathway or the rapid transduction pathway (**Figure 3**) (30). The major mediating non-genomic pathways are the new estrogen membrane receptors (mERs), GPER and ERα-36. The estrogen receptors, related pathway proteins, and effector molecules in the two functional pathways crosstalk with each other, leading to differences in the transcriptional activity of specific tissues and physiological processes; these constitute a complex, multidirectional, and multifunctional estrogen signaling pathway.

3 ANTI-HEPATOCELLULAR CARCINOMA EFFECT AND MECHANISM OF THE ESTROGEN SIGNALING PATHWAY

As noted previously, global epidemiological studies have demonstrated the consistent prevalence of HCC among men, with worse survival than in females, and have concluded that there is a protective impact of the estrogen signaling pathway against liver cancer. It appears that these anti-tumor effects are mediated by different transduction pathways.

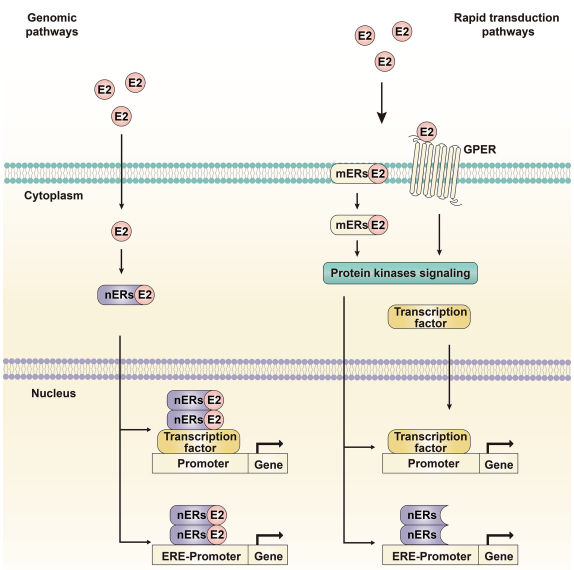

FIGURE 3 | Genomic pathway and rapid transduction pathway. The genomic pathway refers to estrogen binding to nuclear receptors, receptor dimerization and translocation into the nucleus to induce transcriptional changes in estrogen-responsive genes. The rapid transduction pathway refers to estrogen binding to membrane receptors, inducing and activating cytoplasmic events such as intracellular signal transduction cascades and transcription factors. The two pathways crosstalk with each other and mediate the molecular transduction mechanism of the estrogen signaling pathway together.

3.1 Genomic Pathway

The genomic pathway is the classic transduction pathway of the estrogen signaling pathway, which was also the initial pathway targeted for anti-HCC therapy (**Figure 3**).

3.1.1 Cell-Line Studies

Overexpression of ERα can induce cell transformation of ERα-negative human hepatoma Hep3B cells. ERα can bind to the SP1 protein to form a complex, which then binds to the TNF gene promoter and further induces the expression of active Caspase 3 (an executioner in apoptosis) in a ligand replacement manner (31). The promoter of the MTA1 gene has three and a half ERE binding sites. ERα can inhibit the proliferation and invasion of human HCC cells by down-regulating the transcription of MTA1, and the overexpression of MTA1 weakens the proliferation and invasion of HCC cells and tumor formation *in vivo* by the inhibitory effect of ERα (32). E2 can induce the expression of miR-23a by activating ERα and binding to the regulatory region of miR-23a, or by binding to the regulatory region of p53 to induce the expression of miR-23a. MiR-23a then down-regulates the expression of its target gene XIAP, thereby activating the activity of caspase-3 and inducing apoptosis of liver cancer cells (33). E2 can inhibit the hepatocyte cell cycle marker CDK2 and up-regulate the expression of P53, thereby reducing the viability of hepatocytes and HCC cells (34).

3.1.2 Animal Studies

The anti-liver cancer effect of the estrogen signaling pathway has also been reported in animal experiments. Whereas castration of male mice led to a decrease in the incidence of HCC, castration of female mice led to an increase in the incidence of HCC, lending support to the hypothesis that sex hormones play an important role in the occurrence of liver cancer (35, 36). Exogenous and endogenous estradiol were shown to inhibit the occurrence of chemically induced liver cancer, and ER was reportedly involved in inhibiting the early malignant transformation of liver cancer (5). Protein tyrosine phosphatase receptor type O (PTPRO) is one of the receptor types of phosphotyrosine phosphatase (PTP), known to be a tumor suppressor in various cancers. PTPRO was shown to down-regulate the signal transduction that depends on the dephosphorylation of JAK and PI3K and the transcriptional activity of STAT3, thereby inhibiting the occurrence and development of tumors. ERα was used as a transcription factor of PTPRO to up-regulate its expression and enhance its tumor suppressor effect (37). Compared with male mice, female mice injected with diethylnitrosamine (DEN) showed fewer foci of hyperplasia and slower onset of HCC, smaller tumors, higher differentiation, and fewer metastases. Compared with normal male mice, those injected with DEN after castration reduced the expression of cyclin E kinase and enhanced hepatocyte apoptosis. While estradiol and progesterone enhance these effects, the cyclin E kinase activity of normal female mice is lower than that of male mice. The use of testosterone in ovariectomized female mice up-regulates cyclin E, activates cyclin E kinase, and accelerates the occurrence of liver cancer (34). Some researchers have suggested that Foxa faultidirectional, and multifunctional estrogen signalctor and its target are the core of HCC sexual dimorphism. There are obvious gender differences in HCC mice induced by DEN, and the defects of Foxa1 and Foxa2 can reverse this gender difference relative to the incidence of liver cancer. Further studies have found that Foxa1 and Foxa2 can mediate and enhance the regulation of ERα or androgen receptor (AR) on target genes during the formation of liver cancer, thereby inhibiting (ERα) or promoting (AR) the development of liver cancer (38).

3.2 Rapid Transduction Pathway

In addition to the classic genomic pathway, recent studies have found that the rapid transduction pathway is also an important avenue for estrogen signal transmission to produce an anti-liver cancer effect (**Figure 4**).

Leptin is a hormone secreted by white adipose tissue, that can promote the development of liver cancer. E2 and ER antagonize the carcinogenic effect of leptin in HepG2 cells by inhibiting cell proliferation and stimulating apoptosis. This is due to the reversal of leptin-induced SOCS3/STAT3 changes and the increase of p38/MAPK by activating ER-β. Similarly, activation of ER-α and GPER can also increase ERK expression. These findings provide evidence that various estrogen receptors play different roles and mechanisms in the occurrence of HCC (39).

E2 has been shown to significantly inhibit the malignant behavior of HCC cells through the up-regulation of NLRP3 inflammasomes mediated by the ERβ/MAPK signal pathway (40). Further research found that the NLRP3 inflammasome inhibited the protective autophagy of tumors through the E2/ERβ/AMPK/mTOR pathway. In general, E2 can inhibit the onset of HCC by activating caspase 1-dependent apoptosis and inhibiting protective autophagy (41).

In the liver, IL-6 is an important inducer of acute phase response and infection defense, a mitogen of hepatocytes, mediating liver regeneration and other functions, and is related to the metabolic function of the liver. IL-6 is crucial for maintaining hepatocyte homeostasis (42). However, studies have found that the continuous activation of the IL-6 signaling pathway is harmful to the liver, and that IL-6 can promote the occurrence of liver cancer through multiple steps (43–45). IL-6 mediates liver damage and compensatory hyperplasia caused by the carcinogen DEN, and ultimately leads to tumors. The carcinogen DEN mainly promotes the production of IL-6 by Puffer cells (KCs) through MyD88. E2 can inhibit the secretion of IL-6 in KCs and reduce hepatocyte damage and malignant lesions induced by DEN (46).

The activity of Foxo3a is closely related to the oxidative stress response in cells. Activated Foxo3a reduces oxidative stress by binding to the promoters of genes encoding manganese superoxide dismutase (Mn-SOD) and catalase. Our most recent study demonstrated that E2 could reduce the expression of ERα-36 in liver cancer cells and increase phosphorylation of Akt and Foxo3a, preventing Foxo3a from entering the nucleus, thereby preventing synthesis of Mn-SOD and catalase, triggering oxidative stress and ultimately apoptosis. Oxidative stress (defined as excessive production of reactive oxygen species) is one of the important links in the occurrence and development of many

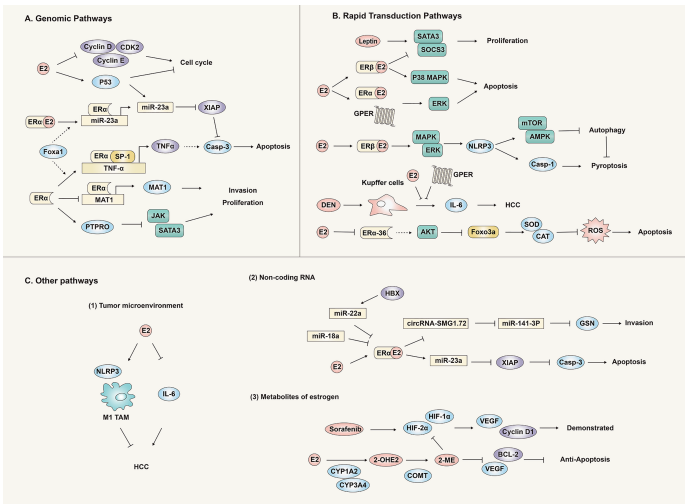

FIGURE 4 | Anti-hepatocellular carcinoma effect and mechanism of the estrogen signaling pathway. Estrogen plays an antagonistic role against liver cancer through genomic pathways **(A)**, rapid transduction pathways **(B)** and other pathways **(C)** (tumor microenvironment, non-coding RNA and metabolites), inhibiting the proliferation, invasion and migration of liver cancer tissues or cells.

diseases, but recently researchers have harnessed this process to develop anti-tumor oxidative therapy and pro-oxidant treatments. The methodology targets the tumor and causes accumulation of active oxygen within it, killing the tumor cells. To our knowledge, we produced the first report that estrogen induces oxidative stress by regulating Foxo3a, which helped clarify the anti-tumor effect and mechanism of the estrogen signaling pathway through the oxidative stress response (6).

GPER is an estrogen membrane receptor located in the plasma membrane that has low expression in liver cancer tissues. In the mouse liver cancer model induced by the carcinogen DEN, knock out of the GPER gene can significantly promote the occurrence of liver cancer, accompanied by immune cell infiltration, fibrosis, and the production of inflammatory factors (such as IL-6). Furthermore, the selective GPER agonist G-1 can reduce the expression of IL-6 in bone marrow-derived macrophages, but this effect is inhibited by GPER knockdown. However, *in vitro* experiments have shown that the viability and proliferation of liver cancer cells were not directly affected by GPER (47). These results indicated that GPER could inhibit HCC through regulation of the inflammatory response rather than direct action on tumor cells. However, a recent study found that GPER was significantly down-regulated in HCC tissues compared with matched non-tumor tissues. Compared with GPER negative patients, GPER positive HCC patients were significantly associated with female sex, HBsAg negative, small tumor size, low serum AFP levels, and longer overall survival. GPER/EGFR/ERK signaling triggered by GPER specific agonist G1 played a crucial role in decreasing the tumor viability of HCC, both *in vitro* and *in vivo*. Clinical analysis indicated that simultaneous high expression of GPER and phosphorylated ERK (P-ERK) predicted improved prognosis of HCC. These findings suggest that specific activation of the GPER/ERK axis could be a therapeutic target for HCC (48). Therefore, activation of GPER could serve as a potential strategy for prevention and treatment of HCC.

3.3 Other Pathways

In addition to the classic genomic pathways and rapid transduction pathways, the estrogen signaling pathway was recently discovered to exert anti-liver cancer effects through multiple pathways such as tumor microenvironment (TEM), non-coding RNA (ncRNA) regulation/small molecule RNA, and metabolites (**Figure 4**).

3.3.1 Tumor Microenvironment

Stromal cells and cytokine-related components of the tumor microenvironment tend to promote tumor cell proliferation, invasion and metastasis, through the action of tumor-associated macrophages (TAM), bone marrow-derived suppressor cells (MDSC), tumor-associated neutrophils (TANs), cancer associated fibroblasts (CAF) and regulatory T cells (Tregs). These immunosuppressive cells can suppress the body's own immune response thereby reducing the effect of immunotherapy, which has opened a new field of research in the treatment of liver cancer. Typically, immune cell regulation by the estrogen signaling pathway enhances normal immune response. Similarly, recent studies have reported that estrogen can regulate the microenvironment of liver cancer to exert its anti-tumor effect (49, 50).

E2 has also been shown to inhibit tumor growth by regulating the polarization of macrophages. The mechanism involves E2 activation of ER-β that interacts with ATPase coupling factor 6 in the presence of IL-4 to up-regulate SOCS1, thereby inhibiting JAK1-STAT6 signal pathways, which attenuates the selective activation of macrophages and the growth of HCC tumors (51).

NLRP3 inflammasome is an intracellular multi-protein complex that participates in the innate immune response to pathogens and other harmful factors. As noted previously, estrogen can inhibit the protective autophagy of tumors by regulating the NLRP3 inflammasome, ultimately inhibiting the progression of HCC (41).

The estrogen signaling pathway has multiple, complex relationships with the tumor microenvironment. Studies have confirmed that estrogen can inhibit tumor progression by regulating the M1 polarization of macrophages, NK cells, CD8+ T cells, Th1 cells and the resultant inflammatory cytokines, IFNγ, TNFα, IL-12. However, estrogen can also regulate the formation of an immunosuppressive microenvironment that can promote tumor immune evasion by regulating CAF, MDSC, Treg cells, Th2 cells and related cytokines IL-4, IL-6 and other components (50, 51). In breast and ovarian cancer as well as other estrogen-dependent tumors, estrogen has been proven to enhance the immunosuppressive microenvironment thereby promoting tumor development (50). Nevertheless, the complete picture of tumor-specific regulation effects and mechanisms of the estrogen signaling pathways on the tumor microenvironment are still not fully clarified. A more complete understanding of the specific mechanisms of the tumor microenvironment regulated by the different functional pathways of the estrogen signaling pathway will most certainly facilitate the development of new treatment strategies related to the estrogen signaling pathway, particularly enhancing immunotherapy (52).

3.3.2 Non-Coding RNA

With the development of high-throughput RNA sequencing technology and bioinformatics, an ever-enlarging number of ncRNA sequences and their functions have been discovered. Such non-coding protein sequences such as ncRNA perform important biological functions in cells. lncRNA, miRNA and eRNA are all non-coding RNAs, proven to play important functions in the occurrence and development of tumors. Critically important, the estrogen signaling pathway can also regulate the occurrence and development of tumors through ncRNAs (53–55).

miRNA is a short non-coding RNA with a base length of 19-25 bp, which acts as a post-transcriptional regulator of gene expression by mediating the degradation and/or translational inhibition of its target mRNA. A single miRNA can target hundreds of mRNAs and affect the expression of many genes through multiple interaction pathways. Multiple studies have reported the involvement of miRNA in the protective effect of the estrogen signaling pathway on liver cancer (53).

The miR-545/374a cluster is a microRNA cluster encoded by the Ftx gene, found to be highly expressed in HBV-related HCC tissues, and is associated with a poor prognosis of HCC patients (56). This cluster originates from tumor tissues, and its expression is positively regulated by HBV infection and may be induced by HBx expression, suggesting that it could potentially be a new diagnostic screening marker for HCC. As might be anticipated, further research found that the miR-545/374a cluster of male HCC patients was much higher than female HCC patients. The target gene prediction program found that estrogen-related receptor γ (ESRRG) was a potential target gene of miR-545/374a, and ESRRG and expression of miR545 are inversely related (56).

Gelsolin (GSN) is an important molecule that mediates metastasis and invasion of liver cancer cells. ERα can bind to the 5'promoter region of SMG1 to inhibit the transcriptional expression of circRNA-SMG1.72, thereby inhibiting the invasion of HCC cells. CircRNA-SMG1.72 can inhibit the expression of miR-141-3p by producing cavernous bodies, which can in turn target the binding of GSN mRNA to reduce the expression of GSN. The end effect, ERα can inhibit the invasion of HCC cells through the ERα/circRNA-SMG1.72/miR-141-3p/GSN signaling pathway (57).

Using miRNA PCR array technology, E2 treatment resulted in up-regulation in 25 and down-regulation in 10 miRNAs of apoptotic HCC cells. Further studies found that E2 could induce miR-23a expression by activating ERα and binding to the regulatory region of miR-23a, or by binding to the regulatory region of p53 to induce miR-23a expression. The effect was to down-regulate the expression of its target gene XIAP, thereby activating caspase-3, inducing apoptosis of liver cancer cells (33).

In addition to the estrogen signaling pathways that can regulate miRNAs to exert anti-liver cancer effects, other studies demonstrated that some miRNAs could act on estrogen signaling pathways ultimately to inhibit anti-liver cancer effects. miR-18a was found to be highly expressed in female HCC patients. Overexpression of miR-18a reduced the expression of ERα and promoted the proliferation of liver cancer cells (58). The gene ESR1 encoding ERα is one of the targets of miR-18a, and miR-18a can inhibit the translation of ERα by binding to its mRNA in the 3'untranslated region. The initial regulatory factor of miR-18a might represent the abnormal expression or mutation of p53, and accumulation of these factors might reduce tumor protection of the estrogen signaling pathway in the development of female liver cancer (58). miR-221 has been found to be highly expressed in various solid and hematological malignancies. Its involvement in the occurrence and development of tumors has been extensively studied and is expected to become a biomarker and therapeutic target for a variety of tumors (59). In liver cancer cells, HBx can promote the proliferation of liver cancer cells by inhibiting ERα and increasing the expression of miR-221. Moreover, further studies found that miR-221 could inhibit ERα expression by directly binding to ERα, resulting in the proliferation of HCC cancer cells and acting as a tumor promoter (60).

3.3.3 Metabolites of Estrogen

In addition to the anti-liver cancer effects mediated by estrogen and estrogen receptors, estrogen metabolites and derivatives also have special anti-tumor effects in liver cancer.

The liver is the main site of estradiol metabolism. Cytochrome P450 CYP1A2 in the liver can convert estradiol into 2-hydroxyestradiol, and then interaction with the enzyme catechol-O-methyltransferase (COMT) will further methoxylate it to produce 2-methoxyestradiol (2-ME) (61). HCC cells express low or almost no CYP1A2. Overexpression of CYP1A2 can increase the level of the estradiol metabolite 2-ME and

enhance the inhibitory effect of estradiol on HCC nuclear xenograft tumors. Both *in vitro* and *in vivo* studies have found that 2-ME could reduce the expression of vascular endothelial growth factor (VEGF) and Bcl-2, promote cell cycle arrest and apoptosis of liver cancer cells; the overall effect: inhibition of liver cancer cell proliferation and tumor growth (61).

Sorafenib is a well-accepted and widely used target drug, approved for the treatment of advanced HCC. Its clinical efficacy, however, has been limited due to drug resistance. The adaptive response of tumor cells to hypoxia is an important mechanism of tumor resistance (62). In liver cancer cells, sorafenib down-regulates the expression of HIF-1α, but up-regulates the expression of HIF-2α, with a final effect of changing the hypoxic response from the HIF-1α-dependent to the HIF-2α-dependent pathway. It promotes the expression of VEGF and Cyclin D1, both being downstream molecules of HIF-2α, and ultimately causes hypoxic HCC cells to lose sensitivity to sorafenib. 2-ME can reduce the expression of HIF-1α, HIF-2α and the downstream molecules VEGF, LDHA and Cyclin D1, to increase the sensitivity of hypoxic HCC cells to 2-ME. *In vivo* and *in vitro* experiments have shown that 2-ME and sorafenib synergistically inhibit the proliferation of HCC cells, induce apoptosis, and inhibit tumor angiogenesis (63).

4 THE ROLE OF THE ESTROGEN SIGNALING PATHWAY IN VIRAL LIVER CANCER

Chronic infection with hepatitis B and C viruses is the principal risk factor for liver cancer. With infection, they cause inflammation, oxidative stress, and often delayed fibrotic reactions, eventuating into cirrhosis. This is accompanied by the appearance of local hypoxia, rearrangement of tissue structure (epithelial mesenchymal transition, EMT) and angiogenesis (64). Chronic viral hepatitis can share characteristics of other viral infections, such as affecting the expression of host genes through processes such as genetic changes, DNA repair inhibition, and microRNA differential expression. These changes include the up-regulation of factors involved in "stemness", indicating that both viruses may promote the development of HCC by promoting stemness (65). In addition to gender differences in the incidence and mortality of liver cancer, significant gender differences have also been found in the prevalence of HBV chronic infection and HBV-related HCC, lending support to the influence of sex hormones in HBV-related HCC (66, 67).

Chronic inflammatory infiltration is an important factor in the progression of HBV infection to HBV-related HCC. It has been confirmed that hepatitis-related inflammatory cytokines such as IL-6, IL-1α and IL-1β are key inflammatory mediators that stimulate the development of HCC (65, 67). In hepatocytes and liver cancer cells, the expression of HBx can activate the downstream signaling proteins IRAK-1, ERKs/p38 and NF-κB of MyD88, thereby promoting the synthesis and secretion of IL-6 and promoting the progress of HBV-related HCC (68). In addition, HBV infection can increase the expression of TGF-β1, IL-1β, TNF-α CTGF and PDGF, thus changing the liver microenvironment and promoting the progression of liver fibrosis (69). Therefore, multiple pathways have been briefly summarized that indicate HBV infection can promote the progress of HBV-related HCC. Counterbalancing these, the estrogen signaling pathway can inhibit the progress of HBV-related HCC by regulating various pathways such as related signal proteins and inflammatory mediators. As noted previously, in addition to inhibiting the secretion of IL-6 by Kupffer cells (46), the estrogen signaling pathway can also regulate the expression of IL-6 by regulating STAT3 and NF-κB signaling molecules. The estrogen signaling pathway can also activate the promoter of ERα binding to IL-1α to reduce its expression (70), thereby regulating the development of HBV-related HCC (**Figure 5**).

Although the estrogen signaling pathway that can regulate progression of HBV infection and HBV-related HCC, the genome and products of HBV can in turn counteract the estrogen signaling pathway and inhibit its protective effect. HBx was reported to inhibit the transactivation function of ERα by forming a trimeric complex with ERα and HDAC1, inhibiting the function of the estrogen signaling pathway, and HDAC inhibitors can reduce the inhibition of HBx on the transactivation function of ERα (71). Moreover, HBx can increase the expression of miR-221, targeting the ERα gene,

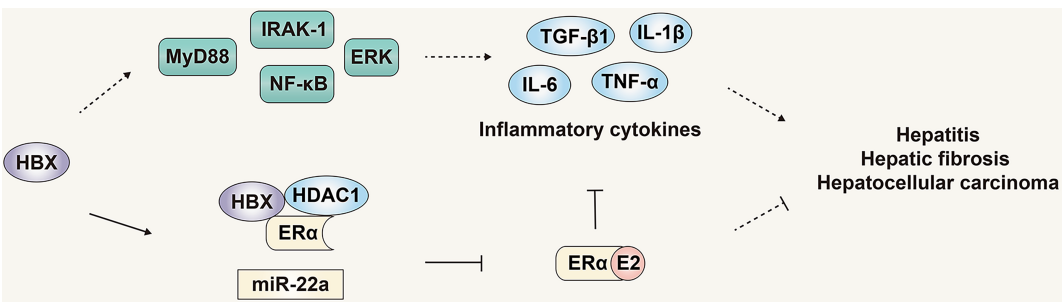

FIGURE 5 | The role and mechanism of the estrogen signaling pathway in viral liver cancer. The estrogen signaling pathway can inhibit the progress of HBV-related HCC by regulating inflammatory mediators. The products of HBV can in turn counteract the estrogen signaling pathway and inhibit its protective effect.

inhibiting expression of ERα, ultimately inhibiting the protective effect of the estrogen signaling pathway on liver cancer (**Figure 5**) (60).

Increasingly, studies have revealed the protective effect and mechanism of the estrogen signaling pathway in the development of HBV-related HCC. Most importantly, the effect of the estrogen signaling pathway on HBV infection and HBV-related HCC is not a single pathway or single effect, but multiple pathways and multiple effects. However, HBV infection can counteract the estrogen signaling pathway and antagonize its protective effects.

Of overall HCV-infected patients, men and postmenopausal women are more likely to develop liver cirrhosis and liver cancer than premenopausal women. Menopause seems to be associated with acceleration of liver fibrosis in HCV-infected women, whereas estrogen replacement therapy can prevent this progression (72).

Comparing liver tissues of normal people, HCV-related cirrhosis and HCV-related HCC patients, the expressions of ERα and ERβ in liver tissues of patients with HCV-related liver disease were increased to varying degrees, but the expression patterns of ERα and ERβ in the cytoplasm and nucleus were different (73). Similarly, the expression of phosphorylated NF-κB and cyclin D1 were significantly higher in tissues with HCV-related liver disease. In HCV-related HCC, the nuclear ER subtype and nuclear cyclin D1 expression were positively correlated, while the cytoplasmic ER subtype was negatively correlated with cytoplasmic phosphorylated IKK. These results indicated that the dysregulation of ER subtype expression and cell sub-localization following chronic HCV infection could lead to the development of HCV-related cirrhosis and HCV-related HCC.

5 CONTROVERSY: THE ROLE AND MECHANISM OF THE ESTROGEN SIGNALING PATHWAY IN PROMOTING LIVER CANCER

In contrast to the multiple studies and different pathways elucidating the protective and preventive roles of the estrogen signaling pathway in liver cancer, some studies have concluded the direct opposite: the estrogen signaling pathway promotes the development of liver cancer. Careful review of these studies reveals the apparent dual role of the estrogen signaling pathway is a function of the different subtypes of the estrogen receptor and the different functional pathways mediated by the spliceosome (74).

ERα-36 is a newly discovered non-classical ERα isoform. Compared with nuclear receptors ERα-66, ERα-36 lacks AF-1 and AF-2 transcription activation domains but retains the DNA binding domain and dimerization domain (**Figure 2**), and ERα-36 is mainly expressed in the cytoplasm and plasma membrane. It mediates non-genomic pathways (or fast signaling pathways) and plays an important role in mitogenic estrogen signaling (75, 76). Of specific relevance to this controversy, the non-genomic transmission pathway mediated by ERα-36 inhibits the genomic transmission pathway mediated by classical nuclear receptors (76).

Initially, the function of ERα-36 was investigated in breast cancer research. ERα (ERα-66) is the most widely used marker for diagnosing human breast cancer, and according to the presence or absence of ERα-66, breast cancer is classified as ER-positive or ER-negative. Anti-estrogens (such as tamoxifen) have been first-line treatments for advanced ER-positive breast cancer. However, recent reports have found that breast cancer is prone to resistance to anti-estrogen therapy, which has an important relationship with ERα-36 (76).

A retrospective study showed that breast cancer patients with high levels of ER-α36 experience less benefit from tamoxifen than those with low levels of ERα-36 expression, and Erα-36 expression is significantly correlated with Her2/Neu expression. These results indicated that ERα-36 might mediate the resistance mechanism of breast cancer to anti-estrogen therapy (77). ERα-36 has been shown to activate downstream signaling pathways through HB-EGF, SRC, EGFR, HER2, IGF-1R, and ultimately to induce the transcription of growth-promoting genes such as c-Myc and Cyclin D1, and finally to stimulate tumor cell proliferation. ERα-36 is also highly expressed in some tumor stem/progenitor cells and participates in their cell maintenance (76). These studies have indicated that this new type of estrogen receptor, ERα-36, mediates an important regulatory role in the occurrence and development of tumors in the estrogen signaling pathway. As such, it serves as a marker for poor prognosis in breast cancer.

The role of ERα-36 in liver cancer has also been explored. In a study of ERα-66 and ERα-36 mRNA expression in non-tumor, cirrhotic and malignant liver tissues and HCC cell lines, it was found that ERα-66 was highly expressed in non-tumor tissues, cirrhotic tissues showed a lower level, whereas its expression decreased or became undetectable in HCC tissues and cell lines. In stark contrast, the expression level of ERα-36 showed just the opposite trend to ERα-66. A high expression of aromatase is an important factor in liver malignancy. It is noteworthy that the expression level of aromatase has the same trend as ERα-36, but opposite to ERα-66. These results emphasize that the principal expression of either ERα-66 to ERα-36 in liver tissues may be directly correlated to the development and/or progression of HCC (78).

Researchers have proposed a new model in which tissue damage and/or inflammatory diseases activate the aromatase-estrogen-ARGE-EGFR axis, eventually leading to liver, breast, and prostate cancers, and other chronic diseases such as diabetes (**Figure 6**) (79), obesity, Alzheimer's disease and heart disease. One such study found that in liver cells, the expression of NF2 was positively correlated with the expression of aromatase, amphiregulin (AREG) and ERα-36, and had a direct correlation with the degree of malignancy, but was inversely correlated with expression of ERα-66. Although estradiol treatment could induce a significant decrease in NF2 expression in HA22T and Huh7 cells, no changes were observed in HepG2 cells. This effect may be negatively related to the expression and activity of aromatase. Aromatase expression in normal and cirrhotic tissue cells is low, while its expression in liver cancer tissues is high. In addition to detecting high levels of ERα-36 in HCC tissues and cells, recent studies

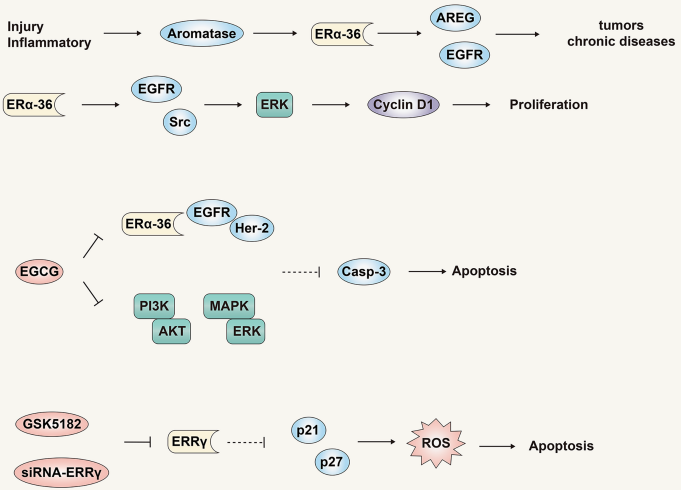

FIGURE 6 | The role and mechanism of the estrogen signaling pathway in promoting liver cancer. ERα -36 is a novel non-classical ERα isotype, which may mediate the estrogen signaling pathway to promote liver cancer. Antagonistic treatment of ERα -36 and ERRγ is expected to become a new therapy for liver cancer.

have revealed the role and mechanism of ERα-36 in the progression of HCC (80). In HCC cells with high expression of ERα-36, the rapid transduction pathway mediated by ERα-36 can be activated by estrogen, which in turn activates EGFR/Src/ERK signal regulation and up-regulates the expression of CyclinD1. In addition, the ERα-36/EGFR signal axis plays an important role in maintaining and actively regulating the growth of HCC tumor cells (**Figure 6**).

EGCG is a natural product with potential anti-cancer properties and has a dose-dependent inhibitory effect on HCC cells that highly express ERα-36 (81). EGCG can activate expression of p-ERK and Caspase-3 by inhibiting the ERα-36/EGFR/Her-2 feedback loop and the PI3K/Akt and MAPK/ERK pathways. This culminates in the induction of HCC cell apoptosis and proliferation inhibition. As noted previously, our most recent study demonstrated that estrogen can down-regulate ERα-36 expression and activate the AKT/Foxo3a signaling axis, triggering oxidative stress and ultimately apoptosis in HCC cells (**Figure 6**). In summary, multiple studies have identified ERα-36 and its mediated rapid transduction pathway might present a logical target for anti-liver cancer drugs.

In addition to the new receptor ERα-36, estrogen-related receptor γ (ERRγ) may also mediate the cell growth and tumorigenesis of various tumors (82). Compared with normal tissues, the expression level of ERRγ in HCC tissues is higher, and the expression level of ERRγ is also closely related to the pathological tumor grade, metastasis and poor prognosis. In addition, siRNA-ERRγ or GSK5182 (ERRγ antagonists) can induce cell cycle arrest and oxidative stress by increasing the expression of p21 and p27, thereby inhibiting the growth and proliferation of HCC cells (**Figure 6**). These results show that, similar to ER-α36, ERRγ might be a potential biomarker for liver cancer, and antagonistic therapy targeting ERRγ is expected to become a new type of therapy for liver cancer.

6 CLINICAL APPLICATION AND RESULTS OF ESTROGEN THERAPY FOR LIVER CANCER

Mounting study results lend support to the application of anti-liver cancer effects of the estrogen signaling pathway to the development of anti-liver cancer therapies. Although anti-estrogen therapy for liver cancer dates back more than 20 years, the early attempts failed to achieve satisfactory results.

As a selective estrogen receptor modulator (SERM) that competes with estrogen for the ER, tamoxifen was used in a small, prospective controlled trial in 1990 that showed it could be effective in treating unresectable or incurable liver cancer (10). Only 38 patients with inoperable HCC were included, but the survival time of the tamoxifen-treated group was statistically prolonged with a survival rate at 12 months of 22% (control, 5%). However, a subsequent large randomized controlled trial showed that tamoxifen did not prolong liver cancer patient survival (9). As an alternative, higher doses of tamoxifen were proposed intending to inhibit HCC in an ER-independent manner (83). To address this, a double-blind randomized trial from the Asia-Pacific region showed that high-dose tamoxifen did not prolong survival of patients with advanced HCC. In fact, on the contrary, its negative impact could increase as the dose was increased (8). Other studies suggested that tamoxifen might have survival benefit for HCC patients who did not have severe liver insufficiency (7). This seemed to restrict anti-estrogen therapy only for early liver cancer and might not be effective for advanced liver disease. According to large trials and Cochrane systematic reviews, tamoxifen was not deemed beneficial in HCC for overall survival or quality of life (84). Therefore, tamoxifen does not justify further testing in HCC, nor should it be used clinically.

Current research results show that the reason for the failure of tamoxifen may be closely related to the main expression of ERα-66

to ERα-36 in HCC tissues. Compared with ERα-66, ERα-36 lacks two transcriptional activation domains, has three potential myristoylation sites located near the N terminus., and has a characteristic 27 amino acid sequence near the C terminus. And this unique amino acid sequence may cause changes in the ligand-binding affinity and specificity of ERα-36 (74). Studies have reported that neither tamoxifen nor another anti-estrogen, ICI-182,780, failed to block ERα-36-mediated ERK1/2 activation and/or ERα-36 degradation in breast cancer cells. And anti-estrogens may more effectively enhance estrogen signal transduction through ERα-36 to activate ERK1/2. The activation of these pathways contributes to the proliferation of tumor cells (25). Another study reported that tamoxifen was found to bind directly to and activate ERα-36 through transcriptional stimulation of aldehyde dehydrogenase 1A1 (ALDH1A1) that enhanced the stemness and ability to metastasize of breast cancer cells (85). These findings support a potential and profound conflict that depends on the which ER isomer has the predominant expression in HCC tissue, ERα-66 or ERα-36, and may explain why tamoxifen fails to inhibit tumors by antagonizing the estrogen signaling pathway as in breast cancer. Instead, it may bind to ERα-36 and activate the rapid transduction pathway mediated by ERα-36 to promote tumor cell proliferation and metastasis. There is no research report to confirm this inference, and relevant research is needed to confirm it.

So, can the estrogen signaling pathway be used in the treatment of HCC? The answer remains to be determined. Strictly anti-estrogen therapy only antagonizes the estrogen signaling pathway. There are many other treatment strategies that could be based on the estrogen signaling pathway, such as estrogen replacement therapy, a treatment strategy based on promoting the estrogen signaling pathway, or targeting a specific estrogen receptor subtype or other key targets in the estrogen signaling pathway (74). Perhaps one or more of these options might be efficacious in the treatment of HCC.

Menopausal hormone therapy (MHT) is estrogen replacement therapy mainly used to treat menopausal symptoms. In a single-center case-control trial of HCC women and female control subjects, estrogen menopausal hormone therapy reduced HCC and HBV-related HCC, and increased overall survival of the HCC patients (11). This study provides epidemiological evidence for estrogen replacement therapy to prevent the occurrence and development of HCC after menopause.

In a systematic review and dose-response meta-analysis of observational studies on reproductive factors and menopausal hormone therapy related to the risk of primary liver cancer, estrogen exposure was found to be associated with the risk of liver cancer in a J-shaped dose response pattern (12). Late menarche and frequent use of MHT were associated with a reduction in the risk. When women with or without a history of oophorectomy were studied, those that had undergone oophorectomy had an increased risk of liver cancer. This study provides epidemiological support for the protective effect of estrogen in the development of liver cancer in females. At present, there are few comprehensive studies of estrogen replacement therapy in the treatment of liver cancer, most of which are retrospective, and most provide only epidemiological evidence. Therefore, research on the basic mechanism and clinical studies of estrogen replacement therapy in the treatment of liver cancer would be of great value.

In summary, estrogen replacement therapy based on the estrogen signaling pathway for HCC remains a valid and important potential therapeutic option. To more effectively develop anti-liver cancer therapies based on the estrogen signaling pathway, it will be important to explore the phenotypes and molecular subgroups of individuals who benefit most from various interventions.

7 DISCUSSION

As an important physiological hormone, estrogen impacts numerous important processes, such as regulating reproductive physiology, cell growth and proliferation, immune response, and metabolism. The estrogen signaling pathway, composed of estrogen and the estrogen receptor, is the main pathway for estrogen to exert its physiological functions. The estrogen signaling pathway is composed of a variety of different estrogen receptor-mediated genomic pathways and rapid transduction pathways. The estrogen receptors and related pathway proteins and effector molecules in the two functional pathways crosstalk with each other. The differences in the transcriptional activity of tissues and physiological processes constitute a complex, multi-functional estrogen signaling pathway.

Epidemiological studies have shown that the incidence and mortality of liver cancer in women are markedly lower than in men, suggesting that the estrogen signaling pathway exerts a protective effect. Recently, evidence has accumulated that has confirmed the anti-liver cancer effect of the estrogen signaling pathway. The estrogen signaling pathway can directly regulate the growth, proliferation, apoptosis and cell cycle of liver cancer cells through genomic and rapid transduction pathways and regulate various cellular stress responses such as cell oxidative stress and autophagy. In addition, tumor microenvironment, non-coding RNA, metabolites and other factors can indirectly regulate tumor growth environment, the immune response to tumors, and epigenetic and genetic changes to exert anti-tumor effects. In addition, the estrogen signaling pathway can directly or indirectly inhibit the progression of hepatitis virus infection and the occurrence and development of hepatitis virus-related liver cancer by regulating host antiviral responses, viral infection pathways, viral replication and transcription.

However, in addition to the inhibitory effect of the estrogen signaling pathway on liver cancer, some studies have also reported promotion of liver cancer by the estrogen signaling pathway. Analysis of these controversial results has revealed that the promotion of estrogen on liver cancer may be mediated by the new estrogen receptor ERα-36 and estrogen-related receptor γ (ERRγ). Analysis of the estrogen signaling pathway and the functional pathway mediated by the estrogen receptor requires analysis of the composition of a specific molecular subgroup of a specific estrogen receptor in a specific environment.

Anti-estrogen therapy based on the anti-estrogen signaling pathway (such as tamoxifen) applied to the treatment of liver cancer has not previously achieved satisfactory results. This may be attributed to the main molecular target being ERα-66, while HCC typically has low expression of ERα-66. Moreover, ERα-66

in HCC usually mediates anti-liver cancer effects. Epidemiological studies have now provided strong basis for the protective effect of estrogen replacement therapy/estrogen therapy based on the estrogen signaling pathway therapy in female liver cancer patients.

In the future, we plan to specifically explore the phenotypes and molecular subgroups of individuals who benefit most from various interventions (such as estrogen therapy). This should facilitate selection of specific interventions for individual patients to obtain maximum benefit. This anti-liver cancer treatment should be directed toward personalized, precision treatment.

Based on previously published reports, we have summarized, analyzed, explored and predicted the potential targets and mechanisms of the estrogen signaling pathway for anti-liver cancer therapy in the future. This should provide a strong theoretical basis for subsequent in-depth research and clinical application. The most appealing initial candidate would be estrogen therapy based on the treatment strategy of the estrogen signaling pathway. Although it has been epidemiologically characterized as having a protective effect in liver cancer, a large randomized multicenter controlled trial would be needed to appropriately answer the efficacy of estrogen therapy on liver cancer. Equally important, because the estrogen signaling pathway is composed of different estrogen receptors and complex functional pathways, it will be necessary to explore which estrogen receptor phenotype and molecular subgroups of liver cancer patients can obtain the most optimal outcomes from estrogen therapy. Gender differences, menopausal status and obesity related to estrogen therapy also deserve further evaluation.

A second treatment strategy could be based on specific estrogen receptor subtypes in the estrogen signaling pathway. Three estrogen receptors, ERα-66, ERβ and GPER, are principally responsible for mediating the anti-tumor effects in liver cancer. In the future, specific agonists developed for these targets have great potential for the clinical treatment of liver cancer. Because ERα-36 has a tumor-promoting effect in liver cancer, and it is highly expressed in cirrhotic and liver cancer tissues, it has great potential as a biomarker for liver cancer diagnosis, and antagonists targeting ERα-36 are expected to become a new type of therapy for liver cancer. The above specific target treatments need to be based on the development or application of more accurate, reliable and convenient estrogen receptor isoform detection methods. Monitoring of changes in estrogen receptor subtypes after treatment will facilitate the precision, efficacy analysis and prognostic evaluation of targeted therapy.

Finally, treatment strategies based on specific key molecules/inflammatory mediators/regulatory pathways in the estrogen signaling pathway also have great potential. The estrogen signaling pathway can regulate the body's inflammatory response to inhibit the progression of liver cancer. The key inflammatory mediators such as IL-6, IL-1α, and IL-1β are expected to become therapeutic targets. The estrogen signaling pathway can regulate the tumor microenvironment of liver cancer through a variety of ways. In the future, can we use the special immune regulation ability of the estrogen signaling pathway to combine with existing tumor immunotherapy to enhance efficacy and overcome problems of acquired drug resistance. This will require a comprehensive and detailed clarification of the regulation mechanism of the estrogen signaling pathway on the tumor microenvironment. In this way, we can distinguish whether the estrogen signaling pathway regulated by different estrogen receptors and functional pathways activates the tumor-promoting microenvironment or the tumor suppressing microenvironment. More precise regulation of tumor microenvironment, combined with tumor immunotherapy should offer a comprehensive plan to obtain maximum benefit.

AUTHOR CONTRIBUTIONS

YG, GW, and JY wrote and edited this manuscript and created figures. LM and XC reviewed and revised the manuscript. LM and XY provided direction and guidance throughout the preparation of the manuscript. QY, WJ, and SL participated in the review and revision of the manuscript during the review. All authors contributed to the article and approved the submitted version.

FUNDING

The authors appreciate the financial support from Natural Science Foundation of China (81800774), Pearl River S&T Nova Program of Guangzhou (201806010166), Natural Science Foundation of Guangdong Province (2214050007824), China Postdoctoral Science Foundation (2017M622660).

REFERENCES

1. Mak LY, Cruz-Ramon V, Chinchilla-Lopez P, Torres HA, LoConte NK, Rice JP, et al. Global Epidemiology, Prevention, and Management of Hepatocellular Carcinoma. *Am Soc Clin Oncol Educ Book* (2018) 38:262–79. doi: 10.1200/EDBK_200939
2. Niu L, Liu L, Yang S, Ren J, Lai P, Chen GG. New Insights Into Sorafenib Resistance in Hepatocellular Carcinoma: Responsible Mechanisms and Promising Strategies. *Biochim Biophys Acta Rev Cancer* (2017) 1868 (2):564–70. doi: 10.1016/j.bbcan.2017.10.002
3. Fuentes N, Silveyra P. Estrogen Receptor Signaling Mechanisms. *Adv Protein Chem Struct Biol* (2019) 116:135–70. doi: 10.1016/bs.apcsb.2019.01.001
4. McGlynn KA, Petrick JL, El-Serag HB. Epidemiology of Hepatocellular Carcinoma. *Hepatology* (2021) 73 Suppl 1:4–13. doi: 10.1002/hep.31288
5. Shimizu I, Yasuda M, Mizobuchi Y, Ma YR, Liu F, Shiba M, et al. Suppressive Effect of Oestradiol on Chemical Hepatocarcinogenesis in Rats. *Gut* (1998) 42 (1):112–9. doi: 10.1136/gut.42.1.112
6. Guo Y, Cai X, Lu H, Li Q, Zheng Y, Lin Z, et al. 17beta-Estradiol Promotes Apoptosis of Hepg2 Cells Caused by Oxidative Stress by Increasing Foxo3a Phosphorylation. *Front Pharmacol* (2021) 12:607379. doi: 10.3389/fphar.2021.607379
7. Barbare JC, Bouche O, Bonnetain F, Raoul JL, Rougier P, Abergel A, et al. Randomized Controlled Trial of Tamoxifen in Advanced Hepatocellular Carcinoma. *J Clin Oncol* (2005) 23(19):4338–46. doi: 10.1200/JCO.2005.05.470
8. Chow PK, Tai BC, Tan CK, Machin D, Win KM, Johnson PJ, et al. High-Dose Tamoxifen in the Treatment of Inoperable Hepatocellular Carcinoma: A Multicenter Randomized Controlled Trial. *Hepatology* (2002) 36(5):1221–6. doi: 10.1053/jhep.2002.36824

9. CLIP Group (Cancer of the Liver Italian Programme). Tamoxifen in Treatment of Hepatocellular Carcinoma: A Randomised Controlled Trial. CLIP Group (Cancer of the Liver Italian Programme). *Lancet* (1998) 352 (9121):17–20. doi: 10.1016/S0140-6736(98)01259-8
10. Farinati F, Salvagnini M, de Maria N, Fornasiero A, Chiaramonte M, Rossaro L, et al. Unresectable Hepatocellular Carcinoma: A Prospective Controlled Trial With Tamoxifen. *J Hepatol* (1990) 11(3):297–301. doi: 10.1016/0168-8278(90)90211-9
11. Hassan MM, Botrus G, Abdel-Wahab R, Wolff RA, Li D, Tweardy D, et al. Estrogen Replacement Reduces Risk and Increases Survival Times of Women With Hepatocellular Carcinoma. *Clin Gastroenterol Hepatol* (2017) 15 (11):1791–9. doi: 10.1016/j.cgh.2017.05.036
12. Zhong GC, Liu Y, Chen N, Hao FB, Wang K, Cheng JH, et al. Reproductive Factors, Menopausal Hormone Therapies and Primary Liver Cancer Risk: A Systematic Review and Dose-Response Meta-Analysis of Observational Studies. *Hum Reprod Update* (2016) 23(1):126–38. doi: 10.1093/humupd/dmw037
13. Osborne CK. Tamoxifen in the Treatment of Breast Cancer. *N Engl J Med* (1998) 339(22):1609–18. doi: 10.1056/NEJM199811263392207
14. Nelson LR, Bulun SE. Estrogen Production and Action. *J Am Acad Dermatol* (2001) 45(3 Suppl):S116–24. doi: 10.1067/mjd.2001.117432
15. Simpson ER. Sources of Estrogen and Their Importance. *J Steroid Biochem Mol Biol* (2003) 86(3-5):225–30. doi: 10.1016/s0960-0760(03)00360-1
16. Miller WL, Auchus RJ. The Molecular Biology, Biochemistry, and Physiology of Human Steroidogenesis and Its Disorders. *Endocr Rev* (2011) 32(1):81–151. doi: 10.1210/er.2010-0013
17. Tsuchiya Y, Nakajima M, Yokoi T. Cytochrome P450-Mediated Metabolism of Estrogens and Its Regulation in Human. *Cancer Lett* (2005) 227(2):115–24. doi: 10.1016/j.canlet.2004.10.007
18. Lakhani NJ, Venitz J, Figg WD, Sparreboom A. Pharmacogenetics of Estrogen Metabolism and Transport in Relation to Cancer. *Curr Drug Metab* (2003) 4 (6):505–13. doi: 10.2174/1389200033489244
19. Cavalieri E, Rogan E. The 3,4-Quinones of Estrone and Estradiol Are the Initiators of Cancer Whereas Resveratrol and N-Acetylcysteine Are the Preventers. *Int J Mol Sci* (2021) 22(15):8238. doi: 10.3390/ijms22158238
20. Samavat H, Kurzer MS. Estrogen Metabolism and Breast Cancer. *Cancer Lett* (2015) 356(2 Pt A):231–43. doi: 10.1016/j.canlet.2014.04.018
21. Tsuchiya Y, Nakajima M, Kyo S, Kanaya T, Inoue M, Yokoi T. Human CYP1B1 Is Regulated by Estradiol *via* Estrogen Receptor. *Cancer Res* (2004) 64(9):3119–25. doi: 10.1158/0008-5472.can-04-0166
22. Liang J, Shang Y. Estrogen and Cancer. *Annu Rev Physiol* (2013) 75(1):225–40. doi: 10.1146/annurev-physiol-030212-183708
23. Kumar R, Zakharov MN, Khan SH, Miki R, Jang H, Toraldo G, et al. The Dynamic Structure of the Estrogen Receptor. *J Amino Acids* (2011) 2011:1–7. doi: 10.4061/2011/812540
24. Ohe K, Miyajima S, Abe I, Tanaka T, Hamaguchi Y, Harada Y, et al. HMGA1a Induces Alternative Splicing of Estrogen Receptor Alpha in MCF-7 Human Breast Cancer Cells. *J Steroid Biochem Mol Biol* (2018) 182:21–6. doi: 10.1016/j.jsbmb.2018.04.007
25. Wang Z, Zhang X, Shen P, Loggie BW, Chang Y. Deuel TF. A Variant of Estrogen Receptor-{Alpha}, Her-{Alpha}36: Transduction of Estrogen- and Antiestrogen-Dependent Membrane-Initiated Mitogenic Signaling. *Proc Natl Acad Sci USA* (2006) 103(24):9063–8. doi: 10.1073/pnas.0603339103
26. Gu Y, Chen T, Lopez E, Wu W, Wang X, Cao J, et al. The Therapeutic Target of Estrogen Receptor-Alpha36 in Estrogen-Dependent Tumors. *J Transl Med* (2014) 12:16. doi: 10.1186/1479-5876-12-16
27. Barton M, Filardo EJ, Lolait SJ, Thomas P, Maggiolini M, Prossnitz ER. Twenty Years of the G Protein-Coupled Estrogen Receptor GPER: Historical and Personal Perspectives. *J Steroid Biochem Mol Biol* (2018) 176:4–15. doi: 10.1016/j.jsbmb.2017.03.021
28. Klinge CM. Estrogen Receptor Interaction With Estrogen Response Elements. *Nucleic Acids Res* (2001) 29(14):2905–19. doi: 10.1093/nar/29.14.2905
29. Hua H, Zhang H, Kong Q, Jiang Y. Mechanisms for Estrogen Receptor Expression in Human Cancer. *Exp Hematol Oncol* (2018) 7(1):24. doi: 10.1186/s40164-018-0116-7
30. Björnström L, Sjöberg M. Mechanisms of Estrogen Receptor Signaling: Convergence of Genomic and Nongenomic Actions on Target Genes. *Mol Endocrinol* (2005) 19(4):833–42. doi: 10.1210/me.2004-0486
31. Tu CC, Kumar VB, Day CH, Kuo WW, Yeh SP, Chen RJ, et al. Estrogen Receptor Alpha (ESR1) Over-Expression Mediated Apoptosis in Hep3B Cells by Binding With SP1 Proteins. *J Mol Endocrinol* (2013) 51(1):203–12. doi: 10.1530/JME-13-0085
32. Deng L, Yang H, Tang J, Lin Z, Yin A, Gao Y, et al. Inhibition of MTA1 by Eralpha Contributes to Protection Hepatocellular Carcinoma From Tumor Proliferation and Metastasis. *J Exp Clin Cancer Res* (2015) 34:128. doi: 10.1186/s13046-015-0248-0
33. Huang FY, Wong DK, Seto WK, Lai CL, Yuen MF. Estradiol Induces Apoptosis *via* Activation of miRNA-23a and P53: Implication for Gender Difference in Liver Cancer Development. *Oncotarget* (2015) 6(33):34941–52. doi: 10.18632/oncotarget.5472
34. Pok S, Barn VA, Wong HJ, Blackburn AC, Board P, Farrell GC, et al. Testosterone Regulation of Cyclin E Kinase: A Key Factor in Determining Gender Differences in Hepatocarcinogenesis. *J Gastroenterol Hepatol* (2016) 31(6):1210–9. doi: 10.1111/jgh.13232
35. Tsutsui S, Yamamoto R, Iishi H, Tatsuta M, Tsuji M, Terada N. Promoting Effect of Ovariectomy on Hepatocellular Tumorigenesis Induced in Mice by 3'-Methyl-4-Dimethylaminoazobenzene. *Virchows Arch B Cell Pathol Incl Mol Pathol* (1992) 62(6):371–5. doi: 10.1007/BF02899706
36. Yamamoto R, Iishi H, Tatsuta M, Tsuji M, Terada N. Roles of Ovaries and Testes in Hepatocellular Tumorigenesis Induced in Mice by 3'-Methyl-4-Dimethylaminoazobenzene. *Int J Cancer* (1991) 49(1):83–8. doi: 10.1002/ijc.2910490116
37. Hou J, Xu J, Jiang R, Wang Y, Chen C, Deng L, et al. Estrogen-Sensitive PTPRO Expression Represses Hepatocellular Carcinoma Progression by Control of STAT3. *Hepatology* (2013) 57(2):678–88. doi: 10.1002/hep.25980
38. Li Z, Tuteja G, Schug J, Kaestner KH. Foxa1 and Foxa2 Are Essential for Sexual Dimorphism in Liver Cancer. *Cell* (2012) 148(1-2):72–83. doi: 10.1016/j.cell.2011.11.026
39. Shen M, Shi H. Estradiol and Estrogen Receptor Agonists Oppose Oncogenic Actions of Leptin in Hepg2 Cells. *PloS One* (2016) 11(3):e151455. doi: 10.1371/journal.pone.0151455
40. Wei Q, Guo P, Mu K, Zhang Y, Zhao W, Huai W, et al. Estrogen Suppresses Hepatocellular Carcinoma Cells Through Erbeta-Mediated Upregulation of the NLRP3 Inflammasome. *Lab Invest* (2015) 95(7):804–16. doi: 10.1038/labinvest.2015.63
41. Wei Q, Zhu R, Zhu J, Zhao R, Li M. E2-Induced Activation of the NLRP3 Inflammasome Triggers Pyroptosis and Inhibits Autophagy in HCC Cells. *Oncol Res* (2019) 27(7):827–34. doi: 10.3727/096504018X15462920753012
42. Schmidt-Arras D, Rose-John S. IL-6 Pathway in the Liver: From Physiopathology to Therapy. *J Hepatol* (2016) 64(6):1403–15. doi: 10.1016/j.jhep.2016.02.004
43. Lokau J, Schoeder V, Haybaeck J, Garbers C. Jak-Stat Signaling Induced by Interleukin-6 Family Cytokines in Hepatocellular Carcinoma. *Cancers (Basel)* (2019) 11(11):1704. doi: 10.3390/cancers11111704
44. Bergmann J, Muller M, Baumann N, Reichert M, Heneweer C, Bolik J, et al. IL-6 Trans-Signaling Is Essential for the Development of Hepatocellular Carcinoma in Mice. *Hepatology* (2017) 65(1):89–103. doi: 10.1002/hep.28874
45. Prieto J. Inflammation, HCC and Sex: IL-6 in the Centre of the Triangle. *J Hepatol* (2008) 48(2):380–1. doi: 10.1016/j.jhep.2007.11.007
46. Naugler WE, Sakurai T, Kim S, Maeda S, Kim K, Elsharkawy AM, et al. Gender Disparity in Liver Cancer Due to Sex Differences in Myd88-Dependent IL-6 Production. *Science* (2007) 317(5834):121–4. doi: 10.1126/science.1140485
47. Wei T, Chen W, Wen L, Zhang J, Zhang Q, Yang J, et al. G Protein-Coupled Estrogen Receptor Deficiency Accelerates Liver Tumorigenesis by Enhancing Inflammation and Fibrosis. *Cancer Lett* (2016) 382(2):195–202. doi: 10.1016/j.canlet.2016.08.012
48. Qiu YA, Xiong J, Fu Q, Dong Y, Liu M, Peng M, et al. GPER-Induced ERK Signaling Decreases Cell Viability of Hepatocellular Carcinoma. *Front Oncol* (2021) 11:638171. doi: 10.3389/fonc.2021.638171
49. Ozdemir BC, Dotto GP. Sex Hormones and Anticancer Immunity. *Clin Cancer Res* (2019) 25(15):4603–10. doi: 10.1158/1078-0432.CCR-19-0137
50. Rothenberger NJ, Somasundaram A, Stabile LP. The Role of the Estrogen Pathway in the Tumor Microenvironment. *Int J Mol Sci* (2018) 19(2):611. doi: 10.3390/ijms19020611
51. Yang W, Lu Y, Xu Y, Xu L, Zheng W, Wu Y, et al. Estrogen Represses Hepatocellular Carcinoma (HCC) Growth *via* Inhibiting Alternative Activation of Tumor-Associated Macrophages (Tams). *J Biol Chem* (2012) 287(48):40140–9. doi: 10.1074/jbc.M112.348763

52. Lu C, Rong D, Zhang B, Zheng W, Wang X, Chen Z, et al. Current Perspectives on the Immunosuppressive Tumor Microenvironment in Hepatocellular Carcinoma: Challenges and Opportunities. *Mol Cancer* (2019) 18(1):130. doi: 10.1186/s12943-019-1047-6
53. Taheri M, Shoorei H, Dinger ME, Ghafouri-Fard S. Perspectives on the Role of Non-Coding RNAs in the Regulation of Expression and Function of the Estrogen Receptor. *Cancers (Basel)* (2020) 12(8):2162. doi: 10.3390/cancers12082162
54. Sedano MJ, Harrison AL, Zilaie M, Das C, Choudhari R, Ramos E, et al. Emerging Roles of Estrogen-Regulated Enhancer and Long Non-Coding RNAs. *Int J Mol Sci* (2020) 21(10):3711. doi: 10.3390/ijms21103711
55. Klingenberg M, Matsuda A, Diederichs S, Patel T. Non-Coding RNA in Hepatocellular Carcinoma: Mechanisms, Biomarkers and Therapeutic Targets. *J Hepatol* (2017) 67(3):603–18. doi: 10.1016/j.jhep.2017.04.009
56. Zhao Q, Li T, Qi J, Liu J, Qin C. The Mir-545/374a Cluster Encoded in the Ftx Lncrna Is Overexpressed in HBV-Related Hepatocellular Carcinoma and Promotes Tumorigenesis and Tumor Progression. *PloS One* (2014) 9(10): e109782. doi: 10.1371/journal.pone.0109782
57. Xiao Y, Liu G, Sun Y, Gao Y, Ouyang X, Chang C, et al. Targeting the Estrogen Receptor Alpha (Eralpha)-Mediated Circ-SMG1.72/Mir-141-3p/Gelsolin Signaling to Better Suppress the HCC Cell Invasion. *Oncogene* (2020) 39 (12):2493–508. doi: 10.1038/s41388-019-1150-6
58. Li CL, Yeh KH, Liu WH, Chen CL, Chen DS, Chen PJ, et al. Elevated P53 Promotes the Processing of Mir-18a to Decrease Estrogen Receptor-Alpha in Female Hepatocellular Carcinoma. *Int J Cancer* (2015) 136(4):761–70. doi: 10.1002/ijc.29052
59. Di Martino MT, Rossi M, Caracciolo D, Gulla A, Tagliaferri P, Tassone P. Mir-221/222 Are Promising Targets for Innovative Anticancer Therapy. *Expert Opin Ther Targets* (2016) 20(9):1099–108. doi: 10.1517/14728222.2016.1164693
60. Chen JJ, Tang YS, Huang SF, Ai JG, Wang HX, Zhang LP. Hbx Protein-Induced Upregulation of Microrna-221 Promotes Aberrant Proliferation in Hbvrelated Hepatocellular Carcinoma by Targeting Estrogen Receptor-Alpha. *Oncol Rep* (2015) 33(2):792–8. doi: 10.3892/or.2014.3647
61. Ren J, Chen GG, Liu Y, Su X, Hu B, Leung BC, et al. Cytochrome P450 1A2 Metabolizes 17beta-Estradiol to Suppress Hepatocellular Carcinoma. *PloS One* (2016) 11(4):e153863. doi: 10.1371/journal.pone.0153863
62. Mendez-Blanco C, Fondevila F, Garcia-Palomo A, Gonzalez-Gallego J, Mauriz JL. Sorafenib Resistance in Hepatocarcinoma: Role of Hypoxia-Inducible Factors. *Exp Mol Med* (2018) 50(10):1–9. doi: 10.1038/s12276-018-0159-1
63. Ma L, Li G, Zhu H, Dong X, Zhao D, Jiang X, et al. 2-Methoxyestradiol Synergizes With Sorafenib to Suppress Hepatocellular Carcinoma by Simultaneously Dysregulating Hypoxia-Inducible Factor-1 and -2. *Cancer Lett* (2014) 355(1):96–105. doi: 10.1016/j.canlet.2014.09.011
64. Maini MK, Bertoletti A. HBV in 2016: Global and Immunotherapeutic Insights Into Hepatitis B. *Nat Rev Gastroenterol Hepatol* (2017) 14(2):71–2. doi: 10.1038/nrgastro.2016.196
65. Arzumanyan A, Reis HM, Feitelson MA. Pathogenic Mechanisms in HBV- and HCV-Associated Hepatocellular Carcinoma. *Nat Rev Cancer* (2013) 13 (2):123–35. doi: 10.1038/nrc3449
66. Montella M, D'Arena G, Crispo A, Capunzo M, Nocerino F, Grimaldi M, et al. Role of Sex Hormones in the Development and Progression of Hepatitis B Virus-Associated Hepatocellular Carcinoma. *Int J Endocrinol* (2015) 2015:854530. doi: 10.1155/2015/854530
67. Liu WC, Liu QY. Molecular Mechanisms of Gender Disparity in Hepatitis B Virus-Associated Hepatocellular Carcinoma. *World J Gastroenterol* (2014) 20 (20):6252–61. doi: 10.3748/wjg.v20.i20.6252
68. Xiang WQ, Feng WF, Ke W, Sun Z, Chen Z, Liu W. Hepatitis B Virus X Protein Stimulates IL-6 Expression in Hepatocytes *via* a Myd88-Dependent Pathway. *J Hepatol* (2011) 54(1):26–33. doi: 10.1016/j.jhep.2010.08.006
69. Yao QY, Feng YD, Han P, Yang F, Song GQ. Hepatic Microenvironment Underlies Fibrosis in Chronic Hepatitis B Patients. *World J Gastroenterol* (2020) 26(27):3917–28. doi: 10.3748/wjg.v26.i27.3917
70. Lee S, Lee M, Kim JB, Jo A, Cho EJ, Yu SJ, et al. 17beta-Estradiol Exerts Anticancer Effects in Anoikis-Resistant Hepatocellular Carcinoma Cell Lines by Targeting IL-6/STAT3 Signaling. *Biochem Biophys Res Commun* (2016) 473(4):1247–54. doi: 10.1016/j.bbrc.2016.04.049
71. Han J, Ding L, Yuan B, Yang X, Wang X, Li J, et al. Hepatitis B Virus X Protein and the Estrogen Receptor Variant Lacking Exon 5 Inhibit Estrogen Receptor Signaling in Hepatoma Cells. *Nucleic Acids Res* (2006) 34(10):3095–106. doi: 10.1093/nar/gkl389
72. Di Martino V, Lebray P, Myers RP, Pannier E, Paradis V, Charlotte F, et al. Progression of Liver Fibrosis in Women Infected With Hepatitis C: Long-Term Benefit of Estrogen Exposure. *Hepatology* (2004) 40(6):1426–33. doi: 10.1002/hep.20463
73. Iyer JK, Kalra M, Kaul A, Payton ME, Kaul R. Estrogen Receptor Expression in Chronic Hepatitis C and Hepatocellular Carcinoma Pathogenesis. *World J Gastroenterol* (2017) 23(37):6802–16. doi: 10.3748/wjg.v23.i37.6802
74. Carruba G. Estrogens in Hepatocellular Carcinoma: Friends or Foes? *Cancers (Basel)* (2021) 13(9):2085. doi: 10.3390/cancers13092085
75. Thiebaut C, Konan HP, Guerquin MJ, Chesnel A, Livera G, Le Romancer M, et al. The Role of Eralpha36 in Development and Tumor Malignancy. *Int J Mol Sci* (2020) 21(11):4116. doi: 10.3390/ijms21114116
76. Wang ZY, Yin L. Estrogen Receptor Alpha-36 (ER-Alpha36): A New Player in Human Breast Cancer. *Mol Cell Endocrinol* (2015) 418 Pt 3:193–206. doi: 10.1016/j.mce.2015.04.017
77. Shi L, Dong B, Li Z, Lu Y, Ouyang T, Li J, et al. Expression of ER-{Alpha}36, a Novel Variant of Estrogen Receptor {Alpha}, and Resistance to Tamoxifen Treatment in Breast Cancer. *J Clin Oncol* (2009) 27(21):3423–9. doi: 10.1200/JCO.2008.17.2254
78. Miceli V, Cocciadiferro L, Fregapane M, Zarcone M, Montalto G, Polito LM, et al. Expression of Wild-Type and Variant Estrogen Receptor Alpha in Liver Carcinogenesis and Tumor Progression. *Omics* (2011) 15(5):313–7. doi: 10.1089/omi.2010.0108
79. Cocciadiferro L, Miceli V, Granata OM, Carruba G. Merlin, the Product of NF2 Gene, Is Associated With Aromatase Expression and Estrogen Formation in Human Liver Tissues and Liver Cancer Cells. *J Steroid Biochem Mol Biol* (2017) 172:222–30. doi: 10.1016/j.jsbmb.2016.05.023
80. You H, Meng K, Wang ZY. The ER-Alpha36/EGFR Signaling Loop Promotes Growth of Hepatocellular Carcinoma Cells. *Steroids* (2018) 134:78–87. doi: 10.1016/j.steroids.2018.02.007
81. Chen J, Chen L, Lu T, Xie Y, Li C, Jia Z, et al. Eralpha36 Is an Effective Target of Epigallocatechin-3-Gallate in Hepatocellular Carcinoma. *Int J Clin Exp Pathol* (2019) 12(9):3222–34.
82. Kim JH, Choi YK, Byun JK, Kim MK, Kang YN, Kim SH, et al. Estrogen-Related Receptor Gamma Is Upregulated in Liver Cancer and Its Inhibition Suppresses Liver Cancer Cell Proliferation *via* Induction of P21 and P27. *Exp Mol Med* (2016) 48:e213. doi: 10.1038/emm.2015.115
83. Tan CK, Chow PK, Findlay M, Wong C, Machin D. Use of Tamoxifen in Hepatocellular Carcinoma: A Review and Paradigm Shift. *J Gastroenterol Hepatol* (2000) 15(7):725–9. doi: 10.1046/j.1440-1746.2000.02235.x
84. Di Maio M, De Maio E, Morabito A, D'Aniello R, De Feo G, Gallo C, et al. Hormonal Treatment of Human Hepatocellular Carcinoma. *Ann N Y Acad Sci* (2006) 1089:252–61. doi: 10.1196/annals.1386.007
85. Wang Q, Jiang J, Ying G, Xie XQ, Zhang X, Xu W, et al. Tamoxifen Enhances Stemness and Promotes Metastasis of Eralpha36(+) Breast Cancer by Upregulating ALDH1A1 in Cancer Cells. *Cell Res* (2018) 28(3):336–58. doi: 10.1038/cr.2018.15

Conflict of Interest: The authors declare that the research was conducted in the absence of any commercial or financial relationships that could be construed as a potential conflict of interest.

frontiers in Oncology

ORIGINAL RESEARCH
published: 31 January 2022
doi: 10.3389/fonc.2021.770918

Profiling and Integrated Analysis of Differentially Expressed MicroRNAs as Novel Biomarkers of Hepatocellular Carcinoma

Yuwei Xie[1], Yixiu Wang[2], Weijie Xue[3], Hao Zou[1], Kun Li[1], Kui Liu[1], Wei Zhao[1], Chengzhan Zhu[1] and Jingyu Cao[1]**

[1] Department of Hepatobiliary and Pancreatic Surgery, The Affiliated Hospital of Qingdao University, Qingdao, China, [2] Department of Hepatic Surgery, Shanghai Cancer Center, Shanghai Medical College, Fudan University, Shanghai, China, [3] Department of Gastrointestinal Surgery, The Affiliated Hospital of Qingdao University, Qingdao, China

OPEN ACCESS

Edited by:
Zongli Zhang,
Qilu Hospital of Shandong University, China

Reviewed by:
Yongsheng Jiang,
Shanghai Jiao Tong University, China
Haizhou Liu,
Guangxi Medical University Cancer Hospital, China
Litu Zhang,
Guangxi Medical University Cancer Hospital, China

***Correspondence:**
Chengzhan Zhu
zhuchengz@qduhospital.cn
Jingyu Cao
cjy7027@163.com

Specialty section:
This article was submitted to Cancer Molecular Targets and Therapeutics, a section of the journal Frontiers in Oncology

Received: *05 September 2021*
Accepted: *29 December 2021*
Published: *31 January 2022*

Citation:
Xie Y, Wang Y, Xue W, Zou H, Li K, Liu K, Zhao W, Zhu C and Cao J (2022) Profiling and Integrated Analysis of Differentially Expressed MicroRNAs as Novel Biomarkers of Hepatocellular Carcinoma. Front. Oncol. 11:770918. doi: 10.3389/fonc.2021.770918

Hepatocellular carcinoma (HCC) is a heterogeneous disease that has multiple etiologies. It is the most common primary liver cancer, the sixth highest cause of cancer incidences, and the fourth highest cause of cancer-related deaths. The discovery of new biomarkers for the early detection, treatment, and prognosis of HCC would therefore be extremely useful. This study investigated differentially expressed ribonucleic acid (RNA) profiles by constructing a genome-wide profile of clinical samples. Differential expression analysis identified 1,280 differentially expressed messenger RNAs (dif-mRNAs), 99 differentially expressed microRNAs (dif-miRNAs), 181 differentially expressed long non-coding RNAs (dif-lncRNAs), and 31 differentially expressed circular RNAs (dif-circRNAs). Gene ontology (GO) analysis and Kyoto Encyclopedia of Genes and Genomes (KEGG) path analysis were then conducted on these differentially expressed RNAs, revealing that they were clearly related to cell division, foreign body metabolism, and ribosome assembly. A competing endogenous RNA (ceRNA) network was then constructed based on the regulatory dif-miRNA-dif-mRNA and dif-miRNA-dif-lncRNA relationships. These results were also verified using HCC data from the Cancer Genome Atlas (TCGA); seven dif-miRNAs were verified in clinical samples by real-time quantitative polymerase chain reaction (RT-qPCR). Kaplan-Meier survival analysis revealed that the expression levels of Hsa-miR-1269a, Hsa-miR-421, and Hsa-miR-190b were correlated with overall survival. (P <0.05). Survival analysis of clinical samples showed that hsa-mir-1269a, hsa-mir-421 were associated with prognosis (p<0.05).This study revealed the general expression characteristics of specific differentially expressed miRNAs using a ceRNA network constructed from HCC samples. Hsa-mir-1269a, hsa-mir-421 may be promising candidates.

Keywords: hepatocellular carcinoma, bioinformatics, whole-transcriptome sequencing, microRNAs, biomarkers

INTRODUCTION

Hepatocellular carcinoma (HCC) is the most common type of primary liver cancer; it is also one of the most common primary malignancies worldwide. According to global cancer statistics, HCC is also the fourth highest cause of cancer death (1–3). HCC usually develops in the context of chronic liver disease; its main causes are alcoholic and non-alcoholic fatty liver, and hepatitis B virus (HBV) and hepatitis C virus (HCV) infections (4). Therefore, it is urgent to better understand HCC tumor biology.

The rapid development of high-throughput next-generation sequencing (NGS) technologies has enabled the complete sequencing of entire genomes, permitting further analysis of the genomic profiles of some cancers (5–7). A recent ribonucleic acid (RNA) sequencing study of HCC found that a new type of vacuolar protein sorting 35 (VPS35) oncogene was significantly reduced in HCC cells. VPS35 plays a carcinogenic role by increasing the sorting and transport of fibroblast growth factor receptor 3 (FGFR3) (8). Recent studies have shown that competitive endogenous RNAs (ceRNAs) can act as natural decoys. The systematic functionalizations of non-coding RNAs (ncRNAs), pseudogenes, and circular RNAs (circRNAs) containing microRNA (miRNA) response elements (MREs) together form a complex miRNA-centered ceRNA network. This network constitutes a common microRNA library that affects gene expression and reveals new mechanisms of RNA interactions (9–12). As a ceRNA mechanism, the long-ncRNA (lncRNA) FAL1 can accelerate cell proliferation and metastasis by competitively binding to miR-1236 (13). However, few studies have used whole-transcriptome sequencing strategies to describe a transcriptional map, which could accurately detect the global gene expression profile.

Here, whole-transcriptome sequencing of tumors and corresponding adjacent non-tumors was conducted for six HCC patients. The expression levels of mRNA, lncRNA, miRNA, and circRNA were then analyzed in the cancer and paracancer groups, and their functional interactions were predicted. In addition, these results were validated using HCC data from the Cancer Genome Atlas (TCGA); a ceRNA network regulatory mechanism was then constructed. This study could offer a new molecular mechanism that could help to reveal the onset and progression of HCC, and its prognosis.

MATERIALS AND METHODS

Patients and Tissue Collection

Cancerous and paracancerous tissue samples were obtained from six male patients with HCC, none of whom had received preoperative radiotherapy or chemotherapy. Patients were selected from the Department of Hepatobiliary and Pancreatic Surgery of the Affiliated Hospital of Qingdao University. All patients participating in the study signed an informed consent form. All specimens were examined for HCC by a pathologist prior to preservation (freezing *via* liquid nitrogen). This research was approved by the Medical Ethics Committee of the Affiliated Hospital of Qingdao University.

RNA Extraction and Quality Control

Total RNA was extracted from frozen tumor tissue and matched paracancerous tissue using TRIzol reagent (Thermofisher Science; Waltham, Massachusetts, USA). RNA degradation and contamination were monitored using 1.5% Sepharose gel, especially for deoxyribonucleic acid (DNA) contamination. RNA concentration and purity were measured using a NanoDrop 2000 spectrophotometer (ThermoFisher Scientific, Wilmington, DE). RNA integrity was assessed using an Agilent Bioanalyzer 2100 system (Agilent Technologies, CA, USA) with the RNA Nano6000 assay kit.

Library Construction and Sequencing

RNA samples (2.5 ng) were used as input material to prepare libraries for RNA sequencing. Sequencing libraries were constructed and generated using the NEBNextR UltraTM small RNA Sample Prep Kit for Illumina R (NEB, USA), according to the manufacturer's instructions. Index codes were added to attribute sequences to each individual sample. Finally, polymerase chain reaction (PCR) products were purified using the AMPure XP system (AMPure XP system); library quality was evaluated using the Agilent Bioanalyzer 2100 system. For clustering and sequencing, index-coded samples were clustered on the cBot cluster generation system, using the TruSeq PE Cluster Kitv3-cBot-HS (Illumina) according to the manufacturer's instructions. After cluster generation, the library was sequenced on the Illumina platform and reads were generated.

Screening of Differently-Expressed (Dif)-Messenger RNAs (mRNAs), Dif-miRNAs, Dif-lncRNAs, and Dif-circRNAs

Samples with biological replicates were screened for differences using DEseq software; samples without biological replicates were screened for differences using EBseq software. Dif-mRNA, dif-circRNA, dif-lncRNA, and dif-miRNA were screened using fold changes greater than or equal to one and a false discovery rate (FDR) of <0.05 as screening criteria. Dif-mRNA, dif-lncRNA, and dif-miRNA were analyzed using the R package "clusterProfiler" for Gene Ontology-Biological Process (GO-BP) enrichment analysis and Kyoto Encyclopedia of Genes and Genomes (KEGG) enrichment of differential genes (14–16).

Protein-Protein Interaction (PPI) Network and Module Analysis of Dif-mRNAs

STRING (version: 11.0; https://www.string-db.org/) was used to analyze the interaction relationships between differential proteins (17). The species was set to human and the import gene set was set to all degrees. To obtain the interaction pairs with the closest interaction relationship, the PPI arguments score was set to 0.99 (high confidence). The PPI network was constructed using Cytoscape software (version 3.8.0; https://cytoscape.org/) and the scores of each node were ranked to

obtain the significant nodes. The most important cluster modules in the network were analyzed using Cytoscape's plugin MCODE (18) (version 2.0.0; PPIMCODE https://apps.cytoscape.org/apps/). The screening threshold was set to 5.0 points, k-core=2, degree cutoff=2, node score cutoff=2, and max depth=100 for screening. GO-BP enrichment analysis was also performed for the important cluster module genes. A GO-BP threshold of $P < 0.05$ was considered to imply a significant difference.

Construction of CeRNA Network

The ceRNA network was constructed using miRDB (V5.0; http://mirdb.org), miRTarBase (V7.0; https://maayanlab.cloud/Harmonizome/resource/MiRTarBase), miRWalk (http://mirwalk.umm.uni-heidelberg.de/) and TargetScan (V7.2; TSCAN.org/VERT_72/). These databases were searched for dif-miRNAs targeting dif-mRNAs to obtain dif-miRNA-dif-mRNA regulatory relationships (19). The dif-miRNA-dif-lncRNA regulatory relationships were obtained by searching for interactions between dif-lncRNAs and dif-miRNAs using the miRcode database (version 11; http://www.mircode.org/), RNAhybrid (https://bibiserv.cebitec.uni-bielefeld.de/rnahybrid/). The dif-miRNA-dif-mRNA and dif-miRNA-dif-lncRNA regulatory relationships were integrated and a composite lncRNA-miRNA-mRNA network was established using Cytoscape, according to the regulatory mechanism of the ceRNA network (20).

TCGA Liver Hepatocellular Carcinoma (LIHC) Database Validation

The data included 374 tumor specimens and 50 paracancerous normal specimens. The expression matrix and annotation information for mRNA, miRNA, and lncRNA were downloaded and the unpaired t-test in LIMMA software package was used to analyze the differential expression of tumor and normal tissues. A |logFC| value of >1 and a p value of <0.05 for mRNA and miRNA were used as cutoff points for the differential expression of lncRNAs. The differential expression results of TCGA data, and the dif-mRNAs, dif-miRNAs, and dif-lncRNAs obtained in this study were subjected to co-expression analysis, and a Venn graph was drawn.

Real-Time Quantitative PCR (RT-qPCR)

Thirty specimens of HCC tissues or normal liver tissues and histopathologically verified paracancerous tissues were selected from the Department of Hepatobiliary and Pancreatic Surgery, Affiliated Hospital of Qingdao University. Total RNA was extracted from HCC tissues and paraneoplastic tissues using Trizol (Takara). Total RNA was reverse transcribed into complementary DNA (cDNA) using a PrimeScript TM RT kit (Takara). RT-qPCR was performed on a LightCycler 480 using ChamQ Universal SYBR qPCR Master Mix (Vazyme) to determine miRNA expression (21). The study was approved by the ethics committee of Affiliated Hospital of Qingdao University.

Survival Analysis

Survival analysis of dif-miRNA using the Kaplan-Meier plotter (http://kmplot.com). The results were evaluated according to RT-qPCR. Grouping by 2^-ΔΔCT into high and low expression groups, survival analysis was performed according to hsa-miR-1269a, hsa-miR-421, and hsa-miR-190b.

RESULT

Dif-RNA Analysis

On the basis of the set screening conditions, a total of 1,280 dif-mRNAs were obtained, of which 904 were up-regulated and 376 were down-regulated. Furthermore, 99 dif-miRNAs were obtained, of which 31 were up-regulated and 68 were down-regulated; 181 dif-lncRNAs were obtained, of which 148 were up-regulated and 33 were down-regulated. Finally, 31 dif-circRNAs were obtained, of which 29 were up-regulated and two were down-regulated. The heat cluster maps of dif-mRNAs, dif-lncRNAs, dif-miRNAs, and dif-circRNAs showed that the tumor samples were clearly divided from the control samples (**Figure 1**), suggesting that the obtained differential expression analysis results were credible.

Functional Enrichment Analysis of Dif-mRNAs

Following GO and KEGG pathway analysis, the top ten most enriched dif-mRNAs were identified. GO term analysis revealed that the genes displayed were related to biological processes such as cell division, and to the xenobiotic metabolism process (**Figure 2A**). KEGG analysis revealed that these genes were significantly related to fatty acid degradation, complement and coagulation cascades, and peroxisome signaling pathways, among other processes (**Figure 2B**).

PPI Network and Module Extraction

The PPI network of dif-mRNAs consisted of 654 nodes and 2262 mutual pairs, among which nodes with high topological structure scores were considered to be the key nodes. Employing the Cytoscape plug-in MCODE, four sub-network modules (score R ≥5.0) were collected and extracted from the PPI network. Module A (score=26) contained 26 nodes and 325 interaction pairs, module B (score = 10.333) contained 19 nodes and 93 interaction pairs, module C (score = 6.8) contained 16 nodes and 51 interaction pairs, and module D (score=5.273) contained 12 nodes and 29 reciprocity pairs (**Figure 3A**). In addition, Go-BP enrichment analysis of the interacting genes in these modules revealed the top five enrichment results of each module; these were selected for display in order of importance. Among them, the genes of module A were found to be closely related to organelle fission and nuclear division, and the genes of module B were found to be related to platelet degranulation and humoral immune response. The genes in module C were revealed to be related to the negative regulation of the cell cycle process, and to the cell cycle G1/S phase transition. The genes in module D, meanwhile, were found to be related to the G1/S phase transitions of the cell cycle and the mitotic cell cycle (**Figure 3B**).

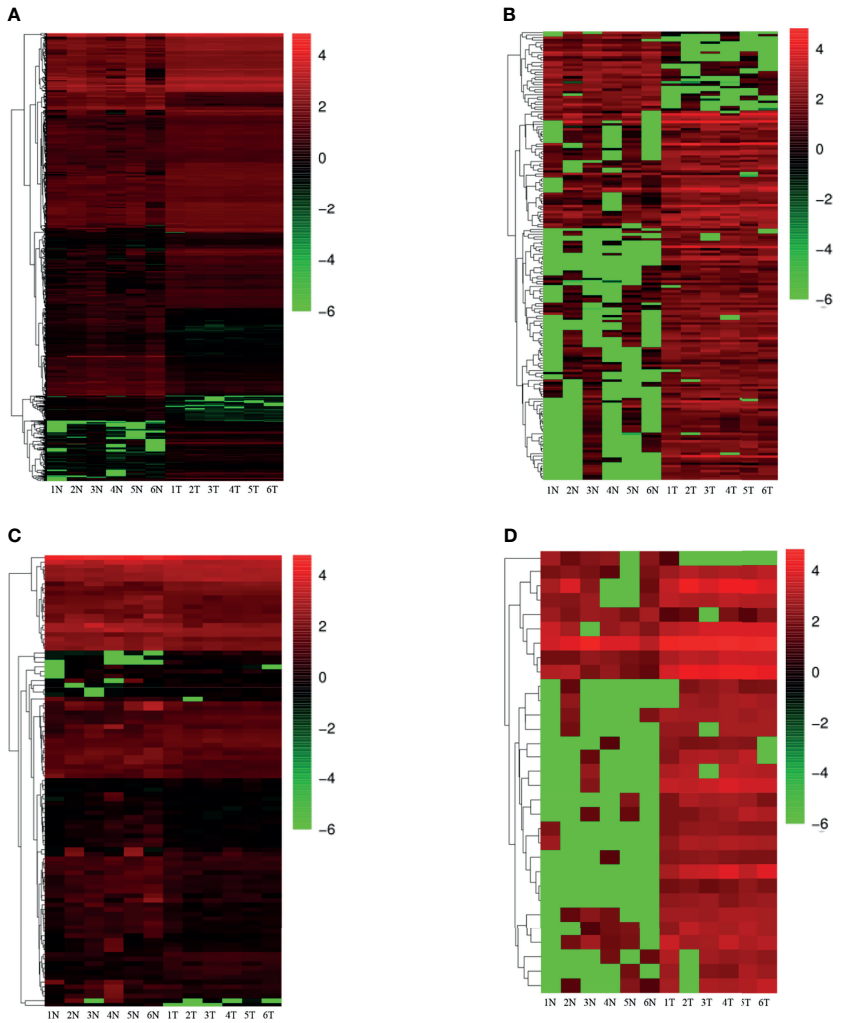

FIGURE 1 | Heatmap of differential expression (N, Normal; T, Tumor) **(A)** differentially expressed mRNAs; **(B)** differentially expressed lncRNAs; **(C)** differentially expressed miRNAs; **(D)** differentially expressed circRNAs. Red indicates up-regulation and green indicates down-regulation.

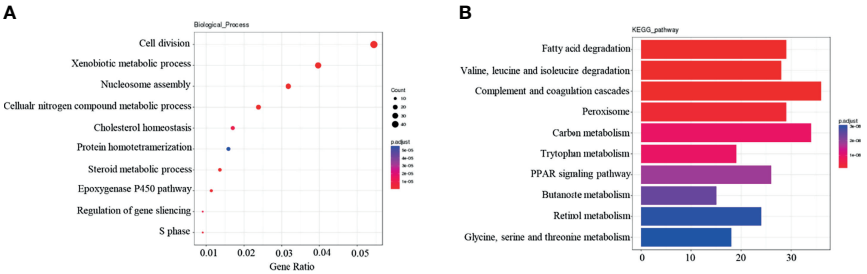

FIGURE 2 | Functional enrichment analysis of Dif-mRNAs: **(A)** Top 10 are enriched for Go-BP terms. **(B)** Top 10 enriched in KEGG pathway.

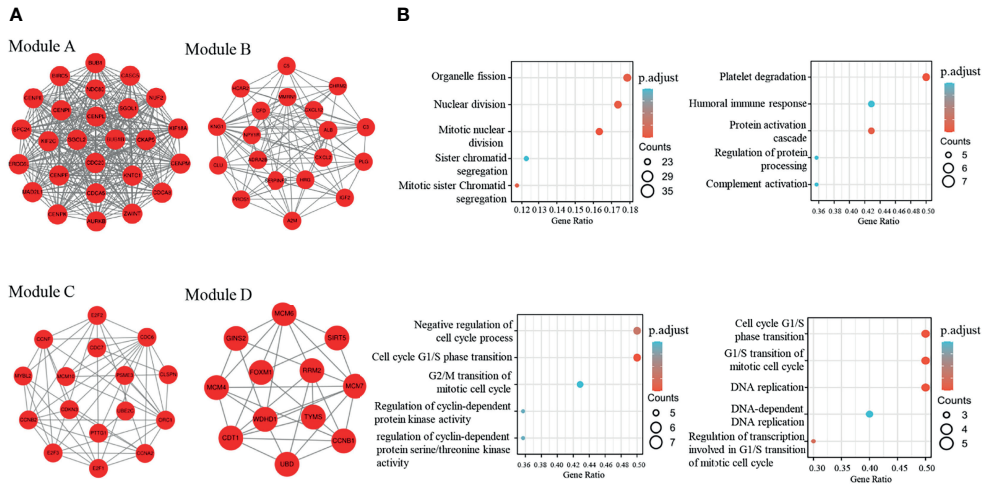

FIGURE 3 | Four modules extracted from the PPI network and GO-BP enrichment analysis of the four modules **(A)** The four modules in the ppi network with a score>5; **(B)** Top5 of GO-BP enrichment analysis of genes in the four modules.

Enrichment Analysis of Dif-lncRNA, Dif-miRNA Targeted Regulation Gene

Functional enrichment analysis of dif-lncRNAs (divided into Cis and Trans dif-lncRNAs) target gene and dif-miRNAs target gene was performed, with the top ten richest results being selected. In GO-BP analysis, Cis dif-lncRNA target gene was found to be significantly related to protein k63-linked ubiquitination and the activation of NF-Kappa B-inducing Kinase activity, among other processes. (**Figure 4A**). Tran dif-lncRNA target gene was shown to be associated with processes such as cell division and the viral modulation of host morphology or physiology (**Figure 4B**). Dif-miRNA target gene was revealed to be significantly related to axon guidance and the neurotrophic tyrosine kinase (Trk) receptor signaling pathway, among other processes (**Figure 4C**). KEGG analysis revealed that Cis dif-lncRNA target gene was significantly correlated with retinol metabolism and chemical carcinogenesis (**Figure 4D**) whereas Tran dif-lncRNA target gene was significantly correlated with the cell cycle and RNA transport (**Figure 4E**). Dif-miRNA target gene was revealed to be associated with pathways in cancer, aldosterone synthesis, and secretion (**Figure 4F**).

CeRNA Network Construction

According to the mutual regulation formation and information of the dif-miRNA-dif-mRNA and dif-miRNA-dif-lncRNA relationships, lncRNAs and mRNAs that were remarkable differentially expressed and mutually regulated on alike miRNAs were screened. Cytoscape was used to construct the lncRNA-miRNA-mRNA ceRNA network (**Figure 5**).

TCGA LIHC Data Verification

After setting the screening thresholds at p <0.05 and fold change >1, screening the TCGA LIHC dif-mRNA, dif-lncRNA, and dif-miRNA data revealed 4,840 dif-mRNAs, 2,616 dif-lncRNAs, and 251 dif-miRNAs. These were compared with the dif-mRNAs, dif-lncRNAs, and dif-miRNAs obtained from Seq analysis and the dif-lncRNAs and dif-miRNAs identified during co-expression analysis. Thus, 805 dif-mRNAs, 6 dif-lncRNAs, and 7 dif-miRNAs were screened; the resulting vine is shown in **Figures 6A–C**. Among these RNAs, all seven dif-miRNAs (**Table 1**) were up-regulated in HCC tissues.

RT-qPCR and Survival Analysis

Seven dif-miRNAs were detected by qRT-PCR, all of which showed significantly higher expression levels in all HCC tissues (**Figures 7A–G**), consistent with the results obtained from the preliminary data. Survival analysis of these seven dif-miRNAs in the Kaplan-Meier database (http://kmplot.com) showed that the overall survival rates of HCC patients with high expression of has-miR-1269a, has-miR-421, and has-miR-190b were significantly lower than those of patients with lower expression of these targets (p<0.05 **Figures 7H–N**). Patients were divided into two groups according to RT-qPCR 2^-ΔΔCT: low expression group and high expression group. Subsequent Kaplan-Meier analysis showed that high expression of has-miR-1269a, has-miR-421 was associated with shorter overall survival (p<0.05, **Figures 8A–C**).

DISCUSSION

HCC is one of the most common malignant tumors of the gastrointestinal tract; it is the sixth-most common malignant tumor worldwide, and has the fourth highest mortality rate. Although surgical resection, radiotherapy, chemotherapy, and liver transplantation have all improved significantly in recent years (22, 23), the prognosis remains unsatisfactory. The recurrence rate remains high five years after surgery (24).

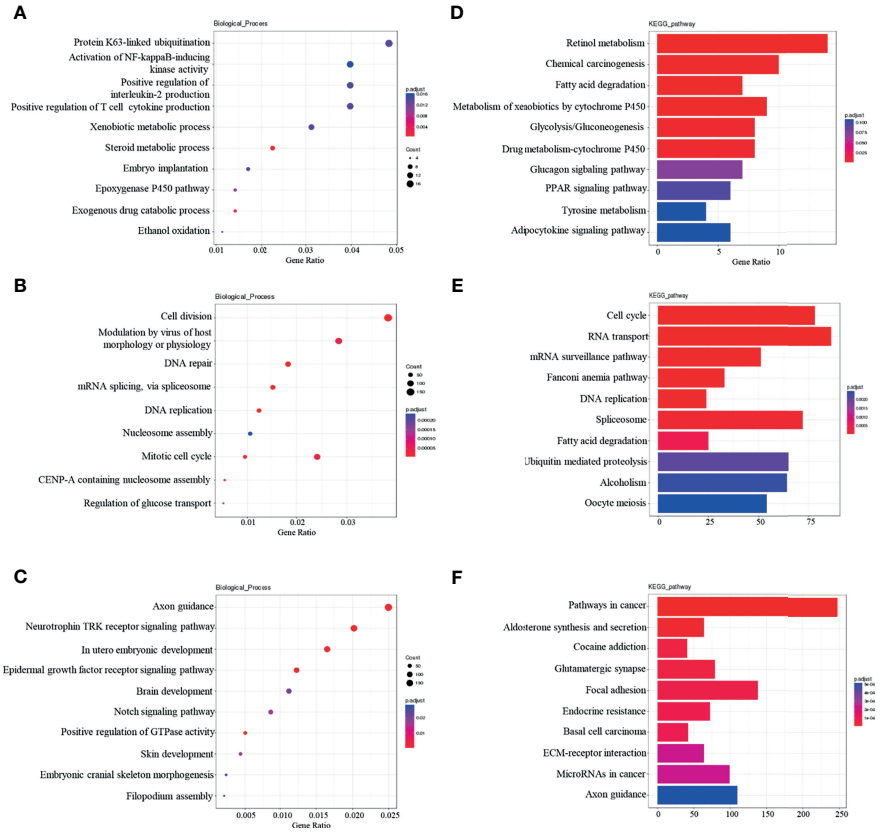

FIGURE 4 | Dif-lncRNAs、Dif-miRNAs GO-BP and KEGG enrichment analysis **(A)** Top10 GO-BP enrichment analysis of cis-lncRNAs target genes; **(B)** Top10 GO-BP enrichment analysis of tran-lncRNAs target genes; **(C)**Top10 GO-BP enrichment analysis of miRNAs target genes; **(D)** Top10 KEGG pathway enrichment analysis of cis-lncRNAs target genes; **(E)** Top10 KEGG pathway enrichment analysis of tran-lncRNAs target genes; **(F)** Top10 KEGG pathway enrichment analysis of miRNAs target genes.

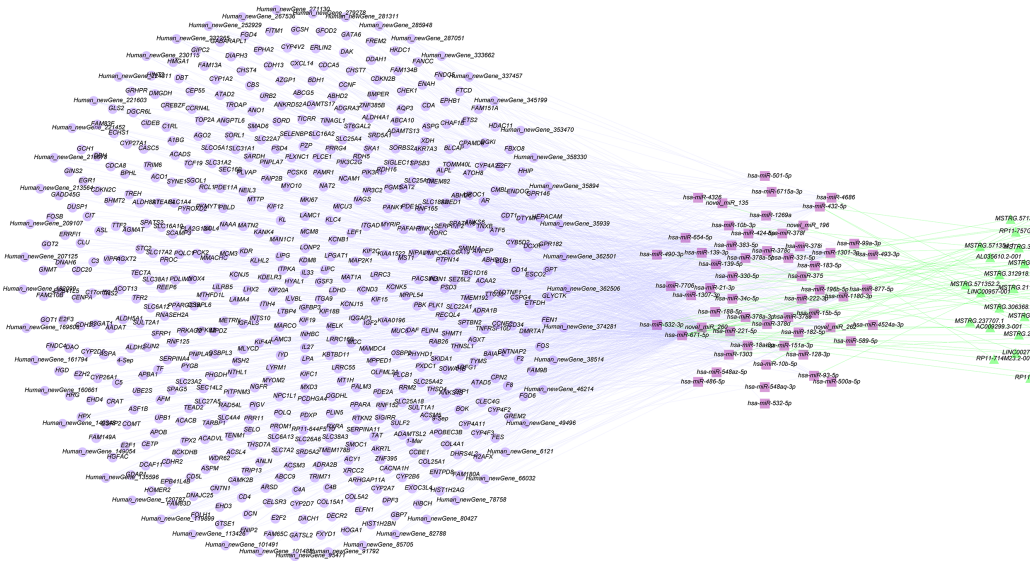

FIGURE 5 | Construction of ceRNA networks by differentially expressed mRNAs, miRNAs and lncRNAs.

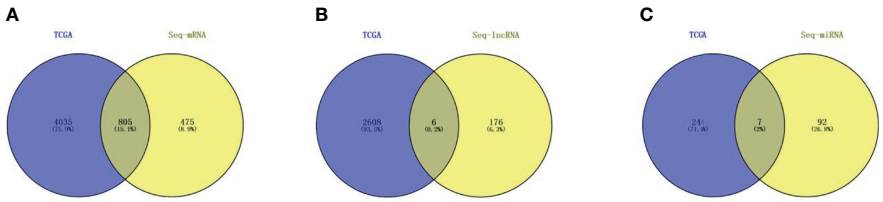

FIGURE 6 | TCGA HCC database and Seq differentially expressed RNAs co-expression analysis **(A)** Dif-mRNAs co-expression analysis; **(B)** Dif-lncRNAs co-expression; **(C)** Dif-miRNAs co-expression.

TABLE 1 | Sequence of each miRNA.

hsa-miR-1269a	5′…CUGGACUGAGCCGUGCUACUGG
hsa-miR-421	5′…AUCAACAGACAUUAAUUGGGCGC
hsa-miR-4326	5′…UGUUCCUCUGUCUCCCAGAC
hsa-miR-7706	5′…UGAAGCGCCUGUGCUCUGCCGAGA
hsa-miR-944	5′…AAAUUAUUGUACAUCGGAUGAG
hsa-miR-190b	5′…UGAUAUGUUUGAUAUUGGGUUG
hsa-miR-217	5′…UACUGCAUCAGGAACUGAUUGGA

Therefore, elucidating the molecular mechanisms and processes of HCC is important for discovering new therapeutic targets and improving the clinical prognoses of patients (13).

CeRNA is a usually used to refer to a class of RNAs, incorporating lncRNAs, miRNAs, mRNAs, and circRNAs. These substances can act as sponges after competitively binding to shared miRNAs. CeRNA networks link protein-coding mRNAs to ncRNAs (e.g., miRNAs and lncRNAs) after participating in the development of tumorigenesis (25, 26).

Here, whole transcriptome sequencing of cancer and paraneoplastic tissues from six HCC patients resulted in the identification of 1,280 dif-mRNAs, 99 dif-miRNAs, 181 dif-lncRNAs and 31 dif-circRNAs. Functional enrichment analysis of dif-mRNAs showed that these differential genes were majorly involved in cell division, xenobiotic metabolic processes, and ribosome assembly. A PPI network was constructed, hub genes were analyzed and identified, and GO-BP enrichment analysis was performed for four modules. These four modules were significantly associated with organelle fission, platelet degranulation, the negative regulation of cell cycle processes, and cell cycle G1/S phase transition. GO-BP and KEGG enrichment analyses were performed for dif-miRNAs, dif-lncRNAs target gene. A ceRNA network of lncRNA-miRNA-mRNA was constructed based on the mutual regulatory dif-miRNA-dif-mRNA and dif-miRNA-dif-lncRNA relationships. In addition, most dif-mRNAs and dif-lncRNAs, and a few dif-miRNAs, were successfully verified by TCGA data. The differences highlighted in both sequencing and TCGA data might be related to sample differences or threshold selection. RT-qPCR validation and survival analysis (using the Kaplan-Meier database) was performed for the seven screened dif-miRNAs.

Few studies have used ceRNA networks to assess the prognosis of HCC, and the discovery of potential biomarkers is crucial to improve the diagnoses and prognoses of HCC patients. It has been shown that the ceRNA networks of breast cancer tissues and matched normal tissues differ, with some ceRNAs being activated in cancerous tissues, leading to the development of breast cancer; they are inactive in normal cells, however (27). Those ceRNAs that are differently expressed in cancer and normal tissues could be used as potential markers. It is well known that miRNAs are an integral part of the cancer development process (28).Thus, studies into the prognostic relevance of miRNA regulatory aspects are essential. In this context, here seven co-expressed dif-miRNAs were validated in HCC tissues, consistent with transcriptome sequencing results and differential miRNA expression in TCGA HCC. Then, survival analysis was performed, revealing that Hsa-miR-1269a, Hsa-miR-421, and Hsa-miR-190b were significantly correlated with overall survival (p <0.05). It has been found that Hsa-miR-1269a is upregulated in advanced colorectal cancer, and that it forms a regenerative feedback loop with the transforming growth factor-beta (TGF-β) signaling pathway to promote metastasis in colorectal cancer (29). Hsa-miR-1269a has been shown to be highly expressed in uveal melanoma and clear cell renal cell carcinoma, interrelated with poor patient prognosis. Therefore, it can be used as a prognostic effect to predict patient survival (30, 31). In serum exosomes, Hsa-miR-1269a plays an oncogenic role in non-small cell lung cancer (NSCLC); it can be used as a diagnostic marker (32). Hsa-miR-421 has been revealed to be highly expressed in NSCLC. Furthermore, upon binding to kelch-like ECH-associated protein 1 (KEAP1) three prime untranslated region (3'UTR), it has been used to forecast low survival in NSCLC (33). On the contrary, the expression of Hsa-miR-421 expression has been found to be downregulated in breast cancer tissues and metastatic cell lines. Decreased levels of its expression have been observed to be associated with lymph node metastasis, recurrence, metastasis, or TNM staging (34). The low expression of Hsa-miR-190b in breast cancer, meanwhile, has been associated with better prognoses (35). Although dif-miRNAs have been validated to some extent, the interconnections of dif-miRNAs in prediction networks have not been discussed. As previously reported, miRNA-1269a facilitates the proliferation and apoptosis of glioma cells by directly targeting ATRX (36). The lncRNA DLEUI increases the expression of rho associated coiled-coil containing protein kinase 1 (ROCK1) *via* Hsa-miR-421, thereby promoting the progress of papillary thyroid carcinoma (37). Furthermore, the lncRNA tumor suppressor candidate 8 (TUSC8) can inhibit the evolution of papillary thyroid carcinoma *via* the miR-190b myosin regulatory light chain interacting protein (MYLIP) axis, which in turn can inhibit breast cancer

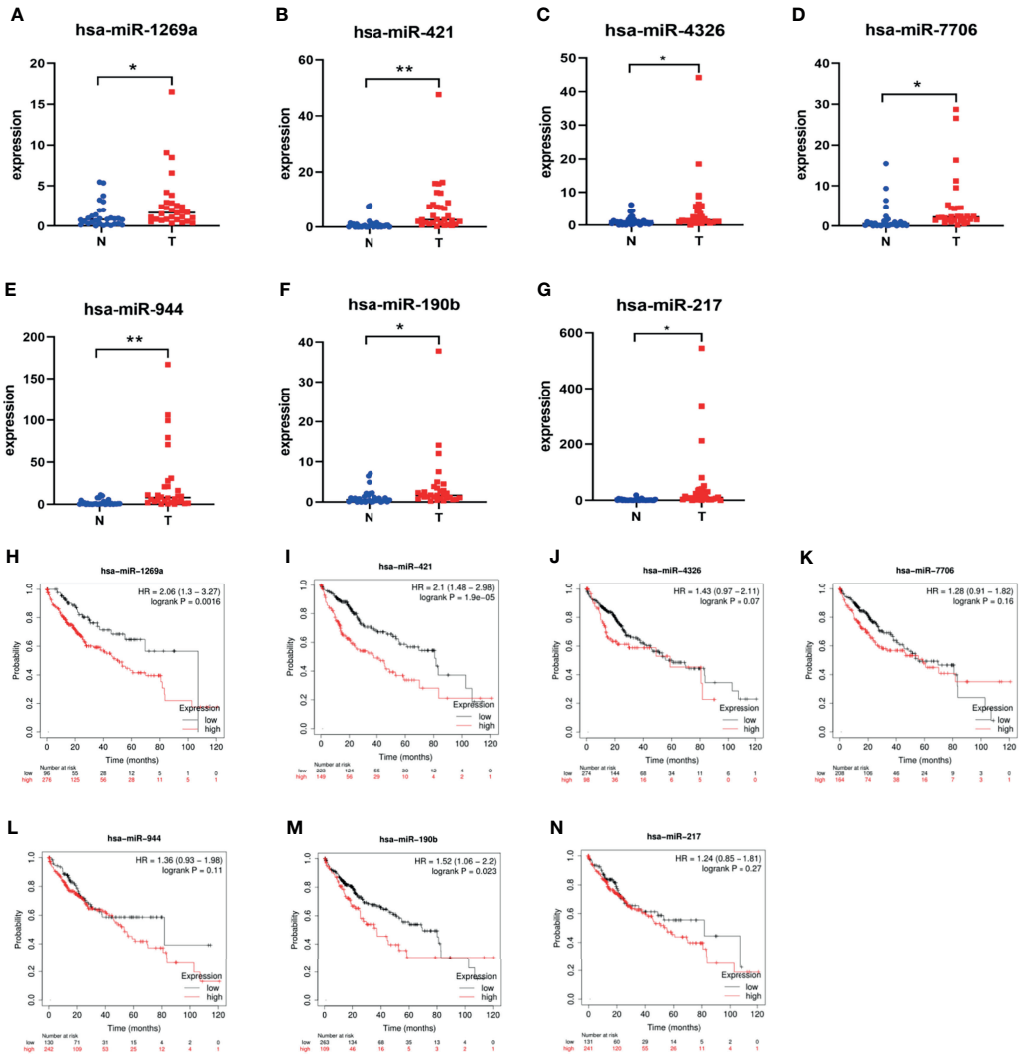

FIGURE 7 | Dif-miRNAs expression in tissue and K-M survival analysis of overall survival (OS) rate **(A)** has-miR-1269a Up-regulation in HCC (*$P < 0.05$); **(B)** has-miR-421 Up-regulation in HCC (**$P < 0.01$); **(C)** has-miR-4326 Up-regulation in HCC (*$P < 0.05$); **(D)** has-miR-7706 Up-regulation in HCC (*$P<0.05$); **(E)** has-miR-944 Up-regulation in HCC (**$P < 0.01$); **(F)** has-miR-190b Up-regulation in HCC ($P < 0.05$); **(G)** has-miR-217 Up-regulation in HCC (*$P < 0.05$); **(H)** Correlation of hsa-miR-1269a with OS ($p < 0.05$); **(I)** Correlation of hsa-miR-421 with OS (*$p < 0.05$); **(J)** Correlation of hsa-miR-4326 with OS; **(K)** Correlation of hsa-miR-7706 with OS; **(L)** Correlation of hsa-miR-944 with OS; **(M)** Correlation of hsa-miR-190b with OS ($p < 0.05$); **(N)** Correlation of hsa-miR-217 with OS.

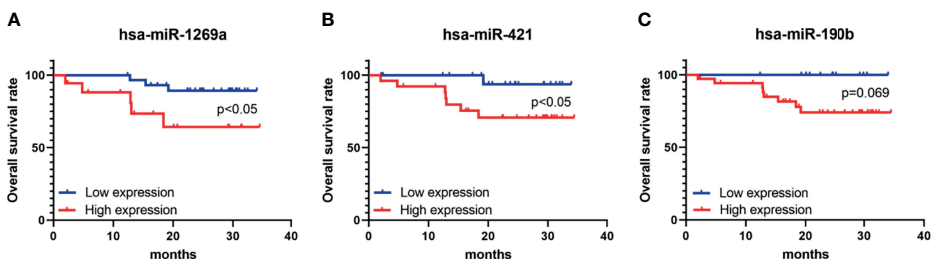

FIGURE 8 | K-M survival analysis of overall survival (OS) of hsa-miR-1269a, hsa-miR-421, and hsa-miR-190b in clinical samples. **(A)** Correlation of hsa-miR-1269a with OS ($p < 0.05$) **(B)** Correlation of hsa-miR-421 with OS ($p < 0.05$) **(C)** Correlation of hsa-miR-4326 with OS.

growth and metastasis (38). Here, miRNA-1269a was found to target binding to six transmembrane epithelial antigen of prostate 4 (STEAP4) and kinase insert domain receptor (KDR). STEAP4 is associated with adipocyte metabolism and mediates hepatocellular carcinogenesis, whereas KDR is a major growth factor of endothelial cells. It is the main mediator in inducing endothelial cell proliferation, survival, migration and tubule morphogenesis; it is also closely related to tumorigenesis and metastasis.

This study also has some limitations, however. First, it is limited by its small sample size regarding the supply of the general situation of the HCC transcriptome; this may have led to analytical bias. In addition, the functions of the identified dif-miRNAs were not been investigated in depth. The predicted lncRNA-miRNA-mRNA interaction networks need to be further confirmed by performing *in vitro* cellular function experiments, and by using animal models to understand the functions and mechanisms behind them. Researchers are currently investigating the direct functions of identified dif-miRNAs and the molecular mechanisms of targeting RNAs.

CONCLUSIONS

In this study, a ceRNA network was constructed based on whole transcriptome sequencing data. When screened in combination with TCGA, seven differentially expressed miRNAs were identified; further validation revealed that three miRNAs Hsa-miR-1269a, Hsa-miR-421, were significantly associated with prognosis. Therefore, these differential miRNAs are expected to be potential biomarkers or therapeutic targets for the prognosis of HCC.

DATA AVAILABILITY STATEMENT

The data presented in the study are deposited in the CNGB Sequence Archive (CNSA) of China National GeneBank DataBase (CNGBdb) repository, accession number CNP0002592.

ETHICS STATEMENT

The studies involving human participants were reviewed and approved by Medical Ethics Committee of the Affiliated Hospital of Qingdao University. The patients/participants provided their written informed consent to participate in this study.

AUTHOR CONTRIBUTIONS

YX, YW, and WX performed the experiments, designed the research, analyzed the data, and wrote the manuscript. HZ, KunL, KuiL, and WZ analyzed the data, and wrote the manuscript. CZ and JC provided reagents and intellectual guidance. All authors contributed to the article and approved the submitted version.

FUNDING

This work was supported by the Taishan Scholars Program of Shandong Province (grant number 2019010668), and the Shandong Higher Education Young Science and Technology Support Program (grant number 2020KJL005).

REFERENCES

1. Yang JD, Hainaut P, Gores GJ, Amadou A, Plymoth A, Roberts LR. A Global View of Hepatocellular Carcinoma: Trends, Risk, Prevention and Management. Nature Reviews. *Gastroenterol Hepatol* (2019) 16(10):589–604. doi: 10.1038/s41575-019-0186-y
2. Global Burden of Disease Cancer Collaboration, Fitzmaurice C, Allen C, Barber RM, Barregard L, Bhutta ZA, et al. Global, Regional, and National Cancer Incidence, Mortality, Years of Life Lost, Years Lived With Disability, and Disability-Adjusted Life-Years for 32 Cancer Groups, 1990 to 2015: A Systematic Analysis for the Global Burden of Disease Study. *JAMA Oncol* (2017) 3(4):524–48. doi: 10.1001/jamaoncol.2016.5688
3. Siegel RL, Miller KD, Jemal A. Cancer Statistics, 2020. *CA: Cancer J Clin* (2020) 70(1):7–30. doi: 10.3322/caac.21590
4. El-Serag HB, Rudolph KL. Hepatocellular Carcinoma: Epidemiology and Molecular Carcinogenesis. *Gastroenterology* (2007) 132(7):2557–76. doi: 10.1053/j.gastro.2007.04.061
5. Ma YS, Huang T, Zhong XM, Zhang HW, Cong XL, Xu H, et al. Proteogenomic Characterization and Comprehensive Integrative Genomic Analysis of Human Colorectal Cancer Liver Metastasis. *Mol Cancer* (2018) 17 (1):139. doi: 10.1186/s12943-018-0890-1
6. Ma YS, Wu ZJ, Zhang HW, Cai B, Huang T, Long HD, et al. Dual Regulatory Mechanisms of Expression and Mutation Involving Metabolism-Related Genes FDFT1 and UQCR5 During CLM. *Mol Ther Oncolytics* (2019) 14:172–8. doi: 10.1016/j.omto.2019.04.008
7. Harding JJ, Nandakumar S, Armenia J, Khalil DN, Albano M, Ly M, et al. Prospective Genotyping of Hepatocellular Carcinoma: Clinical Implications of Next-Generation Sequencing for Matching Patients to Targeted and Immune Therapies. *Clin Cancer Res* (2019) 25(7):2116–26. doi: 10.1158/1078-0432.CCR-18-2293
8. Zhang G, Tang X, Liang L, Zhang W, Li D, Li X, et al. DNA and RNA Sequencing Identified a Novel Oncogene VPS35 in Liver Hepatocellular Carcinoma. *Oncogene* (2020) 39(16):3229–44. doi: 10.1038/s41388-020-1215-6
9. Yu F, Liu JB, Wu ZJ, Xie WT, Zhong XJ, Hou LK, et al. Tumor Suppressive microRNA-124a Inhibits Stemness and Enhances Gefitinib Sensitivity of Non-Small Cell Lung Cancer Cells by Targeting Ubiquitin-Specific Protease 14. *Cancer Lett* (2018) 427:74–84. doi: 10.1016/j.canlet.2018.04.022
10. Ma YS, Lv ZW, Yu F, Chang ZY, Cong XL, Zhong XM, et al. MicroRNA-302a/D Inhibits the Self-Renewal Capability and Cell Cycle Entry of Liver Cancer Stem Cells by Targeting the E2F7/AKT Axis. *J Exp Clin Cancer Res: CR* (2018) 37(1):252. doi: 10.1186/s13046-018-0927-8
11. Sumazin P. Et Al, An Extensive microRNA-Mediated Network of RNA-RNA Interactions Regulates Established Oncogenic Pathways in Glioblastoma. *Cell* (2011) 147(2):370–81. doi: 10.1016/j.cell.2011.09.041
12. Tay Y, Kats L, Salmena L, Weiss D, Tan SM, Ala U, et al. Coding-Independent Regulation of the Tumor Suppressor PTEN by Competing Endogenous mRNAs. *Cell* (2011) 147(2):344–57. doi: 10.1016/j.cell.2011.09.029
13. Long J, Bai Y, Yang X, Lin J, Yang X, Wang D, et al. Construction and Comprehensive Analysis of a ceRNA Network to Reveal Potential Prognostic Biomarkers for Hepatocellular Carcinoma. *Cancer Cell Int* (2019) 19:90. doi: 10.1186/s12935-019-0817-y
14. Ju Q, Zhao YJ, Ma S, Li XM, Zhang H, Zhang SQ, et al. Genome-Wide Analysis of Prognostic-Related lncRNAs, miRNAs and mRNAs Forming a

Competing Endogenous RNA Network in Lung Squamous Cell Carcinoma. *J Cancer Res Clin Oncol* (2020) 146(7):1711–23. doi: 10.1007/s00432-020-03224-8
15. Zhao Y, Zhang H, Ju Q, Li X, Zheng Y. Comprehensive Analysis of Survival-Related lncRNAs, miRNAs, and mRNAs Forming a Competing Endogenous RNA Network in Gastric Cancer. *Front Genet* (2021) 12:610501. doi: 10.3389/fgene.2021.610501
16. Ju Q, Zhao YJ, Dong Y, Cheng C, Zhang S, Yang Y, et al. Identification of a miRNA-mRNA Network Associated With Lymph Node Metastasis in Colorectal Cancer. *Oncol Lett* (2019) 18(2):1179–88. doi: 10.3892/ol.2019.10460
17. Zhang YJ, Ma YS, Xia Q, Yu F, Lv ZW, Jia CY, et al. MicroRNA–mRNA Integrated Analysis Based on a Case of Well–Differentiated Thyroid Cancer With Both Metastasis and Metastatic Recurrence. *Oncol Rep* (2018) 40 (6):3803–11. doi: 10.3892/or.2018.6739
18. Bandettini WP, Kellman P, Mancini C, Booker OJ, Vasu S, Leung SW, et al. MultiContrast Delayed Enhancement (MCODE) Improves Detection of Subendocardial Myocardial Infarction by Late Gadolinium Enhancement Cardiovascular Magnetic Resonance: A Clinical Validation Study. *J Cardiovasc Magn Reson* (2012) 14:83. doi: 10.1186/1532-429X-14-83
19. Du JW, Li GQ, Li YS, Qiu XG. Identification of Prognostic Biomarkers Related to the Tumor Microenvironment in Thyroid Carcinoma. *Sci Rep* (2021) 11 (1):16239. doi: 10.1038/s41598-021-90538-3
20. Smoot ME, Ono K, Ruscheinski J, Wang PL, Ideker T. Cytoscape 2.8: New Features for Data Integration and Network Visualization. *Bioinformatics* (2011) 27(3):431–2. doi: 10.1093/bioinformatics/btq675
21. Xu X, Kong X, Liu T, Zhou L, Wu J, Fu J, et al. Metastasis-Associated Protein 1, Modulated by miR-30c, Promotes Endometrial Cancer Progression Through AKT/mTOR/4E-BP1 Pathway. *Gynecol Oncol* (2019) 154(1):207–17. doi: 10.1016/j.ygyno.2019.04.005
22. Tang A, Hallouch O, Chernyak V, Kamaya A, Sirlin CB. Epidemiology of Hepatocellular Carcinoma: Target Population for Surveillance and Diagnosis. *Abdominal Radiol* (2018) 43(1):13–25. doi: 10.1007/s00261-017-1209-1
23. Rudnick SR, Russo MW. Liver Transplantation Beyond or Downstaging Within the Milan Criteria for Hepatocellular Carcinoma. *Expert Rev Gastroenterol Hepatol* (2018) 12(3):265–75. doi: 10.1080/17474124.2018.1417035
24. Li J, Wu PW, Zhou Y, Dai B, Zhang PF, Zhang YH, et al. Rage Induces Hepatocellular Carcinoma Proliferation and Sorafenib Resistance by Modulating Autophagy. *Cell Death Dis* (2018) 9(2):225. doi: 10.1038/s41419-018-0329-z
25. Salmena L, Poliseno L, Tay Y, Kats L, Pandolfi PP. A ceRNA Hypothesis: The Rosetta Stone of a Hidden RNA Language? *Cell* (2011) 146(3):353–8. doi: 10.1016/j.cell.2011.07.014
26. Qi X, Zhang DH, Wu N, Xiao JH, Wang X, Ma W. ceRNA in Cancer: Possible Functions and Clinical Implications. *J Med Genet* (2015) 52(10):710–8. doi: 10.1136/jmedgenet-2015-103334
27. Conte F, Fiscon G, Chiara M, Colombo T, Farina L, Paci P. Role of the Long Non-Coding RNA PVT1 in the Dysregulation of the ceRNA-ceRNA Network in Human Breast Cancer. *PLoS One* (2017) 12(2):e0171661. doi: 10.1371/journal.pone.0171661
28. Patel N, Garikapati KR, Makani VKK, Nair AD, Vangara N, Bhadra U, et al. Regulating BMI1 Expression *via* miRNAs Promote Mesenchymal to Epithelial Transition (MET) and Sensitizes Breast Cancer Cell to Chemotherapeutic Drug. *PLoS One* (2018) 13(2):e0190245. doi: 10.1371/journal.pone.0190245
29. Bu P, Wang L, Chen KY, Rakhilin N, Sun J, Closa A, et al. miR-1269 Promotes Metastasis and Forms a Positive Feedback Loop With TGF-β. *Nat Commun* (2015) 6:6879. doi: 10.1038/ncomms7879
30. Zhao D-D, Zhao X, Li W-T. Identification of Differentially Expressed Metastatic Genes and Their Signatures to Predict the Overall Survival of Uveal Melanoma Patients by Bioinformatics Analysis. *Int J Ophthalmol* (2020) 13(7):1046–53. doi: 10.18240/ijo.2020.07.05
31. Qin S, Shi X, Wang C, Jin P, Ma F. Transcription Factor and miRNA Interplays Can Manifest the Survival of ccRCC Patients. *Cancers* (2019) 11 (11). doi: 10.3390/cancers11111668
32. Wang X, Jiang X, Li J, Wang J, Binang H, Shi S, et al. Serum Exosomal miR-1269a Serves as a Diagnostic Marker and Plays an Oncogenic Role in Non-Small Cell Lung Cancer. *Thorac Cancer* (2020) 11(12):3436–47. doi: 10.1111/1759-7714.13644
33. Duan FG, Wang MF, Cao YB, Dan Li, Li RZ, Fan XX, et al. MicroRNA-421 Confers Paclitaxel Resistance by Binding to the KEAP1 3'UTR and Predicts Poor Survival in Non-Small Cell Lung Cancer. *Cell Death Dis* (2019) 10 (11):821. doi: 10.1038/s41419-019-2031-1
34. Pan Y, Jiao G, Wang C, Yang J, Yang W. MicroRNA-421 Inhibits Breast Cancer Metastasis by Targeting Metastasis Associated 1. *Biomed pharmacother = Biomed Pharmacother* (2016) 83:1398–406. doi: 10.1016/j.biopha.2016.08.058
35. Gong PJ, Shao YC, Huang SR, Zeng YF, Yuan XN, Xu JJ, et al. Hypoxia-Associated Prognostic Markers and Competing Endogenous RNA Co-Expression Networks in Breast Cancer. *Front Oncol* (2020) 10:579868. doi: 10.3389/fonc.2020.579868
36. Zhang Y, Wang Q, Luo N, Liu J, Ren H, Shao X, et al. MicroRNA-1269a Promotes Proliferation and Arrest of Apoptosis of Glioma Cells by Directly Targeting ATRX. *Front Oncol* (2020) 10:563901. doi: 10.3389/fonc.2020.563901
37. Li R, Wan T, Qu J, Yu Y, Zheng R. Long Non-Coding RNA DLEUI Promotes Papillary Thyroid Carcinoma Progression by Sponging miR-421 and Increasing ROCK1 Expression. *Aging* (2020) 12(20):20127–38. doi: 10.18632/aging.103642
38. Zhao L, Zhou Y, Zhao Y, Li Q, Zhou J, Mao Y. Long Non-Coding RNA TUSC8 Inhibits Breast Cancer Growth and Metastasis *via* miR-190b-5p/MYLIP Axis. *Aging* (2020) 12(3):2974–91. doi: 10.18632/aging.102791

Conflict of Interest: The authors declare that the research was conducted in the absence of any commercial or financial relationships that could be construed as a potential conflict of interest.

frontiers in Oncology

ORIGINAL RESEARCH
published: 07 February 2022
doi: 10.3389/fonc.2022.787897

ARID1A Downregulation Predicts High PD-L1 Expression and Worse Clinical Outcome in Patients With Gallbladder Cancer

Lingxi Nan[1,2,3†], *Changcheng Wang*[1,2,3†], *Jie Wang*[4], *Shulong Zhang*[2,3,5], *Xiaobo Bo*[1,2,3*], *Yueqi Wang*[1,6*] *and Houbao Liu*[1,2,3,5*]

[1] Department of General Surgery, Zhongshan Hospital, Fudan University, Shanghai, China, [2] Biliary Tract Diseases Institute, Fudan University, Shanghai, China, [3] Shanghai Engineering Research Center of Biliary Tract Minimal Invasive Surgery and Materials, Shanghai, China, [4] Department of Thoracic Surgery, Fudan University Shanghai Cancer Center, Shanghai, China, [5] Department of General Surgery, Xuhui District Central Hospital, Shanghai, China, [6] Cancer Center, Zhongshan Hospital, Fudan University, Shanghai, China

Background: Recent studies have confirmed that AT-rich interactive domain-containing protein 1A (ARID1A) plays a critical role in tumorigenesis, but its role in gallbladder cancer (GBC) remains unclear.

Methods: In total, 224 patients from Zhongshan Hospital were recruited for this retrospective study. The clinicopathological and baseline characteristics of the patients were collected. Bioinformatics analysis was performed to reveal variations in genes and signaling pathways, and ARID1A and PD-L1 expression and the number of PD1+ tumor-infiltrating lymphocytes (TILs) were measured by immunohistochemical staining.

Results: ARID1A expression was negatively correlated with overall survival in patients with GBC, and multivariate analysis identified ARID1A as an independent prognostic factor for overall survival. A heatmap and gene set enrichment analysis suggested that cytotoxic T lymphocyte signatures and immune-related signaling pathways were downregulated in ARID1A low tumors. Subsequent immunohistochemical staining confirmed that ARID1A expression was negatively correlated with PD-L1 expression and PD1+ TILs in the tumor microenvironment. The Kaplan–Meier analysis suggested that high ARID1A expression combined with low PD-L1 expression or low PD1+ TIL counts is associated with the best prognosis in patients with GBC.

Conclusion: ARID1A inactivation can lead to a worse prognosis in patients with GBC, potentially by mediating immune evasion through the PD1/PD-L1 pathway.

Keywords: ARID1A, gallbladder cancer, PD-L1, PD1, prognosis, tumor immune

OPEN ACCESS

Edited by:
Yunfei Xu,
Shandong University, China

Reviewed by:
Takeo Toshima,
Kyushu University, Japan
Xiangsong Wu,
Shanghai Jiao Tong University School of Medicine, China

***Correspondence:**
Yueqi Wang
yueqiwang@fudan.edu.cn
Xiaobo Bo
boxiaobo2016@hotmail.com
Houbao Liu
houbaoliu@aliyun.com

†*These authors have contributed equally to this work*

Specialty section:
This article was submitted to Cancer Molecular Targets and Therapeutics, a section of the journal Frontiers in Oncology

Received: *26 October 2021*
Accepted: *05 January 2022*
Published: *07 February 2022*

Citation:
Nan L, Wang C, Wang J, Zhang S, Bo X, Wang Y and Liu H (2022) ARID1A Downregulation Predicts High PD-L1 Expression and Worse Clinical Outcome in Patients With Gallbladder Cancer. Front. Oncol. 12:787897. doi: 10.3389/fonc.2022.787897

INTRODUCTION

Gallbladder cancer (GBC) is a rare malignant tumor of the digestive tract and the most common malignancy of the biliary tract system. Most patients with GBC already have advanced disease at diagnosis, and the 5-year survival rate is less than 5% (1). At present, the prognosis of patients with GBC is mainly predicted according to the clinical and pathological stages, such as TNM and the American Joint Committee on Cancer (AJCC) stage (2). However, the lack of tumor markers represents a significant deficiency of these staging systems. There is thus an urgent need to identify novel biomarkers to facilitate the prediction of prognosis in GBC.

The switch/sucrose non-fermentable (SWI/SNF) chromatin remodeling protein complex, which consists of 12–15 subunits, is assembled from the products of 29 genes (3). The SWI/SNF complex can alter the structure of chromatin and regulate gene expression by utilizing energy generated by ATP hydrolysis (4). The results of gene sequencing illustrated that mutations in the SWI/SNF complex accounted for approximately 20% of mutations in cancers, making it the most frequently mutated tumor suppressor in cancer (5). ARID1A is the core subunit of the SWI/SNF complex, and it can interact with DNA in a sequence-non-specific manner. ARID1A is also the most frequently mutated subunit of the SWI/SNF complex (6, 7). In the last decade, the role of ARID1A in tumors has been widely investigated, and ARID1A mutations were commonly observed in multiple cancers (5, 8). These mutations, which are primarily non-sense or frameshift mutations, can lead to the deficiency of ARID1A and further tumorigenesis (9). Recent genomic studies illustrated that ARID1A is mutated in biliary malignancies at a rate of up to 18% (10–13). Many researchers demonstrated that ARID1A inactivation is correlated with worse prognosis in patients with biliary cancer (11, 14, 15).

Recently, the tumor microenvironment (TME) has emerged as a promising target for cancer treatment, and the PD1/PD-L1 pathway plays an important role in immune evasion in TME. Some recent studies revealed the correlation between ARID1A and the PD1/PD-L1 pathway. In particular, PD-L1 expression was significantly increased in ARID1A-mutated cancers (16, 17), which could lead to impaired tumor immunity, and this might represent a potential mechanism by which ARID1A-deficient tumors escape immune surveillance.

To date, few studies have examined ARID1A mutation in patients with GBC, and its effect on the PD1/PD-L1 pathway and the prognosis of patients with GBC remains unclear. In this study, patients with GBC with low ARID1A expression had a poor prognosis, and further bioinformatics analysis illustrated that certain immune-related pathways were suppressed in ARID1A-low tumors. Immunohistochemistry (IHC) revealed that ARID1A expression was negatively correlated with PD-L1 expression and PD1+ T-cell infiltration in GBC. We propose that ARID1A inactivation could lead to a worse prognosis in patients with GBC, possibly because of impaired immune surveillance in the TME.

MATERIALS AND METHODS

Patient Cohort

This retrospective study enrolled 244 consecutive patients with GBC who underwent surgical resection between January 2008 and December 2013 at Zhongshan Hospital, Fudan University. The diagnosis of GBC was based on preoperative imaging results, intraoperative exploration, and postoperative pathological reports. Written informed consent was obtained from all patients, and the study was approved by the ethics committee of Fudan University. The inclusion criteria were as follows: 1) age ≥ 18 years; 2) confirmation of GBC; 3) complete clinical and baseline data available; and 4) receipt of radical surgery for GBC. The exclusion criteria were as follows: 1) presence of other tumors or chronic diseases; 2) incomplete clinical or follow-up data; and 3) failure of immunohistochemical staining. Among the enrolled patients, four were excluded because of failed immunostaining, and 16 patients were excluded because of incomplete follow-up data. Finally, 224 patients with GBC were included in this cohort.

Data Extraction

The clinicopathological and baseline characteristics of the patients, including age, gender, tumor differentiation, residual tumor, vascular invasion, and TNM stage, were collected retrospectively. The clinical staging of GBC was performed according to the eighth edition of the AJCC staging manual. Follow-up data were collected at an interval of 3 months, and overall survival (OS) was calculated from the date of surgery to that of death or the last visit.

Tissue Microarray and Immunohistochemistry

Tissue microarray (TMA) was established in this study using formalin-fixed, paraffin-embedded surgical specimens, and the specimens were stained immunohistochemically using appropriate antibodies (anti-ARID1A [1:600, ab182560, Abcam, USA]; anti-PD-L1 [1:200, SP142, Roche, Switzerland]; anti-PD1 [1:100, ab52587, Abcam]; anti-CD8 [1:400, ab4055, Abcam]). The ARID1A staining score was calculated as the percentage of positive tumor cells (0%–100%) multiplied by the staining intensity score (0 = negative, 1 = weak, 2 = moderate, and 3 = strong). The calculation of the PD-L1 staining score followed the criteria of the IMpower110 study (18), with some changes (TC% = 0, IHC0; 0 < TC% < 1%, IHC1; 1% < TC % < 50%, IHC2; TC% ≥ 50%, IHC3). Images were acquired using a Nikon Eclipse Ti-S microscope, whereas the numbers of PD1+ tumor-infiltrating lymphocytes (TILs) per field, and CD8+ cells per field were calculated using Image-Pro Plus 6.0 software. The cutoff delineating the high and low expression subgroups was determined by the minimum p-value method using X-title software. Identical settings were applied in each photograph.

Gene Set Enrichment Analysis

Despite the lack of data on GBC in The Cancer Genome Atlas (TCGA), cholangiocarcinoma data were collected for differential expression analysis because the gallbladder shares the same

embryonic origin as bile ducts. This is a routine workaround in the bioinformatics analysis of GBC. In total, 36 cases of cholangiocarcinoma from TCGA were analyzed, and mRNA expression data were downloaded from cBioPortal in the RSEM format. Gene Set Enrichment Analysis (GSEA) was performed to analyze the divergences of biological pathways between high and low ARID1A expression, and the differential gene expression between the high and low expression groups was explored using the edgeR package. The cutoff of ARID1A expression was determined as the median.

Statistical Analyses

Statistical analysis was performed using SPSS (version 25.0), Medcalc Software (version 19.0.4), Stata (version 16.0), and GraphPad Prism 8 (version 8.0.2). Patients' baseline and clinicopathological characteristics were compared using Pearson's chi-square test, Fisher's exact test, and the *t*-test. OS curves were plotted using the Kaplan–Meier method, and the differences between subgroups were analyzed using the log-rank test. Independent prognostic variables were identified by Cox univariate and multivariate regression analyses. All statistical analyses were two-sided, and statistical significance was indicated by $p < 0.05$.

RESULTS

Correlation Between ARID1A Expression and the Prognosis of Patients With Gallbladder Cancer

Immunohistochemical staining was performed using 224 GBC TMAs, and the typical images of high and low ARID1A expression are presented in **Figure 1A**. Based on the cutoff, 98 patients were included in the high ARID1A expression subgroup, and 126 patients were separated into the low ARID1A expression subgroup. The correlations between clinicopathological characteristics and ARID1A expression are presented in **Table 1**. Remarkably, lower ARID1A expression in GBC tissues was positively correlated with the TNM stage ($p = 0.007$, **Figure 1B**), whereas multivariate Cox regression analysis identified ARID1A expression as an independent prognostic factor ($p < 0.001$, **Figure 1C**). The Kaplan–Meier analysis suggested that patients with high ARID1A expression had longer OS than those with low ARID1A expression ($p = 0.002$, **Figure 1D**). We conclude that ARID1A expression is significantly correlated with patient prognosis in GBC, whereas high ARID1A expression predicts a better prognosis.

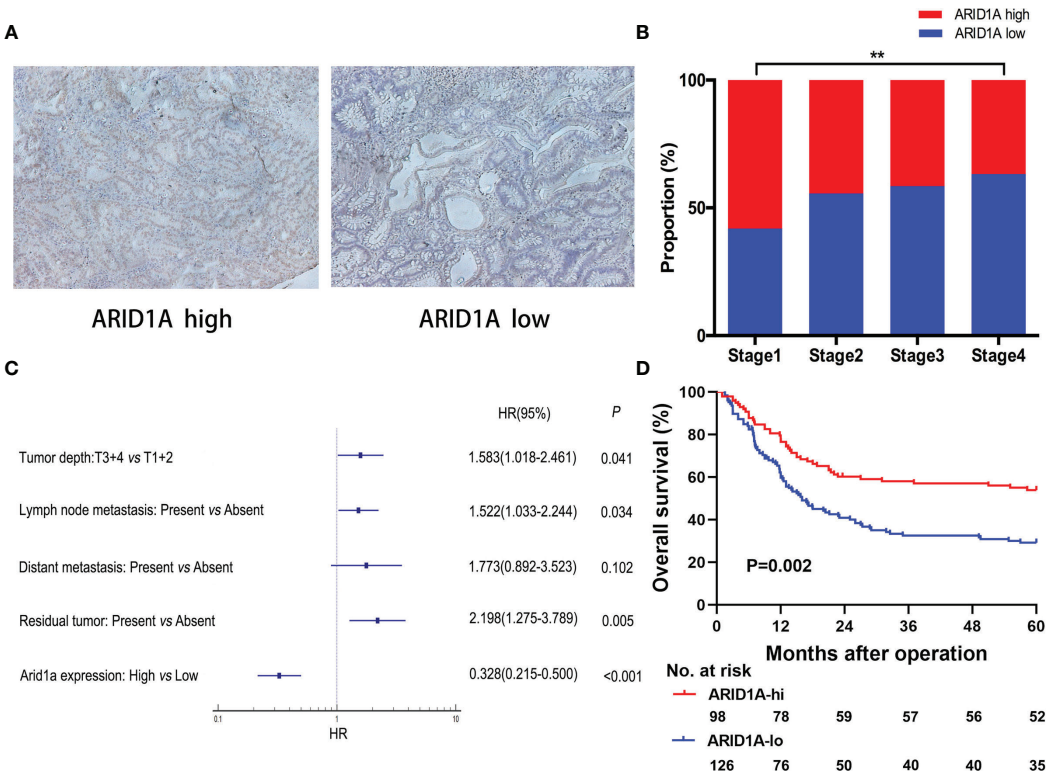

FIGURE 1 | Evaluation of AT-rich interactive domain 1A (ARID1A) expression by immunohistochemical staining in patients with gallbladder cancer (GBC). **(A)** Representative immunohistochemical images of tumor tissues with high or low ARID1A expression. **(B)** Proportions of different TNM stages in patients with high or low ARID1A expression. **(C)** Multivariate Cox regression analysis identified ARID1A expression as an independent prognostic factor for overall survival. **(D)** Kaplan–Meier survival analysis of overall survival in all patients. **P < 0.01.

TABLE 1 | Correlations between ARID1A expression and patient characteristics.

Characteristic	Patients (n = 224)		ARID1A expression		p^a
	Number	%	Low (n = 126)	High (n = 98)	
Age at surgery, years[b]					**0.022**
Mean ± SD	63.55 ± 11.39		62.02 ± 11.28	65.52 ± 11.29	
Gender					0.465
Female	161	71.9	93	68	
Male	63	28.1	33	30	
Tumor location					0.938
Perihilar	26	11.6	14	12	
Distal	29	12.9	17	12	
Gallbladder	169	75.5	95	74	
pT stage					0.791
T2	139	62.1	76	63	
T3	67	29.9	40	27	
T4	18	8	10	8	
pN stage					0.129
N0	181	80.8	97	84	
N1,2	43	19.2	29	14	
M stage					0.167
M0	209	93.3	115	94	
M1	15	6.7	11	4	
TNM stage					0.621
I	27	12.1	13	14	
II	100	44.6	54	46	
III	63	28.1	38	25	
IV	34	15.2	21	13	
Tumor differentiation					0.554
Well, moderate	101	45.1	59	42	
Poor	123	54.9	67	56	
Residual tumor					0.677
R0	201	89.3	114	87	
R1	23	10.7	12	11	
Vascular invasion					0.420
Absent	166	73.4	96	70	
Present	58	26.6	30	28	

ARID1A, AT-rich interactive domain 1A.

[a]*$p < 0.05$ is considered statistically significant.*

[b]*The results of continuous variables are presented as the mean ± SD.*

Bold values represent significant p-values (P <0.05).

ARID1A Downregulation Correlated With T-Cell Inactivation in The Cancer Genome Atlas Dataset

To investigate the potential mechanism of ARID1A in GBC, we investigated gene profiles using TCGA cholangiocarcinoma cohort. As illustrated in **Figure 2A**, ARID1A expression was positively correlated with activated CD8+ T-cell signatures. To further explore the role of ARID1A, differential gene expression analyses were performed. As depicted in **Figure 2B**, genes involved in T-cell activation (e.g., GZMM, CD8A, TIGIT, and IFNG) and T-cell recruitment (e.g., CXCR3) were significantly downregulated in the low ARID1A expression group. We then performed GSEA to determine potential immune lineage changes related to ARID1A expression. Of note, multiple T-cell activation-related processes and signaling pathways were downregulated in tumors with low ARID1A expression, including allograft rejection, inflammatory response, TNF-α, and interferon-gamma (IFN-γ) signaling pathways (**Figure 2C**). These results suggest that ARID1A downregulation mediates immune evasion by impairing T-cell proliferation and activation in the biliary cancer TME.

Decreased ARID1A Expression Is Correlated With High PD-L1 Expression and Increased PD1+ Tumor-Infiltrating Lymphocyte Infiltration in the Gallbladder Cancer Tissue Microarray Dataset

The downregulation of multiple T cell-related pathways, especially the TNF-α and IFN-γ signaling pathways, suggested the possible involvement of the PD1/PD-L1 pathway in the observed mechanism of ARID1A. Thus, we investigated the relationships of ARID1A with PD-L1 expression and PD1+ TIL counts through IHC and found that GBC tissue specimens with low ARID1A expression exhibited increased PD-L1 expression, and they were more likely to display greater PD1+ TIL infiltration (**Figure 3A**). Further, we investigated the correlation between ARID1A and PD-L1 expression, and the result revealed that the proportion of PD-L1-positive GBC tissue

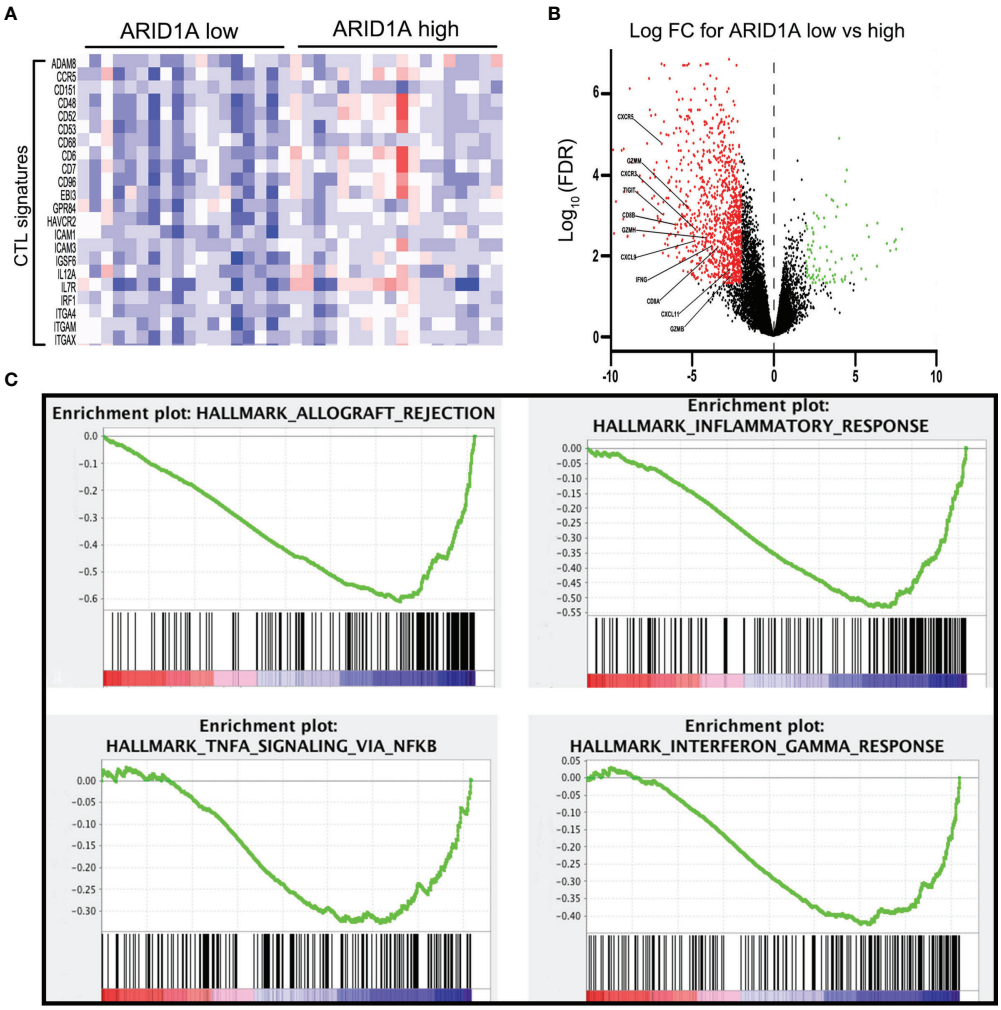

FIGURE 2 | Bioinformatics analysis revealed the regulation of immune-related genes and signaling pathways in AT-rich interactive domain 1A (ARID1A)-inactivated tumors. **(A)** Heatmap of cytotoxic T lymphocyte (CTL) signatures in tumors with high or low ARID1A expression. **(B)** Volcano plot presenting the downregulation of genes involved in CD8+ T-cell activation in ARID1A-inactivated tumors. **(C)** Gene set enrichment analysis revealed the downregulation of the immune-related pathway in ARID1A-inactivated tumors.

specimens was much higher in the ARID1A-low group than in the ARID1A-high group ($p = 0.035$, **Figure 3B**). Meanwhile, the proportion of GBC tissues with strongly positive PD-L1 staining on IHC (IHC score ≥ 2) was also higher in the ARID1A-low group, although the result was not statistically different ($p = 0.150$, **Figure 3C**). We also confirmed a negative correlation between ARID1A expression and the number of PD1+ TILs in GBC tissue ($p < 0.001$, **Figure 3D**).

Low PD-L1 Expression or Reduced PD1+ Tumor-Infiltrating Lymphocyte Infiltration Combined With High ARID1A Expression Is Associated With the Best Prognosis in Gallbladder Cancer

We assessed the impact of ARID1A expression, PD-L1 expression, and PD1+ TIL infiltration on the survival of patients with GBC. According to the Kaplan–Meier analysis, patients with high ARID1A expression and low PD-L1 expression in GBC tissue had the best OS ($p < 0.001$, **Figure 4A**). Further analysis revealed that patients with high ARID1A expression and less PD1+ TIL infiltration had markedly better OS than the other patient subgroups ($p < 0.001$, **Figure 4B**).

DISCUSSION

The SWI/SNF complex utilizes energy from ATP hydrolysis to mobilize nucleosomes and alter the accessibility of DNA (19). Prior studies revealed that mutations in genes encoding SWI/SNF subunits were correlated with multiple malignancies (20, 21). ARID1A, which directly interacts with chromatin as a core

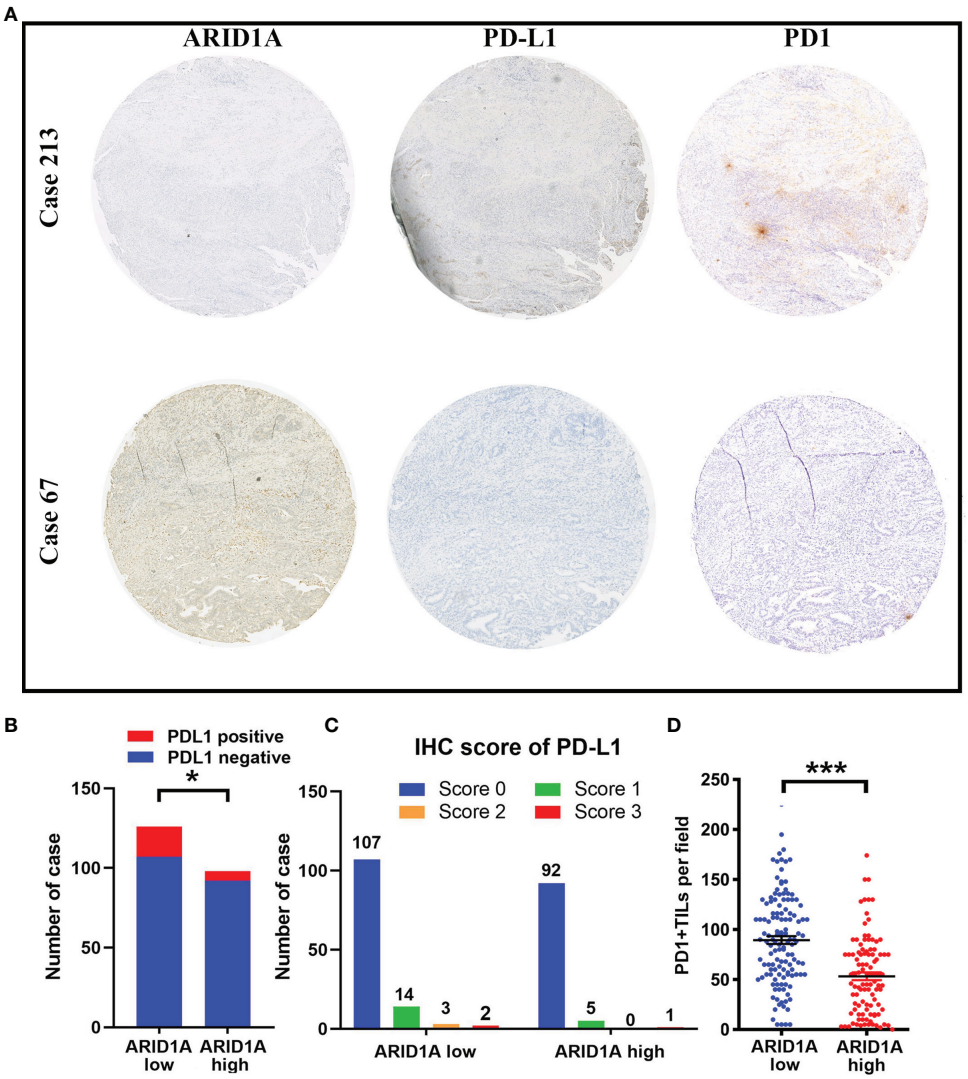

FIGURE 3 | The correlation of AT-rich interactive domain 1A (ARID1A) expression with PD-L1 expression and PD1+ tumor-infiltrating lymphocyte (TIL) counts in patients with gallbladder cancer (GBC). **(A)** Representative immunohistochemical images of PD-L1 expression and PD1+ TILs in patients with low (left upper) or high (left lower) ARID1A expression. **(B)** Distribution of PD1+ TILs in different ARID1A expression groups. **(C)** Proportion of patients with positive PD-L1 staining. **(D)** Distribution of the immunohistochemistry (IHC) score for PD-L1 in the ARID1A-high and ARID1A-low groups. *P < 0.05; ***P < 0.001.

subunit of the SWI/SNF complex, plays critical roles in cancer cell development, differentiation, and proliferation (22, 23). ARID1A is commonly classified as a tumor suppressor, and low ARID1A expression is associated with a poor prognosis in multiple cancers (24–27). However, the relationship between ARID1A expression and the prognosis of patients with GBC remains unclear. In the first part of this study, we observed that loss of ARID1A was correlated with worse OS and TNM stage in patients with GBC. Further multivariate analysis identified ARID1A as an independent prognostic factor for OS. These findings indicate that ARID1A might be a vital factor for predicting prognosis in patients with GBC.

It is known that loss of ARID1A can facilitate tumorigenesis through several mechanisms. Notably, recent studies revealed the vital effect of ARID1A on tumor immunity. One study confirmed that ARID1A plays an important role in lymphocyte development, whereas ARID1A deletion can lead to a developmental arrest in early T cells (28). Loss of ARID1A was found to have a significant correlation with the expression of IFN-γ and checkpoint genes (including PD-L1, CTLA4, and PDCD1) in microsatellite-stable colorectal cancer (29). In addition, ARID1A has been proven to serve as a biomarker for the sensitivity to immune checkpoint inhibitors (29–32).

Considering the role that ARID1A might play in tumor immunity, we examined immune-related signatures and gene sets in TCGA cholangiocarcinoma cohort. In the second part of our study, we found that ARID1A expression was correlated with multiple T cell-related processes, whereas cytotoxic T

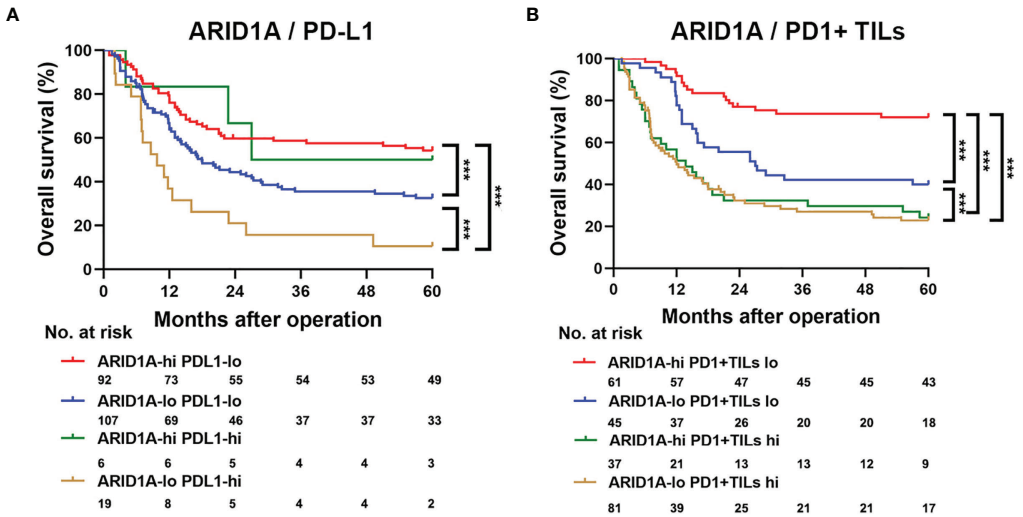

FIGURE 4 | Kaplan–Meier survival analysis of overall survival (OS) according to AT-rich interactive domain 1A (ARID1A) expression, PD-L1 expression, and PD1+ tumor-infiltrating lymphocyte (TIL) counts. **(A)** Kaplan–Meier survival analysis of OS in patients with gallbladder cancer based on ARID1A expression and PD1+ TIL counts. **(B)** Kaplan–Meier survival analysis of OS based on ARID1A expression and PD-L1 expression. ***P < 0.001.

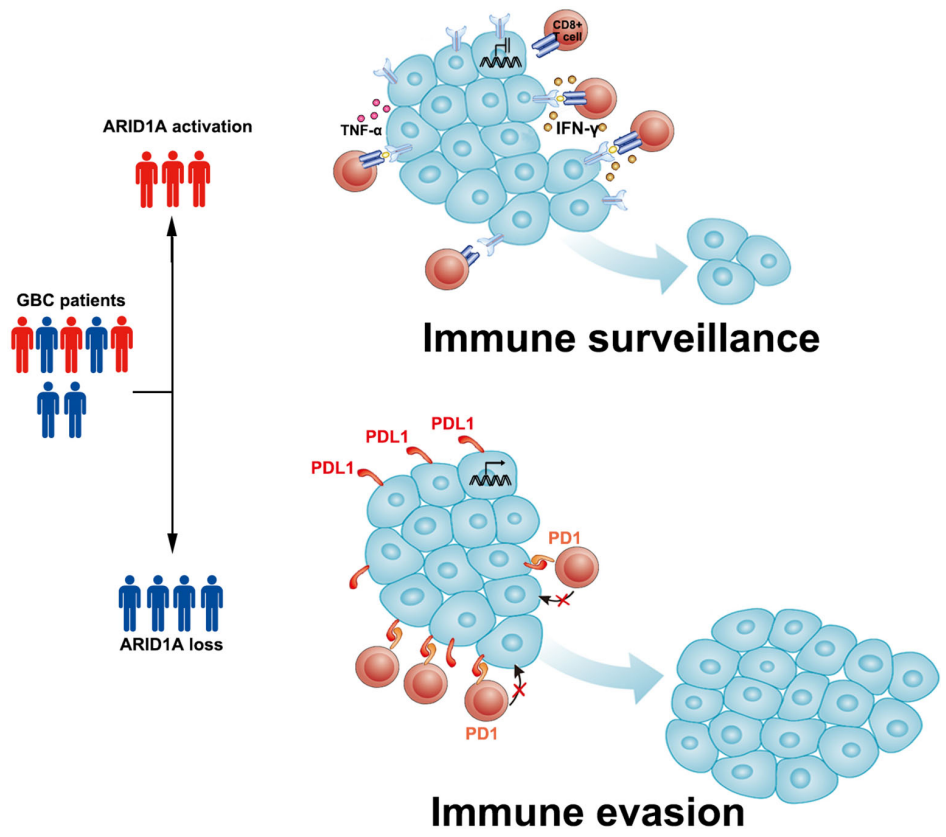

FIGURE 5 | Sketch map depicting the role of AT-rich interactive domain 1A (ARID1A) in patients with gallbladder cancer (GBC). We propose that in ARID1A-activated GBC, the relatively low expression of PD-L1 allows tumor-infiltrating lymphocytes (TILs) to function normally and perform immune surveillance. In ARID1A-inactivated GBC, the upregulation of PD-L1 in tumor cells might lead to immune evasion in the tumor microenvironment *via* the PD1/PD-L1 pathway.

lymphocyte (CTL) signatures were significantly decreased in ARID1A-low tumors. Further differential gene expression analyses also illustrated that genes involved in T-cell activation were downregulated in ARID1A-low tumors. These findings indicate that T cells are potentially depleted in biliary tumors with low ARID1A expression. Combined with the downregulation of several related pathways (such as TNF-α and IFN-γ signaling pathways), we propose that loss of ARID1A may lead to impaired immune surveillance in the TME of biliary cancer by influencing PD1/PD-L1 pathway activity.

ARID1A shares a complex correlation with the PD1/PD-L1 pathway. Loss of ARID1A was proven to be related to high PD-L1 expression in multiple cancers, including non-small cell lung cancer (33), gastric cancer (34), ovarian cancer (35), colorectal cancer (36), and hepatocellular carcinoma (37). Patients with ARID1A-mutated tumors are more likely to benefit from anti-PD1/PD-L1 immunotherapy than patients with wild-type ARID1A tumors (38). Mechanistically, loss of ARID1A can lead to the activation of phosphatidylinositol 3-kinase/AKT signaling, which contributes to the elevated expression of PD-L1 (34, 37). Another scenario holds that ARID1A deficiency results in increased PD-L1 expression by directly removing the antagonistic effect on *Cd274* gene (which encodes PD-L1) (39). Our future goal is to confirm whether the correlation between ARID1A and the PD1/PD-L1 pathway remains valid in GBC.

In the third part of our study, immunohistochemical staining revealed significant increases in PD-L1 expression and PD1+ TIL infiltration in ARID1A-low GBC specimens. Patients with high PD-L1 expression or those with greater PD1+ TIL infiltration had a worse prognosis (**Supplementary Figure S1**). Considering these variables together, the Kaplan–Meier analysis illustrated that high ARID1A expression, low PD-L1 expression, and lower PD1+ TIL infiltration were linked to the best prognosis in GBC. Meanwhile, because it was reported that loss of ARID1A can lead to high CD8+ T-cell infiltration *via* the increased tumor mutation burden (40), we further determined the number of CD8+ T cells in GBC specimens by IHC. The results revealed no significant difference in the number of CD8+ T cells between ARID1A-high and ARID1A-low tumors (**Supplementary Figure S2**). This indicated that the increased number of PD1+ TILs in ARID1A-low GBC tumors was not attributed to an overall increase in the number of TILs, but it was potentially the result of high PD-L1 expression in tumor tissue.

Based on the aforementioned findings, we propose that in GBC, ARID1A might potentially inhibit PD-L1 expression in tumor cells, which allows TILs to function normally in the TME. In ARID1A-inactivated GBC, PD-L1 overexpression and impaired TIL function lead to immune evasion by the tumor and a worse prognosis (**Figure 5**). These results suggest the potentiality of applying anti-PD1/PD-L1 therapy in patients with ARID1A-mutated GBC.

However, a few limitations should be acknowledged. As a single-center retrospective study with a relatively small sample size, it is necessary to validate these findings in a large prospective, multicenter, randomized study. In addition, the results of immunohistochemical staining in this study were based on TMA, which may not completely reflect the actual situation as a semiquantitative method. Currently, we have established an ARID1A-depleted GBC cell line, and we aim to validate these findings in humanized mice. We hope that the exact role of ARID1A in the progression of GBC will be revealed in our future work.

CONCLUSIONS

Our study identified the association of ARID1A downregulation with unfavorable clinical outcomes and prognosis in patients with GBC. Loss of ARID1A predicted increased PD-L1 expression and elevated PD1+ TIL infiltration, which might lead to impaired immune surveillance in the TME of GBC. The combination of high ARID1A expression, low PD-L1 expression, and reduced PD1+ TIL infiltration predicted the best OS in patients with GBC. ARID1A is a prognostic factor, and it might serve as a marker to predict the efficacy of immunotherapy.

DATA AVAILABILITY STATEMENT

The raw data supporting the conclusions of this article will be made available by the authors, without undue reservation.

ETHICS STATEMENT

The studies involving human participants were reviewed and approved by the ethics committee of Fudan University (approval no.: B2018-159R). The patients/participants provided their written informed consent to participate in this study. Written informed consent was obtained from the individual(s) for the publication of any potentially identifiable images or data included in this article.

AUTHOR CONTRIBUTIONS

All authors contributed to the article and approved the submitted version. LN and CW: acquisition of data, analysis, and interpretation of data, statistical analysis, and drafting of the manuscript. JW and SZ: technical and material support. XB, YW, and HL: study concept and design, analysis and interpretation of data, drafting of the manuscript, obtained funding, and study supervision. All authors contributed to the article and approved the submitted version.

FUNDING

This study was supported by grants from the National Natural Science Foundation of China (81872352, 82002525), the Foundation of Shanghai Science and Technology Committee (20JC1418902), the Shanghai Sailing Program (20YF1407300), the Science and Technology Commission of Shanghai Municipality (20DZ2254500), the Clinical Research Project and Outstanding Backbone Scheme of Zhongshan Hospital (2020ZSLC55, 2021ZSGG17), and the Scientific Research Project of Shanghai Municipal Health Commission (201940389).

SUPPLEMENTARY MATERIAL

The Supplementary Material for this article can be found online at: https://www.frontiersin.org/articles/10.3389/fonc.2022.787897/full#supplementary-material

Supplementary Figure S1 | Effects of PD-L1 expression and PD1+ tumor infiltrating lymphocytes (TILs) on overall survival (OS) in patients with gallbladder cancer. **(A)** The OS curves of patients with high or low PD-L1 expression. **(B)** The OS curves of patients with high or low PD1+ TIL infiltration.

Supplementary Figure S2 | The comparison of CD8+ cells and PD1+ tumor infiltrating lymphocytes (TILs) in samples with high/low expression of ARID1A.

REFERENCES

1. D'Hondt M, Lapointe R, Benamira Z, Pottel H, Plasse M, Letourneau R, et al. Carcinoma of the Gallbladder: Patterns of Presentation, Prognostic Factors and Survival Rate. An 11-Year Single Centre Experience. *Eur J Surg Oncol* (2013) 39(6):548–53. doi: 10.1016/j.ejso.2013.02.010
2. Edge SB, Edge SB. *AJCC Cancer Staging Manual. 8th Ed.* New York, USA: Springer (2017).
3. Nakayama RT, Pulice JL, Valencia AM, McBride MJ, McKenzie ZM, Gillespie MA, et al. SMARCB1 Is Required for Widespread BAF Complex-Mediated Activation of Enhancers and Bivalent Promoters. *Nat Genet* (2017) 49 (11):1613–23. doi: 10.1038/ng.3958
4. Clapier CR, Iwasa J, Cairns BR, Peterson CL. Mechanisms of Action and Regulation of ATP-Dependent Chromatin-Remodelling Complexes. *Nat Rev Mol Cell Biol* (2017) 18(7):407–22. doi: 10.1038/nrm.2017.26
5. Kadoch C, Hargreaves DC, Hodges C, Elias L, Ho L, Ranish J, et al. Proteomic and Bioinformatic Analysis of Mammalian SWI/SNF Complexes Identifies Extensive Roles in Human Malignancy. *Nat Genet* (2013) 45(6):592–601. doi: 10.1038/ng.2628
6. Lawrence MS, Stojanov P, Mermel CH, Robinson JT, Garraway LA, Golub TR, et al. Discovery and Saturation Analysis of Cancer Genes Across 21 Tumour Types. *Nature* (2014) 505(7484):495–501. doi: 10.1038/nature12912
7. Wilsker D, Patsialou A, Zumbrun SD, Kim S, Chen Y, Dallas PB, et al. The DNA-Binding Properties of the ARID-Containing Subunits of Yeast and Mammalian SWI/SNF Complexes. *Nucleic Acids Res* (2004) 32(4):1345–53. doi: 10.1093/nar/gkh277
8. Sun X, Wang SC, Wei Y, Luo X, Jia Y, Li L, et al. Arid1a Has Context-Dependent Oncogenic and Tumor Suppressor Functions in Liver Cancer. *Cancer Cell* (2017) 32(5):574–89.e6. doi: 10.1016/j.ccell.2017.10.007
9. Berns K, Caumanns JJ, Hijmans EM, Gennissen AMC, Severson TM, Evers B, et al. ARID1A Mutation Sensitizes Most Ovarian Clear Cell Carcinomas to BET Inhibitors. *Oncogene* (2018) 37(33):4611–25. doi: 10.1038/s41388-018-0300-6
10. Chae H, Kim D, Yoo C, Kim KP, Jeong JH, Chang HM, et al. Therapeutic Relevance of Targeted Sequencing in Management of Patients With Advanced Biliary Tract Cancer: DNA Damage Repair Gene Mutations as a Predictive Biomarker. *Eur J Cancer* (2019) 120:31–9. doi: 10.1016/j.ejca.2019.07.022
11. Javle M, Bekaii-Saab T, Jain A, Wang Y, Kelley RK, Wang K, et al. Biliary Cancer: Utility of Next-Generation Sequencing for Clinical Management. *Cancer* (2016) 122(24):3838–47. doi: 10.1002/cncr.30254
12. Sicklick JK, Fanta PT, Shimabukuro K, Kurzrock R. Genomics of Gallbladder Cancer: The Case for Biomarker-Driven Clinical Trial Design. *Cancer Metastasis Rev* (2016) 35(2):263–75. doi: 10.1007/s10555-016-9602-8
13. Wardell CP, Fujita M, Yamada T, Simbolo M, Fassan M, Karlic R, et al. Genomic Characterization of Biliary Tract Cancers Identifies Driver Genes and Predisposing Mutations. *J Hepatol* (2018) 68(5):959–69. doi: 10.1016/j.jhep.2018.01.009
14. Conci S, Ruzzenente A, Simbolo M, Bagante F, Rusev B, Isa G, et al. Multigene Mutational Profiling of Biliary Tract Cancer Is Related to the Pattern of Recurrence in Surgically Resected Patients. *Updates Surg* (2020) 72(1):119–28. doi: 10.1007/s13304-020-00718-5
15. Sasaki M, Nitta T, Sato Y, Nakanuma Y. Loss of ARID1A Expression Presents a Novel Pathway of Carcinogenesis in Biliary Carcinomas. *Am J Clin Pathol* (2016) 145(6):815–25. doi: 10.1093/ajcp/aqw071
16. Ashizawa M, Saito M, Min AKT, Ujiie D, Saito K, Sato T, et al. Prognostic Role of ARID1A Negative Expression in Gastric Cancer. *Sci Rep* (2019) 9(1):6769. doi: 10.1038/s41598-019-43293-5
17. Li L, Li M, Jiang Z, Wang X. ARID1A Mutations Are Associated With Increased Immune Activity in Gastrointestinal Cancer. *Cells* (2019) 8(7):678. doi: 10.3390/cells8070678
18. Herbst RS, Giaccone G, de Marinis F, Reinmuth N, Vergnenegre A, Barrios CH, et al. Atezolizumab for First-Line Treatment of PD-L1-Selected Patients With NSCLC. *N Engl J Med* (2020) 383(14):1328–39. doi: 10.1056/NEJMoa1917346
19. Euskirchen G, Auerbach RK, Snyder M. SWI/SNF Chromatin-Remodeling Factors: Multiscale Analyses and Diverse Functions. *J Biol Chem* (2012) 287 (37):30897–905. doi: 10.1074/jbc.R111.309302
20. Tessier-Cloutier B, Schaeffer DF, Bacani J, Marginean CE, Kalloger S, Kobel M, et al. Loss of Switch/Sucrose Non-Fermenting Complex Protein Expression in Undifferentiated Gastrointestinal and Pancreatic Carcinomas. *Histopathology* (2020) 77(1):46–54. doi: 10.1111/his.14096
21. Zhou Y, Xu Q, Tao L, Chen Y, Shu Y, Wu Z, et al. Enhanced SMARCD1, a Subunit of the SWI/SNF Complex, Promotes Liver Cancer Growth Through the mTOR Pathway. *Clin Sci (Lond)* (2020) 134(12):1457–72. doi: 10.1042/CS20200244
22. Nagarajan S, Rao SV, Sutton J, Cheeseman D, Dunn S, Papachristou EK, et al. ARID1A Influences HDAC1/BRD4 Activity, Intrinsic Proliferative Capacity and Breast Cancer Treatment Response. *Nat Genet* (2020) 52(2):187–97. doi: 10.1038/s41588-019-0541-5
23. Wang SC, Nassour I, Xiao S, Zhang S, Luo X, Lee J, et al. SWI/SNF Component ARID1A Restrains Pancreatic Neoplasia Formation. *Gut* (2019) 68(7):1259–70. doi: 10.1136/gutjnl-2017-315490
24. He F, Li J, Xu J, Zhang S, Xu Y, Zhao W, et al. Decreased Expression of ARID1A Associates With Poor Prognosis and Promotes Metastases of Hepatocellular Carcinoma. *J Exp Clin Cancer Res* (2015) 34:47. doi: 10.1186/s13046-015-0164-3
25. Kim MJ, Gu MJ, Chang HK, Yu E. Loss of ARID1A Expression is Associated With Poor Prognosis in Small Intestinal Carcinoma. *Histopathology* (2015) 66 (4):508–16. doi: 10.1111/his.12566
26. Yang L, Wei S, Zhao R, Wu Y, Qiu H, Xiong H. Loss of ARID1A Expression Predicts Poor Survival Prognosis in Gastric Cancer: A Systematic Meta-Analysis From 14 Studies. *Sci Rep* (2016) 6:28919. doi: 10.1038/srep28919
27. Yoshino J, Akiyama Y, Shimada S, Ogura T, Ogawa K, Ono H, et al. Loss of ARID1A Induces a Stemness Gene ALDH1A1 Expression With Histone Acetylation in the Malignant Subtype of Cholangiocarcinoma. *Carcinogenesis* (2019) 41(6):734–42. doi: 10.1093/carcin/bgz179
28. Astori A, Tingvall-Gustafsson J, Kuruvilla J, Coyaud E, Laurent EMN, Sunnerhagen M, et al. ARID1a Associates With Lymphoid-Restricted Transcription Factors and Has an Essential Role in T Cell Development. *J Immunol* (2020) 205(5):1419–32. doi: 10.4049/jimmunol.1900959
29. Mehrvarz Sarshekeh A, Alshenaifi J, Roszik J, Manyam GC, Advani SM, Katkhuda R, et al. ARID1A Mutation May Define an Immunologically Active Subgroup in Patients With Microsatellite Stable Colorectal Cancer. *Clin Cancer Res* (2021) 27(6):1663–70. doi: 10.1158/1078-0432.CCR-20-2404

30. Sun D, Tian L, Zhu Y, Wo Y, Liu Q, Liu S, et al. Subunits of ARID1 Serve as Novel Biomarkers for the Sensitivity to Immune Checkpoint Inhibitors and Prognosis of Advanced Non-Small Cell Lung Cancer. *Mol Med* (2020) 26 (1):78. doi: 10.1186/s10020-020-00208-9
31. He Y, Wang X. Identification of Molecular Features Correlating With Tumor Immunity in Gastric Cancer by Multi-Omics Data Analysis. *Ann Transl Med* (2020) 8(17):1050. doi: 10.21037/atm-20-922
32. Li Z, Lin J, Zhang L, Li J, Zhang Y, Zhao C, et al. Comprehensive Analysis of Multiple Parameters Associated With Tumor Immune Microenvironment in ARID1A Mutant Cancers. *Future Oncol* (2020) 16(29):2295–306. doi: 10.2217/fon-2020-0243
33. Naito T, Udagawa H, Umemura S, Sakai T, Zenke Y, Kirita K, et al. Non-Small Cell Lung Cancer With Loss of Expression of the SWI/SNF Complex Is Associated With Aggressive Clinicopathological Features, PD-L1-Positive Status, and High Tumor Mutation Burden. *Lung Cancer* (2019) 138:35–42. doi: 10.1016/j.lungcan.2019.10.009
34. Kim YB, Ahn JM, Bae WJ, Sung CO, Lee D. Functional Loss of ARID1A Is Tightly Associated With High PD-L1 Expression in Gastric Cancer. *Int J Cancer* (2019) 145(4):916–26. doi: 10.1002/ijc.32140
35. Kuroda Y, Chiyoda T, Kawaida M, Nakamura K, Aimono E, Yoshimura T, et al. ARID1A Mutation/ARID1A Loss Is Associated With a High Immunogenic Profile in Clear Cell Ovarian Cancer. *Gynecol Oncol* (2021) 162(3):679–85. doi: 10.1016/j.ygyno.2021.07.005
36. Tokunaga R, Xiu J, Goldberg RM, Philip PA, Seeber A, Battaglin F, et al. The Impact of ARID1A Mutation on Molecular Characteristics in Colorectal Cancer. *Eur J Cancer* (2020) 140:119–29. doi: 10.1016/j.ejca.2020.09.006
37. Iseda N, Itoh S, Yoshizumi T, Yugawa K, Morinaga A, Tomiyama T, et al. ARID1A Deficiency Is Associated With High Programmed Death Ligand 1 Expression in Hepatocellular Carcinoma. *Hepatol Commun* (2021) 5(4):675–88. doi: 10.1002/hep4.1659
38. Okamura R, Kato S, Lee S, Jimenez RE, Sicklick JK, Kurzrock R. ARID1A Alterations Function as a Biomarker for Longer Progression-Free Survival After Anti-PD-1/PD-L1 Immunotherapy. *J Immunother Cancer* (2020) 8(1): e000438. doi: 10.1136/jitc-2019-000438
39. Fukumoto T, Fatkhutdinov N, Zundell JA, Tcyganov EN, Nacarelli T, Karakashev S, et al. HDAC6 Inhibition Synergizes With Anti-PD-L1 Therapy in ARID1A-Inactivated Ovarian Cancer. *Cancer Res* (2019) 79 (21):5482–9. doi: 10.1158/0008-5472.CAN-19-1302
40. Hu G, Tu W, Yang L, Peng G, Yang L. ARID1A Deficiency and Immune Checkpoint Blockade Therapy: From Mechanisms to Clinical Application. *Cancer Lett* (2020) 473:148–55. doi: 10.1016/j.canlet.2020.01.001

Conflict of Interest: The authors declare that the research was conducted in the absence of any commercial or financial relationships that could be construed as a potential conflict of interest.

Publisher's Note: All claims expressed in this article are solely those of the authors and do not necessarily represent those of their affiliated organizations, or those of the publisher, the editors and the reviewers. Any product that may be evaluated in this article, or claim that may be made by its manufacturer, is not guaranteed or endorsed by the publisher.

frontiers in Oncology

ORIGINAL RESEARCH
published: 24 February 2022
doi: 10.3389/fonc.2022.840287

ABCC6 Knockdown Fuels Cell Proliferation by Regulating PPARα in Hepatocellular Carcinoma

Zhicong Zhao[1,2†], *Zhenjun Zhao*[1†], *Jianye Wang*[1,3], *He Zhang*[1,4], *Zhifeng Xi*[1] *and Qiang Xia*[1,5,6*]

[1] Department of Liver Surgery, Renji Hospital, Shanghai Jiao Tong University School of Medicine, Shanghai, China, [2] Department of Systems Biology, Beckman Research Institute of City of Hope, Duarte, CA, United States, [3] Department of Surgery, School of Medicine, Technical University of Munich, Munich, Germany, [4] Department of Surgery, The University of Hong Kong-Shenzhen Hospital, Shenzhen, China, [5] Shanghai Engineering Research Center of Transplantation and Immunology, Shanghai, China, [6] Shanghai Institute of Transplantation, Shanghai, China

The ATP binding cassette (ABC) transporter family is ubiquitous in eukaryotes, specifically in vertebrates, and plays a crucial role in energy homeostasis, cell signaling, and drug resistance. Accumulating evidence indicates that some ABC transporters contribute to cancer cell proliferation and tumor progression; however, relatively little is known about the behavior of the ABC transporter family in hepatocellular carcinoma (HCC). By analyzing two public transcriptomic databases, we evaluated the effect of genes in the ABC transporter family on HCC prognostic prediction; ABCC6 was selected for further study. Notably, ABCC6 was found to be downregulated in HCC tissues and correlated with favorable outcomes in patients with HCC. Moreover, *ABCC6* knockdown not only significantly promoted cell proliferation *in vitro* and *in vivo*, but also inhibited cell cycle arrest and cell apoptosis. Transcriptome analysis revealed that *ABCC6* depletion enhanced the "mitotic cell cycle" and "DNA replication" pathways, and suppressed the "PPAR signaling pathway". Further investigation demonstrated that PPARα, one of the key regulators in peroxisome metabolism, is located downstream of ABCC6. In summary, our study provides profound insights into the behavior of ABC transporter family genes in various HCC cohorts, identifies ABCC6 as a biomarker for early-stage HCC diagnosis, and offers experimental basis for further investigations of targeting ABCC6 in the treatment of patients with HCC.

Keywords: ABC transporter family, ABCC6, biomarker, cell proliferation, hepatocellular carcinoma, PPARα, peroxisome

OPEN ACCESS

Edited by:
Yunfei Xu,
Shandong University, China

Reviewed by:
Zhixiang Jian,
Guangdong Provincial People's Hospital, China
Ning Wei,
University of Pittsburgh Medical Center, United States

***Correspondence:**
Qiang Xia
xiaqiang@shsmu.edu.cn

†These authors have contributed equally to this work

Specialty section:
This article was submitted to Cancer Molecular Targets and Therapeutics, a section of the journal Frontiers in Oncology

Received: *21 December 2021*
Accepted: *28 January 2022*
Published: *24 February 2022*

Citation:
Zhao Z, Zhao Z, Wang J, Zhang H, Xi Z and Xia Q (2022) ABCC6 Knockdown Fuels Cell Proliferation by Regulating PPARα in Hepatocellular Carcinoma. Front. Oncol. 12:840287. doi: 10.3389/fonc.2022.840287

INTRODUCTION

Hepatocellular carcinoma (HCC) is the sixth most common cancer worldwide and accounts for approximately 85% of primary liver cancers (1). Moreover, incidence rates of HCC are significantly higher in China, Southeast Asia, and Africa than the rest of the world (2). Risk factors for HCC include hepatitis B virus infection, cirrhosis, non-alcoholic fatty liver disease, excessive alcohol consumption, autoimmune disease, and accumulation of reactive oxygen species (ROS) (3, 4). Additionally, early diagnosis through surveillance and curative treatment has considerably

improved the 5-year survival of patients with HCC (5). Therefore, it's strongly recommended to systematically screen target populations that are at a particularly high risk for developing HCC.

The ATP binding cassette (ABC) transporter family represents one of the largest families of transmembrane proteins (6). ABC transporters are found among all living organisms, and are classified into seven subfamilies, designated ABCA-ABCG (6). By utilizing the energy from ATP hydrolysis, ABC transporters can translocate specific substrates across the membrane (7). Furthermore, the past few decades have witnessed numerous studies documenting the contribution of ABC transporters to multidrug resistance. Specifically, some ABC transporters, such as ABCC1, ABCG2, and ABCB1, are highly efficient at extruding drugs from cancer cells, resulting in substantial multidrug resistance (8). More recently, accumulating evidence indicates that some ABC transporters also contribute to cancer cell proliferation and tumor progression (6, 7). For example, *ABCC4* knockdown induces cell cycle arrest and apoptosis in acute myeloid leukemia (9). Overexpression of *ABCC1* correlates with reduced overall survival in patients with neuroblastoma (10). Elevated *ABCA13* mRNA levels are linked to poor clinical outcomes in patients with gastric adenocarcinoma (11). At the same time, some ABC transporters (e.g., ABCA1, ABCA2, and ABCA7) are essential for lipid transport and homeostasis (12). However, because ABC transporters perform multiple functions simultaneously, controversial results have been reported (13). Thus, there is a pressing need to understand the overall behavior of ABC transporter family genes in HCC.

ABCC6, primarily localized in the basolateral membrane of hepatocytes, belongs to the ABC transporter C subfamily (14). Several studies have demonstrated that ABCC6 plays an important role in mineralization homeostasis. It's well-established that ABCC6 mutations cause a complex autosomal recessive disease, called pseudoxanthoma elasticum (PXE) (15, 16). Mechanistically, ABCC6 overexpression results in the efflux of ATP, which is rapidly converted into nucleoside monophosphates and pyrophosphate and alters the extracellular environment (17). Moreover, recent studies have suggested that ABCC6 variations correlate with altered plasma triglyceride levels and increased coronary risks (18, 19). Additionally, genetic deletion of *Abcc6* in mice disturbs cholesterol homeostasis and lipid metabolism (20). However, the role of ABCC6 in tumor biology has been poorly investigated.

In the present study, we first analyzed the prognostic value of ABC transporter family genes using the Cancer Genome Atlas (TCGA) and GSE14520 datasets, and then identified ABCC6 as a potential biomarker for early-stage HCC diagnosis and prognostic prediction. Specifically, ABCC6 expression was downregulated in HCC tissues and positively correlated with favorable overall survival in patients with HCC. Functional studies further revealed that ABCC6 knockdown significantly enhanced cancer cell proliferation *in vitro* and *in vivo*. Mechanistically, ABCC6 depletion inhibits the PPARα (Peroxisome proliferator-activated receptor alpha) activity and protects HCC cells from oxidative damage.

MATERIALS AND METHODS

Cell Culture

HCC Cell lines MHCC97H, SMMC7721, and Huh7 were obtained from Cell Resource Center of Shanghai Institutes for Biological Sciences, Chinese Academy of Sciences. Normal human hepatic cell line L-02 and human HCC cell lines MHCC97L and LM3 were kindly given from Huashan Hospital, Cancer Metastasis Institute, Fudan University, Shanghai. All cell lines were grown in DMEM medium (Gibco) supplemented with 10% Fetal bovine serum(FBS)(Gibco), and 1% penicillin-streptomycin (Gibco), incubated at 37°C and 5% CO_2. Mycoplasma contamination was tested every month.

Patients and Samples

Fresh human HCC tumor tissues and adjacent paratumor tissues were collected from patients who underwent surgical resection or liver transplantation at Department of Liver Surgery, Renji Hospital, Shanghai Jiao Tong University School of Medicine. Written informed consent was obtained from each patient. For Clinical analyses, two independent HCC cohorts of HCC patients were retrospectively adopted. HCC cohort 1 (hepatectomy cohort) included 153 HCCs collected between February 2010—August 2015 from Department of Liver Surgery, Renji Hospital, Shanghai Jiao Tong University School of Medicine. HCC cohort 2 (liver transplantation cohort) included 70 HCCs collected between January 2015—April 2016 from Department of Liver Surgery, Renji Hospital, Shanghai Jiao Tong University School of Medicine. All patients were diagnosed with HCC according to the NCCN guidelines and routinely followed up. This study was approved by the Renji Hospital Ethics Committee.

Constructs and Transfections

Human full-length *ABCC6* cDNA was inserted to the lentiviral vector CMV-MCS-3FLAG-SV40- EGFP-IRES-Puromycin plasmid by Fubio company (Shanghai, China). Short hairpin RNA (shRNA) targeting ABCC6 was constructed into PLKO.1 plasmid by Genepharma Company (Shanghai, China), while a non-target shRNA (5'- GCGCGCTTTGTAGGATTCG-3') was used as a negative control. To construct stable cell lines with overexpression or downregulation of *ABCC6*, lentivirus particles were generated based on above plasmids and transfected into HCC cell lines in the presence of polybrene. 48 hours after infection, puromycin (2μg/ml) was added into culture cells. Knockdown and overexpression efficiency was confirmed by western blot. The shRNA target sequences employed in this study are listed as below: shABCC6#1: GTGGCCGAG AATGCTATGAAT; shABCC6#2: CGTAGATGAAAGC CAGAGGAT.

Tissue Microarray Immunohistochemistry Analysis

Two tissue microarrays with definite HCC diagnosis were constructed in this study. All HCC samples were first reviewer histologically by hematoxylin and eosin staining to identify the

border between Tumor and paratumor. Then, representative areas were punched out and mounted onto a recipient block with a semi-automated TMArrayer. Immunohistochemistry assays using tissue microarray were performed according to standard protocol. Briefly, paraffin-embedded tissue microarray slides were deparaffinized and rehydrated for 30 min. Antigen retrieval was done by incubating the slides in citrate buffer (pH 6.0) by boiling for 10 min in the microwave oven. After fully cooled down, the slides were incubated with ABCC6 antibody (Proteintech, 27848-1-AP) overnight at 4°C. After washing three times with PBST, the slides were incubated with HRP-conjugated secondary antibody (Proteintech, SA00001-2). Signals were developed in DAB detection solution (Beyotime, p0203) under microscopic observation and counterstained with hematoxylin. After staining, photographs were captured using Leica microscope. The Image-Pro Plus v6.0 software was used to calculate the integrated optical density (IOD) of each photograph, and the ratio of IOD to total tissue area was calculated as staining intensity.

CCK-8, Colony Formation, and EdU (5-Ethynyl-2'-Deoxyuridine) Incorporation Assays

For CCK-8 assay, HCC cell lines were infected with indicated lentivirus and selected for 1 week to generate stable knockdown or overexpression cells. Then, the cells were seeded into 96-well plates at a density of 3×10^3 cells per well and incubated at 37°C. Every 24 hours, 10% (V/V) CCK-8 (Dojindo, CK04-11) was added to the culture medium and incubated for one hour. Cell viability was measured at OD 450 nm using a SpectraMax i3 microplage reader (Molecular Devices, USA).

Colony formation assay were performed to evaluate the long-term proliferation ability. HCC cell lines were seeded into 60mm dishes at a density of 3×10^3 cells per well and cultured for 14 days. The medium was changed twice a week. Cells were washed gently with PBS and fixed in 4% formaldehyde for 20 minutes followed by staining with 0.1% (w/v) crystal violet. The cell culture plates were scanned to obtain digital images, and the colonies were counted under microscope.

The EdU (5-Ethynyl-2'-Deoxyuridine) incorporation assay was performed using BeyoClick™ EdU Cell Proliferation Kit (Beyotime, C0078S) according to the manufacturer's instructions to further validate cell proliferation ability. Briefly, 1×10^5 cells were planted in 24-well plates with coverslips 24 hours before experiments. Then, 50 mM EdU labeling medium was added into each well and incubated for 2h at 37°C. The cells were fixed using 4% paraformaldehyde for 20 min and treated with 0.5% Triton X-100 for 10 min at room temperature. Then, the cells were stained with Click Reaction mix for 30 min, and the nuclei were stained using DAPI. Proliferation rate was determined by quantifying the percentage of EdU^+ cells using fluorescence microscope.

Transwell-Migration Assay

8μm transwell inserts (Falcon, USA) were used to measure the migratory of cells. Briefly, 5×10^4 HCC cells in 200 μl of DMEM were placed into the upper chamber, 500 μl DMEM medium containing 10% FBS was added to the lower chambers. After 48 h, the non-migrated cells on the top side were wiped carefully and the inserts were fixed in 5% formaldehyde solution for 10 min. After that, each inset was stained with 0.1% crystal violet for 10 min, then washed with PBS for three times. Three random microscopic fields were captured and cells were counted for each group.

Cell Apoptosis and Cell Cycle Assay

Stable 97H and Huh7 cells were seeded into 6-well plates at a density of 5×10^5 cells per well 24 hours before the apoptosis assay. After treating with 20 μM cisplatin (Selleck Chemicals, S1166) for 24 hours, cells were harvested by trypsinization, washed twice with PBS, stained with APC-Annexin V and PI following the manufacturers' instructions (MultiSciences, 70-AP107-100). Flow cytometry was performed using Beckman CytoFLEX and the results were analyzed with FlowJo software.

For cell cycle analysis, cells were harvested and fixed in cold 70% ethanol overnight at 4°C. Cells were then stained with PI staining solution (Sangon Biotech, E607306) for 15min, followed by washing with PBS twice. Flow cytometry was performed using Beckman CytoFLEX and the results were analyzed with FlowJo software.

Intracellular ROS Assay

The intracellular ROS level was detected by CellROX™ Cytometry Assay Kit (Thermo Fisher, C10493). Briefly, cells were harvested and stained with 500 nM CellRox reagent for 60 min at 37°C. After washing the cells once with PBS, immediately analyzed the samples by Beckman CytoFLEX. The results were analyzed with FlowJo software.

Seahorse XF Cell Energy Phenotype Assay

Cellular energy phenotypes and metabolic switching was measured by Seahorse XFe96 Analyzer (Agilent, USA) with Seahorse XF Cell Energy Phenotype Test Kit (Agilent, 103325-100). In brief, $0.5\text{-}1\times10^5$ cells were seeded in 96-well Seahorse plates with XF RPMI medium supplemented with 2 mM glutamine, 10 mM glucose, 1mM pyruvate, and 5 mM HEPES, and then incubated in a CO_2-free incubator for 1 hour prior to the assay. For assessment of energy phenotypes, 100 μM oligomycin and FCCP were used according to the manufacturer's instructions.

β-Galactosidase Staining

The β-galactosidase staining was performed using Senescence β-Galactosidase Staining Kit (Beyotime, C0602) according to the manufacturer's instructions. Briefly, 5×10^5 cells were planted in 6-well plates with coverslips 24 hours before experiments. The cells were fixed using 4% paraformaldehyde for 20 min and then stained with working solution at 37°C overnight. The second day, cells were washed with PBS for three times and observed under microscope. Senescence rate was determined by quantifying the percentage of positive cells.

ATP and Malondialdehyde (MDA) Assay

To measure the intracellular ATP level, we utilized the CellTiter-Glo Cell Viability Assay (Premega, G9241). Control and stable *ABCC6* knockdown HCC cells were seeded into 96-well plates at a density of

1×10^4 cells per well and incubated at 37°C. The second day, added 100μl CellTiter-Glo reagent to the medium in each well, mixed the contents for 2 minutes and incubated at room temperature for 10 minutes. The luminescent signals were measured using a SpectraMax i3 microplage reader (Molecular Devices, USA).

To evaluate lipid peroxidation, we utilized the MDA assay (Beyotime, S0131S). Control and stable *ABCC6* knockdown HCC cells were seeded into 6-well plates at a density of 1×10^6 cells per well and incubated at 37°C. Cells were lysed using Western lysis buffer, and the protein concentration was measured using a BCA protein Assay kit (Thermo Fisher). MDA assay was performed according to the manufacturer's instructions. Signal was measured at OD 532 nm using a SpectraMax i3 microplage reader (Molecular Devices, USA). Relative MDA level was normalized by the protein concentration of each sample.

In Vivo Tumor Growth Assays

NSG (NOD-*scid* IL2Rgamma^{null}) mice were purchased from Shanghai Model Organisms Ltd. and bred at the specific-pathogen-free core facilities in Renji Hospital. All mice were housed on a 12 hours-12 hours light-dark cycle. 5×10^6 shNS and sh*ABCC6* 97H cells were injected subcutaneously into 6-weeks-old NSG mice (n=4 per group). Tumors were measured using a caliper and the tumor volume was calculated as (width × width × length/2). Mice were euthanized when they met the institutional euthanasia criteria for tumor size. At the end-point, tumors were collected and weighted. Animal experimental protocols were approved by the Institutional Animal Care and Use Committee of Renji Hospital, Shanghai Jiao Tong University School of Medicine.

Western Blot

Total protein was extracted using RIPA Lysis Buffer (Thermo Fisher) according to the manufacturer's instructions. The protein concentration was measured using a BCA protein Assay kit (Thermo Fisher). Equal amounts of proteins were separated by 8-10% SDS-PAGE gel and then transferred onto polyvinylidene fluoride membranes. Chemiluminescence signaling was detected by ECL Western Blotting Substrate (Vazyme, E412-01). Antibodies used for western blot were listed below: ABCC6 (Proteintech, 27848-1-AP), β-actin (Cell Signaling Technology, 3700S), PPARα (Novus, NB300-57), Cyclin D1 (Cell Signaling Technology, 2978S), ACOX1 (Proteintech, 10957-1-AP).

Real-Time Quantitative PCR

Total RNA was extracted from cell liens using Trizol (Thermo Fisher) according to the manufacturer's instructions. RNA concentration was measured using Thermo Scientific Nanodrop Spectrophotometer. 0.8-1 μg total RNA was subjected to reverse transcription using HiScript III 1st Strand cDNA Synthesis Kit (Vazyme, R312-01) according to the manufacturer's instructions. The Quantitative real-time PCR (qRT-PCR) was conducted using ChamQ SYBR Color qPCR Master Mix (Vazyme, Q441-02) in the Bio-Rad Real-Time PCR system. Gene expression levels were normalized to the expression of *GAPDH* or *ACTB*. Primers used for qRT-PCR were listed below: ABCC6-F: AGATGGTGCTTGGATTCGCC, ABCC6-R: GCCACACAGTAGGATGAATGAG; ABCA6-F: AAACAGAAAAGCGTGTATCAGCA, ABCA6-R: GAGG AGCCATTCCAGGAAACT; ABCG5-F: TGGACCAGGC AGATCCTCAAA, ABCG5-R: CCGTTCACATACAC CTCCCC; PPARA-F: TTCGCAATCCATCGGCGAG, PPARA-R: CCACAGGATAAGTCACCGAGG; ACOX1-F: GGAAC TCACCTTCGAGGCTTG, ACOX1-R: TTCCCC TTAGTGATGAGCTGG; CCND1-F: GCTGCGAAGTGGA AACCATC, CCND1-R: CCTCCTTCTGCACACATTTGAA; GAPDH-F: GGAGCGAGATCCCTCCAAAAT, GAPDH-R: GGCTGTTGTCATACTTCTCATGG.

RNA-Seq

Total RNA was isolated from shNS and sh*ABCC6* 97H cells using Trizol (Thermo Fisher) according to the manufacturer's instructions. rRNA was subsequently depleted from total RNA using NEBNext rRNA depletion kit (New England BioLabs). After that, NEBNext Ultra Directional RNA Library Prep Kit (New England BioLabs) was used for library preparation. RNA sequencing was performed by Annorad Ltd. using Novaseq 6000 platform. GO and KEGG analysis were performed using David Bioinformatics Resources 6.8 (https://david.ncifcrf.gov/). Gene set enrichment analysis (GSEA) was carried out using GSEA software v2.0.

Statistical Analysis

Data are presented as mean ± standard error of the mean (SEM). Statistical comparisons were performed by using two-tailed t-tests, one-way ANOVA or Kaplan-Meier analysis. *P* values less than 0.05 were considered statistically significant. NS, not significant. All statistical analyses were carried out using R (Version 4.0.1) or Graphpad Prism 8 (GraphPad Software).

RESULTS

ABC Transporter Family Gene Expression and Behavior in HCC

To evaluate the role of ABC family genes in HCC, we first analyzed two public HCC datasets; the Cancer Genome Atlas (TCGA) and the GSE14520 (with the largest number of HCC patients and detailed clinical information) datasets. By comparing the expression levels of ABC family genes in HCC tumors and paratumors, we found that approximately 1/3 of the ABC genes were significantly upregulated, and 1/3 were downregulated (**Figure 1A**). After incorporating the clinical prognosis information into analysis, it was noted that some ABC family genes correlated with overall survival or progression-free survival of patients HCC. However, only *ABCA6*, *ABCB11*, *ABCC6*, and *ABCG5* showed consistent results in both TCGA and GSE14520 datasets (**Tables 1**, **2**). Notably, high *ABCA6*, *ABCB11*, *ABCC6*, and *ABCG5* expression levels were correlated with favorable overall survival (**Figures 1B, C**). Additionally, bioinformatics analyses also showed that the mRNA levels of these genes were attenuated in tumors comparing with those in

paratumor tissues (**Figures 1D, E**). Furthermore, expression levels of these genes gradually decreased as TNM staging advanced in both TCGA and GSE14520 datasets (**Figures 1F, G**). Similarly, we also found that their expression levels decreased with advanced HCC histological staging in the TCGA dataset (**Figure 2A**). Collectively, our data suggest that among all ABC family genes, *ABCA6*, *ABCB11*, *ABCC6*, and *ABCG5* might serve as potential tumor suppressor genes in HCC.

Identification of *ABCC6* as a Biomarker for Early-Stage HCC

It is well-established that overall survival rates are significantly higher in patients with HCC that are diagnosed at an early-stage and receive immediate treatment (21). However, because early-stage HCC does not present significant symptoms, delayed diagnosis and treatment are common and likely contribute to poor cancer outcomes (22). To further assess the clinical value of

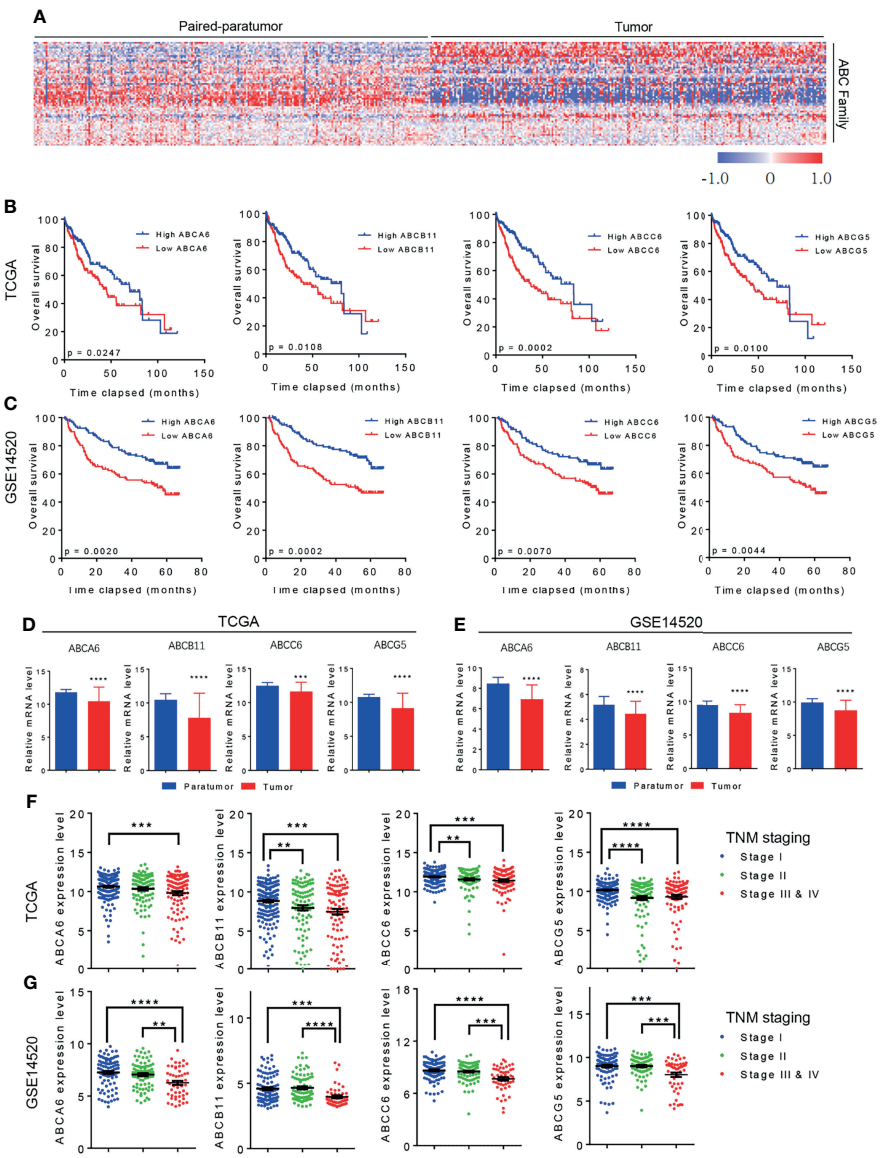

FIGURE 1 | The Role of ABC transporter family genes in HCC. **(A)** Heat map showing the differential expression of ABC transporter family genes in TCGA dataset. **(B)** Kaplan-Meier analysis showing the overall survival of patients with HCC in correlation with high or low ABC family genes level. Data was derived from TCGA dataset. **(C)** Kaplan-Meier analysis showing the overall survival of HCC patients in correlation with high or low ABC family genes level. Data was derived from GSE14520 dataset. **(D)** TCGA dataset showing the differential expression of ABC family genes in HCC paratumor tissues and tumor tissues. **(E)** GSE14520 dataset showing the differential expression of ABC family genes in HCC paratumor tissues and tumor tissues. **(F)** TCGA database showing the expression level of ABC family genes with advanced HCC TNM staging. **(G)** GSE14520 dataset showing the expression level of ABC family genes with advanced HCC TNM staging. Error bars indicate means ± SEM. *P*-values were determined by two tailed *t*-test **(D, E)**, one-way ANOVA **(F, G)** and Kaplan-Meier analysis **(B, C)**. $^{**}P < 0.01$, $^{***}P < 0.001$, $^{****}P < 0.0001$.

TABLE 1 | Cox regression analysis of ABC family genes in GSE14520 cohort.

GSE14520 cohort (n=242)					
Factor	**OS**		**Factor**	**PFS**	
	Relative hazard (95% CI)	***P***		**Relative hazard (95% CI)**	***P***
Low ABCA6 expression	1.884 (1.253 to 2.834)	0.002	Low ABCB11 expression	1.620 (1.153 to 2.277)	0.005
Low ABCB11 expression	2.191 (1.442 to 3.331)	<0.001	High ABCD3 expression	1.437 (1.024 to 2.017)	0.036
Low ABCB4 expression	1.606 (1.072 to 2.405)	0.022	Low ABCG5 expression	1.484 (1.058 to 2.081)	0.022
Low ABCC6 expression	1.739 (1.157 to 2.615)	0.008			
High ABCD3 expression	1.666 (1.108 to 2.505)	0.014			
Low ABCG5 expression	1.797 (1.193 to 2.706)	0.005			

ABCA6, *ABCB11*, *ABCC6*, and *ABCG5* in patients with HCC, we re-analyzed the public datasets and focused on early-stage HCC (TNM stage I & II). Interestingly, Kaplan-Meier analyses showed that *ABCC6* positively correlates with overall survival in TNM stage I and II HCC patients in both datasets, suggesting that *ABCC6* displays significant prognostic value in early-stage HCC. In contrast, *ABCA6*, *ABCB11*, and *ABCG5* did not display consistent prognostic value in early-stage HCC (**Figures 2B, C**).

Furthermore, we measured the expression of *ABCA6*, *ABCC6*, and *ABCG5* in 50 pairs of early-stage tumor tissues and paratumor tissues using quantitative reverse transcription polymerase chain reaction (qRT-PCR). Consistent with our bioinformatic analysis, this assessment also showed significantly lower *ABCC6* expression in tumor tissues than in paratumor tissues (**Figure 2D**), suggesting that *ABCC6* might be a potential diagnostic marker in HCC.

Evaluating the Clinical Effects of ABCC6 Expression in Patients With HCC

Our previous studies have identified *ABCA6*, *ABCC6* and *ABCG5* as potential tumor-suppressor genes in HCC. To further narrow down our candidate gene, we assessed the mRNA level of these genes in normal human tissues using the BioGPS database (http://biogps.org). Only *ABCC6* was found to be specifically expressed in normal liver tissue (**Figure 3A**), highlighting its importance in liver homeostasis. Moreover, western blotting assays confirmed lower ABCC6 expression in tumor tissue than in paratumor tissues (**Figure 3B**). Accordingly, we focused on the function of ABCC6 in the development and progression of HCC.

To further validate our bioinformatic data, we employed two independent HCC cohorts. Cohort 1 (hepatectomy cohort) included 153 individuals who were hospitalized between 2010 and 2015 who underwent liver resection surgery at the Department of Liver Surgery, Renji Hospital, Shanghai Jiao Tong University School of Medicine. Cohort 2 (liver transplantation cohort) included 70 individuals who underwent liver transplantation between 2015 and 2016 at the Department of Liver Surgery, Renji Hospital, Shanghai Jiao Tong University School of Medicine. To evaluate the association between ABCC6 expression and clinicopathological features of HCC, we used immunohistochemistry to detect ABCC6 expression in tissue microarrays of patients from both cohorts. Consistently, ABCC6 was significantly downregulated in tumor tissues compared to paratumor tissues (**Figures 3C–E**). We divided all cases into high and low ABCC6 groups according to the immunohistochemistry expression level, and noticed that patients with high ABCC6 expression displayed increased overall survival and disease-free survival (**Figures 3F, G**), which is consistent with the TCGA and GSE14520 bioinformatic results. Multivariate Cox regression

TABLE 2 | Cox regression analysis of ABC family genes in TCGA cohort.

TCGA cohort (n=365)					
Factor	**OS**		**Factor**	**PFS**	
	Relative hazard (95% CI)	***P***		**Relative hazard (95% CI)**	***P***
Low ABCA6 expression	1.433 (1.012 to 2.028)	0.043	High ABCA2 expression	1.481 (1.060 to 2.070)	0.021
Low ABCA8 expression	1.488 (1.048 to 2.113)	0.026	Low ABCA9 expression	1.493 (1.070 to 2.084)	0.018
Low ABCA9 expression	1.794 (1.255 to 2.564)	0.001	Low ABCD2 expression	1.845 (1.313 to 2.591)	<0.001
Low ABCB11 expression	1.463 (1.033 to 2.071)	0.032	High ABCF2 expression	1.615 (1.152 to 2.265)	0.005
High ABCB6 expression	1.470 (1.036 to 2.085)	0.031			
High ABCC1 expression	1.706 (1.201 to 2.425)	0.003			
High ABCC5 expression	1.587 (1.121 to 2.248)	0.009			
Low ABCC6 expression	2.044 (1.432 to 2.918)	<0.001			
High ABCC8 expression	1.419 (1.001 to 2.011)	0.049			
Low ABCD2 expression	1.586 (1.117 to 2.252)	0.010			
High ABCF2 expression	1.473 (1.037 to 2.092)	0.030			
Low ABCG5 expression	1.561 (1.098 to 2.218)	0.013			
Low ABCG8 expression	1.735 (1.218 to 2.473)	0.002			

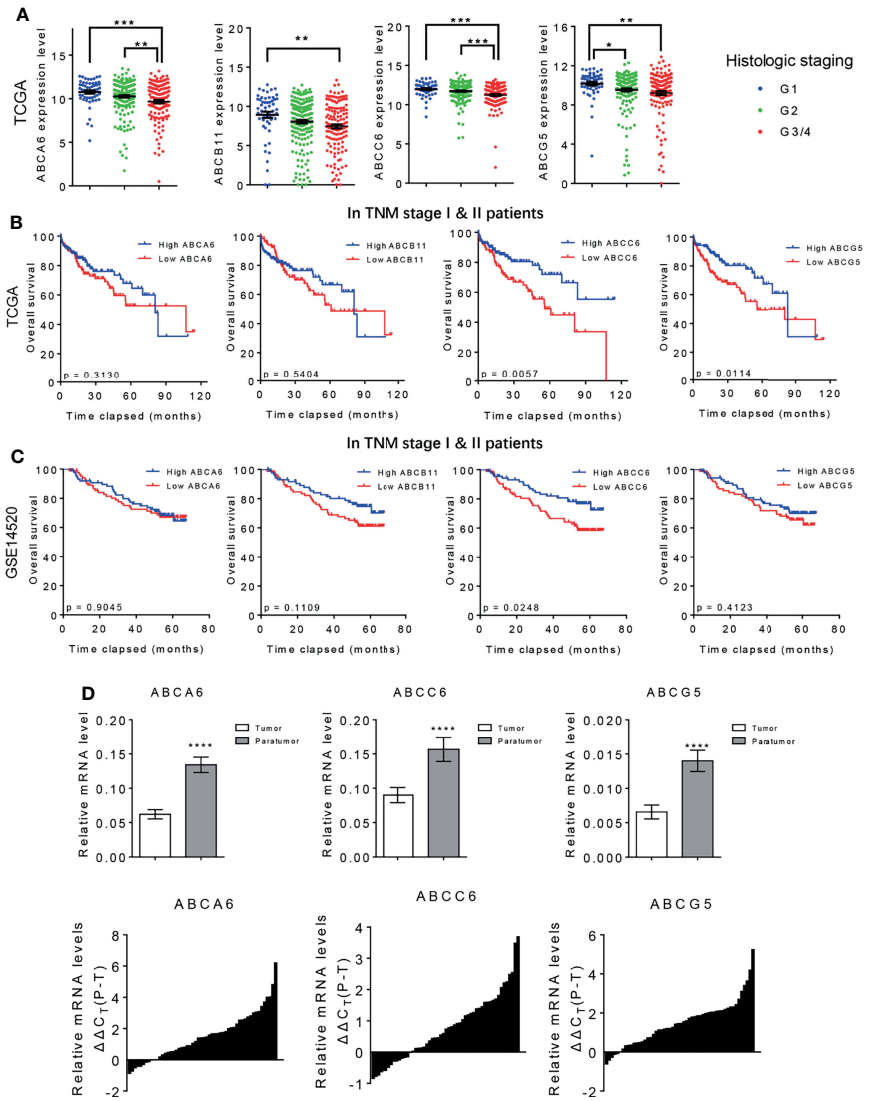

FIGURE 2 | *ABCA6*, *ABCC6*, and *ABCG5* might serve as tumor suppressor genes in HCC. **(A)** TCGA database showing the expression level of ABC family genes in different HCC histologic staging. **(B)** Kaplan-Meier analysis showing the overall survival of early stage HCC patients (TNM I & II) with high or low ABC family genes level. Data was derived from TCGA database. **(C)** Kaplan-Meier analysis showing the overall survival of early stage HCC patients (TNM I & II) with high or low ABC family genes level. Data was derived from GSE14520 dataset. **(D)** qPCR analysis validating the differential expression of *ABCA6*, *ABCC6* and *ABCG5* in 50 pairs of early-stage HCC tumor and paratumor tissues. Error bars indicate means ± SEM. *P*-values were determined by two tailed *t*-test **(D)**, one-way ANOVA **(A)** and Kaplan-Meier analysis **(B, C)**. $^{*}P < 0.05$, $^{**}P < 0.01$, $^{***}P < 0.001$, $^{****}P < 0.0001$.

analysis of clinical prognostic information demonstrated that downregulated ABCC6 was not only an independent prognostic marker, but also correlated with some malignant and aggressive clinicopathological features, such as high AFP values and large tumor size (**Table 3**). Furthermore, we interrogated the TCGA database and analyzed the relationship between *ABCC6* expression and several proliferation markers (e.g., *MKI67*, *CCNB1*, *RRM2*, and *CDC20*). A negative correlation was observed between expression of *ABCC6* and these proliferation markers (**Figure 3H**). Collectively, our data suggest that ABCC6 is downregulated in HCC tumor tissues and correlates with favorable outcomes in patients with HCC.

ABCC6 Knockdown Promotes HCC Proliferation *In Vitro* and *In Vivo*

Next, we investigated the effect of ABCC6 on the biological function of HCC cell lines *in vitro*. ABCC6 expression and protein levels were first examined in five commercial available HCC cell lines (MHCC97H, MHCC97L, SMMC7721, Huh7, and HCC-LM3) and one normal human hepatic cell line (L-02). Enhanced ABCC6 levels were observed in MHCC97H, MHCC97L, and Huh7 cells, while lower ABCC6 levels were observed in SMMC7721 and HCC-LM3 cells. All HCC cell lines displayed lower ABCC6 protein levels than normal hepatic cell line (**Figures 4A, B**). Furthermore, different HCC cell lines were

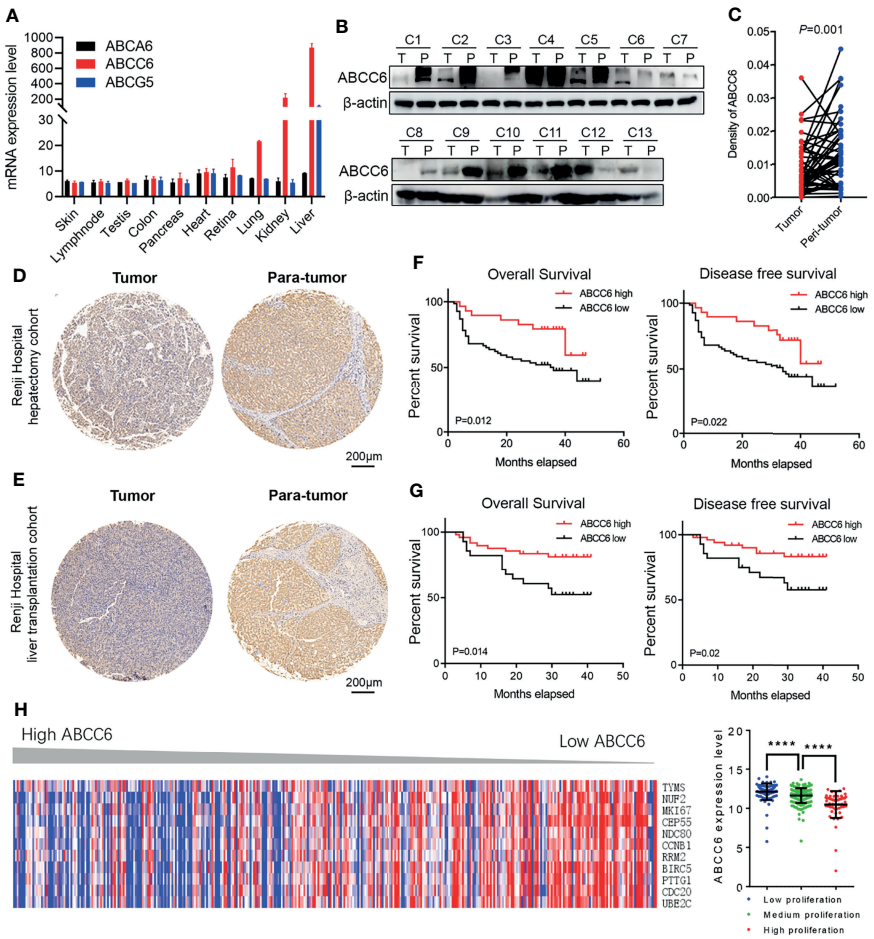

FIGURE 3 | The clinical outcomes of ABCC6 in patients with HCC. **(A)** BioGPS database showing the mRNA expression level of *ABCA6*, *ABCC6*, and *ABCG5* in different normal human tissues. **(B)** Western blotting displaying ABCC6 protein levels in 13 pairs of HCC tumor and paratumor tissues. **(C)** Statistical analysis showing the differential protein level of ABCC6 in Renji Hospital hepatectomy HCC tissue array. **(D)** Representative IHC figure showing the ABCC6 protein level in Renji Hospital hepatectomy HCC tissue array. **(E)** Representative IHC figure showing the ABCC6 protein level in Renji Hospital liver transplantation HCC tissue array. **(F)** Kaplan-Meier analysis showing the overall survival and disease-free survival of HCC patients in correlation with high or low *ABCC6* levels in Renji Hospital hepatectomy cohort. **(G)** Kaplan-Meier analysis showing the overall survival and disease-free survival of HCC patients in correlation with high or low *ABCC6* levels in Renji Hospital liver transplantation cohort. **(H)** Heatmap and histogram showing the expression of proliferation-related genes in correlation with different *ABCC6* expression level. Data was derived from TCGA dataset. Error bars indicate means ± SEM. *P*-values were determined by two tailed *t*-test **(C)**, one-way ANOVA **(H)** and Kaplan-Meier analysis **(F, G)**. ****$P < 0.0001$.

TABLE 3 | Cox regression analysis of risk factors associated with overall survival in Renji Hospital hepatectomy cohort.

Variables	Univariate analysis			Multivariate analysis		
	HR	95% CI	*P* Value	HR	95% CI	*P* Value
ABCC6 expression (High vs. Low)	0.33	0.14-0.78	0.012	0.33	0.14-0.78	0.012
Gender (Male vs. Female)	1.65	0.74-3.72	0.225			
Age (≥50 vs.<50)	0.97	0.52-1.81	0.991			
AFP (≥200 vs.<200)	2.78	1.44-5.33	0.002	1.84	0.93-3.63	0.049
ALT (≥50 vs.<50)	1.82	0.98-3.40	0.058			
Tumor size (≥5 cm vs.<5cm)	2.75	1.44-5.23	0.002	2.18	1.10-4.34	0.026
Tumor nodule number (Multiple vs. Single)	0.50	0.27-0.93	0.027			
Cancer embolus (Presence vs. Absence)	8.18	4.21-15.90	<0.001	6.14	3.04-12.42	<0.001
Pathology grade	1.34	0.74-2.44	0.334			
Tumor necrosis (Presence vs. Absence)	2.36	1.04-5.32	0.039			
Cirrhosis (Presence vs. Absence)	2.41	0.95-6.13	0.066			

chosen for loss- or gain-of-function studies based on their endogenous ABCC6 levels. *ABCC6* knockdown (using two short hairpin RNAs) or overexpression efficiency was confirmed by western blotting (**Figures 4C, D**). CCK-8 assay, colony formation assay and EdU (5-Ethynyl-2'-Deoxyuridine) incorporation assays all showed significantly enhanced proliferation ability in HCC cells with ABCC6 knockdown (**Figures 4E–G**), and the proliferation ability was decreased after ABCC6 overexpression (**Figures 4H–J**). Taken together, these data suggest that ABCC6 plays a tumor-suppressive role by inhibiting HCC proliferation *in vitro*.

We further examined the role of ABCC6 in HCC development and progression *in vivo* using an NSG (NOD-*scid* IL2Rgamma^{null}) xenograft mouse model. The same number of control or *ABCC6* knockdown MHCC97H cells was injected subcutaneously into the left flank of NSG mice. As expected, tumor size, tumor growth curve, and tumor weight were substantially augmented following *ABCC6* knockdown (**Figures 4K–M**), indicating that *ABCC6* depletion also facilitates tumor progression *in vivo*.

ABCC6 Knockdown Influences Cell Cycle and Cell Apoptosis

To further study the role of ABCC6 in tumor biology, we knocked down or overexpressed *ABCC6* in HCC cells and evaluated their migration ability. The results showed that migrative ability was promoted by *ABCC6* depletion and hindered by *ABCC6* overexpression (**Figure 5A**). In addition, cell cycle analysis showed that *ABCC6* knockdown significantly increased the percentage of cells in the G2/M phase and decreased the G0/G1 phase, suggesting that ABCC6 may regulate the cell cycle in cancer cells (**Figures 5B, C**). *ABCC6* depletion also affected the proportion of β gal-positive cells *in vitro* (**Figure 5D**), revealing the possible role of ABCC6 in regulating cell senescence. Furthermore, *ABCC6* knockdown significantly inhibited cisplatin-induced cell apoptosis in both 97H and Huh7 cells (**Figures 5E, F**), implying that *ABCC6* depletion might contribute to HCC growth by ensuring apoptosis resistance.

We then performed gene set enrichment analysis (GSEA) using GSE14520 sequence data. Notably, the "fatty acid metabolism" and "peroxisome" pathways were highly active in samples with high expression of *ABCC6* (**Figure 5G**). Furthermore, to evaluate the potential down-stream targets of ABC family genes, we analyzed the TCGA dataset and overlapped the co-expression gene (R>0.4 or <-0.4) of *ABCC6*, *ABCA6*, *ABCB11*, *ABCG5*. Thirteen genes were identified as co-expression genes through overlapping (**Figure 6A**). Intriguingly, *CAT*, *PPARA*, *ACOX1*, and *ACOX2* are essential peroxisomal genes.

Transcriptome-Wide Analysis of ABCC6 in HCC Cells

Next, we sought to elucidate the mechanism by which ABCC6 regulates HCC cell proliferation. To comprehensively assess the effects of ABCC6 on HCC cells, we performed RNA-sequencing using control and *ABCC6*-knockdown MHCC97H cells. The volcano plot showed that 657 genes were downregulated while 396 genes were upregulated after *ABCC6* depletion (|log2(FC)|>1, P<0.05) (**Figure 6B** and **Supplementary Table 1**). Gene Ontology (GO) analysis showed that "DNA replication" and "cell cycle" pathways were significantly enhanced as a result of *ABCC6* knockdown, while lipid and fatty acid metabolism were significantly inhibited (**Figures 6C, D**). Additionally, the Kyoto Encyclopedia of Genes and Genomes (KEGG) analysis also exhibited the upregulation of "cell cycle" and "DNA replication" pathways, and the downregulation of "PPAR signaling pathway" (**Figures 6E, F**). Finally, we examined the expression of key genes in the "cell cycle" and "fatty acid metabolism" pathways. Strikingly, the expression of *CCND1*, *CCNB1*, *CDK1*, and *CDK2* was all significantly augmented by *ABCC6* knockdown, while *PPARA*, *ACOX1*, *CD36*, *ACSL4* were mitigated (**Figure 6G**). Taken together, these data suggest that *ABCC6* depletion enhances cell proliferation by regulating peroxisome activity.

ABCC6 Knockdown Inhibits PPARα Activity

Peroxisomes are membrane-bound oxidative organelles found in the cytoplasm and involve more than 50 different metabolic enzymes. Peroxisomes play key roles in lipid metabolism and are essential for ROS production (23). Recent studies have reported that cancer cells exhibit remarkable alterations in peroxisome activity (24), and peroxisome metabolism is largely reduced in HCC (25). Our previous results demonstrated that *ABCC6* is positively correlated with both "peroxisome" pathway and essential peroxisomal genes in the HCC public dataset; *ABCC6* knockdown significantly inhibited the expression of *PPARA* and *ACOX1* in HCC cells. Thus, we consider the possibility whether *ABCC6* depletion promotes cell proliferation by inhibiting peroxisome activity.

It is well-established that *ABCC6* overexpression results in the efflux of ATP, which decreases intracellular ATP levels. Accordingly, we found that *ABCC6* knockdown increased intracellular ATP levels (**Figure 7A**). Consistent with our RNA-sequence results, qRT-PCR analysis showed that *PPARA* and *ACOX1* were decreased after *ABCC6* depletion, while the mRNA level of *CCND1* was enhanced (**Figure 7B**). Furthermore, western blotting indicated that *ABCC6* knockdown mitigated the protein levels of PPARα and ACOX1, while enhanced the protein level of CyclinD1, vice versa (**Figures 7C, D**). As PPARα and ACOX1 mainly influence lipid metabolism, we performed the malondialdehyde (MDA) assay to evaluate lipid peroxidation. As expected, *ABCC6* knockdown significantly inhibited lipid peroxidation in HCC cells (**Figure 7E**). Moreover, seahorse assay showed that *ABCC6* depletion affected the cellular energy phenotype and mitigated the oxygen consumption rate (OCR) of cancer cells under stress conditions (**Figure 7F**), most likely due to the lower lipid peroxidation activity. We further examined the intracellular ROS levels and found that *ABCC6* overexpression elevated ROS levels (**Figure 7G**). To determine whether PPARα directly contributes to cell proliferation, we treated *ABCC6* knockdown cells with PPARα agonist fenofibrate and monitored cell growth.

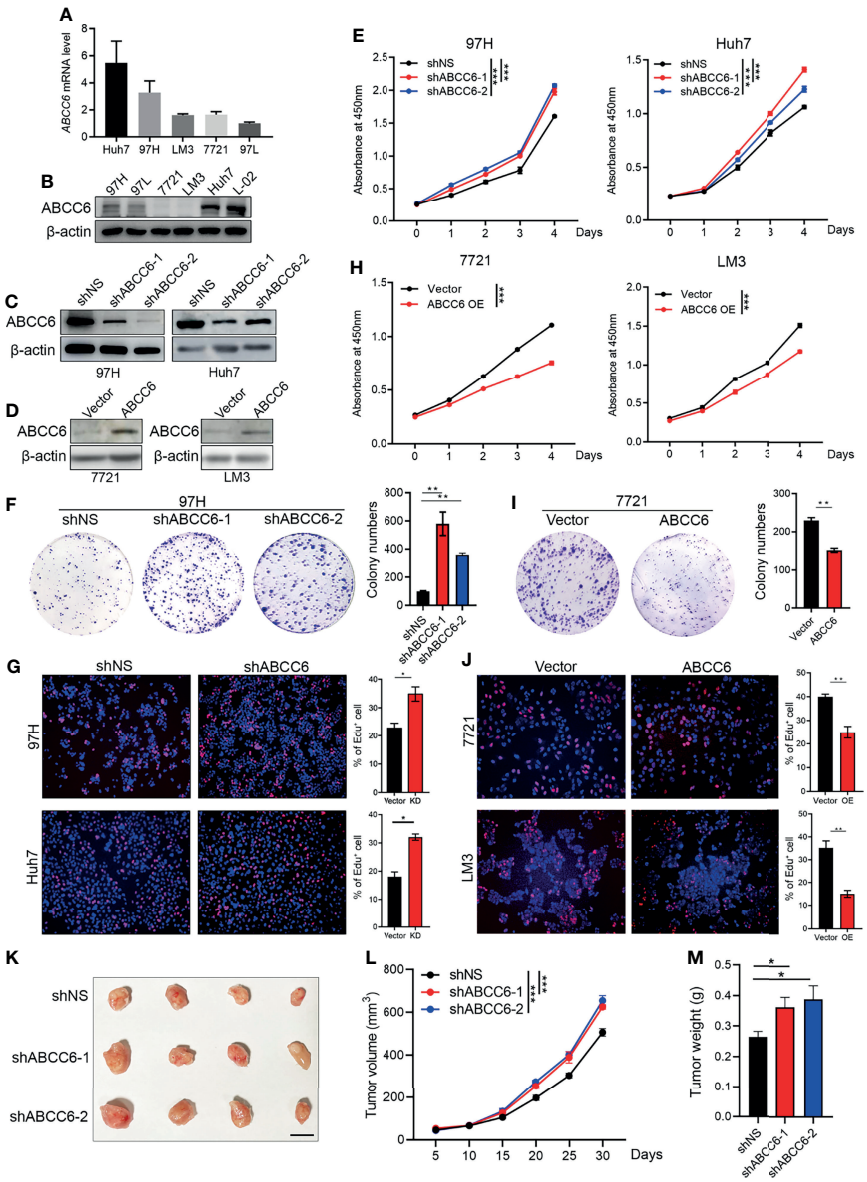

FIGURE 4 | *ABCC6* knockdown promotes HCC cell lines proliferation *in vitro* and *in vivo*. **(A)** qPCR analysis showing *ABCC6* mRNA expression level in different HCC cell lines. **(B)** Western blot displaying ABCC6 protein level in different HCC cell lines as well as one normal human hepatic cell line (L-02). **(C)** Western Blot validating the ABCC6 knockdown efficiency in 97H and Huh7 cell lines. **(D)** Western Blot validating the ABCC6 overexpression efficiency in 7721 and LM3 cell lines. **(E)** CCK-8 assay showing the cell proliferation of *ABCC6* knockdown 97H and Huh7 cells. **(F)** Colony formation assay of *ABCC6* knockdown 97H cells. **(G)** Edu incorporation assay showing the effect of *ABCC6* knockdown on the cell proliferative ability of 97H and Huh7 cells. **(H)** CCK-8 assay showing the cell proliferation of *ABCC6* overexpression 7721 and LM3 cells. **(I)** Colony formation assay of *ABCC6* overexpression 7721 cells. **(J)** Edu incorporation assay showing the effect of *ABCC6* overexpression on the cell proliferative ability of 7721 and LM3 cells. **(K)** Images showing the subcutaneous xenograft of ShNS, ShABCC6-1, and ShABCC6-2 97H cells. n=4; The scale bar indicates 1cm. **(L)** The growth curves of ShNS, ShABCC6-1, and ShABCC6-2 97H cells subcutaneously injected into NSG immunodeficient mice. (M) The weight of tumors collected from xenograft NSG mouse model implanted with ShNS, ShABCC6-1, and ShABCC6-2 97H cells. Error bars indicate means ± SEM. *P*-values were determined by two tailed *t*-test **(E–J)** and one-way ANOVA **(L, M)**. $^{*}P < 0.05$, $^{**}P < 0.01$, $^{***}P < 0.001$.

Consistently, fenofibrate treatment partially rescued the cell proliferation phenotypes (**Figures 7H, I**). Taken together, these findings support the notion that *ABCC6* knockdown inhibits peroxisomal ACOX1 and PPARα to prevent oxidative damage in HCC cells, thereby enhancing cell proliferation.

DISCUSSION

ABC transporter family genes have diverse roles in energy homeostasis, lipid metabolism, drug resistance, and tumor progression. Although several studies suggested that ABC

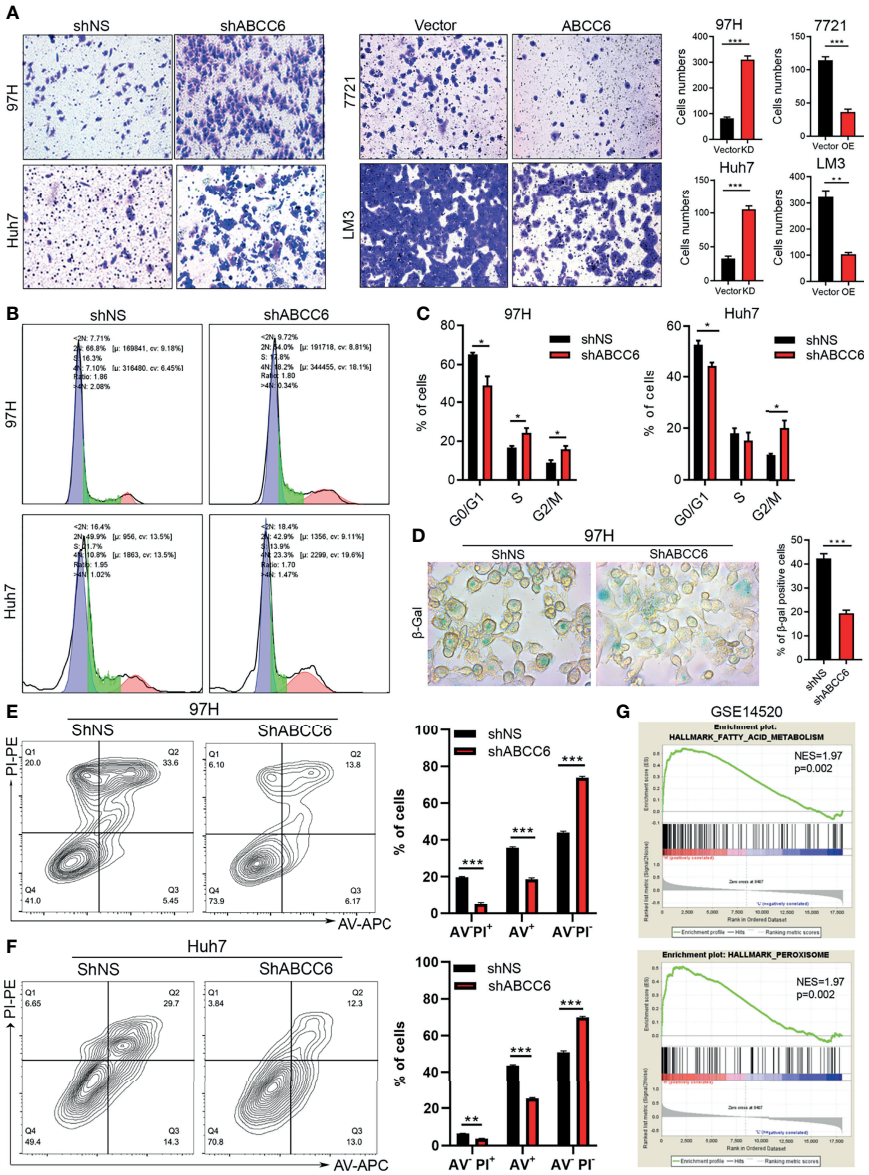

FIGURE 5 | *ABCC6* affect HCC cell lines migration, cell cycle arrest and apoptosis. **(A)** Transwell assay showing the effect of *ABCC6* knockdown and overexpression in the migration ability of HCC cell lines. **(B)** The results of cell cycle analysis by flow cytometry in *ABCC6* knockdown 97H and Huh7 cells. The blue peak and the red peak represents G0-G1, G2-M stage respectively. The middle is S stage. **(C)** Statistical analysis showing the effect of *ABCC6* knockdown in the cell cycle of 97H and Huh7 cells. **(D)** β-galactosidase staining showing the senescence status of HCC cell lines after *ABCC6* knockdown. **(E)** Flow cytometry analysis showing the effect of *ABCC6* knockdown on the apoptosis of 97H cells treating with 20 μM cisplatin for 24 hours. **(F)** Flow cytometry analysis showing the effect of *ABCC6* knockdown on the apoptosis of Huh7 cells treating with 20 μM cisplatin for 24 hours. **(G)** GSEA analysis showing the enrichment pathway of *ABCC6* high samples in GSE14520 dataset. Error bars indicate means ± SEM. *P*-values were determined by two tailed *t*-test **(A, C–F)**. $^{*}P < 0.05$, $^{**}P < 0.01$, $^{***}P < 0.001$.

transporter family genes might serve as cancer drivers in multiple cancer types (7), other studies indicated that some ABC family genes may be tumor suppressors. For example, eight ABC transporter genes (e.g., *ABCA8*, *ABCC6*, and *ABCC9*) were significantly downregulated in prostate cancer tissues compared with noncancerous tissues (26). However, the behavior of ABC transporter family genes in HCC has not been clearly investigated. In this study, we evaluated the expression level and prognostic prediction value of all ABC transporter family members in TCGA and GSE14520 datasets, and found that ABCC6 is significantly downregulated in HCC tumor tissues and correlated with favorable outcomes in patients with HCC. Consistent with our findings, a previous study also demonstrated that the ABCC6 protein was highly expressed in liver tissue, but remained non-detectable in a small panel of human tumor samples (27).

It is well-established that *ABCC6* mutation is responsible for PXE; however, the biological function of ABCC6 in HCC was

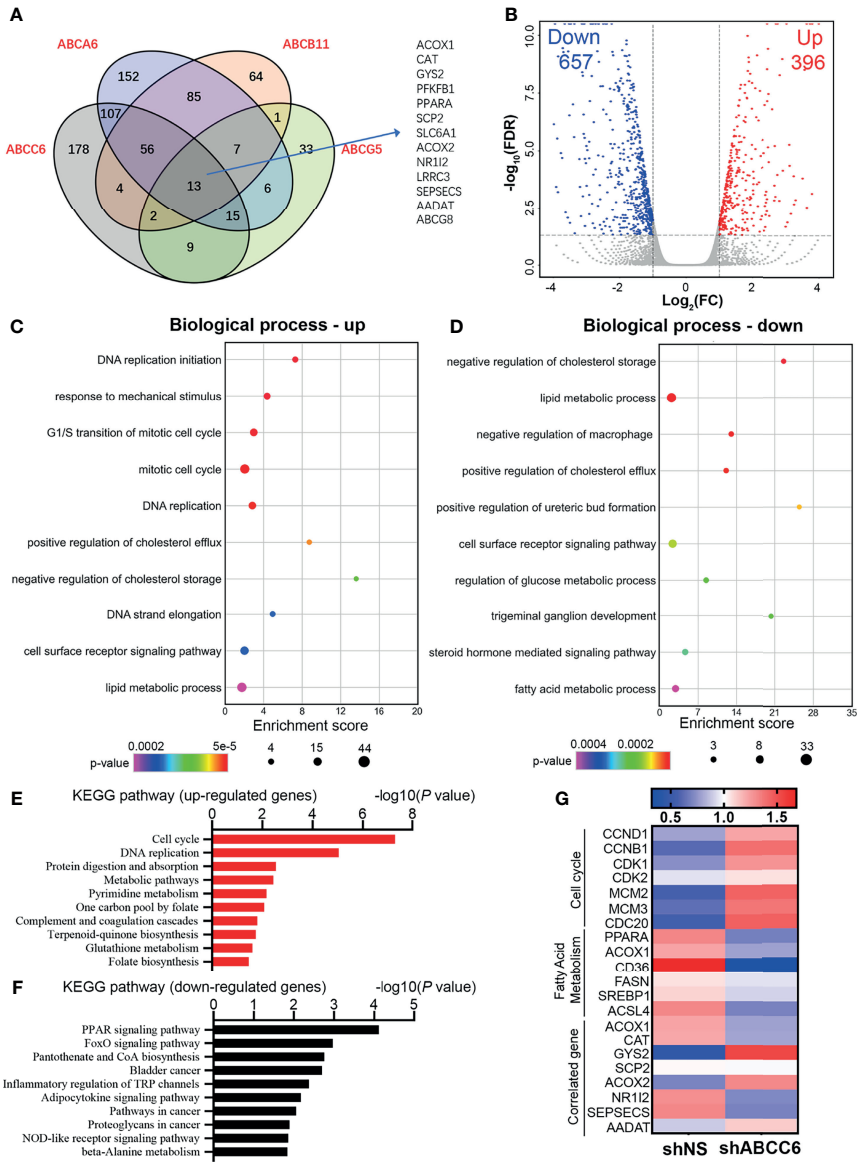

FIGURE 6 | Transcriptome-wide analysis of *ABCC6* knockdown 97H cells. **(A)** Venn diagram showing the overlap among positive correlation (R>0.4) genes of *ABCA6*, *ABCB11*, *ABCC6* and *ABCG5*. Data was derived from TCGA database. **(B)** Volcano plot showing the up-regulated and down-regulated genes in *ABCC6* knockdown 97H cells. Cut-off value: $|\log_2(FC)|>1$, $P<0.05$. **(C)** Gene Ontology (GO) enrichment analysis of up-regulated genes in *ABCC6* knockdown 97H cells. **(D)** Gene Ontology (GO) enrichment analysis of down-regulated genes in *ABCC6* knockdown 97H cells. **(E)** KEGG pathway analysis of up-regulated genes in *ABCC6* knockdown 97H cells. **(F)** KEGG pathway analysis of down-regulated genes in *ABCC6* knockdown 97H cells. **(G)** Heatmap showing the relative expression levels of cell cycle, fatty acid metabolism and *ABCC6* correlated genes based on the RNA-seq results.

largely unexplored. Our *in vitro* and *in vivo* results indicated that *ABCC6* knockdown significantly promoted HCC cell proliferation. Moreover, *ABCC6* depletion suppressed cell cycle arrest and apoptosis. To further investigate the mechanisms of ABCC6 in HCC, we performed GSEA, co-correlation analysis, and transcriptome sequencing. Notably, GO and KEGG analysis indicated that "cell cycle" and "DNA replication" pathways were significantly upregulated, while "PPAR signaling pathway" was downregulated. Furthermore, *PPARA* and *ACOX1* were found to be potential targets of ABCC6.

PPARα, a key regulator of peroxisome metabolism, is closely related to energy homeostasis and lipid metabolism (28). Recent studies have shown that PPARα-deficient mice are remarkably sensitive to DEN(diethylnitrosamine)-induced liver cancer, and PPARα inhibits HCC development by mediating the NF-κB pathway (29). Additionally, the PPARα agonist, fenofibrate, caused inhibitory effects in different cancer cell lines and animal tumor models, including hepatocarcinogenesis (30–32). In our study, we found that *ABCC6* knockdown suppressed PPARα expression transcriptionally, and fenofibrate partially

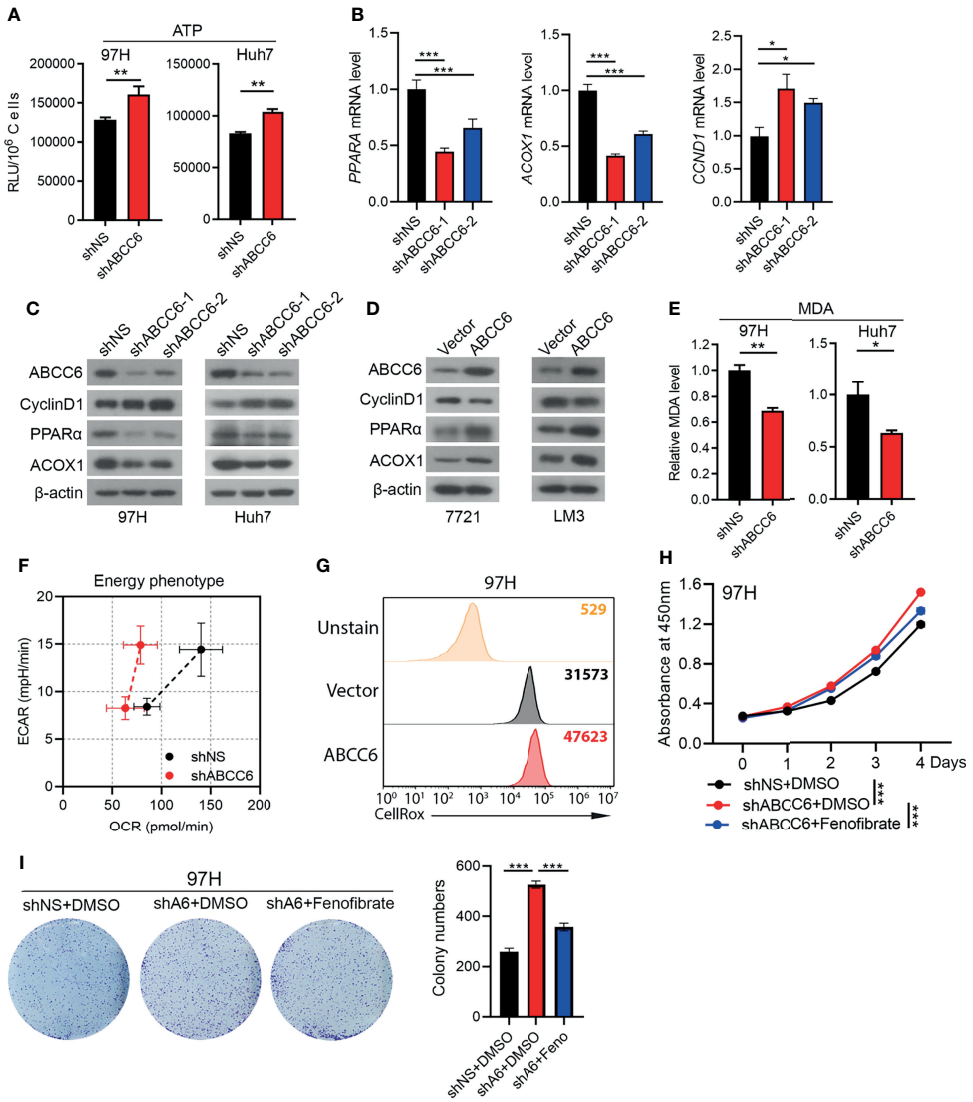

FIGURE 7 | *ABCC6* knockdown suppressed PPARα expression in HCC cells. **(A)** ATP level of *ABCC6* knockdown and control 97H and Huh7 cells. **(B)** qPCR analysis showing the expression of *PPARA*, *ACOX1* and *CCND1* in *ABCC6* knockdown 97H cells. **(C)** Western blot showing the protein levels of ABCC6, Cyclin D1, PPARα and ACOX1 in *ABCC6* knockdown 97H and Huh7 cells. **(D)** Western blot showing the protein levels of ABCC6, Cyclin D1, PPARα and ACOX1 in *ABCC6* overexpression 7721 and LM3 cells. **(E)** MDA assay showing the relative lipid peroxidation level of *ABCC6* knockdown and control 97H and Huh7 cells. **(F)** Seahorse assay displaying the baseline and stressed energy phenotype of *ABCC6* knockdown and control 97H cells. **(G)** Flow cytometry analysis showing the intracellular ROS level of vector and *ABCC6* overexpression 97H cells. **(H)** CCK-8 assay showing the effect of PPARα agonist fenofibrate in the proliferation of *ABCC6* knockdown and control 97H cells. **(I)** Colony formation assay showing the effect of PPARα agonist fenofibrate in the proliferation of *ABCC6* knockdown and control 97H cells. Error bars indicate means ± SEM. *P*-values were determined by two tailed *t*-test **(A, E)** and one-way ANOVA **(B, H, I)**. $^{*}P < 0.05$, $^{**}P < 0.01$, $^{***}P < 0.001$.

rescued the cell proliferation phenotype, suggesting that PPARα is the downstream target of ABCC6. Moreover, ACOX1 is the rate-limiting enzyme in fatty acid β-oxidation. A previous study suggested that ACOX1 is controlled by PPARα, and ACOX1 dysfunction contributes to hepatocarcinogenesis (33). We demonstrated that ABCC6 knockdown mitigated lipid metabolism and oxygen consumption in HCC cells, which could promote cell proliferation by preventing HCC cells from oxidative damage.

The current study still has several limitations. First, it does not address why *ABCC6* is downregulated in tumor tissues. Moreover, although we demonstrated that ABCC6 regulates the activity of peroxisomes in HCC, further studies are required to determine the underlying mechanism by which ABCC6 suppresses the expression of PPARα and ACOX1. Additionally, our study does not investigate whether ABCC6 is responsible for the resistance to clinically approved HCC drugs, such as sorafenib, regorafenib, and lenvatinib.

In conclusion, ABCC6 depletion inhibits peroxisome activity, protects cancer cells from oxidative damage, and therefore promotes cell proliferation. Our study provides profound insights into the behavior of ABC transporter family genes in various HCC cohorts, identifies ABCC6 as a potential biomarker for early-stage HCC diagnosis, and highlights the significance of ABCC6 in liver cancer progression.

DATA AVAILABILITY STATEMENT

The datasets presented in this study can be found in online repositories. The names of the repository/repositories and accession number(s) can be found in the article/**Supplementary Material**.

ETHICS STATEMENT

The studies involving human participants were reviewed and approved by the Renji Hospital Ethics Committee. The patients/participants provided their written informed consent to participate in this study. The animal study was reviewed and approved by the Institutional Animal Care and Use Committee of Renji Hospital, Shanghai Jiao Tong University School of Medicine.

AUTHOR CONTRIBUTIONS

ZCZ designed the study, performed cellular and molecular experiments, interpreted the data and wrote the manuscript. ZJZ performed the bioinformatics analysis. JW, HZ, and ZX performed cellular and molecular experiments or data analyses. QX conceived the project, supervised the study and revised the paper. All authors discussed the results and commented on the manuscript. All authors contributed to the article and approved the submitted version.

FUNDING

This study was supported by National Natural Science Foundation of China (81972205); Major Program of the National Natural Science Foundation of China (92059205); Shanghai Municipal Hospital Three-year-project for Clinical Skills' Promotion and Innovation (SHDC2020CR5012, SHDC2020CR2003A).

ACKNOWLEDGMENTS

We thank Dr. Jiajie Hou for helpful discussion and comment. We thank Jiaxin Li and Yuan Xu in the Department of Liver Surgery, Renji Hospital, Shanghai Jiao Tong University School of Medicine for the collection and follow-up of HCC patients.

SUPPLEMENTARY MATERIAL

The Supplementary Material for this article can be found online at: https://www.frontiersin.org/articles/10.3389/fonc.2022.840287/full#supplementary-material

Supplementary Table 1 | Transcriptome analysis of *ABCC6* knockdown MHCC97H cells versus control cells.

REFERENCES

1. Yang JD, Hainaut P, Gores GJ, Amadou A, Plymoth A, Roberts LR. A Global View of Hepatocellular Carcinoma: Trends, Risk, Prevention and Management. *Nat Rev Gastroenterol Hepatol* (2019) 16(10):589–604. doi: 10.1038/s41575-019-0186-y
2. Gomaa AI, Khan SA, Toledano MB, Waked I, Taylor-Robinson SD. Hepatocellular Carcinoma: Epidemiology, Risk Factors and Pathogenesis. *World J Gastroenterol* (2008) 14(27):4300–8. doi: 10.3748/wjg.14.4300
3. Fujiwara N, Friedman SL, Goossens N, Hoshida Y. Risk Factors and Prevention of Hepatocellular Carcinoma in the Era of Precision Medicine. *J Hepatol* (2018) 68 (3):526–49. doi: 10.1016/j.jhep.2017.09.016
4. Rong G, Wang H, Bowlus CL, Wang C, Lu Y, Zeng Z, et al. Incidence and Risk Factors for Hepatocellular Carcinoma in Primary Biliary Cirrhosis. *Clin Rev Allergy Immunol* (2015) 48(2-3):132–41. doi: 10.1007/s12016-015-8483-x
5. Tang A, Hallouch O, Chernyak V, Kamaya A, Sirlin CB. Epidemiology of Hepatocellular Carcinoma: Target Population for Surveillance and Diagnosis. *Abdom Radiol (NY)* (2018) 43(1):13–25. doi: 10.1007/s00261-017-1209-1
6. Begicevic RR, Falasca M. ABC Transporters in Cancer Stem Cells: Beyond Chemoresistance. *Int J Mol Sci* (2017) 18(11):2362. doi: 10.3390/ijms18112362
7. Domenichini A, Adamska A, Falasca M. ABC Transporters as Cancer Drivers: Potential Functions in Cancer Development. *Biochim Biophys Acta Gen Subj* (2019) 1863(1):52–60. doi: 10.1016/j.bbagen.2018.09.019
8. Fletcher JI, Williams RT, Henderson MJ, Norris MD, Haber M. ABC Transporters as Mediators of Drug Resistance and Contributors to Cancer Cell Biology. *Drug Resist Updat* (2016) 26:1–9. doi: 10.1016/j.drup.2016.03.001
9. Copsel S, Bruzzone A, May M, Beyrath J, Wargon V, Cany J, et al. Multidrug Resistance Protein 4/ ATP Binding Cassette Transporter 4: A New Potential Therapeutic Target for Acute Myeloid Leukemia. *Oncotarget* (2014) 5 (19):9308–21. doi: 10.18632/oncotarget.2425
10. Peaston AE, Gardaneh M, Franco AV, Hocker JE, Murphy KM, Farnsworth ML, et al. MRP1 Gene Expression Level Regulates the Death and Differentiation Response of Neuroblastoma Cells. *Br J Cancer* (2001) 85 (10):1564–71. doi: 10.1054/bjoc.2001.2144
11. Araujo TM, Seabra AD, Lima EM, Assumpcao PP, Montenegro RC, Demachki S, et al. Recurrent Amplification of RTEL1 and ABCA13 and its Synergistic Effect Associated With Clinicopathological Data of Gastric Adenocarcinoma. *Mol Cytogenet* (2016) 9(1):52. doi: 10.1186/s13039-016-0260-x
12. Takahashi K, Kimura Y, Nagata K, Yamamoto A, Matsuo M, Ueda K. ABC Proteins: Key Molecules for Lipid Homeostasis. *Med Mol Morphol* (2005) 38 (1):2–12. doi: 10.1007/s00795-004-0278-8
13. Nobili S, Lapucci A, Landini I, Coronnello M, Roviello G, Mini E. Role of ATP-Binding Cassette Transporters in Cancer Initiation and Progression. *Semin Cancer Biol* (2020) 60:72–95. doi: 10.1016/j.semcancer.2019.08.006
14. Favre G, Laurain A, Aranyi T, Szeri F, Fulop K, Le Saux O, et al. The ABCC6 Transporter: A New Player in Biomineralization. *Int J Mol Sci* (2017) 18 (9):1941. doi: 10.3390/ijms18091941
15. Le Saux O, Martin L, Aherrahrou Z, Leftheriotis G, Váradi A, Brampton CN. The Molecular and Physiological Roles of ABCC6: More Than Meets the Eye. *Front Genet* (2012) 3:289. doi: 10.3389/fgene.2012.00289

16. Terry SF. The Human Face of ABCC6. *FEBS Lett* (2020) 594(23):4151–7. doi: 10.1002/1873-3468.14002
17. Bergen AA, Plomp AS, Schuurman EJ, Terry S, Breuning M, Dauwerse H, et al. Mutations in ABCC6 Cause Pseudoxanthoma Elasticum. *Nat Genet* (2000) 25(2):228–31. doi: 10.1038/76109
18. Wang J, Near S, Young K, Connelly PW, Hegele RA. ABCC6 Gene Polymorphism Associated With Variation in Plasma Lipoproteins. *J Hum Genet* (2001) 46(12):699–705. doi: 10.1007/s100380170003
19. Peloso GM, Demissie S, Collins D, Mirel DB, Gabriel SB, Cupples LA, et al. Common Genetic Variation in Multiple Metabolic Pathways Influences Susceptibility to Low HDL-Cholesterol and Coronary Heart Disease. *J Lipid Res* (2010) 51(12):3524–32. doi: 10.1194/jlr.P008268
20. Ibold B, Tiemann J, Faust I, Ceglarek U, Dittrich J, Gorgels T, et al. Genetic Deletion of Abcc6 Disturbs Cholesterol Homeostasis in Mice. *Sci Rep* (2021) 11(1):2137. doi: 10.1038/s41598-021-81573-1
21. Singal AG, Waljee AK, Patel N, Chen EY, Tiro JA, Marrero JA, et al. Therapeutic Delays Lead to Worse Survival Among Patients With Hepatocellular Carcinoma. *J Natl Compr Canc Netw* (2013) 11(9):1101–8. doi: 10.6004/jnccn.2013.0131
22. Sengupta S, Parikh ND. Biomarker Development for Hepatocellular Carcinoma Early Detection: Current and Future Perspectives. *Hepat Oncol* (2017) 4(4):111–22. doi: 10.2217/hep-2017-0019
23. Waterham HR, Ferdinandusse S, Wanders RJ. Human Disorders of Peroxisome Metabolism and Biogenesis. *Biochim Biophys Acta* (2016) 1863 (5):922–33. doi: 10.1016/j.bbamcr.2015.11.015
24. Kim JA. Peroxisome Metabolism in Cancer. *Cells* (2020) 9(7):1692. doi: 10.3390/cells9071692
25. Litwin JA, Beier K, Volkl A, Hofmann WJ, Fahimi HD. Immunocytochemical Investigation of Catalase and Peroxisomal Lipid Beta-Oxidation Enzymes in Human Hepatocellular Tumors and Liver Cirrhosis. *Virchows Arch* (1999) 435(5):486–95. doi: 10.1007/s004280050432
26. Demidenko R, Razanauskas D, Daniunaite K, Lazutka JR, Jankevicius F, Jarmalaite S. Frequent Down-Regulation of ABC Transporter Genes in Prostate Cancer. *BMC Cancer* (2015) 15(1):683. doi: 10.1186/s12885-015-1689-8
27. Scheffer GL, Hu X, Pijnenborg AC, Wijnholds J, Bergen AA, Scheper RJ. MRP6 (ABCC6) Detection in Normal Human Tissues and Tumors. *Lab Invest* (2002) 82(4):515–8. doi: 10.1038/labinvest.3780444
28. Lefebvre P, Chinetti G, Fruchart JC, Staels B. Sorting Out the Roles of PPAR Alpha in Energy Metabolism and Vascular Homeostasis. *J Clin Invest* (2006) 116(3):571–80. doi: 10.1172/JCI27989
29. Zhang N, Chu ES, Zhang J, Li X, Liang Q, Chen J, et al. Peroxisome Proliferator Activated Receptor Alpha Inhibits Hepatocarcinogenesis Through Mediating NF-κB Signaling Pathway. *Oncotarget* (2014) 5: (18):8330. doi: 10.18632/oncotarget.2212
30. Panigrahy D, Kaipainen A, Huang S, Butterfield CE, Barnés CM, Fannon M, et al. PPARα Agonist Fenofibrate Suppresses Tumor Growth Through Direct and Indirect Angiogenesis Inhibition. *Proc Natl Acad Sci USA* (2008) 105: (3):985–90. doi: 10.1073/pnas.0711281105
31. Yamasaki D, Kawabe N, Nakamura H, Tachibana K, Ishimoto K, Tanaka T, et al. Fenofibrate Suppresses Growth of the Human Hepatocellular Carcinoma Cell *via* PPARα-Independent Mechanisms. *Eur J Cell Biol* (2011) 90: (8):657–64. doi: 10.1016/j.ejcb.2011.02.005
32. Luo Y, Xie C, Brocker CN, Fan J, Wu X, Feng L, et al. Intestinal PPARalpha Protects Against Colon Carcinogenesis *via* Regulation of Methyltransferases DNMT1 and PRMT6. *Gastroenterology* (2019) 157(3):744–59 e4. doi: 10.1053/j.gastro.2019.05.057
33. Lake BG. Mechanisms of Hepatocarcinogenicity of Peroxisome-Proliferating Drugs and Chemicals. *Annu Rev Pharmacol Toxicol* (1995) 35(1):483–507. doi: 10.1146/annurev.pa.35.040195.002411

Conflict of Interest: The authors declare that the research was conducted in the absence of any commercial or financial relationships that could be construed as a potential conflict of interest.

Publisher's Note: All claims expressed in this article are solely those of the authors and do not necessarily represent those of their affiliated organizations, or those of the publisher, the editors and the reviewers. Any product that may be evaluated in this article, or claim that may be made by its manufacturer, is not guaranteed or endorsed by the publisher.

frontiers in Oncology

ORIGINAL RESEARCH
published: 22 March 2022
doi: 10.3389/fonc.2022.855952

Abnormal ECA-Binding Membrane Glycans and Galactosylated CAT and P4HB in Lesion Tissues as Potential Biomarkers for Hepatocellular Carcinoma Diagnosis

*Ying Kong[1], Hao Chen[2], Mengyu Chen[1], Yongshuai Li[1], Jiarong Li[1], Qi Liu[1], Huan Xiong[1], Tangxi Guo[3], Yan Xie[1], Yufeng Yuan[4] and Xiao-Lian Zhang[1,5]**

[1] Hubei Province Key Laboratory of Allergy and Immunology, and Department of Immunology, Wuhan University School of Basic Medical Sciences, Wuhan, China, [2] Department of Pathology, Zhongnan Hospital of Wuhan University, Wuhan, China, [3] Department of Radiation and Medical Oncology, Zhongnan Hospital of Wuhan University, Wuhan, China, [4] Hepatobiliary and Pancreatic Surgery, Zhongnan Hospital of Wuhan University, Wuhan, China, [5] Allergy Department of Zhongnan Hospital, State Key Laboratory of Virology, Medical Research Institute Wuhan University School of Medicine, Wuhan, China

OPEN ACCESS

Edited by:
Yunfei Xu,
Shandong University, China

Reviewed by:
Yongyi Zeng,
First Affiliated Hospital of Fujian Medical University, China
Ning Ren,
Fudan University, China

***Correspondence:**
Xiao-Lian Zhang
zhangxiaolian@whu.edu.cn

Specialty section:
This article was submitted to Cancer Molecular Targets and Therapeutics, a section of the journal Frontiers in Oncology

Received: *16 January 2022*
Accepted: *21 February 2022*
Published: *22 March 2022*

Citation:
Kong Y, Chen H, Chen M, Li Y, Li J, Liu Q, Xiong H, Guo T, Xie Y, Yuan Y and Zhang X-L (2022) Abnormal ECA-Binding Membrane Glycans and Galactosylated CAT and P4HB in Lesion Tissues as Potential Biomarkers for Hepatocellular Carcinoma Diagnosis. Front. Oncol. 12:855952. doi: 10.3389/fonc.2022.855952

Hepatocellular carcinoma (HCC) is one of the most common types of cancer. Despite decades of research efforts, the search for novel biomarkers is still urgently needed for the diagnosis of HCC and the improvement of clinical outcomes. Previous studies of HCC clinical biomarkers have usually focused on serum and urine samples (e.g., serum Alpha-fetoprotein (AFP). However, cellular membrane proteins in lesion tissues are less used in HCC diagnosis. The abnormal expression of membrane glycoproteins in tumor lesions are considered as potential targets for tumor diagnosis and tumor therapies. Here, a lectin array has been employed to screen and identify abnormal glycopatterns and cellular membrane glycans in HCC lesion tissues compared with adjacent non-tumor tissues. We found that there was significantly less expression of *Erythrina cristagalli* (ECA) lectin binding (Galβ1-3/β1-4) glycans on the cellular membrane of HCC lesion tissues compared with those of adjacent non-tumor tissues. Immunohistochemistry analysis further showed that ECA-binding ability on the membrane proteins of HCC tissues progressively decreased in different tumor-node-metastasis (TNM) stages (stage I to stage III) as the malignancy of liver cancer increased. Receiver operating curve (ROC) analysis showed ECA-binding ability yielding a sensitivity of 85% and specificity of 75%, and a combination of ECA and AFP has better clinical diagnostic efficiency, yielding a sensitivity of 90% and specificity of 85%, than ECA or AFP assay alone. ECA pull-down followed by mass spectrometry further showed that there was significantly less expression of ECA binding membrane catalase (CAT) and prolyl 4-hydroxylase beta polypeptide (P4HB) in HCC tissues compared with the adjacent non-tumor tissues. The abnormally increased expression of total CAT and P4HB and decreased expression of galactosylated membrane CAT and P4HB in HCC cell lines were correlated with an HCC metastasis status. Our findings suggest that abnormal declined ECA-binding galatosylated

membrane glycans and two galactosylated-CAT and P4HB glycoproteins in lesion tissues are potential biomarkers in the diagnosis and/or metastasis prediction for HCC.

Keywords: lectin array, *Erythrina cristagalli* (ECA) lectin, hepatocellular carcinoma, catalase (CAT), prolyl 4-hydroxylase beta polypeptide (P4HB), membrane biomarker for diagnosis

INTRODUCTION

Hepatocellular carcinoma (HCC) is the most common type of primary liver cancer and the third leading cause of death among cancers worldwide according to World Health Organization—WHO 2020 (1, 2). The overall 5-year survival rates have been reported to be as low as about 18% around the world (3). The incidence and mortality of HCC have been increasing rapidly for the past several years worldwide, and this represents a considerable public health burden (4–7). The major risk factors of HCC include chronic infection with hepatitis B or C virus (HBV or HCV), type 2 diabetes, heavy alcohol intake, and obesity (8). The poor prognosis of HCC is due to the rapid progression and lack of specific symptoms of HCC and over 60% of patients are diagnosed at an advanced stage or when metastasis has occurred (9).

Several biomarkers have been identified for HCC, such as alpha-fetoprotein (AFP), apyrimidinic endodeoxyribonuclease 1 (APEX1), glypican 3 (GPC3), Dickkopf-1 (DKK1), and Golgi protein-73 (GP73) (10–14). Most clinical HCC biomarkers have usually focused on serum and urine samples (e.g., serum AFP). Among them, AFP is considered currently the most successful diagnostic marker for HCC. Measurement of serum abnormal AFP levels serves as a routine method in clinical HCC surveillance and diagnosis, whereas sensitivity and specificity are still poor (15). Despite decades of research efforts, the search for novel biomarkers is still urgently needed for the diagnosis of HCC and the improvement of clinical outcomes.

In general, membrane proteins play important roles in tumor cell survival and cell communication, as they function as transporters, receptors, anchors, and enzymes. They also served as potential targets for drugs that block receptors or inhibit enzymes related to diseases, and targets for tumor diagnosis and tumor immunotherapies (such as chimeric antigen receptor T cell (CAR-T)). However, to date, membrane proteins are rarely used for HCC diagnosis (16).

Over 50% of proteins in mammal cells and 70–90% of mammal cell membrane proteins and secreted proteins are N-glycosylated (17). Thus, we intended to explore glycoconjugates biomarkers on the cellular surface of human HCC and further assess their value and performance in the diagnosis of HCC.

Lectins are a group of proteins that have a significant carbohydrate-binding ability that could specifically recognize glycan structures on glycoproteins (18). Currently, lectin array and lectin-agarose are usually used for screening and enrichment of low abundant glycoproteins to discover new biomarkers for cancer diagnosis and therapy (19).

In this study, we extracted cell membrane proteins from HCC and adjacent tissues samples and performed lectin array with 35 kinds of different lectins, combined with mass spectrometry (MS), to identify membrane glycoproteins biomarkers for HCC diagnosis. We found significantly decreased *Erythrina cristagalli* lectin (ECA) lectin-binding ability and ECA-binding membrane glycoproteins catalase (CAT) and prolyl 4-hydroxylase beta polypeptide (P4HB) from HCC tissues samples as potential candidates with diagnostic and/or metastasis prediction value for human HCC. Our findings also provide a set of potential targets for HCC diagnostic application and therapeutic strategies.

MATERIALS AND METHODS

Ethics Statements

The collection and use of all human HCC samples for research presented here were approved by the Ethical Committee of Wuhan University School of Medicine in Wuhan, China. Informed consent was obtained from each patient for the collection of the HCC samples. The study methodologies were conducted in accordance with the ethical guidelines of the Declaration of Helsinki.

HCC Tissue Specimens

Surgically resected primary HCC tissues and paired adjacent non-tumor tissues were collected from a total of 41 HCC patients who had not experienced prior chemotherapy or radiotherapy at the Zhongnan Hospital of Wuhan University School of Medicine (Wuhan, China). Medical records were reviewed by study physicians to confirm the diagnosis of HCC and to record patient characteristics [e.g., AFP, tumor size, tumor number, tumor, node, and tumor-node-metastasis (TNM) classification]. A lectin array assay was performed using 10 HCC tissues and paired adjacent non-tumor tissues. Immunofluorescence was performed using 7 HCC tissues and paired adjacent non-tumor tissues. Immunohistochemistry was performed using 5 HCC tissues (TNM = I), 10 HCC tissues (TNM = II), and 5 HCC tissues (TNM = III). ECA pull down assay was performed followed by an LC–MS/MS or Western blot analysis using 4 HCC tissues and paired adjacent non-tumor tissues.

Cell Lines

Human low metastatic liver cell MHCC-97L was a gift from Prof. Fubing Wang from the Hubei Key Laboratory of Tumor Biological Behaviors of the Zhongnan Hospital of Wuhan University School of Medicine, and high metastatic liver cell HCC-LM3 was purchased from the China Center for Type Culture Collection (CCTCC) of Wuhan University, China. Human hepatocellular carcinoma cells Huh7.5.1, normal liver cells L02, MHCC-97L, and HCC-LM3 were maintained in Dulbecco's modified Eagle's medium (DMEM) supplemented

with 10% fetal bovine serum (FBS, Gibco) (Invitrogen, USA) at 37°C in a 5% CO_2 atmosphere as previously described (20, 21).

Membrane Protein Extraction

Membrane protein extraction was performed using a Membrane and Cytosol Protein Extraction Kit (Beyotime, Shanghai, China) (22). Briefly, 30–50 mg tissues or 3×10^6 cells were resuspended in 1 ml of membrane protein isolation solution A and homogenized on ice (for tissue samples) or lysed by two freeze-thaw cycles at liquid nitrogen and 37°C water bath respectively (for cell samples). Cell debris was discarded after centrifugation at 700*g* at 4°C for 10 min. The supernatant was centrifuged at 14,000*g* at 4°C for 30 min to settle the membrane protein debris. The pellet was resuspended in 300 μl solution B and vortexed at a high speed for 5 s twice. After centrifugation at 14,000*g* at 4°C for 5 min, the resulting supernatant was collected as the membrane protein fraction.

Lectin Array Analysis

Lectin array analysis was performed as previously described (20). In brief, 35 kinds of commercially available lectins from the Vector Laboratories (Burlingame, CA) and the Sigma-Aldrich were immobilized onto a microplate. The total membrane proteins (2 mg) from HCC tissues and adjacent non-tumor tissues were labeled with fluorescent dye Cy3 (GE Healthcare; Buckinghamshire, UK) and about 10–15 μg protein was spotted for each individual spot on the lectin microplate. The Mean Fluorescence Intensity (MFI) at 570 nm was determined on a SpectraMax® i3x microplate reader (Molecular Devices, Sunnyvale, CA), and average backgrounds were removed. The lectin microarray data were normalized, and the fold change was evaluated by comparison of the data from HCC tissues with adjacent non-tumor tissues and then analyzed by using GraphPad Prism 9.0.

Immunohistochemistry (IHC) and Image Analysis

The IHC staining was performed as follows. Briefly, the tissue sections were formalin-fixed and paraffin-embedded. Approximately 4 μm of tissue sections were deparaffinized, rehydrated, and subjected to antigen retrieval in boiling citrate buffer (Servicebio) containing 0.05% Tween 20 for 30 min, then blocked with 0.3% peroxide for 10 min and 5% bovine serum albumin (BSA) for 30 min. The sections were incubated with biotin-conjugated ECA (1:250; Vector) overnight at 4°C, and then were incubated with 1:10,000 dilution of horseradish peroxidase (HRP)-conjugated streptavidin at 37°C for 45 min according to the instructions of the manufacturer. Finally, tissue sections were incubated with 3′, 3′-diaminobenzidine (DAB) (Sigma) until a brown color developed, and was counterstained with Harris' modified hematoxylin. The slides were scanned using the Phenoptics™ Vectra 3 System (Akoya Biosciences, Inc., USA), and the digital images were acquired at ×200 magnification using the Phenochart 1.0.2 software. The entire area of the slides was scored and quantified using inForm® 2.4.0 Advanced Image Analysis software. Using supervised machine learning algorithms, images were scored in the mode of 0–3+(4-bin) which was divided into 3 bins as 0/1+, 1+/2+, 2+/3+ after the process of cell segmentation (detecting cells and their nuclear and membranous compartments) (23). Percentage positivity of the cell nuclei and membrane within each bin was presented and the H-score is calculated using the percentages in each bin and range from 0 to 300. The sensitivity and specificity calculations were performed as described in the previous study.

Immunofluorescence (IF) Analysis

The IF staining was performed as follows: 8 μm of frozen sections was set from −80°C to room temperature for 15 min and fixed with 4% paraformaldehyde for 10 min. After washing with 1× PBS, the cells were then incubated with 5% BSA for 30 min at room temperature and with biotin-conjugated ECA (1:25; Vector) overnight at 4°C. After washing with 1× PBS, the cells were incubated with FITC-conjugated streptavidin (1:500; EY) and 4′,6-diamidino-2-phenylindole (DAPI) (1:5,000; Sigma-Aldrich) in the dark for 30 min at room temperature. The coverslips were washed with PBS, mounted, and analyzed with a Leica Aperio VERSA 8 microscope (Leica Biosystems Richmond, Inc., USA).

ECA Lectin Pull-Down Assay

ECA pull-down assay was performed as follows: biotin-ECA was mixed with total membrane proteins to the final concentration of 20 μg/ml and incubated at 4°C overnight. Then 30 μl streptavidin agarose resin (Thermo Scientific, USA) was washed with 1× PBS three times, resuspended with the protein mixture, and incubated at 4°C overnight. After being washed with 1× PBS three times to remove the unbound proteins, the resin was boiled at 100°C for 10 min and followed by SDS-PAGE and western blot analysis. The total membrane protein concentration was measured using a BCA protein assay kit (Fermentas, USA).

TripleTOF/TOF-Mass Spectrum (MS) Analysis

In brief, 25 μl of membrane proteins extracted from HCC tissue and paired adjacent non-tumor tissue were prepared by biotin-conjugated ECA plus streptavidin agarose resin pull down, and then analyzed with SDS-PAGE and stained by commassie blue staining solution. The corresponding protein bonds were excised for MS analysis by the Wuhan Institute of Biotechnology of China. For protein identification, MS/MS spectra acquired by TripleTOF 5600+ were searched with ProteinPilot v.4.5 against the Uniprot-SwissProt human reference proteome database, using the Paragon Algorithm. The parameters were set as below: Sample Type, Identification; Cys Alkylation, Iodoacetamide; Digestion, Trypsin; Search Effort, Rapid ID. Only proteins with a threshold >95% confidence (>1.3 Unused Score) were considered for protein identification.

Western Blot

Approximately 10 μg of total membrane and ECA binding membrane proteins by ECA lectin pull-down assay were subjected to 10% SDS-PAGE. After electrophoresis, the gels were transferred onto PVDF membranes (Millipore, Germany) and the membranes were blocked with 5% skim milk at room temperature for 2 h. The blot was probed with rabbit polyclonal antibody against CAT and P4HB (1:1,000; ABclonal) as primary

antibodies at 4°C overnight, respectively, and incubated with goat anti-rabbit antibody IgG as a secondary antibody (1:10,000; Proteintech) at 37°C for 45 min, and developed using an ECL system (UVP Bioimaging, USA). Na^+/K^+-ATPase (ABclonal, Wuhan, China) was used as an internal membrane control for quantitation, and densitometric analysis of each band was measured using Image J software.

Statistical Analysis

Data were presented as mean ± SD. Differences between the two groups were tested by unpaired Student's t tests. Differences between more than two groups were tested by one-way ANOVA followed by Sidak's multiple comparisons test. GraphPad Prism software (Version 9.0) was used to determine statistical significance. *P*-values under 0.05 were considered statistically significant (*p <0.05, **p <0.01, *** p <0.001, ****p <0.0001). NS represents no statistical significance.

RESULTS

Significantly Declined ECA Binding Membrane Glycans of HCC Lesion Tissues Compared to Adjacent Non-Tumor Tissues With Lectin Array

HCC tissues and paired adjacent non-tumor tissues were collected as described in *Materials and Methods* (**Table 1**). To identify the differentially expressed cellular surface glycoconjugates of HCC tissues compared to adjacent non-tumor tissues, a lectin microarray analysis with 35 kinds of different lectins was performed on 10 pairs of purified membrane proteins from 10 HCC and adjacent non-tumor tissues and analyzed with heatmap by Graphpad Prism 9.0 (**Figures 1A, B**). A total of 35 kinds of lectins and their corresponding binding glycans are shown in **Table 2**. We observed differential expression of glycopatterns of membrane proteins in HCC lesion tissues compared with adjacent non-tumor tissues (**Table 3**). A 1.3-fold change (FC) cut-off was applied to classify glycans binding with lectins as up (≥1.3-fold) or down-regulated (≤0.76-fold). A total of 9 lectins that could bind with cellular membrane glycans of HCC tissues showed up-expressed MFI with 1.3 times (**Table 3**) and a total of 15 lectins showed down-expressed MFI with 0.76 times over adjacent non-tumor tissues (**Table 3** and **Figure 1C**). Among downregulated glycan-binding lectins, 11 lectins showed statistical significance and it is noticeable that ECA was presented the most significant difference (FC = 0.307, ****p <0.0001) (**Table 3**) and was selected to further confirm its association with HCC. Because Galβ1-3GlcNAc/Galβ1-4GlcNAc are usually considered as binding ligands for ECA (25), we postulate that abnormal declined ECA-binding membrane galactosylated glycans expression in lesion tissues of HCC samples compared with adjacent non-tumor tissues.

We then performed immunofluorescence (IF) analysis using FITC-conjugated-ECA staining with 7 paired HCC tissues and adjacent non-tumor tissues to confirm the galactosylated glycan expression profiles. Consistent with the lectin array analysis,

TABLE 1 | Summary of clinical characteristics of human HCC samples.

Groups	For lectin array analysis	For IF analysis	For MS analysis	For IHC analysis	For WB analysis
Cases (24)	10	7	1	20	3
Gender					
Male	8	6	1	18	2
Female	2	1	–	2	1
Age (year)					
<50	5	1	–	2	–
≥50	5	6	1	18	3
AFP (ng/ml)					
<20	4	2	1	12	2
≥20	6	5	–	8	1
HBV-DNA (copies/ml)					
<1.00E+03	8	5	1	16	3
≥1.00E+03	2	2	–	4	–
Tumor size					
<5	5	3	1	9	3
≥5	5	4	–	11	–
Tumor number					
Single	9	7	1	16	3
Multiple	1	0	–	4	–
Vascular invasion					
Absent	9	2	1	16	1
Present	1	5	–	4	2
Metastasis					
Absent	8	5	1	11	3
Present	2	2	–	9	–
TNM stage					
Stage I	4	0	–	5	1
Stage II	4	4	1	10	2
Stage III	2	3	–	5	–

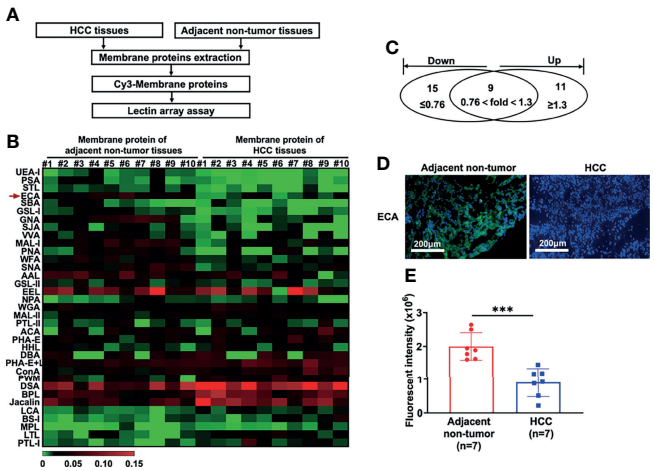

FIGURE 1 | Lectin array and immunofluorescence analysis of glycopatterns on membrane proteins of HCC tissues and adjacent non-tumor tissues. **(A)** Workflow of the strategy for the determination of differentially expressed membrane glycopatterns in HCC tissues compared with adjacent non-tumor tissues. **(B, C)** Expressions of glycans on the membrane proteins between HCC tissues and adjacent non-tumor tissues analyzed by 35 different lectins presented as a heatmap **(B)** and Venn diagram **(C)**. #1 to #10: 10 HCC patients; **(D, E)** Immunofluorescence analysis of fluorescence intensity of glycans binding with ECA on cell membrane proteins between HCC and adjacent non-tumor tissues. Images are stained as FITC-conjugated ECA (green, membrane) and DAPI (blue, nuclei). Fluorescent intensities in **(E)** are presented as the mean ± SD using unpaired Student's t-tests (***$p < 0.001$).

HCC tissues presented dramatically decreased green FITC fluorescence of ECA compared to adjacent non-tumor tissues (**Figures 1D, E**).

Significantly Declined ECA Binding-Glycans in Different TNM Stage of HCC Lesion Tissues

Twenty HCC tissue samples (TNM I = 5, TNM II = 10, TNM III = 5) with paired adjacent non-tumor tissues served to confirm the expression change and evaluate the potential clinical significance of ECA using immunohistochemistry (IHC) (**Table 4**). The staining intensity of ECA showed a significantly lower level in HCC tissues of different TNM stages (from Stage 1 to Stage III) compared with those in adjacent non-tumor tissues (****p <0.0001) (**Figures 2A–F**). The binding affinity of ECA to cellular membrane glycans of HCC decreased with significant progressive from early Stage I to late Stage III (Stage I *vs* late Stage II: ****p <0.0001, Stage I *vs* late Stage III: ****p <0.0001, Stage II *vs* Stage III: ***p = 0.0010, **Figure 2G**). The IHC analysis result is positively correlated with the lectin blot data. These results indicated that decreased β1, 3/β1,4 galactosylated glycans binding with ECA may be related to the malignant progression and differentiation of HCC. Further, an ROC curve analysis was used to test the performance of ECA for HCC diagnosis (**Figure 2H**). The downregulation of ECA showed good performance in distinguishing HCC tissues from adjacent non-tumor tissues control, and the area under the curve (AUC) values are 0.84 (95% confidence interval—CI: 0.7084 to 0.9616), with a sensitivity of 85% (95% CI = 63.96–94.76%) and specificity of 75% (95% CI = 53.13–88.81%).

Then we further analyzed the correlation between HCC serum AFP concentrations and binding affinities of lectin ECA to membrane proteins of HCC tissues. The subjects were divided into two groups according to the serum AFP concentration cut-off value 20 ng/L, as shown in **Figure 2I**. The high concentration AFP group (≥20 ng/L) showed a significantly lower ECA IHC score compared with the low concentration AFP group (≤20 ng/L), which indicates that the binding affinity of lectin ECA with HCC membrane glycoproteins is negatively correlated with HCC serum AFP concentrations.

We further combined decreased ECA with increased AFP to access whether this combination could enhance the diagnostic performance. The results showed that the combination of ECA and AFP results yielded a better clinical diagnostic efficiency between HCC tissues and adjacent non-tumor tissues than ECA or AFP assay alone, and yielded a sensitivity of 90% and specificity of 85%, while the sensitivity of AFP used alone was only 40%. These results imply that declined β1,3/β1,4 galactosylated glycans-binding ECA may be a potential biomarker for HCC diagnosis.

Identification of Significantly Declined ECA-Binding Membrane Galactosylated CAT and P4HB Protein Expression in HCC Tissues

Based on the above results, we then sought to identify specific membrane galactosylated glycoproteins in HCC. For protein identification, we employed the workflow as summarized in **Figure 3A**. ECA-binding membrane proteins from HCC tissues and adjacent non-tumor tissues were pulled down by biotin-ECA plus streptavidin-resin pull-down assay, followed by SDS-PAGE and coomassie blue staining shown in **Figure 3B**. The differentially expressed protein bands (indicated by the red arrow) between HCC tissue and adjacent non-tumor tissue were excised and analyzed by liquid chromatography-tandem mass

TABLE 2 | Different glycan patterns between HCC tissues and adjacent non-tumor tissues by lectin microarray analysis.

No.	Abbr.	Source	Preferred carbohydrate specificity	Company
1	AAL	*Aleuria aurantia*	Fucα1-6GlcNAc, Fucα1-3(Galβ1-4)GlcNAc	Vector (USA)
2	ACA	*Amaranthus caudatus*	Galβ1-3GalNAc	Vector (USA)
3	BPL	*Bauhinia purpurea*	Galβ1-3GalNAc, GalNAc	Vector (USA)
4	BS-I	*Bandeiraea simplicifolia*	α-Gal, α-GalNAc, Galα-1,3Gal, Galα-1,6Glc	Sigma-Aldrich (USA)
5	ConA	*Canavalia ensiformis*	6(Manα1-3)Man, terminal GlcNAc	Calbiochem
6	DBA	*Dolichos biflorus*	αGalNAc	Vector (USA)
7	DSA	*Datura stramonium*	(GlcNAcβ1-4)n, Galβ1-4GlcNAc	Vector (USA)
8	ECA	*Erythrina cristagalli*	Galβ1-3GlcNAc, Galβ1-4GlcNAc	Vector (USA)
9	EEL	*Euonymus europaeus*	Galα3Gal	Vector (USA)
10	GNA	*Galanthus nivalis*	High-Mannose,Manα1-3Man	Vector (USA)
11	GSL-I	*Griffonia simplicifolia*	αMan	Vector (USA)
12	GSL-II	*Griffonia simplicifolia*	Agalactosylated Tri/tetra-antennary glycans	Vector (USA)
13	HHL	*Hippeastrum hybrid*	High-Man, Manα1-3Man, Manα1-6Man	Vector (USA)
14	Jacalin	*Artocapus integrifolia*	Galβ1-3GalNAcα-Ser/Thr(T)	Vector (USA)
15	LCA	*Lens culinaris*	Fucα1-6GlcNAc, α-D-Glc, α-D-Man	Vector (USA)
16	LTL	*Lotus tetragonolobus*	Fucα1-3Galβ1-4GlcNAc	Vector (USA)
17	MAL-I	*Maackia amurensis*	Galβ1-4GlcNAc	Vector (USA)
18	MAL-II	*Maackia amurensis*	Siaα2-3Gal	Vector (USA)
19	MPL	*Maclura pomifera*	Galβ3GalNAc	Vector (USA)
20	NPA	*Narcissus pseudonarcissus*	High-Man, Manα1-6Man	Vector (USA)
21	PHA-E	*Phaseolus vulgaris*	Bisecting GlcNAc	Vector (USA)
22	PHA-E+L	*Phaseolus vulgaris*	Bisecting GlcNAc, bi-antennary N-glycans	Vector (USA)
23	PNA	*Peanut*	Galβ1-3GalNAcα-Ser/Thr(T)	Vector (USA)
24	PSA	*Pisum sativum*	core-fucosylated, trimannosyl structure	Sigma-Aldrich (USA)
25	PTL-I	*Psophocarpus tetragonolobus*	GalNAc	Vector (USA)
26	PTL-II	*Psophocarpus tetragonolobus*	Gal	Vector (USA)
27	PWM	*Sambucus nigra*	N–acetyl–D–glucosamine	Vector (USA)
28	SBA	*Solanum tuberosum*	α or β GalNAc, GalNAcα1-3GalNAc	Sigma-Aldrich (USA)
29	SJA	*Sophora japonica*	βGalNAc	Vector (USA)
30	SNA	*Soybean*	Sia2-6Gal/GalNAc	Vector (USA)
31	STL	*Solanum tuberosum*	GlcNAcβ1-4GlcNAc, Mixture Man5 to Man9	Vector (USA)
32	UEA-I	*Ulex europaeus*	Fucα1-2Galβ1-4GlcNAc	Sigma-Aldrich (USA)
33	VVA	*Vicia villosa*	GalNAcα1-3Gal	Vector (USA)
34	WFA	*Wisteria floribunda*	GalNAcβ1-4GlcNAc, Galβ1-3(-6)GalNAc	Vector (USA)
35	WGA	*Triticum vulgaris*	GlcNAc	Sigma-Aldrich (USA)

spectrometry (LC–MS/MS). A total of 169 differentially expressed proteins were identified, among which 69 proteins were consistent with the molecular weights (MWs) of corresponding excised membrane proteins. The protein list is filtered based on Unused ProtScore, from our MS results (**Table 5**). Both CAT and P4HB are displayed as the two highest coverage and scored with peptides at 95% confidence by MS/MS spectra shown in **Figures 3C, D**. Therefore, decreased ECA binding-galactosylated-CAT and P4HB are selected for further research.

Much Less Membrane Galactosylated CAT and P4HB Expression in High Metastatic HCC Cells Compared to Low Metastatic and Normal Liver Cells

First, we detected the total membrane CAT and P4HB proteins expression by western blot. A higher expression of total membrane CAT and P4HB was found in the Huh7.5.1 cell line compared to L02 (***p <0.001, **Figures 4A–C**). Next, biotin-conjugated ECA pull-down and western blot assay were performed to verify the expressional changes of ECA-binding-membrane-galactosylated CAT and P4HB proteins in HCC Huh7.5.1 cell line and normal L02 liver cell line. ECA-binding-galactosylated-CAT and P4HB protein expressions were dramatically decreased in the HCC Huh7.5.1 cell line compared to the L02 cell line (***p <0.001, **Figures 4A, D, E**). These results reveal that an increased expression of total CAT and P4HB proteins and a decreased β1,3/β1,4 galactosylated-CAT and P4HB on the cell membrane of the HCC cell line correlate with HCC malignancy.

MHCC-97L is a low metastatic liver cell line, while HCC-LM3 cell is a high metastatic cell line. We examined the total membrane CAT and P4HB protein expression and found a relatively higher expression of total CAT and P4HB proteins in the normal L02 liver cell line compared to the low metastatic MHCC-97L and high metastatic HCC-LM3 cell line (***p <0.001, **Figures 4F–H).** However, a progressively decreased expression of ECA-binding-galactosylated-CAT and P4HB was found in the high metastatic HCC-LM3 cell line compared to the low metastatic MHCC-97L and normal L02 liver cell line (***p <0.001, **Figures 4F, I, J**). These results indicated that increased expression of total membrane CAT and P4HB proteins and decreased galactosylated membrane CAT and P4HB proteins may be correlated with HCC malignant metastasis.

TABLE 3 | Lectin binding glycopatterns of membrane glycoproteins between HCC tissues and adjacent non-tumor tissues.

Lectin	Carbohydrate specificity	Fold change (HCC/Adjacent non-tumor)
UEA-I	Fucα1-2Galβ1-4Glc(NAc)	0.147**
PSA	core-fucosylated, trimannosyl structure	0.225**
STL	GlcNAcβ1-4GlcNAc, Mixture Man5 to Man9	–
ECA	Galβ1-4GlcNAc, Galβ1-3GlcNAc	0.307****
SBA	α or β GalNAc, GalNAcα1-3GalNAc	0.372*
GSL-I	αMan	0.394**
GNA	High-Mannose,Manα1-3Man	0.412**
SJA	βGalNAc	0.428*
VVA	GalNAcα1-3Gal	0.514*
MAL-I	Galβ-1,4GlcNAc	0.523**
PNA	Galβ1-3GalNAcα-Ser/Thr(T)	–
WFA	GalNAcβ1-4GlcNAc, Galβ1-3(-6)GalNAc	0.636*
SNA	Sia2-6Gal/GalNAc	0.660*
AAL	Fucα1-6GlcNAc, Fucα1-3(Galβ1-4)GlcNAc	–
GSL-II	Agalactosylated Tri/tetra-antennary glycans	–
EEL	Galα3Gal	–
NPA	High-Man, Manα1-6Man	–
WGA	GlcNAc	–
MAL-II	Siaα2-3Gal	–
PTL-II	Gal	–
ACA	Galβ1-3GalNAc	–
PHA-E	Bisecting GlcNAc	–
HHL	High-Man, Manα1-3Man, Manα1-6Man	–
PHA-E+L	Bisecting GlcNAc, bi-antennary N-glycans	–
DBA	αGalNAc	1.330*
ConA	6(Manα1-3)Man, terminal GlcNAc	1.522*
PWM	N–acetyl–D–glucosamine	1.685*
DSA	(GlcNAcβ1-4)n, Galβ1-4GlcNAc	1.769**
BPL	Galβ1-3GalNAc, GalNAc	1.813**
Jacalin	Galβ1-3GalNAcα-Ser/Thr(T)	1.830*
LCA	Fucα1-6GlcNAc, α-D-Glc, α-D-Man	1.881***
MPL	Galβ1-3GalNAc, GalNAc	–
BS-I	α-Gal, α-GalNAc, Galα-1,3Gal, Galα-1,6Glc	–
LTL	Fucα1-3Galβ1-4GlcNAc	2.490***
PTL-I	Galβ1-3GalNAc, GalNAc	–

*–: no significance; *p < 0.05; **p < 0.01; ***p < 0.001; ****p < 0.0001.*

Consistent with the results from HCC cell lines, the total membrane CAT and P4HB expression were higher in HCC tissues compared with adjacent non-tumor tissues (**Figures 4K–M**). We further measured the expression levels of ECA-binding-galactosylated-CAT and P4HB on the cellular membrane of HCC tissues vs. adjacent non-tumor tissues by using biotin-conjugated ECA pull-down and western blot analysis as shown in **Figures 4K, N, O**. We also found much lower expression levels of ECA-binding-membrane CAT and P4HB in HCC tumor tissues than adjacent non-tumor tissues from three HCC patients (**Figures 4K, N, O**). All the above results reveal a remarkably higher total membrane CAT and P4HB proteins and a significantly lower galactosylated membrane CAT and P4HB proteins expression in both HCC cell lines and HCC tissues compared with normal liver cells and adjacent non-tumor tissues.

TABLE 4 | Immunohistochemistry analysis of ECA in different TNM stages of HCC and adjacent non-tumor tissues.

TNM Stage		N	Scores for ECA		
			Low	Moderate	High
I	HCC	5	0	5	0
	Adjacent	5	0	1	4
II	HCC	10	0	10	0
	Adjacent	10	0	7	3
III	HCC	5	2	3	0
	Adjacent	5	0	5	0

Membrane staining was scored according to four categories: 0 for 'no staining', 1+ for 'light staining visible only at high magnification', 2+ for 'intermediate staining' and 3+ for 'dark staining of linear membrane. Scores = 1 × (% of 1+ cells) + 2 × (% of 2+ cells) + 3 × (% of 3+ cells) (23).
Low: score <100; Moderate: 100<score<200; High: score >200.

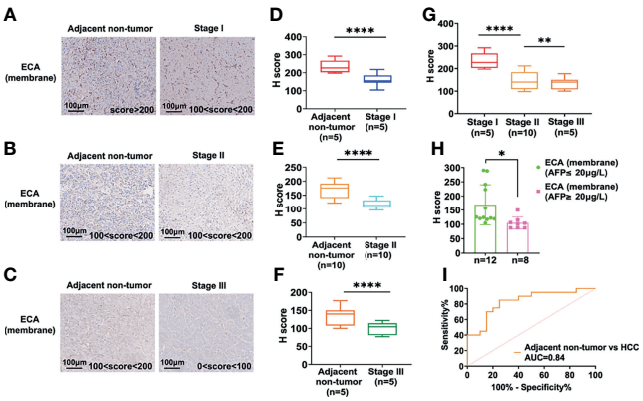

FIGURE 2 | IHC analysis of the ECA-binding galactosylated glycans in the different stages of HCC and adjacent non-tumor tissues. **(A–F)** IHC analysis of staining intensity of glycans binding with ECA on cell membrane proteins among HCC tissues and adjacent non-tumor tissues. Images are stained as brown (HRP-avidin plus biotin-conjugated ECA) and blue (hematoxylin, nuclei). **(A–C)** are representative data for **(D–F)**. **(D, E)** are statistical analysis for **(A–C)**, respectively. **(G)** Comparison of staining intensity of ECA between different stages of HCC tissues. **(H)** Correlation analysis of serum AFP levels and ECA binding affinity. **(I)** ROC curves analysis of ECA between HCC tissues and adjacent non-tumor tissues. Significance analysis for **(D–F)** and **(H)** was performed using unpaired Student's t-tests, and for G with one way ANOVA followed by Sidak's multiple comparisons test (*$p < 0.05$, **$p < 0.01$; ****$p < 0.0001$).

DISCUSSION

Most tumor biomarkers are glycoproteins. In view of the complex relationship between the diversity of glycans and tumors, and the importance of glycosylation in cell migration, proliferation, and differentiation, proteins with specific glycans have been used as valuable diagnostic, prognostic, and therapeutic biomarkers in liver cancer, breast cancer, lung cancer, and other malignant tumors and can further serve as important targets for tumor diagnosis and therapy (26). The high-throughput glycoproteomics technology based on the lectin array for screening tumor biomarkers has been recently widely used in the clinical research of malignant tumors (27). Lectins are biomolecules found in nature with specific affinities toward particular glycan structures, thus forming a relatively strong complex (28, 29). Because of this characteristic, lectins have been used in analytical techniques (e.g., lectin affinity chromatography) for the selective capture or separation of certain glycans in complex samples, or used in lectin microarrays for characterizing glycosylation profiles in diverse clinical situations (30). Lectins have also been developed for the detection of specific aberrant and cancer-associated glycostructures to assist diagnosis, prognosis based on the assessment of patient serum glycoproteins using lectins, such as Sialic acid-binding immunoglobulin-like lectin 15 (Siglec-15) (31), Galectin-8 (32), and Galectin-3 (33).

The lectin ECA was isolated from the *E. cristagalli* seeds, which can specifically recognize and bind with Gal (galactose) β1-3GlcNAc (N-acetylglucosamine)/Galβ1-4GlcNAc glycans (25). From our results, we showed that ECA had a good

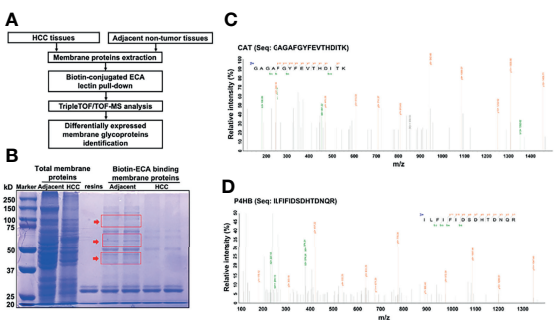

FIGURE 3 | Identification of significantly decreased membrane glycoprotein galactosylated CAT and P4HB in HCC tissues with LC-MS/MS. **(A)** Workflow showing the strategy for the identification of decreased membrane galactosylated CAT and P4HB glycoproteins in HCC tissues. **(B)** SDS-PAGE analysis of the differential membrane proteins between adjacent non-tumor tissues and HCC tissues pull downed by biotin-conjugated ECA. The differentially expressed membrane protein bands indicated by red arrow were excised for MS analysis. **(C)** The amino-acid sequence (GAGAFGYFEVTHDITK) from MS is identified as CAT. **(D)** The amino-acid sequence (ILFIFIDSDHTDNQR) from MS is identified as P4HB.

TABLE 5 | Major results of the mass spectrometry analysis.

Rank	Unuesd score	UniProtKB number	Abbreviation	Full name	Length (aa)	Molecular weight (kD)
1	28.73	P04040	CAT	Catalase	527	59.756
2	26.48	P07237	P4HB	Protein disulfide-isomerase	508	57.116
3	25.31	P07099	EPHX1	Epoxide hydrolase 1	455	52.949
4	22.9	Q13423	NNT	NAD(P) transhydrogenase, mitochondrial	1,086	113.896
5	22.46	P55084	HADHB	Trifunctional enzyme subunit beta, mitochondrial	474	51.294
6	18.61	P27338	MAOB	Amine oxidase [flavin-containing] B	520	58.763
7	17.47	Q02413	DSG1	Desmoglein-1	1,049	113.748
8	12.27	P31930	UQCRC1	Cytochrome b-c1 complex subunit 1, mitochondrial	480	52.646
9	11.29	P07355	ANXA2	Annexin A2	339	38.604
10	10.63	P11021	HSPA5	Endoplasmic reticulum chaperone BiP	654	72.333
11	9.88	P50440	GATM	Glycine amidinotransferase, mitochondrial	423	48.455
12	9.17	P06576	ATP5F1B	ATP synthase subunit beta, mitochondrial	529	56.56
13	8.61	P27797	CALR	Calreticulin	417	48.142
14	8.4	P07327	ADH1A	Alcohol dehydrogenase 1A	375	39.859
15	7.76	P33121	ACSL1	Long-chain-fatty-acid—CoA ligase 1	698	77.943
16	7.74	P01857	IGHG1	Immunoglobulin heavy constant gamma 1	330	36.106
17	7.35	P22695	UQCRC2	Cytochrome b-c1 complex subunit 2, mitochondrial	453	48.443
18	6.67	P22310	UGT1A4	UDP-glucuronosyltransferase 1-4	534	60.025
19	6.53	P11509	CYP2A6	Cytochrome P450 2A6	494	56.501
20	6.45	Q8NBX0	SCCPDH	Saccharopine dehydrogenase-like oxidoreductase	429	47.151

20 proteins with the highest Unuesd scores. aa: amino acid.

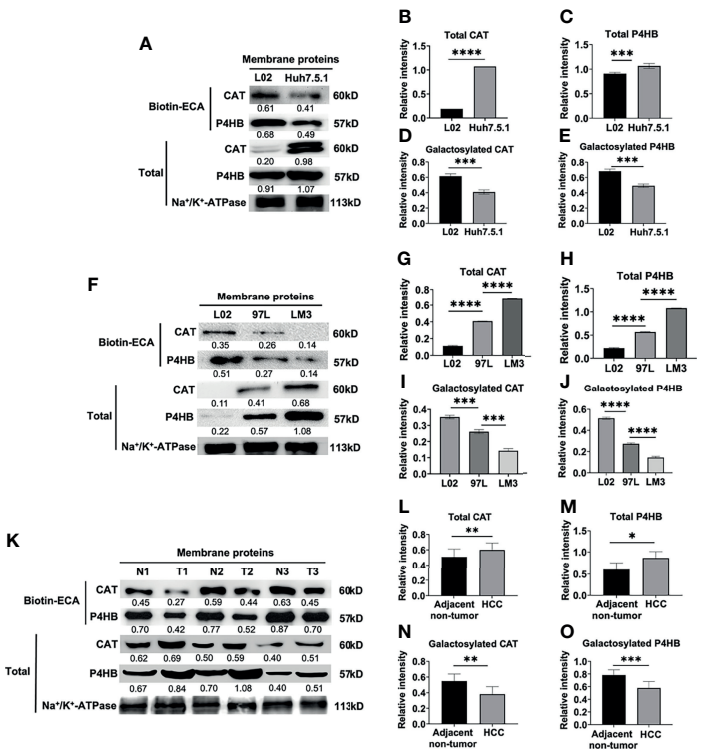

FIGURE 4 | Biotin-conjugated ECA pull down and western blot analysis of decreased membrane glycoproteins CAT and P4HB in different HCC cell lines and HCC tissues. **(A–E)** ECA lectin pull down and western blot analysis of membrane glycoprotein and total CAT and P4HB in human hepatocarcinoma cell line Huh7.5.1 and human normal liver cell L02. **(F–J)** Biotin-conjugated ECA pull down and western blot analysis of membrane glycoprotein and total CAT and P4HB from low metastatic cell (MHCC-97L), high metastatic cell (HCC-LM3) and human normal liver cell L02. **(K–O)** Biotin-conjugated ECA lectin pull down and western blot analysis of membrane glycoprotein and total CAT and P4HB from 3 HCC tissues (T) and adjacent non-tumor tissues **(N)**. P1, P2 and P3 represent HCC tissues from three patients; N1, N2 and N3 represent adjacent-non-tumor tissues from three HCC patients, respectively. **(A, F, K)** are the representative data for **(B–E)**, **(G-J, L-O)**, respectively. **(B, D, I, L, N)** (for CAT), **(C, E, I. J, M, O)** (for P4HB) are statistical analysis. Relative intensities based on endogenous membrane protein Na+/K+-ATPase are presented as the mean ± SD using unpaired Student's t-tests for **(B–E, L–O)**, and using one way ANOVA followed by Sidak's multiple comparisons test for **(G–J)** (*$p <$ 0.05, **$p < 0.01$; ***$p < 0.001$. ****$p < 0.0001$).

diagnostic performance with a statistically significant difference and a high AUC value with a sensitivity of 85% and specificity of 75%, which can efficiently differentiate HCC tissues from adjacent non-tumor tissues. We also showed that the combined application of ECA and serum AFP acquired a much higher specificity at 90% and sensitivity at 85% than ECA or AFP assay alone. To our knowledge, this is the first report showing that abnormal declined β1,3/β1,4 galactosylated membrane glycans-binding ECA can serve as a potential biomarker for HCC diagnosis or malignant prognosis.

In the present study, we also firstly found and determined two abnormal declined membrane galactosylated-CAT and P4HB glycoproteins as potential biomarkers in HCC diagnosis and malignancy progression prediction. CAT is a key enzyme in the metabolism of H_2O_2 and reactive oxygen species (ROS) (34). Previous studies have shown that the functional CAT is mainly located in peroxisomes; moreover, it has also been found in the cytoplasm, mitochondria, and on the cytoplasmic membrane of human cancer cells (35). So far, elevated expression of total CAT protein level has been found on the cell surface of tumor cells such as gastric cancer, skin cancer, colon cancer, and chronic myeloid leukemia (36–39). Consistently, in this study, we also found an increased total CAT expression, and we also firstly found that there was significantly decreased ECA-binding membrane galactosylated CAT of human HCC tissues compared to adjacent non-tumor tissues, and decreased as the malignancy of liver cancer increased accordingly, which suggest that both increased total CAT protein and decreased galactosylated CAT glycoprotein level might be involved in the development of HCC.

P4HB is a multifunctional protein that catalyzes the formation and rearrangement of disulfide bonds. It can act as a molecular chaperone to refine misfolded proteins in response to endoplasmic reticulum (ER) stress (40). It has been reported that P4HB is indicated as a diagnosis and prognosis biomarker and the abnormal higher expression of total P4HB protein level has been found in various tumor types, such as renal cell carcinoma (41), bladder carcinoma (24), gastric cancer (42), diffuse gliomas (43), lung cancer (44), and hepatocellular carcinoma (45). The high P4HB was associated with HCC tumorigenesis and epithelial-to-mesenchymal transition (45, 46). Consistently, in this study, we also found an increased total P4HB expression, and we also firstly identified that membrane galactosylated modification of P4HB in HCC tissues was reduced compared with adjacent non-tumor tissues, and decreased galactosylated-P4HB was associated with HCC malignancy and metastasis. These data clearly suggest that both increased total P4HB and decreased galactosylated P4HB might be involved in the development of HCC.

Our analysis still has some limitations. First, a larger sample size and multicenter study might be needed to further confirm our results. Second, the N/O-glycan profile characteristic of ECA binding galactosylated membrane glycoproteins CAT and P4HB needs further elucidation. Third, the regulation mechanism of decreased galactosylated membrane glycoproteins CAT and P4HB in HCC needs to be further explored. But our study provided comprehensive information of HCC-associated cellular membrane glycopatterns and ECA/ECA-binding membrane CAT and P4HB glycoproteins that may contribute to understanding the complex physiological changes of HCC patients. Our results also provided a new insight for the research of HCC biomarkers and anti-tumor drug targets by using ECA-binding membrane CAT and P4HB glycoproteins, which is conducive to understanding HCC mechanisms and provides a set of potential targets for diagnostic application and therapeutic strategies.

DATA AVAILABILITY STATEMENT

The original contributions presented in the study are included in the article/supplementary material. Further inquiries can be directed to the corresponding author.

ETHICS STATEMENT

The studies involving human participants were reviewed and approved by the Ethical Committee of Wuhan University School of Medicine. The patients/participants provided their written informed consent to participate in this study.

AUTHOR CONTRIBUTIONS

YK, HC, MC, YL, JL and QL performed the experiments and analyzed the data. TG and YY provided the test samples. TG, YY, and YX assisted in the analysis of clinical data. HX contributed IHC stain expertise. XLZ initiated the study, analyzed data, and created and revised the manuscript. All authors listed have made a substantial, direct, and intellectual contribution to the work and approved it for publication.

FUNDING

This work was supported by grants from the National Key R&D Program of China (2018YFA0507603), the National Natural Science Foundation of China (91740120, 22077097, 21721005, and 21572173), the National Grand Program on Key Infectious Disease of China (2017ZX10201301-006), the National Outstanding Youth Foundation of China (81025008), the Medical Science Advancement Program (Basic Medical Sciences) of Wuhan University (TFJC 2018002), the Key R&D Program of Hubei Province (2020BCB020), the Hubei Province's Outstanding Medical Academic Leader Program (523-276003), the Innovative Group Project of Hubei Health Committee (WJ2021C002), and the Foundational Research Funds for the Central University of China.

REFERENCES

1. Zheng R, Qu C, Zhang S, Zeng H, Sun K, Gu X, et al. Liver Cancer Incidence and Mortality in China: Temporal Trends and Projections to 2030. *Chin J Cancer Res* (2018) 30:571–9. doi: 10.21147/j.issn.1000-9604.2018.06.01
2. European Association for the Study of the Liver. EASL Clinical Practice Guidelines: Management of Hepatocellular Carcinoma. *J Hepatol* (2018) 69:182–236. doi: 10.1016/j.jhep.2018.03.019
3. Global Burden of Disease Liver Cancer Collaboration. The Burden of Primary Liver Cancer and Underlying Etiologies From 1990 to 2015 at the Global, Regional, and National Level: Results From the Global Burden of Disease Study 2015. *JAMA Oncol* (2017) 3:1683–91. doi: 10.1001/jamaoncol.2017.3055
4. Befeler AS, Di Bisceglie AM. Hepatocellular Carcinoma: Diagnosis and Treatment. *Gastroenterology* (2002) 122:1609–19. doi: 10.1053/gast.2002.33411
5. Gower E, Estes C, Blach S, Razavi-Shearer K, Razavi H. Global Epidemiology and Genotype Distribution of the Hepatitis C Virus Infection. *J Hepatol* (2014) 61:S45–57. doi: 10.1016/j.jhep.2014.07.027
6. Gao Q, Zhu H, Dong L, Shi W, Chen R, Song Z, et al. Integrated Proteogenomic Characterization of HBV-Related Hepatocellular Carcinoma. *Cell* (2019) 179:561–77.e22. doi: 10.1016/j.cell.2019.08.052
7. Satomaa T, Heiskanen A, Leonardsson I, Angstrom J, Olonen A, Blomqvist M, et al. Analysis of the Human Cancer Glycome Identifies a Novel Group of Tumor-Associated N-Acetylglucosamine Glycan Antigens. *Cancer Res* (2009) 69:5811–9. doi: 10.1158/0008-5472.CAN-08-0289
8. Islami F, Miller KD, Siegel RL, Fedewa SA, Ward EM, Jemal A. Disparities in Liver Cancer Occurrence in the United States by Race/Ethnicity and State. *CA Cancer J Clin* (2017) 67:273–89. doi: 10.3322/caac.21402
9. Craig AJ, von Felden J, Garcia-Lezana T, Sarcognato S, Villanueva A. Tumour Evolution in Hepatocellular Carcinoma. *Nat Rev Gastroenterol Hepatol* (2020) 17:139–52. doi: 10.1038/s41575-019-0229-4
10. Tsuchiya N, Sawada Y, Endo I, Saito K, Uemura Y, Nakatsura T. Biomarkers for the Early Diagnosis of Hepatocellular Carcinoma. *World J Gastroenterol* (2015) 21:10573–83. doi: 10.3748/wjg.v21.i37.10573
11. Cao L, Cheng H, Jiang Q, Li H, Wu Z. APEX1 Is a Novel Diagnostic and Prognostic Biomarker for Hepatocellular Carcinoma. *Aging* (2020) 12:4573–91. doi: 10.18632/aging.102913
12. Zhou F, Shang W, Yu X, Tian J. Glypican-3: A Promising Biomarker for Hepatocellular Carcinoma Diagnosis and Treatment. *Med Res Rev* (2018) 38:741–67. doi: 10.1002/med.21455
13. Jiang K, Shang S, Li W, Guo K, Qin X, Zhang S, et al. Multiple Lectin Assays for Detecting Glyco-Alteration of Serum GP73 in Liver Diseases. *Glycoconj J* (2015) 32:657–64. doi: 10.1007/s10719-015-9614-6
14. Chen L, Li M, Li Q, Wang C-j, Xie S-q. DKK1 Promotes Hepatocellular Carcinoma Cell Migration and Invasion Through β-Catenin/MMP7 Signaling Pathway. *Mol Cancer* (2013) 12:157. doi: 10.1186/1476-4598-12-157
15. Li J, Cheng Y, Guo J, He J, Jiang Z, Liang J, et al. *Guidelines of Chinese Society of Clinical Oncology (CSCO) Hepatocellular Carcinoma* Vol. 98. China: People's Medical Publishing House (2018).
16. Zalba S, ten Hagen TLM. Cell Membrane Modulation as Adjuvant in Cancer Therapy. *Cancer Treat Rev* (2017) 52:48–57. doi: 10.1016/j.ctrv.2016.10.008
17. Han Y, Xiao K, Tian Z. Comparative Glycomics Study of Cell-Surface N-Glycomes of HepG2 Versus LO2 Cell Lines. *J Proteome Res* (2019) 18:372–9. doi: 10.1021/acs.jproteome.8b00655
18. Hirabayashi J, Yamada M, Kuno A, Tateno H. Lectin Microarrays: Concept, Principle and Applications. *Chem Soc Rev* (2013) 42:4443–58. doi: 10.1039/c3cs35419a
19. Badr HA, AlSadek DMM, Darwish AA, ElSayed AI, Bekmanov BO, Khussainova EM, et al. Lectin Approaches for Glycoproteomics in FDA-Approved Cancer Biomarkers. *Expert Rev Proteomics* (2014) 11:227–36. doi: 10.1586/14789450.2014.897611
20. Xiang T, Yang G, Liu X, Zhou Y, Fu Z, Lu F, et al. Alteration of N-Glycan Expression Profile and Glycan Pattern of Glycoproteins in Human Hepatoma Cells After HCV Infection. *Biochim Biophys Acta Gen Subj* (2017) 1861:1036–45. doi: 10.1016/j.bbagen.2017.02.014
21. Li S, Liu XY, Pan Q, Wu J, Liu ZH, Wang Y, et al. Hepatitis C Virus-Induced FUT8 Causes 5-FU Drug Resistance in Human Hepatoma Huh7.5.1 Cells. *Viruses* (2019) 11:378. doi: 10.3390/v11040378
22. Chen H, Shi Y, Sun L, Ni S. Electrospun Composite Nanofibers With All-Trans Retinoic Acid and MWCNTs-OH Against Cancer Stem Cells. *Life Sci* (2020) 258:118152. doi: 10.1016/j.lfs.2020.118152
23. Mazières J, Brugger W, Cappuzzo F, Middel P, Frosch A, Bara I, et al. Evaluation of EGFR Protein Expression by Immunohistochemistry Using H-Score and the Magnification Rule: Re-Analysis of the SATURN Study. *Lung Cancer* (2013) 82:231–7. doi: 10.1016/j.lungcan.2013.07.016
24. Wu Y, Peng Y, Guan B, He A, Yang K, He S, et al. P4HB: A Novel Diagnostic and Prognostic Biomarker for Bladder Carcinoma. *Oncol Lett* (2021) 21:95. doi: 10.3892/ol.2020.12356
25. Wu AM, Wu JH, Tsai MS, Yang Z, Sharon N, Herp A. Differential Affinities of Erythrina Cristagalli Lectin (ECL) Toward Monosaccharides and Polyvalent Mammalian Structural Units. *Glycoconj J* (2007) 24:591–604. doi: 10.1007/s10719-007-9063-y
26. Wang J, Zhou C, Zhang W, Yao J, Lu H, Dong Q, et al. An Integrative Strategy for Quantitative Analysis of the N-Glycoproteome in Complex Biological Samples. *Proteome Sci* (2014) 12:4. doi: 10.1186/1477-5956-12-4
27. Silva MLS. Lectin Biosensors in Cancer Glycan Biomarker Detection. *Adv Clin Chem* (2019) 93:1–61. doi: 10.1016/bs.acc.2019.07.001
28. Silva MLS. Lectin-Based Biosensors as Analytical Tools for Clinical Oncology. *Cancer Lett* (2018) 436:63–74. doi: 10.1016/j.canlet.2018.08.005
29. Yang J, Liu X, Shu J, Hou Y, Chen M, Yu H, et al. Abnormal Galactosylated-Glycans Recognized by Bandeiraea Simplicifolia Lectin I in Saliva of Patients With Breast Cancer. *Glycoconj J* (2020) 37:373–94. doi: 10.1007/s10719-020-09910-6
30. Yu H, Shu J, Li Z. Lectin Microarrays for Glycoproteomics: An Overview of Their Use and Potential. *Expert Rev Proteomics* (2020) 17:27–39. doi: 10.1080/14789450.2020.1720512
31. Li B, Zhang B, Wang X, Zeng Z, Huang Z, Zhang L, et al. Expression Signature, Prognosis Value, and Immune Characteristics of Siglec-15 Identified by Pan-Cancer Analysis. *Oncoimmunology* (2020) 9:1807291. doi: 10.1080/2162402X.2020.1807291
32. Elola MT, Ferragut F, Cardenas Delgado VM, Nugnes LG, Gentilini L, Laderach D, et al. Expression, Localization and Function of Galectin-8, a Tandem-Repeat Lectin, in Human Tumors. *Histol Histopathol* (2014) 29:1093–105. doi: 10.14670/HH-29.1093
33. Dong R, Zhang M, Hu Q, Zheng S, Soh A, Zheng Y, et al. Galectin-3 as a Novel Biomarker for Disease Diagnosis and a Target for Therapy (Review). *Int J Mol Med* (2018) 41:599–614. doi: 10.3892/ijmm.2017.3311
34. Glorieux C, Zamocky M, Sandoval JM, Verrax J, Calderon PB. Regulation of Catalase Expression in Healthy and Cancerous Cells. *Free Radic Biol Med* (2015) 87:84–97. doi: 10.1016/j.freeradbiomed.2015.06.017
35. Heinzelmann S, Bauer G. Multiple Protective Functions of Catalase Against Intercellular Apoptosis-Inducing ROS Signaling of Human Tumor Cells. *Biol Chem* (2010) 391:675–93. doi: 10.1515/bc.2010.068
36. Hwang TS, Choi HK, Han HS. Differential Expression of Manganese Superoxide Dismutase, Copper/Zinc Superoxide Dismutase, and Catalase in Gastric Adenocarcinoma and Normal Gastric Mucosa. *Eur J Surg Oncol* (2007) 33:474–9. doi: 10.1016/j.ejso.2006.10.024
37. Sander CS, Hamm F, Elsner P, Thiele JJ. Oxidative Stress in Malignant Melanoma and Non-Melanoma Skin Cancer. *Br J Dermatol* (2003) 148:913–22. doi: 10.1046/j.1365-2133.2003.05303.x
38. Rainis T, Maor I, Lanir A, Shnizer S, Lavy A. Enhanced Oxidative Stress and Leucocyte Activation in Neoplastic Tissues of the Colon. *Dig Dis Sci* (2007) 52:526–30. doi: 10.1007/s10620-006-9177-2
39. Zelen I, Djurdjevic P, Popovic S, Stojanovic M, Jakovljevic V, Radivojevic S, et al. Antioxidant Enzymes Activities and Plasma Levels of Oxidative Stress Markers in B-Chronic Lymphocytic Leukemia Patients. *J BUON* (2010) 15:330–6.
40. Jang I, Pottekat A, Poothong J, Yong J, Lagunas-Acosta J, Charbono A, et al. PDIA1/P4HB Is Required for Efficient Proinsulin Maturation and ß Cell Health in Response to Diet Induced Obesity. *eLife* (2019) 8:e44528. doi: 10.7554/eLife.44528
41. Xie L, Li H, Ma LZ, Dang Y, Guo J, Liu J, et al. Autophagy-Related Gene P4HB: A Novel Diagnosis and Prognosis Marker for Kidney Renal Clear Cell Carcinoma. *Aging* (2020) 12:1828–42. doi: 10.18632/aging.102715

42. Zhang J, Guo S, Wu Y, Zheng ZC, Wang Y, Zhao Y. P4HB, a Novel Hypoxia Target Gene Related to Gastric Cancer Invasion and Metastasis. *BioMed Res Int* (2019) 2019:9749751. doi: 10.1155/2019/9749751
43. Zou H, Wen C, Peng Z, Shao Y, Hu L, Li S, et al. P4HB and PDIA3 Are Associated With Tumor Progression and Therapeutic Outcome of Diffuse Gliomas. *Oncol Rep* (2018) 39:501–10. doi: 10.3892/or.2017.6134
44. Ercan H, Mauracher L-M, Grilz E, Hell L, Hellinger R, Schmid J, et al. Alterations of the Platelet Proteome in Lung Cancer: Accelerated F13A1 and ER Processing as New Actors in Hypercoagulability. *Cancers* (2021) 13:2260. doi: 10.3390/cancers13092260
45. Dai J, Jiang L, Qiu L, Shao Y, Shi P, Li J. WHSC1 Promotes Cell Proliferation, Migration, and Invasion in Hepatocellular Carcinoma by Activating Mtorc1 Signaling. *Onco Targets Ther* (2020) 13:7033–44. doi: 10.2147/OTT.S248570
46. Xia W, Zhuang 1J, Wang G, Ni J, Wang J, Ye Y. P4HB Promotes HCC Tumorigenesis Through Downregulation of GRP78 and Subsequent Upregulation of Epithelial-to- Mesenchymal Transition. *Oncotarget* (2016) 8:8512–21. doi: 10.18632/oncotarget.14337

Conflict of Interest: The authors declare that the research was conducted in the absence of any commercial or financial relationships that could be construed as a potential conflict of interest.

frontiers in Oncology

ORIGINAL RESEARCH
published: 30 March 2022
doi: 10.3389/fonc.2022.858639

A Panel of Bile Volatile Organic Compounds Servers as a Potential Diagnostic Biomarker for Gallbladder Cancer

*Xin Zhang[1], Xinru Gui[1], Yanli Zhang[2], Qi Liu[1], Liqiang Zhao[3], Jingxian Gao[3], Jian Ji[1] and Yi Zhang[1]**

[1] Department of Clinical Laboratory, Qilu Hospital of Shandong University, Shandong University, Jinan, China, [2] Department of Clinical Laboratory, Shandong Provincial Third Hospital, Jinan, China, [3] Department of Research and Development, Hanon Advanced Technology Group Co., Ltd, Jinan, China

As no reliable diagnostic methods are available, gallbladder cancer (GBC) is often diagnosed until advanced stages, resulting in a poor prognosis. In the present study, we assessed whether volatile organic compounds (VOCs) could be used as a diagnostic tool for GBC. The VOCs in bile samples collected from 32 GBC patients were detected by gas chromatography-ion mobility spectrometry (GC-IMS), and 54 patients with benign gallbladder diseases (BGD) were used as controls. Both principal component analysis and unsupervised hierarchical clustering analysis gave a clear separation of GBC and BGD based on the bile VOC data collected from GC-IMS. A total of 12 differentially expressed VOCs were identified, including four upregulated (cyclohexanone, 2-ethyl-1-hexanol, acetophenone, and methyl benzoate) and eight downregulated [methyl acetate, (E)-hept-2-enal, hexanal, (E)-2-hexenal, (E)-2-pentenal, pentan-1-ol, 1-octen-3-one, and (E)-2-octenal] in GBC compared with BGD. ROC analysis demonstrated a 12-VOC panel con-structed by four machine learning algorithms, which was superior to the traditional tumor marker, CA19-9. Among them, support vector machines and linear discriminant analysis provided the highest AUCs of 0.972, with a sensitivity of 100% and a specificity of 94.4% in the diagnosis of GBC. Collectively, VOCs might be used as a potential tool for the diagnosis of GBC.

Keywords: gallbladder cancer, volatile organic compounds, diagnosis, biomarker, bile

OPEN ACCESS

Edited by:
Xuesong Gu,
Harvard Medical School, United States

Reviewed by:
Huang Guohong,
People's Hospital of Xinjiang Uygur Autonomous Region, China
Mingyi Wang,
Weihai Municipal Hospital, China

***Correspondence:**
Yi Zhang
yizhang@sdu.edu.cn

Specialty section:
This article was submitted to Cancer Molecular Targets and Therapeutics, a section of the journal Frontiers in Oncology

Received: *20 January 2022*
Accepted: *07 March 2022*
Published: *30 March 2022*

Citation:
Zhang X, Gui X, Zhang Y, Liu Q, Zhao L, Gao J, Ji J and Zhang Y (2022) A Panel of Bile Volatile Organic Compounds Servers as a Potential Diagnostic Biomarker for Gallbladder Cancer. Front. Oncol. 12:858639. doi: 10.3389/fonc.2022.858639

INTRODUCTION

Gallbladder cancer (GBC) is one of the most common malignant tumors of the biliary system in Eastern Asia with high mortality (1). In 2020, there are an estimated 115,949 new cases and 84,695 GBC-related deaths worldwide (2). At present, surgical resection is the most effective treatment for GBC (3). Unfortunately, due to the atypical clinical symptoms, the patients often are diagnosed at advanced stages and can not accept surgical treatment, resulting in a poor prognosis for this aggressive disease. Detection in an earlier stage of GBC and removal of precancerous lesions will

reduce the disease burden and mortality rate. However, currently used tumor biomarkers, such as CA 19-9 and CA 242, have low sensitivity and specificity (4–6). Moreover, they have nonspecific elevations in benign gallbladder diseases (BGD), such as gallstones, cholecystitis, polyps, and gallbladder adenomyosis (7, 8). Therefore, it is urgently necessary to identify new biomarkers for the early clinical diagnosis.

Metabolomics is one of the most promising approaches for identifying biomarkers of disease and increasing understanding of metabolic processes in cancer (9). As an important part of metabolism products, volatile organic compounds (VOCs) reflect the metabolic changes produced in a variety of different biochemical reactions in the human body. VOCs are a type of organic matter that exists in the form of steam at room temperature, which can be divided into aromatic hydrocarbons, alkanes, olefins, halohydrocarbons, esters, and ketones. Due to their distinct odors, VOCs emitted from different substrates can be detected by gas chromatography-mass spectrometry (GC-MS), gas chromatography-ion mobility spectrometry (GC-IMS), electronic nose (E-Nose), or even trained sniffer dogs (10–12). Bhatt et al. (13) have studied the plasma metabolomics of 20 patients with esophageal adenocarcinoma and 19 patients with gastroesophageal reflux disease, disclosing nine VOCs and unveiling significant differences between the two groups. Lima et al. (14) have performed the GC-MS to detect the volatile metabolomic signature of urine and established a panel of six volatile biomarkers for the identification of prostate cancer. When compared with other fecal-based techniques, VOCs emitted from feces, such as propan-2-ol, hexan-2-one, and ethyl 3-methyl-butanoate, have a superior diagnostic capability for the diagnosis of colorectal cancer (15, 16). Until now, little is known about VOCs in GBC, and their potential utility to serve as biomarkers for GBC diagnosis remains largely unclear.

In the present study, we performed GC-IMS to obtain the metabolomic profiling of VOCs in bile from patients with GBC and BGD. Moreover, we aimed to develop a volatile biomarker panel that could act as a minimally invasive approach for the early detection of GBC. To the best of our knowledge, we, for the first time, showed that VOCs could be used as bile biomarkers for the diagnosis of GBC.

MATERIALS AND METHODS

Study Population

In the present study, patients who were older than 18 years and histologically diagnosed with GBC were recruited from 2018 to 2021 in Qilu Hospital of Shandong University. Inclusion criteria were set as follows: 1) patients without any history of other malignant tumor or anti-cancer therapy, 2) patients who were cooperative with supplying fresh bile sample and complete medical records, and 3) patients who underwent radical resection and reported GBC by pathological examination. Patients with BGD, such as cholecystitis and gallbladder polyps, who met the above-mentioned conditions except for the pathologically reported GBC, were included as controls. The experimental scheme was approved by the Ethics Committee of Qilu Hospital of Shandong University, and the informed consent were got from each patient.

Sample Preparation

Bile samples were collected when the patient was first treated with endoscopic retrograde cholangiopancreatography (ERCP) or percutaneous transhepatic cholangiodrainage (PTCD). The collected specimens were centrifuged at 3,000 rpm for 10 min at 4°C. The supernatants were aliquoted and stored at -80°C immediately.

Analysis of the VOCs in Bile

VOC profiles from bile samples were detected using GC-IMS (G.A.S. Dortmund, Germany). All samples underwent the same procedure. Briefly, 0.5 mL bile was placed in each headspace bottle and incubated at 80°C for 10 min. Subsequently, 1 mL headspace gas was extracted for analysis. Nitrogen was used as the carrier air. The IMS drift gas was always maintained at 150 mL/min, while the initial flow rate of the carrier air was maintained at 2 mL/min for 2 min, and then it was linearly increased to 150 mL/min in 10 min. Other major experimental parameters were as follows: drift tube temperature: 45°C; gas chromatography column temperature: 60°C; inlet-chromatography column converter temperature: 60°C; column-migration tube converter temperature: 45°C; ion mode: positive ion mode. Each analysis was conducted in triplicate.

Statistical Analysis

The software R (x64 3.6.2) and the software package "ggord" were used for principal component analysis (PCA). The level of each VOC was compared with Mann–Whitney U test. The area under the curve (AUC) was calculated on the receiver operating characteristic (ROC) curve and compared using MedCalc 9.3.9.0. The analysis of machine learning was carried out using Matlab R2016a (Python Software Foundation, Beaverton, USA) based on the Statistics and Machine Learning Toolbox. Based on identified VOCs, decision tree (DT), support vector machines (SVM), linear discriminant analysis (LDA), gradient enhancement machines (GBMs), and K-nearest neighbor (KNN) were used for classification. Hierarchical 10-fold cross-validation was used to optimize the parameters of the training cohort.

RESULTS

Clinical Characteristics of GBC and BGD Patients

A cohort consisting of 86 patients with definite pathological diagnoses, including 32 GBC patients (age 52–77 years, mean 63) and 54 BGD patients (age 56–66 years, mean 59), were included in the present study. Moreover, 70% recruited subjects were randomly selected as a training cohort (n = 24 GBC and n = 36 BGD), while the remaining 26 samples (n = 8 GBC and n = 18 BGD) were set as a test cohort. There were no significant differences between the two cohorts in terms of age, sex, and

some biochemical indexes. **Table 1** lists more detailed clinical characteristics of these patients.

Coefficient of Variation for VOC Analysis With GC-IMS

Room-temperature stability was assessed in the same samples that were measured in parallel every hour within 12 h, with a total of 12 injections. **Figure 1A** shows that the intensity difference of the selected signal peaks in the 12 repeated determinations was little under the same experimental conditions. The average CV for the bile at room temperature for 12 h was within 10% (**Supplementary Table 1**). **Figure 1B** presents that repeated freeze-thaw cycles might affect the VOC composition, while the average CV of VOCs within three freeze-thaw cycles was less than 10% (**Supplementary Table 2**). In the present study, each sample was detected within 3 h after being thawed at room temperature.

VOC Profile Analysis in GBC and BGD Patients

The VOC was characterized by the molecular gas chromatography preservation index, and the migration time of molecular ions was measured and quantified according to the signal peak strength. For each sample, we would generate the 3D data (retention index, migration time, and peak strength) (**Supplementary Figure S1**). Our VOCs were selected from a 2D spectral map (the vertical view of 3D spectra, with color to indicate peak strength), and each point represented a signal peak (**Figure 2A**). **Figure 2A** shows that we could visually see the difference in the VOC between a GBC sample and a BGD sample, with red representing a higher concentration of the substance in the bile of GBC compared with BGD, and blue representing a lower concentration.

Using VOCal software (v0.1.1) with a GC-IMS library, a total of 45 VOC peaks were manually selected based on retention index and migration time in all patients. These species (peaks) included 19 defined substances and six unknown substances (**Figure 2B**). A 3D scatterplot generated from PCA demonstrated that the VOC profile of GBC patients generally differed from that of BGD, and the respective clustering trend could be observed (**Figure 2C**). Unsupervised hierarchical clustering analysis showed a clear separation of GBC and BGD (**Figure 2D**). These data indicated that VOCs had potential as biomarkers for the diagnosis of GBC.

TABLE 1 | Clinical characteristics of GBC and BGD patients.

Charateristics	GBC		BGD	
	Training set	Test set	Training set	Test set
Cases	24	8	36	18
age (years)*	60.6 ± 10.3	58.9 ± 6.5	62.1 ± 10.3	57.4 ± 16.4
Male/Female	16/8	5/3	23/13	10/8
ALB (g/L)#	37.3 (32.7-39.9)	41.0 (35.3-43.2)	42.0 (40.3-45.4)	41.4 (37.8-43.5)
AKP (U/L)#	337.5 (140.3-469.8)	330.0 (261.5-505.3)	119.0 (66.0-131.0)	151.5 (81.3-368.5)
AST (U/L)#	64.0 (32.5-155.8)	85.5 (43.3-121.5)	37.5 (21.0-45.0)	42.0 (17.3-81.0)
ALT (U/L)#	92 (45.5-184.0)	91.5 (68.0-202.3)	38.5 (13.0-74.0)	50.5 (16.5-100.5)

**Data represents mean ± standard deviation; #Data represents the median (interquartile range). GBC, gallbladder cancer; BGD, benign gallbladder diseases; ALB, albumin; AKP, alkaline phosphatase; AST, aspartate aminotransferase; ALT, alanine aminotransferase.*

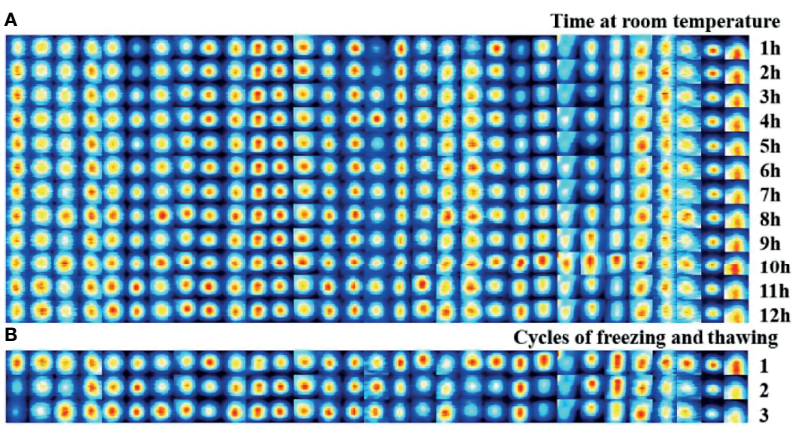

FIGURE 1 | Stability evaluation of bile VOCs analysis with GC-IMS. **(A)** Room-temperature stability was assessed in the same samples that measured in parallel every hour within 12 hours, with a total of 12 injections. **(B)** Freeze/thaw sta-bility evaluation was assessed in the same samples that measured within three freeze-thaw cycles.

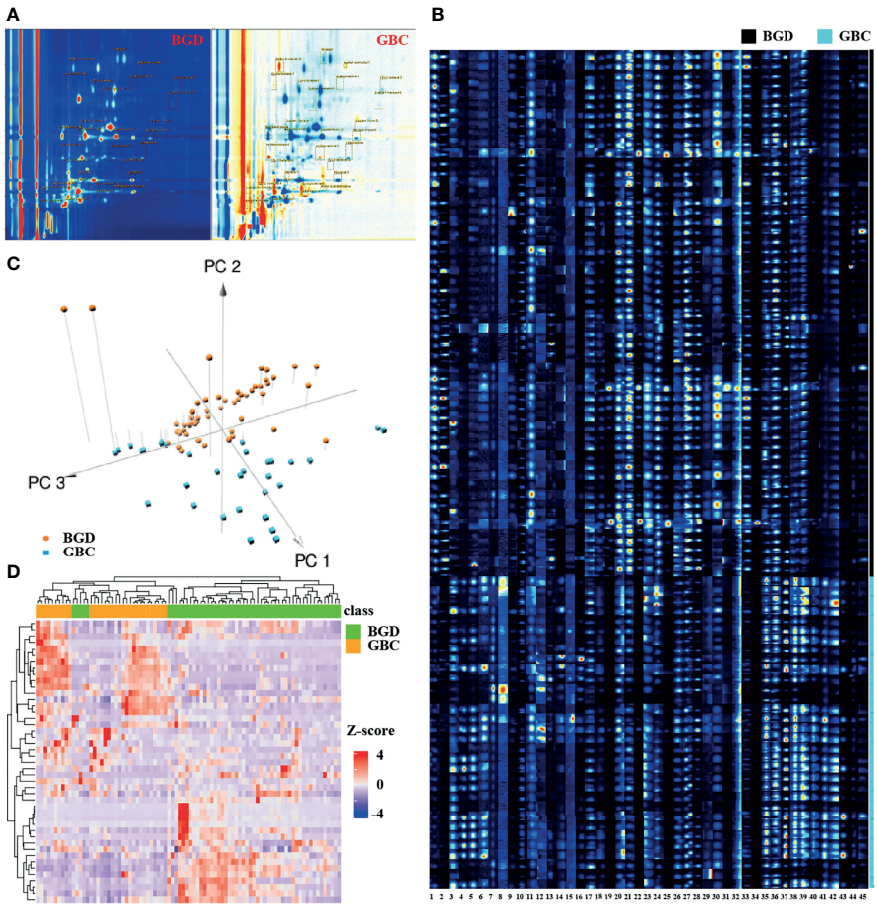

FIGURE 2 | Bile VOCs profile analysis. **(A)** 2D spectral map for BGD and GBC, and each point represent a signal peak. **(B)** GC-IMS signals detected in the bile of BGD and GBC patients. **(C)** A 3-dimensional scatterplot generated from PCA for of VOCs profiles in BGD and GBC patients. **(D)** Heatmap of GC-IMS VOCs profiles in BGD and GBC patients. Note: 1. Unknown-1, 2. Unknown-2, 3. Unknown-3, 4. Unknown-4, 5. Unknown-5, 6. Unknown-6, 7. Methyl benzoate-M, 8. Methyl benzoate-D, 9. pentan-1-o1, 10. 2-heptanone, 11. Nonanal, 12. methyl acetate-M, 13. methyl acetate-D, 14. Methyl isobutyl ketone, 15. 1-propene-3-methylthio, 16. 2-Pentanone, 17. Butyl acetate, 18. 1-octen-3-one-M, 19. 1-octen-3-one-D, 20. (E)-hept-2-enal-1, 21. (E)-hept-2-enal-2, 22. (E)-hept-2-enal-3, 23. (E)-2-octenal-1, 24. (E)-2-octenal-2, 25. (E)-2-octenal-3, 26. Hexanal-1, 27. Hexanal-2, 28. Hexanal-3, 29. (E)-2-pentenal-1, 30. (E)-2-pentenal-2, 31. (E)-2-pentenal-3, 32. (E)-2-hexenal-1, 33. (E)-2-hexenal-2, 34. (E)-2-hexenal-3, 35. cyclohexanone-1, 36. cyclohexanone-2, 37. cyclohexanone-3, 38. 2-ethyl-1-hexanol-1, 39. 2-ethyl-1-hexanol-2, 40. 2-ethyl-1-hexanol-3, 41 Acetophenone-1, 42. Acetophenone-2, 43. Acetophenone-3, 44. Benzaldehy de-M, 45. Benzaldehy de-D.

Quantitative Analysis of VOCs in the Training Cohort

The internal standard method was used for quantification according to the peak volume of VOCs. Briefly, 10 μL 4-methyl-2-pentanol at a concentration of 15 μL/L was used as the internal standard, which was added to each sample. **Figure 3** shows that 12 differentially expressed VOCs were identified, including four up-regulated (cyclohexanone, 2-ethyl-1-hexanol, acetophenone, and methyl benzoate) and eight down-regulated [methyl acetate, (E)-hept-2-enal, Hexanal, (E)-2-hexenal, (E)-2-pentenal, pentan-1-ol, 1-octen-3-one, and (E)-2-octenal] in GBC patients compared with BGD patients. The other seven VOCs showed no significant difference between GBC and BGD (**Supplementary Table 3**).

ROC curve analyses realized that pentan-1-ol, (E)-2-octenal, (E)-hept-2-enal, (E)-2-hexenal, (E)-2-pentenal, cyclohexanone, and acetophenone were robust in distinguishing GBC patients from BGD patients, with AUCs>0.75 (**Table 2**). Among them, (E)-hept-2-enal was significantly superior to CA19-9, a routine clinically used marker in the diagnosis of GBC.

Diagnostic Performance of VOCs With Machine Learning Algorithms

To ensure the accuracy of the diagnostic model under limited data sets, the machine learning method was used to analyze the heterogeneous signal patterns of gallbladder diseases. Coupled with the above-mentioned 12 VOCs, four popular machine learning algorithms (DT, SVM, LDA, and KNN) were used to construct diagnostic models. **Figure 4A** shows the prediction and classification of the model for the training cohort, with each AUC>0.9 in distinguishing GBC patients from BGD patients. In the test cohort, ROC analysis demonstrated that the machine

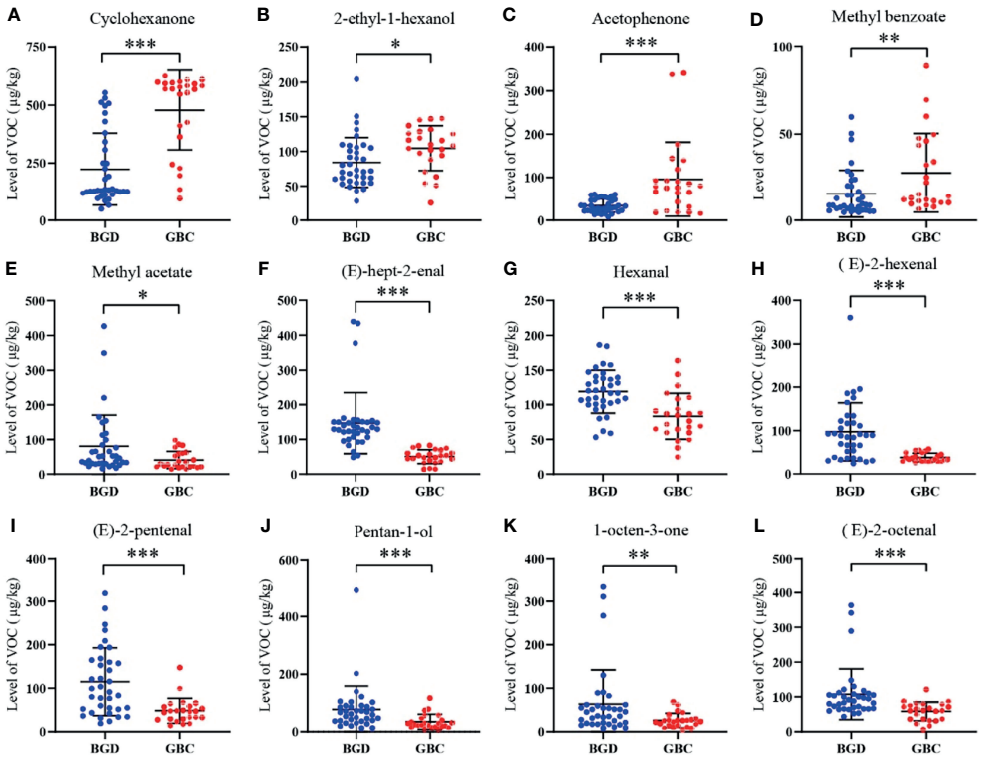

FIGURE 3 | Quantitative analysis of VOCs in the training cohort. The levels of Cyclohexanone **(A)**, 2-ethyl-1-hexanol **(B)**, Acetophenone **(C)**, Methyl benzoate **(D)**, Methyl acetate **(E)**, (E)-hept-2-enal **(F)**, Hexanal **(G)**, (E)-2-hexenal **(H)**, (E)-2-pentenal **(I)**, Pentan-1-ol **(J)**, 1-octen-3-one **(K)**, (E)-2-octenal **(L)**. *P < 0.05, **P < 0.01, ***P < 0.001(Mann–Whitney U test). Data represents the median (interquartile range).

learning models performed better than CA19-9 in differentiating GBC from BGD (**Figure 4B**). Among them, SVM and LDA provided the highest AUCs of 0.972, with a sensitivity of 100% and a specificity of 94.4% (**Supplementary Table 4**).

DISCUSSION

There are still numerous challenges for us to more accurately diagnose GBC. In the present study, we explored the potential role of GC-IMS in the detection of GBC and thus reported several meaningful findings. First, GC-IMS could discriminate between bile samples collected from patients with GBC and BGD. Second, we identified 12 specific VOCs, which might play a relevant role in assessing GBC. Third, the model based on the VOC profile allowed for accurate discrimination between GBC and BGD groups. However, this observation was limited to a small cohort of patients.

There is increasing interest in the application of VOCs in exhaled breath for diagnosing a variety of cancers (17, 18).

TABLE 2 | The AUC, sensitivity and specificity of each VOC for GBC diagnosis.

VOC molecular	AUC (95% CI)	Sensitivity (%)	Specificity (%)	*P**
Methyl benzoate	0.711 (0.580 - 0.821)	87.5	52.8	0.361
Pentan-1-ol	0.774 (0.648 - 0.872)	70.8	80.6	0.790
Methyl acetate	0.675 (0.542 - 0.791)	54.2	80.6	0.166
1-octen-3-one	0.704 (0.572 - 0.815)	79.2	63.9	0.352
(E)-2-octenal	0.799 (0.675 - 0.891)	95.8	52.8	0.995
2-ethyl-1-hexanol	0.694 (0.562 - 0.807)	75.0	66.7	0.156
(E)-hept-2-enal	0.965 (0.883 - 0.995)	100	88.9	0.011
Hexanal	0.787 (0.662 - 0.882)	75.0	83.3	0.903
(E)-2-hexenal	0.834 (0.715 - 0.917)	100	69.4	0.658
(E)-2-pentenal	0.792 (0.667 - 0.886)	91.7	63.9	0.940
Cyclohexanone	0.874 (0.763 - 0.945)	66.7	97.2	0.165
Acetophenone	0.795 (0.671 - 0.888)	70.8	100	0.658

**Compared with CA19-9 using MedCalc 9.3.9.0 software. AUC, area under the curve; CI, confidence interval; VOC, volatile organic compounds; GBC, gallbladder cancer.*

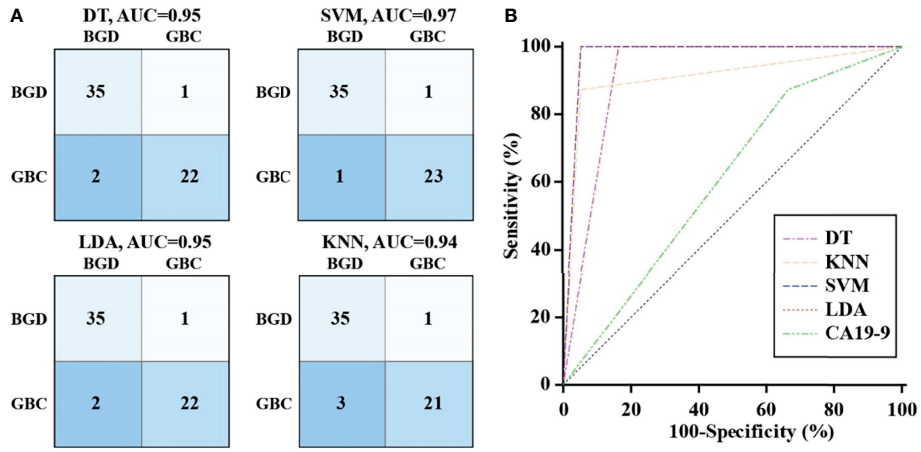

FIGURE 4 | Diagnostic performance of VOCs with machine learning algorithm. **(A)** The confusion matrix of models constructed by DT, SVM, LDA and KNN in the training cohort. **(B)** ROC curves analysis for machine learning models and CA19-9 in differentiating GBC from BGD in the test cohort.

Since VOCs exist in the form of steam, a large number of compounds enter into a gaseous state. Moreover, these molecules diffuse into the blood and are carried to the alveolar membrane, where they spread to the lungs and are exhaled during breathing (19). However, VOCs in exhaled breath may be altered by external factors, such as the surrounding environment, diet, and bacteria (20). Bile is aspirated during ERCP, which is less likely to be affected by confounding factors. Therefore, VOCs in bile may better represent the metabolic activities of surrounding cells in the biliary tract. Navaneethan et al. (21) have reported that the measurement of VOCs in bile is useful to distinguish patients with cholangiocarcinoma from primary sclerosing cholangitis. Recently, they have performed another prospective observational study and found that VOCs in the biliary fluid can help accurately discriminate pancreatic cancer from chronic pancreatitis (22). Our study presented for the first time that bile headspace VOCs were significantly altered in GBC patients. Moreover, both PCA plots and unsupervised hierarchical clustering analysis revealed a clear separation for GBC and BGD cases, suggesting that the VOC profile of GBC patients generally differed from that of BGD patients.

Although GC-IMS has been first used in the detection of bile VOCs, it has been successfully implemented feasibly into others. Maxine and her colleagues have observed a significant difference in fecal VOC profiles using GC-IMS between coeliac disease and refractory coeliac disease (23). Based on urinary VOC profiles, both GC-IMS and GC-TOF-MS methods can establish an interdependence among bladder cancer, prostate cancer, and non-cancerous samples (24). A similar study conducted by Daulton et al. has suggested that GC-IMS and GC-TOF-MS can distinguish pancreatic ductal adenocarcinoma from healthy controls, whereas only GC-IMS can accurately discriminate chronic pancreatitis from healthy controls (25). In the present study, we performed a preliminary analysis to assess the use of the GC-IMS in the diagnosis of GBC. GC-IMS possesses a strong separation capability of complex components with the ultra-high sensitivity of the ion migration spectrum to detect trace volatiles of 10^{-9} or less without enrichment and concentration. Meanwhile, the detection time is shortened to 10 min, which significantly improves the simplicity of detection operation, detection time, and efficiency. In contrast, traditional methods usually need to concentrate the samples, and the detection process can last more than 1 h. It was worth noting that the advantage of this study was to explore the experimental conditions by using orthogonal experiments and to test the effects of room temperature and repeated freeze-thaw cycles on VOCs. The sample was relatively stable within 12 h at room temperature, which facilitated the detection.

In this study, 12 specific VOC molecules linked to GBC were identified. Some of them have also been suggested as potential biomarkers in breath or stool for other diseases. For instance, cyclohexanone is associated with colorectal cancer (26), breast cancer (27), and lung cancer (28). 2-Ethyl-1-hexanol is elevated in the detection of VOCs in patients with lung cancer (28), colorectal cancer (29), and prostate cancer (30). The detailed mechanism of VOC production is not well understood until now, while some researchers have pointed out that these compounds may act directly on the enzyme function (31). Aldehyde dehydrogenase is an important catalyst in the human body, resulting in the oxidization of aldehydes to carboxylic acid (32). Moreover, the carboxylic acids further participate in the synthesis of intracellular lipids, providing materials for the cell membrane (33). With the vigorous metabolism of tumor cells, the activity of acetaldehyde dehydrogenase is increased (34, 35). Therefore, this may explain why the levels of (E)-hept-2-enal, (E)-2-hexenal, (E)-2-pentenal, (E)-2-octenal, and hexanal are reduced in the bile of tumor patients. These findings were

consistent with some studies that volatile aldehydes are decreased in tumor cells (36, 37).

At present, the diagnosis of GBC mainly depends on the clinical manifestations of the disease, CT, B-ultrasound, and other imaging examinations, while these approaches are too subjective, and there are too many external interference factors. Serum CA19-9 test is one of the few non-invasive markers for clinicians to make a preliminary diagnosis (38, 39). However, it only provides limited sensitivity and poor specificity for GBC diagnosis (40). We found that detection of serum CA19-9 had a sensitivity of 87.5% and a specificity of 33.3% using the given cutoff value, with an AUC of 0.604. Among the identified VOCs, (E)-hept-2-enal was superior to CA19-9 in the diagnosis of GBC, while others at most had a considerable diagnostic performance. To ensure the accuracy of the diagnostic model using limited data sets, a machine learning method was used to analyze the heterogeneous signal patterns of gallbladder diseases to obtain higher diagnostic accuracy. In the present study, four popular machine learning algorithms were used to construct the diagnostic model consisting of multiplexed indexes. Besides, the diagnostic accuracy of the VOC combination reached above 90%, which was superior to CA19-9. Support vector machines and linear discriminant analysis provided near 100% accuracy. Thus, we think bile VOCs panel is a suitable biomarker for GBC diagnosis.

CONCLUSIONS

In the present study, our sample size was small, so it was difficult to avoid bias. Therefore, a large sample size and multicenter study should be carried out to further demonstrate the existing data. Meanwhile, it is necessary to further explore the relevant mechanism between the production of endogenous VOCs and the occurrence and development of GBC or BGD. This study provided an experimental basis for the application of VOC analysis in GBC and made it possible to be used in the early diagnosis of GBC, which had an extremely broad application prospect.

DATA AVAILABILITY STATEMENT

The original contributions presented in the study are included in the article/**Supplementary Material**. Further inquiries can be directed to the corresponding author.

ETHICS STATEMENT

The studies involving human participants were reviewed and approved by the Ethics Committee of Qilu Hospital of Shandong University. The patients/participants provided their written informed consent to participate in this study.

AUTHOR CONTRIBUTIONS

Conceptualization, XZ, YiZ; methodology, XG, LZ; validation, XG, JG; investigation, YaZ, QL; data curation, JJ, JG; writing—original draft preparation, XZ; writing—review and editing, YaZ; visualization, LZ; supervision, YiZ; funding acquisition, XZ, JJ, YiZ. All authors have read and agreed to the published version of the manuscript.

FUNDING

This research was funded by National Natural Science Foundation of China, 82172339 and 81972005, Natural Science Foundation of Shandong Province, ZR201910220159, Key Research and Development Program of Shandong Province, 2019GSF108064 and 2021CXGC011105, and Shandong Medical and Health Technology Development Project, 2018WS327.

SUPPLEMENTARY MATERIAL

The Supplementary Material for this article can be found online at: https://www.frontiersin.org/articles/10.3389/fonc.2022.858639/full#supplementary-material

REFERENCES

1. Ferlay J, Soerjomataram I, Dikshit R, Eser S, Mathers C, Rebelo M, et al. Cancer Incidence and Mortality Worldwide: Sources, Methods and Major Patterns in GLOBOCAN 2012. *Int J Cancer* (2015) 136(5):E359–86. doi: 10.1002/ijc.29210
2. Sung H, Ferlay J, Siegel RL, Laversanne M, Soerjomataram I, Jemal A, et al. Global Cancer Statistics 2020: GLOBOCAN Estimates of Incidence and Mortality Worldwide for 36 Cancers in 185 Countries. *CA Cancer J Clin* (2021) 71(3):209–49. doi: 10.3322/caac.21660
3. Kakaei F, Beheshtirouy S, Nejatollahi SM, Zarrintan S, Mafi MR. Surgical Treatment of Gallbladder Carcinoma: A Critical Review. *Updates Surg* (2015) 67(4):339–51. doi: 10.1007/s13304-015-0328-x
4. Garcia P, Lamarca A, Diaz J, Carrera E, Roa JC On Behalf Of The European-Latin American Escalon Consortium. Current and New Biomarkers for Early Detection, Prognostic Stratification, and Management of Gallbladder Cancer Patients. *Cancers* (2020) 12(12):3670. doi: 10.3390/cancers12123670.
5. Rana S, Dutta U, Kochhar R, Rana SV, Gupta R, Pal R, et al. Evaluation of CA 242 as a Tumor Marker in Gallbladder Cancer. *J Gastrointest Cancer* (2012) 43(2):267–71. doi: 10.1007/s12029-011-9288-7
6. Wang YF, Feng FL, Zhao XH, Ye ZX, Zeng HP, Li Z, et al. Combined Detection Tumor Markers for Diagnosis and Prognosis of Gallbladder Cancer. *World J Gastroenterol* (2014) 20(14):4085–92. doi: 10.3748/wjg.v20.i14.4085
7. YU H, Yu T-n, Cai X-j. Tumr Biomarkers: Help or Mislead in the Diagnosis of Xanthogranulomatous Cholecystitis?-Analysis of Serum CA 19-9 Carcinoembryonic Antigen, and CA12-5. *Chin Med J* (2013) 126 (16):30222–7. doi: 10.3760/cma.j.issn.0366-6999.20120341
8. Yu MH, Kim YJ, Park HS, Jung SI. Benign Gallbladder Diseases: Imaging Techniques and Tips for Differentiating With Malignant Gallbladder Diseases. *World J Gastroenterol* (2020) 26(22):2967–86. doi: 10.3748/wjg.v26.i22.2967
9. Garcia-Canaveras JC, Lahoz A. Tumor Microenvironment-Derived Metabolites: A Guide to Find New Metabolic Therapeutic Targets and Biomarkers. *Cancers* (2021) 13(13):3230. doi: 10.3390/cancers13133230

10. Feng X, Wang H, Wang Z, Huang P, Kan J. Discrimination and Characterization of the Volatile Organic Compounds in Eight Kinds of Huajiao With Geographical Indication of China Using Electronic Nose, HS-GC-IMS and HS-SPME-GC-Ms. *Food Chem* (2022) 375:131671. doi: 10.1016/j.foodchem.2021.131671
11. Wang Y, Li J, Wu Y, Yang S, Wang D, Liu Q. Analysis of Volatile Compounds in Sea Bass (Lateolabrax Japonicus) Resulting From Different Slaughter Methods Using Electronic-Nose (E-Nose) and Gas Chromatography-Ion Mobility Spectrometry. *Molecules* (2021) 26(19):5889. doi: 10.3390/molecules26195889
12. Feil C, Staib F, Berger MR, Stein T, Schmidtmann I, Forster A, et al. Sniffer Dogs Can Identify Lung Cancer Patients From Breath and Urine Samples. *BMC Cancer* (2021) 21(1):917. doi: 10.1186/s12885-021-08651-5
13. Bhatt A, Parsi MA, Stevens T, Gabbard S, Kumaravel A, Jang S, et al. Volatile Organic Compounds in Plasma for the Diagnosis of Esophageal Adenocarcinoma: A Pilot Study. *Gastrointestinal Endoscopy* (2016) 84 (4):597–603. doi: 10.1016/j.gie.2015.11.031
14. Lima AR, Pinto J, Azevedo AI, Barros-Silva D, Jeronimo C, Henrique R, et al. Identification of a Biomarker Panel for Improvement of Prostate Cancer Diagnosis by Volatile Metabolic Profiling of Urine. *Br J Cancer* (2019) 121 (10):857–68. doi: 10.1038/s41416-019-0585-4
15. Bond A, Greenwood R, Lewis S, Corfe B, Sarkar S, O'Toole P, et al. Volatile Organic Compounds Emitted From Faeces as a Biomarker for Colorectal Cancer. *Alimentary Pharmacol Ther* (2019) 49(8):1005–12. doi: 10.1111/apt.15140
16. Chandrapalan S, Bosch S, Cubiella J, Guardiola J, Kimani P, Mulder C, et al. Systematic Review With Meta-Analysis: Volatile Organic Compound Analysis to Improve Faecal Immunochemical Testing in the Detection of Colorectal Cancer. *Alimentary Pharmacol Ther* (2021) 54(1):14–23. doi: 10.1111/apt.16405
17. Zhang J, Tian Y, Luo Z, Qian C, Li W, Duan Y. Breath Volatile Organic Compound Analysis: An Emerging Method for Gastric Cancer Detection. *J Breath Res* (2021) 15(4). doi: 10.1088/1752-7163/ac2cde
18. Koureas M, Kalompatsios D, Amoutzias GD, Hadjichristodoulou C, Gourgoulianis K, Tsakalof A. Comparison of Targeted and Untargeted Approaches in Breath Analysis for the Discrimination of Lung Cancer From Benign Pulmonary Diseases and Healthy Persons. *Molecules* (2021) 26(9):2609. doi: 10.3390/molecules26092609
19. Hintzen KFH, Grote J, Wintjens A, Lubbers T, Eussen MMM, van Schooten FJ, et al. Breath Analysis for the Detection of Digestive Tract Malignancies: Systematic Review. *BJS Open* (2021) 5(2):zrab013. doi: 10.1093/bjsopen/zrab013
20. Chen H, Qi X, Zhang L, Li X, Ma J, Zhang C, et al. COVID-19 Screening Using Breath-Borne Volatile Organic Compounds. *J Breath Res* (2021) 15(4). doi: 10.1088/1752-7163/ac2e57
21. Navaneethan U, Parsi MA, Lourdusamy V, Bhatt A, Gutierrez NG, Grove D, et al. Volatile Organic Compounds in Bile for Early Diagnosis of Cholangiocarcinoma in Patients With Primary Sclerosing Cholangitis: A Pilot Study. *Gastrointestinal Endoscopy* (2015) 81(4):943–9.e1. doi: 10.1016/j.gie.2014.09.041
22. Navaneethan U, Spencer C, Zhu X, Vargo JJ, Grove D, Dweik RA. Volatile Organic Compounds in Bile Can Distinguish Pancreatic Cancer From Chronic Pancreatitis: A Prospective Observational Study. *Endoscopy* (2021) 53(7):732–6. doi: 10.1055/a-1255-9169
23. Rouvroye MD, Wicaksono A, Bosch S, Savelkoul E, Covington JA, Beaumont H, et al. Faecal Scent as a Novel Non-Invasive Biomarker to Discriminate Between Coeliac Disease and Refractory Coeliac Disease: A Proof of Principle Study. *Biosensors* (2019) 9(2):69. doi: 10.3390/bios9020069
24. Tyagi H, Daulton E, Bannaga AS, Arasaradnam RP, Covington JA. Urinary Volatiles and Chemical Characterisation for the Non-Invasive Detection of Prostate and Bladder Cancers. *Biosensors* (2021) 11(11):437. doi: 10.3390/bios11110437
25. Daulton E, Wicaksono AN, Tiele A, Kocher HM, Debernardi S, Crnogorac-Jurcevic T, et al. Volatile Organic Compounds (VOCs) for the Non-Invasive Detection of Pancreatic Cancer From Urine. *Talanta* (2021) 221:121604. doi: 10.1016/j.talanta.2020.121604
26. Wang C, Ke C, Wang X, Chi C, Guo L, Luo S, et al. Noninvasive Detection of Colorectal Cancer by Analysis of Exhaled Breath. *Analytical Bioanalytical Chem* (2014) 406(19):4757–63. doi: 10.1007/s00216-014-7865-x
27. Wang C, Sun B, Guo L, Wang X, Ke C, Liu S, et al. Volatile Organic Metabolites Identify Patients With Breast Cancer, Cyclomastopathy, and Mammary Gland Fibroma. *Sci Rep* (2014) 4:5383. doi: 10.1038/srep05383
28. Liu H, Wang H, Li C, Wang L, Pan Z, Wang L. Investigation of Volatile Organic Metabolites in Lung Cancer Pleural Effusions by Solid-Phase Microextraction and Gas Chromatography/Mass Spectrometry. *J Chromatogr B Analytical Technol Biomed Life Sci* (2014) 945-946:53–9. doi: 10.1016/j.jchromb.2013.11.038
29. Wang C, Li P, Lian A, Sun B, Wang X, Guo L, et al. Blood Volatile Compounds as Biomarkers for Colorectal Cancer. *Cancer Biol Ther* (2014) 15(2):200–6. doi: 10.4161/cbt.26723
30. Jimenez-Pacheco A, Salinero-Bachiller M, Iribar MC, Lopez-Luque A, Mijan-Ortiz JL, Peinado JM. Furan and P-Xylene as Candidate Biomarkers for Prostate Cancer. *Urologic Oncol* (2018) 36(5):243 e21– e27. doi: 10.1016/j.urolonc.2017.12.026
31. Ramya M, Jang S, An HR, Lee SY, Park PM, Park PH. Volatile Organic Compounds From Orchids: From Synthesis and Function to Gene Regulation. *Int J Mol Sci* (2020) 21(3):1160. doi: 10.3390/ijms21031160
32. Shortall K, Djeghader A, Magner E, Soulimane T. Insights Into Aldehyde Dehydrogenase Enzymes: A Structural Perspective. *Front Mol Biosci* (2021) 8:659550. doi: 10.3389/fmolb.2021.659550
33. Perchuk I, Shelenga T, Gurkina M, Miroshnichenko E, Burlyaeva M. Composition of Primary and Secondary Metabolite Compounds in Seeds and Pods of Asparagus Bean (Vigna Unguiculata (L.) Walp.) From China. *Molecules* (2020) 25(17):3778. doi: 10.3390/molecules25173778
34. Li G, Li Y, Liu X, Wang Z, Zhang C, Wu F, et al. ALDH1A3 Induces Mesenchymal Differentiation and Serves as a Predictor for Survival in Glioblastoma. *Cell Death Dis* (2018) 9(12):1190. doi: 10.1038/s41419-018-1232-3
35. Grimley E, Cole AJ, Luong TT, McGonigal SC, Sinno S, Yang D, et al. Aldehyde Dehydrogenase Inhibitors Promote DNA Damage in Ovarian Cancer and Synergize With ATM/ATR Inhibitors. *Theranostics* (2021) 11 (8):3540–51. doi: 10.7150/thno.51885
36. Pinto J, Carapito A, Amaro F, Lima AR, Carvalho-Maia C, Martins MC, et al. Discovery of Volatile Biomarkers for Bladder Cancer Detection and Staging Through Urine Metabolomics. *Metabolites* (2021) 11(4):199. doi: 10.3390/metabo11040199
37. Leiherer A, Slefarska D, Leja M, Heinzle C, Mundlein A, Kikuste I, et al. The Volatilomic Footprints of Human HGC-27 and CLS-145 Gastric Cancer Cell Lines. *Front Mol Biosci* (2020) 7:607904. doi: 10.3389/fmolb.2020.607904
38. Yamashita S, Passot G, Aloia TA, Chun YS, Javle M, Lee JE, et al. Prognostic Value of Carbohydrate Antigen 19-9 in Patients Undergoing Resection of Biliary Tract Cancer. *Br J Surg* (2017) 104(3):267–77. doi: 10.1002/bjs.10415
39. Mochizuki T, Abe T, Amano H, Hanada K, Hattori M, Kobayashi T, et al. Efficacy of the Gallbladder Cancer Predictive Risk Score Based on Pathological Findings: A Propensity Score-Matched Analysis. *Ann Surg Oncol* (2018) 25 (6):1699–708. doi: 10.1245/s10434-018-6444-3
40. Kang JS, Hong SY, Han Y, Sohn HJ, Lee M, Kang YH, et al. Limits of Serum Carcinoembryonic Antigen and Carbohydrate Antigen 19-9 as the Diagnosis of Gallbladder Cancer. *Ann Surg Treat Res* (2021) 101(5):266–73. doi: 10.4174/astr.2021.101.5.266

Conflict of Interest: Authors LZ and JG were employed by Hanon Advanced Technology Group Co.,Ltd,.

The remaining authors declare that the research was conducted in the absence of any commercial or financial relationships that could be construed as a potential conflict of interest.

Publisher's Note: All claims expressed in this article are solely those of the authors and do not necessarily represent those of their affiliated organizations, or those of the publisher, the editors and the reviewers. Any product that may be evaluated in this article, or claim that may be made by its manufacturer, is not guaranteed or endorsed by the publisher.

frontiers in Oncology

ORIGINAL RESEARCH
published: 31 March 2022
doi: 10.3389/fonc.2022.829705

The Prognostic Value and Immune Infiltration of USP10 in Pan-Cancer: A Potential Therapeutic Target

Dacheng Gao[1,2], Zhiwen Zhang[2], Rui Xu[2], Ziyang He[2], Fangyi Li[1,2], Yan Hu[2], Hui Chen[2], Jiawei Lu[2], Xingguo Cao[2], Yali Liu[2] and Zengguang Xu[2,3]**

[1] Shanghai East Hospital, Postgraduate Training Base of Jinzhou Medical University, Shanghai, China, [2] Research Center for Translational Medicine, Shanghai East Hospital, School of Medicine, Tongji University, Shanghai, China, [3] Shanghai East School of Clinical Medicine, Jinzhou Medical University, Shanghai, China

Ubiquitin-specific peptidase 10 (USP10) can sustain cellular functions and regulate cellular processes. It plays an essential role in cancer inhibition or facilitation by reversing ubiquitin-proteasome degradation. Studies have identified USP10 to be involved in tumor progression in various cancers. However, the pan-cancer expression pattern of USP10, its prognostic value, and the association between tumor immune cell infiltration and USP10 expression remain to be discussed and thus comprised the aims of the present study. Based on clinical samples and bioinformatic analyses, high *USP10* expression was observed in most cancer tissues except for ovarian cancer. High *USP10* expression correlated with pathological stage and node metastasis and predicted poor patient prognosis. In addition, further analyses at the TIMER and GEPIA databases showed that USP10 is involved in the infiltration of multiple immune cells and regulated the infiltration levels of specific immune cell subpopulations, particularly in pancreatic adenocarcinoma (PAAD) and liver hepatocellular carcinoma (LIHC). Importantly, USP10 might influence survival by modulating immune infiltration in patients with PAAD and LIHC. These results identified USP10 as a potential biomarker for pan-cancer prognosis, and in certain cancers, USP10 could identify clinical prognosis linked to tumor immune infiltration.

Keywords: USP10, prognosis, immune infiltration, pan-cancer, biomarker

OPEN ACCESS

Edited by:
Hongda Liu,
Nanjing Medical University, China

Reviewed by:
Xiang Wang,
Dalian Medical University, China
Shuai Wang,
University of Pittsburgh Medical Center, United States

***Correspondence:**
Yali Liu
yaliliuliu@163.com
Zengguang Xu
xuzg1998@163.com

Specialty section:
This article was submitted to Cancer Molecular Targets and Therapeutics, a section of the journal Frontiers in Oncology

Received: *06 December 2021*
Accepted: *07 March 2022*
Published: *31 March 2022*

Citation:
Gao D, Zhang Z, Xu R, He Z, Li F, Hu Y, Chen H, Lu J, Cao X, Liu Y and Xu Z (2022) The Prognostic Value and Immune Infiltration of USP10 in Pan-Cancer: A Potential Therapeutic Target. Front. Oncol. 12:829705. doi: 10.3389/fonc.2022.829705

INTRODUCTION

Currently, in many human populations and regions, the leading cause of death is cancer, representing a severe threat to human health (1). The malignant phenotype of neoplasms usually correlates with dysregulation of protein synthesis (2). Proteostasis disorders and aberrant gene expression in cancer affect the patients' clinical outcomes. In addition, there has been increasing interest in the role of the tumor microenvironment (TME) in cancer metastasis, in which the infiltration levels of dendritic cells, neutrophils, macrophages, T cells, and B cells, vary significantly. Targeting of immune cells that infiltrate the TME using immunotherapy has become a landmark in the history of tumor therapy and has dramatically advanced the development of oncological immunology (3).

There are various types of post-translational modifications of proteins. Among them, ubiquitination and deubiquitination, which add or remove ubiquitin from target proteins to promote protein degradation or stabilization, are essential to regulate cell cycle processes, cell signaling, the DNA damage response, and the nuclear factor kappa B (NF-κB) pathway (4, 5). Protein ubiquitination is the result of the covalent modification of substrate proteins by ubiquitin-activating enzyme E1, ubiquitin-binding enzyme E2, and ubiquitin-ligase E3.

Deubiquitinating enzymes (DUBs) can mediate and regulate the reversible deubiquitination of substrate proteins and are important factors in regulating the ubiquitin system. On the one hand, they are involved in the recycling of ubiquitin molecules, processing ubiquitin precursors, and editing of ubiquitin chains to regulate the function of conjugated proteins. On the other hand, they can influence proteostasis by removing ubiquitin from substrates and exert pro- or anti-cancer effects (4, 6). In addition, the function of DUBs in cells can be regulated by modifications such as phosphorylation, ubiquitination, and sumoylation, which in turn affect their catalytic activity, cellular localization, or protein abundance.

Ubiquitin-specific peptidase 10 (USP10) is a crucial DUB that is primarily localized in the cytoplasm. The *USP10* gene is situated on chromosome 16q24.1 and encodes a protein product comprising 798 amino acids (relative molecular mass = ~ 93 KDa) (7, 8). Its molecular structure is mainly that of a cysteine-type endopeptidase and a ubiquitin sulfhydryl esterase. USP10 acts as a regulator of the cell cycle and autophagy by deubiquitinating various proteins that are post-translationally transferred to the cytoplasm. USP10 specifically deubiquitinates and stabilizes P53. Under DNA damage stress conditions, USP10 is stabilized by Ataxia Telangiectasia mutated (ATM) kinase phosphorylation modification at Thr42 and Ser337, which drives its entry into the nucleus where it deubiquitinates P53, thereby regulating the P53 downstream network functions (9). In addition, by acting on wild-type P53, USP10 can exercise cancer suppressive functions; however, for some mutant P53s, USP10 might exert cancer-promoting functions.

Studies have shown that the abnormal expression of USP10 in different types of cancer correlates strongly with patient prognosis. High USP10 expression in prostate cancer, breast cancer, non-small cell lung cancer, colon cancer, and melanoma is associated with poor patient prognosis (10–14). However, low expression of USP10 predicts a poor prognosis in patients with ovary cancer (15). Furthermore, USP10 could deubiquitinate sirtuin 6 (SIRT6) to antagonize transcriptional activation of c-Myc oncogenes to inhibit tumor formation (16). In non-small cell lung cancer with mutant P53, targeting USP10 could boost drug sensitivity in patients with lung cancer (17). By contrast, USP10 is closely associated with tumor immunity. USP10 has been identified to be involved in metastasis and can drive tumor-associated macrophage polarization in colorectal cancer (18). Depletion of USP10 markedly reduced apoptosis and immune cell infiltration (19). It also stimulates the production of reactive oxygen species (ROS) in T cells, thereby promoting malignant mutations (20). These studies suggest that USP10 has a critical function in the initiation and progression cancer, and in tumor immunity. Therefore, the design of highly selective inhibitors might bring new hope for anti-cancer immunotherapy.

However, to date, USP10 has not been studied in pan-cancer. Its potential prognostic value and the relevance of immune infiltration are unclear, and there is a lack of macroscopic presentation and discussion. Therefore, this study aimed to determine whether USP10 influences the prognosis of patients with cancer and if such an influence is associated with immune cell infiltration.

MATERIALS AND METHODS

Oncomine Database

The Oncomine cancer database was used to analyze *USP10* mRNA expression levels in different cancer types (https://www.oncomine.org/resource/login.html) (21). The threshold was set as a *P*-value of 0.001, a fold-change of 1.5, and the gene rank of 'all'.

TIMER Database

TIMER (https://cistrome.shinyapps.io/timer/) (22) enables the systematic analysis of immune cell infiltration in various types of cancer. Using TIMER, the association between *USP10* expression in different tumors and six types of immune infiltrates (including B cells, CD4+ T cells, CD8+ T cells, macrophages, neutrophils, and dendritic cells) was explored, as well as the correlation between *USP10* expression and immune cell gene markers after determining the tumor purity. Finally, we determined the associations between the expression of *USP10* and the genetic markers of specific subpopulations of immune infiltrating cells.

HPA Database

The Human Protein Atlas (HPA) (http://www.proteinatlas.org/) was used to assess differences in USP10 expression at the protein level. This database contains immunohistochemical (IHC) data for USP10 protein levels in eight cancer tissues and their normal counterparts (breast, liver, lung, skin, colon, kidney, ovarian, and prostate cancers).

GEPIA Database

Gene Expression Profiling Interactive Analysis (GEPIA) (http://gepia.cancer-pku.cn/) (23) is an online interactive web server for the analysis of tumor samples from The Cancer Genome Atlas (TCGA) and RNA sequencing expression data from the Genotype-Tissue Expression (GTEx) project. We used GEPIA to evaluate the association of *USP10* expression with prognosis in various tumor types, including overall survival (OS) and relapse-free survival (RFS). We further estimated the interaction between *USP10* expression and specific markers related to tumor immune cell infiltration.

PrognoScan Database

The PrognoScan database (http://www.abren.net/PrognoScan/) (24) was used to assess the correlation between *USP10* expression

and survival rate in different types of cancer, and to explore the prognostic value of USP10.

Kaplan-Meier Plotter Database

The Kaplan-Meier plotter database (http://kmplot.com/analysis/) (25) uses meta-analysis data to discover and validate prognosis-related biomarkers. The association between *USP10* expression and patient survival in pan-cancer was investigated.

cBioPortal Database

The open web resource cBioPortal database (http://www.cbioportal.org/) (26) is used to explore multidimensional cancer genome datasets. We used cBioPortal to analyze the impact of *USP10* mutations and copy number variation on various cancers.

UALCAN Database

The UALCAN (http://ualcan.path.uab.edu/) (27) database contains valuable cancer OMICS data and information to help understand tumor staging and node metastasis related to the USP10 protein in a diverse range of cancers, which could inform mechanistic studies.

Tissue Specimens

From May 2008 to Oct 2015, we collected tumors and adjacent non-tumor tissues from 12 patients suffering from different types of cancer who underwent surgical treatment in the Shanghai East Hospital Affiliated to Tongji University. The Ethics Committee of Shanghai East Hospital Affiliated to Tongji University approved this study (No. 2019tjdx110). Exemption from informed consent was granted because of the retrospective nature of the study.

Hematoxylin and Eosin (H&E) Staining

Cancerous and control tissues from the breast, liver, lung, colorectum, kidney, ovary, prostate, stomach, skin, cerebrum, esophagus, and uterus were fixed in 4% paraformaldehyde. After deparaffinization and rehydration, sections were cuts at 4 μm thick and stained with H&E according to the manufacturer's protocol (C0105S, Beyotime, Jiangsu, China). The sections were finally dehydrated and sealed for viewing under a light microscope (×200, Leica DM3000; Wetzlar, Germany).

Immunofluorescence Staining

All tumor sections (4 μm) were deparaffinized and hydrated, quenched in 3% H_2O_2, immersed in citrate buffer, heated to retrieve the antigen, and then stained using immunofluorescence. USP10 primary antibodies (Invitrogen, Waltham, MA, USA; Cat. #PA5-52334) and fluorescently-conjugated secondary antibodies were applied, followed by 4′,6-diamidino-2-phenylindole (DAPI) staining to visualize the nuclei. The sections were observed under a microscope (×200, Leica DM3000).

Statistical Analysis

Data in Oncomine are presented based on gene ranking, fold-change, and *P*-values. Survival curves were plotted using PrognoScan, Kaplan-Meier plotter, and GEPIA, and the results are displayed as the hazard ratio (HR) and *P*-value, or the *P*-value alone, from a log-rank test. Gene expression correlation was estimated using Spearman's correlation, and r values were used to determine the magnitude of the correlation. *P*-values less than 0.05 were considered statistically significant.

RESULTS

Transcriptional and Translational Levels of USP10 in Pan-Cancer

In the Oncomine database, the levels of *USP10* mRNA in various cancers and normal tissues were analyzed. The results showed that *USP10* expression in breast cancer, cervical cancer, colorectal cancer, gastric cancer, head and neck cancer, leukemia, lung cancer, lymphoma, melanoma, myeloma, and prostate cancer was higher than that in normal tissues (**Figure 1A**). By contrast, in some datasets, lower *USP10* expression was observed for brain and CNS cancer, bladder cancer, kidney cancer, ovarian cancer, and sarcoma. **Supplementary Table 1** shows the detailed results for the expression of *USP10* in various cancer types.

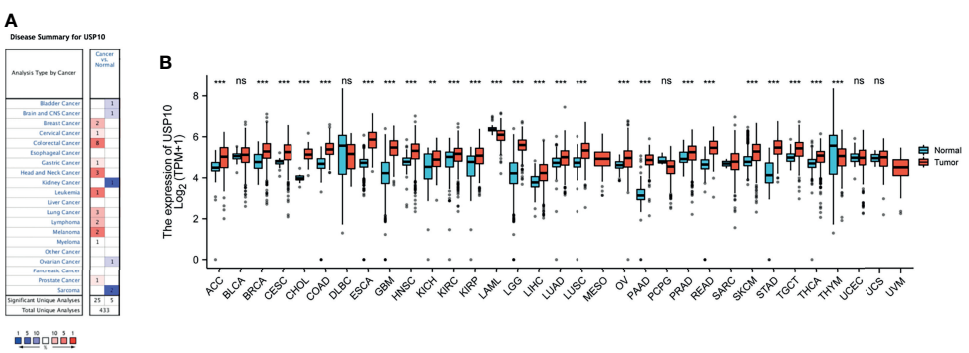

FIGURE 1 | The mRNA expression level of *USP10* in pan-cancer. **(A)** Oncomine data showing enhanced or reduced *USP10* expression in various tumor tissue types and in normal tissues. **(B)** TGCA data showing the expression levels of human *USP10* in different types of cancer, with GTEx data as a control. $^{**}P < 0.01$; $^{***}P < 0.001$. NS, no significance.

Next, TCGA RNA-seq data from multiple malignancies was analyzed for *USP10* expression (**Figure 1B**). Significantly higher *USP10* expression was detected in adrenocortical carcinoma (ACC), breast invasive carcinoma (BRCA), cervical squamous cell carcinoma and endocervical adenocarcinoma (CESC), cholangiocarcinoma (CHOL), colon adenocarcinoma (COAD), (esophageal carcinoma (ESCA), glioblastoma multiforme (GMB), (head and neck cancer (HNSC), (kidney chromophobe (KICH), kidney renal clear cell carcinoma (KIRC), kidney renal papillary cell carcinoma (KIRP), brain lower grade glioma (LGG), liver hepatocellular carcinoma (LIHC), lung adenocarcinoma (LUAD), lung squamous cell carcinoma (LUSC), ovarian serous cystadenocarcinoma (OV), pancreatic adenocarcinoma (PAAD), prostate adenocarcinoma (PRAD), rectum adenocarcinoma (READ), skin cutaneous melanoma (SKCM), stomach adenocarcinoma (STAD), testicular germ cell tumors (TGCT), and thyroid carcinoma (THCA) tissues compared with that in adjacent normal tissues. However, significantly lower *USP10* expression was observed in acute myeloid leukemia (LAML) and thymoma (THYM) compared with that in adjacent normal tissues. The analyses of the two databases were relatively consistent, except for KIRC and OV. These analytical differences were mainly due to the different databases and different sample sizes.

We used immunofluorescence (IF) to examine the expression of USP10 protein in various cancer tissues and their normal counterparts. USP10 protein expression was higher in breast cancer, liver cancer, lung cancer, colorectal cancer, kidney cancer, prostate cancer, stomach cancer, skin cancer, cerebrum cancer, esophagus cancer, and uterus cancer tissues than in normal tissues (**Figure 2** and **Supplementary Figure 1**). However, USP10 protein levels were lower in ovarian cancer tumor tissues compared with those in normal tissues (**Figure 2**), which was in line with the results for the mRNA levels from the Oncomine database (**Figure 1A**). Furthermore, the immunohistochemistry (IHC) results from the HPA database shown in **Supplementary Figure 2** showed similar results. Normal lung, prostate, and liver tissues showed moderate USP10 IHC staining, whereas tumor tissues showed intense staining. Normal breast, colon, kidney, and skin tissue samples showed weak USP10 staining, while tumor tissues showed intense staining. Interestingly, the normal ovary tissue sample had moderate USP10 staining, while tumor tissue had low staining (**Supplementary Figure 2**). These results suggested that USP10 protein levels are generally upregulated in the above tumor tissues but downregulated in ovarian cancer. The transcriptional and translational levels of USP10 in these cancer types were broadly consistent.

Diagnostic Value of USP10 in Representative Tumors

Given that USP10 expression was upregulated in a variety of cancers, we used ROC curves to assess the diagnostic value of USP10 for pan-cancer. The results revealed that USP10 had a certain accuracy (area under the ROC curve (AUC) > 0.7) to predict 12 representative tumors, including BRCA (AUC = 0.749) (**Figure 3A**), CESC (AUC = 0.786) (**Figure 3B**), CHOL (AUC = 1.000) (**Figure 3C**), COAD (AUC = 0.921) (**Figure 3D**), ESCA (AUC = 0.949) (**Figure 3E**), HNSC (AUC = 0.800) (**Figure 3F**), LIHC (AUC = 0.717) (**Figure 3G**), LUAD (AUC = 0.714) (**Figure 3H**), LUSC (AUC = 0.842) (**Figure 3I**), PAAD (AUC = 0.973) (**Figure 3J**), READ (AUC = 0.905) (**Figure 3K**), and STAD (AUC = 0.948) (**Figure 3L**). Among them, USP10 had high accuracy (AUC > 0.9) for PAAD, CHOL, ESCA, STAD, and READ. These results suggested that USP10 has a different diagnostic value depending on the type of cancer.

Prognostic Value of USP10 in Different Cancers

We than investigated whether USP10 expression was linked to the prognosis of patients with cancer. The impact of *USP10* expression on survival rates was evaluated using PrognoScan,

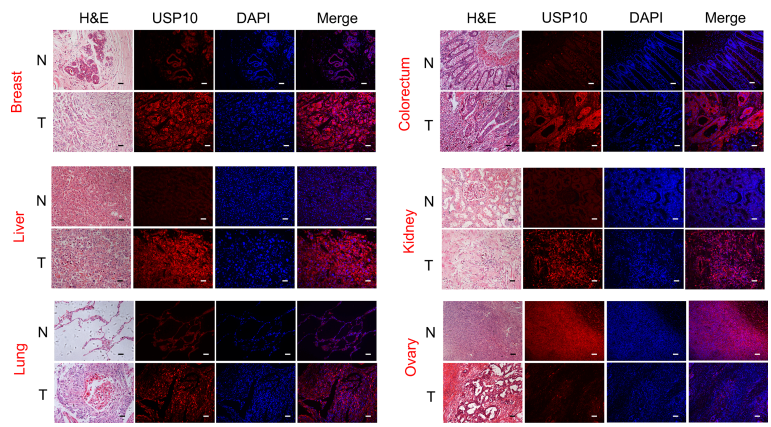

FIGURE 2 | The protein level of USP10 in different types of cancer. Representative images of H&E stained normal and tumor slides (left 1st). Immunofluorescence staining analysis (left 2nd to 4th) showing that an evident fluorescent signal in the tumor tissue sections compared with that in the control group. However, in ovarian cancer, normal tissue has a stronger fluorescent signal than tumor tissue. All scale bars = 50 μm. H&E, hematoxylin-eosin staining. N, normal tissues; T, tumor tissues.

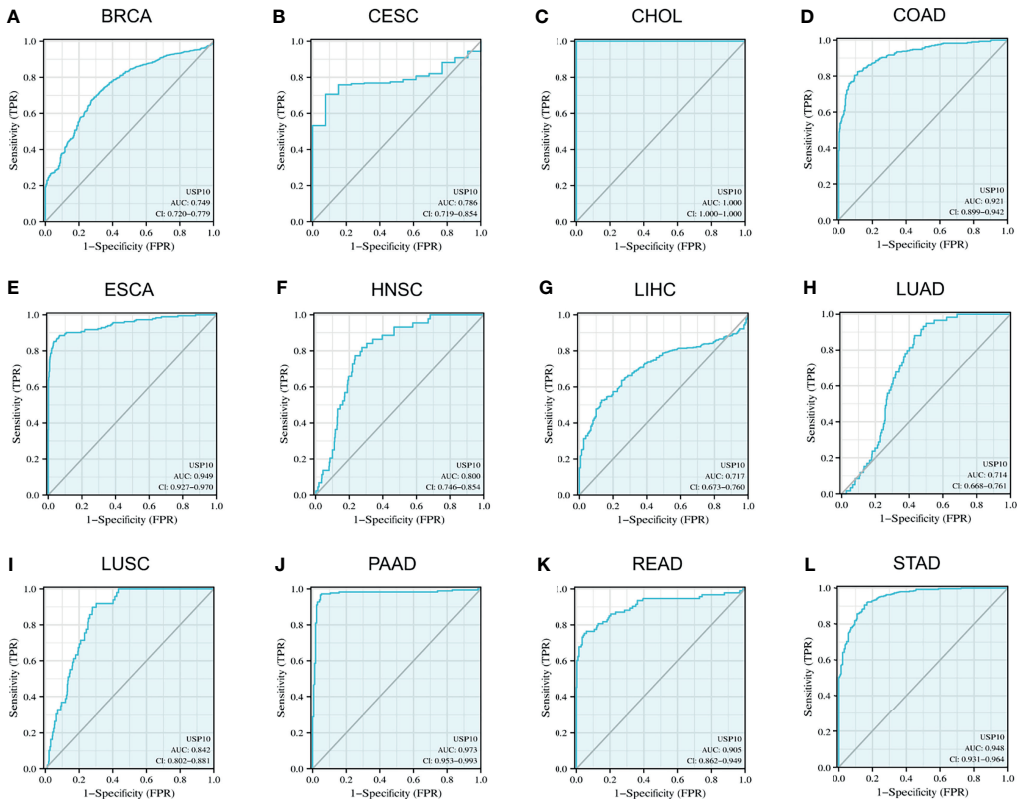

FIGURE 3 | Receiver operating characteristic (ROC) curves for *USP10* in representative tumors. **(A)** BRCA, **(B)** CESC, **(C)** CHOL, **(D)** COAD, **(E)** ESCA, **(F)** HNSC, **(G)** LIHC, **(H)** LUAD, **(I)** LUSC, **(J)** PAAD, **(K)** READ, **(L)** STAD. Values under the ROC curve ranges from 0.5 to 1. The closer the area under the curve (AUC) is to 1, the better the diagnosis. The horizontal coordinate is the False Positive Rate (FPR), and the vertical coordinate is the True Positive Rate (TPR).

primarily using Gene Expression Omnibus (GEO) data. Notably, the expression of *USP10* had a marked effect on the prognosis of six types of cancers, including brain cancer, skin cancer, lung cancer, ovarian cancer, colorectal cancer, and breast cancer (**Figures 4A–L**). In patients with these cancers, high *USP10* expression could be an independent risk factor. Details of the association between *USP10* expression and the prognosis of different cancers are shown in **Supplementary Table 2**.

To further investigate USP10's prognostic potential various cancers, Kaplan-Meier Plotter was employed, which mainly uses TCGA data from Affymetrix microarrays. **Figures 5A–F** show the details of the expression of *USP10* in the different types of cancer. High *USP10* expression correlated with unfavorable prognosis of in terms of OS and RFS in PAAD; OS in BRCA and LUSC; and RFS in LIHC and CESC. However, a favorable prognosis in terms of OS was related to high *USP10* expression in OV. The analysis revealed that USP10 mRNA and protein levels were downregulated significantly in ovarian tumor tissues compared with those in normal tissues, but high USP10 expression improved the OS of patients with ovarian cancer significantly (**Figures 4E**, **5D**). In addition, we examined USP10-related survival (OS and RFS) using the GEPIA database (**Figures 5G–I**). Poor prognosis in PAAD (RFS, HR = 1.6, P = 0.027), LUAD (RFS, HR = 1.4, P = 0.027), and HNSC (OS, HR = 1.4, P = 0.024) correlated with higher *USP10* expression. These results suggest that *USP10* expression has different prognostic values depending on the cancer type.

Genetic Alterations of *USP10* in Pan-Cancer and TMB-Based Survival Analysis of *USP10* Expression in Patients With Tumors

Tumorigenesis is usually accompanied by genetic alterations. Therefore, the genetic alterations of *USP10* were examined in various tumor samples in the TCGA database (**Figure 6A**). *USP10* showed the highest alteration frequency (6.99%) in patients with endometrial tumors with "mutation" as the primary type. Copy number alterations (CAN) of the "deep deletion" type were the predominant type of mutation in prostate adenocarcinoma cases, with a frequency of 5.26%. Noticeably, almost all the tumor cases with genetic alterations had deletions or mutations of *USP10* (**Figure 6A**). *USP10* gene mutations were observed in numerous cancers; therefore, we next explored the potential relationship between the tumor mutational burden (TMB) and *USP10* expression in the clinical survival prognosis of different types of cancer (**Figure 6B**). *USP10* expression correlated significantly with the OS of patients with STAD (HR = 0.57, P = 0.038) and UCEC (HR = 0.47, P = 0.039) with

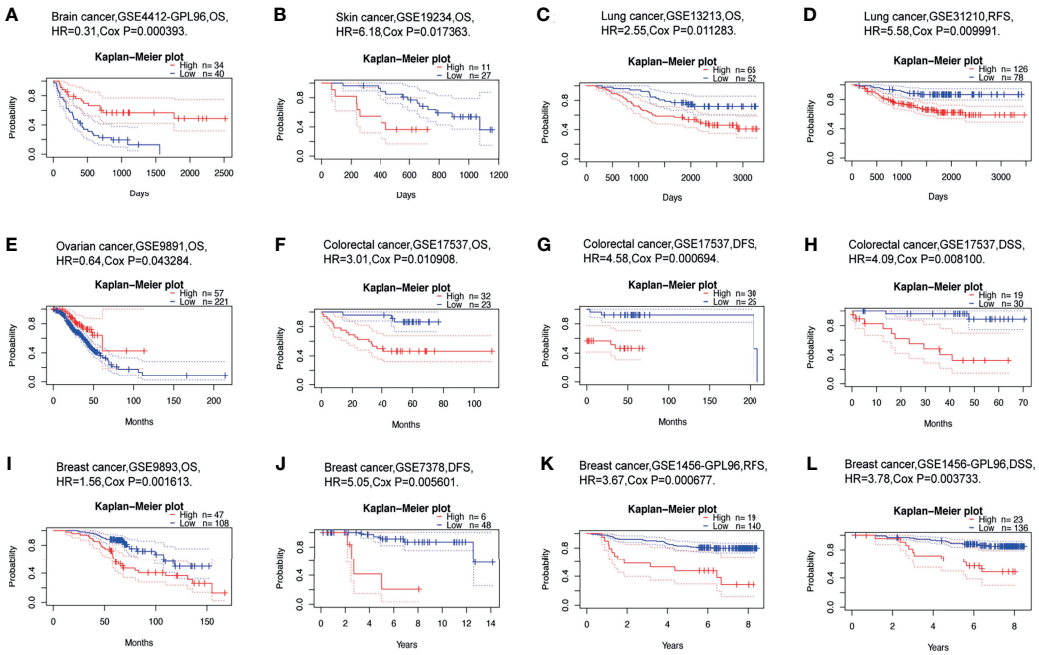

FIGURE 4 | Correlation between *USP10* expression and the prognosis of various types of cancer using data from the PrognoScan database. **(A)** Overall survival (OS) of a cohort of 74 patients with brain cancer (GSE4412-GPL96). **(B)** OS of a cohort of 38 patients with skin cancer (GSE19234). **(C, D)** OS and relapse-free survival (RFS) survival curves for patients in two lung cancer cohorts [GSE13213 (n=117) and GSE31210 (n=204)]. **(E)** OS of a cohort of 278 patients with ovarian cancer (GSE9891). **(F–H)** OS (n = 55), disease-free survival (DFS) (n = 55), disease free survival (DSS) (n = 49) survival curves for a cohort of patients with colorectal cancer (GSE17537). **(I, J)** OS and DFS survival curves for two cohorts of patients with breast cancer [GSE9893 (n =155) and GSE7378 (n =54)]. **(K, L)** RFS (n =159) and DSS (n =159) survival curves for a cohort of patients with breast cancer (GSE1456-GPL96). Patients with high *USP10* expression are represented by the red curve. Significance is indicated by a *P*-value < 0.05.

a high TMB, showing a better prognosis compared with subjects with a low TMB (**Figure 6C**). By contrast, the expression of *USP10* correlated significantly with OS in patients with LUAD (HR = 1.77, P = 0.0074) with a high TMB; however, their prognosis was worse compared with patients with a low TMB (**Figure 6C**). These results suggested that patient prognosis is affected by the association between *USP10* expression and the TMB in certain cancers. Moreover, genetic alterations in *USP10* might play an important role in the genomes of endometrial and prostate cancers. These findings warrant further in-depth investigation.

USP10 Expression and Clinical Parameters of Patients With Different Cancers

To obtain a more detailed understanding of the role of USP10 in the progression of cancers, *USP10* expression was analyzed in patients with multiple cancers based on different clinical parameters using UALCAN. In terms of tumor staging, the expression of *USP10* was increased significantly in patients with LUSC at stages 1, 2, and 3; and in patients with READ and LUAD at stages 1, 2, 3, and 4 (**Figure 7A**). Moreover, patients with STAD had markedly elevated *USP10* expression in stages 1, 2, 3, and 4; and the changes at stage 1 and 3 were statistically significance (P < 0.05) (**Figure 7A**). The expression of *USP10* was upregulated in patients with LIHC. Interestingly, with the deterioration of LIHC, *USP10* expression increased gradually (**Figure 7A**). Notably, patients with HNSC showed significant overexpression of *USP10* in stages 1, 2, 3, and 4. In addition, the comparisons of stage 1 *vs.* 2, stage 1 *vs.* 4, stage 2 *vs.* 3, and stage 3 *vs.* 4 were also statistically significant. However, *USP10* was downregulated significantly in stage 3, possibly influenced by different molecular signaling pathways or different molecular subtypes (**Figure 7A**). For lymph node metastasis, patients with LUSC, READ, and LUAD with N0, N1, or N2 metastasis, *USP10* expression was higher than that in patients with other stages of metastasis (**Figure 7B**). The same *USP10* expression pattern was observed for patients with STAD and HNSC N0, N1, N2, or N3 metastasis and in patients with LIHC with N0 metastasis (**Figure 7B**). Thus, the expression of *USP10* correlated closely with the proliferation and lymph node metastasis of tumors.

The Association of *USP10* Expression With Immune Cell Infiltration in Various Cancers

Numerous inflammatory and immune cells infiltrate cancer tissue, and recent studies have revealed the importance of tumor-infiltrating lymphocytes (TILs) in predicting the prognosis of patient survival (28–31). Therefore, the relationship between *USP10* expression and immune cell

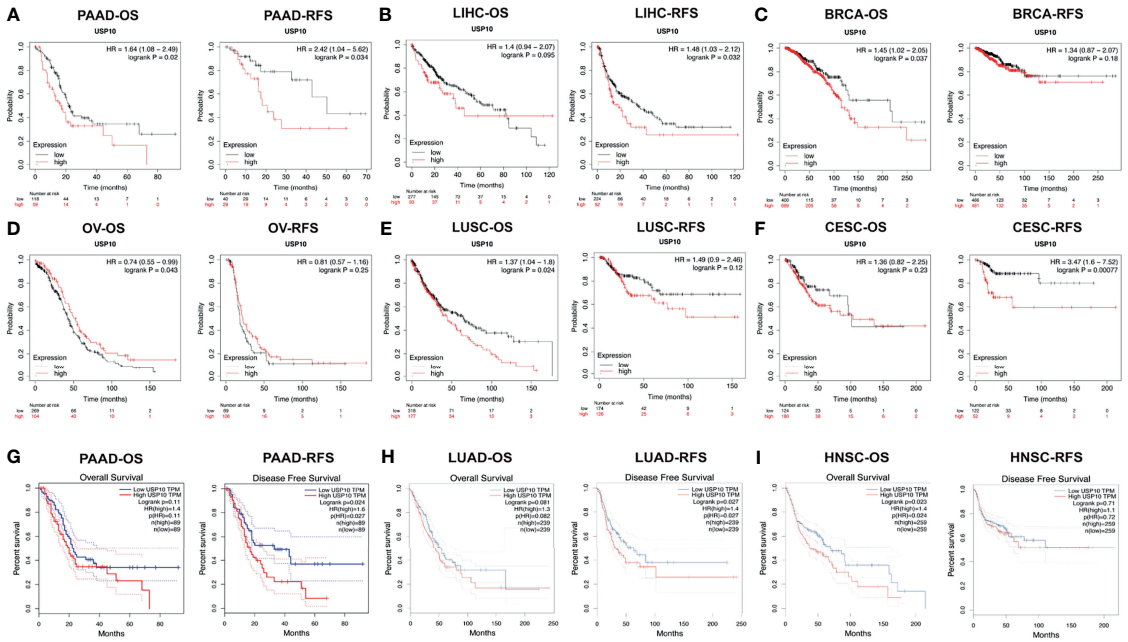

FIGURE 5 | Correlation between *USP10* expression and the prognosis of various types of cancer in the Kaplan–Meier Plotter **(A–F)** and GEPIA **(G–I)** databases. Overall survival (OS) and relapse-free survival (RFS) survival curves of patients with **(A)** pancreatic cancer (PAAD), **(B)** liver cancer (LIHC), **(C)** breast cancer (BRCA), **(D)** ovarian cancer (OV), **(E)** lung squamous cell carcinoma (LUSC), **(F)** cervical squamous cell carcinoma and endocervical adenocarcinoma (CESC), **(G)** pancreatic cancer (PAAD), **(H)** lung adenocarcinoma (LUAD), **(I)** head and neck squamous cell carcinoma (HNSC). Patients with high *USP10* expression are represented by the red curve. Significance is indicated by a *P*-value < 0.05.

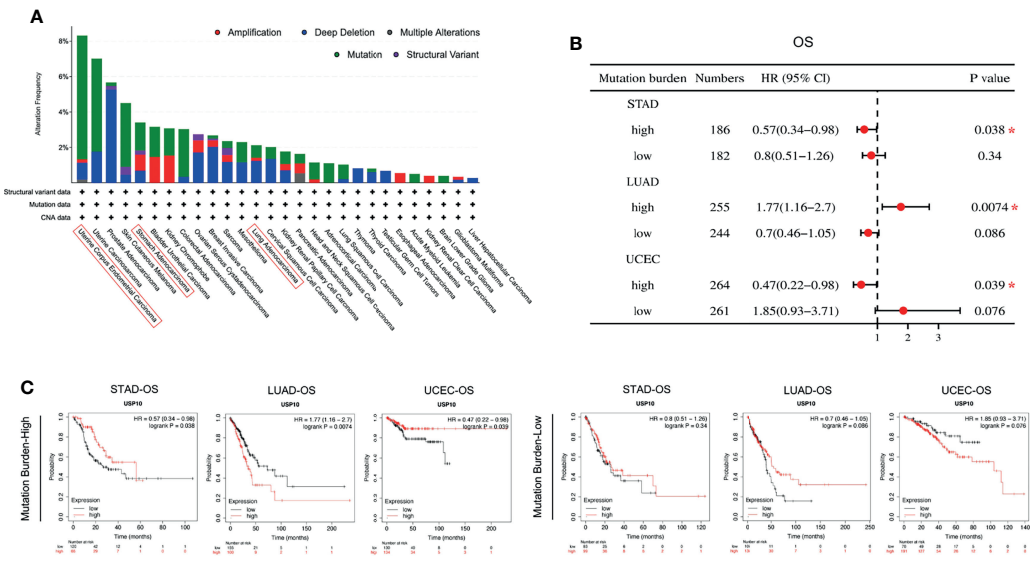

FIGURE 6 | cBioPortal access of TGCA data showing *USP10* mutation features in pan-cancer correlation of the TMB and *USP10* in Kaplan–Meier Plotter. **(A)** Mutation type alteration frequencies. **(B)** The potential associations between the TMB and *USP10* expression in the OS of patients with cancer, shown as a forest plot. **(C)** Survival curves between the TMB and USP10 expression in the OS of patients with cancer. TMB, tumor mutation burden. STAD, stomach adenocarcinoma; LUAD, lung adenocarcinoma; UCEC, uterine corpus endometrial carcinoma. OS, overall survival. *$P < 0.05$.

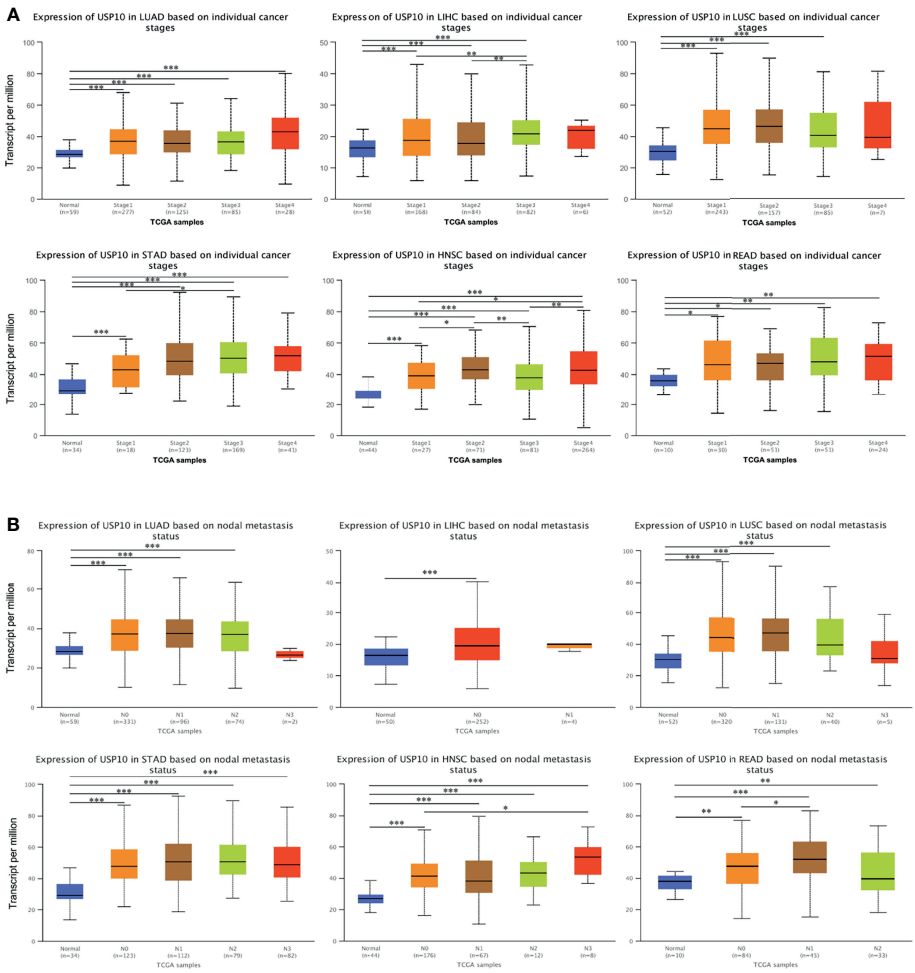

FIGURE 7 | UALCAN database analysis of correlation between clinicopathological parameters and *USP10* expression in multiple cancer types. **(A)** Association between *USP10* expression and tumor stages in patients with different types of cancer. **(B)** The association between *USP10* expression and nodal metastasis status in patients with different types of cancer. LUAD, lung adenocarcinoma; LIHC, liver hepatocellular carcinoma; LUSC, lung squamous cell carcinoma; STAD, stomach adenocarcinoma; HNSC, head and neck squamous cell carcinoma; READ, rectal adenocarcinoma. *$P < 0.05$; **$P < 0.01$; ***$P < 0.001$.

infiltration in 39 types of cancer was assessed using the TIMER database. (**Supplementary Figure 3**). Notably, in 14 cancers, the expression of *USP10* correlated significantly with B cell infiltration levels. Moreover, the expression of *USP10* correlated strongly with the infiltration level of dendritic cells in 10 cancers, with neutrophils in 24 cancers, with macrophages in 18 cancers, with CD4+ T cells in 13 cancers, and with CD8+ T cells in 15 cancers. Notably, *USP10* expression levels in ACC, CHOL, HNSC-HPV+, UCEC, and UCS were not significantly associated with the infiltration of B cells, CD4+ T cells, CD8+ T cells, macrophages, neutrophils, and dendritic cells (**Supplementary Figure 3**). Thus, USP10 might exert a fundamental function in the TME of cancers.

The correlation between the expression of *USP10* and immune cell infiltration in various cancers prompted us to identify those cancers in which prognosis and immune infiltration were associated with *USP10* expression. The effect of immunotherapy and immune cell infiltration can be better evaluated in cancers for which the tumor purity has been determined (32, 33). Therefore, we selected PAAD, LIHC, and LUAD cancers for validation. After determining the tumor purity, we found that for PAAD, high expression of *USP10* correlated significantly and positively with the infiltration levels of CD8+ T cells (r = 0.387, P = 1.67e-07), B cells (r = 0.355, P = 1.94e-06), macrophages (r = 0.318, P = 2.31e-05), neutrophils (r = 0.383, P = 2.32e-07), and dendritic cells (r = 0.417, P = 1.37e-08) (**Figure 8A**). Similarly, there were significant positive correlations with the infiltration levels of dendritic cells (r = 0.34, P = 8.68e-11), neutrophils (r = 0.267, P = 4.64e-07), macrophages (r = 0.273, P = 2.47e-07), CD4+ T cells (r = 0.118, P = 2.81e-02), CD8+ T cells (r = 0.188, P = 4.46e-04), and B cells (r = 0.264, P = 6.78e-07), in LIHC (**Figure 8B**). However, *USP10* expression correlated weakly with immune cell infiltration in LUAD, including only CD8+ T cells (r = 0.134,

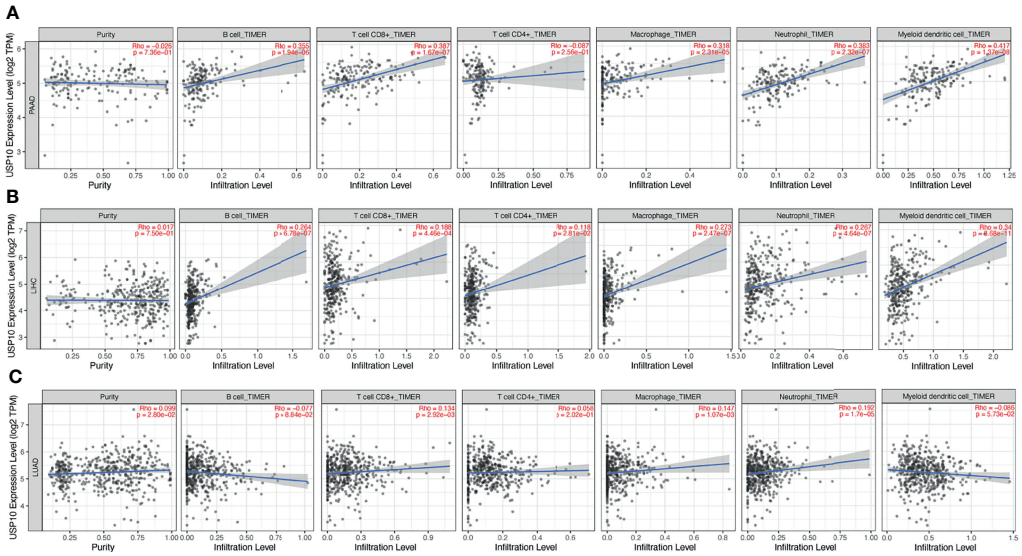

FIGURE 8 | TIMER database analysis of the correlation between *USP10* expression and immune infiltration level in LUAD, LIHC, and PAAD. **(A)** In PAAD, *USP10* expression was not related to tumor purity, but correlated significantly and positively with infiltration levels of dendritic cells, neutrophils, macrophages, CD8+ T cells, and B cells. **(B)** In LIHC, *USP10* expression was not related to tumor purity, but correlated significantly and positively with dendritic cells, neutrophils, macrophages, CD4+ T cells, CD8+ T cells, and B cells. **(C)** In LUAD, *USP10* expression correlated weakly with tumor purity and correlated significantly and positively with CD8+ T cells, macrophages, and neutrophils, but had no significant relationship with the immune infiltration of B cells, CD4+ T cells, and dendritic cells. PAAD, pancreatic adenocarcinoma; LIHC, liver hepatocellular carcinoma; LUAD, lung adenocarcinoma. Significance is indicated by a *P*-value < 0.05.

P = 2.92e-03), macrophages (r = 0.147, *P* = 1.07e-03), and neutrophils (r = 0.192, *P* = 1.7e-05) (**Figure 8C**). These findings suggested that USP10 might play an important part in immune cell infiltration in these cancers.

Assessment of Correlations Between Immune Cell Markers and *USP10* Expression

Next, we used the TIMER database to investigate potential correlations between USP10 and immune cell marker genes in PAAD, LIHC, and LUAD, such as CD8+ T cells, B cells, tumor-associated macrophages (TAMs), monocytes, M1/M2 macrophages, natural killer (NK) cells, DCs, neutrophils, general T cells, and T cell with different functions, e.g., T follicular helper (Tfh) cells, T helper type 1 (Th1) cells, T helper type 2 (Th2) cells, T helper type 17 (Th17) cells, regulatory T cells (Tregs), and exhausted T cells (**Table 1**). The results, which were adjusted for tumor purity, showed that in PAAD and LIHC, the expression level of *USP10* correlated significantly with most immune markers for the various immune cells. However, in LUAD, the expression level of *USP10* was only associated with 23 marker genes (**Table 1**).

Interestingly, USP10 expression correlated significantly with markers of Tregs (*CCR8* (encoding C-C motif chemokine receptor 8) and *STAT5B* (encoding signal transducer and activator of transcription 5B)) in LUAD, LIHC, and PAAD (**Table 1**). The expression of *USP10* was statistically significant for TAMs, monocytes, and M1/M2 macrophages in PAAD and LIHC, but not in LUAD (**Table 1**). Specifically, it was markedly correlated with marker genes of monocytes (*CD86*, *CSF1R* (encoding colony stimulating factor 1 receptor)), marker genes of TAMs (*CD68*, *IL10* (encoding interleukin-10)), marker genes of M1 macrophages (*NOS2* (encoding nitrous oxide synthase 2), *IRF5* (encoding interferon regulatory factor 5), and *PTGS2* (encoding prostaglandin-endoperoxide synthase 2)), marker genes of M2 macrophages (*CD163*, *VSIG4* (encoding V-set and immunoglobulin domain containing 4), and *MS4A4A* (encoding membrane spanning 4-domains A4A)) in PAAD and LIHC (**Figure 9**). Given the homologous data in GEPIA and TIMER from the TCGA, we used the GEPIA database to further assess the associations between the expression of *USP10* and markers genes of monocytes and TAMs in tumor tissues of PAAD, LIHC, and LUAD. Similar results to those obtained using TIMER were observed (**Table 2**). These results indicated that USP10 might participate in immune cell infiltration and regulate the polarization of macrophages in both PAAD and LIHC TMEs. The precise mechanism requires confirmation in further studies.

Analysis of Survival Related to *USP10* Expression Based on Immune Cell Infiltration

USP10 expression correlated significantly with poor prognosis and immune infiltration of patients with PAAD and LIHC; therefore, we investigated whether *USP10* expression could affect the prognosis of patients with PAAD and LIHC *via* immune infiltration (**Figure 10**). Based on *USP10* expression in relevant immune cell subsets, we found that in PAAD, high *USP10* expression was linked to increased infiltration of B cells

TABLE 1 | Analysis of correlations between *USP10* expression and immune cell markers by TIMER.

Description	Gene markers	PAAD				LIHC				LUAD			
		None		Purity		None		Purity		None		Purity	
		Cor	*P*	Cor	*P*	Cor	*P*	Cor	*P*	Cor	*P*	Cor	*P*
CD8+ T cells	CD8A	0.214	*	0.189	0.013	0.173	**	0.191	**	0.071	0.106	0.13	*
	CD8B	0.251	**	0.22	*	0.038	0.388	0.107	0.047	0.038	0.388	0.073	0.107
T cells (general)	CD3D	0.154	0.039	0.12	0.118	0.067	0.196	0.082	0.127	-0.082	0.062	-0.031	0.494
	CD3E	0.194	*	0.162	0.035	0.129	0.013	0.156	*	-0.005	0.910	0.063	0.161
	CD2	0.202	*	0.174	0.023	0.1	0.055	0.121	0.024	-0.028	0.520	0.038	0.398
B cells	CD19	0.146	0.051	0.115	0.134	0.143	*	0.128	0.018	-0.036	0.412	0.002	0.968
	CD79A	0.157	0.035	0.118	0.123	0.077	0.136	0.085	0.114	-0.052	0.236	-0.019	0.681
Monocytes	CD86	0.289	***	0.267	**	0.279	***	0.329	***	-0.055	0.213	0	0.991
	CD115 (CSF1R)	0.257	**	0.255	**	0.266	***	0.315	***	-0.003	0.938	0.051	0.255
TAMs	CCL2	0.016	0.832	-0.012	0.873	0.184	**	0.223	***	-0.02	0.656	0.019	0.675
	CD68	0.325	***	0.312	***	0.225	***	0.245	***	-0.015	0.741	0.037	0.416
	IL10	0.201	*	0.173	0.024	0.245	***	0.27	***	-0.037	0.408	0.014	0.765
M1 Macrophages	INOS (NOS2)	0.224	*	0.184	0.016	0.149	*	0.158	*	0.085	0.055	0.098	0.030
	IRF5	0.261	**	0.237	*	0.33	***	0.323	***	-0.042	0.346	-0.007	0.872
	COX2 (PTGS2)	0.337	***	0.33	***	0.285	***	0.353	***	0.089	0.044	0.081	0.072
M2 Macrophages	CD163	0.342	***	0.337	***	0.277	***	0.317	***	0.092	0.037	0.158	**
	VSIG4	0.26	**	0.261	**	0.218	***	0.259	***	-0.097	0.028	-0.053	0.239
	MS4A4A	0.255	**	0.239	*	0.24	***	0.284	***	-0.08	0.068	-0.026	0.564
Neutrophils	CD66b (CEACAM8)	0.149	0.046	0.124	0.106	0.034	0.514	0.046	0.398	-0.063	0.153	-0.052	0.251
	CD11b (ITGAM)	0.264	**	0.244	*	0.361	***	0.397	***	-0.053	0.230	-0.001	0.984
	CCR7	0.157	0.036	0.128	0.096	0.143	*	0.161	*	-0.012	0.785	0.047	0.295
Natural killer cells	KIR2DL1	0.021	0.779	0.023	0.763	0.091	0.080	0.073	0.177	0.031	0.486	0.047	0.298
	KIR2DL3	0.064	0.398	0.03	0.693	0.176	**	0.189	**	0.122	*	0.162	**
	KIR2DL4	0.215	*	0.115	0.019	0.189	**	0.198	**	0.111	0.012	0.141	*
	KIR3DL1	0.029	0.699	0.006	0.938	0.174	**	0.197	**	0.069	0.120	0.093	0.040
	KIR3DL2	0.226	*	0.198	*	0.063	0.230	0.077	0.154	0.121	*	0.166	**
	KIR3DL3	0.188	0.012	0.166	0.030	0.04	0.437	-0.016	0.774	0.081	0.067	0.095	0.035
	KIR2DS4	0.105	0.163	0.078	0.313	0.101	0.052	0.114	0.034	0.056	0.208	0.087	0.053
Dendritic cells	HLA-DPB1	0.159	0.034	0.126	0.101	0.211	***	0.238	***	-0.198	***	-0.17	**
	HLA-DQB1	0.212	*	0.192	0.012	0.126	0.015	0.147	*	-0.197	***	-0.167	**
	HLA-DRA	0.265	**	0.241	*	0.287	***	0.328	***	-0.205	***	-0.173	**
	HLA-DPA1	0.259	**	0.234	*	0.274	***	0.312	***	-0.139	*	-0.109	0.015
	BDCA-1 (CD1C)	0.137	0.068	0.116	0.132	0.124	0.017	0.142	*	-0.234	***	-0.208	***
	BDCA-4 (NRP1)	0.362	***	0.388	***	0.541	***	0.552	***	0.142	*	0.164	**
	CD11c (ITGAX)	0.15	0.045	0.104	0.177	0.312	***	0.355	***	-0.083	0.065	0.034	0.454
Th1 cells	T-bet (TBX21)	0.108	0.149	0.091	0.237	0.139	*	0.161	*	0.077	0.082	0.152	**
	STAT4	0.097	0.196	0.117	0.128	0.06	0.245	0.07	0.195	-0.073	0.096	-0.026	0.571
	STAT1	0.412	***	0.396	***	0.385	***	0.392	***	0.263	***	0.322	***
	IFN-γ (IFNG)	0.091	0.227	0.078	0.308	0.139	*	0.148	*	0.076	0.084	0.133	*
	TNF-α (TNF)	0.083	0.269	0.069	0.372	0.26	***	0.289	***	-0.001	0.987	0.058	0.200
Th2 cells	GATA3	0.213	*	0.2	*	0.221	***	0.267	***	0.088	0.046	0.15	**
	STAT6	0.436	***	0.417	***	0.429	***	0.404	***	0.137	*	0.147	*
	STAT5A	0.372	***	0.344	***	0.316	***	0.315	***	0.081	0.066	0.146	*
	IL13	-0.019	0.799	-0.025	0.749	0.039	0.451	0.016	0.771	-0.073	0.097	-0.035	0.440
Tfh cells	BCL6	0.458	***	0.444	***	0.432	***	0.427	***	0.155	**	0.156	**
	IL21	0.183	0.015	0.161	0.036	0.087	0.096	0.103	0.057	0.138	*	0.168	**
Th17 cells	STAT3	0.528	***	0.524	***	0.476	***	0.483	***	0.33	***	0.324	***
	IL17A	0.1	0.182	0.1	0.194	0.086	0.097	0.096	0.075	0.001	0.981	0.018	0.686
Tregs	FOXP3	0.235	*	0.213	*	0.257	***	0.278	***	0.019	0.671	0.08	0.075
	CCR8	0.348	***	0.324	***	0.409	***	0.438	***	0.09	0.041	0.153	**
	STAT5B	0.39	***	0.427	***	0.523	***	0.512	***	0.321	***	0.331	***
	TGFβ (TGFB1)	0.129	0.086	0.095	0.216	0.294	***	0.334	***	0.01	0.818	0.048	0.287
Exhausted T cells	PD-1 (PDCD1)	0.18	0.016	0.144	0.060	0.129	0.013	0.13	0.016	0.047	0.286	0.103	0.022
	CTLA4	0.178	0.017	0.145	0.058	0.136	*	0.154	*	-0.009	0.845	0.063	0.163
	LAG3	0.122	0.102	0.114	0.138	0.079	0.128	0.086	0.109	0.108	0.015	0.156	**
	TIM-3 (HAVCR2)	0.247	**	0.226	*	0.287	***	0.342	***	-0.093	0.034	-0.04	0.379
	GZMB	0.196	*	0.156	0.042	0.084	0.105	0.078	0.146	0.089	0.042	0.147	*

*PAAD, pancreatic adenocarcinoma; LIHC, liver hepatocellular carcinoma; LUAD, lung adenocarcinoma. TAM, tumor-associated macrophage; Treg, regulatory T cell; Tfh, follicular helper T cell; Th, T helper cell. Purity, adjusted correlation according to tumor purity; None, non-adjusted correlation. Cor, R value of Spearman's correlation. *P < 0.01; **P < 0.001; ***P < 0.0001.*

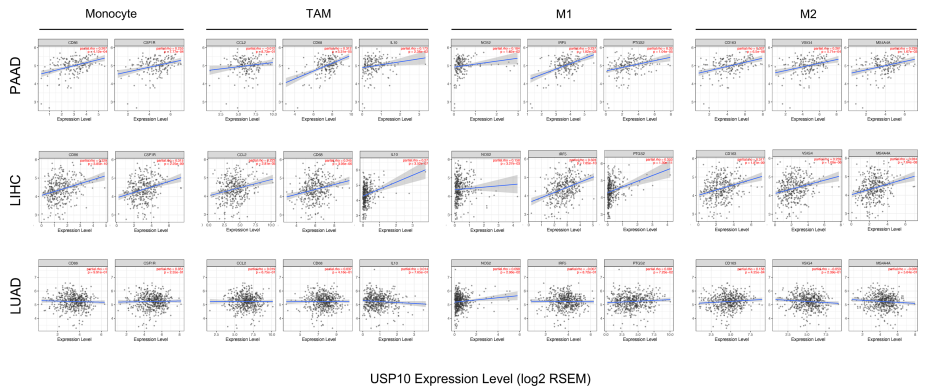

FIGURE 9 | The correlation between the expression of *USP10* and marker genes for M2 macrophages, M1 macrophages, TAMs, and monocytes in LUAD, LIHC, and PAAD, as shown by scatter plots. The monocyte markers were *CSF1R* and *CD86*; the markers for TAMs were *CCL2*, *CD68*, and *IL10*; the markers for M1 macrophages were *PTGS2*, *IRF5*, and *NOS2*; and the markers for M2 macrophages were *MS4A4A*, *VSIG4*, and *CD163*. PAAD, pancreatic adenocarcinoma; LIHC, liver hepatocellular carcinoma; LUAD, lung adenocarcinoma. TAMs, tumor-associated macrophages. Significance is indicated by a *P*-value < 0.05.

(OS, HR = 2.22, *P* = 0.027), NK cells (OS, HR = 2.12, *P* = 0.049), Tregs (OS, HR = 2.14, *P* = 0.021), and Th2 cells (OS, HR = 2.12, *P* = 0.042); and with decreased infiltration of CD4+ T cells, macrophages, and Th1 cells (all *P* < 0.05), and predicted inferior prognostic survival in patients with PAAD (**Figure 10A** and **Supplementary Figure 4A**). In LIHC, overexpression of *USP10* and abundant infiltration of B cells (OS, HR = 4.89, *P* = 0.0061) and Treg cells (OS, HR = 1.63, *P* = 0.038) or reduced infiltration of Th1 cells (OS, HR = 2.22, *P* = 0.019) predicted a worse prognosis (**Figure 10B** and **Supplementary Figure 4B**).

Interestingly, *USP10* expression with increased (OS, HR = 2.41, *P* = 0.027) or decreased (OS, HR = 2, *P* = 0.012) CD8+ T cell infiltration had a marked impact on the survival of patients with PAAD and predicted a worse survival outcome (**Figure 10A** and **Supplementary Figure 4A**). In addition, *USP10* expression in LIHC correlated statistically with enriched infiltration of macrophages (OS, HR = 1.76, *P* = 0.021), indicating a worse prognosis. In contrast, *USP10* expression was associated with reduced infiltration of macrophages (OS, HR = 0.54, *P* = 0.021), predicting a better survival outcome (**Figure 10B** and **Supplementary Figure 4B**). These results further demonstrated that USP10 might regulate macrophage polarization in the TME of LIHC and have an important impact on prognosis. Critically, the potential explanation for how USP10 influences the prognosis of patients with PAAD and LIHC might stem in part from immune infiltration.

DISCUSSION

USP10 specifically cleaves ubiquitin from ubiquitin-conjugated protein substrates and thus affects cellular processes. Although the aberrant expression of USP10 has been reported in many cancers (10–12, 14, 34, 35), and the role of USP10 in tumorigenesis and prognosis has been partially confirmed in several cancers (10–14), a systematic bioinformatic analysis is

TABLE 2 | Analysis of the correlations between *USP10* expression and genetic markers of monocytes and macrophages using GEPIA data.

Description	Gene markers	PAAD				LIHC				LUAD			
		Tumor		Normal		Tumor		Normal		Tumor		Normal	
		R	*P*	R	*P*	R	*P*	R	*P*	R	*P*	R	*P*
Monocytes	CD86	0.340	***	-0.700	0.300	0.320	***	0.380	*	-0.033	0.470	-0.130	0.35
	CD115 (CSF1R)	0.320	***	0.230	0.770	0.280	***	0.410	*	0.034	0.450	0.220	0.091
TAMs	CCL2	0.130	0.079	-0.180	0.820	0.210	***	0.170	0.220	0.005	0.910	0.097	0.46
	CD68	0.400	***	-0.940	0.058	0.230	***	0.430	*	0.064	0.160	0.017	0.9
	IL10	0.180	0.015	-0.910	0.093	0.260	***	0.130	0.350	-0.042	0.360	-0.074	0.58
M1 Macrophages	INOS (NOS2)	0.130	0.080	0.360	*	0.015	0.770	0.110	0.460	0.068	0.140	0.290	0.026
	IRF5	0.320	***	-0.470	**	0.320	***	0.240	0.088	0.009	0.840	0.058	0.66
	COX2 (PTGS2)	0.110	0.140	-0.850	0.150	0.170	*	0.120	0.400	0.097	0.034	0.350	*
M2 Macrophages	CD163	0.310	***	0.037	0.960	0.190	**	0.330	0.018	0.027	0.550	-0.029	0.83
	VSIG4	0.290	***	-0.980	0.017	0.210	***	0.350	0.013	-0.066	0.150	-0.200	0.13
	MS4A4A	0.280	**	-0.950	0.055	0.220	***	0.370	*	-0.054	0.240	-0.200	0.14

*PAAD, pancreatic adenocarcinoma; LIHC, liver hepatocellular carcinoma; LUAD, lung adenocarcinoma. TAM, tumor-associated macrophage. Tumor, association analysis in tumor tissues from TCGA; Normal, association analysis in normal tissues from TCGA. *P < 0.01; **P < 0.001; ***P < 0.0001.*

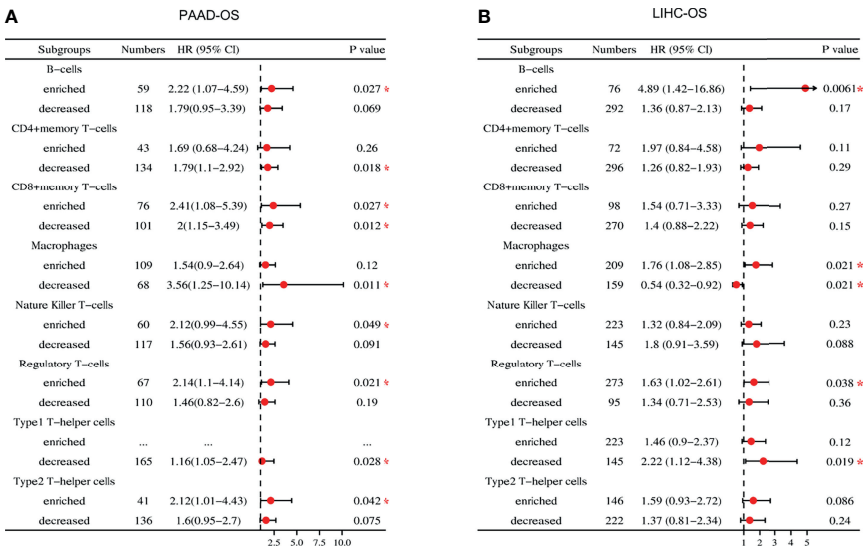

FIGURE 10 | Forest plot of the prognostic value of the expression of *USP10* in immune cell subpopulations of patients with PAAD and LIHC. **(A)** In patients with PAAD, the prognostic benefit of *USP10* expression depends on the patients' different immune cell subsets, according to the forest plot. **(B)** In patients with LIHC, there was an association between the expression of *USP10* and OS for the infiltration of different immune cell subgroups, according to a forest plot. PAAD, pancreatic adenocarcinoma; LIHC, liver hepatocellular carcinoma. OS, overall survival. *$P < 0.05$.

still lacking. Based on bioinformatics, this study investigated USP10 expression in pan-cancer and its correlation with prognosis and analyzed the importance of USP10 in the development of different cancers. Moreover, the association between *USP10* gene expression in the TME and immune cell infiltration was determined. Our findings provide useful insights to further explore the role of USP10 in tumorigenesis and progression *via* mechanistic studies.

In this study, we analyzed the differential expression of *USP10* and its prognostic value in different types of cancer. The results showed that *USP10* mRNA was highly expressed in most tumor types, except for bladder cancer (BLCA), brain and central nervous system cancer, OV, sarcoma (SARC), acute myeloid leukemia (AML), and THYM. The results of the current study suggest that USP10 acts as a therapeutic target for PRAD and AML (36, 37). In addition, IF analysis of 12 clinical samples and the IHC images available through an online database confirmed this trend at the protein level. The results for liver, breast, lung, and colon cancers were similar to those in previous research (11–13, 34). Takayama et al. (10) showed that high expression of USP10 is related significantly to poor prognosis in patients with prostate cancer, which is consistent with our experimental validation. However, Wang et al. (38) showed reduced expression of USP10 in human LUAD tissues, which contradicts the results of the present study, possibly because most of the samples analyzed in Wang's study were derived from metastatic tumor tissues rather than *in situ* tumors. Furthermore, we found that *USP10* was overexpressed in gastric cancer, which is inconsistent with Zang et al.'s (7) findings and might be caused by the different subtypes of cancer and sample differences. Therefore, the sample size needs to be further expanded. Another exciting finding of this study was that the USP10 protein level was significantly lower in ovarian tumor tissues than in adjacent tissues. Furthermore, survival analysis found that low USP10 expression predicted poor prognosis in patients with ovarian cancer. A previous study by Han et al. (15) agreed with our findings and showed that differential *USP10* expression correlated with promoter hypermethylation. Whether USP10 has utility as an independent biomarker of prognosis in OV requires further biological experiments.

Kaplan–Meier survival analysis using the TCGA database demonstrated that in most cancer types (PAAD, LIHC, LUAD, and BRCA), high *USP10* expression was associated with poor prognosis. Similarly, as previously reported, *USP10* overexpression was shown to be associated with a shorter patient survival time (11, 12).. Moreover, *USP10* mutations are closely associated with the development of cancers. We postulated that *USP10* expression might be linked to the TMB in various cancers to influence patient survival and is a useful immunotherapy biomarker for checkpoint blockade selection in many types of cancer (39, 40). Analysis revealed that *USP10* expression was obviously associated with a high TMB in STAD, LUAD, and UCEC, which influenced patient OS. Previous studies have shown that the TMB predicted prognosis in patients with non-small-cell lung and colorectal cancers (41, 42). Further studies showed that high *USP10* expression correlated closely with the stage of cancer and the presence of lymph node metastasis in patients suffering from various types of cancer. These findings suggested that USP10 might serve as a predictable biomarker to determine the prognosis of different cancers. However, more in-depth molecular experimental evidence is needed to verify this.

Importantly, we found that in different types of cancer, *USP10* expression was associated with immune cell infiltration levels and has a critical function in cancer immunity, particularly in PAAD and LIHC. Thus, the results of the present study revealed the possible use of USP10 as a cancer biomarker and its function in tumor immunology. We revealed that the infiltration of dendritic cells, neutrophils, macrophages, CD4+ T cells, CD8+ T cells, and B cells in PAAD and LIHC are associated significantly with *USP10* expression; whereas, there was only a weak correlation between immune cell infiltration and *USP10* expression in LUAD. Interestingly, the association between the expression of *USP10* and the expression levels of marker genes of immune cells (e.g., *CD19*, *CD79A*, *CCL2*, *CD66b*, *HLA-DQB1*, *CD1C*, and *ITGAX*) was not always consistent with the overall trend, suggesting that specific interactions exist between USP10 and certain subtypes of immune cells. Furthermore, the close association between *USP10* expression and immune cell marker gene expression suggested that USP10 might function in PAAD and LIHC tumor immune regulation. DCs and macrophages, which are important antigen-presenting cells (APCs), were most related to the expression of *USP10* in LIHC. Tumor metastasis is promoted by DCs *via* their effects on Treg levels and the reduction in the CD8+ T cell response (43). However, in PAAD, DCs correlated weakly with USP10. These differences suggested heterogeneity between cancers that recruit APCs to the TME. A recent study showed that USP10 promotes tumor progression and TAM polarization in colorectal cancer (18). Therefore, our results revealed that USP10 might regulate TAM polarization.

In addition, Tregs are the most important cell type in the TME. Tregs are believed to suppress the excessive immune response by expressing cytotoxic T-lymphocyte associated protein 4 (CTLA4) and secreting IL-10 and transforming growth factor beta (TGFβ), thereby promoting the immune escape of tumor cells (44, 45). TGFβ signaling can be activated by USP10 depletion (46). Recently, researchers have found that depletion of Tregs does not prevent their suppressive activity. Moreover, the therapeutic effect of programmed cell death-1 (PD-1) and PD-1 ligand-1 (PD-L1) signaling blockade therapy on patients with tumors is still not as beneficial as expected. However, Maj et al. (47) showed that in the TME, Tregs are highly apoptotic and can greatly reduce the efficacy of PD-L1 anti-tumor immunotherapy. We further found a significant positive correlation between USP10 and genetic markers of Tregs (*CCR8* (encoding C-C motif chemokine receptor 8) and *STAT5B* (encoding signal transducer and activator of transcription 5B)) (**Table 1**), suggesting that USP10 could be involved in activating the immunosuppressive activity of Tregs in PAAD and LIHC. Moreover, in PAAD and LIHC, USP10 levels correlated significantly with several T helper cell markers (*STAT1*, *STAT6*, *STAT5A*, and *STAT3*) (**Table 1**). Studies have shown that STAT signaling is involved in numerous aspects of immune regulation, including immune escape and shaping the epigenetic structure of immune cells (48, 49). These findings suggest that USP10 might be closely related to STAT signaling to regulate tumor immune responses. Importantly, the prognosis of PAAD and LIHC was influenced by USP10 through immune cell infiltration. Taken together, USP10 is closely associated with immune cell activity in the TME and might affect patient prognosis through immune infiltration. These findings suggested that USP10 is an immune-related therapeutic target. Nevertheless, USP10's exact role in tumor immunity requires further exploration.

In conclusion, we determined the universal applicability of USP10 in pan-cancer and found that high expression of USP10 is usually associated with poor clinical prognosis. Furthermore, USP10 is intimately linked to immune cell infiltration in certain cancers and might affect the overall survival of patients with PAAD and LIHC *via* immune infiltration. These results will enhance our understanding USP10's vital function in tumorigenesis and serve as a useful basis for future studies.

DATA AVAILABILITY STATEMENT

The datasets presented in this study can be found in online repositories. The names of the repository/repositories and accession number(s) can be found in the article/**Supplementary Material**.

ETHICS STATEMENT

The studies involving human participants were reviewed and approved by The Ethics Committee of Shanghai East Hospital Affiliated to Tongji University. Written informed consent for participation was not required for this study in accordance with the national legislation and the institutional requirements.

AUTHOR CONTRIBUTIONS

DG designed this study. DG, ZZ, RX, ZH, FL, YH, HC, JL, and XC collected the data and performed the bioinformatic analyses and visualization. DG, YH, and HC performed the hematoxylin and eosin staining and immunofluorescence staining experiments. YL and ZX provided study supervision and reviewed the manuscript. All authors contributed to the article and approved the submitted version.

FUNDING

This work was supported by a grant from the National Natural Science Foundation of China [grant number 81972183].

SUPPLEMENTARY MATERIAL

The Supplementary Material for this article can be found online at: https://www.frontiersin.org/articles/10.3389/fonc.2022.829705/full#supplementary-material

Supplementary Figure 1 | The protein level of USP10 in different types of cancer. Representative images of H&E stained normal and tumor slides (left 1st). Immunofluorescence staining analysis (left 2nd to 4th) showing an evident

fluorescence signal in the tumor tissue sections compared with that in the control group. All scale bars = 50 μm. H&E, hematoxylin-eosin staining. N, normal tissues; T, tumor tissues.

Supplementary Figure 2 | Protein expression of USP10 in cancers versus normal tissues as assessed in the HPA database. Compared to normal tissues, USP10 was significantly overexpressed in breast cancer, liver cancer, lung cancer, skin cancer, colon cancer, kidney cancer, and prostate cancer tissues. However, in ovarian cancer, there was a significant low expression of USP10 in tumor tissues compared with that in normal tissues. N, normal tissues; T, tumor tissues.

Supplementary Figure 3 | TIMER database analysis of the correlation between *USP10* expression and immune cell infiltration levels in different cancer types. *USP10* expression levels in PAAD, LIHC, PCPG, PRAD, THCA, KIRC, and BLCA generally correlated positively with immune cell infiltration. However, in ACC, CHOL, HNSC-HPV+, UCEC, and UCS, *USP10* expression levels were not significantly correlated with infiltration of B cells, CD4+ T cells, CD8+ T cells, macrophages, neutrophils, and dendritic cells. Red box, positive Spearman's correlation; blue box, negative Spearman's correlation; gray box, no significant correlation. Significance is indicated by a *P*-value < 0.05.

Supplementary Figure 4 | Analysis of the prognostic value of *USP10* expression in immune cell subsets in patients with PAAD and LIHC using Kaplan–Meier Plotter. **(A)** In PAAD, high *USP10* expression was linked to increased infiltration of B cells, NK cells, Tregs, and Th2 cells (all $P < 0.05$); and with decreased infiltration of CD4+ T cells, macrophages, and Th1 cells (all $P < 0.05$), and predicted inferior prognostic survival in patients with PAAD. However, *USP10* expression with increased (OS, HR = 2.41, $P = 0.027$) or decreased (OS, HR = 2, $P = 0.012$) CD8+ T cell infiltration had a marked impact on the survival of patients with PAAD and predicted a worse survival outcome. **(B)** In LIHC, overexpression of *USP10* and abundant infiltration of B cells and Treg cells (all $P < 0.05$) or reduced infiltration of Th1 cells ($P < 0.05$) predicted a worse prognosis. Interestingly, *USP10* expression in LIHC correlated statistically with enriched infiltration of macrophages (OS, HR = 1.76, $P = 0.021$), indicating a worse prognosis. In contrast, *USP10* expression was associated with reduced infiltration of macrophages (OS, HR = 0.54, $P = 0.021$), predicting a better survival outcome. PAAD, pancreatic adenocarcinoma; LIHC, liver hepatocellular carcinoma. OS, overall survival. HR, hazard ratio. Significance is indicated by a *P*-value < 0.05.

REFERENCES

1. Bray F, Ferlay J, Soerjomataram I, Siegel RL, Torre LA, Jemal A. Global Cancer Statistics 2018: GLOBOCAN Estimates of Incidence and Mortality Worldwide for 36 Cancers in 185 Countries. *CA Cancer J Clin* (2018) 68 (6):394–424. doi: 10.3322/caac.21492
2. Hagner PR, Schneider A, Gartenhaus RB. Targeting the Translational Machinery as a Novel Treatment Strategy for Hematologic Malignancies. *Blood* (2010) 115(11):2127–35. doi: 10.1182/blood-2009-09-220020
3. Zhang Y, Zhang Z. The History and Advances in Cancer Immunotherapy: Understanding the Characteristics of Tumor-Infiltrating Immune Cells and Their Therapeutic Implications. *Cell Mol Immunol* (2020) 17(8):807–21. doi: 10.1038/s41423-020-0488-6
4. Amerik AY, Hochstrasser M. Mechanism and Function of Deubiquitinating Enzymes. *Biochim Biophys Acta* (2004) 1695(1-3):189–207. doi: 10.1016/j.bbamcr.2004.10.003
5. Grabbe C, Husnjak K, Dikic I. The Spatial and Temporal Organization of Ubiquitin Networks. *Nat Rev Mol Cell Biol* (2011) 12(5):295–307. doi: 10.1038/nrm3099
6. Popovic D, Vucic D, Dikic I. Ubiquitination in Disease Pathogenesis and Treatment. *Nat Med* (2014) 20(11):1242–53. doi: 10.1038/nm.3739
7. Zeng Z, Wu HX, Zhan N, Huang YB, Wang ZS, Yang GF, et al. Prognostic Significance of USP10 as a Tumor-Associated Marker in Gastric Carcinoma. *Tumour Biol* (2014) 35(4):3845–53. doi: 10.1007/s13277-013-1509-1
8. Soncini C, Berdo I, Draetta G. Ras-GAP SH3 Domain Binding Protein (G3BP) Is a Modulator of USP10, a Novel Human Ubiquitin Specific Protease. *Oncogene* (2001) 20(29):3869–79. doi: 10.1038/sj.onc.1204553
9. Yuan J, Luo K, Zhang L, Cheville JC, Lou Z. USP10 Regulates P53 Localization and Stability by Deubiquitinating P53. *Cell* (2010) 140(3):384–96. doi: 10.1016/j.cell.2009.12.032
10. Takayama KI, Suzuki T, Fujimura T, Takahashi S, Inoue S. Association of USP10 With G3BP2 Inhibits P53 Signaling and Contributes to Poor Outcome in Prostate Cancer. *Mol Cancer Res* (2018) 16(5):846–56. doi: 10.1158/1541-7786.Mcr-17-0471
11. Deng S, Zhou H, Xiong R, Lu Y, Yan D, Xing T, et al. Over-Expression of Genes and Proteins of Ubiquitin Specific Peptidases (USPs) and Proteasome Subunits (PSs) in Breast Cancer Tissue Observed by the Methods of RFDD-PCR and Proteomics. *Breast Cancer Res Treat* (2007) 104(1):21–30. doi: 10.1007/s10549-006-9393-7
12. Hou J, Aerts J, den Hamer B, van Ijcken W, den Bakker M, Riegman P, et al. Gene Expression-Based Classification of Non-Small Cell Lung Carcinomas and Survival Prediction. *PloS One* (2010) 5(4):e10312. doi: 10.1371/journal.pone.0010312
13. Smith JJ, Deane NG, Wu F, Merchant NB, Zhang B, Jiang A, et al. Experimentally Derived Metastasis Gene Expression Profile Predicts Recurrence and Death in Patients With Colon Cancer. *Gastroenterology* (2010) 138(3):958–68. doi: 10.1053/j.gastro.2009.11.005
14. Guo J, Zhang J, Liang L, Liu N, Qi M, Zhao S, et al. Potent USP10/13 Antagonist Spautin-1 Suppresses Melanoma Growth *via* ROS-Mediated DNA Damage and Exhibits Synergy With Cisplatin. *J Cell Mol Med* (2020) 24 (7):4324–40. doi: 10.1111/jcmm.15093
15. Han GH, Chay DB, Yi JM, Cho H, Chung JY, Kim JH. Loss of Both USP10 and P14arf Protein Expression Is an Independent Prognostic Biomarker for Poor Prognosis in Patients With Epithelial Ovarian Cancer. *Cancer Genomics Proteomics* (2019) 16(6):553–62. doi: 10.21873/cgp.20157
16. Lin Z, Yang H, Tan C, Li J, Liu Z, Quan Q, et al. USP10 Antagonizes C-Myc Transcriptional Activation Through SIRT6 Stabilization to Suppress Tumor Formation. *Cell Rep* (2013) 5(6):1639–49. doi: 10.1016/j.celrep.2013.11.029
17. Hu C, Zhang M, Moses N, Hu C-l, Polin L, Chen W, et al. The USP10-HDAC6 Axis Confers Cisplatin Resistance in Non-Small Cell Lung Cancer Lacking Wild-Type P53. *Cell Death Dis* (2020) 11(5):328. doi: 10.1038/s41419-020-2519-8
18. Li B, Qi ZP, He DL, Chen ZH, Liu JY, Wong MW, et al. NLRP7 Deubiquitination by USP10 Promotes Tumor Progression and Tumor-Associated Macrophage Polarization in Colorectal Cancer. *J Exp Clin Cancer Res* (2021) 40(1):126. doi: 10.1186/s13046-021-01920-y
19. Boumil EF, Castro N, Phillips AT, Chatterton JE, McCauley SM, Wolfson AD, et al. USP10 Targeted Self-Deliverable siRNA to Prevent Scarring in the Cornea. *Mol Ther Nucleic Acids* (2020) 21:1029–43. doi: 10.1016/j.omtn.2020.07.032
20. Takahashi M, Higuchi M, Makokha GN, Matsuki H, Yoshita M, Tanaka Y, et al. HTLV-1 Tax Oncoprotein Stimulates ROS Production and Apoptosis in T Cells by Interacting With USP10. *Blood* (2013) 122(5):715–25. doi: 10.1182/blood-2013-03-493718
21. Rhodes DR, Kalyana-Sundaram S, Mahavisno V, Varambally R, Yu J, Briggs BB, et al. Oncomine 3.0: Genes, Pathways, and Networks in a Collection of 18,000 Cancer Gene Expression Profiles. *Neoplasia* (2007) 9(2):166–80. doi: 10.1593/neo.07112
22. Li T, Fu J, Zeng Z, Cohen D, Li J, Chen Q, et al. TIMER2.0 for Analysis of Tumor-Infiltrating Immune Cells. *Nucleic Acids Res* (2020) 48(W1):W509–w514. doi: 10.1093/nar/gkaa407
23. Tang Z, Li C, Kang B, Gao G, Li C, Zhang Z. GEPIA: A Web Server for Cancer and Normal Gene Expression Profiling and Interactive Analyses. *Nucleic Acids Res* (2017) 45(W1):W98–w102. doi: 10.1093/nar/gkx247
24. Mizuno H, Kitada K, Nakai K, Sarai A. PrognoScan: A New Database for Meta-Analysis of the Prognostic Value of Genes. *BMC Med Genomics* (2009) 2:18. doi: 10.1186/1755-8794-2-18
25. Nagy Á, Munkácsy G, Győrffy B. Pancancer Survival Analysis of Cancer Hallmark Genes. *Sci Rep* (2021) 11(1):6047. doi: 10.1038/s41598-021-84787-5
26. Cerami E, Gao J, Dogrusoz U, Gross BE, Sumer SO, Aksoy BA, et al. The Cbio Cancer Genomics Portal: An Open Platform for Exploring Multidimensional Cancer Genomics Data. *Cancer Discov* (2012) 2(5):401–4. doi: 10.1158/2159-8290.Cd-12-0095

27. Chandrashekar DS, Bashel B, Balasubramanya SAH, Creighton CJ, Ponce-Rodriguez I, Chakravarthi B, et al. UALCAN: A Portal for Facilitating Tumor Subgroup Gene Expression and Survival Analyses. *Neoplasia* (2017) 19 (8):649–58. doi: 10.1016/j.neo.2017.05.002
28. Ohtani H. Focus on TILs: Prognostic Significance of Tumor Infiltrating Lymphocytes in Human Colorectal Cancer. *Cancer Immun* (2007) 7:4.
29. Ravelli A, Roviello G, Cretella D, Cavazzoni A, Biondi A, Cappelletti MR, et al. Tumor-Infiltrating Lymphocytes and Breast Cancer: Beyond the Prognostic and Predictive Utility. *Tumour Biol* (2017) 39(4):1010428317695023. doi: 10.1177/1010428317695023
30. Yusuf M, Gaskins J, Mandish S, May ME, Wall W, Fisher W, et al. Tumor Infiltrating Lymphocyte Grade in Merkel Cell Carcinoma: Relationships With Clinical Factors and Independent Prognostic Value. *Acta Oncol* (2020) 59 (12):1409–15. doi: 10.1080/0284186x.2020.1794033
31. Azimi F, Scolyer RA, Rumcheva P, Moncrieff M, Murali R, McCarthy SW, et al. Tumor-Infiltrating Lymphocyte Grade is an Independent Predictor of Sentinel Lymph Node Status and Survival in Patients With Cutaneous Melanoma. *J Clin Oncol* (2012) 30(21):2678–83. doi: 10.1200/jco.2011.37.8539
32. Yoshihara K, Shahmoradgoli M, Martínez E, Vegesna R, Kim H, Torres-Garcia W, et al. Inferring Tumour Purity and Stromal and Immune Cell Admixture From Expression Data. *Nat Commun* (2013) 4:2612. doi: 10.1038/ncomms3612
33. Aran D, Sirota M, Butte AJ. Systematic Pan-Cancer Analysis of Tumour Purity. *Nat Commun* (2015) 6:8971. doi: 10.1038/ncomms9971
34. Zhu H, Yan F, Yuan T, Qian M, Zhou T, Dai X, et al. USP10 Promotes Proliferation of Hepatocellular Carcinoma by Deubiquitinating and Stabilizing YAP/TAZ. *Cancer Res* (2020) 80(11):2204–16. doi: 10.1158/0008-5472.Can-19-2388
35. Kim K, Huh T, Park Y, Koo DH, Kim H, Hwang I, et al. Prognostic Significance of USP10 and P14arf Expression in Patients With Colorectal Cancer. *Pathol Res Pract* (2020) 216(6):152988. doi: 10.1016/j.prp.2020.152988
36. Liao Y, Guo Z, Xia X, Liu Y, Huang C, Jiang L, et al. Inhibition of EGFR Signaling With Spautin-1 Represents a Novel Therapeutics for Prostate Cancer. *J Exp Clin Cancer Res* (2019) 38(1):157. doi: 10.1186/s13046-019-1165-4
37. Weisberg EL, Schauer NJ, Yang J, Lamberto I, Doherty L, Bhatt S, et al. Inhibition of USP10 Induces Degradation of Oncogenic FLT3. *Nat Chem Biol* (2017) 13(12):1207–15. doi: 10.1038/nchembio.2486
38. Wang X, Xia S, Li H, Wang X, Li C, Chao Y, et al. The Deubiquitinase USP10 Regulates KLF4 Stability and Suppresses Lung Tumorigenesis. *Cell Death Differ* (2020) 27(6):1747–64. doi: 10.1038/s41418-019-0458-7
39. Chan TA, Yarchoan M, Jaffee E, Swanton C, Quezada SA, Stenzinger A, et al. Development of Tumor Mutation Burden as an Immunotherapy Biomarker: Utility for the Oncology Clinic. *Ann Oncol* (2019) 30(1):44–56. doi: 10.1093/annonc/mdy495
40. Fumet JD, Truntzer C, Yarchoan M, Ghiringhelli F. Tumour Mutational Burden as a Biomarker for Immunotherapy: Current Data and Emerging Concepts. *Eur J Cancer* (2020) 131:40–50. doi: 10.1016/j.ejca.2020.02.038
41. Lee DW, Han SW, Bae JM, Jang H, Han H, Kim H, et al. Tumor Mutation Burden and Prognosis in Patients With Colorectal Cancer Treated With Adjuvant Fluoropyrimidine and Oxaliplatin. *Clin Cancer Res* (2019) 25 (20):6141–7. doi: 10.1158/1078-0432.Ccr-19-1105
42. Devarakonda S, Rotolo F, Tsao MS, Lanc I, Brambilla E, Masood A, et al. Tumor Mutation Burden as a Biomarker in Resected Non-Small-Cell Lung Cancer. *J Clin Oncol* (2018) 36(30):2995–3006. doi: 10.1200/jco.2018.78.1963
43. Sawant A, Hensel JA, Chanda D, Harris BA, Siegal GP, Maheshwari A, et al. Depletion of Plasmacytoid Dendritic Cells Inhibits Tumor Growth and Prevents Bone Metastasis of Breast Cancer Cells. *J Immunol* (2012) 189 (9):4258–65. doi: 10.4049/jimmunol.1101855
44. Izcue A, Coombes JL, Powrie F. Regulatory T Cells Suppress Systemic and Mucosal Immune Activation to Control Intestinal Inflammation. *Immunol Rev* (2006) 212:256–71. doi: 10.1111/j.0105-2896.2006.00423.x
45. Boonpiyathad T, Satitsuksanoa P, Akdis M, Akdis CA. Il-10 Producing T and B Cells in Allergy. *Semin Immunol* (2019) 44:101326. doi: 10.1016/j.smim.2019.101326
46. Gillespie SR, Tedesco LJ, Wang L, Bernstein AM. The Deubiquitylase USP10 Regulates Integrin β1 and β5 and Fibrotic Wound Healing. *J Cell Sci* (2017) 130(20):3481–95. doi: 10.1242/jcs.204628
47. Maj T, Wang W, Crespo J, Zhang H, Wang W, Wei S, et al. Oxidative Stress Controls Regulatory T Cell Apoptosis and Suppressor Activity and PD-L1-Blockade Resistance in Tumor. *Nat Immunol* (2017) 18(12):1332–41. doi: 10.1038/ni.3868
48. Owen KL, Brockwell NK, Parker BS. JAK-STAT Signaling: A Double-Edged Sword of Immune Regulation and Cancer Progression. *Cancers (Basel)* (2019) 11(12):2002. doi: 10.3390/cancers11122002
49. Verhoeven Y, Tilborghs S, Jacobs J, De Waele J, Quatannens D, Deben C, et al. The Potential and Controversy of Targeting STAT Family Members in Cancer. *Semin Cancer Biol* (2020) 60:41–56. doi: 10.1016/j.semcancer.2019.10.002

Conflict of Interest: The authors declare that the research was conducted in the absence of any commercial or financial relationships that could be construed as a potential conflict of interest.

Publisher's Note: All claims expressed in this article are solely those of the authors and do not necessarily represent those of their affiliated organizations, or those of the publisher, the editors and the reviewers. Any product that may be evaluated in this article, or claim that may be made by its manufacturer, is not guaranteed or endorsed by the publisher.

frontiers | Frontiers in Oncology

ORIGINAL RESEARCH
published: 02 May 2022
doi: 10.3389/fonc.2022.875097

ACYP1 Is a Pancancer Prognostic Indicator and Affects the Immune Microenvironment in LIHC

Lingyi Zhou[1†], Zheng Fu[1,2†], Shuai Wang[3†], Jing Jia[1,2], Yumeng Cheng[4], Yunxiang Zheng[4], Ningning Zhang[3], Wei Lu[3*] and Zhi Yao[1,5*]*

[1] Department of Immunology, Key Laboratory of Immune Microenvironment and Disease of the Educational Ministry of China, Tianjin Key Laboratory of Cellular and Molecular Immunology, School of Basic Medical Sciences, Tianjin Medical University, Tianjin, China, [2] Innovation and R&D Management Department, Tianjin Kangzhe Pharmaceutical Technology Development Company, Ltd., Tianjin, China, [3] Department of Hepatobiliary Oncology, Liver Cancer Center, Tianjin Medical University Cancer Institute and Hospital, National Clinical Research Center for Cancer, Key Laboratory of Cancer Prevention and Therapy, Tianjin Medical University, Tianjin, China, [4] Department of Clinical Pharmacy, Tianjin Medical University, Tianjin, China, [5] 2011 Collaborative Innovation Center of Tianjin for Medical Epigenetics, Tianjin Medical University, Tianjin, China

Background: ACYP1 plays important physiological and metabolic roles in glycolysis and membrane ion pump activity by catalyzing acyl phosphate hydrolysis. ACYP1 is related to tumorigenesis and progression and poor prognosis in gastrointestinal cancer. However, its pancancer roles and mechanisms are unclear. Our study aimed to understand the ACYP1 expression signature and prognostic value across cancers and investigate immune infiltration patterns in liver hepatocellular carcinoma (LIHC) and verify them in LIHC samples.

Methods: Transcriptional expression profiles of ACYP1 across cancers were analyzed using Oncomine and TIMER. The prognostic value of ACYP1 was assessed across PrognoScan, Kaplan—Meier Plotter, and GEPIA. Significant pathways associated with ACYP1 in LIHC were obtained *via* Gene Set Enrichment Analysis. The correlation between ACYP1 expression and immune infiltration in LIHC was investigated using TIMER. We validated ACYP1 expression, prognostic value, and association with immune cells in tumor tissues by immunohistochemistry and flow cytometry.

Results: ACYP1 was overexpressed across cancers. High expression of ACYP1 correlated with a poor prognosis in most tumor types, especially in LIHC. ACYP1 was significantly implicated in immune and metabolic related pathways. High ACYP1 expression showed significant correlations with the abundances of Th2 cells, Tregs, macrophages, dendritic cells, and myeloid-derived suppressor cells in LIHC. LIHC patients with high ACYP1 expression showed significantly shorter overall survival and relapse-free survival rates concomitant with increased infiltration of CD4+ T cells. Mouse

OPEN ACCESS

Edited by:
Yunfei Xu,
Shandong University, China

Reviewed by:
Yulong Fu,
University of Alabama at Birmingham, United States
Aziz Eftekhari,
Joint Ukraine-Azerbaijan Research Center of Nanobiotechnology, Azerbaijan
Lin Zhang,
University of Pittsburgh, United States

***Correspondence:**
Zhi Yao
yaozhi@tmu.edu.cn
Wei Lu
mail4luwei@163.com
Ningning Zhang
mail4ningning@163.com

[†]These authors have contributed equally to this work

Specialty section:
This article was submitted to Cancer Molecular Targets and Therapeutics, a section of the journal Frontiers in Oncology

Received: *13 February 2022*
Accepted: *29 March 2022*
Published: *02 May 2022*

Citation:
Zhou L, Fu Z, Wang S, Jia J, Cheng Y, Zheng Y, Zhang N, Lu W and Yao Z (2022) ACYP1 Is a Pancancer Prognostic Indicator and Affects the Immune Microenvironment in LIHC. Front. Oncol. 12:875097. doi: 10.3389/fonc.2022.875097

subcutaneous tumors with ACYP1 overexpression exhibited significantly accelerated tumor progression with increased aggregation of CD4+ T cells.

Conclusion: Overall, ACYP1 may serve as a vital prognostic biomarker and play an immunoregulatory role in LIHC.

Keywords: ACYP1, pancancer, liver hepatocellular carcinoma, LIHC, immune infiltration, prognosis, biomarker

INTRODUCTION

Acylphosphatase (ACYP) is a small cytoplasmic enzyme commonly found in many organs and tissues of vertebrates. ACYP is involved in multiple cellular physiological processes by catalyzing the hydrolysis of acylphosphates. Compounds containing carboxyl phosphate bonds are substrates of ACYP and play a crucial role in regulating glycolysis, the tricarboxylic acid (TCA) cycle, and membrane ion pump activity (1, 2). Two isoenzymes of ACYP, namely, the erythrocyte and muscle types, have been identified and are encoded by the ACYP1 and ACYP2 genes, respectively. The erythrocyte type has higher catalytic activity. Recent studies have shown that ACYP is involved in erythrocyte senescence and cell differentiation and is also related to metabolism in the context of hyperthyroidism (3–7). In addition, ACYP expression is involved in colon cancer metastasis and glioblastoma progression by regulating intracellular Ca2+ homeostasis (8). Recently, ACYP1 was reported to be involved in imatinib-resistant gastrointestinal stromal tumors (GISTs) (9). ACYP1 is considered to be a metabolism-related gene used to predict the prognosis of patients with gastric and liver cancer and may become an important candidate target for metabolic therapy (10–12). A recent study revealed that the high expression of ACYP1 was significantly associated with a poor prognosis for cholangiocarcinoma (CHOL) patients, which may be related to the effect of ACYP1 on cell viability and apoptosis (13). However, few pancancer studies have been performed on ACYP1, and its mechanism in different tumors remains unclear.

Abbreviations: ACC, Adrenocortical carcinoma; BLCA, Bladder Urothelial Carcinoma; BRCA, Breast invasive carcinoma; CESC, Cervical squamous cell carcinoma and endocervical adenocarcinoma; CHOL, Cholangio carcinoma; COAD, Colon adenocarcinoma; DLBC, Lymphoid Neoplasm Diffuse Large B-cell Lymphoma; ESCA, Esophageal carcinoma; GBM, Glioblastoma multiforme; HNSC, Head and Neck squamous cell carcinoma; KICH, Kidney Chromophobe; KIRC, Kidney renal clear cell carcinoma; KIRP, Kidney renal papillary cell carcinoma; LAML, Acute Myeloid Leukemia; LGG, Brain Lower Grade Glioma; LIHC, Liver hepatocellular carcinoma; LUAD, Lung adenocarcinoma; LUSC, Lung squamous cell carcinoma; MESO, Mesothelioma; OV, Ovarian serous cystadenocarcinoma; PAAD, Pancreatic adenocarcinoma; PCPG, Pheochromocytoma and Paraganglioma; PRAD, Prostate adenocarcinoma; READ, Rectum adenocarcinoma; SARC, Sarcoma; SKCM, Skin Cutaneous Melanoma; STAD, Stomach adenocarcinoma; TGCT, Testicular Germ Cell Tumors; THCA, Thyroid carcinoma; THYM, Thymoma; UCEC, Uterine Corpus Endometrial Carcinoma; UCS, Uterine Carcinosarcoma; UVM, Uveal Melanoma; TME, Tumor Microenvironment; IHC, Immunohistochemical; OS, Overall Survival; DFS, Disease-free Survival; RFS, Relapse-free Survival; HR, Hazard Ratio; GSEA, Gene Set Enrichment Analysis; GSVA, Gene Set Variation Analysis; DCs, Dendritic Cells; MDSCs, Myeloid-derived Suppression Cells.

The clinical efficacy of immunotherapy is affected by the tumor microenvironment (TME), which includes hypoxia, low pH, and inhibitory metabolites. Therefore, alleviating metabolic inhibition of immune cells in the TME may improve the efficacy. In general, tumor cells tend to use glycolysis for energy, resulting in the production of large amounts of lactic acid, which inhibits the function of effector T cells by reducing proliferation and cytokine production (14). Several studies have shown that ACYP1 is a metabolism-related gene involved in gastric and liver cancer progression (15–17). ACYP1 can affect glycolysis *via* the dephosphorylation of 1,3 bisphosphoglycerate, and glycolysis was found to be highly active in tissues with high ACYP1 expression (1). However, the role of ACYP1 in the TME of LIHC is still unclear.

This study was focused on the prognostic value across cancers, signaling pathways and the TME in LIHC by analyzing the expression of ACYP1. Immunohistochemical (IHC) and flow cytometry were performed to prove its role in the TME of LIHC. Our study aims to elucidate the importance of ACYP1 in LIHC prognosis.

MATERIALS AND METHODS

ACYP1 Expression and Prognostic Value Across Cancers

In this study, the transcriptional signature of ACYP1 across cancers was analyzed based on the Oncomine database, TIMER database, and UALCAN network. The correlation between levels of ACYP1 mRNA and the ending event of patients with different cancer types was analyzed by assessing PrognoScan (microarray data), Kaplan–Meier Plotter (GEO, TCGA and EGA data) and GEPIA (TCGA and GTEx data) datasets. The effect of ACYP1 mRNA expression on overall survival (OS), disease-free survival (DFS), and relapse-free survival (RFS) across cancers was calculated. The relevance of ACYP1 expression and clinical characteristics of LIHC was determined using the Kaplan–Meier Plotter database.

GSEA and GSVA Analysis

RNA-seq data were obtained from the TCGA database (https://portal.gdc.cancer.gov/). GSEA and GSVA were performed to explore potential pathways associated with ACYP1 *via* KEGG and Hallmark terms using R version 4.0.5 (normalized enrichment score (NES) ≥1.0 and false discovery rate (FDR) adjusted p value <0.25).

Correlation Between ACYP1 Expression and Immune Cell Infiltration

The TIMER database used RNA expression profiles to analyze the infiltration of immune cells in tumor tissues. Multiple immune deconvolution methods were used to explore tumor immunological, clinical, and genomic characteristics. The correlation of ACYP1 expression with the abundance of subtypes of immune infiltrating cells, immune cell markers, and tumor purity was analyzed.

Validation of the Role of ACYP1

Tumor tissue slides of LIHC patients at Tianjin Medical University Cancer Hospital were subjected to IHC using the following antibodies at the indicated concentrations: anti-ACYP1 (ab231323, Abcam) 1:100; anti-CD4 (67786-1-Ig, Peprotech) 1:100; and anti-CD8 (66868-1-Ig, Peprotech) 1:100. Stained tissues were scanned and captured using CaseViewer software (3DHISTECH). The H-scores were used to quantify staining intensity (protein expression). The ACYP1 low expression and high expression groups were set based on the median level of ACYP1 expression. Kaplan—Meier survival curves with log-rank tests were used to analyze the effect of high ACYP1 expression. The use of patient information and tissue was approved by Tianjin Medical University Cancer Institute and the hospital ethics committee.

The ACYP1 protein overexpression plasmids were purchased from Genewiz (Suzhou, China). Briefly, HEK293T cells were transfected with a lentiviral plasmid (Plvx-IRES-Puro-ACYP1) along with packaging plasmids using polyethylenemine. Hep1-6 cells were infected with the virus. Hep1-6 control cells (Vector) and hep1-6 ACYP1 overexpressing cells (ACYP1) were injected into the right flanks of mice ($2x10^6$ cells per mouse) to establish a subcutaneous implantation model. From day 8 after injection, tumor size was measured every three days and tumor volume was calculated as length × $width^2/2$. After 30 days, the mice were sacrificed to assess tumor growth. The weight of the tumor was also measured. For flow cytometry analysis of immune cell populations, cells from different mouse tumors were divided into an appropriate number of tubes in 100 μl PBS. Cells were stained with antibodies for 30 minutes at 4°C. Absolute cell numbers and frequency of immune cells were identified with appropriate gating. At least $1x10^6$ cells were recorded for tumor analysis. C57BL/6J mice were obtained from Beijing Vital River Laboratory Animal Technologies. All mice were age-matched and kept under specific pathogen-free conditions. All animal procedures were approved by the Animal Ethics Committee of Tianjin Medical University, Tianjin, China.

Statistical Analysis

All statistics were analyzed using SPSS statistical software (version 24.0.0). $P<0.05$ was considered to indicate statistical significance. The adjusted P value cutoff of 0.01 and the fold change of 1.5 were set in Oncomine. We used a univariate Cox regression model to calculate the HR and Cox P value and the log-rank test to compare survival curves. Spearman's correlation was used to analyze the correlation of gene expression.

RESULTS

The Expression of ACYP1 in Human Cancers

First, we analyzed ACYP1 mRNA expression levels in Oncomine across cancers. ACYP1 expression was higher in a variety of cancer groups than in the respective normal tissues. Decreased expression of ACYP1 was found in the head and neck cancer, breast cancer, etc. (**Figure 1A** and **Supplementary Table S1**). The TIMER database was used to evaluate ACYP1 expression across cancers. ACYP1 expression was significantly higher in most cancers than in their respective adjacent normal tissues (**Figure 1B**). TCGA and GTEx databases were used to identify ACYP1 expression characteristics. ACYP1 was found to be upregulated in lymphoid neoplasm diffuse large B-cell lymphoma (DLBC), pancreatic adenocarcinoma (PAAD), skin cutaneous melanoma (SKCM), thymoma (THYM), etc. ACYP1 was downregulated in some cancers, such as uterine carcinosarcoma (UCS) and brain lower grade glioma (**Supplementary Figure S1**).

Prognostic Potential of ACYP1 Expression

Based on the difference in expression across cancers, the prognostic value of ACYP1 was predicted in different databases. The relationships between ACYP1 expression levels and prognosis for each type of cancer were explored using Kaplan–Meier Plotter. ACYP1 was found to be an adverse prognostic factor for LIHC (OS: HR=2.25, p=2.9e-0.6; RFS: HR=1.82, p=0.0011) (**Figures 2A, B**). ACYP1 also had an adverse effect on OS, but not on RFS for BRCA patients (OS: HR=6.97, p=0.003) (**Figures 2C, D**). For colorectal cancer, ACYP1 was only a favorable prognostic factor in terms of OS, but not RFS in READ (HR=0.39, p=0.029) (**Figures 2E, F**). For HNSC, ACYP1 was a significant protective factor in terms of OS and RFS (OS: HR=0.4, p=0.018; RFS: HR=0.33, p=0.047) (**Figures 2G, H**). In addition, high expression of ACYP1 was beneficial only for LUSC patients (OS: HR=0.73, p=0.028; RFS: HR=0.71, log-rank p=0.18) (**Figures 2I, J**) and not LUAD patients, in which ACYP1 had an adverse effect on RFS (OS: HR=0.82, p=0.18; RFS: HR=1.49, p=0.07) (**Figures 2K, L**). For soft tissue cancer, ACYP1 significantly influenced OS and RFS (OS: HR=1.58, p=0.025; RFS: HR=1.68, p=0.034) (**Figures 2M, N**).

According to the ACYP1 expression level, patients were divided into two groups to assess the role in survival *via* PrognoScan. The results showed that high ACYP1 expression was an adverse prognostic factor for five of these tumor types, including breast, colorectal, brain, soft tissue cancers and skin. Interestingly, in lung cancer and head and neck cancers, ACYP1 played a protective role (**Supplementary Figures S2A–J**). These results suggested that ACYP1 may play variable roles across cancers, while the role of poor prognosis may be predominant.

We also analyzed the RNA sequencing data of ACYP1 in TCGA by using GEPIA. We first analyzed the overall effect of ACYP1 on all 33 cancer types. Of note, high expression of ACYP1 indicated poor prognosis across cancers in a total of

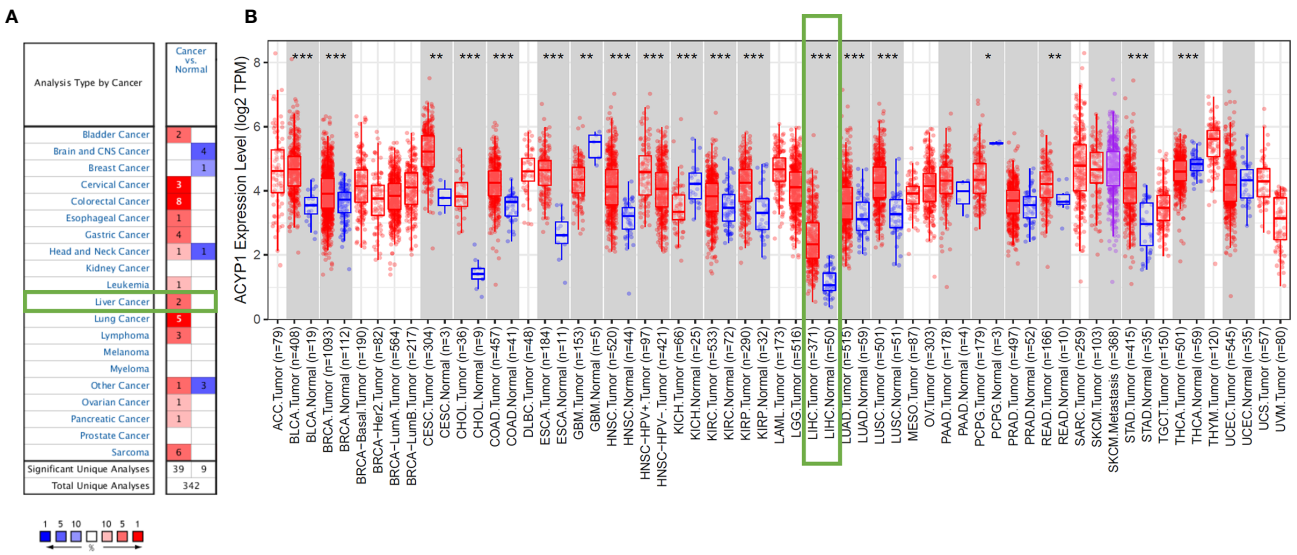

FIGURE 1 | ACYP1 expression levels across cancers. Elevated or decreased levels of ACYP1 expression in multiple cancer types in Oncomine **(A)** and TIMER **(B)**. *P < 0.05, **P < 0.01, ***P < 0.001.

9497 patients, and OS and DFS were significantly different (OS: HR= 1.1, P = 0.039; DFS: HR= 1.1, P = 0.049) (**Supplementary Figures S3A, B**). We then analyzed the role of ACYP1 in each of the cancer types. However, unlike findings from PrognoScan and Kaplan–Meier Plotter, high expression levels of ACYP1 only indicated a poorer prognosis in LIHC (OS: p=0.00015; RFS: p=0.00026) (**Supplementary Figures S3C–P**).

Relationship Between ACYP1 Expression and Clinical Features in LIHC Patients

Then we investigated the relationship between ACYP1 expression and clinicopathologic characteristics. The results showed that male sex, Asian race, stage I tumor, stage, grade, AJCC T stage, microvascular invasion, history of alcohol consumption, and hepatitis virus infection were closely related to high expression of ACYP1, which indicates a worse OS in LIHC (**Figure 3A**). Similarly, high expression of ACYP1 also indicates a worse PFS in LIHC, especially in males, white race, Asian race, stage I to stage III, grade 2 and 3, AJCC T2 and T3, microvascular invasion, alcohol consumption, and hepatitis virus infection (**Figure 3B**).

The results from the Wurmbach mixed liver dataset showed that ACYP1 expression varied significantly by cancer type, grade, hepatitis virus infection status, and vascular invasion (**Supplementary Figures S4A–D**). In the UALCAN database, ACYP1 expression in cancer stage, patient age, tumor grade, and histological subtypes was significantly different. No association was found between ACYP1 expression and the patient's race or sex(**Supplementary Figures S4E–J**). Moreover, ACYP1 was significantly associated with early and late recurrence of LIHC. ACYP1 levels were significantly upregulated in patients with early recurrence (**Supplementary Figure S5**). ACYP1 may be an important factor in the recurrence and prognosis of LIHC.

Significant Pathways Associated With ACYP1 in LIHC

We performed KEGG GSEA and GSVA (**Supplementary Table S2**) to explore the potential role of ACYP1 in signaling pathways. The immune-related pathways were highly enriched in LIHC by KEGG GSEA (NSE≥1.0, FDR<0.25), including Fc-gamma-r-mediated phagocytosis, primary immunodeficiency, TCR signaling pathway, antigen processing and presentation, JAK-STAT pathway, leukocyte transendothelial migration, chemokine signaling pathway and so on, which are shown in red (**Figure 4A**). It also affected several cancer-related pathways, such as DNA replication, the P53 signaling pathway, apoptosis, the WNT signaling pathway, and the MAPK signaling pathway, as shown in blue. ACYP1, as an important enzyme involved in glycolysis (**Supplementary Figure S6D**), was significantly involved in metabolism-related pathways, including glycolysis gluconeogenesis, sphingolipid metabolism, pyruvate metabolism, mTOR signaling, inositol phosphate metabolism, aminoacyl transfer biosynthesis, pyrimidine metabolism, and purine metabolism, as shown in yellow. The top ten signaling pathways related to ACYP1 are shown in **Figure 4B**. The KEGG GSVA analysis showed similar pathways associated with ACYP1 in LIHC (**Figure 4C**). Furthermore, the Hallmark GSEA and GSVA analysis (**Supplementary Table S3**) showed that immune-related pathways, including the TNFα signaling pathway, allograft rejection, inflammatory response, and interferon-gamma response, were highly enriched in LIHC (**Supplementary Figures S6A–C**).

ACYP1 Expression and Immune Infiltration in LIHC

Based on the above analysis, we determined that ACYP1 plays an important role in regulating immune-related pathways in LIHC. Therefore, it is necessary to investigate whether ACYP1 expression is related to immune infiltration in LIHC. The

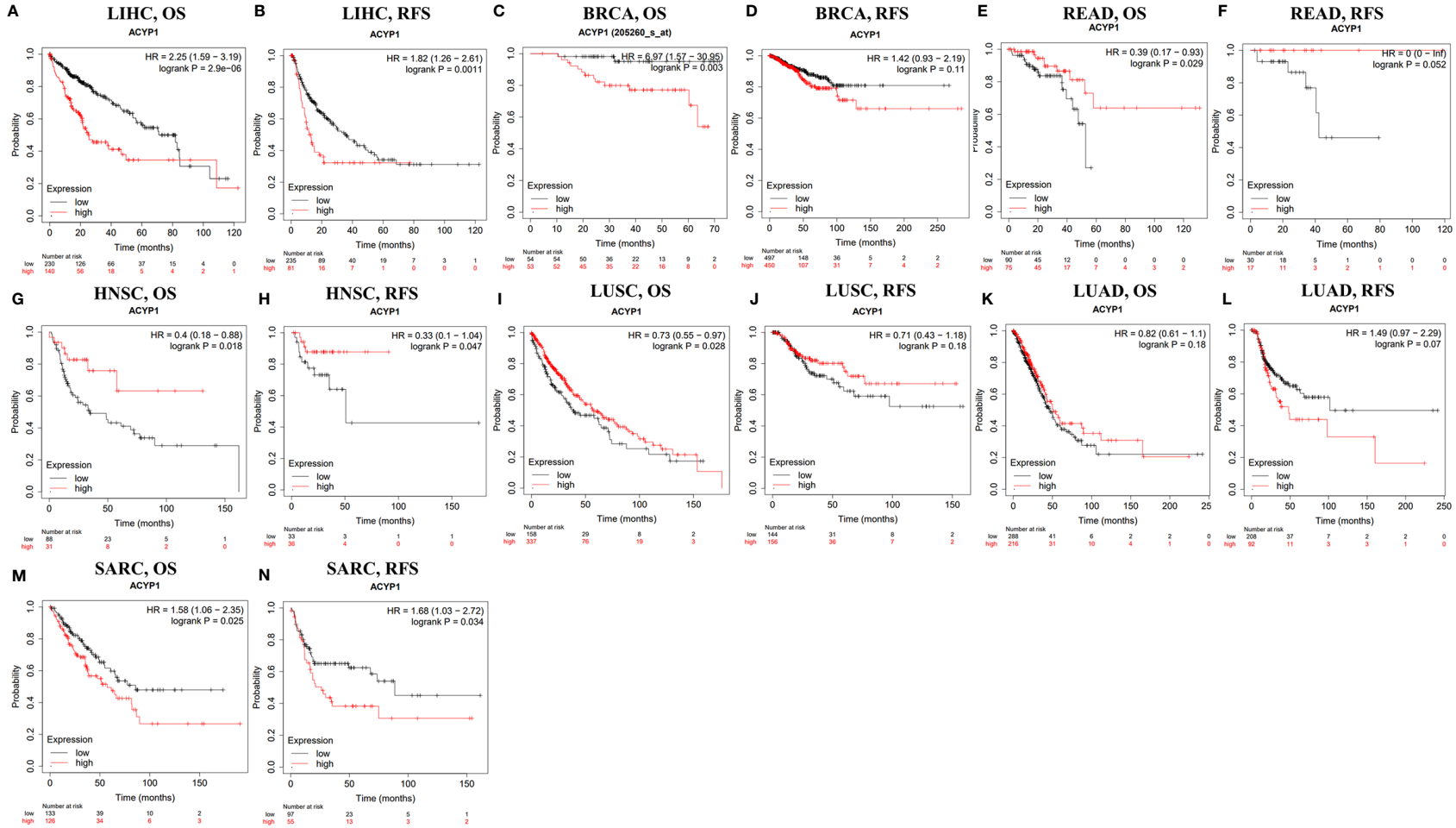

FIGURE 2 | The survival of patients with high and low expression of ACYP1 across cancers in the Kaplan–Meier Plotter database. OS and RFS of liver LIHC **(A, B)**, BRCA **(C, D)**, READ **(E, F)**, HNSC **(G, H)**, LUSC **(I, J)**, LUAD **(K, L)**, and SARC **(M, N)** patients. OS, overall survival; RFS, relapse-free survival.

A

OS(n=364)

Characteristic	Numbe (%)	HR (95%CI)	P value
Gender			
Male	250(67)	2.64(1.67-4.16)	0.000016***
Female	121(33)	1.68(0.92-3.07)	0.088
Race			
White	184(50)	1.65(0.99-2.76)	0.052
Black of african american	17(5)	-	-
Asian	158(43)	3.19(1.74-5.84)	0.000077***
Stage			
1	171(46)	2.24(1.2-4.19)	0.0092**
1+2	257(69)	2.41(1.44-4.02)	0.00054*
2	86(23)	2.7(1.2-6.09)	0.013*
2+3	171(46)	2.48(1.51-4.07)	0.00023***
3	85(23)	2.54(1.33-4.83)	0.0034**
3+4	90(24)	2.38(1.27-4.45)	0.0053**
4	5(1)	-	-
Grade			
1	55(15)	4.22(1.62-11.02)	0.0014**
2	177(48)	2.05(1.15-3.63)	0.013*
3	122(33)	2.21(1.19-4.07)	0.0095**
4	12(3)	-	-
AJCC-T			
1	181(49)	2.16(1.19-3.93)	0.0099**
2	94(25)	2.12(1-4.46)	0.044*
3	80(22)	2.81(1.47-5.37)	0.0012**
4	13(4)	-	-
Vascular invasion			
None	205(55)	1.68(0.94-3.01)	0.077
Micro	93(25)	2.28(1.05-4.93)	0.032*
Macro	16(4)	-	-
Alcohol consumption			
Yes	117(32)	2.29(1.16-4.51)	0.014*
None	205(55)	2.77(1.7-4.52)	0.000021***
Hepatitis			
Yes	153(41)	3.05(1.56-5.96)	0.00062***
None	169(46)	2.17(1.35-3.49)	0.0011**

B

PFS(n=370)

Characteristic	Numbe (%)	HR (95%CI)	P value
Gender			
Male	250(67)	3.16(2.1-4.74)	0.0000000056***
Female	121(33)	1.19(0.69-2.04)	0.53
Race			
White	184(50)	1.82(1.19-2.79)	0.0052**
Black of african american	17(5)		-
Asian	158(43)	2.4(1.47-3.92)	0.0003***
Stage			
1	171(46)	0.8(0.48-1.33)	0.38
1+2	257(69)	2.07(1.37-3.13)	0.0004***
2	86(23)	2.88(1.54-5.38)	0.00054***
2+3	171(46)	1.96(1.29-2.96)	0.0012**
3	85(23)	1.58(0.9-2.77)	0.11
3+4	90(24)	1.6(0.93-2.77)	0.087
4	5(1)	-	-
Grade			
1	55(15)	2.14(0.95-4.85)	0.061
2	177(48)	2.1(1.31-3.38)	0.0017**
3	122(33)	1.75(1.02-3)	0.041*
4	12(3)	-	-
AJCC-T			
1	181(49)	0.77(0.47-1.26)	0.3
2	94(25)	2.8(1.57-5)	0.00028***
3	80(22)	1.81(1-3.27)	0.045*
4	13(4)	-	-
Vascular invasion			
None	205(55)	1.41(0.85-2.35)	0.18
Micro	93(25)	2.61(1.45-4.7)	0.00092*
Macro	16(4)	-	-
Alcohol consumption			
Yes	117(32)	2.24(1.31-3.84)	0.0025**
None	205(55)	2.06(1.34-3.17)	0.00072***
Hepatitis			
Yes	153(41)	1.83(1.1-3.02)	0.018*
None	169(46)	2.29(1.45-3.61)	0.00026***

FIGURE 3 | Correlation of ACYP1 expression from LIHC patients in various clinicopathologies with OS (n=364) **(A)** and RFS (n=370) **(B)**. Red dots represent the hazard ratio. OS, overall survival; PFS, progression-free survival. *P < 0.05, **P < 0.01, ***P < 0.001.

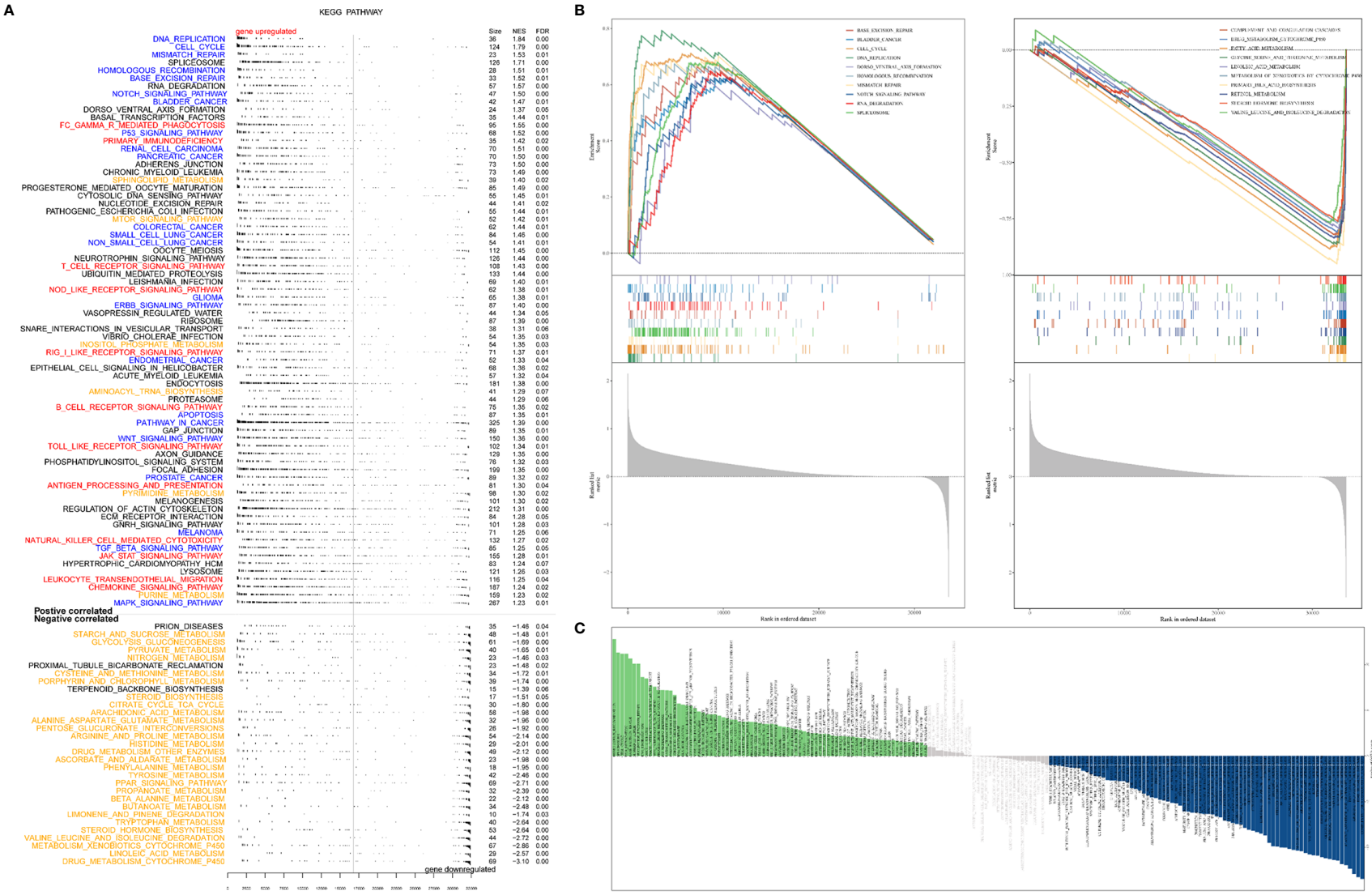

FIGURE 4 | Signal pathways involved in ACYP1. **(A)** Correlation between ACYP1 expression and KEGG pathways in LIHC analyzed *via* GSEA. **(B)** The top ten signaling pathways with significant positive and negative correlations with ACYP1 in LIHC. **(C)** Relationships between ACYP1 expression and KEGG pathways in LIHC performed *via* GSVA (NSE≥1.0, FDR<0.25).

results indicated that ACYP1 expression had no significant correlations with tumor purity. In addition, the ACYP1 expression level was closely related to the infiltration of B cells (R=0.264, p=6.66e-07) and other B-cell subtypes; including CD8+ T cells (R=0.125, p=2.05e-02), CD4+ T cells (R=0.201, p=1.75e-04) and their subtypes, Tregs (R=0.361, p=4.42e-12), NK cells (R=0.201, p=1.70e-04), macrophages (R=-0.414, p=9.43e-16), monocytes (R=-0.253, p=1.87e-06), macrophages/monocytes (R=0.274, p=2.38e-07), dendritic cells (DCs) (R=0.419, p=4.19e-16), myeloid-derived suppressor cells (MDSCs) (R=0.565, p=1.84e-30), neutrophils (R=0.309, p=4.60e-09) and cancer-associated fibroblasts (R=0.271, p=3.06e-07) (**Figure 5**). We created a heatmap and lollipop plot of the correlation between ACYP1 and infiltration of various immune cell types *via* CIBERSORT (**Supplementary Figure S7**, **Supplementary Table S4**). Moreover, correlation analysis of ACYP1 in all other tumors with various immune cell infiltrations was performed in TIMER1.0 (**Supplementary Figure S8**) and TIMER2.0 (**Supplementary Figure S9**), respectively. These results revealed that ACYP1 expression affects patient survival by affecting the infiltration of various immune cell types in LIHC, with the strongest correlations with CD4+ Th2 T cells, Tregs, DCs, macrophages, and MDSCs.

Then the correlation between ACYP1 expression and the expression of biomarkers of immune cell subsets was investigated in LIHC patients. Some representative markers were selected to characterize various infiltrating immune cells in LIHC. We analyzed T-cell subsets, such as CD8+ T cells, Th1 cells, Th17 cells, Tregs, exhausted T cells, and different types of macrophages, such as M1, M2, and tumor-associated macrophages. The results showed that ACYP1 expression was significantly associated with the expression of 45 of the 49 assessed markers in LIHC. Similarly, ACYP1 expression was significantly correlated with the infiltration levels of MDSCs, Th2 cells, DCs, and macrophages and respective markers for these four immune cell types (**Table 1**). Moreover, ACYP1 expression was correlated with the infiltration of B cells, T cells and other subtypes, neutrophils, and NK cells infiltration to varying degrees. Therefore, these results confirmed that ACYP1 expression may influence the infiltration of various immune cell types in different ways and ultimately comprehensively affect the prognosis of LIHC patients.

Preliminary Experimental Verification of the ACYP1 Signature in LIHC

IHC was performed to evaluate the expression of ACYP1 in 50 LIHC specimens. According to ACYP1 expression level, all specimens were classified as either high expression (ACYP1 high) or low expression (ACYP1 low). Images of representative samples were taken at 100× and 400× magnification and ACYP1 expression is shown (**Figures 6A, B**). Of note, we investigated the prognostic role of ACYP1 in LIHC patients and revealed that patients with high expression of ACYP1 had worse OS (p=0.0141) and RFS (p=0.0131) (**Figure 6E**). The relative levels of immune cell infiltration showed that the infiltration of CD4+ T cells, but not CD8+ T cells was stronger in the ACYP1 high expression group than in the other group (p<0.05) (**Figures 6A–D**). Then, we extended our studies to the subcutaneous implantation tumor model of Hep1-6 (mouse hepatoma cells) to explore the potential roles of ACYP1 in tumor progression and the TME. The expression of ACYP1 was significantly up-regulated in ACYP1-overexpressing stable cell lines (**Supplementary Figure S10A**). Remarkably, ACYP1 overexpression significantly accelerated tumor growth under the skin (**Figure 6F**). The tumor in the ACYP1 overexpression group were significantly larger and weighted more than those in the vector group (**Figures 6G, H**). Moreover, we explored whether immune cells were involved in the high ACYP1 expression-mediated LIHC progression. In comparison with the vector group, a prominent accumulation of CD4+ T cells was found in ACYP1 overexpressing mice, while no obvious changes were found in CD8+ T cells (**Figures 6I, J** and **Supplementary Figure S10B**). These results indicated that ACYP1 expression was positively related to CD4+ T cells, which is consistent with the results from TCGA.

DISCUSSION

Acylphosphatase, as a cytoplasmic enzyme, widely exists in a variety of vertebrate tissues and can catalyze the hydrolysis of carboxyl phosphate bonds in carboxyl phosphate. These carboxyl phosphate bonds mainly exist in two forms: metabolic products, such as 1,3-bisphosphoglyceric acid, and acetyl phosphate, and membrane ion pump intermediates, such as active intermediates of K+, Ca2+, and Na+-ATPase (18–20). The hydrolytic activity of ACYP on 1,3 diphosphoglyceric acid suggests that ACYP plays a regulatory role in glycolysis. It has been confirmed that ethanol production is significantly increased in yeast cells overexpressing the ACYP gene. ACYP plays a regulatory role in the ion transport system. It affects membrane pumps *via* hydrolyzing the phosphate of aspartic acid under the action of Ca2+, Na+, and K+-ATPase in neuronal erythrocyte membranes, cardiac sarcolemmas, and skeletal muscle sarcolemmas (19–23).

The roles of the ACYP in cancer have not been well studied, and a few studies have explored this topic. ACYP expression is associated with the metastatic phenotype of human colorectal cancer and plays an oncogenic role in gliomas *via* activating the c-MYC signaling pathway (8, 24). Recent studies have shown that high expression of ACYP1 can affect the prognosis of CHOL, and hepatocellular CHOL patients *via* affecting cell proliferation *in vitro* (13).

As a metabolism-related gene with prognostic value in gastric cancer and liver cancer, ACYP1 may become an important candidate target for metabolic therapy (10–12). Our study revealed that ACYP1 plays an adverse role in LIHC patients, although its implication may vary depending on clinical characteristics such as sex, race, tumor stage, tumor grade, vascular invasion, alcohol consumption, and hepatitis status according to multifactor regression analysis. The TME is likely to help elucidate the underlying mechanisms of tumor progression. In this study, ACYP1 overexpression in LIHC tumors may result in much more immune suppressive cell

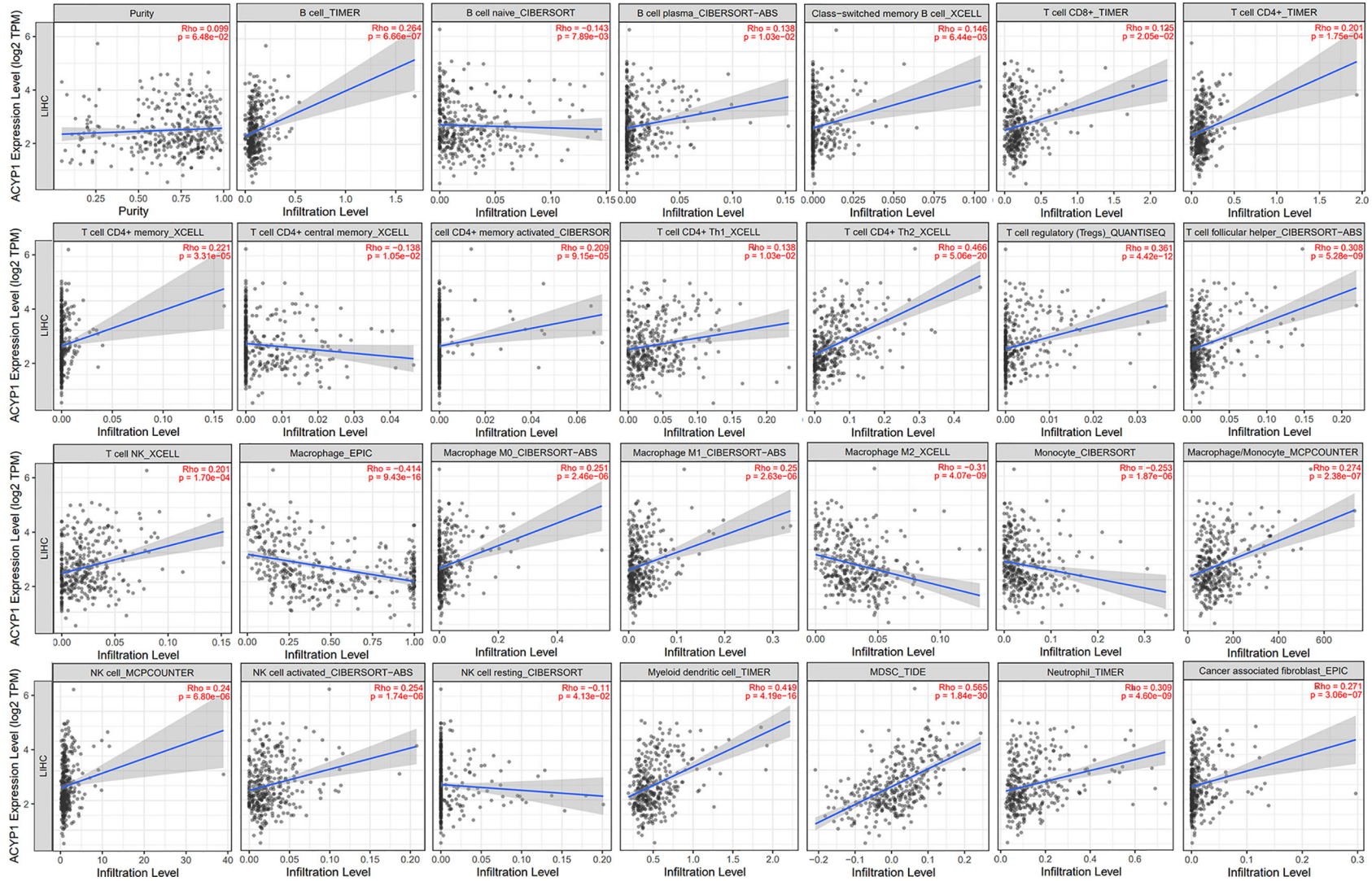

FIGURE 5 | Effects of ACYP1 expression on the TME in LIHC by using TIMER. ACYP1 expression had a significant correlation with the infiltration of various immune cells, including B cells, CD8+ T cells, CD4+ T cells, Tregs, Tfh cells, macrophages, monocytes, macrophages/monocytes, NK cells, DCs, MDSCs, neutrophils, cancer-associated fibroblasts, and their respective subtypes. LIHC, liver hepatocellular carcinoma.

TABLE 1 | Correlation between ACYP1 expression and immune cell markers in LIHC.

Cell type	Gene markers	Cor	*p*	
B cell	CD19	0.238	0.000008	***
	CD79A	0.167	0.001880	**
T cell	CD3D	0.303	0.000000	***
	CD3E	0.24	0.000007	***
	CD2	0.223	0.000029	***
CD8+ T cell	CD8A	0.205	0.000128	***
	CD8B	0.208	0.000099	***
Th1	T-bet	0.096	0.074700	
	IL-2	0.116	0.031700	*
	IFN-γ	0.243	0.000005	***
	TNF	0.272	0.000000	***
Th2	GATA3	0.261	0.000001	***
	STAT5A	0.242	0.000005	***
	IL13	0.178	0.000896	***
Th17	STAT3	0.147	0.006170	**
	IL17A	0.08	0.137000	
Tfh	BCL6	0.212	0.000075	***
	IL21	0.071	0.189000	
Treg	FOXP3	0.214	0.000061	***
	CCR8	0.312	0.000000	***
	STAT5B	0.187	0.000495	***
	TGFβ	0.325	0.000000	***
T cell exhaustion	PD-1	0.237	0.000009	***
	CTLA-4	0.359	0.000000	***
	LAG3	0.274	0.000000	***
	TIM-3	0.379	0.000000	***
	GZMB	0.152	0.004630	**
	TOX	0.228	0.000019	***
	TIGIT	0.305	0.000000	***
TAM	CCL2	0.232	0.000013	***
	CD68	0.205	0.000122	***
	IL10	0.239	0.000007	***
M1 macrophage	iNOS	0.087	0.109000	n.s.
	IRF5	0.366	0.000000	***
	COX2	0.276	0.000000	***
M2 macrophage	CD163	0.109	0.042400	*
	VSIG4	0.185	0.000547	***
	MS4A4A	0.172	0.001380	**
Neutrophils	CD66b	0.094	0.081200	n.s.
	CD11b	0.337	0.000000	***
NK	CD16	0.330	0.000000	***
	CD56	0.346	0.000000	***
DC	CD1c	0.103	0.057100	n.s.
	CD83	0.37	0.000000	***
	CD209	0.104	0.053600	n.s.
	MHCII	0.219	0.000042	***
Monocyte	CD14	-0.301	0.000000	***
	CD64	0.338	0.000000	***
	CD15	0.368	0.000000	***

*LIHC, liver hepatocellular carcinoma; Tfh, follicular helper T cell; Th, T helper cell; Treg, regulatory T cell; TAM, tumor associated macrophage; NK, natural killer cell; DC, dendritic cell; Cor, R value of Spearman's correlation. *P < 0.05, **P < 0.01, ***P < 0.001. n.s. "no significance".*

infiltration, while the molecular mechanism needs to be further investigated.

There are some studies have explored biomarkers of prognosis or treatment in pancancer based on public databases. The results suggested that single gene may deeply involve in the immunological features and cancer prognosis. Chao Deng et al. performed multidimensional bioinformatics analysis to examine the relationship between NRP genes and prognostic in pancancer, and finally found the NRP family genes are significantly correlated with cancer prognosis and immune infiltration in bladder urothelial carcinoma (25). Xiaoyu Zhang and colleagues reported MXD3 played an important role in predict prognosis of glioma, and may expected to be as a clinical therapeutic target *via* analyzing public databases and experimental validation (26). To facilitate researchers exploring the prognosis associated genetic features in multi-omic levels in pancancer and finding critical genes for drug discovery and precision medicine, an online platform was developed by Ouyang Jian and colleagues. Our results were further validated on this platform (27). In this study, we analyzed the expression levels of ACYP1 and its prognostic value across cancers using multiple databases. First, in Oncomine, ACYP1 expression was higher in a variety of cancer groups versus their corresponding normal control groups. Moreover, reduced expression of ACYP1 was found in brain cancer, breast cancer, head and neck cancer, and other cancers, while TCGA database analysis results *via* TIMER were not the same. The differences may be due to different algorithms in the two databases. We further explored the effect of ACYP1 on the prognosis of various cancers. In PrognoScan, high ACYP1 expression was a risk factor for adverse outcomes in breast, colorectal, brain, skin, and soft tissue cancers. In Kaplan–Meier Plotter and GEPIA, ACYP1 was closely related to a poor prognosis in LIHC and was related to the following clinical characteristics: male sex, Asian race, all tumor stages, all tumor grades, AJCC T stage, microvascular invasion, alcohol consumption (yes or no), and hepatitis virus infection (yes or no). Thus, at present, we have evidence that ACYP1 has the potential to be a pancancer prognostic biomarker, especially in LIHC.

The TME can inhibit immune responses *via* multiple mechanisms. Aerobic glycolysis, known as the Warburg effect, the most common type of tumor metabolic reprogramming, the results in a TME characterized by hypoxia, low pH, low nutrient status and the production of inhibitory metabolites such as lactic acid, which promote tumor progression by affecting immune cell function. Aerobic glycolysis is a hallmark of liver cancer, which involves cancer progression, and even induces an immunosuppressive TME *via* key enzymes (28). In breast cancer, aerobic glycolysis affects MDSCs and maintains tumor immunosuppression (29). Macrophages promote tumor growth *via* regulating tumor cell aerobic glycolysis with PGK1 phosphorylation (30). The glycolysis pathway is actively regulated during the differentiation of Tregs, providing necessary biological energy sources for Tregs biosynthesis, proliferation, and migration (31–33). Therefore, addressing the metabolic limitations of immune responses in the tumor immune microenvironment may improve the effectiveness of cancer immunotherapy. Given that ACYP1 is an important metabolic enzyme in glycolysis, we hypothesized that the upregulation of ACYP1 in LIHC may affect immune cell infiltration *via* increasing the glycolysis rate. In our study, the pathway analysis suggested that ACYP1 was highly related to immune-related pathways in LIHC. The higher expression of ACYP1 may be closely related to negative immunity in the tumor

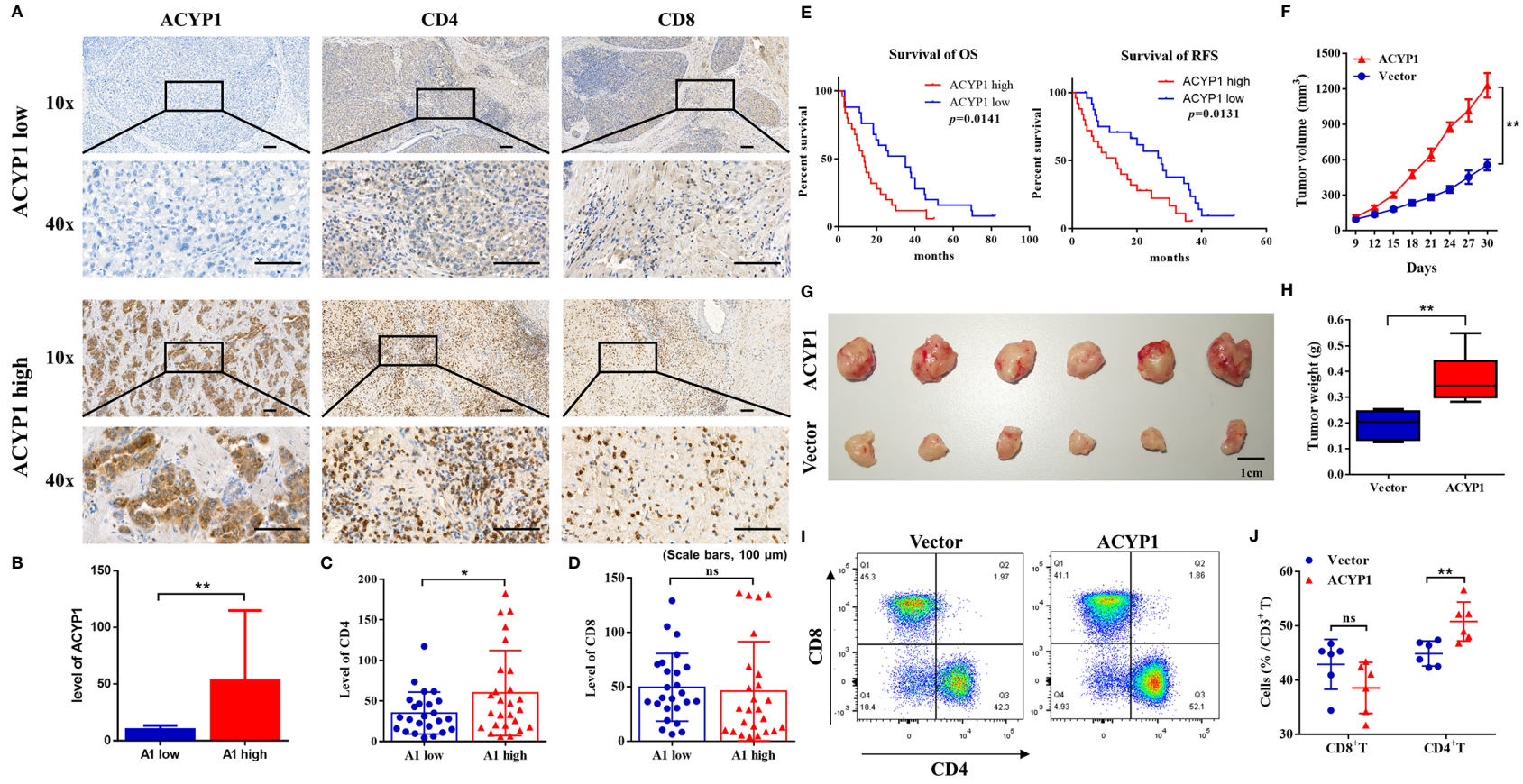

FIGURE 6 | Preliminary experimental verification of the ACYP1 signature in LIHC. **(A)** Representative samples with low and high ACYP1 expression for IHC staining of ACYP1, CD4+ and CD8+ T cells in the ACYP1 low and high group were taken at 100x and 400x magnification. **(B–D)** Relative quantitative analysis of ACYP1 **(B)**, CD4 **(C)** and CD8 **(D)** levels by IHC staining. **(E)** Survival analysis of the ACYP1 high group and the ACYP1 low group in 50 LIHC patients. **(F)** Subcutaneous growth of Hep1-6 tumors in the vector group and ACYP1 overexpression group (n=6). **(G)** Representative images of subcutaneous Hep1-6 tumors in the vector group and ACYP1 overexpression group (n=6). **(H)** The weight of subcutaneous Hep1-6 tumors in vector group and ACYP1 overexpression group (n=6). **(I, J)** The relative content of CD4+ T cells and CD8+ T cells in subcutaneous Hep1-6 tumors from vector mice and ACYP1 overexpressing mice (n=6). Positive cell percentages are shown. *P < 0.05, **P < 0.01, n.s. "no significance".

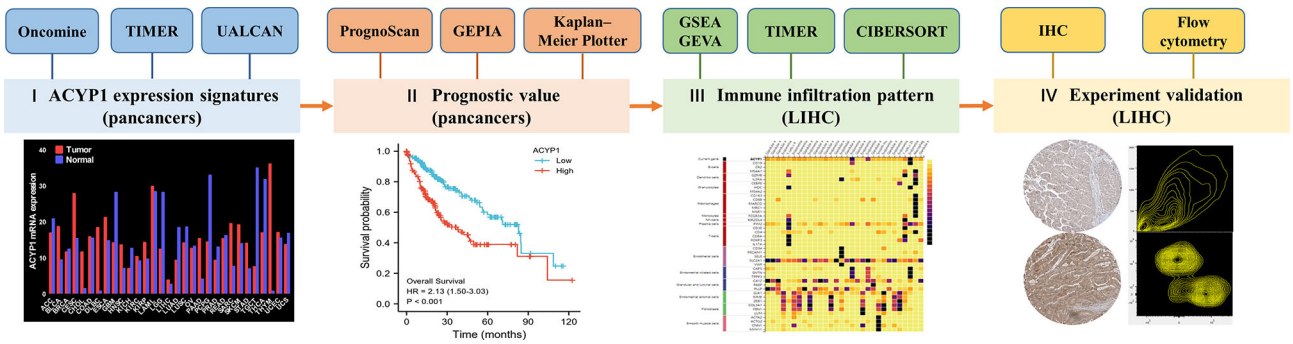

FIGURE 7 | Study flow-chart. I ACYP1 expression patterns explored *via* Oncomine, TIMER, and UALCAN; II Survival analysis of ACYP1 in PrognoScan, Kaplan—Meier Plotter, and GEPIA; III Signaling pathways and TME affected by ACYP1 *via* GSEA, GSVA, and TIMER; IV Experimental validation in human and mice tumor samples of LIHC.

itself. ACYP1 expression was also significantly correlated with the gene markers of these four immune cell types. The strength of the correlation between different markers and ACYP1 expression varied, suggesting that ACYP1 has characteristic interactions with certain immune cell subtypes.

The results from public data analysis were verified *via* using human LIHC tumor specimens and mouse subcutaneous tumor specimens. First, in LIHC patients, high expression of ACYP1 indicates a poor OS. In a mouse subcutaneous tumor model, high expression of ACYP1 was closely related to tumor progression. Moreover, immune infiltration was assessed by IHC in human tumor specimens and flow cytometry in mouse tumor samples. The results were consistent with the TCGA data, in which high expression of ACYP1 was positively associated with CD4+ T cells, but was not correlated with CD8+ T cells. Our results suggest the possibility that the immunosuppressive TME resulting from by ACYP1 may be the culprits of LIHC progression.

In this study, we investigated the roles of ACYP1 in pancancer and eventually showed an important role in the development of LIHC (**Figure 7**). Based on its physiological role and ectopic expression in liver cancer, our analysis integrated metabolism-related pathways and the immune microenvironment. The results showed that ACYP1 was an enzyme in the progress of glycolysis and promoted tumor progression *via* participating in the glycolysis and immunosuppression. Interestingly, glycolysis was closely associated with immune microenvironment and affect the prognosis of patients. The liver itself is an immune organ, with rich populations of immune cells, and it is also a key organ in regulating glucose metabolism (34). In the process of LIHC development and treatment, changing in metabolism and immune cells play a crucial role. So, a bridge between glucose metabolism and immunotherapy was necessary. According to our results, ACYP1 could be that link, and as a candidate drug target for LIHC intervention.

In conclusion, we demonstrated for the first time the role of ACYP1 in predicting prognosis, and the TME, and associated pathways across cancers. To this end, we confirmed that ACYP1 predicts a poor prognosis and an immunosuppressive TME in LIHC. Overall, ACYP1 has potential as a pancancer prognostic marker from the perspective of tumor immunology and provides a novel target for the treatment of LIHC.

DATA AVAILABILITY STATEMENT

The datasets presented in this study can be found in online repositories. The names of the repository/repositories and accession number(s) can be found in the article/**Supplementary Material**.

ETHICS STATEMENT

The studies involving human participants were reviewed and approved by Tianjin Medical University Cancer Institute and the hospital ethics Committee. The patients/participants provided their written informed consent to participate in this study. The animal study was reviewed and approved by Animal Ethics Committee of Tianjin Medical University.

AUTHOR CONTRIBUTIONS

LZ: Formal analysis, Investigation, Writing - Original Draft. ZF: Methodology, Data Curation. SW: Conceptualization, Software. JJ: Validation, Visualization. YC: Data Curation, Resources. YZ: Resources. NZ: Software, Resources. WL: Supervision. ZY: Writing - Review & Editing, Supervision, Funding acquisition. All authors contributed to the article and approved the submitted version.

FUNDING

This work was supported by a grant from the General Program of National Natural Science Foundation of China [82173199].

ACKNOWLEDGMENTS

We would like to acknowledge Tianjin Medical University Cancer Institute and Hospital for providing us with paraffin tissue specimens from LIHC patients.

SUPPLEMENTARY MATERIAL

The Supplementary Material for this article can be found online at: https://www.frontiersin.org/articles/10.3389/fonc.2022.875097/full#supplementary-material

REFERENCES

1. Stefani M, Taddei N, Ramponi G. Insights Into Acylphosphatase Structure and Catalytic Mechanism. *Cell Mol Life Sci CMLS* (1997) 53(2):141–51. doi: 10.1007/pl00000585
2. Fiaschi T, Raugei G, Marzocchini R, Chiarugi P, Cirri P, Ramponi G. Cloning and Expression of the Cdna Coding for the Erythrocyte Isoenzyme of Human Acylphosphatase. *FEBS Lett* (1995) 367(2):145–8. doi: 10.1016/0014-5793(95)00553-l
3. Liguri G, Nassi P, Degl'Innocenti D, Tremori E, Nediani C, Berti A, et al. Acylphosphatase Levels of Human Erythrocytes During Cell Ageing. *Mech Ageing Dev* (1987) 39(1):59–67. doi: 10.1016/0047-6374(87)90086-8
4. Degl'Innocenti D, Marzocchini R, Rosati F, Cellini E, Raugei G, Ramponi G. Acylphosphatase Expression During Macrophage Differentiation and Activation of U-937 Cell Line. *Biochimie* (1999) 81(11):1031–5. doi: 10.1016/s0300-9084(99)00333-8
5. Cecchi C, Liguri G, Fiorillo C, Bogani F, Gambassi M, Giannoni E, et al. Acylphosphatase Overexpression Triggers Sh-Sy5y Differentiation Towards Neuronal Phenotype. *Cell Mol Life Sci CMLS* (2004) 61(14):1775–84. doi: 10.1007/s00018-004-4192-y
6. Nassi P, Liguri G, Nediani C, Taddei N, Ramponi G. Increased Acylphosphatase Levels in Erythrocytes, Muscle and Liver of Tri-Iodothyronine Treated Rabbits. *Hormone Metab Res* (1990) 22(1):33–7. doi: 10.1055/s-2007-1004843
7. Chiarugi P, Raugei G, Marzocchini R, Fiaschi T, Ciccarelli C, Berti A, et al. Differential Modulation of Expression of the Two Acylphosphatase Isoenzymes by Thyroid Hormone. *Biochem J* (1995) 311(Pt 2):567–73. doi: 10.1042/bj3110567
8. Li M, Ruan B, Wei J, Yang Q, Chen M, Ji M, et al. Acyp2 Contributes to Malignant Progression of Glioma Through Promoting Ca(2+) Efflux and Subsequently Activating C-Myc and Stat3 Signals. *J Exp Clin Cancer Res: CR* (2020) 39(1):106. doi: 10.1186/s13046-020-01607-w
9. Cao J, Wei J, Yang P, Zhang T, Chen Z, He F, et al. Genome-Scale Crispr-Cas9 Knockout Screening in Gastrointestinal Stromal Tumor With Imatinib Resistance. *Mol Cancer* (2018) 17(1):121. doi: 10.1186/s12943-018-0865-2
10. Wen F, Huang J, Lu X, Huang W, Wang Y, Bai Y, et al. Identification and Prognostic Value of Metabolism-Related Genes in Gastric Cancer. *Aging* (2020) 12(17):17647–61. doi: 10.18632/aging.103838
11. Ye Z, Zheng M, Zeng Y, Wei S, Huang H, Wang Y, et al. A 13-Gene Metabolic Prognostic Signature Is Associated With Clinical and Immune Features in Stomach Adenocarcinoma. *Front Oncol* (2021) 11:612952. doi: 10.3389/fonc.2021.612952
12. Cui L, Xue H, Wen Z, Lu Z, Liu Y, Zhang Y. Prognostic Roles of Metabolic Reprogramming-Associated Genes in Patients With Hepatocellular Carcinoma. *Aging* (2020) 12(21):22199–219. doi: 10.18632/aging.104122
13. Sakano Y, Noda T, Kobayashi S, Kitagawa A, Iwagami Y, Yamada D, et al. Clinical Significance of Acylphosphatase 1 Expression in Combined Hcc-Icca, Hcc, and Icca. *Dig Dis Sci* (2021). doi: 10.1007/s10620-021-07266-x
14. DePeaux K, Delgoffe GM. Metabolic Barriers to Cancer Immunotherapy. *Nat Rev Immunol* (2021) 21(12):785–97. doi: 10.1038/s41577-021-00541-y
15. Oliff A. The Role of Tumor Necrosis Factor (Cachectin) in Cachexia. *Cell* (1988) 54(2):141–2. doi: 10.1016/0092-8674(88)90543-0
16. Strickland FM, Kripke ML. Immune Response Associated With Nonmelanoma Skin Cancer. *Clinics Plast Surg* (1997) 24(4):637–47.
17. Rago L, Saano V, Auvinen T, Adojaan A, Holma R, Airaksinen MM. The Effect of Chronic Treatment With Peripheral Benzodiazepine Receptor Ligands on Behavior and Gabaa/Benzodiazepine Receptors in Rat. *Naunyn-Schmiedeberg's Arch Pharmacol* (1992) 346(4):432–6. doi: 10.1007/BF00171086
18. Nediani C, Formigli L, Perna AM, Pacini A, Ponziani V, Modesti PA, et al. Biochemical Changes and Their Relationship With Morphological and Functional Findings in Pig Heart Subjected to Lasting Volume Overload: A Possible Role of Acylphosphatase in the Regulation of Sarcoplasmic Reticulum Calcium Pump. *Basic Res Cardiol* (2002) 97(6):469–78. doi: 10.1007/s00395-002-0367-6
19. Nassi P, Nediani C, Liguri G, Taddei N, Ramponi G. Effects of Acylphosphatase on the Activity of Erythrocyte Membrane Ca2+ Pump. *J Biol Chem* (1991) 266(17):10867–71. doi: 10.1016/S0021-9258(18)99099-X
20. Nediani C, Fiorillo C, Marchetti E, Pacini A, Liguri G, Nassi P. Stimulation of Cardiac Sarcoplasmic Reticulum Calcium Pump by Acylphosphatase Relationship to Phospholamban Phosphorylation. *J Biol Chem* (1996) 271(32):19066–73. doi: 10.1074/jbc.271.32.19066
21. Hokin LE, Sastry PS, Galsworthy PR, Yoda A. Evidence That a Phosphorylated Intermediate in a Brain Transport Adenosine Triphosphatase Is an Acyl Phosphate. *Proc Natl Acad Sci USA* (1965) 54(1):177–84. doi: 10.1073/pnas.54.1.177
22. Nassi P, Marchetti E, Nediani C, Liguri G, Ramponi G. Acylphosphatase Induced Modifications in the Functional Properties of Erythrocyte Membrane Sodium Pump. *Biochim Biophys Acta* (1993) 1147(1):19–26. doi: 10.1016/0005-2736(93)90311-m
23. Nassi P, Nediani C, Fiorillo C, Marchetti E, Liguri G, Ramponi G. Modifications Induced by Acylphosphatase in the Functional Properties of Heart Sarcolemma Na+,K+ Pump. *FEBS Lett* (1994) 337(1):109–13. doi: 10.1016/0014-5793(94)80639-x
24. Riley HD, Macnab J, Farrell TJ, Cohn K. The Expression of Acylphosphatase Is Associated With the Metastatic Phenotype in Human Colorectal Tumors. *Carcinogenesis* (1997) 18(12):2453–5. doi: 10.1093/carcin/18.12.2453
25. Deng C, Guo H, Yan D, Liang T, Ye X, Li Z. Pancancer Analysis of Neurovascular-Related NRP Family Genes as Potential Prognostic Biomarkers of Bladder Urothelial Carcinoma. *BioMed Res Int* (2021). doi: 10.1155/2021/5546612
26. Zhang X, He X, Li Y, Xu Y, Chen W, Liu X. MXD3 as an Immunological and Prognostic Factor From Pancancer Analysis. *Front Mol Biosci* (2021) 8:702206. doi: 10.3389/fmolb.2021.702206
27. Ouyang J, Qin G, Liu Z, Jian X, Shi T, Xie L. ToPP: Tumor Online Prognostic Analysis Platform for Prognostic Feature Selection and Clinical Patient Subgroup Selection. *iScience* (2021) 39. doi: 10.2139/ssrn.3900664
28. Feng J, Li J, Wu L, Yu Q, Ji J, Wu J, et al. Emerging Roles and the Regulation of Aerobic Glycolysis in Hepatocellular Carcinoma. *J Exp Clin Cancer research: CR* (2020) 39(1):126. doi: 10.1186/s13046-020-01629-4
29. Li W, Tanikawa T, Kryczek I, Xia H, Li G, Wu K, et al. Aerobic Glycolysis Controls Myeloid-Derived Suppressor Cells and Tumor Immunity *Via* a Specific Cebpb Isoform in Triple-Negative Breast Cancer. *Cell Metab* (2018) 28(1):87–103.e6. doi: 10.1016/j.cmet.2018.04.022
30. Zhang Y, Yu G, Chu H, Wang X, Xiong L, Cai G, et al. Macrophage-Associated Pgk1 Phosphorylation Promotes Aerobic Glycolysis and Tumorigenesis. *Mol Cell* (2018) 71(2):201–15.e7. doi: 10.1016/j.molcel.2018.06.023
31. Li L, Liu X, Sanders KL, Edwards JL, Ye J, Si F, et al. Tlr8-Mediated Metabolic Control of Human Treg Function: A Mechanistic Target for Cancer Immunotherapy. *Cell Metab* (2019) 29(1):103–23.e5. doi: 10.1016/j.cmet.2018.09.020
32. Shi LZ, Wang R, Huang G, Vogel P, Neale G, Green DR, et al. Hif1alpha-Dependent Glycolytic Pathway Orchestrates a Metabolic Checkpoint for the Differentiation of Th17 and Treg Cells. *J Exp Med* (2011) 208(7):1367–76. doi: 10.1084/jem.20110278
33. Kempkes RWM, Joosten I, Koenen H, He X. Metabolic Pathways Involved in Regulatory T Cell Functionality. *Front Immunol* (2019) 10:2839. doi: 10.3389/fimmu.2019.02839
34. Keenan BP, Fong L, Kelley RK. Immunotherapy in Hepatocellular Carcinoma: The Complex Interface Between Inflammation, Fibrosis, and The Immune Response. *J Immunother Cancer* (2019) 7(1):267. doi: 10.1186/s40425-019-0749-z

Conflict of Interest: Authors ZF and JJ were employed by Tianjin Kangzhe Pharmaceutical Technology Development Company, Ltd.

The remaining authors declare that the research was conducted in the absence of any commercial or financial relationships that could be construed as a potential conflict of interest.

Publisher's Note: All claims expressed in this article are solely those of the authors and do not necessarily represent those of their affiliated organizations, or those of the publisher, the editors and the reviewers. Any product that may be evaluated in this article, or claim that may be made by its manufacturer, is not guaranteed or endorsed by the publisher.

frontiers | Frontiers in Oncology

ORIGINAL RESEARCH
published: 17 May 2022
doi: 10.3389/fonc.2022.877194

The Acquired Vulnerability Caused by CDK4/6 Inhibition Promotes Drug Synergism Between Oxaliplatin and Palbociclib in Cholangiocarcinoma

*Orawan Suppramote[1,2], Sunisa Prasopporn[1], Satinee Aroonpruksakul[1], Ben Ponvilawan[1], Jiradej Makjaroen[3], Monthira Suntiparpluacha[1], Krittiya Korphaisarn[4], Komgrid Charngkaew[5], Rawisak Chanwat[6], Trairak Pisitkun[3], Seiji Okada[7], Somponnat Sampattavanich[1] and Siwanon Jirawatnotai[1]**

[1] Siriraj Center of Research Excellence (SiCORE) for Systems Pharmacology, Department of Pharmacology, Faculty of Medicine Siriraj Hospital, Mahidol University, Bangkok, Thailand, [2] Princess Srisavangavadhana College of Medicine, Chulabhorn Royal Academy, Bangkok, Thailand, [3] Center of Excellence in Systems Biology, Faculty of Medicine, Chulalongkorn University, Bangkok, Thailand, [4] Division of Medical Oncology, Department of Medicine, Faculty of Medicine Siriraj Hospital, Mahidol University, Bangkok, Thailand, [5] Department of Pathology, Faculty of Medicine Siriraj Hospital, Mahidol University, Bangkok, Thailand, [6] Hepato-Pancreato-Biliary Surgery Unit, Department of Surgical Oncology, National Cancer Institute, Bangkok, Thailand, [7] Division of Hematopoiesis, Joint Research Center for Human Retrovirus Infection, Kumamoto University, Kumamoto, Japan

OPEN ACCESS

Edited by:
Zongli Zhang,
Qilu Hospital of Shandong University, China

Reviewed by:
Philipp Kaldis,
Lund University, Sweden
Jinghan Wang,
Shanghai East Hospital, China

***Correspondence:**
Siwanon Jirawatnotai
siwanon.jir@mahidol.ac.th

Specialty section:
This article was submitted to Cancer Molecular Targets and Therapeutics, a section of the journal Frontiers in Oncology

Received: *16 February 2022*
Accepted: *12 April 2022*
Published: *17 May 2022*

Citation:
Suppramote O, Prasopporn S, Aroonpruksakul S, Ponvilawan B, Makjaroen J, Suntiparpluacha M, Korphaisarn K, Charngkaew K, Chanwat R, Pisitkun T, Okada S, Sampattavanich S and Jirawatnotai S (2022) The Acquired Vulnerability Caused by CDK4/6 Inhibition Promotes Drug Synergism Between Oxaliplatin and Palbociclib in Cholangiocarcinoma. Front. Oncol. 12:877194. doi: 10.3389/fonc.2022.877194

Cholangiocarcinoma (CCA) is one of the most difficult to treat cancers, and its nature of being largely refractory to most, if not all, current treatments results in generally poor prognosis and high mortality. Efficacious alternative therapies that can be used ubiquitously are urgently needed. Using acquired vulnerability screening, we observed that CCA cells that reprofile and proliferate under CDK4/6 inhibition became vulnerable to ribosomal biogenesis stress and hypersensitive to the anti-ribosome chemotherapy oxaliplatin. CCA cells overexpress the oncogenic ribosomal protein RPL29 under CDK4/6 inhibition in a manner that correlated with CDK4/6 inhibitor resistance. Depletion of RPL29 by small interfering RNAs (siRNAs) restored the sensitivity of CCA cells to CDK4/6 inhibition. Oxaliplatin treatment suppressed the RPL29 expression in the CDK4/6 inhibitor treated CCA cells and triggered RPL5/11-MDM2-dependent p53 activation and cancer apoptosis. In addition, we found that combination treatment with oxaliplatin and the CDK4/6 inhibitor palbociclib synergistically inhibited both parental and CDK4/6 inhibitor-resistant CCA, and prevented the emergence of CDK4/6 and oxaliplatin-resistant CCA. This drug combination also exerted suppressive and apoptosis effects on CCA in the *in vitro* 3-dimensional culture, patient-derived organoid, and *in vivo* xenograft CCA models. These results suggest the combination of the CDK4/6 inhibitor palbociclib and the anti-ribosome drug oxaliplatin as a potentially promising treatment for cholangiocarcinoma.

Keywords: acquired vulnerability, ribosomal biogenesis stress, CDK4/6 inhibitor, oxaliplatin, cholangiocarcinoma (CCA), palbociclib

INTRODUCTION

Cholangiocarcinoma (CCA) is a highly lethal gastrointestinal malignancy that has one of the worst prognoses among solid tumors. Most patients with CCA are diagnosed at a late stage. Although, surgery is the only curative treatment; most patients are ineligible for tumor resection. Gemcitabine plus cisplatin is recommended as first-line treatment for advanced stage disease with objective response rate only 25 percent (1).

Although novel molecular targetable mutations, such as activating IDH1/2 mutations and FGFR fusions, have been identified, these mutations present in only a small percentage of patients (2). Almost all patients eventually experience disease progression while on first-line systemic therapy and succumb to their disease. Therefore, novel therapeutic drugs/strategies to treat CCA are urgently needed. Targeted therapies that can be broadly applied do not yet exist, because CCA includes genetically heterogeneous tumors with no single major molecular driver (3–8).

Previously reported evidence showed that deregulation of genes that encode cell cycle regulators is common in CCA, which highlights cell cycle inhibition as a logical strategy for CCA treatment (9), and several preclinical studies, including our work, have reported corroborating evidence (10–12). However, a clinical study in CDK4/6 inhibitor monotherapy for CCA fell short of expectations (13). There are some hypotheses that may explain the aforementioned disappointing results. For one thing, the shortcoming in clinical level may be a result of a failure to identify the CCA with suitable molecular profiles for the CDK4/6 inhibition. Second, the efficacy of CDK4/6 inhibitor monotherapy may be compromised by the emergence of acquired drug resistance, which can develop rapidly. These challenges will need to be overcome to leverage the benefit of the cell cycle inhibitors in CCA. Considering the inevitable emergence of drug resistance, identification of rational combinations is an appealing concept, and one of the most active fields of study in cancer drug resistance (14).

It has been demonstrated that cancer cells that are being treated with drugs try to adapt and reprofile their molecular networks to survive, proliferate, and become drug-resistant. This adaptation comes at a fitness cost of some collateral physical characters, which may result in an acquired vulnerability (acquired sensitivity) within the drug-resistant cancer cell (15).

In the present study, we hypothesized that while under strong CDK4/6 inhibition, CCA cells would reprofile their molecular networks and, as a result, become dependent on a new converged biological process/pathway to survive the inhibition. We then set forth to identify the newly emerging therapeutic targets in CDK4/6 inhibitor-resistant cancer cells by leveraging the acquired vulnerability of the cancer cells that grew under CDK4/6 inhibition in the hope that inhibition of the novel target would synergize with CDK4/6 inhibition and prohibit the escape of CCA from CDK4/6 inhibition. We performed acquired vulnerability screening and analyzed pathway reprofiling in CDK4/6 inhibitor-resistant CCA. Our results revealed an acquired vulnerability of resistant CCA cells to ribosome biogenesis stress, and drug synergism between CDK4/6 inhibitor and a drug already used in the treatment of CCA, oxaliplatin. We also uncovered the mechanistic basis for the observed drug synergism, and validated the efficacy of this drug combination in both *in vitro* and *in vivo* CCA models, which facilitates direct translation for clinical investigation of these findings.

MATERIALS AND METHODS

Cell Culture and the Establishment of Resistant Cell Lines

KKU-055 and KKU-213B cell lines were obtained from the Japanese Collection of Research Bioresources (JCRB) Cell Bank (Osaka, Japan). The culture methods were previously described (10). Cell lines were routinely tested for mycoplasma. Palbociclib-resistant cell lines and single-resistant clones were generated as previously described (16, 17).

Cell Viability Assay

Palbociclib, ribociclib, abemaciclib, oxaliplatin, cisplatin, and actinomycin D were purchased from Selleck Chemicals (Houston, TX, USA). Phenanthriplatin was generously provided by Professor Stephen J Lippard of the Department of Chemistry, Massachusetts Institute of Technology, Boston, MA, USA. Drug testing in resistant cell lines and 3-demensional (3D) spheroids was performed as previously described (10).

Western Blotting and Immunoprecipitation Assay

The whole-cell lysates were prepared by lysis in 0.5% NP-40 buffer (NP-40, 1 M HEPES pH 7.4, 5M NaCl, 0.5M EDTA pH 8) supplemented with a protease inhibitor and a phosphatase inhibitor (Thermo, 78420, USA). The nuclear-cytoplasmic fractionation lysates were prepared using cytoplasmic buffer (10 mM HEPES, 1.5 mM MgCl2, 10 mM KCl, 0.5 mM DTT, 0.05% NP-40, pH 7.9) and nucleoplasmic buffer (5 mM HEPES, 1.5 mM MgCl2, 0.2 mM EDTA, 0.5 mM DTT, 26% glycerol, pH 7.9). Equal amounts of lysate were used for Western blotting as previously described (10). Immunoprecipitation was performed according to standard protocol (18).

Immunofluorescence Staining

Cells were seeded in six-well plates at a 2,000 cell/well density and incubated for 24 hours. The next day, the culture medium was removed and new culture medium treated with 5 μM oxaliplatin, 0.5 μM cisplatin, or Vehicle was added into different wells and reincubated for 24 hours (10).

Proteomic Analysis by Quantitative Mass Spectrometry

Two palbociclib-resistant clones (KKU-055R29 and KKU-055R30) and the KKU-055wt were selected for 3-plex dimethyl labeling proteomic analysis. The cells were lysed in 8 M urea lysis buffer containing protease and phosphatase inhibitors (Thermo, 78420, USA). Equal amounts of whole-cell lysate were digested,

labeled, fractionated, and subjected to liquid chromatography-tandem mass spectrometry (LC-MS/MS) using the Q Exactive™ Plus Hybrid Quadrupole-Orbitrap™ mass spectrometer as previously described (19). The raw data were analyzed for protein identification and relative quantification using MaxQuant software (Max Planck Institute of Biochemistry, Planegg, Germany). The files were searched against the human UniProt database (August 2019) using previously described search parameters (19). Proteins matched the reverse database and contaminants were excluded, and imputed missing values were derived from the normal distribution (width: 0.3, downshift: 0.5). The pathway analysis was performed and the statistics were calculated using Perseus software (version 1.6.14.0, Max Planck Institute of Biochemistry).

Gene Set Enrichment Analysis

Gene expression profile from the Kyoto Encyclopedia of Genes and Genomes (KEGG) ribosome signature gene set (88 genes by gene family) analysis was performed as previously described (10). The normalized enrichment score was calculated, and the genes with a positive rank metric score were specified.

In Vivo Studies

The protocols for all *in vivo* experiments in this study were approved by the Mahidol University – Institute Animal Care and Use Committee. Experiments were performed as previously described (10). A total of 10×10^6 of KKU-055 cells was subcutaneously injected into female 2-month-old non-obese diabetic/severe combined immunodeficiency (NOD/SCID) mice, and the resulting tumor was allowed to grow to 0.5 cm in diameter. After that, 75 mg/kg palbociclib was administered daily *via* oral gavage until the tumor re-grew during treatment to obtain a palbociclib-resistant tumor. The palbociclib-resistant tumor was then excised and engrafted into a new cohort of study mice. After confirmation of tumor engraftment, 75 mg/kg palbociclib daily *via* oral gavage, 5 mg/kg oxaliplatin weekly *via* intraperitoneal injection, or the combination of both was given to tumor engrafted study mice. Hematoxylin and eosin (H&E) staining of mouse tumor tissues was performed according to standard protocol (10).

Drug Testing in Patient-Derived Organoids

The study protocol was approved by the Institutional Review Board for Human Research (SI494/2019 and NCI006/2020). Intrahepatic CCA tissues were pasted using surgical blades and then washed with 12 ml of wash media (advanced DMEM/F12 containing 1 x Glutamax™ (Thermo, 10565018, USA), 10 mM HEPES, and 100 U/ml Penicillin/Streptomycin). The tissue paste was collected by centrifugation at 400 x g, 4°C for 5 min, then digested with 5 ml of the wash media containing 2 mg/ml collagenase D at 37°C for 30 min. Undigested tissues were filtered out with cell strainers. The cells were embedded in 70% matrigel and cultured in organoid culture media (20) until organoids formed. The organoids were dissociated into single cells by incubating with 1 ml of TrypLE™ Express (Gibco, 12604021, USA) at 37°C for 5 min. In a 384-well plate format, the cells suspended in organoid culture media containing 5% matrigel were plated at 1000 cells/well, and incubated for 72 h. Eight concentrations of each drug with the following final concentrations: Palbociclib at 10, 5, 1, 0.5, 0.25, 0.125, 0.062, and 0.031 mM; Oxaliplatin at 100, 50, 10, 5, 2.5, 1.25, 0.62, and 0.31 mM; Palbociclib plus Oxaliplatin combination at 1:1 ratio, were added and incubated for 5 days. Cell viability was measured using ATPlite™ Luminescence Assay System (Perkin Elmer, Waltham, MA, USA) following the manufacturer's instruction, and the cell viability percentages were calculated by normalizing with non-treated control (0.05% DMSO).

Statistical Analysis

Unless otherwise stated, comparison was made and statistical significance was determined between groups using a two-sided Student's t-test. A p-value of less than 0.05 was considered statistically significant for all tests. Data are shown as the mean ± standard deviation (SD) of at least 3 experiments. Analysis of variance (ANOVA) or Kruskal-Wallis test was used for comparisons among 3 or more groups.

RESULTS

Characterization of CDK4/6 Inhibitor-Resistant CCA Cells

To investigate acquired vulnerability in CCA cells that proliferate despite CDK4/6 inhibition, we developed the CDK4/6 inhibitor-resistant CCA cell lines KKU-055R and KKU-213BR from parental KKU-055 (KKU-055wt) and KKU-213B (KKU-213Bwt) cells by culturing the parental cells with the CDK4/6 inhibitor palbociclib using a step-wise dosing protocol (**Figure 1A**). The KKU-055R and KKU-213BR palbociclib GR50s were 18.57- and 15.53-fold higher than that of the parental cells, respectively (**Figure 1B**). We isolated and expanded up to 29 single cells (clones) from KKU-055R, and 13 clones from KKU-213BR to study various mechanisms of CDK4/6 inhibitor resistance (**Figure 1A**). We validated that these drug-resistant clones were resistant to the all of the FDA-approved CDK4/6 inhibitors (i.e., palbociclib, ribociclib, and abemaciclib) (**Figures 1C, D**, and **Supplementary Figures 1A, B**). The resistant clones divided under CDK4/6 inhibitor treatments with varied rates and doubling times, which suggests heterogeneous behavior among the cells (**Figures 1E, F**). We then explored the mechanisms of drug resistance in 12 randomly selected KKU-055R clones by immunoblotting (**Supplementary Figure 1C**). Virtually all of the representative clones demonstrated altered levels of proteins previously reported to be associated with CDK4/6 inhibitor resistance (21). More specifically, clones 8, 18, and 30 showed pRB downregulation; clones 12, 15, 18, 27, 28, and 29 showed CDK4-Cyclin Ds downregulation and cyclin E upregulation; and, clones 12, 15, 27, 28, and 30 showed CDK6 overexpression that correlated with slight upregulation of phospho-S6 kinase. These results indicated that we had established CDK4/6 inhibitor-resistant CCA clones that had

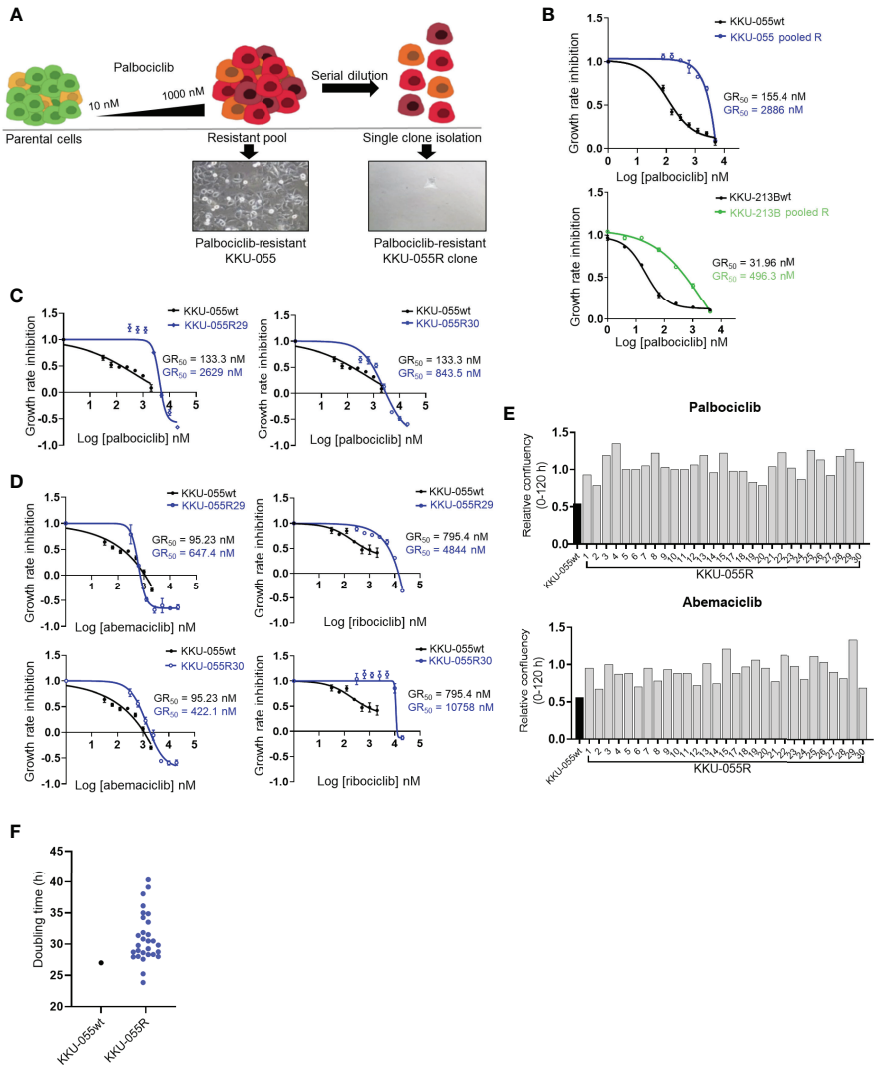

FIGURE 1 | Characterization of CDK4/6 inhibitor-resistant CCA cells. **(A)** Palbociclib-resistant KKU-055 and KKU-213B CCA cells (KKU-055 pooled R, and KKU-213B pooled R) were generated using a step-wise dosing protocol, and then isolated into single clones *via* serial dilution. All resistant cells were maintained in 1 μM palbociclib. **(B)** Palbociclib dose-response curves for parental KKU-055wt and pooled resistant cells. Error bars represent standard deviation of triplicate cultures. **(C)** Palbociclib dose-response curves for KKU-055wt and resistant clones. Error bars represent standard deviation of triplicate cultures. **(D)** Abemaciclib and ribociclib dose-response curves for KKU-055wt and resistant clones. Error bars represent standard deviation of triplicate cultures. **(E)** Relative confluencies of resistant KKU-055 clones compared to KKU055wt under 140 nM palbociclib or 100 nM abemaciclib treatment at 120 hours. **(F)** Doubling time of KKU-055wt and twenty-nine KKU-055-resistant clones.

developed varied adaptive molecular profiles to survive under CDK4/6 inhibitor treatment.

Acquired Vulnerability Screening Uncovered Hypersensitivity of CDK4/6 Inhibitor-Resistant Clones to Ribosome Biogenesis Stress

We used the IncuCyte® Live-Cell Analysis System to perform acquired vulnerability screening by comparing the 5-day growth curves of twenty-nine resistant KKU-055R clones to the growth curves of KKU-055wt while under treatment with individual drugs from a small cancer drug library that covered 25 cancer pathways plus commonly used chemotherapies. We defined acquired vulnerability as positive when the average (n=4) area under the curve (AUC) of a resistant clone was smaller than the AUC of the parental cell by at least two fold (**Figure 2A**). As expected, we found all of the KKU-055R clones to universally resistant to all 3 of the CDK4/6 inhibitors (i.e., palbociclib, ribociclib, and abemaciclib) [**Figure 2B** (blue color indicates less sensitivity to a drug compared to the sensitivity observed in KKU-055wt]. None of the resistant clones acquired vulnerability to the standard first-line CCA chemotherapy gemcitabine or cisplatin, except clone 12, which developed sensitivity to cisplatin (shown in red). We also found

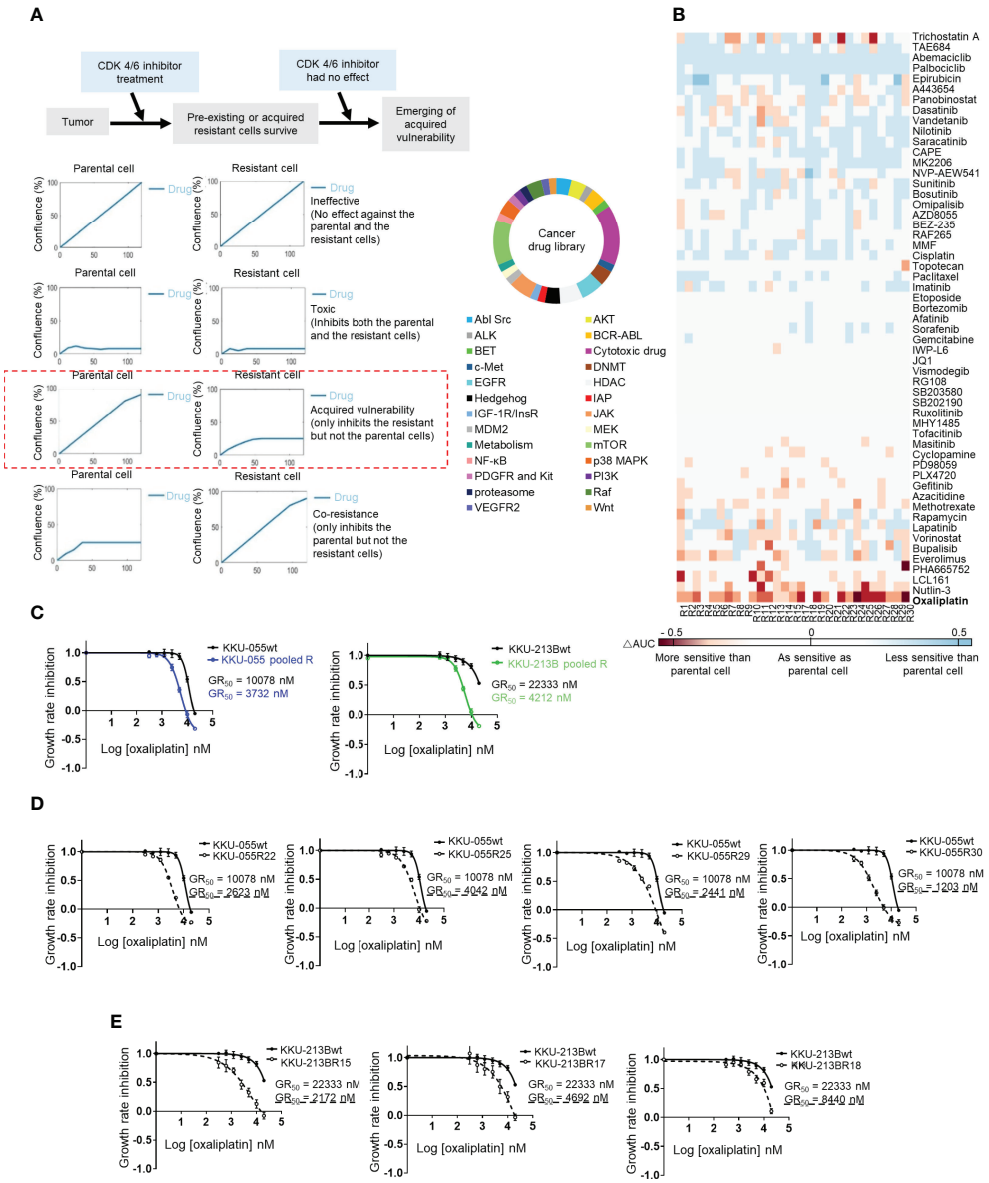

FIGURE 2 | Cancer drug library screening reveal the acquired vulnerability of CDK4/6 inhibitor-resistant clones to ribosome biogenesis stress. **(A)** Acquired vulnerability concept (top). Drugs were considered to be acquired vulnerability-positive when the 5-day area under the cell proliferation curve (AUC) of a resistant clone was lower than 50% of the AUC of the parental cell (left). A small cancer drug library (right). **(B)** Heat map showing the relative sensitivity of each KKU-055-resistant clone compared to KKU-055wt (less sensitive: blue, more sensitive: red). **(C)** Oxaliplatin dose-response curves for KKU-055wt, KKU-213B, and their pooled resistant cells. **(D)** Oxaliplatin dose-response curves for KKU-055wt and resistant clones. **(E)** Oxaliplatin dose-response curves for KKU-213Bwt and resistant clones.

that several resistant clones became hypersensitive to mTOR inhibitors [i.e., everolimus (13/29 clones), and rapamycin (6/29 clones)] (**Figure 2B**), which is consistent with previous findings from breast cancer studies that investigated whether targeting activated PI3K/mTOR signaling may overcome acquired resistance to CDK4/6-based therapies (21–23). Unexpectedly, we found that most of the resistant clones (25/29 clones, 86.2%) had acquired sensitivity to oxaliplatin, which is a platinum agent that is used in combination with fluoropyrimidine, or gemcitabine as one of the standard second-line CCA treatment (**Figure 2B**, **Supplementary Figure 2A**). To validate the acquired vulnerability to oxaliplatin, we generated oxaliplatin dose-response curves for several KKU-055R and KKU-213BR clones, as well as for pools of KKU-055R, and KKU-213BR cells. We found a consistent reduction in oxaliplatin GR50s in all the clones and pooled resistant cells (**Figures 2C–E**). Oxaliplatin is an atypical platinum agent, which unlike the prototypical cisplatin, kills cancer cells by interfering with ribosome biogenesis (24). Clonogenic survival assay confirmed that the resistant clones were more sensitive to oxaliplatin compared to KKU-055wt cells (**Supplementary**

Figure 2B). We then tested the relative sensitivity of the resistant clones to other drugs known to interfere with ribosomal biogenesis, such as phenanthriplatin (24) and actinomycin D. We found most of the KKU-055R and 213BR clones tested and the pooled resistant clones to be vulnerable to anti-ribosome biogenesis drugs (**Supplementary Figures 2C–H**). To further confirm the target of oxaliplatin in the ribosomal pathway, we also treated CCA cells with omacetaxine, which is a ribosome inhibitor whose anti-cancer function relies on intact ribosome function. We found that increasing the dose of oxaliplatin antagonized the anti-cancer activity of omacetaxine, which suggests that both drugs exploit a similar biological pathway to inhibit cancer cells (**Supplementary Figure 3A**). Of note, the observed antagonism was more noticeable in resistant KKU-055R cells compared to the parental cells, which suggests a more pronounced ribosomal dependency in the resistant cells. In addition, to exclude the possibility that resistant cells acquired a vulnerability to DNA damage-induced killing, we treated KKU-055R clones with various doses of cisplatin. We found that none of the resistant clones acquired sensitivity to cisplatin compared to the KKU-055wt (**Supplementary Figure 3B**). We, therefore, concluded that our acquired vulnerability screen had uncovered an acquired vulnerability to ribosomal biogenesis stress that may be targeted by oxaliplatin, an anti-ribosomal biogenesis drugs.

Altered Ribosome Expressions in CDK4/6 Inhibitor-Resistant CCA Cells

To understand the acquired sensitivity to anti-ribosome biogenesis agents, we quantitatively analyzed the proteomic profiles of resistant clones. We selected KKU-055R30 with a low level of pRB, and KKU-055R29 with cyclin E overexpression to compare with KKU-055wt cells. We found quite similar proteomic changes in both resistant clones. Top changes that were shared between the two resistant clones were cell cycle (p=0.0000017 vs. p=0.0000013), amino acid and glucose metabolism (p=0.0000014 vs. p=0.0000085), phagocytosis (p=0.0000031 vs. p=0.000023), regulation of actin (p=0.00000078 vs. p=0.0000058), and ribosomal proteins (p=0.0000044 vs. p=0.000013), all respectively (**Figure 3A**). As a result of the acquired vulnerability to anti-ribosomal biogenesis agents observed in the resistant cells, we focused on common changes in ribosomal proteins. We found significant enrichment of 15, and 10 ribosomal proteins in KKU-055R29, and KKU-055R30, respectively (**Figure 3B**). Individually, Ribosomal Protein (RP) Large subunit 29 (RPL29) was the most significantly upregulated in both resistant cells compared to KKU-055wt (**Figure 3C**).

Interestingly, we found the levels of RPL29 in resistant cells to be associated with drug treatment. More specifically, RPL29 was upregulated under palbociclib treatment, but it was downregulated under oxaliplatin treatment (**Figure 3D** and **Supplementary Figures 4A, B**). This finding suggests a functional role of RPL29 in CCA survival under these two treatments. Interestingly, the level of RPL29 was also suppressed in oxaliplatin treatment in spite of palbociclib treatment (**Supplementary Figure 4B**). The drug-induced ribosomal changes were specific to RPL29, but not to the other key RPs in the ribosome checkpoint pathway, such as RPL5, RPL11, and RPS14 (**Figure 3D**). Of note, cisplatin treatment did not cause any noticeable change in RPL29 expression (**Figure 3E**). Interestingly, we also observed drug-induced changes in RPL29 in the CDK4/6 inhibitor sensitive KKU-055wt cells, in a lesser extent (**Supplementary Figure 4B**), which suggests that drug-induced changes in RPL29 are a consequence of molecular reprofiling in resistant cells. RPL29 is a long half-life protein that was stable for 96 hours under cycloheximide treatment. We found that oxaliplatin significantly shortened the half-life of RPL29 to 20 hours (**Figures 3F, G**). Oxaliplatin had no effect on the half-life of RPL5 or RPL11 (**Figure 5F**). Therefore, to survive CDK4/6 inhibition, CCA cells reprofiled their molecular networks as reflected by drug-induced changes in RPL29. To further investigate whether RPL29 plays an essential role in the survival of the resistant clones, we partially depleted RPL29 by 2 independent sequences of RPL29 siRNA (**Supplementary Figure 4C**). We found that RPL29 siRNA-a, and b, which depleted 50% of the endogenous RPL29, significantly decreased the survival of the resistant clones, and the addition of palbociclib further decreased the survival of the resistant clones (**Figures 3H-J**).

Ribosome Biogenesis Checkpoint-Mediated Activation of p53 in CDK4/6 Inhibitor-Resistant Clones Under Oxaliplatin Treatment

Ribosomal biogenesis is tightly linked to cellular activities, such as growth and cell cycle progression. Perturbation of ribosomal biogenesis can cause nucleolar stress. The process through which RPs transmit nucleolar stress signals *via* MDM2-p53 has been described as a crucial tumor suppression mechanism (25). Downregulation of RPL29 has been linked to p53 activation by RPL5/11 sequestration of MDM2 in the nucleus (18, 26–28). Since we found that oxaliplatin promotes downregulation of RPL29, we hypothesized that oxaliplatin triggers RPL5/11-mediated MDM2 sequestration and p53 activation in CDK4/6 inhibitor-resistant cells.

As shown by the immunoblots in **Figure 4A**, oxaliplatin downregulated RPL29 in all of the resistant clones tested (to a lesser extent in wild-type cells), and promoted relocation of RPL5 and RPL11 from the cytoplasm to the nucleus. We also detected activation of p53 as indicated by elevated p53 S9 phosphorylation, and upregulation of the p53 functional target p21 (**Figure 4A**). Translocation of RPL5 and RPL11 was also confirmed by immunofluorescence staining (**Figure 4B** and **Supplementary Figure 5A**). The drug-induced relocalizations of RPL5 and RPL11 were specific to oxaliplatin – not cisplatin (**Figure 4C** and **Supplementary Figure 5B**).

We demonstrated by co-immunoprecipitation an increase in MDM2-RPL5/11 complex in the resistant cells upon oxaliplatin treatment (**Figure 4D** and **Supplementary Figure 5C**). We also observed the departure of p53 from the MDM2 complex upon oxaliplatin treatment (**Figure 4D**). We, therefore, concluded that under oxaliplatin treatment, RPL29 was suppressed, and RPL5/11 were relocalized to the nucleus to sequestrate MDM2, which caused p53-mediated growth inhibition in the resistant cells (**Figure 4E**).

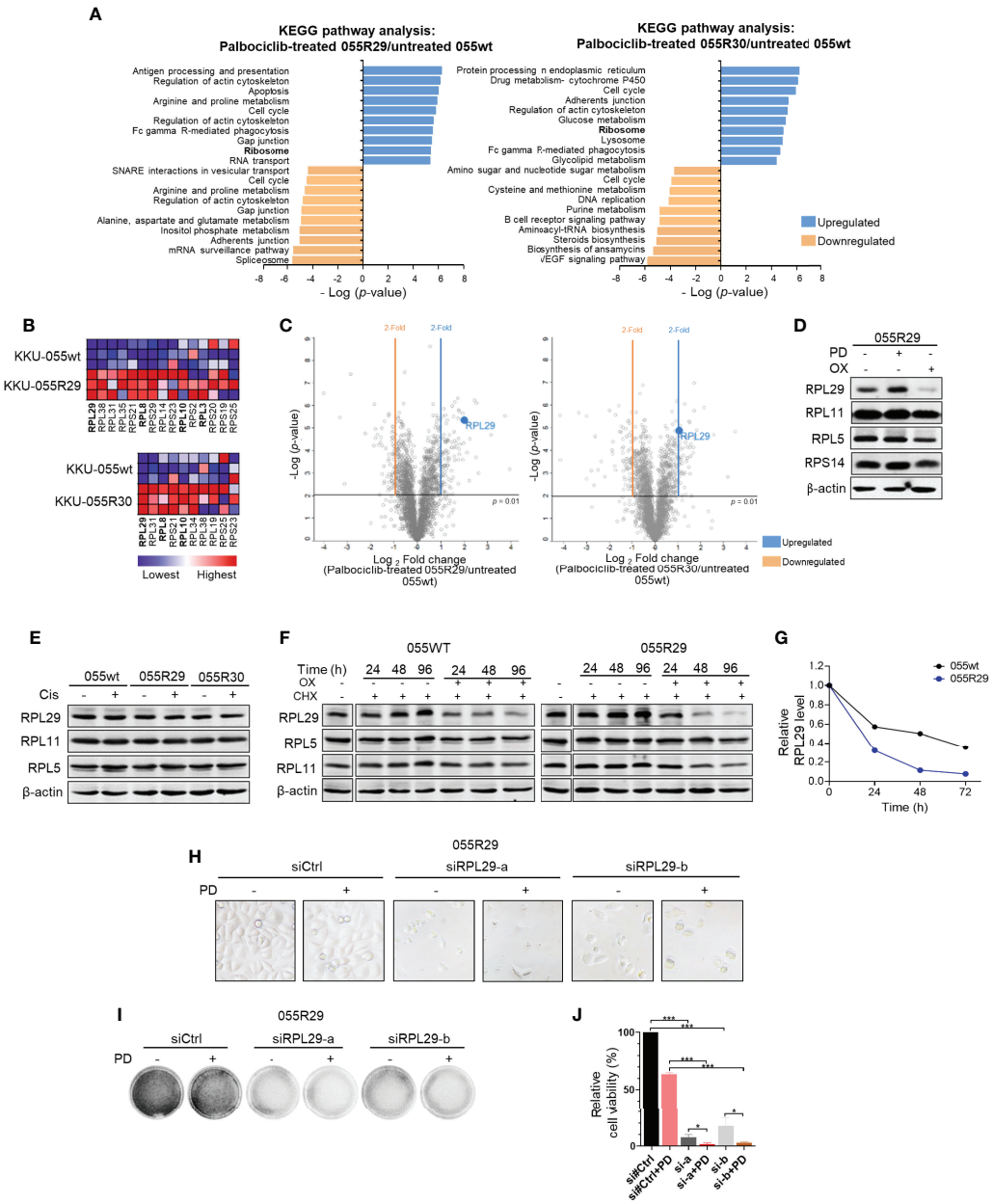

FIGURE 3 | Dysregulated expression of specific ribosomal protein in CDK4/6 inhibitor-resistant CCA cells. **(A)** Kyoto Encyclopedia of Genes and Genomes (KEGG) pathway enrichments in palbociclib-treated KKU-055R29 (left) and KKU-055R30 (right) compared to untreated KKU-055wt. **(B)** Ribosome gene set enrichment shows significant ribosomal protein enrichment in palbociclib-treated KKU-055R29 and KKU-055R30 compared to untreated KKU-055wt ($p<0.05$). The heat map shows the enrichments in triplicate (highest in red, lowest in blue). Ribosomal proteins in the RPL29 complex are shown in bold. **(C)** Volcano plots of protein expressions in palbociclib-treated KKU-055R29 (left) and KKU-055R30 (right) compared to untreated KKU-055wt. **(D)** Western blot analysis of ribosomal proteins in KKU-055-resistant clone R29 after 24 hours of treatment with 1 μM palbociclib, 5 μM oxaliplatin, or vehicle. β-Actin was used as the loading control. **(E)** Western blot analysis of ribosomal proteins in KKU-055wt and KKU-055-resistant clones after 24 hours of treatment with 0.5 μM cisplatin or vehicle. **(F)** Western blot analysis of ribosomal proteins in KKU-055-resistant clone R29 (right) after 24-, 48-, and 96-hours of treatment with vehicle, 0.5 μM cycloheximide, or 0.5 μM cycloheximide combined with 5 μM oxaliplatin. **(G)** Quantitation of RPL29 half-life in KKU-055wt compared to that of KKU-055R. At each time point, the protein amount was quantitated and normalized relative to β-actin. **(H)** Phase-contrast images of KKU-055-resistant clone R29 treated with non-targeting siRNA (siCtrl) or RPL29 siRNAs (siRPL29-a, siRPL29-b) for 48 hours, and then treated with 0.5 uM palbociclib (PD) or vehicle for 72 hours. **(I)** Images of crystal violet staining from H. **(J)** Relative survival from F was quantified. The bars represent the average of 3 replicates ± standard deviation (SD). Analysis for statistical significance was performed using Student's t-test (*p≤0.05, and ***p≤0.001).

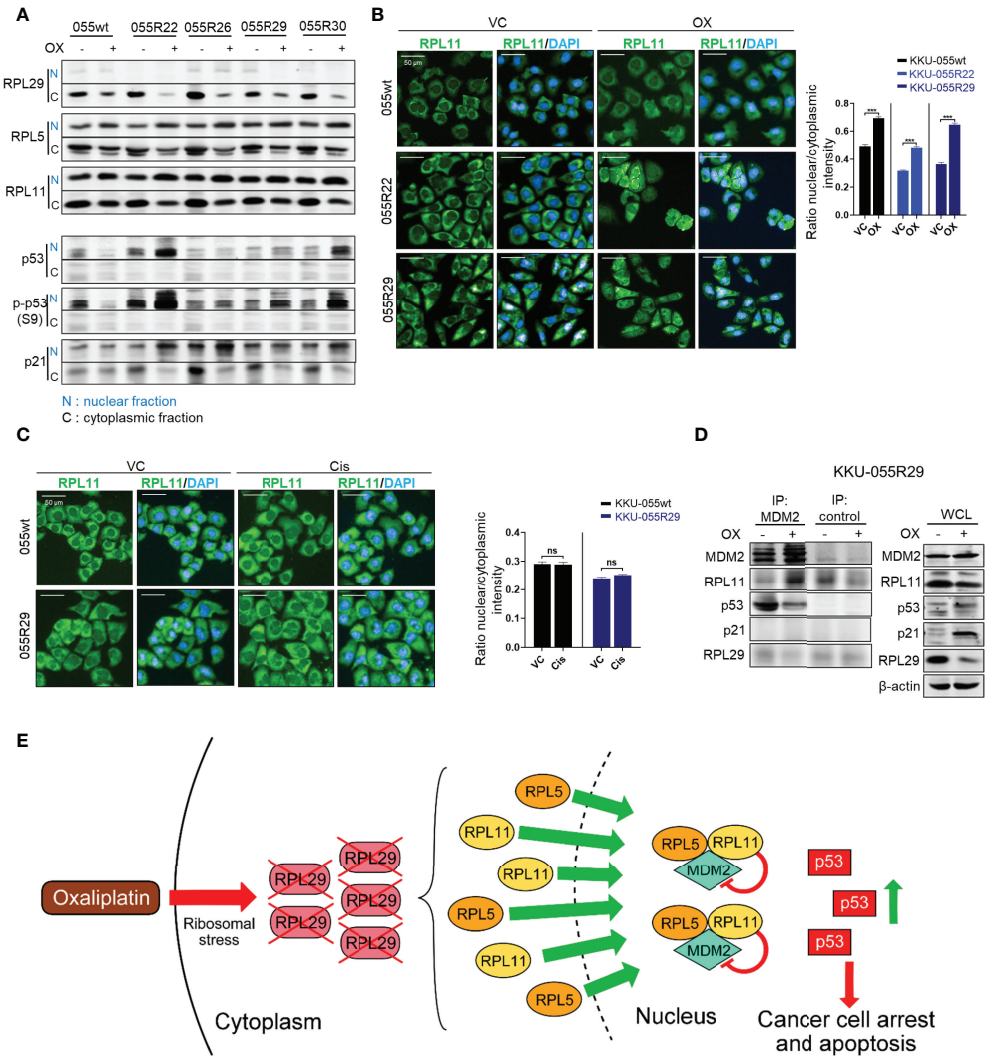

FIGURE 4 | Oxaliplatin treatment promotes growth inhibition in the CDK4/6 resistant clones through p53 activation. **(A)** Western blot analysis of RPL29, RPL5, RPL11, p-p53 (S9), and p21 in the nucleus (N) and cytoplasm **(C)** of KKU-055wt and KKU-055-resistant clones after 24-hours of treatment with 5 μM oxaliplatin or vehicle. **(B, C)** Fluorescence images of RPL11 in KKU-055wt and KKU-055-resistant clones after 24 hours of treatment with 5 μM oxaliplatin (B) or 0.5 μM cisplatin **(C)** compared to vehicle control (VC). DAPI (4′,6-diamidino-2-phenylindole) staining was performed to identify the nucleus. Percent intensity quantification is shown in bar graphs. The bars represent the averages of 3 replicates ± SD. Analysis for statistical significance was performed using Student's t-test (***p≤0.001, ns; not statistically significant). **(D)** Immunoprecipitation of MDM2 interacting proteins in a resistant clone under 24-hours of oxaliplatin treatment. Western blot analysis of the MDM2 interactors is shown on the left, and expressions of endogenous proteins are shown on the right. β-Actin was used as the loading control. **(E)** Schematic of oxaliplatin-induced RPL29 degradation and RPL5/11-MDM2-mediated p53 activation in palbociclib-resistant cells.

Oxaliplatin Synergizes With Palbociclib to Inhibit CDK4/6 Inhibitor-Resistant CCA

We set forth to evaluate the efficacy of CDK4/6 inhibitor and oxaliplatin combination therapy for preventing cancer drug resistance. We performed *in vitro* cancer inhibition assays of different oxaliplatin+palbociclib combinations, and we calculated the combination index (CI) for each combination. We found that most of the evaluated combinations generated synergistic effect (CI <1), and that a higher dose of oxaliplatin produced stronger synergism (**Figure 5A**). Similar results were observed in the phenanthipatin+palbociclib combination (**Supplementary Figure 6A**). Results from isobologram confirmed the synergistic effect between oxaliplatin and palbociclib with 90%, 75%, and 50% growth inhibition (Fa 90, 75, 50, respectively) (**Figure 5B**). These results were also validated in 3D spheroid models (**Supplementary Figure 6B**).

Mechanistically, palbociclib exerts a cytostatic effect *in vitro* (**Figure 5C**). The addition of low-dose oxaliplatin (GR50 of parental KKU-055wt cells) effectuated small upregulation of the dying annexin V-positive KKU-055wt cells. In contrast, it caused

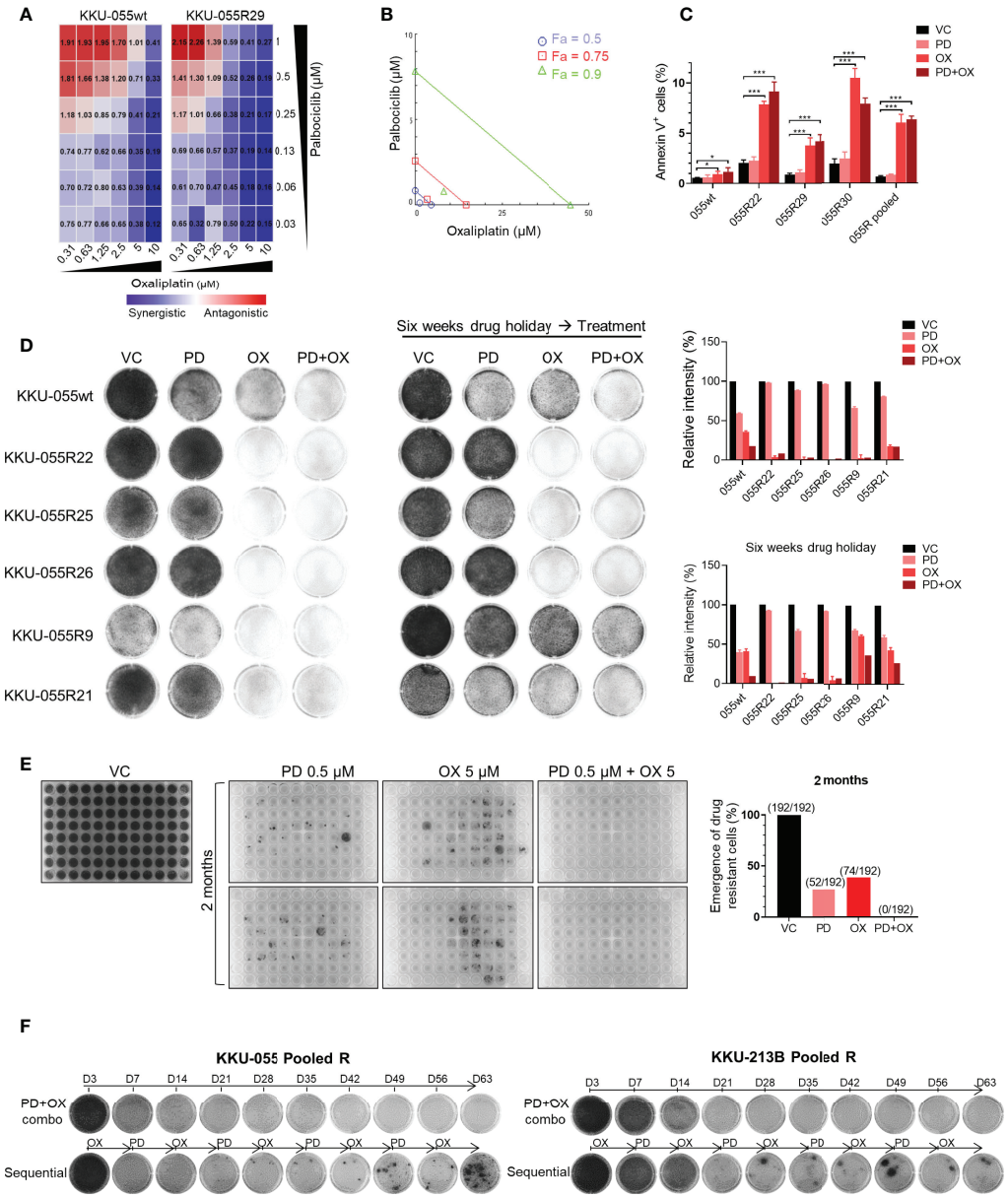

FIGURE 5 | Dual oxaliplatin plus palbociclib synergistically inhibited emergence of drug-resistant cells. **(A)** Combination index matrices of indicated doses of palbociclib and oxaliplatin combination treatment in KKU-055wt and resistant clone R29. Colors in the matrix indicate different levels of drug effect (synergistic: blue, antagonistic: red). **(B)** Isobologram of 0.13 μM palbociclib and 1.25 μM oxaliplatin combination treatment in KKU-055 resistant clone R29. **(C)** Annexin V assay of the KKU-055wt and resistant clones treated with 0.13 μM palbociclib, 4 μM oxaliplatin, the combination of both, or vehicle for 48 hours. Percent annexin V-positive cells quantification is shown in bar graphs. The bars represent the average of 4 replicates ± SD. Analysis for statistical significance was performed using Student's *t*-test (*$p \leq 0.05$, **$p \leq 0.01$, and ***$p \leq 0.001$). **(D)** Clonogenic survival assay of KKU-055wt and resistant clones that were treated with 1 μM palbociclib, 5 μM oxaliplatin, the combination of both, or vehicle (left). The resistant clones were cultured in medium without drug for six weeks (drug holiday), and then treated with 1 μM palbociclib, 5 μM oxaliplatin, the combination of both, or vehicle (middle). The results are representative wells of triplicates. Percent intensity quantification is shown in bar graphs (right), and the bars represent the average of 3 replicates ± SD. **(E)** The emergence of drug-resistant cells was demonstrated by crystal violet staining. Two-month cultures of KKU-055wt cells under 0.5 μM palbociclib, 5 μM oxaliplatin, and the combination of both in 2 of 96-well plates (192 wells). The number of emergences well was counted and plotted in a bar graph (right). **(F)** KKU-055 pooled R and KKU-213B pooled R were treated with the combination of 0.5 μM palbociclib and 5 μM oxaliplatin (upper), or sequentially treated with 5 μM Oxaliplatin for 7 days and followed by 0.5 μM Palbociclib for another 7 days (lower) for 2 months. The emergence of the drug-resistant cell were shown in crystal violet staining.

significant increases in annexin V-positive cells in all resistant clones, as well as in the pooled cells. Similar results were observed in the oxaliplatin + plabociclib combination (**Figure 5C**).

Drug resistance, whether preexisting or acquired, is largely thought to be a stable and heritable process. However, over the past few decades, clinical evidence has suggested the role of unstable (reversible) non-heritable mechanisms of acquired drug resistance that affect chemotherapy and targeted agents. We, therefore, examined whether oxaliplatin can overcome both stable and reversible types of CDK4/6 inhibitor resistance. After a 6-week drug holiday, several CDK4/6 inhibitor-resistant clones (i.e., 22, 25, and 26) retained their CDK4/6 inhibitor resistance, which indicated stable resistance in these clones. In contrast, the resistance to palbociclib was reversed in some clones, such as 9 and 21 (**Figure 5D**), which indicates reversible resistance.

We found oxaliplatin to be effective against both stable and reversible resistance when given to the cells without drug holiday, or when given in combination with palbociclib (**Figure 5D**, left panel). After a 6-week drug holiday, oxaliplatin was still effective against the clones with stable resistance (clones 22, 25, 26). However, oxaliplatin monotherapy was not effective against the cells with reversible resistance. Interestingly, only the oxaliplatin+palbociclib combination was relatively effective against the reversed clones (**Figure 5D**, right panel). These findings indicate that continuous pressure from CDK4/6 inhibition is required to maintain acquired vulnerability to oxaliplatin. We then investigated the application of CDK4/6 inhibitor and oxaliplatin combination for preventing the emergence of drug-resistant cells. We performed long-term cultures of KKU-055wt cells under high doses of palbociclib, oxaliplatin, and the combination of the two for 2 months in 2 of 96-well plates (192 wells) (**Figure 5E**). Within 2 months, we found that 52 (27.1%) and 74 (38.5%) colonies of drug-resistant cells emerged in palbociclib and oxaliplatin monotherapy, respectively; however, there was no emergence (0%) of resistant cells from the combination treatment, which indicates a complete block of drug resistance by this drug combination. In contrast, complete suppression of resistant cells was not achieved by the palbociclib+cisplatin combination (**Supplementary Figure 6C**). Lastly, we found that the combination regimen was more effective compared to the sequential regimen in suppression of the pool drug resistant KKU-055R, and KKU-214BR cells (**Figure 5F**).

Effect of Oxaliplatin+Palbociclib Combination Treatment in an *In Vivo* Model for CDK4/6 Inhibitor-Resistant CCA and Patient-Derived Organoid Models

To assess the physiological effect and relevance of the oxaliplatin +palbociclib combination, we developed a mouse xenograft model for CDK4/6 inhibitor-resistant CCA. CDK4/6 inhibitor-sensitive KKU-055wt cells were implanted into the flanks of NOS/SCID mice, and the tumor was allowed to grow to 0.5 cm in diameter. To obtain a CDK4/6 inhibitor-resistant tumor, we treated the mice with 75 mg/kg/day palbociclib until the tumor regrew under the treatment. The CDK4/6 inhibitor-resistant tumor was then engrafted into a cohort of NOD/SCID mice to generate the CDK4/6 inhibitor-resistant model (**Figure 6A**). Although 13/16 (81.3%) and 16/16 (100%) of the drug-resistant tumors developed under palbociclib monotherapy and oxaliplatin monotherapy, respectively, only half (10/20, 50%) of the palbociclib-resistant tumors grew under the oxaliplatin +palbociclib combination treatment, which suggests that the combination therapy was more effective than monotherapy in the *in vivo* setting (**Figure 6B**). This combination treatment was also effective in suppressing tumor invasion and metastasis. We did not detect any tumor metastasis or invasion in the mice under combination therapy (0/20 tumors injected). In contrast, we found 12/16 and 3/16 metastasis sites/tumor injected in mice treated with palbociclib and oxaliplatin monotherapy, respectively (**Figure 6C**). In agreement with the *in vitro* cell death results, tumors extracted from combination treated mice and oxaliplatin monotherapy treated mice contained a large proportion of cancer cell death and necrosis (**Figures 6D, E**). To evaluate the clinical relevance of the combination, we tested it against 2 models of drug-naïve patient-derived intrahepatic CCA organoid, and we found that the combination was effective against the CCA organoids and lowered of the effective dose of each drug (**Figures 6F, G**). Taken together, these results indicate the comparative effectiveness of oxaliplatin+palbociclib combination therapy against drug-naïve CCA and CDK4/6 inhibitor-resistant CCA cells in the *in vivo* settings.

DISCUSSION

Acquired vulnerability screening in CCA clones under CDK4/6 inhibitor treatment revealed that while attempting to survive and proliferate under CDK4/6 inhibition, CCA cells alter their ribosomal balance, which results in a novel drugable weakness. Our approach did not focus on identification of the drug-resistant mechanism, but rather on the exploitable profile of the resistant cells. The resistant clones that we developed reflected clonal heterogeneity, and possessed several possible CDK4/6 inhibitor-resistant mechanisms. Fortunately, we found that almost all of them succumbed to the anti-ribosome biogenesis drug oxaliplatin. *Via* a series of experiments, we demonstrated that different CDK4/6 inhibitor-resistant mechanisms may translate into a common weakness in ribosome biogenesis that can be targeted by oxaliplatin, one of the standard drug used in CCA treatment.

In addition to their primary function in ribosome biogenesis, many RPs have extraribosomal functions (22, 23), such as apoptosis, cell cycle arrest, cell migration, and invasion (24). RPL29 was identified as an oncoprotein because of its ability to promote cancer cell proliferation, to promote tumor angiogenesis, and to inhibit cell differentiation (25–28). Expression of RPL29 was also reported to be associated with cancer drug resistance (29). In this study, we showed that RPL29 is a central protein that enables the survival of CCA under CDK4/6 inhibition, and that oxaliplatin treatment results in early degradation of RPL29 and cancer cell death, which is mediated at least partly by p53-mediated cell death. A functional link between ribosome biogenesis stress and cell cycle control was recently established. Imbalanced expression of ribosomal proteins can trigger cell cycle arrest or cell death as a

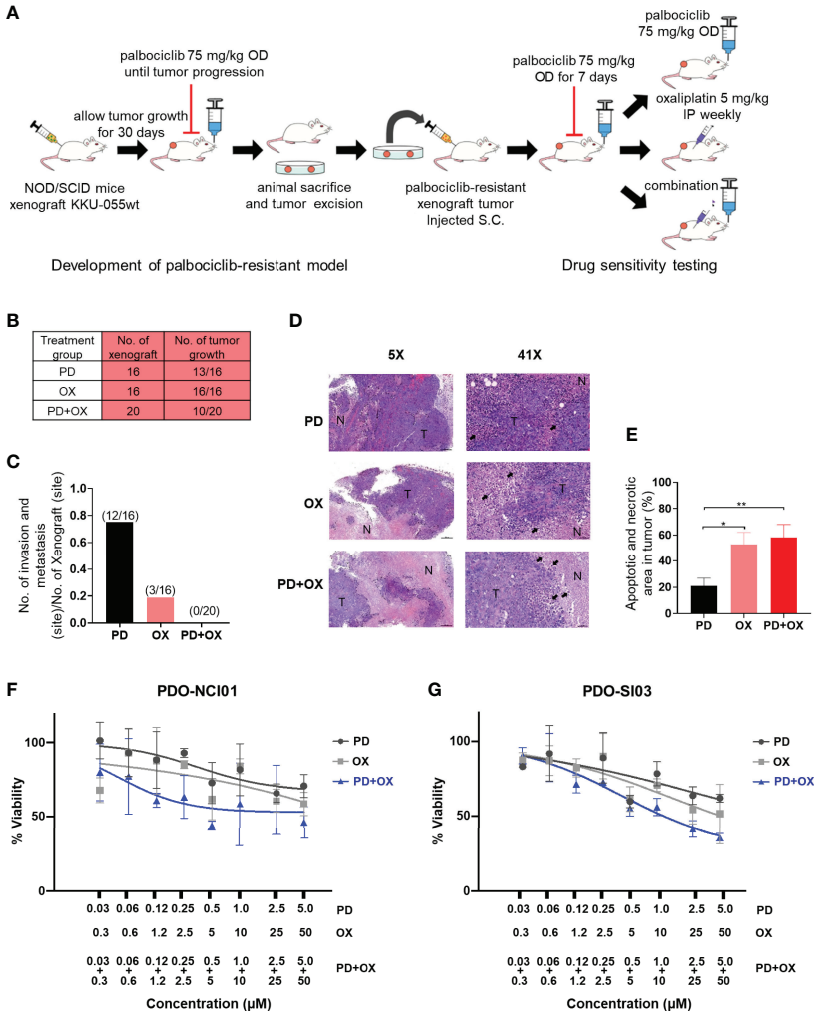

FIGURE 6 | Palbociclib treatment enhances the antitumor effect of oxaliplatin in an in vivo model. **(A)** Schematic of the in vivo study. **(B)** The number of drug-resistant tumors that developed under Palbociclib (PD), oxaliplatin (OX), or palbociclib and oxaliplatin combination (PD+OX) treatment. **(C)** The number of invasion and metastasis sites in mice treated with palbociclib, oxaliplatin, or palbociclib and oxaliplatin combination treatment. **(D)** Hematoxylin and eosin (H&E) staining was used to identify areas of necrosis/apoptosis. (tumor area: T, coagulative necrosis area: N, apoptotic cell: black arrow). **(E)** Percent apoptotic and necrotic areas in each tumor were calculated and are shown in a bar graph. The bars represent the average of each treatment ± standard error of the mean (SEM). Analysis for statistical significance was performed using Student's t-test (*p≤0.05, and **p≤0.01). **(F–G)** Dose response curves of patient-derived CCA organoids (PDO). The PDOs were treated with Palbociclib, Oxaliplatin, or combination of Palbociclib+Oxaliplatin as indicated. Error bars represent standard deviation of triplicate cultures.

result of CDK4 binding and blocking by RPS14 or RPL22, or p53 activation by RPL5 or RPL11 (30–32). Interestingly, we showed a novel feedback mechanism by which cell cycle arrest by drug inhibitor stimulates upregulation of an oncogenic ribosomal protein. Further study is needed to elucidate how CDK4/6 inhibition causes RPL29 upregulation.

CDK4/6 inhibitors have shown great potential as new resources against cancer. However, their effect as single agents is limited, and the focus now is on identifying novel drug combination strategies. The cooperation between CDK4/6 inhibitors and endocrine therapy has been quite successful in estrogen-positive breast cancers. Other pathways that depend on CDK4-cyclin D complex, such as RAS-ERK and PI3K-AKT-mTOR, may also be good options for combination with CDK4/6 inhibition (33). Our results demonstrate a new approach in which we induced acquired dependency of CCA cells on ribosome biogenesis created by CDK4/6 inhibition. In agreement with this notion, our results showed that continuous pressure from CDK4/6 inhibition is needed to produce optimum anti-cancer activity. By way of example, we found that the oxaliplatin+palbociclib combination outperformed oxaliplatin monotherapy in resistant mouse model.

Since oxaliplatin is already a component of some of the standard regimens for CCA. i.e. FOLFOX, FOLFIRINOX, GemOx, the addition of a CDK4/6 inhibitor to oxaliplatin is an appealing possibility.

We showed that oxaliplatin treatment can accelerate RPL29 degradation, but we still do not know how RPL29 is upregulated by

CDK4/6 inhibition, especially in CDK4/6 inhibitor-resistant cells. One possible explanation is that the activated PI3K-AKT-mTOR pathway in the resistant clones causes collateral overproduction of RPs (34). However, this cannot be a comprehensive explanation because only about half of the clones contained an activated PI3K-AKT-mTOR pathway. Disturbed ribosome biogenesis could also be the result of altered RB or p130 activities in a cell trying to survive under CDK4/6 inhibition (35) thereby causing derangement in rRNA expression. We also do not know whether CDK4/6 inhibition-induced acquired vulnerability to oxaliplatin also occurs in other types of cancer cells, or in cells with inherited resistance to CDK4/6 inhibition.

DATA AVAILABILITY STATEMENT

The raw data supporting the conclusions of this article will be made available by the authors, without undue reservation.

ETHICS STATEMENT

The studies involving human participants were reviewed and approved by The Institutional Review Board for Human Research. The patients/participants provided their written informed consent to participate in this study. The animal study was reviewed and approved by The Faculty of Medicine, Siriraj Hospital Mahidol University – Institute Animal Care and Use Committee.

AUTHOR CONTRIBUTIONS

OS, SP, SA, BP, JM, MS performed the experiments KK, KC, RC, TP, SO, SS, SJ supervised and provided critical comments, experimental framework, and experimental design. RC, SO provided important resources and clinical specimens. OS, JM, TP, SS, SJ analyzed and interpreted the data. OS, SJ wrote and edited the manuscript. SJ provided financial support to the project. All authors contributed to the article and approved the submitted version.

FUNDING

This study was funded by grants from the National Science and Technology Development Agency (NSTDA) of Thailand, the Japan Science and Technology Agency, and the National Institute of Allergy and Infectious Diseases of the United States as part of the e-ASIA Joint Research Program (e-ASIA JRP); the NSTDA (P-15-50208); the Thailand Research Fund (RSA5880038); the Siriraj Research Fund; the Foundation for Cancer Care, Siriraj Hospital; and, the Advanced Research in Pharmacology Fund, Siriraj Foundation (D003421). The aforementioned funding agencies had no influence on the interpretation of data, the final conclusions drawn, or the decision to publish this report.

ACKNOWLEDGMENTS

SP, MS, KK, SS, and SJ are part of the R.E.D program, Faculty of Medicine, Siriraj Hospital, Mahidol University.

SUPPLEMENTARY MATERIAL

The Supplementary Material for this article can be found online at: https://www.frontiersin.org/articles/10.3389/fonc.2022.877194/full#supplementary-material

REFERENCES

1. Eckel F, Schmid RM. Chemotherapy and Targeted Therapy in Advanced Biliary Tract Carcinoma: A Pooled Analysis of Clinical Trials. *Chemotherapy* (2014) 60:13–23. doi: 10.1159/000365781
2. Rizvi S, Khan SA, Hallemeier CL, Kelley RK, Gores GJ. Cholangiocarcinoma - Evolving Concepts and Therapeutic Strategies. *Nat Rev Clin Oncol* (2018) 15:95–111. doi: 10.1038/nrclinonc.2017.157
3. Jiao Y, Pawlik TM, Anders RA, Selaru FM, Streppel MM, Lucas DJ, et al. Exome Sequencing Identifies Frequent Inactivating Mutations in BAP1, ARID1A and PBRM1 in Intrahepatic Cholangiocarcinomas. *Nat Genet* (2013) 45:1470–3. doi: 10.1038/ng.2813
4. Chan-On W, Nairismagi ML, Ong CK, Lim WK, Dima S, Pairojkul C, et al. Exome Sequencing Identifies Distinct Mutational Patterns in Liver Fluke-Related and Non-Infection-Related Bile Duct Cancers. *Nat Genet* (2013) 45:1474–8. doi: 10.1038/ng.2806
5. Borad MJ, Champion MD, Egan JB, Liang WS, Fonseca R, Bryce AH, et al. Integrated Genomic Characterization Reveals Novel, Therapeutically Relevant Drug Targets in FGFR and EGFR Pathways in Sporadic Intrahepatic Cholangiocarcinoma. *PloS Genet* (2014) 10:e1004135. doi: 10.1371/journal.pgen.1004135
6. Jusakul A, Cutcutache I, Yong CH, Lim JQ, Huang MN, Padmanabhan N, et al. Whole-Genome and Epigenomic Landscapes of Etiologically Distinct Subtypes of Cholangiocarcinoma. *Cancer Discov* (2017) 7:1116–35. doi: 10.1158/2159-8290.CD-17-0368
7. Nakamura H, Arai Y, Totoki Y, Shirota T, Elzawahry A, Kato M, et al. Genomic Spectra of Biliary Tract Cancer. *Nat Genet* (2015) 47:1003–10. doi: 10.1038/ng.3375
8. Zou S, Li J, Zhou H, Frech C, Jiang X, Chu JS, et al. Mutational Landscape of Intrahepatic Cholangiocarcinoma. *Nat Commun* (2014) 5:5696. doi: 10.1038/ncomms6696
9. Banales JM, Marin JJG, Lamarca A, Rodrigues PM, Khan SA, Roberts LR, et al. Cholangiocarcinoma 2020: The Next Horizon in Mechanisms and Management. *Nat Rev Gastroenterol Hepatol* (2020) 17:557–88. doi: 10.1038/s41575-020-0310-z
10. Sitthithumcharee G, Suppramote O, Vaeteewoottacharn K, Sirisuksakun C, Jamnongsong S, Laphanuwat P, et al. Dependency of Cholangiocarcinoma on Cyclin D-Dependent Kinase Activity. *Hepatology* (2019)70:1614–30. doi: 10.1002/hep.30704
11. Kitchen P, Lee KY, Clark D, Lau N, Lertsuwan J, Sawasdichai A, et al. A Runaway PRH/HHEX-Notch3-Positive Feedback Loop Drives Cholangiocarcinoma and Determines Response to CDK4/6 Inhibition. *Cancer Res* (2020) 80:757–70. doi: 10.1158/0008-5472.CAN-19-0942
12. Saqub H, Proetsch-Gugerbauer H, Bezrookove V, Nosrati M, Vaquero EM, de Semir D, et al. Dinaciclib, a Cyclin-Dependent Kinase Inhibitor, Suppresses

Cholangiocarcinoma Growth by Targeting CDK2/5/9. *Sci Rep* (2020) 10:18489. doi: 10.1038/s41598-020-75578-5
13. Al Baghdadi T, Halabi S, Garrett-Mayer E, Mangat PK, Ahn ER, Sahai V, et al. Palbociclib in Patients With Pancreatic and Biliary Cancer With CDKN2A Alterations: Results From the Targeted Agent and Profiling Utilization Registry Study. *CO Precis Oncol* (2019) 3:1–8. doi: 10.1200/PO.19.00124
14. Lim JS, Turner NC, Yap TA. CDK4/6 Inhibitors: Promising Opportunities Beyond Breast Cancer. *Cancer Discov* (2016) 6:697–9. doi: 10.1158/2159-8290.CD-16-0563
15. Wang L, Leite de Oliveira R, Huijberts S, Bosdriesz E, Pencheva N, Brunen D, et al. An Acquired Vulnerability of Drug-Resistant Melanoma With Therapeutic Potential. *Cell* (2018) 173:1413–1425.e1414. doi: 10.1016/j.cell.2018.04.012
16. Jansen VM, Bhola NE, Bauer JA, Formisano L, Lee KM, Hutchinson KE, et al. Kinome-Wide RNA Interference Screen Reveals a Role for PDK1 in Acquired Resistance to CDK4/6 Inhibition in ER-Positive Breast Cancer. *Cancer Res* (2017) 77:2488–99. doi: 10.1158/0008-5472.CAN-16-2653
17. Zhao X, Ren Y, Lawlor M, Shah BD, Park PMC, Lwin T, et al. BCL2 Amplicon Loss and Transcriptional Remodeling Drives ABT-199 Resistance in B Cell Lymphoma Models. *Cancer Cell* (2019) 35:752–766.e759. doi: 10.1016/j.ccell.2019.04.005
18. Sun XX, Wang YG, Xirodimas DP, Dai MS. Perturbation of 60 S Ribosomal Biogenesis Results in Ribosomal Protein L5- and L11-Dependent P53 Activation. *J Biol Chem* (2010) 285:25812–21. doi: 10.1074/jbc.M109.098442
19. Makjaroen J, Somparn P, Hodge K, Poomipak W, Hirankarn N, Pisitkun T. Comprehensive Proteomics Identification of IFN-Lambda3-Regulated Antiviral Proteins in HBV-Transfected Cells. *Mol Cell Proteomics* (2018) 17:2197–215. doi: 10.1074/mcp.RA118.000735
20. Nuciforo S, Fofana I, Matter MS, Blumer T, Calabrese D, Boldanova T, et al. Organoid Models of Human Liver Cancers Derived From Tumor Needle Biopsies. *Cell Rep* (2018) 24:1363–76. doi: 10.1016/j.celrep.2018.07.001
21. Alvarez-Fernandez M, Malumbres M. Mechanisms of Sensitivity and Resistance to CDK4/6 Inhibition. *Cancer Cell* (2020) 37:514–29. doi: 10.1016/j.ccell.2020.03.010
22. Warner JR, McIntosh KB. How Common are Extraribosomal Functions of Ribosomal Proteins? *Mol Cell* (2009) 34:3–11. doi: 10.1016/j.molcel.2009.03.006
23. Zhou X, Liao WJ, Liao JM, Liao P, Lu H. Ribosomal Proteins: Functions Beyond the Ribosome. *J Mol Cell Biol* (2015) 7:92–104. doi: 10.1093/jmcb/mjv014
24. Xu X, Xiong X, Sun Y. The Role of Ribosomal Proteins in the Regulation of Cell Proliferation, Tumorigenesis, and Genomic Integrity. *Sci China Life Sci* (2016) 59:656–72. doi: 10.1007/s11427-016-0018-0
25. Li C, Ge M, Yin Y, Luo M, Chen D. Silencing Expression of Ribosomal Protein L26 and L29 by RNA Interfering Inhibits Proliferation of Human Pancreatic Cancer PANC-1 Cells. *Mol Cell Biochem* (2012) 370:127–39. doi: 10.1007/s11010-012-1404-x
26. Jones DT, Lechertier T, Reynolds LE, Mitter R, Robinson SD, Kirn-Safran CB, et al. Endogenous Ribosomal Protein L29 (RPL29): A Newly Identified Regulator of Angiogenesis in Mice. *Dis Model Mech* (2013) 6:115–24. doi: 10.1242/dmm.009183
27. Liu JJ, Huang BH, Zhang J, Carson DD, Hooi SC. Repression of HIP/RPL29 Expression Induces Differentiation in Colon Cancer Cells. *J Cell Physiol* (2006) 207:287–92. doi: 10.1002/jcp.20589
28. Miller SA, Brown AJ, Farach-Carson MC, Kirn-Safran CB. HIP/RPL29 Down-Regulation Accompanies Terminal Chondrocyte Differentiation. *Differentiation* (2003) 71:322–36. doi: 10.1046/j.1432-0436.2003.7106002.x
29. Furlan T, Kirchmair A, Sampson N, Puhr M, Gruber M, Trajanoski Z, et al. MYC-Mediated Ribosomal Gene Expression Sensitizes Enzalutamide-Resistant Prostate Cancer Cells to EP300/CREBBP Inhibitors. *Am J Pathol* (2021) 191:1094–107. doi: 10.1016/j.ajpath.2021.02.017
30. Lohrum MA, Ludwig RL, Kubbutat MH, Hanlon M, Vousden KH. Regulation of HDM2 Activity by the Ribosomal Protein L11. *Cancer Cell* (2003) 3:577–87. doi: 10.1016/S1535-6108(03)00134-X
31. Zhang Y, Wolf GW, Bhat K, Jin A, Allio T, Burkhart WA, et al. Ribosomal Protein L11 Negatively Regulates Oncoprotein MDM2 and Mediates a P53-Dependent Ribosomal-Stress Checkpoint Pathway. *Mol Cell Biol* (2003) 23:8902–12. doi: 10.1128/MCB.23.23.8902-8912.2003
32. Dai MS, Lu H. Inhibition of MDM2-Mediated P53 Ubiquitination and Degradation by Ribosomal Protein L5. *J Biol Chem* (2004) 279:44475–82. doi: 10.1074/jbc.M403722200
33. Malumbres M. CDK4/6 Inhibitors: What Is the Best Cocktail? *Clin Cancer Res* (2019) 25:6–8. doi: 10.1158/1078-0432.CCR-18-2177
34. Mayer C, Grummt I. Ribosome Biogenesis and Cell Growth: mTOR Coordinates Transcription by All Three Classes of Nuclear RNA Polymerases. *Oncogene* (2006) 25:6384–91. doi: 10.1038/sj.onc.1209883
35. Ciarmatori S, Scott PH, Sutcliffe JE, McLees A, Alzuherri HM, Dannenberg JH, et al. Overlapping Functions of the pRb Family in the Regulation of rRNA Synthesis. *Mol Cell Biol* (2001) 21:5806–14. doi: 10.1128/MCB.21.17.5806-5814.2001

Conflict of Interest: The authors declare that the research was conducted in the absence of any commercial or financial relationships that could be construed as a potential conflict of interest.

Publisher's Note: All claims expressed in this article are solely those of the authors and do not necessarily represent those of their affiliated organizations, or those of the publisher, the editors and the reviewers. Any product that may be evaluated in this article, or claim that may be made by its manufacturer, is not guaranteed or endorsed by the publisher.

frontiers | Frontiers in Oncology

ORIGINAL RESEARCH
published: 25 May 2022
doi: 10.3389/fonc.2022.882372

LncRNA USP2-AS1 Promotes Hepatocellular Carcinoma Growth by Enhancing YBX1-Mediated HIF1α Protein Translation Under Hypoxia

Shi-Ping Chen[1†], Gui-Qi Zhu[1†], Xiao-Xia Xing[2,3†], Jing-Lei Wan[2], Jia-Liang Cai[2], Jun-Xian Du[4], Li-Na Song[2], Zhi Dai[2,3] and Jian Zhou[1*]*

[1] Department of Liver Surgery and Transplantation, Liver Cancer Institute, Zhongshan Hospital, Fudan University; Key Laboratory of Carcinogenesis and Cancer Invasion of Ministry of Education, Shanghai, China, [2] Liver Cancer Institute, Zhongshan Hospital, Fudan University, Shanghai, China, [3] State Key Laboratory of Genetic Engineering, Fudan University, Shanghai, China, [4] Department of General Surgery, Zhongshan Hospital, Fudan University, Shanghai, China

OPEN ACCESS

Edited by:
Hongda Liu,
Nanjing Medical University, China

Reviewed by:
Zhao Li,
Peking University People's Hospital, China
Yang Deng,
Shandong First Medical University, China

***Correspondence:**
Jian Zhou
zhou.jian@zs-hospital.sh.cn
Zhi Dai
dai.zhi@zs-hospital.sh.cn

†These authors have contributed equally to this work

Specialty section:
This article was submitted to Cancer Molecular Targets and Therapeutics, a section of the journal Frontiers in Oncology

Received: 23 February 2022
Accepted: 25 April 2022
Published: 25 May 2022

Citation:
Chen S-P, Zhu G-Q, Xing X-X, Wan J-L, Cai J-L, Du J-X, Song L-N, Dai Z and Zhou J (2022) LncRNA USP2-AS1 Promotes Hepatocellular Carcinoma Growth by Enhancing YBX1-Mediated HIF1α Protein Translation Under Hypoxia. Front. Oncol. 12:882372. doi: 10.3389/fonc.2022.882372

Recently, the role of lncRNAs in tumorigenesis and development has received increasing attention, but the mechanism underlying lncRNAs-mediated tumor growth in the hypoxic microenvironment of solid tumors remains obscure. Using RNA sequencing, 25 hypoxia-related lncRNAs were found to be upregulated in HCC, of which lncRNA USP2-AS1 were significantly increased under hypoxia. We further confirmed that USP2-AS1 was significantly upregulated in liver cancer using FISH assay and that USP2-AS1 was associated with advanced liver cancer and increased tumor size. Furthermore, overexpression of USP2-AS1 under hypoxia dramatically increased HCC proliferation and clone formation, whereas the opposite results were observed after USP2-AS1 knockdown. We also found that overexpression of USP2-AS1 increased migration and invasion of HCC cells, while USP2-AS1 knockdown led to the opposite effect. In addition, USP2-AS1 knockdown can increase the efficacy of lenvatinib in our mice tumor xenograft model. Our findings also suggest that USP2-AS1 could increase the protein level of HIF1α by enhancing YBX1 protein binding to HIF1α mRNA under hypoxia and the therapeutic effect of lenvatinib can be enhanced by combination with HIF1α inhibitors in liver cancer.

Keywords: TME: tumor microenvironment, USP2-AS1: ubiquitin specific peptidase 2 antisense RNA 1, YBX1: Y-box binding protein 1, lncRNA, HIF1α, Lenvatinib, hypoxia, HCC

Abbreviations: HCC, Hepatocellular carcinoma; OS, Overall survival; TME, Tumor microenvironment; DFS, Disease-free survival; USP2-AS1, ubiquitin specific peptidase 2 antisense RNA 1; RIP, RNA immunoprecipitation; TCGA, The Cancer Genome Atlas; YBX1, Y-box binding protein 1; HIF1α, hypoxia inducible factor 1 subunit alpha; FISH, Fluorescent *in situ* hybridization; Edu,5-Ethynyl-2'-deoxyuridine; ECL, Enhanced Chemiluminescence; LIHC, Liver Hepatocellular Carcinoma; GO, Gene oncology; NC, Normal Contrast.

INTRODUCTION

Liver cancer, including hepatocellular carcinoma (HCC) (80% of cases), is the fourth most common cancer and one of the leading causes of cancer-related mortality. About 50% of all liver cancer cases and deaths worldwide occur in China (1). HCC can be treated by different treatments, including liver transplantation, surgical resection, chemotherapy and radiation, targeted therapy, and immunotherapy. However, drug resistance and recurrence are common. Liver cancer has a five-year survival of less than 30% (2, 3). Therefore, insights into hepatocarcinogenesis are urgently needed to find effective therapeutic targets for HCC.

Hypoxia is one of the important features of the tumor microenvironment (TME) and is essential for tumor growth and progression (4). Hypoxia affects tumor angiogenesis (5), metabolic reprogramming (6), enhancing tumor invasion and metastasis ability (7), and immune escape (8, 9) by regulating different genes. Hypoxia-induced resistance to drug therapy has attracted a lot of attention from researchers (10–13). Hypoxia-inducible factor-1α (HIF1α) is a master regulator and interacts with upstream binding sites (called HIF regulatory elements) of hypoxia-responsive genes. Increased level of HIF1α has been shown to contribute to resistance to sorafenib and lenvatinib in HCC since antiangiogenic drug treatment results in insufficient oxygen supply, and elevated HIF1α and mediate the hypoxic adaptation of tumor cells (13, 14). Hypoxia-induced sorafenib resistance has been extensively investigated and METTL3 (methytrans ferase-like 3), HSP90α (heat shock protein 90 alpha), ATAD3A (ATPase family AAA domain-containing 3A), FOXO3A (forkhead box O3), have all been found to be involved in hypoxia-associated therapy resistance (15–18). However, the association of hypoxia-mediated abnormal lncRNAs expression and lenvatinib resistance remains uninvestigated.

Long non-coding RNAs (LncRNAs) are defined as non-coding RNA molecules that are longer than 200 nucleotides in length with limited or no protein-coding capacity and they have been shown to play significant roles in cancer (19, 20). Abnormal expression of lncRNAs mediates carcinogenesis, tumor progression, and invasion. Olivero et al. demonstrated that p53 activates the lncRNA Pvt1b to inhibit Myc and suppress tumorigenesis (21). SATB2-AS1 inhibits tumor metastasis by regulating SATB2 (22). LncRNAs also affect immunotherapeutic and chemotherapy efficacy and have different clinical and prognostic implications (23–26). However, the effect of hypoxia on the expression of lncRNAs remains elusive.

In this study, we identified 25 hypoxia-associated lncRNAs by RNA sequencing (RNA-seq) that are both upregulated in HCC tissues and Huh7 cells treated with hypoxia (1% O2) for 48 hours. We found that HCC patients with higher USP2-AS1 expression had a worse prognosis. We confirmed that lncRNA USP2-AS1 promoted the proliferation and invasion of HCC by enhancing YBX1-mediated HIF1α translation under hypoxia. In combination with USP2-AS1 knockdown, the efficacy of lenvatinib increased in a mouse model of subcutaneous liver cancer.

MATERIALS ND METHODS

Cells Culture

The human hepatoma cell lines MHCC97H, Huh7, PLC, MHCCLM3, Hep3B and human normal liver cells LO2 were from Liver Cancer Institute, Zhongshan Hospital, Fudan University. Cells were cultured in Dulbecco's modified Eagle's medium (DMEM High Glucose Pyruvate, Gibco) with 10% fetal bovine serum (FBS, Sigma) and 1% antibiotics in an incubator with 5% CO2 at 37°C. For hypoxic treatment, cells were cultured in a hypoxia incubator with 1% O2, 5% CO2, and 94% N2 for 48h, then were harvested. All cells used in this study have tested negative for mycoplasma.

In Vivo Proliferation Assay

Five-week-old female BALB/c nude mice housed in a suitable environment according to the protocols approved by the Animal Ethics Committee of Zhongshan Hospital. 3×10^6 Huh7 cells with USP2-AS1 overexpression or normal control after treated with hypoxia (1% O_2) for 48h were subcutaneously injected into either side of the flank of each female nude mouse (n=4 mice per group). All mice were sacrificed after 4 weeks for tumor weight and volume measurement.

To explore the anti-tumor effect of lenvatinib combined with USP2-AS1 knockdown, the mice were randomly divided into two groups (n=4 mice per group), 3×10^6 Huh7 cells with USP2-AS1 knockdown or Normal Contrast (NC) after treated with hypoxia (1% O_2) for 48h were subcutaneously injected into either side of the flank of each female nude mouse. When the tumor volume exceeded 50 mm^3, lenvatinib solvent diluted with PBS (22.6mg/kg per time for each nude mouse according to the manufacturer's instructions) or PBS (as Normal Contrast) was administered by oral gavage, five times a week. Two weeks after the injection of lenvatinib, the mice were sacrificed for tumor weight and volume measurement.

Protein Extraction and Immunoblotting

The cells were plated in a six-well plate and washed twice with PBS, then SDS-PAGE Sample Loading Buffer,1X 200uL (purchased from Shanghai Beyotime Biotechnology Company) was directly added to lyse the cells for protein extraction. The samples were then heated at 95°C for 10 minutes and then loaded onto a sodium dodecyl sulfate-polyacrylamide gel electrophoresis (SDS-PAGE) to separate proteins based on their different molecular weights. The gel was then transferred to a nitrocellulose membrane. The membrane was incubated with the corresponding primary and secondary antibodies, and the signals were visualized by ECL (Enhanced Chemiluminescence). The film was scanned by the ImageStudio system, photographed, and preserved for follow-up analysis.

RNA Extraction and qRT-PCR

The RNA was extracted from cells or tissues with RNAeasy™ Animal RNA Isolation Kit with Spin Column (purchased from Shanghai Beyotime Biotechnology Company, China) according to the manufacturer's protocol. Following the manufacturer's instructions, Hifair®II 1st Strand cDNA Synthesis SuperMix

(YEASEN Biotechnology, Shanghai, China) PCR premix was used for qRT-PCR. The gene expression level relative to GAPDH was calculated by the $2^{-\Delta\Delta CT}$ method. Each experiment was performed in triplicates. The sequences of primers used in qRT-PCR are listed in **Supplementary Table 2**.

Lentivirus, siRNA, and Cell Transfection

USP2-AS1 overexpression and knockdown lentiviral expression vectors are provided by Tsingke Biotechnology Co., Ltd (Beijing, China). Transfection was performed with corresponding transfection reagents when the cell density reached 30%-50%. 6-8h after transfection, the medium was changed, and puromycin was used for 48h for selection. After 2 weeks, a stably transfected cell line was obtained. YBX1-siRNAs and negative control siRNAs were provided by Ribobio Biotechnology Co., Ltd (Guangzhou, China). Viral transfections were carried out using the corresponding viral transfection reagents, Polyplus jetPRIME transfection reagents were used for all siRNAs transfection.

Cell Proliferation and Colony Formation Assay

Cell proliferation assays were carried out using the BeyoClick™ EdU Cell Proliferation Kit with Alexa Fluor 555(EdU-555, Beyotime, China), according to the manufacturer's protocols. In brief, 5000 cells were cultured in a 96-well plate. After the adherence of the cells, the 2 × Edu culture medium was added and incubated for 2 hours. After fixing, washing, and permeating, the configured Click Additive Solution was added and incubated at room temperature in the dark for 30 minutes. The nuclei were stained with Hoechst 33342 and incubated at room temperature in the dark for 10 minutes. Finally, the cells were observed and photographed using a fluorescence microscope.

Clone Formation Assay

A total of 2000 cells were inoculated in a six-well plate. After the cells adhered to the wall, they were cultured in the anoxic incubator of 1% O_2, and the culture medium was changed twice a week. Cells were harvested after 15 days. Each experiment was performed with three replicates.

Migration and Invasion Assay

Cell migration and invasion assays were carried out using the Boyden chamber (BD Bioscience) with an aperture of 8um with or without Matrigel, and the experiments were performed according to the manufacturer's protocols. The cells were washed with PBS and digested into a single-cell suspension. 1×10^5 cells (suspended in 200ul medium containing 10%FBS) were added to the upper chamber and 600ul containing 30% FBS was added to the lower chamber and cultured in the hypoxia incubator for an appropriate time. The cells were fixed with 4% paraformaldehyde, stained with crystal violet, and washed by PBS. The cells on the surface of the upper chamber were observed and photographed using a microscope. The experiments were repeated three times.

RNA-Protein Immunoprecipitation

RIP was performed by the MagnaRIPTM RNA-Binding Protein Immunoprecipitation Kit (Merck Millipore) according to the manufacturer's protocols. 2×10^7 cells were lysed by Complete RIP Lysis Buffer, centrifuged and the supernatant was incubated with magnetic beads conjugated to antibody (Five micrograms per analysis) against Y-box binding protein 1 (YBX1) at 4°C overnight. After the protein was digested by protease K, RNA was purified by phenol-chloroform. Finally, the qRT-PCR test was performed with specific primers for quantitative analysis of lncRNA USP2-AS1 and HIF1α mRNA.

RNA Pulldown

LncRNA pulldown assay was performed by the Pierce™ Magnetic RNA-Protein PullDown Kit from Thermo according to the manufacturer's protocols. Approximately 50 pmol of the RNA 3' end desthiobiotinylation labeled lncRNA USP2-AS1 full-length or its truncated probes (synthesized by BersinBio, Guangzhou, China) were incubated with 50ul of streptavidin magnetic beads for 30 minutes at room temperature. The beads were then washed by using an equal volume of 20 mM Tris (pH 7.5). 100ul 1× RNA-protein binding buffer (Containing 100ug total protein) was added to the tube containing streptavidin magnetic beads and gently mixed and incubated at room temperature for 60 minutes. After washing the beads 1-2 times with an equal volume of 1x wash buffer (100ul), the beads were mixed with 50ul Elution Buffer and incubated at 37°C for 30 minutes. Supernatants were collected for silver staining or WB analysis.

Tissue Microarrays and Liver Cancer Samples

HCC tissue microarrays were purchased from Shanghai Outdo Biotech Company (T16-339 TMA1, T16-339 TMA2, T16-T16-TMA3) for the FISH experiment. The clinical information was statistically analyzed based on the high and low USP2-AS1 positive cell rates. A total of 208 pairs of non-duplicate liver cancer paired samples and 216 liver cancer tissue samples (8 samples were repeated) were collected on the three tissue microarrays, of which the third tissue microarray had a small number of duplicate samples. These samples were included in the analysis of USP2-AS1 expression in normal liver and HCC tissues. In the survival and prognostic analysis, we excluded the duplicate samples. Two liver cancer samples used in the USP2-AS1 FISH experiment and 36 paired samples of HCC used in the qRT-PCR experiment came from Zhongshan Hospital Fudan University (approved by the Institutional Review Board (IRB) at Zhongshan Hospital Fudan University).

RNA *In Situ* Hybridizations

LncRNA USP2-AS1 *in situ* hybridization kit was provided by Wuhan Servicebio technology Co., Ltd. Briefly, the dehydrated and fixed tissue microarray was dripped with a probe specific for lncRNA USP2-AS1 and hybridized overnight at 55°C in a thermostat. After hybridization, tissue microarray was washed by 2 × SSC at 37°C for 10 minutes, 1 × SSC at 37°C for 2 × 5

minutes and 0.5 × SSC for 10 minutes at room temperature, or formamide was added to wash nonspecific hybrids. Then the microarray was blocked with BSA and incubated with anti-DIG-488 at 37°C for 50 minutes, washed 4 times (5 minutes per wash). Finally, DAPI dye was added and incubated for 8 minutes, protected from light. After being washed, anti-fluorescence quenching tablets were added to seal. The rate of USP2-AS1 positive cells was counted using a fluorescence microscope.

Related Web Tools

The protein-coding ability of USP2-AS1 has displayed by PhyloCSF (PhyloCSF in the UCSC Genome Browser (https://genome.ucsc.edu/). We use the lncATLAS (https://lncatlas.crg.eu/) to predict the location of USP2-AS1 in HCC cells. The binding site of USP2-AS1 with YBX1 was predicted through the online website catRAPID (http://service.tartaglialab.com/update_submission/380192/4af202c73a). We also used the RNAfold Webserver (http://rna.tbi.univie.ac.at/cgi-bin/RNAWebSuite/RNAfold.cgi) to predict the secondary structure of USP2-AS1. TCGA-LIHC (The Cancer Genome Atlas-Liver hepatocellular carcinoma) was used for verifying the overexpression of lncRNA USP2-AS1 in liver cancer and the correlation between YBX1 and HIF1A, YBX1 and USP2-AS1.

Statistical Analysis

All experiments in this study were performed at least three times. Data were expressed as mean± SD. Differential comparisons of data between two groups were performed using paired or unpaired two-tailed t-tests. Statistical analysis was performed using GraphPad Prism 8.0.2 and R 4.0.5. The results were considered statistically significant when $p < 0.05$.

RESULTS

USP2-AS1 Is Significantly Up-Regulated in Hepatocellular Carcinoma

To find hypoxia-associated lncRNAs with potential promoting effect on HCC, RNA sequencing analysis was performed using HCC tissues and adjacent normal tissues from 4 patients and HCC cell line Huh7 treated with hypoxia for 48h (**Figures 1A, B**). A total of 2722 lncRNAs were significantly up-regulated in HCC tissues, and 101 lncRNAs were up-regulated in hypoxia-treated Huh7 cells, the intersection between the two categories included 25 lncRNAs (**Figure 1B**).

Given that lncRNA USP2-AS1 (ubiquitin specific peptidase 2 antisense RNA 1) has the most pronounced fold change in the two categories, so we focused on the role of USP2-AS1 in HCC in our following studies. USP2-AS1 is a long non-coding RNA with 3798 nucleotides in length (USP2-AS1-208, ENST00000659432.1). Similar to other lncRNAs, we found USP2-AS1 has almost no protein-coding ability by PhyloCSF (**Figure S1A**). We also found that USP2-AS1 is likely entirely located in HCC cytoplasm by lncATLAS. (**Figure S1B**), which is confirmed by Fluorescent *in situ* hybridization (FISH) assay (**Figure S1C**).

To explore the relationship between USP2-AS1 and liver cancer, we analyzed the expression of USP2-AS1 in 36 pairs of HCC and adjacent non-tumor specimens by RT-qPCR.

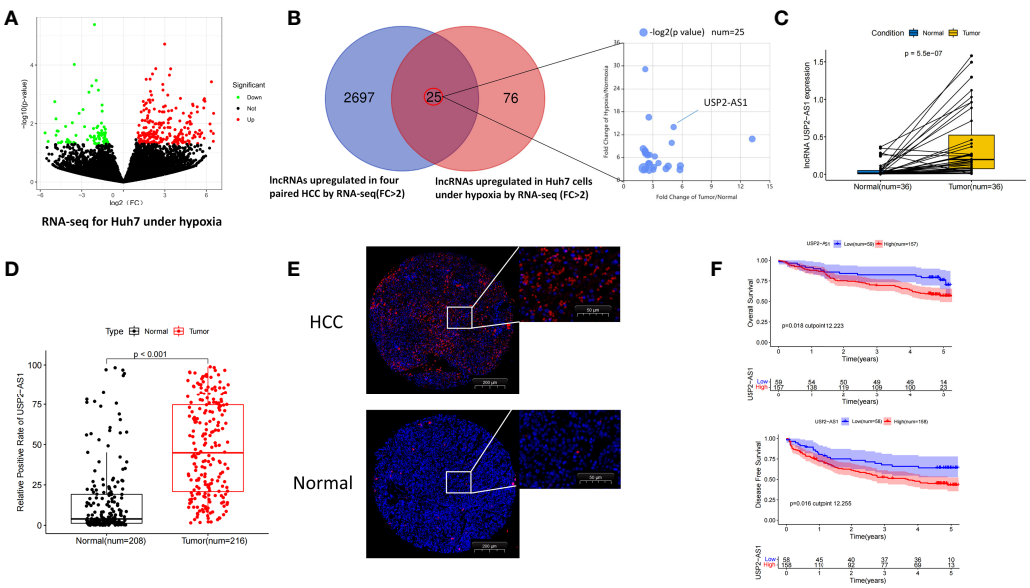

FIGURE 1 | USP2-AS1 is significantly up-regulated in hepatocellular carcinoma. **(A)** Molecules differentially expressed under normoxia and hypoxia in Huh7 cells identified by RNA-seq. **(B)** 25 intersection candidate genes obtained by hypoxia-treated Huh7 cells and HCC tissue sequencing. **(C)** The relative expression of USP2-AS1 in 36 pairs of HCC and adjacent non-tumor specimens by RT-qPCR. **(D)** Relative expression of USP2-AS1 in the HCC chips by FISH experiments, unpaired Student's t-test. **(E)** The relative positive cell rate of USP2-AS1 in the HCC chips by FISH experiments. **(F)** Kaplan–Meier analysis of overall survival time and disease-free survival time in HCC patients with high USP2-AS1 expression versus low USP2-AS1 expression.

As expected, the expression of USP2-AS1 in HCC was significantly higher than in para-cancer tissues (**Figure 1C**). It was also confirmed in the FISH experiment using three tissue chips of human liver cancer (**Figures 1D, E**), which is consistent with the TCGA-LIHC (The Cancer Genome Atlas, Liver Hepatocellular Carcinoma) data (**Figure S1D**).

USP2-AS1 was differentially upregulated in hepatoma cell lines (Huh7, MHCC97H, HCCLM3, PLC) compared with normal human hepatocyte LO2 under both normoxic and hypoxic conditions (**Figures S2A, B**). We also found that the expression of USP2-AS1 was significantly up-regulated in these cell lines following 48h hypoxia (**Figure S2C**), which was consistent with our RNA sequencing results (**Figure 1A**). By analyzing the positive cell rate of USP2-AS1 in human liver cancer tissue microarrays and determining the cutoff value of USP2-AS1 by X-Tile software, we observed that patients with low expression of USP2-AS1 had better prognosis while patients with high expression of USP2-AS1 had shorter OS (Overall Survival) and DFS (Disease-Free Survival) time (**Figure 1F**).

Notably, clinical information of the tissue microarrays showed that USP2-AS1 remarkably correlated with tumor size and the TNM stage of HCC (**Table 1**). Importantly, ROC curve analysis showed lncRNA USP2-AS1 had a high AUC (Area Under Curve, 0.824) for HCC diagnosis (**Figure S2D**). The above results indicate that hypoxia-related lncRNA USP2-AS1 is up-regulated in HCC. USP2-AS1 positively correlated with worse outcomes in HCC patients and may be a potential prognostic tool.

USP2-AS1 Enhances HCC Proliferation, Migration, and Invasion *In Vitro* Under Hypoxia

To investigate the role of USP2-AS1 in HCC, we constructed stable transfectants of MHCC97H and Huh7 cell lines overexpressing USP2-AS1 and knocked down USP2-AS1 in Huh7 cell lines by lentiviral transfection (**Figure 6A**). Under normoxic conditions, overexpression or knockdown of USP2-AS1 did not affect the proliferation, migration, and invasion ability of HCC (data not given). However, our previous RNA sequencing and FISH experiments have confirmed a significant difference in the expression of USP2-AS1 between liver cancer and para-cancer tissues (**Figures 1C–E**). And given that hypoxia treatment can increase USP2-AS1 expression in HCC cell lines (**Figure S2C**), we hypothesized USP2-AS1 promotes the progression of tumors by affecting tumor hypoxic metabolism.

After being treated with hypoxia for 48h, overexpression of USP2-AS1 dramatically increased HCC proliferation and clone formation *in vitro* (**Figures 2A, B**). Conversely, USP2-AS1 knockdown significantly inhibited the proliferation and clone formation ability of HCC (**Figures 2A, B**). We observed that the migration and invasion of HCC cells decreased after knockdown of USP2-AS1, while the reverse was observed with USP2-AS1

TABLE 1 | The clinic pathological factors of HCC patients.

Features	All cases	lncRNA USP2-AS1 exxpression		P-value
		Low	High	
Total number	216	59	157	
Age				0.7978
≤60	150	43	107	
>60	66	16	50	
Gender				0.6328
Male	170	49	121	
Female	46	10	36	
Liver cirrhosis				0.8716
with	89	26	63	
without	127	33	94	
Tumor size (cm)				**0.0109***
≤5	89	34	55	
>5	127	25	102	
Tumor number				0.2343
solitary	198	51	147	
multiple	18	8	10	
Edmondson grade				0.8823
I + II	137	39	98	
III	79	20	59	
TNM stage				**0.0098***
I + II	110	40	70	
III + IV	106	19	87	
HBsAg				0.6818
positive	102	25	77	
negative	114	34	20	
Recurrence				0.7515
with	144	37	107	
without	72	22	50	

**Statistical significant results.*

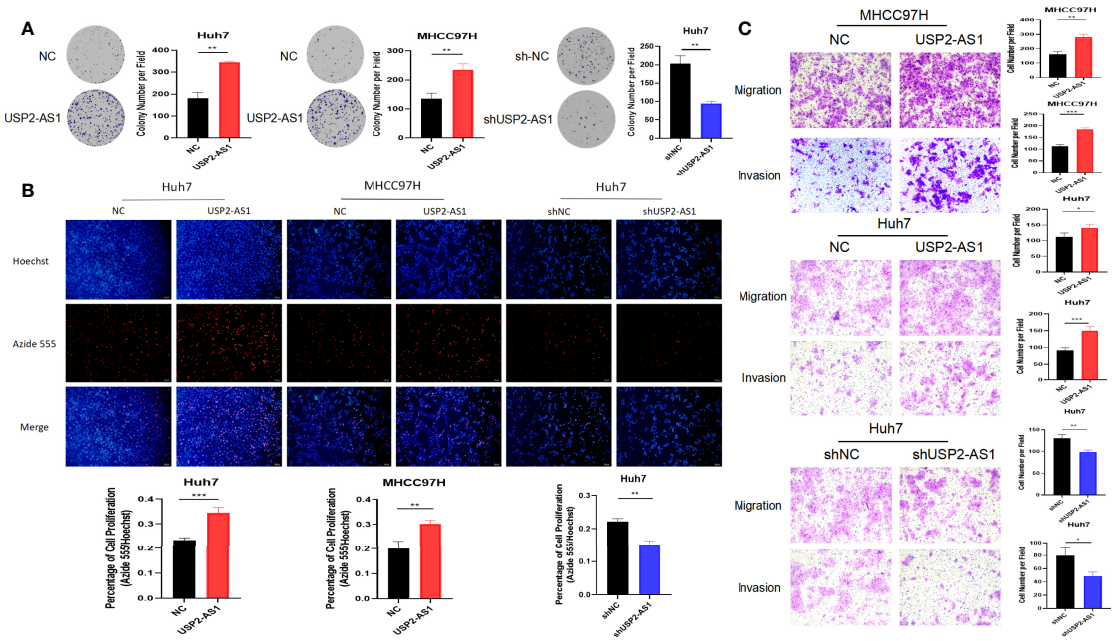

FIGURE 2 | USP2-AS1 promotes HCC proliferation, migration, and invasion under hypoxia *in vitro*. **(A)** The effect of USP2-AS1 on the clonogenic capacity of HCC cell lines Huh7 and MHCC97H *in vitro* was verified under hypoxia. **(B)** EdU cell proliferation assays confirmed USP2-AS1 affected the proliferative capacity of hepatoma cell lines Huh7 and MHCC97H, under hypoxia, *in vitro*. **(C)** Overexpression or knockdown of USP2-AS1 under hypoxic conditions affected the migration and invasion ability of HCC cell lines Huh7 and MHCC97H *in vitro*. Two-tailed Student's t-test, *p < 0.05, **p < 0.01, and ***p < 0.001.

overexpression (**Figure 2C**). These results indicate that USP2-AS1 significantly enhances the proliferation, migration, and invasion of liver tumor cells *in vitro* under hypoxia.

USP2-AS1 Physically Interacts With YBX1 Under Hypoxia

To understand the mechanism of USP2-AS1 in HCC progression under hypoxia, we performed RNA pulldown assays on Huh7 cells cultured in hypoxia for 48 hours (**Figures 3A** and **S3A, B**). A total of 75 proteins were identified as potential molecules that may bind to USP2-AS1 by using mass spectrometry (**Table S1**). We conducted GO enrichment analysis as well as KEGG pathway enrichment analysis of these 75 protein molecules. GO enrichment results showed that MF (Molecular Function) principally included protein binding and RNA binding, BP (Biological Process) mainly comprised of mRNA Splicing, cell-cell adhesion, and translation, and CC (Cellular Component) was primarily in the cytoplasm and nucleus (**Figures 3B, C**). Among these protein molecules, we noticed that YBX1(Y-box binding protein 1) is highly likely to bind to USP2-AS1 with the highest protein spectrum score (**Figure 3D**). The binding of YBX1 to USP2-AS1 was confirmed by YBX1-RIP assay in the MHCC97H cell line (**Figure 3E**), and in the Huh7 cell line (**Figure 3F**).

To investigate how USP2-AS1 binds to YBX1, we predicted the binding site of USP2-AS1 with YBX1 through the online website catRAPID It indicated the segment 500nt-1000nt of USP2-AS1 was likely to bind to YBX1 (**Figure S2E**). We also found USP2-AS1 contains 6 fragments with specific secondary structures by the RNAfold Webserver (**Figure 4A**). We hypothesized that these secondary structures (A-F fragments) are the binding sites of USP2-AS1 with YBX1. We designed six truncated probes (corresponding to A-F fragments, respectively) of USP2-AS1, such as A (1-790nt), B (791-1370nt), C (1371-1960nt), D (1961-2450nt), E (2451-3330nt) and F (3331-3798nt) for RNA pulldown assays (**Figures 4B** and **S3B, C**). We demonstrated that fragment A and C are necessary to mediate the binding of USP2-AS1 and YBX1 (**Figure 4C**). These results show USP2-AS1 physically interacts with YBX1 by the A and C fragments under hypoxia.

USP2-AS1 Enhances HIF1α Translation Under Hypoxia

Hypoxia-inducible factors (HIFs) are critical transcriptional activators mediating tumor hypoxia metabolism, and their imbalance plays an important role in tumor development (27), so we explored whether the expression of USP2-AS1 affects the levels of HIF1α under hypoxia. However, the overexpression of USP2-AS1 did not affect the levels of HIF1α mRNA in Huh7 or MHCC97H cells, and the knockdown of USP2-AS1 also did not affect the HIF1α mRNA in Huh7 (**Figure 4D**). Interestingly, we found that overexpression of USP2-AS1 increased HIF1α protein levels under hypoxia while USP2-AS1 knockdown reduced the protein levels of HIF1α compared with the control group (**Figures 4E** and **S4A**). However, no changes in HIF2α mRNA and protein levels were observed after knockdown or

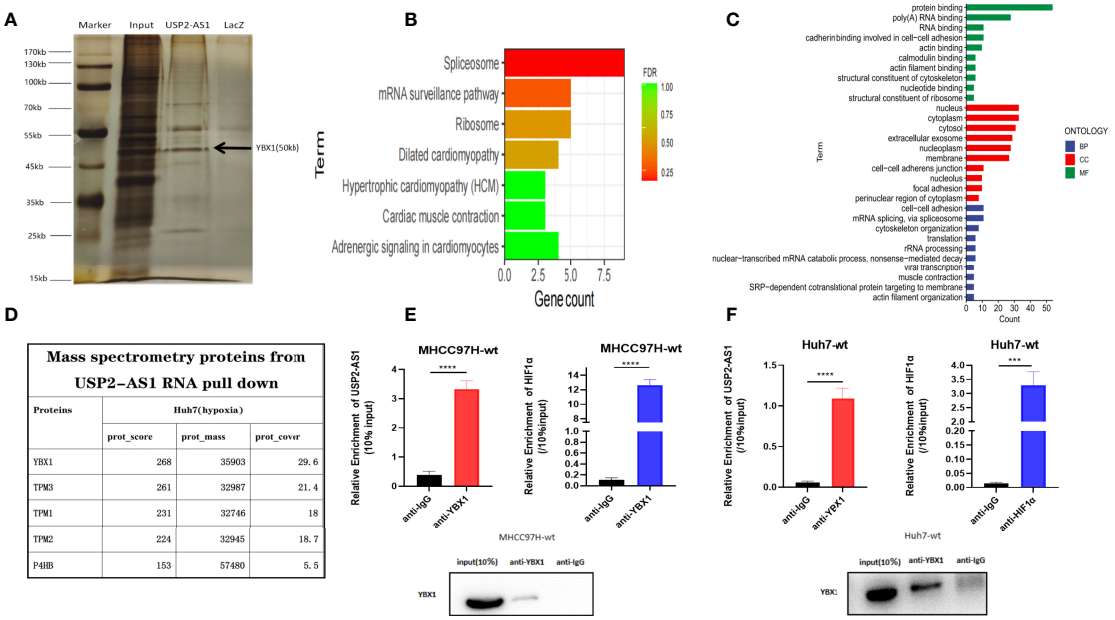

FIGURE 3 | USP2-AS1 physically interacts with YBX1 under hypoxia. **(A)** Silver staining and mass spectrometry analysis following RNA pull-down of USP2-AS1 or Laz (as negative control probe) in Huh7 cells after exposed to hypoxia for 48 hours. **(B)** KEGG pathway enrichment analysis for differential protein molecules from mass spectrometry analysis. **(C)** GO enrichment analysis for differential protein molecules from mass spectrometry analysis. **(D)** The top 5 differential proteins from mass spectrometry analysis. **(E)** YBX1 associated HIF1α and USP2-AS1 as measured by qRT-PCR following RIP YBX1 in MHCC97H cells. **(F)** YBX1 associated HIF1α and USP2-AS1 as measured by qRT-PCR following RIP YBX1 in Huh7 cells after being treated with hypoxia for 48 hours. ***p < 0.001, ****p < 0.0001.

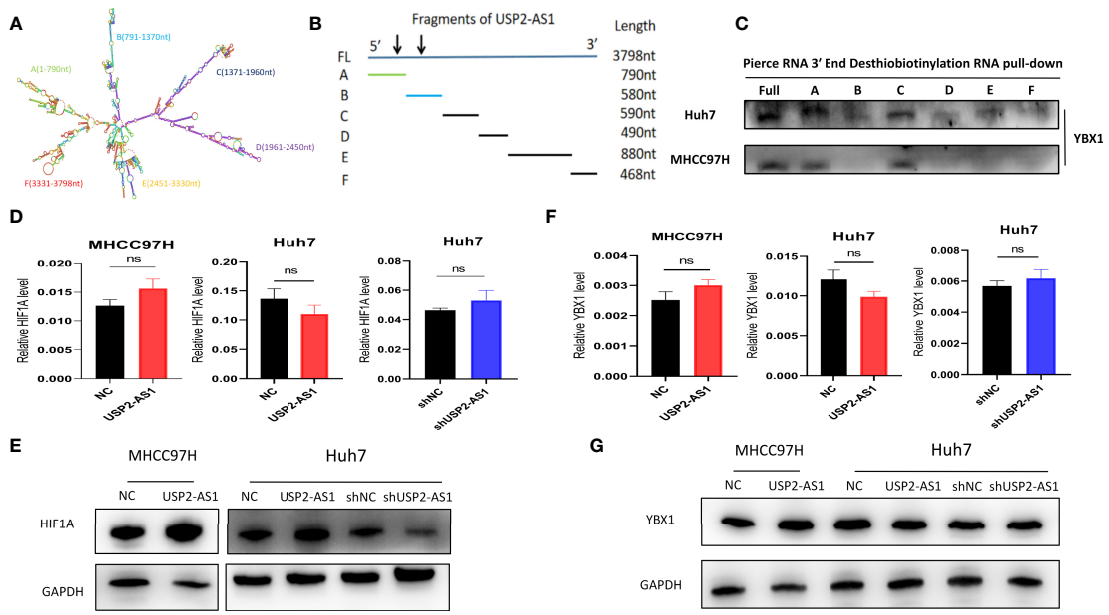

FIGURE 4 | USP2-AS1 increases HIF1α translation under hypoxia. **(A)** The secondary structure of USP2-AS1 was predicted by RNAfold Webserver. **(B)** Six truncated probes (**A–F** fragments) of USP2-AS1 were designed to perform RNA pulldown assays. **(C)** USP2-AS1 physically interacts with YBX1 by the A and C fragments under hypoxia measured by WB. **(D)** USP2-AS1 overexpression or knowdown failed to cause significant changes in HIF1α mRNA measured by qRT-PCR. **(E)** USP2-AS1 affects HIF1α protein levels, as measured by WB. **(F)** USP2-AS1 overexpression or knowdown failed to cause significant changes in YBX1 mRNA measured by qRT-PCR. **(G)** USP2-AS1 overexpression or knockdown does not affect YBX1 protein levels compared with the controls, ns means not significant.

overexpression of USP2-AS1 (data not shown), indicating that the effect of USP2-AS1 on HIF1α protein levels is specific.

Previous studies have indicated that YBX1 promotes the translation of HIF1α protein by directly binding to the 5' UTR of HIF1α mRNA to mediate the metastasis of osteosarcoma (28). At the same time, it indicated that the expression of YBX1 and HIF1α showed a significant positive correlation in the TCGA-LIHC (**Figure S4B**), which is consistent with previous studies. In this study, we confirmed USP2-AS1 binds to YBX1, but whether USP2-AS1 changed the protein levels of HIF1α by affecting the transcription or translation level of YBX1 remains unclear. We found a positive correlation of expression between YBX1 and USP2-AS1 in TCGA-LIHC (**Figure S4C**), so we hypothesized USP2-AS1 may increase HIF1α protein levels by affecting the expression of YBX1. Unfortunately, We further demonstrated that overexpression or knockdown of USP2-AS1 failed to cause significant changes in YBX1 mRNA or protein levels (**Figures 4F, G** and **S4D**). These results suggested that USP2-AS1 did alter the protein levels of HIF1α under hypoxia, but not affected the transcriptional or translation levels of YBX1.

USP2-AS1 Enhances YBX1 Binding to HIF1α mRNA Under Hypoxia

LncRNAs can inhibit or promote the translation of HIF1α by binding to YBX1 protein without changing the expression level of YBX1 protein itself (29–31). We investigated whether USP2-AS1 could enhance the effect of YBX1 on the translation of HIF1α protein by binding to YBX1. RIP experimental results indicated HIF1α mRNA did bind to YBX1 protein (**Figures 3E, F**), which was consistent with the previous outcomes. We observed that under hypoxic conditions, overexpression of USP2-AS1 increased the binding efficiency of YBX1 to USP2-AS1 and significantly increased the effective binding of YBX1 to HIF1α mRNA (**Figures 5A, B**). The knockdown of USP2-AS1 had the opposite effect on the binding level of YBX1 and HIF1α mRNA (**Figure 5C**).

We used small interference RNA to change the expression of YBX1 in USP2-AS1 overexpression or knockdown cell lines (**Figure 5D**). The effect of overexpression or knockdown of USP2-AS1 on the translation level of HIF1α protein under hypoxia was significantly abrogated after the knockdown of YBX1 (**Figure 5D**). Cell proliferation, migration, and invasion experiments also showed that knockdown of YBX1 eliminated the effect of USP2-AS1 on the growth of HCC cells (**Figures S5A, B**, **S6A, B**). The results suggest that USP2-AS1 can increase the protein levels of HIF1α by enhancing YBX1 protein binding to HIF1α mRNA under hypoxia, ultimately promoting the growth and development of HCC.

USP2-AS1 Knockdown Enhances the Efficacy of Lenvatinib on HCC in Mice Tumor Xenograft Model

To further explore the role of USP2-AS1 acting on the growth of HCC *in vivo*, we constructed tumor xenograft model in mice by

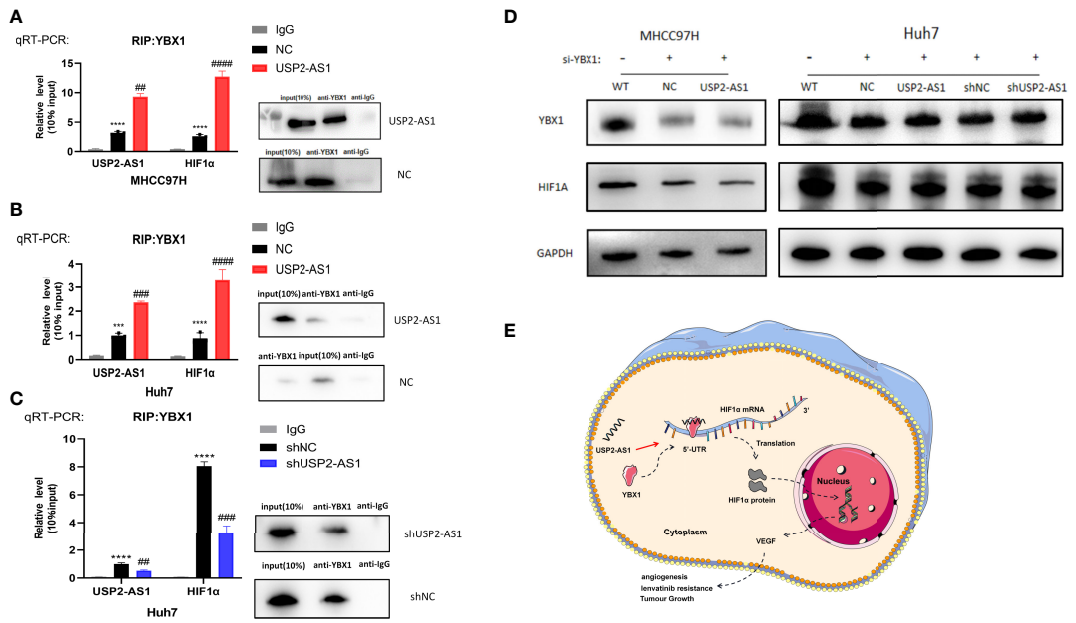

FIGURE 5 | USP2-AS1 enhances YBX1 protein binding to HIF1α mRNA under hypoxic conditions. **(A)** RIP assays were performed to confirm that USP2-AS1 overexpression in MHCC97H can increase the effective binding of YBX1 to HIF1α mRNA. **(B)** RIP assays showed that USP2-AS1 overexpression in Huh7 increases the binding of YBX1 protein to HIF1α mRNA. **(C)** USP2-AS1 knockdown in Huh7 significantly inhibits the binding of YBX1 protein to HIF1α mRNA by RIP assays. HIF1α mRNA and USP2-AS1 were measured by RT-qPCR after RIP. WB assays were performed to test the experiment quality (10%input used as a positive control and IgG was the negative control). **(D)** WB assays were performed to analyze the effect of USP2-AS1 on HIF1α protein in MHCC97H and Huh7 after YBX1 was knocked down by siRNA, GAPDH as protein loading controls, WT as the controls. **(E)** The possible mechanism of USP2-AS1 regulating HIF1α protein translation by YBX1 under hypoxia in HCC, $^{\#\#}p < 0.01$, and *** or $^{\#\#\#}p < 0.001$, **** or $^{\#\#\#\#}p < 0.0001$.

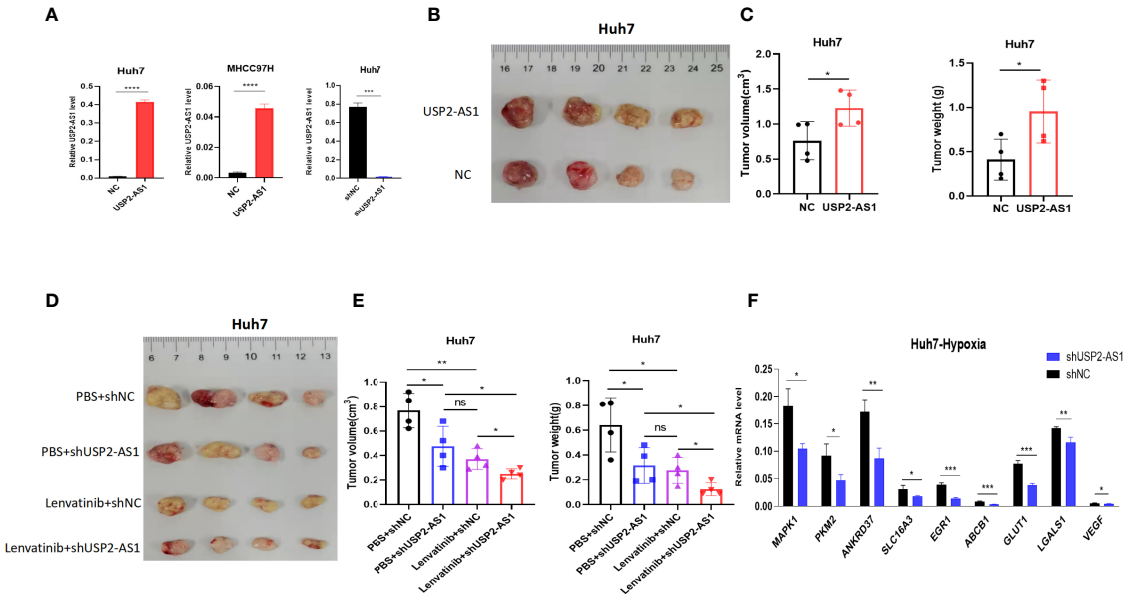

FIGURE 6 | USP2-AS1 knockdown can increase the efficacy of lenvatinib in mice tumor xenograft model. **(A)** Construction of Huh7 and MHCC97H cell lines overexpressing USP2-AS1 and Huh7 USP2-AS1 knockdown cell lines. **(B, C)** Tumor volume and tumor weight of NC (Normal Contrast) or USP2-AS1 overexpressing Huh7 cells in the xenograft mouse model (n = 4). **(D, E)** Tumor volume and tumor weights of NC or USP2-AS1 overexpressing Huh7 cells in a xenograft mouse model (n = 4) with PBS or Lenvatinib. **(F)** Several downstream target genes of HIF1α were down-regulated following USP2-AS1 knockdown in Huh7 cell under hypoxia. Two-tailed Student's t-test, *p < 0.05, **p < 0.01, ***p < 0.001, ****p < 0.0001, and ns, no statistically significant differences.

using USP2-AS1 overexpression or knockdown Huh7 cell line. The tumor xenograft model showed that overexpression of USP2-AS1 promoted the growth of tumor while USP2-AS1 knockdown inhibited the proliferation of HCC *in vivo* (**Figures 6B–E**). These results suggest USP2-AS1 overexpression or knockdown can affect the growth of tumor in our mice tumor xenograft model.

Hypoxia often mediates the resistance of solid tumors to chemotherapeutic drugs. Lenvatinib is a multikinase inhibitor like sorafenib, which was developed in Japan as a multitargeted kinase inhibitor for the treatment of advanced-stage HCC in 2018. Lenvatinib significantly improved the overall survival and progression-free survival time of patients with advanced HCC compared with sorafenib treatment (32). Sorafenib treatment is also limited by drug resistance. Under hypoxic conditions, transcription factor HIF1α can mediate the transcriptional activation of some genes related to glucose uptake, metabolism, and cell proliferation, such as MAPK1, VEGF, MDR1 (ABCB1), GLUT1, to facilitate the adaptive response of liver tumor cells to hypoxia, thereby increasing the therapeutic resistance of HCC to sorafinib (14). Therefore, the therapeutic effect of sorafenib is increased in liver cancer when it is combined with HIF1α inhibitors (33, 34). However, the mechanisms of HCC resistance to lenvatinib are poorly understood.

Our previous study showed that USP2-AS1 increased the protein levels of HIF1α in an anoxic environment, RT-qPCR also showed that the expression of target genes downstream of HIF1α was also significantly down-regulated in USP2-AS1 knockdown Huh7 cell line (**Figure 6F**), suggesting that USP2-AS1 knockdown may enhance the efficacy of lenvatinib. Therefore, we further explored whether USP2-AS1 knockdown enhanced the therapeutic effect of lenvatinib on HCC in mice tumor xenograft model. We observed that the tumor volume and tumor weights of mice treated with lenvatinib were significantly lower than those of the control group in the HCC xenograft model (**Figures 6D, E**). Importantly, compared with control groups, the tumors' weight and volume were the smallest in the group treated with lenvatinib and USP2-AS1 knockdown (**Figures 6D, E**), indicating that USP2-AS1 knockdown can enhance the therapeutic effect of lenvatinib in HCC in our mice tumor xenograft model.

DISCUSSION

Although a large number of studies mainly focus on protein-coding genes and their anti-tumor roles, recent studies have shown that mutations and abnormal expression of non-coding genes, especially long non-coding RNA play an important role in tumor development (35). Exploring the specific molecular mechanisms of lncRNAs in cancer is instrumental in understanding the complex process of cancer occurrence and development, and provides promising targets for tumor drug treatment.

Our study identified a hypoxia-associated lncRNA USP2-AS1.And we observed USP2-AS1 was significantly up-regulated in HCC compared with normal liver tissue, patients with low expression of USP2-AS1 had better prognosis while patients with

high expression of USP2-AS1 had shorter OS and DFS time. Moreover, clinical information showed that USP2-AS1 related with tumor size and the TNM stage of HCC. And ROC curve analysis showed USP2-AS1 had a potential for HCC diagnosis. *In vitro* and *in vivo* results, USP2-AS1 knockdown significantly inhibited the growth of HCC, while USP2-AS1 overexpression promoted the proliferation, migration, and invasion ability of liver cancer cells.

In addition, we confirmed that USP2-AS1 increases the level of HIF1α protein, by enhancing HIF1α mRNA binding to YBX1 protein under hypoxia. We also observed that USP2-AS1 knockdown decreased the transcript level of some downstream target genes of HIF1α under hypoxia, such as MAPK1, VEGF, MDR1(ABCB1), GLUT1, whose transcriptional activation play an important role in tumor hypoxia metabolism (36–39). These results suggest that USP2-AS1 promotes the growth and development of HCC by increasing the expression of HIF1α proteins and its downstream target genes.

The mechanism of tumor development is complex and different tumors have unique metabolic processes and tumor micro-environments. Solid tumors often suffer from hypoxia due to rapidly growing cells. Hypoxia-related factors or metabolic pathways are activated by tumor cells to adapt to the hypoxic environment (40). HIF1α, which is significantly up-regulated under hypoxia, is a critical regulatory factor of hypoxia metabolism in tumor cells. It contributes to the development of tumors under hypoxia by promoting the transcription of many downstream target genes related to hypoxia (41). Hydroxylation, acetylation, ubiquitination, and phosphorylation regulate the transcriptional activity of HIF1α (42), but there are few direct regulatory mechanisms of its translation level. However, it has been shown that certain RNA binding proteins, such as YBX1, can directly bind to HIF1α mRNA to regulate its protein translation (28). Our study observed hypoxia-associated lncRNA USP2-AS1 binds to YBX1 protein to enhance its binding to HIF1α mRNA and directly promotes the protein translation of HIF1α (**Figure 5E**).

In recent years, some lncRNAs mediating the translation of HIF1α through YBX1 have been reported. For example, the PERK/eIF2 signal pathway inhibits the expression of downstream target genes of HIF1α *via* YBX1-dependent regulation of HIF1α translation (29). LncRNA SNHG6 promotes carcinogenesis by enhancing the translation of YBX1-mediated HIF1α in clear cell renal cell carcinoma (31). LncRNA HITT can reduce HIF1α protein translation through YBX1 in colorectal tumors and cervical cancer while forming a feedback regulatory loop with HIF1α to regulate angiogenesis and tumor growth (30). However, the direct effect of hypoxia-associated lncRNAs on the protein translation of HIF1α in HCC has not been reported. Despite USP2-AS1 is up-regulated under hypoxia, USP2-AS1 specifically increases the protein level of HIF1α but not HIF2α, suggesting that the molecular mechanisms of hypoxia metabolism in tumor growth are complex and need further research.

The resistance of HCC to drug treatment is an important reason for the poor prognosis of HCC patients. The mechanisms of drug resistance in HCC therapy are complex (43, 44). Transcriptional activation of molecules such as VEGF induced by HIF1α under hypoxia is one of the most important mechanisms that mediate drug resistance to lenvatinib in HCC. Alternatively, it has been reported that EGFR-activated mutant NSCLC cells change the regulation of VEGF. In EGFR mutated cells, EGFR is the main regulator of HIF1α and VEGF (45). Patients with hypoxic tumors may benefit from EGFR inhibitors already available in the clinic (46). Also, it has been proved that PLAGL2-EGFR-HIF1/2A signaling pathway promotes the progression of HCC and affects the response of cancer cells to anti-EGFR drug erlotinib (47). These studies suggest complex relationships exist between HIF1α, VEGF, and EGFR, so the combination of one or more inhibitors of HIF1α, VEGR, EGFR with lenvatinib may enhance their therapeutic effect in hepatocellular carcinoma (48). The hypoxia-associated lncRNA USP2-AS1 knockdown significantly inhibited the translation of HIF1α protein and the transcriptional activation of its downstream target gene, such as VEGF, and increased the inhibitory effect of lenvatinib on the growth of HCC mice xenograft tumors. So, the combination of HIF1α inhibitors and lenvatinib may hold therapeutic potential in HCC.

In summary, our study identified a hypoxia-associated lncRNA USP2-AS1, which promotes the growth of hepatocellular carcinoma under hypoxia. In mechanism, USP2-AS1 physically interacts with YBX1 to increase the protein translation of HIF1α under hypoxia. We also found that the USP2-AS1 knockdown can enhance the inhibitory effect of lenvatinib on the growth of HCC in our mice tumor xenograft model.

DATA AVAILABILITY STATEMENT

The datasets presented in this study can be found in online repositories. The names of the repository/repositories and accession number(s) can be found in the article/ **Supplementary Material**.

ETHICS STATEMENT

The studies involving human participants were reviewed and approved by Ethics Committee of Zhongshan Hospital affiliated to Fudan University. The patients/participants provided their written informed consent to participate in this study. The animal study was reviewed and approved by Animal Ethics Committee of Fudan University.

AUTHOR CONTRIBUTIONS

S-PC and G-QZ conceived and designed the study. L-NS and X-XX collected the data, analyzed the data, and wrote the manuscript. J-LW, J-XD and J-LC assisted with the data analyses and participated in the writing of manuscript. ZD and JZ coordinated the study. All authors read and approved the final

manuscript. All authors contributed to the article and approved the submitted version.

FUNDING

This study was jointly supported by the National Key R&D Program of China (2019YFC1315800, 2019YFC1315802), National Natural Science Foundation of China (No.82150004, 81830102, 81772578, 81802991), Fudan University and Shanghai Municipal Key Clinical Specialty (IDF152064/014), The Leading Project of the Science and Technology Committee of Shanghai Municipality (Grant number: No. 21Y21900100).

SUPPLEMENTARY MATERIAL

The Supplementary Material for this article can be found online at: https://www.frontiersin.org/articles/10.3389/fonc.2022.882372/full#supplementary-material

REFERENCES

1. Torre LA, Siegel RL, Ward EM, Jemal A. Global Cancer Incidence and Mortality Rates and Trends–An Update. *Cancer Epidemiol Biomark Prev* (2016) 25:16–27. doi: 10.1158/1055-9965.EPI-15-0578
2. Goh GB, Chang PE, Tan CK. Changing Epidemiology of Hepatocellular Carcinoma in Asia. *Best Pract Res Clin Gastroenterol* (2015) 29:919–28. doi: 10.1016/j.bpg.2015.09.007
3. Siegel RL, Miller KD, Jemal A. Cancer Statistics, 2019. *CA Cancer J Clin* (2019) 69:7–34. doi: 10.3322/caac.21551
4. Harris AL. Hypoxia–a Key Regulatory Factor in Tumour Growth. *Nat Rev Cancer* (2002) 2:38–47. doi: 10.1038/nrc704
5. Befani C, Liakos P. The Role of Hypoxia-Inducible Factor-2 Alpha in Angiogenesis. *J Cell Physiol* (2018) 233:9087–98. doi: 10.1002/jcp.26805
6. Jain RK. Antiangiogenesis Strategies Revisited: From Starving Tumors to Alleviating Hypoxia. *Cancer Cell* (2014) 26:605–22. doi: 10.1016/j.ccell.2014.10.006
7. Rankin EB, Giaccia AJ. Hypoxic Control of Metastasis. *Sci (New York NY)* (2016) 352:175–80. doi: 10.1126/science.aaf4405
8. Mohme M, Riethdorf S, Pantel K. Circulating and Disseminated Tumour Cells - Mechanisms of Immune Surveillance and Escape. *Nat Rev Clin Oncol* (2017) 14:155–67. doi: 10.1038/nrclinonc.2016.144
9. Palazon A, Goldrath AW, Nizet V, Johnson RS. HIF Transcription Factors, Inflammation, and Immunity. *Immunity* (2014) 41:518–28. doi: 10.1016/j.immuni.2014.09.008
10. Jing X, Yang F, Shao C, Wei K, Xie M, Shen H, et al. Role of Hypoxia in Cancer Therapy by Regulating the Tumor Microenvironment. *Mol Cancer* (2019) 18:157. doi: 10.1186/s12943-019-1089-9
11. Lu Y, Liu Y, Oeck S, Zhang GJ, Schramm A, Glazer PM. Hypoxia Induces Resistance to EGFR Inhibitors in Lung Cancer Cells *via* Upregulation of FGFR1 and the MAPK Pathway. *Cancer Res* (2020) 80:4655–67. doi: 10.1158/0008-5472.CAN-20-1192
12. Prabhakar NR, Peng YJ, Nanduri J. Hypoxia-Inducible Factors and Obstructive Sleep Apnea. *J Clin Invest* (2020) 130:5042–51. doi: 10.1172/JCI137560
13. Xu K, Zhan Y, Yuan Z, Qiu Y, Wang H, Fan G, et al. Hypoxia Induces Drug Resistance in Colorectal Cancer Through the HIF-1alpha/miR-338-5p/IL-6 Feedback Loop. *Mol Ther* (2019) 27:1810–24. doi: 10.1016/j.ymthe.2019.05.017
14. Zhu YJ, Zheng B, Wang HY, Chen L. New Knowledge of the Mechanisms of Sorafenib Resistance in Liver Cancer. *Acta Pharmacol Sin* (2017) 38:614–22. doi: 10.1038/aps.2017.5
15. Liang C, Dong Z, Cai X, Shen J, Xu Y, Zhang M, et al. Hypoxia Induces Sorafenib Resistance Mediated by Autophagy *via* Activating FOXO3a in Hepatocellular Carcinoma. *Cell Death Dis* (2020) 11:1017. doi: 10.1038/s41419-020-03233-y
16. Liao Y, Yang Y, Pan D, Ding Y, Zhang H, Ye Y, et al. HSP90alpha Mediates Sorafenib Resistance in Human Hepatocellular Carcinoma by Necroptosis Inhibition Under Hypoxia. *Cancers (Basel)* (2021) 13(2):243. doi: 10.3390/cancers13020243
17. Lin Z, Niu Y, Wan A, Chen D, Liang H, Chen X, et al. RNA M(6) A Methylation Regulates Sorafenib Resistance in Liver Cancer Through FOXO3-Mediated Autophagy. *EMBO J* (2020) 39:e103181. doi: 10.15252/embj.2019103181
18. Wu H, Wang T, Liu Y, Li X, Xu S, Wu C, et al. Mitophagy Promotes Sorafenib Resistance Through Hypoxia-Inducible ATAD3A Dependent Axis. *J Exp Clin Cancer Res* (2020) 39:274. doi: 10.1186/s13046-020-01768-8
19. Huarte M. The Emerging Role of lncRNAs in Cancer. *Nat Med* (2015) 21:1253–61. doi: 10.1038/nm.3981
20. Quinn JJ, Chang HY. Unique Features of Long Non-Coding RNA Biogenesis and Function. *Nat Rev Genet* (2016) 17:47–62. doi: 10.1038/nrg.2015.10
21. Olivero CE, Martinez-Terroba E, Zimmer J, Liao C, Tesfaye E, Hooshdaran N, et al. P53 Activates the Long Noncoding RNA Pvt1b to Inhibit Myc and Suppress Tumorigenesis. *Mol Cell* (2020) 77:761–74.e768. doi: 10.1016/j.molcel.2019.12.014
22. Xu M, Xu X, Pan B, Chen X, Lin K, Zeng K, et al. LncRNA SATB2-AS1 Inhibits Tumor Metastasis and Affects the Tumor Immune Cell Microenvironment in Colorectal Cancer by Regulating SATB2. *Mol Cancer* (2019) 18:135. doi: 10.1186/s12943-019-1063-6
23. Dong H, Hu J, Zou K, Ye M, Chen Y, Wu C, et al. Activation of LncRNA TINCR by H3K27 Acetylation Promotes Trastuzumab Resistance and Epithelial-Mesenchymal Transition by Targeting MicroRNA-125b in Breast Cancer. *Mol Cancer* (2019) 18:3. doi: 10.1186/s12943-018-0931-9
24. Lu C, Wei Y, Wang X, Zhang Z, Yin J, Li W, et al. DNA-Methylation-Mediated Activating of lncRNA SNHG12 Promotes Temozolomide Resistance in Glioblastoma. *Mol Cancer* (2020) 19:28. doi: 10.1186/s12943-020-1137-5
25. Zhang L, Li L, Zhan Y, Wang J, Zhu Z, Zhang X. Identification of Immune-Related lncRNA Signature to Predict Prognosis and Immunotherapeutic Efficiency in Bladder Cancer. *Front Oncol* (2020) 10:542140. doi: 10.3389/fonc.2020.542140
26. Zhang Y, Liu Q, Liao Q. Long Noncoding RNA: A Dazzling Dancer in Tumor Immune Microenvironment. *J Exp Clin Cancer Res* (2020) 39:231. doi: 10.1186/s13046-020-01727-3
27. Semenza GL. Oxygen Sensing, Hypoxia-Inducible Factors, and Disease Pathophysiology. *Annu Rev Pathol* (2014) 9:47–71. doi: 10.1146/annurev-pathol-012513-104720
28. El-Naggar AM, Veinotte CJ, Cheng H, Grunewald TG, Negri GL, Somasekharan SP, et al. Translational Activation of HIF1alpha by YB-1 Promotes Sarcoma Metastasis. *Cancer Cell* (2015) 27:682–97. doi: 10.1016/j.ccell.2015.04.003
29. Ivanova IG, Park CV, Yemm AI, Kenneth NS. PERK/eIF2alpha Signaling Inhibits HIF-Induced Gene Expression During the Unfolded Protein Response *via* YB1-Dependent Regulation of HIF1alpha Translation. *Nucleic Acids Res* (2018) 46:3878–90. doi: 10.1093/nar/gky127
30. Wang X, Li L, Zhao K, Lin Q, Li H, Xue X, et al. A Novel LncRNA HITT Forms a Regulatory Loop With HIF-1alpha to Modulate Angiogenesis and Tumor Growth. *Cell Death Differ* (2020) 27:1431–46. doi: 10.1038/s41418-019-0449-8
31. Zhao P, Deng Y, Wu Y, Guo Q, Zhou L, Yang X, et al. Long Noncoding RNA SNHG6 Promotes Carcinogenesis by Enhancing YBX1-Mediated Translation of HIF1alpha in Clear Cell Renal Cell Carcinoma. *FASEB J* (2021) 35:e21160. doi: 10.1096/fj.202000732RR

32. Kudo M, Finn RS, Qin S, Han K-H, Ikeda K, Piscaglia F, et al. Lenvatinib Versus Sorafenib in First-Line Treatment of Patients With Unresectable Hepatocellular Carcinoma: A Randomised Phase 3 Non-Inferiority Trial. *Lancet* (2018) 391:1163–73. doi: 10.1016/S0140-6736(18)30207-1
33. Feng J, Dai W, Mao Y, Wu L, Li J, Chen K, et al. Simvastatin Re-Sensitizes Hepatocellular Carcinoma Cells to Sorafenib by Inhibiting HIF-1alpha/PPAR-Gamma/PKM2-Mediated Glycolysis. *J Exp Clin Cancer Res* (2020) 39:24. doi: 10.1186/s13046-020-1528-x
34. Mendez-Blanco C, Fondevila F, Garcia-Palomo A, Gonzalez-Gallego J, Mauriz JL. Sorafenib Resistance in Hepatocarcinoma: Role of Hypoxia-Inducible Factors. *Exp Mol Med* (2018) 50:1–9. doi: 10.1038/s12276-018-0159-1
35. Bhan A, Soleimani M, Mandal SS. Long Noncoding RNA and Cancer: A New Paradigm. *Cancer Res* (2017) 77:3965–81. doi: 10.1158/0008-5472.CAN-16-2634
36. Comerford KM, Wallace TJ, Karhausen J, Louis NA, Montalto MC, Colgan SP. Hypoxia-Inducible Factor-1-Dependent Regulation of the Multidrug Resistance (MDR1) Gene. *Cancer Res* (2002) 62:3387–94.
37. Deng R, Zhang HL, Huang JH, Cai RZ, Wang Y, Chen YH, et al. MAPK1/3 Kinase-Dependent ULK1 Degradation Attenuates Mitophagy and Promotes Breast Cancer Bone Metastasis. *Autophagy* (2021) 17:3011–29. doi: 10.1080/15548627.2020.1850609
38. Liu J, Wang W, Wang L, Chen S, Tian B, Huang K, et al. IL-33 Initiates Vascular Remodelling in Hypoxic Pulmonary Hypertension by Up-Regulating HIF-1alpha and VEGF Expression in Vascular Endothelial Cells. *EBioMedicine* (2018) 33:196–210. doi: 10.1016/j.ebiom.2018.06.003
39. Xia H, Chen J, Gao H, Kong SN, Deivasigamani A, Shi M, et al. Hypoxia-Induced Modulation of Glucose Transporter Expression Impacts (18)F-Fluorodeoxyglucose PET-CT Imaging in Hepatocellular Carcinoma. *Eur J Nucl Med Mol Imaging* (2020) 47:787–97. doi: 10.1007/s00259-019-04638-4
40. Mennerich D, Kubaichuk K, Kietzmann T. DUBs, Hypoxia, and Cancer. *Trends Cancer* (2019) 5:632–53. doi: 10.1016/j.trecan.2019.08.005
41. Masoud GN, Li W. HIF-1alpha Pathway: Role, Regulation and Intervention for Cancer Therapy. *Acta Pharm Sin B* (2015) 5:378–89. doi: 10.1016/j.apsb.2015.05.007
42. Kallio PJ, Pongratz I, Gradin K, McGuire J, Poellinger L. Activation of Hypoxia-Inducible Factor 1alpha: Posttranscriptional Regulation and Conformational Change by Recruitment of the Arnt Transcription Factor. *Proc Natl Acad Sci USA* (1997) 94:5667–72. doi: 10.1073/pnas.94.11.5667
43. Butler EB, Zhao Y, Munoz-Pinedo C, Lu J, Tan M. Stalling the Engine of Resistance: Targeting Cancer Metabolism to Overcome Therapeutic Resistance. *Cancer Res* (2013) 73:2709–17. doi: 10.1158/0008-5472.CAN-12-3009
44. Llovet JM, Villanueva A, Lachenmayer A, Finn RS. Advances in Targeted Therapies for Hepatocellular Carcinoma in the Genomic Era. *Nat Rev Clin Oncol* (2015) 12:408–24. doi: 10.1038/nrclinonc.2015.103
45. Nilsson MB, Robichaux J, Herynk MH, Cascone T, Le X, Elamin Y, et al. Altered Regulation of HIF-1α in Naive- and Drug-Resistant EGFR-Mutant NSCLC: Implications for a Vascular Endothelial Growth Factor-Dependent Phenotype. *J Thorac Oncol* (2021) 16:439–51. doi: 10.1016/j.jtho.2020.11.022
46. Mamo M, Ye IC, DiGiacomo JW, Park JY, Downs B, Gilkes DM. Hypoxia Alters the Response to Anti-EGFR Therapy by Regulating EGFR Expression and Downstream Signaling in a DNA Methylation-Specific and HIF-Dependent Manner. *Cancer Res* (2020) 80:4998–5010. doi: 10.1158/0008-5472.CAN-20-1232
47. Hu W, Zheng S, Guo H, Dai B, Ni J, Shi Y, et al. PLAGL2-EGFR-HIF-1/2alpha Signaling Loop Promotes HCC Progression and Erlotinib Insensitivity. *Hepatology* (2021) 73:674–91. doi: 10.1002/hep.31293
48. Jin H, Shi Y, Lv Y, Yuan S, Ramirez CFA, Lieftink C, et al. EGFR Activation Limits the Response of Liver Cancer to Lenvatinib. *Nature* (2021) 595:730–4. doi: 10.1038/s41586-021-03741-7

Conflict of Interest: The authors declare that the research was conducted in the absence of any commercial or financial relationships that could be construed as a potential conflict of interest.

Publisher's Note: All claims expressed in this article are solely those of the authors and do not necessarily represent those of their affiliated organizations, or those of the publisher, the editors and the reviewers. Any product that may be evaluated in this article, or claim that may be made by its manufacturer, is not guaranteed or endorsed by the publisher.

frontiers | Frontiers in Oncology

ORIGINAL RESEARCH
published: 24 June 2022
doi: 10.3389/fonc.2022.898156

Designer Exosomes for Targeted Delivery of a Novel Therapeutic Cargo to Enhance Sorafenib-Mediated Ferroptosis in Hepatocellular Carcinoma

Xiaoju Li[1†], Qianqian Yu[2†], Runze Zhao[1†], Xinyan Guo[1], Chenlin Liu[1], Kuo Zhang[1], Wangqian Zhang[1], Jinghan Liu[1], Jinzheng Yu[1], Shuning Wang[1], Qiang Hao[1], Weina Li[1], Wei Zhang[1], Meng Li[1], Yingqi Zhang[1], Cun Zhang[1*] and Yuan Gao[1*]*

[1] State Key Laboratory of Cancer Biology, Biotechnology Center, School of Pharmacy, The Fourth Military Medical University, Xi'an, China, [2] Department of Oncology, Tongji Hospital, Tongji Medical College, Huazhong University of Science and Technology, Wuhan, China

Sorafenib is one of the few effective first-line drugs approved for the treatment of advanced hepatocellular carcinoma (HCC). However, the development of drug resistance is common among individuals with HCC. Recent evidence indicated that the anticancer activity of sorafenib mainly relies on the induction of ferroptosis. Furthermore, in our study, genes that suppress ferroptosis, especially GPX4 and DHODH, were enriched in sorafenib-resistant cells and primary tissues and were associated with poor prognosis of HCC patients who received sorafenib treatment. Therefore, a new ferroptosis inducer comprising a multiplex small interfering RNA (multi-siRNA) capable of simultaneously silencing GPX4 and DHODH was created. Then, exosomes with high multi-siRNA loading and HCC-specific targeting were established by fusing the SP94 peptide and the N-terminal RNA recognition motif (RRM) of U1-A with the exosomal membrane protein Lamp2b. The results from the *in vitro* and *in vivo* experiments indicate that this tumor-targeting nano-delivery system ($Exo^{SP94\text{-}lamp2b\text{-}RRM}$_multi-siRNA) could enhance sorafenib-induced ferroptosis and overcome sorafenib resistance. Taken together, HCC-targeted exosomes ($Exo^{SP94\text{-}Lamp2b\text{-}RRM}$) could specifically deliver multi-siRNA to HCC tissues, enhance sorafenib-induced ferroptosis by silencing GPX4 and DHODH expression and consequently increase HCC sensitivity to sorafenib, which opens a new avenue for clinically overcoming sorafenib resistance from the perspective of ferroptosis.

Keywords: hepatocellular carcinoma, resistance, sorafenib, engineered exosome, ferroptosis

OPEN ACCESS

Edited by:
Yunfei Xu,
Shandong University, China

Reviewed by:
Qiang Wang,
Nanjing Drum Tower Hospital, China
Feng Zhang,
Nanjing University of Chinese Medicine, China

***Correspondence:**
Yuan Gao
gaoyuan321@fmmu.edu.cn
Cun Zhang
zhangcun@fmmu.edu.cn
Yingqi Zhang
zhangyqh@fmmu.edu.cn

†These authors have contributed equally to this work

Specialty section:
This article was submitted to Cancer Molecular Targets and Therapeutics, a section of the journal Frontiers in Oncology

Received: *17 March 2022*
Accepted: *24 May 2022*
Published: *24 June 2022*

Citation:
Li X, Yu Q, Zhao R, Guo X, Liu C, Zhang K, Zhang W, Liu J, Yu J, Wang S, Hao Q, Li W, Zhang W, Li M, Zhang Y, Zhang C and Gao Y (2022) Designer Exosomes for Targeted Delivery of a Novel Therapeutic Cargo to Enhance Sorafenib-Mediated Ferroptosis in Hepatocellular Carcinoma. Front. Oncol. 12:898156. doi: 10.3389/fonc.2022.898156

INTRODUCTION

Hepatocellular carcinoma (HCC) was ranked as the sixth most commonly diagnosed cancer and the fourth leading cause of cancer-related death worldwide in 2018 (1, 2). In the early stages of HCC, curative treatment can be achieved with tumor ablation, resection, or liver transplantation (3). However, the majority of HCC patients are already in the middle or late stages at the time of

diagnosis, missing the optimal window for curative treatment. Sorafenib is the first systemic therapy shown to improve survival in HCC and has been approved by the U.S. Food and Drug Administration (FDA) for treatment of unresectable HCC (4). Despite their initial response, sorafenib-treated tumors rarely regress completely, and most patients develop disease progression. Therefore, to improve the survival and quality of life of patients with HCC, combination therapies should be considered as a potentially superior treatment option.

Ferroptosis is a recently discovered form of programmed cell death characterized by iron-dependent accumulation of lipid peroxides to lethal amounts (5). A growing amount of evidence indicates that ferroptosis can be induced by inhibiting cystine/glutamate transporter (system x_c-) activity, downregulating GPX4 or DHODH expression, and accumulating reactive oxygen species (ROS) (6). Recent reports have shown that sorafenib can induce ferroptosis by inhibiting system x_c- (7). Moreover, numerous studies suggest that the anticancer activity of sorafenib mainly relies on inducing ferroptosis (5, 8–11). Therefore, targeting constituents of ferroptosis might be a promising strategy to increase sorafenib efficacy and overcome sorafenib resistance.

Herein, we first found that ferroptosis suppressor genes, especially GPX4 and DHODH, are enriched in sorafenib-resistant cells and primary tissues from patients and are associated with poor prognosis of HCC patients who receive sorafenib treatment. Then, we created a novel ferroptosis inducer comprising a multiplex small interfering RNA (multi-siRNA) suitable for simultaneously silencing GPX4 and DHODH. Then, exosomes ($Exo^{SP94\text{-}lamp2b\text{-}RRM}$) with high tumor targeting ability and high multi-siRNA loading efficacy were constructed to deliver the multi-siRNA cargo. Using *in vitro* and *in vivo* models, we demonstrated that this tumor-targeting nanodrug ($Exo^{SP94\text{-}lamp2b\text{-}RRM}$-multi-siRNA) could enhance sorafenib-induced ferroptosis and overcome sorafenib resistance, suggesting that it is a promising therapeutic strategy for treating sorafenib-resistant HCC.

MATERIALS AND METHODS

Antibodies and Inhibitors

The antibodies used targeted the following proteins (dilutions used are included):

GAPDH (CW0101: immunoblotting, 1:1000) from CWBIOTECH; F-actin (40734ES75: immunofluorescence, 1:100) from YEASEN; U1A (10212: immunoblotting, 1:500) from Proteintech; CD63 (67605-1-Ig: immunoblotting, 1:5000) from Proteintech; CD9 (60232-1-Ig: immunoblotting, 1:5000) from Proteintech; TSG101 (14497-1-AP: immunoblotting, 1:1000) from Proteintech; GPX4 (67763-1-Ig: immunoblotting, 1:5000; IHC, 1:1000) from Proteintech; and DHODH (14877-1-AP: immunoblotting, 1:2000; IHC, 1:100) from Proteintech.

The inhibitors used are as follows:

Sorafenib (HY-10201: 10 μM for the *in vitro* assay and 30 mg/kg for the *in vivo* assay) and Ferrostatin-1 (HY-100579: 60 nM for the *in vitro* assay), and ferrostatin-1 (HY-100579: 5 mg/kg, intraperitoneal injection for the *in vivo* assay) were obtained from MedChem Express.

Cell Lines and Culture

The HepG-2 and HEK-293T cell lines were obtained from the Type Culture Collection of the Chinese Academy of Sciences (Shanghai, China). These cell lines were authenticated by the analysis of short tandem repeat (STR) profiles, and all of them matched those of the standard cell lines in the DSMZ data bank. These cells tested negative for cross-contamination of other human cells and mycoplasma contamination. The sorafenib-resistant HepG-2 cell line (HepG-2R) was generated by continuous treatment of HepG2 cells with sorafenib up to 10 μM and maintained as previously described (12). HepG-2, HepG-2R and HEK-293T cells were cultured in DMEM containing 10% fetal bovine serum and 1% penicillin-streptomycin.

Plasmid Construction

Briefly, the sequences for SP94 peptide (SFSIIHTPILPL), the CDS sequences of Lamp2b and the CDS sequences of the N-terminal RNA recognition motif (RRM) of U1-A were orderly arranged from N-terminal to C-terminal. Then the sequence encoding the above fusion protein was digested with BamHI-XhoI and cloned into pcDNA3.1(+) vector. The clones were confirmed by DNA sequencing and stored for the following experiments.

Exosome Purification

For exosome isolation from HEK-293T cells, cells were transfected with control or SP94-Lamp2b-RRM expressing plasmids with Lipofectamine3000. 12 h later, cells were further cultured in DMEM with 10% exosome-depleted FBS (ultracentrifugation at 120,000 ×g for 16 h) for 24–36 h. Then, the culture medium was precleared by centrifugation at 500×g for 15 min and then at 10000×g for 20 min. Exosomes were isolated by ultracentrifugation at 110000×g for 70 min at 4°C and washed in PBS using the same centrifugation conditions. The concentration of exosomes was determined by measuring total exosomal protein using a Pierce BCA Protein Assay Kit (Thermo Scientific, USA) according to the manufacturer's instructions. NanoSight and transmission electron microscopy were used to determine the size distribution, concentration and morphology of the exosomes. For siRNA loading experiments, 100 nM corresponding siRNAs were transfected with Lipofectamine 3000. Twenty-four hours later, the cells were further cultured in DMEM with 10% exosome-depleted FBS for another 24 h, followed by exosome isolation.

Transmission Electron Microscope Assay

Cells were collected and fixed with 2.5% glutaraldehyde. Subsequently, cells were postfixed in 2% tetroxide and dehydrated through a series of gradient ethanol solutions. Samples were embedded in epoxy resin, cut into thin slices, and placed onto a nickel grid. Images were acquired using a Tecnai G2 Spirit transmission electron microscope (Thermo Fisher).

Intracellular ROS Measurements

A lipid ROS assay was performed as described previously. Briefly, cells were incubated with PBS containing 10 μM DCFDA dye in a cell culture incubator for 30 min. Cells were then collected and washed twice with PBS followed by resuspension in 200 μl of PBS. ROS levels were analyzed using a Beckman CytoFLEX system through the FITC channel.

Detection of Malondialdehyde (MDA)

Analysis of lipid peroxidation was assessed by quantifying the MDA concentration in cell lysates using a Lipid Peroxidation MDA Assay Kit (S0131, Beyotime) in accordance with the manufacturer's instructions.

Animal Study

Six-week-old, male, athymic BALB/c nude mice were used. All animal experiments were carried out under protocols approved by the Animal Care and Use Committee of Fourth Military Medical University.

For *in vivo* tracking of exosomes, purified exosomes with the indicated modifications were labeled with the fluorescent dye DiR at a final concentration of 8 μM (Invitrogen). Labeled exosomes were collected by ultracentrifugation after washing with saline and stored in saline before use. Mice were injected with labeled exosomes (100 μg at the protein level in 100 μL) *via* tail vein injection. Mice were subjected to fluorescent living imaging 6 h after injection with an *in vivo* imaging system (IVIS lumina II).

For orthotopic implantation, six-week-old male nude mice were anesthetized with 3% (w/v) pentobarbital sodium by intraperitoneal injection. Then, 2×10^6 sorafenib-resistant HepG-2 cells stably expressing luciferase were surgically implanted into the left liver lobes of mice. Tumor growth was monitored by bioluminescence with an *in vivo* imaging system (IVIS lumina II). Two weeks after inoculation, mice were randomized to each group and began to receive different treatments. In the sorafenib treatment group, sorafenib (30 mg/kg) was given every 3 days. In the sorafenib and exosome combination treatment group, sorafenib was administered at the same dose, and 100 μg of the indicated exosomes (at the protein level) was injected *via* the tail vein 24 h after every sorafenib administration. At the end of the experiment, mice were sacrificed. Tumor bearing liver tissues and the main organs were collected for the following experiments.

Immunohistochemistry

This experiment was performed as previously described (13). Briefly, sections (4 μm thick) of paraffin-embedded samples were deparaffinized and rehydrated in a graded series of ethanol. After inactivation of endogenous peroxidase activity with 3% H_2O_2 in methanol for 10 min, the sections were washed three times in PBS and blocked with goat serum for 20 min. Then, they were incubated with primary antibodies in a humid container at 4°C overnight. After the addition of the PowerVision™ complex, tissue sections were incubated at 37°C for 20 min followed by treatment with DAB. PBS in place of primary antibody was used as a negative control.

Statistical Analysis

The data are presented as the mean ± s.e.m. from at least three independent experiments. Statistical analysis was performed using GraphPad Prism software. A random number table was used to randomize the mice into control and treatment groups. The numbers of mice were determined on the basis of our pretests and previous experience with similar experiments. A value of $P<0.05$ was considered statistically significant. The statistical tests were two-sided.

RESULTS

Suppressed Ferroptotic Activity During Sorafenib Treatment Is Associated With Compromised Therapeutic Efficiency

To confirm whether sorafenib could induce ferroptosis in HCC cells, we performed a CCK-8 assay. Our data showed that sorafenib-mediated cell death in the human HCC cell line HepG-2 was blocked by ferrostatin-1 (a ferroptosis inhibitor) (**Figure 1A**, **Figure S1A**). The accumulation of reactive oxygen species (ROS) and lipid peroxidation are key events in ferroptosis (14); thus, we analyzed the levels of ROS and the end products of lipid peroxidation (i.e., MDA) in HepG-2 cells. The results indicated that sorafenib increased the levels of ROS and MDA in HepG-2 cells (**Figures 1B, C**). Apart from ferroptosis-suppressing agents, numerous genes have been identified as key ferroptosis suppressors. For example, glutathione peroxidase 4 (*GPX4*) resides in the center of a network that functions to prevent the accumulation of lipid hydroperoxides, thereby strongly suppressing ferroptosis (15). Interestingly, we constructed a ferroptosis suppressor gene signature and discovered that ferroptosis suppressor genes were enriched in sorafenib-resistant cells and primary tissues from HCC patients (**Figure 1D**, **Figure S1B**). Moreover, the results indicated that the high expression level of the ferroptosis suppressor gene signature was associated with poor prognosis of HCC patients who received sorafenib treatment (**Figure 1E**, **Figure S1C**). Therefore, the results suggest that suppressed ferroptotic activity is associated with sorafenib resistance.

Gene-Silencing Activities of the Multi-siRNA Against GPX4 and DHODH

The above data suggest that silencing key ferroptosis suppressor genes increases the therapeutic effect of sorafenib. Among the ferroptosis suppressor genes, *GPX4* and DHODH can directly remove the dangerous products of iron-dependent lipid peroxidation and consequently protect the cell membrane from damage; when *GPX4* and DHODH expression and/or function are dysregulated, ferroptosis ensues (16, 17). Moreover, we found that the expression of GPX4 and DHODH was upregulated in sorafenib-resistant patients (**Figures 2A, B**) and associated with

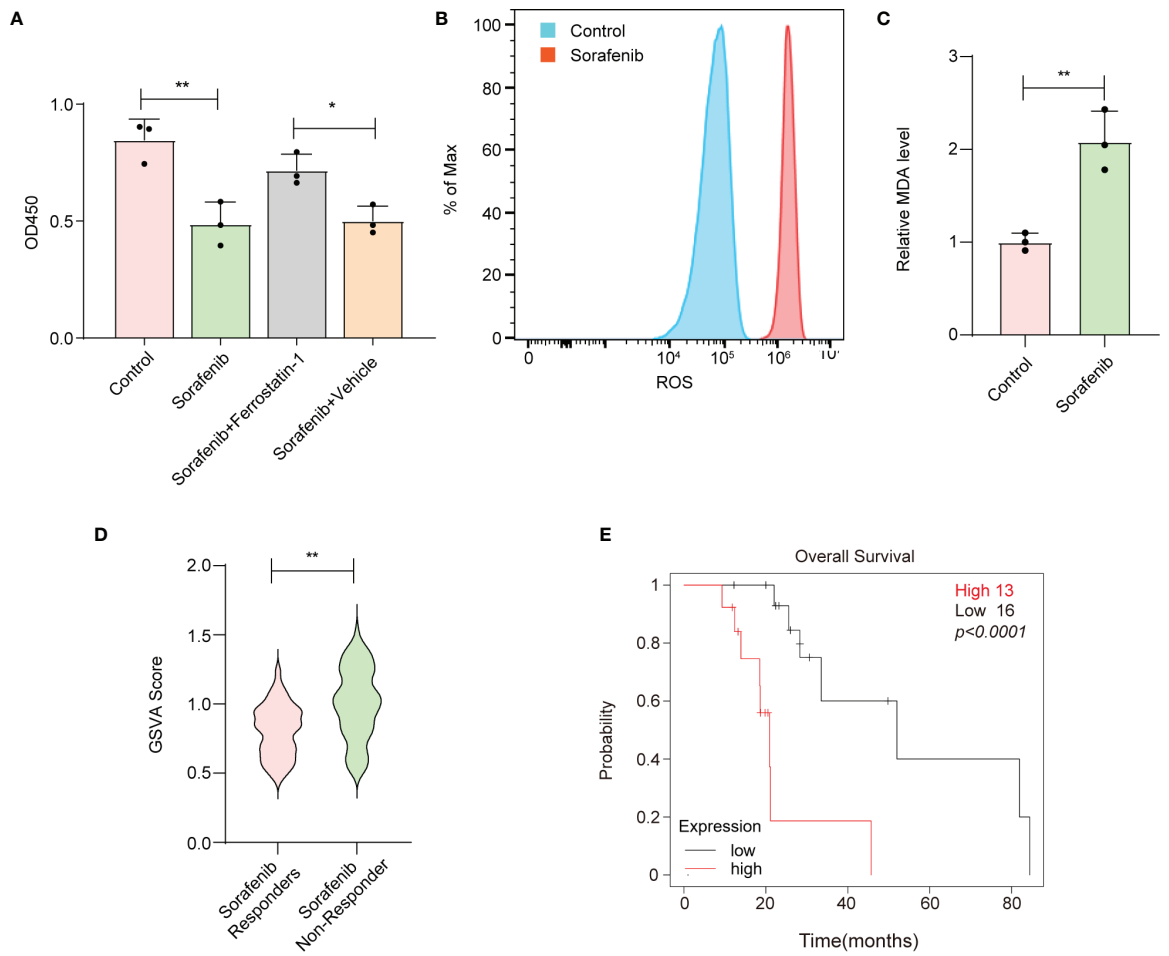

FIGURE 1 | Reduced ferroptotic activity during sorafenib treatment is associated with compromised therapeutic efficiency. **(A)** Viability of HepG-2 cells as measured by the CCK-8 assay. Ferrostatin-1 is a ferroptosis inhibitor. Sorafenib (10 μM). **(B)** HepG-2 cells were treated with 10 μM sorafenib, and ROS production was assessed by DCFH-DA staining followed by flow cytometry. **(C)** MDA levels in HepG-2 cells treated with vehicle or 10 μM sorafenib for 24 h. **(D)** GSVA was conducted to calculate the score for enrichment of ferroptosis suppressor genes. HCC tissues from sorafenib responders or sorafenib nonresponders were obtained from the Gene Expression Omnibus (GSE1109211). **(E)** Kaplan–Meier analysis of overall survival based on the expression signature of ferroptosis suppressor genes. **(A, C)** The data are shown as the means ± S.E.M. **(A)** ANOVA with Dunnett's t-test. **(C, D)** Unpaired t-test. **(E)** Log-rank test. *p < 0.05, **p < 0.01.

poor prognosis of HCC patients who received sorafenib treatment (**Figures 2C, D**). Meanwhile, GPX4 and DHODH expression was upregulated in sorafenib-resistant HCC cell line (HepG-2R) (**Figure 2E**). In light of these findings, we sought to interfere with the expression and function of these two genes at the same time. First, siRNAs targeting the human *GPX4* gene and human *DHODH* gene were designed and screened to determine their effectiveness. As shown in **Figures 2F, G** and **Figures S2A, B**, si-GPX4#1 and si-DHODH#1 were the most effective siRNAs in knocking down their respective proteins. Then, we designed a multi-siRNA containing the sequences corresponding to si-GPX4#1 and si-DHODH#1; the sequence "AUUGCAC" was used as a linker to connect si-GPX4#1 to si-DHODH#1. The results showed that this multi-siRNA could simultaneously suppress GPX4 and DHODH expression (**Figure 2H**).

Preparation and Characterization of SP94-Lamp2b-RRM Fusion Protein-Engineered Exosomes

Exosomes have been considered a good siRNA delivery vehicle to reduce drug resistance (18). However, low cargo encapsulation efficiency and the lack of cell-type specific targeting remain major hurdles for their potential clinical application. Recently, some RNA-binding proteins have been shown to significantly promote exosomal miRNA cargo loading *via* interaction with common short sequence motifs present in miRNAs (19). Therefore, we hypothesized that fusion of specific RNA-binding proteins with the exosomal membrane proteins can increase the loading efficiency of the desired RNAs. We fused the N-terminal RNA recognition motif (RRM) of U1-A with the C-terminus of Lamp2b (exosomal

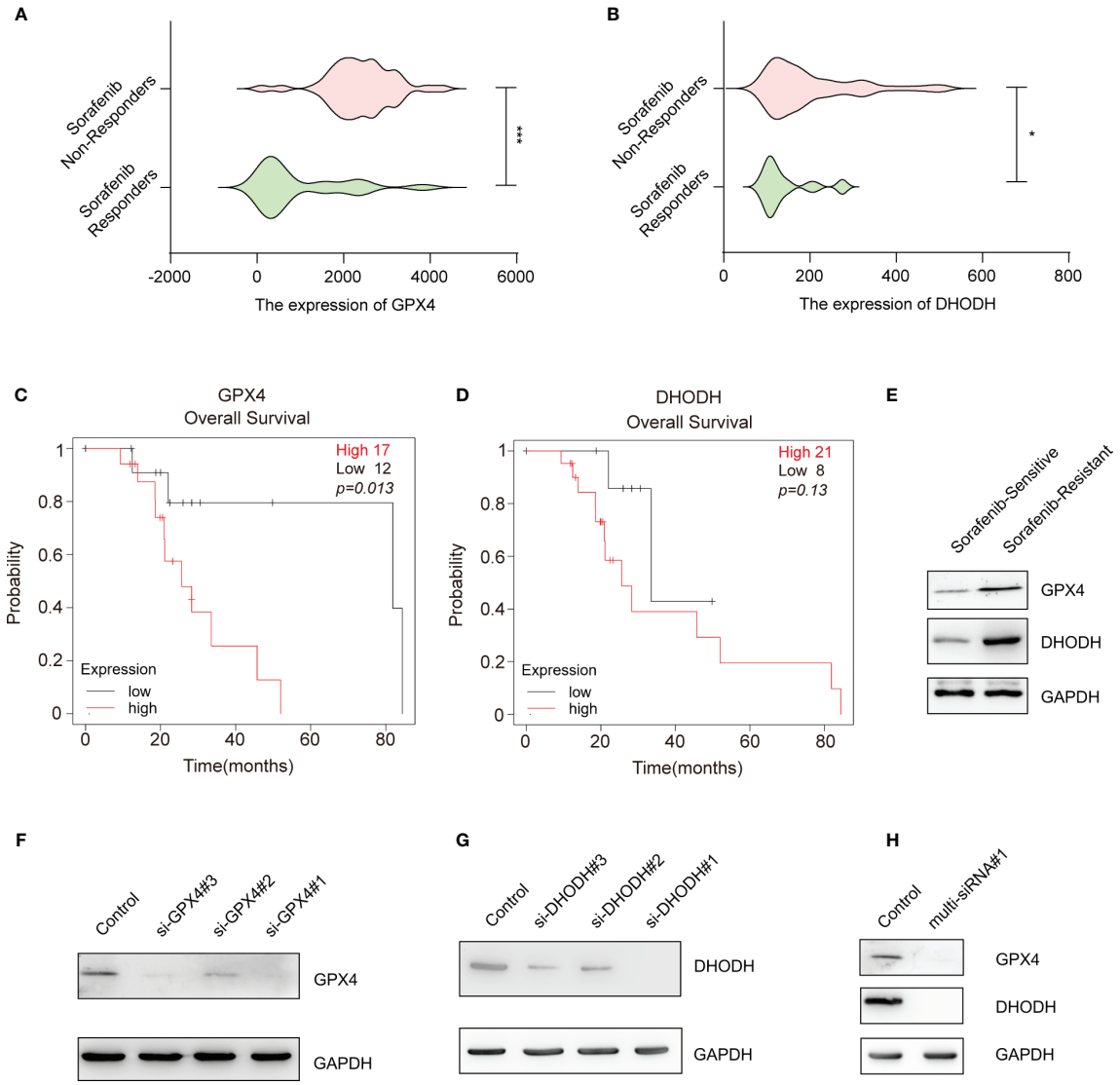

FIGURE 2 | Gene-silencing activities of multi-siRNA against GPX4 and DHODH genes. **(A)** GPX4 expression in HCC tissues from sorafenib responders (n=21) or sorafenib nonresponders (n=43) (gse109211). **(B)** That of DHODH in the HCC tissues of sorafenib responders (n=21) or sorafenib nonresponders (n=43) (gse109211). **(C)** Kaplan–Meier overall survival analysis of the GPX4 gene in HCC patients who received sorafenib treatment. **(D)** Kaplan–Meier overall survival analysis of the DHODH gene in HCC patients who received sorafenib treatment. **(E)** Western blotting for assessment of the protein levels of DHODH and GPX4 in sorafenib-sensitive HepG-2 or sorafenib-resistant HepG-2 (HepG-2R) cells. **(F)** Western blotting was conducted to detect GPX4 expression in HepG-2R cells transfected with scramble or GPX4 siRNAs. **(G)** Western blotting was conducted to detect DHODH expression in HepG-2R cells transfected with scramble or DHODH siRNAs. **(H)** HepG-2R cells were transfected with scramble siRNA or multi-siRNA#1 containing the si-GPX4#1 and si-DHODH#1 target sequences, and Western blotting was conducted to detect GPX4 and DHODH expression. **(A, B)** Unpaired *t*-test. **(C, D)** Log-rank test. *p <0.05, ***p <0.001.

surface protein) (**Figures 3A, B**). U1-A can bind the highly conserved sequence "AUUGCAC" in RNA *via* its N-terminal RRM (20). SP94 (protein sequence, SFSIIHTPILPL), is a novel peptide that has been reported to specifically bind to HCC cells (21). Therefore, we fused SP94 with the N-terminus of Lamp2b to enhance the tumor-targeting ability of the engineered exosomes (**Figures 3A, B**). The recombinant vector produced abundant expression of the fusion protein in transfected cells (**Figure 3C**). As the engineered SP94-Lamp2b-RRM fusion protein could express on exosomes (**Figure 3D**), we analyzed the binding ability of these exosomes to HCC cells. The results showed that exosomes derived from HEK-293T cells transfected with SP94-Lamp2b-RRM could bind strongly to HCC cells (**Figure 3E**), indicating that the SP94-Lamp2b-RRM fusion protein was incorporated into exosomes. In addition, specific exosome markers (CD63, TSG101 and CD9) were

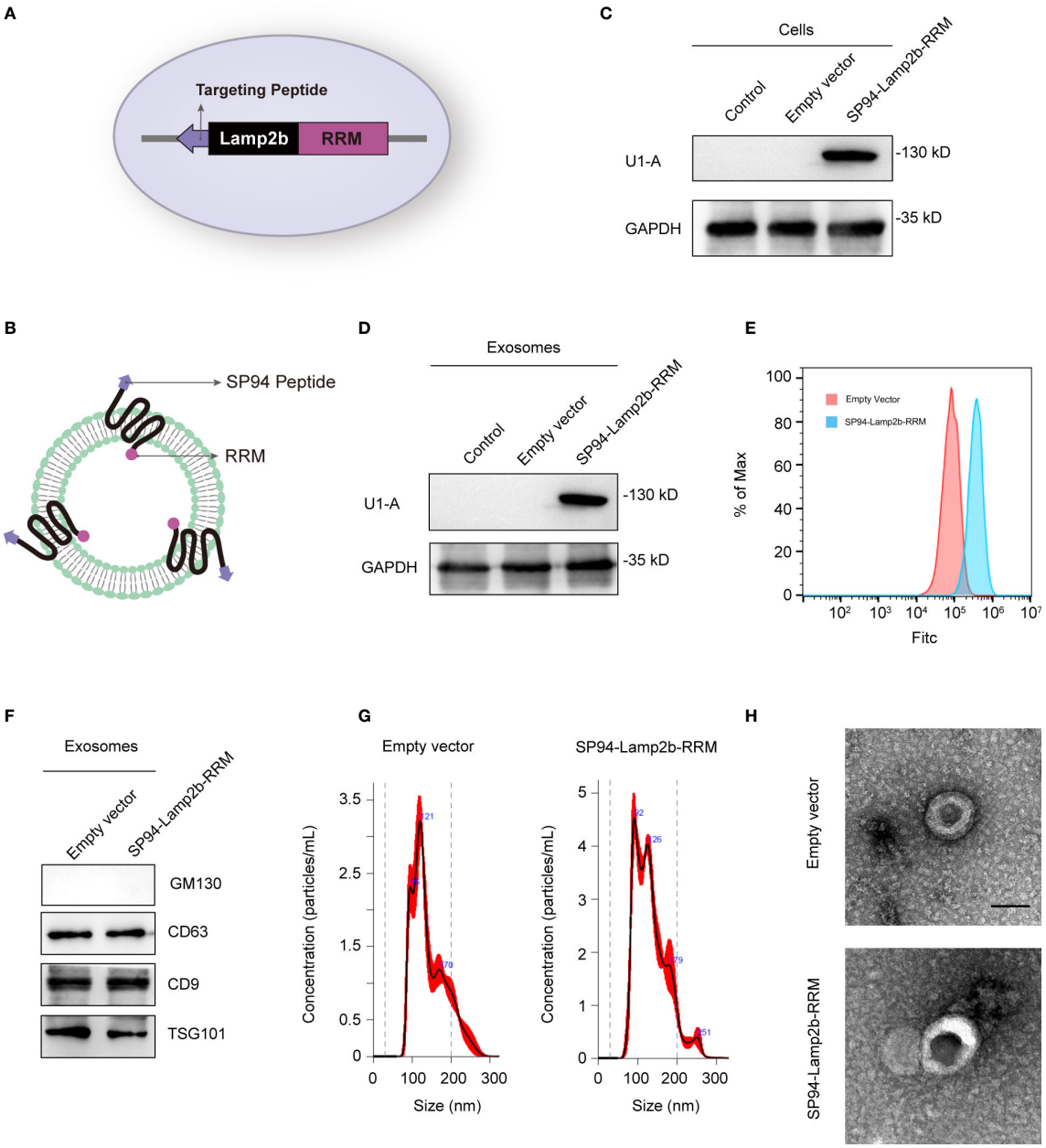

FIGURE 3 | Preparation and characterization of SP94-Lamp2b-RRM fusion protein-engineered exosomes. **(A)** Schematic representation of the hepatoma-cell-targeting peptide SP94 and the RRM of U1-A fused to the N-terminus and C-terminus of Lamp2b. **(B)** Schematic representation of the structure of the SP94-Lamp2b-RRM fusion protein and the engineered exosomes. **(C)** Western blot analysis of U1-A expression in HEK-293T cells transfected with empty vector or SP94-Lamp2b-RRM plasmids. **(D)** U1-A expression in exosomes derived from HEK-293T cells transfected with empty vector or SP94-Lamp2b-RRM plasmids. **(E)** Equal amount of DiO-labeled exosomes were incubated with $1*10^6$ immobilized HepG-2 cells for 1h. After washing, unbound exosomes were removed. HepG-2 cells were used for flow cytometry after trypsinization. The binding of different exosomes to HepG-2 cells was then quantitated by flow cytometry (FITC channel). **(F)** Western blot analysis of the exosome markers CD63, CD9 and TSG101, and the exclusive exosome marker GM130 on exosomes derived from HEK-293T cells transfected with different plasmids. **(G)** Nanoparticle tracking analysis shows the size distribution of exosomes derived from HEK-293T cells transfected with different plasmids. **(H)** Representative TEM images of exosomes derived from control or SP94-Lamp2b-RRM plasmid-transfected HEK-293T cells (scale bar, 100 nm).

detected in the purified samples, while the Golgi marker GM130 was barely detectable (**Figure 3F**). Nanoparticle tracking analysis (NTA) revealed that the exosomes were similar in number and had a similar size distribution between the groups (**Figure 3G**). Transmission electron microscopy (TEM) confirmed that the purified exosomes exhibited a typical round-shaped vesicular morphology and were within the appropriate size range (**Figure 3H**).

Efficient Therapeutic Cargo Encapsulation Into SP94-Lamp2b-RRM Fusion-Protein-Engineered Exosomes

Next, we explored whether the engineered SP94-Lamp2b-RRM fusion protein could promote RNA loading during exosome biogenesis. First, HEK-293T cells overexpressing the SP94-Lamp2b-RRM fusion protein were transfected with 100 nM corresponding FITC-tagged multi-siRNA (**Figure 4A**). Then, an equal number of exosomes from each group was evaluated by flow cytometry. The results showed that a higher amount of multi-siRNA containing the RRM recognition motif "AUUGCAC" could be sorted into exosomes compared to that of multi-siRNA#2 without the RRM binding sequence (**Figure 4B**). HEK-293T cells were then cocultured with HepG-2 cells (**Figure 4C**). Images from the confocal microscope showed a higher level of multi-siRNA containing the RRM "AUUGCAC" in HepG-2 cells (**Figure 4D**). Consistent

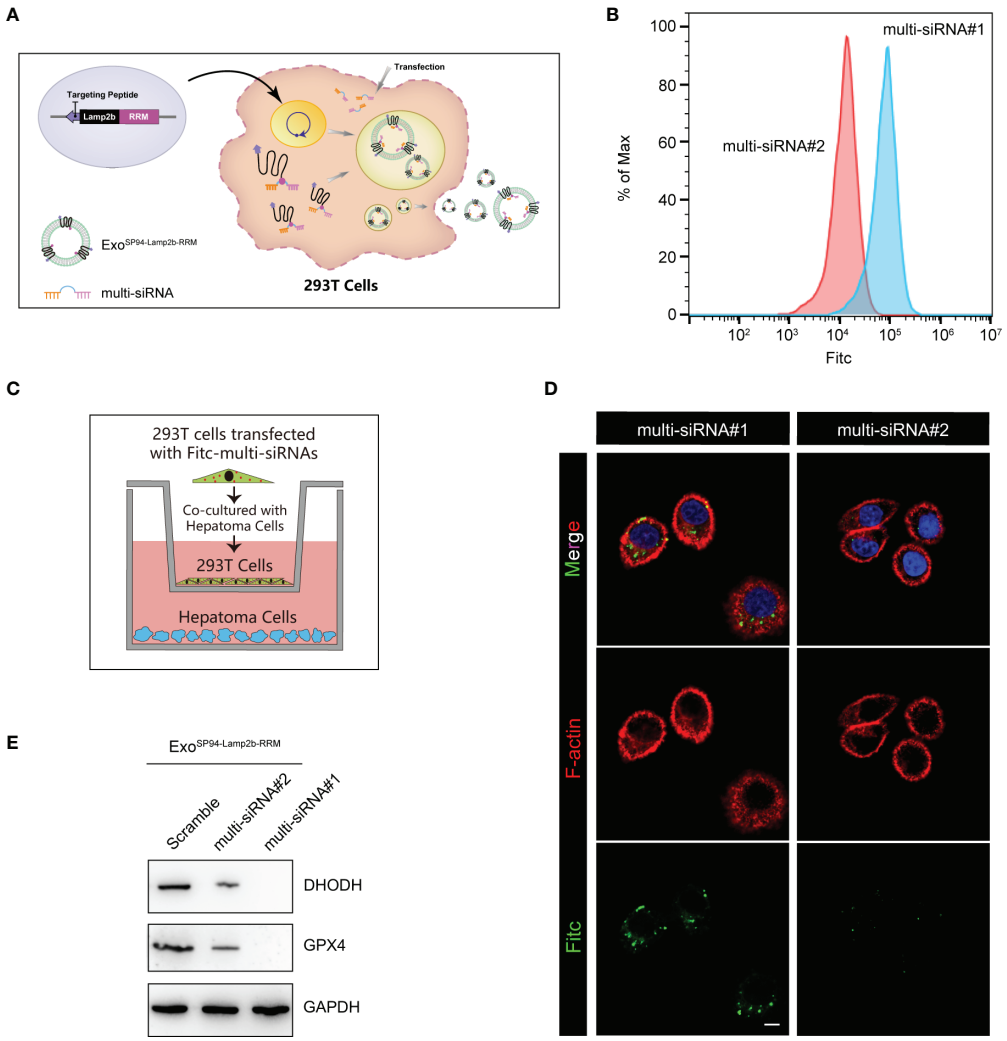

FIGURE 4 | Efficient therapeutic cargo encapsulation into engineered exosomes expressing SP94-Lamp2b-RRM fusion protein. **(A)** Schematic diagram of the process of multi-siRNA encapsulation into exosomes *via* the SP94-Lamp2b-RRM fusion protein in HEK-293T cells. The SP94-Lamp2b-RRM fusion protein recruits multi-siRNA containing the sequence "AUUGCAC" to exosomes *via* RNA-RRM recognition. **(B)** HEK-293T cells transiently transfected with FITC-tagged multi-siRNA#1 or FITC-tagged multi-siRNA#2. Then, exosomes were collected for the flow cytometry assay (multi-siRNA#1, contains si-GPX4#1, si-DHODH#1 and the RRM binding sequence; multi-siRNA#2, contains si-GPX4#1 and si-DHODH#1 without the RRM binding sequence). **(C, D)** HEK-293T cells transiently transfected with FITC-tagged multi-siRNAs were cocultured with HepG-2 cells for 24 h. **(C)** Schematic illustration of HepG-2 and HEK-293T cell coculturing. **(D)** Representative confocal images of FITC (green) and F-actin (red) staining in HepG-2 cells. The nuclei were counterstained with DAPI (blue) (scale bar, 10 μm). **(E)** HepG-2 cells were treated with functionalized exosomes derived from HEK-293 T cells and containing SP94-Lamp2b-RRM, and Western blot assays were conducted to detect GPX4 and DHODH expression in HepG-2 cells. Scramble: $1*10^6$ HEK-293T cells were treated with the same amount of scramble siRNA; multi-siRNA#2: $1*10^6$ HEK-293T cells were treated with the same amount of multi-siRNA#2; multi-siRNA#1: $1*10^6$ HEK-293T cells were treated with the same amount of multi-siRNA#1. After 24 h, the exosomes were collected and added to HepG-2 cells.

with this finding, exosomes derived from HEK-293T cells transfected with the multi-siRNA containing the "AUUGCAC" sequence could significantly suppress the expression of GPX4 and DHODH in HCC cells (**Figure 4E**). These results suggest that the SP94-Lamp2b-RRM fusion protein promotes the exosomal loading of the "AUUGCAC" sequence linked to the multi-siRNA *via* RNA-protein interactions.

SP94-Lamp2b-RRM-Functionalized Exosomes Could Overcome Sorafenib Resistance by Enhancing Sorafenib-Induced Ferroptosis in HCC Cells

To investigate whether $Exo^{SP94\text{-}Lamp2b\text{-}RRM}$ can bind to HCC cells, blank exosomes or $Exo^{SP94\text{-}Lamp2b\text{-}RRM}$ were labeled with DiO and added to sorafenib-resistant HepG-2 cell cultures. Confocal assay showed that green fluorescence appeared within 15 min and intensified over time (up to 60 min) in the SP94-Lamp2b-RRM-functionalized exosomes treated group. By contrast, relatively low level of green fluorescence was observed in control exosomes treated cells up to 60 min, confirming the targeting ability of SP94-Lamp2b-RRM-functionalized exosomes to HCC cells (**Figures 5A, B**). Then, we treated sorafenib-resistant HepG-2 cells with exosomes ($Exo^{SP94\text{-}Lamp2b\text{-}RRM}$-multi-siRNA#1). The results showed that $Exo^{SP94\text{-}Lamp2b\text{-}RRM}$-multi-siRNA#1 could significantly enhance the effect of sorafenib (**Figure 5C**). Then, we further measured ROS and lipid peroxidation levels, which are the primary drivers of ferroptosis. The results showed that treatment with $Exo^{SP94\text{-}Lamp2b\text{-}RRM}$-multi-siRNA#1 significantly increased ROS and MDA levels in sorafenib-resistant cells (**Figures 5D, E**). In addition to biochemical analyses, TEM was used to observe morphological changes. $Exo^{SP94\text{-}Lamp2b\text{-}RRM}$-multi-siRNA#1-treated cells displayed diminished or vanished mitochondrial cristae and condensed mitochondrial membrane densities compared to $Exo^{SP94\text{-}Lamp2b\text{-}RRM}$-scramble-treated cells (**Figure 5F**). Moreover, we also found that $Exo^{SP94\text{-}Lamp2b\text{-}RRM}$-multi-siRNA#1 could enhance sorafenib-induced ferroptotic cell death (**Figure 5G**). Taken together, these results suggested that $Exo^{SP94\text{-}Lamp2b\text{-}RRM}$-multi-siRNA#1 could enhance sorafenib-induced ferroptosis in HCC cells by silencing the expression of GPX4 and DHODH.

SP94-Lamp2b-RRM-Functionalized Exosomes Could Efficiently Target Hepatocellular Carcinoma *In Vivo*

To confirm whether SP94-Lamp2b-RRM-functionalized exosomes could target HCC *in vivo*, we tracked the distribution of DiR-labeled exosomes. First, we established an orthotopic liver injection model and observed that SP94-Lamp2b-RRM-functionalized exosomes were mainly distributed to the liver (**Figures 6A–C**). Meanwhile, SP94-Lamp2b-RRM-functionalized exosomes could target HCC (**Figures 6A–C**). Next, sorafenib-resistant HepG-2 cells were subcutaneously inoculated into the left backs of mice. In the subcutaneous HCC model, we found that SP94-Lamp2b-RRM-functionalized exosomes were mainly distributed in the liver and subcutaneous tumor tissues (**Figure 6D**, **Figure S3A**). The results from the different HCC models suggest that the SP94 targeting peptide dramatically enhances the ability of exosomes to bind HCC cells and tissues.

Therapeutic Effects of Cotreatment With SP94-Lamp2b-RRM-Functionalized Exosomes and Sorafenib in an HCC Mouse Model

Next, we explored the therapeutic effect of SP94-Lamp2b-RRM-functionalized exosomes combined with sorafenib *in vivo*. While the tumors of mice treated with sorafenib and $Exo^{SP94\text{-}Lamp2b\text{-}RRM}$ containing scramble multi-siRNA grew rapidly, those of mice treated with sorafenib and $Exo^{SP94\text{-}Lamp2b\text{-}RRM}$ containing multi-siRNA#1 were significantly reduced after 21 days of treatment (**Figures 7A–C**). However, the effect of sorafenib and $Exo^{SP94\text{-}Lamp2b\text{-}RRM}$ containing multi-siRNA#1 on inhibiting tumor growth was diminished when cells were treated with the ferroptosis inhibitor ferrostatin-1 (**Figures 7A–C**). Similarly, mice from the sorafenib and $Exo^{SP94\text{-}Lamp2b\text{-}RRM}$ containing multi-siRNA#1 cotreatment group had a longer life expectancy than did mice from the sorafenib and $Exo^{SP94\text{-}Lamp2b\text{-}RRM}$ containing scramble multi-siRNA treatment group (**Figure 7D**). To examine the knockdown efficiency in each group, GPX4 and DHODH expression in primary tumor lesions was investigated by immunohistochemistry. The results showed that multi-siRNA#1 could significantly suppress GPX4 and DHODH expression *in vivo* (**Figure 7E**). Taken together, these results suggested that $Exo^{SP94\text{-}Lamp2b\text{-}RRM}$-multi-siRNA#1 could overcome sorafenib resistance *in vivo* by silencing the ferroptosis suppressor genes GPX4 and DHODH.

Systemic Toxicity Evaluation

To evaluate the systemic toxicity of $Exo^{SP94\text{-}Lamp2b\text{-}RRM}$, exosomes containing scramble or multi-siRNA#1 were injected into nude mice *via* tail vein. There was no significant difference in the body weights of mice in the two groups (**Figure S4A**). In addition, compared to the control group, the $Exo^{SP94\text{-}Lamp2b\text{-}RRM}$ group showed relatively normal tissue structure and morphology (**Figure 8**). These results indicate that there was no obvious adverse effect after treatment with $Exo^{SP94\text{-}Lamp2b\text{-}RRM}$.

DISCUSSION

Our study demonstrated that sorafenib could induce ferroptosis in HCC cells, which is in line with the literature stating that the anticancer activity of sorafenib mainly relies on the induction of ferroptosis. What's more, we found that the expression of ferroptosis suppressor genes, especially GPX4 and DHODH, was enriched in sorafenib-resistant HCC cells and patient samples, which suggests that suppressed ferroptotic activity is associated with compromised therapeutic efficiency of sorafenib. Thus, precise elimination of ferroptosis suppressor genes might be a new promising strategy to enhance sorafenib efficacy and improve patient prognosis.

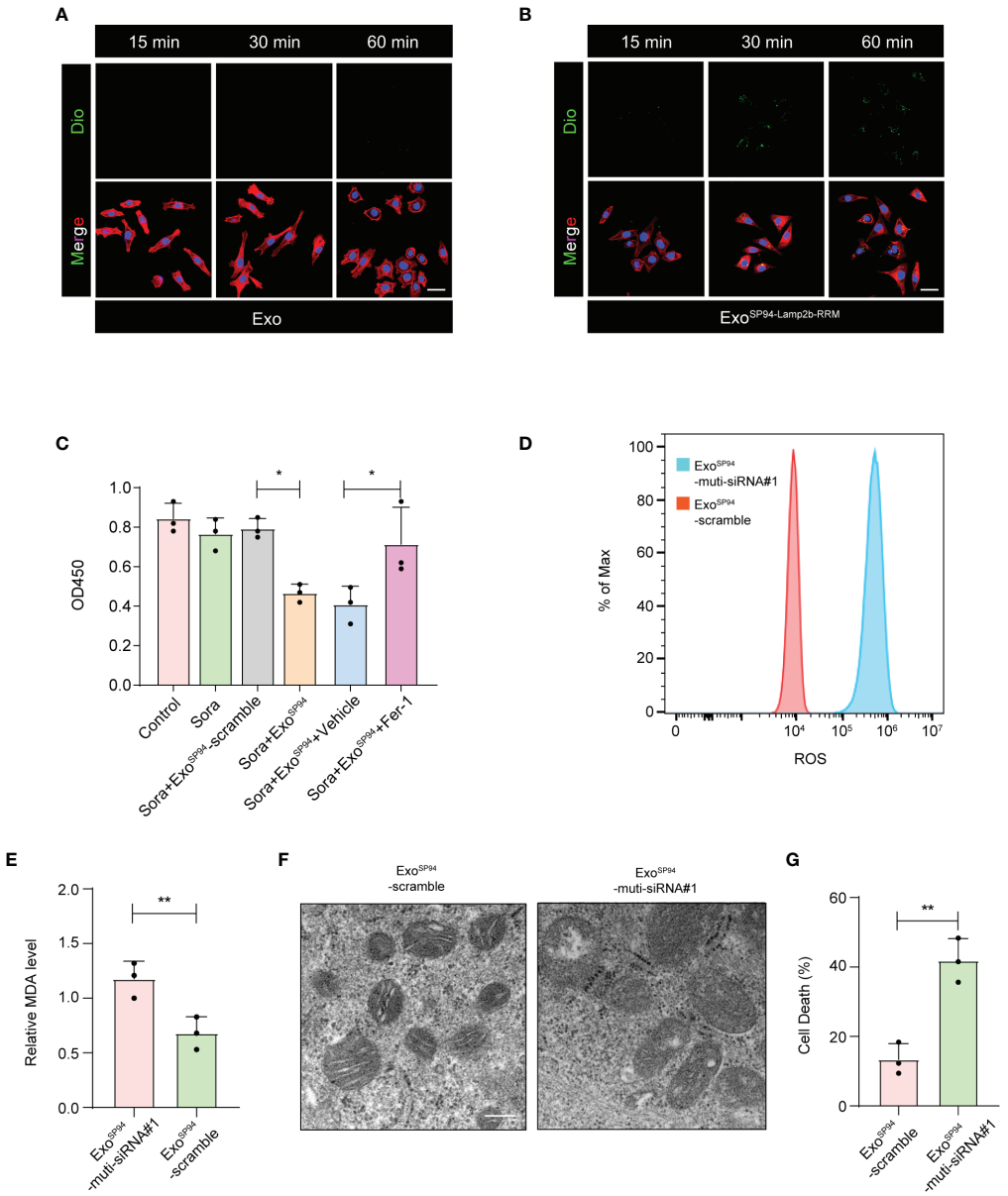

FIGURE 5 | SP94-Lamp2b-RRM-functionalized exosomes could overcome sorafenib resistance by enhancing sorafenib-induced ferroptosis in HCC cells. **(A–B)** Dio labeled engineered exosomes or control exosomes were incubated with HCC cells for 15, 30 or 60 min at 37°C. Then unbound exosomes were removed by PBS washing. Exosome endocytosis was analyzed by confocal microscopy. The nuclei and F-actin were counterstained with DAPI (blue) and TRITC phalloidin (red), respectively, (scale bar, 50 μm). **(C)** Sorafenib-resistant HepG-2 cells treated with sorafenib and SP94-Lamp2b-RRM-functionalized exosomes containing scramble or multi-siRNA#1. Viability of sorafenib-resistant HepG-2 cells as measured by the CCK-8 assay. **(D)** Sorafenib-resistant HepG-2 cells were treated with sorafenib in combination with SP94-Lamp2b-RRM-functionalized exosomes containing scramble or multi-siRNA#1, and the ROS production was assessed by DCFH-DA staining followed by flow cytometry. **(E)** MDA levels of sorafenib-resistant HepG-2 cells treated with sorafenib and SP94-Lamp2b-RRM-functionalized exosomes containing scramble or multi-siRNA#1. **(F)** TEM images of mitochondria in sorafenib-resistant HepG-2 cells cotreated with sorafenib and SP94-Lamp2b-RRM-functionalized exosomes containing scramble or multi-siRNA#1. **(G)** Sorafenib-resistant HepG-2 cells were treated with sorafenib and SP94-Lamp2b-RRM-functionalized exosomes containing scramble or multi-siRNA#1. Cell death was determined by PI staining coupled with flow cytometry. **(C, E, G)** The data are shown as the means ± S.E.M. **(C)** ANOVA with Dunnett's *t*-test. **(E, G)** Unpaired *t*-test. $^{*}p < 0.05$, $^{**}p < 0.01$.

Ferroptosis is a form of regulated cell death that is induced by excessive lipid peroxide accumulation in cellular membranes (22–24). Cells have developed at least two major defensive arms to detoxify lipid peroxides: GPX4 and DHODH. Consequently, disabling one arm forces cells to be more dependent on the other. For example, inhibition of either DHODH or GPX4 alone did not induce ferroptosis in HT-1080 cells, which is likely due to the relatively high endogenous expression of GPX4 and DHODH (25);

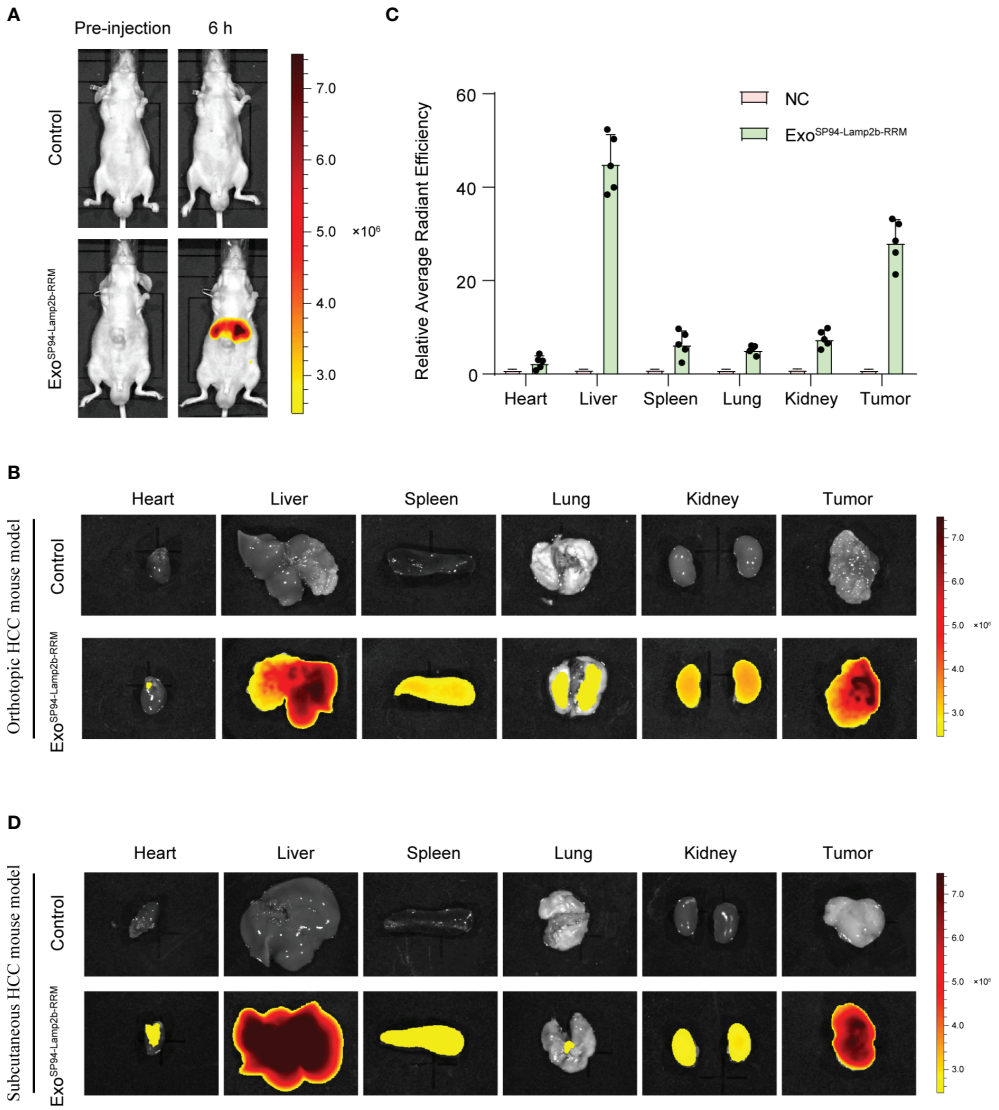

FIGURE 6 | SP94-Lamp2b-RRM-functionalized exosomes could efficiently target HCC *in vivo*. ***(A–C)*** Sorafenib-resistant HepG-2 cells were orthotopically inoculated into the left liver lobes of nude mice. SP94-Lamp2b-RRM-functionalized exosomes (100 μg) were injected into nude mice *via* tail vein. **(A)** Mice were evaluated with a fluorescent live imaging system 6 h after injection. **(B)** Representative *ex vivo* fluorescence images of DiR-labeled exosomes in the main organs and HCC tissues. **(C)** Relative fluorescence intensity of DiR-labeled exosomes in different organs and liver cancer tissues. **(D)** Sorafenib-resistant HepG-2 cells were subcutaneously inoculated on the left backs of mice. SP94-Lamp2b-RRM-functionalized exosomes were loaded with DiR, and 100 μg of exosomes was injected into mice *via* tail vein. Different organs and tumors were harvested to conduct fluorescence imaging. **(C)** The data are shown as the means ± S.E. M; n=5.

interestingly, a GPX4 inhibitor combined with a DHODH inhibitor could synergistically suppress HT-1080 tumor growth. Similarly, in our study, the sorafenib-resistant cells and tissue samples exhibited high levels of GPX4 and DHODH expression. Therefore, disabling both arms might better enhance sorafenib-induced ferroptosis. Here, we created a multi-siRNA that can simultaneously knock down GPX4 and DHODH *in vitro* and *in vivo*. To our knowledge, this is the first ferroptosis inducer that can directly target two genes. Additionally, this novel construct provides a new approach for the clinical treatment of sorafenib-resistant cancer.

Because of their intrinsic nature, exosomes are biocompatible with the host immune system and have an innate ability to protect and transport small RNAs and other critical molecules across biological barriers *in vivo*; they have been increasingly recognized as promising vehicles to deliver siRNA *in vivo* (26, 27). At present, the most common way to load nucleic acids into exosomes is *via* electroporation or direct encapsulation in donor cells (28); however, these methods have relatively low loading efficiencies. Meanwhile, *in vitro* loading of naked siRNAs into exosomes by electroporation could cause extensive siRNA aggregation and significantly reduce the level of bioactive siRNAs (29). Thus, there is an urgent need to develop a strategy for efficient loading of nucleic acids, especially siRNA. Recently, research conducted by our laboratory and others have observed that some RNA-binding

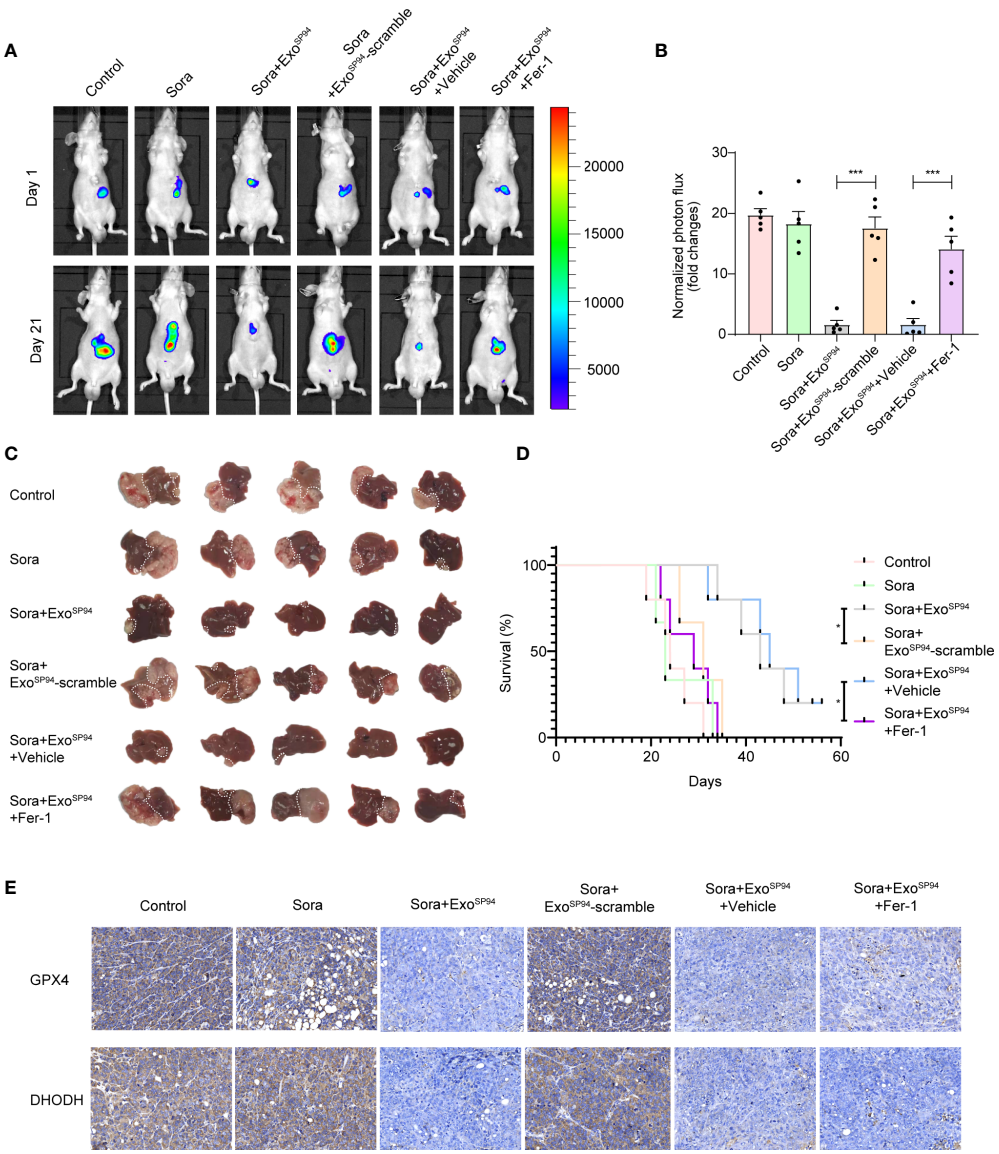

FIGURE 7 | Therapeutic effects of SP94-Lamp2b-RRM-functionalized exosomes and sorafenib in an HCC mouse model. Sorafenib-resistant HepG-2 cells were orthotopically injected into the left liver lobes of nude mice. Mice with a similar tumor size were used. Control: saline; Sora: sorafenib; Sora+Exo^{SP94}: sorafenib plus SP94-Lamp2b-RRM-functionalized exosomes containing multi-siRNA#1; Sora+Exo^{SP94}-scramble: sorafenib plus SP94-Lamp2b-RRM-functionalized exosomes containing scramble siRNA; Sora+Exo^{SP94}+Vehicle: sorafenib plus SP94-Lamp2b-RRM-functionalized exosomes containing multi-siRNA#1 in vehicle; Sora+Exo^{SP94}+Fer-1: sorafenib plus SP94-Lamp2b-RRM-functionalized exosomes in multi-siRNA#1 combined with ferrostatin-1. Tumor growth was measured with an IVIS imaging system. **(A)** Representative tumor imaging on days 1 and 21 after the first treatment. **(B)** The normalized photon flux at day 21 was analyzed (n=5). **(C)** Image of resected xenografts of nude mice injected intrahepatically with Sorafenib-resistant HepG-2 cells. **(D)** Survival of mice from different groups (n=5). **(E)** Representative immunohistochemical staining for GPX4 and DHODH in HCC tissues from different groups (scale bar, 25 μm). **(B)** The data are shown as the means ± S.E.M. ANOVA with Dunnett's *t*-test. **(D)** Log-rank test. ***$p < 0.001$.

proteins can efficiently sort miRNAs and other RNAs into exosomes *via* protein-RNA interactions (30, 31). In light of these data, we hypothesized that fusion of an exosomal membrane protein with a specific RNA-binding protein would increase the loading efficiency of the siRNA of interest; therefore, we fused the RNA recognition motif of U1-A with the C-terminus of Lamp2b, which interacts with the sequence "AUUGCAC" in the target RNA with a relatively high affinity. Then, a multi-siRNA was engineered to harbor the consensus "AUUGCAC" sequence. The preliminary data here indicate that the fusion protein helps sort multiple siRNAs containing the "AUUGCAC" sequence into exosomes during exosome biogenesis, especially when the RNA of interest is exogenously overexpressed. It is worth noting that due to the limitation of the present siRNA detection technology, the biological loading rate of multi-siRNA cannot be accurately detected in live cells and exosomes. Here, in the preparation of

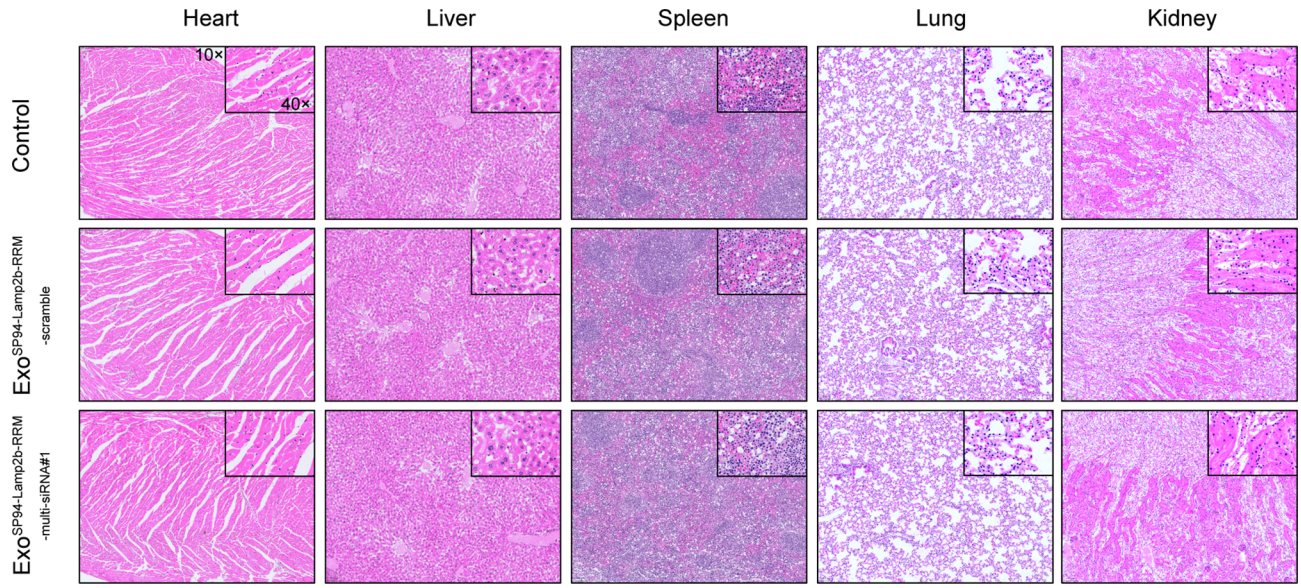

FIGURE 8 | Systemic toxicity evaluation. One hundred micrograms of SP94-Lamp2b-RRM-functionalized exosomes were injected into nude mice *via* tail vein every 3 days for 21 days. Control: saline; Sora+Exo$^{SP94\text{-}Lamp2b\text{-}RRM}$-scramble: sorafenib plus SP94-Lamp2b-RRM-functionalized exosomes containing scramble siRNA; Sora+Exo$^{SP94\text{-}Lamp2b\text{-}RRM}$-multi-siRNA#1: sorafenib plus SP94-Lamp2b-RRM-functionalized exosomes containing multi-siRNA#1; Representative hematoxylin-eosin (H&E) staining of the main organs from different treatment groups (scale bar, 100 μm).

functionalized exosomes, saturated amount of multi-siRNAs were transfected into cells to ensure that engineered exosomes were loaded with sufficient multi-siRNAs. Further experiments also confirmed that a large amount of multi-siRNAs could be effectively encapsulated into engineered exosomes and delivered to HCC cells, thus inducing down-regulation of GPX4 and DHODH. Our study established a novel strategy to efficiently load therapeutic multi-siRNA cargos into exosomes.

Currently, the poor solubility and potential off-target toxicity to normal cells and tissues preclude the systematic use of traditional ferroptosis inducers *in vivo* (32–34). Nanoscale exosomes are considered a good choice as a drug vehicle because exosomes could be engineered toward better targeting specificity *via* exosome surface protein modifications (35–39). For example, exosomes expressing the αγ integrin-specific iRGD peptide fused to LAMP-2b efficiently delivered doxorubicin to integrin-positive breast cancer cells *in vitro* and *in vivo* (40). Here, an HCC-specific targeting peptide, SP94, was fused to the extracellular domain of LAMP-2B at the N-terminus (21). Our data show that functionalized exosomes (Exo$^{SP94\text{-}lamp2b\text{-}RRM}$-multi-siRNA) can selectively deliver therapeutic cargos to human HCC cells with no obvious adverse effects. This is the first report of tumor-targeted exosome delivery of ferroptosis inducers, which might open a new avenue for the systematic use of ferroptosis inducers to treat cancer.

In summary, this study firstly identified that ferroptosis suppressor genes GPX4 and DHODH were enriched in sorafenib-resistant HCC and associated with compromised therapeutic efficiency of sorafenib. In addition, we described the use of multi-siRNA to enhance sorafenib-induced ferroptosis by simultaneously knocking down GPX4 and DHODH. More importantly, we designed HCC-targeted engineered exosomes (Exo$^{SP94\text{-}Lamp2b\text{-}RRM}$) to deliver multi-siRNA, thus overcoming acquired resistance to sorafenib from the perspective of ferroptosis.

DATA AVAILABILITY STATEMENT

The datasets presented in this study can be found in online repositories. The names of the repository/repositories and accession number(s) can be found in the article/**Supplementary Material**.

ETHICS STATEMENT

The animal study was reviewed and approved by Animal Care and Use Committee of Fourth Military Medical University.

AUTHOR CONTRIBUTIONS

XL, QY, and RZ contributed equally to this work. YG, CZ, and YZ contributed to project conceptualization and supervision. YG, XL, QY, CL, XG, RZ, and KZ contributed to the investigation. WQZ, SW, QH, WL, and ML contributed to the data curation; YG and XL contributed to writing the original draft; YG, CZ, YZ, WZ, and XL contributed to writing, reviewing, and editing the manuscript; and

YG, CZ, and SW contributed to funding acquisition. All authors contributed to the article and approved the submitted version.

FUNDING

This work was financially supported by grants from the Hong Kong Scholar Program; the National Natural Science Foundation of China (NSFC), NO. 81902678, 81802632, 82072910; the Key Research and Development Program of Shaanxi Province (NO. 2017ZDCXL-SF-01-03); and the Young Elite Scientist Sponsorship Program by CAST (No. YESS20210177).

ACKNOWLEDGMENTS

We thank Ms. Wang Wei for drawing the Graphical Abstract.

SUPPLEMENTARY MATERIAL

The Supplementary Material for this article can be found online at: https://www.frontiersin.org/articles/10.3389/fonc.2022.898156/full#supplementary-material

REFERENCES

1. Siegel RL, Miller KD, Jemal A. Cancer Statistics, 2018. *CA Cancer J Clin* (2018) 68:7–30. doi: 10.3322/caac.21442
2. Bray F, Ferlay J, Soerjomataram I, Siegel RL, Torre LA, Jemal A. Global Cancer Statistics 2018: GLOBOCAN Estimates of Incidence and Mortality Worldwide for 36 Cancers in 185 Countries. *CA Cancer J Clin* (2018) 68:394–424. doi: 10.3322/caac.21492
3. Yang JD, Hainaut P, Gores GJ, Amadou A, Plymoth A, Roberts LR. A Global View of Hepatocellular Carcinoma: Trends, Risk, Prevention and Management. *Nat Rev Gastroenterol Hepatol* (2019) 16:589–604. doi: 10.1038/s41575-019-0186-y
4. Cheng AL, Kang YK, Chen Z, Tsao CJ, Qin S, Kim JS, et al. Efficacy and Safety of Sorafenib in Patients in the Asia-Pacific Region With Advanced Hepatocellular Carcinoma: A Phase III Randomised, Double-Blind, Placebo-Controlled Trial. *Lancet Oncol* (2009) 10:25–34. doi: 10.1016/S1470-2045(08)70285-7
5. Chen X, Kang R, Kroemer G, Tang D. Broadening Horizons: The Role of Ferroptosis in Cancer. *Nat Rev Clin Oncol* (2021) 18:280–96. doi: 10.1038/s41571-020-00462-0
6. Wang Q, Bin C, Xue Q, Gao Q, Huang A, Wang K, et al. GSTZ1 Sensitizes Hepatocellular Carcinoma Cells to Sorafenib-Induced Ferroptosis *via* Inhibition of NRF2/GPX4 Axis. *Cell Death Dis* (2021) 12:426. doi: 10.1038/s41419-021-03718-4
7. Su Y, Zhao B, Zhou L, Zhang Z, Shen Y, Lv H, et al. Ferroptosis, a Novel Pharmacological Mechanism of Anti-Cancer Drugs. *Cancer Lett* (2020) 483:127–36. doi: 10.1016/j.canlet.2020.02.015
8. Sun X, Ou Z, Chen R, Niu X, Chen D, Kang R, et al. Activation of the P62-Keap1-NRF2 Pathway Protects Against Ferroptosis in Hepatocellular Carcinoma Cells. *Hepatology* (2016) 63:173–84. doi: 10.1002/hep.28251
9. Lachaier E, Louandre C, Godin C, Saidak Z, Baert M, Diouf M, et al. Sorafenib Induces Ferroptosis in Human Cancer Cell Lines Originating From Different Solid Tumors. *Anticancer Res* (2014) 34:6417–22.
10. Dixon SJ, Patel DN, Welsch M, Skouta R, Lee ED, Hayano M, et al. Pharmacological Inhibition of Cystine-Glutamate Exchange Induces Endoplasmic Reticulum Stress and Ferroptosis. *Elife* (2014) 3:e2523. doi: 10.7554/eLife.02523
11. Coriat R, Nicco C, Chereau C, Mir O, Alexandre J, Ropert S, et al. Sorafenib-Induced Hepatocellular Carcinoma Cell Death Depends on Reactive Oxygen Species Production *In Vitro* and *In Vivo*. *Mol Cancer Ther* (2012) 11:2284–93. doi: 10.1158/1535-7163.MCT-12-0093
12. Dietrich P, Koch A, Fritz V, Hartmann A, Bosserhoff AK, Hellerbrand C. Wild Type Kirsten Rat Sarcoma is a Novel microRNA-622-Regulated Therapeutic Target for Hepatocellular Carcinoma and Contributes to Sorafenib Resistance. *Gut* (2018) 67:1328–41. doi: 10.1136/gutjnl-2017-315402
13. Gao Y, Wang Z, Hao Q, Li W, Xu Y, Zhang J, et al. Loss of ERalpha Induces Amoeboid-Like Migration of Breast Cancer Cells by Downregulating Vinculin. *Nat Commun* (2017) 8:14483. doi: 10.1038/ncomms14483
14. Dixon SJ, Stockwell BR. The Role of Iron and Reactive Oxygen Species in Cell Death. *Nat Chem Biol* (2014) 10:9–17. doi: 10.1038/nchembio.1416
15. Seibt TM, Proneth B, Conrad M. Role of GPX4 in Ferroptosis and its Pharmacological Implication. *Free Radic Biol Med* (2019) 133:144–52. doi: 10.1016/j.freeradbiomed.2018.09.014
16. Feng H, Stockwell BR. Unsolved Mysteries: How Does Lipid Peroxidation Cause Ferroptosis? *PloS Biol* (2018) 16:e2006203. doi: 10.1371/journal.pbio.2006203
17. Wang F, Min J. DHODH Tangoing With GPX4 on the Ferroptotic Stage. *Signal Transduct Target Ther* (2021) 6:244. doi: 10.1038/s41392-021-00656-7
18. Herrmann IK, Wood M, Fuhrmann G. Extracellular Vesicles as a Next-Generation Drug Delivery Platform. *Nat Nanotechnol* (2021) 16:748–59. doi: 10.1038/s41565-021-00931-2
19. Wozniak AL, Adams A, King KE, Dunn W, Christenson LK, Hung WT, et al. The RNA Binding Protein FMR1 Controls Selective Exosomal miRNA Cargo Loading During Inflammation. *J Cell Biol* (2020) 219:e201912074. doi: 10.1083/jcb.201912074
20. Bolduc F, Turcotte MA, Perreault JP. The Small Nuclear Ribonucleoprotein Polypeptide a (SNRPA) Binds to the G-Quadruplex of the BAG-1 5'utr. *Biochimie* (2020) 176:122–7. doi: 10.1016/j.biochi.2020.06.013
21. Zhou T, Liang X, Wang P, Hu Y, Qi Y, Jin Y, et al. A Hepatocellular Carcinoma Targeting Nanostrategy With Hypoxia-Ameliorating and Photothermal Abilities That, Combined With Immunotherapy, Inhibits Metastasis and Recurrence. *ACS Nano* (2020) 14:12679–96. doi: 10.1021/acsnano.0c01453
22. Garcia-Bermudez J, Birsoy K. A Mitochondrial Gatekeeper That Helps Cells Escape Death by Ferroptosis. *Nature* (2021) 593:514–5. doi: 10.1038/d41586-021-01203-8
23. Stockwell BR, Friedmann AJ, Bayir H, Bush AI, Conrad M, Dixon SJ, et al. Ferroptosis: A Regulated Cell Death Nexus Linking Metabolism, Redox Biology, and Disease. *Cell* (2017) 171:273–85. doi: 10.1016/j.cell.2017.09.021
24. Zhang Y, Shi J, Liu X, Feng L, Gong Z, Koppula P, et al. BAP1 Links Metabolic Regulation of Ferroptosis to Tumour Suppression. *Nat Cell Biol* (2018) 20:1181–92. doi: 10.1038/s41556-018-0178-0
25. Mao C, Liu X, Zhang Y, Lei G, Yan Y, Lee H, et al. DHODH-Mediated Ferroptosis Defence is a Targetable Vulnerability in Cancer. *Nature* (2021) 593:586–90. doi: 10.1038/s41586-021-03539-7
26. Fu Z, Zhang X, Zhou X, Ur-Rehman U, Yu M, Liang H, et al. *In Vivo* Self-Assembled Small RNAs as a New Generation of RNAi Therapeutics. *Cell Res* (2021) 31:631–48. doi: 10.1038/s41422-021-00491-z
27. van Niel G, D'Angelo G, Raposo G. Shedding Light on the Cell Biology of Extracellular Vesicles. *Nat Rev Mol Cell Biol* (2018) 19:213–28. doi: 10.1038/nrm.2017.125
28. Ohno S, Takanashi M, Sudo K, Ueda S, Ishikawa A, Matsuyama N, et al. Systemically Injected Exosomes Targeted to EGFR Deliver Antitumor microRNA to Breast Cancer Cells. *Mol Ther* (2013) 21:185–91. doi: 10.1038/mt.2012.180
29. Kooijmans S, Stremersch S, Braeckmans K, de Smedt SC, Hendrix A, Wood M, et al. Electroporation-Induced siRNA Precipitation Obscures the Efficiency of siRNA Loading Into Extracellular Vesicles. *J Control Release* (2013) 172:229–38. doi: 10.1016/j.jconrel.2013.08.014
30. Gao Y, Li X, Zeng C, Liu C, Hao Q, Li W, et al. CD63(+) Cancer-Associated Fibroblasts Confer Tamoxifen Resistance to Breast Cancer Cells Through Exosomal miR-22. *Adv Sci (Weinh).* (2020) 7:2002518. doi: 10.1002/advs.202002518
31. Zhang H, Deng T, Liu R, Ning T, Yang H, Liu D, et al. CAF Secreted miR-522 Suppresses Ferroptosis and Promotes Acquired Chemo-Resistance in Gastric Cancer. *Mol Cancer* (2020) 19:43. doi: 10.1186/s12943-020-01168-8

32. Yu M, Gai C, Li Z, Ding D, Zheng J, Zhang W, et al. Targeted Exosome-Encapsulated Erastin Induced Ferroptosis in Triple Negative Breast Cancer Cells. *Cancer Sci* (2019) 110:3173–82. doi: 10.1111/cas.14181
33. Lu B, Chen XB, Ying MD, He QJ, Cao J, Yang B. The Role of Ferroptosis in Cancer Development and Treatment Response. *Front Pharmacol* (2017) 8:992. doi: 10.3389/fphar.2017.00992
34. Stockwell BR, Jiang X. The Chemistry and Biology of Ferroptosis. *Cell Chem Biol* (2020) 27:365–75. doi: 10.1016/j.chembiol.2020.03.013
35. Yi J, Minikes AM, Jiang X. Aiming at Cancer *In Vivo*: Ferroptosis-Inducer Delivered by Nanoparticles. *Cell Chem Biol* (2019) 26:621–2. doi: 10.1016/j.chembiol.2019.05.002
36. Terasawa K, Tomabechi Y, Ikeda M, Ehara H, Kukimoto-Niino M, Wakiyama M, et al. Lysosome-Associated Membrane Proteins-1 and -2 (LAMP-1 and LAMP-2) Assemble *via* Distinct Modes. *Biochem Biophys Res Commun* (2016) 479:489–95. doi: 10.1016/j.bbrc.2016.09.093
37. Armstrong JP, Holme MN, Stevens MM. Re-Engineering Extracellular Vesicles as Smart Nanoscale Therapeutics. *ACS Nano* (2017) 11:69–83. doi: 10.1021/acsnano.6b07607
38. Yang J, Wu S, Hou L, Zhu D, Yin S, Yang G, et al. Therapeutic Effects of Simultaneous Delivery of Nerve Growth Factor mRNA and Protein *via* Exosomes on Cerebral Ischemia. *Mol Ther Nucleic Acids* (2020) 21:512–22. doi: 10.1016/j.omtn.2020.06.013
39. Kim H, Yun N, Mun D, Kang JY, Lee SH, Park H, et al. Cardiac-Specific Delivery by Cardiac Tissue-Targeting Peptide-Expressing Exosomes. *Biochem Biophys Res Commun* (2018) 499:803–8. doi: 10.1016/j.bbrc.2018.03.227
40. Tian Y, Li S, Song J, Ji T, Zhu M, Anderson GJ, et al. A Doxorubicin Delivery Platform Using Engineered Natural Membrane Vesicle Exosomes for Targeted Tumor Therapy. *Biomaterials* (2014) 35:2383–90. doi: 10.1016/j.biomaterials.2013.11.083

Conflict of Interest: The authors declare that the research was conducted in the absence of any commercial or financial relationships that could be construed as a potential conflict of interest.

Publisher's Note: All claims expressed in this article are solely those of the authors and do not necessarily represent those of their affiliated organizations, or those of the publisher, the editors and the reviewers. Any product that may be evaluated in this article, or claim that may be made by its manufacturer, is not guaranteed or endorsed by the publisher.

Frontiers in Oncology

Advances knowledge of carcinogenesis and tumor progression for better treatment and management

The third most-cited oncology journal, which highlights research in carcinogenesis and tumor progression, bridging the gap between basic research and applications to imrpove diagnosis, therapeutics and management strategies.

Discover the latest Research Topics

See more →

Frontiers

Avenue du Tribunal-Fédéral 34
1005 Lausanne, Switzerland
frontiersin.org

Contact us

+41 (0)21 510 17 00
frontiersin.org/about/contact